

KfK 3880/3
December 1984

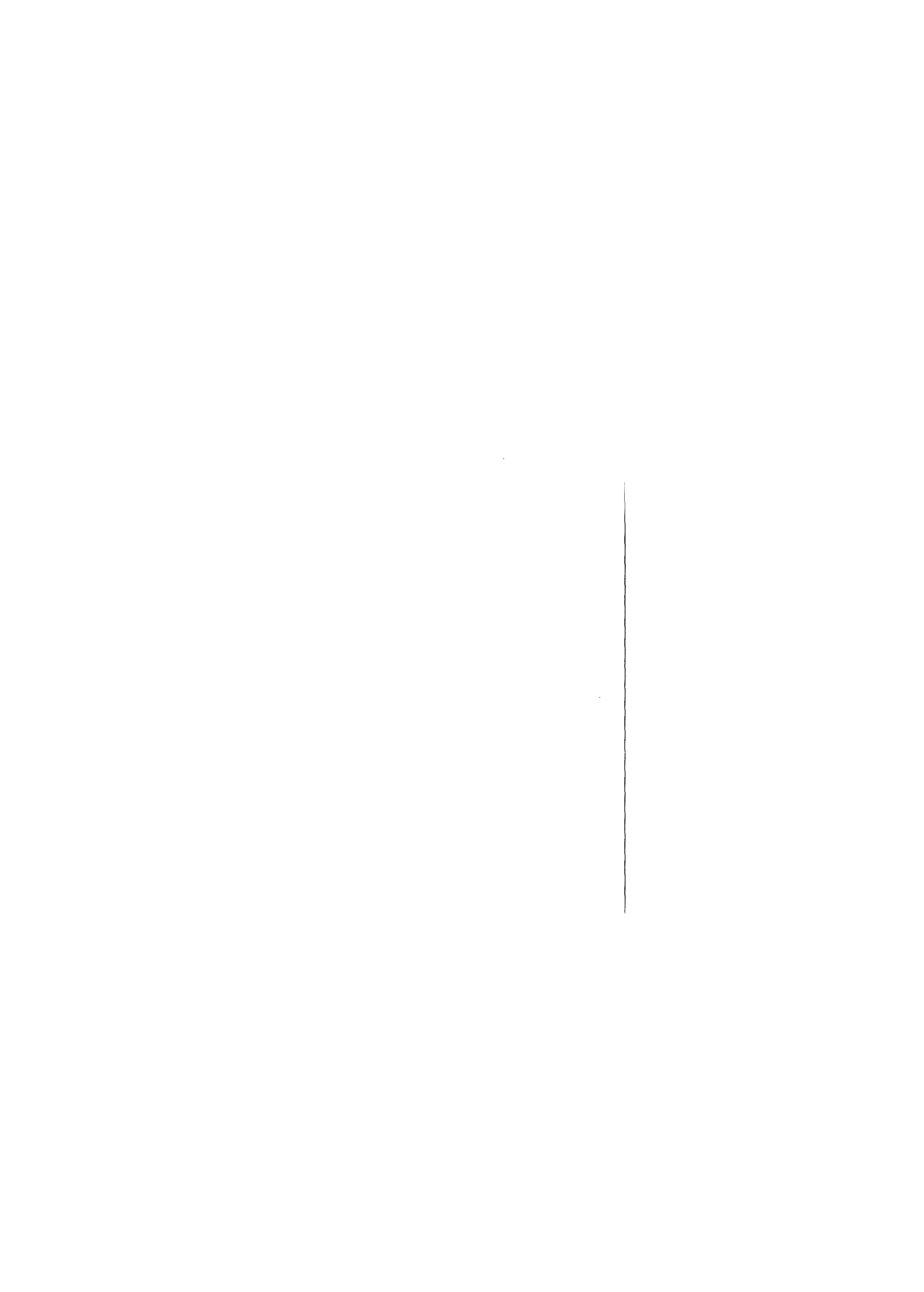
Fifth International Meeting on Thermal Nuclear Reactor Safety

Held at Karlsruhe Sept. 9-13, 1984

Proceedings Vol 3



**Nuclear Research Center
Karlsruhe**



FIFTH INTERNATIONAL MEETING
ON THERMAL NUCLEAR REACTOR SAFETY

KfK 3880/3 B

held at KARLSRUHE, September 9 - 13, 1984

VOLUME 3

Chapter 9: Fission Product Behavior
Chapter 10: Code Development and Verification
Chapter 11: Probabilistic Risk Assessment

Compiled by G. Bork and H. Rininsland
Karlsruhe Nuclear Research Center
Project Nuclear Safety

© Copyright 1984 by
Kerntechnische Gesellschaft e. V., Bonn
All rights reserved
Available from
Kernforschungszentrum Karlsruhe GmbH
Literaturabteilung
Postfach 3640 · D-7500 Karlsruhe 1
Printed in the Federal Republic of Germany

ISSN 0303-4003

Foreword

The 5th International Meeting on Thermal Nuclear Reactor Safety was held in Karlsruhe on September 9-13, 1984; it was attended by some 500 scientists and engineers from 25 countries. The conference was jointly sponsored by the European Nuclear Society (ENS), the American Nuclear Society (ANS), the Canadian Nuclear Society (CNS) and the Japan Atomic Energy Society (JAES). The meeting was further endorsed by, and organized in cooperation with, the Nuclear Energy Agency (NEA) of the Organization for Economic Cooperation and Development, the International Atomic Energy Agency (IAEA), and the Commission of the European Communities (CEC). Host organizations were the Kerntechnische Gesellschaft (KTG) and the Kernforschungszentrum Karlsruhe (KfK). The meeting was the fifth in a series of international meetings in the same subject areas with ANS and ENS as primary sponsors.

The Karlsruhe reactor safety meeting was held to reflect on the present status of engineered safety systems in nuclear power plants and to represent the findings of international safety research.

Seven invited experts of international reputation outlined the present state of the art in survey lectures. Moreover, more than 200 technical and scientific papers selected from 280 submitted papers, dealt with recent findings in reactor safety technology and research in the following areas: safety systems and functions optimization; man machine interface and emergency response; code development and verification; system and component behavior; fuel behavior during severe accidents; core debris and core concrete interaction; fission product behavior; containment response; probabilistic risk assessment. We wish to thank all speakers for their valuable contributions.

The meeting was concluded by a panel discussion on "Progress and Trends in Reactor Safety Technology and Research - What Has Been Achieved to Date? - What Remains to Be Done?"

It is not possible to acknowledge individually all persons who contributed to the meeting. We are greatly indebted to H.H. Hennies, President of the German Kerntechnische Gesellschaft (KTG), and J.M. Hendrie, President of the American Nuclear Society (ANS) who served as General Chairmen, and to A. Birkhofer as Chairman of the Technical Program Committee. Many thanks are due to the members of the Steering Committee, the Technical Program Committee, the Review Committee and the Organizing Committee.

The 6th International Meeting on Thermal Nuclear Reactor Safety was announced to take place in February 1986 at San Diego, California.

Volume 1Chapter 1

Opening Addresses and Invited Papers (Plenary Sessions)

Opening Addresses:	pages
1.1 H.H. Hennies, General Chairman	3 - 8
1.2 G. Weiser, Baden-Württemberg State Minister	9 - 19
1.3 K.H. Narjes, Member of the Commission of the European Communities	21 - 34
Invited Papers (Plenary Sessions):	
1.4 A. Gauvenet: Nuclear Reactor Operation Across the World	35 - 54
1.5 W. Dircks, G. Naschi: Regulatory Trends in OECD Member Countries	55 - 72
1.6 D.O. Pickman, A. Fiege: Fuel Behavior Under DBA Conditions	73 - 94
1.7 W.R. Stratton: Review of Recent Source Term Investigations	95 - 110
1.8 W.G. Morison, W.J. Penn: Containment Systems Capability	111 - 138
1.9 H.W. Lewis: Probabilistic Risk Assessment - Merits and Limitations	139 - 148
1.10 J.H. Gittus, F.R. Allen: Safety Goals Approaches	149 - 164
1.11 A. Birkhofer: Advances and Trends in Reactor Safety Research and Technology	165 - 178

Chapter 2

Safety Related Operation Experience

	pages
2.1 K.J. Laakso: Systematic Analysis of Plant Disturbances with a View to Reducing Scram Frequency	181 - 190
2.2 R. Japavaire, B. Fourest: An Example of Operating Experience in France: The Tricastin 1 Incident on August 3, 1982	191 - 198
2.3 G. Gros, D. Perrault: Control Rod Guide Tube Support Pin Cracking at French Plants	199 - 209
2.4 P.J. Amico: Fault Tree Analysis of Westinghouse Solid State Protection System Scram Reliability	210 - 219
2.5 T. Meslin, A. Carnino, B. Payen, A. Cahuzac: Station Blackout: A Test on a Plant at Power Lessons Learned for Safety Studies	220 - 229
2.6 P. Cassette, G. Giroux, H. Roche, J.J. Seveon: Evaluation of Primary Coolant Leaks and Assessment of Detection Methods	230 - 238
2.7 G. Dredemis, B. Fourest: Systematic Safety Evaluation of Old Nuclear Power Plants	239 - 247
2.8 J. Magdalinski, R. Ivars: Hydrogen Water Chemistry - A Proven Method to Inhibit Intergranular Stress Corrosion Cracking in Boiling Water Reactors	248 - 257

	pages
2.9 R. Schraewer, B. Wintermann: The Fine Motion Control Rod Drive and Reactor Scram System of KWU; Design, Long Term Operational Behaviour and Experiences	258 - 267
2.10 E. Legath: Power Uprates in ASEA-ATOM Boiling Water Reactors	268 - 272
2.11 K. Fischer, H. Kastl, M. Kurzawe: Dose Reduction by Application of Advanced Methods for Testing and Repairing of Steam Generator Tubes	273 - 282
2.12 R.G. Sauvé, W.W. Teper Investigation of A Liquid Zone Control Assembly Failure at a Nuclear Generating Station	283 - 294

Chapter 3

System and Component Behavior

3.1 F.J. Erbacher: Interaction Between Fuel Clad Ballooning and Thermal- Hydraulics in a LOCA	299 - 310
3.2 M.A. Bolander, C.D. Fletcher, C.B. Davis, C.M. Kullberg, B.D. Stitt, M.E. Waterman, J.D. Burttt: RELAP5 Thermal-Hydraulic Analyses of Overcooling Sequences in a Pressurized Water Reactor	311 - 319
3.3 J.E. Koenig, R.C. Smith: TRAP-PF1 Analyses of Potential Pressurized-Thermal-Shock Transients at a Combustion-Engineering PWR	320 - 329
3.4 W. Häfner, L. Wolf: Review and Assessment of American Experiments and Theoretical Models for Thermal Mixing PTS-Phenomena as Basis for Designing HDR-Experiments TEMB	330 - 347

	pages
3.5 J.Q. Howieson, L.J. Watt, S.D. Grant, P.G. Hawley, S. Girgis: CANDU LOCA Analysis with Loss of Offsite Power to Meet LWR Acceptance Criteria as Applied in Japan	348 - 356
3.6 U.S. Rohatgi, C. Yuelys-Miksis, P. Saha: An Assessment of Appendix K Conservatism for Large Break LOCA in a Westinghouse PWR	357 - 365
3.7 P. Gulshani, M.Z. Caplan, N.J. Spinks: THERMOSS: A Thermohydraulic Model of Flow Stagnation in a Horizontal Fuel Channel	366 - 375
3.8 N.J. Spinks, A.C.D. Wright, M.Z. Caplan, S. Prawirosoehardjo, P. Gulshani: Thermosyphoning in the CANDU Reactor	376 - 384
3.9 K.H. Ardron, V.S. Krishnan, J.P. Mallory, D.A. Scarth: Studies of Hot-Wall Delay Effects Pertinent to CANDU LOCA Analysis	385 - 396
3.10 J.T. Rogers: A Study of the Failure of the Moderator Cooling System in a Severe Accident Sequence in a CANDU Reactor	397 - 408
3.11 S.E. Meier: Fluid-Structure Interaction in Pressure Water Reactors	409 - 415
3.12 J.A. Kobussen, R. Mylonas, W.X. Zheng: RETRAN Predictions for Pressure Transients Following a Feedwater Line Break and Consequent Check Valve Closing	416 - 425
3.13 J.A. Desoisa, C.P. Greef: Reactor Fault Simulation at the Closure of the Windscale Advanced Gas-Cooled Reactor: Analysis of Transient Tests	426 - 435

	pages
3.14 G. Herbold, E.J. Kersting: Analysis of a Total Loss of AC-Power in a German PWR	436 - 447
3.15 C.A. Dobbe, R. Chambers, P.D. Bayless: Thermal-Hydraulic and Core Damage Analysis of the Station Blackout Transient in Pressurized Water Reactors	448 - 456
3.16 R. Bisanz, B. Burger, U. Lang, M. Schindler, F. Schmidt, H. Unger: Analysis of Severe LOCA Problems Using RELAP5 and TRAC	457 - 466
3.17 R.R. Schultz, Y. Kukita, Y. Koizumi, K. Tasaka: A LSTF Simulation of the TMI-2 Scenario in a Westinghouse Type Four Loop PWR	467 - 476
3.18 E.F. Hicken: Results from the OECD-LOFT Consortium Tests	477
3.19 P.J. Fehrenbach, I.J. Hastings, J.A. Walsworth, R.C. Spencer, J.J. Lipsett, C.E.L. Hunt, R.D. Delaney: Zircaloy-Sheathed UO ₂ Fuel Performance During In-Reactor LOCA Transients	478 - 487
3.20 V.I. Nath, E. Kohn: High Temperature Oxidation of CANDU Fuel During LOCA	488 - 497
3.21 R.M. Mandl, B. Brand, H. Schmidt: The Importance of End-of-Blowdown Phase on Refill/ Reflood for the Case of Combined ECC Injection. Results from PKL Tests	498 - 507
3.22 M. Spiga: Heat Transfer in PWR U-Tube Steam Generators	508 - 515
3.23 F.J. Erbacher, P. Ihle, K. Rust, K. Wiehr: Temperature and Quenching Behavior of Undeformed, Ballooned and Burst Fuel Rods in a LOCA	516 - 524

	pages
3.24 D.G. Reddy, C.F. Fighetti: A Study of Rod Bowing Effect on Critical Heat Flux in PWR Rod Bundles	525 - 534
3.25 H. Kianjah, V.K. Dhir, A. Singh: Enhancement of Heat Transfer in Disperse Flow and Downstream of Blockages in Rod Bundles	535 - 545
3.26 D. Saphier, J. Rodnizky, G. Meister: Transient Analysis of an HTGR Plant With the DSNP Simulation System	546 - 555

Chapter 4

Safety Systems and Function Optimization

4.1 R. Martin, H. Guesnon: Safeguard Pumps Qualification for French Nuclear Plants The EPEC Test Loop	559 - 573
4.2 P. Wietstock: Hydrodynamical Tests with an Original PWR Heat Removal Pump	574 - 580
4.3 G. Depond, H. Sureau: Steam Generator Tube Rupture Risk Impact on Design and Operation of French PWR Plants	581 - 587
4.4 L. Cave, W.E. Kastenberg, K.Y. Lin: A Value/Impact Assessment for Alternative Decay Heat Removal Systems	588 - 596
4.5 H.A. Maurer: Cost Benefit Analysis of Reactor Safety Systems	597 - 606

	pages
4.6 A. Renard, R. Holzer, J. Basselier, K. Hnilica, Cl. Vandenberg: Safety Assessment from Studies of LWR's Burning Plutonium Fuel	607 - 616
4.7 J.L. Platten: Periodic (Inservice) Inspection of Nuclear Station Piping Welds, for the Minimum Overall Radiation Risk	617 - 625
4.8 P. Grimm, J.M. Paratte, K. Foskolos, C. Maeder: Parametric Studies on the Reactivity of Spent Fuel Storage Pools	626 - 633
4.9 W. Geiger: The CEC Shared Cost Action Research Programme on the Safety of Thermal Water Reactors: Results in the Sub-Area "Protection of Nuclear Power Plants Against External Gas Cloud Explosions"	634 - 642
4.10 G.P. Celata, M. Cumo, G.E. Farello, P.C. Incalcaterra: Physical Insight in the Evaluation of Jet Forces in Loss of Coolant Accidents	643 - 654
4.11 A. Singh, D. Abdollahian: Critical Flow Thru Safety Valves	655 - 665
4.12 A. Aust, H.-R. Niemann, H.D. Fürst, G.F. Schultheiss: Chugging-Related Load Reduction for Pressure Suppression Systems	666 - 674
4.13 S.A. Andersson, S. Helmersson, L.-E. Johansson: Improved Fuel Cycle Flexibility and Economy: Verification Tests with BWR Coolant Flow Range Extension	675 - 682

	pages
4.14 M. Bielmeier, M. Schindler, H. Unger, H. Gasteiger, H. Stepan, H. Körber: Investigation of the ECC-Efficiency in the Case of Small Leaks in a 1300 MW _{e1} Boiling Water Reactor	683 - 692
4.15 H. Fabian, K. Frischengruber: Safety Concept and Evaluation of the 745 MW KWU- Pressurized Heavy Water Reactor (PHWR)	693 - 711
4.16 P. Antony-Spies, D.Göbel, M. Becker: Survey of KWU's Safety Related Containment Work for American Boiling Water Reactors	712 - 719

Volume 2

Chapter 5

Man Machine Interface and Emergency Response

5.1 W. Aleite, K.H. Geyer: Safety Parameter Display System Functions are Integrated Parts of the KWU KONVOI Process Information System (SPDS Functions are parts of the KWU-PRINS)	723 - 732
5.2 R. Marcille: Man-Machine Interface Enhancement Undertaken by EDF to Minimize Human Errors	733 - 739
5.3 B. Wahlström, G. Mancini: International Research and Information Dissemination in the Field of Human Factors of Nuclear Power	740 - 751
5.4 K. Hartel: Simulator Modelling of the PWR	752 - 761
5.5 J.D. Lewins: Simulation for Nuclear Reactor Technology	762 - 765

	pages
5.6 T. Eckered, W. Essler: Emergency Planning and Preparedness in EC Countries	766 - 775
5.7 S. Hassanien: Bruce Nuclear Generating Station 'A' Operational Review for Loss of Coolant Accident with Fuel Failure Scenario	776 - 785
5.8 E. Hussein, J.C. Luxat: Heat Transport Inventory Monitoring for CANDU-PHW Reactors	786 - 795
5.9 S. Guarro, D. Okrent: Logic Flowgraph Model for Disturbance Analysis of a PWR Pressurizer System	796 - 803
5.10 R.C. Knobel: A Symptom Based Decision Tree Approach to Boiling Water Reactor Emergency Operating Procedures	804 - 813
5.11 R.T. Curtis, B.B. Agrawal: Recent Results from the U.S. Severe Accident Sequence Analysis (SASA) Program	814 - 823
5.12 T.S. Margulies, J.A. Martin, Jr.: Precalculated Doses for Emergency Response	824 - 832
5.13 H. Sureau, J. Mesnage: Physical State Approach to PWR Emergency Operating Procedures: Recent Developments in France	833 - 841
5.14 A. Brunet, T. Meslin: Validation of Event Oriented Procedures	842 - 846

Chapter 6

Fuel Behavior during Severe Accidents

	pages
6.1 R.W. Wright, M. Silberberg, G.P. Marino: Status of the Joint Program of Severe Fuel Damage Research of the USNRC and Foreign Partners	851 - 857
6.2 J.N. Lillington: Assessment of SCDAP by Analysis of In-Pile Experiments; Power Burst Facility - Severe Fuel Damage Scoping Test	858 - 875
6.3 P.E. MacDonald, C.L. Nalezny, R.K. McCardell: Severe Fuel Damage Test 1-1 Results	876 - 887
6.4 L.J. Siefken: SCDAP Code Analysis of the Power Burst Facility Severe Fuel Damage Test 1-1	888 - 896
6.5 C.M. Allison, D.L. Hagrman, G.A. Berna: The Influence of Zircaloy Oxidation and Melting Behavior on Core Behavior during a Severe Accident	897 - 907
6.6 R. Bisanz, F. Schmidt: Analysis of the PBF Severe Fuel Damage Experiments with EXMEL-B	908 - 916
6.7 A.C. Marshall, P.S. Pickard, K.O. Reil, J.B. Rivard, K.T. Stalker: DF-1: An ACRR Separate Effects Experiment on Severe Fuel Damage	917 - 927
6.8 G. Schanz, H. Uetsuka, S. Leistikow: Investigations of Zircaloy-4 Cladding Oxidation under Steam Starvation and Hydrogen Blanketing Conditions	928 - 937
6.9 S. Saito, S. Shiozawa: Severe Fuel Damage in Steam and Helium Environments Observed in In-Reactor Experiments	938 - 947

	pages
6.10 U. Lang, F. Schmidt, R. Bisanz: Analysis of the Fuel Heatup and Melting Experiments NIELS- CORA with the Code System SSYST-4	948 - 957
6.11 S.H. Kim, R.P. Taleyarkhan, M.Z. Podowski, R.T. Lahey, Jr.: An Analysis of Core Meltdown Accidents for BWRs	958 - 967
6.12 P. Cybulskis: In-Vessel Hydrogen Generation Analyses with MARCH 2	968 - 977
6.13 C. Blahnik, W.J. Dick, D.W. McKean: Post Accident Hydrogen Production and Control in Ontario Hydro CANDU Reactors	978 - 987
6.14 G.I. Hadaller, R. Sawala, E. Kohn, G.H. Archinoff, S.L. Wadsworth: Experiments Investigating the Thermal-Mechanical Behaviour of CANDU Fuel under Severely Degraded Cooling	988 - 998
6.15 M.S. El-Genk, S.-H. Kim, D. Erickson: Post-Accident Heat Removal Analysis: An Assessment of the Composition of Core Debris Beds	999 - 1014
6.16 P. Hofmann, H.J. Neitzel: External and Internal Reaction of Zircaloy Tubing with Oxygen and UO ₂ and its Modeling	1015 - 1025
6.17 A. Denis, E.A. Garcia: Simulation of the Interaction Between Uranium Dioxide and Zircaloy	1026 - 1034
6.18 A. Skokan: High Temperature Phase Relations in the U-Zr-O System	1035 - 1042
6.19 H.E. Rosinger, K. Demoline, R.K. Rondeau: The Dissolution of UO ₂ by Molten Zircaloy-4 Cladding	1043 - 1056

	pages
6.20 W. Eifler: Thermal Hydraulic Severe Accident Phenomena in Small Fuel Rod Bundles during Simulation Experiments	1057 - 1066
6.21 A.W.P. Newbigging, A.I. Russell, E. Turner: Post-Irradiation Examination of Fuel Subjected to Pressurized High Temperature Transients in WAGR	1067 - 1075

Chapter 7

Core Debris Behavior and Core Concrete Interaction

7.1 B.W. Spencer, L.M. McUmber, J.J. Sienicki: Results and Analysis of Reactor-Material Experiments on Ex-Vessel Corium Quench and Dispersal	1079 - 1089
7.2 T. Schulenberg, U. Müller: A Refined Model for the Coolability of Core Debris with Flow Entry from the Bottom	1090 - 1097
7.3 B.J. Kim, M.L. Corradini: Recent Film Boiling Calculations: Implication on Fuel-Coolant Interactions	1098 - 1107
7.4 T. Ginsberg, J.C. Chen: Quench Cooling of Superheated Debris Beds in Containment during LWR Core Meltdown Accidents	1108 - 1117
7.5 B.D. Turland, N.J. Brealey: Improvements to Core-Concrete Interaction Models	1118 - 1127
7.6 S.B. Burson: Contributions to Containment Threat from High-Temperature Core-Debris Cavity Interactions	1128 - 1137
7.7 P.G. Kroeger, Y. Shiina: Transient Moisture Migration in Concrete During Severe Reactor Accidents	1138 - 1147

	pages
7.8 R.S. Denning: Interactions and Feedback Effects in Severe Accident Analysis	1148 - 1157
7.9 H. Pförtner, H. Schneider, W. Drenkhahn, C. Koch: The Effects of Gas Explosions in Free and Partially Confined Clouds on Nuclear Power Plants	1158 - 1166
7.10 M. Bürger, C. Carachalios, D.S. Kim, H. Unger, H. Hohmann, H. Schins: Description of Vapor Explosions by Thermal Detonation and Hydrodynamic Fragmentation Modeling	1167 - 1176
7.11 H. Alsmeyer: Core-Concrete Interaction: Status of BETA Experimental Program	1177 - 1185
7.12 T.Y. Chu, J.E. Brockmann: Large-Scale Melt/Material Interaction Experiments	1186 - 1195
7.13 J.E. Kelly, M.F. Young, J.L. Tomkins, P.J. Maudlin, W.J. Camp: The MELPROG Model for Integrated Melt Progression Analysis	1196 - 1205
7.14 K.R. Boldt, P.A. Kuenstler, Jr., T.R. Schmidt: Results of the In-Pile Degraded Core Coolability Experiments: DCC-1 and DCC-2	1206 - 1215
7.15 L. Barleon, K. Thomauske, H. Werle: Extended Dryout and Rewetting of Particulate Core Debris Beds	1216 - 1224

Chapter 8
Containment Response

		pages
8.1	M.H. Fontana, A.R. Buhl: Improving our Understanding of Nuclear Power Plant Response to Severe Accidents: Summary of IDCOR Results	1227 - 1241
8.2	T. Ishigami, M. Nishi, H. Horii, K. Kobayashi, K. Muramatsu, K. Soda: Analysis of Containment Response after Vessel Failure with Corium Ejection into a Reactor Cavity	1242 - 1251
8.3	R. Blomquist, A. Enerholm, J. Engström, F. Müller, G. Nordgren: Containment Response during Postulated Severe Accidents in First Generation of Swedish BWR's	1252 - 1258
8.4	J. Fermandjian, J.M. Evrard, G. Cenerino, Y. Berthion, G. Carvallo: Containment Loading during Severe Core Damage Accidents	1259 - 1271
8.5	S.G. Krishnasamy, W.W. Koziak: Structural Integrity of CANDU Reactor's Vacuum Building	1272 - 1281
8.6	M. Berman, J.T. Larkins: Recent Progress on NRC-Supported Hydrogen Research	1282 - 1290
8.7	H. Karwat: Scaling Problems Associated to the Extrapolation of Containment Experiments	1291 - 1300
8.8	K. Almenas, U.-C. Lee, S.A. Traiforos: Scaling Aspects of Subcompartment Analysis	1301 - 1311
8.9	T.E. Blejwas: Testing and Analysis of Containment Models	1312 - 1321

	pages
8.10 R. Avet-FlanCARD, B. Barbe, J.-L. Costaz, J. Dulac: PWR Containment Behaviour Beyond the Design Conditions	1322 - 1326
8.11 R.K. Kumar, H. Tamm: The Effect of Fan-Induced Turbulence on the Combustion of Hydrogen-Air Mixtures	1327 - 1336
8.12 K. Fischer, W. Häfner: Analysis and Prediction of Jet Loads	1337 - 1344
8.13 K. Müller, G. Katzenmeier: Behavior of Containment and Structures during Blowdown and Other Tests at the HDR Plant	1345 - 1352

Volume 3

Chapter 9

Fission Product Behavior

9.1 M.F. Osborne, J.L. Collins, R.A. Lorenz, K.S. Norwood: Measurement and Characterization of Fission Products Released from LWR Fuel	1357 - 1366
9.2 D.J. Osetek, A.W. Cronenberg, D.L. Hagrman, J.M. Broughton, J. Rest: Behavior of Fission Products Released from Severely Damaged Fuel during the PBF Severe Fuel Damage Tests	1367 - 1376
9.3 E. Groos, R. Förthmann: Determination of Iodine 131 Release from Defect Irradiated Fuel Rods under Simulated LOCA Conditions	1377 - 1386
9.4 P. Beslu, C. Leuthrot, A. Brissaud, A. Harrer, G. Beuken: Solid Fission Products and Actinides Release and Deposition Inside PWR's Primary Circuits	1387 - 1397

	pages
9.5 H. Sévéon, C. Leuthrot, J.P. Stora, P. Chenebault, R. Warlop: Release of Fission Products by Defective Pressurized Water Reactor Fuel	1398 - 1404
9.6 R. Kohli: Thermochemical Interactions of Fission Products in an LWR Accident	1405 - 1414
9.7 M. Furrer, R.C. Cripps, T. Gloor: Determination of Partition Coefficients for Iodine Between Water and Vapour Phase with I-131 as Tracer	1415 - 1422
9.8 J.A. Garland, A.C. Wells, E.J. Higham, I.C. Smith: Experimental Study of the Deposition of Iodine and Other Fission Products in the Coolant Circuit of a CAGR	1423 - 1431
9.9 E.M. Hood, P.N. Clough: The Behaviour of Iodine in Advanced Gas-Cooled Reactor (AGR) Circuits	1432 - 1441
9.10 F. Abbey, W.O. Schikarski: Recent Developments in Nuclear Aerosol Research Related to Thermal Reactor Safety	1442 - 1457
9.11 W. Schöck, H. Bunz, W. Schikarski, J.P. Hosemann, D. Haschke, T.F. Kanzleiter, T. Schröder, M. Fischer, K. Hassmann, M. Peehs, H. Ruhmann: The DEMONA Project: Objectives, Results and Significance to LWR Safety	1458 - 1467
9.12 J.A. Gieseke, H. Chen, P. Cybulskis, R.S. Denning, M.R. Kuhlman, K.W. Lee, M. Silberberg, M. Jankowski: Radionuclide Release to the Environment under Specific LWR Accident Conditions	1468 - 1477

	pages
9.13 E.A. Warman: Parametric Study of Factors Affecting Retention of Fission Products in Severe Reactor Accidents	1478 - 1491
9.14 K. Hassmann, M. Fischer, J.P. Hosemann, H. Bunz: Current Results of Radioactive Source Term Analyses for Melt Down Sequences in KWU-Type PWR's	1492 - 1504
9.15 H. Deuber, H.-G. Dillmann, K. Gerlach: Retention of Gaseous Radioiodine with Sorbents under Accident Conditions	1505 - 1513
9.16 V. Rüdinger, J.G. Wilhelm: Confinement of Airborne Particulate Radioactivity in the Case of an Accident	1514 - 1522
9.17 W. Morell, W. Kastner, R. Rippel, F. Richter: Experimental Investigations Simulating Iodine Release at Design Basis Accident in PWR	1523 - 1534
9.18 D. Cubicciotti, B.R. Sehgal: Fission Product and Material Vapor Transport during Molten Corium-Concrete Interactions	1535 - 1553
9.19 H. Kodaira, S. Kondo, Y. Togo: An Application of the Monitoring and Diagnostic System to Plant Diagnosis of FP Transport and Release in NPPS	1554 - 1563
9.20 K.-D. Hocke, R. Bisanz, F. Schmidt, H. Unger: Fission Product Release and Transport Modeling in KESS-2	1564 - 1571
9.21 C.I. Ricketts, V. Rüdinger, J.G. Wilhelm: HEPA-Filter Response to High Differential Pressures and High Air Velocities	1572 - 1582

	pages
9.22 K. Vinjamuri, D.J. Osetek, R.R. Hobbins: Tellurium Behaviour During and After the TMI-2 Accident	1583 - 1592
9.23 H.-G. Dillmann, H. Pasler: A Containment-Venting Filter Concept and its Implementation at Stainless-Steel Fiber Filters	1593 - 1605

Chapter 10

Code Development and Verification

10.1 T. Kervinen, H. Purhonen, H. Kalli: REWET-II Experiments to Determine the Effects of Spacer Grids on the Reflooding Process	1609 - 1617
10.2 H. Kalli, T. Kervinen, J. Rossi: Reflooding in a Tight-Pitch Rod Lattice	1618 - 1627
10.3 D.R. Glynn, D. Kirkcaldy, N. Rhodes: Prediction of Reflooding in Single Channels and Partially- Blocked Rod Bundles	1628 - 1636
10.4 M. El-Shanawany, C.G. Kinniburgh, K.T. Routledge: Comparison of Calculations Using the Best Estimate Reflood Heat Transfer Code BART-A1 with Data from the FEBA and REBEKA Facilities	1637 - 1644
10.5 J. Duco, M. Reocreux, A. Tattegrain, Ph. Berna, B. Legrand, M. Trotabas: In-Pile Investigations at the PHEBUS Facility of the Behavior of PWR-Type Fuel Bundles in Typical L.B. LOCA Transients Extended to and beyond the Limits of ECCS Criteria	1645 - 1655
10.6 H. Staedtke, W. Kolar, B. Worth: RELAP5/MOD1 Assessment with LOBI-MOD1 Test Results	1656 - 1665

	pages
10.7 J.C. Rousseau, G. Houdayer, M. Reocreux: The CATHARE Code Development	1666 - 1678
10.8 J.M. Healzer, E. Elias, A. Singh, F.J. Moody: A Model for Two-Phase Jet Expansion and Impingement	1679 - 1688
10.9 L. Szabados, I. Toth, L. Perneczky: The PMK-NVH Experimental Facility and the Phenomena to be Investigated	1689 - 1701
10.10 R.J. Salm: Post Analysis of a 10 cm ² SBLOCA Test in the OTSG Equipped GERDA Facility Using a BBR Version of RELAP4/MOD6	1702 - 1710
10.11 P.C. Hall: Post Test Calculations of Semiscale Pump Suction Small Break LOCE, S-PL-4, Using RELAP5/MOD1.5	1711 - 1720
10.12 J. Miettinen: Small Break Analyses with Computer Codes SMABRE and RELAP5/MOD1	1721 - 1730
10.13 M. Andreani, P.C. Cacciabue, M. Mazzini, F. Oriolo: The Analysis of LOFT Test L9-3 Using RELAP4/MOD6 and ALMOD-JRC Computer Codes	1731 - 1740
10.14 C.L. Nalezny, T.-H. Chen: Analysis of Recovery Procedures for a Single Steam Generator Tube Rupture	1741 - 1749
10.15 G.G. Loomis: Steam Generator Tube Rupture in an Experimental Facility Scaled from a Pressurized Water Reactor	1750 - 1759

	pages
10.16 G.C. Slovik, P. Saha: A RAMONA-3B Code Description and Nodalization Study for the Peach Bottom-2 Turbine Trip Test 3	1760 - 1769
10.17 S. Børresen, L. Moberg: Systematic Procedures for Core Neutronics Modelling in the 3-D BWR System Transient Code RAMONA-3B	1770 - 1979
10.18 C.S. Lin, W.E. Kastenberg: A Quick Running Dynamic Simulation Code for BWR Transients	1780 - 1790
10.19 Y. Waaranperä, H. Svensson: A BWR Stability Prediction Model and its Qualification Against Tests in Operating Reactors	1791 - 1800
10.20 K.C. Wagner, R.J. Dallman: A Comparison of RELAP5/MOD1.6, TRAC-BD1/Version 12, and TRAC-BD1/MOD1 Assessments with Data from a ROSA III Small Break Test	1801 - 1810
10.21 M. Kato, N. Abe, H. Aoki, K. Tasaka: ROSA-III Large Break Test Analysis by TRAC-BD1	1811 - 1820
10.22 G.Th. Analytis, S.N. Aksan: TRAC-BD1 Assessment under Severe Accident Boil-off Conditions	1821 - 1830
10.23 P. Saha, L. Neymotin, U.S. Rohatgi: Analysis of Single and Parallel Tube Counter-Current Flow Limiting Experiments with TRAC-BD1 Code	1831 - 1839
10.24 P.D. Wheatley, K.C. Wagner: Posttest Data Analysis and Assessment of TRAC-BD1/MOD1 with Data from a Full Integral Simulation Test (FIST) Power Transient Experiment	1840 - 1849

	pages
10.25 D.A. Schauer: Transient Condensation Heat Transfer Coefficient Expressions during and after Blowdown	1850 - 1858
10.26 E.W. McCauley, E. Aust, H. Schwan: Multivalent Effects in a Large Scale Boiling Water Reactor Pressure Suppression System	1859 - 1866
10.27 M.J. Thurgood, K. Fischer, L. Wolf: Verification of the 3-D, 2-FLUID, 3-FIELD Containment Code COBRA-NC with HDR- and Battelle-Frankfurt Data Sets	1867 - 1875

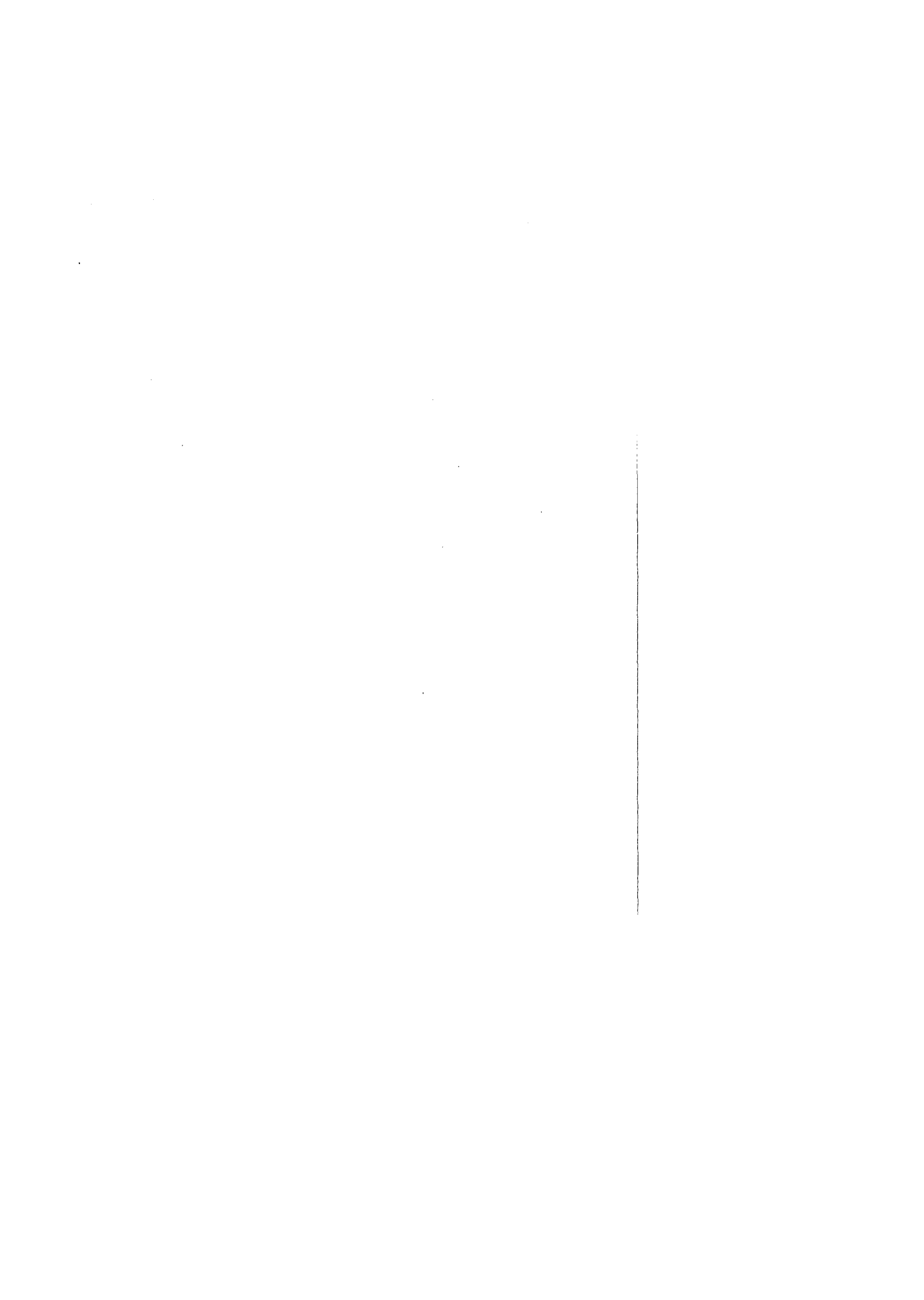
Chapter 11

Probabilistic Risk Assessment

11.1 A. Thadani, F. Rowsome, T. Speis: Applications of Probabilistic Techniques at NRC	1881 - 1890
11.2 E.P. O'Donnell, T.J. Raney: A Proposed Approach to Backfit Decision-Making Using Risk Assessment and Benefit-Cost Methodology	1891 - 1897
11.3 L. Cave, W.E. Kastenberg, J.N. Tweedy: The Development and Application of Quantitative Methods in Licensing Nuclear Power Plants	1898 - 1907
11.4 M.P. Rubin, B. Atefi, D.W. Gallagher, R.T. Liner: Application of Probabilistic Risk Assessment Techniques as a Decision Tool in the U.S. Nuclear Regulatory Commission's Systematic Evaluation Program	1908 - 1917
11.5 H. Fuchs, L. Miteff: PRA - to what Depth? (The "Bed of Nails" Effect)	1918 - 1926
11.6 A.S. Benjamin, V.L. Behr, F.E. Haskin, D.M. Kunsman: Severe Accident Reactor Risks and the Potential for Risk Reduction	1927 - 1936

	pages
11.7 R.A. Bari, I.A. Papazoglou, W.T. Pratt, K. Shiu, H. Ludewig, N. Hanan: Severe Accident Analysis and Risk Assessment for two Boiling Water Reactors	1937 - 1946
11.8 J.E. Wells: Seismic Risk Assessment as Applied to the Zion Nuclear Generating Station	1947 - 1956
11.9 F.T. Harper, M.T. Drouin, E.A. Krantz: Classification of United States Light Water Reactors by Dominant Core Melt Frequency Contributors	1957 - 1966
11.10 G. Bars, J.M. Lanore, G. Villeroix: Introduction of Operator Actions in the Event Trees	1967 - 1973
11.11 G. Ericsson, S. Hirschberg: Treatment of Common Cause Failures in the Barsebäck 1 Safety Study	1974 - 1982
11.12 J.C. Luxat, A.P. Firla, E. Hussein, A.P. Mazumdar, B.C. Choy: Probabilistic Transient Simulation Methodology in Support of Probabilistic Safety Evaluation Studies for Ontario Hydro Reactors	1983 - 1991
11.13 S.L. Israel: How Firm are PRA Results?	1992 - 1999
11.14 P.J. Amico, W.L. Ferrell, M.P. Rubin: The Significance of Water Hammer Events to Public Dose from Reactor Accidents: A Probabilistic Assessment	2000 - 2008
11.15 H. Fabian, A. Feigel, O. Gremm: The Probabilistic Approach and the Deterministic Licensing Procedure	2009 - 2015

	pages
11.16 P. Wittek, W.G. Hübschmann, S. Vogt: Influence of the Atmospheric Dispersion Model Modifications on the Results of the German Reactor Risk Study	2016 - 2024
11.17 J.A. Martin, Jr.: Effectiveness of Early Evacuation of Small Areas, Shelter and Relocation in Reducing Severe Accident Consequences	2025 - 2027
11.18 R.P. Burke, D.C. Aldrich, N.C. Rasmussen: Modeling the Economic Consequences of LWR Accidents	2028 - 2037
11.19 D.A. Lappa: Impact of Assumptions Concerning Containment Failure on the Risk from Nuclear Power Plants	2038 - 2047
11.20 J.G. Kollas: An Estimation of the LOCA Consequences of a Research Reactor Located Within a Large Population Centre	2048 - 2056



LIST OF AUTHORS

Abbey, F.	Vol. 3, P. 1442	Buhl, A.R.	Vol. 2, P. 1227
Abdollahian, D.	Vol. 1, P. 655	Bunz, H.	Vol. 3, P. 1458
Abe, N.	Vol. 3, P. 1811	Bunz, H.	Vol. 3, P. 1492
Agrawal, B.B.	Vol. 2, P. 814	Burger, B.	Vol. 1, P. 457
Aksan, S.N.	Vol. 3, P. 1821	Burke, R.P.	Vol. 3, P. 2028
Aldrich, D.C.	Vol. 3, P. 2028	Burson, S.B.	Vol. 2, P. 1128
Aleite, W.	Vol. 2, P. 723	Burt, J.D.	Vol. 1, P. 311
Allen, F.R.	Vol. 1, P. 149	Bürger, M.	Vol. 2, P. 1167
Allison, C.M.	Vol. 2, P. 897	Cacciabue, P.C.	Vol. 3, P. 1731
Almenas, K.	Vol. 2, P. 1301	Cahuzac, A.	Vol. 1, P. 220
Alsmeyer, H.	Vol. 2, P. 1177	Camp, W.J.	Vol. 2, P. 1196
Amico, P.J.	Vol. 1, P. 210	Caplan, M.Z.	Vol. 1, P. 366
Amico, P.J.	Vol. 3, P. 2000	Caplan, M.Z.	Vol. 1, P. 376
Analytis, G.Th.	Vol. 3, P. 1821	Carachalios, C.	Vol. 2, P. 1167
Andersson, S.A.	Vol. 1, P. 675	Carnino, A.	Vol. 1, P. 220
Andreani, M.	Vol. 3, P. 1731	Carvalho, G.	Vol. 2, P. 1259
Antony-Spies, P.	Vol. 1, P. 712	Cassette, P.	Vol. 1, P. 230
Aoki, H.	Vol. 3, P. 1811	Cave, L.	Vol. 1, P. 588
Archinoff, G.H.	Vol. 2, P. 988	Cave, L.	Vol. 3, P. 1898
Ardron, K.H.	Vol. 1, P. 385	Celata, G.P.	Vol. 1, P. 643
Atefi, B.	Vol. 3, P. 1908	Cenerino, C.	Vol. 2, P. 1259
Aust, A.	Vol. 1, P. 666	Chambers, R.	Vol. 1, P. 448
Aust, E.	Vol. 3, P. 1859	Chen, H.	Vol. 3, P. 1468
Avet-Flancard, R.	Vol. 2, P. 1322	Chen, J.C.	Vol. 2, P. 1108
Barbe, B.	Vol. 2, P. 1322	Chen, T.-H.	Vol. 3, P. 1741
Bari, R.A.	Vol. 3, P. 1937	Chenebault, P.	Vol. 3, P. 1398
Barleon, L.	Vol. 2, P. 1216	Choy, B.C.	Vol. 3, P. 1983
Bars, G.	Vol. 3, P. 1967	Chu, T.Y.	Vol. 2, P. 1186
Basselier, J.	Vol. 1, P. 607	Clough, P.N.	Vol. 3, P. 1432
Bayless, P.D.	Vol. 1, P. 448	Collins, J.L.	Vol. 3, P. 1357
Becker, M.	Vol. 1, P. 712	Corradini, M.L.	Vol. 2, P. 1098
Behr, V.L.	Vol. 3, P. 1927	Costaz, J.-L.	Vol. 2, P. 1322
Benjamin, A.S.	Vol. 3, P. 1927	Cripps, R.C.	Vol. 3, P. 1415
Berman, M.	Vol. 2, P. 1282	Cronenberg, M.W.	Vol. 3, P. 1367
Berna, G.A.	Vol. 2, P. 897	Cubicciotti, D.	Vol. 3, P. 1535
Berna, Ph.	Vol. 3, P. 1645	Cumo, M.	Vol. 1, P. 643
Berthion, Y.	Vol. 2, P. 1259	Curtis, R.T.	Vol. 2, P. 814
Beslu, P.	Vol. 3, P. 1387	Cybulskis, P.	Vol. 2, P. 968
Beuken, G.	Vol. 3, P. 1387	Cybulskis, P.	Vol. 3, P. 1468
Bielmeier, M.	Vol. 1, P. 683	Dallman, R.J.	Vol. 3, P. 1801
Birkhofer, A.	Vol. 1, P. 165	Davis, C.B.	Vol. 1, P. 311
Bisanz, R.	Vol. 1, P. 457	Delaney, R.D.	Vol. 1, P. 478
Bisanz, R.	Vol. 2, P. 908	Demoline, K.	Vol. 2, P. 1043
Bisanz, R.	Vol. 2, P. 948	Denis, A.	Vol. 2, P. 1026
Bisanz, R.	Vol. 3, P. 1564	Denning, R.S.	Vol. 2, P. 1148
Blahnik, C.	Vol. 2, P. 978	Denning, R.S.	Vol. 3, P. 1468
Blejwas, T.E.	Vol. 2, P. 1312	Depond, G.	Vol. 1, P. 581
Blomquist, R.	Vol. 2, P. 1252	Desoisa, J.A.	Vol. 1, P. 426
Bolander, M.A.	Vol. 1, P. 311	Deuber, H.	Vol. 3, P. 1505
Boldt, K.R.	Vol. 2, P. 1206	Dhir, V.K.	Vol. 1, P. 535
Borresen, S.	Vol. 3, P. 1770	Dick, W.J.	Vol. 2, P. 978
Brand, B.	Vol. 1, P. 498	Dillmann, H.-G.	Vol. 3, P. 1505
Brealey, N.J.	Vol. 2, P. 1118	Dillmann, H.-G.	Vol. 3, P. 1593
Brissaud, A.	Vol. 3, P. 1387	Dircks, W.	Vol. 1, P. 55
Brockmann, J.E.	Vol. 2, P. 1186	Dobbe, C.A.	Vol. 1, P. 448
Broughton, J.M.	Vol. 3, P. 1367	Dredemis, G.	Vol. 1, P. 239
Brunet, A.	Vol. 2, P. 842	Drenkhahn, W.	Vol. 2, P. 1158

Drouin, M.T.	Vol. 3, P. 1957	Gremm, O.	Vol. 3, P. 2009
Duco, J.	Vol. 3, P. 1645	Grimm, P.	Vol. 1, P. 626
Dulac, J.	Vol. 2, P. 1322	Groos, E.	Vol. 3, P. 1377
Eckered, T.	Vol. 2, P. 766	Gros, G.	Vol. 1, P. 199
Eifler, W.	Vol. 2, P. 1057	Guarro, S.	Vol. 2, P. 796
El-Genk, M.S.	Vol. 2, P. 999	Guesnon, H.	Vol. 1, P. 559
El-Shanawany, M.	Vol. 3, P. 1637	Guishani, P.	Vol. 1, P. 366
Elias, E.	Vol. 3, P. 1679	Göbel, D.	Vol. 1, P. 712
Enerholm, A.	Vol. 2, P. 1252	Hadaller, G.I.	Vol. 2, P. 988
Engström, J.	Vol. 2, P. 1252	Hagrman, D.L.	Vol. 2, P. 897
Erbacher, F.J.	Vol. 1, P. 299	Hagrman, D.L.	Vol. 3, P. 1367
Erbacher, F.J.	Vol. 1, P. 516	Hall, P.C.	Vol. 3, P. 1711
Erickson, D.	Vol. 2, P. 999	Hanan, N.	Vol. 3, P. 1937
Ericsson, G.	Vol. 3, P. 1974	Harper, F.T.	Vol. 3, P. 1957
Essler, W.	Vol. 2, P. 766	Harrer, A.	Vol. 3, P. 1387
Evrard, J.M.	Vol. 2, P. 1259	Hartel, K.	Vol. 2, P. 752
Fabian, H.	Vol. 1, P. 693	Haschke, D.	Vol. 3, P. 1458
Fabian, H.	Vol. 3, P. 2009	Haskin, F.E.	Vol. 3, P. 1927
Farello, G.E.	Vol. 1, P. 643	Hassanien, S.	Vol. 2, P. 776
Fehrenbach, P.J.	Vol. 1, P. 478	Hassmann, K.	Vol. 3, P. 1458
Feigel, A.	Vol. 3, P. 2009	Hassmann, K.	Vol. 3, P. 1492
Fernandjian, J.	Vol. 2, P. 1259	Hastings, I.J.	Vol. 1, P. 478
Ferrell, W.L.	Vol. 3, P. 2000	Hawley, P.G.	Vol. 1, P. 348
Fiege, A.	Vol. 1, P. 73	Healzer, J.M.	Vol. 3, P. 1679
Fighetti, C.F.	Vol. 1, P. 525	Helmersson, S.	Vol. 1, P. 675
Firla, A.P.	Vol. 3, P. 1983	Hennies, H.H.	Vol. 1, P. 3
Fischer, K.	Vol. 1, P. 273	Herbold, G.	Vol. 1, P. 436
Fischer, K.	Vol. 2, P. 1337	Hicken, E.F.	Vol. 1, P. 477
Fischer, K.	Vol. 3, P. 1867	Higham, E.J.	Vol. 3, P. 1423
Fischer, M.	Vol. 3, P. 1458	Hirschberg, S.	Vol. 3, P. 1974
Fischer, M.	Vol. 3, P. 1492	Hnilica, K.	Vol. 1, P. 607
Fletcher, C.D.	Vol. 1, P. 311	Hobbins, R.R.	Vol. 3, P. 1583
Fontana, M.H.	Vol. 2, P. 1227	Hocke, K.-D.	Vol. 3, P. 1564
Foskolos, K.	Vol. 1, P. 626	Hofmann, P.	Vol. 2, P. 1015
Fourest, B.	Vol. 1, P. 191	Hohmann, H.	Vol. 2, P. 1167
Fourest, B.	Vol. 1, P. 239	Holzer, R.	Vol. 1, P. 607
Frischengruber, K.	Vol. 1, P. 693	Hood, E.M.	Vol. 3, P. 1432
Fuchs, H.	Vol. 3, P. 1918	Horii, H.	Vol. 2, P. 1242
Furrer, M.	Vol. 3, P. 1415	Hosemann, J.P.	Vol. 3, P. 1458
Förthmann, R.	Vol. 3, P. 1377	Hosemann, J.P.	Vol. 3, P. 1492
Fürst, H.D.	Vol. 1, P. 666	Houdayer, G.	Vol. 3, P. 1666
Gallagher, D.W.	Vol. 3, P. 1908	Howieson, J.Q.	Vol. 1, P. 348
Garcia, E.A.	Vol. 2, P. 1026	Hunt, C.E.L.	Vol. 1, P. 478
Garland, J.A.	Vol. 3, P. 1423	Hussein, E.	Vol. 2, P. 786
Gasteiger, H.	Vol. 1, P. 683	Hussein, E.	Vol. 3, P. 1983
Gauvenet, A.	Vol. 1, P. 35	Häfner, W.	Vol. 1, P. 330
Geiger, W.	Vol. 1, P. 634	Häfner, W.	Vol. 2, P. 1337
Gerlach, K.	Vol. 3, P. 1505	Hübschmann, W.G.	Vol. 3, P. 2016
Gieseke, J.A.	Vol. 3, P. 1468	Ihle, P.	Vol. 1, P. 516
Ginsberg, T.	Vol. 2, P. 1108	Incalcaterra, P.C.	Vol. 1, P. 643
Girgis, S.	Vol. 1, P. 348	Ishigami, T.	Vol. 2, P. 1242
Giroux, G.	Vol. 1, P. 230	Israel, S.L.	Vol. 3, P. 1992
Gittus, J.H.	Vol. 1, P. 149	Ivars, R.	Vol. 1, P. 248
Gloor, T.	Vol. 2, P. 1415	Jankowski, M.	Vol. 3, P. 1468
Glynn, D.R.	Vol. 3, P. 1628	Japavaire, R.	Vol. 1, P. 191
Grant, S.D.	Vol. 1, P. 348	Johansson, L.-E.	Vol. 1, P. 675
Greef, C.P.	Vol. 1, P. 426	Kalli, H.	Vol. 3, P. 1609

Kalli, H.	Vol. 3, P. 1618	Legrand, B.	Vol. 3, P. 1645
Kanzleiter, T.F.	Vol. 3, P. 1458	Leistikow, S.	Vol. 2, P. 928
Karwat, H.	Vol. 2, P. 1291	Leuthrot, C.	Vol. 3, P. 1387
Kastenberg, W.E.	Vol. 1, P. 588	Leuthrot, C.	Vol. 3, P. 1398
Kastenberg, W.E.	Vol. 3, P. 1780	Lewins, J.D.	Vol. 2, P. 762
Kastenberg, W.E.	Vol. 3, P. 1898	Lewis, H.W.	Vol. 1, P. 139
Kastl, H.	Vol. 1, P. 273	Lillington, J.N.	Vol. 2, P. 858
Kastner, W.	Vol. 3, P. 1523	Lin, C.S.	Vol. 3, P. 1780
Kato, M.	Vol. 3, P. 1811	Lin, K.Y.	Vol. 1, P. 588
Katzenmeier, G.	Vol. 2, P. 1345	Liner, R.T.	Vol. 3, P. 1908
Kelly, J.E.	Vol. 2, P. 1196	Lipsett, J.J.	Vol. 1, P. 478
Kersting, E.J.	Vol. 1, P. 436	Loomis, G.G.	Vol. 3, P. 1750
Kervinen, T.	Vol. 3, P. 1609	Lorenz, R.A.	Vol. 3, P. 1357
Kervinen, T.	Vol. 3, P. 1618	Ludewig, H.	Vol. 3, P. 1937
Kianjah, H.	Vol. 1, P. 535	Luxat, J.C.	Vol. 2, P. 786
Kim, B.J.	Vol. 2, P. 1098	Luxat, J.C.	Vol. 3, P. 1983
Kim, D.S.	Vol. 2, P. 1167	MacDonald, P.E.	Vol. 2, P. 876
Kim, S.H.	Vol. 2, P. 958	Maeder, C.	Vol. 1, P. 626
Kim, S.H.	Vol. 2, P. 999	Magdalinski, J.	Vol. 1, P. 248
Kinniburgh, C.G.	Vol. 3, P. 1637	Mallory, J.P.	Vol. 1, P. 385
Kirkcaldy, D.	Vol. 3, P. 1628	Mancini, G.	Vol. 2, P. 740
Knobel, R.C.	Vol. 2, P. 804	Mandl, R.M.	Vol. 1, P. 498
Kobayashi, K.	Vol. 2, P. 1242	Marcille, R.	Vol. 2, P. 733
Kobussen, J.A.	Vol. 1, P. 416	Margulies, T.S.	Vol. 2, P. 824
Koch, C.	Vol. 2, P. 1158	Marino, G.P.	Vol. 2, P. 851
Kodaira, H.	Vol. 3, P. 1554	Marshall, A.C.	Vol. 2, P. 917
Koenig, J.E.	Vol. 1, P. 320	Martin, Jr., J.A.	Vol. 2, P. 824
Kohli, R.	Vol. 3, P. 1405	Martin, Jr., J.A.	Vol. 3, P. 2025
Kohn, E.	Vol. 1, P. 488	Martin, R.	Vol. 1, P. 559
Kohn, E.	Vol. 2, P. 988	Maudlin, P.J.	Vol. 2, P. 1196
Koizumi, Y.	Vol. 1, P. 467	Maurer, H.A.	Vol. 1, P. 597
Kolar, W.	Vol. 3, P. 1656	Mazumdar, A.P.	Vol. 3, P. 1983
Kollas, J.G.	Vol. 3, P. 2048	Mazzini, M.	Vol. 3, P. 1731
Kondo, S.	Vol. 3, P. 1554	McCardell, R.K.	Vol. 2, P. 876
Kozlak, W.W.	Vol. 2, P. 1272	McCauley, E.W.	Vol. 3, P. 1859
Krantz, E.A.	Vol. 3, P. 1957	McKean, D.W.	Vol. 2, P. 978
Krishnan, V.S.	Vol. 1, P. 385	McUmbur, L.M.	Vol. 2, P. 1079
Krishnasamy, S.G.	Vol. 2, P. 1272	Meier, S.E.	Vol. 1, P. 409
Kroeger, P.G.	Vol. 2, P. 1138	Meister, G.	Vol. 1, P. 546
Kuenstler, Jr., P.A.	Vol. 2, P. 1206	Meslin, T.	Vol. 1, P. 220
Kuhlman, M.R.	Vol. 3, P. 1468	Meslin, T.	Vol. 2, P. 842
Kukita, Y.	Vol. 1, P. 467	Mesnager, J.	Vol. 2, P. 833
Kullberg, C.M.	Vol. 1, P. 311	Miettinen, J.	Vol. 3, P. 1721
Kumar, R.K.	Vol. 2, P. 1327	Miteff, L.	Vol. 3, P. 1918
Kunsman, D.M.	Vol. 3, P. 1927	Moberg, L.	Vol. 3, P. 1770
Kurzawe, M.	Vol. 1, P. 273	Moody, F.J.	Vol. 3, P. 1679
Körber, H.	Vol. 1, P. 683	Morell, W.	Vol. 3, P. 1523
Laakso, K.J.	Vol. 1, P. 181	Morison, W.G.	Vol. 1, P. 111
Lahey, Jr., R.T.	Vol. 2, P. 958	Muramatsu, K.	Vol. 2, P. 1242
Lang, U.	Vol. 1, P. 457	Mylonas, R.	Vol. 1, P. 416
Lang, U.	Vol. 2, P. 948	Müller, F.	Vol. 2, P. 1252
Lanore, J.M.	Vol. 3, P. 1967	Müller, K.	Vol. 2, P. 1345
Lappa, D.A.	Vol. 3, P. 2038	Müller, U.	Vol. 2, P. 1090
Larkins, J.T.	Vol. 2, P. 1282	Nalezny, C.L.	Vol. 2, P. 876
Lee, K.W.	Vol. 3, P. 1468	Nalezny, C.L.	Vol. 3, P. 1741
Lee, U.-C.	Vol. 2, P. 1301	Narjes, K.H.	Vol. 1, P. 21
Legath, E.	Vol. 1, P. 268	Naschi, G.	Vol. 1, P. 55

Nath, V.I.	Vol. 1, P. 488	Rust, K.	Vol. 1, P. 516
Neitzel, H.J.	Vol. 2, P. 1015	Rüdinger, V.	Vol. 3, P. 1514
Newbigging, A.W.P.	Vol. 2, P. 1067	Rüdinger, V.	Vol. 3, P. 1572
Neymotin, L.	Vol. 3, P. 1831	Saha, P.	Vol. 1, P. 357
Niemann, H.-R.	Vol. 1, P. 666	Saha, P.	Vol. 3, P. 1760
Nishi, M.	Vol. 2, P. 1242	Saha, P.	Vol. 3, P. 1831
Nordgren, G.	Vol. 2, P. 1252	Saito, S.	Vol. 2, P. 938
Norwood, K.S.	Vol. 3, P. 1357	Salm, R.J.	Vol. 3, P. 1702
O'Donnell, E.P.	Vol. 3, P. 1891	Saphier, D.	Vol. 1, P. 546
Okrent, D.	Vol. 2, P. 796	Sauve, R.G.	Vol. 1, P. 283
Oriolo, F.	Vol. 3, P. 1731	Sawala, R.	Vol. 2, P. 988
Osborne, M.F.	Vol. 3, P. 1357	Scarth, D.A.	Vol. 1, P. 385
Osetek, D.J.	Vol. 3, P. 1367	Schanz, G.	Vol. 2, P. 928
Osetek, D.J.	Vol. 3, P. 1583	Schauer, D.A.	Vol. 3, P. 1850
Papazoglou, I.A.	Vol. 3, P. 1937	Schikarski, W.O.	Vol. 3, P. 1442
Paratte, J.M.	Vol. 1, P. 626	Schikarski, W.O.	Vol. 3, P. 1458
Pasler, H.	Vol. 3, P. 1593	Schindler, M.	Vol. 1, P. 457
Payen, B.	Vol. 1, P. 220	Schindler, M.	Vol. 1, P. 683
Peehs, M.	Vol. 3, P. 1458	Schins, H.	Vol. 2, P. 1167
Penn, W.J.	Vol. 1, P. 111	Schmidt, F.	Vol. 1, P. 457
Perneckzy, L.	Vol. 3, P. 1689	Schmidt, F.	Vol. 2, P. 908
Perrault, D.	Vol. 1, P. 199	Schmidt, F.	Vol. 2, P. 948
Pförtner, H.	Vol. 2, P. 1158	Schmidt, F.	Vol. 3, P. 1564
Pickard, P.S.	Vol. 2, P. 917	Schmidt, H.	Vol. 1, P. 498
Pickman, D.O.	Vol. 1, P. 73	Schmidt, T.R.	Vol. 2, P. 1206
Platten, J.L.	Vol. 1, P. 617	Schneider, H.	Vol. 2, P. 1158
Podowski, M.Z.	Vol. 2, P. 958	Schraewer, R.	Vol. 1, P. 258
Pratt, W.T.	Vol. 3, P. 1937	Schröder, T.	Vol. 3, P. 1458
Purhonen, H.	Vol. 3, P. 1609	Schulenberg, T.	Vol. 2, P. 1090
Raney, T.J.	Vol. 3, P. 1891	Schultheiss, G.F.	Vol. 1, P. 666
Rasmussen, N.C.	Vol. 3, P. 2028	Schultz, R.R.	Vol. 1, P. 467
Reddy, D.G.	Vol. 1, P. 525	Schwan, H.	Vol. 3, P. 1859
Reil, K.O.	Vol. 2, P. 917	Schöck, W.	Vol. 3, P. 1458
Renard, A.	Vol. 1, P. 607	Sehgal, B.R.	Vol. 3, P. 1535
Reocreux, M.	Vol. 3, P. 1645	Seveon, H.	Vol. 3, P. 1398
Reocreux, M.	Vol. 3, P. 1666	Seveon, J.J.	Vol. 1, P. 230
Rest, J.	Vol. 3, P. 1367	Shiina, Y.	Vol. 2, P. 1138
Rhodes, N.	Vol. 3, P. 1628	Shiozawa, S.	Vol. 2, P. 938
Richter, F.	Vol. 3, P. 1523	Shiu, K.	Vol. 3, P. 1937
Ricketts, C.I.	Vol. 3, P. 1572	Siefken, L.J.	Vol. 2, P. 888
Rippel, R.	Vol. 3, P. 1523	Sierricki, J.J.	Vol. 2, P. 1079
Rivard, J.B.	Vol. 2, P. 917	Silberberg, M.	Vol. 2, P. 851
Roche, H.	Vol. 1, P. 230	Silberberg, M.	Vol. 3, P. 1468
Rodnizky, J.	Vol. 1, P. 546	Singh, A.	Vol. 1, P. 535
Rogers, J.T.	Vol. 1, P. 397	Singh, A.	Vol. 1, P. 655
Rohatgi, U.S.	Vol. 1, P. 357	Singh, A.	Vol. 3, P. 1679
Rohatgi, U.S.	Vol. 3, P. 1831	Skokan, A.	Vol. 2, P. 1035
Rondeau, R.K.	Vol. 2, P. 1043	Slovik, G.C.	Vol. 3, P. 1760
Rosinger, H.E.	Vol. 2, P. 1043	Smith, I.C.	Vol. 3, P. 1423
Rossi, J.	Vol. 3, P. 1618	Smith, R.C.	Vol. 1, P. 320
Rousseau, J.C.	Vol. 3, P. 1666	Soda, K.	Vol. 2, P. 1242
Routledge, K.T.	Vol. 3, P. 1637	Speis, T.	Vol. 3, P. 1881
Rowsome, F.	Vol. 3, P. 1881	Spencer, B.W.	Vol. 2, P. 1079
Rubin, M.P.	Vol. 3, P. 1908	Spencer, R.C.	Vol. 1, P. 478
Rubin, M.P.	Vol. 3, P. 2000	Spiga, M.	Vol. 1, P. 508
Ruhmann, H.	Vol. 3, P. 1458	Spinks, N.J.	Vol. 1, P. 366
Russell, A.I.	Vol. 2, P. 1067	Spinks, N.J.	Vol. 1, P. 376

Staedtke, H.	Vol. 3, P. 1656	Wolf, L.	Vol. 3, P. 1867
Stalker, K.T.	Vol. 2, P. 917	Worth, B.	Vol. 3, P. 1656
Stepan, H.	Vol. 1, P. 683	Wright, A.C.D.	Vol. 1, P. 376
Stitt, B.D.	Vol. 1, P. 311	Wright, W.R.	Vol. 2, P. 851
Stora, J.P.	Vol. 3, P. 1398	Young, M.F.	Vol. 2, P. 1196
Stratton, W.R.	Vol. 1, P. 95	Yuelys-Miksis, C.	Vol. 1, P. 357
Sureau, H.	Vol. 1, P. 581	Zheng, W.X.	Vol. 1, P. 416
Sureau, H.	Vol. 2, P. 833		
Svensson, H.	Vol. 3, P. 1791		
Szabados, L.	Vol. 3, P. 1689		
Taleyarkhan, R.P.	Vol. 2, P. 958		
Tamm, H.	Vol. 2, P. 1327		
Tasaka, K.	Vol. 3, P. 1811		
Tattegrain, A.	Vol. 3, P. 1645		
Teper, W.W.	Vol. 1, P. 283		
Thadani, A.	Vol. 3, P. 1881		
Thomuske, K.	Vol. 2, P. 1216		
Thurgood, M.J.	Vol. 3, P. 1867		
Togo, Y.	Vol. 3, P. 1554		
Tomkins, J.L.	Vol. 2, P. 1196		
Toth, I.	Vol. 3, P. 1689		
Traiforos, S.A.	Vol. 2, P. 1301		
Trotabas, M.	Vol. 3, P. 1645		
Turland, B.D.	Vol. 2, P. 1118		
Turner, E.	Vol. 2, P. 1067		
Tweedy, J.N.	Vol. 3, P. 1898		
Uetsuka, H.	Vol. 2, P. 928		
Unger, H.	Vol. 1, P. 457		
Unger, H.	Vol. 1, P. 683		
Unger, H.	Vol. 2, P. 1167		
Unger, H.	Vol. 3, P. 1564		
Vandenberg, Cl.	Vol. 1, P. 607		
Villeroix, G.	Vol. 3, P. 1967		
Vinjamuri, K.	Vol. 3, P. 1583		
Vogt, S.	Vol. 3, P. 2016		
Waaranderä, Y.	Vol. 3, P. 1791		
Wadsworth, S.L.	Vol. 2, P. 988		
Wagner, K.C.	Vol. 3, P. 1801		
Wagner, K.C.	Vol. 3, P. 1840		
Wahlström, B.	Vol. 2, P. 740		
Walsworth, J.A.	Vol. 1, P. 478		
Warlop, R.	Vol. 3, P. 1398		
Warman, E.A.	Vol. 3, P. 1478		
Waterman, M.E.	Vol. 1, P. 311		
Watt, L.J.	Vol. 1, P. 348		
Weiser, G.	Vol. 1, P. 9		
Wells, A.C.	Vol. 3, P. 1423		
Wells, J.E.	Vol. 3, P. 1947		
Werle, H.	Vol. 2, P. 1216		
Wheatley, P.D.	Vol. 3, P. 1840		
Wiehr, K.	Vol. 1, P. 516		
Wietstock, P.	Vol. 1, P. 574		
Wilhelm, J.G.	Vol. 3, P. 1514		
Wilhelm, J.G.	Vol. 3, P. 1572		
Wintermann, B.	Vol. 1, P. 258		
Wittek, P.	Vol. 3, P. 2016		
Wolf, L.	Vol. 1, P. 330		

Chapter 9

Fission Product Behavior

	pages
9.1 M.F. Osborne, J.L. Collins, R.A. Lorenz, K.S. Norwood: Measurement and Characterization of Fission Products Released from LWR Fuel	1357 - 1366
9.2 D.J. Osetek, A.W. Cronenberg, D.L. Hagrman, J.M. Broughton, J. Rest: Behavior of Fission Products Released from Severely Damaged Fuel during the PBF Severe Fuel Damage Tests	1367 - 1376
9.3 E. Groos, R. Förthmann: Determination of Iodine 131 Release from Defect Irradiated Fuel Rods under Simulated LOCA Conditions	1377 - 1386
9.4 P. Beslu, C. Leuthrot, A. Brissaud, A. Harrer, G. Beuken: Solid Fission Products and Actinides Release and Deposition Inside PWR's Primary Circuits	1387 - 1397
9.5 H. Sévéon, C. Leuthrot, J.P. Stora, P. Chenebault, R. Warlop: Release of Fission Products by Defective Pressurized Water Reactor Fuel	1398 - 1404
9.6 R. Kohli: Thermochemical Interactions of Fission Products in an LWR Accident	1405 - 1414
9.7 M. Furrer, R.C. Cripps, T. Gloor: Determination of Partition Coefficients for Iodine Between Water and Vapour Phase with I-131 as Tracer	1415 - 1422
9.8 J.A. Garland, A.C. Wells, E.J. Higham, I.C. Smith: Experimental Study of the Deposition of Iodine and Other Fission Products in the Coolant Circuit of a CAGR	1423 - 1431

	pages
9.9 E.M. Hood, P.N. Clough: The Behaviour of Iodine in Advanced Gas-Cooled Reactor (AGR) Circuits	1432 - 1441
9.10 F. Abbey, W.O. Schikarski: Recent Developments in Nuclear Aerosol Research Related to Thermal Reactor Safety	1442 - 1457
9.11 W. Schöck, H. Bunz, W. Schikarski, J.P. Hosemann, D. Haschke, T.F. Kanzleiter, T. Schröder, M. Fischer, K. Hassmann, M. Peehs, H. Ruhmann: The DEMONA Project: Objectives, Results and Significance to LWR Safety	1458 - 1467
9.12 J.A. Gieseke, H. Chen, P. Cybulskis, R.S. Denning, M.R. Kuhlman, K.W. Lee, M. Silberberg, M. Jankowski: Radionuclide Release to the Environment under Specific LWR Accident Conditions	1468 - 1477
9.13 E.A. Warman: Parametric Study of Factors Affecting Retention of Fission Products in Severe Reactor Accidents	1478 - 1491
9.14 K. Hassmann, M. Fischer, J.P. Hosemann, H. Bunz: Current Results of Radioactive Source Term Analyses for Melt Down Sequences in KWU-Type PWR's	1492 - 1504
9.15 H. Deuber, H.-G. Dillmann, K. Gerlach: Retention of Gaseous Radioiodine with Sorbents under Accident Conditions	1505 - 1513
9.16 V. Rüdinger, J.G. Wilhelm: Confinement of Airborne Particulate Radioactivity in the Case of an Accident	1514 - 1522

	pages
9.17 W. Morell, W. Kastner, R. Rippel, F. Richter: Experimental Investigations Simulating Iodine Release at Design Basis Accident in PWR	1523 - 1534
9.18 D. Cubicciotti, B.R. Sehgal: Fission Product and Material Vapor Transport during Molten Corium-Concrete Interactions	1535 - 1553
9.19 H. Kodaira, S. Kondo, Y. Togo: An Application of the Monitoring and Diagnostic System to Plant Diagnosis of FP Transport and Release in NPPS	1554 - 1563
9.20 K.-D. Hocke, R. Bisanz, F. Schmidt, H. Unger: Fission Product Release and Transport Modeling in KESS-2	1564 - 1571
9.21 C.I. Ricketts, V. Rüdinger, J.G. Wilhelm: HEPA-Filter Response to High Differential Pressures and High Air Velocities	1572 - 1582
9.22 K. Vinjamuri, D.J. Osetek, R.R. Hobbins: Tellurium Behaviour During and After the TMI-2 Accident	1583 - 1592
9.23 H.-G. Dillmann, H. Pasler: A Containment-Venting Filter Concept and its Implementation at Stainless-Steel Fiber Filters	1593 - 1605

MEASUREMENT AND CHARACTERIZATION OF FISSION PRODUCTS RELEASED
FROM LWR FUEL

M. F. Osborne, J. L. Collins, R. A. Lorenz, and K. S. Norwood*

Chemical Technology Division
Oak Ridge National Laboratory
Oak Ridge, Tennessee 37831

R. V. Strain

Materials Science and Technology Division
Argonne National Laboratory
Argonne, Illinois 60439

ABSTRACT

Samples of commercial LWR fuel have been heated under simulated accident conditions to determine the extent and the chemical forms of fission product release. This project was sponsored by the USNRC under a broad program of reactor safety studies. Of the five tests discussed, the fractional releases of Kr, I, and Cs varied from ~2% at 1400°C to >50% at 2000°C; much smaller fractions of Ru, Ag, Sb, and Te were measured in some tests. The major chemical forms in the effluent appeared to include CsI, CsOH, Sb, Te, and Ag.

INTRODUCTION

Accurate information about the quantities and chemical forms of fission products released from light-water reactors (LWRs) during overheating incidents is required for the reliable assessment of potential hazards. For several years, the U.S. Nuclear Regulatory Commission (USNRC) has sponsored experimental studies of these phenomena at Oak Ridge National Laboratory (ORNL).¹⁻³ In all these tests, small segments of commercial LWR fuel rods were heated under simulated accident conditions, and the released material was collected and analyzed. The most recent test series used a new furnace design which permitted testing at temperatures up to 2000°C. The primary objectives of the study were: to determine the release rates and the chemical forms of the most significant fission products, to relate these results to changes in the fuel microstructure, and to compare these data with results from other experimental work. With the exception of detailed studies of the fuel and cladding microstructure, which was conducted at Argonne National Laboratory (ANL), all of this work was carried out at ORNL. The results will be used by the USNRC in computer modeling studies of various accident scenarios to evaluate the resulting consequences.

*Guest scientist from UKAEA-Harwell.

EXPERIMENTAL APPARATUS AND TECHNIQUES

In the recent test series, the fuel specimens (15 to 20-cm-long segments of LWR rods of 10 to 40 MWd/kg burnup) were heated in an induction furnace (Fig. 1) at 1400 to 2000°C for 20 min.⁴⁻⁷ An atmosphere of steam and helium at 0.1 MPa pressure flowed across the heated specimens, oxidizing the Zircaloy cladding and transporting released material to the collection system, comprised of a thermal gradient tube lined with platinum, an aerosol sampler, a series of glass-fiber filters, heated charcoal, and cooled charcoal. The temperature in the thermal gradient tube varied from about 850°C at the inlet to 150°C at the outlet. The other collector components were maintained at ~150°C to prevent steam condensation.

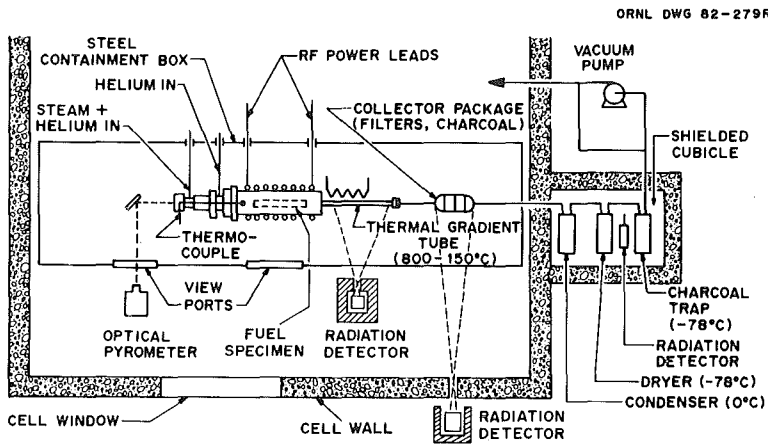


Fig. 1. Fission product release and collection system.

Data were obtained before, during, and after each test. The principal methods for analysis were (1) gamma spectrometry (GS) for the radionuclides, (2) neutron activation analysis (NA) for ^{129}I , (3) spark-source mass spectrometry (SSMS), and (4) energy-dispersive x-ray analysis (EDX) via scanning electron microscopy for all except the lighter elements. All four methods have been valuable in studying fission product release and transport, and, in addition, the SSMS and EDX analyses have provided data on the behavior of structural and impurity elements that influence fission product behavior. Fission product inventories in the fuel were determined by ORIGEN calculations, based on the reactor operating histories and on mass spectrometric analysis of the irradiated fuel. The accumulations of ^{134}Cs and ^{137}Cs on the thermal gradient tube and the filters and of ^{85}Kr on the cooled charcoal were measured during the tests by gamma spectrometry. Posttest examinations included GS analysis of the entire fuel specimen and all apparatus components, as well as optical microscopy and scanning electron microscopy of selected areas (especially the fuel/cladding interfaces and areas of melting and/or reaction).

RESULTS AND INTERPRETATION

The principal test parameters and the fractional release data for the five tests in this series are summarized in Table I. Significant releases of fission

Table I. Fission product release data from tests of LWR fuel

Test No.	Temperature (°C)	Time (min)	Steam flow rate (L/min)	Fraction of inventory ^a found (%)				
				⁸⁵ Kr ^b	¹³⁷ Cs	¹²⁹ I	¹²⁵ Sb ^c	^{110m} Ag ^c
HI-1	1400	30	1.0	3.13	1.75	2.04	0.018	0
HI-2	1700	20	1.0	51.8	50.5	53.0	1.55	3.13
HI-3	2000	20	0.30	59.3	58.8	35.4	0.001	0.015
HI-4	1850	20	0.32	31.3	31.7	24.7	0.009 ^d	0.094
HI-5	1700	20	0.41	19.8	20.8	22.9	0.315 ^d	18.07 ^d

^aBased on ORIGEN calculation.

^bIncludes Kr released during irradiation.

^cMeasurable only after Cs removal; values represent minima only.

^dAbout 99% of released Sb and Ag remained in the furnace.

product Kr, I, and Cs occurred in all tests; smaller and more variable fractions of Mo, Ru, Ag, Cd, Sb, Te, Ce, and Eu were detected also. The very high levels of radiocesium interfered with GS analyses for the less abundant gamma emitters, such as ¹⁰⁶Ru, ^{110m}Ag, and ¹²⁵Sb. The release fractions for rubidium and bromine were similar to those for cesium and iodine, their chemical analogs. The release and transport of Ag, Sb, and Te appeared to be influenced by the extent of cladding oxidation by the steam.

In addition to these fission products, a number of structural elements (Zr, Sn, Mg, Ca) and impurities (S, Cl, Pb, Bi) were identified by SSMS and EDX. These structural and impurity elements were significant contributors to the masses of aerosol deposited on the thermal gradient tubes and filters. Since some of these elements are not present in LWRs, however, their behavior in our tests is not relevant to safety considerations.

The mass distributions of fission product Cs, I, Sb, and Ag in the platinum thermal gradient tube varied significantly. This is illustrated in Fig. 2.^{8,9} In all tests, the iodine was deposited in a single broad peak at temperatures ranging between 400 and 600°C. These results indicate the existence of a single form of iodine, apparently CsI, in association with some other form of cesium. The iodine form was somewhat less volatile than pure CsI.⁹ Based on our knowledge of the materials present and on their thermochemical properties,¹⁰ we believe the CsI forms a solid solution with a less volatile cesium compound. Very little elemental or organic iodine was present, as evidenced by the small fractions of released iodine (0.4% maximum) found on the charcoal.

The behavior of antimony was markedly different; as shown in Fig. 2, the surface concentration decreased exponentially with distance along the platinum tube. Our data indicate that antimony was released in elemental form, and that gas-phase diffusion was the limiting step in deposition onto the platinum. The antimony reacted rapidly and irreversibly with the platinum, probably forming a solid solution of PtSb₂ in platinum.¹¹ In addition, the antimony release exceeded 1% only in test HI-2, indicating a correlation with cladding oxidation. Although our data for tellurium release are limited, the release of this element appeared to be strongly dependent on the extent of cladding oxidation, as reported by Albrecht and Wild¹², and by Lorenz et al.¹³ Only in tests where cladding oxidation was nearly complete, was tellurium release appreciable.

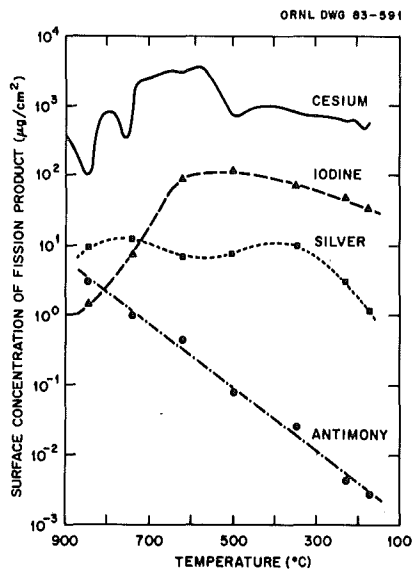


Fig. 2. Mass distribution of fission products in thermal gradient tube after test HI-2.

Cesium profiles in the thermal gradient tube have usually been complex, indicating two or more chemical forms. In our tests, only ~30% of the released cesium deposited in the thermal gradient tubes; the remainder either deposited on the ZrO_2 at the outlet end of the furnace or was collected on the filters. Although a large fraction of the released cesium may have existed as $CsOH$, the deposition profiles indicated the presence of other, less volatile forms. Spark-source mass spectrometry data have revealed sufficient masses of other elements to form less volatile mixed oxides of cesium; the major possibilities are zirconium (from the cladding), molybdenum (fission product), and sulphur (from furnace ceramics).

In the most recent test (HI-5), a miniature deposition sampler was used to collect aerosol samples continuously in a form convenient for posttest examination. A small graphite rod, driven by a screw, traveled across the effluent stream prior to the filters, collecting material in a spiral path on its surface. After the test, the rod was analyzed by GS, then examined by scanning electron microscopy with EDX analysis. Particle sizes ranging from ~1 to 100 μm were measured. A number of apparently crystalline particles with Cs/I ratios of ~1.7 were observed with a general background of cesium, suggesting that the particles were primarily CsI . Other elements identified by EDX included Cd, Zr, Fe, Si, S, and Cu, listed in order of declining concentrations.

Gamma spectrometric analysis of the fuel specimen provided supplementary data about fission product release and test temperature. The ratios of ^{134}Cs

(1365 keV) to ^{154}Eu (1274 keV) for four sets of measurements are plotted in Fig. 3. Europium was chosen for comparison because it should behave like the UO_2 fuel and be relatively immobile, while the cesium should be released in large quantities during the test. In order to minimize attenuation effects in the fuel, similar gamma ray energies for ^{134}Cs and ^{154}Eu were measured both before and after testing. Measurements were made on both the entire specimen (through a 3.8-cm-thick lead plate) and on 1-cm-long sections (unshielded, as through a collimator). Cesium release values obtained by this method and by the conventional "summation of components" method are shown in Table II for the last three tests of the series.

ORNL DWG 84-850

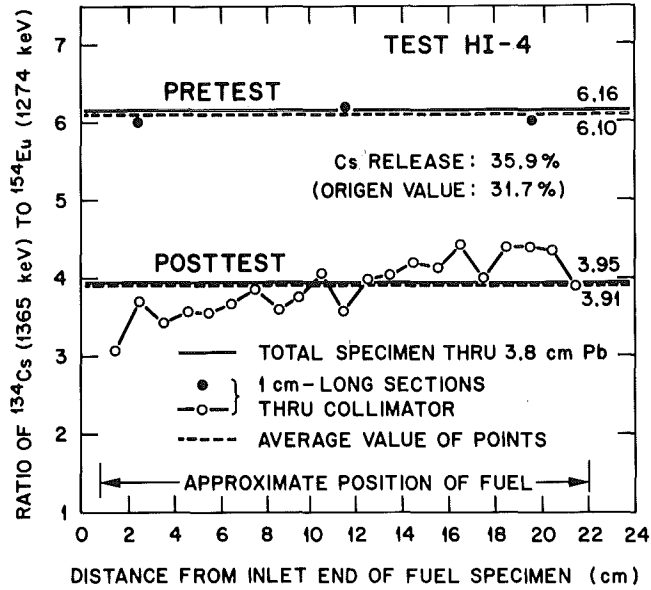


Fig. 3. Cesium-134 content of the fuel before and after test HI-4.

Table II. Cesium release values found by GS analysis and by summation of components

Test No.	Reactor	Cesium released from the fuel (%)	
		Component analysis/ORIGEN	Gamma spectrometric pre- and post-test fuel analysis
HI-3	Robinson	58.8	60.2
HI-4	Peach Bottom	31.7	35.9
HI-5	Oconee	20.8	24.5

These data show that (1) the two independent techniques for determining cesium release agree reasonably well for three types of fuel with a burnup range of 10 to 40 MWd/kg; (2) the slightly higher cesium release indicated for the inlet end of the specimen is in good agreement with the predicted temperature profile in the furnace; and (3) results from the two types of measurement of fission products in the fuel (short sections unshielded vs total specimen with lead attenuation) are consistent and comparable. The absence of appropriate gamma ray energies and the generally lower release rates of elements other than cesium, however, limits the usefulness of this technique in determining the release of other fission products.

Posttest examination of the fuel specimens at ANL included optical and scanning electron microscopy and scanning Auger microprobe analysis. Changes in the fuel microstructure correlated reasonably well with the measured fission product release values.¹⁴ Test-induced increases in UO₂ grain size varied from ~20% at 1400°C to ~50% at 2000°C. Fuel fractography showed the development of bubbles, both on the grain faces and within grains, as shown in Fig. 4. The

ORNL PHOTO 5072-84

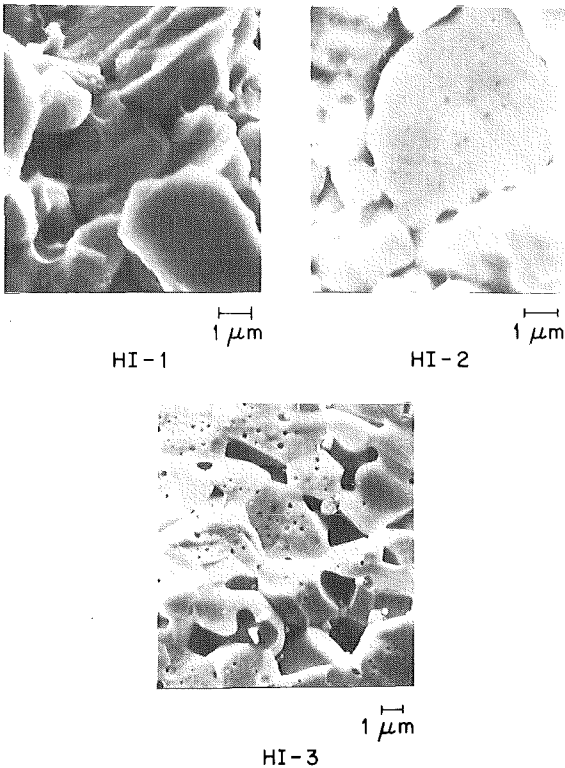


Fig. 4. Fractographs of intragranular fractures in the UO₂ in tests HI-1, HI-2, and HI-3, illustrating the development of porosity both internal and on the surfaces of the grains.

observed increases in porosity, which resulted from bubble growth and inter-linkage, correlated reasonably well with test temperatures and measured fission gas releases. Energy-dispersive x-ray analysis determined that observed intergranular metallic beads consisted of the noble metal fission products Zr, Ru, Rh, and Pd.

Examination of the Zircaloy cladding showed essentially complete oxidation to ZrO_2 for test HI-2 and less, but extensive, oxidation in the other tests. Considerable chemical interaction between the fuel and cladding was observed in the 2000°C test (HI-3); although local uranium concentrations were quite high in some areas of the cladding, the average content was estimated to be <3 wt %. Compared to the observations of Hofmann and Kerwin-Peck,¹⁵ our results indicate that the oxidizing atmosphere (steam), reduced the extent of fuel-cladding interaction and liquifaction by converting Zr to ZrO_2 .

A recent NRC-sponsored review of all applicable fission product release work¹⁶ compared the data on the basis of fractional release rate, k , using a model proposed by Albrecht and Wild¹⁷ of the form

$$F = 1 - e^{-kt} . \quad (1)$$

This equation, where F is the total fractional release, t is time, and k is a function of temperature, can be solved for k :

$$k = -\frac{1}{t} \ln(1 - F) . \quad (2)$$

Because the release of fission products from UO_2 should be closely related to the vapor pressures of the particular species, we chose to compare the data in the Arrhenius fashion, as suggested by Andriessse and Tanke,¹⁸ rather than directly vs temperature, as done previously.⁸ However, the comparison of total release data from experiments of varying duration (20 to 30 min in this test series vs 0.5 to 10 min in a previous series²) introduced a significant uncertainty in the release rate, k . In an effort to compare all tests more equally, we derived k 's for Kr and Cs from the on-line release data, using results for only a short period (generally 5 min) at the beginning of the maximum temperature phase of each test. These data, which are plotted in Fig. 5, show consistent dependence on reciprocal absolute temperature, with curves from the two types of tests exhibiting slightly different slopes. Experimental differences that might contribute to the higher release rates found in the earlier HT tests² are: (1) expanded cladding, which could reduce any cladding restraints on release and increase the accessibility of steam to the UO_2 , and (2) direct induction heating of the cladding, which resulted in faster heatup rates. The data points for test HI-2 appear high by all methods of comparison; the complete oxidation and large fracture of the cladding may have resulted in some oxidation of the UO_2 , a potential cause of increased fission product release.

CONCLUSIONS

These tests of commercial LWR fuel have shown that ~50% of the fission product cesium, iodine, and krypton may be released within a matter of minutes at temperatures of 1700 to 2000°C. Smaller, but significant, fractions of the Ru, Ag, Sb, and Te were released also. Rubidium and bromine release fractions were similar to those for their respective chemical analogs, cesium and iodine. Release rates calculated from these total release fractions compare reasonably well with previous experimental values, and the release rates for cesium and krypton correlate well with classical reciprocal temperature behavior. Observed

ORNL DWG 84-847

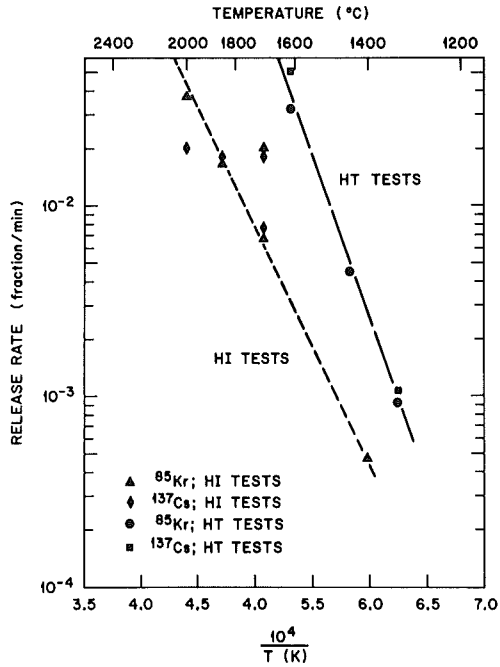


Fig. 5. Krypton and cesium release rates based on initial 5 min at test temperature.

changes in fuel microstructure, such as grain growth and the growth and interlinkage of bubbles, were consistent with test temperatures and fission product releases. These results indicate that the kinetic processes controlling inert gas release apply similarly to the behavior of the volatile fission products, cesium and iodine.

The released iodine behaved in all cases like a mixture of CsI and a less-volatile cesium compound; only very small fractions of iodine (<0.4%) passed through the filters as I_2 , HI, and/or organic iodides. Cesium, however, seemed to exist in several different forms, and the dominant cesium species probably depended on the availability of such elements as molybdenum, zirconium, and sulphur, any of which may react with CsOH. Antimony, and probably silver and tellurium, were released in elemental form. Apparently the release of these elements was strongly inhibited in cases where metallic zirconium was present, suggesting the formation of alloys with the cladding until most of the zirconium had been converted to ZrO_2 .

A technique for the direct measurement of fission products in the fuel, both before and after testing, was demonstrated to be reliable and produced independent verification of fission product release and of temperature distribution in the fuel specimen.

REFERENCES

1. R. A. Lorenz, J. L. Collins, A. P. Malinauskas, O. L. Kirkland, and R. L. Towns, Fission Product Release from Highly Irradiated LWR Fuel, NUREG/CR-0722 (ORNL/NUREG/TM-287/R2), February 1980.
2. R. A. Lorenz, J. L. Collins, A. P. Malinauskas, M. F. Osborne, and R. L. Towns, Fission Product Release from Highly Irradiated LWR Fuel Heated to 1300-1600°C in Steam, NUREG/CR-1386 (ORNL/NUREG/TM-346), November 1980.
3. R. A. Lorenz, J. L. Collins, M. F. Osborne, R. L. Towns, and A. P. Malinauskas, Fission Product Release from BWR Fuel Under LOCA Conditions, NUREG/CR-1773 (ORNL/NUREG/TM-388), July 1981.
4. M. F. Osborne, R. A. Lorenz, J. R. Travis, and C. S. Webster, Data Summary Report for Fission Product Release Test HI-1, NUREG/CR-2928 (ORNL/TM-8500), December 1982.
5. M. F. Osborne, R. A. Lorenz, J. R. Travis, and C. S. Webster, Data Summary Report for Fission Product Release Test HI-2, NUREG/CR-3171 (ORNL/TM-8667), February 1984.
6. M. F. Osborne, R. A. Lorenz, K. S. Norwood, J. R. Travis, and C. S. Webster, Data Summary Report for Fission Product Release Test HI-3, NUREG/CR-3335 (ORNL/TM-8793), March 1984.
7. M. F. Osborne, J. L. Collins, R. A. Lorenz, K. S. Norwood, J. R. Travis, and C. S. Webster, Data Summary Report for Fission Product Release Test HI-4, NUREG/CR-3600 (ORNL/TM-9011) June 1984.
8. M. F. Osborne et al., "Fission Product Release from Fuel Under LWR Accident Conditions," p. 4.1-1, Proceedings of the International Meeting on Light-Water Reactor Severe Accident Evaluation, Cambridge, Mass., Aug. 28-Sept. 1, 1983.
9. K. S. Norwood, J. L. Collins, M. F. Osborne, R. A. Lorenz, and R. P. Wichner, "Characterization and Chemistry of Fission Products Released from LWR Fuel Under Accident Conditions," Proceedings of the ANS Topical Meeting on Fission Product Behavior and Source Term Research, Snowbird, Utah, July 15-19, 1984.
10. I. Barin and O. Knacke, Thermochemical Properties of Inorganic Substances, Springer-Verlag, 1973, p. 659.
11. M. Hansen and K. Anderko, Constitution of Binary Alloys, 2nd ed., McGraw-Hill, 1958, p. 138.
12. H. Albrecht and H. Wild, "Behavior of Cs, I, Te, Ba, Ag, In, and Cd During Release from Overheated LWR Cores," Proceedings of the International Meeting on Light-Water Reactor Severe Accident Evaluation, pp. 4.2-1-6, Cambridge, Mass., Aug. 28-Sept. 1, 1983.
13. R. A. Lorenz, E. C. Beahm, and R. P. Wichner, "Review of Tellurium Release Rates from LWR Fuel Element Under Accident Conditions," Proceedings of the International Meeting on Light Water Reactor Severe Accident Evaluation, pp. 4.4-1-9, Cambridge, Mass., Aug. 28-Sept. 1, 1983.

14. R. V. Strain, J. E. Sanecki, and M. F. Osborne, "Fission Product Release from Irradiated LWR Fuel Under Accident Conditions," Proceedings of the ANS Topical Meeting on Fission Product Behavior and Source Term Research, July 15-19, 1984, Snowbird, Utah.
15. P. Hofmann and D. K. Kerwin-Peck, "Chemical Interactions of Solid and Liquid Zircaloy-4 with UO_2 Under Transient Nonoxidizing Conditions," Proceedings of the International Meeting on Light Water Reactor Severe Accident Evaluation, pp. 1.8-1-7, Cambridge, Mass., Aug. 28-Sept. 1, 1983.
16. Technical Bases for Estimating Fission Product Behavior During LWR Accidents, NUREG-0772, U.S. Nuclear Regulatory Commission, June 1981.
17. H. Albrecht and H. Wild, "Investigation of Fission Product Release by Annealing and Melting of LWR Fuel Pins in Air and Steam," Proceedings of the ANS Topical Meeting on Reactor Safety Aspects of Fuel Behavior, Sun Valley, Idaho, August 2-6, 1981.
18. C. D. Andriessse and R. H. J. Tanke, Dominant Factors in the Release of Fission Products from Overheated Urania, KEMA Laboratories, Arnhem, the Netherlands (to be published).

BEHAVIOR OF FISSION PRODUCTS RELEASED FROM SEVERELY DAMAGED FUEL
DURING THE PBF SEVERE FUEL DAMAGE TESTS

D. J. Osetek,¹ A. W. Cronenberg,² D. L. Hagrman,¹
J. M. Broughton¹ and J. Rest,³

EG&G Idaho, Inc.
Idaho Falls, ID 83415

ABSTRACT

The results of fission product behavior during the first two Power Burst Facility Severe Fuel Damage tests are presented. Measured fission product release is compared with calculated release using temperature dependent release rate correlations and FASTGRASS analysis. The test results indicate that release from fuel of the high volatility fission products (Xe, Kr, I, Cs, and Te) is strongly influenced by parameters other than fuel temperature; these are fuel/fission product morphology, fuel and cladding oxidation state, extent of fuel liquefaction, and quench induced fuel shattering. Fission product transport from the test fuel through the sample system was strongly influenced by chemical effects. Holdup of I and Cs was affected by fission product chemistry and transport time. Analysis demonstrates that such integral test data can be used to confirm physical, chemical, and mechanistic models of fission product behavior for severe accident conditions.

INTRODUCTION

The United States Nuclear Regulatory Commission has initiated an internationally sponsored severe fuel damage research program⁴ to investigate light water reactor (LWR) fuel rod and core response, and the release and transport of fission products and hydrogen during degraded core cooling accidents. The principal in-pile testing portion of this program is a series of severe fuel damage (SFD) tests being performed in the Power Burst Facility (PBF) at the Idaho National Engineering Laboratory.

The principal test conditions for the four bundle experiments are summarized in Table I, and a cross-sectional view of the bundle configuration is shown in Figure 1. The test bundle consists of zircaloy-clad UO₂ fuel rods arranged in a 6 x 6 array, without corner rods. The first two tests, the SFD Scoping Test (SFD-ST) and SFD 1-1, used fresh fuel which was trace-irradiated to approximately 90 MWd/MTU prior to initiation of the SFD transient; the last two tests incorporate rods previously irradiated to approximately 36,000 MWd/MTU. Ag-In-Cd control rods will be incorporated into the last test. This paper summarizes results for the first two experiments. Further details of the test program are described in References 1 and 2.

The on-line fission product sampling and monitoring system is shown schematically in Figure 2. The test effluent, consisting of steam, hydrogen, and fission products, was routed from the fuel bundle to the monitoring system through a 1.3 cm diameter stainless steel pipe. Six effluent steam samples were remotely opened at various times during the tests to provide samples for posttest analysis. The remaining effluent was cooled to a temperature below 340 K. The effluent then entered a separator vessel, where nitrogen purge gas

TABLE I. SUMMARY OF THE PBF-SFD PHASE-I TEST CONDITIONS

Test (Status)	Heating Rate	Fuel Burnup (at.%)	Nominal Coolant Flow (g/s)	Cooldown Mode	Test Conditions
SFD-ST (Oct, 1982)	0.13 K/s to 1700 K 10.0 K/s to 2400 K	0.0089	16.0	Quench	Steam rich, 100% oxidation partial fuel liquefaction generated
SFD 1-1 (Sept 1983)	0.45 K/s to 1300 K 1.3 K/s to 1700 K 30 K/s to 2400 K	0.0079	0.7	Slow	Steam starved 30% oxidation extensive liquefaction
SFD 1-3 (July 1984)	0.5 K/s to 1200 3.7 K/s to 1700 30 K/s to 2400	3.6	0.7	Slow	Similar to SFD 1-1, but 4 empty guide tubes
SFD 1-4 (Jan 1985)	Similar to SFD 1-1	3.6	0.7	Slow	4 AgInCd Control Rods

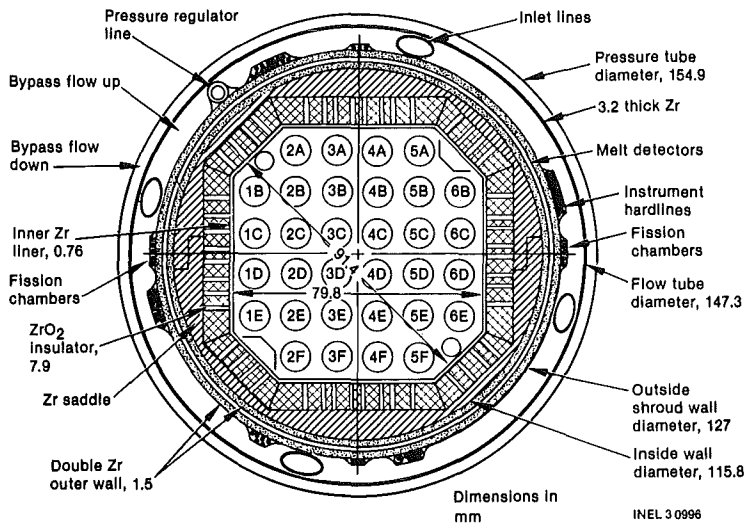


Figure 1. Cross section of the severe fuel damage test train.

PBF Transient Release System

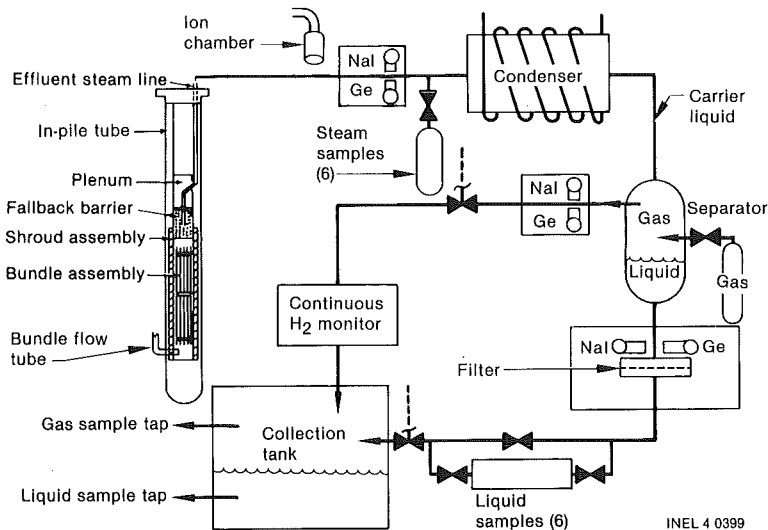


Figure 2. SFD Fission product and hydrogen monitoring system for test 1-1.

swept hydrogen, fission gases, and other noncondensables from the separator, past a gamma spectrometer and a hydrogen monitor, into a collection tank. The liquid from the separator was also monitored continuously by gamma spectroscopy, then passed through a particle filter and into a collection tank. Six liquid grab samples were collected at specific times during the tests to assess fission products carried with the liquid.

The principal differences between test SFD-ST and test SFD 1-1 were the mass flow rates of coolant and the cooldown mode. The higher mass flow during the SFD-ST (16 gm/s) resulted in a steam rich environment within the fuel bundle, a high volumetric flow rate leaving the bundle ($\sim 550 \text{ cm}^3/\text{s}$), and relatively low fission product concentrations. The low mass flow during the SFD 1-1 test (0.7 gm/s) resulted in a predominately hydrogen blanketed fuel bundle and a low volumetric flow rate leaving the bundle ($\sim 20 \text{ cm}^3/\text{s}$). The rapid quench and reflow of the SFD-ST bundle resulted in extensive fuel shattering, whereas the slow cooling of the SFD 1-1 bundle minimized fuel shattering and changes in the high temperature geometry.

In the following sections, fission product behavior observed during the first two tests are correlated with fuel/fission product morphology, and system chemistry and transport conditions.

EFFECTS OF FUEL/FISSION PRODUCT MORPHOLOGY

Released fission products are monitored downstream of the bundle exit after the test effluent flows through approximately 30 meters of piping. Thus the released fission products can interact physically and chemically with the steam/hydrogen atmosphere, or the metal components of the system, before activity measurements are obtained. Such transport effects probably influenced

the measured behavior of I, Cs, and Te which are highly reactive. However, the noble gases are essentially inert both physically and chemically under these conditions, and their on-line measured activity, corrected for transport time, should provide an accurate signature of real-time release from the fuel.

The noble gas release rates from the fuel for both tests, as a function of fuel temperature are shown in Figure 3. A small burst release was noted in both tests at fuel temperatures of ≈ 1100 K, which corresponds to the gap inventory of noble gases at the time of cladding rupture. Fission product release was low during both tests after the burst release until the fuel temperatures reached ≈ 1700 K. The indicated fractional release rates increased from 10^{-6} to 10^{-3} min^{-1} above 1700 K as fuel temperatures approached the $\alpha\text{-Zr(O)}/\text{UO}_2$ eutectic melting temperature of ≈ 2170 K. Significant fuel liquefaction would be expected at temperatures above ≈ 2170 K. A spike in the release of noble gases was detected at the time of bundle quench during the scoping test. Extensive fuel fracturing along grain boundaries is believed to be the reason for the enhanced fission product release. The total fractional release of noble gases was approximately 0.5 during the Scoping Test and approximately 0.2 during Test 1-1. Most of the fission gas release measured during the Scoping Test occurred during quench of the fuel bundle from high temperature; however, during Test 1-1, most of the fission gas release was measured when the bundle was cooling, and is probably related to fuel liquefaction.

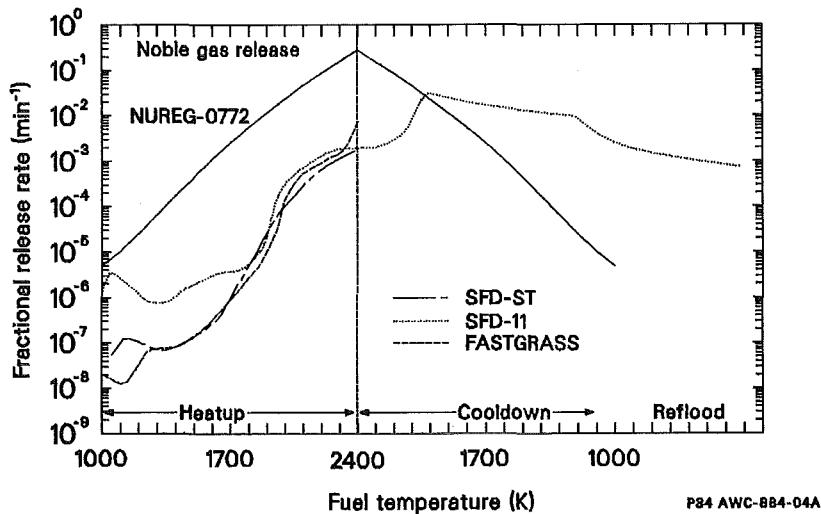


Figure 3. Comparison of the noble gas behavior during the SFD-ST and test SFD 1-1.

The mobility of the fission gases, Xe and Kr, within the fuel matrix is primarily controlled by the local temperature, temperature gradient, and burnup related fuel/fission product morphology. The mobility of the fission gas atoms at temperatures less than about 1300 K is too low to permit appreciable movement. However, motion of the gas atoms is significant at temperatures above 1300 K. Gas bubbles will form within grains and gradually collect at grain boundaries. Bubble motion can occur due to thermal gradients or by sweeping of grain-boundaries[3]. Gas that collects at grain boundaries is

released from the pellet interior only if the intergranular bubble density is large enough to cause bubble interlinkage and pathways to open porosity, or to sufficiently weaken the grain boundaries so that stress in the fuel causes cracking. If such interlinkage is absent, the noble gases are effectively trapped within the fuel pellet interior at the grain boundaries. Above 1900 K, gas bubbles and closed pores are sufficiently mobile to be driven by the thermal gradient to grain boundaries or open cracks where the gas is released. Thus, the gas release during a transient might be greatly enhanced if grain boundaries were disrupted by mechanisms such as the quench during the scoping test or fuel liquefaction during 1-1.

The fission gas release rate correlations from NUREG-0772 [4] and FASTGRASS [5] calculations of noble gas release are also shown in Figure 3. Measured release rates for the SFD-ST and 1-1 Tests are, in general, much lower during the fuel heatup than the NUREG-0772 release rate correlation. These tests were performed with trace-irradiated fuel that acquired only 80 to 90 MWd/MT burnup during preconditioning at relatively low power and temperature. Therefore, trace quantities of fission products were essentially distributed uniformly within the fuel grains, with almost no accumulation (concentration) at grain boundaries before the transient. Under these conditions, limited release of noble gases would be expected. A FASTGRASS analysis was performed for the SFD-ST and 1-1 test transients and the results indicate that the vast majority of both the noble gases and volatiles I and Cs were retained within the interior of individual grains as either individual atoms or newly nucleated intergranular microbubbles during most of the heatup phase. Because atomic or intergranular microbubble fission products are readily accommodated within the solid fuel microstructure, they experience little release from solid fuel, even at relatively high temperatures. The FASTGRASS calculations indicate that such conditions probably existed up until the time grain growth caused sweeping of intergranular atoms and microbubbles to grain boundaries (starting at about 1900 K). The predicted behavior using FASTGRASS and a model for oxidation accelerated grain growth, indicates rather good agreement with the SFD-ST and 1-1 data during fuel heatup to 2400 K, as shown in Figure 3.

The SFD Test 1-1 was terminated with a slow cooldown requiring approximately 16 minutes. The measured fission-gas release is in sharp contrast with the NUREG-0772 release rates which decrease as the bundle cools. The SFD Test 1-1 release rates and estimated fuel temperatures are plotted on a linear scale against time in Figure 4. The linear scale places release during heatup in perspective with the peak release during cooldown; cooldown started at about 41 min and was complete by about 57 min. The sharp increase in fission product release at about 41 min was at least partly induced by fuel liquefaction. The process of clad melting and fuel liquefaction provides an important mechanism for enhanced fission product release from the UO_2 matrix. However, the fission product atoms and bubbles must coalesce to form bubbles with sufficient buoyancy to overcome viscosity within the liquefied core material and rise to a free surface. The fission gas release during cooldown is further complicated because the U-Zr-O mixture does not freeze at constant temperature. Instead, as the mixture slowly cools, uranium and zirconium oxides precipitate in a uranium-zirconium liquid matrix, gradually increasing the solid content of the original slurry. Movement of the fission-gas bubbles would be progressively more difficult as they attempt to coalesce and migrate to a free surface, because the effective viscosity of the slurry gradually increases with decreasing temperature. The final U-Zr component freezes at about 1600 K, which correlates well with the exponential decay and eventual cessation of measured fission product release.

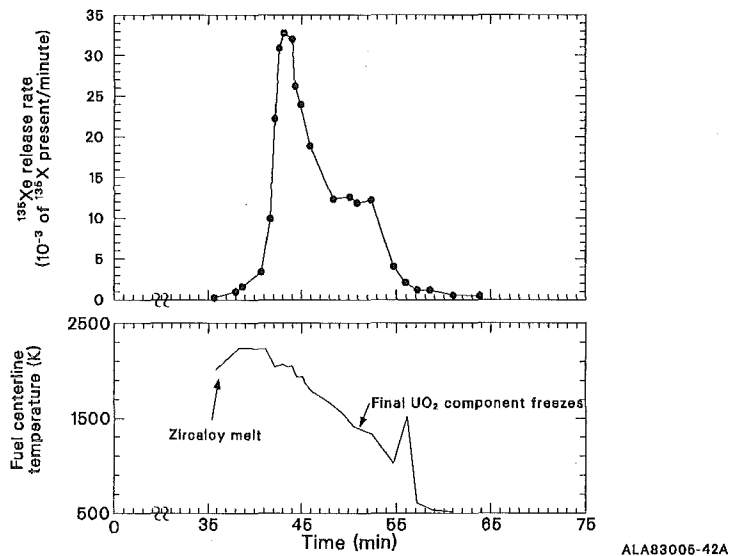


Figure 4. SFD 1-1 Xe release rates and estimated fuel temperatures.

In summary, the sequence of events leading to fission product release for the trace-irradiated fuel employed in the SFD-ST and 1-1 Tests appears to be as follows:

- o Initially high fission-product retention within individual fuel grains as individual atoms or intergranular microbubbles, with nil gas release.
- o Sweeping of fission products from the grain interior to grain boundaries at fuel temperatures above ~ 1900 K, which can be enhanced by rapid grain growth under fuel oxidation conditions.
- o Destruction of the grain structure via fuel liquefaction or quench-induced grain boundary shattering, with rapid fission gas release.
- o Sustained gas release during cooldown as the liquefied U-Zr-O mixture remains molten to lower temperatures (~ 1600 K).

In addition to fuel/fission product morphology, fission product behavior is also strongly influenced by chemical effects after release from the fuel. These effects are discussed below.

CHEMICAL BEHAVIOR OF FISSION PRODUCTS

The measured I and Cs activity as a function of test fuel temperatures is shown in Figure 5. Large differences in I and Cs behavior are noted between the two tests. Such discrepancies can be explained in terms of the differences in the chemical and effluent flow conditions for the ST versus 1-1 tests.

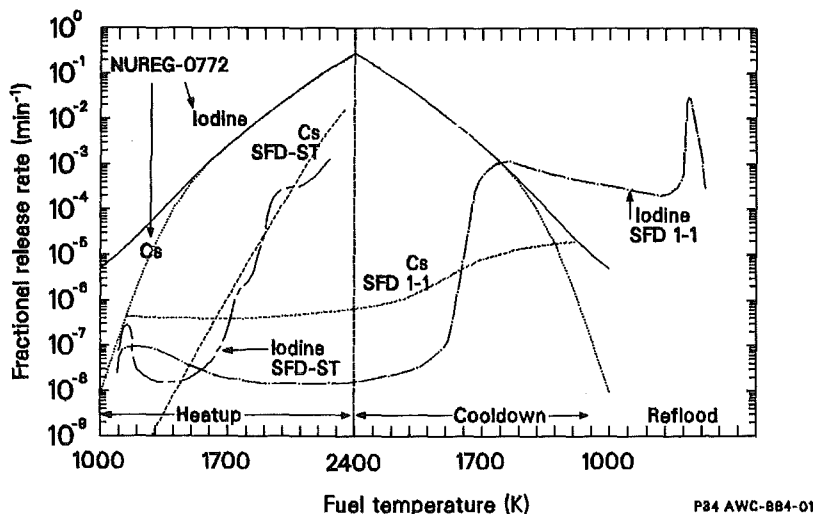


Figure 5. Comparison of iodine and cesium release behavior noted during the SFD-ST and 1-1 Tests.

Cs and I will mix and react with the steam and hydrogen released by the steam-zircaloy reaction after release from the fuel. The ultimate chemical composition of this vapor mixture depends on specie concentration, temperature, pressure and oxidation/reduction conditions. The equilibrium composition, at a particular temperature and pressure, can be found by noting that the total free energy of formation (ΔG_f°) approaches zero, this is:

$$\Delta G_f^\circ (\text{Products}) - \Delta G_f^\circ (\text{Reactants}) \approx 0$$

For an ideal gas, ΔG_f° can be expressed as:

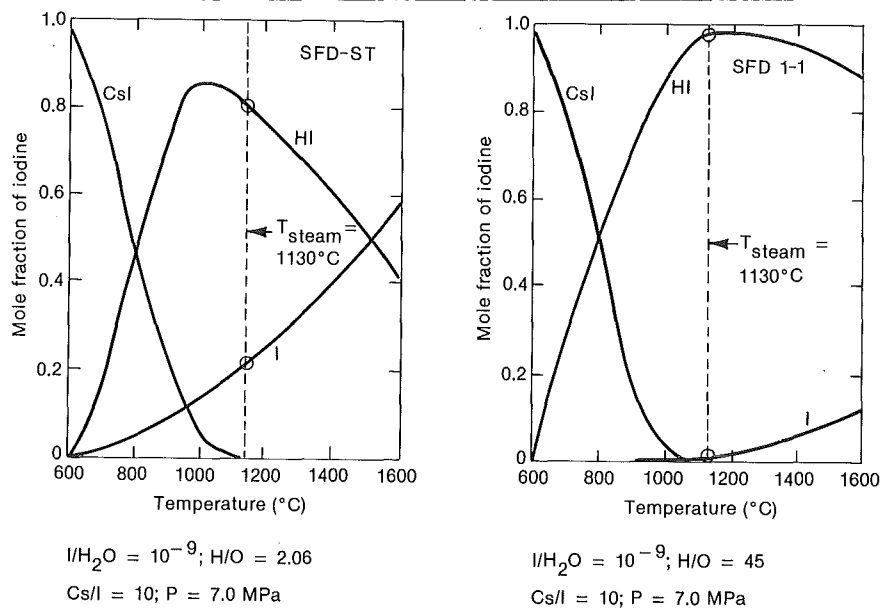
$$\Delta G_f^\circ = RT \ln (p_i)$$

where p_i is the partial pressure of a particular gaseous component of the reacting mixture. Changes in reactant concentration and H/O ratio will produce a change in the product composition. The results of Sallach's equilibrium analysis [6] for the Cs-I-O-H system, were used to assess the primary chemical forms for the SFD-ST and SFD 1-1 test conditions.

Table II is a summary of the fission product concentration and thermalhydraulic conditions in the high temperature region of the test bundle at the beginning of enhanced fission product release. The fractional I species concentrations as calculated by Sallach [6], at the corresponding fission product concentration levels, H/O ratio and test pressure conditions are shown in Figure 6. It is important to note that for trace-irradiated fuel, the release concentrations of I in H₂O are on the order of 10⁻⁹ to 10⁻⁶ mole fraction. Since the effect of decreasing iodine and cesium concentration is toward a diminished abundance of CsI at thermochemical equilibrium, the results plotted in Figure 6 may not be typical of what would be expected during an accident with higher burnup fuel, where higher fission product concentrations may exist. Nevertheless, for the ST and 1-1 trace irradiation conditions the fractional partitioning of I and Cs species are estimated from Figure 6. The

TABLE II. SUMMARY OF THERMODYNAMIC AND CONCENTRATION CONDITIONS FOR THE SFD-ST AND 1-1 TESTS AT THE TIME OF ENHANCED FISSION PRODUCT RELEASE

Parameter	SFD-ST	SFD 1-1
Steam temperature	$\approx 1400 \text{ K}$ ($\approx 1130^\circ\text{C}$)	$\approx 1400 \text{ K}$ ($\approx 1130^\circ\text{C}$)
System pressure	$\approx 7.0 \text{ MPa}$ ($\approx 70 \text{ bar}$)	$\approx 6.6 \text{ MPa}$ ($\approx 66 \text{ bar}$)
H/O mole ratio	≈ 2.06	≈ 45
Cs/I mole ratio	≈ 10	≈ 10
I/H ₂ O mole ratio	$\approx 10^{-9}$	$\approx 10^{-8}$
Cs/H ₂ O mole ratio	$\approx 10^{-8}$	$\approx 10^{-7}$



INEL 4 0901

Figure 6. Relative abundance of iodine species in the Cs-I-H-O system for the conditions of the SFD-ST (A) and 1-1 (B) tests as predicted from thermochemical equilibrium.

low boiling point volatiles I and HI predominate for both cases and probably more for the ST case where the steam supply diluted the cesium and iodine more than it did in the 1-1 test. In the near neutral environment (i.e., H/O ≈ 2.06) of the SFD-ST test, iodine in the high temperature (1400 K)

region is predicted to exist as 20 percent atomic iodine and 80 percent HI. In the highly reducing environment of Test SFD 1-1 ($H/O \approx 45$), approximately 98 percent of the iodine is predicted to be in the form of HI.

The high mole fractions of volatile iodine species HI and I (assumed to behave similar to I_2) in the SFD-ST and their low vaporization temperatures (see Table III) suggest limited condensation potential during the rapid transport (≈ 3 s) through the effluent line to the detectors. However, due to the relatively low flow rate for the SFD 1-1 test and long transport times (≥ 60 s), cooldown of the effluent in the piping causes transformation of I and HI to CsI. Calculations performed with a modified version of the TRAP MELT code [7] show that the iodine which transforms to CsI will condense on the inlet side of the condenser while the HI and I pass through the condenser. This is the reason for the nil iodine and cesium measured at the downstream detector location during the SFD 1-1 Test. Only upon bundle reflood and washout of reversible CsI deposits was significant iodine measured for Test SFD 1-1.

TABLE III. VAPORIZATION TEMPERATURES OF I AND Cs SPECIES

	<u>HI</u>	<u>I_2</u>	<u>CS</u>	<u>CsI</u>	<u>CsOH</u>
T_{vap} (K) at 1 atm	238	457	951	1553	1263
T_{vap} (K) at 70 atm	410	860	2275	2745	2180

In summary, the high mole fractions of HI and I, and the rapid transport conditions account for the high iodine measurement during the SFD-scoping test. However, the transformation of I and HI to CsI, due to higher concentration and to cooldown effects during the long transport time associated with the low flow rate of the 1-1 test, explain the observation that only upon bundle reflood was significant iodine measured for Test SFD 1-1.

CONCLUSIONS

From the foregoing analysis, the following conclusions can be drawn relative to noble gas and volatile fission product release from fuel and transport behavior in the SFD-ST and 1-1 tests:

- o Fission product release is strongly influenced by prior irradiation induced fuel/fission product morphology. Analysis of the SFD-ST and SFD-1-1 data for trace-irradiated fuel indicates limited release on heatup to fuel temperatures up to 2000 K, where the majority of the noble gases and volatiles are retained within the grain interior as individual atoms. Only upon grain growth and sweeping of fission products to grain boundaries is enhanced noble gas and volatile release predicted for trace-irradiated fuel in the solid state. Subsequent fuel liquefaction and quench-induced grain boundary shattering result in rapid fission product release
- o Iodine and cesium chemistry are strongly influenced by concentration and oxidation/reduction conditions. The low I and Cs concentrations and the relatively neutral ($H/O \approx 2.06$) high steam flow rate conditions of the Scoping Test resulted in predominately free iodine and CsOH transport in steam. However, the low flow rate, highly reducing ($H/O \approx 45$) environment of Test 1-1 combined with the concentration and cooldown-induced transformation of I and HI to CsI accounts for the observation of limited iodine detection during the

heatup phase of this test. Only upon posttransient reflood of the Test SFD 1-1 bundle was significant iodine release observed, which was probably washout of reversible CsI deposits

REFERENCES

1. P. E. MacDonald et al., "PBF Severe Fuel Damage Program: Results and Comparison to Analysis," Proc. Int. Mtg. on LWR Severe Accident Evaluation, Cambridge, MA, August 28-September 1, 1983.
2. D. J. Osetek, A. W. Cronenberg, R. R. Hobbins, and K. Vinjamuri, "Fission Product Behavior During the First Two PBF Severe Fuel Damage Tests," Proc. ANS Topical Mtg. Fission Product Behavior and Source Term Research, Snowbird, Utah, July 15-19, 1984.
3. D. R. Olander, Fundamental Aspects of Nuclear Reactor Fuel Elements, Technical Information Center, Office of Public Affairs ERDA, 1976.
4. United States Nuclear Regulatory Commission, Technical Bases for Estimating Fission Product Behavior During LWR Accidents, NUREG-0772, 1981.
5. J. Rest "The Mechanistic Prediction of Iodine and Cesium Release from LWR Fuel," Proc. Mtg. on Fission Product Behavior and Source Term Research, Snowbird, Utah, July 15-19, 1984.
6. R. A. Sallach, Chemistry of Fission Products Elements in High Temperature Steam: Thermodynamic Calculations of Vapor Composition, SAND81-0534, 1984.
7. H. Jordan et al., TRAP-MELT Users Manual, NUREG/CR-0632, February 1979.

FOOTNOTES

1. EGG Idaho, Inc., P. O. Box 1625, Idaho Falls, ID 83415.
2. Engineering Science and Analysis, 836 Claire View, Idaho Falls, ID 83402.
3. Material Science Division, Argonne National Laboratory, 9700 South Cass Ave., Argonne, IL 60439.
4. Sponsors of the program include Belgium, Canada, Federal Republic of Germany, Italy, Japan, Netherlands, United Kingdom, and United States.

NOTICE

This paper was prepared as an account of work sponsored by an agency of the United States Government. Neither the United States Government nor any agency thereof, or any of their employees, makes any warranty, expressed or implied, or assumes any legal liability or responsibility for any third party's use, or the results of such use, of any information, apparatus, product or process disclosed in this report, or represents that it use by such third party would not infringe privately owned rights. The views expressed in this paper are not necessarily state or reflect those of the United States government or any agency thereof.

Work supported by the U.S. Nuclear Regulatory Commission, Office of Nuclear Regulatory Research under DOE Contract No. DE-AC07-76ID01570.

DETERMINATION OF IODINE 131 RELEASE FROM DEFECT IRRADIATED
FUEL RODS UNDER SIMULATED LOCA CONDITIONS

E. Groos and R. Förthmann

Kernforschungsanlage Jülich GmbH, W.-Germany

ABSTRACT

In an attempt to obtain realistic and reliable values for the I 131 release in a PWR-LOCA, nineteen test fuel rods, irradiated under power reactor conditions, were heated with deliberately caused leaks to temperatures between 800 and 1000°C.

I 131 release showed a dependence on burn up and/or specific power and could be separated in a volatile and a non-volatile fraction. For fuel rods with normal load, the volatile fraction was 3×10^{-6} of the I 131 inventory at the most and the average total release over several hours of heating was about 10^{-4} .

1. INTRODUCTION

Iodine 131 is to our present knowledge the radiologically most significant radionuclide among those possibly released during a reactor incident. Theoretical assessment however is very difficult because of the complicated chemistry of the iodine, yet the chemical form is decisive for the release behaviour. Accordingly the I 131 release values assumed in the appropriate safety regulations are rather conservative by nature. To render possible a more realistic assessment the availability of reliable realistic experimental data is essential.

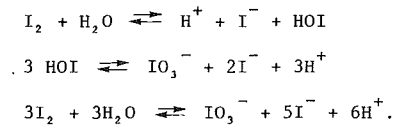
When breakage of a main coolant pipe of a PWR occurs, i.e. loss of coolant accident (LOCA), the pressure drop in the core and the superheating of the fuel cause the claddings of some fuel rods to burst before they are reflooded by the emergency coolant /1/. Fission products accumulated in the gap between fuel and cladding can be released spontaneously (gap release). It was the aim of this investigation to measure the gap release of iodine 131, being decisive for any further iodine release in the course of the accident /2,3/.

Emphasis was placed on simulating the accident conditions as realistic as possible in a post irradiation experiment. Temperatures, pressures and environment conditions were adjusted similar to those in a reactor core and the test fuel rods used had realistic burn up and specific power and still contained I 131 produced by fission.

2. IODINE CHEMISTRY

Iodine belongs to the group of the halogens, which are the most reactive chemical elements. It is however less aggressive than fluorine, chlorine and bromine. The elemental iodine (I_2) is a crystalline substance with a boiling point of 184,4°C though it sublimates noticeably at room temperature. This quality has led to the fact, that in nuclear reactor accident assessment iodine is treated like a noble gas.

Taking its chemical reactivity into account, the behaviour of the iodine in contact with the coolant water and the structural materials in the reactor core must be considered. The reaction with water produces iodide (I^-), hypoiodite (HOI) and iodate (IO_3^-)



All three reactions depend on various parameters (temperature, pH-value, radiation, oxygen concentration and others). Different from I_2 , the two iodine species I^- and IO_3^- are not volatile and - in a loss of coolant accident - remain dissolved in the sump-water. Only if the acidity of the water reaches pH-values of < 6 and lower, the equilibria shift to the left side to form again I_2 , resp. can I^- be oxydized to I_2 by oxygen from the air /4/.

With metals I_2 reacts - particularly at higher temperatures resp. in the presence of water - to form non-volatile iodides



for example with Zr the ZrI_4 (boiling point about $430^\circ C$). This compound as well as non-volatile compounds with metallic fission products (CsI) can be formed in the intact fuel rod, thus making only a small fraction of the iodine available in volatile, elemental form for instant gap release when a rupture of the canning occurs /5/.

3. TEST FACILITY

Figure 1 is a schematic presentation of the apparatus used for the experiments. It had to be placed in a hot cell and consisted of four main parts:

- a pressure tube (1) in a furnace to take the test fuel rod (tube length 60 mm, diameter 2,5 cm); the temperature ($1200^\circ C$ max.) was measured and registered by a thermocouple (2), the pressure (6 bar max.) by a pressure gauge (3);
- a gas/water feed system (4) could feed through the inlet pipe (5) either a gas (6) or - by means of an injection pump (7) - water in small measured portions to the hottest point in the pressure tube; through the compensation pipe (8) an adjustable gas pressure could be put on the
- cooled condensate trap (9). In this receptable steam coming from the pressure tube through the outlet pipe (10) was condensed and the gas pressure was necessary to compensate the resulting underpressure. When the pressure tube was swept with an inert gas instead of steam, the condensate trap contained sodium hydroxide solution (0,1 % NaOH) to dissolve soluble iodine. The content of the condensate trap could be sampled for analysis through the pipe (11);
- any iodine in the gas from the condensate trap was collected in the filter system (12). The gas stream could be adjusted by the valve (13) before it passed through a fibre filter (14) and a charcoal filter (15), containing KJ impregnated charcoal in four separable partitions. Before releasing it into the hot cell atmosphere, the gas passed a safety filter (16), mainly for the adsorption of fission gases.

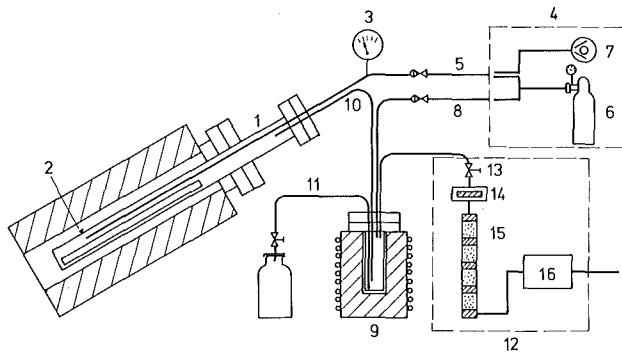


FIGURE 1: TEST APPARATUS (SCHEMATIC)

4. TEST PROCEDURE

The test parameters were chosen to simulate the conditions in a reactor pressure vessel during a LOCA as close to reality as possible in an out of pile experiment.

That comprises:

- test fuel rods with realistic burn up and specific power
- test temperatures between 800 and 1100°C
- test pressures between 1 and 6 bar
- test fuel rod in a steam atmosphere and an environment of structural material corresponding to the core structure (stainless steel, zircaloy).

4.1 Test Fuel Rods

The test fuel rods were provided by KWU, who had irradiated them in the KKW-Obrigheim to burn ups between 8 and 44 GWd/tU. The length was only a tenth of that of the original 4 m fuel rods. They had been stored for over a year so that the shorter lived fission products, including the I 131, had decayed. The rods were therefore reirradiated in the HFR-Petten, at specific powers between 210 and 400 W/cm to an I 131 inventory of 5 to 11 x 10¹² Bq (140 to 300 Ci) per rod.

4.2 Cladding Leak

The leak in the cladding was produced by one of three methods:

- sawing of a slit (30 mm long, 2 mm wide) before heating into the cladding in the region of the temperature maximum in the pressure tube (fig. 2)
- making a preset breaking point by milling the cladding wall thin (30 mm long) (fig. 3) and bursting the cladding during heating, detectable by a pressure peak
- bursting of the cladding during heating without any pretreatment (fig. 4)

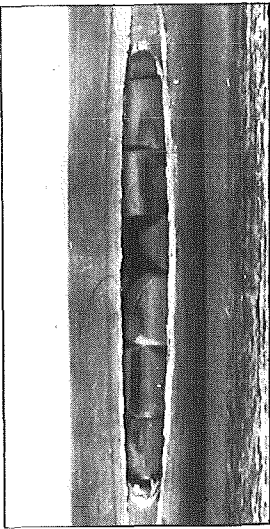


FIGURE 2

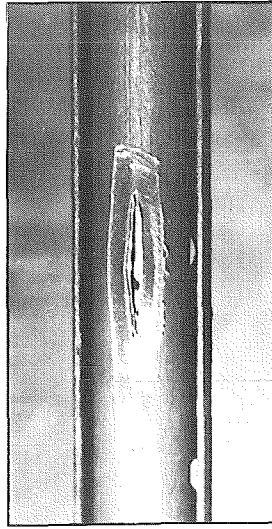


FIGURE 3

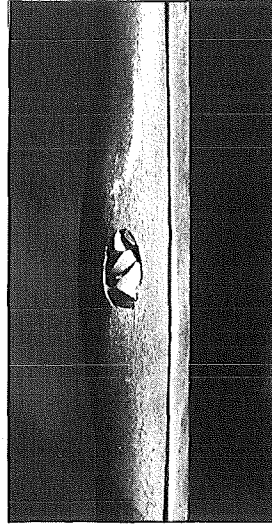


FIGURE 4

DIFFERENT TYPES OF CLADDING LEAKS

Bursting of the fuel rod wall occurred between 730 and 780°C with the exception of the two rods with the highest load, which ruptured at 640 resp. 620°C. In table I the relevant test parameters are compiled. Any influence of the way the leak was produced on the release of I 131 could not be observed.

4.3 Heating

The temperature in the furnace was controlled by an automatic regulator in combination with the thermocouple. Heating up to 800°C took about 1 hour, to 1100°C about 1 1/2 to 2 hours. During the heating the fuel rods in the pressure tube were either swept with steam (16 rods) or with an inert gas (3 rods).

Sweeping with Steam

When the temperature in the pressure tube had reached 200°C, water was injected in small portions of 0,2 to 0,5 ml into the hot tube, thus filling it with steam. The throughput was between 200 and 300 ml of water per hour. There were three possibilities to adjust the pressure in the system:

- amount of water injected fig. 1 (7)(5)
- outlet valve (13) and
- compensation gas pressure (6)(8).

Most of the I 131 released from the defect fuel rod that did not deposit on the hot metals in the pressure tube was dissolved in the water condensed in the condensate trap and could be withdrawn by means of the sampling pipe (11) without interruption of the test. This rendered possible the measurement of the time dependence of the I 131 release from the pressure tube. Some negligible small amounts of I 131 were found in the filter system, mainly in the first partition of the charcoal filter.

Sweeping with Inert Gas

Three test rods were heated in an atmosphere of helium instead of steam to check the iodine behaviour in the absence of water. The helium was swept through the inlet pipe (5), the condensate trap was filled with 150 ml of 0,1 % sodium hydroxide solution through the pipe (8). This solution was chosen to avoid oxidation of I^- by air. It was changed regularly and the I 131 measured. In addition, exchangeable charcoal traps with a volume of about 20 cm³ were placed between the condensate trap (9) and the outlet valve (13) to measure the iodine not dissolved in the sodium hydroxide solution.

4.4 Post Heating Treatment

Water Leach

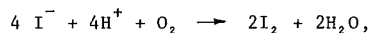
In some tests (table I) the pressure tube with the ruptured fuel rod inside was filled with water after cooling to room temperature (25 to 30°C) and left for four hours in order to measure the non-volatile soluble I 131 (reflood phase).

Cleaning of the Pressure Tube

With each test some of the I 131 remained in the pressure tube. It could not be removed even at temperatures up to 1000°C with either steam or inert gas and could therefore not have been I₂, but non-volatile iodine compounds, presumably iodides. This iodine could be removed completely with diluted nitric acid (0,5% HNO₃) injected into the pressure tube at about 200°C. The I 131 was collected in the condensate trap and the charcoal filter.

4.5 Analysis of the Iodine Species

Regarding the chemical form of the I 131 released from the fuel rod, two different forms could be distinguished: the iodine retained in the pressure tube even at high temperatures in a non-volatile form and that found in the condensate trap and the charcoal filters. The first kind, deposited in the pressure tube, is not elemental iodine or it would have been evaporated out of the tube during the heat treatment. It could, however, be converted into volatile iodine with nitric acid, proving it was retained in the tube as non-volatile I^- formed either with the metallic walls of the tube or with fission metals (reduction of I₂ to I^-). In an acidic medium, I^- can easily be oxidized to I₂



which was here achieved with nitric acid but is also possible with air.

In the charcoal traps the iodine can occur in three forms:

- adsorbed as elemental iodine (I₂)
- adsorbed as organic iodine compound (R-I)
- deposited on aerosoles as iodide (I^-) or iodate (IO₃⁻).

Since the fraction of this iodine is negligible compared with that in pressure tube and condensate trap - less than 1 %, except during heating in helium - it is of no significance in connection with the results discussed later and is - to be on the safe side - treated as "volatile" iodine.

In the condensate trap iodine can appear both as non volatile I^- and as volatile elemental I_2 . Liquid/liquid extraction was employed to separate I_2 and $I^- + IO_3^-$. The distribution between an aqueous phase ($5 < pH < 6$) and an organic phase, not miscible with each other, leads to the concentration of I_2 in the organic phase, whereas I^- and IO_3^- remain in the aqueous phase. The I_2 is then reextracted from the organic phase into an aqueous phase of $pH = 12$ as in the form of $I^- + IO_3^-$. By this method volatile I_2 and non volatile $I^- + IO_3^-$ can be distinguished.

4.6 Measurement of I 131

In all samples I 131 was determined by gamma spectrometry, using the area of the photopeak at 364 keV as a measure for the I 131 activity. There was no interference by other radionuclides.

5. RESULTS

Two groups of results have been obtained:

- I 131 release values for different sections of the test apparatus summed up to the total release for the ruptured fuel rod (table I and II) and
- time dependent releases curves of I 131 from the pressure tube, describing the transport with steam into the aqueous solution in the condensate trap (figures 5 to 8).

In both groups volatile I_2 and non-volatile I^- were separated. All release values are expressed as "Fractional Release", i.g. the quotient between I 131 released and I 131 inventory of the test fuel rod.

Both burn up and specific power influence the release of fission products from the fuel. The higher the burn up, the easier the fission product transport in the fuel due to the increasing distortion of its structure. Higher specific power means higher fuel temperature and steeper temperature gradients across the fuel pellets, both resulting in a faster fission product transport. According to the actual tendency of the release values to increase with both increasing burn up and specific power, an empirical "load factor" was defined as the product of total burn up (GWd/tU) and specific power (W/cm) during reirradiation:

$$K_B = B \text{ (GWd/tU)} \times P \text{ (W/cm)}.$$

For the fuel rods considered this number was between 1900 and 17600, in a nuclear power reactor, however, with a mean burn up of about 30 GWd/tU and an average specific power of 200 W/cm, a fuel rod under normal conditions will not exceed a K_B of 6000.

Table I summarizes all results obtained from 19 fuel rods. They are placed in the table in the order of increasing K_B . According to the experimental technique it contains four columns with "sectional" results (column 7 to 10) and one with the fractions of I_2/I^- found in the condensate trap are shown in table II.

5.1 Condensate (1. Sample)

Best representative for the "gap" release is the I 131 found in the sample first taken from the condensate trap. Ideally it should have been taken 2 to 3 minutes after the burst of the fuel rod, which was not possible due to the experimental conditions. For the test rods with the saw cut applied before heating, no time of burst could be defined; the first condensate sample was taken when the rod reached 800°C. For the rods bursting inside the pressure tube, the first condensate sample was taken between 2 minutes (D 66 and 457) and about 30 minutes (D 225 and 451) after the burst. However, time does not seem to play a significant role, as comparison between D 225 and D 457 shows. In spite of the different sampling times no significant differences in the I 131 release could be observed ($1,4 \times 10^{-5}$ resp. $4,0 \times 10^{-5}$. This difference complies rather with the general trend of the values in this column to increase with increasing load factor).

The most remarkable feature of these figures is the altogether very low fractional release of only 4×10^{-5} of the I 131 inventory and less - only exceeded from the fuel rod D 338 with the unrealistically high load of 400 W/cm at a burn up of 44 GWd/tU ($K_B = 17\ 600$) which released 2×10^{-4} of its inventory. The values in the corresponding column in table 2 show that the fraction of volatile iodine is even less, namely a fifth at the most. This fraction decreases further with increasing fuel rod load and heating temperature. The gap release of volatile iodine was below 10^{-5} for the test rod with the highest load (D 338, $K_B = 17\ 600$), for rods with normal load ($K_B \leq 6000$) it was 3×10^{-6} at the most (D 451).

5.2 Condensate (Total)

The rods were heated between three and six hours. Every 15 to 30 minutes the content of the condensate trap was sampled in order to establish the time dependence of the I 131 transport out of the pressure tube by steam or gas resp. into the condensate trap. Figure 5 presents three typical release curves for 800°C which show the burn up resp. power dependence. A separation of the influence of burn up and specific power was not possible due to the insufficient small number of fuel rods. For the upper curve of figure 5 the fractions of I_2 and I^- are plotted in figure 6. Almost all of the I_2 was released into the first sample, the following samples containing merely less than 1% I_2 each.

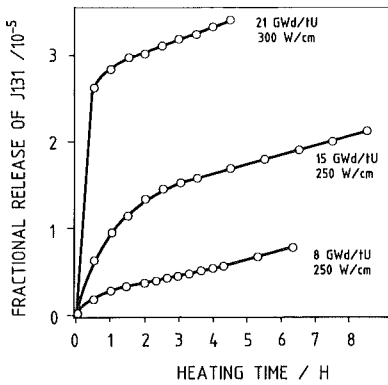


FIG. 5: RELEASE OF I 131 FROM PRESSURE TUBE AT 800°C

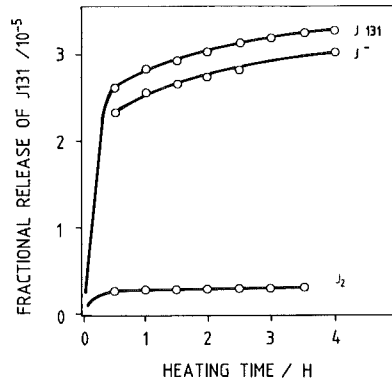


FIG. 6: FRACTIONS OF I_2 AND I^- AT 800°C (21 GWd/tU, 300 W/cm)

The corresponding curves of the rods heated up to 1100°C are plotted in figures 7 and 8, in fig. 7 together with the temperature curves. The I₂ fraction is markedly smaller than it is at 800°C (fig. 6).

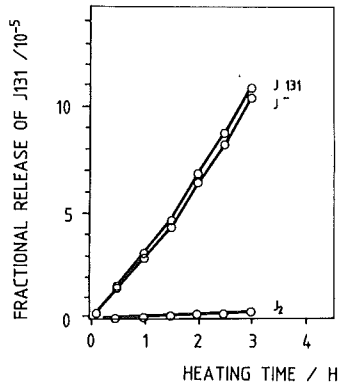
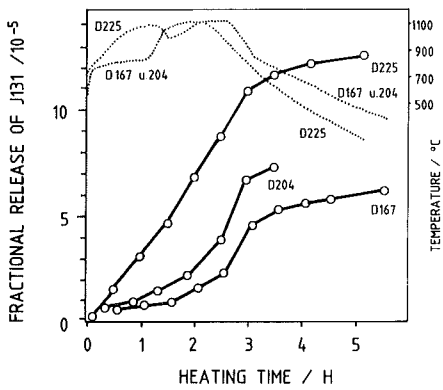


FIG. 7: RELEASE OF I 131 FROM PRESSURE TUBE AT 1100°C

FIG. 8: FRACTIONS OF I₂ AND I⁻ AT 1100°C (SAMPLE D 225)

5.3 Total Release

Fig.9 gives a graphical summary of the release results of all 19 test fuel rods. The results are split in three groups: condensate (l. sample), condensate (total) and total release and are plotted against the burn up. From this graph it is apparent, that except for fuel rods with both high burn up and high specific power the overall I 131 release will be less than 10⁻⁴ of the inventory. Bearing in mind that only a tenth of this iodine is in the elemental, volatile form, I 131 release into the air in a LOCA should not exceed 10⁻⁵ of the inventory of the ruptured fuel rods.

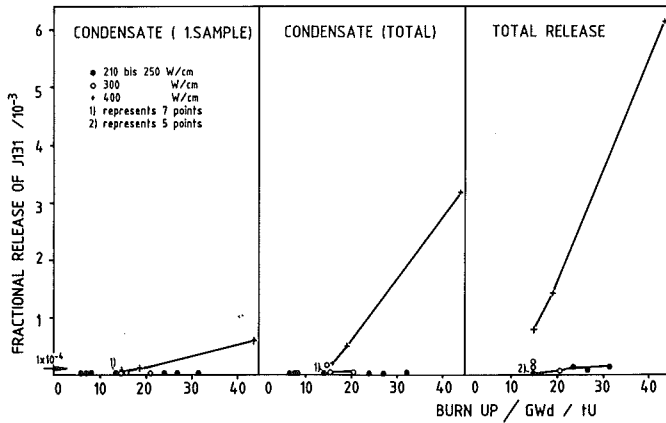


FIGURE 9: I 131. RELEASE FROM 19 TEST FUEL RODS HEATED UNDER LOCA CONDITIONS

The total I 131 release from the fuel rods over several hours of heating is presented in column 10 (table I) as the sum of the columns 7, 8 and 9. Neglecting as a rough approximation both temperature and heating time - and with the relatively small number of samples no better evaluation was possible - the average total release of I 131 from fuel rods under normal load ($K_B < 6000$) was about 1×10^{-4} of the inventory. The heating times were up to 8 hours at 800°C , with peak temperatures up to 1100°C . The release figures vary between 3×10^{-5} (D 66, $K_B = 3000$) and 1×10^{-6} (D 408, $K_B = 6000$). The release fraction of volatile I₂ from these rods is about 3×10^{-6} at the most; only rod D 338 with the unrealistic high K_B of 17 600 exceeds this value with a release of 2×10^{-4} . This total balance includes also the rods heated in helium (table III).

The portions of I 131 dissolved out of the pressure tube (including the fuel rod) with water and those from the empty pressure tube with diluted nitric acid were about equal and similar to those transported out of the tube by steam (or helium) (table I).

6. CONCLUSIONS

The results obtained from heating experiments with defect test fuel rods demonstrate plainly, that the release of I 131 is significantly lower than assumed in the appropriate safety regulations. Other authors /6/ and the evaluation of the TMI accident came to similar results, indicating that there is at least a factor of 100, more probable 500 to 1000, between the measurable and the assumed release of I 131 from a ruptured fuel rod under LOCA conditions.

The reason for this discrepancy is the neglect of the chemical reactivity of the iodine, which not only reacts with other fission products in the fuel rod and structural material in the reactor-core but also with the H_2O omnipresent in all water reactors. Iodine can therefore not be treated like a noble gas, which is unlimitedly volatile and chemically inert but rather like a reactive substance, able to form compounds in the environment of a LWR, which are not volatile and - most of them - easily soluble in water.

7. LITERATURE

- /1/ H. Watzinger:
"Analyse des Kühlmittelverlust-Störfalls beim LWR im Hinblick auf seine Auswirkung auf den Brennstab", Fachtag der Fachgruppe "Brennelemente" der KTG, Erlangen, 14. November 1975
- /2/ F. Lange, H. Friedrichs, W. Ullrich, J.P. Hosemann:
"Neuere Analysen des Spaltproduktverhaltens nach einem Kühlmittelverlust-Störfall", Atomwirtschaft 27 (1982) 82-88
- /3/ J.P. Hosemann, K.H. Neeb, J. Wilhelm:
"Neuere Bewertung der Freisetzung und des Transports von Jod bei schweren Reaktorstörfällen", Fachsitzung Sicherheit von Kernkraftwerken, Jahrestagung Kerntechnik 83, Berlin, 14.-16. Juni 1983
- /4/ C. Keller:
"Radiojod in Kerntechnik und Nuklearmedizin", Chemiker-Zeitung 5/83, S. 145
- /5/ T.M. Besmann, T.B. Lindemer:
"Chemical Thermodynamics of the System Cs-U-Zr-H-I-O in der LWR Fuel-Clad Gap", ORNL/TM-6130 (Jan. 1978)
- /6/ B.A. Lorenz, J.L. Collins, A.P. Malinauskas, O.L. Kirkland, R.L. Towns:
"Fission Product Release from Highly Irradiated LWR Fuel", Report NUREG/CR (ORNL/NUREG/TM-287/R1) (1980)

TEST FUEL ROD	BURN UP GMd/c	SPECIFIC POWER W/cm	LOAD FACTOR $K_B/10^3$	TEMPERATURE °C		HEATING TIME HRS.	FRACTIONAL RELEASE OF I 131/10 ⁻⁵				
				MAX.	LEAK		CONDENSATE		WATER LEACH	NITRIC ACID PURGE	TOTAL
							I. SAMPLE	TOTAL			
D 31	7.5	250	1.9	800	25	6.8	0.2	0.8			
D 81	7.5	250	1.9	800	25	7.2	0.2 ¹⁾	1.5 ¹⁾			
D 90	7.5	250	1.9	800	25	8.2	0.2 ¹⁾	1.5 ¹⁾			
D 66	15	200	3.0	800	750	5.8	<0.1	0.2		2.4	2.6
D 175	15	210	3.2	800	25	7.5	0.4	2.5			
D 190	15	210	3.2	800	25	8.5	0.7	2.2		2.5	4.7
D 74	15	250	3.8	800	25	7.2	0.2 ¹⁾	1.5 ¹⁾			
D 197 ²⁾	15	250	3.8	1000	780	3.1	<0.1	2.8 ³⁾		6.5	9.3
D 212 ²⁾	15	250	3.8	800	780	5.5	<0.1	1.0 ³⁾	5.0	1.5	7.4
D 374 ²⁾	15	250	3.8	800	780	4.5	0.1	1.8 ³⁾	4.9	1.3	8.0
D 106	15	300	4.5	800	760	5.3	2.0	6.3		8.7	15
D 112	15	300	4.5	1000	770	4.3	1.2	24		3.6	28
D 204	24	210	5.0	1100	740	3.5	0.6	7.2	6.1	9.5	23
D 167	27	210	5.7	1100	740	5.6	0.3	6.1	1.8	5.6	14
D 408	15	400	6.0	800	770	4.0	4.0	16		89	105
D 451	21	300	6.3	800	740	4.5	2.6	3.4		2.2	5.6
D 225	32	210	6.7	1100	730	5.2	1.4	12.6	0.7	5.9	19
D 457	19	400	7.6	800	640	4.7	4.0	50		130	180
D 338	44	400	17.6	800	620	4.0	20	320		280	600

TABLE I Experimental Parameter and I 131 Release Results

TEST FUEL ROD	LOAD FACTOR $K_B/10^3$	FRACTIONAL RELEASE OF I 131/10 ⁻⁵						
		CONDENSATE (I. SAMPLE)			CONDENSATE (TOTAL)			TOTAL
		I ₂	I ⁻	I ₂ +I ⁻	I ₂	I ⁻	I ₂ +I ⁻	I ₂ +I ⁻
D 66	3.0	<0.001	0.001	0.001	0.002	0.12	0.12	2.6
D 190	3.2	0.15	0.79	0.94	0.27	1.7	2.0	4.7
D 374 ²⁾	3.8	0.002	0.13	0.13	0.02	0.51	0.53	8.0
D 451	6.3	0.29	2.3	2.6	0.32	3.0	3.4	5.6
D 225	6.7	0.02	1.5	1.5	0.30	10	11	19
D 338	17.6	0.92	17	18	18 ⁴⁾	260 ⁴⁾	280 ⁴⁾	600 ⁵⁾

1) Values corrected for contamination

2) Heated in inert gas (helium)

3) Sum of NaOH solution and charcoal

4) After 3 hrs. heating

5) After 4 hrs. heating

TABLE II Fractions of I₂ and I⁻ in total I 131 Release

TEST ROD	NaOH SOLUTION	CHARCOAL	WATER LEACH	HNO ₃ PURGE	TOTAL	I 131		FRACTION OF I 131	
						I ₂	I ⁻	I ₂	I ⁻
D 197	0.4	2.4	-	(6.5)	9.3	2.4	6.9	26 %	74 %
D 212	0.3	0.6	(5.0)	(1.5)	7.4	0.6	6.8	8 %	92 %
D 374	0.7	1.1	4.9	1.3	8.0	1.1	6.9	14 %	86 %

TABLE III I 131 Release in Helium

(all values 10⁻⁵ of the I 131 inventory; values in brackets uncertain due to experimental difficulties)

SOLID FISSION PRODUCTS AND ACTINIDES RELEASE
AND DEPOSITION INSIDE PWR's PRIMARY CIRCUITS

P. Beslu* - C. Leuthrot* - A. Brissaud** - A. Harrer** - G. Beuken***

* CEA/IRDI/DRE

** EDF/SEPTEN

*** SEMO/Centrale de Tihange

ABSTRACT

Release of solid fission products and actinides in the primary coolant mainly occurs in case of large cladding defects such as those induced by baffle jetting. Fissile materials as well as solid fission products (Sr, Ba, Zr, Ru, Ce, La) are released in the primary circuit where they deposit on the surfaces. Measurements performed by CEA, EDF and SEMO on PWR reactors allowed a better understanding of the mechanisms of deposition and to find relationships between the release of these species, the dose rate and alpha contamination on the primary circuit.

Modeling has been deduced from these studies and included in the PROFIP 4 computer code.

INTRODUCTION

The behaviour and release of volatile fission products (gas, iodines and cesiums) have been extensively studied both in normal and accidental conditions, and reliable data are available for safety, health physics and project purposes.

Other fission products, produced in large quantities in the fuel as those belonging to the alkaline - earth group (barium, strontium) to the lanthanides group (cerium, praseodymium) and some metallic fission products (zirconium, ruthenium) are not volatile and have a very low diffusivity in uranium dioxide; therefore, they do not migrate easily out of the fuel and are not released in appreciable quantity in the primary coolant if there are only very small cladding defects as those generally observed during normal operating conditions.

Nevertheless, in the case of large cladding defects (for example baffle jetting induced defects) it may happen that water is in direct contact with oxide fuel pellets, leading to a fuel erosion. The fissile material is then dispersed in the primary coolant together with the fission products included in the fuel.

The uranium dioxide present in the primary coolant is, of course, responsible for the release of actinides and alpha contamination, but also for solid fission products as well by two processes :

- 1) - Fission products atoms included in the fissile materials which have been dispersed in the primary coolant.
- 2) - Fission products created in the uranium contamination deposited on the primary circuit area under neutron flux.

Due to their beta or gamma energies and long half lives or toxicities, some of these fission products are of interest in several fields such as safety, health physics or waste package.

The studies, presented in this paper, pertain mainly to :

- alkaline earth group : ^{90}Sr , ^{140}Ba and its daughter ^{140}La
- lanthanides group : ^{141}Ce , ^{144}Ce , ^{144}Pr
- metallic fission products : ^{95}Zr , ^{95}Nb , ^{103}Ru , ^{160}Ru + ^{106}Rh
- actinides responsables for alpha activity : ^{238}Pu , ^{239}Pu , ^{240}Pu , ^{241}Am , ^{242}Cm ,
 ^{244}Cm .

I - BEHAVIOUR OF ACTINIDES OUTSIDE THE FUEL CLADDING

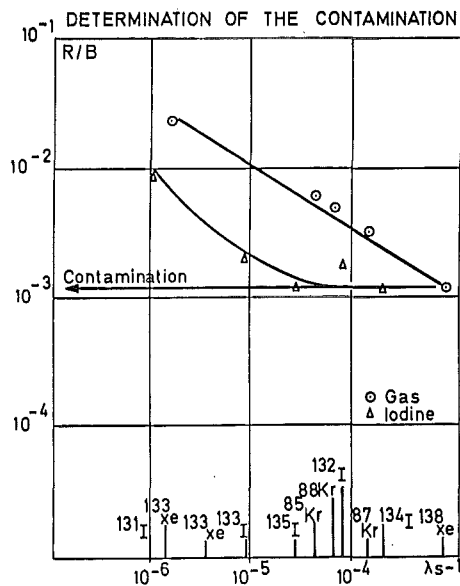
In a PWR fissile material is always present outside the fuel cladding ; even if there is no cladding defect, the material uranium contained as impurities in zircaloy and the unavoidable cladding pollution which occurs during the assembly manufacture lead to a small but measurable quantity of fissile material in direct contact with the primary coolant. In case of cladding defects where the water is in contact with the pellets, UO_2 may be released in the coolant and deposit on the primary circuit.

I.1 - Estimation of the uranium contamination

The estimation of the quantity of uranium in the primary circuit has been realized by appropriate analyses performed both on scrapping on the primary circuit and on primary water sampling. The calculation of the amount which is deposited under neutron flux, can be deduced from the fission products activities in the coolant (mainly from rare gas and iodines).

Fission products are created in the contamination deposited under neutron flux and directly released without delay in the primary water by the recoil process ; the release fraction of these fission products are independant of their half-life and therefore, it is possible (see figure 1) to determine the contribution of the contamination to the total fission products release and furthermore to estimate the quantity of fissile material responsible for the contamination ; typical values of the UO_2 mass deposited under neutron flux are :

- "clean" reactor (first cycle - without defect) : < 1 g
- reactor with small defects (size < 50 μ) : 1 to 10 g
- reactor with broken rods (due to baffle jetting): 50 to 200 g (or more)



For large values of the contamination, an estimation of the mass balance in the primary circuit has been done ; typical values are given on Table I.

TABLE I

Contamination mass balance in the PWR primary circuits

Reactor cycle	Total mass (g U)	Balance (%)		
		in flux	out of flux	in the coolant
TIHANGE 1 cycle 4	60	67	33	$1.7 \cdot 10^{-3}$
TIHANGE 1 cycle 5	620	37	63	$6.0 \cdot 10^{-3}$
TIHANGE 1 cycle 6	300	47	53	$3.0 \cdot 10^{-3}$
TIHANGE 1 cycle 7	310	48	52	$6.4 \cdot 10^{-3}$
BUGEY 2 cycle 2	200	65	35	$4.1 \cdot 10^{-2}$

It shows :

- a) that Uranium contamination is quite uniformly deposited in the primary circuit
- b) in steady state conditions and with normal water chemistry, uranium is always in an insoluble form and the quantity of particles in the primary coolant is only 10^{-5} to 10^{-4} of the total deposited mass.

I.2 - Actinides composition of the contamination

The initial isotopic composition of the contamination is identical to this one of the defected assembly. Because there is no self-shielding for the plutonium production in the oxide deposited under neutron flux, the fissile isotopes increase during irradiation more rapidly in the contamination than in the fuel itself. Therefore the evolution with burnup of the quantities and the ratio of the main fissile isotopes ^{235}U and ^{239}Pu is different in the contamination and in the fuel. The direct experimental checking of this phenomena is not easy because the very small quantities of nuclides and the difficulty of sampling. On the other hand the amount of fission products created and released from the contamination is directly related to his isotopic composition ; because ^{239}Pu and ^{235}U fission yields for xenons and iodines are similar but very different for kryptons, it is possible to verify experimentally the theoretical evolution of the contamination through the analysis of the fission products activities in the primary coolant.

I.2a - Theoretical model

Calculations have been performed, using the cell computer code APOLLO in which we described a PWR 17 x 17 assembly. Because it is not possible to strictly solve the problem, we assigned in the calculations cross sections values without self-shielding ; the corresponding results will be an upper limit for the ^{239}Pu formation ; they are summarized in the table II where the ratios $^{235}\text{U}/^{238}\text{U}$ and $^{239}\text{Pu}/^{238}\text{U}$ in the fuel and in the contamination are reported for several values of the burnup.

TABLE II
Evolution of actinides ratio in the fuel and in the contamination

Burnup (MWJ/t)	$^{235}\text{U}/^{238}\text{U}$ (%)		$^{239}\text{Pu}/^{238}\text{U}$ (%)	
	Fuel	Contamination	Fuel	Contamination
4400	2.23	2.24	0.223	1.42
9500	1.79	1.80	0.374	2.39
15300	1.39	1.40	0.472	3.01
21600	1.04	1.05	0.531	3.36
28500	0.750	0.762	0.564	3.55
35800	0.516	0.529	0.582	3.63
43700	0.341	0.352	0.591	3.66

Using these results and the PROFIP 4 computer code which allow to calculate the fission products activities in the primary coolant due to the release from defected rods or to the contamination, we calculated the activity evolution of ^{85m}Kr , ^{133}I and ^{134}I in the primary water for a 900 MWe PWR. Hypothesis used for the calculations are :

- ^{235}U initial enrichment for the fuel and the contamination : 3.1 %
- contamination in the water / deposited contamination : $1 \cdot 10^{-4}$
- CVCS flow rate : $13.7 \text{ m}^3/\text{h}$
- average linear power in the core : 175 W/cm.

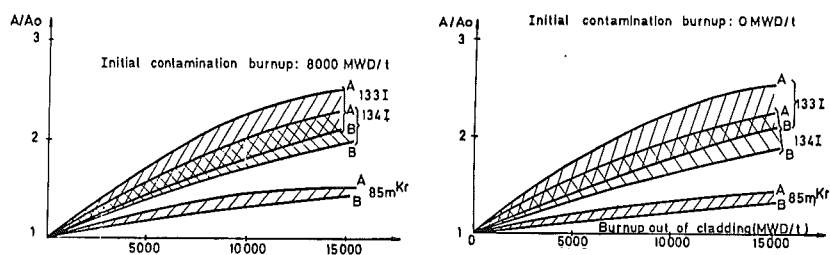
Because the gap in our actual knowledges about the uranium transfer in the primary circuit, calculations have been performed for two drastic hypothesis

- A - the contamination do not transfer during irradiation and lay under neutron flux ; this case occurs probably for the low contamination values (manufacture contamination).
- B - the transfer of the contamination leads to an homogeneous isotopic composition for the in core and out of core contamination ; this case occurs probably with large values of contamination due to baffle jetting.

Results are summarized on the figure 2 where the increase of the water activities for ^{85m}Kr , ^{132}I and ^{134}I due to a constant mass of uranium contamination, is reported versus burnup.

FIGURE 2

Evolution of the fission products activities due to the contamination



We can notice that :

- 1) - the activities evolution is nearly independent of the initial contamination burnup ;
- 2) - the increase is about 2 for iodines and only 30 % for kryptons.

I.2b - Experimental checking

The experimental checking of this theoretical model has been realised with data, concerning reactors without cladding defects in which the contamination is the only fission products activities source.

- a) - contamination less than 1 g U : FESSENHEIM 2 and GRAVELINES 1 cycle 1
- b) - contamination due to small defects in a previous cycle (≈ 5 g) : TRICASTIN 1 cycle 2
- c) - large contamination due to baffle jetting in a previous cycle (> 30 g)
BUGEY 2 - cycle 3 and TIHANGE 1 - cycle 8.

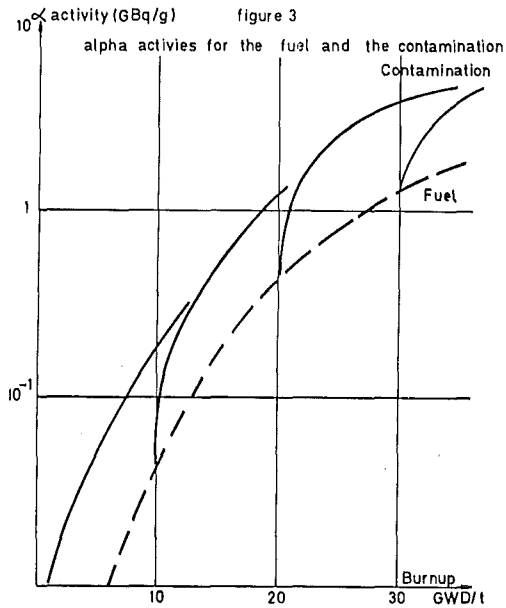
The comparison between the experimental results and the calculations are presented in Table III for the A and B hypothesis ; A calculation seems to be very close the experimental data, which means that very low transfer of uranium in the primary circuit occurs during the irradiation cycle.

Table III
Evolutions of ^{85m}Kr and ^{134}I activities in the primary coolant during an irradiation cycle.

Reactor cycle	Estimated burnup (MWD/t)		activities ratio (end of cycle/start of cycle)			
	Start of cycle	End of cycle	Measurements		calculations A/B	
			^{134}I	^{85m}Kr	^{134}I	^{85m}Kr
FESSENHEIM 2 cycle 1	0	14000	2.2	1.5	2.1/1.7	1.4/1.3
GRAVELINES 1 cycle 1	0	13000	2.0		2.1/1.7	1.4/1.3
BUGEY 2 cycle 3	9000	20000	2.0	1.4	2.1/1.8	1.5/1.3
TIHANGE 1 cycle 8	8000	19000	1.6	1.4	2.1/1.7	1.5/1.3
TRICASTIN 1 cycle 2	11500	20000	2.0	1.3	2.0/1.7	1.5/1.3

I.3 - Alpha activities

The theoretical model of evolution has been used in order to calculate the alpha activity of the contamination. Several calculations have been performed for different initial burnup of the contamination. Figure 3 where are reported the results shows that after a transitory period of about 2 to 3 GWD/t U following the release of the contamination, the alpha activity in the contamination is 3 to 4 times higher than in the fuel at the same burnup.



II - BEHAVIOUR OF SOLID FISSION PRODUCTS

The release fractions of several fission products have been measured on PWR's fuel at nominal power and in steady state conditions. Typical values for long lives fission products ($T > 10$ days) are shown on Table IV.

Table IV
Fission products released fractions for PWR'S
in steady state conditions at nominal power
(900MWe)

chemical species	released fractions
rare gases	1.10^{-2} to 5.10^{-2} *
iodine	1.10^{-2} to 5.10^{-2} *
cesium	1.10^{-2} to 5.10^{-2} *
baryum	1.10^{-3}
strontium	1.10^{-3}
zirconium	0
niobium	0
ruthenium	0
lanthanides	0

* depending on the defected rod power

Species such as Zr, Nb, Ru, Ce, Pr, La are not directly released from the defected rod and are always present in the primary circuit together with uranium contamination ; they are not soluble and the fraction of activity in the primary coolant is as for uranium, 10^{-5} to 10^{-4} of the total deposited amount of these species.

Direct release of strontium and baryum is low (10 times lower than volatiles fission products) and these species are mainly insolubles with normal operating conditions, but they can partly dissolve during chemical transients such as pH decreases, as shown on Table V.

Table V
TIHANGE 1 - Cycle 7

Solubilities of alkaline earth fission products during a pH transient

Nuclide	Water activity / Deposited activity	
	pH = 7.2	pH = 6.6
90Sr	$1 \cdot 10^{-3}$	$2 \cdot 10^{-2}$
140Ba	$1.5 \cdot 10^{-3}$	$5 \cdot 10^{-2}$

III - DOSE RATES INDUCED BY SOLID FISSION PRODUCTS

The PROFIP computer code which calculates the deposited fission products activities around the primary circuit allow us to estimate dose rates induced by these fission products for simple geometries as those of the primary pipes ; calculations have been checked by appropriate dose rates measurements around the primary pipes and estimations of deposited fission products activities by gamma spectrometry. Typical values of these measurements and calculations for the TIHANGE 1 reactor are given on Tables VI and VII

Table VI
TIHANGE 1
Dose rates induced by fission products

cycle		4	5	6	7
contamination (gU)		60	630	300	310
dose rates (mRem/h)	hot pipes	1 to 2	20 to 70	10	10
	cold pipes	15	25	5	5
	heat exchanger	0.15	5 to 20	2 to 10	2 to 5
	CVCS (B3)		70	25	50

Table VII
 TIHANGE 1 - cycle 6
 Dose rates around the primary circuit

PLACE	Dose rate (mRem/h)			FP dose rate total dose rate (%)	
	calculations		measurement		
	F.P.	total	total		
Hot pipes	1	16	171	170	9.4
	2	20	163	240	12
Cold pipes	1	4.3	86	54	5.0
	2	4.3	92	54	4.7
	3	4.3	70	66	6.1
Heat exchanger (hot side)	1	4.4	215	180	2.0
	2	1.8	108	110	1.7
Heat exchanger (cold side)	1	105	161	150	6.5
	2	105	108	96	9.7
CVCS (B3)		31	153	380	2.0
CVCS (exchanger outlet)		2.8	77	60	3.6

Participation of fission products to the total dose rates is only important for large uranium contamination and mainly around CVCS and RHRS.

Roughly, the dose rates due to solid fission products may be estimated from the uranium mass deposited in the primary circuit ; with 1 g U uniformly deposited the dose rates close the heat insulator are about $3 \cdot 10^{-2}$ mRem/h for the hot pipes, $2 \cdot 10^{-2}$ mRem/h for the cold pipes and the heat exchangers and 10^{-1} mRem/h for CVCS and RHRS.

CONCLUSION

Experimental data obtained on TIHANGE and French PWR reactors in the field of fission products and uranium contamination allowed us to improve the understanding of the release and behaviour of solid fission products in the primary circuit and to propose theoretical model and correlations for the PROFIP-4 computer code which is used at the Safety French Energy Commission (CEA/DSN) and the National Electric Company (EDF). It is now possible to calculate deposited alpha and beta activities as well as dose rates out of the primary pipes.

RELEASE OF FISSION PRODUCTS BY DEFECTIVE PRESSURISED WATER REACTOR FUEL

H. Sév on (CEA) C. Leuthrot (CEA) J.P. Stora (EDF/SEPTEN)
P. Chenebault, R. Warlop

Centre d'Etudes Nucl aires de Grenoble
D partement de M tallurgie de Grenoble
85 X - 38041 GRENOBLE Cedex FRANCE

ABSTRACT

The fission products released in reactors are compared with the quantities available in the pellet-cladding gap, calculated from recommended release values obtained from an experimental programme. The comparison shows that these values can be applied to reactors.

I - EXPERIMENTAL PROGRAMME.

With a view to defining the fission products (FP) in pressurised water reactor (PWR) primary circuits, an experimental programme was implemented by the D partement de M tallurgie de Grenoble, Service de Recherches sur les Mat riaux, Section d'Etudes du Comportement des Combustibles (DMG/SRM/SECC) from 1975 to 1984. This programme was financed by the Institut de Protection et de S ret  Nucl aire, D partement des Analyses de S ret  (IPSN/DAS) and Electricit  de France, Service d'Etudes des Projets Thermiques et Nucl aires (EdF/SEPTEN).

The experimental programme consisted of 12 experiments conducted in the Silo  reactor. The fuel rods were of standard geometry of the PWR type : 17x17 and short in length (about 300 mm). Two types irradiation devices were used :

- a) The Bouffon device is a small thermo-siphon loop in which the cladding temperature is controlled by the saturation temperature for a linear fuel power greater than 20 KW.m^{-1} . Nine experiments were conducted with this system.
- b) The Jet Pump device is a water loop in which the cladding temperature control is independent of the linear power, thereby giving more representative values of the fuel rod internal temperature for all power values, especially under 20 KW.m^{-1} . Three experiments were carried out using this system.

Two types of defect were studied :

- defects located in the upper plug made before irradiation, simulating a large construction defect (six experiments),

- defects located in the fuel column, obtained by fatigue before irradiation (one experiment) or by external mechanical stress during irradiation (three experiments), or by pellet-cladding interaction.

The experiments were conducted either with stable power levels between 10 and 40 KW.m⁻¹ over a period of several days, or at daily varying power levels corresponding to the load following regime.

The burnups reached are between 1000 and 5000 Mwd.t⁻¹ for the ten experiments with fresh fuel, and between 20 000 and 30 000 Mwd.t⁻¹ for the two experiments run with fuel pre-irradiated in power reactors.

II - MAIN RESULTS OF THE EXPERIMENTAL PROGRAMME.

II.1 - Release rate.

FP release by UO₂ is greater for defective rods than for clean rods. For example, if the release of gaseous species, especially 133 Xe, is compared for the same type of fuel operating at the same powers, it is found experimentally that the release rate is 10 times greater for defective fuel rods than for rods in normal condition. This fact is attributed to oxidation of the UO₂ by chemical interactions with water vapour and, in particular, the influx of oxygen formed by radiolysis of the water in the fuel-cladding gap.

II.2 FP emission with time.

It has been observed that FP release under steady power and temperature conditions is not permanent but consists of "bursts" separated by periods without any fission products. This phenomenon can be observed only under "favourable conditions" (irradiation loop where the water renewal time is a matter of a few minutes, low conductance cladding defect). The simultaneous measurement of the fuel rod internal pressure showed that these "bursts", which occur at varying frequency averaging two per hour, correspond to internal pressure drops and the absence of release to pressure increases. From this observation, there is reason to believe that the radiolysis gases are the driving force for release, thus implying necessary idle periods for accumulation and decomposition of a sufficient quantity of water. It seems highly probable that this mechanism exists at all times, but is too rapid to be observed with larger size defects. The response time (about 10 h) of the primary circuit of a reactor makes it impossible to observe this mechanism.

The experimental programme also highlighted regimes during which FP release varied more slowly (several hours to dozens of hours). Figure 1 illustrates this type of release. After the peak which accompanies the power rise, a release level can be seen which lasts a maximum of 30 hours. This is followed by a release level three times lower that is interrupted only by a power variation. This type of release can be observed in reactors.

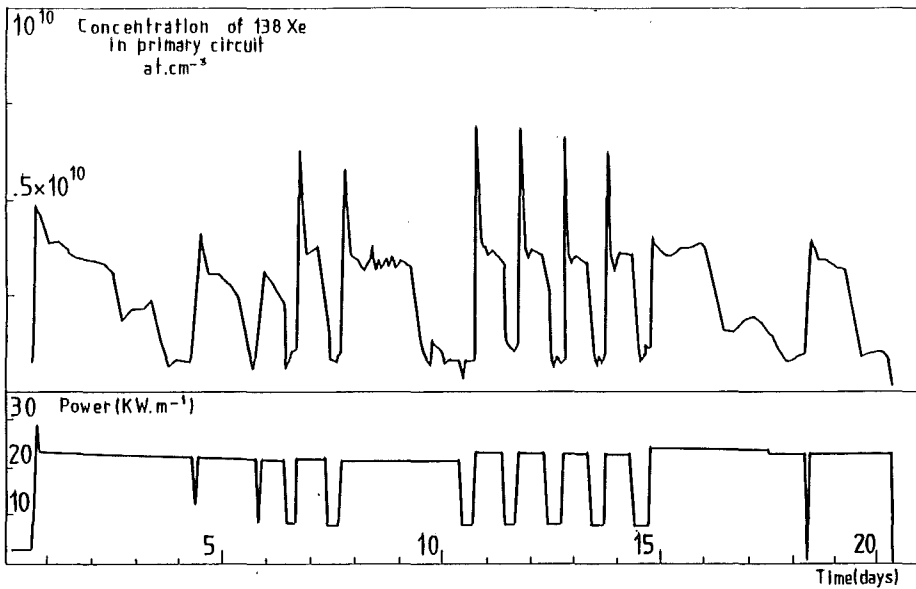


FIG.1 CRUSIFON 5_ Evolution of fission product release during irradiation

II.3 - Existence of a critical regime.

During the experimental programme, it was found that, at a certain power level, release outside the fuel rod was higher, especially for short-lived nuclides. Figure 2 shows the activity of primary circuit water and fuel rod power in relation to time. It is to be noted that, at 16.4 KW.m^{-1} , release is much higher than at 10 and 20 KW.m^{-1} . The high activity of short-period nuclides can be explained only by the existence of a critical regime which corresponds to the rapid vaporisation and condensation of water in the fuel-cladding gap. Within a very tight power range, it is in fact possible to have simultaneously an internal cladding temperature lower than the saturation temperature and a pellet surface temperature higher than the saturation temperature. Such conditions may arise in reactors and give birth to the same release rate in the case of a defect located in front of the fuel, and large enough to allow the inlet and outlet of water.

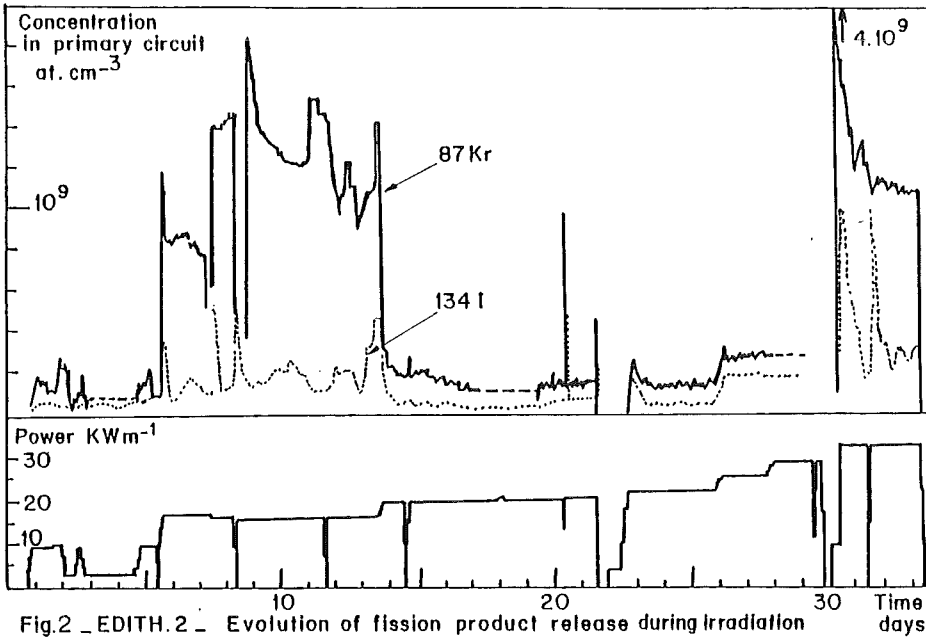


Fig.2 _EDITH.2_ Evolution of fission product release during irradiation

III - RELEASE BY UO_2 .

The measures taken during the experimental programme concerned FP release outside the fuel rod, which is a function of the fuel rate and transfer rate through the rod. It has been shown in section II that this transfer is complex. However, in the transients or in the critical regime periods, this transfer is rapid and enables the release by UO_2 to be quantified.

Figure 3 and 4 represent the R/B release rates of gases and halogens in relation to the linear power. R/B is defined as the ratio between the number of atoms released per second by the fuel and the number of atoms born per second in the fuel at radioactive equilibrium. These values, obtained from the experimental programme, represent the recommended values of release by UO_2 pellets placed in a defective cladding. They are in good agreement with those published elsewhere /1/.

The recommended values for halogens are derived from values obtained with xenon of equivalent periods and were observed only in the case of liquid water expulsion likely to entrain the halogens.

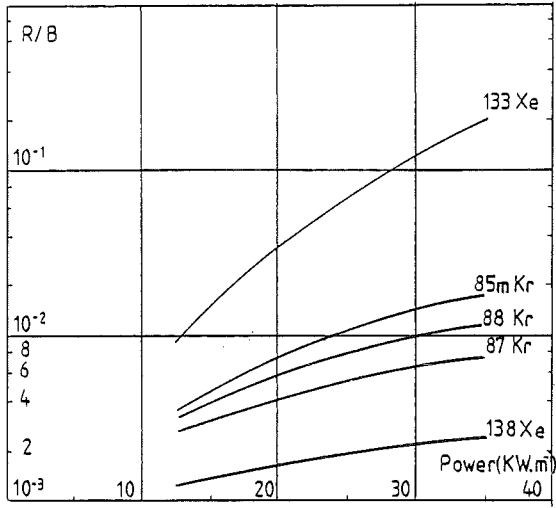


FIG. 3. Release rate of noble gases vs linear power

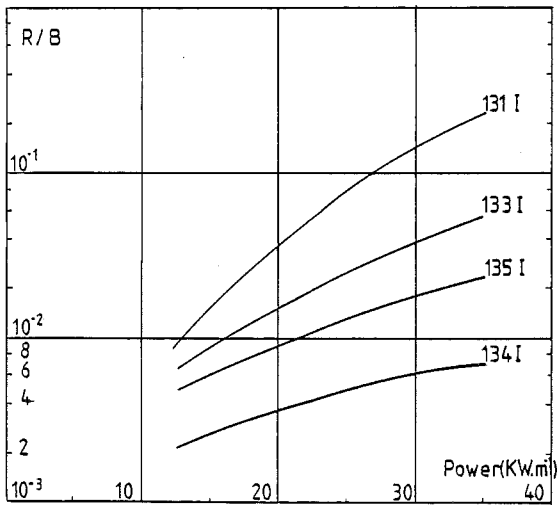


FIG. 4. Release rate of halogens vs linear power

IV - COMPARISON OF RESULTS ON POWER REACTORS.

The activity of the primary reactor circuit is measured during operation and during normal shut-down periods, which include a pressure drop stage, followed by a period of temperature and pressure drop of the cooling water. Subjected to these conditions, the defective fuel rods release most of the radioactive species in the fuel-cladding gap. The ratio of activities released in operation to those released in transients is variable. This variation is due to the size and position of the defects, to the power of the defective fuel rods and to the composition of the internal atmosphere.

For certain reactors, sipping tests on assemblies during unloading operations give an idea of the number of defective rods as well as their position in the core and thus their operating power.

In addition, on the basis of primary circuit activity measurements taken during operation and during shut-down, the total activities released by the defective rods are calculated for the various nuclides, taking into account the purification rates and losses. It should be noted that the measurements with the reactors shut-down were taken for a primary circuit depressurisation range of 15.5 to 2.7 MPa only. A calculation based on simple hypotheses (water vapour and gaseous atmosphere at 15.5 MPa inside the fuel rods in operation) shows that only 70% of the available activity can be released under these conditions. The corresponding correction has been made.

The mean value A of the ratio between the total activity measured in the reactor and the calculated activity available is represented in Table 1 for the various nuclides measured.

Nuclides	A
133 Xe	0.87
131 I	1.40
133 I	0.87
134 I	1.23
135 I	0.69

Table 1

$$A = \frac{\text{Total activity measured in the reactor}}{\text{Calculated available activity}} \quad \text{for different nuclides.}$$

If the recommended values correctly represent the release rates from the UO_2 in defective rods of reactors, then the ratio A should be equal to 1. Table I shows that deviations of up to $\pm 40\%$ in this value were measured.

V - CONCLUSIONS.

The agreement between released activity in a reactor and calculated available activity based on the recommended values of the experimental programme is quite good. These recommended values correctly represent release by UO_2 in defective pressurised water reactor fuel rods.

REFERENCE

- /1/ E. Schuster, F. Garzarolli, K.H. Neeb and H. Stehle.
Release of fission products from defective fuel rods of light water reactors.
AIEA Specialists Meeting - Chalk River, Sept. 1979.

THERMOCHEMICAL INTERACTIONS OF FISSION
PRODUCTS IN AN LWR ACCIDENT

Rajiv Kohli

Battelle Columbus Laboratories
Columbus, Ohio 43201, U.S.A.

ABSTRACT

The presence of a large number of fission products in a fuel rod results in a very complex chemical system. The chemical states of the fission products released from the fuel during a severe core damage accident are determined by the nature of the immediate environment which is generally oxidizing. The oxygen potential and the temperature of the system affect the relative stabilities of the potential vapor species of the fission products. Using chemical thermodynamic data, the stable vapor species of the fission products Cs, Rb, I, Br, Te, Se, Sr, Ba, Sb, Ru and Mo released from failed fuel rods were evaluated for three conditions in the temperature range 1000 - 3000K: a) water/steam/hydrogen environment (oxygen potential ~ -150 to -380 kJ/mol); b) water/steam/air environment (oxygen potential ~ -15 to -40 kJ/mol); c) air environment (oxygen potential ~ -10 to -40 kJ/mol). The oxides, hydrides, hydroxides, molybdates, molybdites, halides, chalcogenides and the elemental forms of these fission elements were considered. Following release of the volatile species from the fuel rods, their interactions with the liquid water coolant were evaluated by means of electrochemical stability (Eh-pH) diagrams for the individual fission products to 600 K. The results of the calculations suggest that small amounts of selenium, tellurium, ruthenium, molybdenum, and possibly, bromine and iodine, may be released to the environment.

INTRODUCTION

During irradiation of an LWR fuel rod over forty individual fission products are released, resulting in a very complex chemical system within the rod. In the event of a severe core damage accident, release of the volatile fission products to the environment becomes a matter of prime concern. The behavior of the fission products can be modeled most reliably by comparing their observed release in simulated or actual reactor accidents with that anticipated from their chemistry.

The chemical state of a fission product is determined by the nature of its immediate environment because the amounts of fission products released are small in relation to the amount of host environment. In an accident

the temperature of the fuel rods rises rapidly and they may fail by cladding rupture. Steam will then enter the fuel rods where it reacts with the fuel and the zircaloy cladding liberating hydrogen. If now the primary pressure boundary is also breached, air could be present. This means that the ruptured fuel rods could be exposed to a water-steam-hydrogen-air atmosphere.

Within an intact fuel rod, the chemical environment is generally reducing. However, in a reactor accident where the cladding balloons and bursts, the environment becomes progressively more oxidizing and one needs to consider the temperature and the oxygen potential of the environment to predict the chemically stable fission product species released from the hot fuel. Following their release, the fission products will interact with the coolant water which then dominates their behavior. Most of the fission products released will dissolve in water, while the insoluble species will tend to plate out on the cooler surfaces. Since subsequent release of the fission products from the aqueous solution will be by vaporization, the equilibrium chemical states of the fission products in aqueous solution must also be considered in detail.

Other recent treatments of the problem have considered only a limited number of fission elements: Cs and I [1]; Cs, I and Te [2]; or Cs, I, Te, Sr and Ru [3]. Also, aqueous solution chemistry is not treated at all in these earlier models. The emphasis in this paper is on the vaporization and aqueous solution chemistry of the high yield (Cs, Sr, Ba, Ru, Mo), radiotoxic (I, Cs, Te, Sb, Ru, Sr, Ba) fission elements which are also volatile or form volatile compounds (Cs, Rb, I, Br, Te, Se, Sr, Ba, Mo, Ru). The stable volatile species have been evaluated from equilibrium chemical thermodynamic calculations for intact fuel rods and various accident situations. The interactions of the fission products with liquid water are considered in terms of high temperature electrochemical stability diagrams (Eh-pH diagrams).

FUEL ROD CHEMICAL CONDITIONS

Four principal scenarios were considered in which to assess the vaporization behavior of the fission products from LWR fuel rods. The general chemical conditions prevailing in each situation are described below.

A. Intact fuel rods. The interior of an intact fuel rod is chemically reducing since the UO_2 fuel and the zircaloy cladding react with the oxygen generated during fissioning. As a result, the oxygen potential varies during the life of a fuel rod. Based on experimental measurements and theoretical estimates, the oxygen potential assumes a value in the range of -400 to -500 kJ/mol [4,5].

B. Failed fuel rods in water/steam atmosphere containing hydrogen. In this case it is assumed that the fuel rods have failed by cladding rupture, but the primary pressure boundary is intact. Steam and water react with the hot fuel and the cladding liberating H_2 . The oxygen potentials are set

by the H_2/H_2O partial pressure ratios and are of the order of -380 kJ at 1000K, -275 kJ at 2000K and -155 kJ at 3000K for $p(H_2)/p(H_2O) = 1$. In addition to the oxidizing environment, the presence of steam could lead to the formation of volatile hydroxide species. This system is substantially more oxidizing than situation A above.

C. Failed fuel rods in water/steam environment containing air. In a more severe accident where the primary pressure boundary is breached, air can enter the system. The oxygen potentials will then be set by the steam/air mixture and may attain values as high as in air (0.2 atm of O_2): -13 kJ at 1000K, -26 kJ at 2000K, and -40 kJ at 3000K. This system has significantly higher oxygen potentials than system B.

D. Failed fuel rods exposed to air. In accidents which occur in dry atmospheres, the fuel rods could be exposed to air. The fuel could attain temperatures as high as 3000K due to the absence of any effective cooling. The oxygen potentials are of the order of -3 to -37 kJ/mol. Since there is no liquid water present, there can be no dissolution of the fission products in the liquid phase.

THERMODYNAMIC DATA AND CALCULATION PARAMETERS

A free energy minimization technique was employed to determine the equilibrium distribution of the fission products in the present eleven component system. The calculation technique is based on the theoretical treatments of Brinkley [6] and White et al [7], and incorporated into recent computer programs [8-10] for calculation of complex chemical equilibria. Where available experimentally measured thermodynamic properties as a function of temperature for various condensed and vapor species were used [8,11-20]. In all other cases, the thermodynamic data were estimated by various methods: extrapolation of room temperature data [3, 18, 21]; general parametrization schemes [22]; bond energy correlations [11, 17, 23,24].

The calculations were performed for the situations described above for the following conditions: $H_2/H_2O = 1$; 1000 - 3000K; total pressure = 170 atm.

FISSION PRODUCT VAPORIZATION CHEMISTRY

The results of the calculations are shown in Tables 1 and 2. These tables list the partial pressures of the predominant volatile species of the fission products considered for each of the situations A - D.

Situation A. Inspection of Table 1 suggests that of the fission products considered, the following volatile species could be released at very high fuel temperatures in intact rods: Cs, Rb, Cs_2O , Rb_2O , CsI, RbI, CsBr,

Table 1. Calculated Partial Pressures of the Major Volatile Fission Product Species for the Scenarios A and B

Fission Product	Scenario A			Scenario B		
	Temp. K	Species ^a	Partial Pressure (atm)	Temp. K	Species ^a	Partial Pressure (atm)
Cs, Rb ^b	1000	M	$10^{-2} - 10^{-5}$	1000	M, MOH, $M_2(OH)_2$	$10^{-5}, 10^{-2} - 10^{-3}$
	2200	M, M_2O	>1	3000	M, MOH, MO	$10^{-1}, >1, 10^{-3}$
Cs, Rb ^c	1000	M	$10^{-5} - 10^{-8}$	1000	M, MOH, $M_2(OH)_2$, M_2MoO_4	$10^{-8}, 10^{-3} - 10^{-5}, 10^{-7}$
	2200	M, H_2O , M_2MoO_4	>1	3000	M, MOH, MO, M_2MoO_4	$10^{-3}, >1, 10^{-4}, >1$
Te	1000	Te_2	10^{-2}	1000	H_2Te	10^{-5}
	2200	Te	>1	3000	Te, H_2Te , TeO	$10^{-1}, 10^{-2}, 10^{-2}$
Se	1000	Se_2 , Se_5 , Se_6	$10^{-3} - 10^{-4}$	1000	H_2Se	10^{-8}
	2200	Se	>1	3000	Se, H_2Se , SeO	$10^{-1}, 10^{-4}, 10^{-2}$
I, Br	1000	MI, MBr	10^{-3}	1000	HX	10^{-3}
	2200	MI, MBr	1	3000	HX, X, HX	$>1, 10^{-2} - 10^{-3}$
Mo ^d	1000	-	-	1000	H_2MoO_4	10^{-7}
	2200	H_2MoO_4	>1	3000	H_2MoO_4	>1
Ru ^d	1000	-	-	1000	-	-
	2200	Ru	10^{-6}	3000	Ru, RuOH, $Ru(OH)_2$	$10^{-3} - 10^{-5}$
Sb	1000	Sb	10^{-3}	1000	Sb	10^{-3}
	2200	Sb	>1	3000	Sb	>1
Sr ^d	1000	-	-	1000	-	-
	2200	-	-	3000	SrOH, $Sr(OH)_2$	$10^{-3} - 10^{-4}$
Ba	1000	-	-	1000	-	-
	2200	-	-	3000	BaOH, $Ba(OH)_2$	$10^{-1} - 10^{-2}$

^a M is either Cs or Rb, X is either I or Br.

^b Cs_2UO_4/Rb_2UO_4 is assumed to be the stable solid phase.

^c Cs_2MoO_4/Rb_2MoO_4 is assumed to be the stable solid phase.

^d No vapor species of Ba and Sr are expected in scenario A.

Table 2. Calculated Partial Pressures of the Major Volatile Fission Product Species for the Scenarios C and D

Fission Product	Scenario C			Scenario D		
	Temp. K	Species ^a	Partial Pressure (atm)	Temp. K	Species ^a	Partial Pressure (atm)
Cs, Rb ^b	1000	M, MOH, M ₂ (OH) ₂	10 ⁻⁸ , 10 ⁻³ - 10 ⁻⁴	1000	M	10 ⁻⁴
	3000	M, MOH, MO	>1	3000	M, MO	>1
Cs, Rb ^c	1000	M, MOH, M ₂ (OH) ₂ , M ₂ MoO ₄	10 ⁻¹¹ , 10 ⁻⁵ - 10 ⁻⁷ , 10 ⁻⁷	1000	M, M ₂ MoO ₄	10 ⁻⁶ , 10 ⁻⁷
	3000	M, MOH, MO, M ₂ MoO ₄	10 ⁻⁵ , 1, 10 ⁻⁶ , 1	3000	M, MO, M ₂ MoO ₄	>1
Te	1000	H ₂ Te	10 ⁻⁶	1000	TeO, TeO ₂	10 ⁻⁴ - 10 ⁻⁵
	3000	TeO, TeO ₂ , TeO(OH) ₂	10 ⁻¹ - 10 ⁻²	3000	TeO, TeO ₂	10 ⁻¹ - 10 ⁻²
Se	1000	H ₂ Se	10 ⁻⁹	1000	SeO, SeO ₂	10 ⁻⁴ - 10 ⁻⁵
	3000	SeO, SeO ₂	10 ⁻¹ - 10 ⁻²	3000	SeO, SeO ₂	10 ⁻¹ - 10 ⁻²
I, Br	1000	MX	10 ⁻³	1000	MX, X	10 ⁻¹ , 10 ⁻³
	3000	MX, X, HX	10 ⁻² - 10 ⁻³	3000	MX, X	>1
Mo	1000	M ₂ MoO ₄ , MoO ₃	10 ⁻⁷ , 10 ⁻⁸	1000	M ₂ MoO ₄ , MoO ₃	10 ⁻⁷ , 10 ⁻⁸
	3000	M ₂ MoO ₄ , MoO ₃	>1, 10 ⁻¹	3000	M ₂ MoO ₄ , MoO ₃	>1, 10 ⁻¹
Ru	1000	RuO ₃ , RuO ₄	10 ⁻⁶	1000	RuO ₃ , RuO ₄	10 ⁻⁶
	3000	RuO ₃ , RuO ₄	10 ⁻² , >1	3000	RuO ₃ , RuO ₄	10 ⁻² , >1
Sb	1000	Sb, Sb ₄ O ₆	10 ⁻³ , 10 ⁻²	1000	Sb, Sb ₄ O ₆	10 ⁻³ , 10 ⁻²
	3000	Sb, Sb ₄ O ₆	>1	3000	Sb, Sb ₄ O ₆	>1
Sr	1000	-	-	1000	-	-
	3000	SrOH, Sr(OH) ₂	10 ⁻³ - 10 ⁻⁴	3000	SrO	10 ⁻⁶
Ba	1000	-	-	1000	-	-
	3000	BaOH, Ba(OH) ₂	10 ⁻¹ - 10 ⁻²	3000	BaO	10 ⁻⁴

^a M is either Cs or Rb; X is either I or Br.

^b Cs₂UO₄/Rb₂UO₄ is assumed to be the stable solid phase.

^c Cs₂MoO₄/Rb₂MoO₄ is assumed to be the stable solid phase.

RbBr, Cs₂MoO₄, Rb₂MoO₄, Te, Se₆ and Sb. Since the vapor pressures of these species are small at fuel periphery (~900K) and cladding temperatures (~600K), they will tend to plate out at those cooler regions. On the other hand, if the cladding now balloons and bursts, the volatile species above will be swept out along with the fission gases Xe and Kr, and He (most LWR fuel rods are pre-pressurized with He).

Situation B. In the event of cladding failure the first fission products released from the rods will prevent initial ingress of steam. When steam enters the fuel rod it will oxidize the fuel, further releasing fission products. Also, the steam will react with the zircaloy cladding liberating H₂. As shown in Table 1, the principal volatile species released to the steam/hydrogen environment will be CsOH, RbOH, CsI, RbI, CsBr, RbBr, Cs₂MoO₄, Rb₂MoO₄, H₂Te, H₂Se, Se₆, although at high temperatures (>2000K) Cs, Rb, CsO, RbO, I₂, HI, Br₂, HBr, Sb, Ba(OH)₂, BaOH, SrOH, Sr(OH)₂, Ru, RuOH, TeO, SeO, Te and Se will also become important. These species tend to dissolve in the liquid water or they will plate out on the cooler surfaces.

Situation C. In this situation, the presence of oxygen from air ingress provides a significantly more oxidizing system than situation B. For these conditions, Table 2 shows that the predominant species are still the same as in situation B, but now release of RuO₃, RuO₄, Sb₄O₆, TeO₂, SeO₂ and MoO₃ must also be considered. At lower temperatures, the contributions of elemental iodine and bromine are relatively small, since the ratio of the alkali halides to the halogens is estimated to be 10³ to 10⁴. However, at temperatures above 2500K the halogen pressures are comparable to those calculated for the halides. Again, the released fission product species have either low enough vapor pressures to condense on the cooler surfaces, or they will dissolve in the liquid water. However, there may be some release as aerosols through the primary containment rupture.

Situation D. The predominant species are essentially the same as in situation C, except for the absence of any hydroxides. In addition, SeO₂, TeO₂ and Sb₄O₆ dominate for these elements and SrO and BaO must also be considered. Significant partial pressures of elemental iodine and bromine are also calculated to develop at very high temperatures. The released fission products should condense at the cooler regions of the fuel or of the cladding.

FISSION PRODUCT AQUEOUS SOLUTION CHEMISTRY

In each of the two accident scenarios B and C, there is a large amount of liquid water present in the system. The equilibrium chemical states of the fission products in aqueous solution are most conveniently evaluated by means of Eh-pH diagrams for the individual fission products in the temperature range 300-600K and a pH range 5-11. Since the only fission product Eh-pH diagrams currently available are those at room temperature [25], a technique was developed to estimate the thermodynamic data for the relevant fission product aqueous species to 600K [26, 27]. Using these estimated

values, Eh-pH diagrams at 323, 373, 423, 473, 523, and 600K have been constructed for the fission elements in aqueous solution. As an example, figure 1 shows the ruthenium - water system at 298, 373 and 523K.

The information on the dominant chemical species released from the failed fuel rods in accidents B and C is combined with the Eh-Ph diagrams to describe their behavior in aqueous solutions.

Cesium and Rubidium. The only thermodynamically stable species are the ions Cs^+ and Rb^+ over the entire region in which water is stable. Since the species released from the ruptured fuel rods are all compounds of Cs^+ and Rb^+ , they will dissolve without reaction. Elemental Cs and Rb react with water to form M^+ ions. Hence, Cs and Rb will not volatilize from aqueous solution.

Tellurium. The stable forms in water are solid Te, TeO_2 , TeO_3 , H_2TeO_4 (HTeO_4^-), HTeO_3 and TeO_3^{--} which are generally non-volatile. The species released from the fuel rods, H_2Te , Te_2 and TeO_2 , interact with H_2O to form one of the stable forms. Hence, any release of tellurium species will be very small.

Selenium. Se_6 , SeO and SeO_2 are the species released from the fuel rods, which are also the stable forms in aqueous solution together with SeO_3 , SeO_4^{--} and HSeO_3^- . Hence, there may be some release of selenium as vapor (vapor pressure of Se = 10^{-3} atm at 600K).

Iodine and Bromine. The thermodynamically stable forms of I and Br in H_2O are $(\text{I,Br})^-$ and $(\text{I,Br})\text{O}_3^-$. The alkali halide species released from the fuel rods and HI and HBr dissolve in the water to form stable $(\text{I,Br})^-$ and $(\text{I,Br})\text{O}_3^-$ ions and possibly, HOI and HOBr. The latter species may release small amounts of fission-product halogens to the environment.

Molybdenum. MoO_3 has a relatively low vapor pressure at 600K and it is slightly soluble in H_2O . The molybdates, on the other hand, are completely soluble. The stable forms of Mo in H_2O are MoO_2 and MoO_4^{--} which are generally nonvolatile. Hence, any release of Mo as vapor to the environment will be extremely small.

Antimony. For the two scenarios considered here, elemental Sb, Sb_2O_3 , and HSbO_2 are the thermodynamically stable forms in water. These substances have vapor pressures of the order of 10^{-20} atm at 600K, and release of volatile forms of Sb to the environment will be negligible.

Ruthenium. The Ru - H_2O system shows that Ru and RuO_2 are the thermodynamically stable forms, both of which are nonvolatile. Of the species released from the ruptured fuel rods, Ru is nonvolatile and insoluble in H_2O , and RuO_4 (and, possibly RuO_3) reacts with H_2O to precipitate non-volatile RuO_2 . Release of RuO_3 as vapor to the environment will be only partial, but it is likely.

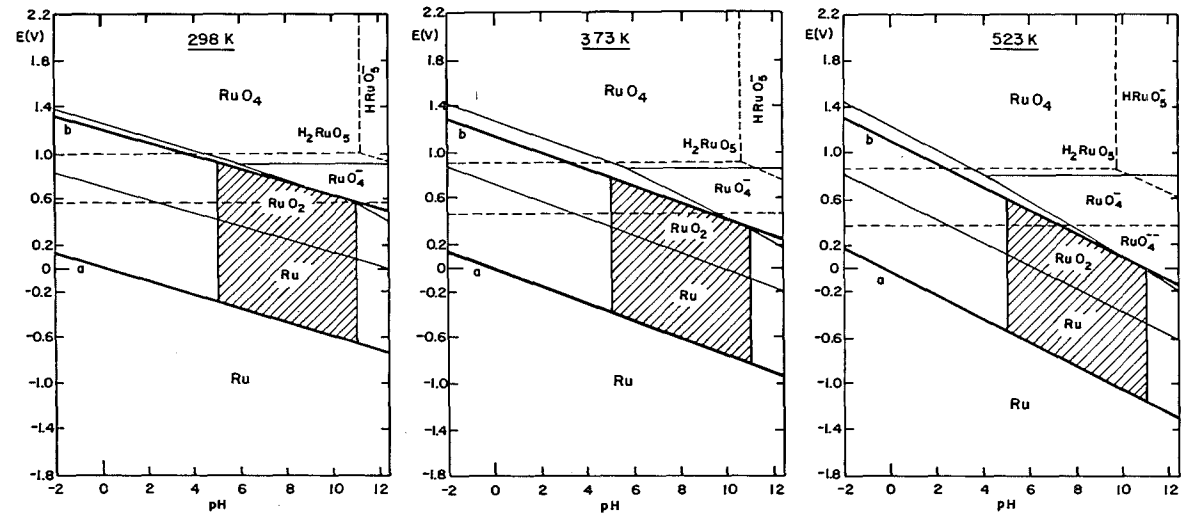


FIGURE 1. POTENTIAL—pH DIAGRAMS FOR THE RUTHENIUM-WATER SYSTEM AT (i) 298K, (ii) 373K, AND (iii) 523K. SHADED REGION INDICATES AREA OF INTEREST. LINE a REPRESENTS THE REDUCTION EQUILIBRIUM OF WATER AND LINE b REPRESENTS ITS OXIDATION EQUILIBRIUM. DISSOLVED SPECIES ACTIVITY IS 10^{-8}

Barium and Strontium. Barium and strontium hydroxides are highly soluble in water, and will dissolve without reaction. Since Ba^+ and Sr^+ are the only stable species in water, release of Ba and Sr vapor species to the environment is highly unlikely.

SUMMARY AND CONCLUSIONS

Three fuel rod accident scenarios (exposure to steam/hydrogen/water, exposure to steam/air/water, and exposure to air) and intact fuel rods were used to assess the vaporization and aqueous solution chemistry of fission product species of Cs, Rb, I, Br, Se, Te, Ba, Sr, Mo, Ru and Sb. Equilibrium thermodynamic calculations and Eh-pH diagrams were used to analyze the behavior of the chemical species. The results of this analysis showed that small amounts of selenium, tellurium, ruthenium, molybdenum iodine and bromine could be released to the environment.

The analysis presented here suffers from a lack of reliable thermodynamic data at high temperatures, particularly on the gaseous oxides and hydroxides. Similarly, there is very little experimental thermochemical or solubility data on most of the fission product compounds in aqueous solution at high temperatures. Hence, accurate quantitative predictions of fission product chemistry in accident situations must await the availability of reliable thermochemical information. Furthermore, the formation of nitrogen and carbon-bearing species of the fission products, such as nitrates, nitrites, and carbonyls must also be considered.

ACKNOWLEDGMENT

The author is grateful to Linda Watts for assistance with manuscript preparation.

REFERENCES

1. T. M. Besman and T. B. Lindemer, Nucl. Technol., 40 (1978) 297.
2. Technical Bases for Estimating Fission Product Behavior During LWR Accidents, NUREG-0772, U.S. Nuclear Regulatory Commission (June 1981).
3. D. Cubicciotti and B. R. Sehgal, Nucl. Technol., 65 (1984) 266.
4. M. G. Adamson, E. A. Aitken, S. K. Evans and J. H. Davies, "Oxygen Redistribution and its Measurement in Irradiated Oxide Fuels", in Proc. Symp. Thermodynamics of Nuclear Materials 1974, IAEA, Vienna (1975), p. 59.
5. H. Kleykamp, J. Nucl. Mater., 84 (1979) 109.
6. S. R. Brinkley, J. Chem. Phys., 15 (1947) 107.
7. W. B. White, S. M., Johnson and G. B. Dantzig, J. Chem. Phys., 28 (1958) 751.

8. S. Gordon and B. J. McBride, "Computer Program for Calculation of Complex Chemical Equilibrium Compositions, Rocket Performance, Incident and Reflected Shocks, and Chapman-Jouguet Detonations", NASA SP-273, National Aeronautics and Space Administration (Feb. 1971).
9. G. Ericksson, *Chemica Scripta*, 8 (1975) 100.
10. T. M. Besman, "SOLGAS MIX-PV, A Computer Program to Calculate Equilibrium Relationships in Complex Chemical Systems", ORNL/TM-5775, Oak Ridge National Laboratory (1977).
11. D. R. Stull and H. Prophet, *JANAF Thermochemical Tables 2nd Edition*, NSRDS-NBS 37, National Bureau of Standards, Washington, D.C. (1971); see also 1974, 1975, 1978 and 1982 JANAF Supplements.
12. I. Barin, O. Knacke and O. Kubaschewski, *Thermochemical Properties of Inorganic Substances*, Springer Verlag, Berlin and New York (1973 and 1977).
13. D. D. Wagman, W. H. Evans, V. B. Parker, I. Halow, S. M. Bailey and R. H. Schumm, "Selected Values of Chemical Thermodynamic Properties", NBS Technical Notes 270-3 to 270-8, National Bureau of Standards (1968-1981).
14. K. C. Mills, *Thermodynamic Data for Inorganic Sulphides, Selenides and Tellurides*, Butterworths, London (1974).
15. CODATA Recommended Key Values for Thermodynamics, ICSU Central Office, Frankfurt (April 1978).
16. O. Kubaschewski and C. B. Alcock, *Metallurgical Thermochemistry 5th Edition*, Pergamon Press, New York (1979).
17. R. C. Feber, "Thermodynamic Data for Selected Gas Impurities in the Primary Coolant of High-Temperature Gas-Cooled Reactors", LA-NUREG-6634, Los Alamos Scientific Laboratory (April 1977).
18. T. B. Lindemer, T. M. Besman and C. E. Johnson, *J. Nucl. Mater.*, 100 (1981) 178.
19. R. Kohli, "Ein thermodynamischer Beitrag zum Verständnis des Vielstoffsystems Uranoxid-Spaltprodukte-Zircaloy", SGAE-3014, Austrian Research Center Seibersdorf, Austria (Dec. 1978).
20. R. Kohli, in *Chemical Metallurgy - A Tribute To Carl Wagner*, N. A. Gokcen (Ed.), Publ. Met. Soc. AIME, Warrendale, Pennsylvania (June 1981), p. 309.
21. P. E. Blackburn and C. E. Johnson, "Light Water Reactor Fission Product Data Assessment", ANL-82-42, Argonne National Laboratory (Sept. 1982).
22. R. Kohli, *Thermochim. Acta*, 65 (1983) 285.
23. D. D. Jackson, "Thermodynamics of the Gaseous Hydroxides", UCRL-51137, University of California (Dec. 1971).
24. O. Krikorian, "Predictive Calculations of Volatilities of Metals and Oxides in Steam-Containing Environments", UCRL-85553, Lawrence Livermore Laboratory (Aug. 1981).
25. M. Pourbaix, *Atlas of Electrochemical Equilibria in Aqueous Solutions*, NACE Publication, 2nd Edition (1974).
26. R. Kohli, *Electrochem. Soc. Extended Abstracts*, 82-1 (1982) 1094.
27. R. Kohli, "Thermodynamic Stability of Aqueous Electrolytes at High Temperatures: Eh-pH Diagrams to 600K", IUPAC Conference on Chemical Thermodynamics, Hamilton, Canada, August 1984.

DETERMINATION OF PARTITION COEFFICIENTS FOR IODINE
BETWEEN WATER AND VAPOUR PHASE WITH I-131 AS TRACER

M.Furrer , R.C.Cripps and T.Gloor

Materials Technology Dept. (Hot Laboratory)
Swiss Federal Institute for Reactor Research (EIR)
CH-5303 Wuerenlingen , Switzerland

ABSTRACT

The calculation of reliable iodine partition coefficients: $P = ([I]_{\text{tot.aq.}} / [I]_{\text{tot.gas}})$ is hindered by basic uncertainties in both thermodynamic and kinetic data. Experimental determinations of P as a function of various parameters (concentration, temperature, pH, redox potential) provide data for risk analysis studies and also allows a verification of computing models.

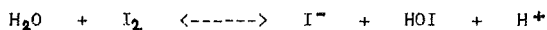
A steel autoclave arrangement is described, which allows the determination of P values up to 10^6 at temperatures from ambient up to 200 °C. Emphasis is placed on experiments which show the influence of pH and redox potential on the thermodynamics and kinetics of the iodate formation. Iodate is one of the dominant factors leading to very high partition coefficients.

Experimental results are compared with P values obtained from recently published computing models.

INTRODUCTION

In the current quest to obtain reliable source term information, the distribution coefficient (P) for iodine between the liquid and the vapour phase is a most important parameter.

Calculations of P are hampered by uncertainties in the thermodynamic and kinetic data despite extensive studies over the last decades. A comprehensive set of thermodynamic data is compiled in [1]. The validity of the "classical" equation for the hydrolysis of iodine in water:



is questionable. To date it has not been possible to prove the existence of HOI in the gas phase [2]. HOI will be the only volatile iodine species besides elemental iodine. Extensive calculations of kinetic parameters [3] are partly based on the existence of HOI.

In view of these uncertainties, the need for experimental measurement of P values is clear. Experimental determinations of P have been carried out under varying physical and chemical conditions in a number of research institutes. Recent EIR work concerning a re-evaluation of the merits of an external containment spray cooling has shown that the partition coefficient for iodine plays an important role. Associated calculations require reliable P values up to 200°C. The uncertainties shown and the high temperatures required have resulted in the present experiments being carried out using a stainless steel autoclave system.

EXPERIMENTAL

One litre of aqueous iodine/iodide solution was placed in the glass inner container (1) of the autoclave, shown in Fig.1. A few mCi of I-131 were added as tracer.

The pH value and redox potential of the solution was measured before the autoclave was closed.

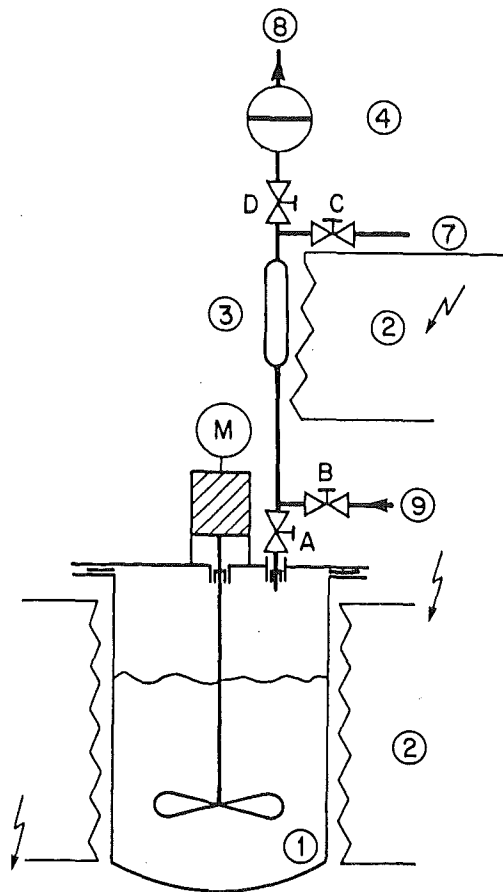


Fig. 1: Sketch of the EIR autoclave system for the

 determination of iodine partition between water
 and vapour phase up to 200°C.

Sampling of the gas for activity measurements was carried out at various temperatures. Each gas sample was taken after about one hour of stirring at constant temperature in order to obtain equilibrium conditions. The gas sampling tube (3) was held at a higher temperature than the autoclave. The tube was evacuated before sampling. Rapid operation of valve (A) provided a 5 ml sample of gas. This gas in the sampling tube was transferred with the help of an inert carrier gas into the filter capsule (4). The filter was charged with 50 ml of activated charcoal. At the end of each experiment, an aqueous sample was taken as a control.

Irradiation tests proved that the small tracer concentration of less than 10 mCi/l did not produce significant changes in iodine species distribution due to radiolysis.

From the (high) partition coefficients and the small volume of the gas sample it can be seen that less than 0.1% of the total iodine is removed per gas sample. Thus a very large number of samples can be taken without significant changes in the concentration of the liquid and the gaseous phases.

A good approximation of a "clean condition" experiment was achieved by heavily gold plating all of the internal steel surfaces in order to avoid irreversible deposition/absorption reactions.

RESULTS AND DISCUSSION

The first data set shows the influence of temperature on the partition coefficient P , with pH and redox potential as constants.

In Fig.2, the resulting partition coefficients for five temperatures between 21 and 115°C are represented as solid dots.

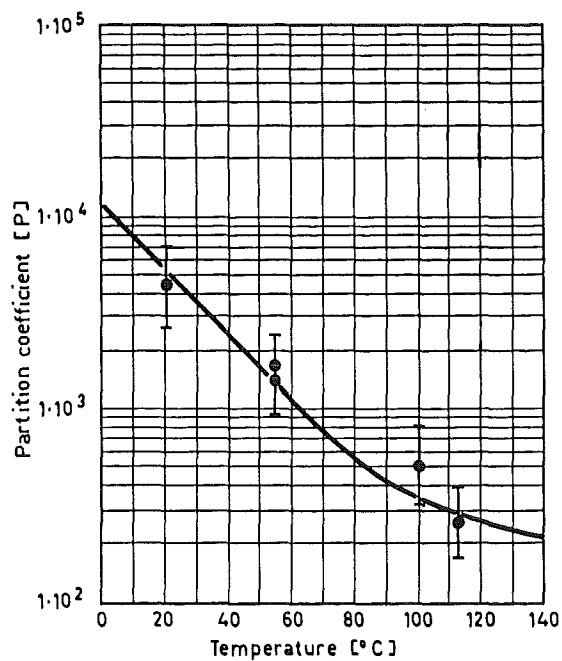


Fig. 2: Iodine partition as a function of temperature

 $[I_2]_{\text{tot.aq.}} = 0.001 \text{ M}$ (added as I_2)
 pH (25°C) = 5.1
 E (25°C) = 0.67 V vs. SHE

The curve on Fig.2 represents the theoretical data calculated using the thermodynamic constants out of [4] derived from the free energy data in [2] including HOI hydrolysis and volatility values. Fig.2 shows a good fit between experimental and calculated data values.

Since these calculations show insignificant HOI and iodate equilibrium values, little information concerning these two problem areas could be deduced.

Due to dissimilar experimental conditions and lack of sufficiently detailed information (redox potential measurements), no attempt was made to compare the data shown here with other experimental P determinations.

A second data set compiled in Fig.3 shows the relationship between pH and partition coefficient at constant temperature and constant redox potential. The experimental P values remain constant up to about pH 6.5, then rapidly increase by several orders of magnitude, with only minor increase in pH.

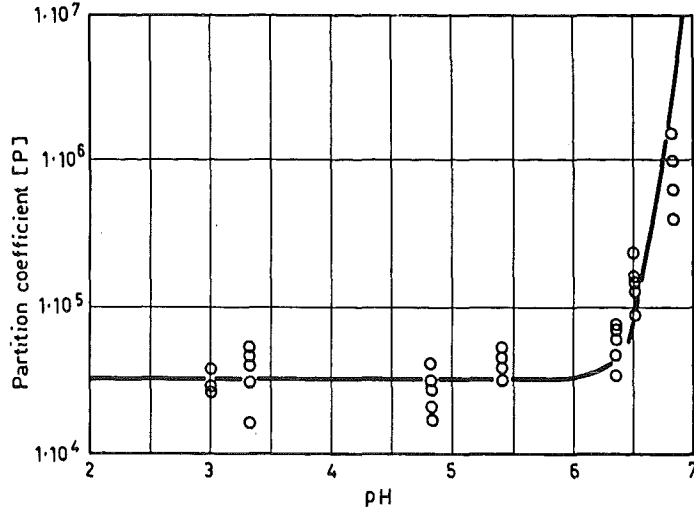


Fig. 3: Iodine partition as a function of pH

in CsI solution

[CsI]_{aq.} = 0.0001 M
Buffer (Phosphate) = 0.1 M
Temperature: 110°C
E (25°C) = 0.61 V vs. SHE

The bend in the experimental data at pH 6.5 does not correlate well with results of calculations of kinetic parameters, based on theoretical models in a recent report [3]. This shows that iodate should be a major species and that iodate equilibrium is

CONCLUSIONS

The data described here provide some contribution to the discussion of thermodynamic and kinetic parameters in "clean condition" systems. A good fit with clean systems is a prerequisite for investigations of complex realistic systems. Such an advanced experiment is now underway at EIR.

It must consider, for example solutions which approximate to a "core melt" sump. This could contain a large number of dissolved species and suspended solids such as fuel, silicates and structure material. Contributory effects of a strong radiation field must also be considered.

A calculation of iodine distribution is hardly achievable on thermodynamic grounds. Using the autoclave system shown, combined with a radiation field, reliable partition coefficients can be determined at temperatures up to 200°C.

REFERENCES

- [1] R.J. Lemire, J. Paquette, D.F. Torgerson, D.J. Wren and J.W. Fletcher
AECL-6812 (1981)
- [2] J. Paquette, S. Sunder, D.F. Torgerson, C.J. Wren and D.J. Wren
Water Chemistry 3, BNES, London (1983)
- [3] J.T. Bell, M.H. Lietzke and D.J. Palmer
NUREG/CR-2900 ORNL-5876 (1982)
- [4] R.J. Bawdwen, A.M. Deane, K. Garbett, B.J. Handy and N.R. Large
AERE-R-10494 (Rev. 1) (1983)

EXPERIMENTAL STUDY OF THE DEPOSITION OF IODINE AND OTHER
FISSION PRODUCTS IN THE COOLANT CIRCUIT OF A CAGR

J.A. Garland and A.C. Wells

AERE Harwell, Oxon OX11 0RA, UK

E.J. Higham

WNPDL, Sellafield, Cumbria CA20 1PF, UK

I.C. Smith

Hinkley Point Power Station, Somerset TA5 1UD, UK

ABSTRACT

Deposition of activity in the coolant circuit of a Commercial Advanced Gas-Cooled Reactor reduces the amount that might escape in the event of an accident.

In a continuing programme, iron oxide particles of 0.6, 2 and 5 μm diameter, 17 μm alumina particles and methyl iodide vapour have each been injected into the CO_2 coolant of a reactor at Hinkley Point, England. Subsequent changes of concentration provide information on the rate of deposition.

Initially, rapid deposition occurred for all the tracers. Methyl iodide was removed with an initial half-life of 12 s. The corresponding half-life was about 20 s for the particles up to 5 μm diameter, and 120 s for 17 μm particles. After the first few minutes the removal became slower, but concentrations fell by factors of several hundred to some tens of thousands during a period of 3 h following each injection. The potential escape of fission products in an accident could be reduced several hundred times by deposition.

In one experiment, 17 μm particles were injected with the reactor shut down and the coolant flow rate reduced. The particles deposited more rapidly than at full flow. On increasing the flow rate to full flow most of the particles were resuspended into the gas stream.

The results imply that the metal-oxide particles deposit onto, but also bounce and blow off, the internal surfaces of the coolant circuit. Methyl iodide is converted, at least in part, into one or more chemical forms of iodine, which also disappear rapidly from the gas stream. Although the mechanisms for removal are not fully understood, the benefit of deposition in reducing the amount of circulating activity is clearly very great.

INTRODUCTION

In analysing the safety of operation of commercial advanced gas-cooled reactors (CAGR) a number of possible accidents are postulated in which iodine and other volatile fission products escape from damaged fuel to the coolant gas, without damage to the coolant circuit. The iodine could be present in two forms; either as methyl iodide, or attached to particles which are circulating in the coolant [1]. These materials could escape from the intact coolant circuit with the two or three percent of the gas that leaks daily from the circuit, until the reactor could be blown down. However, experiments in the prototype Windscale AGR, under a range of operating conditions, have shown that methyl iodide and particles are removed from the gas stream by deposition onto the internal surfaces of the coolant circuit, thus reducing the fraction that might leak out by a large factor [2,3,4]. Further experiments are in progress in a CAGR at Hinkley Point. They enable the magnitude of this decontamination factor to be evaluated, and provide some information on the behaviour of particulate matter and iodine compounds in the reactor coolant.

EXPERIMENTAL

Methyl iodide and particles of iron oxide or alumina were injected rapidly into the coolant gas stream, and the rate of deposition was deduced from the decrease with time of the concentration in the gas. The injection point for all the experiments entered a duct of 30 cm diameter returning gas from the coolant treatment plant to the reactor pressure vessel, upstream of one of the eight circulators (see Fig 1). A sample collected downstream of the injection point allowed estimation of the quantity injected.

Methyl iodide, labelled with ^{131}I , was prepared and sealed in a small silica capsule, which, at the appropriate time, was broken in a stream of helium. The methyl iodide evaporated rapidly and was carried into the reactor duct within 1 minute. Sequential samples of the coolant were collected in several locations, both from sampling pipes installed in the circulators, and also from selected fuel channels via the Burst Cartridge Detection Pipes, penetrating the pile cap. These pipes were long and of narrow bore. At each sampling point coolant gas was drawn at 1 to 2 g s⁻¹ through traps of 35 or 65 ml volume, packed with activated charcoal impregnated with KI. A manifold arrangement was used to permit continuous sampling. In addition a few samples were taken at 80 g s⁻¹ through a pipe of wider bore only 2 m long at sampling point 2 (see Fig 1). At this sampling point, the gas was passed through a pack containing six or more charcoal-impregnated glass fibre filters in series. A fraction of the gas penetrating these filters was sampled by a charcoal trap. The amounts of ^{131}I collected on the samples were deduced from the gamma ray spectra recorded using Germanium-Lithium detectors.

Monodisperse particles of 2, 5 and 17 μm diameter were labelled with ^{59}Fe . In each experiment, particles of the selected size were dispersed within a small pressure vessel connected at the injection point, and the resulting aerosol was carried into the reactor in a stream of helium. In an additional experiment a submicron aerosol of mass median diameter 0.6 μm , geometric standard deviation 2.5 with the same radioactive label was generated by atomising a colloidal suspension in the pressure vessel. The variation in concentration of the injected particles was followed for

about 200 minutes at sampling point 2 only. Glass fibre filters, supported on both sides by stainless steel gauzes were used to collect particulate material from the gas at a flow rate of about 115 g s^{-1} . Gamma spectrometry was used to determine the ^{59}Fe content of the samples. The techniques for generation, injection and sampling of the test aerosols have been described elsewhere [5].

The methyl iodide and particle injection experiments were carried out during normal operation of the reactor. One additional particle injection experiment was performed with the reactor shut down and with the coolant circulation rate reduced to 47 per cent of normal. Four hours after injecting the particles the circulation rate was raised to the normal value, to determine whether the deposited particles could be raised from the surfaces by an increase in gas velocity. Information regarding the background ^{59}Fe raised into the gas stream during this operation was obtained by collecting samples during a similar change in flow the day before the particles were injected. The concentration ratios of ^{59}Fe to other activation products found on the filter samples (particularly ^{58}Co and ^{54}Mn), were used to estimate the contribution of background ^{59}Fe circulating in the coolant gas during the following experiment.

EFFECT OF MIXING

The circulators drive about 4000 kg s^{-1} of coolant around the reactor circuit, so that the total $1.2 \times 10^5 \text{ kg}$ pass around the circuit once every 30 s. There is a tendency for the gas that has passed through a given circulator to return to that circulator on the next pass. Thus, the tracers, injected effectively into the inlet to one circulator, do not appear immediately at sampling points in different parts of the circuit. Experiments were conducted in which helium, an inert tracer, was injected for 30 s or 1 min at the injection point and was measured in samples of reactor coolant collected at the particulate sampling point and at some selected circulators. The results (Fig 2) show the time required for the tracer to disperse uniformly around the circuit, and the variation in concentration due to mixing alone at selected sampling points. Data from the methyl iodide and the particulate injection experiments could be corrected for the effect of mixing, to reveal the effects of deposition alone on the concentration of the injected tracer.

BEHAVIOUR OF IODINE INJECTED AS METHYL IODIDE

Fig. 3 shows examples of the variation in concentration following an injection of methyl iodide. The results have been normalised by dividing by the concentration that would have resulted, had all the injected activity been uniformly mixed throughout the coolant.

Measurements at different locations in the reactor circuit showed the large variations in peak concentration that would be expected for a tracer with a deposition half-life that is much shorter than the time required for mixing throughout the reactor circuit. Measurements at the circulator which received the injected methyl iodide, showed that initially the ^{131}I disappeared from the gas stream with a half-life of about 12 s. Within two or three minutes the concentration had declined several hundred times, but the rate of decline of concentration had diminished substantially. After 3 hours the concentration was less than

Table I. Iodine collected on the components of the samplers used to study iodine compounds

Sample Point mean time ^a of sample	1	2	2	2	2	2
	0.5 ^b	1.0	4.7	14.3	52.9	217.7
charcoal ^d papers	47	0.053	4.4x10 ⁻³	3.8x10 ⁻³	2.8x10 ⁻³	3.2x10 ⁻³
Conc. ^c Charcoal pack	187	0.15	1.3x10 ⁻³	4.9x10 ⁻⁴	3.3x10 ⁻⁴	2.7x10 ⁻⁴

^a Measured in minutes from start of injection

^b During injection

^c Concentrations normalised as for Fig.3

^d Six charcoal-loaded filter papers in series

10⁻⁴ of the initial value, and it approached the background level, present before injection, over a period of a few days.

Samples collected using sampling trains of several elements in series gave some evidence of the presence of more than one chemical form of ¹³¹I. Measurements at the sampling point 1 (Fig 1), close to the injection point, showed that charcoal-loaded filter papers each retained only about 4 per cent of the incident methyl iodide. The remainder penetrated to the following charcoal trap. In contrast, measurements at sampling point 2, showed substantial fractions of iodine retained on the filters. After a few minutes the fraction collected on a stack of six charcoal-loaded filter papers was consistently 80 to 90 per cent of the total retained by the sampling train. (See Table I).

In some samples a plain glass-fibre filter was included at the front of the stack of filters. This retained only a few per cent of the total iodine, showing that there was little absorption on the particulate material suspended in the coolant.

The results imply the presence of at least two chemical forms of iodine. The more easily absorbed was retained with an efficiency of sixty to seventy per cent by each of the filters, so that the fraction of this form penetrating the six filters in series would be negligible. The more penetrating form of iodine, behaving in this respect like methyl iodide, was absorbed inefficiently by the filters and was mostly collected by the following charcoal trap. This was confirmed by the fact that the last of the six papers often retained only a few per cent of the quantity held by the trap.

It would be reasonable to conjecture that the injected methyl iodide constituted the penetrating form. However, for the samples collected at sampling point 2, measurements indicated that the rear of the charcoal pack (divided into halves by a gauze) collected on average, less than 12 per cent of the iodine retained by the whole pack, while in the sample exposed to methyl iodide, just downstream of the injection at sampling point 1, the corresponding fraction was 23 per cent. This comparison suggests the presence of yet another form of iodine.

The variation of composition of the iodine suggests a complex mechanism for the interconversion and deposition of the species present,

and the results do not provide an understanding of this process. However the results clearly indicate a large and rapid reduction in total concentration due to loss to surfaces within the coolant circuit.

BEHAVIOUR OF TRACE AEROSOLS

Figure 4 shows examples of the results for two experiments conducted at full flow.

The results for submicron, 2 and 5 μm diameter particles showed many similarities. For all three the concentration of ^{59}Fe declined rapidly at first, with a deposition half-life of about 20 s. After a few minutes, the decline slowed, but deposition continued, and when 3 hours had elapsed the concentration was less than one thousandth of the concentration that would have resulted had the injected particles become uniformly mixed throughout the coolant. The results were generally similar to those obtained in the prototype AGR at Windscale [2] for 2 and 5 μm particles, but the initial deposition half-life at Windscale was about 1 min.

The 17 μm alumina particles deposited more slowly, with an initial half-life of 2 minutes. After 15 min the half life extended to 2 hours, and decay was still proceeding at this rate when sampling was discontinued some 3 h after injection.

In several experiments (eg see Fig 4), occasional fluctuations were imposed on the general trend of ^{59}Fe concentration. Sometimes these coincided with changes in other activation products, indicating that the fluctuations were related to the background material in the reactor. On other occasions, ^{59}Fe variations did not correlate with other tracers, and preferential resuspension of the injected particles, due perhaps to small changes in coolant flow, or movement of reactor components is a plausible explanation.

The results appear to imply that several processes combined to determine the variation of concentration. Initially, mixing causes an early peak in concentration, but explains little of the subsequent decline. Particles in the size region represented in these measurements are expected to arrive at surfaces chiefly due to impaction, a mechanism which increases in effectiveness with particle size. The fact that the deposition half-life does not vary inversely with particle size is strongly suggestive that bounce-off (or possibly rapid resuspension) is occurring, its frequency increasing with particle size. The slower variation in concentration that occurred after the tenth minute following each injection can be explained by a progressive process of resuspension and deposition, particles ultimately accumulating in locations from which resuspension is very slow.

The experiment at low flow provided further evidence of the nature of the processes occurring (Fig 5). When the 17 μm aerosol was injected at 47 per cent flow, the initial deposition half-life (50 s) was shorter than the equivalent value at full flow. As impaction is expected to increase in frequency with flow rate, this inverse variation of deposition with flow suggests an increase of bouncing with velocity. Increases in flow rate, both before and after the deposition experiment, gave clear evidence of resuspension of activated component elements of steel and of the injected test particles. At least a half of the injected particles must have become suspended again to explain the observed concentrations.

CONCLUSIONS

Experiments on such a large, complex system as a power reactor, with limited access for sampling, provide valuable evidence regarding the behaviour of vapours and particles, but cannot alone give a full understanding of the physical and chemical changes involved. However, the results described above clearly indicate that methyl iodide (and the products of its chemical changes in the coolant gas) and particulate tracers are rapidly removed onto surfaces. Within three hours of release, concentrations are reduced by factors from hundreds to tens of thousands, and the potential for escape of fission product iodine from a reactor in the event of an accident is reduced by a comparable degree.

ACKNOWLEDGEMENTS

The authors gratefully acknowledge the essential assistance rendered by the Station Superintendent and CEBG personnel at Hinkley Point Power Station and also at Berkeley Nuclear Laboratories, and by UKAEA staff at Windscale and Harwell. The project was funded jointly by the UKAEA and the CEBG.

REFERENCES

1. Collins D.A., McIntosh A.E., Taylor R. and Yuille W.D. (1966) *J. Nuclear Energy Parts A/B* 20, 97-122.
2. Garland J.A., Wells A.C. and Higham E.J. (1982) AERE-R 10491.
3. Brightman F.G., Chapman C.J., Garland J.A., Hargreaves R. and Higham E.J. (1982) *Gas Cooled Reactors Today*, BNES London 3, 43-52.
4. Hillary J.J. and Taylor J.C. (1975) *J. British Nuclear Energy Soc.* 14, 159-165.
5. Wells A.C., Garland J.A. and Hedgecock J.B. (1984) Techniques used in the experimental study of the deposition of aerosol particles to surfaces in the coolant of a commercial carbon dioxide cooled reactor. CSNI Specialist Meeting on nuclear aerosols in reactor safety, Karlsruhe, 1984.

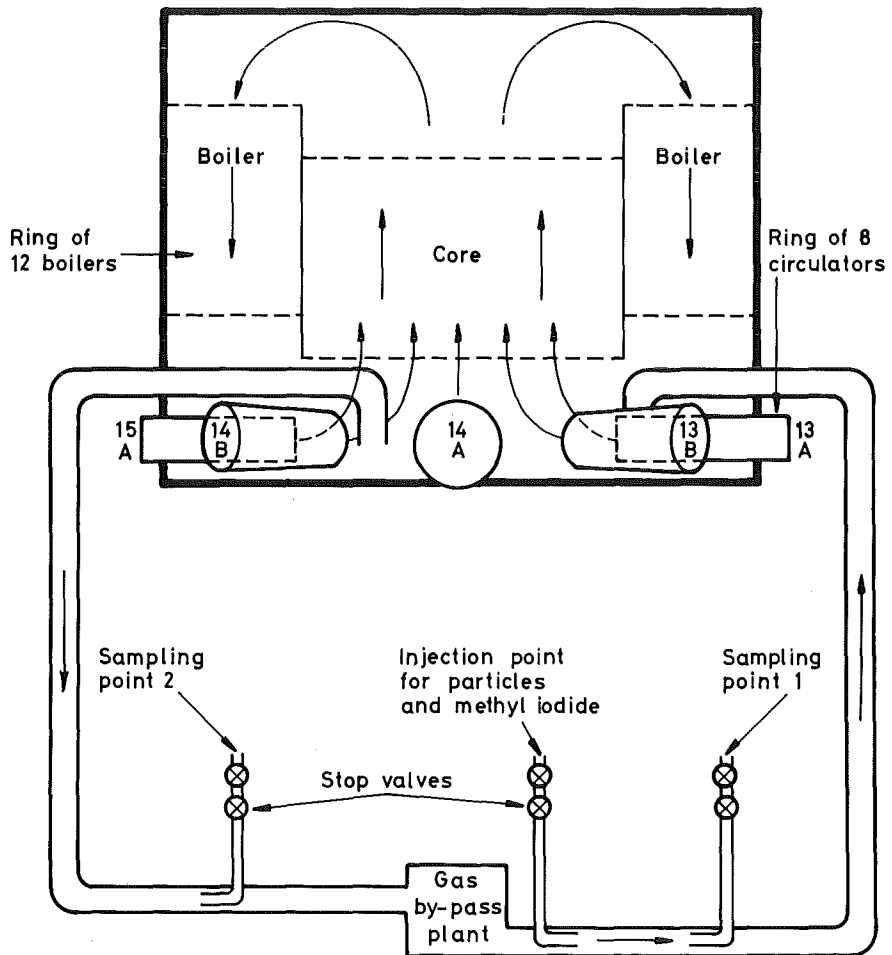


Fig. 1. Schematic diagram of coolant flows and sampling and injecting positions

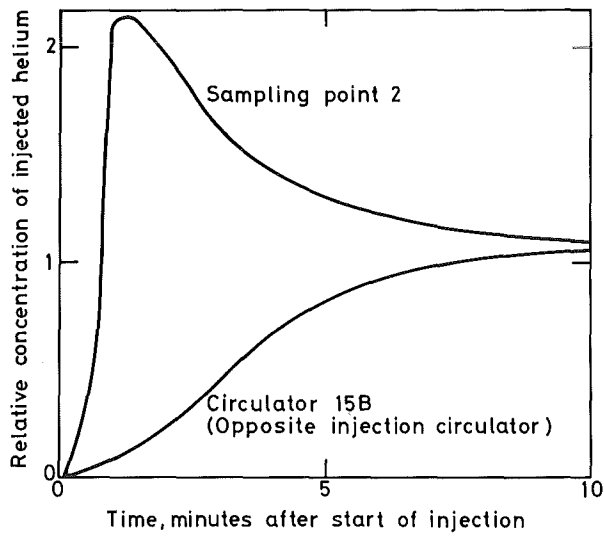


Fig. 2. Some results from a helium injection experiment

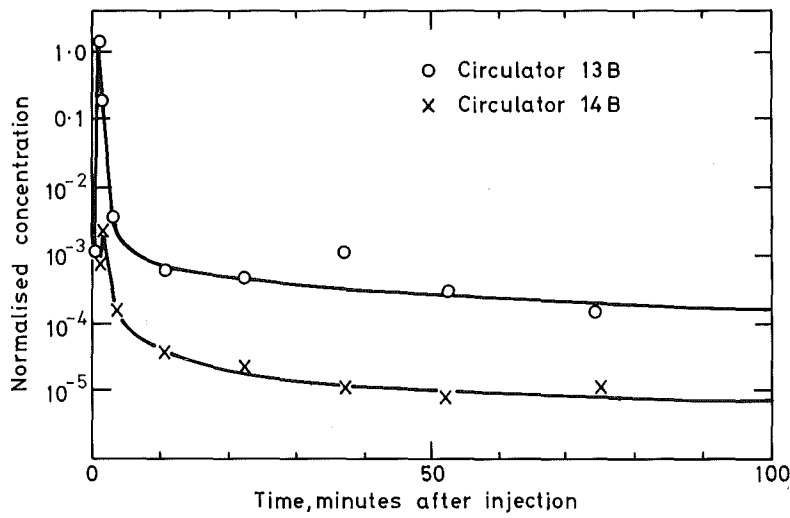


Fig. 3. Variation of the concentration of ^{131}I at two sampling points following an injection of $\text{CH}_3^{131}\text{I}$. The concentration has been corrected for background and normalised by dividing by $\left(\frac{\text{activity injected}}{\text{mass of coolant}}\right)$

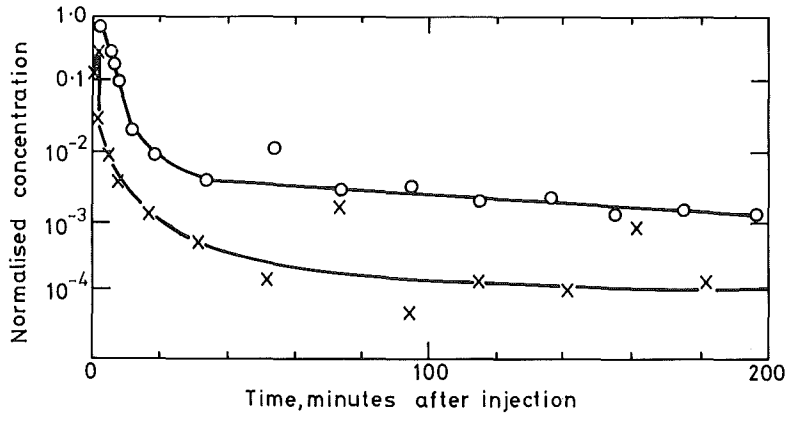


Fig. 4. Variation in concentration at sampling point 2 following injections of 2µm iron oxide (—x—) and 17µm alumina (—o—) particles. The results are corrected for background and normalised as in Fig. 3.

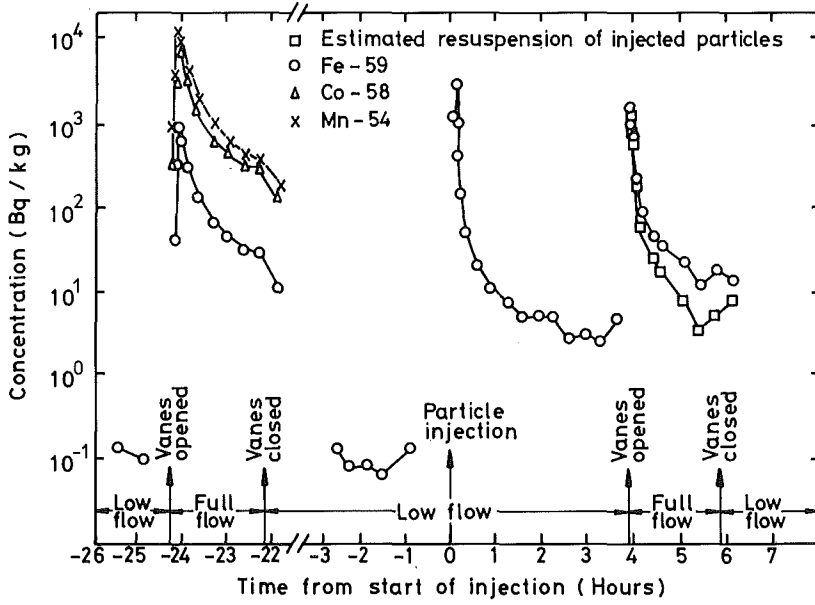


Fig.5.17 Micron alumina experiment - injection and resuspension

THE BEHAVIOUR OF IODINE IN ADVANCED GAS-COOLED REACTOR (AGR) CIRCUITS

by

E. M. Hood and P. N. Clough

Safety and Reliability Directorate, UKAEA,
Culcheth, Warrington, U.K.

ABSTRACT

Evidence on the behaviour of iodine in the coolant circuits of AGR is reviewed, and suggests that several iodine species are important with respect to the overall plate-out behaviour. Interconversion of these species by radiolysis in the core is a key process. An approach to the modelling of iodine plate out which takes account of the coolant radiolytic chemistry is described.

1. INTRODUCTION

Understanding the behaviour of fission product iodine in the coolant circuit, and particularly the potential for retention by surface plate-out in abnormal conditions, represents an important area in the safety assessment of Advanced Gas-Cooled Reactors (AGR). For some time, we have been developing a computer code (AGRIPA) for modelling the plate-out of iodine in AGR's under a wide range of conditions. The model for iodine surface deposition originally employed was based on the prevailing view that methyl iodide is the dominant form of iodine in AGR coolants, and is the plating-out species [1]. However, this approach proved incompatible with some of available experimental evidence, in particular the results of methyl iodide injection experiments at Windscale AGR. We were led to propose a new model in which at least two iodine species have important roles, the interconversion of these playing a key part. This preliminary work included a number of arbitrary assumptions about the nature and rate of the interconversion processes.

In this paper, we re-examine old evidence and review new results which point to the importance of several iodine species in AGR circuits. A detailed analysis of the radiolytic mechanism by which methyl iodide may be converted to other iodine species confirms that this is an important process, even in shut-down reactor conditions. The need to include a proper treatment of the gas-phase chemistry of the coolant in iodine plate-out modelling is emphasized, and approaches to an improved modelling code are examined.

2. IODINE SPECIES AND THEIR INTERCONVERSION IN AGR CIRCUITS

The importance of methyl iodide in AGR circuits was demonstrated in early reactor coolant sampling measurements. Maypack measurements from burst cartridge detection (BCD) pipes on core channels containing defected fuel pins at Windscale AGR (WAGR) showed more than 90% of the total radioiodine to be organic [2]. Gas chromatographic measurements confirmed that methyl

iodide was the major organic component. This evidence was further supported by elemental iodine injection experiments at the French Chinon reactor [3], with similar coolant chemistry to an AGR. Rapid conversion of a proportion of the elemental iodine to organic form was observed, accompanied by a fast overall removal of iodine from the coolant by plate-out. The quantitative extent of organic conversion was not determined, however.

Earlier laboratory studies by Collins et al [4] were in accord with these reactor observations. Irradiated miniature fuel pins heated to clad melting temperature in flowing CO_2/CO carriers were found to release most of their iodine attached to particulate, but the 10-25% gaseous component was largely organic. Methane added to the carrier increased the organic iodine fraction, but added air resulted in 60-80% of the released iodine being characterised as elemental. The accumulated evidence some ten years ago thus pointed strongly to methyl iodide as the dominant form of iodine in AGR circuits. On this basis, methyl iodide was chosen as representative of iodine behaviour in the first series of injection experiments to measure plate-out at WAGR [5].

Our modelling studies [1] of the WAGR methyl iodide injections [5,6] suggested that this is an oversimplified picture. Our conclusions that several iodine species play important roles are supported by new experimental results and a re-examination of older data. BCD pipe measurements alone are not a reliable diagnostic of chemistry in the coolant circuit, since investigations have shown that up to 90% of the total iodine entering the pipes from failed fuel core channels may become absorbed on the pipe walls [7]. Recent measurements show that the proportion depositing can vary from near zero up to 80%, depending on reactor operating conditions and the particular fuel failure. It is probable that long, narrow sampling pipes act as selective filters, trapping reactive forms of iodine and transmitting the less reactive methyl iodide. Plate-out of methyl iodide itself cannot account for the extent and variability of the observed deposition in BCD pipes. Recent results from a special sampling point installed at Hinkley Point B commercial AGR confirm this view [8]. This point accesses the coolant circuit through a short length of wide-bore pipe, so greatly reducing plate-out en route to the Maypack sampler. Under normal operation, the background iodine in the circuit is found to consist of a mixture of iodine species in which the reactive component exceeds the methyl iodide by about a factor of 10. Samples taken in conjunction with injections of methyl iodide into the circuit show a rapid conversion of a proportion of this to the reactive form.

Recently revised thinking on the chemistry of iodine in oxide fuels also points to a need to consider several iodine species which can interconvert in the coolant circuits of AGR's. Detailed assessment of iodine chemistry in LWR oxide fuel [9] has led to the conclusion that caesium iodide will be the predominant iodine form. The in-pin chemistry of AGR fuel should differ very little from that of LWR fuel, the effects of the different cladding being slight. Releases of iodine from AGR fuel pins with minor defects where fuel chemistry is unperturbed by coolant penetration is thus expected to be as caesium iodide. Caesium iodide will be thermodynamically stable in AGR coolants ($\text{CO}_2/1\% \text{CO}$ with a few hundred ppm of CH_4 , H_2 and H_2O) [10], but may be radiolytically converted to other iodine species including methyl iodide by processes of the type discussed in Section 4 below. Direct measurements of iodine release from AGR fuel are not inconsistent with CsI. Hillary and Taylor [11] found that most of the iodine and caesium released from irradiated WAGR pins heated in CO_2/CO deposited in the high temperature region of their system, consistent with CsI. The earlier experiments of

Collins et al [4] probably involved some extraneous effects. CsI may have been decomposed on the hot silica walls of the apparatus [12], and the free iodine released reacted with trace hydrocarbon impurities to yield methyl iodide. With air in the carrier, fuel oxidation could have led to caesium uranate formation and corresponding decomposition of CsI.

It is reasonable to conclude that several iodine species, of which the most important are caesium iodide, atomic iodine, hydrogen iodide and methyl iodide, are important in AGR circuits, and must be considered in improved modelling of iodine behaviour.

3. THE PLATE-OUT BEHAVIOUR OF IODINE

There is abundant reactor evidence that iodine plates out strongly in AGR's. The observations at the Chinon reactor, and the measurements on WAGR BCD pipes, have been referred to already. Further evidence from WAGR is based on the iodine concentration measured in coolant from core channels containing fuel failures compared with that from clean channels [2]. A ratio of about 30 was typically found, which could only be explained on the basis of substantial loss of iodine to surfaces in the circuit. Steel specimens retrieved from WAGR boilers following a fuel failure showed positive evidence of deposited iodine [2]. The series of methyl iodide injection experiments at WAGR [5,6], though difficult to interpret in detail, demonstrate that overall iodine is rapidly removed from the coolant by plate-out. They are supported by the recent measurements at the special sampling point at Hinkley Point B following a methyl iodide injection [8], which show that the different iodine species present all plate-out rapidly.

Models describing iodine behaviour in AGR's must include a valid treatment of the basic surface deposition processes of the various iodine species. In this respect, controlled laboratory measurements are a valuable source of information. The deposition of elemental iodine onto steel and other surfaces has been much studied [13,14], but under conditions relevant to LWR and HTGR, rather than AGR. Data on other iodine species are very sparse. Measurements currently in progress at Windscale Nuclear Laboratories [15] specific to AGR conditions should do much to improve this situation. Meanwhile, results from experiments employing inert carriers are of closest relevance. Ideally, the rate constants for adsorption and desorption are required as functions of temperature, the ratio of these determining the equilibrium state for conditions below surface saturation. However, most measurements have been concerned with determining the equilibrium isotherms of elemental iodine onto a range of steels, and so are of limited value for reactor modelling. Early results have been reviewed by Hoinkins [13], and recently Osborne et al [16] have published new measurements for low chrome steel in conjunction with a further review of earlier data. Osborne et al's work also includes some measurements of the rates of adsorption and desorption. The principal conclusions which can be drawn from this combined evidence are:

- i) Two main mechanisms operate for elemental (atomic) iodine on steel. For low iodine pressures and high temperatures where condensed FeI_2 and CrI_2 phases are unstable, reversible chemisorption operates up to surface loading approaching monolayer coverage, when saturation effects set in. These conditions will apply for normal AGR operation, but not necessarily when enhanced iodine levels are present. For higher iodine concentrations, iodides of steel components will form on the cooler circuit surfaces, and saturation effects do not then arise.

- ii) Material type and surface condition are important. Equilibrium loadings on heavily oxidized surfaces are much lower than on bare metals, and are lower on stainless steel than on carbon steel. There is some evidence that the rate of adsorption is lower on oxidized surfaces than on bare metals. The oxygen content or oxygen potential of the carrier gas also plays a role.
- iii) The adsorption process is non-activated and is generally fast. Deposition velocities are typically in the range 10^{-4} - 10^{-2} ms^{-1} . Alternatively deposition can be represented in terms of a gas kinetic sticking probability, for which values of 10^{-3} and 10^{-4} are indicated by the work of Osborne et al at temperatures 400°C and 700°C respectively.
- iv) Desorption is an activated process, and the activation energy appears to depend on surface condition. For slightly oxidized surfaces, values are in excess of 200 kJ mol^{-1} [16], but for heavily oxidized surfaces such as those in AGR's, values in the range 100 - 150 kJ mol^{-1} appear likely based on plant measurements [1,7].

Hydrogen iodide is expected to exhibit very similar plate-out characteristics to elemental iodine. Of the remaining species important in AGR circuits, caesium iodide deposition rates onto steel have been measured by Nicolosi and Baybutt [17], but only in steam atmospheres and under poor mass transport conditions. Very recent measurements in an inert carrier by Bowsher et al [18] suggest that unsaturated CsI vapour does not deposit significantly onto oxidized steel surfaces. No data on methyl iodide deposition rates at relevant temperatures have been published, but there is evidence that at 115°C the rate is orders of magnitude slower than for elemental iodine [19]. Since elemental iodine is known to plate-out rapidly, it seems a reasonable modelling assumption to attribute the dominant role in AGR circuits to this species.

4. THE ROLE OF RADIATION AND A RADIATION CHEMISTRY MODEL

A treatment of the interconversion of iodine species is needed in a fully-developed plate-out model. Earlier, we suggested that radiolysis probably plays the key role in this [1], and the modelling studies now described confirm this view. In an AGR core under normal operation, neutron and γ -fields are very high, and even under shut-down conditions substantial γ -fields persist for long periods. Both CH_3I and CsI are decomposed by γ irradiation [20,21], but at the very low concentrations involved, direct radiolysis will be negligible. The dominant decomposition mechanisms will involve reactions with the primary radiolysis products of CO_2 , analogous to the hydrocarbon radiolyses which have been much studied in the context of graphite oxidation and carbon deposition on fuel pins [22, 23].

AGR coolant radiolysis chemistry is extremely complex and incompletely understood. No data on iodine species behaviour in this environment are available. Numerous mechanisms for the decomposition of CsI and CH_3I could be postulated. We confine attention here to the latter species, mainly because of its importance in interpreting the results of CH_3I injection experiments at WAGR, but also because very reasonable assumptions about its behaviour can be based on the established radiolysis mechanisms for methane.

In order to assess the extent of methyl iodide destruction on passage through the core, it is necessary to incorporate the important coolant chemistry reactions into a description of a fuel channel. The main difficulty lies in

selecting representative reactions, otherwise the problem becomes too big to solve efficiently. The reaction scheme in the model is limited to 20 chemical species:-

- a) Coolant constituents - CO_2 , CO , H_2O , H_2 , CH_4 , C_2H_6 , C_2H_4
- b) 1° Radiolysis products - CO_2^+ , $\text{O}(^3\text{P})$
- c) 2° Radiolysis products - $(\text{CO}_2)_2^+$, $(\text{CO}_2 \cdot \text{CO})^+$, $(\text{CO})_2^+$, $(\text{CO}_2 \cdot \text{CO} \cdot \text{CO})^+$, $(\text{CO})_3^+$
- d) Organic radicals - $\text{CH}_3\cdot$, $\text{C}_2\text{H}_5\cdot$, $\text{C}_2\text{H}_3\cdot$
- e) Iodine species - CH_3I , $\text{C}_2\text{H}_5\text{I}$, I

Reactions leading to the primary and secondary radiolysis products are shown schematically in Fig. 1. The CO_2^+ ions and the $\text{O}(^3\text{P})$ atoms are the primary products of CO_2 radiolysis and the secondary products are formed by clustering of the CO_2^+ ion. Fig. 2 shows diagrammatically the reactions involving other species. Briefly, the scheme involves reaction of radiolysis products with hydrocarbons to produce free radicals and with organic iodides to produce radicals and I atoms; hydrogen stripping reactions between radicals and hydrocarbons; radical recombination and recombination of I atoms with radicals to re-form organic iodides. The rate constants for all these reactions are either best literature values or best estimates.

The fuel channel is divided up into 50 equal volume compartments, which are assumed to be well-mixed in all species and with a uniform temperature. The energy deposition rate in each compartment, $E(z)$, is calculated from a standard expression for a WAGR fuel channel, involving E_{max} the peak rating. The production rates of O atoms and CO_2^+ ions can then be calculated using the equation:-

$$\text{Production rate} = 6.2418 \times 10^{16} \cdot \rho \cdot G \cdot E(z) \text{ molecules cm}^{-3} \text{ s}^{-1}$$

$$\text{where: } \rho = \text{density of } \text{CO}_2 \text{ in g cm}^{-3}$$

$$G = \text{G-value for production of species in } (100 \text{ eV})^{-1}$$

$$E(z) = \gamma\text{-energy deposition rate in W g}^{-1}.$$

Chemical reactions within each compartment and the transport of each species from one compartment to the next are modelled. This involves a total of 1000 variables, requiring the use of a sophisticated differential equations solver. The FACSIMILE code [24] is used since it was originally developed for the solution of large, stiff problems such as this.

Calculations have been performed for four of the injection experiments in WAGR [5, 6], for which details of coolant composition are available, in order to assess the extent of conversion of methyl iodide to ethyl iodide and iodine atoms. Energy deposition rates were estimated as a fraction of full power rating from the length of time from shut-down to injection and the variation of decay heat with time. The results for the appropriate conditions can be seen in Table 1. Fig. 3 shows profiles of iodine species and radicals up the channel for the high temperature injection. The results are obviously very sensitive to both coolant composition and reactor conditions. The fractional destruction of methyl iodide is, however, almost independent of the channel inlet concentration over several decades, which simplifies application of the results in a plate-out model.

It is interesting to note that the destruction of methyl iodide is predicted to be higher under cold shutdown conditions than at normal operation. This could be due, in part, to the very low methane concentration (5 vpm) in the former experiment.

TABLE 1 : PREDICTION OF CH₃I CONVERSION IN WAGR INJECTION EXPERIMENTS

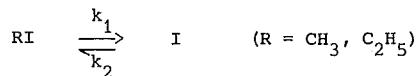
(The fractions of iodine species at the channel outlet following a single pass are shown)

EXPERIMENT	COOLANT* COMPOSITION	RATING (% FULL POWER)	E _{max} (mW/g)	FRACTION OF IODINE (%)		
				CH ₃ I	C ₂ H ₅ I	I
'High' Temperature	1.24 44 410 80	100	350	53.75	14.76	31.49
'Medium' Temperature	1.01 56 290 200	0.84	2.94	86.53	1.04	12.43
180°C	1.05 880 550 580	0.9	3.15	90.17	1.40	8.43
55°C low flow	0.12 5 35 50	0.4	1.40	13.98	1.71	84.31

*The coolant composition is shown in order as:- CO in volume %, CH₄, H₂O, H₂ in vpm respectively.

5. THE IMPACT OF RADIOLYSIS CHEMISTRY ON PLATE-OUT PREDICTIONS

The detailed reaction scheme outlined above is too complex to be included in a plate-out model of the whole reactor circuit. In our preliminary two species model [1], radiolysis in the core was represented by arbitrary first order rate constants for processes destroying and reforming methyl iodide. It is possible to cast the results of the detailed analysis in this form and derive pseudo-first-order rate constants specific to the experimental conditions, so eliminating the arbitrary element. Considering the scheme:



k_2 can be found from the product of the aggregate radical concentration (effectively constant) and the estimated recombination rate constant for R and I

($10^{-11} \text{ cm}^3 \text{ molecule}^{-1} \text{ s}^{-1}$ [25]). k_1 can then be adjusted to give the correct fraction of I atoms leaving the channel. Recombination of I atoms and radicals outside the core is negligible. The reactor circuit model therefore allows organic iodide/I atom interconversion only in the fuel channels and moderator graphite channels in the main radiation field.

The present version of the plate-out model itself involves only iodine atom deposition on the boiler steels, and is based on the conclusions of section 3 above. Adsorption is treated as non-activated, with a rate equal to a sticking probability times a surface collision rate. Desorption is treated as a simple activated process with an Arrhenius-type rate constant, although it is clear that a more complex desorption mechanism is needed.

Initial attempts at fitting the WAGR injection experiments using the overall model are promising. In particular, the initial removal rates for methyl iodide are in broad agreement with experiment, and the weak temperature dependence observed can be rationalised.

REFERENCES

1. E. M. Hood, A. R. Taig and P. N. Clough. "Plate-out Modelling in Assessing Fission Product Retention in Advanced Gas-Cooled Reactor Primary Circuits". Proc. International Meeting on Thermal Nuclear Reactor Safety, Chicago, August 1982 p 131. (NUREG/CP-0027).
2. J. J. Hillary. "The Behaviour of Iodine Species in the Windscale AGR". TRG Report 2012(W), 1970.
3. J. Barbier, G. Benezech, B. Cadet, J. Miribel and P. Sigli. "Piégeage et Desorption de l'Iode dans les Reacteurs Graphite Gaz". IRPA Proceedings, 1973.
4. D. A. Collins, A. E. McIntosh, R. Taylor and W. D. Yuille. "Experiments Relating to the Control of Fission-Product Release from Advanced Gas-Cooled Reactors". Journal of Nuclear Energy Parts A/B, 1966, Vol. 20, pp 97-122.
5. J. J. Hillary and J. C. Taylor. "Behaviour of Methyl Iodide in the Windscale AGR". Journal of the British Nuclear Energy Society, Vol 14, Number 2, pp 159-165, 1975.
6. F. J. Brightman, C. J. Chapman, J. A. Garland, R. Hargreaves and E. J. Higham. "The Windscale AGR Concluding Experiments: Circuit Activity Measurements". BNES Conference 'Gas Cooled Reactors Today', Bristol, Sept. 1982. Paper 120.
7. C. J. Chapman, D. V. Freck and R. L. Woolley. "Progress in Research on the Retention of Caesium and Iodine Fission Products by the Gas Circuit Surfaces in AGR's". Ibid. Paper 122.
8. J. A. Garland, A. C. Wells, E. J. Higham and I. C. Smith. "Experimental Study of the Deposition of Iodine and Other Fission Products in the Coolant Circuit of a CAGR". This Conference.
9. USNRC. "Technical Bases for Estimating Fission Product Behaviour During LWR Accidents". NUREG-0772 1981.

10. G. W. Horsley. "A Thermodynamic Appraisal of the Chemical Forms of Caesium and Iodine After Release from Defective Fuel Pins into the CAGR Coolant Circuit". AERE-R11197, 1984.
11. J. J. Hillary and J. C. Taylor. "The Release of Fission Products from AGR Type Fuel at Around 1000°C". TRG Report 2317(W), 1972.
12. R. A. Lorenz, M. F. Osborne, J. L. Collins, S. R. Manning and A. P. Malinauskas. "Behaviour of Iodine, Methyl Iodide, Caesium Oxide and Caesium Iodide in Steam and Argon". ORNL/NUREG/TM-25 1976.
13. E. Hoinkis. "A Review of the Adsorption of Iodine on Metal and Its Behaviour in Loops". ORNL-TM-2916, 1970.
14. J. M. Genco, W. E. Berry, H. S. Rosenberg, and D. L. Morrison. "Fission-Product Deposition and its Enhancement Under Reactor Accident Conditions: Deposition on Primary-System Surfaces". BMI-1863, 1969.
15. J. J. Hillary and M. G. Evans. Windscale Nuclear Laboratories. Unpublished Results.
16. M. F. Osborne, R. B. Briggs and R. P. Wichner. "Iodine Sorption on Low-Chromium Alloy Steel". ORNL/TM-7755, 1982.
17. S. L. Nicolosi and P. Baybutt. "Vapour Deposition Velocity Measurements and Correlations for I₂ and CsI". NUREG/CR-2713 (BMI-2091), 1982.
18. B. R. Bowsher, S. Dickinson, A. L. Nichols, J. S. Ogden and P. E. Potter. "Chemical Aspects of Fission Product Transport in the Primary Circuit". ANS Topical Meeting: Fission Product Behaviour and Source Term Research. Snowbird, July 1984.
19. H. S. Rosenberg, J. M. Genco, and D. L. Morrison. "Fission-Product Deposition and Its Enhancement Under Reactor Accident Conditions: Deposition on Containment-System Surfaces". BMI-1865, 1969.
20. D. Cubicciotti and J. H. Davis. "Release of Iodine from Iodide Salts by Gamma Radiolysis". Nuclear Science and Engineering Vol. 60, p 314, 1976.
21. L. F. Parsly, "Chemical and Physical Properties of Methyl Iodide and its Occurrence Under Reactor Accident Conditions". ORNL-NSIG-82, 1971.
22. D. J. Norfolk, R. F. Skinner and W. J. Williams. "Hydrocarbon Chemistry in Irradiated CO₂/CO/CH₄/H₂O/H₂ Mixtures". Radiation Physics and Chemistry Vol. 21, p 307, 1983.
23. A. Dyer (Ed). "Gas Chemistry in Nuclear Reactors and Large Industrial Plant". Sections III and IV, Publ. Heyden, 1980.
24. E. M. Chance, A. R. Curtis, I. P. Jones and C. R. Kirby. "Facsimile: A Computer Program for Flow and Chemistry Simulation, and General Initial Value Problems". AERE-R 8775, 1977.
25. T. F. Hunter and K. S. Kristjansson. "Optoacoustic Method of Measuring Reaction Rates of the Radicals CH₃, CD₃, C₂H₅ and CH₂I with I and I₂". Journal of the Chemical Society, Faraday Transactions 2, Vol. 78, p 2067, 1982.

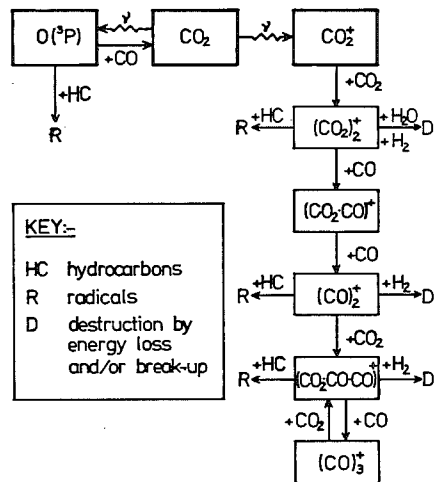


FIGURE 1 : Schematic of CO₂ Radiolysis Product Reactions.

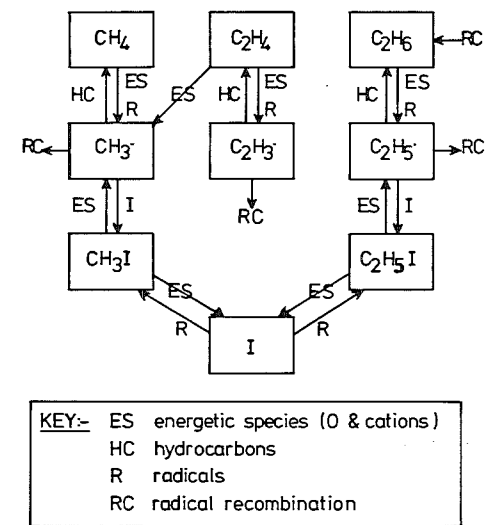


FIGURE 2 : Schematic of Organic Species Reactions.

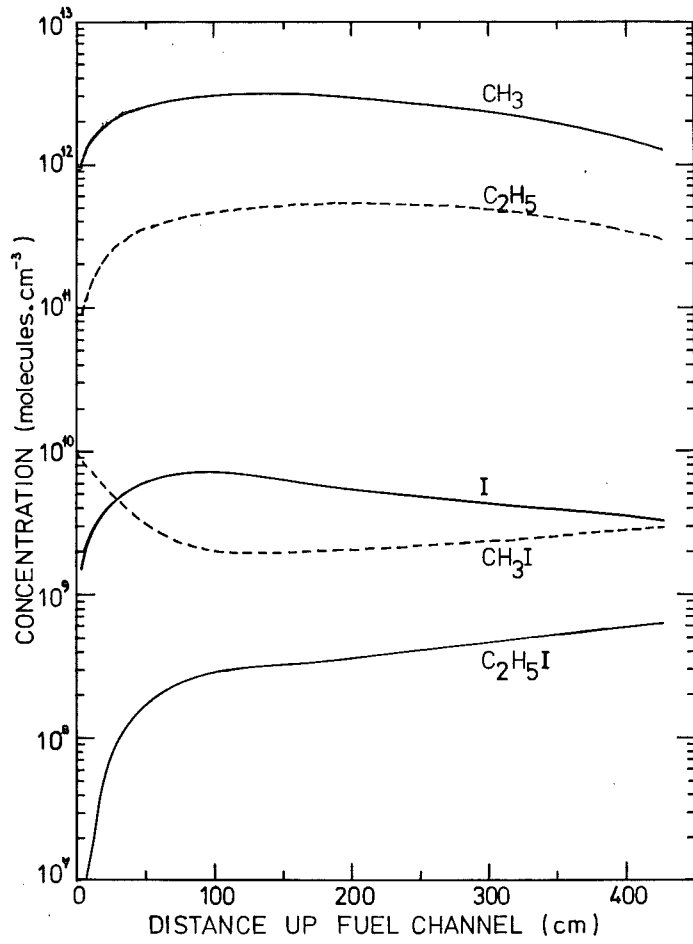


FIGURE 3 : Profiles of Radical and Iodine Species Concentrations in a WAGR Fuel Channel for the High Temperature Injection. (Concentration of methyl iodide at channel inlet is 10^{10} molecules cm^{-3})

Recent Developments in Nuclear Aerosol Research
Related to Thermal Reactor Safety

by

F. Abbey
Safety and Reliability Directorate, UKAEA
Culcheth, Warrington, UK

and

W. O. Schikarski
Kernforschungszentrum Karlsruhe GmbH
Laboratorium für Aerosolphysik und Filtertechnik I
7500 Karlsruhe, W.-Germany

ABSTRACT

This paper reports on the outcome of a Specialist Meeting on Nuclear Aerosols in Reactor Safety held at KfK Karlsruhe, 4-6th September, 1984, under the joint sponsorship of the Committee on the Safety of Nuclear Installations of the NEA, The German Nuclear Society and the Association for Aerosol Research, and under the co-chairmanship of the present authors. Although the Specialist Meeting covered nuclear aerosols in all reactor systems, and some fuel cycle facilities, this report is limited to aspects relevant to thermal reactors, and in particular LWR's. The paper is structured on the same basis as the meeting and reviews the highlights, including important results presented and recommendations for further research.

1. Introduction

The purpose of this paper is to report on a specialist meeting on nuclear aerosols in reactor safety held at KfK under the co-chairmanship of the authors immediately prior to the present ENS/ANS meeting (4-6th September, 1984), insofar as the topics discussed at the meeting are relevant to thermal reactor systems.

The prediction of fission product transport, deposition and release associated with postulated nuclear accidents is necessary for the assessment of radiological consequences, and hence is an essential element in reactor safety evaluation. And, since many of the fission products transport and deposit as aerosols, the study of aerosol behaviour is an important part of this problem. Nuclear aerosols can also affect the course as well as the consequences of reactor accidents, for example via their effect on the performance of engineered safety features such as the containment and air-cleaning systems.

Because of the high concentrations and extreme environments in which nuclear aerosols may exist they exhibit very dynamic physical and chemical behaviour and pose special analytical and experimental problems different from those associated with aerosols found under industrial and ambient conditions. In 1978 an expert group on nuclear aerosols in reactor safety was established by the Committee on the Safety of Nuclear Installations (CSNI) of the NEA. In June of 1979 this group issued a state-of-the-art report /1/, and a specialist meeting was held subsequently in April, 1980, at Gatlinberg in the USA. The emphasis in these early activities was on nuclear aerosol behaviour in LMFBR systems, and in 1981 following the TMI-2 accident, CSNI reconvened the expert group with a request to prepare a supplementary state-of-the-art report /2/ with particular reference to new information which had become available since the original document and which is relevant to accidents involving extensive core damage in LWR's. The

final meeting of the group, held in March 1983, recommended that a second specialist meeting be held in mid-1984.

It is this meeting, jointly sponsored by CSNI, the German Nuclear Society, and the Association for Aerosol Research, to which the present paper refers. The objectives of the meeting were to provide a forum for the exchange of information between aerosol research specialists, reactor designers and regulators. The paper reviews the highlights of the meeting and notes important results presented and recommendations made for further research related to nuclear aerosols in LWR safety. The treatment follows the main topic areas adopted for the meeting.

2. Aerosol Formation (Session I)

Aerosol formation, in this context, is concerned with the nature of the gas-borne particulate matter generated in a nuclear accident immediately after and in the immediate vicinity of its initial formation by vaporisation/nucleation/condensation or fragmentation processes, i.e. it is concerned to define the input to the subsequent treatment of the transport and release of the aerosol through the reactor system to the environment. In severe LWR accidents liquid (water) aerosols may be formed in the containment by blowdown of the coolant. Solid aerosols can also be formed in the reactor coolant circuit (RCS) by vaporisation and condensation of volatile materials from an overheated core, and in the containment as a result of discharging the core materials from the reactor pressure vessel (RPV) when the failure occurs at pressure, or by interaction between the core materials and the concrete of the containment.

Both the chemical and physical forms of the aerosols will, in principle, influence their subsequent transport and release. Apart from the more obvious characteristics of particle size etc, the solubility of the solid aerosols in water may have an

important influences on steam condensation in the containment in the case of the LWR.

Substantial programmes of research are currently in progress worldwide in all these areas, and need to be continued.

The work of Albrecht et al in Germany, which provides the principal data base for evaluating the amounts of core materials released during the in-vessel core melt phase of a severe LWR accident, has recently been extended /3/ to include measurements of the chemical speciation of the aerosols formed, using X-ray photo-electron spectroscopy. In these experiments with simulated core mixtures, the materials principally released as aerosol were fission product iodine, caesium and tellurium, and cadmium, indium and silver from the neutron absorber rods. Over most of the temperature range (1275 - 1900°C) the neutron absorber materials were the dominant contributors, and at the higher temperatures there was a significant enrichment of the less volatile indium and silver. The principal chemical forms detected were caesium and silver iodides, caesium hydroxide, tellurium metal, cadmium hydroxide, indium oxide and silver metal. For the principal hazardous fission products iodine and caesium this is in accord with predictions based on thermodynamic and kinetic studies. For the aerosols generated at the higher temperatures the surface composition was significantly different from the bulk, showing an enrichment of the more volatile iodine, caesium, cadmium and indium.

Other experiments have placed emphasis on the physical form of the aerosols generated from the neutron absorber materials. Experiments in the UK /4/ in which the steel cladding of the absorber rod was simulated showed that, at low pressure in argon, the aerosols were composed of spherical submicron particles which rapidly coagulate to form chain-like structures. The primary particle size distribution is in good agreement with the measurements of Parker /5/ on aerosol

formed in a hydrogen-argon atmosphere by the condensation of cadmium vapour from a plasma torch. However, the formation of such extensive agglomerates in a steam environment is questionable.

3. Aerosol Processes (Session II)

The modelling of aerosol processes is of great significance for the development of nuclear aerosol codes applicable to the primary or containment systems of nuclear power plants. A review of the most important aerosol processes is given in /1/. Continued research has provided a better understanding of some processes and generated a large amount of new information which was not discussed in /1/ but which is included in /2/. In this section we report only on some new developments in the research on nuclear aerosol processes which are relevant to thermal reactor safety.

It has long been recognized that the shape factors of nuclear aerosols are important for most aerosol processes. Under LWR accident conditions steam condensation leads to compaction and spherification of agglomerates. Small spatial and temporal inhomogeneities in the containment atmosphere are sufficient to cause a permanent condensation and evaporation on and from particles and, therefore, a continuous compaction. This spherification effect leads under most LWR accident conditions to a value of unity for the dynamic coagulation and condensation shape factor /6/. There are also new results on shape factors under dry conditions. As reported in /7/ the coagulation shape factor of UO_2 particles has been measured for the first time. It is interesting to note that according to these experiments the dynamic shape factor and the coagulation shape factor have approximately the same value.

Diffusiophoresis and/or thermophoresis can be of major importance for the wall plate-out of nuclear aerosols under LWR accident conditions. Diffusiophoresis occurs when steam condenses on the wall, thermophoresis may occur also without steam, if a temperature gradient exists in the boundary layer at the wall. The

temperature gradient causing the particle movement primarily induces a sensible heat flux in the case of thermophoresis and a latent heat flux in the case of diffusiophoresis. It has been shown that the diffusiophoretic deposition rate is proportional to the mass flux of condensing steam and the thermophoretic deposition rate is proportional to the sensible heat flux. These fluxes can be obtained with reasonable accuracy from thermodynamic calculations compared to earlier deposition rate estimates by means of the boundary layer thicknesses. Furthermore, it has been shown that for the diffusiophoretic deposition the mass flux can be substituted by the overall condensation rate /8/, which was verified experimentally. A satisfactory mathematical description of diffusiophoresis and thermophoresis is now possible, at least under the conditions of a LWR accident scenario.

Another aerosol process still under consideration is the gravitational coagulation. Here the formulation of the collision efficiency of particles under coagulation has been discussed. Different aerosol codes use different factors in the gravitational collision kernel which leads to large discrepancies in code predictions when gravitational coagulation is important. Further experimental and theoretical work seems to be necessary.

A number of other aerosol processes important under the special conditions of a nuclear aerosol system were discussed at the meeting. Since they are relevant to LMFBR safety only or of minor importance for the accuracy of aerosol code predictions in LWR scenarios no detailed discussion is given. Rather, the reader is referred to the literature /2/, /9/.

4. Inter-relation of Thermal-hydraulics and Aerosol Behaviour (Session III)

The sensitivity of aerosol behaviour predictions to the estimated thermal-hydraulic conditions has always been recognized. For example, uncertainty regarding the thermal-hydraulic conditions in the upper plenum is one of the major uncertainties in predicting aerosol transport and retention in the primary system of a LWR. Additional or improved data are required in a number of areas.

However, current computer codes generally make two further basic assumptions 1) each control volume within the code is treated as well mixed up to any surface boundary layers, so that a single node treatment will suffice, 2) thermal-hydraulics and aerosol behaviour are regarded as separable in the sense that there is no back coupling from aerosol behaviour to thermal-hydraulics; hence the thermal-hydraulic conditions can be evaluated separately and are then used as input data for the aerosol equations. The validity of both of these assumptions may now be open to question.

Recent thermal-hydraulic measurements taken on the DEMONA model containment facility (see Section 7) show that convective mixing is often not strong enough to overcome stratification effects /10/. Further DEMONA evaluation will show what degree of accuracy can be achieved in this situation using single node aerosol codes, and which simplifications appear permissible.

It has also been suggested /11/ that aerosol behaviour may affect the thermal-hydraulics in a number of ways and that it may not always be possible to neglect the back coupling, e.g. as a determinant of the spatial distribution of the associated decay heat, (the question of possible revaporisation of fission products initially deposited in the primary system mentioned in Section 6 may be a case in point here), or, as suggested in Section 2, by solubility effects on steam condensation in the containment. This is an area which needs further attention.

A detailed theoretical investigation has been made /12/ of aerosol nucleation and growth by condensation in the formation and cooling of vapour-gas mixtures, applicable for example to the condensation of fission product vapours in the primary system or steam condensation in the environment. It is shown that experimental and computer modelling must accurately represent heat as well as mass transfer processes. There is room for improvement in this respect in the current modelling of the condensation of fission product vapours in the primary system, which may significantly overestimate the amount of aerosol formed.

5. Aerosol Measurement and Generation Techniques for Large Scale Experiments (Session IV)

Nuclear aerosol measurement techniques comprise most other aerosol measurement techniques if they comply with the conditions which usually occur for nuclear aerosols, namely high concentrations, high temperature and pressure and eventually high humidity. Of particular significance is the application of nuclear aerosol instrumentation in experiments where aerosol formation, behaviour and retention is investigated, since then the accuracy of aerosol measurement is in competition with the accuracy of code calculations.

In this context intercomparison tests of various aerosol measurement techniques for sodium fire aerosols/13/ have been carried out. Groups of five countries participated with six cascade impactors of different type, one spiral centrifuge, one sedimentation battery and one inertial spectrometer. Two groups also performed image analysis of particles. The aerosol investigated was NaOH and Na₂CO₃ particles with Na-mass concentrations between 60 and 1,200 mg/m³. All instruments used produced aerosol data that were in reasonable agreement. The individual aerodynamic mass median diameters were within approximately $\pm 20\%$ and the σ 's were generally within $\pm 50\%$ of the sample mean values. This indicates that sodium aerosol measurement techniques of sufficient accuracy are available and major problems could be judged to be solved.

Particle size distribution measurements for high mass concentrations of test aerosols and for high temperatures have been carried out by means of a cascade cyclone aerosol sampler. It was found that the cyclone performance depends not only upon the gas viscosity but also on the gas density/14/. The cascade cyclone seems to be a new method of nuclear aerosol classification, where high particle loads in high temperature streams are involved.

Another example of the successful application of nuclear aerosol measurement techniques is the aerosol measurement system used in the DEMONA Experiments /15/. The system is designed to perform under extreme conditions (high pressure, high temperature, high aerosol concentration and steam saturated atmosphere) in the 640 m³ vessel. This almost excludes the use of conventional aerosol measurement techniques which are commercially available. Additionally, the aerodisperse system to be measured consists of solid particles, liquid particles (droplets), and an air-steam mixture carrier gas, and the mass concentration, particle size distribution, density and form of particles and the mass of condensed water are to be determined as function of time and location. The solution of this complex aerosol measurement task consists of different techniques, namely

- filtration devices of special design to prevent steam entrainment
- cascade impactors protected against steam
- inertial spectrometers protected against steam
- photometers for integral aerosol concentration measurement protected against temperature and steam
- optical spectrometer for droplet measurement protected against steam and temperature
- calorimeter for measurement of airborne water content

It could be judged as a major accomplishment that all these new nuclear aerosol measurement techniques have been developed and pretested successfully. The use of these techniques in the dry DEMONA tests has so far demonstrated reasonable performance. Application to the wet tests of DEMONA is scheduled later this year.

Nuclear aerosol behaviour simulation experiments require the production of high aerosol mass concentrations in large volumes. For the DEMONA tests an aerosol generator system has been developed with an aerosol production rate of about 100 g/min metal oxide particles. Based on an aerosol generator design developed at ORNL three 80 kW plasma guns blowing the metal powder into a burning chamber resulting in wall temperatures of up to 1500°C have been developed. The heating in the plasma provides melting of the powder and subsequent oxidation and evaporation of the particles, which finally recondense. The performance of the generator has been demonstrated up to 3 bars system pressure. This aerosol generation method for producing high mass concentrations and high production rates has been tested and shown to produce adequate aerosols of reasonable size and shape. There are, however, still improvements necessary in order to avoid aerosol material losses due to insufficient material transport through the feedline of the system.

6. Aerosol Behaviour in the Primary System, Experimental Investigations (Session V)

Studies of aerosol transport and deposition in the primary system have not progressed to the same degree as the equivalent containment studies.

One of the important recommendations of the Supplementary Report of the OECD-CSNI expert group on nuclear aerosols in reactor safety was to perform realistic, large scale experiments on aerosol transport in the primary system of an LWR. An international series of experiments of this kind has recently been

initiated and is in progress using the Marviken reactor in Sweden. The objectives of the experiments are to provide a demonstration of aerosol retention, and to establish a data base for code validation purposes. An attempt is being made to provide as realistic conditions as possible, particularly thermal-hydraulic conditions, though high pressures are excluded by the limitations of the facility. The behaviour of the volatile fission products (iodine and caesium - "fissium") and the more refractory constituents of the core ("corium") are being studied separately and in combination, the aerosols being generated respectively by means of a furnace and a plasma torch. A programme of supporting separate effects test is associated with the Marviken experiments.

A primary circuit code validation test programme is also being carried out at ORNL in the USA /16/ incorporating both aerosol transport tests to simulate upper-plenum transport and deposition, and aerosol resuspension tests. The major results to date of the aerosol transport tests show that the fraction of aerosol transported out of the vertical pipe which is used to simulate the upper plenum is influenced by the flow residence time, and, via thermophoresis, by the thermal gradients produced at the walls. So far code comparisons with measured aerosol plate-out have been better than comparisons with aerosol settling. By contrast with earlier experiments the resuspension test have been performed with a range of particle sizes and with dense deposits of the kind which may be produced in reactor accidents. The results show that smaller particles ($< 1\mu\text{m}$ diameter) are more difficult to resuspend. Both transport and resuspension tests will be continued.

The research programmes described provide for most of the questions related to aerosol behaviour in the primary system. However, one question not addressed, by definition since the simulant aerosols used are inactive, is the effect of the decay heat associated with the deposited materials on the thermal-hydraulic conditions prevailing in the primary system. If the temperature

of the deposited material increases sufficiently there may be the possibility of re-vaporisation, particularly in the later stages of an accident. The potential importance of this problem needs to be established.

7. Aerosol Behaviour in the Containment - Large Scale Experiments, Comparison to Aerosol Codes (Session VI & VII)

The OECD-CSNI expert group on nuclear aerosols in reactor safety /1/ also recommended large scale experiments on aerosol behaviour, in LWR containments under accident conditions. This has been implemented recently by several laboratories. In addition, research has been done on aerosol behaviour under LMFBR accident conditions. Although in both cases different types of nuclear aerosols have been used the main aerosol processes involved (see section 3) are the same except the steam condensation process for LWR accident conditions. For LWR conditions the large scale experiments which have been carried out or are underway, include the ORNL-program in the Nuclear Safety Pilot Plant (NSPP), the HEDL-program (LACE) in the Containment Systems Test Facility (CSTF) and the KfK-program in the Model Containment of Battelle-Frankfurt (DEMONA). In addition, the FAUNA-program at KfK and the ABCOVE-program at HEDL should be mentioned although not directly related to LWR safety.

Preliminary results of the NSPP, LACE and DEMONA programs show typical decay curves of aerosol mass concentration as predicted by aerosol codes. A strong influence of steam condensation was observed. Questions to be answered by these experimental programs are:-

- Is the aerosol mass concentration time function influenced by the chemical properties of the aerosol (as suggested by NSPP data)?
- What are the resuspension mechanism and are they sufficient to resuspend significant quantities of radioactive aerosols? What are the physical nature and the aerosol characteristics of resuspended material (as investigated in the LACE and the NAUA program)?

- Are there significant aerosol depletion processes in the primary system piping and/or in the auxiliary building path ways to reduce the aerosol source term into the containment (as investigated in the LACE program)?
- Is the homogenous mixing hypothesis - as applied in all aerosol codes so far - valid for all significant accident scenarios (as investigated in the DEMONA program)?
- What is the influence of accident scenario dependent thermal hydraulics on aerosol behaviour (as investigated in the DEMONA, NSPP and LACE programs)?

The intercomparison of aerosol codes has been done for the case of sodium oxide aerosol behaviour by an expert group in cooperation with the CEC /17/. Except for the code AEROSOLS/A2, which uses the assumption of a lognormal particle size distribution, all codes predict the leaked aerosol mass within a range of 10% (reference case). The sensitivity analysis showed that the aerosol code results depend strongly on the collision efficiency, the coagulation shape factor, the turbulent energy density dissipation rate and the dynamic shape factor. In order to reduce uncertainties further analysis should be devoted to these parameters.

Similar intercomparisons of aerosol codes related to core melt scenarios in LWR accidents is underway in cooperation with OECD-CSNI and CEC. For the first dry experiments in the DEMONA program pre-test calculations of the aerosol mass concentration time function were made /18/. Here the uncertainty was about a factor 2 reflecting the lack of knowledge in the initial particle size distribution, aerosol production rate etc. The post-test calculation of aerosol mass concentration time function, however, lies within the error band width due to uncertainties in the measurement techniques. Whether this favourable result will hold also for the forthcoming wet tests in the DEMONA program cannot be decided at this time, since additional uncertainties could occur due to the influence of thermal hydraulics on aerosol behaviour.

8. Conclusions

Very substantial progress has been made in the understanding of nuclear aerosol behaviour in LWRs, since the previous CSNI Specialist Meeting held in Gatlinburg, USA, in 1980. However, further research is required in a number of specific areas.

The conclusion and recommendations of the CSNI supplementary SOAR /2/ regarding areas where further research is required were generally endorsed by papers at the meeting.

REFERENCES

1. Nuclear Aerosols in Reactor Safety, NEA/OECD, June, 1979.
2. Supplement to Nuclear Aerosols in Reactor Safety, NEA/OECD, to be published 1984.
3. H. Moers et al., Chemical State Evaluation of the Constituents of Aerosol Particles Formed in LWR Core Melting Experiments, Specialist Meeting on Nuclear Aerosols in Reactor Safety, Karlsruhe, F.R. Germany, 4th-6th September, 1984, NEA/OECD.
4. J. P. Mitchell, A.L. Nichols and J. A. H. Simpson, The Characterisation of Ag-In-Cd Control Rod Aerosols Generated at Temperatures below 1500 °C, *ibid.*
5. G.W. Parker, G. E. Creek and A. L. Sutton, in NUREG/CR-2299, Vol. 4, 12, 1982.
6. W.Schöck, Recent Developments in Research on Nuclear Aerosol Processes, Specialist Meeting on Nuclear Aerosols in Reactor Safety, Karlsruhe, F. R. Germany, 4th-6th September, 1984, NEA/OECD.
7. W. Zeller, Direkte Messung von Aerosolformfaktoren, KfK 3560, Dez. 1983.
8. W. Schöck et al., Spatial Distribution of an Aerosol in a Large Structured Building, First Joint International Aerosol Conference, Minneapolis, Minnesota, USA, 17th - 21th September, 1984
9. W. Schikarski et al., DEMONA, Forschungsprogramm zur Demonstration nuklearen Aerosolverhaltens, KfK 3636, EIR 502, Dez. 1983
10. T. F. Kanzleiter, Thermal-Hydraulic Behaviour of a Containment Atmosphere Measured in the DEMONA Experiments, Specialist Meeting on Nuclear Aerosols in Reactor Safety, NEA/OECD
11. T. S. Kress, Simultaneous Coupled Solution of the Thermal-Hydraulic and Aerosol Behaviour Equations for Source Term Determination, *ibid.*
12. C. F. Clement, Aerosol Nucleation and Growth and Their Coupling to Thermal-Hydraulics, *ibid.*

13. S. Jordan et al., Intercomparison Test of Various Aerosol Measurement Techniques for Sodium Fire Aerosols, *ibid.*
14. K. W. Lee, A. Gieseke, W. H. Piispanen, Calibration of Cascade Cyclone Aerosol Sampler, *ibid.*
15. G. Friedrich et al., Aerosol Measurement System for the DEMONA Experiment, *ibid.*
16. A. L. Wright and W. L. Pattison, Results from Simulated Upper-Plenum Aerosol Transport and Aerosol Re-suspension Experiments, *ibid.*
17. I. H. Dunbar, Aerosol Behavior Codes: Development, Inter-comparison, and Application, *ibid.*
18. H. Bunz, W. Schöck, Comparison of Measured Aerosol Behaviour during DEMONA Experiments to NAUA Code Predictions, *ibid.*

THE DEMONA PROJECT

OBJECTIVES, RESULTS AND SIGNIFICANCE TO LWR SAFETY

W. Schöck, H. Bunz, W. Schikarski
KfK/LAF I, Karlsruhe, Germany

J. P. Hosemann
KfK/PNS, Karlsruhe, Germany

D. Haschke
EIR, Würenlingen, Switzerland

T. F. Kanzleiter, T. Schröder
Battelle-Institut e.V., Frankfurt, Germany

M. Fischer, K. Hassmann, M. Peehs, H. Ruhmann
KWU, Erlangen, Germany

ABSTRACT

The development of the NAUA code has been finalized with the completion of version Mod5. The code calculates aerosol behaviour in the containment system of an LWR during core melt accidents. As a final demonstration of the ability of the code to calculate the overall aerosol behaviour correctly, the large scale experimental project DEMONA is underway. The experiments are conducted in the model containment facility at Battelle Frankfurt. Accident conditions during the aerosol depletion phase in the containment are reproduced as closely as possible, because also the thermodynamics code COCMEL is being validated. DEMONA is supported and conducted as an international project with participations from Switzerland and Germany.

A thermodynamic test of the facility and the instrumentation was conducted and the leak rate of the (unlined) containment was measured to be 70 %/d. Two dry aerosol behaviour test are reported using tin oxide and iron oxide aerosol. In both cases the agreement of measured mass concentration with post test calculations was excellent. For the tin oxide aerosol test pre test predictions with the NAUA code were in good agreement with measured data, too.

INTRODUCTION

In the years following the publication of the Reactor Safety Study /1/ and the German Risk Study Phase A /2/ extensive analytical and experimental work has been carried out in the field of fission product retention capability of the reactor containment system. These worldwide efforts have been stimulated further by the TMI 2 accident which demonstrated possible low consequences of severe accidents. The efforts were first concentrated on particulate fission products which had not been treated very detailed in the risk studies. A much larger retention of aerosols in the containment than expected earlier was found in model calculations and partly confirmed by experiments. As a consequence the highly volatile fission products, mainly iodine, then dominated the risk associated to nuclear accidents. This in turn triggered more work in the field of iodine chemistry in particular, or fission product chemistry in general. The today's picture is that the volatile forms of iodine are much less likely to occur and persist than assumed previously and that non-volatile iodides will be formed by reactions with airborne particulates or in the sump provided they have not already been released to the containment in particulate form.

So, except for the noble gases, all fission products are in the form of or may react with particulate airborne matter, aerosols, in the containment. The prediction of aerosol behaviour in the containment, therefore, is a central part in all calculations of fission product transport and depletion in nuclear accidents.

DEMONA, OBJECTIVES AND METHODS

At present three large scale ($>100 \text{ m}^3$) experimental aerosol projects in the field of LWR safety are being conducted: MARVIKEN V, LACE and DEMONA. The necessity of coordinating these efforts has been recognized from the beginning to avoid duplications and to provide the links between them. The interest of the DEMONA project is only in aerosol behaviour in the containment, to demonstrate the effectiveness of natural aerosol depletion processes as calculated with the NAUA code. The NAUA code development is considered to be completed with version Mod5 which, in addition to Mod4 /3/, contains a module for diffusio-phoretic deposition /4/. An additional aim of the DEMONA project is to validate a suitable thermodynamics code which generates the required input data for NAUA. In DEMONA the single volume code COCMEL /5/ and the multi zone code FIPLC /6/ are being applied. The DEMONA project is jointly conducted by KfK Karlsruhe, Battelle Frankfurt, The Swiss Federal Institute for Reactor Research Würenlingen, and KWU Erlangen /7/.

The experiments are conducted in the model containment test facility at Battelle Frankfurt which is a 1 : 4 scale model of the Biblis containment (Fig. 1). The model containment is constructed of concrete (without liner) which gives thermodynamic characteristics very similar to a real power plant.

Table I contains the test matrix for DEMONA. The tests are variations of the base case which is a simulation of a low pressure core melt accident with late overpressure failure of the containment. This is simultaneously the scenario with the highest probability of occurrence and the situation in which the aerosol behavior has to be calculated over the longest period of time and is therefore best suited to check the validity of the results.

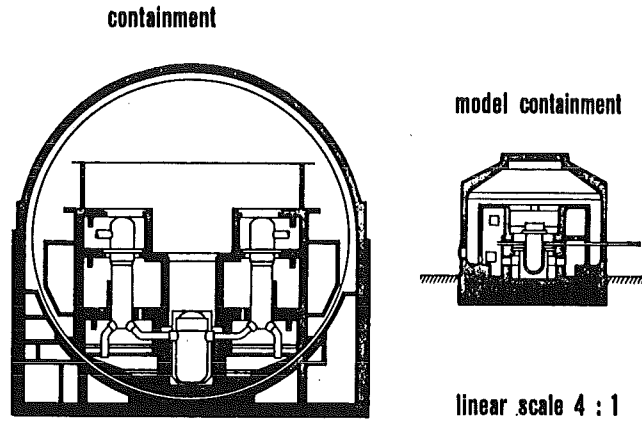


Fig. 1: Size Comparison of PWR and DEMONA containments

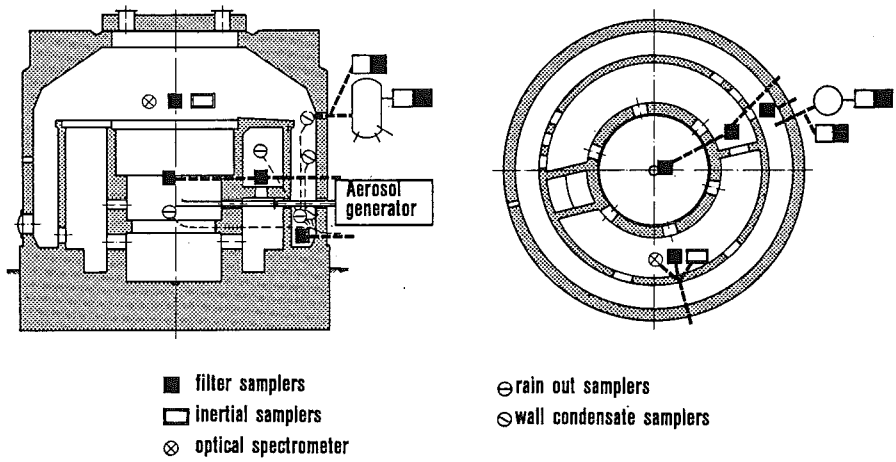


Fig. 2: Aerosol measurement instrumentation in the DEMONA containment

1. Thermodynamic test of the model containment
2. Dry aerosol test
3. Base experiment
4. Variation: weak aerosol source
5. Variation: transient thermodynamics
6. Variation: complex geometry
- 7.-9. Spare tests, if needed
10. Final demonstration experiment

Table I: DEMONA test matrix

The aerosols for the experiments are non-radioactive metal oxides. Three plasma torch aerosol generator units of 80 kW each have been installed to vaporize and oxidize metal powders /8/. The oxide vapor condenses when cooled and forms an aerosol of aggregates of very fine primary particles which is fed into the containment. The mass concentration of the aerosol is up to approximately 10 g/m³. The containment atmosphere is a condensing saturated steam air mixture at 115 °C temperature and 3 Bar total pressure.

Considerable efforts have been made in the development of the instrumentation of the test facility. The thermodynamic instrumentation /9/ measures temperatures of gas, walls and sump at many locations, pressure and composition of the atmosphere, mass and heat input rates, leak rates, heat transfer coefficients and the concentration of liquid airborne droplets. The aerosol instrumentation /10/ measures mass concentration, particle size distribution, spatial distribution and deposits on walls and floors. Chemical composition and morphology can be evaluated from samples taken at different locations in the containment. Besides the mass concentration of airborne droplets also their size distribution will be measured.

In Fig. 2 the locations of some of the instruments are shown. In the containment filter sampling stations, inertial devices, an optical size spectrometer and wall and floor samplers are distributed. An extraction line with an auxiliary dilution tank feeds additional instruments such as mass monitor, impactor, samplers etc. Not shown in Fig. 2 are ten identical photometers which measure the spatial distribution of the aerosol.

Pre test calculations of the thermodynamics and of the aerosol behaviour are being conducted for each experiment. After the experiment post test calculations are done using the actual experimental parameters. Both calculations are compared to the measured data. For each individual experiment of the test matrix a separate report is published.

RESULTS OF THE THERMODYNAMICS TEST

The thermodynamics test /11/ was performed to check the function of the facility and of the instrumentation under the conditions of the planned experiments. The behaviour of the containment was tested and its thermodynamic behaviour was measured and compared with calculations with the codes COCMEL and FIPLOC. Further the aerosol instrumentation was tested under layout conditions.

The course of the experiment, which is representative for most of the experiments of the test matrix, can be subdivided into four phases:

1. Heat up phase: The model containment is heated by steam injection until a steady state is reached. At the beginning of this phase the air is expelled and the heating of the structures and walls is performed with pure steam which gives a very uniform temperature increase. At the end of this phase, after approximately two days, the temperature is 115 °C and the internal structures are almost saturated.
2. Air injection phase: Air is injected to establish the desired atmospheric composition. This phase corresponds to the aerosol generation period in the later experiments. Air, steam and aerosol is injected until the total pressure is 3 Bars after about 2 hours.
3. Measurement phase: This is, in the later experiments, the period of interest in which the aerosol depletion will be measured. In this phase the total pressure is kept constant at 3 Bars by steam injection to make up for pressure losses due to condensation and leakages. During the thermodynamics test the leak rate of the containment was measured in this phase.
4. Cooling phase: Cooling and venting of the model containment after the end of the measurement phase will last approximately 3 days until the temperatures are low enough to enter the facility and recover the instruments and in situ samples.

The main aim of the thermodynamics test, besides testing the performance of the equipment, was to measure the leak rate of the model containment. The leak rate has to be known for the NAUA calculations and was postulated not to exceed 200 %/d. It has to be recalled that the model containment has concrete walls without liner. The leak rate was determined by measuring the change in the composition of the atmosphere with four independent methods. Since only steam is added during the measurement phase the steam air ratio will increase slowly as air leaks out of the containment. From the decrease of the air partial pressure the leak rate can be calculated.

During the phases 2 and 3, however, a significant gradient in the atmospheric composition developed in a few hours. In the lower dead volumes steam was depleted by condensation, in the upper part steam was enriched and could not be transported to the depleted zones. Since the total pressure was kept constant this also led to a temperature gradient, the temperature increasing from bottom to top. In the given geometric configuration of the test this effect was stronger than the counteracting mixing effects of natural convection.

As a result of all this the atmospheric composition varied not only with time but also with space. However, since it was measured at 14 different locations a weighted mean could be determined and a value of 70 %/d was obtained for the leak rate which is well below the postulated limit.

The comparison of measured thermodynamic data with model calculations was of course complicated by the inhomogeneous conditions in the containment. The single volume model COCMEL could only calculate average values which, nevertheless, were in good agreement with measured data, especially for temperature and pressure build up during the heat up phase and for steam condensation rates. For further experiments with stronger natural convection COCMEL is expected to give representative results. On the other hand a FIPLC calculation with 22 zones modelled showed the observed inhomogeneities very well. Therefore, the thermodynamic behaviour of the model containment can be considered as completely understood.

RESULTS OF DRY TESTS

The dry test of the test matrix, without the influence of condensation and diffusiophoresis on aerosol behaviour, is intended to serve as a comparison case for the wet tests. The dry test is conducted at ambient temperatures but with 3 Bars pressure which are built up during the aerosol generation. Two different dry tests will be reported here:

- V 23 with tin oxide aerosol with a peak concentration of 5 g/m^3
- V 20 with iron oxide aerosol with a peak concentration of 1.6 g/m^3

Fig. 3 shows measured and calculated mass concentrations of the aerosol during test V 23. The aerosol generation was essentially in two periods the first producing 5 g/m^3 of aerosol the second adding 1 g/m^3 after 4 hrs. The dashed line is a pre test calculation with constant source and leak rate. The solid curve represents a NAUA post test calculation taking into account the measured time functions for aerosol source and leak rate. The other data are measured concentrations at five different locations in the model containment.

First of all and most important it can be seen that pre test calculation as well as post test calculation and measured data all agree within a factor of 2 (shaded area), which is a very encouraging result. The differences between pre test calculation on the one side and post test calculation and measured data on the other can be fully explained by unexpected deviations in the experiment which could not have been taken into account for the pre test calculation. These are:

- In the first four hours of technical problems lead to an intermittent operation of the aerosol generators. Consequences to the aerosol system were enhanced convection and input of sensible heat both resulting in an increased overall depletion rate. This explains the steeper slope of the mass concentration curve during the first four hours as compared to the pre test calculation.
- The leak rate of the containment decreased from initial 110 %/d to 50 %/d after 20 hours due to pressure drop and clogging of the leak paths. This explains the slower decrease of the long term mass concentration as compared to the pre test calculation for which a constant leak rate of 100 %/d had been assumed.

These two corrections in the input data for NAUA proved to be sufficient to give the good agreement between measured data and post test calculations. Another experimental result which was different from the pre test assumptions but had very little influence on the calculated mass concentration concerns the particle shape. For a "dry" test no condensation was assumed and particle shape factors of 2 were used in the pre test calculation. However, the compressed air which was used to cool the aerosol generators and to transport the aerosol contained enough excess humidity to condense temporarily on the particle. No indication of a condensational growth of the particles was obtained but all particles showed the well known spherification process during the early phases of the experiment. Aggregates formed later were not spherified again. Thus in the post test calculation shape factors of 1 were used with an effective density of 50 % of the aerosol material density.

Another case of deviations from pre test assumptions was observed in test V 20. Fig. 4 shows pre test calculation, measured data at eight locations and post test calculation of the mass concentration during V 20. Here a very rapid decrease of the aerosol concentration during the first hours of the experiment

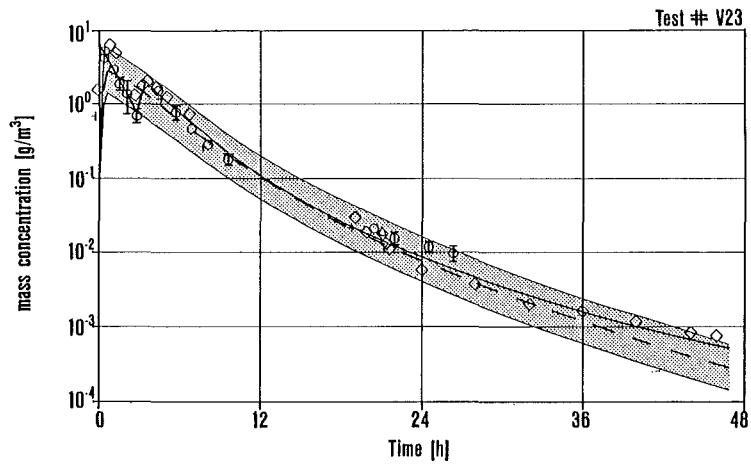


Fig. 3: Pre test calculation (dashed line), post test calculation (solid line) and measured data for DEMONA test V23

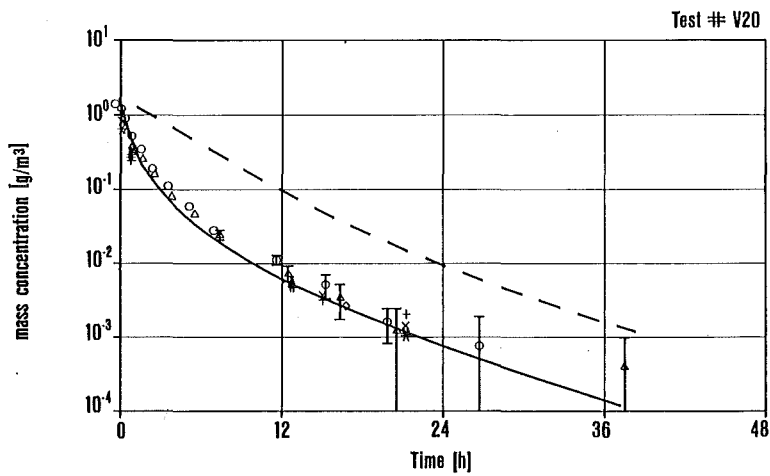


Fig. 4: Pre test calculation (dashed line), post test calculation (solid line) and measured data for DEMONA test V20

was measured although there was no further energy input as in V23. The explanation is that in contrast to test V 23 the aerosol contained an unwanted coarse fraction of powder residues which had not been completely vaporized. This fraction is removed from the airborne state much faster than a finely dispersed aerosol. The post test calculation using the measured bimodal source particle size distribution then gives a complete agreement with the measured data.

These results indicate that NAUA calculations agree well with the observed aerosol behaviour when the parameters of the aerosol source are known, which seems to be difficult to forecast in experiments.

CONCLUSIONS

When judging the quality of the results of code calculations we have to answer two different questions: How good is the physical modelling in the code and how good are the predictions to be used in risk assessments of reactor accidents?

The physical modelling of the code can be judged only by comparing experimental results with calculations that use identical boundary conditions. For an aerosol behaviour code this means that the input data for aerosol sources, thermodynamics and containment properties should be known in detail. As was shown above these complex data can sometimes not be predetermined with the necessary precision before the experiment. So a rigid check of the correct performance of the code is only possible by post test calculations. For the examples discussed above the agreement was excellent then.

On the other hand the more important question pertains to the quality of predictions in case conditions are only roughly known as will be the most likely case in severe accident analysis. Pre-test calculations offer an unique possibility to answer this question because actual large scale tests deviate frequently from planned conditions. This has been observed during the DEMONA tests but also in other large scale experimental programs.

Certainly the confidence band width of computed results which depend on uncertain input parameters could be evaluated by parameter variations alone, but experimental evidence is sometimes more convincing. Concerning the DEMONA experiments two statements have been verified which had been based on analytical work before.

Firstly, the initial source particle size distribution influences the long time aerosol behaviour only when the particles are relatively coarse. This was analytically predicted by calculations with the NAUA code /12/. In an accident aerosols are generated by vaporization of the core and no such coarse fragments can exist in the aerosol as have been observed in test V20. With that respect experiment V20 is not representing real accident conditions, and the discrepancy between pre test calculation and measurement has no significance for the code's predicting capabilities. In test V23, when the aerosol was generated by complete vaporization of the material, the pre test calculation predicted the measured aerosol behaviour very well.

Secondly, the relative insensitivity of the long time aerosol concentration on the aerosol source function which can be seen in the pre and post test calculations for test V23 is due to the dry test conditions. In dry atmosphere the aerosol behaviour is dominated by dry interaction and dry deposition processes which tend to level out initial differences and lead to almost identical

states of the aerosol system after some time. This interesting confirmation of the 'enveloppe concept' /13/ developed for LMFBRs, however, has no bearing on LWR aerosol behaviour because in steam atmospheres condensation and diffusio-phoresis will establish a component depending on thermodynamics. Long time aerosol behaviour then depends mainly on thermodynamics.

For accident analysis, finally, long time aerosol behaviour is of lesser importance in many cases. The total accumulated leakage from the containment mainly originates from the early period of the accident when the aerosol concentration is high. Therefore, the mass released into the containment is one of the most important factors influencing the leakage and the consequences. Once the release function is known, the subsequent aerosol behaviour was found to be calculated correctly with NAUA.

REFERENCES

1. Reactor Safety Study, "An Assessment of Accident Risks in U.S. Commercial Nuclear Power Plants", WASH 1400, NUREG 75/014, 1975
2. Deutsche Risikostudie Kernkraftwerke, BMFT Editor, Verlag TÜV-Rheinland, 1980
3. H. Bunz, M. Koyro, W. Schöck, NAUA Mod4, A code for Calculating Aerosol Behaviour in LWR Core Melt Accidents, Code Description and Users Manual, KfK 3554, August 1983
4. H. Bunz, W. Schöck, Direct Measurement of Diffusiophoretic Deposition of Particles at Elevated Temperatures, in Aerosols: Science, Technology and Industrial Applications of Airborne Particles, B.Y.H. Liu, D.Y.H. Pui and H. Fissan editors, Elsevier 1984
5. K. Hassmann, M. Reimann, Analysis of Hypothetical Core Melt Down Accidents, ENS/ANS Topical Meeting on Reactor Safety Aspects of Fuel Behaviour, Sun Valley, Idaho, August 1981
6. FIPLC - calculations on the CSE experiments A5 and A11, G. Weber, H. Jahn, ANS Topical Meeting on Fission Product Behavior and Source Term Research, Snowbird, Utah, July 15-19, 1984
7. W. O. Schikarski ed., DEMONA Forschungsprogramm zur Demonstration nuklearen Aerosolverhaltens - Grundlagen, Ziele, Auslegung, KfK 3636, EIR 502 (1983)
8. H. Ruhmann, M. Peehs, Development and Performance Testing of an Aerosol Generator System for DEMONA, Proceedings of the Specialist Meeting on Nuclear Aerosols in Reactor Safety, Karlsruhe, September 4-6, 1984, KfK 3800, in preparation
9. T.F. Kanzleiter, Thermal-Hydraulic Behaviour of a Containment Atmosphere Measured in the DEMONA Aerosol Experiments, loc. cit.
10. G. Friedrich et al., Aerosol Measurement System for the DEMONA Experiment, loc. cit.
11. T. F. Kanzleiter, DEMONA-Versuche Kalibrierversuch A1, Battelle-Institut e.V., Frankfurt, BTeV-R-65.523-30-1 (1984)
12. H. Bunz, M. Koyro, W. Schöck, Influence of the Source Term Parameters on Aerosol Behaviour in Core Melt Down Accidents in LWRs, CSNI Specialist Meeting on Nuclear Aerosols in Reactor Safety, Gatlinburg/Tenn., April 15-17, 1980, ORNL/NUREG/TM-404, CSNI-45
13. B. Y. Underwood, B. C. Walker, R. J. Williams, Development of Interpolations Formulae for Rapid Evaluation of the Attenuation Due to Aerosol Processes of Radioactive Releases Following Hypothetical Fast Reactor Accidents, Loc. cit.

RADIONUCLIDE RELEASE TO THE ENVIRONMENT UNDER
SPECIFIC LWR ACCIDENT CONDITIONS

J. A. Gieseke, H. Chen, P. Cybulskis, R. S. Denning,
M. R. Kuhlman, and K. W. Lee

Battelle's Columbus Laboratories
Columbus, Ohio 43201, U.S.A.

and

M. Silberberg and M. Jankowski

U.S. Nuclear Regulatory Commission
Silver Spring, Maryland, U.S.A.

ABSTRACT

Analyses were performed to obtain more realistic estimates of the release of radionuclides to the environment in severe accidents. Results are presented for a variety of accident sequences in five different LWR plant designs. The predicted environmental release fractions obtained in these analyses are in most cases significantly lower than those in the WASH-1400 study. The methodology developed for this study is expected to form the technical basis for upgrading the methods used to analyze source terms in regulatory practice.

INTRODUCTION

The potential for the release of radionuclides to the environment in severe accidents has long been a source of public concern about the safety of nuclear power plants and the focus of regulatory research. For most operating reactors, research report TID-14844 /1/ formed the technical basis for licensing analyses involving radionuclide release in severe accidents. Published in 1962, TID-14844 makes certain assumptions about the release of fission products during a hypothetical severe accident which were representative of the state of knowledge at the time. From 1972-1975 the Nuclear Regulatory Commission conducted the Reactor Safety Study to assess the accident risks in U.S. commercial nuclear power plants. The report of that study, designated WASH-1400, /2/ was published in 1975 and provided a more comprehensive and physically accurate description of fission product behavior. The amount of fission product release to the environment (the "source term") estimated in WASH-1400 has since been used extensively in planning and evaluating reactor operations.

The WASH-1400 source term for accident sequences has had broad implications for operating LWRs--in licensing, emergency planning, safety goals, and indemnification policy. However, additional research continued to provide improved methods for estimating fission product release and transport. In 1981, the Nuclear Regulatory Commission issued the report "Technical Bases for Estimating Fission Product Behavior During LWR Accidents" /3/ which reviewed the state of knowledge at the time. As part of the Technical Bases report, the

assumptions, analytical procedures, and available data were evaluated, and new estimates were made. One improvement of the new estimates over previous ones was that they took into account the retention of radioactive material within the reactor coolant system. But, because of the limitations of the computer codes available at that time, these new estimates could not follow the transport of fission products along their flow path from the core to the environment by applying the various codes sequentially. This resulted in piecemeal, parametric estimates of release.

The research effort described in this paper was undertaken to provide such a systematic, sequential application of the codes as well as to present analyses performed with computational procedures improved since the "Technical Bases" report. It is to be recognized that in this study, an analytical approach was developed for estimating radionuclide transport and deposition which incorporates individual physical and chemical processes or mechanisms. When verified, these methods are expected to replace the generalized source term of TID-14844 and the tabular release fractions in WASH-1400 which were used for broad classes of accidents. The results presented in this paper are reported in greater detail in the first six volumes of the report BMI-2104 /4/.

METHODS OF ANALYSIS

In the approach developed for this study, the calculations provide a consistent analysis of radionuclide behavior by following fission product transport along flow paths, starting with release into the core region and ending with final release to the environment. The general approach consists of a series of steps performed in sequence such that in the combined analysis, the results are specific to an individual set of accident conditions, and each step is based on results from analyses of the previous step.

Overall time-dependent thermal-hydraulic conditions were estimated with the MARCH 2 code, /5/ and detailed thermal-hydraulic conditions for the primary system were estimated with the MERGE /6/ code developed specifically for this program.

The time-dependent core temperatures were used as input to another code developed for this program, CORSOR, which predicts time- and temperature-dependent mass releases or vaporization of radionuclides from the fuel and control rod and structural materials within the pressure vessel. Releases during core-concrete interactions of radionuclides and other materials remaining with the melt were estimated by Sandia National Laboratories using the VANESA code.

Using the MARCH/MERGE-predicted thermal-hydraulic conditions and the CORSOR-predicted radionuclide release rates as input, the TRAP-MELT 2 /7/ code was used to predict vapor and particulate transport in the primary coolant circuit.

Transport and deposition of radionuclides in the containment were calculated using the NAUA-4 /8/ code. The NAUA code was modified for this study by including mechanisms for spray wash-out of aerosols, Stefan-flow deposition of aerosols with condensing steam, and homogeneous nucleation of fog droplets when the water vapor saturation ratio exceeded a value of approximately three.

The basic stepwise procedure described above is illustrated in Figure 1, which shows the relationships among the computational models. The calculations

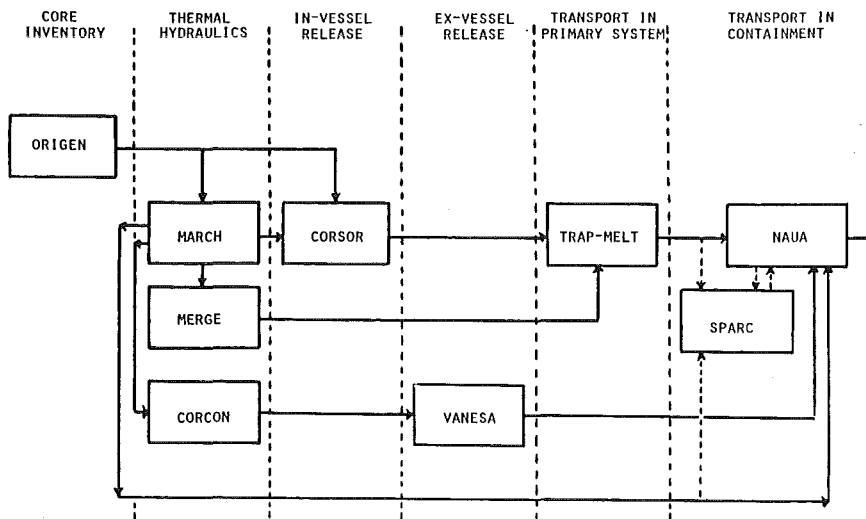


FIGURE 1. SEQUENCE OF COMPUTER ANALYSES

were of a "best estimate" type using input derived from experimental measurements whenever possible. Types of data employed in the analyses include vapor deposition velocities, aerosol deposition rates, aerosol agglomeration rates, fission product release rates from fuel, particle sizes formed from vaporizing/condensing fuel materials, engineering correlations for heat and mass transfer, and physical properties of various fuel, fission product, and structural materials.

SEQUENCES ANALYZED

A variety of accident sequences were examined in this study for a number of different plant designs. Five different plant designs were investigated: two large, dry PWR designs, Surry and Zion; an ice condenser PWR design, Sequoyah; a Mark I BWR design, Peach Bottom; and a Mark III BWR design, Grand Gulf. Accident sequences were selected for analysis based upon risk significance and the intent to cover a broad spectrum of accident conditions.

RESULTS OF ANALYSES

The quantities of important chemical species predicted to be released to the environment for the accident sequences analyzed in this study are tabulated in Tables I through V. For the two plants analyzed in WASH-1400 the corresponding source terms are also indicated.

TABLE I. RELEASE FRACTIONS FOR PWR - LARGE, DRY CONTAINMENT (SURRY)

Sequence	Species	RCS	Containment ^(a)	Safeguards Building	Environment	WASH 1400
AB-β	CsI	0.027	0.59	0.29	0.087	0.7
	CsOH	0.038	0.59	0.29	0.085	0.5
	Te	0.26	0.19	0.12	0.070	0.3
AB-β _m ^(b)	CsI	0.027	0.92		0.050	0.7
	CsOH	0.038	0.92	(c)	0.049	0.5
	Te	0.26	0.34		0.042	0.3
AB-γ	CsI	0.027	0.92		0.057	0.7
	CsOH	0.038	0.90	(c)	0.059	0.5
	Te	0.26	0.31		0.14	0.3
AB-ε	CsI	0.027	0.97		4.8×10^{-5}	8×10^{-4}
	CsOH	0.038	0.96	(c)	4.7×10^{-5}	8×10^{-4}
	Te	0.26	0.45		4.0×10^{-5}	1×10^{-3}
TMLB ¹ -δ	CsI	0.85	0.11		0.046	0.7
	CsOH	0.86	0.10	(c)	0.039	0.5
	Te	0.30	0.16		0.11	0.3
TMLB ¹ -ε	CsI	0.85	0.15		2.8×10^{-3}	8×10^{-4}
	CsOH	0.86	0.14	(c)	1.7×10^{-4}	8×10^{-4}
	Te	0.30	0.19		8.1×10^{-2}	1×10^{-3}
S ₂ D-γ	CsI	0.48	0.52		4.2×10^{-5}	3×10^{-2}
	CsOH	0.57	0.43	(c)	6.4×10^{-5}	9×10^{-3}
	Te	0.91	0.058		3.3×10^{-2}	5×10^{-3}
S ₂ D-ε	CsI	0.74	0.26		1.5×10^{-8}	2×10^{-5}
	CsOH	0.76	0.24	(c)	1.4×10^{-8}	1×10^{-5}
	Te	0.69	0.15		7.7×10^{-8}	2×10^{-5}
V with water ^(d)	CsI	0.50	0.018	0.40	0.079	0.7
	CsOH	0.51	0.017	0.40	0.073	0.5
	Te	0.13	0.71	0.14	0.025	0.3
V no water	CsI	0.50	0.018	0.069	0.41	0.7
	CsOH	0.51	0.017	0.071	0.40	0.5
	Te	0.13	0.71	0.044	0.12	0.3

(a) Balance of Te to add total to 1.0 is predicted to remain in the melt.

(b) Containment volume divided into four compartments.

(c) Safeguards building not considered for this sequence.

(d) Release point in safeguards building assumed to be under 3 feet of saturated water.

TABLE II. RELEASE FRACTIONS FOR PWR - LARGE, DRY CONTAINMENT (ZION)

Sequence	Species	RCS	Containment ^(a)	Environment	WASH 1400
TMLB ^{1-ε}	CsI	0.98	2.5×10^{-2}	1.9×10^{-6}	8×10^{-4}
	CsOH	0.98	2.5×10^{-2}	1.9×10^{-6}	8×10^{-4}
	Te	0.28	0.64	7.8×10^{-5}	1×10^{-3}
S ₂ D-ε	CsI	0.34	0.66	2.5×10^{-8}	2×10^{-5}
	CsOH	0.42	0.58	2.3×10^{-8}	1×10^{-5}
	Te	0.93	1.7×10^{-2}	3.6×10^{-8}	2×10^{-5}

(a) Balance of Te to add total to 1.0 is predicted to remain in the melt.

TABLE III. RELEASE FRACTIONS FOR PWR - ICE CONDENSER CONTAINMENT (SEQUOYAH)

Sequence	Species	RCS	Lower ^(a) Containment	Ice Bed	Upper Containment	Environment
TMLB ^{1-γ}	CsI	0.82	6.1×10^{-2}	0.10	1.5×10^{-3}	1.7×10^{-2}
	CsOH	0.83	3.9×10^{-2}	0.12	2.9×10^{-3}	2.3×10^{-2}
	Te	0.25	2.4×10^{-2}	3.7×10^{-2}	6.2×10^{-4}	1.4×10^{-2}
TMLB ^{1-δ}	CsI	0.82	8.6×10^{-3}	0.17	5.5×10^{-3}	3.9×10^{-4}
	CsOH	0.83	5.4×10^{-2}	0.13	5.0×10^{-3}	4.5×10^{-4}
	Te	0.25	4.0×10^{-2}	3.1×10^{-2}	3.8×10^{-3}	2.0×10^{-3}
TML-γ	CsI	0.82	4.2×10^{-2}	9.4×10^{-2}	4.6×10^{-2}	1.3×10^{-3}
	CsOH	0.83	3.1×10^{-2}	0.11	3.4×10^{-2}	7.0×10^{-3}
	Te	0.25	3.1×10^{-4}	1.2×10^{-2}	8.6×10^{-3}	5.5×10^{-4}
TML-δ	CsI	0.82	5.7×10^{-2}	8.5×10^{-2}	3.4×10^{-2}	6.9×10^{-9}
	CsOH	0.83	5.8×10^{-2}	9.4×10^{-2}	3.5×10^{-2}	7.4×10^{-9}
	Te	0.25	8.1×10^{-3}	1.0×10^{-2}	9.5×10^{-3}	1.6×10^{-8}
S ₂ HF	CsI	0.73	4.5×10^{-2}	8.3×10^{-2}	0.11	3.3×10^{-2}
	CsOH	0.75	4.2×10^{-2}	7.6×10^{-2}	0.10	3.2×10^{-2}
	Te	0.69	6.4×10^{-2}	6.5×10^{-2}	4.5×10^{-2}	5.5×10^{-2}

(a) Balance of Te to add total to 1.0 is predicted to remain in the melt.

TABLE IV. RELEASE FRACTIONS FOR BWR - MARK I (PEACH BOTTOM)

Sequence	Species	RCS	Pool	Drywell ^(a)	Hotwell	Reactor Building	SGTS	Environment	WASH 1400
AE-y'	CsI	0.19	0.35	0.12	0	--	--	0.34	0.9
	CsOH	0.19	0.34	0.14	0	--	--	0.33	0.5
	Te	2.9×10^{-2}	3.2×10^{-3}	0.32	0	--	--	0.65	0.3
TC-y'	CsI	0.06	0.69	1.5×10^{-2}	0	--	--	0.24	0.9
	CsOH	0.22	0.56	1.4×10^{-2}	0	--	--	0.21	0.5
	Te	0.34	7.9×10^{-3}	0.16	0	--	--	0.37	0.3
TC-y	CsI	0.06	0.69	1.5×10^{-2}	0	6.9×10^{-2}	6.8×10^{-2}	0.10	0.1
	CsOH	0.22	0.56	1.4×10^{-2}	0	6.1×10^{-2}	5.8×10^{-2}	9.1×10^{-2}	0.1
	Te	0.34	7.9×10^{-3}	0.16	0	0.11	1.3×10^{-2}	0.25	0.3
TM-y'	CsI	0.14	0.80	5.4×10^{-3}	0	--	--	4.8×10^{-2}	0.9
	CsOH	0.15	0.79	5.0×10^{-3}	0	--	--	4.5×10^{-2}	0.5
	Te	0.40	8.6×10^{-3}	0.2	0	--	--	0.19	0.3

(a) Balance of Te to add total to 1.0 is predicted to remain in the melt.

TABLE V. RELEASE FRACTIONS FOR BWR - MARK III (GRAND GULF)

Sequence	Species	RCS	Drywell ^(a)	Pool	Containment	Environment
TC	CsI	0.19	3.6×10^{-2}	0.77	1.9×10^{-4}	6.8×10^{-3}
	CsOH	0.51	1.4×10^{-3}	0.49	9.2×10^{-6}	3.5×10^{-4}
	Te	0.22	6.0×10^{-2}	0.45	4.3×10^{-4}	8.8×10^{-3}
TPI	CsI	8.4×10^{-2}	3.9×10^{-3}	0.91	7.5×10^{-7}	2.4×10^{-4}
	CsOH	0.24	3.7×10^{-3}	0.76	9.0×10^{-7}	3.1×10^{-4}
	Te	0.45	6.0×10^{-2}	0.14	1.4×10^{-5}	1.3×10^{-3}
TQUV	CsI	6.3×10^{-2}	3.8×10^{-6}	0.94	6.8×10^{-4}	8.4×10^{-4}
	CsOH	0.54	2.8×10^{-6}	0.46	3.5×10^{-4}	4.4×10^{-4}
	Te	0.40	8.0×10^{-2}	0.21	1.6×10^{-3}	2.1×10^{-3}
S ₂ E (nominal pool bypass)	CsI	9.1×10^{-2}	1.4×10^{-2}	0.89	9.6×10^{-4}	7.0×10^{-3}
	CsOH	0.16	1.3×10^{-2}	0.82	8.6×10^{-4}	6.3×10^{-3}
	Te	0.26	3.5×10^{-2}	0.32	6.5×10^{-3}	2.4×10^{-2}
S ₂ E (high pool bypass)	CsI	9.1×10^{-2}	1.1×10^{-2}	0.86	5.9×10^{-3}	4.2×10^{-2}
	CsOH	0.16	9.8×10^{-3}	0.79	5.4×10^{-3}	3.8×10^{-2}
	Te	0.26	3.5×10^{-2}	0.11	0.10	0.14

(a) Balance of Te to add total to 1.0 is predicted to remain in the melt.

The release of fission products from fuel during the period of fuel heatup and melting in-vessel and during ex-vessel attack of the concrete predicted in this study is not markedly different from the results in WASH-1400. Essentially all of the volatile fission products are predicted to be released from the fuel in all cases.

Retention of fission products during transport through the reactor coolant system was not credited in the WASH-1400 study. In the current study the amount of retention in the reactor coolant system is in many cases substantial (e.g., 85 percent of the iodine in TMLB') depending on the thermal-hydraulic conditions in the system. The uncertainty regarding the ultimate fate of fission products deposited within the reactor coolant system is very great, however. Follow-on analyses of decay heating of reactor coolant system surfaces and the reevolution of fission products are in progress.

The release of fission products from the fuel and transport in the reactor coolant system vary with accident sequence and plant type (BWR versus PWR) but are relatively insensitive to the containment design. Containment design was, however, found to have a dramatic effect on the magnitude of the predicted environmental source terms.

Surry Plant

The results of the containment transport analyses performed for this study indicate that the potential for retention in the containment building and secondary buildings is somewhat greater than predicted in WASH-1400. This is partially because of an underestimation of removal processes in the WASH-1400 CORRAL code and partially because of an increased time to containment failure in the current analyses.

In general, the results of the current study indicate that for many important accident sequences the source term in WASH-1400 is overestimated by approximately an order of magnitude. The effect of a reduction of this magnitude on estimated risk would be essentially proportional for the risk of latent fatalities (i.e., an order of magnitude) but would be even more dramatic for the risk of early fatalities because of the threshold behavior of this measure.

Of the important sequences analyzed, the one in which a major reduction in consequences was not observed is the interfacing LOCA sequence, V, for the assumption of no overlying pool of water at the entry point into the safeguards building. If there is an overlying water layer, the source term is considerably reduced. Although this is no longer considered a risk-dominant sequence because of steps taken to suppress its likelihood, the existence of credible sequences with potentially large consequences can have public perception and regulatory implications regardless of the risk significance of the sequence.

Zion Plant

The issue of whether or not early containment failure can occur in some accident sequences in large, dry PWR containment designs largely overshadows most of the other uncertain aspects of source term analysis. If the containment remains intact for an extended period of time following core meltdown, the potential human health consequences will be minor and the

character of off-site emergency response will differ substantially from the high-consequence, early containment failure sequences of WASH-1400. It has not been the purpose of this paper to determine the likelihood of early containment failure in the Zion or Surry plants. This topic is being investigated in other work being performed for the NRC. The potential benefits of a high failure pressure and a large containment volume are, however, evident.

By comparing the predicted releases of aerosols from the containment in the two sequences analyzed, the effects of spray scrubbing and reduced containment pressure on release can be observed in the lower releases for S₂D. Although the release of fission products in aerosol form appears to dominate the consequences of large-release accidents with early containment failure, the release of more volatile forms of iodine (e.g., I₂ or methyl iodide) formed by interactions within pools and on surfaces in the containment building along with the release of noble gases tend to dominate the predicted releases in the accidents with delayed failure and smaller releases.

Sequoyah Plant

The results of the containment transport analyses in the present study indicate significant potential for fission product attenuation. As would be expected, the environmental source terms are seen to depend on the timing of containment failure, with earlier failure leading to larger releases. The ice condenser was found to typically remove about half of the airborne radioactivity passing through it. The operation of containment sprays and air return fans was found to lead to substantial reduction in the potential release to the environment.

The ice condenser containment was found to be potentially vulnerable to large hydrogen burns. For the accident conditions and modeling assumptions considered, significant pressure loads were predicted even considering operation of the hydrogen igniters; large pressure loads resulted when the burning was predicted to propagate into the upper compartment of the containment. The prediction of containment failure mode likelihood was not an objective of this study, however. The potential for early containment failure is being investigated in other tasks being performed for the NRC.

Peach Bottom Plant

The retention of fission product aerosols during their transport through the reactor coolant system in the present study was found to be on the order of 10-20 percent of that released from the fuel. Primary system retention of tellurium was found to be quite high, but since only a fraction of the total tellurium release occurred during the in-vessel phase of the accidents, the effect on the overall tellurium release from the plant was not great. In general, the predicted retention for Peach Bottom is not as high as for some of the PWR sequences considered in this study; the differences in the predicted primary system retention are associated with differences in accident thermal-hydraulics for the two types of designs.

Fission product aerosol removal by the BWR pressure suppression pool has been found to be sensitive to the aerosol particle size distribution, the nature of the flows through the pool, and the thermodynamic state of the pool.

For accident sequences such as AE, in which the suppression pool remains sub-cooled, quite high pool decontamination factors are predicted. Due to the timing and location of the predicted containment failure in this sequence, however, not all of the released fission products pass through the pool, thus limiting overall decontamination and resulting in substantial releases to the environment. In sequences such as TC and TW, all of the melt releases are discharged in the suppression pool, but here the pool is boiling or saturated at the time of core melting, greatly reducing its effectiveness for fission product retention. Overall approximately one-half of the aerosol releases were predicted to have been retained in the suppression pool for these accident sequences.

In the accident sequences evaluated in this study, the failure of the primary containment was assumed to lead to the failure or bypass of the secondary containment (reactor building). The potential effectiveness of the secondary containment and the Standby Gas Treatment System (SGTS) were explicitly considered for one of the accident sequences. The potential for retention in the reactor building and removal by the SGTS was found to be limited by outleakage from the reactor building, as the gas and vapor inputs carrying the fission products exceeded the flow capacity of the SGTS. The inclusion of the secondary containment was found to result in only a fractional reduction in the predicted fission product source term to the environment. The effectiveness of the secondary containment could vary greatly, however, depending on the accident sequence and assumptions made about the flow path following primary containment failure.

Grand Gulf

Transient accident sequences were emphasized for the Mark III containment design because they are expected to be major contributors to risk. Two variations of a pipe break sequence were included, however, to investigate the effects of suppression pool bypass.

Because the suppression pool was not bypassed in the transient sequences, major fractions of the fission products are collected there. Nearly all of the fission products not deposited in the reactor coolant system or drywell are deposited in the suppression pool. The subcooled pool in the pipe break sequence is also an effective attenuating factor for flow through the pool but the pool bypass flow has a major influence on release from the plant. The two bypass flow cases considered were a nominal leakage flow and an assumed stuck-open vacuum breaker. The nominal leakage and vacuum breaker cases gave source terms about a factor of 10 higher than the source terms predicted for the transient cases with no bypass flow.

SUMMARY AND COMMENTS

The magnitudes of the environmental fission product source terms predicted in this study are significantly lower than those of earlier assessments, such as WASH-1400. It is important, however, to recognize that the uncertainties associated with these results could be quite large. The prediction of fission product release has been shown to be sensitive to accident thermal-hydraulics as well as to the mechanisms of fission product release and transport. It should also be recognized that the prediction of the course and consequences of the low probability hypothetical situations considered here is inherently

uncertain; at best, the smaller number of accident scenarios considered here can only be representative of a wide spectrum of possible outcomes in the event of an accident.

Some potentially important aspects of fission product release and transport have been treated superficially in this study which require further consideration. The potential for the reevolution of fission products from surfaces in the reactor coolant system as the result of decay heating could lead to larger environmental source terms than predicted. Similarly, fission products deposited in the containment could be reevolved and released from the containment over the long term, perhaps in a different chemical form such as methyl iodide or elemental iodine.

REFERENCES

1. DiNunno, J. J., et al, "Calculation of Distance Factors for Power and Test Reactor Sites", TID-14844 (March 23, 1962).
2. "Reactor Safety Study--An Assessment of Accident Risks in U.S. Commercial Nuclear Power Plants", WASH-1400, NUREG-75/014 (October, 1975).
3. "Technical Bases for Estimating Fission Product Behavior During LWR Accidents", NUREG-0772 (June, 1981).
4. Gieseke, J. A., et al, "Radionuclide Release Under Specific LWR Accident Conditions, Volumes 1-6 (BMI-2104 (July, 1983; July, 1984).
5. Wooton, R. O., et al, "MARCH 2 Code Description and Users' Manual", Draft (December, 1982).
6. Freeman-Kelly, R., "A Users' Guide for MERGE", Battelle's Columbus Laboratories, (October, 1982).
7. Jordan, H., Gieseke, J. A., and Baybutt, P., "TRAP-MELT Users' Manual", NUREG/CR-0632, BMI-2017 (February, 1979).
8. Bunz, H., Kopyro, M., and Schock, W., "A Code for Calculating Aerosol Behavior in LWR Core Melt Accidents Code Description and Users' Manual", KFK 3554 (Aug. 1983)

Parametric Study of Factors Affecting Retention
of Fission Products In Severe Reactor Accidents

E. A. Warman

Stone & Webster Engineering Corporation
Boston, Massachusetts, 02107, U.S.A.

ABSTRACT

During the past year and a half, a parametric study of factors affecting retention of fission products in containments and contiguous structures has been conducted by Stone & Webster Engineering Corporation (SWEC) in support of the American Nuclear Society's (ANS) Special Committee on Source Terms.¹ This paper summarizes the results of that study and discusses the application of the results in the formulation of source terms for severe core damage accidents. The study reported here is for a large pressurized water reactor (PWR). The Surry station was selected for the study because it was the PWR plant analyzed in the Reactor Safety Study (WASH-1400).² A similar parametric study of the Peach Bottom Mark I plant, the boiling water reactor plant analyzed in WASH-1400, is in progress.

This study represents a careful appraisal of a number of parameters and phenomena which have been neglected to oversimplified in some analyses. Inclusion of the effects analyzed results in a large overall reduction in releases of fission products to the environment, when the effects are considered together, although the reduction from any single effect is not large when considered alone.

When these relatively large reductions in releases are combined with the reductions from studies of fission product retention in the reactor coolant system (RCS), such as those reported in the recent U.S. Nuclear Regulatory Commission (USNRC) sponsored work at Battelle Columbus Laboratories (BMI-2104),³ substantial overall reductions in releases to the environment result.

Based on the results of this study and studies by others, a downward revision is proposed to the interim source term first proposed by the author at the Second International Conference on Nuclear Technology Transfer ICONTT-II.⁴ The revised interim source term includes the release to the environment of the following fractions of the core inventory of specific fission product groups: noble gases-1.00, volatiles-(iodine (I), cesium-rubidium (Cs-Rb), and tellurium-antimony (Te-Sb)-0.01, and nonvolatiles barium-strontium (Ba-Sr)-0.004, ruthenium (Ru)-0.003, and lanthanum (La)-0.0002. The release fractions of the nonvolatile groups have been reduced based on analyses of aerosol retention within the power plant.

STONE & WEBSTER



INTRODUCTION

The study reported here included analyses of releases of fission products with: (1) postulated pre-existing openings in the containment (e.g., resulting from failure to isolate the containment completely, (2) hypothetical early breach of the containment pressure boundary (i.e., during or shortly after core degradation), and (3) postulated late breach of the containment because of the slow pressure buildup resulting from the generation of noncondensable gases associated with the core/concrete interaction processes. The results indicate that the releases for hypothetical early breaches of the containment are comparable to those for pre-existing openings. Without a pre-existing opening or early breach, containment breach is not expected to occur in less than one day, if at all. The releases associated with late containment openings are observed to be small in comparison with those of pre-existing openings. Thus, the focus of the study is on the potential releases associated with pre-existing openings.

The following phenomena and parameters were included in the study:

- | | |
|----------------------------|----------------------------------|
| o Containment Opening Size | o Aerosol Particle Size |
| o Timing of Opening | o Aerosol Concentration |
| o Diffusiophoresis | o Timing of Te Release from Core |
| o Suspended Liquid | o Core Degradation Without |
| o Contiguous Structures | Vessel Melthrough |
| o Multicompartamentation | o Fission Product Decay Heating |
| o Release of Non Volatiles | o Timing of Injection into |
| | Containment |

Because of the length limitations for this paper, results are presented only for the parameters and phenomena listed in the left column. Results of analyses of the parameters listed in the right column are presented in Chapter 6 and Appendix B of the ANS Committee Report.¹

Analyses were performed for three accident sequences described in WASH-1400:² AB (large break LOCA in containment with loss of all AC power), TMLB (a transient with loss of all AC power followed by the failure of the power conversion system and the loss of the capability of the secondary system to remove heat from the RCS), and V (an interfacing system LOCA in the low-pressure emergency core cooling system at a location outside the containment). The results presented in this paper are limited to the AB and TMLB sequences.

APPROACH AND ANALYTICAL METHODS

This study concentrated on the retention of fission products in the containment and contiguous structures. Analyses were performed first by neglecting retention of fission products in the RCS. Subsequently, some analyses were repeated with the RCS retention factors reported in Volume V of BMI-2104.³ Finally, some analyses were performed assuming retention in the RCS with subsequent delayed injection into the containment.



The release rates from the core and their timing were taken from the initial draft report of the BMI study of the Surry plant, Volume I of BMI-2104.⁵ Some subsequent analyses were performed with the later data reported by BMI.³ Complete release of the volatile species from the core was assumed. The release fractions from the core of the non-volatile species are similar to those reported in WASH-1400, as listed below:

<u>Fission Product</u> <u>Group</u>	<u>WASH-1400</u> <u>PWR Analysis</u>	<u>Present</u> <u>Analysis</u>
Volatiles	1.00	1.00
Nonvolatiles		
Barium-Strontium	0.11	0.27*
Ruthenium	0.033	0.022*
Lanthanum	0.013	0.017*

* Taken from BMI-2104.

The approach used was to first perform analyses of the thermal hydraulic conditions as a function of time for each phase of the accident sequence being analyzed and then perform aerosol behavior analyses. The thermal hydraulic calculations were performed with a combination of mass and energy calculations using the RELAP-4 Mod5 computer program,⁶ core/concrete interaction data obtained from Sandia,⁷ and thermal hydraulics analyses with the THREED computer program.⁸ The THREED program incorporates the thermal hydraulic formulations of RELAP-4 and the treatment of passive heat sinks from CONTEMPT-LT.⁹ Portions of the analyses, such as the boiloff phase for the AB sequence, were calculated manually. The aerosol transport and behavior were then analyzed using the NAUA-4 computer program,¹⁰ as modified by SWEC to include diffusio-phoretic removal based on the volumetric removal rate of steam due to condensation on passive heat sinks as computed by THREED.

SUMMARY OF RESULTS

A. Size of Opening In Containment

Figure 1 presents the results of analyses of the relative cumulative leakage of iodine and cesium for various size postulated pre-existing openings in the containment. Data are presented for both the AB and TMLB sequences. The data are normalized to a relative leakage of 1.0 for a 1.0 ft² (0.093m²) pre-existing opening. Leakage is seen to increase rapidly with increasing opening sizes in the range from near zero to ~ 1.0 ft² (0.093m²) and to decrease for larger openings for the AB sequence and increase only slightly for larger opening sizes for the TMLB sequence. The unexpected behavior observed for larger opening sizes results from the effects of in-leakage which was observed for these opening sizes.

Figure 2 depicts the volumetric leakage rate as a function of time for the TMLB sequence with two different pre-existing containment openings - 1.0 ft² (0.093m²) and 0.1 ft² (0.0093m²). In-leakage is seen to occur because of the expulsion of air and noncondensable gases, and the continuing steam condensation in the containment. For a period of one hour

to one and one-half hours following the postulated vessel meltthrough, the containment acts as a condenser with air being taken in from outside of the containment. For the smaller size opening, in-leakage is not observed over the time period presented in this figure. The volumetric leak rates are combined with the NAUA analysis of aerosol transport and behavior to result in the cumulative leakage of fission products for each opening size studied. The cumulative leakages were observed to be asymptotic within approximately three hours after the start of core melting. The data presented in Figure 1 represent the cumulative (or total) leakage for each containment opening size studied.

B. Timing of Opening in Containment

Figure 3 presents the relative cumulative leakage of iodine and cesium as a function of the time at which a 1.0 ft² (0.093m²) opening in the containment is postulated to occur. The t=0 data represents a pre-existing opening, i.e., an opening resulting from failure to isolate the containment completely or created coincident with the onset of the accident. The data are normalized to a relative cumulative leakage of 1.0 for a pre-existing opening. Data are presented for aerosol loadings corresponding to the amount reported in BMI-2104 Volume I or one-fifth (i.e., multiplier of 0.2) and one-tenth (i.e., multiplier of 0.1) times the nominal loading reported by BMI, to investigate the effect of the large uncertainties associated with those quantities at the present time. The total mass of "other" aerosols, i.e., other than the 168kg represented by the iodine, cesium, and tellurium species, is summarized below:

	Mass of Other Aerosols (kg)	
	<u>AB Sequence</u>	<u>TMLB Sequence</u>
Nominal (BMI-2104 Volume I)	5,500	6,130
0.2 x Nominal	1,100	1,230
0.1 x Nominal	550	513

An unexpected finding in the parametric study is that the relative cumulative releases of iodine and cesium for postulated early breaches of containment are not much different than for pre-existing openings. Figure 3 shows that the releases are only approximately 30% higher for a 1.0 ft² (0.093m²) opening at the start of core melt (0.5 hr) for the AB sequence compared with the releases with a pre-existing opening. For the TMLB sequence, no appreciable difference in releases was calculated for pre-existing openings and openings coincident with the start of core melting (~ 3 hr) or at vessel meltthrough (4.6 hr). The cumulative releases are observed to decrease exponentially with the timing of postulated containment breach following the injection of fission products into containment. The injection periods during which severe core degradation is calculated to occur are ~ 0.5 to 1.0 hr for the AB sequence and ~ 3 to 4 hr for the TMLB sequence. The slopes of the curves in Figure 3 are related primarily with aerosol settling rates. It should also be noted that the core/concrete aerosol loading does not affect the volatile fission product releases for containment openings up to ~ 1 1/2 hr after the start of severe fuel damage.



Figure 4 illustrates the results of an analysis of the release of volatile fission products due to a postulated late overpressure breach of the containment for a TMLB sequence. The curves to the left of the figure depict the fraction of the cesium (as a representative fission product) which is airborne in the containment as a function of time. Three curves are presented, representing the airborne cesium fraction with the nominal loading of "other" aerosols and with 0.2 and 0.1 times the nominal loadings. These curves are seen to decrease when the postulated openings occur at 27 hr. The cumulative cesium leakage fraction (i.e., mass leaked divided by mass injected into the containment) is shown in the curves at the right of the figure. In this analysis the containment is assumed to develop either a 0.1 ft² (0.0093m²) or 1.0 ft² (0.093m²) opening 24 hr after the start of core damage, i.e., 27 hr into the accident sequence. The cumulative cesium leakage fractions for the three loadings of "other" aerosols are summarized below:

Loading of "Other" Aerosols	Cumulative Cesium Leakage Fraction	
	0.1 ft ² (0.0093m ²)	1.0 ft ² (0.093m ²)
Nominal	3.0 x 10 ⁻⁵	4.5 x 10 ^{-5*}
0.2 x Nominal	2.6 x 10 ⁻⁴	3.6 x 10 ⁻⁴
0.1 x Nominal	5.7 x 10 ⁻⁴	7.6 x 10 ⁻⁴

* Not shown in Figure 4.

Note: These data assume no retention in the RCS.

The effect of timing of openings in the containment is illustrated by the following data for the TMLB sequence including retention in the RCS:

Timing of Containment Breach	Fraction of Inventory of Iodine Released*	
	0.1 ft ² (0.0093m ²)	1.0 ft ² (0.093m ²)
Pre-existing (Prior to core degradation)	2.1 x 10 ⁻³	1.5 x 10 ⁻²
Early (During or shortly after core degradation)	2.1 x 10 ⁻³	1.5 x 10 ⁻²
Late (Substantially after core degradation - 27 hr)	2.6 x 10 ^{-5**}	3.6 x 10 ^{-5**}

* Includes retention in RCS from BMI-2104 Volume V.

** Based on 0.2 x nominal aerosol loading, which is close to the BMI-2104, Volume V aerosol loading.

C. Diffusiophoresis

Enormous quantities of steam are condensed on passive heat sinks in light water reactor containments during accidents. A total of 54,600 lb (24,800kg) of steam is calculated to be condensed on the containment heat sinks during the period of injection of fission products in the TMLB sequence, i.e., from 3 to 4:6 hr. The average condensation rate is ~ 9.6 lb/s (4.4 kg/s).



Analyses were performed to quantify the amount of aerosol removal from the atmosphere because of this steam condensation, a process which has come to be described as diffusiophoresis.¹¹ The removal of aerosols from the containment atmosphere was calculated within NAUA by adding a volumetric removal rate term based on the steam condensation rate calculated with THREED. Diffusiophoresis was found to have a different effect on the fission product mass distribution depending on the containment opening size as illustrated below:

Pre-existing Containment Opening Size		Fraction of Injected Mass of Cesium Removed via Diffusiophoresis	
(ft ²)	(m ²)	AB	TMLB
0	0	0.23	0.34
0.1	0.0093	0.21	0.29
0.35	0.033	0.16	0.28
1.0	0.093	0.18	0.20
2.0	0.19	0.26	0.17
4.0	0.37	0.29	0.15
7.0	0.65	0.32	0.21

D. Suspended Liquid

Severe accidents at light water reactor nuclear power plants include the ejection of a two phase mixture of steam and liquid water at the location of the break in the RCS.¹² For example, during the AB (large break LOCA) sequence approximately 247,000 lb (112,000 kg) of liquid water was calculated to be injected into the containment during the blowdown and refill/reflood portions of the sequence. A significant fraction of this water is aerosolized.¹³ For purposes of analysis it was assumed that fractions of the injected liquid were airborne in the containment atmosphere as suspended liquid water droplets. These water droplets were modeled in the NAUA-4 analyses with a log-normal source distribution with a number median diameter (NMD) of 1.0 μ m and a standard deviation σ of 2.0. The water droplets were observed to settle rather quickly. However, due to the large number of particles involved, a significant number density remains airborne at the time of injection of fission product aerosols, @ 1,680 sec in the AB sequence analysis.

A parametric study was conducted in which the initial mass of suspended liquid droplets was varied from a few to 25% of the injected liquid mass. The resulting release of volatile fission products with a 1.0 ft² (0.093m²) pre-existing opening was observed. Figure 5 presents the results of the analysis for the AB sequence, with and without diffusiophoresis in the NAUA-4 analyses. Similar sensitivity analyses were conducted for the TMLB sequence. Analyses indicate that water droplets with larger diameters (e.g., NMD-10 μ m) did not effect the fission product behavior appreciably. The conclusions reached from these studies was that initial airborne concentration of suspended liquid on the order of 10% or more of the injected amount result in reduction in iodine and cesium leakage by about a factor of 2.

Figure 6 presents a comparison of the effects on airborne concentration of cesium due to "other" aerosols (i.e., other than the volatile species),

diffusiophoresis, and suspended liquid. These data are for the AB sequence with no opening in containment. Case (1) in this figure is based on only the volatile fission products being injected into the containment. Case (2) includes the addition of the 434 kg of "other" aerosols reported to be released from the RCS prior to vessel meltthrough in BMI-2104 Volume I.⁵ Case (3) is a repeat of case (1) with diffusiophoresis and suspended liquid water droplets, as discussed above. Case (4) is the baseline nominal set of conditions for the AB sequence in the parametric study, with masses obtained from the BMI study but with no diffusiophoresis and no suspended liquid. Case (5) shows the effect of adding diffusiophoresis and suspended liquid to Case (4). The effect of diffusiophoresis and suspended liquid, as shown in Cases (3) and (5) is to substantially reduce the amount of time required for a given reduction in the airborne fraction. The figure also illustrates (by comparing Cases (4) and (5)) that the "other" aerosols do not influence the airborne fraction of cesium during the first few hours of the sequence. As noted earlier, the cumulative leakage for pre-existing openings is asymptotic in less than 3 hr. Thus, the leakage for pre-existing openings is essentially unaffected by the core/concrete aerosol loading.

E. Contiguous Structures

Penetrations in PWR containments, with the exception of the equipment hatch and purge system, lead into contiguous structures outside containment. Retention of fission products due to aerosol behavior in contiguous structures was investigated using the quench spray pump house and main steam valve house configurations at the Surry plant. Analyses were performed in which a single node (single control volume) model of the containment was coupled serially with a four node model of the lower and upper levels of the structures mentioned above. The ratio of the cumulative leakage fractions from the contiguous structures to the leakage fractions from the containment indicate the amount of retention in these structures as summarized below:

Ratio, Leakage from Contiguous Structures
to Leakage from Containment

Size of Pre-existing Containment Opening	AB Sequence	TMLB Sequence
0.1 ft ² (0.0093m ²)	0.42	0.42
1.0 ft ² (0.093m ²)	0.55	0.65

F. Multicompartmentation within Containment

The analyses discussed previously in this paper are based on a single control volume representation of the containment. Thermal hydraulics analyses for the AB sequence were also performed with a multi-node model of the containment, which includes 14 nodes and 28 internodal junctions, using the THREED program. The results of these analyses were used to reduce the representation of the multicompartmentation within the containment to 6 nodes, based on taking advantage of symmetry and combining flows across several junctions. The 6 node model was employed in a series of serial calculations using NAUA. The resultant cumulative leakage of

iodine and cesium, as calculated with the multinode model, was 0.6 times the leakage calculated with the single-node model.

The multinode thermal hydraulics analyses indicate that the containment is well mixed at the time of injection of fission products in the present analysis. The analyses also indicate that, as time progresses, the residence time in each node increases. Thus, if the injection of fission products into the containment is delayed, the effect of multicompartimentation would be much greater than it appears to be in the present analysis.

This analysis of the effect of multicompartimentation should be viewed as a first estimate. Detailed quantification of this effect should be obtained with a multinode program which couples the thermal hydraulics and aerosol behavior analyses. Recent calculations with the CONTAIN program represent the first such undertaking.¹⁴ Additional analyses are required to develop a more refined estimate of the effects of multicompartimentation.

G. Combined Effects of Several Parameters

Figure 7 depicts the cumulative leakage fraction of cesium and iodine as a function of time for a TMLB sequence with no retention in the core or RCS. The results of six separate analyses are presented as shown in this figure.

Each succeeding curve represents a separate NAUA run with a change in or addition of a parameter to the previous case, with Curve 5 including all of the changes and additions considered. Curve 6 represents a multiplication of the results from Curve 5 by a factor of 0.6 to account for the effects of multicompartimentation, as previously described. These multicompartimentation analyses were performed for an AB sequence and are applied here to the TMLB case as a first order approximation.

It is observed that the leakage fraction (0.72) depicted in Curve 1 is essentially the same as the 0.7 leakage fraction reported in WASH-1400 for iodine. However, by including the other effects depicted in this figure the leakage fraction is reduced to 0.015 with no retention in the core or RCS.

Another way of analyzing these effects is to consider the effect on leakage with a 1.0 ft² (0.093m²) pre-existing opening and reduce the containment opening size at the end of the analysis. Both approaches were used in studying the effects for the AB and TMLB sequences, as summarized in Figure 8. Cases 1 through 5 represent analyses with THREED and NAUA in which each effect was introduced into the analysis sequentially, with no retention in the RCS. Case 6 includes retention in the RCS as reported in BMI-2104 Vol. V, pending completion of SWEC analyses of RCS retention.¹⁵

H. Retention of Non Volatile Fission Products

In WASH-1400, the release fractions for the non volatile fission product groups for the highest release category (PWR-2) were based on an analysis of the TMLB' sequence with early overpressure breach of the containment. These release fractions resulted from a combination of release fractions from the core and the containment, neglecting retention in the RCS.



They are summarized as follows:

Nonvolatile Fission Product Group	Fraction of Inventory Released From Core	Containment Leakage Fraction	Fraction of Inventory Released to Environment
Barium-Strontium	0.11	0.6	0.06
Ruthenium	0.033	0.6	0.02
Lanthanum	0.013	0.3	0.004

The effects of retention of nonvolatile fission products can be determined approximately by assuming that they would be released in direct proportion to the "other" aerosols as illustrated below for a 0.1 ft² pre-existing opening:

Nonvolatile Fission Product Group	Fraction of Inventory Released From Core*	Fraction Retained In RCS**	Cont. Leakage Fraction***	Fraction Released To Environ.
Barium-Strontium	0.27	0.90	0.035	3.7x10 ⁻³
Ruthenium	0.27	0.90	0.035	3.0x10 ⁻⁴
Lanthanum	0.017	0.90	0.035	2.3x10 ⁻⁴

* Taken from BMI-2104, Volume V.

** Taken from BMI-2104, Volume V. Applies only to portion released prior to vessel meltthrough.

*** From present study, including retention in contiguous structures.

APPLICATIONS OF RESULTS TO SOURCE TERMS

In view of the analysis results discussed above, Stone & Webster Engineering Corporation proposes that the Interim Source Term, first proposed at the ICONTT-II Conference,⁴ be revised as follows to account for a more realistic assessment of the release fractions of the nonvolatile fission product groups. The noble gases and volatile fission product groups are unaffected by this revision.

Fission Product Group	Fraction of Core Inventory Released to Environment		
	WASH-1400 PWR-2	Interim Source Term*	Revised Interim Source Term
Xenon & Krypton	0.90	1.00	1.00
Iodine	0.70	0.01	0.01
Cesium-Rubidium	0.50	0.01	0.01
Tellurium-Antimony	0.30	0.01	0.01
Barium-Strontium	0.06	0.01	0.004**
Ruthenium	0.02	0.01	0.003**
Lanthanum	0.004	0.004	0.0002**

* Proposed at ICONTT-II, November 1982.⁴

** Revision based on conservative interpretation of analyses of aerosol retention.

REFERENCES

1. Report of the American Nuclear Society's Special Committee on Source Terms, Chapter 6 and Appendix B (in printing).
2. "Reactor Safety Study: An Assessment of Accident Risks in U.S. Commercial Nuclear Power Plants", WASH-1400, NUREG-75/014, U.S. Nuclear Regulatory Commission (1975).
3. Gieseke, J.A. et al, "Radionuclide Release Under Specific LWR Accident Conditions - Vol. V - PWR Large Dry Containment (Surry Recalculations), Draft Report, BMI-2104, Vol. V, Battelle Columbus Laboratories (Jan.1984)
4. Warman, E.A., "Assessment of Radiological Consequences of Postulated Reactor Accidents", Presented at Second International Conference on Nuclear Technology Transfer, ICONTT-II, Buenos Aires, Argentina (Nov.1982).
5. Gieseke, J.A. et al, "Radionuclide Release Under Specific LWR Accident Conditions - Vol. I - PWR Large Dry Containment, Draft Report, BMI-2104, Vol. I, Battelle Columbus Laboratories (July 1983).
6. Moore, K.V. and Pettey, W.H., "RELAP4-Mod5: A Computer Program for Transient Thermal Hydraulic Analysis of Nuclear Reactors and Related Systems", User's Manual, Vol. I-III, Aerojet Nuclear Company, ANCR-NUREG-1355 (Sept. 1976).
7. Powers, D., Sandia National Laboratories, Personal Communication.
8. "THREED: A Subcompartment Transient Response Code", Stone & Webster Engineering Corporation, Proprietary Computer Program, NU-092 (Mar. 1975).
9. Wheat, L.L. et al, "CONTEMPT-LT, A Computer Program for Predicting Containment Pressure - Temperature Response to a Loss-of-Coolant Accident", Aerojet General Corporation, ANCR-1219 (1975).
10. Bunz, H., Kayro, M. and Schock, W., "NAUA-Mod4, A Code for Calculating Aerosol Behavior in LWR Core Melt Accidents, Code Description and User's Manual", Kernforschungszentrum Karlsruhe (KfK) (Mar. 1982).
11. Dunbar, I.A. "The Role of Diffusiophoresis in LWR Accidents", UKAEA Safety and Reliability Directorate, Proceedings of the International Meeting on Light Water Reactor Severe Accident Evaluation, Cambridge, MA (Aug. 1983).
12. Almenas, K.K. and Marchello, J.M., "The Physical State of Post Loss-of-Coolant Accident Containment Atmosphere", Nuclear Technology, Vol. 44 (Aug. 1979).
13. Koestel, A., Gido, R.G., and Lamkin, D.E., "Drop-Size Estimates for a Loss-of-Coolant-Accident", NUREG/CR-1607, LA-8449-MS, Los Alamos Scientific Laboratory (Aug. 1980).
14. Williams, D.C., Murata, K.K., and Tills, J.L., "Phenomenological Uncertainties in the Suspended Radionuclide Concentrations in Containment During Severe LWR Accidents", Sandia National Laboratories, Presented at ANS Topical Meeting on Fission Product Behavior and Source Term Research, Snowbird, Utah (July 1984).
15. Warman, E.A., Metcalf, J.E., Drozd, A., and Donahue, M.L., "Fission Product Transport and Retention in PWR Reactor Coolant and Containment Systems", Specialists Meeting on Nuclear Aerosols in Reactor Safety, Committee on the Safety of Nuclear Installations (CSNI) of the Organization for Economic Cooperation and Development (OECD) Nuclear Energy Agency, Karlsruhe, FRG, (Sept. 1984).



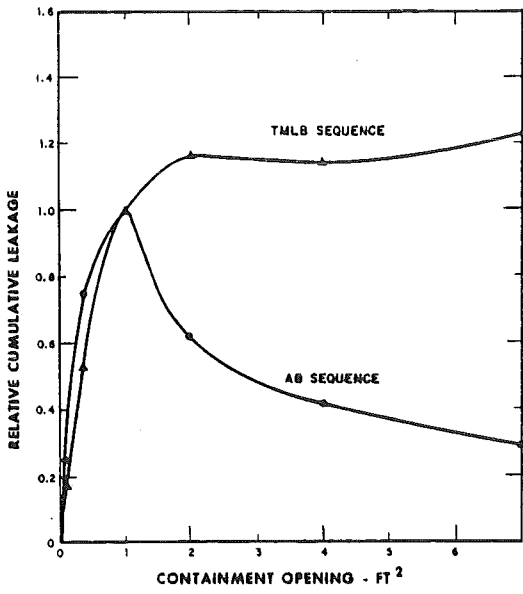
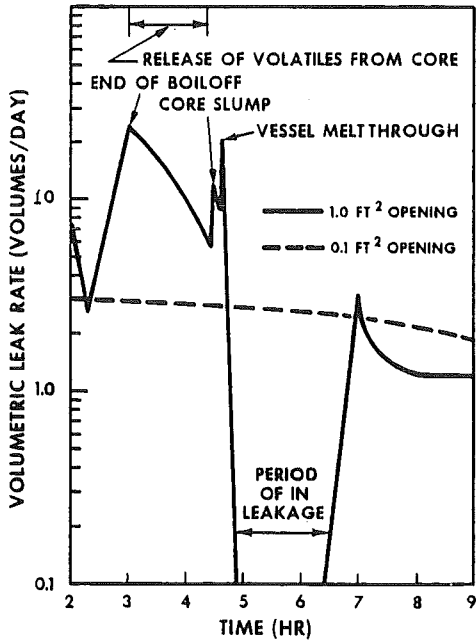


Figure 1
EFFECT OF SIZE OF
PRE-EXISTING
OPENING ON
LEAKAGE OF IODINE
AND CESIUM

NOTE:
NORMALIZED TO A LEAKAGE
FRACTION OF 1.0 FOR
1.0 FT² OPENING

STONE & WEBSTER ▲

Figure 2



VOLUMETRIC LEAK RATES
WITH 1.0 OR 0.1 FT²
PRE-EXISTING OPENING
IN CONTAINMENT
TMLB SEQUENCE

STONE & WEBSTER ▲

STONE & WEBSTER ▲

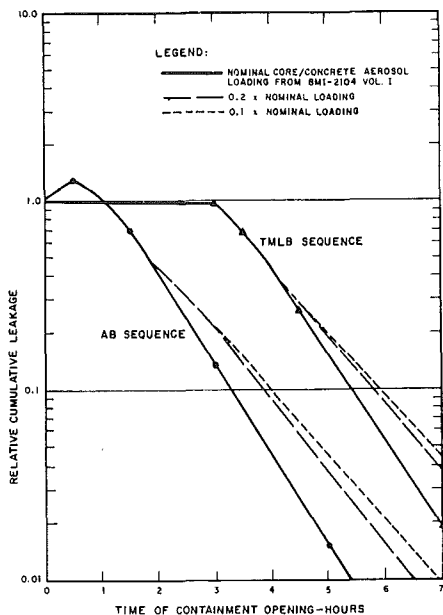
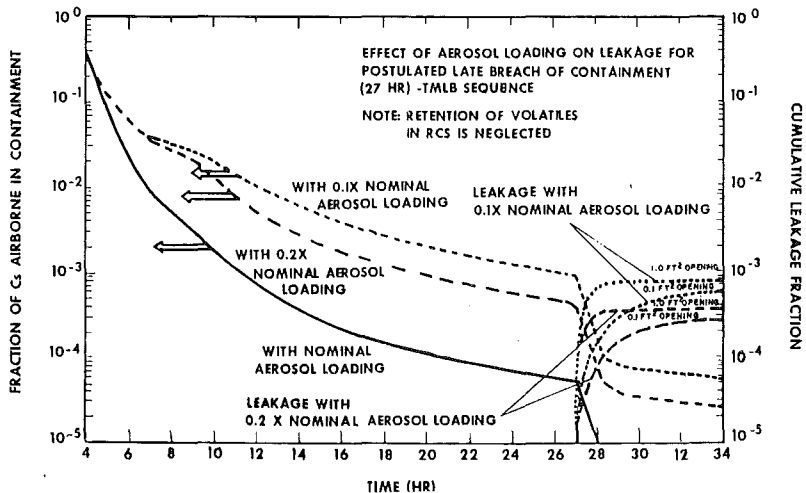


Figure 3
**EFFECT OF TIMING OF 1.0 FT²
 OPENING IN CONTAINMENT
 ON LEAKAGE OF
 IODINE AND CESIUM**

NOTE:
 NORMALIZED TO A LEAKAGE FRACTION OF
 1.0 FOR A PRE-EXISTING OPENING

Figure 4



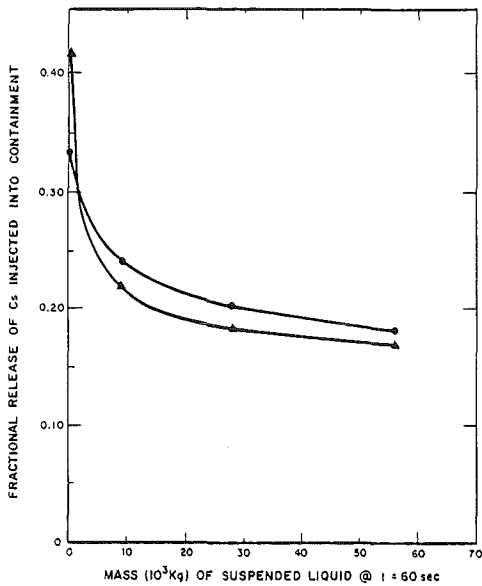


Figure 5
EFFECT OF SUSPENDED LIQUID ON RELEASE OF Cs WITH AND WITHOUT DIFFUSIOPHORESIS

LEGEND:
● DIFFUSIOPHORESIS CONSIDERED
▲ DIFFUSIOPHORESIS NOT CONSIDERED

CONDITIONS:
AB SEQUENCE 1.0 FT² OPENING @ t = 0
DEPLETION OF SUSPENDED LIQUID
AFTER t = 60 sec CALCULATED BY
NAUA-MOD 4
MONODISPERSE LOG NORMAL
DISTRIBUTION WITH 1.0 MICMMD
AND $\sigma_g = 2.0$

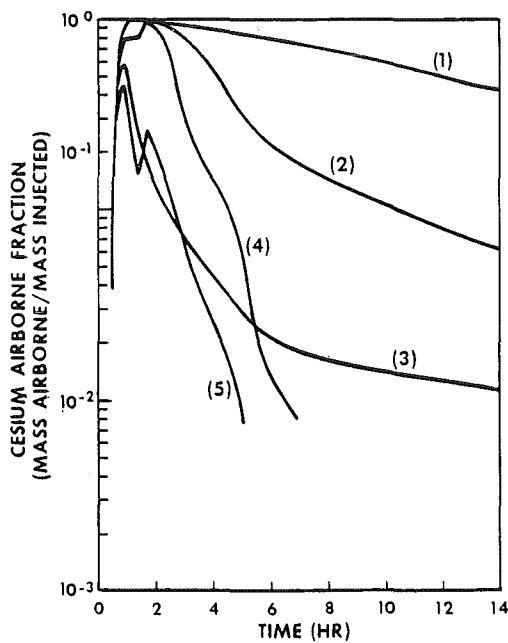
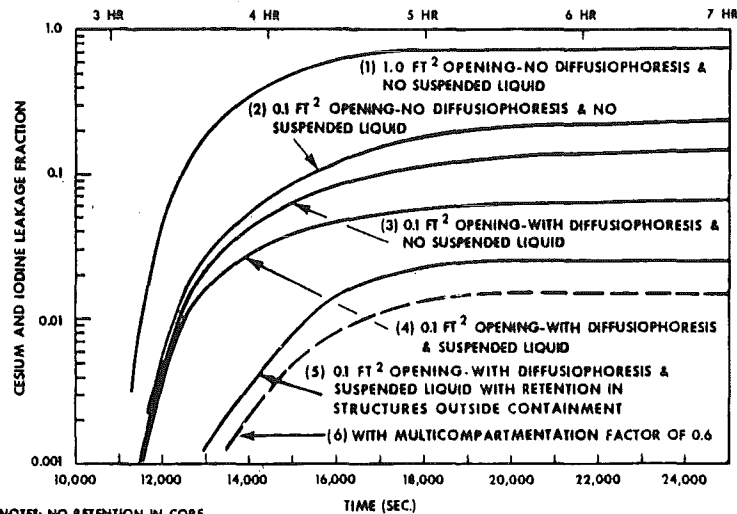


Figure 6
EFFECT OF 'OTHER' AEROSOLS AND DIFFUSIOPHORESIS AND SUSPENDED LIQUID ON AIRBORNE CONCENTRATION OF CESIUM FOR AB SEQUENCE WITH NO CONTAINMENT BREACH

LEGEND OF CASES STUDIED
(1) IN-VESSEL RELEASE OF VOLATILES (10.3 kgI, 106.2 kgCs, AND 18.3 kgTe)
(2) IN-VESSEL RELEASE OF VOLATILES AND 'OTHER' AEROSOLS (SAME AS CASE 1 PLUS 434 kg OF 'OTHER' AEROSOLS)
(3) CASE 1 WITH DIFFUSIOPHORESIS AND SUSPENDED LIQUID
(4) IN-VESSEL RELEASES FROM CASE 2 AND EX-VESSEL RELEASES TOTALING 12.4 kgI, 130.6 kgCs, 25.4 kgTe, AND 5500 Kg OF 'OTHER' AEROSOLS, NEGLECTING DIFFUSIOPHORESIS AND SUSPENDED LIQUID
(5) CASE 4 WITH DIFFUSIOPHORESIS AND SUSPENDED LIQUID

Figure 7

EFFECT OF RETENTION FACTORS ON CUMULATIVE CESIUM AND IODINE LEAKAGE FRACTIONS WITH PREEXISTING CONTAINMENT OPENING-TMLB SEQUENCE



NOTE: NO RETENTION IN CORE
NO RETENTION IN REACTOR COOLANT SYSTEM

Figure 8

CUMULATIVE EFFECTS OF VARIOUS PHENOMENA ON IODINE RELEASE

ANALYSIS CASE	PHENOMENA INCLUDED IN ANALYSIS						FRACTION OF CORE INVENTORY RELEASED TO ENVIRONMENT			
	AGGLOMERATION & SETTLING	DIFFUSIOPHORESIS	SUSPENDED LIQUID	STRUCT. OUTSIDE CONT.	MULTI-COMPARTMENTS IN CONT.	RETENTION IN ACE*	AB SEQUENCE		TMLB SEQUENCE	
							PREEXISTING OPENING SIZE (FT ²)	PREEXISTING OPENING SIZE (FT ²)	PREEXISTING OPENING SIZE (FT ²)	PREEXISTING OPENING SIZE (FT ²)
							1.0	0.1	1.0	0.1
1	X						0.43	0.16	0.72	0.23
2	X	X					0.35	0.11	0.55	0.15
3	X	X	X				0.20	0.049	0.36	0.061
4	X	X	X	X			0.11	0.020	0.23	0.026
5	X	X	X	X	X		0.066	0.012	0.14	0.015
6	X	X	X	X	X	X	0.064	0.012	0.014	0.0015

*RETENTION IN RCS TAKEN FROM BMI-2104 VOLUME V.

CURRENT RESULTS OF RADIOACTIVE SOURCE TERM ANALYSES
FOR MELT DOWN SEQUENCES IN KWU-TYPE PWR'S

K. Hassmann, M. Fischer

Kraftwerk Union AG, P.O.Box 3220,
D-8520 Erlangen, F.R.G

J. P. Hosemann, H. Bunz

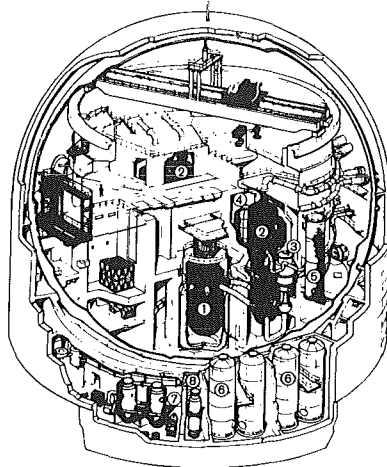
Karlsruhe, Nuclear Research Center,
P.O.Box 3640, D-7500 Karlsruhe, F.R.G

ABSTRACT

Core melt accidents in nuclear power plants are analysed to occur with an extremely low probability. In spite of this fact the public interest concentrates on the radioactive material which may be released during these highly improbable hypothetical events. Therefore, the objective of the R+D-work sponsored by the Federal Ministry of Research and Technology focus on the development of the analytical basis for radioactive source term predictions. It is the purpose of this paper - on the basis of 1300 MWe KWU type PWR's - to summarize and to compare the results of current analyses performed in the Federal Republic of Germany.

INTRODUCTION

The investigations into core meltdowns conducted for more than ten years in the Federal Republic of Germany (FRG) currently have been concentrated on the source term for risk dominant accident sequences. To determine the radioactive fission product releases to the environment, thermohydraulics and thermodynamics are needed as well as comprehensive computations to evaluate the aerosol and iodine fractions and their physical and chemical behavior. Additionally, single problems - such as the pressure level beyond that the steel shell fails during pressurization as well as the flow paths of the gases within the reactor building before and after containment failure - influence the results and therefore have to be identified. Recent analyses performed currently demonstrate that the consequences of melt downs had been considerably overestimated in previous basic studies such as the German Risk Study / 1 /. The above statement is based not the least on the particular features of the containment and the entire building with respect to the retention of radioactivity. A typical German containment is shown in Fig. 1.



<u>Primary Circuit</u>	<u>Emergency Cooling Circuit</u>
① Reactor Pressure Vessel	⑤ Accumulator
② Steam Generator	⑥ Borated Water Storage
③ Reactor Coolant Pump	⑦ Safety Injection Pump
④ Pressurizer	⑧ Residual Heat Exchanger

Fig. 1: Reactor Building Biblis

ACCIDENT SEQUENCES

With a view of the considerations to be made later in this paper, it is appropriate to present first a review of the melt-down sequence. In general, two cases can be distinguished as typical examples: the low pressure and the high pressure paths, which with respect to the radioactive source term are expected to be the enveloping bounds for all other melt-down scenarios.

Low Pressure Path

After a large leak as initiating event this sequence proceeds at low pressure in the primary system. Representative of this category, the sequence will be described following a double-ended break of the hot main coolant line and complete failure of the low pressure emergency core cooling systems if the operation changes from the feed to the sump recirculation mode. As a consequence of this hypothesis the evaporation from the reactor pressure vessel flooded up to the main coolant line level starts 20 minutes after blow-down. Subsequently, the water level after 0.6 h has dropped down to the upper edge of the core followed by failure of the core support structure after another 1.2 h.

The interaction of core melt with the foundation concrete starts immediately after failure of the reactor pressure vessel about 1.9 h after blow-down. Evaporation of the sump-water starts after about eight hours, immediately after the concrete shielding in the reactor cavity is penetrated which, initially, keeps the sump separate from the melt. The long-term build-up of pressure in the containment is determined by the evaporation of the sump-water. With the containment isolated - which exhibits only the design leakage of 0.25 Vol%/d - this gives rise to a pressure build-up in the long run.

High Pressure Path

Contrary to the low pressure path, this sequence is characterized by events taking place at high pressure in the primary system. If, after an emergency power case additionally the whole set of redundant Diesel generators fails, no electricity supply is available. In that case, the decay heat is initially removed from the core to the steam generators which, on the secondary side, evaporate their water inventory until after about 1.5 h all steam generators are getting dry. This results in a pressure and temperature rise in the primary circuit onto the set point of the pressurizer pressure relief valves.

Closing and opening cycles of the pressure relief valves are repeated until the dropping water level has rendered bare parts of the core in the reactor pressure vessel. The core is further heated and later there will be indications of melting. If the reactor pressure vessel fails due to contact of molten material with the RPV, substantial energy and mass transport takes place from the primary system into the containment. Depressurization upon failure of the reactor pressure vessel is followed by flooding of the molten material and of the still unmolten core parts slumped on the concrete foundation through accumulator water. Depending on whether the liquid and solid core parts are coolable or not coolable in water, the water evaporates at a slightly faster or slower rate. For both, the low and the high pressure cases Table 1 compares the most important results of the sequence analyses. The lowest three lines contain important information which is needed to value the fission product release rates presented in the following sections.

In conformity with the results reported in the German Risk Study on Nuclear Power Plants it can be assumed that in much more than 90 % of all conceivable cases the containment is tight at the onset of an accident (except for the design leakage to be considered) and that it remains tight until overpressure failure. Therefore, the calculations presented in the paper concentrate on this scenario.

	Low Pressure Case	High Pressure Case
Initiating event, h	0.3	0
Core heat up, failure of core support structure after, h	1.3	5.0
RPV-heat up, until h	1.9	5.0
Sump water ingress, h	8	5.0
Integral aerosol release into containment, kg	3460	22.4
Failure of steel shell, d	5	Melt coolable yes no 4.3 5
Sump evaporated, d	12/8.5*	6/7*

* depending upon failure mode of the steel shell (20/300 cm²)

Table 1: RESULTS OF MELT DOWN SEQUENCES

THERMODYNAMICS IN THE CONTAINMENT AND IN ADJACENT VOLUMES

The calculations have been performed with the computer code WAVCO / 2 / which has been developed in order to predict the thermodynamics and the distribution of gases and other constituents within a subdivided building. Based upon the main features illustrated in Fig. 2, an equation system consisting of separate mass- and energy-balances for the state of the atmosphere and sump of each zone is set-up. Furtheron, additional balances for the mass of each component must be solved to determine the actual gas distribution. All possible thermodynamic states of the atmospheric steam are commonly covered by the same equation-system. Since the conditions inside different zones are strongly dependent from each other all the zone-specific equations have to be combined to form a coupled non-linear differential equation system.

Fig. 3 illustrates the overall reactor building as well as the flow paths which have to be considered in core melt situations of release category 6 sequences (containment intact within the first couple of days until overpressurization of the steel shell). Fission products approaching the annulus can be released to the environment through the air extraction system via the stack - or - at slight overpressure conditions - via leakages through penetrations in the outermost concrete structure. After containment failure the pressure in the annulus increases beyond the 0.1 bar limit. Then, a large leak with an area of 12 m² which has been identified to be the weakest point fails resulting in a pressure equalisation between the annulus and the auxiliary building. During this blow-down procedure the pressure in the auxiliary building increases up to the 0.05 bar level initiating failure of a connection to the environment and to the turbine hall.

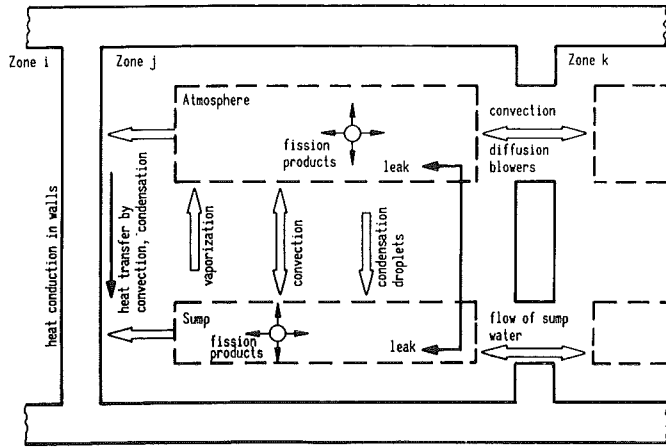


Fig. 2: WAVCO, SCHEME OF CONSIDERED PHYSICAL PROCESSES

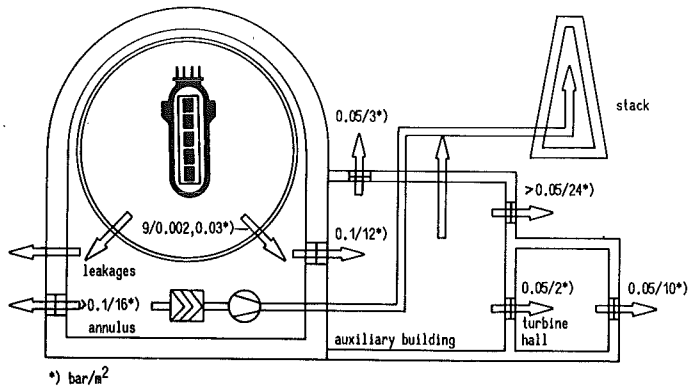


Fig. 3: SKETCH OF THE REACTOR BUILDING

From that point on, containment atmosphere enters the environment through several connections. The time dependent flow rates via the different flow paths has been calculated and have been used as the basis for aerosol and iodine calculations.

The containment failure mode, in particular, the cross section, influences the flow rate out of the containment into adjacent areas and therefore determines the released radioactive source term. As a matter of fact, experts in the FRG agree today that failure of the undisturbed steel shell of a German 1300 MWe Standard PWR will occur at about 14 bars and that in the realistic case at a lower pressure level leakages before failure are expected. Therefore, investigations of the load carrying capability were performed at different locations of the containment, the goal being to quantify the type of failure for a steadily rising internal pressure and to indicate the associated cross sections of the openings.

At a pressure of 11 bar and a temperature of 170 °C radial expansions of as much as approx. 40 cm and vertical tangential displacements at the equator of about 30 cm occur in the undisturbed shell zone. Deformations of this size are not tolerated by the surrounding structure; even before attaining the loading condition indicated before, substantial constrained deformations take place at the disturbed points and hence leakages develop. The results show that failure of the steel shell must be expected to occur first at the material lock which is bolted to the steel shell of the reactor containment. For verification a cheap experiment will be performed / 3 /, the results of which could be transferred directly to real conditions without requiring to develop and run an expensive computer program.

According to the present state of knowledge a leak of limited size is expected. The leak size ranges between 300 cm² and a value which is sufficiently high to prevent a further continuous pressure rise in the reactor containment. This value depends exclusively on thermodynamic parameters because just the energy and mass flows generated in the containment at the time of overpressure failure must be removed through the leak. The leak is also strongly influenced by the layout of the containment. For containments of German standard PWR's a 20 cm² cross section is sufficient to prevent a further pressure increase in the containment.

On the basis of the energy and mass release into the containment and the two limit cases encountered for overpressure failure (20 cm² leak and 300 cm² leak) Fig. 4 shows the pressure plot for the low (LPC) and the high pressure case (HPC). For the LPC a pressure increase up to the 9 bar load limit of the steel shell must be expected after about five days only. Because of the fact the core material has been assumed to be coolable, a slightly shorter time interval of 4.3 days has been calculated for the HPC.

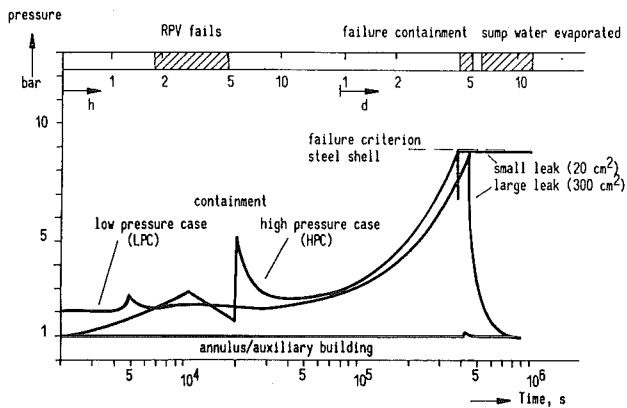


Fig. 4: CONTAINMENT HISTORIES FOR RELEASE CATEGORY 6 SEQUENCES

For the HPC the maximum pressure occurring during pressurization of the primary circuit is well below the design pressure of the containment. As already mentioned, the pressure can be stabilized with a 20 cm^2 leak whilst a leak cross section of 300 cm^2 leads to complete depressurization. The pressure in the annulus and the auxiliary building stays at the atmospheric level. Only immediately after failure of the steel shell the pressure within the annulus exceeds to the 0.1 bar level causing failure of the connection between annulus and auxiliary building. This fact has been predicted to occur for both the small and the large leak size.

FISSION PRODUCT BEHAVIOR

Until overpressurization of the steel shell only the design leakage from the containment into the annulus is effective (about $7 \text{ m}^3/\text{h}$). In the low pressure case fission gases, iodine and particles are transported to the stack passing the filter system via the annulus suction system (about $600 \text{ m}^3/\text{h}$). Because of the loss of power this system doesn't operate in the high pressure sequence. For all cases the filter itself has been assumed to be ineffective at the time of overpressurization failure. This is a very conservative assumption because the situation within the annulus during and after this time period will probably only cause a degradation of the filter's behavior to retain iodine and aerosols.

Aerosols

Data derived from the SASCHA experiments / 4 / have been used in order to compute the release of aerosols particles from the core and the primary circuit into the containment. The behavior of the aerosol system within the containment and in the adjacent volumes have been analysed by the NAUA-code / 5 /. The code is based on physical aerosol processes summarized in Tab. 2 which also includes the sensitivity of each individual process on the basis of the conditions typical for LWR-scenarios.

Aerosol Process	Integrated in NAUA	Sensitivity
sedimentation	yes	very important
diffusion	yes	minor effective
thermophoresis	no	insignificant for LWR-szenarios
diffusiophoresis	yes	important
turbulence	no	not important for LWR-szenarios
agglomeration	yes	very important
steam condensation	yes	important, if thermodynamics available

Table 2: SENSITIVITY OF DIFFERENT AEROSOL DEPLETION MECHANISMS

For the high and the low pressure case Fig. 5 shows the instantaneous airborne particle mass in the containment.

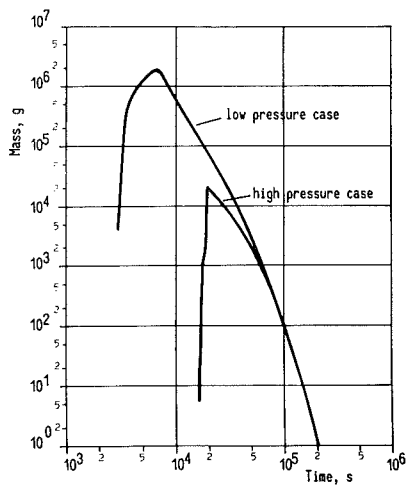


Fig. 5: AIRBORNE AEROSOL MASS IN THE CONTAINMENT

It should be pointed out that, obviously, by far the highest amount of airborne particle mass are non-radioactive elements and isotops. For the low pressure case (LPC) as a result of the large aerosol source the airborne mass decreases by more than five orders of magnitude within five days through aerosol-physical removal mechanisms. At the time of containment failure only those substances can still be released at the maximum which continue to be airborne. Starting with a less dense aerosol atmosphere the removal in the high pressure sequence (HPC) is slower and in the long term period equals the situation in the LPC. At the time of overpressurization of the containment which is not shown in Fig. 5 even higher aerosol concentrations are calculated for the HPC.

Fig. 6 shows the integral particle mass transported to the environment via all open connections as calculated on the basis of the flow paths illustrated in Fig. 3.

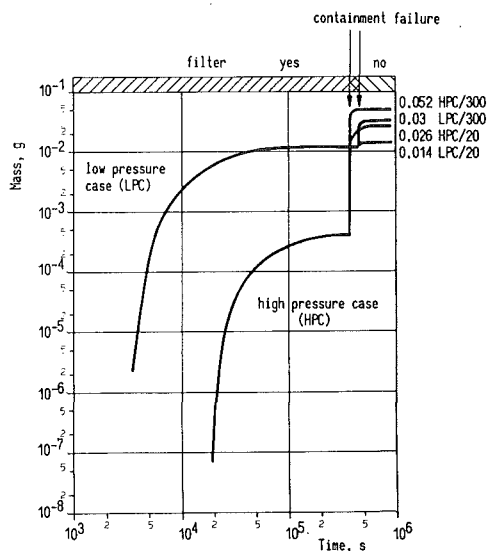


Fig. 6: ACCUMULATED AEROSOL MASSES LEAKED TO THE ENVIRONMENT

Compared with the small leak cases the results indicate about a factor of 2 higher releases for the 300 cm² leak. As a consequence of the shorter time interval until containment failure and of the higher amount of aerosol still airborne a slightly larger mass will be released to the environment in the HPC. It also can be concluded that failure of the filters as pessimistically assumed is more sensitive in the HPC.

Iodine

The iodine behavior within the containment and adjacent volumes has been calculated using the iodine model IMPAIR. The main features of the model / 6 / are summarized in Tab. 3.

During Release out of the Fuel and within the Primary System
 =====

- Constant release rates and homogenous mixing
- 99 % of I₂ instantaneously reacts in Cs/H₂O/H₂ atmosphere to form CsI
- no AgI reaction
- no retention
- in the high pressure case max. concentration of aerosols 200 g/m³ containing 2 % I

In the containment
 =====

- I₂-partition coefficient 200
- secondary reactions neglected which result in higher pH-values as f.i. impurities, I₂-formation, Redox-potential, radiolysis
- I₂ reacts in sumpwater to form AgI, equilibrium after 3.5 h with 10 % of the I₂ available
- airborne I₂ reacts with organic material to form organic I, at the maximum 90 % I₂ and 10 % organic I

In Adjacent Volumes
 =====

- carry over of I-species corr. to leak rates and composition within the "source-volume"
- no I⁻ release to adjacent volumes via water droplets in the steam flow generated by sump-water evaporation
- partition coefficient of 5000 for the overall I
- organic I released to adjacent volumes doesn't react any more. Additional organic I is formed by airborne I₂ (after 10 h 50 % of each)
- I-release continues until all the sump-water is evaporated.

Tab. 3 cont.: IMPAIR (IODINE MODEL), IMPORTANT ASSUMPTIONS

Table 3: IMPAIR (IODINE MODEL), IMPORTANT ASSUMPTIONS

These assumptions are based on the actual knowledge in this extremely complex science and represent the commonly agreed opinion of experts in the FRG and abroad. Nevertheless, important assumptions which usually include some conservatism need final experimental verification. The numbers which are reported in this paper will change in the future and therefore should be taken as a preliminary orientation.

Analogous to Fig. 6 representing the aerosol release rates Fig. 7 shows the total iodine releases to the environment for the low and the high pressure case (HPC). Because of the uncertainties as well as the only small differences in the calculated results the influence of the different containment failure modes on the iodine behavior is not presented. Similar to the results of the NAUA calculations, larger iodine releases - at the end in the one/two orders of magnitude range - have been analysed for the HPC.

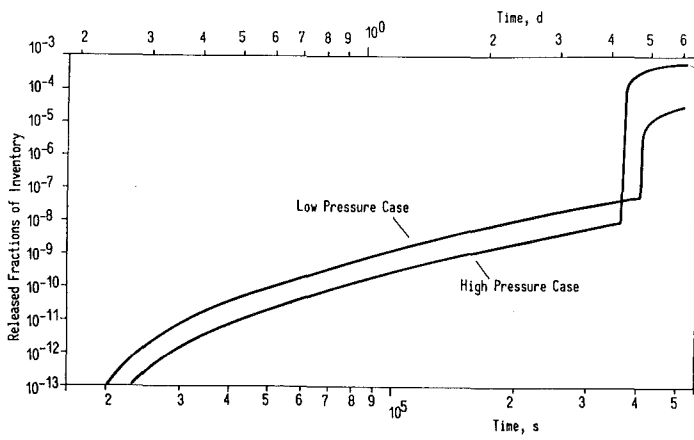


Fig. 7: COMPARISON OF THE TOTAL IODINE RELEASE TO THE ENVIRONMENT

On the basis of the HPC the fraction of the different iodine species is given in Fig. 8.

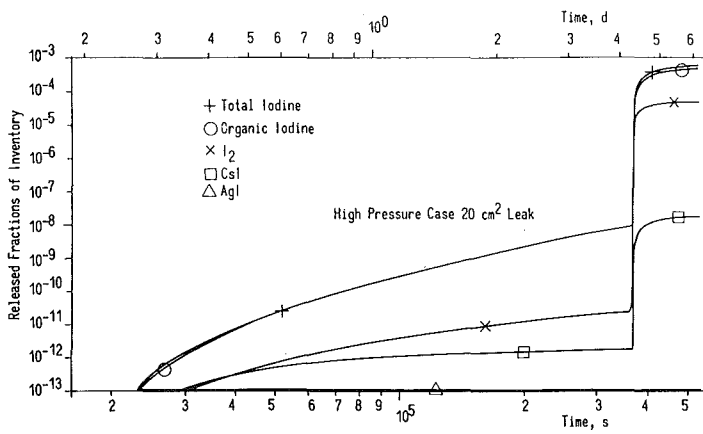


Fig. 8: IODINE RELEASE TO THE ENVIRONMENT

This tendency demonstrating the importance of organic iodine and I_2 has been identified for all scenarios.

CONCLUSION

Finally, Table 4 summarizes the integral release of Cs 137 and I 131 as the isotopes dominating the melt-down consequences, I 131 determining the early fatalities, Cs 137 the late cancers and the ground contamination. Although care should be taken as a consequence of important assumptions which may change in the future, it can be concluded that - compared with the results of the German Risk Study - the consequences of core melt-downs will be much lower than previously estimated.

	Cs 137		I integral	I 131	
	g	Ci	g	g	Ci
Low Pressure Case					
- case 1	$3 \cdot 10^{-4}$	$3 \cdot 10^{-2}$	1	0.04	$5 \cdot 10^3$
- case 2	$7 \cdot 10^{-4}$	$7 \cdot 10^{-2}$			
High Pressure Case					
- case 1	$3 \cdot 10^{-3}$	0.3	10	0.5	$6 \cdot 10^4$
- case 2	$5 \cdot 10^{-3}$	0.5			

case 1 = 20 cm^2 leak
case 2 = 300 cm^2 leak

Table 4: CAESIUM AND IODINE RELEASE TO THE ENVIRONMENT (WITHOUT DECAY)

To confirm the expected tendency ongoing research work on specific aspects related to severe accidents has to be completed. In particular, this includes: sensitivity studies, consequence analyses for other dominant sequences, improvements of fission products behavior and demonstration of aerosol plate-out (DEMONA-experiments). In addition, work is being performed to clarify hydrogen distribution and explosion phenomena as well as the long term melt/concrete behavior (BETA-experiments). All the R & D work mentioned above has been initiated and is expected to be completed in the near term future.

LITERATURE

- / 1 / "Deutsche Risikostudie Kernkraftwerke",
Herausgeber Bundesminister für Forschung und
Technologie, Verlag TÜV Rheinland, Köln 1979
- / 2 / M. Fischer et al, The Multi Compartment Code
WAVCO, Status and Validation, International
Conference on Containment Design, June 17 - 20,
1984, Toronto, Ontario
- / 3 / H. H. Hennies et al, The Reactor Containment of
German Pressurized Water Reactors of Standard
Design, as / 2 /
- / 4 / H. Albrecht, H. Wild, "Behavior of I, Cs, Te, Ba,
Ag, In, and Cd during Release from Overheated PWR
Cores", International Meeting on Light Water Reactor
Severe Accident Evaluation, Aug. 29 - Sept. 1, 1983,
Cambridge, Mass.
- / 5 / H. Bunz, W. Schikarski, W. Schöck, The Role of
Aerosol Behavior in LWR Core Melt Accidents,
Nuclear Technology, Vol. 53, pp. 141-146, May 1981
- / 6 / J. P. Hosemann, K. H. Neeb, J. Wilhelm, Neuere
Bewertung der Freisetzung und des Transportes von
Jod bei schweren Reaktorstörfällen, Jahrestagung
Kerntechnik 1983, Berlin

RETENTION OF GASEOUS RADIOIODINE WITH SORBENTS
UNDER ACCIDENT CONDITIONS

H. Deuber, H.-G. Dillmann, K. Gerlach

Kernforschungszentrum Karlsruhe GmbH
D-7500 Karlsruhe 1, Postfach 3640
Federal Republic of Germany

ABSTRACT

Under moderate filtration conditions ($<150^{\circ}\text{C}$) impregnated activated carbons can be used to efficiently retain radioiodine. With a residence time of about 1 s in the carbon, for elemental radioiodine a retention of $\geq 99.99\%$ can be anticipated because the desorbing iodine is in a nonelemental form. For methyl iodide a retention of $>99\%$ can be assumed under the same conditions. An extremely low retention has to be expected for certain unidentified iodine species which according to recent measurements may occur in high proportions in the exhaust air of light water reactors in rare cases. Under extreme filtration conditions (temperature $\geq 150^{\circ}\text{C}$) silver zeolites are eligible for efficiently trapping radioiodine.

INTRODUCTION

In light water reactors (LWRs) the release of gaseous radioiodine has in general to be mitigated by filtration in both normal operation and accidents /1/. This paper deals with work which in recent years has been performed in our laboratory on the retention of gaseous radioiodine with sorbents under accident conditions. Both eligible sorbents and achievable retention are covered. Only some important results are given. Details can be found in the papers cited below. Work which is being initiated in our laboratory, e.g. on the influence of fire, is not dealt with.

GENERAL

This chapter contains some general remarks on gaseous radioiodine species, filtration conditions in LWR accidents and iodine sorbents.

The iodine species which in general have to be taken into account are elemental iodine (I_2), methyl iodide (CH_3I) and similarly behaving organic iodine compounds. Moreover, unidentified penetrating iodine species have to be reckoned with (see below). The occurrence of gaseous hypoiodous acid (HOI) is questionable /2/. The formation of gaseous hydriodic acid (HI) can not be excluded in accidents when hydrogen is present.

I_2 exhibits a much higher sorption tendency than CH_3I . Therefore, in general I_2 can be much better retained by sorbents than CH_3I . Radiologically, I_2 is much more important than CH_3I with respect to ingestion. As for inhalation, these species are of similar importance.

The retention of iodine volatilized from aqueous solutions ("HOI") by sorbents has been treated in some publications /3,4,5,6/. There are virtually no data on the retention of HI by sorbents. Corresponding investigations are being initiated in our laboratory.

As for the retention to be achieved with accident filters, it is mentioned here that German guidelines for pressurized water reactors (PWRs) require a minimum retention of 99.99 % for elemental radioiodine and of 99 % for organic radioiodine in a design basis accident /7/.

The challenges of accident filters in various LWR accident scenarios have been described /2/. In the present paper two filtration conditions are distinguished: moderate conditions (e.g. filtration of PWR annulus exhaust air) and extreme conditions (e.g. exventing of PWR containment). In the first case, the temperature is below 150 °C. The relative humidity is low as long as the temperature is high. In the second case, the temperature is in the region of 150 °C or higher. The relative humidity may be both low and high.

As for iodine sorbents, both activated carbons and inorganic sorbents are eligible for efficiently trapping radioiodine /1,8/.

RETENTION WITH ACTIVATED CARBONS

The activated carbons employed to capture radioiodine are usually impregnated with KI, TEDA, derivatives of TEDA or similar compounds. Mixtures of these impregnants are also used.

In this chapter some results are presented from laboratory tests on the activated carbons 207B (KI) and 207B (TEDA) (base material: coal; grain size: 8-12 mesh) with I_2 -131 and CH_3I -131 as the test agents. Moreover, some results pertaining to penetrating I-131 in the exhaust air of LWRs are given.

The conditions in the laboratory tests which are dealt with in some detail are indicated in Table I.

Table I: Parameters in the laboratory tests on the retention of $^{131}I_2$ and $CH_3^{131}I$ with activated carbons

Parameter	Unit	Value
Carrier concentration	mg/m ³	1
Temperature	°C	130 or 180
Relative humidity ^{a)}	%	2 or < 1
Pressure ^{b)}	bar	1
Face velocity	cm/s	50
Bed depth ^{c)}	cm	25
Residence time	s	0.5
Preconditioning Time	h	1
Injection time	h	1
Purging time	h	2

a) 2 % at 130 °C, < 1 % at 180 °C (dew point: 30 °C)

b) absolute (also in the following tables)

c) section depth: 1.25 or 2.5 cm (diameter: 2.5 cm)

Figs. 1 and 2 show the penetration as a function of the bed depth in the tests with I_2 -131. Two parts of the penetration curves can be distinguished. The steep part (bed depth: ≤ 5 cm) can be ascribed to I_2 , the flat part (bed depth: ≥ 5 cm) at least largely to more penetrating iodine species present as impurities or formed in the test bed.

Figs. 1 and 2 illustrate that under the test conditions chosen there was practically no influence of both the impregnant and the temperature on the extent of the penetration. At a residence time of about 0.1 s the penetration was well below 10^{-2} % with fresh carbons.

With aged carbons qualitatively similar results were obtained (not shown). However, the penetration exceeded 10^{-2} % in some cases, even at a residence time of 0.5 s (purging time: 1 week in the tests at 130 °C). It has to be mentioned that in one test with aged 207B (TEDA) at 180 °C ignition occurred.

The most important finding of the tests with I_2 -131 is that at 130 °C the iodine passing through deep carbon beds (residence time: 0.5 s) was in a non-elemental form in all cases, even with aged carbon. At 180 °C, however, also elemental iodine passed through equivalent beds of aged carbon.

With activated carbons other than 207B (KI) and 207B (TEDA) similar results were obtained. It is therefore concluded that at moderate filtration conditions (< 150 °C) a minimum retention of 99.99 % for elemental radioiodine can be equally well achieved with various commercial impregnated activated carbons.

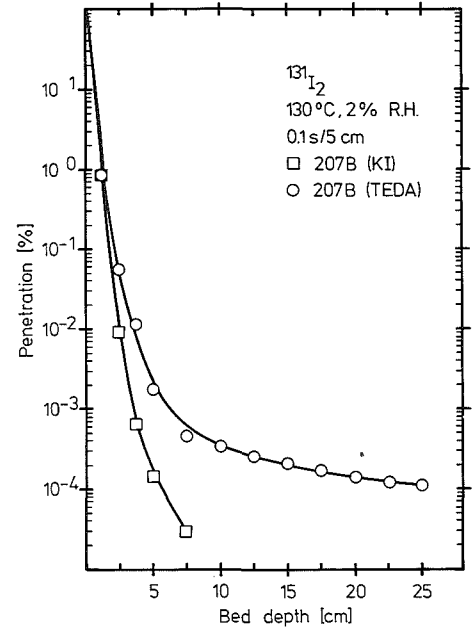
Details of the tests with I_2 -131 can be found elsewhere /9,10,11,12/.

Figs. 3 and 4 display the penetration as a function of the bed depth in the tests with CH_3I -131. As with I_2 -131, steep and flat parts of the penetration curves can be distinguished. Again, there was practically no influence of both the impregnant and the temperature on the extent of the penetration. At a residence time of about 0.1 s the penetration was several orders of magnitude lower than 1 %. It can be concluded that at moderate filtration conditions (< 150 °C) a minimum retention of 99 % for methyl radioiodide can be equally well achieved with various commercial impregnated activated carbons.

As for penetrating iodine species, the above mentioned experiments illustrate that in laboratory tests their proportions are generally extremely low. It has been found that in the exhaust air of LWRs the proportions of penetrating iodine species are usually low too (order of magnitude: 1 %) /5/. However, as discussed below, recent measurements in a boiling water reactor (BWR5) have shown that much higher proportions can not be entirely excluded.

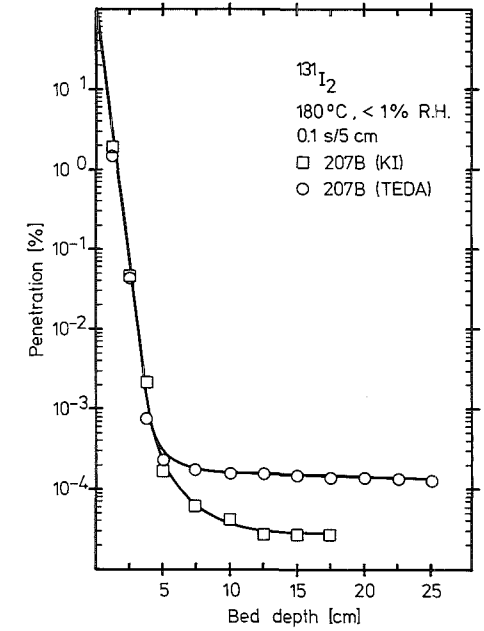
The measurements in BWR5 were made after an unusually high release of radioiodine into the reactor water due to fuel element damages. Table II contains the retention of gaseous I-131 from the reactor by a purge air filter. (The purge air originates in particular from the containment and other rooms containing reactor water.) The filter, which had been filled with fresh carbon shortly prior to the beginning of the investigations, exhibited a very low retention of total and organic I-131, in spite of the favorable filtration conditions. In two sampling periods the retention was numerically even negative.

The relatively high retention of elemental I-131 proves that the poor performance of the purge air filter was not caused by leakage. The results of a laboratory test on the carbon of the filter with CH_3I -131 show that also aging was unimportant.



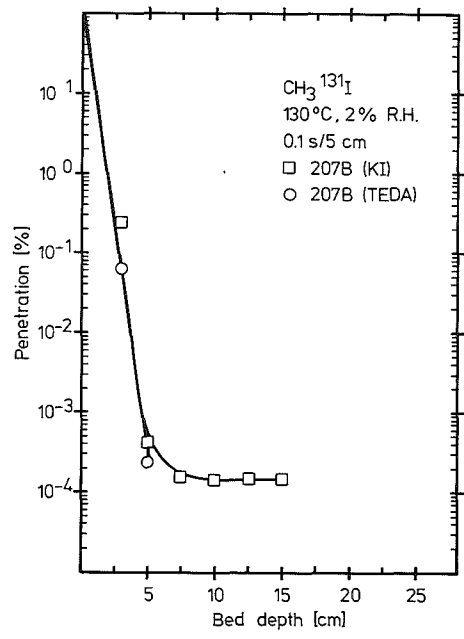
Penetration as function of bed depth

Fig. 1



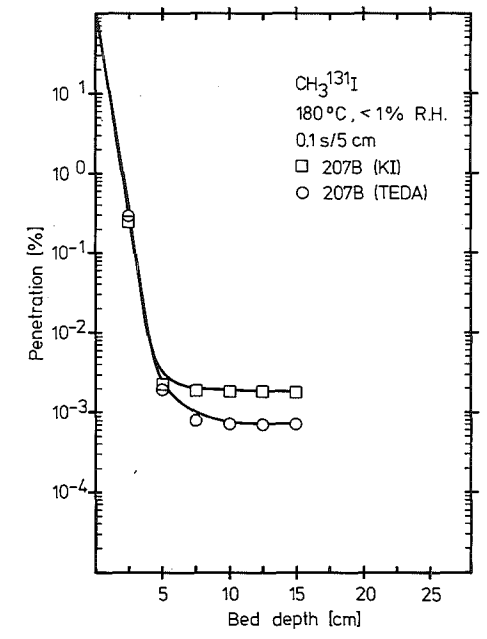
Penetration as function of bed depth

Fig. 2



Penetration as function of bed depth

Fig. 3



Penetration as function of bed depth

Fig. 4

Table II: Retention of the gaseous ^{131}I from the reactor by the purge air filter^{a)} of BWR5

Temperature : ≈ 30 °C Face velocity : 50 cm/s
 Relative humidity: ≈ 40 % Bed depth : 25 cm
 Pressure : 1 bar Residence time: 0.5 s

Sampling period ^{b)}	Retention [%]		
	Total ^{131}I	Elemental ^{131}I	Organic ^{131}I
1	76	> 99.9	71
2	55	> 99.9 ^{c)}	41
3	< 0	> 99.9 ^{c)}	< 0
4	< 0	> 99.8 ^{c)}	< 0

a) activated carbon: 207B (KI), 8-12 mesh

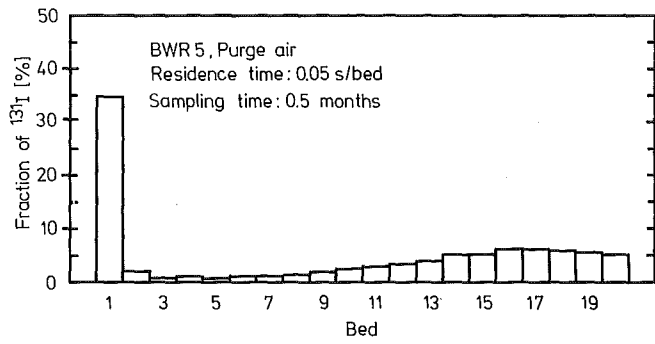
b) duration: 1 week each

c) detection limit for elemental ^{131}I in outlet air not exceeded

Hence, only the occurrence of penetrating I-131 species has to be considered. Indeed, high proportions of penetrating I-131 (order of magnitude: 50 %) result from the distribution of the I-131 from the reactor on (sectioned) activated carbon beds run in parallel to the purge air filter in the sampling periods 2 and 3. The distribution obtained with 207B (KI) and 207B (TEDA) is presented in Figs. 5 and 6. No significant difference is discernible. With another KI impregnated activated carbon (RKJ1) a better retention was observed.

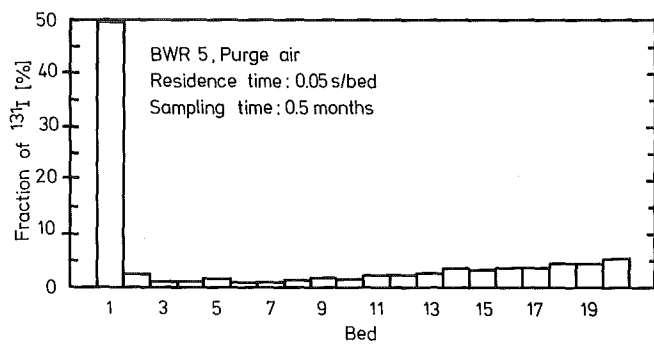
With mass spectrometric measurements the nature of the penetrating I-131 could not be elucidated. However, from the distribution of the I-131 on the carbon beds it can be concluded that "HOT" and compounds such as $\text{C}_6\text{H}_5\text{I}$ (iodine benzene) played no significant part /5/. The source of the penetrating I-131 is unknown.

The investigations on the penetrating I-131 in BWR5 are described in detail elsewhere /13/.



Distribution of ^{131}I on activated carbon beds: 207B(KI)

Fig. 5 a)



Distribution of ^{131}I on activated carbon beds: 207B(TEDA)

Fig. 6 a)

a) ^{131}I from the reactor

RETENTION WITH INORGANIC SORBENTS

Under extreme filtration conditions (temperature ≥ 150 °C), silver containing inorganic sorbents can be used instead of impregnated activated carbons to retain radioiodine. Zeolites in the silver form and materials impregnated with silver compounds are eligible.

Apart from inflammability, the inorganic sorbents exhibit a very low desorption of iodine under extreme conditions because the iodine is bound in stable silver compounds (e.g. AgI). However, the structure and/or the impregnant of the inorganic sorbents may be adversely affected under extreme conditions.

With a particular silver zeolite, however, only a very low deterioration was found. Table III contains the retention of CH_3I - ^{131}I with this sorbent under conditions which are much more serious than those to be expected e.g. during exventing of a PWR containment. At a bed depth of 5 cm (residence time: 0.2 s) a retention of <99 % was found only at the most adverse conditions. It has to be mentioned that a hydrogen purge of the silver zeolite after exhaustive loading with I-131 had no deleterious influence at high temperatures.

Inorganic materials impregnated with AgNO_3 (e.g. AC6120) should not be used at temperatures above 200 °C because of the possible decomposition of the impregnant.

Details of the investigations on inorganic sorbents can be found elsewhere /14/.

Table III: Retention of CH_3I ^{131}I with a silver zeolite

Dew point	: ≈ 150 °C	Residence time:	0.1 s/2.5 cm
Pressure	: 5 bar	Injection time:	≈ 0.1 h
Face velocity	: 25 cm/s	Purging time	: 2 h

Temperature [°C]	Exposure time [h]	Retention [%]	
		2.5 cm ^{a)}	5.0 cm ^{a)}
160	5	96.0	99.8
	96	95.4	99.7
300	5	97.8	99.9
	96	83.9	97.4

^{a)} bed depth

REFERENCES

- /1/ Wilhelm, J.G.,
Iodine Filters in Nuclear Installations, Commission of the European Communities, V/2110/83 (1982)
- /2/ OECD (NEA),
Air Cleaning in Accident Situations (to be published)
- /3/ Kabat, M.J.,
Testing and Evaluation of Absorbers for Gaseous Penetrative Forms of Radioiodine, 13th AEC Air Cleaning Conference, San Francisco, 12-15.8.74, CONF- 740807 (1975) 765
- /4/ Kabat, M.J.,
Selective Sampling of Hypoiodous Acid, 14th ERDA Air Cleaning Conference, Sun Valley, 2 -4.8.1976, CONF-760822 (1977) 490
- /5/ Deuber, H., Wilhelm, J.G.,
Occurrence of Penetrating Iodine Species in the Exhaust Air of PWR Power Plants, 16th DOE Nuclear Air Cleaning Conference, San Diego, 20-23.10.1980, CONF- 801038 (1981) 1354
- /6/ Deuber, H.,
Retention of ^{131}I Volatilized from Aqueous Solutions, by Sorbents, KfK 3778 (to be published)
- /7/ Reaktorsicherheitskommission,
RSK-Leitlinien für Druckwasserreaktoren, Gesellschaft für Reaktorsicherheit (1981)
- /8/ Kovach, J.L.,
The Evolution and Current State of Radioiodine Control, 16th DOE Nuclear Air Cleaning Conference, San Diego, 20-23.10.1980, CONF-801038 (1981) 417
- /9/ Deuber, H., Wilhelm, J.G.,
Retention of Elemental Radioiodine by Deep Bed Carbon Filters Under Accident Conditions, 17th DOE Nuclear Air Cleaning Conference, Denver, 2-5.8.1982, CONF-820833 (1983) 248
- /10/ Deuber, H.,
Influence of Aging on the Retention of Elemental Radioiodine by Deep Bed Carbon Filters Under Accident Conditions, 18th DOE Nuclear Airborne Waste Management and Air Cleaning Conference, Baltimore, 12-16.8.1984
- /11/ Deuber, H.,
Abscheidung von elementarem ^{131}I an Aktivkohlen unter Störfallbedingungen, KfK 3776 (1984)
- /12/ Deuber, H.,
Abscheidung von elementarem ^{131}I an Aktivkohlen unter extremen Bedingungen, KfK 3796 (1984)
- /13/ Deuber, H. et al.,
Investigations on the Extremely Low Retention of ^{131}I by an Iodine Filter of a Boiling Water Reactor, 18th DOE Nuclear Airborne Waste Management and Air Cleaning Conference, Baltimore, 12-16.8.1984
- /14/ Dillmann, H.-G., Pasler, H.,
Theoretical and Experimental Investigations Into the Filtration of the Atmosphere Within the Containment of Pressurized Water Reactors After Serious Reactor Accidents, 16th DOE Nuclear Air Cleaning Conference, San Diego, 20-23.10.1980, CONF-801038 (1981) 373

CONFINEMENT OF AIRBORNE PARTICULATE RADIOACTIVITY
IN THE CASE OF AN ACCIDENT

V. Rüdinger, J.G. Wilhelm
Laboratorium für Aerosolphysik und Filtertechnik
Kernforschungszentrum Karlsruhe GmbH,
Postfach 3640, D-7500 Karlsruhe 1
Federal Republic of Germany

ABSTRACT

In the case of an accident, the filter elements in the inlets and exhausts of the air-cleaning systems of a nuclear facility may become a part of the remaining fission product barrier. Among others, the Project Nuclear Safety is pursuing the information necessary to insure safe operation of air-cleaning systems under accident conditions.

Experimental investigations into the response of HEPA filters to differential pressures involving both dry and moist air have demonstrated the occurrence of structural failure with subsequent loss of efficiency at low values of differential pressures. Contributions are being made to the development and verification of computer codes used to calculate those fluid-dynamic and thermodynamic conditions expected to prevail in an air-cleaning system as a result of potential accident situations.

With regard to further investigations, a new test facility was put into operation for the realization of superimposed challenges and a new method for testing particulate removal efficiency under high temperature or high humidity was developed.

Further work will concentrate on experimental investigations of aged filters under combined challenges, development of improved filter elements, and the development of codes to model air-cleaning systems.

INTRODUCTION

The High Efficiency Particulate Air (HEPA) filters within the air-cleaning systems of nuclear installations play an important role in the confinement of airborne particulate radioactivity. The performance of these filter elements must be guaranteed not only during normal service but also under accident conditions.

In order to be able to evaluate the risk of an increased release of radioactivity to the environment, a thorough understanding of HEPA-filter behavior under possible accident conditions is needed. The necessary data, however, are in general very limited. Within this context it should be noted that relatively frequent failures of HEPA filters during normal service have been reported /1, 2/. For the more stringent possible challenges posed during accidents, more failures can be expected. Therefore, two aims of our investigations are in the field of HEPA-filter performance and include the establishment of filter performance under possible accident conditions as well as the development of improved filter designs, where found to be necessary. A requirement in this regard is that present filter dimensions and air-flow specifications should in general be maintained.

As of this time, comprehensive requirements regarding filter service under accident conditions cannot be specified because the possible conditions challenging the filter units within the Air-Cleaning Systems (ACS) are largely unknown. This is due to the lack of computer codes able to reliably estimate the conditions inside the ACS. Two additional aims fall within the context of modelling such systems. These include obtaining the required input data on ACS components, in particular the filter units, as well as contributing to the development and experimental verification of ACS codes.

In the following, a brief overview of the current status of these investigations, that are performed within the scope of the Project Nuclear Safety, are given.

HEPA-FILTER STRUCTURAL LIMITS

If a HEPA filter fails structurally the removal efficiency is usually reduced to values below 90 %, even to zero. Therefore in the case of an accident, above all the filters structural integrity must be maintained. Mechanical loads endangering the filter units can result, among others, from increased differential pressures that are induced by a tornado depressurization or a LOCA, or that develop due to filter loading with moisture from a LOCA or soot from a fire.

Response to High Air Flow Velocities: The response to high air velocities was investigated with a blowdown facility /3/. Altogether more than 250 individual tests with approximately 30 types of filters from 10 different manufacturers were performed at ambient temperature and low relative humidity; in order to establish structural limits and to measure flow resistance characteristics. Both new, commercially-available filters and improved prototypical units were tested. Some of the filters were preloaded with polystyrene latex of 0.3 μ m aerodynamic diameter; up to a pressure drop of 1 kPa at rated flow /4-6/.

The results obtained allow the actual structural limits of the major designs of commercial filters at high air velocity to be defined. They are summarized in Table I with the range of the average differential pressure at failure for the different designs.

Table I: Structural Limits of Commercial HEPA Filters of Standard Size With Glass-Fiber Media

Filter Design		Temp. of Operation (°C)	Range of Average Failure Differential Pressure (kPa)
Pack	Frame		
Deep Pleat	Wood	< 130	11 - 23
Deep Pleat	Metal	< 220	4 - 11
Mini Pleat	Wood, Metal or Plastic	< 130	6 - 19

The test results demonstrate that the structural strength of HEPA filters currently available is rather low even under the relatively benign conditions of ambient temperature and low relative humidity. It can be further stated that the filter units with deeply pleated medium and separators, sustain the highest differential pressure before failure occurs. It was found that preloading the new filters with polystyrene latex particulate led to a slight reduction in failure pressure, on the average, with two exceptions of - 27 % and - 40 %.

Response to Moist Air: The response of standard-size HEPA filters to moist air was investigated using the test facility TAI-FUN /7/. It is a closed loop facility that allows accurate control of the relative humidity up to 151 °C. With a spray system, fog conditions can also be simulated.

To establish the mechanical loads that result from exposure to flows of moist air, the measurements were oriented to determine how filter differential pressure increases as a function of the relative humidity of the air to be filtered as well as the liquid moisture content for air at > 100 % rel. humidity. In Figure 1 the results obtained from HEPA filters preloaded with room-air dust during service operation, are summarized, /8/. The tests were performed at 50 °C and the rated air flow of 1700 m³h⁻¹.

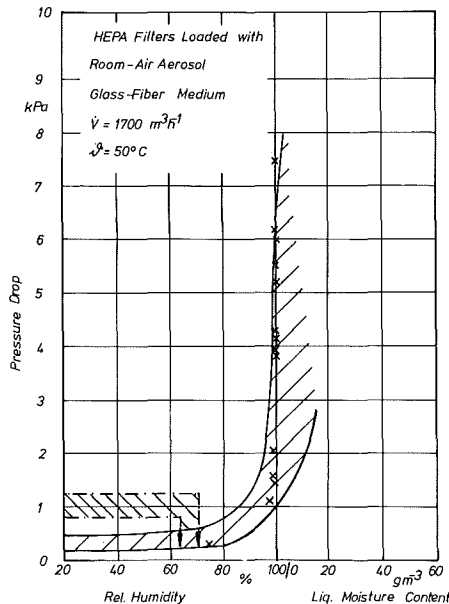


Fig. 1: Pressure drop of preloaded HEPA filters as a function of air-stream rel. humidity and liquid moisture content (50 °C, 1700 m³h⁻¹).

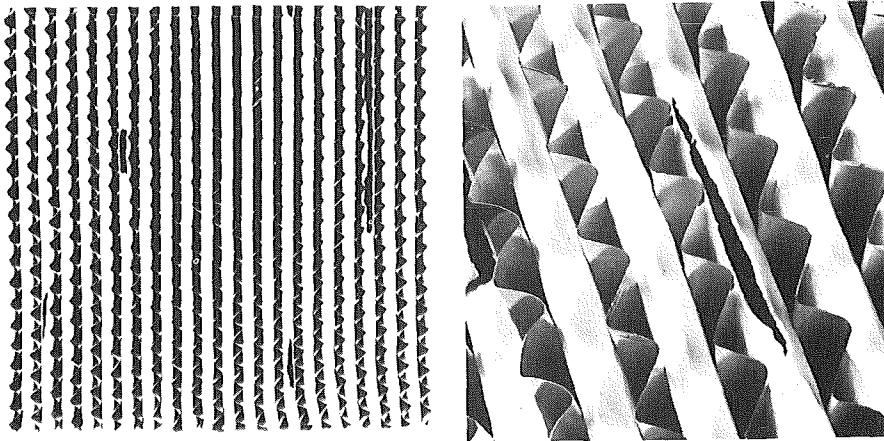
In the first phase of all the tests with loaded filters, an unexpected irreversible decrease in flow resistance was observed when the relative humidity exceeded approx. 70 % for the first time. This effect, which is not relevant with regard to the structural limits, is attributed to compaction of the particles deposited within the fiber matrix of the filter medium due to condensing water vapor. The filter medium loaded with the compacted dust only begins at about 70 % rel. humidity to incorporate water to such an amount that the flow resistance starts to rise measurably.

drop attained at 100 % rel. humidity fall within a range of 1 to approx. 7 kPa, in part dependent upon the quantity of accumulated dust. From these results it can be concluded that below 90 % rel. humidity, loaded filters are not seriously affected by extended exposure to moist air. At 100 % rel. humidity however, high differential pressures occur, and thus impose elevated mechanical loads on the filter medium. Due to the resulting stresses, the filter units usually failed at differential pressures between 1.7 and 6.3 kPa, after extended exposure to saturated air flow. Since mist eliminators, usually installed upstream of HEPA filters, can in the ideal case only reduce the moisture content only to that of saturation, they will not be able to fully protect loaded filters from failure. This conclusion was experimentally proven.

High air humidity does not only create elevated mechanical loads in the filter units, it additionally weakens the filter pack and reduces the tensile strength of the medium. Both factors cause the HEPA filters made with glass fiber media to fail structurally at the relatively low differential pressures already noted above.

Response to High Temperature: Pratt and Green /9/ reported on dynamic tests of HEPA filters during which the temperature was increased stepwise from ambient up to 500 °C over a period of approx. 30 min. Whereas the filter units of one type remained intact, the filters of two other designs failed structurally at differential pressures on the order of only 1 kPa.

Failure Modes and Filter Improvement: Different modes of failures were observed for the experiments reported on here. One mode of failure which seems to limit the structural strength of the deep-pleat design that showed the highest structural strength, is the rupture of downstream ends of the folds of the filter paper, which is illustrated in Figures 2 and 3.



Figs. 2 and 3: Failed folds of deep pleat HEPA filters

This mode of failure was observed during tests with high air velocities with high air humidities as well as under hot dynamic conditions. These failures are due to the combined effects of elevated tensile stresses within the filter medium at the ends of the folds and a reduction in the tensile strength of the medium during the exposure to the extreme operating conditions.

Based on the information gained about the modes and mechanisms of failures, first successful improvements were achieved with HEPA filters made with glass-fiber media /4-6/. The potential for further improvement in this concept of filter design is judged to be considerable. For special purposes, where the requirements for fire resistance are not very high, HEPA filters with high structural strength and high resistance to the effects of humidity and acid can be manufactured using a polycarbonate microfiber medium /10/. Particulate filters with high removal efficiency and potentially high temperature resistance, that also function as flame arrestors, can be made with stainless-steel fiber pads as the filter medium /11/. With the aid of a strong construction supporting the fiber mats, high structural strength can be achieved in spite of the very low tensile strength of the fiber pads.

NEW FACILITIES AND METHODS

The investigations into the behavior of HEPA filters under possible accident conditions also require the construction of new test facilities and the development of new test methods. In France /12/ and in the United Kingdom /9/ two new facilities were built in order to test the behavior of HEPA filters operated under high temperature.

Nearly all existing facilities only allowed HEPA filters to be tested under individual challenges, i.e., combinations of challenges were not possible. Therefore, the fluid-dynamic test facility BORA was specially designed and built at the Karlsruhe Nuclear Research Center to fill this need. With this facility, that has recently been put into operation, HEPA filters and other components of air-cleaning systems can be exposed to the combined challenges of high differential pressure and flow rate, together with high relative humidity, in a temperature range from 30 °C up to approx. 110 °C. For temperatures up to 350 °C, challenges by high temperature can be combined with high air-flow velocities. The schematic of the closed-loop facility BORA is shown in Fig. 4.

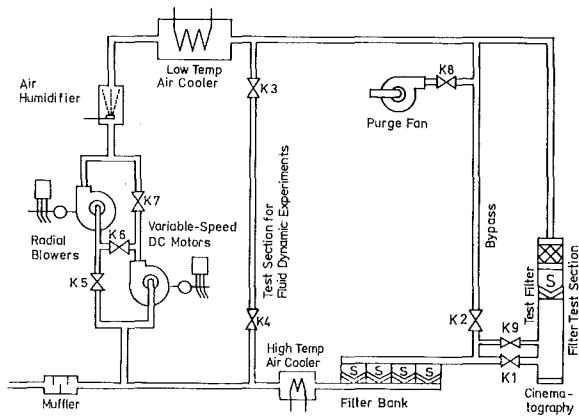
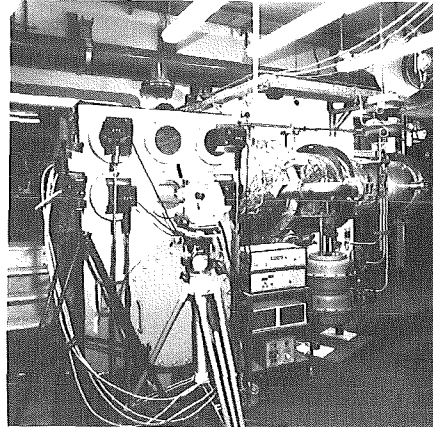
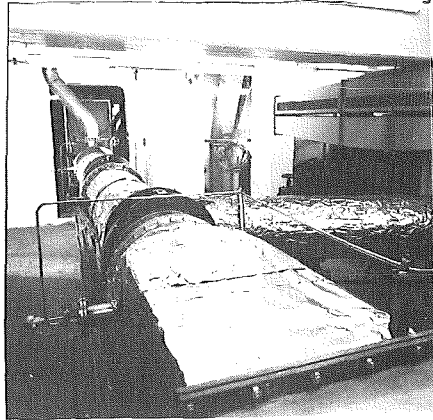
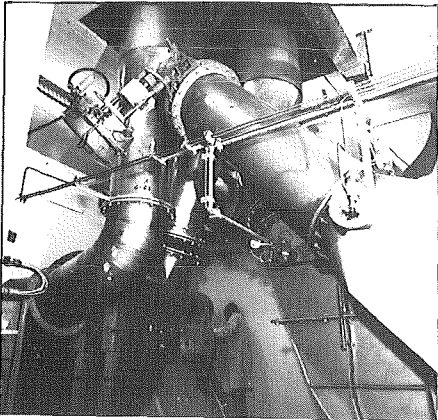


Fig. 4.: Schematic of the test facility BORA.

The facility has a maximum electrical power requirement of 900 kW and uses up to 50 m³/h of cooling water. The photos in Figs. 5-7 give an impression of the size and the character of the test facility BORA.



Figs. 5-7: Views of the test facility BORA before mounting of the thermal insulation: (5) Blowers and connecting ductwork. (6) Low temperature cooler, main duct and by-pass duct. (7) End wall of the component test section with the high-speed cinematographic equipment.

The test facility BORA was designed to analyze the behavior of air cleaning system components, namely particulate filters under extreme test-air conditions at steady and unsteady flows, as well as to help develop and to verify numerical computer codes that can model the response of air-cleaning systems to design-basis and hypothetical accident conditions. The results of the successful first test program are reported on in Ref. 13.

Another development need involves filtration efficiency, that is, verifying fission-product confinement once the structural integrity of the filter elements is assured. Whereas the NaCl method seems to be satisfactory for the measurement of filter removal efficiency at temperatures up to 350 °C /9 including discussion of Dorman, 12, 14/ no test method has been available, until now, to test full-scale HEPA filters under challenges that include high air humidity.

The newly developed procedure to test HEPA-filter efficiency under simulated conditions of high temperature and high humidity /14/ uses a condensation aerosol which is generated with the aid of an argon plasma using TiO_2 or MoO_3 powders. These aerosol substances are insoluble in water, are thermally stable, and have a high melting point. Efficiency measurements are accomplished by the collection of test-aerosol samples onto Nuclepore filters and by subsequent atomic absorption analysis. The schematic of the test method is shown in Fig. 8.

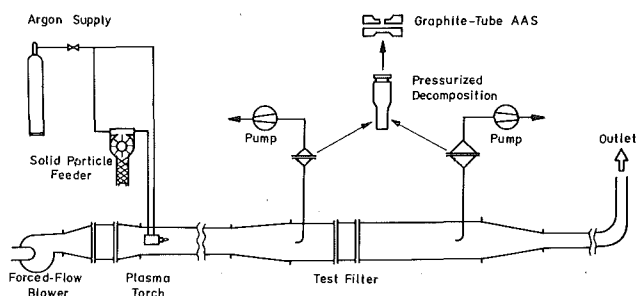


Fig. 8: Schematic of the plasma-aerosol efficiency test method for HEPA filters.

The new test method has been successfully evaluated and checked against two standard procedures at room-air conditions. The sensitivity of the method allows decontamination factors as high as 10^4 to be determined.

CONTRIBUTIONS TO AIR-CLEANING-SYSTEM CODE DEVELOPMENT

To evaluate whether the confinement of fission products is also assured during an accident, reliable data on the behavior of particulate filters are needed, in addition to knowledge of the challenges that the filter units would be exposed to, at the places within the air-cleaning system where they are mounted. There are only a few relatively simple codes available to model air-cleaning systems' response to, e.g., gas-dynamic transients. These codes include TVENT /15/ for tornado simulation, or EVENT /16/ for explosion simulation. In different institutions, fire codes are under development /17/.

In preparation for further code development, both above-mentioned gas-dynamic codes were modified so that active components with time-dependent flow-resistance characteristics can be modelled. Additionally, a more accurate description of HEPA-filter flow resistance was introduced. In order to verify the accuracy of the calculations, the gas-dynamic characteristics of the test facility BORA were modelled with both codes. Subsequently, the predictions of different gas-dynamic transients simulated with this facility were compared with the corresponding experimental measurements /18/.

As a typical result of these investigations, Fig. 9 shows the variation in the static pressure upstream of the component test section as well as across the test section, where a HEPA filter was mounted. The predictions of both codes are almost identical for the range in static pressure of this test. Apart from the time delay of approx. 0.25 s the calculations are in very close agreement with the experimental data.

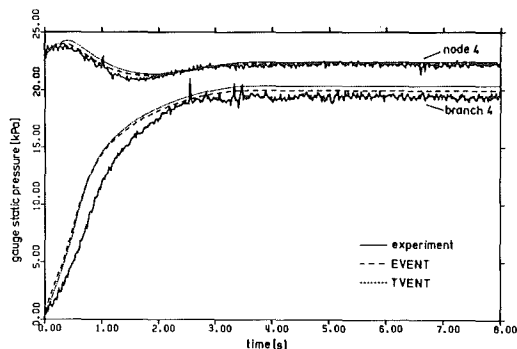


Fig. 9: Some results of modelling the gas-dynamic behavior of the test facility BORA with the codes TVENT and EVENT. Comparison of calculated and measured gage static pressures.

Given the effectiveness of TVENT and EVENT in predicting gas-dynamic transients, neither was originally developed to take into account the process of water condensation or the transport of liquid-water aerosols that may occur during a LOCA in a water-cooled nuclear power facility. In order to obtain realistic data regarding the challenges to the filters within air-cleaning systems, additional code-development work is necessary.

CONCLUSIONS

Based on the results obtained so far, it can be concluded that safe HEPA-filter operation seems to be limited to conditions close to normal. No information is available yet on the behavior of aged filter units or the response of new and aged filters, to combined challenges, both of which indicate the need for further investigations. Additionally, the ongoing work for filter improvement is considered necessary, where the conventional filter concept with glass-fiber media seems to offer good possibilities. Furthermore, the challenges to the filter units inside the air-cleaning systems need to be estimated before credit for the particulate removal efficiency of the filters can be taken into account in source-term calculations. This implies additional work in the field of code development.

REFERENCES

- /1/ Ohlmeyer, M.; "Vor-Ort-Prüfung von Schwebstofffiltern und Entnahme von Sorptionsmaterialien bei Iod-Sorptionsfiltern," Atomenergie - Kerntechnik 40 (1982) p. 259.
- /2/ Carbaugh, E.H.; "A Survey of HEPA-Filter Experience," CONF 820833 (1983) p. 790.

- /3/ Gregory, W.S. et al.; "Investigations of HEPA Filters Subject to Tornado Pressure Pulses; Initial Structural Testing;" LA-7202, Los Alamos Scientific Laboratory, 1978.
- /4/ Ruedinger, V.; Wilhelm, J.G.; "HEPA-Filter Response to High Air Flow Velocities," CONF 820833 (1983) p. 1069.
- /5/ Ruedinger, V.; Ensinger, U.; "Studium des Verhaltens von Schwebstofffiltern unter Störfallbedingungen;" KfK 3350 (1983) p. 4400/20.
- /6/ Ruedinger, V. et al.; "Studium des Verhaltens von Schwebstofffiltern der Klasse S unter simulierten Störfallbedingungen;" KfK 3450 (1984) p. 4400/..
- /7/ Wilhelm, J.G. et al.; "Testing of Iodine-Filter Systems Under Normal and Post-Accident Conditions," CONF 720823 (1972) p. 434.
- /8/ Ruedinger, V.; Ricketts, C.I. and Wilhelm, J.G.; "Limits of HEPA-Filter Application Under High-Humidity Conditions," Proc. 18th DOE Nuclear Airborne Waste Management and Air Cleaning Conference, Baltimore 1984, (to be published).
- /9/ Pratt, R.P.; Green, B.L.; "Performance Testing of HEPA Filters Under Hot Dynamic Conditions," ibida.
- /10/ Alken, W. et al.; "Development of a HEPA Filter With High Structural Strength and High Resistance to the Effects of Humidity and Acid," ibida.
- /11/ Dillmann, H.-G.; Pasler, H.; "Experimental Investigation of Aerosol Filtration With Deep Bed Fiber Filters," CONF 820833 (1983) p. 1160.
- /12/ Du Poux, . et al.; "SIMOUN: High Temperatur Dynamic Test Rig For Industrial Air Filters," Proc. 18th DOE Nuclear Airborne Waste Management and Air Cleaning Conference, Baltimore 1984, (to be published).
- /13/ Ruedinger, V. et al.; "BORA - A Facility for Experimental Investigation of Air Cleaning During Accident Situations," ibida.
- /14/ First, M.W.; "Performance of Absolute Filters at Temperatures from Ambient to 1000 °F," CONF 721038 (1972) p. 677.
- /15/ Duerre, K.H. et al.; "TVENT - A Computer Program for Analysis of Tornado-Induced Transients in Ventilation Systems," LA 7397-M (1978).
- /16/ Tang, P.K. et al.; "EVENT User's Manual - A Computer Code for Analyzing Explosion-Induced Gas-Dynamic Transients in Flow Networks," LA 9624-M (1983).
- /17/ Los Alamos National Laboratory; "Proc. of the CSNI Specialist Meeting on Interaction of Fire and Explosion with Ventilation Systems in Nuclear Facilities," LA-9911-C (1983).
- /18/ Hartig, S.H. et al.; "Comparison and Verification of two Computer Programs Used to Analyze Ventilation Systems Under Accident Conditions," Proc. 18th DOE Nuclear Airborne Waste Management and Air Cleaning Conference, Baltimore 1984, (to be published).

EXPERIMENTAL INVESTIGATIONS SIMULATING IODINE RELEASE
AT DESIGN BASIS ACCIDENT IN PWR

W. Morell, W. Kastner, R. Rippel, F. Richter

KRAFTWERK UNION
Hammerbacherstraße 12 + 14
D-8520 Erlangen
FR Germany

ABSTRACT

After failure of an effective pressure line in the transducer compartment of the annulus of a PWR fission products, especially I131 contained in the primary coolant, are released in the compartment atmosphere.

Depressurization experiments in a 1 : 1 scale test facility were performed using cesium-tracer simulating the ionic dissolved fission product behaviour.

During the test-phase of about 50 minutes corresponding to the initial accident phase, the humidity-born tracer release is less than 1 % of the discharged amount.

INTRODUCTION

The calculation of the radiological consequences of design basis accidents with primary-coolant release presumes reliable data on the behaviour of important radionuclides (iodine, cesium) under the accident conditions.

The guidelines by the Federal Ministry of the Interior on evaluating the design of nuclear power stations with pressurized-water reactors against accidents within the scope of § 28, section 3 of the radiation protection regulations dated 18th October, 1983 prescribe which accidents are decisive for technical safety design and which forms of proof are to be furnished.

One of these accidents to be analysed radiologically in accordance with the accident guidelines is a "leak in an instrument line bearing primary coolant (effective pressure line)" in the annulus of the reactor building. In such an accident, part of the hot primary coolant discharged from the site of the leak evaporates very rapidly, and it is necessary to clarify which proportion of the radionuclides is released under these conditions. The parameters to be used for this accident are given in the "Fundamentals on accident calculation for the guidelines ..." published as supplement to the accident guidelines. An essential assumption is based on the fact that the activity concentration with relation to mass in the steam arising on discharge comprises 10 % of the discharged, un-vaporised coolant with respect to iodine and other impurities.

The research project jointly financed by the Federal Ministry for Research and Technology and KWU and conducted by KWU furnished proof that this model is sufficiently conservative.

PROBLEM AND OBJECTIVES

Experimental findings on the release of droplets after a break in an effective pressure line in the annulus are determined in depressurisation experiments.

The broken effective pressure line, the transducer room and the cross-section of the vent chimney are hereby simulated in the geometrical scale 1 : 1 (Fig. 1). The discharge time in the experiments is selected so that more than the initial phase of the accident (30 minutes) is covered.

The radionuclide I131 plays the radiologically dominant role in the initial phase of the accident. As the experimental facility is not situated inside a controlled area, it was not possible to employ radionuclides in their reactor-equivalent concentration as tracers, but nonradioactive substances must be employed in a comparatively high concentration.

It has been determined in parallel examinations that iodine is dominantly (90 %) present in the chemical form of the water-soluble, non-volatile iodide (I^-) in the real primary-coolant of PWR. It is thus possible to employ the ionogeneous alkaline salt $CsNO_3$ as tracer which is also easily soluble in water.

The most important objective of the experiments is to determine which proportion of the tracer is released from the leakage

space surrounding the leak within the first accident phase of 30 min. Two pilot tests were performed to test the measurement and sampling techniques, as well as two main experiments.

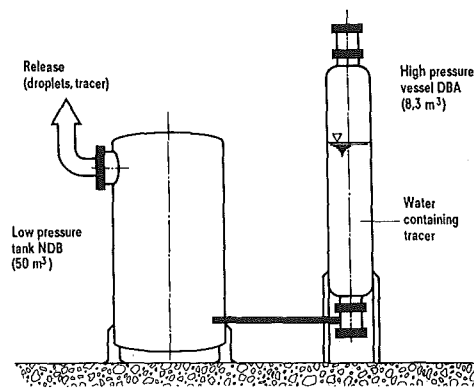


Fig. 1

Break of an Effective Pressure Line:
Test Facility Simulating the Iodine Release

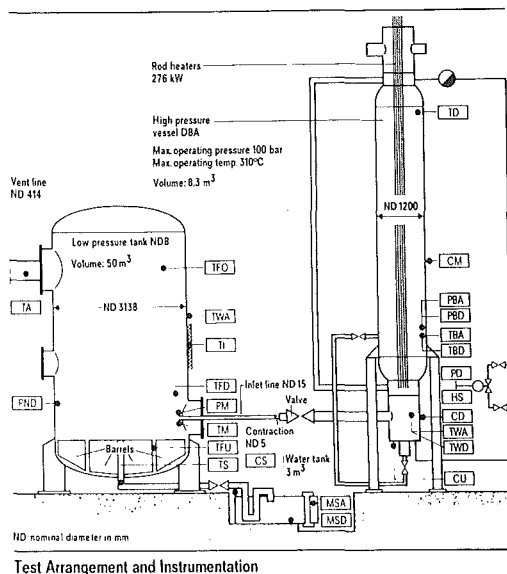
TEST ARRANGEMENT

The experiments were performed on a high pressure vessel (DBA) with following 50 m³ container (low pressure tank; NDB). Figs. 2 and 3 show the test arrangement.

The system consists essentially of four components:

- high pressure vessel (DBA),
- inlet line,
- low pressure tank (NDB),
- vent line.

The high pressure vessel DBA simulates the primary circuit. This is heated by rod heaters placed vertically in the lower vessel part. The water mass usable for discharge is approx. 3500 - 4000 kg and enables an experiment time $t > 50$ min.



The discharge of the saturated water takes place from the lower part of the DBA via a pipe ND 150, followed by an electrically operated sliding valve to which the actual inlet line ND 15 is connected.

The inlet line ND 15 represents the broken effective pressure line leading to the transducer compartment, the contraction ND 5 corresponds to the cross-section of the welded connection to the main coolant line which limits the flow.

The nozzle of the inlet line is situated in the lower part of the low pressure tank, which represents the transducer compartment.

The water separated in the NDB is led through a pipe from the lowest point of the vessel into the sump tank and collected there.

In the upper part, the vent line ND 414 is connected to the NDB. The cross-section area corresponds to that of the grills areas of feed exhaust air openings in the transducer compartment of a power station.

The vent line, consists of an approx. 5.7 m long vertical and a 5.4 m long horizontal tubing and forms the connection between NDB and environment.

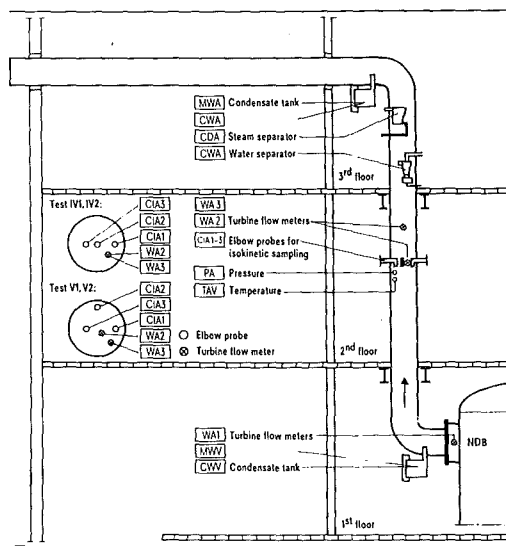


Fig. 3

Measurement Positions in the Vent Line ND 414

In order to determine the transport of the tracer through the vent line, the system of isokinetic sampling of a representative partial mass flow was selected as sampling technique (Fig. 4).

For this purpose, three elbow probes (inner diameter 20 mm) arranged in counter flow direction were fitted to different positions in the cross-section. In order to configurate the sampling of the steam-droplet mixture isokinetically, knowledge of the flow speed is necessary which was determined with a turbine flow meter. In two experiments, one elbow probe was adjusted close to the wall in order to determine possible concentration profiles across the cross-section.

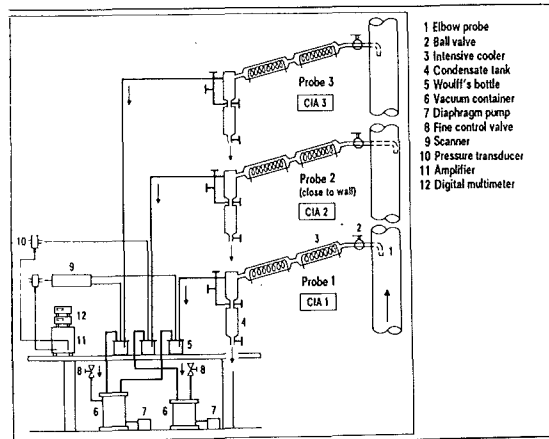


Fig. 4

Test Arrangement for
Isokinetic Sampling of Steam/Droplet-Samples

During sampling of the steam-droplet mixture through the elbow probes, the two-phase mixture from the appropriate probe is condensed completely with an intensive cooler.

A carry-over of humidity into the Woulff's bottles was not observed. In order to make certain, the tube connections and the Woulff's bottles were rinsed with deionised water after completing the experiments and the Cs content was measured. The Cs mass rinsed from the surfaces was approx. 2,5 μg . The error on account of carry over is thus only 2.5 o/oo of the determined value.

No statement can however be made from the isokinetic sampling on the water separated in the vent line which consists of steam condensate and droplets. In order to determine the quantity and to make a chemical analysis of this water (wall-condensate) collection vessels were fitted (Fig. 3) at the entry to the vertical and horizontal line section.

For a separate examination of the phases, a steam separator and a droplet separator (cyclone) were additionally installed.

The steam separator consists of a hollow body open on one side which is partly filled with wire wool. The water droplets are here separated from the fluid sucked up (water jet pump). The remaining steam flows to a condenser. Samples are taken from the condensed steam. As the tracer is non-volatile, the concentration in the steam sample should be zero.

THE PROCEDURE

Two pilot tests were carried out to check and improve the measuring and sampling procedure. As these experiments were satisfactory, they were also fully evaluated.

In this way, four experiments are available under almost equal initial conditions.

To perform the experiments, the high pressure vessel (DBA) was filled with approx. 6 m³ deionised water and a CsNO₃ solution of a known composition added in order to obtain the required Cs-concentration in the DBA.

Homogenous distribution was checked by analysing water samples taken at three points of different geodetic heights (CM, CD, CU).

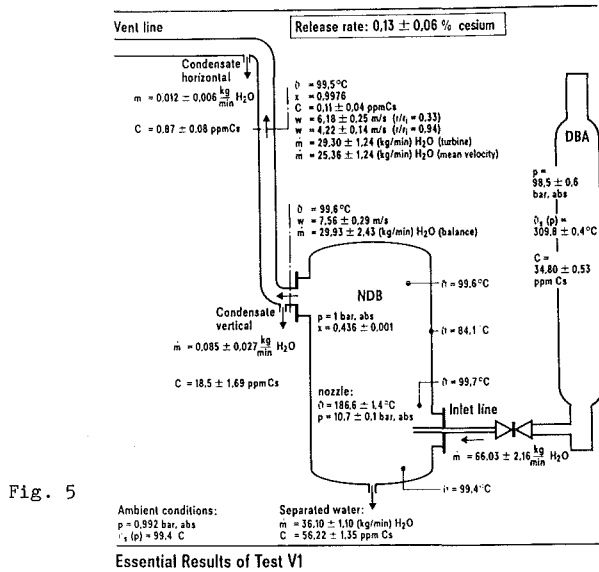
The partly filled DBA was then heated to saturation point at approx. 310 deg C, 100 bar.

After opening the sliding valve the saturated water expanded into the low pressure tank NDB from the DBA via the inlet line ND 15 fitted with a contraction to ND 5.

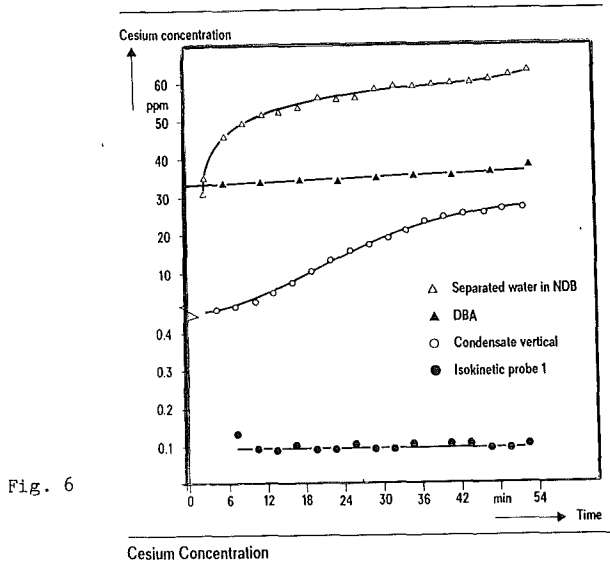
The discharging process was stopped after appr. 50 min in order to keep the rod heaters in the DBA covered. The DBA heating was controlled during the discharge phase so that pressure and temperature were constant as possible during the total period.

RESULTS

The essential results of the experimental phase at steady-state conditions which begins after 12 minutes and which is only to be observed here, are shown for the experiment V 1 in Fig. 5.



The trend for the measured results of Cs-concentration for this experiment is represented in Fig. 6: the small increase of the tracer concentration in the DBA is caused by evaporation of the fluid inside DBA during the flashing.



The cesium concentration of the water separated in the NDB reaches approximately twice the concentration of the DBA; the reasons are the enthalpy values during evaporation and the non-volatility of the cesium tracer. The increase in cesium concentration in the wall condensate of the vertical part of the vent line is caused by the decreasing condensation (reason: warming up of the line) and an assumed constant amount of droplets.

As can be further seen the cesium concentration in the isokinetic samples - compared with the given concentration originally in the DBA - is very small.

The most important parameter for the problem posed in this project is nevertheless represented by the release of cesium. In order to be independent of the given tracer-concentration, the outflowing Cs mass flow rate $\dot{m}_A \cdot C_{ISO}$ was related to the inflowing mass flow rate $\dot{m}_E \cdot C_{DBA}$. This parameter is characterized as release ϕ and given in percent.

$$\phi = \frac{\dot{m}_A \cdot C_{ISO}}{\dot{m}_E \cdot C_{DBA}}$$

Thus the following measured values are necessary to calculate the release.

- concentration in the DBA: C_{DBA}
- inflowing mass in the NDB: \dot{m}_E
- concentration in the isokinetic samples: C_{ISO}
- mass flow in the vent line: \dot{m}_A

Purely the mass flow rate \dot{m}_A could not be directly measured but can be determined from the following values:

- specific enthalpy on saturation
 - $h' = f(p_{DBA})$
 - $h' = f(p_U \approx 1 \text{ bar})$
 - $h'' = f(p_U \approx 1 \text{ bar})$
- saturation density of water
 - $\rho' = f(p_U)$
 - $\rho'' = f(p_U)$
- velocity in the vent line w_A

or alternatively by employing the sump water mass separated per time unit (mass balance).

Summarizing the results including the error propagation in the calculation, the following values are received for the cesium release (Fig. 7):

			IV 1	IV 2	V 1	V 2
Mass flow rate vent line	$\dot{m}_A = \frac{f(w_1)}{f(bal.)}$	kg/min	26.93 ± 1.18	28.64 ± 1.25	29.30 ± 1.24	29.58 ± 1.36
			23.31 ± 1.18	24.81 ± 1.25	25.36 ± 1.24	25.59 ± 1.36
			29.21 ± 3.76	30.61 ± 3.31	29.93 ± 2.43	29.69 ± 2.86
Concentration vent line	C_{150}	ppm	0.06 ± 0.04	0.06 ± 0.05	0.10 ± 0.04	0.11 ± 0.04
Mass flow rate inlet line	m_E	kg/min	67.32 ± 2.89	67.30 ± 2.35	66.30 ± 2.16	66.27 ± 2.45
Initial Concentration DBA	C_{DBA}	ppm	10.44 ± 0.23	15.74 ± 0.22	34.80 ± 0.53	33.30 ± 0.44
Release	Φ	%	0.22 ^{+0.21} -0.19	0.15 ^{+0.16} -0.13	0.13 ± 0.06	0.14 ± 0.06

Fig. 7

Calculation of the Cesium-Release Φ

RÉSUMÉ

Experimental results were determined in four depressurization experiments on a technical scale for the droplet release in the primary coolant dissolved non-volatile substances after a failure in an effective pressure line in the annulus.

The broken effective pressure line, the transducer compartment and the cross-section of the vent chimney were simulated on the geometric scale 1 : 1. The primary coolant was simulated by deionized water in saturated state at approx. 100 bar/310 °C, the behaviour of the non-volatile, dissolved radionuclides (iodide) simulated by employing cesium ions (CsNO_3).

The experimental period of at least 50 minutes covers more than the necessary first phase to be observed for the accident of approx. 30 minutes. After a non-steady state starting phase of about 12 minutes, which is of subordinate importance for the tracer release, steady-state conditions take place in the system.

If the release \emptyset , i. e. the quotient of the rate of outflowing and inflowing cesium mass in percent, is examined, the results for all experiments performed ly within the range

$$0,02 \% \leq \emptyset \leq 0,43 \%$$

If the pilot tests are not regarded (larger error range, measuring techniques employed were tested), then the release \emptyset for the two main experiments V 1 and V 2 is at

$$0.07 \% \leq \emptyset \leq 0.20 \%$$

CONCLUSION

If these values are compared with the basis for accident calculation, it can be seen that the release of such radionuclides as iodine and cesium is considerably overestimated for the accident examined.

FISSION PRODUCT AND MATERIAL VAPOR TRANSPORT
DURING MOLTEN CORIUM-CONCRETE INTERACTIONS

D. Cubicciotti and B.R. Sehgal

Electric Power Research Institute
Palo Alto, California 94303 USA

ABSTRACT

The ex-vessel progression of a postulated core melt-down accident leads to molten corium concrete interactions (MCCI), during which the gases generated from concrete decomposition and the concrete solids react with the corium melt. Fission product and reactant-material sparging and aerosol formation occurs due to vaporization-condensation processes. The timing, the magnitude and the chemical and physical form of the products of MCCI are extremely important in determining the overall source term resulting from postulated severe accidents. This paper presents a methodology based on equilibrium thermodynamics, in which a free energy minimization treatment was used to estimate partial pressures of gases in a many component, multi-phase system. The amounts of the fission products and condensable materials vaporized and their chemical form were calculated for an example case of basalt-aggregate concrete. The MCCI reaction rate model embodied in the CORCON-1 code was used to provide the thermal-hydraulic conditions.

I. INTRODUCTION AND BACKGROUND

Postulated risk-dominant accidents [1], by current definition, lead to a core melt down. An accident starts with postulated faults, which result in undercooling of the core, which in turn leads to core heat up, degradation and eventual melting. This in-vessel progression of the accident ends with the failure of the vessel by the attack of the molten core on the lower head. The molten material consisting of UO_2 fuel, Zircaloy clad and stainless steel from the vessel internals is ejected out of the lower head penetrations into the containment cavity and the ex-vessel phase of the accident ensues.

Fission products contained in the UO_2 fuel are subject to release while the core heats up during the in-vessel progression of the accident. Indeed, it is very likely that most of the volatile fission products, i.e., iodine (I), cesium (Cs), and tellurium (Te) which pose the most biohazard would be released [2], during the core heat up. However, recent tests [3] at Oak Ridge National Laboratory have indicated that some fraction of the tellurium inventory may be retained in the melt, if some of the zirconium escapes oxidation during the core heat up and melt-down periods. This retained Te, then, may become available for release during the ex-vessel progression of the accident.

The debris formed in containment cavity melts due to decay heat generation and attacks the concrete base-mat. The molten corium concrete interaction (MCCI) results in decomposition and melting of the concrete with production of very large quantities of carbon dioxide and steam. A cavity forms, advancing both

axially downwards and radially outwards in time, through and alongsides which gas bubbles and gas streams will pass and emerge at the top of the corium melt.

The carbon dioxide and steam react with the contents of the corium melt to produce a variety of chemical reactions and the resulting products. For example, they partially oxidize the metals in the melt to produce heat, which adds to the decay heat being generated. The gases, the fission products and other materials in the melt form various chemical compounds, which may vaporize and be carried away with the flowing gases. These vaporized materials after emerging from the corium melt will form an aerosol source as they condense in the containment atmosphere.

The magnitude, the content and the physical and chemical character of the MCCI aerosol source are extremely important in estimating the source term due to postulated accidents. In addition to these parameters, the timing of the MCCI aerosol release, relative to that of the fission product aerosol release from the primary system, and to that of the containment failure, is of great importance. If the timing is opportune, the relatively copious and large-particle MCCI aerosol will help scrub the relatively dilute and small-particle aerosol that may be discharged from the vessel on revolatilization of the fission products deposited on the primary system surfaces. Similarly, if containment failure does not follow soon after the start of the MCCI, there is little danger of having a large airborne source in the containment, since natural processes of aerosol removal from the containment atmosphere would have been active for a sufficiently long time.

Corium concrete interactions are modeled by several codes developed somewhat independently. The German codes WECHSEL [4] and KAVERN [5] and the U.S. code CORCON [6] are similar in concept, but have differences in submodels. The code MAAP [7] developed under Industry Degraded Core (IDCOR) Program employs similar physical concepts about the MCCI albeit both in a somewhat simplified manner. Predictions from these codes for the thermal-hydraulic parameters in some typical MCCI events during postulated accidents have been different from each other.

The CORCON code models the MCCI chemistry and thermal-hydraulics in a coupled fashion. However, the chemical treatment is limited in its scope and extent and a model named VANESA [8] has been developed at Sandia National Laboratories in which a chemical-kinetic treatment involving many chemical reactions has been employed. The VANESA code has been used [9] for prediction of the MCCI aerosol source for some postulated accident scenarios.

In this paper, the vaporization of the fission products and the corium components is considered on the basis of equilibrium chemical thermodynamics combined with the thermal-hydraulic treatment embodied in the CORCON code. The CORCON models are briefly described in Section II with the results of their application to the example case of corium interactions with concrete containing basalt aggregate. Section III gives a description of the chemical model employed and gives results for the releases in the example case chosen and calculated in Section II; and Section IV summarizes the results and presents some conclusions.

II. CORIUM-CONCRETE INTERACTION: THERMAL-HYDRAULIC MODEL

The CORCON code treats the MCCI as occurring in a concrete cavity containing an axisymmetric pool of molten corium surrounded by a gas atmosphere. The corium pool is treated as a set of layers (each with spatially-homogeneous properties) consisting of metallic and oxidic components of the molten corium. The

relative axial positions of these layers are determined by their bulk densities. In most cases, three layers are assumed: a heavy oxide layer, a metallic layer and a light oxidic layer. The calculations are performed in two dimensional axisymmetric geometry.

The interaction of the molten corium with the concrete cavity proceeds on the bottom and on the sides of the concrete cavity. CORCON assumes that the gases generated at the bottom are transported through the corium pool, while the gases generated on the sides are allowed to bypass the pool. The initial configuration of the pool is assumed as a two layered system with the heavy oxide layer at the bottom and a metallic layer on the top. The solids of the concrete melted on the sides of the cavity are presumed by the CORCON model to float on the metal and form a third layer in the pool, which is termed as the light-oxide layer. The solids of concrete melted on the bottom mix with the heavy oxide layer and reduce its density. At some point in time the heavy oxide layer becomes light enough and is assumed to 'float-through' the metallic layer and join the light oxide layer. Thus, the thickness, content and the material properties of these layers change with time as the MCCI proceeds.

The CORCON code employs empirical models for heat transfer in the downward, sideways and upward directions. The proper partitioning of the heat generated is of importance, since that determines the rate of the progression of the melt in the cavity, the rate of gas bubbling through the corium pool and thus the rate of vapor transport out of the pool. It is suspected, presently, that empirical heat transfer models employed in the code may not be correct, since the predicted downward progression of the corium melt has not agreed [10] with the measurements from the first BETA test [11].

The chemical interactions, the decay heat generation, and the heat transfer between layers determine the temperature histories of the layers. The three layers have significantly different histories of heat generation (decay heat in heavy oxide layer, chemical energy in metallic layer) as the interaction proceeds. The temperatures of the molten layers are very important relative to the vaporization processes.

The example treated in our paper for MCCI considers reactor core melt falling on to a concrete base-mat containing basaltic aggregate whose composition was obtained from Reference 6. The core was presumed to melt through the reactor vessel at 13,000 seconds after initiation of the accident and onto the concrete base-mat. We have not considered the initial interactions of the melt with concrete, in which significant dispersal may or may not occur. The period of time considered is after when the core debris has settled down and reheated again.

The core material initially consists of UO_2 fuel (3.63 E5 g moles or 98T), the Zircaloy cladding (2.48 E5 g moles or 31T), of which about 20% was assumed to be metallic and the rest oxidized to ZrO_2 , for this calculation, stainless steel structural material (2E6 g at. or 112 T Fe; 3.35 E5 g at. or 17T Cr, 1.8 E5 g at. or 10T Ni, and 4E4 g at. or 2.2T Mn), and fission products, this is similar to the values used in BMI-2104 [9] which is the reference for this simple case. (The terminology XEY is used in this paper to represent the number $X10^Y$). To limit the extent of the calculations, only certain fission products were considered; based on their amounts, radioactivity, and availability of chemical information. Those included and their amounts were: La (826 g at. or 114 Kg), Mo (3870 g at. or 372 Kg), Nb (719 g at. or 67 Kg), Sb (16 g at. or 2 Kg), Sr (860 g at. or 76 Kg), Ru (2270 g at. or 231 Kg), Te (213 g at. or 27 Kg). Also included were Ag (10,000 g at. or 1080 Kg) and Sn (2155 g at. or 254 Kg). The bulk of the Ag was from control blade alloy, but there is some fission product Ag. The Sn came from the Zircaloy cladding but also included some fission-generated material.

The molten core separates into two layers: an oxide, which is the denser, and contains UO_2 , ZrO_2 , La_2O_3 , SrO , Sb_2O_3 , SnO_2 , NbO_2 , MoO_2 , and the metal, which floats, and contains Fe , Cr , Ni , Mn , Zr , Ag , Ru , Te . (The Te is presumed to have been associated with the Zircaloy cladding as a telluride, and is therefore carried to the metal layer; this is also based on the assumption in BMI-2104 [9]). Some Cs (360 g at.) and I (40 g at.) were included in the MCCI phase of the accident. Also, the Sb , which is quite volatile, was included because it had not been in the earlier treatment. All three of these substances were found to be very volatile and vaporized from the melt soon after melt through.

Figure 1 shows the CORCON estimate of the temperatures from 13,000 seconds into the accident, when the vessel melt-through occurred to 20,000 seconds, where a significant amount of freezing of corium pool has occurred and the CORCON model is not applicable. The figure shows that the dense oxide joins the light oxide layer (termed the 'oxide-flip') above the metallic layer, slightly after 15,000 seconds i.e., approximately 2,000 seconds after the start of the MCCI. The large and growing difference in temperatures between the oxide and the metallic layers is apparent from Figure 1. Concrete constituents including the gases CO_2 and H_2O released in the CORCON calculation are shown in Figure 2. The amounts of other metal oxides introduced during concrete melting were assumed to be proportional to the SiO_2 .

III. VAPORIZATION THERMODYNAMICS CALCULATIONS

III.1 METHOD

The procedure used for the early stages after melt-through, while there were two oxide layers and one metal layer, i.e. before the 'oxide-flip', was as follows. The gas entering the bottom was equilibrated with the dense oxide. Then, the gas from that calculation was equilibrated with the metal layer. During the first time step (500 seconds), it was assumed that there was no light oxide layer present. During the subsequent time steps (1,000 seconds each), that gas was equilibrated with the light oxide layer above the metallic layer. The side gas was equilibrated only with the concrete entering the sides to represent their interaction before the concrete mixed with the melt. After the 'oxide-flip', which occurred sometimes after 15,000 seconds in this case, the following steps were used. The gas entering the bottom was equilibrated with the metal; then the gas from the metal plus the side gas was equilibrated with the oxide layer, which was less dense than the metal at that time.

The amounts of material vaporized from the system, were considered to be the moles of gas in equilibrium with the light oxide melt during each time step for the bulk materials; but for the fission products, the amounts vaporized were taken as the moles in any gas phase. This was done partly to reduce the number of elements involved in the calculations and partly with the concept that the small amounts of vaporized fission products might be aerosolized and pass into the final gas leaving the system. The additional simplifications made were that the sodium would behave chemically like potassium and magnesium like calcium. Thus, the gram atoms of sodium were added to those of potassium and magnesium to calcium. The free energy minimization computer code SOLGASMIX-PV was used to calculate these equilibria. A version [12] that treats as many as 20 elements was employed.

The species considered can affect the calculated equilibria. The calculation must include all of the important species. Those employed in the calculations reported here are listed in Table I. The thermochemical values used for these calculations were taken from References 13 to 21. In general, they are

measured values; however, values for the hydroxides taken from Jackson [15] are mostly estimated. No values were available for trihydroxides, which may play a role with trivalent elements.

III.2 FREE ENERGY MINIMIZATIONS

A sample flowsheet for a calculation before the 'oxide-flip' is shown in Figure 3. The amounts of gas (H_2O and CO_2) and concrete (SiO_2 , K_2SiO_3 , $CaSiO_3$) added to the dense oxide from the bottom, were taken from the CORCON calculation at the current time step. The earlier dense oxides were obtained from the earlier time step calculation (or initial inputs for the first time step calculation). These amounts of material were input into the SOLGASMIX-PV program, along with the temperature of the dense oxide layer obtained from the CORCON calculation. The output from the calculation gave the numbers of moles of gas and the moles of condensed phase dense oxide used for the next time step calculation.

The moles of gas phase generated in the dense oxide layer were used as part of the input to the metal layer calculation. Interaction of the gases with the metal constituents from the earlier time step calculation was evaluated by the free energy minimization program with formation of the three phases indicated: a gas phase, which went to the light oxide layer, an oxide phase which was added to the light oxide layer and a metal phase which went to the next time step calculation.

Calculation of the equilibrium in the light oxide layer included the gas and oxide from the metal layer, as well as the oxides from the light oxide (earlier time step) calculation and the oxide from earlier time step side calculation. Gas resulting from this calculation was included in the final gas issuing from the core-concrete interaction and the oxides produced went to the next time step light oxide calculation.

The side calculation represented interaction of the concrete with its own gas as it was added to the light oxide layer. The amounts of gas and concrete were taken from the CORCON calculation. The gas resulting from the calculation was added to the final gas and the oxide to the light oxide for the next time step calculation.

The flow paths considered for the conditions after the 'oxide-flip' are similar to those in Figure 3. Only two layers were considered, the molten metal which was at the bottom of the cavity, and the molten oxide which floated on it. The concrete and gases added from the bottom were input into the calculation for the metal layer. The gas and oxide from that calculation was added to the light oxide layer. The gas and concrete added from the side were mixed with the other constituents of the light oxide calculation.

In brief, the amounts of bulk materials vaporized from the system were taken to be the moles of gas in equilibrium with the light oxide melt during each time period; but for the fission products, the amounts vaporized were taken as the moles in any gas phase.

III.3 COMPOSITION OF LAYERS

III.3.1 Oxide Layers. The compositions calculated for the oxide layers are shown in Figure 4. It was assumed that there was no significant amount of light oxide during the first 500 seconds. The composition of the oxide melt after the 'flip' is also shown in the figure. During the time period from 15,000 to 16,000 seconds, the two oxide phases were mixing, and compositions

were not calculated. After the 'oxide-flip', the main constituents continue to be UO_2 and ZrO_2 , although significant amounts of concrete are added. Most of the oxides of the concrete remain in the melt, but the alkali metal oxides are vaporized out.

III.3.2 Molten Melt Layer. The composition of the molten metal is shown in Figure 5. The major constituents are the stainless steel metals (Fe, Cr, Ni). It was assumed that the steel contained about 2% Mn. It was also assumed that about 20% of the zirconium of the cladding entered the melt as metal when the core melted through the reactor vessel. Half of the original inventory of fission product tellurium was assumed to go to the molten metal layer with zirconium. Also, about half of the original inventory of control rod silver was assumed to be carried by the cladding to the metal layer. The Sn originally in the Zircaloy cladding was assumed to be in the dense oxide and collected in the metal. Fission product Ru was assumed to be in the metal layer initially, and it remained there throughout the scenario. Fission product Mo was initially added to the dense oxide and it was slowly vapor-transported to the molten metal. The H_2O and CO_2 added to the system from the bottom of the cavity, after passing through the dense oxide, interacted with the molten metal. They oxidized the metal and passed onto the light oxide phase. The fraction of Zr in the metal decreased rapidly after about 15,000 seconds. Then the next most reactive metal, Mn, began to be oxidized.

III.3.3 Gases Released. Figure 6 shows the amounts of H_2O , H_2 , CO, and CO_2 released from the system during the course of the core-concrete interaction. The H_2O arises mainly from the gas added by the side concrete. The H_2 comes from the H_2O added at the bottom which is reduced when it interacts with the metal (and is partly reoxidized in the light oxide). The CO_2 and CO come from the side gas and the bottom gas, respectively. Some O_2 (about 3000 moles) is released as part of the thermal decomposition of the concrete added from the side. The amount is approximately equivalent to the amount of K released from the side concrete before the 'oxide-flip'. No significant amounts of O_2 were released from any other layer in the calculation.

In addition to the semipermanent gases mentioned above, quite large amounts of certain condensable gases were released. Figure 6 shows these species, mainly K, KOH, and $Fe(OH)_2$, and their amounts. Most of the alkali metal oxides and the Fe_2O_3 from the side; and part of the alkali metal oxides from the concrete added to the bottom became vaporized.

III.3.4 Fission Product Vaporization. Fission products were introduced into the system either in the dense oxide or in the molten metal layers. The amounts used in the calculations are shown in the second column of Table II. Some of them were essentially completely vaporized in the first time step considered, namely Cs, I and Sb. These were assumed to enter the gas phase from the dense oxide and to be vapor-transported out of the system with no further significant interactions with the melt.

Two of the elements involving fission products in the dense oxide (Mo, Sn) were found to vaporize partially. Before the 'oxide-flip', some of them were found to be vapor transported into the metal. After the 'oxide-flip', that process did not occur. The remaining fission products in the dense oxide (La, Nb, Sr) were so slightly volatile that they were not included in other calculations for a given time step. It was assumed that the amount vaporized from the dense oxide was carried with the final gas transported out of the cavity. The elements added to the metal (Ag, Te, Ru), and those transported in (Mo, Sn), were included in the calculation for the molten metal-gas phases. The amounts of those elements, in the gas phase, in equilibrium with the metal were presumed to be vapor transported out of the cavity before the 'oxide-flip'.

The total amounts vapor transported are given in Tables II and III and the releases of some of the fission products with time are shown in Figure 7. The dominant vapor species for each element is indicated in the last column of Table II. Table III shows the amounts of materials vaporized from the melt-concrete system and corresponds to Figure 6. The first five entries are permanent, or semipermanent gases, which are released as the concrete is decomposed. The quantities of alkali metals released are noteworthy because their removal from the concrete melt is expected to impact the model for the thermal-hydraulics. A rather large amount of iron was vapor-released. These condensable materials (alkali metals and Fe) would probably influence aerosol formation and transport in regions outside the cavity.

IV. SUMMARY AND CONCLUSIONS

A methodology to predict the source of vaporized fission products and component materials during the interaction of molten corium and concrete was developed. Such an interaction might occur in the containment cavity of a light water reactor, if a postulated core-melt accident is allowed to proceed to breach the reactor vessel. The time frame of the interactions is after the corium debris has settled down in the containment cavity, remelted and started to attack the concrete base-mat.

The methodology developed is based on the assumption of the interaction proceeding under thermodynamic equilibrium conditions. The thermal-hydraulic conditions for evaluation of the rates of the chemical reactions were derived from the model embodied in the CORCON-1 code. The methodology considered spatial layers of corium containing materials of different density (e.g., oxides, metals), which underwent chemical reactions with the gases and other materials generated from melting concrete. The dynamics of the interactions was modeled as batch processes in each time step with coupling between the chemistry and thermal-hydraulics taken into account. The source of the fission products and component materials emerging at the top of the corium melt into the containment atmosphere was calculated.

An example of the application of the methodology considered almost a whole core melt (along with molten structure from the bottom of the reactor vessel) interacting with the concrete base-mat containing basalt aggregate. The results of the calculations for this example are shown in Tables II and III and in Figures 6 and 7, in terms of the amounts of gases and vapors released at the top surface of the corium melt as a function of time. The vapors released are precursors to the aerosol source in the containment, as they reach the cooler parts of the containment. For the example considered large amounts of gases: H_2O , H_2 , CO_2 and CO were released. Some fission products and quite large amounts of condensable concrete materials accompanied these gases.

Among the fission products considered it was found that Cs, I and Sb were very volatile and if present in the melt would volatilize completely in the chemical forms of CsOH, CsI and Sb_2 respectively. Most of the fission product tellurium, if present in the corium melt due to the reaction with zirconium, would be vaporized during the MCCI. Other fission products e.g. La, Sr, Mo, Nb and Ru were not vaporized out of the MCCI system to any appreciable degree.

The vaporization of the alkali metals constitutes a heat removal process, which could influence the progression of the MCCI. A rough estimate of the heat removal is shown in Table IV, which shows the vaporization reaction, the reaction enthalpy change, the total heat absorbed and the megawatts of heat removed. The heat removal by alkali metal and iron vaporization is greater than that by vaporization of H_2O and CO_2 from the concrete.

The results presented here are specific to the example chosen. The amounts and compositions of the gases generated are strong functions of the composition of concrete aggregates. The results shown here for the gas and vapor source from MCCI apply only to the compositions employed here for the corium melt and the concrete. It has not been possible to make direct comparisons of the present results to those presented in Reference 9; although the major features of both analyses are similar to each other.

ACKNOWLEDGEMENTS

The authors are indebted to Professor M. Corradini of the University of Wisconsin for providing thermal-hydraulic information from the CORCON-1 code for the example treated in the paper, and to Glen Snyder for computer programming assistance.

REFERENCES

1. B.R. Sehgal and J.J. Carey, "Degraded Core Accidents--An Overview," Proc. Int. Mtg. Light Water Reactor Severe Accident Evaluation, Cambridge, Massachusetts, August 28-September 1, 1983. American Nuclear Society (1983).
2. D. Cubicciotti and B.R. Sehgal, Nuclear Technology, 65, 266, (1984). See also.

D. Cubicciotti, B.R. Sehgal, D. Hausknecht, H. Morewitz, R. Ritzman, and R.C. Vogel, "Estimation of the Fission Product and Core Material Source Characteristics," Final Report, Industry Degraded Core Program, Subtasks 11.1, 11.4 and 11.5, Atomic Industrial Forum, (1984).
3. G.W. Parker, A.L. Button, Jr., and G.E. Creek, "LWR Core Melt Studies," Oak Ridge National Laboratory Technical Highlights Report for August 1982, Oak Ridge National Laboratory (1982).
4. M. Reimann, W.B. Murfin, "The WECHSEL Code" KFK 2890, Kernforschungszentrum Karlsruhe (1981).
5. W. Schwarzott et al., "KAVERN Code Users Manual," KWU-914/83/006, Kraftwerk Union Erlangen Germany (April 1983).
6. J.F. Muir, R.K. Cole, Jr., M.L. Corradini, and M.A. Ellis, "CORCON-MOD1: An Improved Model for Molten-Core/Concrete Interactions," NUREG/CR-2142, U.S. Nuclear Regulatory Comm., Washington, D.C. (1981).
7. A. Buhl, M. Fontana, "IDCOR, the technical foundation and process for Severe Accident Decisions", Proceedings Atomic Industrial Forum Conference (Sept. 18-21, 1983)
8. D.A. Powers and J.E. Brockman, "Release of Fission Products and Generation of Aerosols Outside the Primary System." Draft Report Fin. No. A1227, Sandia National Laboratories (1983). See also D.A. Powers and J.E. Brockman, "Status of VANESA Validation." Draft Report Fin. No. A1227, Sandia National Laboratories (1983).
9. J.A. Gieseke, P. Cybulskis, R.S. Denning, M.R. Kuhlman, H. Chen and K.W. Lee, "Radio-Nuclide Release Under Specific LWR Accident Conditions - Volume V. PWR Large Dry Containment (Surry Recalculations)". BMI-2104 Vol 5, Battelle Columbus Laboratories, Columbus, Ohio (Jan. 12, 1984).

10. J.P. Hoseman, Personal Communication (1984).
11. H. Rininsland, "Beta (Core-Concrete Interaction) and DEMONA (Demonstration of NAUA)--Key Experimental Programs for Validation and Demonstration of Source Terms in Hypothetical Accident Situations," Proc. Int. Mtg., Light Water Reactor Severe Accident Evaluation, Cambridge, Massachusetts, August 28-September 1, 1983. American Nuclear Society (1983).
12. T.M. Besmann, "SOLGASMIX-PV, A Computer Program to Calculate Equilibrium Relationships in Complex Chemical Systems," ORNL/TM 5775, Oak Ridge National Laboratory, Tenn. (1977) and T.M. Besmann, revision of SOLGASMIX-PV for 20 elements, personal communication (1983).
13. O. Kubaschewski and C.B. Alcock, Metallurgical Thermochemistry, 5th ed., Pergamon Press, New York (1979).
14. JANAF Thermochemical Tables, the Dow Chemical Company, Midland, Michigan (1981 rev.).
15. D.D. Jackson, "Thermodynamics of Gaseous Hydroxides," UCRL-51137, Lawrence Livermore National Laboratory (December 1971).
16. L. Brewer and G. Rosenblatt, "Dissociation Energies and Free Energy Functions of Gaseous Monoxides," in Advances in High Temperature Chemistry, Vol. 2, Academic Press, N.Y. (1969).
17. R.C. Feber, "Thermodynamic Data for Selected Gas Impurities in the Primary Coolant of High-Temperature Gas-Cooled Reactors," LA-NUREG-6635, Los Alamos National Laboratory (April 1977).
18. R. Ackermann and M.S. Chandrasekhariah, Thermodynamics of Nuclear Materials-1974, Vol. 2, p. 3, International Atomic Energy Agency, Vienna, 1975.
19. S.R. Dharwadkar, S.N. Tripathi, M.D. Karkhanavala, and M.C. Chandrasekhariah, Thermodynamics of Nuclear Materials-1974, Vol. 2, p. 455, International Atomic Energy Agency, Vienna, 1975.
20. T.B. Lindemer, T.M. Besmann, and C.E. Johnson, "Thermodynamic Review and Calculations--Alkali-Metal Oxide Systems with Nuclear Fuels, Fission Products and Structural Materials," J. Nucl. Mater., 100, 178 (1981).
21. K.C. Mills, "Thermodynamic Data for Inorganic Sulfides, Selenides and Tellurides," Butterworths and Company, London (1974).

Table II. Vapor transport of fission products and related elements

	Original Amount (moles)	Amount ^a Released as Vapor (moles)	Percent Vapor Transport	Dominant Gas Species
<u>Dense oxide:</u>				
Cs	360	360	100 ^c	CsOH
I	40	40	100 ^c	CsI
La	826	1.7E-2	<0.1	
Mo	3870	56	2	MoO ₃
Nb	719	2.7E-3	<0.1	
Sb	16	16	100 ^c	Sb ₂
Sn ^b	2155	4.3	0.2	Sn
Sr	860	5.3E-3	<0.1	
<u>Molten Metal:</u>				
Ag ^b	10,000	275	3	Ag
Te	213	168	79	Te
Ru	2270	3.3E-5	<0.1	Ru

^aAmount released during the scenario considered (i.e., 13,000 to 20,000 sec.)

^bFission product Ag and Sn constitute only a small fraction of the amount of these elements used in the calculation.

^cThese were released in the first time period considered.

Table III. Material vapor transported during melt-concrete reaction

	<u>Total moles</u>	<u>Percent</u> ^b
H ₂ O	100,300	65
H ₂	34,270	22
CO ₂	6,410	40
CO	10,050	60
O ₂	3,035	--
K	53,620	68
KOH ^a	22,600	29
SiO	2,930	--
Fe(OH) ₂	13,400	--
Mn	2,930	10
UO ₃	150	--

^aK represents the alkali metals (K + Na).

^bPercent of element (i.e., H, C, K, Mn) introduced into entire system that was vaporized.

Table IV. Heat Removal Effects of Vaporization Reactions

	<u>Δ H,</u> <u>(kj/mole)</u>	<u>Total Heat (j)</u>	<u>Power</u> <u>(MW)</u>
$K_2SiO_3 + H_2O(g) = 2 KOH(g) + SiO_2$	414	4.8×10^9	0.7
$K_2SiO_3 + H_2(g) = 2K(g) + SiO_2 + H_2O(g)$	575	1.6×10^{10}	2.2
$FeO + H_2O(g) = Fe(OH)_2(g)$	188	2.6×10^9	0.4
$H_2O(l) = H_2O(g)$	44	7×10^9	1.0
$CaCO_3 = CaO + CO_2(g)$	180	3×10^9	0.4

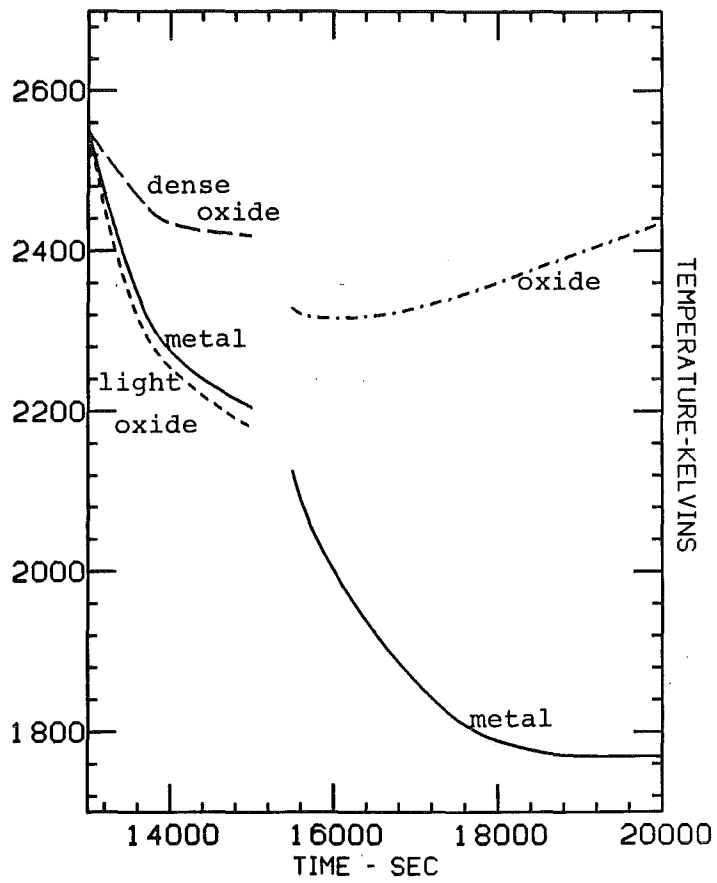


Figure 1. Temperatures of molten layers for Basalt concrete estimated from the CORCON Model. The light and dense oxides mix to form a single oxide that floats on the metal after about 15,000 sec.

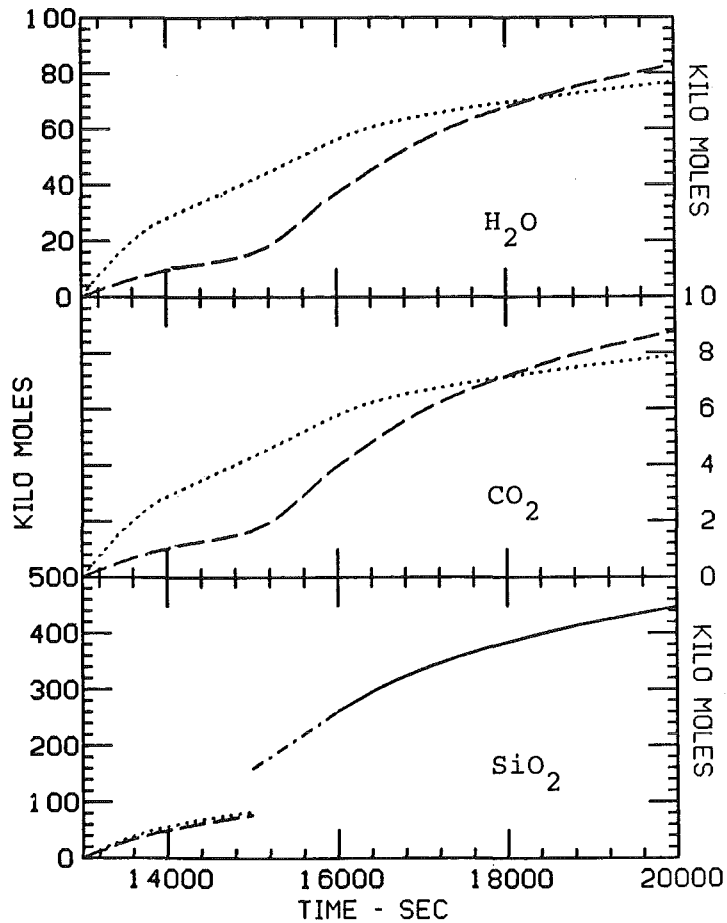


Figure 2. Concrete Constituents introduced during Molten Core-Concrete Interaction Period from CORCON Model (in thousands of moles). Top box represents H_2O , the middle box CO_2 , and the bottom the SiO_2 part of the concrete. In each case the dashed curve is material released from the bottom of the molten pool and the dotted curve from the sides. The full curve in the SiO_2 box represents the sum from the bottom and sides after 'oxide-flip'.

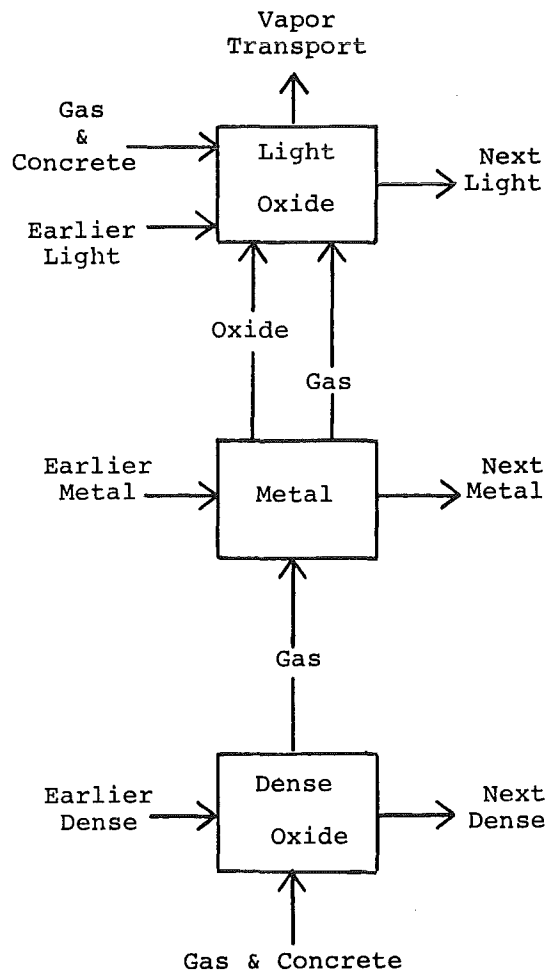


Figure 3. Schematic flow sheet before 'oxide-flip'. Boxes indicate the calculation steps for each time step.

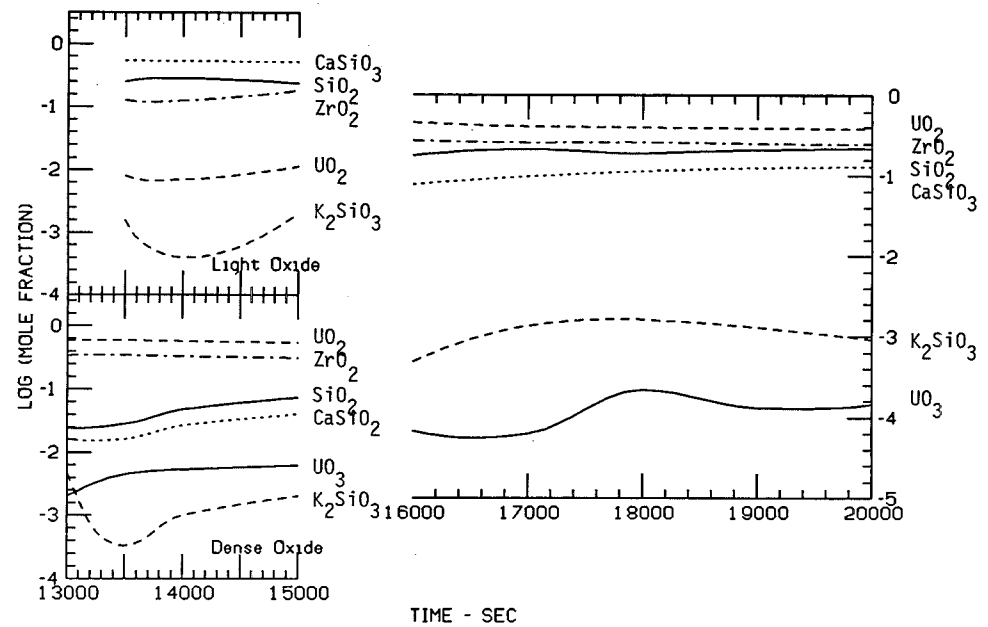


Figure 4. Compositions of molten oxide layers. The formulas on the right hand side of each curve identify the components.

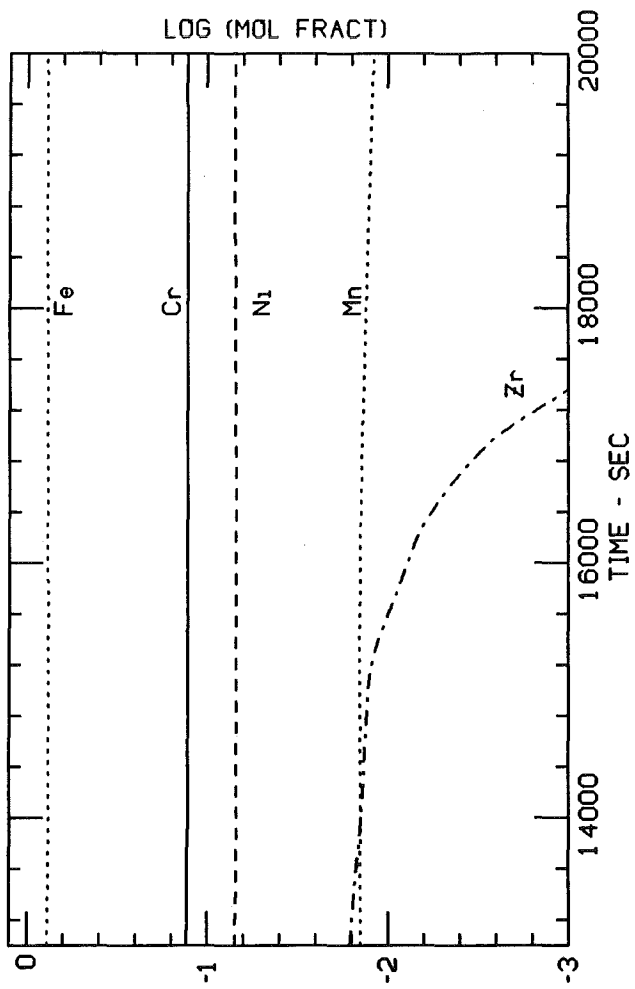


Figure 5. Composition of metal layers.

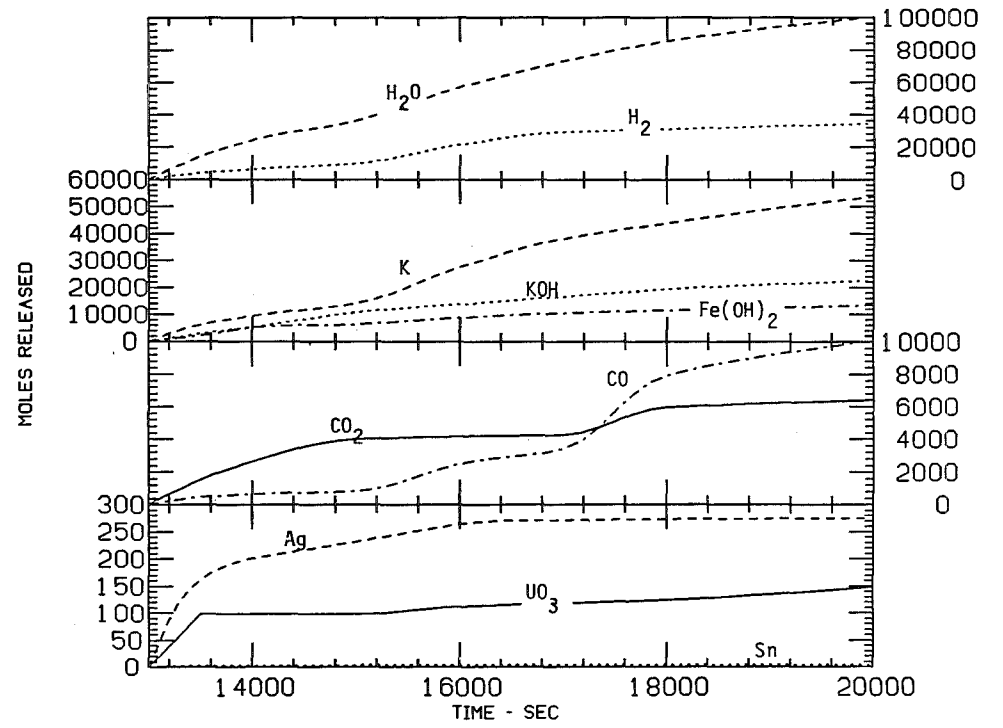


Figure 6. Gases released from basalt concrete/core melt as a function of time.

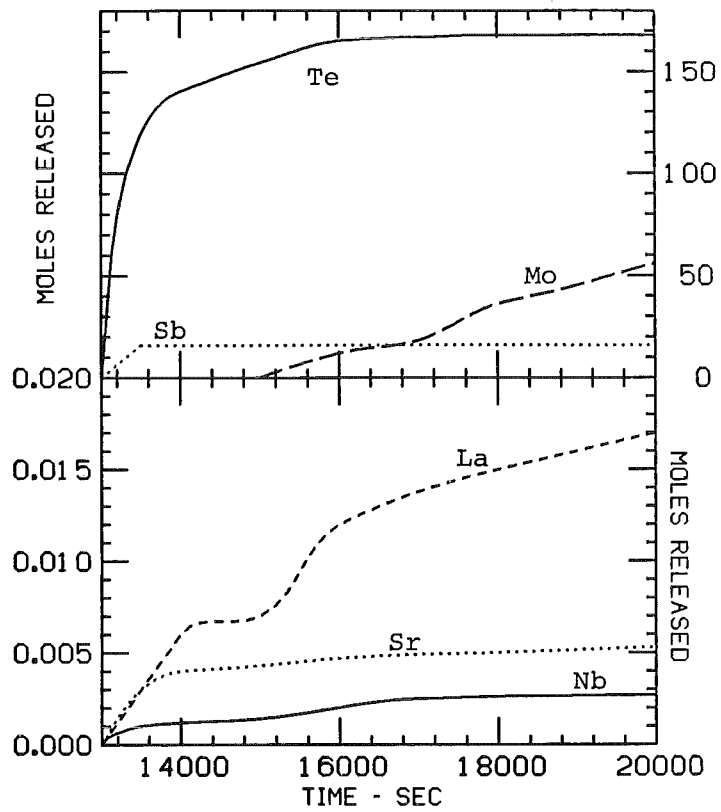


Figure 7. Release of fission products from the total system as a function of time. Upper box - moderately volatile fission products. Lower box - relatively involatile fission products.

AN APPLICATION OF THE MONITORING AND DIAGNOSTIC SYSTEM
TO PLANT DIAGNOSIS ON FP TRANSPORT AND RELEASE IN NPPS

H. Kodaira, S. Kondo and Y. Togo

University of Tokyo
7-3-1, Hongo, Bunkyo-ku, Tokyo, Japan

ABSTRACT

A monitoring and diagnostic system (MADS) of FP transport and release in NPPs is applied to plant diagnosis in combination with the computational code "SACHET", which evaluates the dynamic FP inventories in the multiple compartment system of PWR plants. MADS introduces an algorithm of the stochastic approximation for the adaptive pattern classification of the dynamic disturbed parameter system, using a non-linear functional of the set of monitored data and the system parameters. By the use of MADS, it becomes possible to understand PWR plant states precisely in the view of FP transport and release during normal operation, to identify the occurrences of the unusual events clearly, and to forecaste the potential hazards reasonably and updatedly.

INTRODUCTION

High power levels and fuel exposures of modern nuclear reactor power plants have resulted in core inventories that may exceed 10 billion curries (Ci) of radioactive material, and the potentially severe consequences of the release of a major part of them are serious problems that must be addressed if nuclear reactors are to be used successfully as a large-scale source of power for the near future.

During normal operation of NPPs, a major part of the FP inventories is retained in the core and the very small fractions of them escape to the primary system. The radioactive materials in the primary system then escape to the secondary system and/or to the reactor containment and the major part of them is removed by the purification systems. The radioactive materials cannot, however, disappear in the plants except for radioactive decay, and when an unusual event will happen, all of them may become the source terms of the environment. As the occurrence of an unusual event may be hardly forecasted, we must be prepared for it.

Various kinds of man/machine systems in NPPs have been proposed and developed after Three Miles Island Accident. These systems can be described as computer-based information processing systems which take in plant data, analyze the plant dynamics, estimate the resulting damage to fission product barriers, and display the results to the NPP's operating crew to help their control of the plant.

A monitoring and diagnostic system (MADS) of FP transport and release in NPPs has been proposed, and our primary objective of MADS is to monitor the distribution of the radioactive FP and to diagnose the plant state in the view of FP transport during the NPP's lifetime. MADS can provide the NPP's operating crew with the information of the dynamic distribution of the whole radioactive FPs at all times, and in case of an unusual event, these informations may become the accurate initial conditions for the evaluation of the radiological consequences.^{1,2)}

Equations of The Multiple Compartment Model

As the flow terms assume uniform mixing within each compartment, the changes of FP inventories are described by a set of equations of the form:

$$dC_i/dt = \sum_j H_{ij} C_j + \lambda' C'_i + P * U \quad (1)$$

where C_i = inventories of nuclide C in compartment i
 H_{ij} = transport coefficient of nuclide C from compartment j to compartment i
 $H_{ij} = -\sum H_{ji} - \lambda$
 λ_{ii} = decay constant of nuclide C
 C'_i = inventories of mother nuclide C' in compartment i
 λ' = decay constant of mother nuclide C'
 P = constant according to the thermal power and fission yield
 U = 1 if compartment i is the core fuel
 0 in other cases

These equations are solved exactly and the FP distribution after t is obtained as follows.

$$C(t) = \exp(Ht) C_0 - (1 - \exp(Ht)) H^{-1} * (\lambda' C'_0 + P * U) \\ = (I + Ht + \frac{1}{2} H^2 t^2 + \frac{1}{6} H^3 t^3 + \dots) C_0 + (t + \frac{1}{2} Ht^2 + \frac{1}{6} H^2 t^3 + \dots) * (\lambda' C'_0 + P * U) \quad (2)$$

As the estimation of the whole FP core inventories needs a relatively large computer code such as ORIGEN, and a long computational time, FP core inventory matrix is used in SACHET, which is previously calculated by ORIGEN code.

In normal operation, operating power equilibrium FP source term and FP escape rate coefficient are used in SACHET.³⁾

Iodine spiking phenomena after the reactor shutdown are considered in SACHET, in which original empirical model obtained by the Davidson-Fletcher-Powell method, using the data of the experiments in OWL-1 in-pile loop of JMTR, is used. The model is a nonlinear function with such variables as reactor power, fuel burnup, FP inventories, and changes of linear heat rate, coolant temperature, and coolant pressure.⁴⁾

In case of further fuel defect, from gap release to core explosion, the release fractions of the core inventories are referred to the data from Refs.5&6.

Transport Coefficient

Transport coefficients of the matrix H are defined by the several system parameters of NPP, such as decontamination factor, filter efficiency, partition factor, etc., which are summarized as follows.

$$\text{Purification system } i \text{ (decontamination factor DF) } FI(j-i), FO(i-1) \\ H_{ij} = (FI - FO/DF)/V_j, H_{ii} = 0, \text{ and } H_{1j} = FO/DF/V_j \quad (3)$$

$$\text{Filtration system } i \text{ (filter efficiency EF) } G(j-i, i-1) \\ H_{ij} = EF * G/V_j, H_{ii} = 0, \text{ and } H_{1j} = (1 - EF) * G/V_j \quad (4)$$

$$\text{(partition factor) } F(j-i, 1) \\ H_{ij} = PF * F/V_j, \text{ and } H_{1j} = (1 - PF) * F/V_j \quad (5)$$

METHOD OF MADS

Schematic flow diagrams of MADS and SACHET, and the interrelation of them are given in Fig. 1. The software of MADS consists of codes as follows.

Data Input

In the process of data input, three kinds of data set are took in, plant process data, control data, and radiological data. Process data such as temperatures, pressures, flow rates, etc. are used to determine the transport coefficients. Control data such as valve open/close, pump on/off, etc. are used to recognize the NPP's state, and also to determine the transport coefficients.

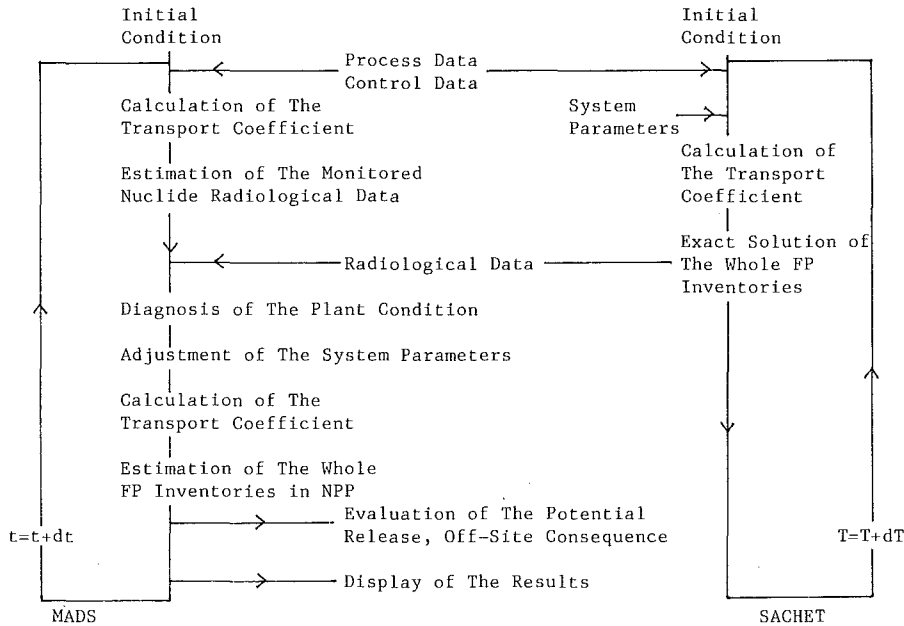


Fig. 1 Schematic Flow Diagrams and Interrelation of MADS and SACHET

Radiological data are monitored after evaluating them, and those values are compared at the next diagnosis phase.

The equations to be solved are the ones described in the previous chapter, and the solution of them is also given previously. Numerical approximation is adopted in MADS by the truncation of the third order matrix, and this approximation is valid for the product of t by the norm of the matrix H is small.

Diagnosis of The Plant State

Example plant conditions of FP transport in MADS are shown in Table III, where the damages to the FP barriers are summarized.

Table III Example Conditions of FP Transport in MADS

Class	Normal Operation	Unusual Event	Alert	Site Emergency
Fuel Damage	~0.25%	0.1%(30 min)	1%(30 min) 5%	Degraded Core
SG Leak	50kg/day	1250kg/day	1250kg/min	
Primary Coolant Leak	75kg/day	2.5kg/min	125kg/min	
Steam Line Break			with SG Leak 25kg/min	with SG Leak 125kg/min
SG Leak with Off-Site Power Down			125kg/min	1250kg/min

The monitored radiological data, in some cases the activities of the mixture of the radiological nuclides are measured, such as inventory vector of the reference radioactive nuclide, and the estimated value of it are used to diagnose the plant condition and to identify the occurrence by the pattern recognition method. The threshold of each condition is given by the results of SACHET.

Adjustment of The System Parameters

At the estimation phase of MADS and SACHET, there are a lot of system parameters which are defined approximately, and according to the experiences of the plant operation, such values as decontamination factors have varied widely with the plant operation. These parameters can be adapted properly at the adjustment phase of MADS using the following asymptotic equations.

A functional of the system parameter x and measured data \tilde{C} is defined as follows.

$$Q(C, x) = \frac{1}{2} \sum g_i (\tilde{C}_i - C_i(x))^2 \quad (6)$$

where C is the estimated data using the system parameter x , and g_i is the factor of the values and errata of C and \tilde{C} . At the time step n , the data \tilde{C} is measured, and system parameter is adjusted according to the equations.

$$x[n, m] = x[n, m-1] + \Gamma[m] \sum g_i \{ \tilde{C}_i[n] - C_i[n, x[n, m-1]] \} \frac{\partial C[n, x[n, m-1]]}{\partial x} \quad (7)$$

$$C[n, m] = C[n-1] + H(x[n, m]) C[n-1] * t \quad (8)$$

$$Q[n, m] = \frac{1}{2} \sum g_i (\tilde{C}[n] - C[n, m])^2 \quad (9)$$

where $x[n, 0] = x[n-1]$, $x[n] = x[n, m]$.

The system parameters adjusted at this step are:

- (1) common parameters: failed fuel rate, leak rate from the primary coolant to the containment, leak rate from the primary to the secondary coolant,
- (2) elementary parameters: leak rate with cladding failure, removal rate by sprays or natural deposition, transport coefficient with evaporation, and
- (3) parameters of every nuclide: decontamination factor of demineralizer, stripping factor of CVC tank, etc.

These parameters are drawn up from the fuel to the environment, from the common to the individual, and from the inert gas to the particle, for the adjustment in sequence.

Estimation of The Unmonitored FP Distribution and The Potential Releases

At this step unmonitored FP distributions are evaluated using the adjusted transport coefficient matrixes.

In an unusual event, the FP distribution after long period can be evaluated and especially in case of a rare occurrence, the potential release in addition to a loss of one of three FP barriers is also evaluated.

RESULTS AND DISCUSSION

Normal Operation

The estimated radioactive FP inventories during normal operation are shown in Table IV. These evaluations are based on the fuel burnup 19800 MWD/UMT, 0.25% failed fuel, and other operating parameters. During normal operation, as the FP leakage from the fuel to the primary coolant is very small, the quasi-steady condition is considered in the multiple compartment system, and the inventories are evaluated on the ratio of the source terms to the rates of removal by radioactive decay, purification, and leakage. These values have been used as the initial conditions of the following calculations.

The results show that the consideration of the fission decay chain and the source terms of the mother nuclide decay is not negligible. In case of alkali metals such as Cs and Rb, the greater parts of their inventories are derived from the decay of their mother nuclides. There are a lot of NPPs, whose radioactivity monitoring systems adopt Cs-137 as the reference radioactive nuclide and the analysis of the transport of it to the monitoring system in consideration of the fission decay chain is necessary.

Change of System Parameters

Table IV FP Inventories in Compartments at Quasi-Steady State

	I 131	I 133	I 135	Kr 85	Kr 87	Kr 88	Xe 133	Xe 135	Xe 137	Cs 135	Cs 136	Cs 137	Rb 87	Halogen	Inert gas	Parti- cle
Whole core inventory	2.72 *E24	5.79 *E23	1.66 *E23	1.25 *E25	9.32 *E21	3.00 *E22	3.48 *E24	6.22 *E22	1.71 *E21	7.80 *E25	1.88 *E23	2.91 *E26	9.67 *E24	5.75 *E25	1.62 *E25	7.70 *E26
1ry coolant inventory	2.79 *E18	4.95 *E17	1.00 *E17	4.30 *E18	9.91 *E15	5.98 *E16	1.72 *E20	3.50 *E17	3.68 *E14	2.17 *E19	2.52 *E17	8.19 *E19	2.69 *E19	3.08 *E18	1.80 *E20	1.46 *E20
(Decay chain)							1.74 *E20	4.37 *E17		2.20 *E19		8.19 *E19	2.69 *E19		1.82 *E20	1.46 *E20
Holdup tank inventory	5.97 *E15	1.27 *E14	6.61 *E12	3.81 *E18	3.01 *E13	4.33 *E14	5.11 *E19	8.60 *E15	1.65 *E10	6.47 *E12	4.01 *E16	5.67 *E17	8.02 *E12	6.10 *E15	5.62 *E19	4.41 *E18
(Decay chain)							5.15 *E19	1.08 *E16		9.45 *E17		5.73 *E17	4.36 *E16		5.66 *E19	5.40 *E18
CVC tank inventory	9.11 *E15	1.57 *E15	2.95 *E14	7.97 *E16	1.04 *E14	1.05 *E15	6.06 *E18	9.77 *E15	7.92 *E11	7.98 *E14	1.57 *E15	1.04 *E16	9.90 *E14	1.10 *E16	6.26 *E18	6.72 *E16
(Decay chain)							6.11 *E18	1.23 *E16		3.69 *E15		1.05 *E16	1.37 *E15		6.31 *E18	7.06 *E16
Gas decay tank inventory	5.76 *E14	1.40 *E12	1.60 *E10	1.76 *E18	9.28 *E12	1.65 *E14	2.40 *E19	3.80 *E15	6.33 *E08	0.0	0.0	0.0	0.0	5.77 *E14	2.64 *E19	0.0
(Decay chain)							2.42 *E19	5.09 *E15		2.87 *E17		4.94 *E12	3.63 *E15		2.66 *E19	2.83 *E17
Waste holdup tank inventory	7.55 *E14	3.58 *E12	7.61 *E10	1.19 *E13	1.02 *E08	1.81 *E09	2.39 *E14	4.15 *E10	6.97 *E03	4.14 *E05	1.00 *E14	1.87 *E15	3.56 *E05	7.59 *E14	2.56 *E14	1.44 *E16
(Decay chain)							2.41 *E14	6.98 *E10		1.65 *E15		1.88 *E15	1.08 *E14		2.59 *E14	1.62 *E16
Reactor containment inventory	2.20 *E11	3.77 *E10	7.03 *E09	2.54 *E13	7.23 *E10	5.48 *E11	1.97 *E15	3.73 *E12	1.40 *E08	5.71 *E07	1.72 *E08	1.03 *E09	7.07 *E07	2.66 *E11	2.03 *E15	7.05 *E09
(Decay chain)							1.98 *E15	4.69 *E12		1.63 *E11		1.69 *E09	1.79 *E10		2.05 *E15	1.93 *E11
2ry coolant (liq.) inventory	6.21 *E12	1.07 *E12	2.02 *E11	0.0	0.0	0.0	0.0	0.0	0.0	2.86 *E11	3.29 *E13	1.62 *E14	3.54 *E11	7.51 *E12	0.0	1.32 *E15
(decay chain)							1.03 *E09	6.10 *E08		5.71 *E13		1.64 *E14	8.27 *E12		1.65 *E09	1.39 *E15

19800 MWD/UMT, 0.25% failed fuel

As MADS is not installed in an actual NPP yet, the validity of the software of MADS is tested in combination with SACHET code.

Some results are shown in Table V (CASE I - VIII), where several parameters are changed at the first step of calculation ($t=0.0$), and in CASE V - VIII, reactor has been stopped at the third step of calculation ($t=20.0$). The adjustment of the system parameters are not shown in Table V explicitly, however, in the use of the equations (7), (8), and (9), the numbers of iteration m are only three or four in most cases as shown in Fig. 2 (a).

In CASE I and II, where fuel cladding failures are increased by the rate of 0.1%/30min as shown in Table III (unusual event), the increases of the fuel failure are identified at the first step of the adjustment, and only the inventory of each element in the primary coolant is necessary for the adjustment.

In CASE III and V, where the primary coolant leaks to the reactor containment, at the rates of 2.5kg/min and 125kg/min respectively, as shown in Table III, the leak rates are adjusted by the monitored data of the inventories of inert gas in the reactor containment. The partition factor of iodine in CASE V is adjusted after the adjustment of the leak rate, by the monitored data of the inventories of iodine in the reactor containment.

In CASE IV and VI, where the primary coolant leaks through SG to the secondary coolant, at the rates of 1250kg/day and 1250kg/min respectively, as shown in Table III, the SG leak rates are adjusted by the monitored data of inert gas in the primary coolant and the secondary coolant(gas).

In CASE VII and VIII, where both the primary and secondary coolant leak at the nearly same time, the two leak rates are adjusted by the monitored data of the inventories in the primary and secondary coolant and the turbine building. The convergence of the parameter estimations are not so good as compared with the other cases, as shown in Fig. 2 (b).

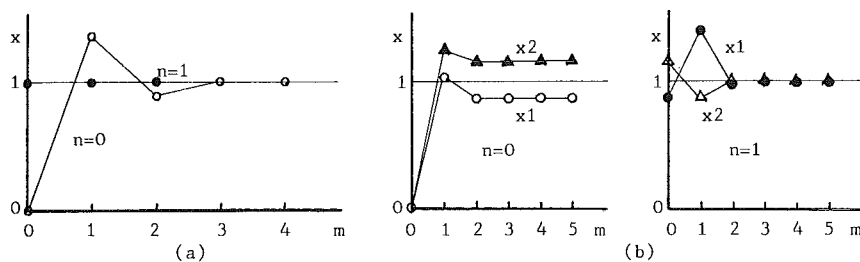


Fig. 2 Adjustment of the system parameters by MADS

Bypass Factor

In case of steam line break, transport coefficient from the second compartment to the third compartment (R_2) is larger than that from the first compartment to the second compartment (R_1), where those compartments have become in a state of transient equilibrium, in a short time. As FP increase in the third compartment (turbine building) has been proportional to the inventories of the first compartment (primary coolant), the transport coefficient from the first compartment to the third compartment (H_{31}) has been significant, and the value of it is as follows.

$$H_{31} = \frac{1}{2} R_1 (R_2 - R_1) * t \quad (10)$$

In similar cases of the purification system and the filtration system, bypass factor (BF) is defined as follows.

$$BF = \frac{1}{2} (R_2 - R_1) * t \quad (11)$$

Table V FP Inventories after The Change of The System Parameters

CASE I (Cladding Failure)					
t=0.0; 5.56*E-07/sec					
	t=0.0	t=100.0	t=200.0	t=300.0	sec
Halogen					
Primary Coolant	2.96*E+02	8.98*E+02	1.49*E+03	2.07*E+03	Ci
CVC Tank	1.03*E+00	1.12*E+00	1.40*E+00	1.84*E+00	
Reactor Building	2.45*E-05	2.60*E-05	3.05*E-05	3.76*E-05	
Inert Gas					
Primary Coolant	7.74*E+03	8.85*E+03	9.87*E+03	1.08*E+04	Ci
CVC Tank	2.67*E+02	2.67*E+02	2.70*E+02	2.75*E+02	
Reactor Building	8.78*E-02	8.81*E-02	8.88*E-02	9.00*E-02	
Particle					
Primary Coolant	5.76*E+01	6.63*E+02	1.26*E+03	1.83*E+03	Ci
CVC Tank	3.41*E-01	5.58*E-01	1.17*E+00	2.39*E+00	
Reactor Building	4.54*E-05	4.66*E-05	5.44*E-05	7.26*E-05	
CASE II (Cladding Failure - No Decay Chain)					
t=0.0; 5.56*E-07/sec					
	t=0.0	t=100.0	t=200.0	t=300.0	sec
Halogen					
Primary Coolant	2.96*E+02	8.98*E+02	1.49*E+03	2.07*E+03	Ci
CVC Tank	1.03*E+00	1.12*E+00	1.40*E+00	1.84*E+00	
Reactor Building	2.45*E-05	2.60*E-05	3.05*E-05	3.76*E-05	
Inert Gas					
Primary Coolant	7.63*E+03	8.75*E+03	9.76*E+03	1.07*E+04	Ci
CVC Tank	2.63*E+02	2.64*E+02	2.67*E+02	2.72*E+02	
Reactor Building	8.65*E-02	8.68*E-02	8.76*E-02	8.87*E-02	
Particle					
Primary Coolant	2.77*E+01	6.24*E+02	1.19*E+03	1.74*E+03	Ci
CVC Tank	1.62*E-01	3.70*E-01	9.60*E-01	1.85*E+00	
Reactor Building	1.91*E-08	3.44*E-08	7.73*E-08	1.44*E-07	
CASE III (Primary Coolant Leak)					
t=0.0; 4.167*E-05 ton/sec					
	t=0.0	t=100.0	t=200.0	t=300.0	sec
Halogen					
Reactor Building	2.45*E-05	5.67*E-04	1.08*E-03	1.55*E-03	Ci
Inert Gas					
Reactor Building	8.78*E-02	2.31*E-01	3.68*E-01	4.98*E-01	Ci
Particle					
Reactor Building	4.54*E-05	5.61*E-05	8.45*E-05	1.26*E-04	Ci
CASE IV (SG Leak)					
t=0.0; 1.447*E-05 ton/sec					
	t=0.0	t=100.0	t=200.0	t=300.0	sec
Halogen					
Secondary Coolant(l)	7.11*E-04	2.30*E-03	3.76*E-03	5.10*E-03	Ci
Secondary Coolant(g)	1.07*E-05	2.54*E-04	4.76*E-04	6.78*E-04	
Inert Gas					
Secondary Coolant(l)	4.37*E-07	7.88*E-07	1.52*E-06	2.53*E-06	Ci
Secondary Coolant(g)	2.82*E-03	3.76*E-02	5.45*E-02	6.26*E-02	
Particle					
Secondary Coolant(l)	2.43*E-03	2.78*E-03	3.13*E-03	3.47*E-03	Ci
Secondary Coolant(g)	1.46*E-06	5.16*E-06	9.58*E-06	1.29*E-05	

Table V (continued)

CASE V (Primary Coolant Leak)					
t=0.0; 2.08*E-03 ton/sec					
0.2 (Iodine Partition Factor in Reactor Building)					
t=20.0; shutdown					
	t=0.0	t=100.0	t=200.0	t=300.0	sec
Halogen					
Reactor Building	2.45*E-05	5.40*E-02	1.04*E-01	1.51*E-01	Ci
Inert Gas					
Reactor Building	8.78*E-02	7.23*E+00	1.40*E+01	2.05*E+01	Ci
Particle					
Reactor Building	4.54*E-05	5.63*E-04	1.87*E-03	3.66*E-03	Ci
CASE VI (SG Leak)					
t=0.0; 2.08*E-02 ton/sec					
t=20.0; shutdown					
	t=0.0	t=100.0	t=200.0	t=300.0	sec
Halogen					
Secondary Coolant(l)	7.11*E-04	2.39*E+00	4.55*E+00	6.52*E+00	Ci
Secondary Coolant(g)	1.07*E-05	2.91*E-01	5.81*E-01	8.50*E-01	
Turbine Building	9.75*E-07	3.11*E-05	1.22*E-04	2.72*E-04	
Inert Gas					
Secondary Coolant(l)	4.37*E-07	4.99*E-04	1.58*E-03	2.84*E-03	Ci
Secondary Coolant(g)	2.82*E-03	5.21*E+01	7.72*E+01	8.94*E+01	
Turbine Building	4.31*E-04	6.54*E-03	2.04*E-02	3.79*E-02	
Particle					
Secondary Coolant(l)	2.43*E-03	5.36*E-01	1.04*E+00	1.53*E+00	Ci
Secondary Coolant(g)	1.46*E-06	3.67*E-03	8.81*E-03	1.23*E-02	
Turbine Building	3.33*E-08	3.32*E-07	2.00*E-06	5.38*E-06	
CASE VII (Steam Line Break with SG Leak)					
t=0.0; 3.62*E-02 ton/sec (Steam Release)					
4.17*E-04 ton/sec (SG Leak)					
t=20.0; shutdown					
	t=0.0	t=100.0	t=200.0	t=300.0	sec
Halogen					
Secondary Coolant(l)	7.11*E-04	4.84*E-02	9.15*E-02	1.31*E-01	Ci
Secondary Coolant(g)	1.07*E-05	5.82*E-03	1.15*E-02	1.69*E-02	
Turbine Building	9.75*E-07	4.20*E-05	1.67*E-04	3.73*E-04	
Inert Gas					
Secondary Coolant(l)	4.37*E-07	1.04*E-05	3.18*E-05	5.63*E-05	Ci
Secondary Coolant(g)	2.82*E-03	1.03*E+00	1.51*E+00	1.72*E+00	
Turbine Building	4.31*E-04	8.67*E-03	2.73*E-02	5.10*E-02	
Particle					
Secondary Coolant(l)	2.43*E-08	1.31*E-02	2.32*E-02	3.30*E-02	Ci
Secondary Coolant(g)	1.46*E-06	7.51*E-05	1.74*E-04	2.38*E-04	
Turbine Building	3.33*E-08	4.40*E-07	2.70*E-06	7.24*E-06	
CASE VIII (SG Leak with Off-Site Power Down)					
t=0.0; 2.08*E-03 ton/sec (SG Leak)					
2.91*E-02 ton/sec (Steam Dump)					
t=20.0; shutdown					
	t=0.0	t=100.0	t=200.0	t=300.0	sec
Halogen					
Secondary Coolant(l)	7.11*E-04	2.40*E-01	4.55*E-01	6.51*E-01	Ci
Secondary Coolant(g)	1.07*E-05	2.90*E-02	5.77*E-02	8.44*E-02	
Turbine Building	9.75*E-07	1.65*E-04	6.63*E-04	1.49*E-03	
Inert Gas					
Secondary Coolant(l)	4.37*E-07	5.02*E-05	1.58*E-04	2.80*E-04	Ci
Secondary Coolant(g)	2.82*E-03	5.17*E+00	7.59*E+00	8.68*E+00	
Turbine Building	4.31*E-04	3.34*E-02	1.09*E-01	2.34*E-01	
Particle					
Secondary Coolant(l)	2.43*E-08	5.57*E-02	1.07*E-01	1.55*E-01	Ci
Secondary Coolant(g)	1.46*E-06	3.66*E-04	8.64*E-04	1.19*E-03	
Turbine Building	3.33*E-08	1.65*E-06	1.07*E-05	2.90*E-05	

$$H_{21}=R_1*(1-BF) \quad (12)$$

$$H_{31}=R_1*BF \quad (13)$$

In such cases as steam line break and large LOCA, monitoring the second compartment has not become essential.

Computational Time

The software of MADS is not so simple as to perform the real time operation by a process (mini) computer, even though computational time is shorter than real time in the use of M-280H. To shorten it, the software of MADS have been tuned for the vector calculation, and the ratio of it becomes less than 0.3 as compared with the scalar calculation. Process computer with an array processor can realize the real time operation of MADS.

CONCLUSION

Computerized code "SACHET" which simulates the dynamical FP transport and release in PWR plant has been developed, and the software of MADS has been studied, and the effectiveness of MADS is shown in this study.

REFERENCES

1. H. Kodaira et al, "A monitoring and diagnostic system of fission product transport and release in nuclear power plants," Report NUREG/CP-0027,(1983).
2. H. Kodaira et al, "A method of computer-based operator instruction system for diagnosing fission product transport and release in nuclear power plants," Journal of the faculty of engineering, UT(B) XXXVII,3, (1984).
3. "Calculation of release of radioactive materials in liquid and gaseous effluents from pressurized water reactors (PWRs)," DRAFT REGULATORY GUIDE 1.BB, (1974).
4. H. Kodaira, "Analysis of iodine spike activity in ATR primary coolant by Togo-Kondo-Kodaira (TKK) model," (in Japanese) NEUT Report 80-09, (1980).
5. "Release of radioactivity in reactor accidents, Appendix VII to reactor safety study," Report WASH-1400, (1975).
6. R. A. Lorenz et al, "Fission product source terms for light water reactor Loss-Of-Coolant Accident," *Nucl. Tech.* 46, (1979).
7. J. E. Fialkovich et al, "Compilation of reported noble gas effluent monitor capabilities at operating nuclear power plants," Report NUREG-0592, (1980).

FISSION PRODUCT RELEASE AND TRANSPORT MODELING IN KESS-2

K.-D. Hocke, R. Bisanz, F. Schmidt, H. Unger

Institut für Kernenergetik und Energiesysteme (IKE)
University of Stuttgart, Pfaffenwaldring 31, 7000 Stuttgart 80, FRG

ABSTRACT

The modular core melt system KESS-2 is being developed to analyze the course of severe accidents. The major volatile fission products are released during the early phase of the meltdown accident and transported through the primary system into the containment. The fission product decay and release is modeled by the module FIPREM-2 of KESS-2.

The code is coupled to the transient thermalhydraulic and core models. The results are then fed into the transport code TRAP-MELT.

The model FIPREM-2, its validation and the results of the KESS-2 analysis will be described with respect to the fission product release and transport for different accident scenarios.

INTRODUCTION

The core meltdown system KESS-2 is being developed in order to analyze the course of severe accidents in light water reactors /1/. The main objectives of the KESS-2 modeling are the following:

- Provide activity and aerosol source terms during severe accidents for the risk assessment.
- In depth analysis of the course of severe accident phenomena and the physical processes involved.
- Analysis of experiments in the severe fuel/core damage area and extrapolation to reactor conditions.
- Identification of key phenomena and operator actions to terminate accidents.

Since one of the major objectives of severe accident analysis with KESS-2 is to determine the space and time dependent release of fission products to the environment, the physical processes which significantly influence the

fission product release will be modeled and coupled adequately in KESS-2. The current concept of KESS-2 and the modular programs are shown in Fig. 1. Investigations based on a 2F-LOCA indicate, that almost all fission products were retained in the containment, if the containment failed due to overpressurization a few days after the initiation of the accident /2/. Assuming a prior leak in the safety building (FK2-FK4 in the German Risk Study /3/) and/or a small break in the primary system, the major fission products may be released continuously from the containment. The major volatile fission products are released during the early phases of the meltdown accident (Phases 1 - 3, in-vessel phenomena). Thus, the transport and deposition of fission products in the primary system are strongly coupled to the thermal-hydraulics and the core heatup and slumping phenomena until failure of the pressure vessel.

FISSION PRODUCT RELEASE MODELING IN KESS-2

Fig. 2 shows the modeling approach of the fission product and aerosol release within KESS-2 and the connection to other KESS-2 models the dashed lines indicate, that only a weak coupling exists.

The inventory of the nuclides considered is required as input at the beginning of the accident. Such an information may be contributed by the ORIGEN code.

The space and time dependent temperatures in the fuel rods and structure are provided by the MELSIM3 and LUECKE3 code systems of KESS-2. In MELSIM and LUECKE the geometry is represented in a two-dimensional geometry.

The module FIPREM-2 models the fission product decay and release from the fuel rods and structural materials within the reactor pressure vessel.

In spite of the uncertainties in the experimental results, a rate type equation is assumed. The model considers the space dependency of the temperatures, the reduction of local heat sources and the redistribution of fuel rod material due to the slumping fuel rods within the two dimensional geometry.

However, the complex chemical behavior of the released fission products is not well understood, but under investigation elsewhere /4/.

It is assumed that the released fission products are not retained in the core region. The transport through the steam line of the primary system (e.g. pipes and components) is modeled by the TRAP-MELT code. The code requires the mass flow rates and temperatures of the flowing steam and the temperatures on the piping walls. These data are provided by the primary system module PRIMOD of KESS-2.

The releases from the primary system into the containment are input for the aerosol behavior codes, like the NAUA code /5/. The thermodynamic state in the containment is modeled by the codes COCMEL or ASTRO of KESS-2.

The main features of the fission product release and transport modeling in KESS-2 can be summarized as follows:

- Time and space dependent concentration and activities for an arbitrary number of nuclides, its decay and build-up.
- Release of fission products from the core and structural material based on measured release rates (coupling to the core behavior codes in KESS-2).
- Transport through and deposition of aerosols in the primary system (coupling to thermalhydraulics).
- Aerosol behavior in the containment (coupling to containment codes).
- Easy updating in the view of physical and experimental insights.
- Validation of the code by parts.
- Easily adaptable to experimental conditions.

APPLICATIONS

In order to demonstrate the sensitivity of temperature uncertainties on the release fractions of J, the module FIPREM-2 has been applied to an experiment performed by Albrecht /6/. The release rates were derived from experimental data taken from Fig. 3 /7/ (dashed lines). Based on the temperature history shown in Fig. 4, the accumulated release fractions with release rates basing on SASCHA experiments and the proposed NUREG-0772 were applied. It should be mentioned that the release rates are based on different experimental conditions and have not been corrected to achieve the same results. The results shown in Fig. 4 demonstrate that it is not sufficient to model the temperature dependency of the release rates only. One should additionally at least consider burn-up and geometric conditions. The sensitivity of a +/- 100 K deviation in the temperatures is shown to be less important compared to the influence of the fuel burn-up, for instance.

With respect to the fission product release and transport models in KESS-2 various accident scenarios have been investigated. A disadvantage to date is the lack in modeling the chemical behavior of significant radioactive isotopes. This part will be incorporated in the future /4/. The advantages of the analysis are:

- Determination of the fission product and structural material release on a best estimate basis.
- Information about the reduction of heat sources in the core calculations.

- Coupling to sophisticated codes with respect to thermalhydraulics, containment and core behavior.
- Continuous analysis starting at the initiation of the accident.
- Capability of validating the codes on a stand-alone basis.

REFERENCES

- /1/ F. Schmidt, R. Bisanz: "KESS-2 - Recent Development and Perspectives", Int. Meeting on Light Water Reactor Severe Accident Evaluation, Vol. II, Cambridge, Mass., USA, Aug./Sept. 1983
- /2/ J.P. Hosemann: "Neuere Ergebnisse zum Ablauf und zu den Auswirkungen hypothetischer DWR-Kernschmelzunfälle", KFK-Nachrichten, 14, 4/82
- /3/ Deutsche Risikostudie Kernkraftwerke, Verlag TÜV Rheinland, Dezember 1979
- /4/ J.P. Hosemann, K.H. Neeb, J. Wilhelm: "Neuere Bewertung der Freisetzung und des Transports von Jod bei schweren Reaktorstörfällen", Jahrestagung Kerntechnik, Juni 1983
- /5/ A. Bunz, M. Koyro, W. Schöck: "NAUA Mod 4 - A Code for Calculating Aerosol Behavior in LWR Core Melt Accidents", Code Description and Users Manual, KFK 3554, Aug. 1983
- /6/ H. Albrecht, H. Wild: "Freisetzungsquellterme bei hypothetischen LWR-Störfällen", KTG-Fachtagung "Freisetzung und Transport von Spaltprodukten bei hypothetischen Störfällen von Leichtwasserreaktoren", KFK, 8.-9. 6. 1982
- /7/ Technical Bases for Estimating Fission Product Behavior During LWR Accidents, NUREG-0772, June 1981

KESS 2

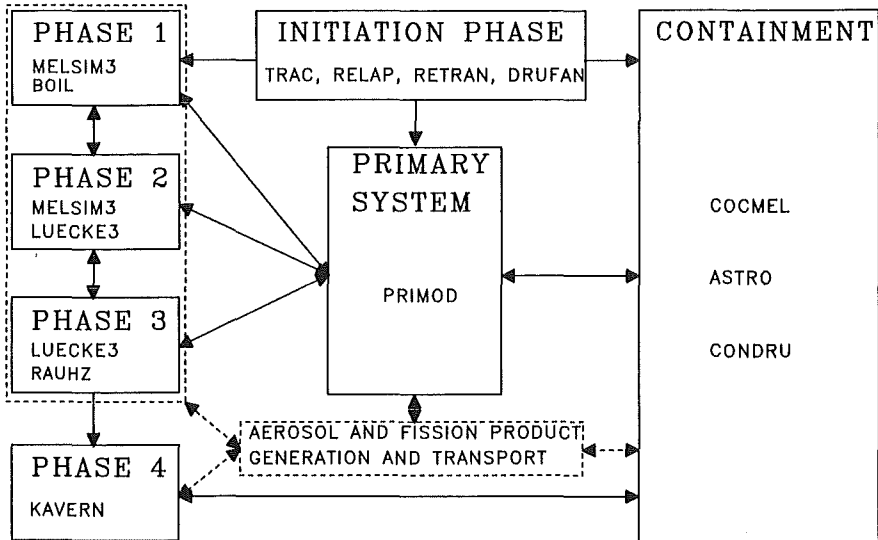


FIG. 1

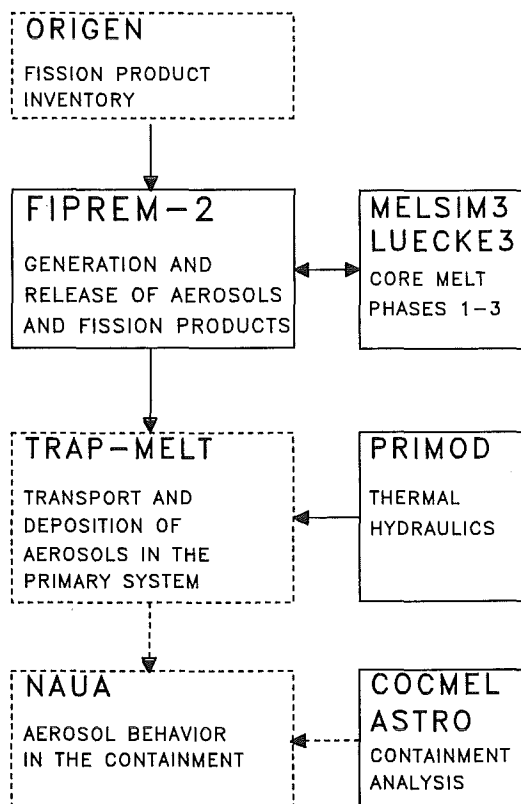


FIG.2:
 MODELING OF AEROSOL AND FISSION
 PRODUCT RELEASE IN KESS-2

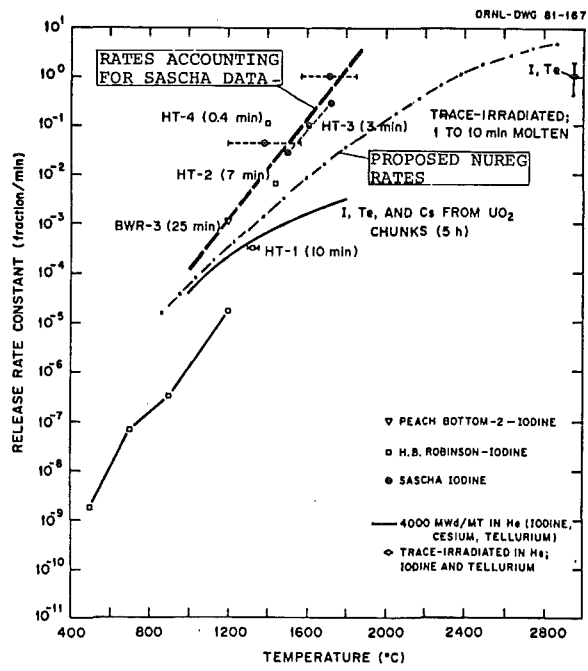
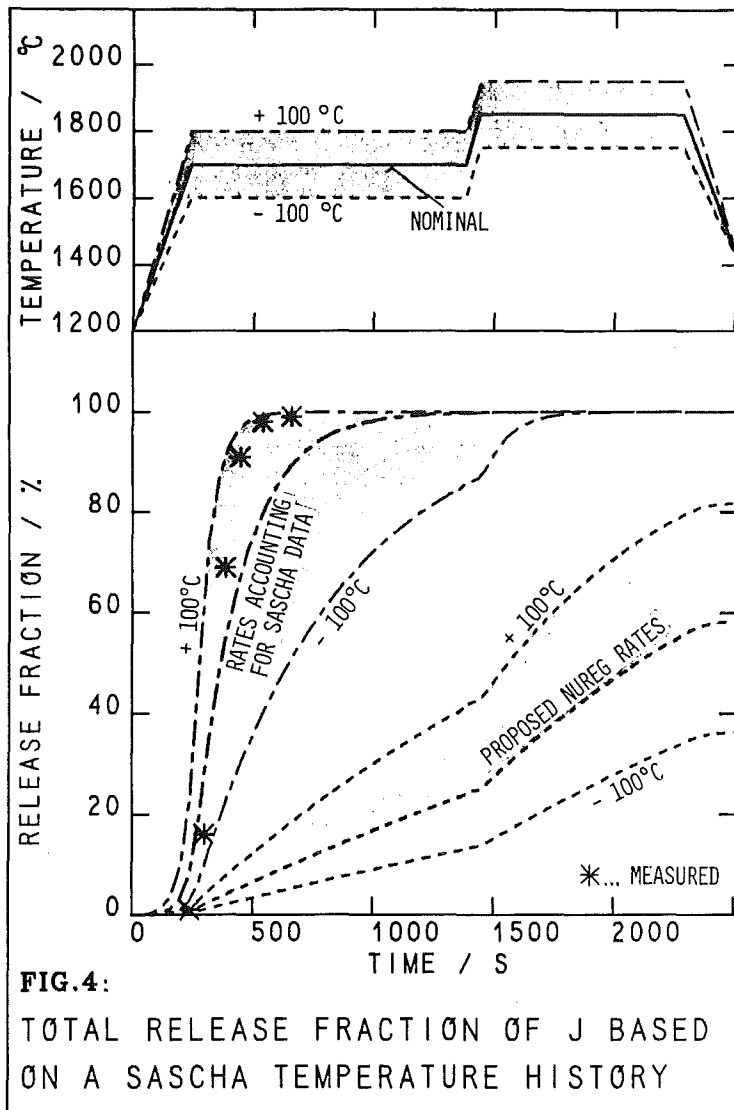


Fig. 3: Iodine release rate constants from fuel



HEPA-FILTER RESPONSE TO HIGH DIFFERENTIAL PRESSURES
AND HIGH AIR VELOCITIES

C.I. Ricketts, V. Rüdinger, J.G. Wilhelm
Laboratorium für Aerosolphysik und Filtertechnik
Kernforschungszentrum Karlsruhe GmbH
Postfach 3640, D-7500 Karlsruhe 1
Federal Republic of Germany

ABSTRACT

As part of a study aimed at the evaluation and improvement of the performance of HEPA filters under possible accident conditions, the structural limits and flow resistances of commercial and prototypical filter units, during exposure to high air velocities, were investigated.

Full-size, clean and preloaded, unused filters were exposed to air flows with differential pressures up to 28 kPa and filter-entrance velocities up to 35 m/s, at ambient temperatures and relative humidities.

Test results include the range of average differential pressures at which present-day commercial HEPA filters can be expected to fail, 4 - 23 kPa, as well as the flow-resistance data required for input to computer codes used in safety analysis. Test results are applicable to the design, safety analysis, and licensing of nuclear facilities.

INTRODUCTION

The High Efficiency Particulate Air (HEPA) filters within the air-cleaning systems of nuclear facilities form part of the barrier between contaminated zones and the ambient environment. Protection of human health from the effects of airborne radioactive material relies upon an effective air-cleaning process, not only during normal operation but particularly during accident situations. A loss of coolant, a fire, or a tornado depressurization could challenge HEPA filters at their service locations with high differential pressure, high flow rate, high temperature, or high relative humidity. Mechanical stresses within the filter medium can be expected to occur, followed by possible loss of effective filtration or release of previously captured particulate. Contingent upon accident type and scenario, these challenges could be imposed individually or in combination, i.e., superimposed. A Loss-of-Coolant Accident (LOCA), for example, could superimpose all of the above challenges on filters in service.

The amount of radioactive material released to the environment via an air-cleaning system during an accident situation is in part determined by the resultant behavior of the filters. To investigate this behavior, other authors have exposed HEPA filters to conditions that simulate the effects of a number of accident types /1-9/.

These studies provide general, though sometimes restricted orientation toward the evaluation of HEPA-filter behavior during individual challenges to filter performance. Often, the numbers, the manufacturers, and the designs of the filters tested have been limited. In addition, tests have been performed almost exclusively with new filter units. Limits in filter-performance characteristics have not always been discussed within the context of possible improvements to such characteristics, e.g., maximum differential pressure, flow resistance, filtration efficiency, dust holding capacity, and resistance to the effects of exposure to moisture, high temperature, or shock waves.

Reported on here are the results of a first step toward goals of evaluating the performance of commercial HEPA filters under individual and superimposed challenges, and improving filter performance where considered necessary. A third objective is to obtain the experimental data required for numerical simulations of transient flows in air-cleaning systems. In addition to the structural limits, the failure mechanisms, and the flow resistance characteristics of HEPA filters at room temperatures and humidities, some relevant improvements in structural limit and flow resistance are discussed.

STRUCTURAL TESTS

Effective HEPA filtration depends first of all upon preservation of the structural integrity of the filter medium. Hence, the differential pressure (ΔP) at rupture of the medium in a HEPA filter is an important criterion of filter performance. Filter structural failure can be defined to occur with the first visible rupture in the glass-fiber medium that normally has a thickness of 0.5 mm. The differential pressure associated with this initial failure is then designated as the structural limit of the filter.

Structural limits were determined by subjecting each test filter to a differential pressure pulse, of up to 28 kPa in magnitude and for as long as 5 s in duration, by the use of compressed air and a blowdown test facility /3, 10/. During these structural tests, the differential pressure and structural failure were recorded by an oscillograph chart recorder and a high speed camera, respectively. All tests including the flow-resistance tests described below were conducted at air temperatures of $< 40^{\circ}\text{C}$ and relative humidities of $< 60\%$.

FLOW-RESISTANCE TESTS

The flow-resistance curve of a filter describes filter differential pressure as a function of flow rate or average air velocity at the filter entrance. HEPA-filter flow resistances are relevant for two reasons. Computer codes /11-12/ that numerically simulate transient flows in air-cleaning systems require these functions in order to model filter differential pressures and flow rates under accident conditions. Secondly, the mechanical stresses in a filter pack are proportional to the differential pressure and hence related to the flow rate by the flow-resistance function. Desirable, low mechanical stresses at high flow rates depend upon low differential pressure and thus are to be obtained with filters which have flow resistances characterized by flat, rather than steep curves.

Flow-resistance tests of HEPA filters were performed at conditions of quasi-steady flow and at differential pressures of up to 20 kPa with the same test facility employed for the structural tests. From each filter type to be structurally tested, one filter was exposed to a sequence of about 10 different flow rates, while the flow and pressure data needed to generate a flow-resistance curve were registered with a chart recorder. The duration of a test was usually less than 30 s.

TEST FILTERS

The majority of filters tested were 610x610x292-mm commercial units that represent 3 current designs from the major European and American manufacturers. A closely related group included similar units that had been factory modified by reinforcement of the glass-fiber medium. In a third test category were 2 types of prototypical filters with filter medium of metal fiber and polycarbonate microfiber, respectively. A few commercial units in standard sizes smaller than 610x610x292-mm were also evaluated. All test filters were new and some had been preloaded with particulates during exposure to air flows containing a polystyrene-latex (PSL) aerosol with a count median geometric diameter of some 0.3 μm .

STRUCTURAL-TEST RESULTS

Relevant to filter structural performance under high differential pressure are measures of performance as well as parameters that influence this performance. Additionally of interest are methods by which performance can be improved. Structural limit as well as the progressive structural damage that follows initial structural failure are two measures of performance. Parameters with potential influence include the design, the manufacturer, and the size of the filter, and also the presence of particulate loading. Filter structural performance can be improved by modifications to current designs or development of new, less conventional designs.

In Table I are listed the location and the ΔP range of structural failure for clean HEPA filters of 3 current commercial designs. A total of 72 test filters from 8 manufacturers are represented here. The ΔP range of average failures in the fourth column is a quantitative measure of the differential pressures, on the average, which will cause structural failure for a given filter design. The parameter responsible for the width in the ranges is filter manufacturer, since the averages were calculated for groups of filters based upon manufacturer. For example, from the first design listed, the value of 11 kPa is the average differential pressure at structural failure for five filters from one manufacturer and correspondingly, 23 kPa is the value of the same parameter for 4 filters from another manufacturer. Average values by manufacturer, for other tested filters of this design, fall within these two bounds. In addition to an average structural limit, each group of filters also has an associated standard deviation. The average standard deviation for each of the designs listed, from first to third, respectively, is 12, 7, and 12 %. Because the values of Table I are averages, some failures at both somewhat lower and somewhat higher ΔP 's than those listed, can be expected.

Table I: Structural limits for 3 Designs of Commercial
New Clean 610x610x292-mm HEPA Filters.

Filter Design		Structural Failure Location in Filter	ΔP Range of Average Failures (kPa)
Pack	Frame		
Deep Pleat (270 mm) Separators	Wood	Fold of Medium	11 - 23
Deep Pleat (270 mm) Separators	Metal	Adhesive, Pack- to-frame	4 - 11
Mini Pleat (20-40 mm) V Panels	Wood, Metal, or Plastic	Panel of Medium	6 - 19

An additional, yet qualitative measure which can be used to compare the performance of the 3 filter designs, is how quickly and to what extent structural damage progresses after the initial structural failure. The ability to qualify filter performance on this basis is made possible by further analysis of the same high-speed films which were taken of the downstream side of the test filters and used to establish the initial structural failures. Study of the films shows that each of the 3 commercial filter designs typically exhibits a different mode of progression in structural damage. These modes relate in part to the respective locations of structural failure in the filter, listed in the third column of Table I.

For deep-pleat filters with a wooden frame, initial failure typically occurs as the result of a 2-4 cm rupture in one of several swollen folds of medium on the downstream side of the filter /13/. Damage usually progresses relatively slowly by an increase in length of the original rupture, up to as much as 40 cm, and/or by additional rupture in a second or third swollen fold. Even after exposure to maximum ΔP 's approx. 5 kPa greater than those at initial failure, generally > 99 % of the filter medium remained intact, as shown typically in Fig. 1. The tensile strength of the glass-fiber medium has been implicated as the point of weakness for this design /3,10,14/.

The relatively low structural limit as well as the early occurrence of catastrophic failure in deep-pleat filters with a metal frame, for service at >120 °C, is mostly attributed to the lack of adhesive between pack and frame /10/. Visible failure begins with horizontal lines of small ruptures in the downstream folds of the medium. This is followed suddenly by ejection of the entire filter pack from the frame at ΔP 's less than about 1 kPa greater than those of initial failure. Essentially no medium remains in the frame as illustrated in Fig. 2.

The structural limits as well as the extent of progressive damage for the mini-pleat filters with multiple panels mounted in 'V' configurations, lie between those of the two designs described above. Initial failure typically begins when the downstream edge of a swollen medium panel shears at the vertical sheet-metal rib to which it is glued /10/. Progressive damage spreads relatively quickly with failure of other panels, as the ΔP increases. The lack of structural support for the medium panels is responsible for this failure type. Mini-pleat filters exposed to maximum

ΔP 's of approx. 5 kPa greater than those at initial failure generally retained about 50 % of the filter medium intact as indicated typically in Fig. 3. Such damage reduces the removal efficiency to essentially zero.

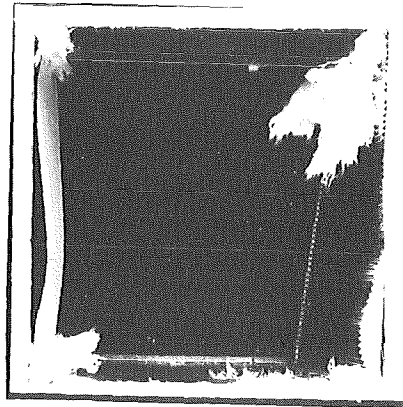
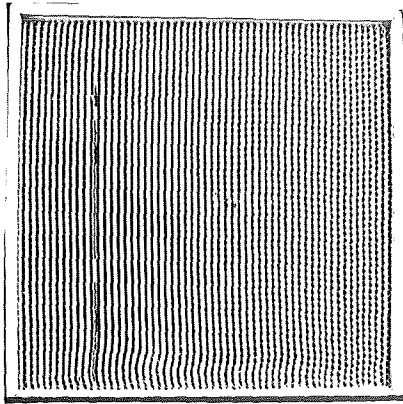
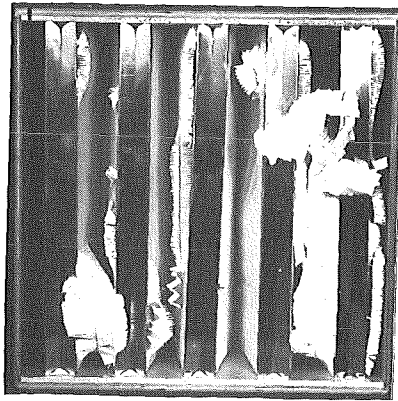


Fig. 1: Damage to a Deep-Pleat Wooden-Frame Filter After ΔP of 18 kPa.

Fig. 2: Damage to a Deep-Pleat Metal-Frame Filter After ΔP of 6 kPa.

Fig. 3: Damage to a Mini-Pleat Wooden-Frame Filter After ΔP of 20 kPa.



Other parameters which showed some influence on the structural limits for the filter design with deep pleats, aluminium separators, and wooden frame, were filter cross section, filter depth, and particulate loading. As shown in Table II for filters of the same depth with two different cross sections, and from both of two manufacturers, structural limits increased with decreases in filter cross section. Increases are also seen for filters with the 305x305-mm cross section for a decrease in filter depth. But with the same decrease in depth for filters with the 610x610-mm cross section, a decrease in structural limit is evident.

Table II: Variation of the Structural Limits with Filter Cross Section and Depth; for New Commercial Deep-Pleat Wooden-Frame Clean HEPA Filters.

Filter Size		Average Break Pressure $\bar{\Delta P}$, Standard Deviation σ , and Number of Tests n .					
		Filter Type A			Filter Type C		
Cross Section (mm x mm)	Depth (mm)	$\bar{\Delta P}$ (kPa)	σ (%)	n (Ea.)	$\bar{\Delta P}$ (kPa)	σ (%)	n (Ea.)
610x610	150	10	14	3	13	27	3
610x610	292	13	5	4	23	17	4
305x305	150	26	2	7	25	6	5
305x305	292	17	11	8	24	7	8

The 610x610x150-mm size is characterized not only by the lowest structural limit but also by a catastrophic initial failure of the pack /13/, rather than the localized initial failure of folds in the medium, as is the case for the other three sizes. Both the early catastrophic failure and the relatively low ΔP 's that cause it, may be attributed to higher structural stresses in the pack due to geometry. If the pack is modeled as an average thickness plate under a distributed load, a geometric ratio proportional to the maximum stresses in the pack is pack cross-sectional area divided by the square of pack depth /15/. For the 610x610x150-mm size this ratio is greater than those of the other three sizes, by factors of between 4 and 20. The susceptibility to failure of the pack as a whole is, for any given ΔP , greatest for this size.

Not yet clear is why the highest structural limits appear for filters with a 150-mm depth, i.e., those with the 305x305-mm cross section. This may be attributed to changes, with pack depth, in the not-yet-defined distributions of air flow and pressure within the pack at high air velocities. Or, another possibility is that of a more stable pack in this size, due to geometry or manufacturing processes. These possibilities would be applicable for the localized initial failure in medium folds, not the catastrophic failure of the 610x610x150-mm size.

The effect of a preload of PSL, to a ΔP of 1 kPa at rated flow, on the structural limits of filters with deep pleats and wooden frame was to increase structural limits by an average of < 10 %. This compares with average decreases of 14 % and 40 %, respectively, for deep-pleat filters with metal frame and one type of mini-pleat filter. Taken altogether the results indicate a slight trend toward lower structural limits due to a preload with PSL.

The structural limits of the filters listed in Table III illustrate the results of several approaches taken to improve filter design. First noted are the results of several respective reinforcements of the filter medium that show an increase in the structural limits for one filter type of one manufacturer; from 11 to 23 kPa in one case and from 11 to 24 kPa for

another case. Two types of filters with deep-pleat medium that had been reinforced by a fiber-glass scrim exhibited the highest structural limit of any 610x610x292-mm modified filter with a glass-fiber medium. Three filters from each of these two types supplied by another manufacturer were tested and all six remained undamaged after exposure to differential pressures > 27 kPa.

Additional modified commercial designs tested but not shown in Table III included a deep-pleat, separatorless and several mini-pleat types, both with wooden frames. The separatorless type was reinforced by a fiber-glass scrim for which test outcomes showed an increase in average ΔP at failure, from 11 kPa /4/ up to 18 kPa. Perforated steel sheets on the downstream side of the medium panels, of one type of modified mini-pleat filter, also resulted in an increase in structural limit: to 22 kPa from the 11 kPa /10/ of the standard type.

Results from 2 categories of prototypical HEPA filters which were tested are also shown in Table III. The one deep-bed metal-fiber filter /16/ evaluated, withstood undamaged, the maximum differential pressure of the test facility, 27-28 kPa, as did 24 filters with several types of deep-pleat polycarbonate microfiber media /17/. One additional filter in the latter category sustained without structural damage a differential pressure of 30 kPa in another test facility /18/. The widespread application of the filters with the metal-fiber and polycarbonate medium, respectively, remains yet limited by flow-rate and temperature performance characteristics.

Table III: Structural Limits of Modified Deep-Pleat, and Prototypical, New Clean 610x610x292 mm HEPA Filters.

Modification to Filter Pack	Design Flow Rate (m ³ /h)	Average ΔP at Failure (kPa)
<u>Improved Deep-Pleat Glass-Fiber</u>		
None: Commercial Medium	1700	11
Protective Fiber Mat Pleated with Medium	1700	23
Protective Strip in Folds + Long-Fiber Medium	1700	24
Medium Reinforced with Fiber-Glass Scrim	1700	> 27 *
<u>Prototypical</u>		
Deep-Bed Metal-Fiber Medium	40	> 28 *
Deep-Pleat Polycarbonate Microfiber Medium	1700	> 27 *

* No observed structural failure.

The comparison of structural-test results with similar tests by Gregory and coworkers /3,4/ shows that the structural limits for approx. 100, of 120, other similiary tested commercial filters lie within the ranges given in Table I . The exceptions, results for approx. 20 test filters of the first design in Table I and from one manufacturer, showed an average 9-kPa differential pressure at failure and a different characteristic failure mode, both attributed to a medium with an unusually low tensile strength /5/.

Over 200 filters of 30 types from 10 manufactureres were tested to obtain the results presented for structural tests. A summary of these results indicates that structural limits varied significantly with both design and manufacturer for representative samples of new commercial 610x610x292-mm nuclear-grade HEPA filters procured in Europe and in the U.S.A. The degree of progressive structural damage at several kPa above that required to cause initial structural failure, was observed to depend primarily upon filter design. The filter design typified by the highest structural limits and least progressive damage is that with deep pleats, separators, and wooden frame. The versions of this design with metal frames for applications above 120 °C, were found to exhibit not only the lowest structural limits but also the most progressive damage after initial failure. Most of the factory-modified commercial-type filters of the deep-pleat and mini-pleat designs tested, demonstrated structural limits higher than their commercial counterparts. Comparable structural limits of > 27 kPa were also observed for two types of prototypical filters tested.

RESISTANCE-TEST RESULTS

The flow-resistance characteristics of a filter are usually illustrated graphically by differential pressure across the filter plotted against the average air velocity at the filter entrance. This format is also employed for the flow-resistance curves of Figs. 4-7, where the results from flow-resistance tests of commercial and modified 610x610x292-mm filters are presented.

The curves in Fig. 4 illustrate flow resistances for a number of clean filters with deep pleats and separators. The "S" filters are modified units, the group "AM-VM" refers to metal-frame filters, and the other types are commercial filter units. Differences among the curves are primarily due to slight variations in construction of the filter pack. The flow resistances of a number of identical filters, which had been preloaded with PSL to 1 kPa at a flow rate of 1700 m³/h, are shown in Fig. 5. Steeper and more linear flow-resistance curves are seen to be characteristic of the preloaded filters, in comparison to the clean filters.

The influence of the number of folds in the medium can be recognized by comparison of the two resistance curves drawn with solid lines in Fig. 6 for filters of 64 and 95 folds, respectively. Flow resistance was found to increase with the number of folds, for air velocities above approx. 15 m/s and for the range in the number of folds, 50-95, investigated. The dotted lines of Fig. 6 show the contribution of the flow resistance in the pack, i.e., in the channels formed between the pleats of medium and the adjacent separators, to the total flow resistance of the filter. The test data for these curves was obtained by testing each filter a second time after the ends of the folds had been removed.

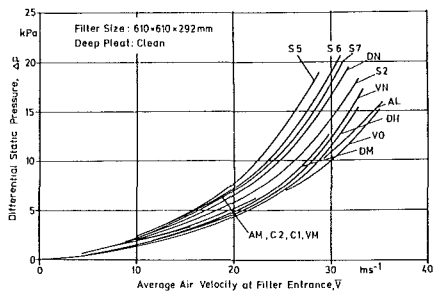


Fig. 4: Flow-Resistance Curves for Clean Deep-Pleat HEPA Filters.

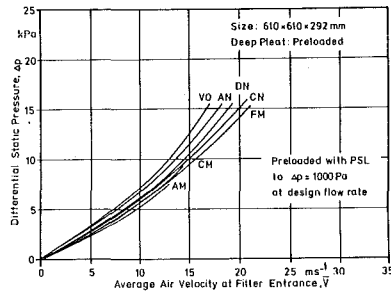


Fig. 5: Flow-Resistance Curves for Preloaded Deep-Pleat HEPA Filters.

In Fig. 7 are shown the flow resistance curves for several types of clean mini-pleat filters, and one separatorless filter, "FS", all of which are characterized by steep increases in resistance for air velocities between 10 and 20 m/s. This is undesirable from the standpoint of low mechanical stresses in the filter medium at high air velocities. An improvement in flow resistance for the structurally reinforced "DSV" filter, compared to the standard "DV" filter, is also evident. Ruedinger has shown curves for mini-pleat filters with higher resistances due to a preload of PSL /10/.

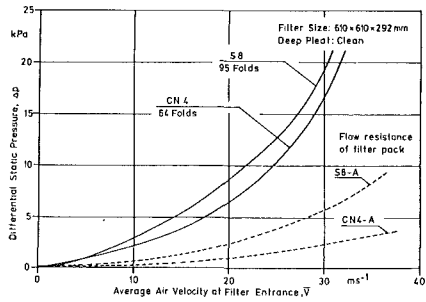


Fig. 6: Curves Showing Influence of Folds and Pack on Flow Resistance.

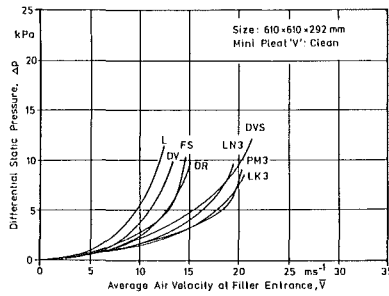


Fig. 7: Flow-Resistance Curves for Mini-Pleat Clean HEPA Filters.

The test results for the flow-resistance curves illustrated here can also be used to determine differential pressure as a function of the average air velocity at the filter entrance. It is these functions that are required by computer codes used to numerically simulate fluid-dynamic accident-induced transients within air-cleaning systems. The flow resistance of deep-pleat 610x610x292-mm commercial HEPA filters with separators can be modeled by

$$\Delta P = 0.079\bar{V} + 0.012\bar{V}^2 \tag{1}$$

for clean filters and

$$\Delta P = 0.370\bar{V} + 0.021\bar{V}^2 \tag{2}$$

for filters loaded to 1 kPa at a flow rate of 1700 m³/h, where: ΔP is in kPa, \bar{V} is < 35 m/s, and φ is < 70 % relative humidity.

A summary, of the over 80 flow-resistance tests performed, shows that based on the criterion of minimum mechanical stresses at high flow rates, the filter design with the least desirable flow-resistance characteristics is that with mini pleats. From the same standpoint, the most desirable design is that with deep pleats and separators. The flow resistances for filters of the latter design vary with both manufacturer and number of folds in the medium. At average filter-entrance air velocities of 20-35 m/s, the optimum number of folds for minimum flow resistance for clean filters is between 50 and 60.

CONCLUSIONS

Test results indicate that new commercial HEPA filters of current designs are probably not structurally suitable for all possible conditions of operation during accident situations. The structural limits of HEPA filters during superimposed challenges of high differential pressure, high flow rate, high relative humidity, and high temperature remain untested. Also unknown are the effects of filter aging as a factor in filter response to these challenges. Additional investigations into the behavior of both new and used filter units, during exposure to some individual and particularly to combined challenges, are needed.

Further improvements in filter structural strength, in addition to those already demonstrated, are considered necessary and possible. Some improvement in the flow-resistance characteristics of deep-pleat filters at air velocities above 20 m/s is considered feasible.

ACKNOWLEDGMENTS

The authors wish to express their appreciation to Dr. W.S. Gregory of Los Alamos National Laboratory for having made possible the use of the LANL test facility and to Dr. P.R. Smith of New Mexico State University for his support during the test programs.

REFERENCES

- /1/ Peters, A.H.; "Application of Moisture Separators and Particulate Filters in Reactor Containment," USAEC DP-812, Savannah River Laboratory 1962.
- /2/ Stratmann, J.; "Bericht eines Grossverbrauchers von Schwebstofffiltern Klasse S," Proc. Seminar on High Efficiency Aerosol Filtration, Comm. European Community, Luxembourg (1977) p. 411 ff.
- /3/ Horak, H.L. et al.; "Structural Performance of HEPA Filters Under Simulated Tornado Conditions," NUREG/CR-2565, LA-9197-MS, Los Alamos National Laboratory (LANL) 1982.
- /4/ Gregory, W.S and Smith, P.R.; "Response of Standard and High-Capacity HEPA Filters to Simulated Tornado and Explosive Transients", LA-9210-M, LANL 1982.
- /5/ Cuccuru, A. et. al. "Effects of Shock Waves on High-Efficiency Filter Units," CONF-820833 (1983) p. 1093 ff.

- /6/ Alvares, N.J., Beason, D.G., and Ford, H.W.; "In-Duct Countermeasures for Reducing Fire-Generated-Smoke-Aerosol Exposure to HEPA Filters," CONF-780819 (1979) p. 653 ff.
- /7/ Fenton, D.L. et al.; "The LANL/NMSU Filter Plugging Test Facility," LA-9929-MS, LANL 1983.
- /8/ Hackney, S.; "Fire Testing of HEPA Filters Installed in Filter Housings," CONF-820833 (1983) p.1030 ff.
- /9/ Pratt, R.P. and Green, B.L.; "Performance Testing of HEPA Filters Under Hot Dynamic Conditions," Proc. of the 18th DOE Nuclear Airborne Waste Management and Air Cleaning Conference (to be published 1985).
- /10/ Ruedinger, V. and Wilhelm, J.G., "HEPA-Filter Response to High Air Flow Velocities," CONF-820833 (1983) p. 1069 ff.
- /11/ Martin, R.A. et al.; "Material Transport Analysis for Accident-Induced Flow in Nuclear Facilities", NUREG/CR-3527, LA-9913-MS, LANL 1983.
- /12/ Hartig, S.H. et al.; "Comparison and Verification of Two Computer Programs Used to Analyze Ventilation Systems Under Accident Conditions," Proc. of the 18th DOE NAWM and AC Conf. (to be published 1985).
- /13/ Gregory, W.S., et al.; "Investigations of HEPA Filters Subjected to Tornado Pressure Pulses: Initial Structural Testing," LA-7202-MS, LANL 1978.
- /14/ Ruedinger, V., Ricketts, C.I., and Wilhelm, J.G.; "Limits of HEPA-Filter Application Under High-Humidity Conditions," Proc. of the 18th DOE NAWM and AC Conf. (to be published 1985).
- /15/ Vidosic, J.P.; "Mechanics of Materials" in "Standard Handbook for Mechanical Engineers," 7th ed.; Edited by T. Baumeister, McGraw-Hill, New York (1967) pp. 5-68 to 5-70.
- /16/ Dillmann, H.-G.; "Ergebnisbericht über Forschungs- und Entwicklungsarbeiten 1981 des Laboratoriums für Aerosolphysik und Filtertechnik," KfK 3294 Kernforschungszentrum Karlsruhe 1982 p. 12.
- /17/ Alken, W. et al.; "Development of a HEPA Filter with High Structural Strength and High Resistance to the Effects of Humidity and Acid," Proc. Of the 18th DOE NAWM and AC Conf. (to be published 1985).
- /18/ Ruedinger, V. et al.; "BORA - A Facility for Experimental Investigation of Air Cleaning During Accident Situations," Proc. of the 18th DOE NAWM and AC Conf. (to be published 1985).

TELLURIUM BEHAVIOR DURING AND AFTER THE TMI-2 ACCIDENT

K. Vinjamuri, D. J. Osetek, R. R. Hobbins

EG&G Idaho, Inc.
P.O. Box 1625
Idaho Falls, ID 83415

ABSTRACT

The estimated behavior of tellurium during and after the accident at the Three Mile Island Unit-2 is presented. The behavior is based on all available measurement data for ^{129m}Te , ^{132}Te , Stable tellurium (^{126}Te , ^{128}Te and ^{130}Te), and best estimate calculations of tellurium release and transport. The predicted release was calculated using current techniques that relate release rate to fuel temperature and holdup of tellurium in zircaloy until significant oxidation occurs. The calculated release fraction was low, approximately 7%, but the total measured release for samples analyzed to date is about 4.0%. Of the measured tellurium about 2.4, 0.88, 0.42, 0.17 and 0.086% of core inventory were in the containment sump water, containment solids in water, makeup and purification demineralizer, containment inside surface, and the reactor primary coolant, respectively. A significant fraction (54%) of the calculated tellurium retained on the upper plenum surfaces (4.61% of the core inventory) was deposited during the high pressure injection of coolant at about 200 minutes after the reactor scram. Comparison of tellurium behavior with in-pile and out-of-pile tests strongly suggests that zircaloy holds tellurium until significant cladding oxidation occurs. Analyses of samples from the core region of TMI-2 may provide an assessment of the large fraction of tellurium retained there, thus validating the zircaloy-oxidation-dependent tellurium release models.

INTRODUCTION

Until recently, studies of tellurium release from the core were based on temperature, and its volatility in comparison with other potentially important radionuclides (I, and Cs)[1]. However, tests at the core melt facility at Oak Ridge National Laboratory (ORNL), the severe fuel damage tests at the Idaho National Engineering Laboratory (INEL), and the SASCHA tests at Karlsruhe, suggest that tellurium may be held up by zircaloy cladding which results in significantly lower releases from the core. These tests also demonstrated that tellurium releases increase significantly when the zircaloy cladding is oxidized and the previously held up tellurium is released. Lorenz et al.,[2] emphasized that a lower-than-expected tellurium release does not necessarily mean a lower calculated release to the environment, but rather that the tellurium transport pathway is different from previously envisioned and higher or lower releases to the environment may result, depending on zircaloy oxidation during an accident progression. The study of tellurium behavior during and after the Three Mile Island-Unit 2 accident may shed further light on tellurium transport during a severe accident.

The objectives of this paper are to: present the results of tellurium analyses performed to date on TMI-2 samples; estimate the tellurium distribution, release and retention factors; and compare the data with current best estimate behavior models and data from out-of-reactor and in-reactor tests.

MEASUREMENT OF TELLURIUM RELEASED FROM TMI-2 CORE

A summary of tellurium measured in all samples taken from the TMI-2 plant systems and components is listed in Table I. The systems and components included in the tellurium investigation were: (a) reactor primary coolant,[3,4] (b) reactor coolant bleed tank water[5] (c) containment inside surface,[4,6] (d) containment sump water and solid debris,[7-10] (e) containment atmosphere,[11] (f) auxiliary building sump water[12] (g) makeup and purification filter,[13,14] (h) upper plenum surfaces[15] (samples from the H8 and B8 leadscrews), and (i) core debris (grab samples). The largest tellurium releases measured in the above plant systems and components were summed to give a total fractional release of about 4% of the core inventory.

TABLE I. SUMMARY OF TELLURIUM RELEASE FRACTIONS IN TMI-2 SYSTEMS

System or Component	Sampling Date	Tellurium Isotope	Percent of Initial Core Inventory ^a	Reference	
1. Reactor primary coolant	3-29-79	¹³² Te	0.086	[3]	
	3-30-79	¹³² Te	0.086	[3]	
	4-10-79	¹³² Te	0.010	[3]	
	6-21-79	¹³² Te	0.014	[4]	
2. Reactor coolant bleed tank water	12-18-79	¹²⁹ Te	0.009	[5]	
3. Containment inside surface	8-29-79	^{127m} Te	0.045	[6]	
	8-29-79	^{129m} Te	0.12	[4]	
	9-09-79	^{129m} Te	0.17	[6]	
4. Containment sump water	6-20-79	¹²⁹ Te	1.06	[7]	
	6-20-79	¹³² Te	2.40	[7]	
	8-29-79	^{129m} Te	0.008	[8]	
	Solids in water	8-28-79	^{129m} Te	0.47	[8]
				0.88	[9]
Sludge ^b	10-26-82	¹³⁰ Te	765 ppm	[10]	
		¹²⁸ Te	108 ppm	[10]	
		¹²⁶ Te	27 ppm	[10]	
		^{129m} Te	4.0 x 10 ⁻⁷	[11]	
5. Containment atmosphere	5-1-80	^{129m} Te	4.0 x 10 ⁻⁷	[11]	
6. Auxiliary building sump tank water sample	3-25-80	^{127m} Te	1.3 x 10 ⁻⁴	[12]	
		^{129m} Te	1.5 x 10 ⁻³	[12]	
7. Makeup and purification demineralizer	May 1983	Stable Te	4.2 x 10 ⁻¹	[13,14]	
	May 1983	Stable Te	3.1 x 10 ⁻¹	[13,14]	
8. Upper plenum surface (Leadscrew data)	c	Stable Te	c	[15]	
9. Core debris	d	Stable Te	d		

a. Core inventory calculated by ORIGEN-2 code [16].

b. Not analyzed.

c. Analysis is underway and will be discussed in the EG&G report [Reference 15].

d. Analysis is underway and will be reported in 1985.

Control rod mechanism leadscrew samples from the H8 and B8 positions are being analyzed by induction coupled plasma technique for elemental tellurium, at INEL.[15] The radioactive tellurium nuclides except ^{125m}Te , are expected to have been decayed to negligibly small amounts and the measured tellurium would be the stable tellurium nuclides (^{126}Te , ^{128}Te and ^{130}Te) from fission products and the doped tellurium added to stainless steels as a free-machining agent. The precise quantity of doped tellurium is generally proprietary information, however, tellurium weight percentages of 0.0005- 0.1 % are typical. Analyses of grab samples from the core are underway, but these data are not available for this paper.

CALCULATION OF TELLURIUM RELEASE FROM TMI-2 CORE

The details of the TMI-2 accident sequence have been discussed in several reports.[17-21] Some of the key events[9] in the accident sequence for the time period 100 to 213 minutes are shown in Table II. The critical period of the accident sequence from the point of view of core damage and fission product release is believed to be between 113 and 208 minutes after the reactor trip.[9] The 113-minute time corresponds to the beginning of core uncovering following phase separation in the reactor coolant when the reactor coolant pumps were turned off at about 100 minutes. The 208-minute time corresponds to the core refill following the resumption of sustained high pressure injection at about 200-minutes.

For the purpose of estimating the tellurium release fraction from the core, the TMIBOIL temperature data[9] were used in the fractional release rate calculations using the Lorenz model[2].

The SCDAP computer code[22] was used to calculate the extent of zircaloy cladding oxidation. The core was divided into seven axial and three radial nodes. The radial nodes are denoted by cold (C), Average (A)

TABLE II. SUMMARY OF PERTINENT EVENTS IN THE TMI-2 ACCIDENT SEQUENCE

Time, Minutes	Event
100	Last Reactor Coolant (RC) pumps turned off in Loop A.
113	Beginning of core uncovering.
139	Pilot Operated Release Valve (PORV) closed.
145	Iodine in the reactor building air sample (HP-P-227) began to increase rapidly.
150	A radiation detector (in core instrument panel area monitor) showed response indicating release of activity to the primary system.
174	RC pump 2B was started and run until 193 minutes.
192	The PORV block valve was opened and cycled several times in the next period.
200	Sustained High Pressure Injection (HPI) and core reflooded.
208	Core refill.

and Hot (H) regions, and the axial nodes were numbered from 1 through 7. As shown in Figure 1 the cladding in nodes H6 and A6 were oxidized to >90%. The rest of the cladding in the core was oxidized to <90%. The estimated fractional releases from nodes H6 and A6, and from the rest of the core were 4.36, 1.14 and 1.46%, respectively. These estimates were made based on Lorenz's model, and weighting the core inventory according to the axial flux distribution. The total release fraction is therefore approximately 7%.

This low estimated tellurium release fraction is in reasonable agreement with the low measured tellurium release fraction and suggests that most of the tellurium was retained within the core, probably in the zircaloy cladding.

TRAP-MELT Calculations

Preliminary calculations of tellurium transport and deposition during the TMI-2 accident were made using the TRAP-MELT computer code[23]. Input parameters were obtained from various TMI-2 reports published[9, 19, 21, 24] during the last five years. The primary coolant system was divided into eight control volumes as shown in Figure 2. The control volume geometries were obtained either from the final safety analysis report (FSAR)[25] or estimated. These parameters include length, hydraulic diameter, flow area, settling area and height. Thirteen 5 minute time intervals starting from 153 minutes and ending with 213 minutes were used. Steam temperatures and steam flow rates reported in [Reference 21] were used and system pressures were obtained from the measurements charts reported in [Reference 24]. The tellurium source term (0.07) estimated in the previous section was used.

The fraction of the core inventory deposited on lower plenum, core, upper plenum upper head, hotleg, pressurizer, steam generator and cold leg surfaces are, 1.60×10^{-4} , 0.0, 4.61, 1.46, 0.69, 0.087, 0.084, and 0.0026%, respectively. The fraction of the core inventory of tellurium deposited on upper plenum surfaces versus time is shown in Figure 3. Out of a total deposition of 4.6% on upper plenum surfaces, about 2.5% was deposited after the event at 200 minutes, when the core was reflooded (see Table II for accident sequence). A large steam flow rate[21] at reflood transported much tellurium from the core and deposited on the upper plenum surfaces.

COMPARISON OF TMI-2 TELLURIUM BEHAVIOR WITH INPILE AND OUT-OF-PILE TESTS

In this section, the fractional release rates and release fractions estimated and measured during the TMI-2 accident are compared with measurements from the two PBF Severe Fuel Damage Tests[26, 27], and the ORNL[2] and SASCHA[29-31] out-of-pile tests. The modified tellurium release model of Lorenz et al[2], was used to estimate the fractional release rates for TMI-2 in the temperature range of 1300 to 2550 K for two regions in the core: 3.05 to 3.66m (10 to 12 feet) and 2.44m to 3.05m (8 to 10 feet) from the bottom of the core, where the cladding oxidation was ≥ 90 and < 90 %, respectively. The fractional release rates versus temperature are shown in Figure 4 and compared with the data from the PBF Tests (SFD-ST and SFD 1-1), ORNL Tests (HI-1, HI-2, and HI-3) and the SASCHA Tests. The PBF SFD-ST result at 2400 K, the ORNL Test HI-2 and the SASCHA Tests lie above the lower line. The SFD-ST results at 2000 K, the SFD 1-1 and the ORNL Tests HI-1 and HI-3 show low tellurium release because of low cladding oxidation.

The release fractions measured and estimated from TMI-2 are compared with the inpile and out-of-pile tests in Table III. The calculated and measured tellurium release fractions for TMI-2 are low. The measured tellurium fraction in the TMI-2 accident simulation test (SFD 1-1) in the PBF is lower. The PBF

C7	A7	H7	A7	C7
C6	A6	H6	A6	C6
C5	A5	H5	A5	C5
C4	A4	H4	A4	C4
C3	A3	H3	A3	C3
C2	A2	H2	A2	C2
C1	A1	H1	A1	C1

 Cladding oxidized to >90%
 Cladding oxidized to <90%

P36 KXV-884-09

Figure 1. Extent of TMI-2 cladding oxidation.

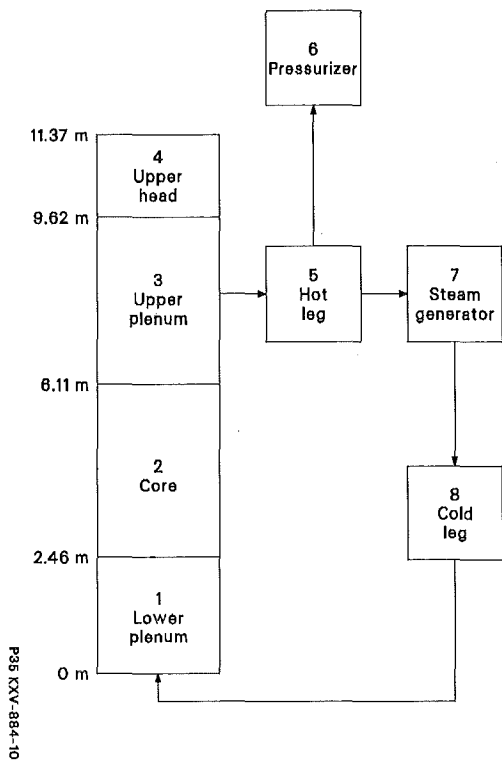


Figure 2. TMI-2 control volumes for TRAP-MELT calculations.

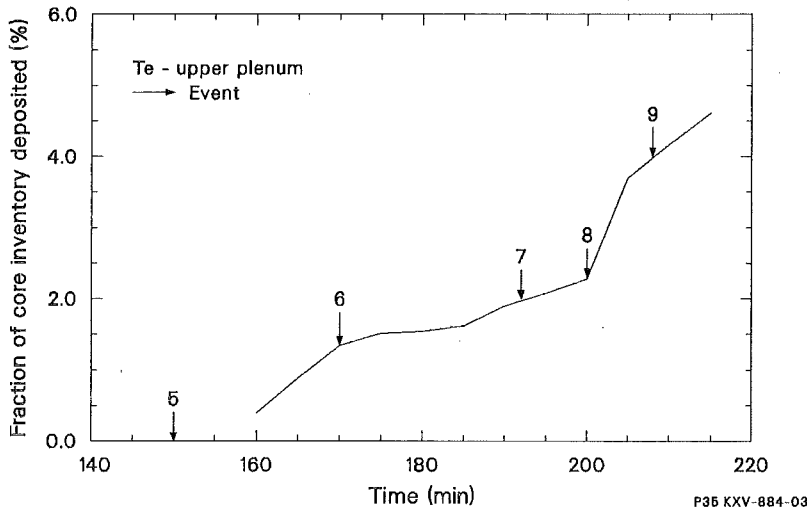


Figure 3. TRAP-MELT calculated tellurium retention on TMI-2 upper plenum surfaces.

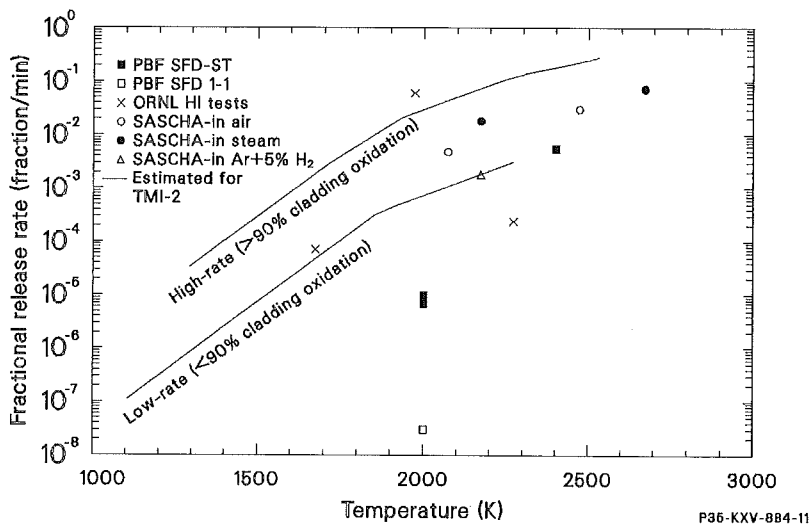


Figure 4. Comparison of fractional release rates.

TABLE III. COMPARISON OF TMI-2 Te RELEASE FRACTIONS WITH INPILE AND OUT-OF-PILE TESTS

Event	Maximum Fuel Temperature (K)	Cladding Oxidation (%)	Release Fraction	Reference
TMI-2 Accident	2600	Low	4.0×10^{-2} (measured) 7.0×10^{-2} (estimated)	Present Study
<u>PBF Tests</u>				
SFD-ST	2400	100	4.0×10^{-1}	
SFD 1-1	2400	30	1.1×10^{-2}	
<u>ORNL Tests</u>				
HI-1	1673	40	3.0×10^{-3}	[2]
HI-2	1973	100	0.5 to 1.0	
HI-3	2273	35	6.0×10^{-3}	
<u>SASCHA Tests</u>				
Low Steam Flow (1.5 L/m)	2573	Low	3.3×10^{-1}	[2]
High Steam Flow (30 L/m)	2733	High	6.5×10^{-1}	
Ar + 5% H ₂	2173	0	3.6×10^{-2}	
Ar + 5% Steam	2200	Low	2.0×10^{-1}	

SFD 1-1 test closely approximated the thermal hydraulic conditions of the TMI-2 accident, and the results of this test indicate very small tellurium release ($\sim 1.1\%$), which is attributed to the holdup of tellurium by unoxidized zircaloy in the test bundle. Also the low tellurium release is consistent with ORNL tests, where the cladding oxidation was low and tellurium was tied up with the zircaloy cladding. The tellurium release in SASCHA test (Ar + 5% H₂) is in good agreement with TMI-2. Also in SASCHA tests, the tellurium release was higher in a test where the steam flow is high. Analyses of samples from the core region may provide an assessment of the large fraction of tellurium retained in the core, thus validating the zircaloy-oxidation dependent tellurium release models.

CONCLUSIONS

A number of available TMI-2 samples were analyzed, best estimate calculations were performed, and the data were compared with results from inpile and out-of-pile tests. The following conclusions are drawn from the analysis:

1. Very little ($\sim 4.0\%$) tellurium was released and transported from the TMI-2 core, probably as a result of holdup by zircaloy cladding and structural materials. Analyses of samples from the core region may provide an assessment of the large fraction of tellurium retained there.
2. Best estimate calculations suggest that a significant fraction of the total tellurium deposited on the upper plenum surfaces was due to high pressure injection at about 200 minutes after the reactor scram, resulting in high steam flow.

3. Comparison of tellurium release fractions and fractional release rates from the TMI-2 accident with in-pile and out-of-pile test results suggests that zircaloy holds tellurium until the cladding is oxidized significantly.

ACKNOWLEDGMENTS

The authors thank Mrs. Pushpa Bhatiya for running the TRAP-MELT computer code and G. S. Reilly for plotting the figures. The authors acknowledge D. O. Campbell and R. A. Lorenz of ORNL for providing TMI-2 data.

REFERENCES

1. Technical Bases for Estimating Fission Product Behavior During LWR Accidents, NUREG--0772, June 1981.
2. R. A. Lorenz et al., "Review of Tellurium Release Rates from LWR Fuel Elements Under Accident Conditions," Proceedings of the International Meeting on Light Water Reactor Severe Accident Evaluation, Cambridge, Massachusetts, August 18 to September 1, 1983.
3. C. A. Pelletier et al., Iodine 131 Behavior During the TMI-2 Accident, NSAC-30, September 1981.
4. R. A. Lorenz et al., "Review of Tellurium Release Rates from LWR Fuel Elements and Aerosol Formation from Silver Control Rod Materials," An informal letter to M. Jankowski, ORNL, Chemical Technology Division, Oak Ridge, Tennessee, 37830, February 28, 1983.
5. Letter from J. E. Emery to J. A. Carter, Interoffice Correspondence, Oak Ridge National Laboratory, Oak Ridge, Tennessee, 37830, March 28, 1980.
6. R. J. Davis, Information on Reactor Building Surface Contamination, NUS-IM-352, September 1983.
7. M. P. Morrell, "The Three Mile Island Unit 2 (TMI-2) containment assessment task force program," ANS thermal reactor safety meeting, Knoxville, Tennessee, April 1980, conference No. 800403/volume II, P. 1140.
8. Letter from W. D. Shults to J. A. Daniel, Analytical Chemistry Division, Oak Ridge National Laboratory, Oak Ridge, Tennessee 37830, September 4, 1979.
9. J. C. Cunnane and S. L. Nicolosi, Characterization of the Contamination in the TMI-2 Reactor Coolant System, EPRI NP-2722 November 1982.
10. Letter from J. A. Carter to D. O. Campbell, interlaboratory correspondence, Oak Ridge National Laboratory, Oak Ridge, Tennessee 37830, October 27, 1982.
11. J. K. Hartwell et al., Characterization of the Three Mile Island Unit-2 Reactor building Atmosphere Prior to the Reactor Building Purge, GEND-005, May 1981.
12. Letter from J. E. Emery to J. A. Carter, interoffice correspondence, Oak Ridge National Laboratory, Oak Ridge, Tennessee 37830, March 3, 1980.

13. E. J. Renkey and W. W. Jenkins, Planning Study: Resin and Debris Removal System-Three Mile Island Nuclear Station Unit 2 Makeup and Purification Demineralizers, Hanford Engineering Development Laboratory, HEDL-7377, June 1983.
14. J. D. Thomson and T. R. Osterhoudt, TMI-2 Purification Demineralizer Resin Study, GEND-INF-013, May 1984.
15. K. Vinjamuri, D. W. Akers and R. R. Hobbins, Examination of H8 and B8 Leadscrews from TMI-2, EG&G informal report, September 1984.
16. M. J. Bell, ORIGEN, ORNL Isotope Generation and Depletion Code, ORNL-4628, 1973.
17. M. Rogovin, Three Mile Island-A Report to the Commissioners and to the Public, NUREG/CR-1250.
18. G.P.U. Technical Data Report 044, Annotated Sequence of Events, March 28, 1979.
19. J. R. Ireland, et al., "Thermal-Hydraulic and Core-Damage Analysis of the TMI-2 Accident", Nuclear Safety, Vol. 22, 5, September-October, 1981.
20. J. Rest and C. R. Johnson, A Prediction of TMI-2 Core Temperatures from the Fission Product Release History, NASC-12, November, 1980.
21. K. H. Ardron and D. G. Cain, TMI-2 Accident: Core Heatup Analysis, EPRI-NSAC-24, January, 1981.
22. C. M. Allison et al., SCDAP/MOD1 Analysis of the progression of core damage during the TMI-2 Accident, EG&G report No. SE-CMD-009, June 19, 1984.
23. H. Jordan et al., TRAP-MELT Users Manual, NUREG/CR-0632, February 1979.
24. Analysis of Three Mile Island-Unit 2 Accident, NSAC-80-1, March 1980.
25. Three Mile Island Nuclear Station, Unit 2 License Application, FSAR, Metropolitan Co., 1974.
26. P. E. MacDonald, B. J. Busher, R. R. Hobbins, R. K. McCardell, and G. E. Gruen, "PBF Severe Fuel Damage Program: Results and Comparison to Analysis," International Meeting on Light-Water Reactor Severe Accident Evaluation, Cambridge, MA, August 28-September 1, 1983.
27. P. E. MacDonald, C. L. Nalezny, R. K. McCardell, "Severe Fuel Damage Test 1-1 Results," American Nuclear Society Annual Meeting Vol. 46, P478, New Orleans, Louisiana, June 3-8, 1984.
28. K. Vinjamuri, D. J. Osetek and R. R. Hobbins, "Fission Product Release Rates Measured During the in-pile Fuel Damage Tests," American Nuclear Society Annual meeting, New Orleans, Louisiana, June 3-8, 1984, Vol. 46, P. 480.
29. H. Albrecht and H. Wild, "Investigation of fission Product Release by Annealing and Melting of LWR Fuel Pins in Air and Steam," ANS Topical Meeting, Sun Valley, Idaho, August 2-6, 1981.

30. H. Albrecht and H. Wild, "Behavior of I, Cs, Te, Ba, Ag, In and Cd During Release from overheated PWR Cores," International Meeting on Light Water Reactor Severe Accident Evaluation, Cambridge, MA, August 28-September 1, 1983.
31. H. Albrecht and H. Wild, "Review of the main Results of the SASCHA Program on Fission Product Release under Core Melting Conditions," ANS topical Meeting on Fission Product Behavior and source Term Research, Snowbird, UT, July 15-19, 1984.

NOTICE

This paper was prepared as an account of work sponsored by an agency of the United States Government. Neither the United States Government nor any agency thereof, or any of their employees, makes any warranty, expressed or implied, or assumes any legal liability or responsibility for any third party's use, or the results of such use, of any information, apparatus, product or process disclosed in this report, or represents that its use by such third party would not infringe privately owned rights. The views expressed in this paper are not necessarily state or reflect those of the United States government or any agency thereof.

A CONTAINMENT-VENTING FILTER CONCEPT AND ITS IMPLEMENTATION

AT STAINLESS-STEEL FIBER FILTERS

H.-G. Dillmann, H. Pasler
 Laboratorium für Aerosolphysik und Filtertechnik
 Kernforschungszentrum Karlsruhe GmbH
 Postfach 3640, D-7500 Karlsruhe 1
 Federal Republic of Germany

ABSTRACT

Bursting of the containment of pressurized water reactors as a result of severe reactor accidents can be avoided by installation of accident filter systems which fulfill the function of a safety valve. This greatly reduces contamination of the environment by fission product release. The filter concept and its implementation using stainless-steel fiber filters and silver molecular sieves are described.

INTRODUCTION

Following severe reactor accidents a reaction between concrete and the melted core could give rise to the buildup of pressures in the reactor containment of LWRs which, depending on the development of the accident and on the types of concrete used, could lead after some days to bursting of the reactor containment /1/. This implies a near-ground release of radioactivity from the containment which, at the time of burst, would be an airborne radioactivity. The process might even be aggravated by a fraction of activity released from the boiling sump as a result of resuspension.

AN ACCIDENT FILTER CONCEPT

German PWR power plants are designed for a maximum containment pressure of 6 bar. The burst pressure is assumed to be 8-9 bar. The operating point of an accident filter system should lie in the pressure range of 6-8 bar. The volumetric flow rate of the gas resulting from the reaction of melted core and concrete is known from computations made in /1/ and amounts to about 3000-5000 m³/h. The demister (Fig. 1) of the venting system is installed within the reactor containment. In this way it is ensured that the outflowing gas stream leaves the

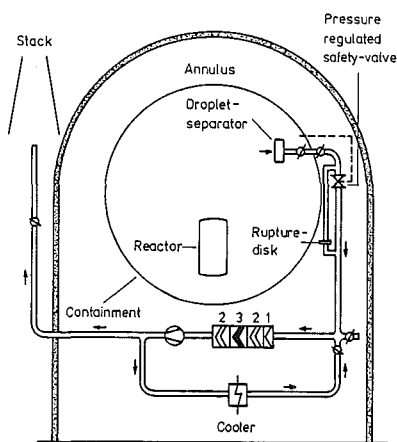


FIG. 1 1 Prefilter 2 HEPA Filter 3 Iodine Filter

CONCEPT OF AN ACCIDENT FILTER SYSTEM FOR
 CONTAINMENT VENTING AGAINST BURSTING

reactor containment with a maximum gas relative humidity of 100 % and without the presence of water droplets. Data of droplet separators are given below.

The second essential component is a pressure control valve actuated via the internal pressure; it allows only the same volume of gas to escape as is newly generated. In this way, the pressure in the reactor containment is kept at a constant value and the activity confined in the reactor containment for as long as possible. Moreover, by aerosol physical processes the fraction of airborne activity is reduced through agglomeration. Another important function of the valve is to produce an isenthalpic expansion of the containment atmosphere and thus effect a strong drying of the gas, from 160 °C and 100 % relative humidity to 145 °C with a 45 °C distance from the dew point (Fig. 2).

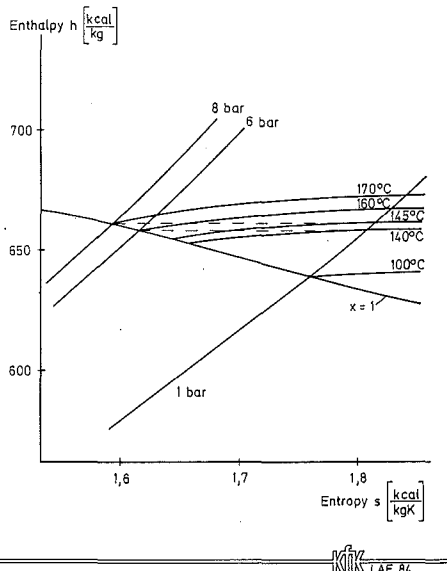


FIG. 2 DRY-EFFECT OF THE SAFETY VALVE BY ISENTHALPIC PRESSURE DECREASE

Except for the short start-up phase of about 10 s duration when only about 8 l of condensate are produced in the HEPA filter section, until the 100 °C limit (dew point 1 bar) is attained, the filter components are exposed exclusively to superheated steam. As a backup for the valve a burst diaphragm connected in parallel which does not open until a pressure of about 8 bar is attained. After the onset of an accident about 4 to 5 days will pass until the filter system is put into operation. During this time interval the filter system can be inertized with N₂, if required, in order to prevent H₂ deflagration.

The first filter stage is a pre-filter consisting of stainless-steel fibers and made up of several layers of different fiber diameters for removal of the majority of the coarse aerosols. The measured values will be indicated below. The second stage consists of 2 µm stainless-steel

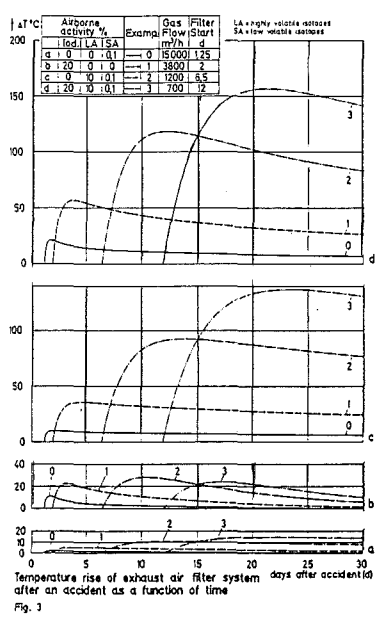


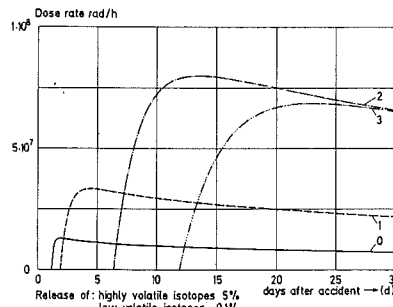
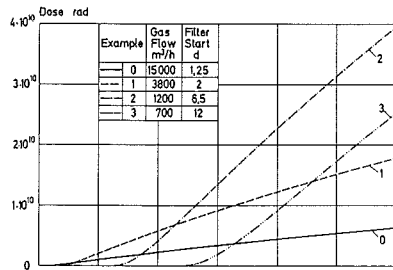
Fig. 3

fibers comparable with HEPA glass-fiber media. At this stage, the very fine aerosols of less than 1 μm diameter are removed. The temperature and radiation burden of the HEPA filter are given in Fig. 3 and 4.

It is possible to connect another HEPA filter downstream of the iodine filter in order to remove any contaminated abrasion material from the iodine filter stage. The offgas is subsequently carried via a fan and a flame arrester (on account of the H_2 fraction) to the stack.

In addition, a device will be provided which allows filtration of the air in the annulus, in the case that the latter is contaminated by air leaking from the reactor containment into the annulus.

A bypass of the filter system will be provided to be used during the period after the pressure buildup has come to an end, the pressure in the containment has dropped to values < 6 bar, and the exventing filter system is no longer required for the reactor containment. This bypass allows the removal of the decay heat of the plated-out fission products without releasing any more vent air to the outside. And in fact, failure of this bypass cooling would not pose problems since no organic adhesives and sealants are used for the filter components and temperatures up to 500 $^\circ\text{C}$ can be accommodated. At these temperatures, cooling by heat radiation alone should be sufficient.



Dose and Dose rate of the HEPA filter after an accident as a function of time
Fig. 4

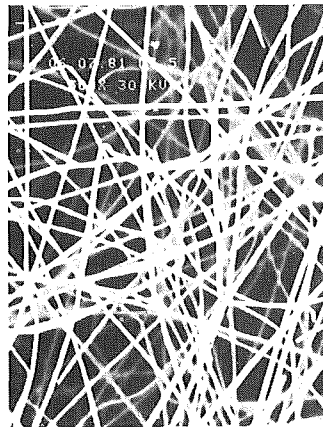


Fig. 6

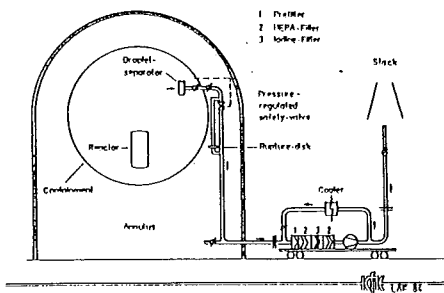


Fig. 3 TRANSPORTABLE FILTER SYSTEM (CONCEPT)

Another solution consists of a mobile filter system as represented in Fig. 5 because about 4 days will pass until the filter systems would be put into operation. Only installation of the demister, control valve, internal pipework, and appropriate connections will be required. The largest weight to be handled in a mobile system will undoubtedly be the required radiation shield, but that could be built up by using bricks of concrete at the site.

FIBER MATERIALS

Both the prefilters and the HEPA filter stages use stainless steel fibers, which are temperature resistant up to 550 °C and resistant to some acids. Their radiation resistance is practically unlimited. The metal fibers come in the following diameters: 22, 12, 8, 4, and 2 μm. For filters with removal efficiencies corresponding to those of HEPA filters, only fibers of 2 μm, respectively, can be employed to ensure a minimum depth of the fiber pack. The usual fiber material used is No. 1.4404 stainless steel (AISI TP 316L), but also such materials as inconel 601, titanium and nickel are being applied although they have not yet been made available in all diameters. The fibers can be supplied in flats, coils, unsintered and sintered or as yarns and fabrics. At present, only unsintered fleeces produced in coils are being used. Sintering reduces the porosity. Although the product is easier to process, it has a lower storage capacity because of the lower porosity.

Stainless steel fibers can be used up to some 550 °C; they additionally offer flame protection, e. g. in fires, and are resistant to moisture and acid according to specifications. Fig. 6 shows a scanning electron micrograph of the fiber structure.

TEST EQUIPMENT AND TEST METHODS

Two test rigs are available for studies of aerosol filters. Test rig No. 1, which is called "TAIFUN", has been presented at the 12th USAEC Air Cleaning Conference. /2/ It allows all main accident parameters to be set. The second test duct is designed for normal conditions, and loading tests.

The removal efficiencies of metal fiber filters were determined by the uranine method, with which readers are assumed to be familiar /3/. Fig. 7 shows an aerosol spectrum typical of the tests conducted. According to Dorman /4/, the uranine method results in a penetration which is approx. a factor of 5 higher than that for DOP, which means that the measured values should be regarded as conservative compared with DOP.

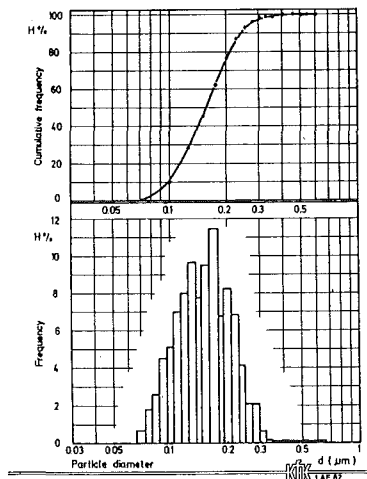


Fig. 7 URANINE PARTICLE SPECTRUM

THE HEPA FILTER STAGE

Six layers of 750 g/m^2 with $2 \mu\text{m}$ fibers allowed DF values up to $> 10^7$ to be measured at face velocities of 40 cm/s (Fig. 8, curve 1). Since the data measured with clean air were only slightly above the limit of detection within the period of exposure, the filter pack was cut in half for some further studies. This filter, which was covered with three layers of 750 g/m^2 each, produced the bottom curve in Fig. (8). This can be explained by a selective change in the aerosol spectrum on the way through such a fiber pack filter.

In two test series the influence of temperature on the DF was studied. In the range up to 200°C , the DF was found to increase with rising temperature. The face velocity was set at 30 and 40 cm/s . The results are shown in Fig. 9. The higher DF can be explained by increased diffusion-controlled removal. Moreover, the pressure dependence of the DF was studied.

Fig. 10 indicates the results. The DF decreases with rising pressure. At 5 bar , a factor of approx. 0.5 is attained. For this test series, a fiber layer of 1500 g/m^2 with $2 \mu\text{m}$ fibers was used. This drop can be explained by diffusion-controlled removal being impeded by the higher density of the air.

STUDIES WITH STEAM IN THE HEPA FILTER SECTION

Previous investigations into the HEPA filter section dealt mainly with filters exposed to air /5/. However, since in a severe accident the major fraction of the containment atmosphere consists of steam, measurements of the removal efficiency under conditions of steam exposure were performed. Superheated steam, 1 bar and 140°C , was assumed and the steam temperature was reduced in steps in order to increase the steam moisture until condensation occurred. The values have been entered in Table 1. No significant difference was observed in comparison to tests performed with air.

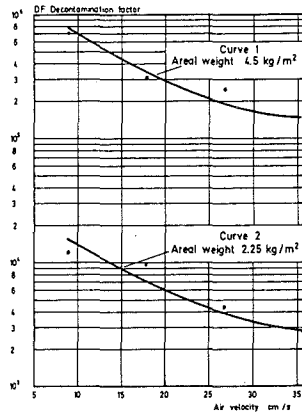


Fig. 8 DECONTAMINATION FACTOR OF $2 \mu\text{m}$ FIBERS

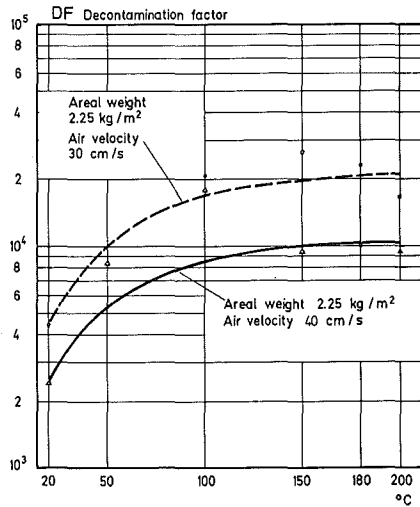


Fig. 9 DECONTAMINATION FACTOR AS A FUNCTION OF THE OPERATING TEMPERATURE OF A STAINLESS STEEL $2 \mu\text{m}$ FIBER FILTER

This demonstrates that, at least over several weeks, filtration efficiency can be maintained with the use of stainless- steel fiber filters.

Table 1

Decontamination factors of stainless-steel fiber filters exposed to steam.

Filter loading	: 1.5 kg/m ² fibers
Fiber diameter	: 2 μm
Face velocity	: 30 cm/s
Volumetric flow rate	: 350 m ³ /h
Pressure differential	: 27 mbar
Pressure	: 1 bar
Test gas	: Superheated steam
Tracer aerosol	: Uranine

Temperature (°C)	Decontamination factor	Removal Efficiency	Decontamination factor with air ⁺
140	5650	99.98	
130	4100	99.98	
130	4900	99.95	
120	2050	99.95	
120	3500	99.97	
110	1800	99.94	
110	1400	99.93	
102	1070	99.9	
102	1010	99.9	
140 ⁺		99.97	4000
100 ⁺		99.93	1400

THE PRESSURE BURST RESISTANCE

In a test series conducted at the LANL in Las Cruces, USA, two filter cartridges of the cell design (610 mm x 610 mm x 290 mm), equipped with 30 layers of 4 μm fibers of 300 g/m² each, were subjected to a pressure burst test. The test facility allows a maximum differential pressure of 0.28 bar to be applied across the test filter. This pressure was not sufficient to destroy the filter. If the rupture resistance of the fibers is sufficiently high and the design to support the fibers and the casing are made appropriately, a pressure burst resistance of 1 bar or more can be achieved.

SOME REMARKS ABOUT METAL FIBER FILTER DESIGNS

A filter to be used in accident situations can be expected to be exposed to dose rates of a few 10^1 rad/h, and to integral doses of a few 10^0 rad. For this reason, such filters should not incorporate organic sealing compounds and seals between the upstream and the downstream sides. A design similar to the deep bed adsorption filters has been developed and the cell structure abandoned for such uses. A housing design has been made in which the fiber packs are pressed only mechanically. Several elements have been built which are meant to optimize the design. Fig. 11 is a sketch of the housing and one filter insert. The face area is 2 to 2.5 m^2 , depending on the element used. As a function of the design, volume flows between approx. 1500 and $3000 \text{ m}^3/\text{h}$ can be filtered. The only gasket is installed between the filter element and the upstream side of the housing, which means that any leakage air penetrating would also be filtered.

A special advantage of fiber pack filters is due to the possibility to combine in one housing the HEPA filter section and a roughing separator. The vertical position of the fiber packs and the design of the fiber clamping system ensures that condensate and precipitated droplets will be collected on the upstream side, where they can be removed, e. g., by means of a drain pipe.

THE IODINE FILTER STAGE

For the iodine filter, the maximum temperature increases to about 160°C which is above the 100°C temperature of the influent gas. This can be controlled with iodine sorption materials (molecular sieves in the silverform) over a period of 100 h according to the test conducted. /6/

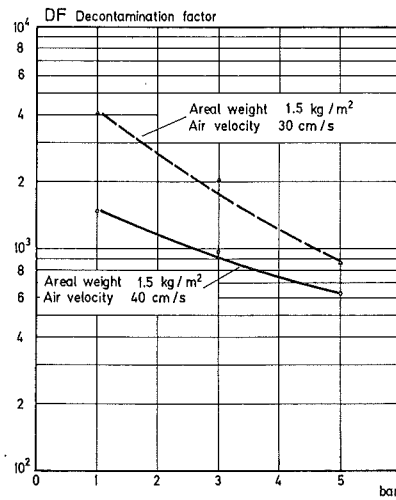


Fig. 10 DECONTAMINATION FACTOR OF $2 \mu\text{m}$ FIBER FILTERS AS A FUNCTION OF THE OPERATING PRESSURE AT 30°C

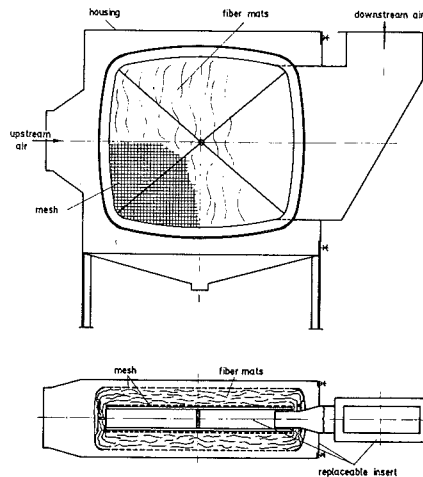


Fig. 11: DEEP-BED PARTICLE FILTER HOUSING WITH ONE TYPE OF REPLACEABLE INSERT

The calculated dose and dose rate values vary over a wide range because only relative arbitrary assumptions can be made on the geometries and activity distributions. However, the magnitudes can be indicated (Fig. 12).

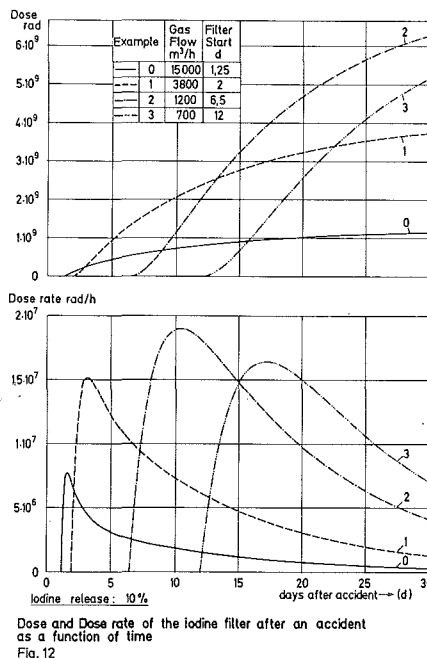
100 % of the β -radiation, and 10 % of the γ -radiation were taken into account in the calculations. The dose burdens of the iodine sorption material and of the particulate air filter are indicated.

For the iodine sorption unit a material had to be found which has a high removal efficiency for iodine over the whole range of possible conditions and is not characterized by significant desorption also at elevated temperatures and high radiation burden. The activated carbon used in normal exhaust air iodine filters is not eligible because of its easy inflammability and high desorption.

Two materials were tested; firstly, inorganic sorption materials based on catalyzer carriers with a silver nitrate impregnation and, secondly, silver molecular sieves. With both materials the reaction between iodine, iodine compounds and silver gives rise to temperature resistant iodine silver compounds having practically the same desorption behavior. One of the most important parameters influencing removal is the relative humidity.

The AC 6120 sorption material contains less silver than the molecular sieves. Already with 7 g Ag/100 g of basic material the removal efficiencies are sufficient at humidities of the air < 80 % RH. Silver zeolites do not attain this value until a silver content of about 30 g/100 g of material has been attained.

In a laboratory scale apparatus tests were performed at different humidities, temperatures and pressures with molecular sieves in the silver form from different supplies and with impregnated catalyzer carriers (designation AC 6120). The materials must attain minimum removal efficiencies both at high and low temperatures and humidities. This means that design measures have to be taken against droplet storage and reduction in the humidity of the air.



The sorption materials behave differently with respect to changes in the parameters of pressure and temperature. Up to a limit temperature of about 250 °C the AC 6120 removal efficiency increases with increasing temperature because the reaction rate rises. Above this temperature the impregnation material undergoes thermal decomposition at a relatively high rate, whilst molecular sieves are more temperature resistant because of the different bonding of the silver in the sorption material. The removal efficiency decreases with increasing pressure. But this effect is much smaller than the influence exerted by the temperature. Since the temperature and the pressure are coupled via the vapor pressure curve in a first approximation and since the (positive) influence by the temperature dominates over the influence exerted by pressure, rising pressure will normally not cause a reduction in the removal efficiency of an exventing air filter.

For the reasons stated above exhaust air filters will be operated at normal pressure outside the safety containment since throttling will lower the pressure and in addition diminish the relative humidity of the air.

The service life is an essential parameter with respect to accident filter operation. From the plots showing the development versus time of the airborne activity in the safety containment about 100 h of safe operation can be expected under conditions of elevated pressure and temperature.

Table 2 shows the removal efficiencies as a function of the temperature and time of vapor loading. Results of radiation and desorption tests are given in /6/.

TABLE 2

REMOVAL EFFICIENCY OF AN A6 MOLECULAR SIEVE FOR $\text{CH}_2^{131}\text{I}$ UNDER EXTREME CONDITIONS

FACE VELOCITY : 25 CM/S

LOADING TIME : 5 MIN.

PURGING TIME : 2 H

TEMPERATURE (°C)	DEW POINT TEMPERATURE (°C)	PRESSURE (BAR)	EXPOSURE (H)	REMOVAL EFFICIENCY (%) BED DEPTH (CM)	
				2,0	5,0
150	105	1,2	5	99,2	99,99
			96	99,9	99,99
160	151	5	5	96,0	99,77
			96	95,4	99,71
300	151	5	5	97,8	99,89
			96	83,9	97,4

DEMISTER

Above all two boundary conditions are decisive for the use of a droplet separator.

1. Great quantities of water must be expected since in an accident up to about 300 tons of water get released and when escaping a large volume of it is in the vapor phase and recondenses subsequently.

2. Over a rather long period during the condensation phase very small droplets must be expected which might lead to an inadmissible storage of water in the particulate air filters and in the iodine filter.

Moreover, a droplet separator must have the lowest possible resistance to air and must be radiation resistant.

These conditions can be fulfilled by using demisters made of stainless steel fiber separators. After optimization a configuration of droplet separators of 22 and 8 μm fibers by four layers each has proved to be suitable for use in coarse and fine droplet separators. The results have been indicated in Table 3.

TABLE 3
REMOVAL EFFICIENCY OF A DROPLET SEPARATOR CONTAINING STAINLESS STEEL FIBER PACKS

DIAMETER OF DROPLETS : 2-5 μm

LOADING RATE : ~ 3 kg/h

FIBER DIAMETER

PACK 1 : 22 μm

PACK 2 : 8 μm

AIR FLOW RATE (M^3/H)	FACE VELOCITY (M/s)	TOTAL PRESSURE DROP (PA)	REMOVAL EFFICIENCY (%)		
			PACK 1	PACK 2	PACKS 1 + 2
200	0.23	250	99.6	98.9	99.996
300	0.34	320	99.4	97.3	99.98
400	0.46	480	99.5	89.3	99.94

THE PROBLEM OF CORROSION

The stainless-steel fibers have been exposed to steam and steam-air mixtures at temperatures between 100 and 180 $^{\circ}\text{C}$ in endurance tests which lasted for several months. No corrosion whatsoever appeared on the fibers. Therefore, it can be assumed that no critical corrosion phenomena will occur during an estimated service life of 2 - 4 weeks, not even when the filters are exposed to the offgas of a reactor containment. Repeated use of such a filter system is certainly not to be anticipated.

VALUES MEASURED AT THE PREFILTERS

Prefilters have been investigated with a respect to loading capacity and removal efficiency. The tracer aerosol was a commercial fire-extinguishing powder with an aerosol size distribution between approx. 1 and 10 μm .

Given the long waiting time until the filter is put into operation the fraction of fine aerosols $< 1 \mu\text{m}$ should not make a substantial contribution to filter loading because agglomeration takes place. The values are given in Table 4.

TABLE 4
LOADING AND REMOVAL EFFICIENCY OF PREFILTERS
VOLUMETRIC FLOW RATE : 200 m^3/h , 4 400 m^3/h
EXPOSURE AREA : 0.31 m^2
TRACER AEROSOL : 1 - 10 μm

FIBER DIAMETER (μm)	FIBER LOADING (g/m^2)	INITIAL VALUE OF ΔP (HBAR)	FINAL VALUE OF ΔP (HBAR)	EFFICIENCY (%)	LOADING (g)	LOADING (kg/m^2)
30	2500	0.1	6	78	3293	10.5
22	1500	0.15	7	85	2348	7.6
12	1500	0.25	8.8	96	2288	7.3
8	1500	0.5	13.5	> 99	1080	3.5
4	1500	2.3	17.2	> 99	488	1.56
4 8	1500	1.7	24.9	90	1430	4.6
4 4	1500	5.1	31	> 99	790	2.5

Since an exventing filter with an exposure area of about 5 m^2 will be necessary for a volumetric flow rate of 3000-5000 m^3/h in order to realize a HEPA filter section with 2 μm fibers, a theoretical loading of about 50 kg can be expected. However, according to results previously obtained from other investigations such a high aerosol loading is not to be expected so that in this respect also there exists no limit in the application of the filter.

The investigations will be continued at different flow rates in order to cover possible changes in volumetric flow rates as well.

SUMMARY

By this demonstration of performance of an accident filter system it can reasonably be supposed that hypothetical accidents in LWRs can also be controlled and the environmental burden reduced by a factor of ≥ 1000 . Using this filter concept, both aerosol- and iodine activities can be contained. Only the noble gases with low radiological impact would be released. The cost of such a filter system should amount to 0.5 to 1 million dollars. This means that, compared with condensation systems, a cost-advantage factor of about 20 could be achieved./7,8,9/

REFERENCES

- /1/ M. Reimann,
The Erosion Behavior of Different Types of Concrete
Interacting with a Core Melt,
Proc. Thermal Reactor Safety, April 6-9, 1980
Knoxville, Tenn., pp. 197-204.
- /2/ J. G. Wilhelm, H.-G. Dillmann, K. Gerlach,
Testing of Iodine Filter Systems Under Normal
and Post-Accident Conditions,
CONF - 720 823, pp. 434 (1972).
- /3/ J. Dupoux,
Insitu Measurement of the Efficiency of Filtration
Installation in the Nuclear Industry, by the Soda-Fluorescein (Ura-
nin) Aerosol Method - AFNOR Standard NFC 44.011,
CONF - 801 038, pp. 17 (1980).
- /4/ R. G. Dorman,
A Comparison of the Methods Used in the Nuclear Industry
to Test High Efficiency Filters,
Commission of the European Communities,
June 1981, V/3603/81 EN.
- /5/ H.-G. Dillmann, H. Pasler,
Experimental Investigations of Aerosol Filtration with
Deep Bed Fiber Filters,
CONF - 820 833, pp. 1160 (1982).
- /6/ H.-G. Dillmann, H. Pasler,
Theoretical and Experimental Investigations into the
Filtration of the Atmosphere within the Containments of
Pressurized Water Reactors after Serious Reactor Accidents,
CONF 801 038, pp. 373 (1980).
- /7/ R.K. Owen, A.K. Postma, Hanford Engineering Laboratory
Development of a Passive, Self-Cleaning Scrubber for
Containment Venting Applications,
CONF 801 038, pp. 335 (1980).
- /8/ H.C. Walling*, A.S. Benjamin*, P. Cybulskis**,
*Sandia National Laboratories, **Battelle Columbus Lab.
CONF 801 038, pp. 353 (1980).
- /9/ C. Gräslund, K. Johansson, L. Nilsson, I. Tiren,
FILTRA, Filtered Atmospheric Venting of LWR Containments,
A Status Report, IAEA-CN-39/74, 1980-10-20-24.

Chapter 10

Code Development and Verification

	pages
10.1 T. Kervinen, H. Purhonen, H. Kalli: REWET-II Experiments to Determine the Effects of Spacer Grids on the Reflooding Process	1609 - 1617
10.2 H. Kalli, T. Kervinen, J. Rossi: Reflooding in a Tight-Pitch Rod Lattice	1618 - 1627
10.3 D.R. Glynn, D. Kirkcaldy, N. Rhodes: Prediction of Reflooding in Single Channels and Partially- Blocked Rod Bundles	1628 - 1636
10.4 M. El-Shanawany, C.G. Kinniburgh, K.T. Routledge: Comparison of Calculations Using the Best Estimate Reflood Heat Transfer Code BART-A1 with Data from the FEBA and REBEKA Facilities	1637 - 1644
10.5 J.Duco, M. Reocreux, A. Tattegrain, Ph. Berna, B. Legrand, M. Trotabas: In-Pile Investigations at the PHEBUS Facility of the Behavior of PWR-Type Fuel Bundles in Typical L.B. LOCA Transients Extended to and beyond the Limits of ECCS Criteria	1645 - 1655
10.6 H. Staedtke, W. Kolar, B. Worth: RELAP5/MOD1 Assessment with LOBI-MOD1 Test Results	1656 - 1665
10.7 J.C. Rousseau, G. Houdayer, M. Reocreux: The CATHARE Code Development	1666 - 1678
10.8 J.M. Healzer, E. Elias, A. Singh, F.J. Moody: A Model for Two-Phase Jet Expansion and Impingement	1679 - 1688
10.9 L. Szabados, I. Tóth, L. Perneczky: The PMK-NVH Experimental Facility and the Phenomena to be Investigated	1689 - 1701

- 10.10 R.J. Salm: 1702 - 1710
Post Analysis of a 10 cm² SBLOCA Test in the OTSG
Equipped GERDA Facility Using a BBR Version of
RELAP4/MOD6
- 10.11 P.C. Hall: 1711 - 1720
Post Test Calculations of Semiscale Pump Suction Small
Break LOCE, S-PL-4, Using RELAP5/MOD1.5
- 10.12 J. Miettinen: 1721 - 1730
Small Break Analyses with Computer Codes SMABRE and
RELAP5/MOD1
- 10.13 M. Andreani, P.C. Cacciabue, M. Mazzini, F. Oriolo: 1731 - 1740
The Analysis of LOFT Test L9-3 Using RELAP4/MOD6 and
ALMOD-JRC Computer Codes
- 10.14 C.L. Nalezny, T.-H. Chen: 1741 - 1749
Analysis of Recovery Procedures for a Single Steam
Generator Tube Rupture
- 10.15 G.G. Loomis: 1750 - 1759
Steam Generator Tube Rupture in an Experimental Facility
Scaled from a Pressurized Water Reactor
- 10.16 G.C. Slovik, P. Saha: 1760 - 1769
A RAMONA-3B Code Description and Nodalization Study for
the Peach Bottom-2 Turbine Trip Test 3
- 10.17 S. Borresen, L. Moberg: 1770 - 1979
Systematic Procedures for Core Neutronics Modelling in
the 3-D BWR System Transient Code RAMONA-3B
- 10.18 C.S. Lin, W.E. Kastenber: 1780 - 1790
A Quick Running Dynamic Simulation Code for BWR
Transients

- 10.19 Y. Waaranperä, H. Svensson: 1791 - 1800
A BWR Stability Prediction Model and its Qualification
Against Tests in Operating Reactors
- 10.20 K.C. Wagner, R.J. Dallman: 1801 - 1810
A Comparison of RELAP5/MOD1.6, TRAC-BD1/Version 12, and
TRAC-BD1/MOD1 Assessments with Data from a ROSA III
Small Break Test
- 10.21 M. Kato, N. Abe, H. Aoki, K. Tasaka: 1811 - 1820
ROSA-III Large Break Test Analysis by TRAC-BD1
- 10.22 G.Th. Analytis, S.N. Aksan: 1821 - 1830
TRAC-BD1 Assessment under Severe Accident Boil-off
Conditions
- 10.23 P. Saha, L. Neymotin, U.S. Rohatgi: 1831 - 1839
Analysis of Single and Parallel Tube Counter-Current
Flow Limiting Experiments with TRAC-BD1 Code
- 10.24 P.D. Wheatley, K.C. Wagner: 1840 - 1849
Posttest Data Analysis and Assessment of TRAC-BD1/MOD1
with Data from a Full Integral Simulation Test (FIST)
Power Transient Experiment
- 10.25 D.A. Schauer: 1850 - 1858
Transient Condensation Heat Transfer Coefficient
Expressions during and after Blowdown
- 10.26 E.W. McCauley, E. Aust, H. Schwan: 1859 - 1866
Multivalent Effects in a Large Scale Boiling Water Reactor
Pressure Suppression System
- 10.27 M.J. Thurgood, K. Fischer, L. Wolf: 1867 - 1875
Verification of the 3-D, 2-FLUID, 3-FIELD Containment
Code COBRA-NC with HDR- and Battelle-Frankfurt Data Sets

REWET-II EXPERIMENTS TO DETERMINE THE EFFECTS OF
SPACER GRIDS ON THE REFLOODING PROCESS

Timo Kervinen, Heikki Purhonen,

Technical Research Centre of Finland,
Nuclear Engineering Laboratory,
P.O. Box 169, SF-00181 Helsinki 18, Finland

Heikki Kalli,

Lappeenranta University of Technology,
Department of Energy Technology,
P.O. Box 20, SF-53851 Lappeenranta 85, Finland

ABSTRACT

25 reflooding experiments have been carried out in the REWET-II test facility for studying the influence of spacer grids on the reflooding process during a postulated LOCA. The test section of the REWET-II facility contains 19 indirectly electrically heated full-length fuel rod simulators in a triangular array equipped with ten honeycomb type spacer grids. The first 15 experiments have been carried out in the standard test section i.e. with all the 10 spacer grids. In the last 10 experiments two spacer grids (the 6th and the 8th) have been removed from the upper half of the rod bundle. Experimental results indicate that spacer grids improve the cooling of the fuel rod simulators. The main reason for the improved cooling is the entrained droplets adhering to the spacer grids and forming new downstream and upstream moving quenching fronts.

INTRODUCTION

The REWET-II facility has been designed to investigate the reflooding phenomena during a postulated LOCA in an LWR. The reference plant is the Loviisa VVER-440 plant in Finland. The VVER-reactors have certain unique features differing from other PWRs. Fuel rods are in hexagonal geometry, fuel rod bundles of 127 rods are in BWR-like channels. The fuel rod bundle has 10 honeycomb type spacer grids. The emergency core cooling (ECC) system consists of two separate systems having two LPCI-pumps each. The ECC water is injected directly into both the upper plenum and the downcomer of the reactor vessel.

During recent years several authors have published papers dealing with the effect of spacer grids on reflooding phenomena during a LOCA [1,2,3].

Also the earlier REWET-experiments indicated that the spacer grids may have an important effect on the reflooding phenomenon [4]. In this paper two new series of reflooding experiments are presented. The REWET-II facility and experiments are described in the second and third sections. In the two last sections the results of experiments are presented and the effects of spacer grids are discussed.

REWET-II TEST FACILITY AND TEST CONDITIONS

The layout of the REWET-II test facility is presented in Fig. 1. The scaling ratio between REWET-II facility and the reference reactor is 1:2333. In the facility all the elevations of different components are the same as in the reference reactor. The reactor core is simulated with a bundle of 19 electrically heated fuel rod simulators in the actual hexagonal fuel rod geometry (Fig. 2). Hence, the heated length (2420 mm), the outer diameter (9.1 mm) and the lattice pitch (12.2 mm) of the simulators are also the same as in the reference reactor. The power distribution of the fuel rod simulators is a chopped cosine with a peaking factor of 1.5. The number and the construction of the honeycomb type spacer grids are the same as in the actual fuel bundles. The heating coil of the fuel rod simulator is inside a stainless steel cladding tube filled with magnesium oxide. The facility contains also a pipe simulating the broken loop and a connection line between the upper plenum and downcomer simulating the 5 intact loops. The REWET-II facility has been described in detail in Ref. [5].

The parameters of interest in the experiments were the rod surface temperatures measured with thermocouples. Areas around the 6th (at the elevation of 1341 mm) and the 8th (at the elevation of 1821 mm) spacer grids were especially well-instrumented (Fig. 3.). Other parameters to be measured were system pressure, differential pressures, coolant flow rates, coolant temperature and heating power.

Before the experiment the facility was preheated by steam and the lower plenum was filled with water. A specified electrical power was then switched on and when the maximum cladding temperature had reached a specified value the test was initiated by starting the injection of the ECC water into the downcomer and/or to the upper plenum.

EXPERIMENTS

The two test series reported here included 25 reflooding experiments. In the first test series SGI (Spacer Grid Test I) 15 experiments were carried out using the standard rod bundle equipped with 10 honeycomb type spacer grids. In the second test series SGII (Spacer Grid Test II) 10 experiments were repeated using the same rod bundle with only 8 spacer grids, i.e., the 6th and 8th spacer grids were removed from the upper half of the test section.

The parameters in the experiments have been chosen in accordance with the reference plant. Hence, e.g. the coolant injection rates have been scaled down from the ECC system of the Loviisa plant. The heating power used in the experiments corresponds to about 5 % of the thermal power of the reference plant. Coolant temperature (50 °C) is the same as in the reference plant. The ranges of the parameters are shown in Table I.

Table I. Ranges of test parameters in REWET-II spacer grid experiments.

System pressure	0.1 - 0.3 MPa
Heating power of rod bundle	30-40 kW
Average linear heating power	6.5-8.7 W/cm
Total flow rate (cold level rise)	4-20 cm/s
Initial maximum cladding temperature	600 °C
Relative flow rate distribution, downcomer/upper plenum	100/0 % - 50/50 %
Coolant injection temperature	50 °C

RESULTS

Effect of Spacer Grids on Cladding Temperature and Quenching Times

In the reflooding process the most significant parameter is the cladding temperature of fuel rods. Temperature rise and quenching time are typical characteristics used to describe the cladding temperature behavior and the cooling of the rod bundle during the reflooding process.

The cladding temperatures measured in the experiments indicated that in the lower half of the test section the differences between the corresponding temperatures in the two test series SGI and SGII were insignificant (Fig. 4). In the upper part of the test section (where two spacer grids were removed in test series SGII) local temperature rise was lower and quenching earlier in test series SGI than in the corresponding experiments in test series SGII. The largest differences in quenching time and local temperature rise between corresponding experiments at the elevations of the 6th spacer grid were 50 s and 105°C and at the elevation of the 8th spacer grid 150 s and 150°C, respectively.

Maximum initial temperature, local temperature rise, turnaround time and quenching time for selected experiments are summarized in Table II. Figs. 5 - 6 show quenching times at different elevations and maximum local temperatures for two compared experiments.

Table II. Summary of reflooding characteristics in four pairs of REWET-II spacer grid experiments.

	SGI	SGII
Total flow rate: 4 cm/s ,ECC injection to downcomer,		
Average heating power: 6.5 W/cm , Pressure: 0.1 MPa		
T_{imax}	630°C	600°C
T_i	580°C	570°C
ΔT	30°C	105°C
t_t	15 s	153 s
t_q	325 s	365 s
Total flow rate: 8 cm/s ,ECC injection to downcomer and upper plenum,		
Average heating power: 6.5 W/cm , Pressure: 0.1 MPa		
T_{imax}	595°C	610°C
T_i	480°C	550°C
ΔT	0°C	105°C
t_t	0 s	242 s
t_q	305 s	361 s
Total flow rate: 20 cm/s ,ECC injection to downcomer,		
Average heating power: 6.5 W/cm , Pressure: 0.1 MPa		
T_{imax}	600°C	610°C
T_i	540°C	575°C
ΔT	0°C	0°C
t_t	0 s	0 s
t_q	78 s	83 s
Total flow rate: 4 cm/s ,ECC injection to downcomer,		
Average heating power: 8.7 W/cm , Pressure: 0.3 MPa		
T_{imax}	640°C	630°C
T_i	590°C	560°C
ΔT	35°C	133°C
t_t	12 s	78 s
t_q	170 s	174 s

T_{imax} = maximum initial temperature at elevation 1195 mm (midplane)
 T_i = initial temperature at elevation 1341 mm
 ΔT = maximum temperature rise at elevation 1341 mm
 t_t = turnaround time at elevation 1341 mm
 t_q = time for quenching at elevation 1341 mm

Effect of Spacer Grids on Reflooding Mechanism

The temperature histories measured in the experiments indicated irregular quenching near the spacer grids; a distinct positive temperature difference was found between the upstream and downstream side of the spacers (Fig. 7a). The largest temperature difference measured was 250°C, and in all the experiments with the standard rod bundle the difference rose to more than 100°C. The effect of spacer grid on the axial temperature profile of the cladding was clearest just above the spacer (curve 1356 mm in Fig. 7a); the temperature began to recover as the distance from the spacer increased (cf. curve 1376 mm). In the experiment with the corresponding spacer grid removed the quenching occurred in the natural order from upstream to downstream and the temperature profile was smooth (Fig. 7b).

There are two reasons for the better cooling on the downstream side of the spacer grids. By restricting the flow area and acting as heat transfer fins in the rod bundle the spacer grids increase turbulence and flow velocity of the coolant and enlarge the heat transfer area of the rods. Further, the

droplets entrained by the steam may adhere to the spacer grids or break into smaller droplets thus altering the steam-to-liquid heat transfer. The droplets attached to the spacer grids increase local heat transfer and form new upstream falling and downstream rising quenching fronts, finally improving the total rewet of the fuel rod simulators.

CONCLUSION

The two test series have been carried out in the REWET-II test facility to study the effect of spacer grids on the reflooding phenomena. The first test series was performed with a hexagonal bundle of 19 fuel rod simulators equipped with ten honeycomb type spacer grids. In the second test series the same rod bundle was used but with only eight spacer grids i.e. the 6th and 8th spacer grid were removed from the upper half of the test section. From the results obtained in these test series the following conclusions can be drawn.

The spacer grids improve the cooling of the fuel rod simulators during the reflooding process in two ways. First, the spacer grids reduce the flow area and, hence, increase turbulence and coolant flow velocity. Second, entrained droplets adhere to the spacer grids and form new downstream rising and upstream falling quenching fronts. The combined effect is that spacer grids alter the local axial temperature profile of the cladding. Near the spacer grids film boiling, transition boiling and nucleate boiling take place earlier than elsewhere. There are several downstream and upstream moving quenching fronts in the rod bundle improving the cooling and rewetting of the rods. The phenomenon described above can actually be seen in the REWET-III facility, which consists of three 1500 mm long fuel rod simulators inside a glass tube.

In the REWET-II reflooding experiments both pure downcomer ECC-injection and combined downcomer and upper plenum ECC-injection were used to determine the effect of spacer grids on reflooding phenomena. However, significant differences near the spacer grids were not found between these two injection modes. The effect of the spacer grids on the cooling of the test rod bundle was clearest with low pressure, low flow rate and high heating power.

REFERENCES

1. P. IHLE and K. RUST, "Einfluss von Abstandhaltern auf den Wärmeübergang während der Flutphase eines DWR Kühlmittelverluststörfalles", KfK 3178, Juni 1981.
2. R. DERUAZ, P. CLEMENT and J.M. VETEAU, "Reflooding of a PWR Bundle. Effect of Inlet Flow Rate Oscillations and Spacer Grids", European Two Phase Flow Group Meeting, Paris 1982.
3. G. L. YODER et al., "Dispersed-Flow Film Boiling Heat Transfer Data Near Spacer Grids in a Rod Bundle", Nuclear Tehnology, vol 60, Feb. 1983, pp. 304-313.
4. T. KERVINEN, "Reflood Experiments with Simultaneous Upper and Lower Plenum Injection in the REWET-II Rod Bundle Facility", International Meeting on Thermal Nuclear Safety, ANS/ENS/JAES, Chicago 1982.
5. H. KALLI, T. KERVINEN and A. HÄMÄLÄINEN, "REWET-II Facility for Experiments on the Loss-Of-Coolant Accident in Nuclear Reactors", Acta Polytechnica Scandinavica, Ph138, Helsinki 1983.

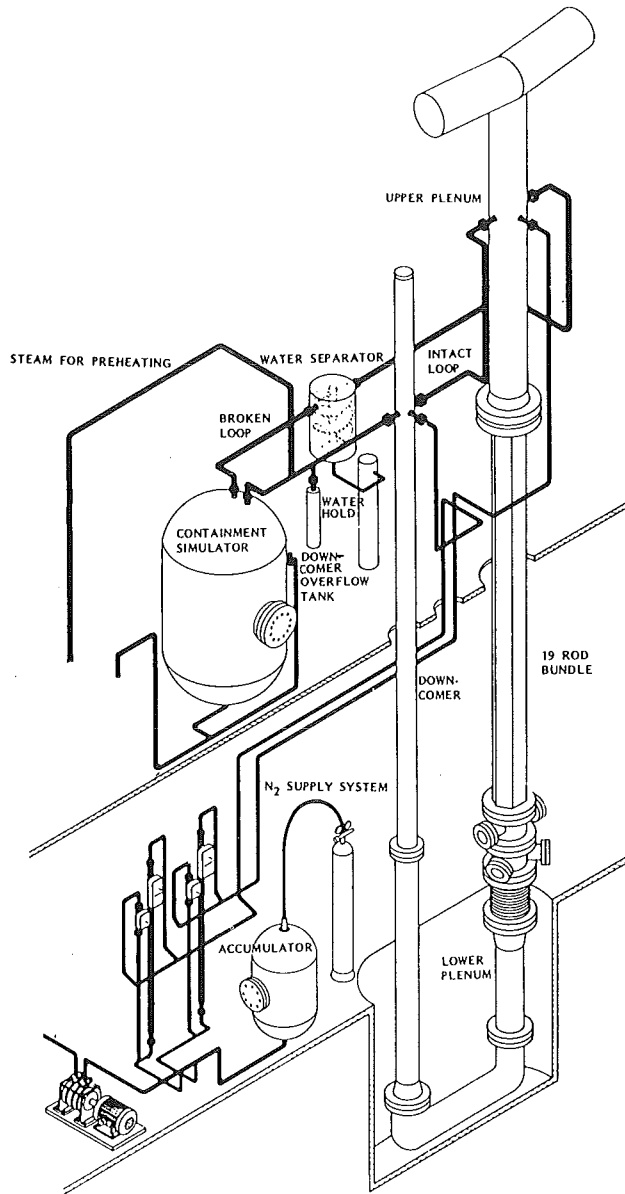


Figure 1. REWET-II facility.

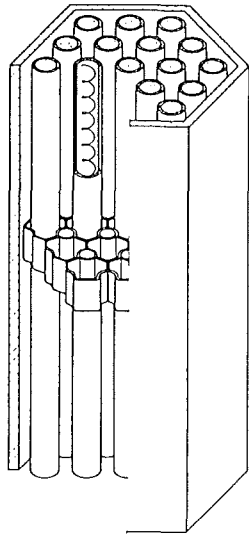


Figure 2. Reactor core simulation in the REWET-II facility.

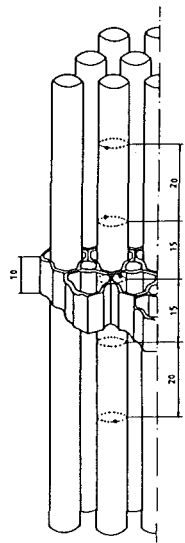


Figure 3. Example of thermocouple locations near spacer grids in REWET-II experiments, in millimetres.

REWET-II EXPERIMENT

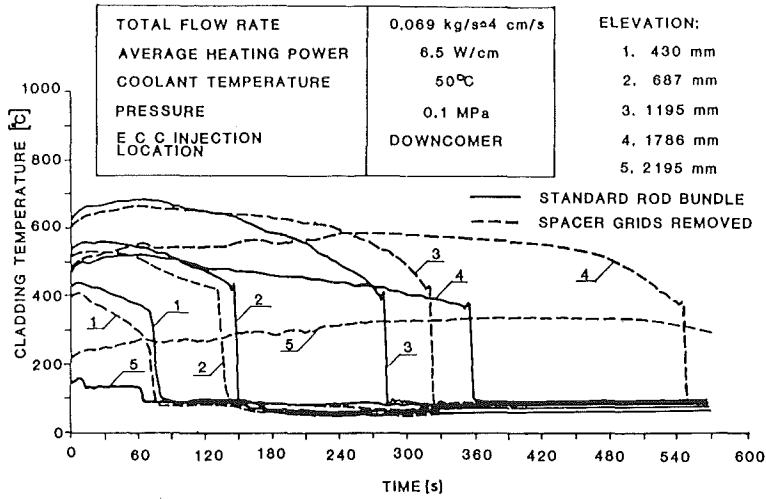


Figure 4. Comparisons of cladding temperature histories in REWET-II experiments. (Note: the elevation of the 4th thermocouple in the experiment with spacer grids removed is slightly different, 1821 mm).

TOTAL FLOW RATE	4 cm/s=0.069 kg/s
AVERAGE HEATING POWER	6.5 W/cm
COOLANT TEMPERATURE	50°C
PRESSURE	0.1 MPa
E.C.C. INJECTION LOCATION	DOWNCOMER

TOTAL FLOW RATE	4 cm/s=0.069 kg/s
AVERAGE HEATING POWER	6.5 W/cm
COOLANT TEMPERATURE	50°C
PRESSURE	0.1 MPa
E.C.C. INJECTION LOCATION	DOWNCOMER

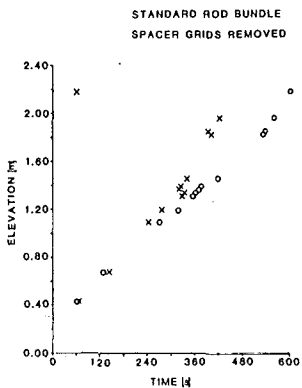


Figure 5. Comparisons of quenching times in a pair of REWET-II experiments.

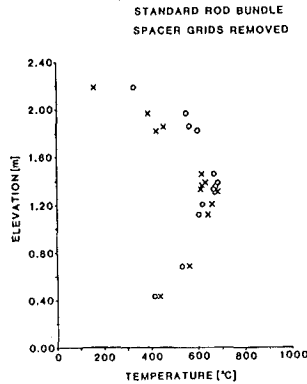


Figure 6. Comparisons of maximum local temperatures in a pair of REWET-II experiments.

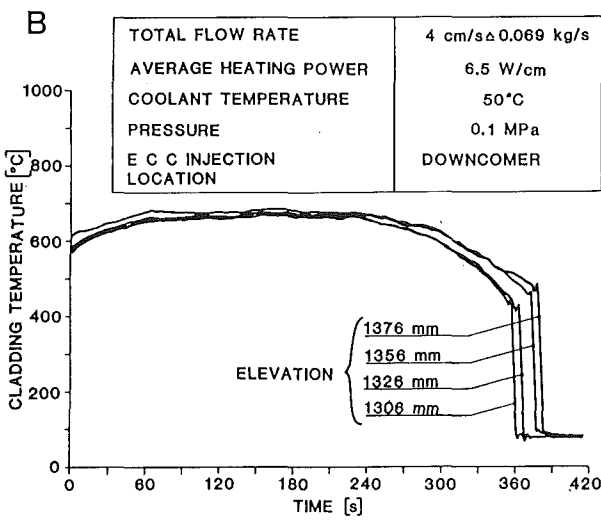
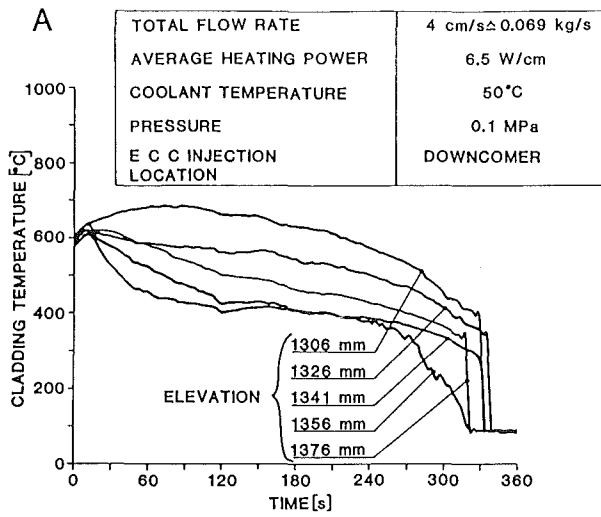


Figure 7. Comparisons of cladding temperature histories near the spacer grids in REWET-II experiments, A with all the spacer grids and B with two spacer grids removed.

REFLOODING IN A TIGHT-PITCH ROD LATTICE

Heikki Kalli*, Timo Kervinen** and Jukka Rossi**

*Lappeenranta University of Technology, Dept. of Energy Technology
P.O.Box 20, SF-53851 Lappeenranta 85, Finland**Technical Research Centre of Finland, Nuclear Engineering Laboratory
P.O.Box 169, SF-00181 Helsinki 18, Finland

ABSTRACT

Several authors have proposed improving the fuel utilization of the PWRs by reducing the moderator-to-fuel volume ratio (V_{H_2O}/V_{UO_2}). The low water volume fraction is achieved with a triangular fuel rod array. In this paper a calculational study on the reflooding phenomena in a tight-pitch rod lattice is presented. Two reflood computer codes, FLOOD4 and NORCOOL-I, are first verified against results obtained in experiments with the REWET-II facility which has a triangular array of fuel rod simulators. Using these computer codes, the reflooding is then investigated in a tight-pitch rod bundle. The results seem to indicate that the emergency core cooling in the tight-pitch lattice is no more difficult than the emergency cooling of the core lattice in the VVER-440 reactor simulated by the REWET-II facility.

1. INTRODUCTION

During recent years several authors (e.g. [1...5]) have proposed to improve the fuel utilization of the pressurized water reactors by reducing the moderator-to-fuel volume ratio (V_{H_2O}/V_{UO_2}) from about 1.5-2.0 to about 0.5. The low moderator volume fraction is achieved with a triangular fuel rod arrangement. By using PuO_2/UO_2 fuel, high conversion ratios (>0.9) are possible in this kind of advanced pressurized water reactor (APWR) core, cf. especially reference [5]. In Table 1 typical characteristics of APWR fuel assemblies are given.

Table 1. Data of APWR fuel assemblies [3, 4, 5]

Fuel rod	
- array	triangular
- outer diameter	0.8-0.95 cm
- active length	1.5-2.3 m
- cladding material	stainless steel
Spacer	helical fins or wires
- wire diameter	~ 1 mm
Fuel assembly	hexagonal
V_{H_2O}/V_{UO_2}	~ 0.5

Thermal-hydraulics of the APWR during a loss-of-coolant accident (LOCA) have been studied in references [3] and [6]. In this paper the same problemacy is approached from a different direction. Our starting point will be the experiments in the REWET-II reflood facility on the emergency core cooling (ECC). The REWET-II test section resembles in certain aspects the APWR core configuration. The experiments will serve to verify two reflood codes, FLOOD4 and NORCOOL-1. Using these codes, the reflooding will then be investigated in a tight-pitch rod bundle.

2. REWET-II REFLOOD EXPERIMENT FACILITY

The REWET-II reflood facility [7], jointly built by the Technical Research Centre of Finland and Lappeenranta University of Technology, has been operational since fall 1981. First results have been published in references [8] and [9]. In Table 2 the main characteristics of the facility are given. The reference power plant is the Loviisa VVER-440 plant, Figure 1.

Table 2. REWET-II facility characteristics

Fuel rod simulator	
- array	triangular
- outer diameter	0.91 cm
- heated length	2.42 m
- pitch	1.22 cm
- axial power distribution	chopped cosine
- axial peaking factor	1.5
- cladding material	stainless steel
Spacer	honeycomb
Rod bundle geometry	hexagonal
Number of rods in bundle	19
ECC injection locations	upper plenum and/or downcomer
Heating power of fuel rod simulators	0-90 kW
Average linear heating power	0-20 W/cm
Flow rate (cold level rise)	0-15 cm/s
System pressure	0.1-1.0 MPa
Maximum surface temperature of fuel rod simulators	~ 1000 °C
Coolant temperature	15-120 °C

As seen in Tables 1 and 2, the REWET-II test section, Figure 2a, is quite similar to the APWR configuration. The fuel rod simulators are in the triangular array, their length and outer diameter are close to the dimensions of the APWR fuel rods. The REWET-II spacer grids are different and, of course, the lattice pitch is larger than in the APWR fuel assembly.

3. REFLOOD CALCULATIONS

Two computer codes, FLOOD4 and NORCOOL-I, have been used to analyze the REWET-II reflood experiments [9]. The FLOOD4 code has been developed at the INEL, U.S.A., in the Semiscale program [10]; the NORCOOL-I code is a product of the Nordic reactor safety project [11].

3.1 Verification of the Computer Codes

Two standard experiments have been chosen to represent typical REWET-II experiments. The results and main parameters of these experiments are given in Figures 3a and 4a. In the beginning of the experiments the lower plenum is full of cooling water. In the first experiment, Figure 3a, the ECC water is injected into the downcomer only. In the second experiments, Figure 4a, the same total flow of ECC water is divided between the downcomer and the upper plenum (combined injection).

These standard experiments have been calculated using the codes FLOOD4 and NORCOOL-I. The results are given in Figures 3b and 3c for the first experiment, and in Figures 4b and 4c for the second experiment.

The two codes can reproduce relatively well the first standard experiment, especially the quenching times in the hottest region of the test section (cf. curves 3 and 4 in Figures 3) are close to the measured values. In the second experiment, Figures 4, the agreement between the measured and calculated results is more qualitative. In both cases, FLOOD4 seems to give more reliable results than NORCOOL-I.

3.2 Calculations with a Tight-Pitch Test Section

In what follows the REWET-II test section in Figure 2a is replaced by a fictitious "APWR test section" shown in Figure 2b. The rods remain exactly the same, but the lattice pitch is reduced from 12.2 mm to 10.1 mm. Consequently, the water-to-rod volume ratio of the test section is reduced from about 1.2 to 0.47. Helical wires are used instead of the honeycomb spacers.

With this APWR test section in the REWET-II facility, the two standard experiments have been calculated for two values (600 °C and 700 °C) of the maximum initial cladding temperature. The case of the higher initial temperature (700 °C) is illustrated in Figures 5.

In the first standard experiment both codes agree in the quenching behavior of the hottest region (Figures 5a and 5b). As earlier in Figures 3b and 3c, the top quenching (cf. curve 5) predicted by FLOOD4 is not seen in the NORCOOL-I results. Hence, the maximum cladding temperatures differ in the upper part of the test section. In the second standard experiment NORCOOL-I did not manage to give reasonable results; only FLOOD4 results are shown here in Figure 5c.

Compared with the experiments in Figures 3 and 4, the results in Figures 5 seem to indicate that under similar conditions the quenching times are slightly shorter in the APWR test section than in the normal REWET-II test section, especially in the hottest region near and above the test section mid-plane.

FLOOD4 calculations of the two standard experiments have been performed also with reduced linear heating power and ECC flow rate in the APWR test section. This reduction corresponds to the fact that in a given core volume there would be more fuel rods in the APWR case. Sample results of these calculations are shown in Figures 6a and 6b. Compared with Figures 5a and 5c, the quenching rate of the hottest region is even still higher in this case.

4. CONCLUSIONS

An investigation on reflooding in a tight-pitch rod lattice has been performed using two codes, FLOOD4 and NORCOOL-I. The codes have been verified against the results obtained in two "standard" experiments with the REWET-II facility. This reflood facility is designed to simulate the LOCA conditions in a VVER-440 reactor. The REWET-II test section resembles in certain aspects the APWR configurations proposed.

The results obtained in chapter 3.2 seem to indicate that the emergency core cooling in the tight-pitch lattice is no more difficult than in the VVER-440 core lattice, the rod dimensions being the same in the two cases. Under similar conditions even slightly higher reflooding rates are obtained in the tight-lattice case. Although parallel to results in [3] these results are not directly comparable with the earlier studies [3] and [6].

Finally, the need for experiments should be pointed out. In addition to the eventual verification of the results obtained, these experiments would offer a severe test problem to the reflood computer codes.

REFERENCES

1. Edlund, M.C., High conversion ratio plutonium recycle in pressurized water reactors. *Annals of Nuclear Energy* 2 (1975), pp. 801-807.
2. Driscoll, M.J. and Correa, F., The reactor physics of tight-pitch PWR cores. *Trans. Am. Nucl. Soc.* 33 (1979), pp. 807-808.
3. Uotinen, V.O. et al., Technical feasibility of pressurized water reactor design with a low-water-volume-fraction lattice. EPRI-NP-1833, May 1981.
4. Oldekop, V., Berger, H.-D. and Zeggel, W., General features of advanced pressurized water reactors with improved fuel utilization. *Nuclear Technology* 59 (1982), pp. 212-227.
5. Millot, J.-P., Considérations sur les réacteurs PWR sous-modérés. *Revue Générale Nucléaire Année 1982*, n° 4, pp. 405-408.
6. Schumann, S. and Oldekop, W., Untersuchungen zur Flutphase nach einem Kühlmittelverlust bei hochkonvertierenden fortgeschrittenen Druckwasserreaktoren (FDWR). *Atomkernenergie-Kerntechnik* 42 (1983) 2, pp.80-91.
7. Kalli, H., Kervinen, T. and Hämäläinen, A., REWET-II facility for experiments on the loss-of-coolant accident in nuclear reactors. *Acta Polytechnica Scandinavica Ph138* (1983), pp. 66-71.
8. Kervinen, T., Reflood experiments with simultaneous upper and lower plenum injection in the REWET-II rod bundle facility. *International Meeting on Thermal Nuclear Reactor Safety*, Chicago, U.S.A., Aug. 29- Sept. 2, 1982.
9. Kervinen, T., Hämäläinen, A. and Miettinen, J., Reflood experiments in the REWET-II rod bundle facility including comparisons with computer calculations. *Second International Topical Meeting on Nuclear Reactor Thermal-Hydraulics*, Santa Barbara, California, Jan. 11-14, 1983.
10. Shumbway, R.W., Core reflood dynamics code-FLOOD4. EGG-SEMI-505, October 1979.
11. Andersson, J.G.M. et al., NORCOOL-I, a model for analysis of a BWR under LOCA conditions, a revised report. NORHAV-D-47, August 1977.

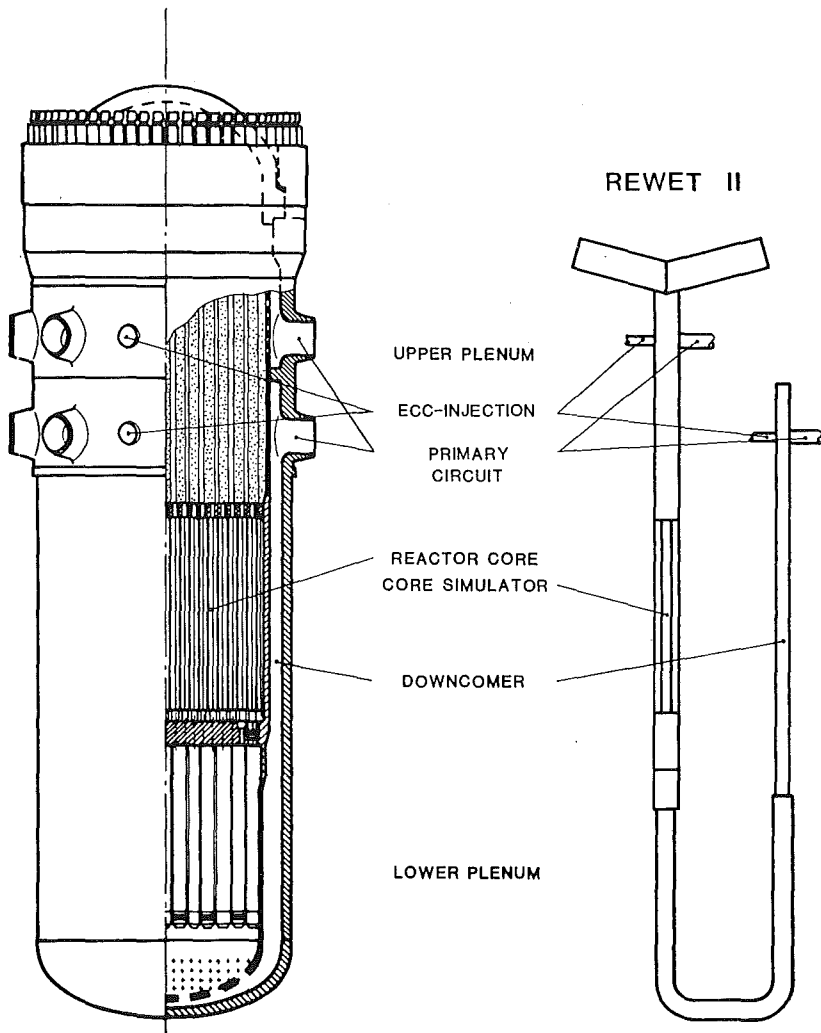


Figure 1. Simulation of the VVER-440 reactor vessel in the REWET-II facility.

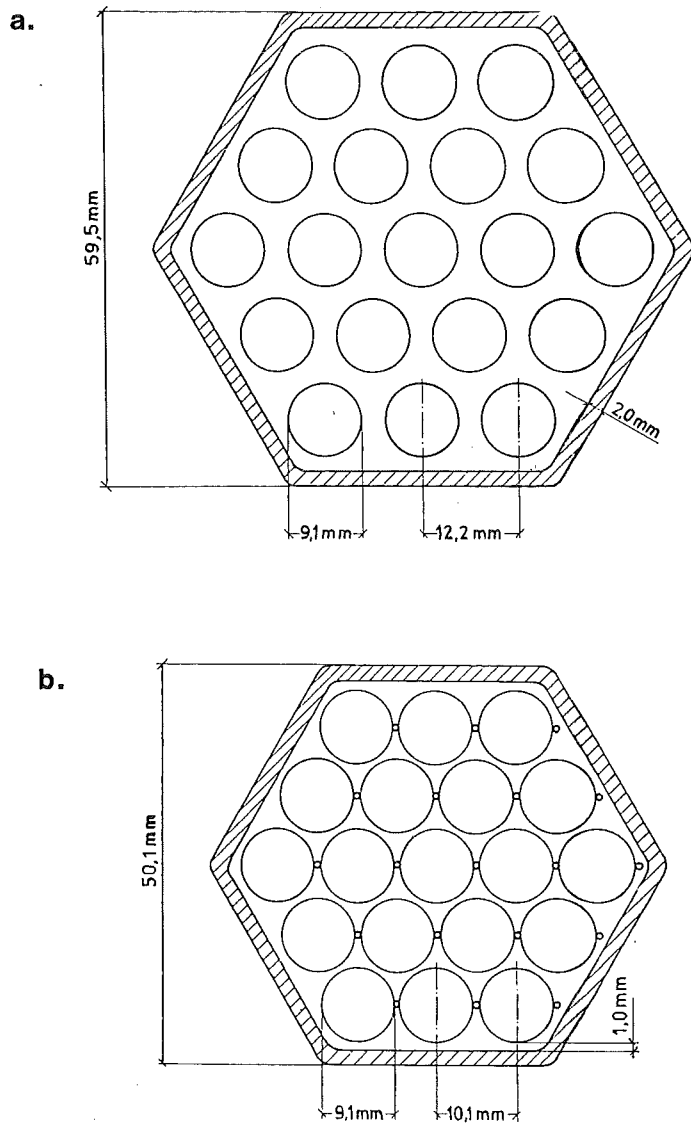


Figure 2. a) Cross section of the REWET-II test section.
b) Cross section of the APWR test section used in the calculations.

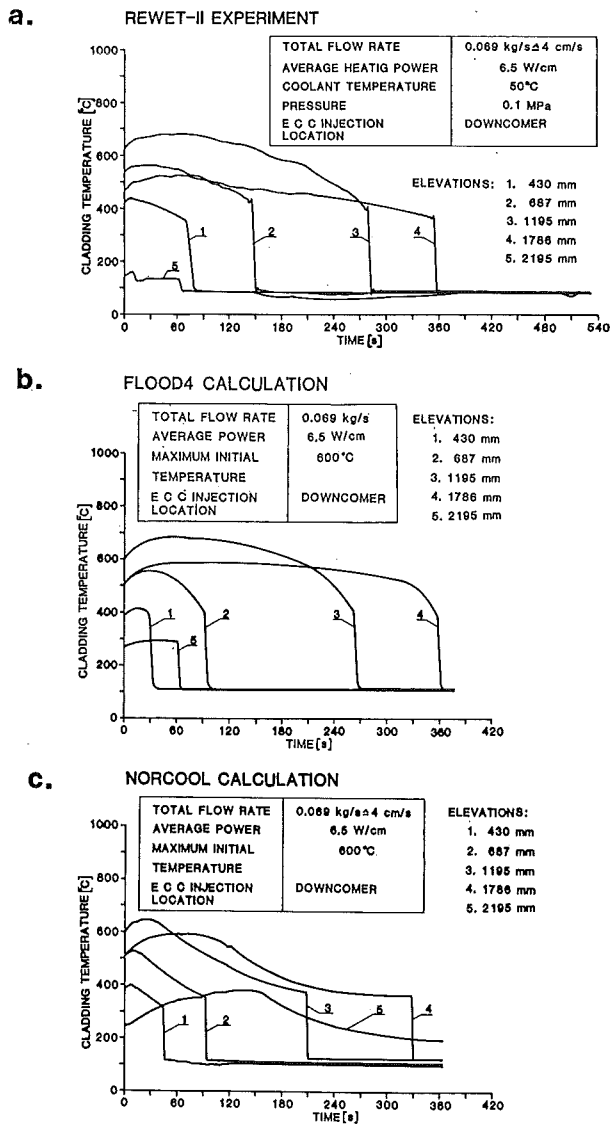


Figure 3. Results and parameters of the first standard experiment (downcomer ECC injection)

- a) REWET-II experimental results
- b) FLOOD4 calculation
- c) NORCOOL-I calculation.

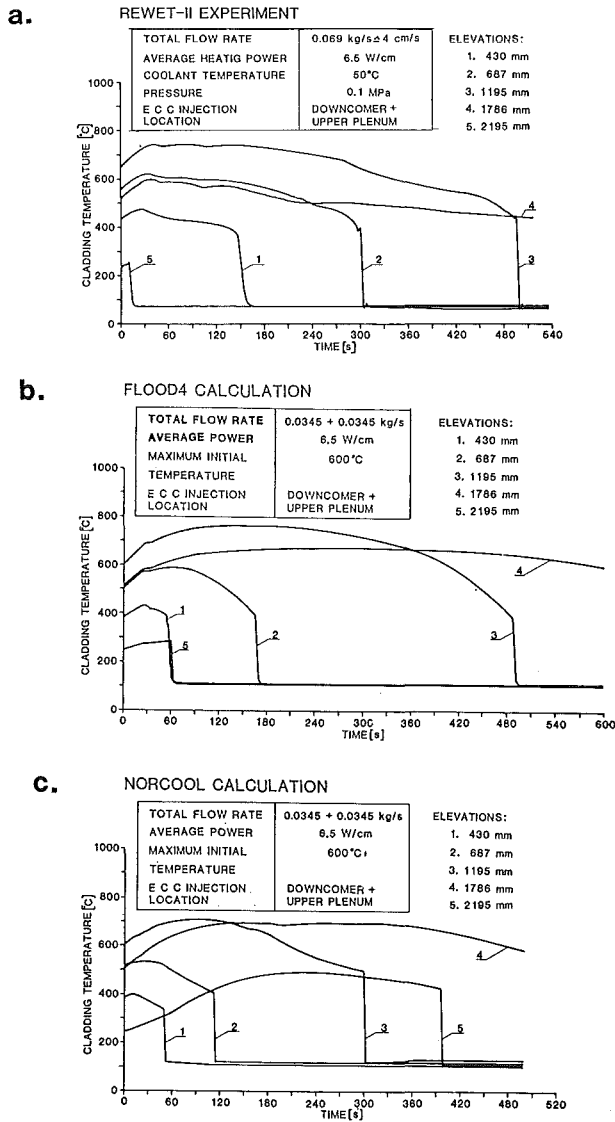


Figure 4. Results and parameters of the second standard experiment (combined ECC injection)

- a) REWET-II experimental results
- b) FLOOD4 calculation
- c) NORCOOL-I calculation.

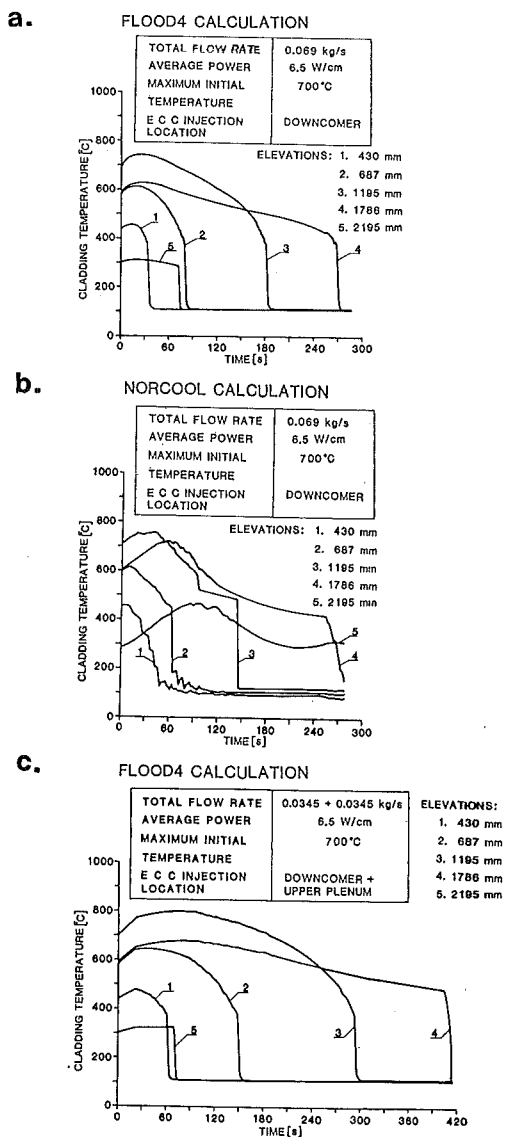
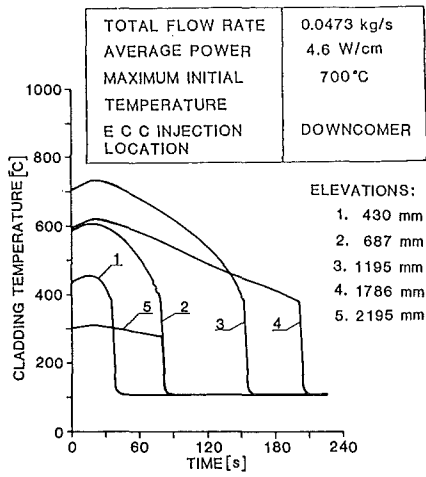


Figure 5. Results of the APWR test section

- a) FLOOD4 calculation of the first standard experiment
- b) NORCOOL-I calculation of the first standard experiment
- c) FLOOD4 calculation of the second standard experiment.

a. FLOOD4 CALCULATION



b. FLOOD4 CALCULATION

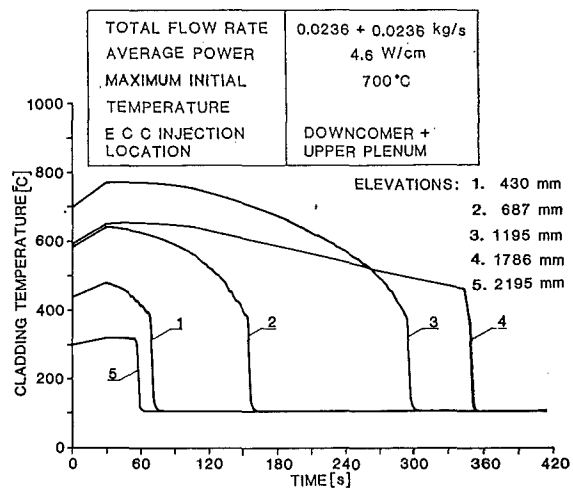


Figure 6. Results of the APWR test section; average linear power and total flow rate have been reduced by a factor 0.685

- a) FLOOD4 calculation of the first standard experiment
b) FLOOD4 calculation of the second standard experiment.

PREDICTION OF REFLOODING IN SINGLE CHANNELS
AND PARTIALLY-BLOCKED ROD BUNDLES

D R Glynn, D Kirkcaldy & N Rhodes

CHAM Limited, Bakery House, 40 High Street,
Wimbledon, London SW1 5AU UK

ABSTRACT

A mathematical model to investigate the influence of system parameters on the flow and heat transfer during reflooding is described. The model employs equations for momentum and enthalpy of vapour and liquid phases; correlations are used to determine fluid friction and heat transfer as functions of flow regime and local conditions. Calculations which predict a selection of the UKAEA REFLEX single-channel experiments are reported. These show the effects of pressure, heat generation, inlet subcooling and flow rate. Reasonably good agreement with experiment has been obtained. The three-dimensional flow in a partially-blocked rod bundle is also examined. Calculations for a geometry typical of current designs with flow and boundary values based on the PWR-FLECHT tests are reported.

INTRODUCTION

The reflooding of a reactor core is an important stage in the recovery from a Loss-of-Coolant-Accident. It begins when emergency core cooling water first reaches the fuel rods and continues until the core is quenched. Prior to reflood, cladding temperatures may rise to values at which water cannot wet the wall. The heat-transfer processes occurring during reflood are therefore very complex and consideration of several flow regimes is required.

Much experimental work has been carried out to gain a deeper understanding of the fluid-flow and heat-transfer mechanisms which occur during reflood. This work usually involves tests on single heated rods or channels, [1] and [2], and in some cases rod bundles [3], although the latter are usually aimed at providing overall information for safety analysis rather than detailed insights into the flow behaviour. Analytical models of reflood also fall broadly into two categories, those which rely heavily on large-scale experimental data, and those which employ detailed mathematical descriptions of the local physical processes, using empirical correlations to model local heat, mass and momentum transfer.

The reflood model used in the present study is of the latter kind, and was developed using a general, multi-dimensional, two-phase flow program PHOENICS [4]. The model was first used to investigate the effect on predicted reflooding behaviour of different heat-transfer assumptions. In particular, the flow regimes and corresponding correlations for wall-to-fluid heat-transfer used in codes such as RELAP and TRAC were examined. A previous study [5] showed that the quench rate predicted for CSNI standard problem number 7 [6] varied between one-half and four

times the experimental value, depending on the correlations employed. Of the correlations which were studied, those used in the TRAC code appeared to give closest agreement with this experimental case.

The present paper describes further applications of the model to single-channel reflood experiments, and an extension to a three-dimensional case in which a rod bundle is partially blocked. The results of the UKAEA REFLEX experiments [2] show the influence of pressure, heat generation, subcooling and inlet flow rate on reflooding. The purpose of the one-dimensional calculations was to assess whether the assumptions used for flow regimes and empirical correlations remained valid over a range of conditions.

The three-dimensional study was aimed at determining the two-phase flow behaviour in a partially blocked rod bundle. Results are reported for a typical bundle geometry, the inlet flow rates and boundary conditions being based on the PWR-FLECHT tests. Attention is focussed on the stage of reflood before the quench front reaches the ballooned region, the flow conditions at this time being the most crucial in terms of maximum cladding temperatures obtained.

ANALYSIS AND SOLUTION METHOD

Governing Differential Equations

The general two-phase, three-dimensional transient conservation equations solved in PHOENICS may be written in the form:

$$\frac{\partial}{\partial t} (\rho_i R_i \phi) + \text{div}(\rho_i R_i \vec{u}_i \phi + \Gamma_\phi \text{grad} \phi) = S_\phi$$

where ϕ is the dependent variable, ρ the density, u the vector velocity, R the volume fraction, Γ_ϕ the diffusive exchange coefficient for ϕ , S_ϕ the source of ϕ per unit volume, and the subscript i denotes the phase concerned.

In the three-dimensional cases considered, equations of the above form are solved for six velocity components (one for each phase in each coordinate direction) and for the enthalpy of each phase. The pressure, which is presumed common to both phases, and the volume fractions, are determined from the continuity equations, which are of the same form as above with $\phi=1$. In the one-dimensional model of the single-channel experiments, only two velocity equations are required. However, a wall temperature equation of the form:

$$\frac{\partial}{\partial t} (\rho_w T_w) - \text{div}(k_w \text{grad} T_w) = S_T$$

is also solved so that the effect of axial conduction, which is significant in the region of the quench front, can be included.

The effects of pressure and gravity are included as source terms. Additional source terms represent the effects of interphase and wall-to-fluid momentum, heat and mass transfer; these contain coefficients which are obtained in most instances from empirical correlations, which in turn depend on the flow regime. The flow regimes considered in the model are shown in Table 1. It can be seen that the local wall temperature and the void fraction are the most important parameters in determining the regime. The wall temperatures at which regime changes occur are the liquid-saturation temperature, T_{sat} , the critical-heat-flux temperature, T_{CHF} and the minimum-film-boiling temperature, T_{min} .

The wall-to-fluid heat-transfer coefficients for the various regimes are taken from the TRAC code [8], and are outlined in Table 2. The mathematical forms of the exchange coefficients and source terms, together with the correlations for interphase friction and heat transfer, and for wall-fluid friction, are described in detail by Glynn, Rhodes and Tatchell [5].

Solution Method

The calculation domain is divided into a number of grid cells. The differential equations are approximated by finite-domain equations which are solved using the IPSA algorithm of Spalding 1981 [9]. The solution is obtained by a time-marching method which is fully implicit. This means that at each time step during the solution, all quantities (except of course the previous-time value in the transient term) are evaluated at the new time level. This necessitates iteration at each time step, but ensures that stable solutions can be obtained even when large time steps are used. Flow regimes are, however, fixed according to previous-time-step values.

Computer Program

The solution scheme outlined above is embodied in a general-purpose fluid-flow computer code called PHOENICS [4]. The use of a general code has allowed much of the reflow problem to be set up through standard 'switch-on' options. The empirical information built into the model is provided in special user subroutines.

PRESENTATION OF RESULTS

Predictions of the UKAEA-REFLEX Experiments

(a) Definition of the test cases

The test section in the REFLEX rig comprises a vertical heated tube made of Inconel 600, which is 3.59m long, 12.56mm inside diameter and 15.87mm outside diameter. A range of tests has been performed with varying pressure, inlet water subcooling, flow rate and tube wall heating. Three tests have been chosen for analysis, these being Runs 92, 107 and 129. The test conditions are given in Table 3.

(b) Computational details

In order to resolve the steep gradients of temperature and heat flux in the quench front region, and hence account accurately for heat conduction in the tube wall, a fine grid is required. A moving grid treatment is used which employs a fine-grid region of uniformly-spaced cells, centred on the quench front and moving with it. The remainder of the tube is divided into larger cells, which are redistributed as necessary so as to preserve an approximately uniform distribution. The grids and time steps used for the three runs are set out in Table 4. These values were chosen after some initial calculations had shown that they were adequate for the predictions to be substantially independent of grid and time step.

(c) Comparison of predictions with experiments

The flow regime which is established at the beginning of reflood depends on the rate of injection of liquid, the wall temperature, liquid subcooling, and system pressure. For example, with large subcooling and high flow rate, a column of liquid would develop, thus forming an inverse-annular flow regime. If the wall temperature is above the minimum film-boiling temperature, as is usually the case, then water cannot wet the wall, and cooling is obtained by convection of the steam generated from boiling of the liquid column and dispersed droplets. The heat-transfer coefficients associated with this flow regime are relatively low, and it is not until the wall temperature reaches T_{min} that alternative flow regimes bring into play mechanisms which permit greater heat-transfer. When this occurs, the wall temperature falls rapidly to near the liquid saturation temperature, thus forming a quench front which moves gradually up the channel. Ahead of the quench front, the wall temperature may rise if there is sufficient heat generation. Eventually, however, it begins to fall as the quench front approaches.

The predicted variations of quench front position, pressure-drop and wall temperature at 1.25m are compared with experimental data, for the three cases considered, in Figures 1 to 3.

The predicted quench front positions, Figure 1, all show a rate of quenching which is slower than experiment at the beginning of reflood, but which increases later on. The overall heat-transfer is evidently too low in the early stages. An extreme example is Run 129, where the onset of quenching is delayed because the heat-transfer coefficient predicted by the film-boiling correlation appears to be too low for the local conditions, and some time was taken for the tube to cool to T_{min} . The rapid quenching in the later stages of reflood, particularly for Runs 92 and 129 may be a result of too high a value predicted for T_{min} as mentioned below.

The overall pressure drop data are given in Figure 2. It can be seen that the predicted values are lower than those measured, particularly for Run 92. The pressure-drop is approximately equal to the hydrostatic head in the tube. The under-prediction may, therefore, indicate that interphase friction is too high, and that water passes through the tube too quickly. It should be noted, however, that the measured value at the beginning of the transient has, for each case, a value of about 10^4 N/m². It may be that this offset is a feature of the instrumentation and should be subtracted from the data before comparison with the predictions. If this is the case, then the two sets of data are in quite good agreement.

It is interesting to note the predicted fluctuation in pressure drop in Run 129 at about 30s. This is caused by a change in flow regime from inverse-annular to annular. A similar change was predicted at about the same time for Run 107. Run 92, however, was predicted to have an annular flow regime from the beginning, probably due to the low flooding rate and zero subcooling.

The wall temperature variations at 1.25m height are shown in Figure 3. These compare reasonably well with experimental data. The most notable feature is the wall temperature at which quenching occurs. The predictions indicate a value of T_{min} of about 400°C or slightly above. The experiment shows a somewhat lower value, in the region of 350°C. This difference in T_{min} may explain the more rapid rate of quenching predicted, the tube wall not having to cool to such a low temperature before the correlations which predict a higher heat-transfer coefficient are brought into use by the regime selection criteria.

Overall, the predictions are in reasonable agreement with the experimental data, particularly if the discrepancy in pressure drop can be explained by a constant offset in the experimental data. More importantly, the heat-transfer and

friction correlations used in the model appear to have responded correctly to the varying reflood conditions.

Blocked Rod-Bundle Analysis

(a) Definition of the test case

The system considered is a regular square matrix of closely-spaced fuel pins in an 11x11 array. A blocked region has been assumed to form in the central region of the bundle, due to clad ballooning. A 360mm length of the bundle is considered, the blockage being located in the middle, and having a length of 120mm. The diameter of the underformed rods is 9.5mm and the pitch 12.6mm. It is assumed that the deformed rods swell until they just touch. This results in a blockage of about 60%. Figure 4 gives the geometry considered, other parameters are as follows:

Heat generation :	719 W/m,	Droplet diameter :	1 mm,
Inlet gas velocity :	10 m/s,	System pressure :	3 bar,
Inlet liquid velocity :	5 m/s,	Inlet gas temperature :	300 °C,
Inlet liquid temperature :	133 °C (saturation).		

(b) Computational details

One quarter of the rod bundle was considered, as shown in Figure 4. One grid cell per sub-channel was used in the cross-stream plane, with 18 divisions in the axial direction. Thus, the grid used was 6x6x18. Steady-state and transient calculations were performed, the former with fixed amounts of liquid-droplet mass inflow, and the latter with a varying liquid inflow.

(c) Typical results

Typical results from the model are shown in Figures 5 and 6 in the form of gas and liquid velocity vector plots, and graphs showing the axial variations of rod temperature.

The gas phase velocities, Figure 5, show that the gas is deflected around the blockage, causing an increase in velocity at the outside of the bundle. Within the blockage, the gas velocity is similar to that at inlet, although the mass flow is reduced by the deflection of gas into the outer region. Directly above the blockage, where the flow area once again expands to the normal value, the gas velocities are much reduced. The liquid droplet velocities are not unduly influenced by the gas deflection, therefore the inertia of the droplets at inlet carry them through the blocked region at the same rate. Within and directly above the blocked region, the liquid velocities gradually reduce due to the influence of gravity and the low gas velocities providing relatively little interphase friction.

Axial distributions of rod temperature are shown in Figure 6 for the seven rods indicated in Figure 4. Outside the blockage, rods 6 and 7, the temperatures do not vary greatly. A reduction to about 420°C is evident in the centre of the bundle, where the gas velocity is higher. The rods associated with the blocked region all show a similar behaviour. Their temperature increases up to the blockage, fall within the blockage where a greater heat-transfer area is available, and rise outside the blockage where gas velocities are low and areas are reduced. The highest temperature, about 680°C, occurs in the rod nearest the centre of the blockage. Towards the exit of the bundle the rod temperatures fall due to the crossflow of cooler gas expanding into the region above the blockage.

The predicted behaviour of the three-dimensional flow in a blocked rod bundle appears to be qualitatively similar to that observed experimentally. In particular, the blocked region is, perhaps contrary to expectation, reasonably well cooled. The presence of water droplets ensure that the steam does not become superheated in the blockage, and hence good cooling is maintained despite the reduced steam flow. This general behaviour has been confirmed experimentally [3].

Concluding Remarks

This paper has presented reflood predictions for single-channel and partially-blocked rod-bundle cases. Single channel modelling studies have shown that reasonable agreement between prediction and experiment for quench front position and wall temperature is obtained, but that pressure-drop is somewhat underpredicted. Further work is required to provide some fine tuning of the heat-transfer and friction correlations employed. However, the basic set appear to respond reasonably well to changes in reflood conditions.

The three-dimensional predictions of a partially blocked rod bundle show encouraging qualitative agreement with experimental data. Prediction of particular experimental cases and more detailed comparisons would provide greater insight into the flow behaviour and heat transfer. A three-dimensional model, thus validated, could then be used to predict behaviour in reactor conditions.

ACKNOWLEDGEMENT

The single-channel reflood study described in this paper was funded by the United Kingdom Atomic Energy Authority, Winfrith. The authors are grateful to the UKAEA for permission to publish their experimental data.

REFERENCES

1. Yadigaroglu G (1977) 'The Reflooding Phase of the LOCA - State of the Art (1)'. Two-Phase Flows and Heat Transfer, Ed: Kakac S & Veziroglu T N. Proceedings NATO Advanced Study Institute, Istanbul, Hemisphere Publishing.
2. Denham M K, Elliott D F & Shawyer K J (1980) 'Fundamental Studies of the Reflooding of an Inconel Tube in the REFLEX Rig'. AEEW - R1353.
3. Pearson K G, Cooper C A, Jowitt D & Kinneir J H (1983) 'Reflooding Experiments on a 49-Rod Cluster Containing a Long 90% Blockage'. AEEW-R1591.
4. Spalding D B (1981) 'A General-Purpose Computer Program for Multi-Dimensional One and Two-Phase Flows'. Math. Comp. Sim., Vol 23, pp267-276.
5. Glynn D R, Rhodes N & Tatchell D G (1983) 'Numerical Modelling of Reflood Processes. IMechE Conference on Nuclear & Process Plant Safety.
6. Deruaz R & Tellier N (1979) 'An Analysis of a Reflooding Experiment. Comparison Report on OECD-CSNI LOCA Standard Problem No 7'. CSNI Rept 55.
7. Kirkcaldy D & Rhodes N (1982) 'Computer Modelling of the Flow in a Partially Blocked Rod Bundle During Reflood'. CHAM Report Number 2491/3.
8. TRAC-PD2 Manual (1980) 'An Advanced Best-Estimate Computer Program for PWR LOCA Analysis'. Los Alamos Scientific Lab, Report LA-8709-MS.
9. Spalding D B (1981) 'Numerical Computation of Multiphase Fluid Flow and Heat Transfer'. Recent Advances in Numerical Methods in Fluids, Vol 1, Editors: Taylor C & Morgan K, Pineridge Press, pp 139-167.

$\alpha=1$	convection to single-phase liquid	forced-convection annular flow	transition boiling (high quality)	dispersed flow
$\alpha=0.2$		nucleate boiling	transition boiling (low quality)	inverse-annular film boiling
$\alpha=0$		T_{sat}	T_{chr}	T_{min} wall temperature

Table 1 - Regime Map

Regime	Correlations	
	Gas	Liquid
Dispersed, inverse-annular	Maximum (Bromley, natural convection, Dougall-Rohsenow)	Radiation + Forstund-Rohsenow
Transition	Maximum (Bromley, natural convection, Dougall-Rohsenow) $\times (T_w - T_{chr}) / (T_{min} - T_{chr})$	Forstund-Rohsenow + quadratic interpolation + radiation $\times (T_w - T_{chr}) / (T_{min} - T_{chr})$
Nucleate, annular (forced-convection)	-	Chen
Single-phase liquid	-	Dittus-Boelter
Critical heat flux	Blast	
Minimum film boiling	Homogeneous nucleation or film	

Table 2 - Wall-to-Fluid Heat-Transfer Correlations

Run	92	107	129
Pressure (bar)	4	4	2
Heat generation (W/m)	600	100	600
Subcooling (°C)	0	40	40
Inlet flow (kg/m ² s)	40	40	160

Table 3 - REFLEX Test Cases

Run	92	107	129
Total number of cells	100	100	50
Number of fine cells	40	40	20
Cell length (mm)	2.5	2.5	2.5
Time step (s)	0.5	0.25	0.125

Table 4 - Grids and Time Steps Used

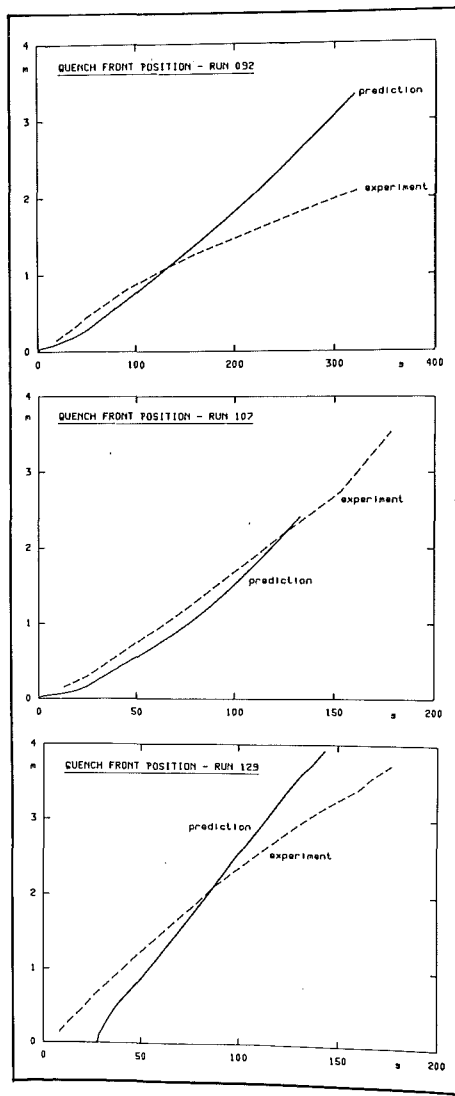


Figure 1: Quench Front Position Versus Time.

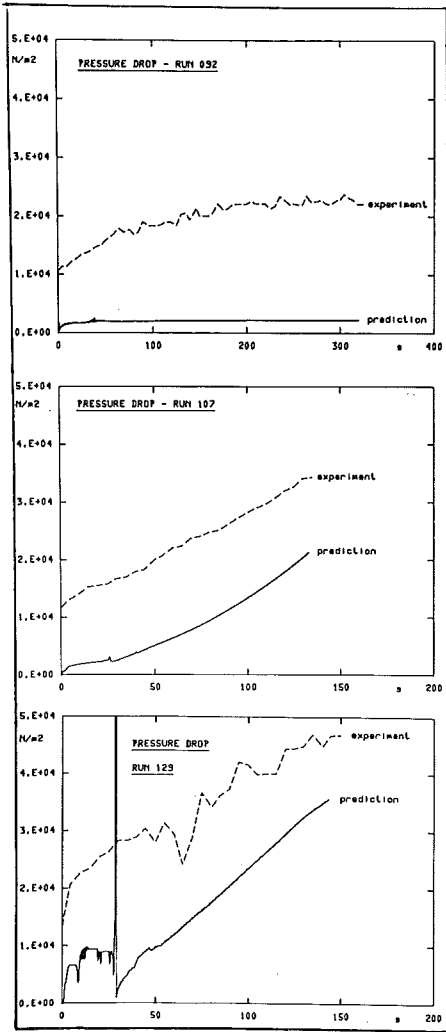


Figure 2 : Overall Pressure Drop Versus Time.

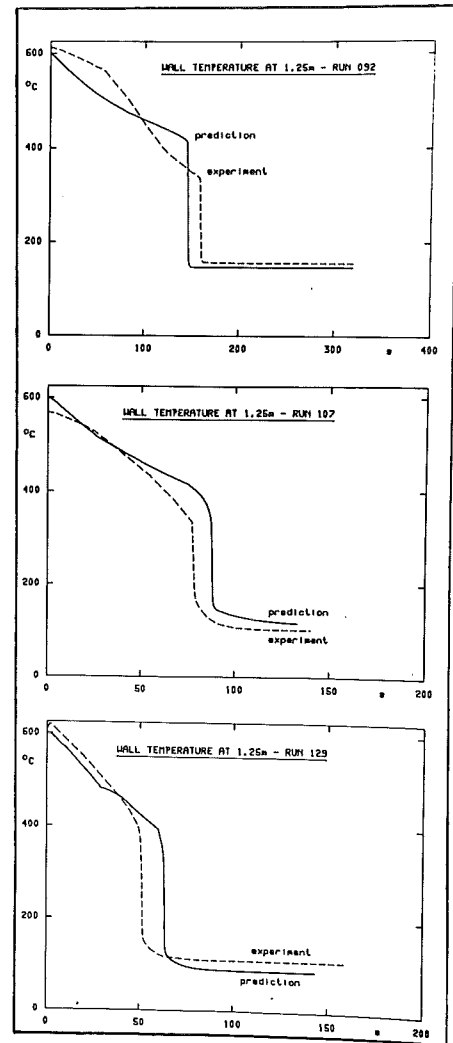


Figure 3 : Wall Temperature at 1.25 m Versus Time.

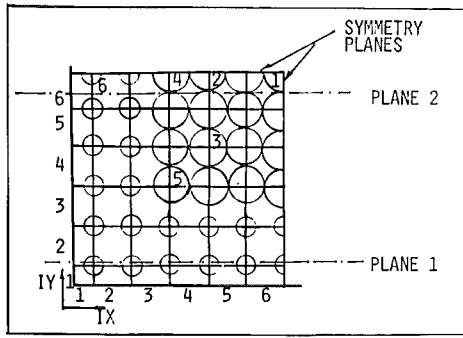


Figure 4 : Blocked Rod-Bundle Geometry.

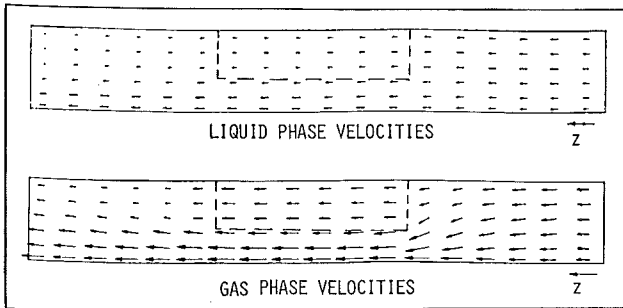


Figure 5 : Gas and Liquid Velocity Vectors in Plane through the Blockage.

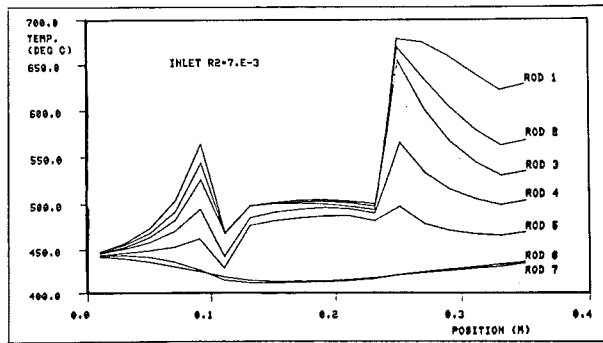


Figure 6: Axial Temperature Variations of Selected Rods.

COMPARISON OF CALCULATIONS USING THE BEST ESTIMATE REFLOOD HEAT
TRANSFER CODE BART-A1 WITH DATA FROM THE FEBA AND REBEKA FACILITIES

M. El-Shanawany, C.G. Kinniburgh and K.T. Routledge

National Nuclear Corporation
Whetstone, Leicester, England

ABSTRACT

BART-A1 is a Westinghouse computer code which provides a mechanistic evaluation of heat transfer during the reflood stage of a large Loss of Coolant Accident (LOCA) in a Pressurised Water Reactor. The code has been used by NNC in support of the reactor safety case with respect to the consequences of fuel clad swelling or ballooning during a LOCA. In support of this application of the code to the safety case, an extensive programme of validation of all aspects of the modelling is in progress. In this paper, the results of comparisons of the code with experimental data from two FEBA tests (0% and 90% sub-channel flow area blockage) and with the REBEKA6 experiment are presented.

Reasonable agreement with the data is obtained and the results confirm that the code provides a generally adequate description of the heat transfer process during core reflood.

INTRODUCTION

The safety case for LOCA in the UK is based on the use of an Evaluation Model, which complies with the requirements of Appendix K to 10CFR50. In the development of the safety case, all aspects of the modelling in the Evaluation Model have been investigated in detail to assess the conservatism embodied in calculations using this methodology. An aspect that has received considerable attention in the UK is the phenomenon of fuel clad ballooning during a LOCA. A considerable programme of model development, experimental work and calculations have been undertaken to confirm that this phenomenon will not result in calculated clad temperatures in excess of the appropriate limit. The Evaluation Model calculates the consequences of ballooning via a strain and blockage definition using the NUREG-0630 prescription coupled with a blockage steam cooling assumption prescribed by Appendix K. To determine the adequacy of this modelling technique, an alternative calculational method was developed which evaluated clad burst strain and rupture via a more mechanistic approach and which resulted in a conservative estimate of the flow blockage which was greater in axial and radial extent than via NUREG-0630. To determine the coolability of such a blockage the Westinghouse mechanistic reflood heat transfer code BART [1] was used which models explicitly the effect of entrained drops in the steam flow in reflood heat transfer. In support of this application an extensive programme of further validation of the BART code has been undertaken, particularly related to ballooning and flow blockage experiments. This paper discusses the results of comparisons of the code with data from two FEBA tests and from the REBEKA 6 experiment.

THE BART CODE

The BART code is a non-equilibrium, non-homogeneous two phase fluid model. Details of the code have been described elsewhere [2] and thus only a brief outline will be provided below.

Moving up the channel the code models a variety of flow regimes from subcooled liquid at the bottom of the test section or fuel bundle to a saturated boiling region, a quench front, an inverted annular film boiling region, a transition flow region, and in the upper part of the bundle, a dispersed flow region. Early in the transient, if conditions are such that entrainment of drops is not possible, then a single phase vapour region is modelled.

The dispersed flow region is a very important regime for reflood blockage heat transfer process. The dispersed region consists of a highly superheated steam phase with entrained liquid drops. The mechanisms for heat transfer from the rod surface to the fluid that are modelled in the code, are forced convection to vapour and direct radiation to the fluid. The forced convection coefficient accounts for the presence of drops in the steam flow. Desuperheating of the vapour is accounted for by droplet to vapour heat transfer.

Specific models are incorporated in the code to account for the effects of spacer grids, both in terms of their effects on the clad axial strain profile and on the reflood heat transfer process. The grid heat transfer effects include improved heat transfer due to the reduced sub-channel flow area and due to flow disturbances, and grid rewetting which improves heat transfer by desuperheating the steam.

A strain and blockage model is also incorporated in BART. The code calculates clad temperatures circumferentially around the clad as well as axially along the rod and clad rupture is calculated via a local clad strain limit. This limit will be exceeded locally due to calculated variations in temperature around the clad due to assumed eccentricity of the fuel pellet or heater rod. The strain is calculated to translate into a subchannel flow blockage via several optional idealised flow blockage models. A two channel model is employed to calculate flow diversion around the blockage.

THE FEBA TESTS

The FEBA facility (Ref. 2) at Kernforschungszentrum Karlsruhe has been designed to provide data on the effects of grids and subchannel flow blockage on the reflood heat transfer process. The bundle consists of a 5x5 array of full length rods and the test section is forced flooded from the bottom at a constant flood rate. Two tests are examined in this paper, Test 229 which modelled six grids and no flow blockage, and Test 239 which had identical fluid boundary conditions to Test 229, and modelled a short 90% flow blockage across a 3x3 array in one corner of the bundle at the midplane.

Several parameters from Test 229 are shown in Figure 1. The quench front advance up the bundle is well predicted by the code as are the steam temperatures. This is an indication that BART is modelling the details of the two phase heat transfer process reasonably well. The clad temperature comparisons indicate that the code accurately calculates lower and mid bundle temperatures while overpredicting temperatures near the top of the bundle by $\sim 100^{\circ}\text{C}$. It is noted that no model of the FEBA shroud is incorporated in the code which can be expected to have some influence on temperatures in the small

FEBA bundle.

Figure 2 shows comparisons of key parameters from Test 239. Two BART calculations are presented. In one all the entrained drops in the steam flow were assumed to carry on through the blockage. In the other some drops are diverted from the blockage in a manner nominally analogous to that assumed in safety case modelling. The drops are assumed to remain in the bypass channel once diverted.

The clad axial profile comparison shows that BART reasonably accurately predicts the temperature variation along the rod for the case with all drops assumed to carry through the blockage. The effect of the grids in the calculation can be seen as dips in the calculated clad temperature transient at the appropriate elevations. The blockage is seen to have a small effect on the clad temperature in both the calculation and data with the temperature just downstream of the blockage overpredicted by $\sim 60^{\circ}\text{C}$ and further downstream by $\sim 100^{\circ}\text{C}$, as in Test 229. It is noted that the shroud introduces strong radial temperature gradients across the FEBA blockage and thus care must be taken in comparing calculated clad temperatures with data from different blocked rods. The indications from interpolations of available data are that BART would overpredict the data by less than 60°C just downstream of the blockage if the appropriate thermocouple measurements were available.

The case with some drops diverted from the blocked channel substantially overpredicts the clad temperatures within and downstream of the blockage. The overprediction can be seen in Figure 2 to be of order $200\text{--}250^{\circ}\text{C}$. This latter result shows the importance of the presence of drops in the steam flow in limiting steam superheat and thus reducing clad temperatures.

THE REBEKA 6 EXPERIMENT

The REBEKA 6 experiment [3] is an out-of-pile test at Kernforschungszentrum Karlsruhe designed to investigate fuel rod straining, rupture and flow blockage heat transfer in rod bundle during a simulated large LOCA reflood transient. REBEKA models a large 7×7 full length fuel bundle and all but three of the rods were pressurised. The bundle was force reflooded at a constant rate and at a constant system pressure. All the pressurised rods strained and ruptured.

The test was designated a blind standard problem (German Standard Problem No.7 and International Standard Problem No.14) and BART predictions of the test were made without access to any of the thermohydraulic or mechanical data. The BART model assumes an eccentricity of the heater element within the clad which results in a temperature difference around the clad and thus non-uniform strain and rupture based on a local burst strain criterion. An appropriate eccentricity for input to BART was derived by separate BART and TAPSWEL analysis of the REBEKA 5 test. The latter code is a two-dimensional thermal conduction code which uses input heat transfer parameters from BART and a range of eccentricities to calculate a range of burst strains. BART requires a single value of eccentricity to represent an average rod in the bundle.

The BART blind analysis provided predictions of a number of parameters including clad temperatures, rupture strains, rupture times and flow blockage. Burst of all the rods occurred as was predicted. Key parameters from the test are shown in Figure 3. Reasonable predictions of clad rupture strain and clad to coolant heat transfer were made. However the clad burst temperatures, pressures and times were less well predicted and BART overestimated the time to initiation of entrainment of water drops early in the

reflood. The latter is a characteristic of many BART forced reflood test predictions. The quench front progression was also significantly underestimated by the code.

Temperatures downstream of the blockage were significantly overpredicted. This was partly due to the quench front underprediction but was mainly influenced by the premature wetting of the burst sites which occurred in the test. No codes are available which can calculate appropriately this powerful beneficial feature of this dynamic ballooning experiment.

Further calculations have been undertaken post-test after results of the data were released. These further calculations were based on a better definition of the test boundary conditions, included some changes to the BART modelling, and incorporated some further developments to the code, particularly related to the modelling of the initiation of droplet entrainment. These calculations have resulted in a significant improvement in the quench front modelling and reduced clad temperatures somewhat at upper elevations, though the code still overpredicts the data. More importantly, the post-test analysis has provided an accurate simultaneous calculation of burst strain, rupture time, burst temperature and burst pressure.

Flow blockage was overpredicted somewhat in both sets of analysis. This is to be expected since the calculational model assumes coplanar strain and rupture. There is some evidence that the external thermocouples may have influenced to a small extent the amount of non-coplanarity in the test. The premature quenching of burst sites is an obviously important feature of the REBEKA experiment that can significantly affect clad temperature results. The reproducibility of such effects for other fluid conditions is an area worth further investigation.

CONCLUSIONS

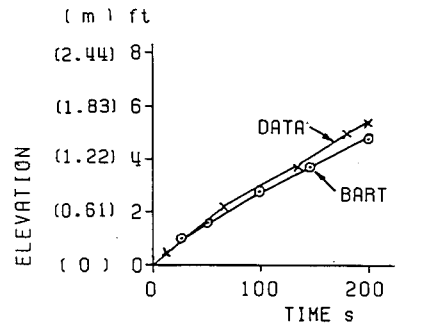
1. BART calculations of flow blockage tests in the FEBA and REBEKA facilities have been presented. These results indicate that the code can produce reasonably accurate or conservative predictions of the key data for the fluid conditions in these tests.
2. The comparison with test data had led to improvements in the code modelling. These improvements will, of course, also be tested against other experimental data.
3. The calculations and detailed examination of the data has led to increased understanding of a number of characteristics of the tests not modelled by the code including the influence of the shroud in FEBA, premature quenching of burst sites and possible effects of external thermocouples in REBEKA.

ACKNOWLEDGEMENTS

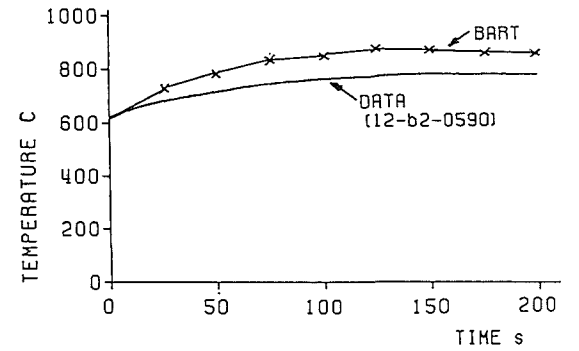
The authors would like to acknowledge the work of a number of Westinghouse staff involved in development of the BART code, particularly Mr. M.Y. Young and Dr.L.E. Hochreiter and other NNC staff including Dr. D.B. Utton, Dr. B.J. Holmes and Dr. G. Ahmed. Useful comments have been provided by a number of CEGB(UK) staff. In addition, valuable discussions on the data interpretation have been made with a number of KFK staff.

REFERENCES

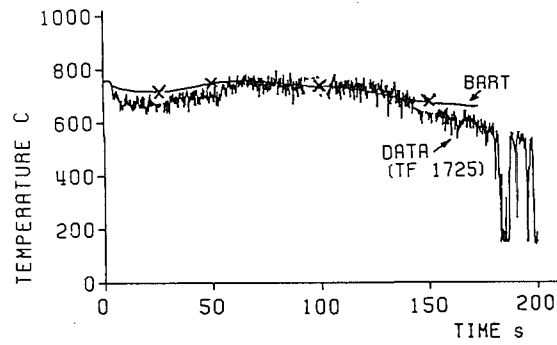
- [1] Spencer, A.C. and Young, M.Y.
"A Mechanistic Model for the Best Estimate Analysis of Reflood Transients (The BART Code)." 19th National Heat Transfer Conference (ASME), Orlando, July 22-30 (1980).
- [2] Ihle, P., et. al
"FEBA - Flooding Experiments with Blocked Arrays - Heat Transfer in Partly Blocked 25 Rod Bundle". 19th National Heat Transfer Conference (ASME), Orlando, July 22-30 (1980).
- [3] Karwat, H.
"International Standard Problem (ISP)14 - Behaviour of a Fuel Bundle Simulator During a Specified Heat-Up and Flooding Period (REBERA 6 Experiment)". 18th February, 1983. CSNI/OECD-Document SINDOC (83) 229.



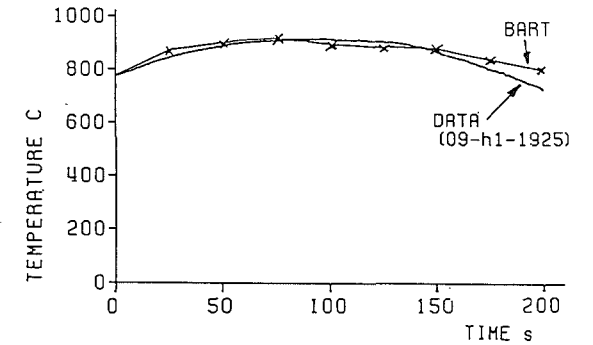
Quench Front Progression



Clad Temperature At 3.20 m (10.5 ft) Elevation

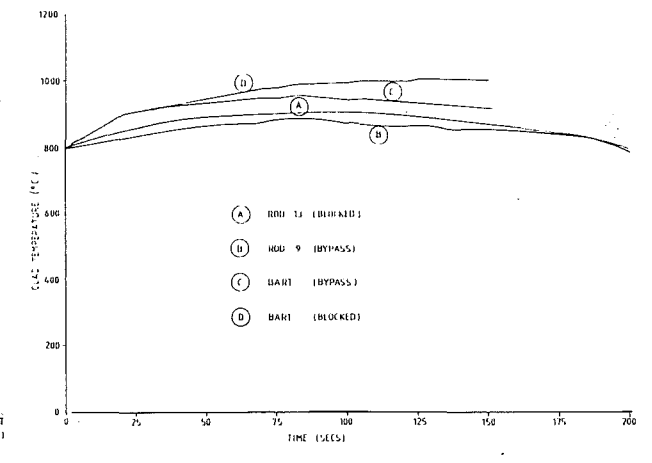
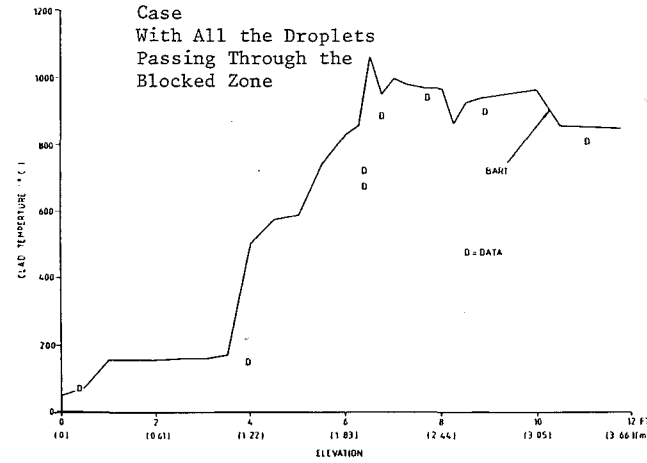
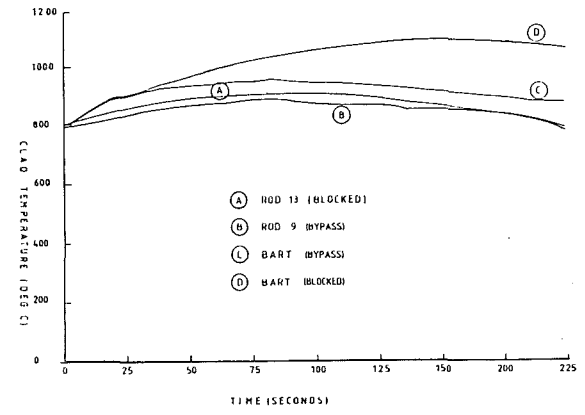
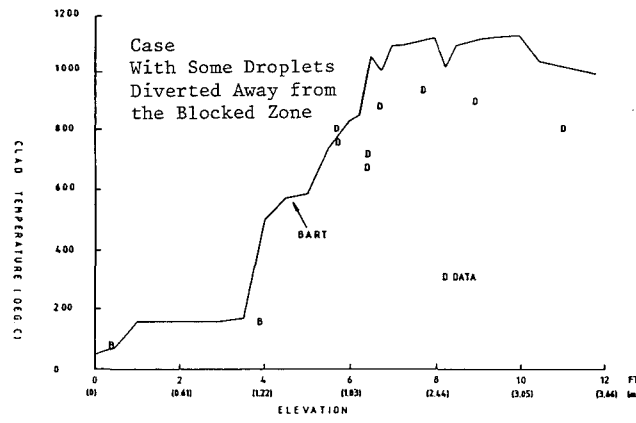


Steam Temperature At 2.29 m (7.5 ft) Elevation



Clad Temperature At 2.13 m (7 ft) Elevation Just Above Midplane

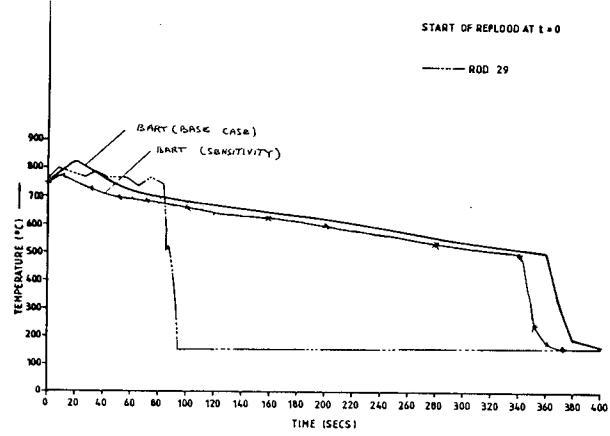
Figure 1 FEBA test 229 and BART results



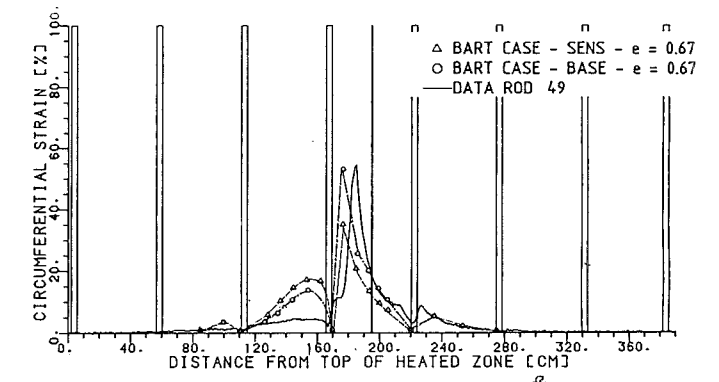
CLAD TEMPERATURE PROFILE AT 150 SECS IN THE TRANSIENT BLOCKED CHANNEL

CLAD TEMPERATURE FOR BLOCKED AND BYPASS CHANNELS
AT 2.13m (7.0ft) ELEVATION
JUST ABOVE BLOCKAGE

FIGURE 2 FEBA TEST 239 RESULTS

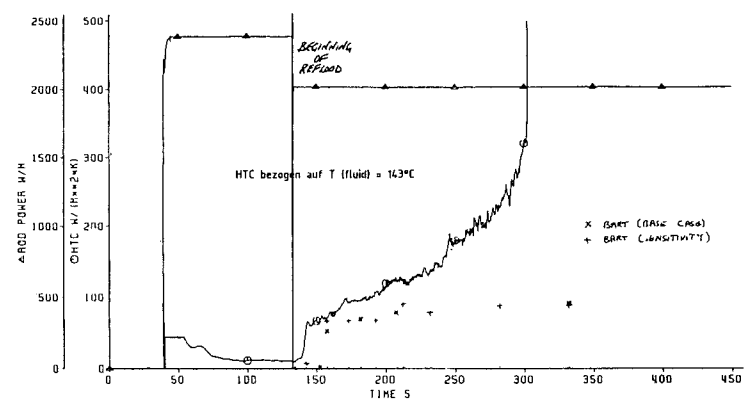


CLAD TEMPERATURE AT 2150mm — TIME (2225)



REBEKA 6

Comparison of BART Strain Profiles with That Measured for Rod 49



Comparison of BART/REBEKA 6 Heat Transfer Coefficients - Rod 14, Elevation 195 cm
FIGURE 3 REBEKA 6 RESULTS

IN-PILE INVESTIGATIONS AT THE PHEBUS FACILITY OF THE BEHAVIOR
OF PWR-TYPE FUEL BUNDLES IN TYPICAL L.B. LOCA TRANSIENTS
EXTENDED TO AND BEYOND THE LIMITS OF ECCS CRITERIA

J. DUCO, M. REOCREUX, A. TATTEGRAIN
Ph. BERNA, B. LEGRAND, M. TROTABAS

Commissariat à l'Energie Atomique, France

ABSTRACT

An in-pile investigation is currently carried out at the PHEBUS facility of the behavior of .8m active height, 25-rod PWR-type fuel bundles during simulated large-break LOCA (L.B. LOCA) reactor transients. A first series of six tests using pressurized rods is to be completed by the end of 1984, relative to a conservatively calculated 2-peak cladding temperature transient at the hot point, as considered in the French 900 MW(e) PWR standard safety report. The severity of such a transient has been increased in the tests so as to check the bundle behavior at the limits of the first two NRC ECCS criteria, which were, in fact, locally exceeded in one test. Three of the tests are reported on hereunder. Short coplanar cladding ballooning was observed at the hot point level, which resulted in maximum flow blockage ratios of about 50%. Severe cladding embrittlement against thermal shock and subsequent handling was observed in the test where the criteria were exceeded. Prediction of the overall thermal-hydraulic behavior in the bundle was good, using the RELAP 4 MOD 6 code. Cladding strains are generally overevaluated by codes such as FRAPT 4 or CUPIDON, which currently do not take into account azimuthal cladding temperature gradients. Other L.B. LOCA test series are envisaged from 1986 on, based on transients calculated with "physical" models.

OBJECTIVES

The general objective of stage 2 part 1 of the PHEBUS programme to be completed by the end of 1984 is to investigate the actual in-pile behaviour of .8m active height, 25-rod PWR-type pressurized fuel bundles, during the course of conservatively calculated L.B. LOCA 2-peak transients, such as those considered in the French 900 MW(e) PWR standard safety reports. The severity of the 2nd peak of such transients has been intentionally increased, by an adequate control of the driver core power and delaying bundle reflooding, so as to reach the NRC ECCS criteria limits, as regards maximum cladding temperature and maximum cladding oxidation (Fig.1); this is expected to provide insight into the adequacy and the possible margins of conservatism of such limits for zircaloy embrittlement against thermal shock on reflooding, once the cladding has endured the full 2-peak-type transient.

The particular objectives can be identified as follows :

a) the qualification in a bundle-type geometry of the cladding deformation and rupture models as derived from the single-rod EDGAR tests, and the supplying of adequate data sets for the qualification of any further development of these models which could be required ; a possible residual

effect on deformation of the brief cladding temperature foray beyond the α/β metallurgical phase transus at the first peak is particularly to be investigated ;

b) The assessment of the maximum flow blockage ratios that could be reached during the transient, their impact on possible cladding failure propagation modes, and the obtention of data which could be used to evaluate the coolability of damaged reactor assemblies ;

c) The supplying of data as regards cladding oxidation behavior : verification of the predictions given by current zircaloy oxidation models, axial extent of internal oxidation in failed rods, structure of oxidized cladding (extent of ZrO_2 , $\alpha - Zr(O)$ brittle layers, etc...) ;

d) The assessment of the actual capability of deformed claddings, oxidized up to 17% wall thickness according to a given temperature history, to withstand thermal shock during PWR prototypical refloodings ; the capability at ambient temperature for the bundle to resist other loads which might arise from post-test handling, storage and transport is also to be assessed.

The above objectives appear as the best compromise between some current safety analysis issues and the existing capabilities of the PHEBUS facility. PHEBUS will be stopped for one year at the end of 1984 and upgraded. The test campaign will be resumed in early 1986, involving L.B. LOCA (stage 2 part 2) and SFD experiments (stages 3 and 4 of the program). Among the new LOCA test series considered for implementation at that time, two serious candidates could be the following :

a) tests for assessing the impact of a significant burn-up on bundle behavior,

b) tests liable to give major long-ballooning channel blockages during blowdown. The latter case refers to milder transients than those considered in the current series, such as those which could be calculated with "physical" models. Flattening the present "peaky" axial power profile in the test bundle is a prerequisite, for which some technical solutions are being examined.

TEST MATRIX

The basic cladding temperature history to be simulated in this test series is a two-peak curve vs time after the onset of depressurization (Fig. 1). At the hot point, the temperature rockets within 10 sec to about 920°C at the first peak (which is 100°C higher than the α/β metallurgical transus of zircaloy), then drops rapidly below 800°C, before rising briskly to a maximum value which is attained in about 40-50 sec ; this maximum value is 1100°C or 1200°C as a goal, depending on the test. A temperature plateau is maintained at that level during such a calculated time interval as to attain a given oxidized fraction of the deformed cladding wall near the balloon ; in view of particular objective c, the chosen oxidized fractions cover a domain up to the 17% limit of NRC ECCS criteria as a goal. Then, depending on the test, the bundle is cooled slowly to preserve the deformed bundle geometry, or more rapidly aiming at the same reflooding velocity as in the PWR case (objective d). Cladding burst temperature is a test parameter which is chosen either at 810°C or 890°C as a goal. 890°C refers to the burst temperature as calculated for the reactor reference transient at the hot point and corresponds to the $\alpha+\beta$ phase of

zircaloy, whereas 810°C is a tentative to get a larger strain at burst, which derives from the fact that in the high α -phase, around 810°C, deformations at burst are larger (objectives a and b). The choice for these temperatures is based on characteristic values of metallurgical equilibrium states. Actually there will be in fact probable effects of phase change dynamic which will result from the quick temperature excursion beyond the α/β transus at the first peak during blowdown.

Six tests with pressurized bundles (test numbers 215 P and 215 R, 216, 217, 218 and 219) have been scheduled until the end of 1984- stoppage of PHEBUS.

Up to now, tests 215 P to 218 have been completed, but the last two too recently (test 217 carried out on 21 June and test 218 on 19 July) to provide more than general information. Test results presented hereinafter will therefore refer to tests 215 P, 215 R and 216, for which significant analysis work has been accomplished.

TEST PERFORMANCE

In order to apply to the fuel rods the desired transients as regards the cladding temperatures and the differential pressures across the clads, the test train is put in a loop (Fig.2) where the initial conditions reproduce steady state conditions of the power plant for pressure and temperatures. The transient conditions are obtained by insulating the test section of the loop containing the fuel bundle, then by opening two breaks, one on the cold leg and the other on the hot leg. The total area of the breaks is adjusted in order to get the desired system pressure history. The break area ratio is set up to simulate the flows on a power reactor which move to the break through the cold and hot legs, and therefore the flow through the core. The latter adjustment allows the control of the position of the stagnation point and thus the control of the heat transfer from the rods to the coolant, which means the obtention of the desired cladding temperature transient. At the end of the blowdown, the refill of the lower part of the loop is initiated, and is followed by the bundle reflooding at a controlled inlet flow-rate.

The adjustment of this operational procedure has been obtained during stage 1 of the PHEBUS program by an iterative approach between thermal-hydraulic code predictions and experimental results. 15 hydraulic tests with unpressurized rods have been performed to reach a satisfactory control of the transients applied to the bundle.

TESTS RESULTS

TEST 215 P

This test, which was the first to use 22 pressurized rods in a bundle, was carried out on 8 July 1982, with the 2-peak reference transient of Fig.1 as a goal, and relevant experimental results were reported on at the OECD-NEA-CSNI/IAEA Specialists Meeting at Riso, Denmark in May 1983. The fresh fuel was just preconditioned by previous adequate power cycling to fragment UO₂ pellets. The anticipated thermal evolution of the cladding was disturbed firstly by an early, unexpected, non-homogeneous rewet of the bundle during the

blowdown, which prevented the goal temperature of 920°C from being reached at the first peak, and secondly by three minor entrainments of water onto the bundle during the heat-up phase of the transient (Fig. 3), causing the downwards flow through the bundle to reverse at about 60 sec. The first event resulted in the enhanced development of large heterogeneities on cladding temperature histories which led to unsynchronized, anisotropic cladding deformations, and eventually to flow blockage ratios of 83% (six center rods with coplanar short balloons), 65% (nine center rods), and 48% for the whole bundle (apart from the unpressurized rods). The latter low value, which is of no concern for bundle cooling, is partly due to the flow reversal at about 60 sec, which caused the hot part of the bundle temperature profile - a rather peaky axial shape indeed - to move upwards and subsequently to provoke the ballooning and burst of outer rods at a level higher than the elevation where the central rods burst.

PIE results proved that maximum cladding oxidation is 5% close to the bundle power peak ; the extent of internal axial oxidation on both sides of the burst exceeds 50 mm for the center rods and is about 30 mm for the outer rods. UO₂ pellets are divided into 3 or 4 large fragments, which materially hinders any significant fuel relocation as the cladding balloons.

Five extra hydraulic tests with nuclear power, using unpressurized test trains, were conducted between October 1982 and April 1983, to adjust test parameters so as to avoid unwanted early rewet and insure all the phases of the reference transient. These led to the successful test 213 G on 14 April 1983, the parameters of which were used for the specification of test 215 R with a pressurized bundle.

TEST 215 R

This test was performed on 5 May 1983 with 22 pressurized rods. On Fig. 3 a typical cladding temperature history is represented for test 215 R. The cladding temperatures at the first peak of the reference transient attained the maximum value of 1030° C on central rod n° 18, but their average values were estimated at 850°C and 730°C for the central and external rods, respectively. After the expected temperature drop of 150 to 250°C at about 15 sec, due to the full opening of the hot leg break, the heat-up ramp, starting at a rate of 10°C/sec, caused a maximum temperature plateau of 1050°C to be reached without refill disturbances, which was maintained about 35 sec, before a progressive reflooding.

All rods actually pressurized burst at about 25 sec at a mean temperature of 850°C. Unexpectedly rods n°10, 15 and 18 did not burst, revealing an initial lack of tightness. PIE showed a better coplanarity in the bundle of the short balloons of the rods, just below core mid-plane, than in test 215 P. Unlike test 215 P, where the burst points of rods were turned towards the bundle center, ruptured parts of the claddings in test 215 R faced undeformed rods n°10 or 18 (Fig. 4) ; this is due to the fact that these last two rods are presumably the hottest in test 215 R. Due to large azimuthal cladding temperature differences, strains at burst and relevant sub-channel blockage ratios are similar to those obtained in test 215 P (Fig. 5). Total cladding oxidation reached a maximum of 15% of initial cladding thickness on rods n°8 and 13 at core mid-plane. Internal oxidation extended to 113 mm of the burst point on rod n°13, but a standard penetration is rather 70 to 80mm.

TEST 216

This test was intended to be a repetition of test 215 R on a new test train with 23 pressurized rods, more reactor specific as regards some fuel assembly features, like the metallurgical cladding variety or the use of mixing grids. As it so happened, on 1st December 1983, the first cladding peak temperature was attained as expected, but the temperature failed then to drop significantly, due to some misoperation of the break valves, so that cladding bursts were detected at the first peak. The subsequent heat-up phase procured unexpected plateau temperatures of 1350°C on the hottest rods, at the limit of the capacity of cladding thermocouples. Test control at the end of the 120 sec duration plateau was achieved by small repeated water injections, but the induced disturbances caused for some claddings rewets followed by dry-outs before final quenching (Fig.6). It has to be noted that throughout the test no temperature rise occurred which could not be finally controlled.

PIE revealed smaller cladding strains at burst than in the two previous tests, resulting in a maximum channel blockage ratio of about 40% for the external rods just below core mid-plane. Fractured claddings and free pellet fragments in the bundle (Fig.7) give evidence of severe embrittlement, but it is presently difficult to attribute such a damage to thermal shock or subsequent handling of the bundle.

Micrographic examinations of the claddings show that the maximum zirconia thickness reaches 75 μm and 62 μm on the external and internal sides of rod 9 cladding, respectively. The $\alpha\text{-Zr(O)}$ layer attains a maximum thickness of 140 μm on rod 9 and appears in general more severely cracked than the adjacent zirconia. Some indication of pellet-cladding reaction is visible on rod 17.

Although test 216 did not reach its original goals, it procures valuable information as regards the amplitude of cladding deformation at the first temperature peak where bursting occurred. Besides, cladding oxidation on some rods went beyond the relevant ECCS criteria limits, which resulted in significant embrittlement: further analysis should give additional insight into the actual margins of such criteria.

TEST INTERPRETATION

Due to the global character of the PHEBUS experiments, the interpretation has been focused on physical phenomenology and on global code verification.

Physical phenomenology is derived directly from the detailed analysis of the measurements and of the post irradiation examinations (PIE). After trying to understand qualitatively what happened, it was seen physically very clearly that the phenomena governing most of the fuel behavior are the thermalhydraulic events, including those occurring at the sub-channel scale.

Coplanarity of bursts depends upon each displacement of the hot spot. In test 215 P, flow reversal occurs between the burst of inner rods with a downwards flow and the burst of outer rods (upwards flow), which explains the location of bursts in two distinct regions (Fig. 5). In 215 R, flow remains upwards and leads logically to a better coplanarity at a higher level compared to 215 P.

Times of bursts depend upon times at which rupture temperatures are reached. In 215 P, a large scatter in times is observed due to early rewet which gives very heterogeneous initial conditions at the onset of the heat-up phase. In 215 R, temperatures are closer to each other, resulting in burst time differences as low as 2 sec for some categories of rods. Azimuthal cladding temperature differences are the cause of burst orientation and of large oxidation differences around a rod. Oxidation is more advanced on the parts of the rods which are expected to be the hottest as indicated by the burst orientation.

Tests 215 P and 215 R also show mechanical bundle effects, i.e. mechanical interactions between rods which depend on times of ballooning and burst.

Code verification is the second objective of test interpretation. The codes concerned are those which can currently be used for power plant safety evaluation in the LOCA case. The codes used are RELAP 4 MOD 6 for thermalhydraulics and fuel behavior, FRAPT 4 and CUPIDON - which constitutes the basis of the CATHARE fuel module - for fuel behavior, once the thermalhydraulic input is defined. Some CATHARE verification is envisaged in the future.

Successful prediction by RELAP 4 MOD 6 has been confirmed by the correct assessment of the overall thermalhydraulic behavior in PHEBUS tests (pressures, break flow, densities...) insofar as PHEBUS features could be adequately modelled.

When measured temperatures are used as an input data to the fuel codes or are calculated by RELAP 4 MOD 6 by some artifice, thermal behavior of the rods is predicted accurately (Fig. 8) provided all the details are correctly modelled (e.g. the thermocouple holes, power profile, ...). Oxidation is also correctly predicted using the usual correlations of these codes. However, the mechanical behavior is not as well predicted.

Table I shows that for test 215 P times and temperatures at burst are under-evaluated by FRAPT 4, slightly over-estimated by CUPIDON, quite correctly predicted by RELAP 4 MOD 6. The strains are in most cases significantly over-evaluated.

For 215 R test, times at rupture (Fig.9) seem to be better predicted : this could be due to a more rapid crossing of the rupture conditions resulting in less sensitivity to the models. Deficiencies in strain prediction are obviously due to azimuthal temperature differences which are not taken into account in these codes. Some calculations with RODSWELL show that introducing azimuthal heterogeneities on heat transfer and power generation improves strain predictions.

It is clear that the description of azimuthal effects must be introduced in codes if one wants to obtain realistic predictions. As the PHEBUS facility allows for global experiments only, where many effects are combined, a separate effect test program has been defined on the EDGAR rig. The following items are to be studied : impact of the actual material properties and geometry of the cladding, effect of azimuthal temperature gradient, axial stress and internal pressure feedback.

This separate-effect program as well as the next PHEBUS tests are due to give a better physical understanding of individual phenomena and provide challenging data for modelling improvements.

	Time t at rupture sec	Temperature at rupture °C	Internal pressure at rupture M Pa	Average strain (1)	Total strain (2)
RELAP 4	54	840	7.3	35%	-
FRAP T4	46	766	5.5	23%	-
CUPIDON	62	890	4.8	34%	65%
EXPERIMENT INNER RODS	46 < t < 66	~ 840	-	21%-34%	~ 52%
FRAP T 4	86	770	4.9	30%	139%
CUPIDON	170	847	3.5	50%	90%
EXPERIMENT OUTER RODS	-	≤ 830°C	-	8%-20%	15%-37%

(1) at the limit of the ballooned part of the cladding

(2) on the ballooned part of the cladding

TABLE I : PHEBUS TEST 215 P

CONCLUSION

A detailed control of the PHEBUS facility has been obtained, which eventually affords a substantial in-pile experiment potential for reproducing complex LOCA-type, thermal-hydraulic transients.

Although a full prototypicality of PHEBUS tests cannot be obtained, due to some peculiarities of the facility, such as its atypical bundle power profiles, L.B. LOCA experiments yield three kinds of valuable results :

- a) they provide additional elements of proof as regards the global core coolability in the LOCA case ;
- b) they constitute a research tool for identifying governing physical phenomena in complex real-life transients ; such an understanding is a prerequisite for insuring a comprehensive safety analysis ;
- c) they procure data sets for code verification and for improvement.

As regards item a) the main results of the PHEBUS tests reported on are the following : no runaway of Zr oxidation and no bundle coolability impairment were observed - no cladding embrittlement occurred provided the criteria were respected, but cladding fractured during reflood if they were not satisfied

(central part in test 216) - early cladding burst resulted in aborted deformation - there was no fuel relocation in deformed claddings, but only fresh fuel was used.

From these results two further themes are serious candidates for the definition of future tests :

- a slower transient in test trains with more uniform power profiles, so as to maximize flow blockage ;
- the possible relocation in significantly irradiated fuel, liable to procure a larger flow blockage.

For item b), PHEBUS tests highlighted the acute sensitivity of individual cladding histories, and resulting cladding burst strains, to the 3-D local, transient boundary conditions, such as the sub-channel flow fluctuations. As such similar variations are expected to occur to some degree in power reactor fuel assemblies, one may question if they do not definitely preclude a detailed, accurate code prediction of the phenomena happening in the reactor core during a LOCA transient. However, such heterogeneities enhance azimuthal cladding temperature variations and will lead to smaller channel blockage ratios than expected in a uniform temperature field.

As concerns item c), PHEBUS tests results confirmed the good quality of the RELAP 4 MOD 6 predictions for the overall thermal-hydraulics. Conversely fuel rod mechanical behavior in the bundle is not correctly predicted by currently available codes (FRAPT 4, CUPIDON). Some code improvements are presently achieved such as the modelling of the impact of azimuthal heterogeneities on cladding deformation. Besides, an out-of-pile, separate-effects test campaign has been initiated in the EDGAR fuel test rig for clarifying individual effects. A reasonable code development should ensue.

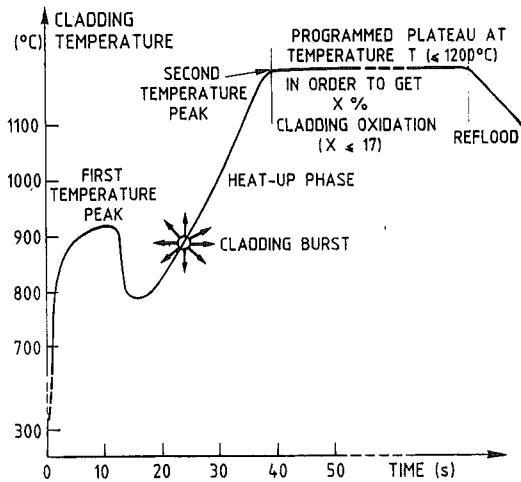


Fig. 1 : CLADDING TEMPERATURE TRANSIENT

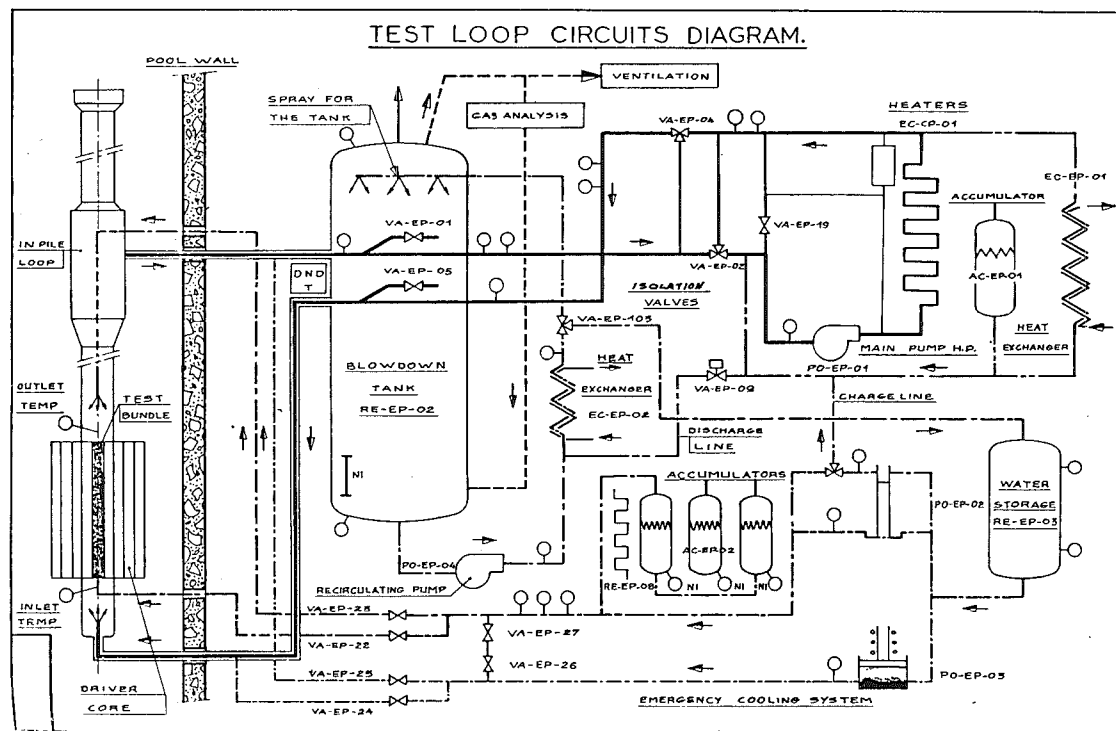


FIGURE 2

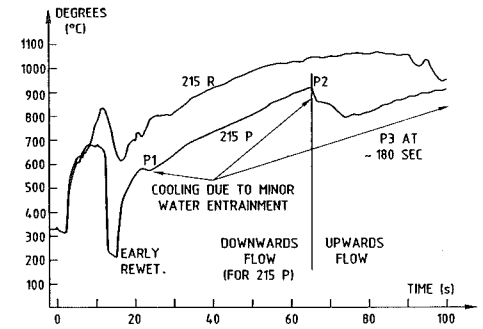


Fig. 3 : COMPARISON OF 215 P AND 215 R CLADDING TEMPERATURE TRANSIENTS

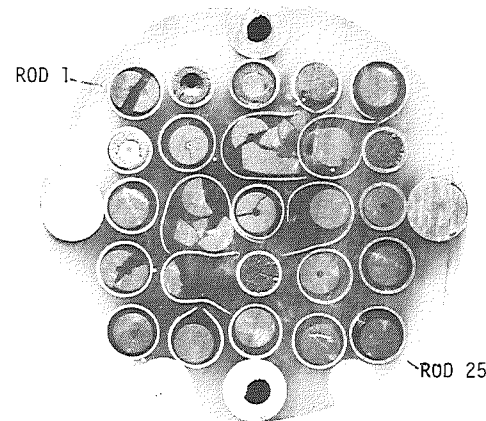


Fig.4 : PHEBUS TEST 215 R
BUNDLE SECTION AT ELEVATION - 7537
(37MM BELOW CORE MID-PLANE)

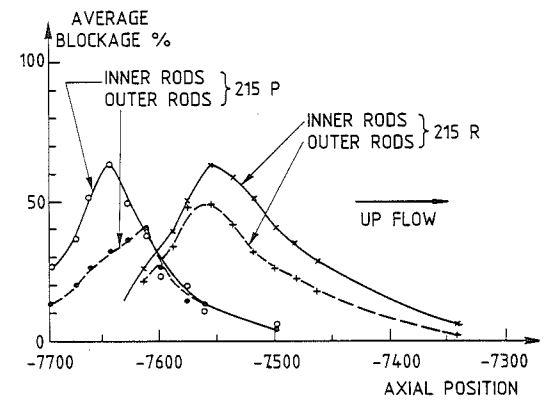


Fig. 5 : COMPARISON OF FLOW BLOCKAGE IN 215 P AND 215 R

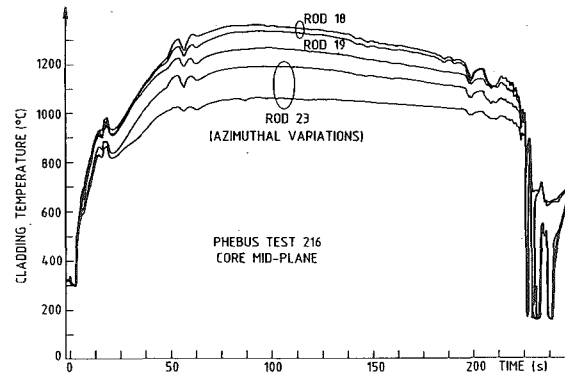


Fig. 6 : CLADDING TEMPERATURE - TEST 216

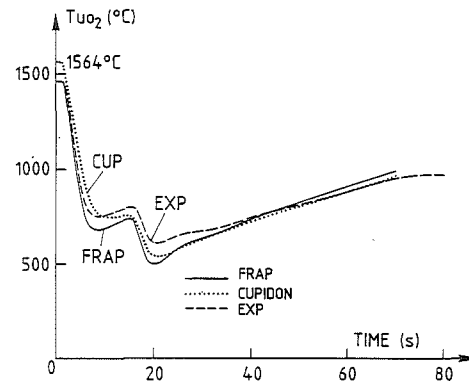


Fig. 8 : FUEL CENTRAL TEMPERATURE
TEST 215 P
ROD 9 ELEVATION - 7660

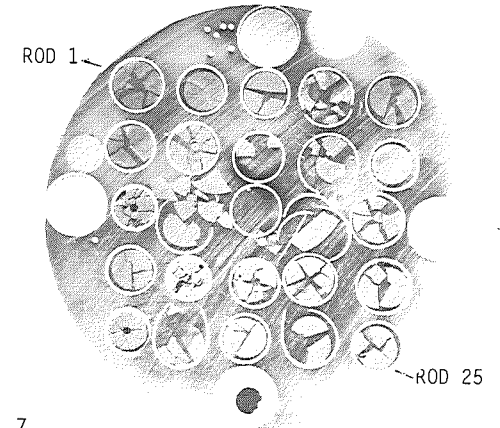


Fig. 7
PHEBUS TEST 216
BUNDLE SECTION AT ELEVATION - 7545
(45MM BELOW CORE MID-PLANE)

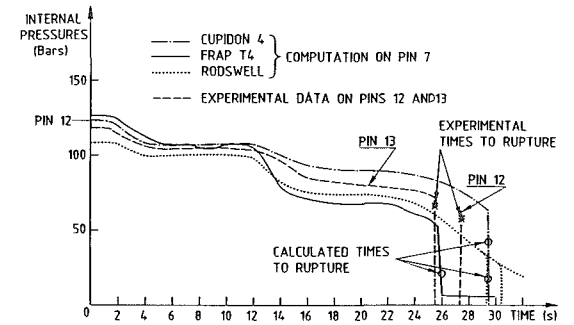


Fig. 9 : COMPARISONS OF EXPERIMENTAL DATA WITH
COMPUTATIONS BY CUPIDON 4, FRAP T4 AND RODSWELL
OF 215 R EXPERIMENT

RELAP5/MOD1 ASSESSMENT WITH LOBI-MOD1 TEST RESULTS

H.Staedtke, W.Kolar, B.Worth

Commission of the European Communities
EURATOM Joint Research Centre - LOBI Project,
Ispra Establishment, I-21020 ISPRA/Varese, Italy

ABSTRACT

Results of RELAP5 post-test calculations of selected LOBI-Tests, from the large and intermediate break LOCA test programme, are described. For each of these tests, two predictions have been performed using two different code versions of RELAP5/MOD1: (1) the original version of RELAP5/MOD1/Cycle 19 as received from INEL/Idaho and converted to the IBM/AMDAHL computer system at Ispra and (2) an updated version of RELAP5/MOD1 which includes several model improvements implemented at Ispra. Measured key parameters are compared with the predicted results and the existing discrepancies are analysed. Recommendations are given for further code improvements needed to increase the reliability of the code prediction and to speed up the calculation.

INTRODUCTION

The RELAP5/MOD1 code is at present extensively used at JRC-Ispra, within the framework of the LOBI Project, for pre-test and post-test analyses. The predicted results are mainly used to support the ongoing LOBI test programme. The experience gained with the code represents in addition a substantial contribution to the independent assessment of RELAP5.

The LOBI test facility shown in Fig. 1, is built and operated to investigate the thermal-hydraulic behaviour of a PWR under off-normal and accident conditions. The main aim of the LOBI test programme is to provide experimental data for the independent assessment and verification of large LWR safety codes /1/.

The LOBI test facility was originally designed to investigate large break LOCA transients (LOBI-MOD1 configuration). Within the period from December 1979 to June 1982, 25 large and intermediate break LOCA tests were performed. The

LOBI-MOD1 test programme covered the influence of break size, break location, downcomer configuration, pump control and ECC injection mode. During 1982/83, the test facility was substantially modified to meet the requirements for the investigation of small break LOCA and special transients (LOBI-MOD2 configuration). The LOBI-MOD2 small break LOCA test programme started in June 1984. The results of the small break experiments will not be released prior to the calculation deadline for International Standard Problem No. 18 (LOBI 1% break in the cold leg pipe).

LOBI TESTS SELECTED FOR RELAP5/MOD1 ASSESSMENT

From the LOBI large and intermediate break LOCA programme /2/ as carried out in the period 1979-82, the following tests have been selected as assessment cases:

Test A1-04, which was the first test of the programme, simulated a 2A-break in the cold leg pipe of a PWR. For this test, the power to the electrically heated bundle was shut off two seconds after the initiation of the blowdown. For this reason, the heater rod temperatures showed only a short period of deviation from nucleate boiling. The test is of interest for code assessment because there exists only a very small coupling between the thermal behaviour of the heater rod bundle and the fluid dynamics in the primary system. For the test, the upper head simulator was disconnected from the system. The test A1-04 was used for a Prediction Exercise (PREX) with international participation.

Test A1-04R was a repetition of test A1-04, but with an electrical power input which simulated the thermal behaviour of nuclear fuel rods including the effect of stored heat. The power to the bundle was shut off completely at 50 s transient time. In this test the upper head simulator was connected to the downcomer upper annulus and upper plenum. Both test A1-04 and test A1-04R were performed with the large downcomer gap width of 50 mm. As typical for the LOBI facility with this downcomer configuration, an extended positive core mass flow resulted in an early rewet of the heater rods during the blowdown period.

Test A1-66 was the first test after the gap width of the internal downcomer had been reduced from 50 mm to 12 mm. The test was a simulation of a 2A-break in the cold leg pipe of a PWR. The reduced downcomer volume resulted in a more reactor typical core mass flow and heater rod temperature behaviour during the blowdown period. However, the small downcomer gap width of 12 mm led to a delay in the penetration of the ECC water into the pressure vessel.

Test A1-06 was a repetition of test A1-66 with nearly the same initial and boundary conditions. The only difference to test A1-66 was the combined ECC injection as typical for the German KWU PWR power plants. The ECC water from the accumulators was injected into the intact loop hot and cold leg and into the broken loop hot leg. For both tests A1-66 and A1-06, the electrical power to the heater rod bundle was shut off at 30 s after blowdown initiation.

CODE VERSIONS USED FOR TEST PREDICTIONS

For the selected tests, post-test predictions were performed with two different versions of the RELAP5/MOD1 code /3/.

- (i) the original INEL, Idaho, version of RELAP5/MOD1 converted to run on the IBM/AMDAHL computer system at Ispra /4/. The conversion of the code started with the CDC version of RELAP5/MOD1/006 distributed at the RELAP5 Workshop at Idaho Falls in 1981. Several updates were later incorporated into this code version. The predicted results shown were performed with RELAP5/MOD1/019. A number of test cases have been performed using both the CDC and the IBM/AMDAHL version to ensure the correct implementation of the code on the AMDAHL computer. The Ispra-IBM/AMDAHL version of RELAP5/MOD1/019 is available via the NEA Data Bank in Paris.
- (ii) the updated version of RELAP5/MOD1/019 which includes various JRC model improvements.

The main improvements in the JRC updated version of RELAP5/MOD1 concern changes to the following models and subroutines:

- In the non-equilibrium evaporation and condensation model the mass transfer equation was re-written taking into account a clear distinction between the transport coefficient and the 'driving force', e.g. the difference between the actual vapour quality and the corresponding equilibrium value. The equilibrium vapour quality was redefined to give finite 'driving forces' also in cases when one phase vanishes. Subroutines changed: MDOT and EQFINL.
- New relations have been introduced to calculate junction properties for low flow velocities (near stagnation conditions). A relaxation technique is applied for the transition from near stagnant junction properties to the donor volume approach for large flow velocities. The reason for this modification is to avoid discontinuities in cases of flow reversals which frequently occur during the transient, especially in bypass junctions and in connections to dead-end volumes. Subroutine changed: JPROP.
- The finite difference form of the momentum flux form was re-written to avoid unrealistic flow behaviour in case of large density (void) differences between adjacent volumes. Subroutine changed: VEXPLT.
- In the following cases, the criteria for flow regime selection were changed:

Annular flow map: the lower limit for the occurrence of pure annular flow (without any entrainment or de-entrainment of droplets) was increased from $\alpha_g = 0.2$ to $\alpha_g = 0.65$.

Horizontal flow map: the upper boundary of the transition region between stratified flow and various other flow regimes was enlarged from $G = 200 \text{ kg/m}^2 \text{ s}$ to $G = 600 \text{ kg/m}^2 \text{ s}$.

A more continuous interpolation was introduced for the transition regions between different flow regimes.

- The averaging procedure for the interphase drag was changed for junctions incorporated in branch components to avoid unrealistic mass distribution during ECC injection.

- In the original INEL version of the code the thermodynamic fluid quantities within a volume are evaluated from a set of steam-water property tables by interpolation routines which leads to inherent discontinuities in state derivatives. In the JRC Ispra version of RELAP5 the property tables and interpolation subroutines have been replaced by analytical formulations based on the Helmholtz equation. The new method has been proven to be as fast as the table interpolation procedure with the advantage of consistent property data, high accuracy and reduced core memory.

All these modifications are directed towards increasing the reliability of the predicted data and reducing the large CPU time needed for slow transients.

The test predictions were performed with frozen load modules of the original INEL version of RELAP5/MOD1/Cycle 19 and the JRC-Ispra updated version of this code. No further updates have been incorporated between the test predictions. For all the predictions the same base input data set was used for the LOBI test facility. A total of 146 control volumes and 147 heat structures were used to model the primary system and the secondary sides of the two steam generators. The large number of heat structures were necessary to model properly the heat release from the structural material of the test facility to the fluid. The input data were modified only to describe hardware modifications or different initial and boundary conditions between the different tests. The nodalization scheme as used in the predictions is shown in Fig. 2.

COMPARISON OF PREDICTED AND MEASURED DATA

Examples of predicted and measured key parameters are shown in Figs. 3 to 14 for tests A1-04 and A1-04R. Both tests show a similar behaviour for the fluid dynamic parameters. However, considerable differences in the heater rod temperature response are indicated due to the differences in the electrical power curve.

Blowdown Period prior to ECC Injection

During the high pressure blowdown phase prior to ECC injection from the accumulator ($p > 2.7$ MPa) the predicted parameters of both RELAP5 versions used show a good agreement with the corresponding measured data. This good agreement includes absolute pressures, differential pressures, fluid temperatures, fluid densities and mass flows. For the electrically heated bundle (directly heated rods) the time to DNB, the first temperature maximum and the subsequent rewet behaviour (if rewet occurred) was correctly predicted.

During the intermediate blowdown period (system pressure $6.0 \text{ MPa} > p > 2.5$ MPa) a tendency exists in all calculations to overpredict the depressurization of the primary system (Figs. 3 and 4). This could not be corrected by a reasonable break flow multiplier (all predictions were performed with break flow multipliers of 1.00 for subcooled and 0.85 for saturated conditions upstream of the break). The overprediction of the depressurization seems to be caused by the choking model of the code which does not correctly calculate the mass and energy release through the break for the wide range of pressure values and vapour qualities as occur upstream of the break during the LOCA transient. For example the choking model does not account properly for the steep pressure gradient near the break and the related changes of fluid properties between the upstream volume and the break junction.

Refill Period after Start of the ECC Injection

Due to the overpredicted depressurization, the start of the ECC injection from the accumulator(s) was calculated to occur 2 to 3 s earlier compared with the experiments. For all the 2A-break test predictions, the original INEL version of RELAP5/MOD1 failed due to inherent flow instabilities which occurred after the pipe near the ECC injection point was nearly filled with subcooled water. The predictions were terminated with steam property errors after unrealistic high fluid temperatures occurred in the pipe between the intact loop pump (still running with 60% of nominal speed) and the ECC injection point.

With the JRC version of RELAP5/MOD1, the predictions could be continued through the refill period of the transient without any stability problems. The predicted thermal-hydraulic parameters agreed reasonably well with the measured data. However, during the late blowdown/refill period ($p = 1.0$ MPa) some of the measurement signals (e.g. differential pressure, flow velocities, flow drags) are reduced to very low values which are of the same order of magnitude as the uncertainty band of the measurement. For this reason, no data evaluation could be done for the mass flows, flow velocities and flow directions during the low pressure period of the transient.

Relatively large uncertainties have been obtained for the prediction of heater rod temperatures during the later period of the transient, as shown in Figs. 12 to 14 for test A1-04R. Although the time to dry-out (if dry-out occurred), was reasonably well calculated, the predicted heater rod temperatures deviated from the measured values by up to 150 deg C for test A1-04R and even more for the tests with the small downcomer gap width (tests A1-66 and A1-06). A general tendency exists to overestimate the heater rod temperature in the lower bundle region and to underpredict the heater rod temperature in the upper part of the bundle. This discrepancy, which indicates insufficient phase separation in the core region, could be reduced in the JRC version of the code. Parametric studies which have been performed for test A1-66 show that the predicted heater rod temperatures are very sensitive to small variations of the vessel and pump side break flows. For this reason it is believed that the deviations of the predicted heater rod temperature are mainly caused by incorrectly calculated fluid conditions in the core region, e.g. mass flows, phase velocities and vapour qualities. Other contributions to the deviation of the predicted heater rod temperatures might be the underestimated extent of phase separation (i.e. two-phase flow conditions are treated as being too homogeneous) and the restriction that the least massive phase is always saturated. This assumption of a partial equilibrium prevents the prediction of superheated vapour for low qualities but high void fractions ($g = 0.96$) in the low pressure region.

CONCLUSIONS AND RECOMMENDATIONS

Post-test predictions have been performed for selected tests from the LOBI-MOD1 large break LOCA test programme with two different code versions of RELAP5/MOD1: (1) the original INEL version of RELAP5/MOD1/Cycle 19 and (2) an updated version which includes several model improvements implemented at JRC-Ispra. Apart from a slight overprediction of the depressurization rate, both code versions showed a good agreement with measured data during the blowdown period prior to the ECC injection.

Due to inherent flow instabilities, the INEL version of RELAP5/MOD1 failed to predict the refill period of the transient. The JRC version of the code continued through the refill period without any stability problems and gave satisfactory agreement with most of the measured data. However, relatively large uncertainties have been obtained in predicting the heater temperatures for the intermediate and late period of the transient.

To increase the reliability of the RELAP5 code for large break LOCA predictions, a further effort is needed to improve the following code models:

- non-equilibrium evaporation/condensation models
- critical mass flow calculation (choking model)
- flow regime criteria (flow maps) and interphase drag calculation
- heat transfer during transition and film boiling

Some of these items are addressed in the development of RELAP5/MOD2.

REFERENCES

- /1/ W. L. Riebold, H. Staedtke:
LOBI-Influence of PWR Primary Loops on Blowdown. First Results.
ANS 27th Annual meeting, June 7-11, 1981, Bal Harbour, Florida/USA.
- /2/ W. L. Riebold:
LOBI Experimental Programme A, Test Matrix Part A1 and A2
Technical Note No. I.06.01.111.79, November 1979.
- /3/ V. H. Ransom et al:
RELAP5/MOD1 Code Manual, Volume 1: System Models and Numerical
Methods; Volume 2: User Guide and Input Requirements,
NUREG/CR-1826, EGG-2070, Idaho National Engineering Laboratory,
March, 1982.
- /4/ W. Kolar, W. Brewka:
The IBM-Version of RELAP5/MOD1, EUR 6977 EN, Joint Research
Centre, Ispra Establishment, Italy, 1983.

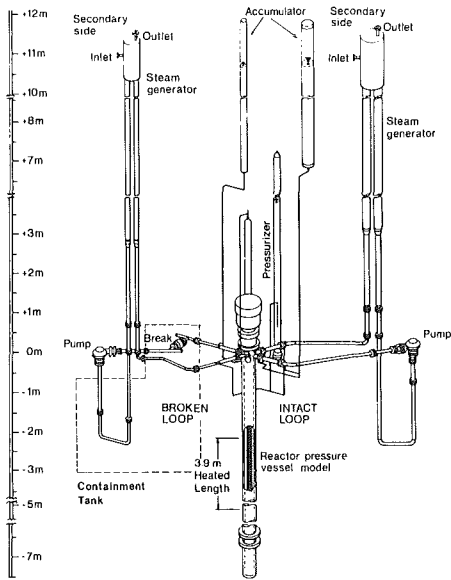


Fig. 1 LOBI MOD1 Test Facility with

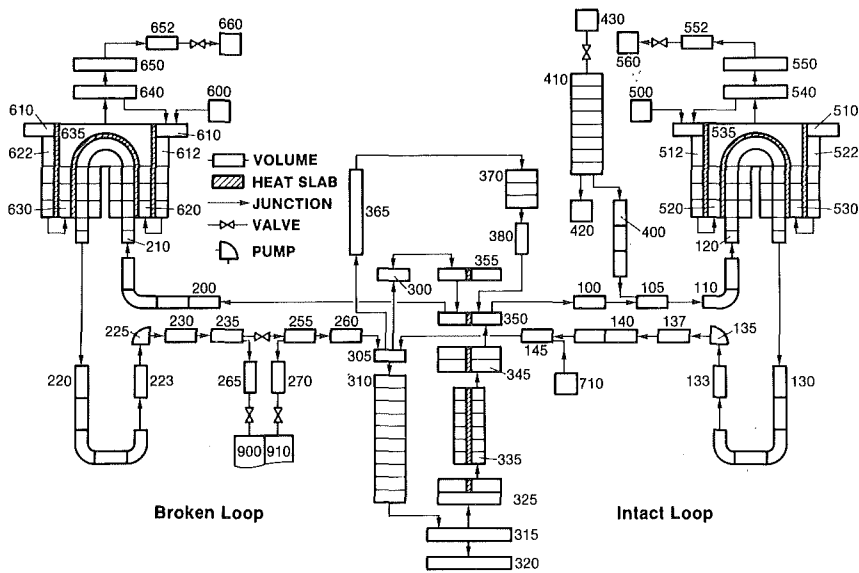


Fig. 2 LOBI-MOD 1 RELAP5-Nodalization Scheme

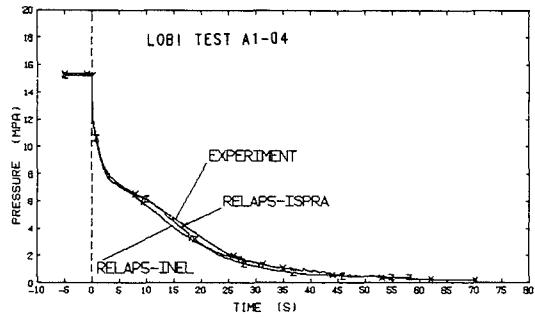


FIG 3 PRIMARY SYSTEM PRESSURE INTACT LOOP HOT LEG

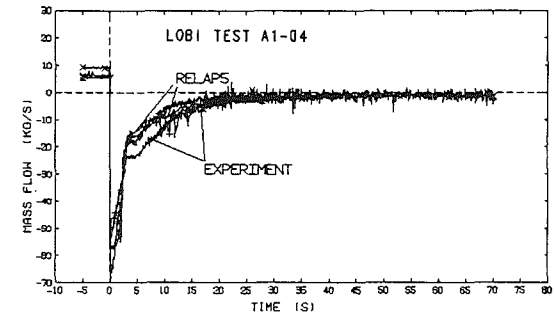


FIG 4 MASS FLOW IN BROKEN LOOP COLD LEG UPSTREAM VESSEL SIDE BREAK

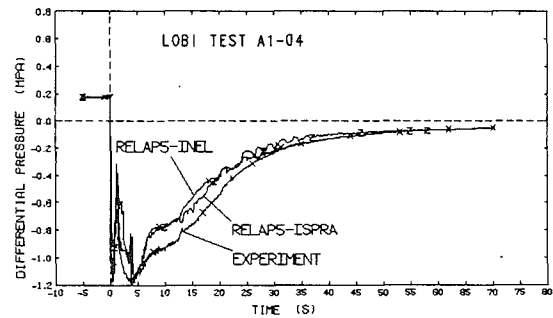


FIG 5 DIFFERENTIAL PRESSURE OVER BROKEN LOOP PUMP

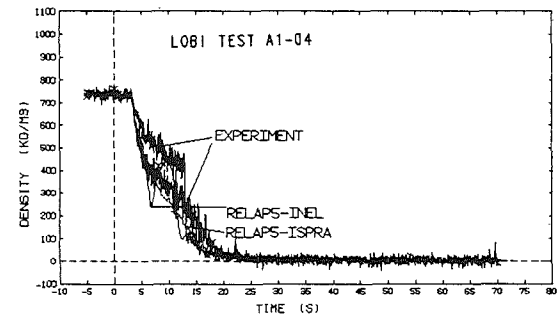


FIG 6 FLUID DENSITY IN INTACT LOOP COLD LEG PUMP INLET

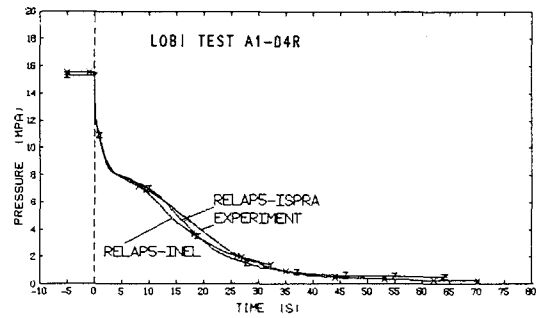


FIG 7 PRIMARY SIDE SYSTEM PRESSURE
INTACT LOOP HOT LEG

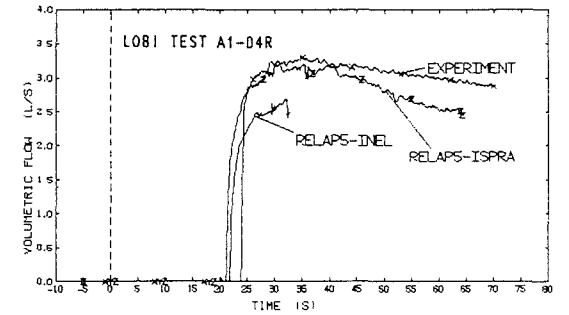


FIG 8 ECC INJECTION MASS FLOW FROM ACCUMULATOR

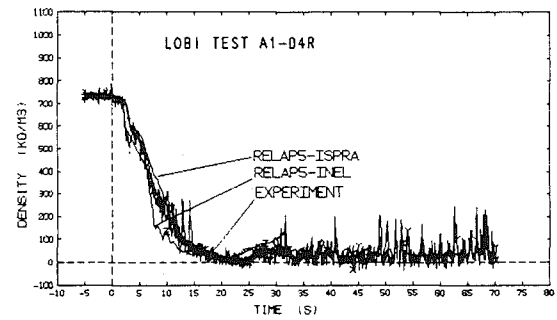


FIG 9 FLUID DENSITY IN BROKEN LOOP COLD LEG
BETWEEN BREAK AND PRESSURE VESSEL

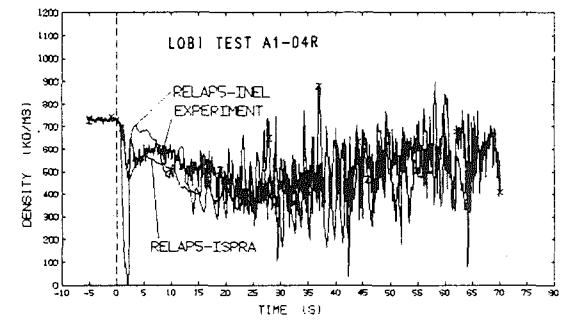


FIG 10 FLUID DENSITY AT CORE ENTRANCE

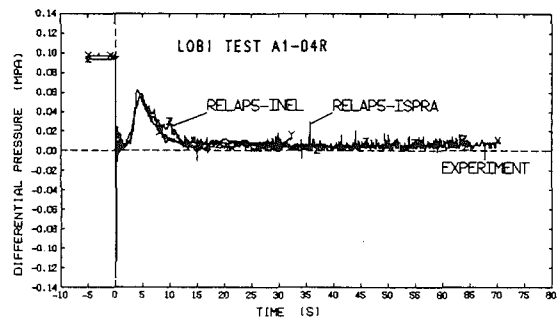


FIG 11 DIFFERENTIAL PRESSURE OVER CORE HEATED LENGTH

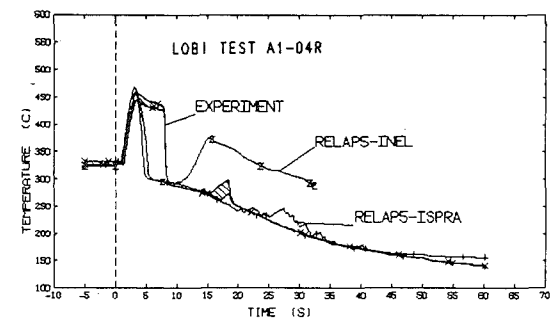


FIG 12 HEATER ROD SURFACE TEMPERATURES LOWER INTERMEDIATE SECTION OF HEATED LENGTH

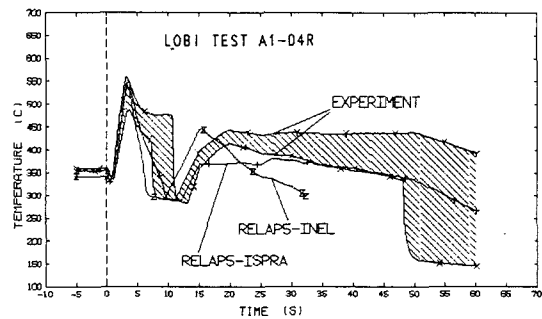


FIG 13 HEATER ROD SURFACE TEMPERATURES UPPER MIDDLE SECTION OF HEATED LENGTH

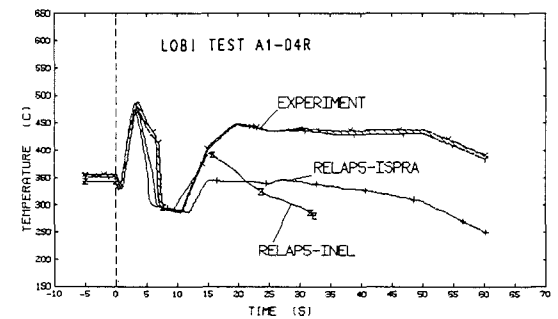


FIG 14 HEATER ROD SURFACE TEMPERATURES UPPER INTERMEDIATE SECTION

THE CATHARE CODE DEVELOPMENT

J.C. ROUSSEAU*, G. HOUDAYER**, M. REOCREUX***

Centre d'Etudes Nucléaires de Grenoble

Abstract

The CATHARE code is a best estimate code for simulation of PWR loss of coolant accidents. It is developed by the french CEA, EDF and FRAMATOME

This paper deals with the objectives and fundamental characteristics of the code. The assessment strategy is presented, based on a large analytical experiment program (qualification) then on a verification procedure on global experiments.

Finally some reactor calculations with CATHARE are presented.

I. CATHARE FRAME AND OBJECTIVES

The CATHARE code development is a joint effort of CEA* (Both IPSN* and IRDI* institutes) and EDF*, with the participation of FRAMATOME.

CATHARE is a best estimate code aimed to the simulation of pressurized water Reactor loss of coolant (large and small break) and any transient.

Moreover, CATHARE is used as a basis for a simulator development.

In order to develop the CATHARE code, an important experimental program has been carried out over the ten past years ; this program includes analytical experiments upon two-phase flow behaviour, heat transfer and component tests.

CEA : Commissariat à l'Energie Atomique
IPSN : Institut de protection et de Sécurité Nucléaire
IRDI : Institut de Recherche et Développement Industriel
EDF : Electricité de France

*J.C. ROUSSEAU - CEA-IRDI-DEDR-STT Centre d'Etudes Nucléaires de Grenoble

**G. HOUDAYER - EDF-SEPTEN (69) Villeurbanne

***M. REOCREUX - CEA-IPSN Fontenay aux Roses

Finally, the verification of the CATHARE code will be partially based on the BETHSY integral test program.

II. CATHARE CHARACTERISTICS

Physical Characteristics

CATHARE simulates all the thermalhydraulics phenomena which occur in the primary circuit of a PWR during a loss of coolant accident. (Some other phenomena which are strongly connected to the thermalhydraulics are also described, such as : neutron kinetics, fuel thermal mechanical and chemical behaviour).

In order to get a good representation of any two-phase flow behaviour, the physical model must take into account all the mechanical and thermal non equilibria of each phase.

Consequently, the thermalhydraulics 1D. two fluid model is needed.

In such a model, the mass, energy and momentum conservation equations are written for each phase (six partial differential equations).

Energy and momentum interactions between liquid and vapor appear in these equations and constitute the constitutive laws of the model.

The constitutive laws are the actual physical basis of the model. CATHARE contains a very specific and unique set of constitutive laws, which are issued from a very large analytical experiment program.

Numerical and structural characteristics of the code

The CATHARE code is structured such that it can describe different types of installations : Reactors with 3 or 4 loops, integral loops, experimental test sections etc...

This objective led to a modular structure of the code ; any circuit is decomposed into components, which are linked together in order to represent any topology.

These components can be pipes, volumes, pumps, or tees, etc...

CATHARE contains an actual steady state calculation, using the same physical model as the transient calculation. For transient, a fully implicit finite difference scheme is used, which allows generally large time steps, with no stability limit.

Finally CATHARE contains a specific software for data acquisition and for post-processing (graphics, CRT display) which makes the code very easy to handle, and facilitates the analysis of a calculated sequence.

III. REPRESENTATION OF A REACTOR CIRCUIT WITH CATHARE

One-dimension component : (1.D : 2 fluid model). This component is used for representation of any pipe of the reactor, associated with a 1D radial conduction for simulation of the walls. The reactor core is represented by one or several parallel channels. (No cross flows are simulated in the present CATHARE version). A 2D (r, z) conduction calculation is used for computation of the quench front velocity.

Clad deformation is calculated by a mechanical model up to the rupture. Nevertheless, this deformation does not affect the pipe geometry for flow calculation.

Clad oxydation and energy release are taken into account.

The secondary circuit of the steam generators is point in the present version of CATHARE. A complete representation of the secondary system with a 1D model is underway.

Volumes :

A simulation of the volumes (upper or lower plenum) with a 3D two-phase flow model has not been considered, taking account of its complexity and no evidence of physical improvement (entrainment or de-entrainment in a geometry with complex internal structures).

A two point model has been preferred. The volume is then divided into two parts separated by a moving interface. The lower sub-volume simulates a liquid continuum with rising bubbles ; the upper sub-volume simulates a vapor continuum with falling droplets. Both sub-volumes may be in non-equilibrium.

Pumps :

They are simulated by local momentum and energy source terms on a pipe. These source terms come from homologous curves for head and torque, with possible degradation due to two-phase flow.

A scheme for a reactor primary circuit with CATHARE is presented on figure 1.

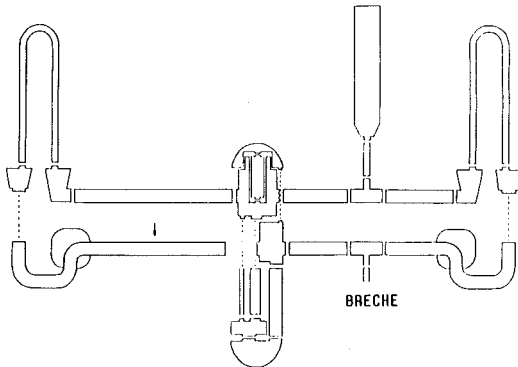


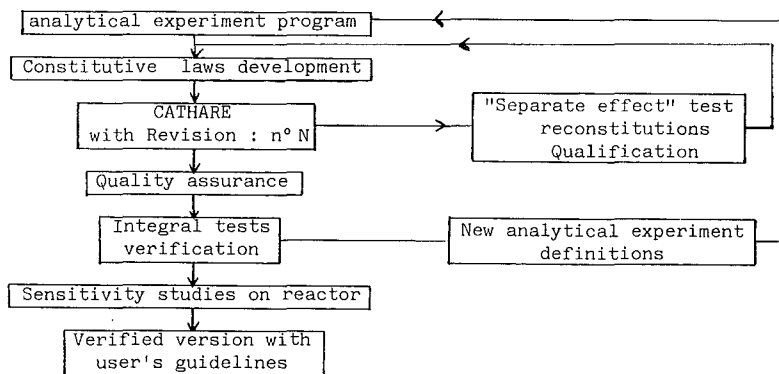
Fig. 1 : REACTOR PRIMARY CIRCUIT REPRESENTATION

IV. ASSESSMENT STRATEGY OF CATHARE

Preliminarily, some peculiar definitions of the CATHARE assessment have to be specified :

- 1 - A Revision of the CATHARE physical laws corresponds to a coherent set of constitutive laws, issued from the analysis of analytical or "separate effect" tests of the CATHARE experimental program.
- 2 - Qualification procedure :
A given Revision, introduced in CATHARE is submitted to reconstitution of "separate effect" tests. This confrontation identifies the physical imperfections of the model and defines the points which need new physical developments.
- 3 - The quality assurance procedure is a planned and systematic pattern of analytical experiment reconstitutions, which is attached to a Revision and is used as a quality reference.
- 4 - Tests on integral experiments constitute the verification procedure. The observed discrepancies between experiment and calculation during this procedure have no direct impact on the physical model of the code. They only may suggest new analytical studies for analysis of new phenomena, or give user's guidelines.

The assessment strategy can be represented on the following scheme :



IV.1 The CATHARE analytical experiment program

The two fluid model contains constitutive laws which must be established by means of analytical experiments. These constitutive laws are the mass, momentum and energy transfers between phases, and the wall.

Experiments were designed in such a way that these transfers could be separately studied.

Then, the program consists of four types of experiments, of increasing complexity :

- . Momentum transfer experiments
- . Mass transfer experiments
- . Heat transfer experiments
- . Component experiments

IV.1.1. Momentum transfer experiments :

- Air water Moby Dick experiments ($\alpha < 0.6$)

These experiments are performed at low pressure, low void fraction and high velocities, in tubes 0.014 m ID.

- For higher void fraction, ($\alpha > 0.6$), the DADINE experiment simulates steady state flows in a tubular test section (0.012 m ID) at low pressure. Mass flow rates and heat fluxes are low (0.2 to 1 kg/m²/s, 10⁴ To 5.5.10⁴ W/m²). The original feature of this experiment is the void fraction measurement technique, which uses the scattering property of a thermal neutron beam. This technique gives a high resolution in the range of high void fractions in dispersed flow.

- Mist flows at high velocities up to the critical conditions, low pressure, very high void fractions ($\alpha > 0.96$) are studied in REBECA experiment

- The ECTHOR experiments simulate steady state air-water flows in a tubular horizontal test section at atmospheric pressure. They give informations upon stratification occurrence and mechanical interactions in stratified flows.

- Finally, in order to cover the whole range of pressure and dimension parameters, different test sections have been introduced in the Super Moby Dick loop, in vertical and horizontal conditions, pressure varying from 20 bars to 120 bars and diameter up to 0.135 m.

IV.1.2. Mass transfer experiments

The mass transfer model for CATHARE is essentially issued from the analysis of the MOBY DICK CF and SUPER MOBY DICK CF experiments.

Both test sections consist of a vertical channel (0.014 or 0.02 m ID) followed by a 7 degree straight divergent. The inlet flow is subcooled and a steam water flow develops in the test section by flashing. Downstream pressure is decreased to obtain critical conditions. Pressure and void fraction are measured along the test section. A large range of pressure from 1 bar to 120 bars is investigated.

IV.1.3. Heat transfer experiments

The OMEGA loop is used for tubular or rod cluster blowdown tests in order to study transient two-phase flow heat transfers.

The blowdown experiments consist in depressurizing a highly pressurized vertical electrically heated test section (tube or 36 rod cluster) in full length. The test section is strongly equipped with wall thermocouples. Spool pieces are set at both ends of the test section. They consist of

a γ beam densitometer, a venturi and a turbine allowing a good evaluation of transient two-phase mass flow rates.

The ERSEC experiments are used to evaluate the quench front velocity and the heat transfer downstream of the quench front in reflooding conditions. The tests are performed with an electrically heated tube (0.012 m ID) and a 36 electrically heated rod bundle. Wall temperatures, test section pressure drop, carry-over and vapor temperature at the outlet are measured.

For these reflooding tests, inlet mass flow rate and quality are set. More recently, the PERICLES experiment (357 heated rods) investigates reflooding complex effects due to radial power distribution.

IV.1.4. Component experiments

- Pumps behaviour in two-phase flow have been studied in the EVA (1/3 scale) and EPOPEE (1/10 scale) apparatus.

- Two-phase flow in the lower plenum of the vessel has been analysed in the 1/4 scale air-water PIERO experiment.

IV.2. General approach for the constitutive laws development

The momentum transfer experiments (see IV.1.1) have been used to elaborate a set of coherent mechanical interaction laws involving : wall-liquid friction, wall vapor friction and interfacial friction. The method of elaboration is very systematic : It uses an "inverse" version of the 1D module of CATHARE which is applied to any experimental result .

This method gives rise to the realization of data banks :

$$[\tau_i, \alpha, v_l, v_v, h_l, h_v, p]$$

Then correlations are developed by taking account of some pre-established structures :

$$\tau_i = \xi(\alpha, p, v_l, v_v, D) \cdot \rho_l \cdot \frac{(v_v - v_l)^2}{D}$$

A representation of the interfacial friction factor ξ introduced in the current CATHARE revision is presented on figure 2

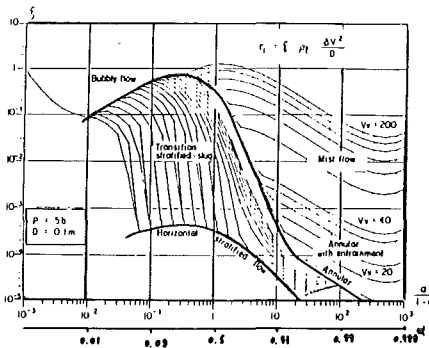


Fig. 2 : CATHARE INTERFACIAL FRICTION FACTOR

The method of analysis of the mass transfer experiments is very similar to the previous ones.

Assuming that mechanical laws are still valid in case of interfacial mass and energy exchanges, the use of the "inverse" 1.D. CATHARE module provides a new data bank.

$$[\Gamma, \alpha, v_l, v_v, h_l, h_v, p]$$

which leads to correlations under the form :

$$\Gamma = f(\alpha, p, v_l, v_v), (h_l - h_{l\text{sat}})$$

Finally, wall heat transfer correlations are developed from the diabatic experiments by using the evaluated values of the local state of fluid $(\alpha, h_l, h_v, v_l, v_v)$ resulting from the interfacial transfer laws.

IV.3. Code qualification

The comparison of CATHARE calculations with "separate effect" test results constitutes the qualification procedure. It allows the determination of the interval of confidence for each physical correlation, the identification of the weaknesses and the definition of new needs for the next revisions.

The "separate effect" test comparison deals with the following topics :

- critical flow
- blowdown of an unheated test section
- swell level
- reflood
- blowdown of a heated test section
- wall condensation

. critical flow : Tests belonging to the Moby Dick and Super Moby Dick program are selected. They cover the range of parameters $1 \text{ bar} < p < 120 \text{ bar}$

$$0 < \Delta T_{\text{sub}} < 70^\circ\text{K}$$

$$0 < X < 10\%$$

with long or short nozzles.

Figure 3 presents typical results of pressure and void fraction evolutions along the nozzle.

Marviken CFT tests (nozzle alone) are also involved in the qualification matrix, for large dimension nozzles.

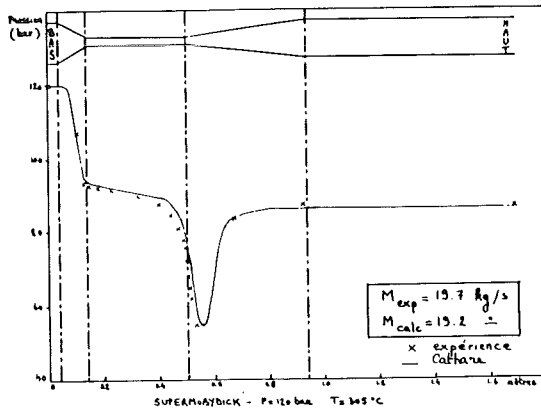


Fig. 3 a. : SUPER MOBY DICK TEST SECTION PRESSURE PROFILE

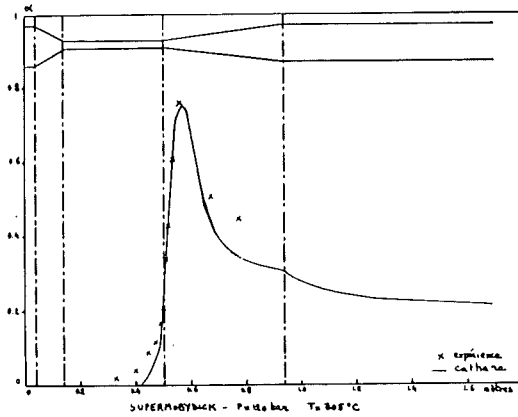


Fig. 3 b. : SUPER MOBY DICK TEST SECTION VOID FRACTION PROFILE

As a conclusion, it can be said that prediction of critical mass flow rate is generally good for long or short nozzles (error < 3%) for high inlet subcooling or positive inlet qualities. The error can reach 10% or 20% for low inlet subcooling (- 0 to - 3°K).

. Blowdown of an unheated test section :

- Marviken CFT in full geometry
- Horizontal CANON : tests covering a large area of break size and initial water temperatures
- Vertical CANON : Vertical pipe (0.10 m ID, 4 m long), depressurized by a small break (form \emptyset 0.003 to 0.015 m) at the top.

As an exemple, figures 4 (a,b) represent the compared mass inventories and level evolutions.

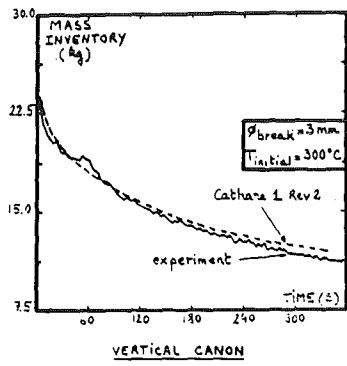
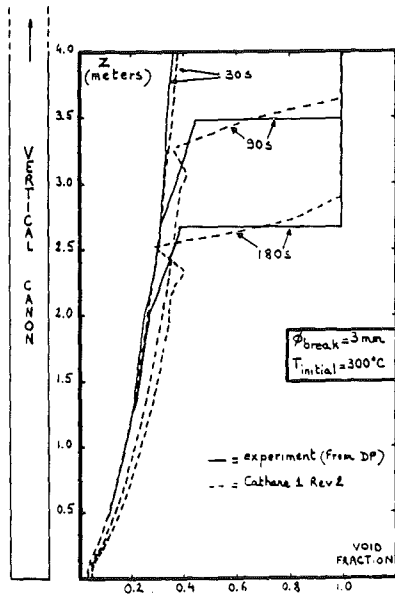


Fig. 4 a. : VERTICAL CANON MASS INVENTORY

Fig. 4 b. : VERTICAL CANON VOID FRACTION PROFILE
AT DIFFERENT TIMES

- TAPIOCA experiment similar to vertical CANON, but in a larger dimension :
0.35 m ID. 2.4 m long. Breaks at different elevations, from the top to a
low lateral position.

. Swell level :

G2 experiment : 19 x 19 rod bundle, with axial cosine flux ($0.5 \cdot 10^4 < \dot{q} < 2.8 \cdot 10^4 \text{ W m}^{-2}$), at pressures between 1 and 55 bars.

These tests consisted in measuring a swell level for a given froth level in a rod bundle. The CATHARE model failed in predicting a good swell level and the analysis led to the conclusion that the interfacial friction had a different structure in rod bundle than in a tubular pipe. Such an improvement is necessary to be introduced in the next CATHARE revision.

. Reflood : DADINE and ERSEC (tubular and rod bundle) tests enter in the qualification matrix for CATHARE.

Figure 5 represents a reconstitution of one of the reflooding tests.

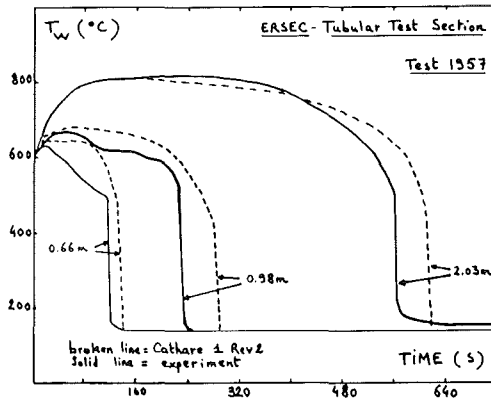


Fig. 5 : ERSEC TUBULAR TEST SECTION. WALL TEMPERATURES EVOLUTION AT DIFFERENT ELEVATIONS

The general conclusions on this topic are :

- The quench front rises a little too slowly
- The pressure drop is underestimated

Nevertheless, the maximum wall temperatures and the carry-over are in reasonable agreement.

All these anomalies are now well understood and should be eliminated in the next Revision.

. Blowdown of a heated test section :

several tests of the OMEGA blowdown program (tube and rod bundle) are involved in the CATHARE qualification.

. Wall condensation : PATRICIA GV1

PATRICIA GV1 consists of a unique steam generator pipe in small break LOCA conditions, with condensation inside the tube. Minor modifications concerning wall condensation have to be introduced in the next CATHARE revision.

As a general conclusion for the CATHARE qualification it can be said that no deep imperfection is observed in the present CATHARE Revision. Only local improvements are needed for future revisions.

IV.4. CATHARE quality assurance

The systematic pattern of analytical experiments used for the CATHARE quality assurance belongs to the above qualification program.

The tests have been selected following several criterion :

- the thermalhydraulics conditions must be near those encountered during a reactor accident
- The largest range of parameters must be covered
- Tests presenting very peculiar physical phenomena (level formation, grid effect for instance)
- A particularly good quality of the experimental measurements is required (The selection of the tests has been made with the experimentalists themselves).

The number of tests is limited to forty.

IV.5. Code verification

Since the beginning of 1984, date of release of the CATHARE version 1 (with Revision 2), the verification program is underway.

This program concerns small break tests :

LOFT 3.5 and 3.6
 LOBI SDSL 03
 BETHSY (for future)

and large break tests :

LOFT 1.5 and 2.5
 PKL K5.a and K9

Presently, LOFT 3.5 (See figure 6) is the only global test for which the interpretation has been completed, with CATHARE.

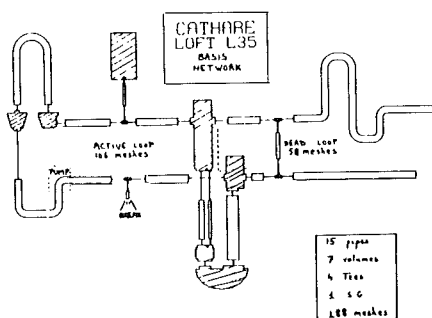


Fig. 6 : LOFT CIRCUIT REPRESENTATION

The general conclusions are : ① the calculated mass flow rate at the break is generally greater than the measured mass flow rate, during the 300 first seconds (fig. 7). The lack of physical model (entrainment or pull-through) at the tee near the break could be the reason of this difference.

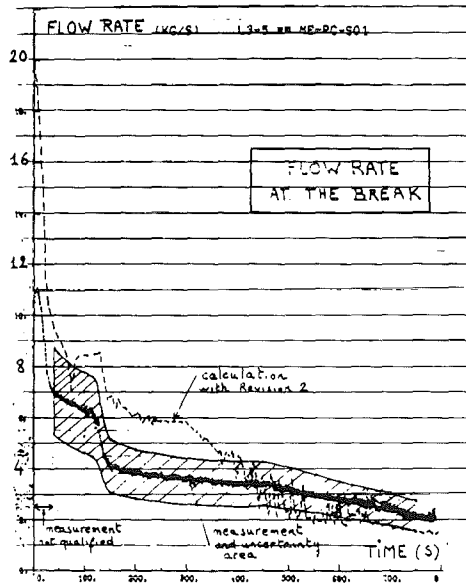


Fig. 7 : LOFT 3.5 MASS FLOW RATE AT THE BREAK

An experimental program on two-phase flows in tees on the Super Moby Dick apparatus is underway to investigate these phenomena.

② The calculations show a rupture of natural circulation at about 140 sec and occurrence of reflux boiling in the active loop.

Instrumentation in LOFT 3.5 is not able to give precise enough informations on these phenomena.

V. CATHARE PROGRESS

CATHARE version 1 is presently fully operational and several CPI reactor accident calculations have been performed.

. A large break calculation is now over, up to the end of the reflood phase. However the physical results during refilling and reflooding are questionable, due to a lack of consistency of the condensation laws and probably some other physical parameters such as singular pressure drops. Significant efforts have to be made in order to improve these models.

. Several small break (3' and 6') calculations have been completed. The different sequences are directly visualized on CRT display, and analysed. They allow improvement in understanding the physical phenomena which can lead to core uncover and recovery.

Several objectives are now planned in the frame of CATHARE development :

. A maintenance of the code : The code being released to the partners CEA, EDF and FRAMATOME, it consists in maintaining a user's assistance, editing new versions and new procedures, updating the user's handbook, and organizing workshops and seminars. A user's club has been created in which user's experiences are exchanged.

. The code verification :
This action is underway, the objective being to obtain a verified version with user's guidelines at the end of 1985.

. Numerical improvement :
One of our short term major objectives concerns optimisation of the code.

For a reactor small break calculation, the average time step is high ($\approx 0,3$ sec, due to the fully implicit method), however the CPU computing time per mesh and per time step is rather important : ≈ 20 msec on CRAY.1.

The simulator which is being developed on the CATHARE basis, has demonstrated that a significant factor on the computing time, is possible. CATHARE is now taking account of this experience.

. Physical developments :
A new revision of the physical laws is in progress. Its introduction in the code is planned for end 1985.

. New modules developments :
A short term priority is devoted to an axial secondary circuit description.

For long term, the following new modules are planned :

- two dimension description of the downcomer
- introduction of non condensable gas in all the elements of the circuit
- one-dimension pump.

A MODEL FOR TWO-PHASE JET EXPANSION AND IMPINGEMENT

J. M. Healzer
E. Elias

S. Levy Incorporated, Campbell, California 95008, U.S.A.

A. Singh

Electric Power Research Institute, Palo Alto, California 94303, U.S.A.

F. J. Moody

General Electric Company, San Jose, California 95125, U.S.A.

ABSTRACT

In this paper, data from large scale two-phase jet impingement tests at Marviken are compared to a two-phase jet model. This jet model applies conventional single-phase compressible flow methods to predict the jet expansion and pressures. A method-of-characteristics solution technique is used to predict jet behavior from the jet discharge to an impingement target in the jet path, where a standing shock is assumed to occur. The jet model uses standard steam and water properties to calculate jet behavior, assuming the phases remain in equilibrium.

Model predictions of jet centerline static pressure compare well with data for jets with steam and two-phase stagnation conditions. Predictions of jet behavior for jets with subcooled stagnation conditions in the region near the jet discharge are less favorable because non-equilibrium at the jet discharge makes it difficult to define consistent equilibrium properties for the jet model. For these cases, the model tends to overpredict jet centerline pressures. Jet impingement pressures predicted by the model tends to be below the data, although general trends predicted by the model agree with the data.

NOMENCLATURE

D	= nozzle diameter	v	= radial velocity component
c	= speed of sound	V	= $u^2 + v^2$, jet velocity
G	= $V\rho$, mass flow	x	= quality
h	= enthalpy	z	= jet axial coordinate
L	= distance to target	α	= $\arcsin(c/V)$, Mach angle
M	= c/V , Mach number	θ	= $\arctan(v/u)$, angle of velocity
p	= pressure	ρ	= density
r	= jet radial coordinate	ϕ	= velocity potential
s	= entropy	()	I,II conditions along characteristics
u	= axial velocity component		

INTRODUCTION

The evaluation of two-phase jet impingement loads plays an important role in the design of light water reactor containment and piping systems. A relatively simple but conservative model is the presently recommended design standard. This model for jet impingement loads and reaction loads on the pipe which has ruptured is given in the American Nuclear Society Standard ANS-58.2 [1]. In view of the importance of this particular design basis to the containment and piping design of the nuclear plant, there has been much interest in better quantifying jet reaction and impingement loads.

There have been several experiments, most at small scale, to study the behavior of two-phase jets and, along with these experiments, jet models which have been largely empirical. More recent experiments, performed in 1980-1 are the Marviken Jet Impingement Tests (JIT) conducted by Studsvik Engergiteknik at the Marviken Power Station, Sweden [2]. Unique features of these tests are the large pipe sizes tested (20 to 50 cm.) and initial pressures (50 bar) and range of subcooling (30°C subcooled to saturated steam).

Since the completion of the Marviken tests, there have been several theoretical investigations of two-phase jets using advanced numerical simulation techniques which have relied at least in part on the Marviken data for verification. These include a study by Kashiwa and others [3] at Los Alamos using the K-FIX code and the SALE code. In another study by Weigand [4] and others at Sandia, the CSQ code has been used to predict two-phase jet behavior. In addition to these studies, a recent paper by Kawasaki [5] has described the analysis of a jet using a "fluid-in-cell" method. The details of the model are not given, but it is said that the jet is assumed to be homogeneous equilibrium flow.

The present study is also a theoretical analysis of the two-phase jet. This study, however, models the two-phase jet with the much simpler analysis methods which are used for single-phase compressible jets. By treating the jet as a homogeneous equilibrium mixture, the governing equations for the jet reduce to a much simpler form which can be solved by the method of characteristics.

JET MODELING

In an earlier paper [6] the governing equations for the two-phase jet are discussed in more detail. The following is a summary of this discussion.

The governing equations of steady, axisymmetric and irrotational flow in cylindrical coordinates z and r are [7].

$$\left(1 - \frac{u^2}{c^2}\right) \phi_{zz} - 2 \frac{uv}{c^2} \phi_{zr} + \left(1 - \frac{v^2}{c^2}\right) \phi_{rr} + \frac{\phi_r}{r} = 0 \quad (1)$$

where c is the speed of sound and

$$u = \frac{\partial \phi}{\partial z} = \phi_z \quad (2)$$

$$v = \frac{\partial \phi}{\partial r} = \phi_r$$

Using standard mathematical procedures [7], the following differential equations for the characteristic curves of Equation (1) can be obtained:

$$\left(\frac{dr}{dz}\right)_{I,II} = \frac{-uv \pm c \sqrt{u^2 + v^2 - c^2}}{c^2 - u^2} \quad (3)$$

$$\left(\frac{dv}{du}\right)_{I,II} = \frac{uv \pm c \sqrt{u^2 + v^2 - c^2}}{(c^2 - v^2)} - \frac{c^2 v}{(c^2 - v^2)} \frac{1}{r} \left(\frac{dr}{du}\right)_{I,II} \quad (4)$$

where the subscripts I and II refer to family I and II of the characteristic curves, respectively. These equations can be rewritten in terms of the velocity components V and θ by setting

$$u = V \cos \theta ; \quad v = V \sin \theta \quad \text{and noting that } \sin \alpha = \frac{c}{V} .$$

The equations for the characteristic curves are then transformed into

$$\left(\frac{dr}{dz}\right)_{I,II} = \tan(\theta \mp \alpha) \quad (5)$$

$$\frac{1}{V} \left(\frac{dV}{d\theta}\right)_{I,II} = \mp \tan \alpha + \frac{\sin \alpha \tan \alpha \sin \theta}{\sin(\theta \mp \alpha)} \frac{1}{r} \left(\frac{dr}{d\theta}\right)_{I,II} \quad (6)$$

Equation (5) represents the directions in the physical plane of the right (I) and left (II) running Mach lines. Equation (6) represents the corresponding hodograph plane. Thus, the simultaneous solution of Equations (5) and (6) for given initial conditions is equivalent to solving the original partial differential equation for the jet, Equation (1).

Since Equations (5) and (6) each contains terms in both velocity and physical coordinates, it is necessary to solve them simultaneously. A detailed description of the calculation procedure for ideal gas is given in [7]. The following is an outline of the procedure used for a two-phase jet. The solution scheme generally consists of utilizing the solution in the physical and hodograph planes at two points in the jet to calculate the solution at a third point downstream. Given the location of the two points in the physical and hodograph planes, the location and conditions at a downstream point which is located at the intersection of the two Mach lines, can be determined from solving the finite difference form of Equations (5) and (6). The pressure and thermodynamic state at the downstream point in the jet are computed from the velocity, using the following relationships for isentropic expansion:

$$V^2 = 2(h_0 - h) \quad (7)$$

$$h = h_f + x h_{fg} \quad (8)$$

$$x = \left[\frac{s_0 - s_f}{s_g - s_f} \right] \quad (9)$$

where h is the flow enthalpy, s is the entropy, x is the quality, and the subscripts o , f and g refer to stagnation condition and saturated liquid and gas, respectively. To compute the pressure corresponding to a given velocity, Equations (7) to (9) are solved by trial and error. A pressure is assumed and the flow quality and enthalpy are calculated using a thermodynamic properties

model. A velocity is then computed by Equation (7) and compared to the actual velocity. If the computed velocity is too large, then a larger pressure is chosen and the process is repeated until the velocities match within a pre-determined convergence criterion.

The boundary conditions for the jet are defined by a constant ambient pressure at the jet outer boundary and by the critical pressure at the nozzle exit. The critical pressure is determined by considering a homogeneous equilibrium (HEM) critical flow at the nozzle. The mass flow rate in the nozzle is given by:

$$G = V\rho \quad (10)$$

where V and ρ are the velocity and density of the mixture, respectively. Combining Equations (10) and (7) yields the homogeneous equilibrium mass flux expression:

$$G = \rho[2(h_0 - h)]^{1/2} \quad (11)$$

Expressing the enthalpy and density in terms of the static quality x and liquid and vapor specific enthalpies and densities and using Equation (8) yields:

$$G = \frac{[2(h_0 - [(1-x)h_f + xh_g])]^{1/2}}{(1-x)/\rho_f + x/\rho_g} \quad (12)$$

The homogeneous equilibrium critical flow rate for a given set of stagnation conditions is the maximum value obtained when Equation (12) is evaluated at different pressure states having entropies equal to the stagnation entropy. The pressure at which the mass flux is a maximum is the critical pressure which is used as a boundary condition in the free jet calculations.

The speed of sound c is calculated at each mesh point in the jet by

$$c^2 = \left(\frac{\partial p}{\partial \rho} \right)_s \quad (13)$$

For saturated stagnation conditions, the value of c calculated by equation (13) at the critical nozzle exit pressure is equal to the mixture velocity calculated by maximizing Equation (12). Consequently, the nozzle exit Mach number is unity for saturated and slightly subcooled stagnation conditions. For subcooled stagnation conditions, the pressure corresponding to the maximum flow prediction yields a speed of sound at the choke point which is less than the flow velocity. This anomaly has been discussed by several authors, i.e., D. G. Hall [8]. To avoid this difficulty in the present model, the flow is assumed to choke at the critical pressure predicted by the HEM and the flow velocity is taken equal to that predicted by the HEM and not to the value calculated by Equation (13).

Analysis of the two-phase jet using the method-of-characteristics approach proceeds much as for a single phase underexpanded supersonic jet. Flow out the nozzle exit expands downstream until the free jet boundary turns in. Reflected characteristics from this boundary begin to intersect each other indicating the formation of a shock wave. The coalescence of the characteristics first occurs at the jet boundary forming an incident shock which curves inward downstream forming a normal shock at some point in the jet flow. The characteristic net cannot be extended past the shock wave without some information about the shock structure and pattern of shock waves beyond the initial shock. In the present

analysis, the characteristic net is only extended to the point where right running characteristic line from the point in the characteristics net where the first intersection occurs is propagated to the jet centerline. For conditions typical of those tested at Marviken, the characteristics net is extended several meters past the nozzle discharge, including the region of the jet, where impingement loads are largest.

From experience with single-phase supersonic jets it is known that a standing shock wave will form in the flow approaching a target in the jet path. Although the present jet is two-phase, this flow will also experience a rapid irreversible compression as it approaches a target. There have been several models proposed for shock waves in two-phase flow. A good summary can be found in the book by Wallis [9]. In the present jet model, it has been assumed that the shock is parallel to the target and that the two-phase mixture remains in equilibrium as it passes through the shock. For a target perpendicular to the jet centerline, the flow at the jet centerline will encounter a normal shock while flow at the target edge may encounter an oblique shock. This is illustrated in Figure 1. The governing equations for flow across the normal shock are the same as for single phase flow:

$$\text{mass:} \quad \rho_1 V_1 = \rho_2 V_2 \quad (14)$$

$$\text{momentum:} \quad p_1 + \rho_1 V_1^2 = p_2 + \rho_2 V_2^2 \quad (15)$$

$$\text{energy:} \quad h_{01} = h_{02} \quad (16)$$

where subscripts 1 and 2 refer to upstream and downstream of the shock.

For an oblique shock, the above equations are solved for the flow velocity component normal to the shock.

Solution of these equations for a two-phase mixture is by trial-and-error. Once conditions behind the shock are obtained, the impingement pressure is taken to be the stagnation pressure based on the component of the flow which is perpendicular to the target. At the jet centerline, the full stagnation pressure behind the shock is recovered. At the target edge, the stagnation pressure is based on the flow velocity normal to the target.

COMPARISON TO DATA

The first six tests in the Marviken JIT series were free-jet tests with instrumentation to determine jet axial and radial pressures. These were followed by six tests where pressures on impingement targets were measured. Each test was conducted as a blowdown experiment so that, as the system depressurized, stagnation conditions for the jet varied from test initial conditions which were typically 30°C subcooled to saturated conditions to nearly all steam as the level in the pressure vessel dropped below the standpipe which delivers flow to the jet nozzle. Since the change in stagnation conditions occurred relatively slowly compared to the transient time through the pipe and nozzle, the tests have been analyzed as a series of quasi-steady states, using the nominal stagnation conditions which were measured at various times during the blowdown.

One of the free jet tests and one of the impingement tests were steam blowdowns, with the pressure vessel standpipe above the liquid or two-phase

level during the blowdown. These tests provide an ideal basis for comparison to the method of characteristics solution since the steam jet should exhibit perfect gas behavior. From the other tests, jet behavior and impingement loads with both saturated and subcooled stagnation conditions is available by selecting different times in the blowdown transient.

Comparisons of model predictions with jet centerline pressures for several of the free jet tests are shown in Figures 2 through 4. The data shown in Figure 4 are from two different times in the steam blowdown test. Note that the homogeneous equilibrium model of the jet does a good job of representing the data.

The top two curves in Figure 2 are for two different times in a blowdown where jet stagnation conditions were subcooled. The agreement with this data is not as good as for the steam blowdown. Note that the HEM critical flow model is still able to predict the jet discharge flow. Using the HEM critical flow model to predict jet velocity forces the same pressure in the jet as would be predicted by the HEM critical flow model. This results in an exit Mach number greater than 1.0 and a large initial expansion out the nozzle as can be seen by the delay in the jet to depressurize at the nozzle exit in Figure 2. Later in this same blowdown, shown in the lower curve of Figure 2, stagnation conditions are saturated and the static pressure predictions at the jet discharge are a much better match to the data. Figure 3 shows jet centerline pressure late in another free jet test with initial stagnation conditions which were subcooled, but with different nozzle size. These predictions are also a reasonably good match to the data.

Figures 5 through 7 show data from the impingement tests. Three of the tests in this series were nearly identical blowdowns with the impingement plate target at different locations from the nozzle discharge. All of these tests were initially subcooled blowdowns with a large diameter nozzle. Figure 5 shows data and predictions for three different times in these blowdowns. In general, the model underpredicts the data. An interesting feature of this data is that the impingement pressure on the target at its most distant location has delayed to nearly the ambient pressure. The prediction for the data from these tests is the worst match to the data late in the blowdowns at 50 seconds. During this period, conditions in the pressure vessel are rapidly changing near the end of the test. Prediction of the data late in the blowdown was found to be difficult for all the tests.

Figure 6 shows impingement pressures on the plate for a steam blowdown. Target distance for this test was $L/D = 2.15$ and the target impingement pressures, both predicted and measured are but a small fraction of the vessel stagnation pressure.

Figure 7 shows data for impingement pressures on a cylinder in the two-phase jet. Nozzle to target distance for this test was $L/D = 2.97$, and again, the impingement pressures are only a small fraction of the stagnation pressures.

For each of these comparisons, the impingement pressures predicted by the model fall below the data. A possible reason for this is that the impingement pressure is calculated from the jet velocity component, normal to the target. This is a difficult pressure to measure even in single phase flow. Most total pressure measurement devices attempt to be independent of incoming flow angle. In this case, the probe would have to measure the pressure for flow only normal to the plate. The test reports however show comparisons between the plate load based on integrated pressure measurements and the load cells. The data from

these two independent measurements agree very well, supporting the accuracy of the pressure data. Another possible explanation for the under prediction is the model assumption that the jet expands fully. In the Marviken tests, the jet centerline pressure typically recovers back to the ambient pressure within a meter or two from the nozzle exit. This is likely related to the confinement of the jet inside the test facility. The jet centerline static pressure is under predicted by model by about this same amount since the model does not account for the jet confinement. This error in static pressure also carries through to the impingement pressures. The data predictions in both Figures 6 and 7, where the impingement pressures are very low, miss the data by nearly the same as the difference in the static pressures for these two cases.

SUMMARY

Modeling of two-phase jets as a homogeneous equilibrium mixture and applying standard method-of-characteristics techniques provides good predictions of the Marviken JIT data with both two-phase and steam jets. Calculation of stagnation pressures on targets within the jet requires modeling of the shock wave which would be formed in front of any target in the jet path. Impingement pressures calculated by the model fall below the Marviken data.

REFERENCES

1. American National Standard--Design Basis for Protection of Nuclear Power Plants Against Effects of Postulated Pipe Rupture, ANS-58.2, ANSI N176, American Nuclear Society, La Grange Park, Illinois (January, 1979).
2. "The Marviken Full-Scale Jet Impingement Tests, Fourth Series," Report Series MXD-200, Joint Reactor Safety Experiments in the Marviken Power Station Sweden (1980-81).
3. Kashiwa, B. A., et al., "Steam-Water Jet Analysis," Los Alamos Scientific Laboratory Report LA-UR-82-958 (March, 1982).
4. Weigand, A. A., S. L. Thompson, and D. Tomasko, "Two-Phase Jet Loads," Sandia National Laboratory Report NUREG/CR-2913 (SAND82-1925, 124) (January, 1983).
5. Kawasaki, T., A. Yamanouchi, and M. Nartoh, "Numerical Analysis of Two-Phase Jet Impingement," American Nuclear Society Transactions, p 428, Vol. 45, TANSO 45 1-184 (1983).
6. Elias, E., et al., "Modeling Two-Phase Jet Flow," presented at the ASME 1984 Pressure Vessel and Piping Conference, San Antonio, Texas.
7. Shapiro, A. H., The Dynamics and Thermodynamics of Compressible Fluid Flow, Vols. 1,2, The Ronald Press Co., New York (1953).
8. Hall, D. G. and L. S. Czapy, "Tables of Homogeneous Equilibrium Critical Flow Parameters for Water in SI Limits," Idaho National Engineering Laboratory Report, EGG-2056 (September 1980).
9. Wallis, G. B., One-Dimensional Two-Phase Flow, McGraw Hill, Inc., New York (1969).

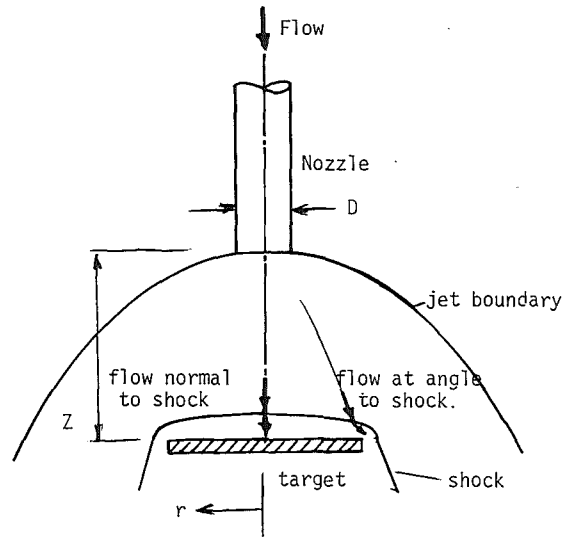
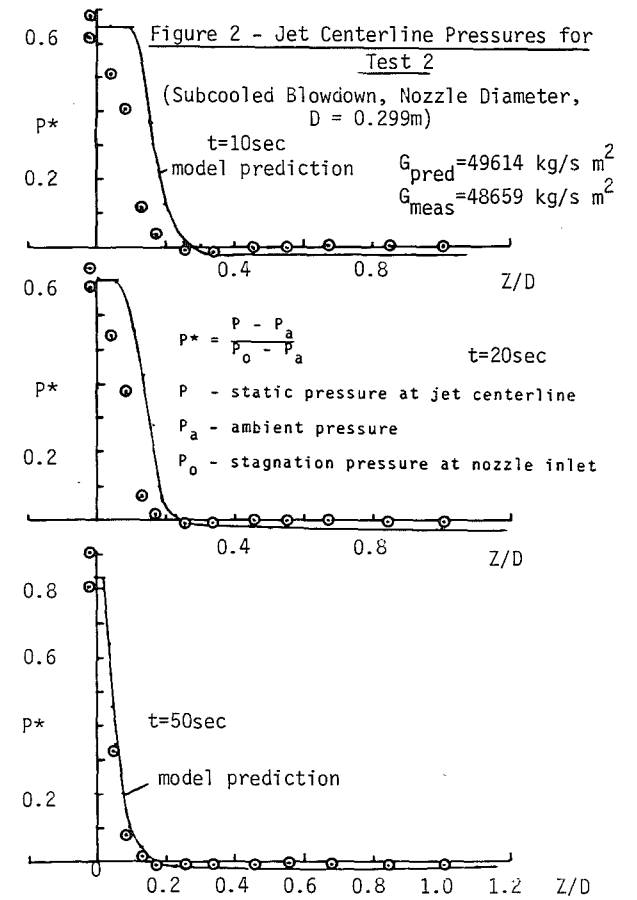


Figure 1 - Jet Schematic



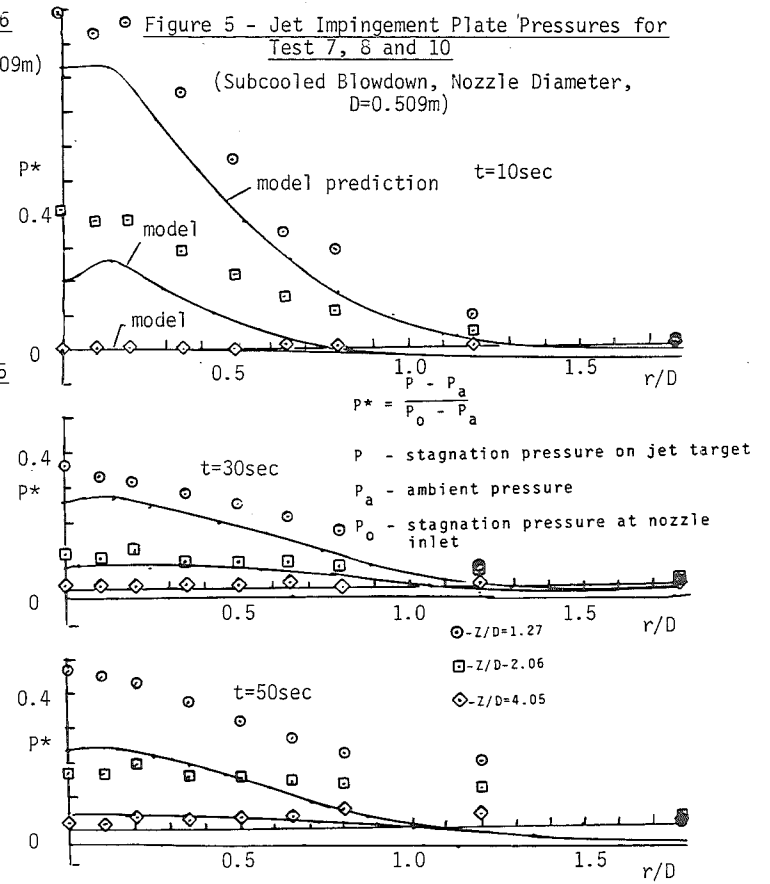
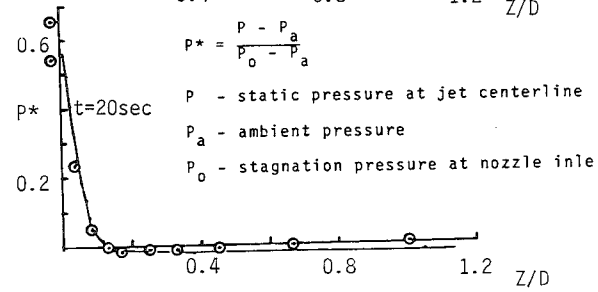
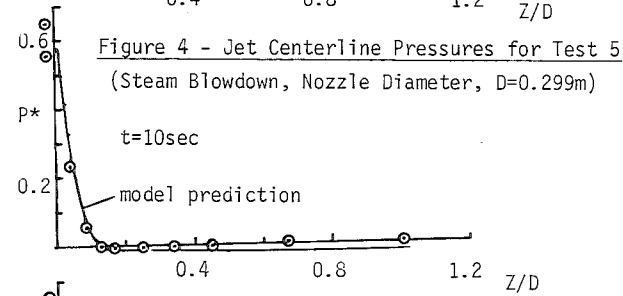
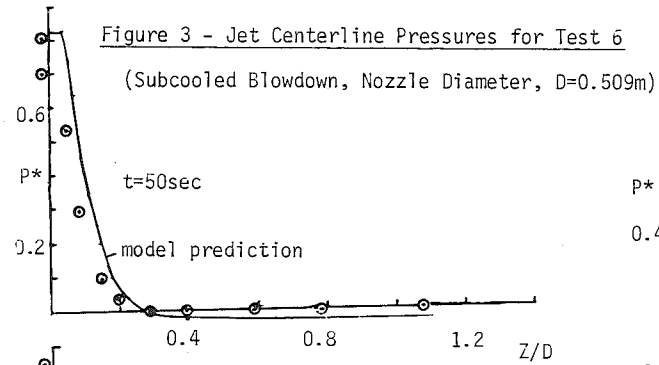


Figure 6 - Jet Impingement Plate Pressures for

Test 11

(Steam Blowdown, Nozzle Diameter, D=0.299m,
Target at Z/D = 2.15)

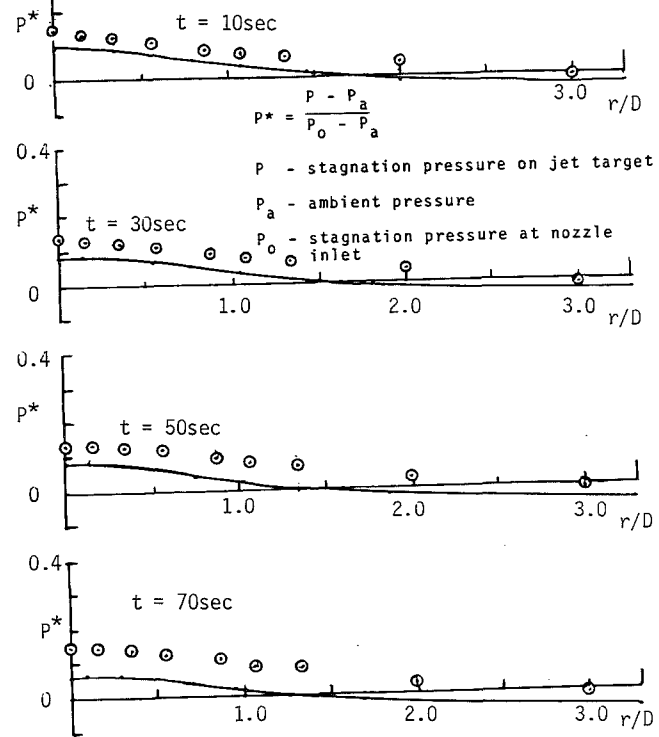
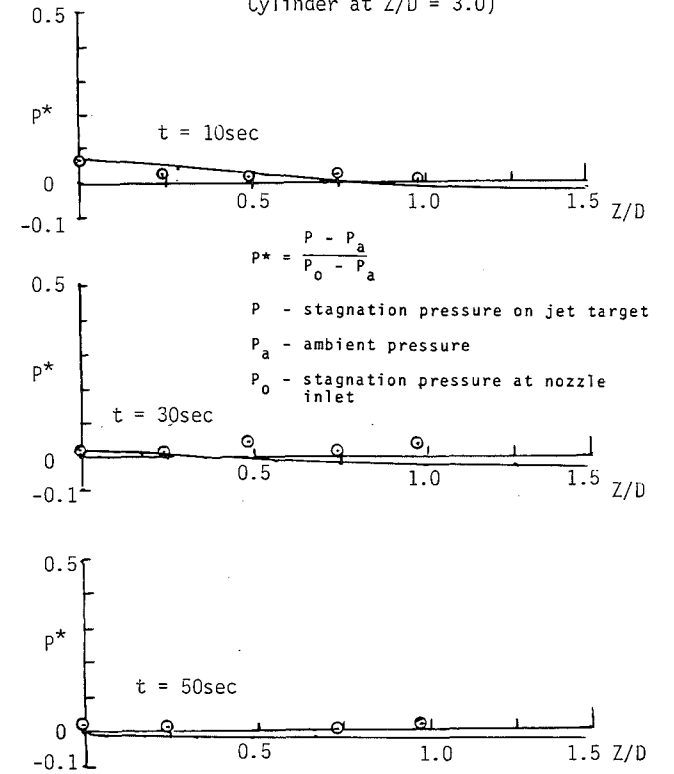


Figure 7 - Jet Impingement Cylinder Pressures

for Test 12

(Subcooled Blowdown, Nozzle Diameter, D=0.509m
Cylinder at Z/D = 3.0)



THE PMK-NVH EXPERIMENTAL FACILITY AND
THE PHENOMENA TO BE INVESTIGATED

L. Szabados, I. Tóth, L. Perneczky

Central Research Institute for Physics
H-1525 Budapest, P.O.Box 49, Hungary

ABSTRACT

The integral-type PMK-NVH test facility is a 1:2070 scaled model of the primary circuit of the WWER-type Paks Nuclear Power Plant. The operating pressure and temperature are 16 MPa and 623 K, respectively. The elevations are the same as in the plant. The scheduled time for the start-up is the end of 1984. The loop was designed for SB LOCA experiments above all, but operational transients can also be investigated.

Paper presents the system description including instrumentation, control system and data acquisition. Some important phenomena to be expected from SB tests as they could be derived from pre-test calculations are also presented. The effect of the loop seals on the natural circulation, normal or reverse heat transfer in steam generators, core heat transfer at reduced primary circuit inventory are included.

INTRODUCTION

In Hungary a government-sponsored safety research programme has been initiated for nuclear reactor safety analysis in 1980 for a 5-year period of 1981-1985. The thermohydraulic part of the programme was aimed at creating a set of selected computer codes tested by experiments, that would allow analyses to be performed under different accident conditions for the Paks Nuclear Power Station. In support of these purposes an integral-type experimental facility called PMK-NVH is under construction.[1]

As it is known four units of the Paks NPP are under construction on the same site, all being equipped with a WWER-440 MW pressurized water reactor. The first unit has been running at nominal power for a year. These reactors are slightly different from other PWRs as: 6-loop primary circuit, horizontal steam generators, loop seals in hot and cold legs, safety injection tank set-point pressure higher than secondary pressure.

The PMK-NVH facility is a model of the primary circuit of the Paks NPP and designed mainly to investigate processes following small breaks in the primary circuit, but it was conceived in a way that allows simulation of a variety of different plant transients. Small break processes are felt to be important since relatively few results have been published on these phenomena of the Soviet PWR-type plants.

Because of the loop seals the natural circulation behaviour is also important. According to these considerations a planned test matrix is given in

Table 1 for the time interval of 1985-86. In order to compare the experimental programme of PMK-NVH to that of other test programmes, a set of similar experiments had been studied for LOFT, PKL, LOBI and SEMISCALE. [1] It can be stated that the aims of the experiments and processes considered to be important are very similar in case of different facilities.

A short system description is given in the paper and results of modelling problems and pre-test analyses are presented.

In the framework of a cooperation between the International Atomic Energy Agency /IAEA/ and the Central Research Institute for Physics /CRIP/, Budapest Hungary an IAEA organized and coordinated Standard Problem has been selected for member states. The experiment chosen is a 7,4% cold leg break from full power covering the blowdown phase of the transient.

SYSTEM DESCRIPTION, MODELLING ASPECTS

In order to perform the experimental programme summarized above a full pressure test loop was designed, considering the appropriate modelling aspects and scaling criteria. [1]

SYSTEM DESCRIPTION

The PMK-NVH facility is a model of the primary circuit of the Paks NPP. The 6-loop PC is equipped with a WWR-440 reactor and a horizontal steam generator in each loop. There are three parallel high pressure injection systems /HPIS/ and four safety injection tanks /SIT/. HPIS systems are activated by low system pressure and water level in the pressurizer. The SIT set-point pressure is 60 bar, higher than the secondary pressure of 46 bar. The inlet and outlet temperatures are 267 and 297 °C, respectively, while the operating pressure is 123 bar; the core thermal power is 1375 MW.

The PMK-NVH model system consists of the same components as it is shown in Fig.1. Because of the gravity dominated processes in small break LOCA the elevations are the same as in the plant with the exception of the lower plenum and pressurizer. Scaling ratios of volumes and power are 1:2070. A core model of 19 rods is used. The 6 loops of the NPP are modelled by a single loop. The pressure drop in the model is approximately the same as in the plant. On the secondary side of the steam generator the steam volume ratio is kept. The PMK loop is connected to the NVH loop as it is shown in Fig. 1. The NVH loop is the secondary circuit of the PMK, resulting in the PMK-NVH facility. The operating pressure and temperature of the model are 160 bar and 350 °C, respectively. A list of instrumentation is also presented in Fig.1. The control and data acquisition system is completely computerized.

MODELLING ASPECTS

The design of an integral type test facility is a compromise between the strict scaling criteria and the economical and experimental requirements. In case of the PMK-NVH loop the volume scaling criteria were selected. Particular attention was given to satisfy the volume distribution requirement in the system, flow area relationships in the core and the steam generator, elevations, pressure drops and heat losses.

Table 1.

Test matrix for the PMK-NVH test facility
in the time interval of 1985-86.

Type	Experiment	Aims / Remarks
Steady state tests	One-phase flow natural circulation	Comparison of the results with measured Paks NPP data. A "testing" of the test facility. Different core powers and coolant levels. Constant secondary side pressure.
	Two-phase flow natural circulation	Effect of mixture level on the flow rate. Mixture levels in upper plenum, hot leg and steam generator. The maximum value of power transported from the core. Constant secondary side pressure.
Transient tests	7,4% cold leg break without SITs and with one HPIS	Investigation of the blowdown process. Initial conditions are the nominal operating conditions, one HPIS and constant secondary side pressure.
	7,4% cold leg break with SITs and one HPIS	Aims and initial conditions are the same as the first 7,4% break case. Effect of SITs on the process.
	7,4% hot leg break without SITs and with one HPIS	Aims and initial conditions are the same as the first two 7,4% break cases. Effect of break location on the process.
	1% cold leg break without SITs and with one HPIS	Investigation of the blowdown process in case of long process time. Real small break case. Initial conditions are the nominal operating conditions.
	1% cold leg break without SITs and with three HPIS	Aims and initial conditions are the same as in case of the first 1% break experiment. Effect of the three HPIS on the process.
	3.3% break on the pressurizer /TMI case/	Investigation of the blowdown process in case of such a special break location.

In a reduced scale system the surface area to volume ratios are larger than those in the reference system. For this reason the heat losses in the model system will be larger than in the NPP. The heat loss for the PMK should be kept as low as 2,5 kW. Losses from tubings and components can be minimized by appropriate insulation, however, experience with similar loops shows that instrumentation penetrations and structural supports are sources of much higher losses that are very difficult to evaluate beforehand. In order to mitigate the consequences of the latter, additional heating is applied in areas where the losses are important. As an example, surface area to coolant volume ratios for the Semiscale MOD3-FWR and PMK-NVH-Paks NPP are presented in Table 2. It can be seen, that the two systems give similar values.

Surface area to coolant volume ratios

Table 2.

Primary Circuit Components	FWR /4-loop/	Semiscale MOD-3	Semiscale FWR	WWER-440 Paks	PMK-NVH	PMK-NVH WWER-440
Core	301.9	295.3	0.98	410.7	431.0	1.04
Hot leg				8.1	87.0	10.7
Intact loop	5.6	60.0	10.7			
Broken loop	5.6	117.5	21.0			
Cold leg				8.1	87.0	10.7
Intact loop	5.74	60.0	10.5			
Broken loop	5.74	117.5	20.5			
Steam generator primary				303.0	526.3	1.7
Intact loop	203.4	390.4	1.9			
Broken loop	203.4	203.4	1.0			

The time history of the transients is effected by the axial volume distribution. A comparison was made between PMK-NVH and the Paks NPP /Fig.2/. It can be observed that there is almost complete agreement for the whole elevation range, with the exception of lower plenum and pressurizer.

SB LOCA PRE-TEST RESULTS

In order to prepare SB-LOCA PMK-tests a large number of pre-test calculations have been performed using the RELAP4/mod6 computer code [2], [3]. The analyses covered break sizes from 0.5 to 7,4% located on the cold, hot leg or the pressurizer, the steam generator secondary side being held at constant pressure or cooled down. As to the safety injection systems, the effect of 1 or 2 of the three HPIS not being available was investigated and calculations were done with and without injection from the hydroaccumulators.

The most important phenomena to be expected during SB LOCEs on the PMK-NVH facility are discussed by presenting calculated results for a 1% cold leg break case. In the calculations no SIT injection was considered and it was

assumed that only one of the three HPSI pumps is available. The pressure on the secondary side was kept constant throughout the transient.

The basic processes can be explained with the aid of the pressure-time diagram in Fig.3. /The corresponding results for the Paks NPP are shown for comparison in Fig.4./ After scram at about 40 s the depressurization rate increases. The pressurizer empties at 78 s and this continues to enhance depressurization until steam generated in the core begins to accumulate in the upper plenum thereby resulting in a slight increase of system pressure. At 400 s the mixture level in the upper plenum drops to the hot leg elevation and the steam in the hot leg forces down the liquid level on the reactor side of the loop seal that leads to increased repressurization of the primary circuit.

One detrimental effect of the hot leg loop seal is that it depresses core mixture level [4]. On the other hand, system behaviour in this period is governed by the evolution of loop seal pressure drop versus total loop pressure drop. Figure 5 shows changes in elevation head losses in the loop seal $/H_{LS}/$ and the core $/H_C/$ versus total loop pressure loss. /Arrows indicate decreasing loop seal mixture level./ Both losses vary several times that of the loop pressure loss, the loop seal elevation loss increasing somewhat faster than core elevation loss decreasing. The difference of these two $/H_{LS}/$ keeps almost the balance with the total loop pressure loss the remaining amount decreasing the loop flow rate.

The decreasing flow rate leads to increased steam production in the core. Figure 6 shows the variation of core steam flow as a function of the relative mixture level in the loop seal. Earlier to loop seal mixture level decrease the volumetric loss through the break is balanced by the HPSI and the steam produced in the core. However, with decreasing mixture level the core volumetric steam flow rate soon exceeds the break flow rate that leads to an increase in system pressure. System pressure behaviour prior to hot leg loop seal clearing depends on core power, break size and position. The pressure build-up is enhanced with higher core power, while the opposite is true if the break size increases or the break position is at higher elevation, since both lead to increased volumetric mass flow rate through the break.

After all, the mixture level in the loop seal decreases sufficiently to permit the steam to pass to the steam generator collector. The calculations indicate that steam first accumulates in the upper part of the collector and only enters the steam generator tubings, when the mixture level of the collector drops to the elevation of the latter /Fig.3/. It is only then that system pressure is rapidly decreasing very near to the secondary pressure, because of the steam being condensed in the steam generator.

It is expected that the processes on the PMK-NVH facility will differ in this period from those in the plant, due to some asymmetric behaviour between broken and intact loops that can not be reproduced with the single loop test facility. Figure 4 shows the variation of the collector mixture level both in the broken and the intact loops. While the former drops to 2.62 m at 850 s thereby allowing steam to pass to the steam generator, the latter does so only at 1100 s. The broken loop steam generator can not condense all the steam produced by the core - that is why system pressure does not decrease here as radically as in the PMK calculations.

Hot leg loop seal clearance and steam condensation temporarily increases natural circulation flow rates. However, after 730 s loop and core flow rates

are again decaying because of the mixture level decrease in the cold leg steam generator collector and soon the cold leg loop seal is getting effective. This leads to increased steam production in the core and a decrease of the mixture level in the reactor vessel, that is also reflected in fuel rod temperatures. /The PMK rod simulators were modelled in the calculation as real fuel rods./ Figure 7 shows average fuel rod center line, and cladding temperatures: while in the early part of the transient they closely followed the saturation temperature, at about 1120 s they rapidly climb to about 740 K due to DNB.

At 1420 s the cold leg loop seal is cleared and loop and core flows recover. This leads to quenching of the fuel rods and increased steam generator heat transfer. As a consequence system pressure drops below the secondary one and the direction of steam generator heat flow is reversed that, in turn, has a detrimental effect on natural circulation flow rates. In Fig. 8 the core flow is plotted versus the relative primary mass /i.e. mass at a given time divided by the initial mass in the system/ for the discussed transient. The flow rate is mainly governed by core power and loop seal resistance.

After 1550 s another effect is superimposed on these processes: the downcomer mixture level drops to the elevation of the break and this is reflected by a sudden decrease in the break mass flow rate. The primary circuit processes show a periodic behaviour that can be explained as follows: when steam is leaving the system through the break, the critical mass flow rate is lower than the amount injected by the HPSI pump and mixture level in the downcomer begins to rise. Since the HPSI pump delivers cold water the gravitational head of downcomer water column is increasing that forces coolant into the core leading to a weak positive flow rate. The relatively low quality coolant entering the steam generator is evaporated because of the higher temperature on the secondary side, the steam produced pushes water from the pump seal into the downcomer. These effects lead to the fact that the breach is covered again, this, in turn, along with the steam production in the steam generator, provokes a rather fast increase in the system pressure. At the same time, the higher mass flow rate through the breach makes the downcomer level to fall again and the whole process is repeated. Because of the sawtooth-like behaviour in system pressure the average depressurization rate is very low.

It is evident from the above results that the steam generator plays an important role during hot and cold leg loop seal clearing as well as when the break is uncovered. Calculations indicate that the reflux condensation mode, so effective at reduced primary inventory in PWRs with vertical U-tube heat exchangers, is not existing in the WWER geometry, but already a very small positive pressure drop across the steam generator is sufficient to push the condensed water into the cold leg.

When the break is uncovered or, with larger break sizes, when the break flow becomes two-phase the primary system behaviour very much depends on break size and elevation: while in the case of a 1% break the energy removed through the break is not sufficient to render the primary pressure independent of the secondary one, the 7,4% case shows a different picture. When there is two-phase flow at the break, primary pressure falls below the secondary one, but steam produced by the reverse heat flow in the steam generators maintains the former very near the secondary level. This situation lasts until the break becomes uncovered, this leading to fast depressurization of the system.

The effect of the steam generator in different small-break transients is illustrated by Fig. 9, where the primary system pressure variation is plotted versus power to steam generator/core power. Reverse steam generator heat flow is a consequence of two-phase or steam break flow in all cases, but the one with 0,55% break: here, due to 3 HPIS pumps injecting, the system subcooling is getting so high that the primary temperature is lower than secondary already at a pressure of 8.4 MPa. The loop seal effects are reflected by loops on the 1%-1 HPIS curve.

CONCLUSIONS

Pre-test analyses of SB-LOCs to be performed on the PMK-NVH facility indicate that test results will reproduce the important processes in the plant during such transients. The single-loop design of the facility will, of course, not represent asymmetric behaviour among the six loops but, on the other hand, it does not suffer from shortcomings that would arise if five intact loops were lumped into one. To keep heat losses as low as possible the loop will be adequately insulated and heater bands will be applied at instrument penetrations.

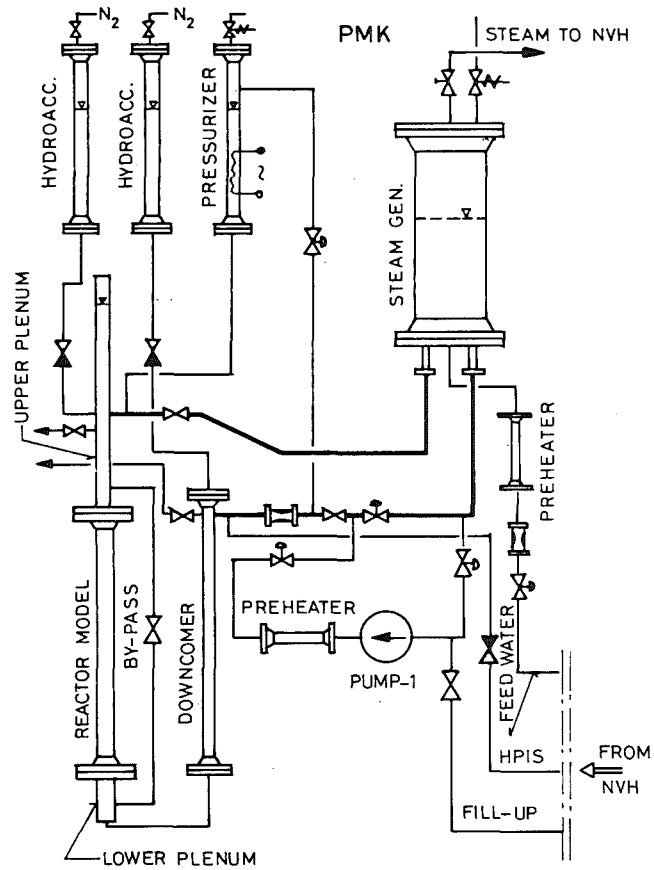
Calculation results obtained with RELAP4/mod6 are regarded as tentative: the main aim of the PMK tests is to produce experimental data for computer code validation. The main areas where RELAP4/mod6 results should be checked are the following:

- Phase separation in the upper plenum and loop seals has an important effect on natural circulation flow rates, while in the volume next to the break it greatly influences break flow rate. It also determines heat transfer in the core.
- Condensation on the steam generator primary side is of great importance. /RELAP4/mod6 does not contain any condensation model, the number of steam generator control volumes may also have an influence./
- Thermal non-equilibrium processes are encountered at SIT and HPIS injection, as well as at pressurizer refill. Since RELAP4 is a thermal equilibrium code it is to be checked, whether these processes have an important effect on overall system behaviour.

PMK instrumentation was designed to give extensive information on most of these processes. Mixture level in the upper plenum and loop seals will be tracked by using impedance void probes and Δp transducers. 26 thermocouples are mounted on the uppermost part of the electrically heated fuel rod simulators in order to give information on heat transfer in this part of the core. A spool piece containing a symmetric venturi, a turbine flow meter and a γ -densitometer is being calibrated at the two-phase test-loop of Österreichisches Forschungszentrum Seibersdorf, in order to measure the low, two-phase natural circulation flow rates.

REFERENCES

- [1] Szabados, L., PMK-NVH - An Integral-Type Test Facility for PWRs. Technical Committee on Thermal Reactor Safety Research, Vienna, 1984.
- [2] Tóth, I., Szabados, L., IAEA-Assisted Research Work in the Field of Operational Safety for Hungary's First NPP, Proc. Operational Safety of Nuclear Power Plants, Marseille, 1983.
- [3] Perneczky, L., Tóth, I., Pre-Test Analysis of PMK Experiments, IAEA Specialists' Meeting on Experimental and Modelling Aspects of SB LOCA, Budapest, 1983.
- [4] Bukrinsky, A.M., Transient processes in NPPs with WWER /in Russian/, Energoizdat, Moscow, 1982.



LIST OF MEASUREMENTS

Measurements	Temperature	Level	Flow	Pressure diff. pr.	Density
Reactor vessel	43	8	1	3	3
Pressurizer	1	1		1	
Steam generator	2	2		2	
Loops		9	2	5	2
Hydroaccumulators	2	2		2	
Feed water line	1		1	1	
Steam line	1		1		
Total:	96	50	22	5	14

Control and Data Acquisition:

- computer system based on mini computer for control
- computerized monitoring system to help the operator
- data acquisition system based on microprocessor and mega-mini computer

Fig. 1 PMK-NVH facility with list of measurements. Control and data acquisition.

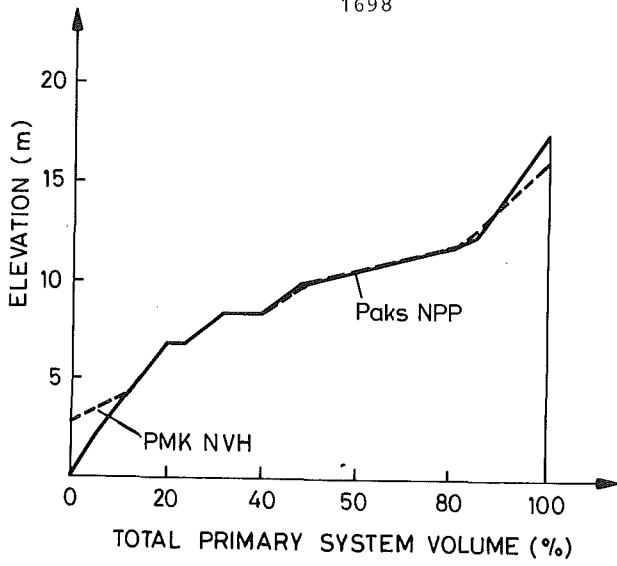


Fig. 2 Comparison of axial volume distributions for PMK-NVH and Paks NPP

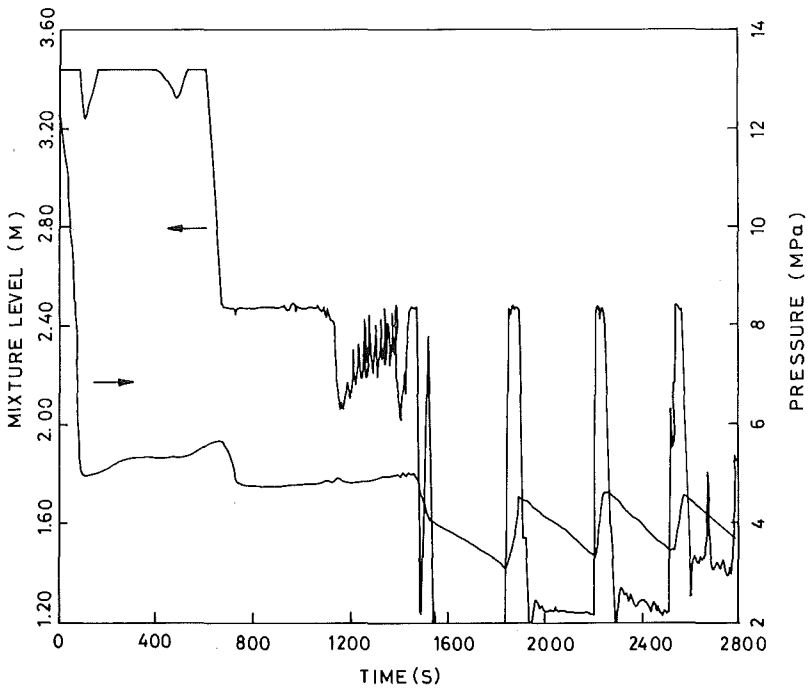


Fig. 3 Variation of PMK-NVH system pressure and steam generator hot collector level /1% cold-leg break/

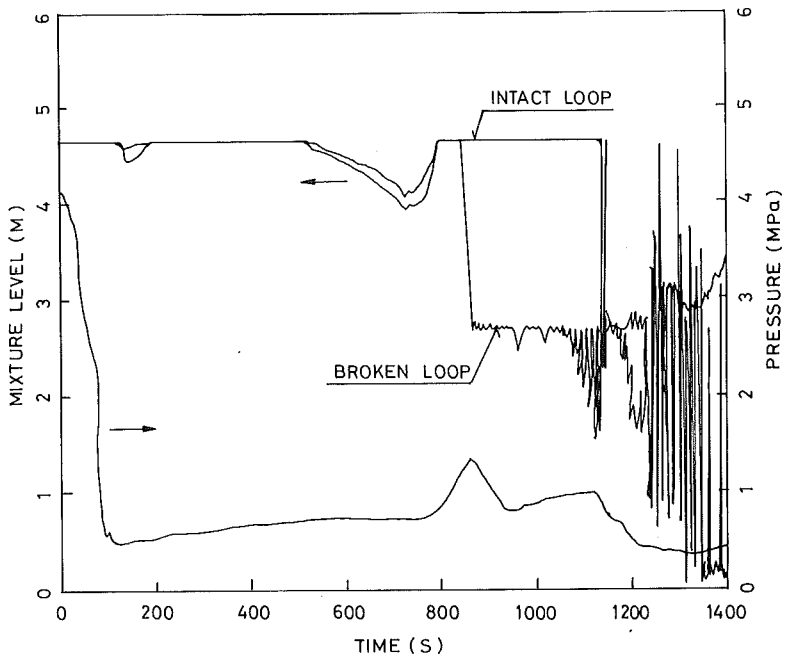


Fig. 4 Variation of Paks NPP system pressure and steam generator hot collector levels in broken and intact loops /1% cold-leg break/

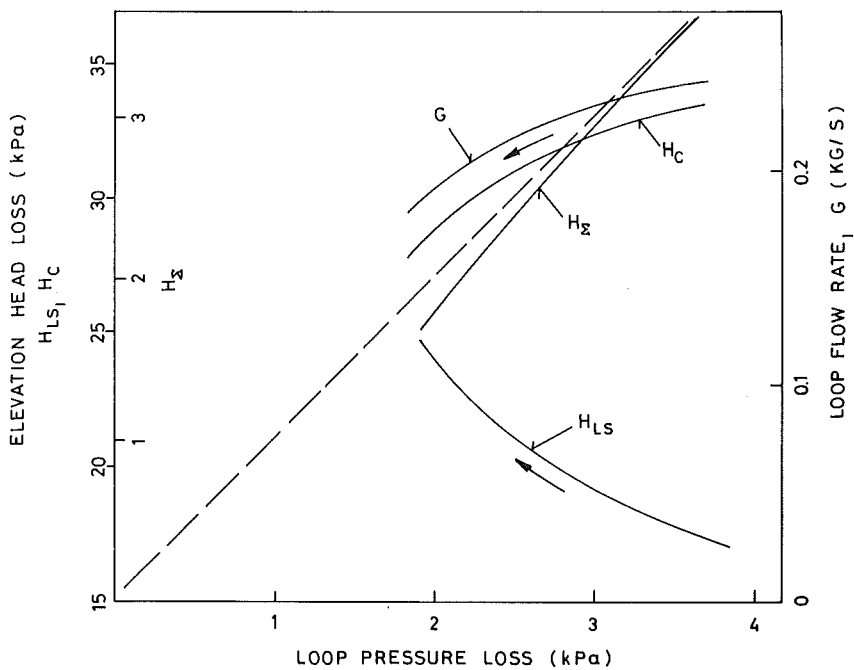


Fig. 5 Elevation head losses and loop flow rate during hot-leg loop-seal clearing

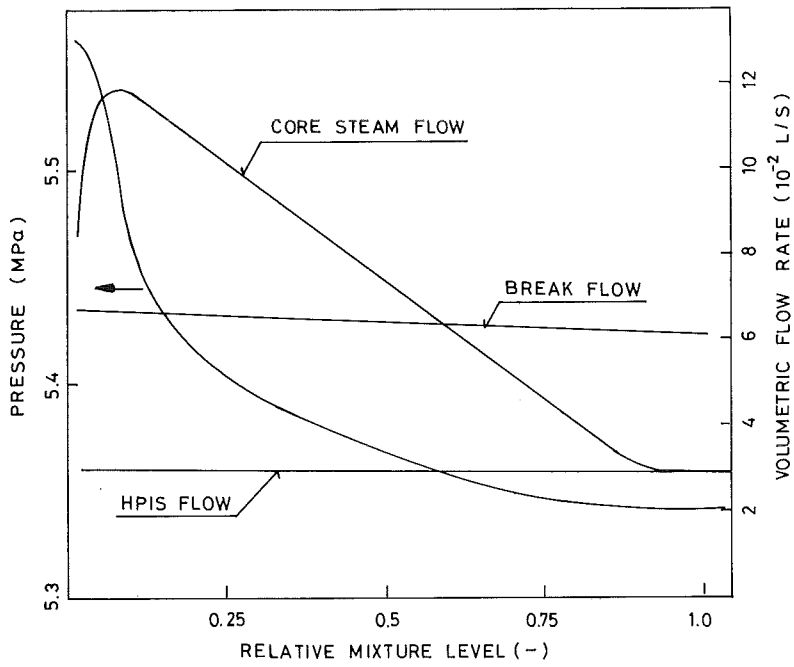


Fig. 6 Leak and fill flow rates and system pressure during hot-leg loop-seal clearing

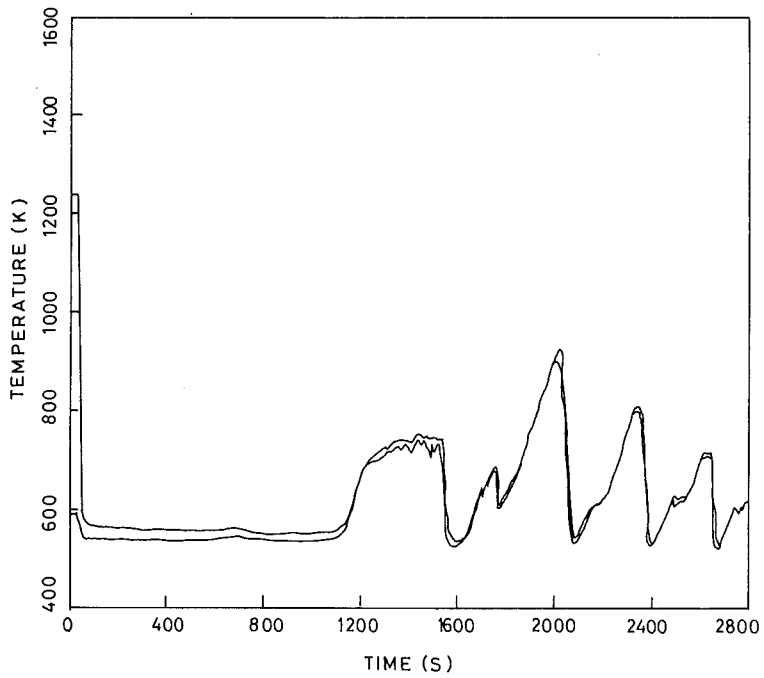


Fig. 7 PMK-NVH fuel rod temperature evolution

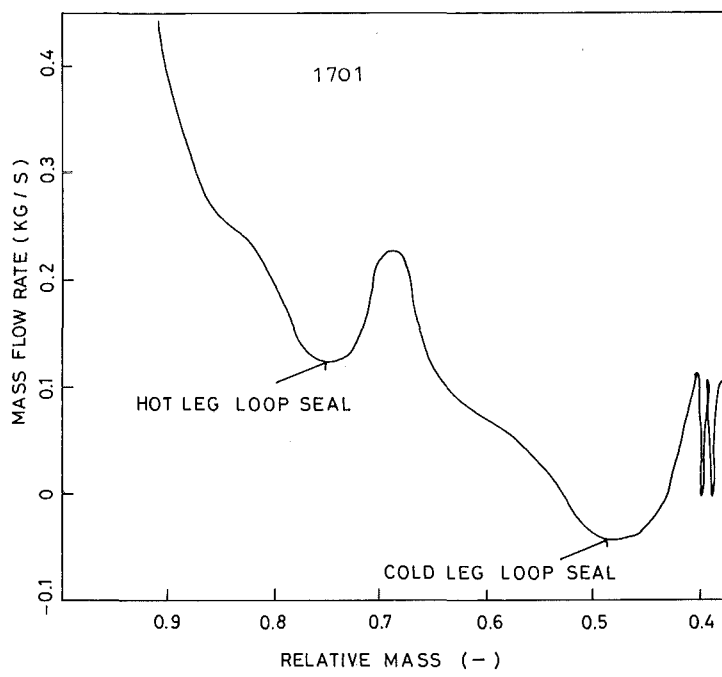


Fig. 8 PMK-NVH natural circulation core flow rate

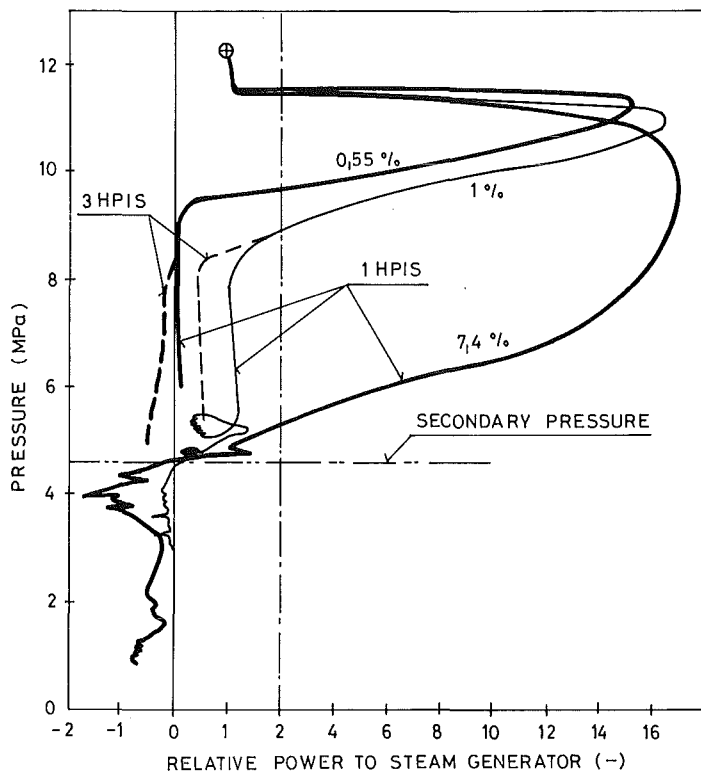


Fig. 9 Effect of relative steam generator power on system pressure with different break sizes

POST ANALYSIS OF A 10 CM² SBLOCA TEST IN THE OTSG
EQUIPPED GERDA FACILITY USING A BBR VERSION OF RELAP4/MOD6

Robert J. Salm

Brown Boveri Reaktor GmbH
Dudenstraße 44
Mannheim, West Germany

ABSTRACT

The paper evaluates a post analysis of a 10 cm² SBLOCA test performed in the BBR / B&W research facility GERDA. The facility is a one-loop, full elevation, 1/1686 scale representation of the BBR PWR design, a design which incorporates once-through-steam-generators and reactor internals vent valves.

The analysis, performed with an extensively modified version of RELAP4/MOD6, shows good agreement with the data. It follows the transient from its start in forced circulation on through the SBLOCA phases of natural circulation, intermittent circulation and the boiler-condenser mode. It ends with the transient under control and the primary loop refilling.

INTRODUCTION

The GERDA project, a joint venture of Brown Boveri Reaktor GmbH and the Babcock & Wilcox Company, provided integral effects test data on SBLOCA phenomena in PWR designs incorporating once-through-steam-generators and reactor vessel internals vent valves. This paper compares data from a 10 cm² reactor vessel leak test to the results of a post analysis with a special BBR version of RELAP4/MOD6.

GERDA

GERDA (figure 1) is a full pressure, single-loop, single-cold leg, full elevation, 1/1686 scale test facility. It has a functioning once-through-steam-generator and an electrically heated core supplying decay heat. The reactor vessel internals vent valves are simulated and enable steam venting from the core outlet plenum to the downcomer. Forced circulation of up to 20 % of plant design is provided by an external pump connected ahead of the reactor coolant pump simulator.

ANALYTICAL TECHNIQUES

The purpose of this benchmark analysis was to demonstrate the suitability of not only the code, a modified version of RELAP4 / MOD6, but also the modeling techniques used by BBR in plant licensing work. Therefore, in spite of known simplifications and conservatisms, the established techniques were not altered except to account for GERDA heat losses, and for the characteristics of the GERDA leak simulation. The RELAP nodalization scheme is shown in figure 2.

Model features include:

- "Double flowpaths":
Horizontally, this technique enables a simple simulation of stratified flow over short distances. Vertically, it prevents steam / mixture "pancaking".
- Vertical slip:
A newly formulated model includes correlations for both bubbly and annular flow regimes.
- Phase separation model:
Enables formation of distinct mixture / steam interfaces.
- 3-region non-equilibrium pressurizer:
Improves simulation of pressurization transients.
- Dynamic heat transfer package:
Covers all major heat transfer mechanisms including filmwise condensation.
- Modified enthalpy transport model:
Adjusts outlet junction properties to account for heat transfer induced temperature gradients within control volumes.
- Vertically non-uniform control volumes:
Reduces the noding detail required to preserve the relationship between fluid volume, level and driving head.

A notable weakness of this particular nodalization scheme (figure 2) is the use of only a single node to simulate the steam generator secondary side. Because of the thermoequilibrium nature of the control volume, there is an underprediction of steam generator performance. Heat transfer to the steam region must be neglected (region cannot superheat) and the model cannot simulate the subcooled heat transfer zone created by the injection of cold auxiliary feedwater. While this is an acceptable, conservative situation for SBLOCA licensing purposes, its effect on the transient is discernable next to test data.

COMPARISON OF ANALYSIS RESULTS TO DATA

The 10 cm² SBLOCA transient described in this paper is typical for breaks of between 5 cm² and 50 cm² and is characterized by three distinct phases:

1. Forced and natural circulation,
2. Intermittant circulation, and
3. Boiler-condenser mode.

Phase 1: Forced and natural circulation

The test is initialized with the primary loop having 9 % forced circulation and fluid conditions which will later key to those in the plant at the time of pressurizer draining. The test is started by opening the leak, a 10 cm² break at the bottom of the reactor vessel, and tripping the external circulation pump. Primary pressure (figure 3) immediately begins to fall as the pressurizer slowly drains. Without a flywheel on the circulation pump, there is a sharp drop in loop flow and a transition to natural circulation (figure 4). The vent valve opens and establishes an internal circulation path through the downcomer and core. By 4 minutes, the pressurizer is empty and safety actions are taken: HPI is actuated, and secondary side level and pressure control setpoints are switched from 3 to 8 m, and 7.9 MPa to 4.8 MPa. Primary pressure stabilizes at 11.7 MPa as steam begins to form and collect in the hot leg U-bend. Loop circulation diminishes and soon boiling begins in the core. Steam accumulates in the vessel (figure 5) and liquid is displaced out into the loop. As circulation recovers, the resulting flow of subcooled liquid into the vessel now condenses steam and draws liquid out of the loop. By 7 minutes (analysis: 8 minutes), loop flow is fully interrupted.

Phase 2: Intermittant circulation

Although there is no longer sufficient liquid in the primary system to support uninterrupted natural circulation, the shifting of inventory between the reactor vessel and the loop continues to provide regular pulses of loop circulation. Because individual flow cycles are comprised of distinct steps that do not vary too much from cycle to cycle, only the first flow cycle will be described.

1. The hot leg mixture level falls below the hot leg U-bend and loop circulation is interrupted. See flow (figure 4) at 7 minutes (analysis: 8 minutes).
2. Subcooling in the cold leg discharge piping / downcomer region is not adequate to condense core steam (via vent valve path). Primary pressure begins to increase as steam accumulates in the reactor vessel. Liquid is displaced from the vessel region into the loop. See both pressure (figure 3) and vessel level (figure 5) at 7 minutes (analysis: 8 minutes).
3. The hot leg mixture level increases until liquid spills over the hot leg U-bend and initiates loop circulation. See flow (figure 4) at 9 minutes (analysis: 9.5 minutes).

4. Primary pressure falls as subcooled fluid circulated from the steam generator to the vessel condenses steam. Secondary side pressure momentarily increases as hot primary fluid enters the heat transfer zone. See pressure (figure 3) and vessel level (figure 5) at 9.5 minutes (analysis: 10 minutes).
5. As vessel steam is condensed, liquid is drawn from the loop back into the vessel and the hot leg mixture level falls below the U-bend. Loop circulation is again interrupted and the first flow cycle is completed. See flow (figure 4) at 11 minutes (analysis: 12 minutes).

Phase 3: Boiler-condenser mode

Since primary pressure is still too high for the HPI to overfeed the leak, the loop continues to drain. At 32.5 minutes (analysis: 31 minutes), the primary side steam generator level drops below the secondary level, thereby initiating the condensation of primary steam. Primary pressure falls sharply while secondary side pressure rises (figure 3). The analysis ends at 46 minutes with HPI exceeding leak flow and primary pressure still decreasing.

COMMENTS TO COMPARISON

The differences between the analysis results and the test data are in most cases attributable to the underprediction of steam generator heat transfer. It explains for example,

- . the somewhat greater degree of primary system pressurization during the intermittent circulation phase (figure 3),
- . the markedly lower rate of depressurization in the boiler-condenser mode,
- . the relatively small secondary side pressure rise that accompanies each pulse of intermittent circulation and the start of the boiler-condenser mode, and
- . the small shifts in event timing that result from the inadequate subcooling of cold leg fluid.

Because the root cause of these differences is the simple one-node secondary side model, switching to a best estimate multi-node secondary side would markedly improve the analytical results.

The oscillatory flow behavior starting in the RELAP calculation at 22 minutes (figure 4) is not numerical instability. It is a 10 second period cyclic process characteristic of the full elevation, small scale GERDA loop when the vessel mixture level is within the hot leg nozzle and the loop is draining. It is not as evident in the plot of test data because of a low data storage frequency and the tendency for the flow metering orifice to uncover under these conditions and go out of range.

CONCLUSION

Although using conservative licensing techniques, the quantitative differences between the data and the analysis are not large. Further, the BBR version of RELAP4/MOD6 reproduces all major phenomena starting from the circulation pump trip, through intermittent circulation, to the boiler-condenser mode. Taken as a whole, the calculation demonstrates a fundamental capability to perform this type of analysis.

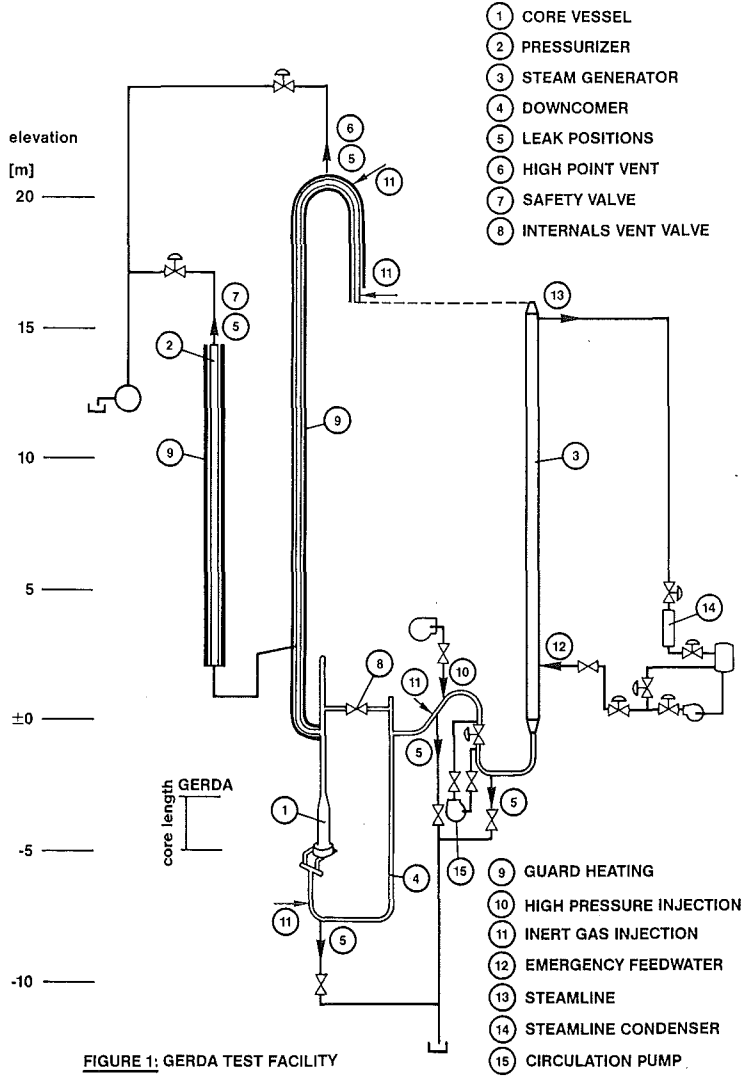
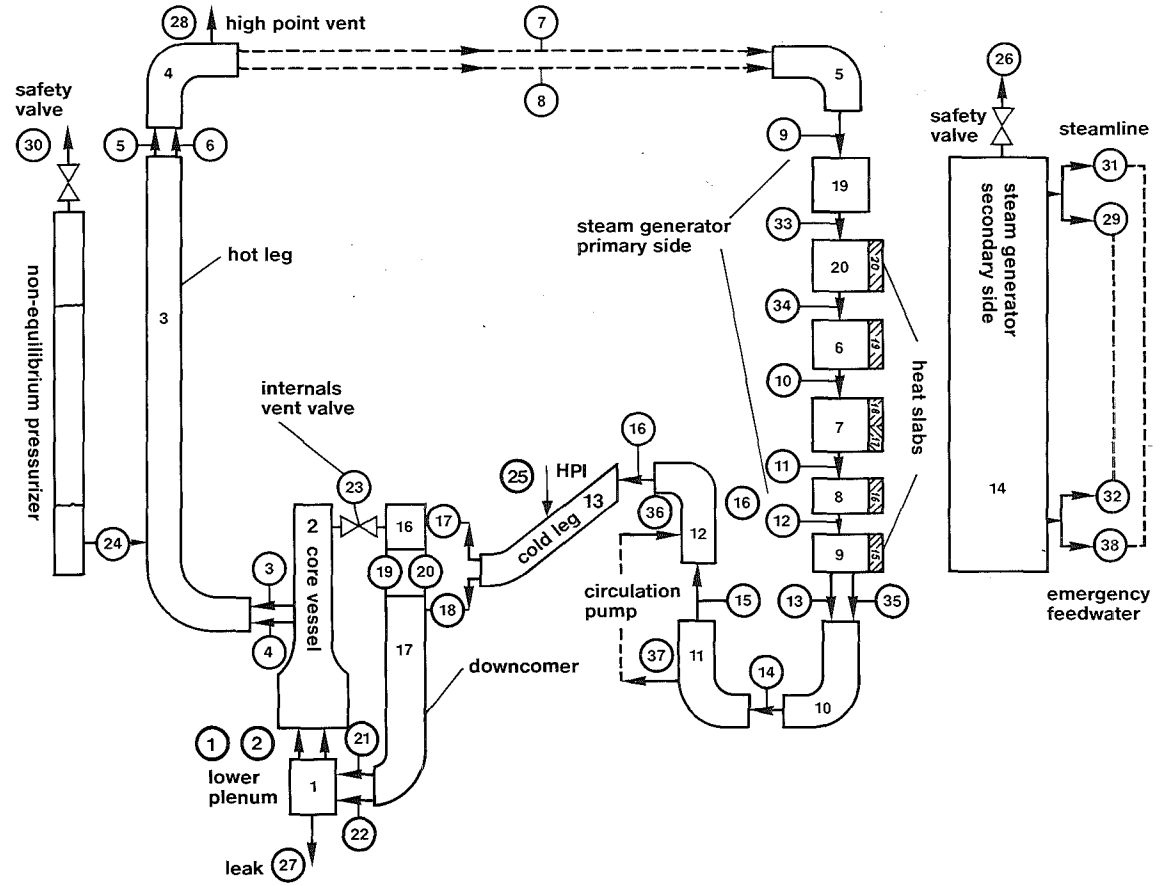


FIGURE 1: GERDA TEST FACILITY

FIGURE 2: RELAP NODALIZATION SCHEME FOR GERDA ANALYSIS



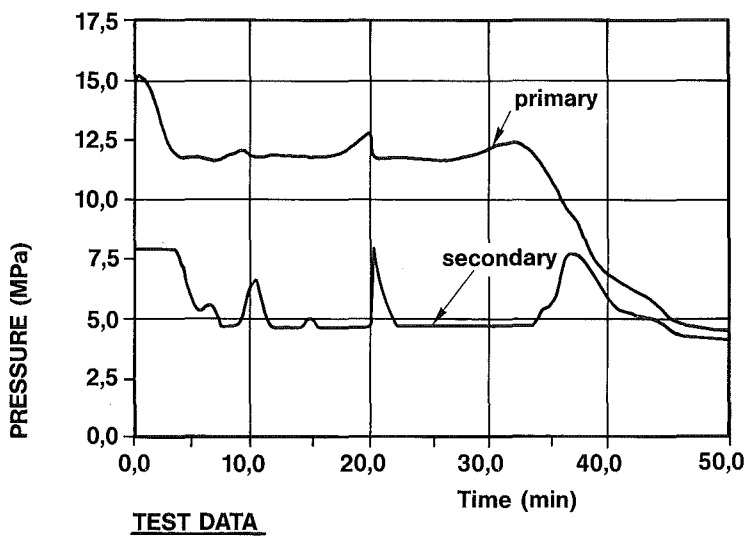
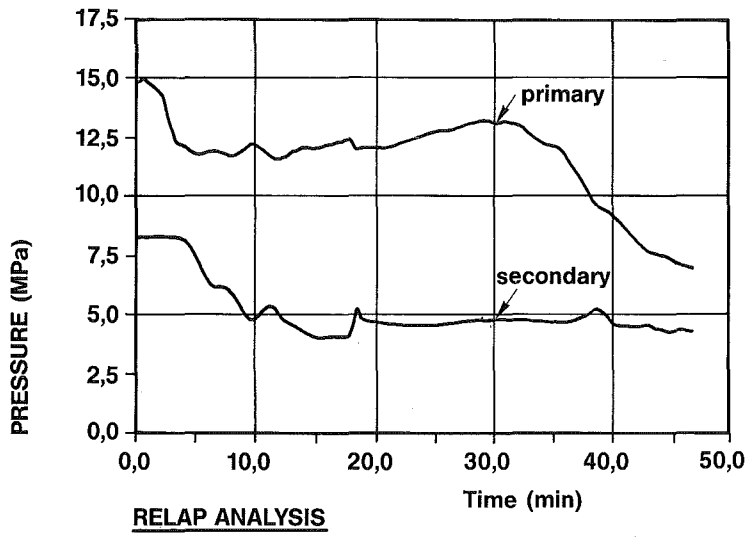


FIGURE 3: PRIMARY AND SECONDARY PRESSURE
- 10 cm² REACTOR VESSEL LEAK
- GERDA TEST 1605AA

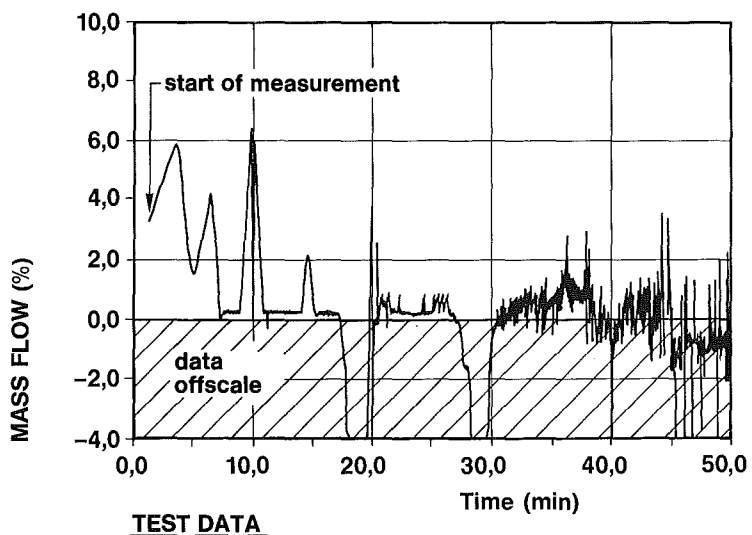
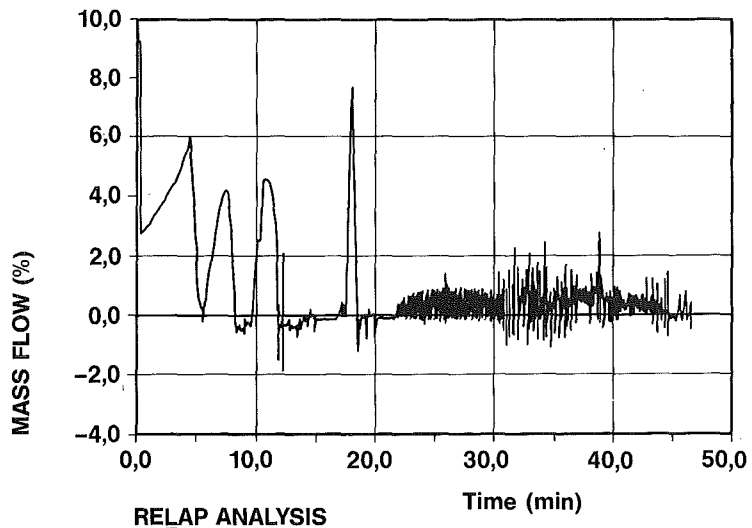


FIGURE 4: COLD LEG MASS FLOW
 - 10 cm² REACTOR VESSEL LEAK
 - GERDA TEST 1605AA
 1 % = 0,12 kg/s

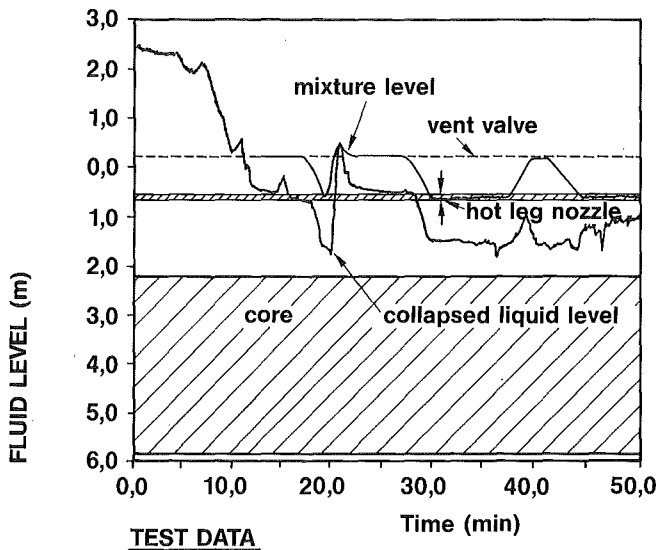
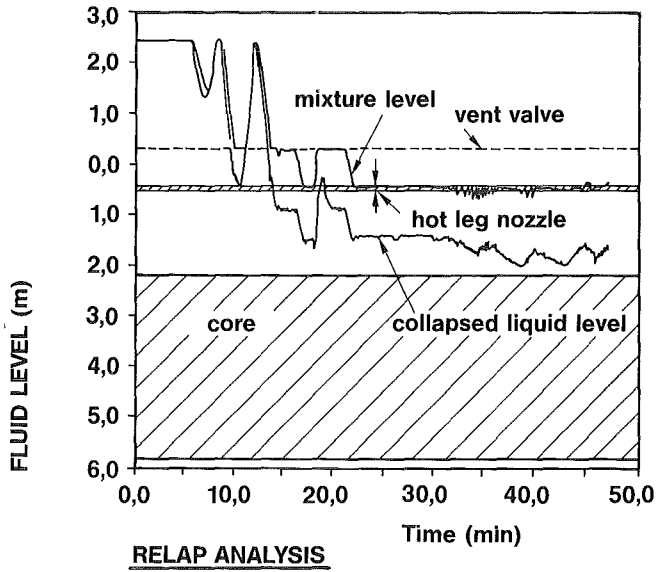


FIGURE 5: MIXTURE LEVEL AND COLLAPSED LIQUID LEVEL IN THE CORE VESSEL
 - 10 cm² REACTOR VESSEL LEAK
 - GERDA TEST 1605AA

POST TEST CALCULATIONS OF SEMISCALE PUMP SUCTION SMALL
BREAK LOCE, S-PL-4, USING RELAP5/MOD1.5

P C Hall

Central Electricity Generating Board
Berkeley Nuclear Laboratories
(current address: CEGB, Generation Development and Construction Division
Barnwood, Gloucester, UK)

ABSTRACT

This report describes posttest analysis of the Semiscale 5% pump suction break experiment, S-PL-4, using RELAP5/MOD1.5. MOD1.5 is a direct development of MOD1, with more sophisticated treatment of thermal disequilibrium and interphase drag. It embodies many of the improvements subsequently included in RELAP5/MOD2, though it retains the use of only five conservation equations. Apart from requiring special modelling to overcome a suspected code error in the break flow calculation, the code ran without difficulty and accurately reproduced the measured primary mass inventory, pressure history and overall chronology. Potentially important errors in the calculated water distribution within the primary system were observed, and were concluded to be related both to difficulties in the calculation of the timing of clearing of the intact loop pump suction pipework and to the calculation of voidage distribution in a boiling channel. However, actual errors in calculated clad temperature were less than 50K.

INTRODUCTION

The test considered in this report is S-PL-4, which was a 5% area LOCE, with the break located in the pump suction, conducted on the Semiscale MOD-2B facility, at the Idaho National Engineering Laboratory. Semiscale is scaled to a reference 4-loop PWR based on a power-to-volume ratio of 1/1705.5. The system consists of a pressure vessel with a simulated PWR core and internals, an external pipe downcomer and two primary coolant loops, each with an active steam generator. The intact loop is scaled to represent three primary loops, while the broken loop represents the fourth. In order to scale the facility correctly and to preserve important phenomena, component elevations, dynamic pressure heads and liquid distributions were maintained as close to the reference PWR values as possible. Test S-PL-4 is the first in an integral facility to model a break in the pump suction pipework, and may be seen as extending the existing Semiscale data base on 5% breaks, which includes the cold leg break tests S-UT-6, 7, and 8.^{1,2} This paper compares the results of test S-PL-4 with calculations performed using RELAP5/MOD1.5, with the objective of assessing the capabilities of the code.

DESCRIPTION OF FACILITY, AND CONDUCT OF TEST

Full details of the Semiscale MOD2B facility as configured for this test can be found in references 3 and 4. The main feature particular to this test was that the break orifice was positioned in the horizontal leg of a tee, approximately half way up the upflow leg of the broken loop pump

suction pipe. Flow leaving the break was routed via a condenser to vented collection tanks. Break flow rate was derived by measuring the rate of change of hydrostatic head in these tanks.

The initial conditions for this test are summarized in Table 1. A comprehensive compilation of data from Test S-PL-4 is available.⁵ The primary was at normal 100% power with a core temperature rise of 32K. The secondary pressures were allowed to float. The course of the test was relatively straightforward. Blowdown was initiated at time zero, and a SCRAM signal was generated on low pressurizer pressure (12.6 MPa) at 13s. This signal activated core power shutdown, and the closing of the SG feed and steam valves. Primary pumps were tripped at 43s, and high pressure injection commenced at 44s. No further operator actions or trips were simulated before the initiation of Low Pressure Injection at about 2400s. The experiment was terminated at 2697s.

Table I Initial Conditions for S-PL-4

		Measured	Calculated/Input
Cold leg flow	Broken loop	3.5 μ /s	3.5 μ /s
	Intact loop	10.5 μ /s	10.5 μ /s
Pressurizer pressure		15.6 MPa	15.9 MPa
Core power		2.00 MW	1.96 MW
Cold leg temp.	Broken loop	560.0 K	557.5 K
	Intact loop	557.5 K	560.1 K
Lower plenum fluid temperature		558.4 K	559.3 K
Core fluid temperature rise		31.7 K	32.9 K
SG pressure	Broken loop	5.2 MPa	5.68 MPa
	Intact loop	5.6 MPa	5.60 MPa
SG Secondary Mass	Broken loop	32.4 kg	32.6 kg
	Intact loop	126.3 kg	126.6 kg

RELAP5 MODEL DESCRIPTION

The Semiscale MOD2B system RELAP5 model is represented by the nodalization diagram in Figure 1. It is generally based on the Semiscale MOD2A Standard RELAP5 Model⁶, with Improved modelling of the guard heaters. The model used for these analyses consists of 162 hydrodynamic volumes, 168 junctions, and 227 heat structures. All volume parameters are calculated with non-equilibrium code models. Steam generator secondaries, ECC systems, system environmental heat loss, and piping guard heaters (which were switched off in this test) are modelled in detail. The core axial power profile is modelled with twelve continuous heat structures over six axial hydrodynamic volumes.

The steam generator secondaries are modelled with four hydrodynamic volumes in the U-tube region and nine in the downcomer. Previous Semiscale models^{1,7} have used more detailed nodalization than this, but have involved tests in which the SG secondaries played a dominant role (feed and steamline breaks, 2½% area LOCE). In this test, the secondaries are sealed early in

the transient and the primary-to-secondary heat transfer is expected to be much less important in a 5% break. The riser and downcomer are modelled as pipe components.

Two discharge coefficients are applied to the RELAP5 critical flow model at the break, one (CD1) for subcooled flow and another (CD2) for two phase and vapour flow. In the analysis of the 5% breaks in the UT series of tests (which used the same orifice plate as this test) Leonard^{1,2} found appropriate values for these coefficients to be 0.9 and 0.8 - 0.84 respectively, when using RELAP5/MOD1. Preliminary checks indicated that, at 1000 psia, two phase critical flow rates calculated with MOD1.5 were approximately 40% less than those calculated using MOD1. Brief investigation suggested that this discrepancy resulted from a probable error in the break flow modelling in the present cycle of RELAP5/MOD1.5. In view of the different behaviour of the two MODs it would not be appropriate to use the break flow multipliers developed by Leonard, (with MOD1) in this (MOD1.5) calculation. Instead, it was decided to minimize the effects of the suspected code error by attempting to force MOD1.5 to give break flow behaviour similar to that experienced by Leonard, modelling this orifice plate with MOD1. A close match to MOD1 performance could be achieved by adopting a single velocity model within the break junction, and in order to force still closer correspondence between the two MODs, the value of CD2 was increased to 0.88.

Initial Conditions

To simplify the finding of a steady state calculation, a simple control system was modelled using RELAP5 control variables. For example, desired loop flow was achieved by adjusting the speed of the primary pumps. Other items controlled in this way were the secondary steam valve position (to achieve desired pressure); and feed flow rate (to control secondary mass inventory). During the approach to steady state, the primary pressure was held at the required value using a very large dummy pressurizer, which was deleted from the calculation 20s before the start of the transient. Calculated primary and secondary conditions just before the start of the transient were somewhat steadier than those obtained in the test.

The initial conditions obtained by these means are summarized in Table I, and most parameters are shown to be within the experimental uncertainty. The main discrepancy is in the broken loop SG secondary pressure (and therefore, temperature). This temperature was purposely raised to reduce an error of -9K in the calculated broken loop cold leg liquid temperature. The error introduced into the initial pressure and temperature must, of course, affect the calculation, but subsequent scrutiny of the calculated results suggested that the effect was small.

Boundary Conditions

Core power was entered, using an input table of power versus time after reactor scram. In this test, the pumps were coasted down manually. Measured values of pump speed versus time after break opening were inserted via a table. Secondary steam and feed flows were ramped to zero after scram, in accordance with the measured valve closure times. HPIS injection was calculated from an input table of flow rate versus pressure, constructed from measured data. The accumulators were modelled using the RELAP5 accumulator component. Environmental heat losses were calculated mechanistically, and were within the experimental uncertainty quoted by Loomis.⁸

Table II. Sequence of Events

	Measured Time (s)	Calculated Time (s)
Blowdown initiated	0	0
Pressurizer pressure reached reactor trip set point (12.6 MPa [1827 psi])(SCRAM)	13	13.0
Broken loop pump suction down-flow leg clears	120	220
Break flow demonstrates sharp reduction (indicates two phase upsteam conditions)	120	85
Upper head drains	190	Does not completely drain
Void fraction in broken loop pump suction exceeds 90%	200	250
Core starts to uncover (dryout heatups start)	430	-
Intact loop accumulator injection starts	460	450
Broken loop accumulator injection starts	469	460
Core level starts to recover	505	505
Intact loop pump suction upflow leg clears	540	180
Broken loop accumulator empties	1044	>1411
Experiment terminated	2697	

COMPARISON OF EXPERIMENTAL AND CALCULATED RESULTS

The measured and calculated pressure histories are shown to be in excellent agreement in Figure 2. This is, in large part, a consequence of the good agreement between measured and calculated break flows, especially beyond 200s (Figure 3). Before 85s, the calculated discharge flow is somewhat too high, but as soon as steam appears at the break (void fraction >2%) discharge flow falls by about 60% and remains too low until about 210s. In terms of integrated mass discharge, these two errors fortuitously cancel giving very accurate system mass inventory. Anomalies in the behaviour of the RELAP5 critical flow calculation were noted above. The accurate pressure and mass discharge calculations enable the code to calculate the chronology of the experiment very accurately also, as illustrated in Table II.

The first major process of the transient, the draining of the pressurizer was calculated within the experimental uncertainty and this led to accurate timing of the reactor trip signal (scram) at 13s. Several other events are related to this trip (i.e., isolation of SG secondaries, starting of HPI, and tripping of the primary pumps) and are therefore accurately timed also. After the pumps coasted down, (54-58s) flows in the primary fell close to zero enabling the vertical differential pressure measurements to be used to assess liquid inventory. Measured and calculated drainage of both sides of the SG U-tubes were in reasonable agreement, calculated emptying times typically being within 25s of measured values.

The collapsed liquid levels in the pump suction pipework are shown in Figures 4, 5, 6, and 7. Figures 4 and 6 illustrate the reversal of order of

emptying the down side of the pump suction. The broken loop pump suction downside began to empty, but at about 85s, the draining was halted. Since the calculated break flow fell sharply at this time, it was suspected that errors in the break flow might have contributed to the errors in clearing the pump suction. A sensitivity calculation was performed in which the break flow was forced to exceed data until 140s. The result was somewhat more rapid emptying of both loops, but the reversal in the order of draining, and the large delay in clearing the broken loop pump suction downside persisted. In the base case calculation, draining of the downside of the intact loop pump suction (Figure 4) is very accurately calculated until 190s. In the calculation, this pump suction cleared, whereas in the experiment it refilled. A possible contribution to this behaviour is the ability of "homogeneous node" codes to pass steam through the pump suction before the liquid level falls to the bottom. Davis⁹ has previously observed this behaviour, and Summers¹⁰ has shown that finer nodding of the downside can ameliorate the difficulty. Consequences of the early clearing of the intact loop pump suction included a maldistribution of steam flow in the loops in the period 200-600s (the intact loop pump suction actually cleared at 600s); and the delivery of a slug of water to the downcomer and also to the broken loop pump suction, delaying its clearance still further.

In spite of the detailed errors in the calculated clearing of the loops, the overall behaviour was reasonably accurate. In particular, errors in the calculated broken loop upside density were relatively minor. Hence, the pressure and integrated break flow were in good agreement with data by the time agreement between measured and calculated conditions near the break was achieved (250s). In consequence, the timing of initiation of accumulator injection was also calculated within 20s. Furthermore, since the calculated total primary inventory was correct as the accumulators began to inject, the pressure fluctuations caused by condensation on the cold water were also accurately calculated.

Since the primary pressure and inventory were calculated reasonably accurately, we might expect calculation of other features within the system to be accurately calculated also. This does not prove to be the case. For example, the measured heater rod temperatures at the top of the core indicate a minor dryout commencing at about 460s, which does not appear in the calculated results. Figure 8 shows that the mixture level fell below the top of the core at this time, a feature which the calculation failed to reproduce. Indeed the calculated mixture density at the top of the core is higher than that in the middle in spite of monotonically increasing steam flow rate. This feature is at odds with a wide range of experimental data¹¹, including that of the present test. However, the calculated core water inventory is only slightly too high at the time dryouts are observed, suggesting the errors in the calculated water distribution within the core may contribute to the core's failure to reproduce dryout. Excessive liquid is also held in the upper plenum, and both hot legs for significant portions of the calculation. This excess vessel inventory prior to accumulator injection is consistent with the erroneous clearing of the intact loop pump suction pipe work. A consequence of the calculated existence of excess water at outlet from the core is failure to reproduce the steam superheating observed in these areas (see, for example, Figure 9). This unfortunately precludes any test of the ability of the improved treatment of superheat implemented in MOD1.5.

The calculated pressure response of the secondary side of the steam generator is broadly correct, except in the broken loop SG after it became a heat source. The test data imply that its coupling to the primary was rather loose, whereas calculated secondary pressure followed that of the primary. This erroneous close coupling occurred because a small amount of water, incorrectly calculated to reside in the lowest node of the inlet side of the U-tube, permitted a region of transition or nucleate boiling, which greatly enhanced the calculated heat removal from this secondary, and led to overestimation of the depressurization rate within it.

The calculation was terminated at 1411s, with the calculated pressure approximately 0.15 MPa too high, at 1.9 MPa, and falling too slowly. The reason for this fairly minor departure is suspected to be due to errors in the measured HPIS flow rate starting at about 900s. In view of this uncertainty it was considered unworthwhile to extend the calculation.

DISCUSSION OF PERFORMANCE OF RELAP5/MOD1.5

This calculation was performed as part of the independent assessment of RELAP5/MOD1.5, and no special modelling of the Semiscale facility, nor special code updates were used, with the exception of the changes made to discharge flow modelling noted earlier. With this proviso, the calculation of discharge flow and primary inventory was excellent, although some evidence exists of cancelling errors in the calculation of discharge flow in the subcooled and very low quality regions. It is considered that the use of finer noding in the pump suction near the break would not ameliorate these problems, and is therefore unnecessary.

The accumulator model worked satisfactorily, though neither accumulator had ceased injecting water at the time the transient was terminated. The weak area of the calculation was in the water distribution around the system. In particular too much water was held in the upper core, upper plenum and hot legs, and too little in the intact loop pump suction and the lower part of the core. Although it has not been possible to identify particular causes of this behaviour, an obvious candidate is the interfacial drag modelling, allowing too much slip, and permitting steam generated within the core and hot legs in the period 80-120s to pass round the loops without entraining water with it. Several alternative explanations, relating to break flow modelling and initial conditions in the SG secondaries were investigated, but found not to improve the representation of the loop flows or clearance of the pump suction.

For the initial part of the transient, the maximum time step was set at 0.5s, and the RELAP5 time step control system functioned to keep the actual maximum time step below this limit. The minimum time step (10^{-7} s) was used on a number of occasions during the first 100s of the calculation, and time step dependent oscillations were observed, but the code did not fail. RELAP5/MOD1.5 cycle 34 includes a mass error mitigation scheme, and so no significant mass errors were sustained at any point in the calculation. The calculation proceeded without major difficulty until its termination at 1411s. The average ratio of cpu:real time was approximately 8:1, on a cyber 176 computer.

CONCLUSIONS

1. Excellent agreement between calculated and measured pressure history, and chronology of events was obtained for this pump suction break. No special modelling of the broken loop pump suction was required.
2. Loop pump seal clearing was calculated reasonably well. Minor errors in calculated loop density led however to errors in timing of the clearing event.
3. Significant errors in the water distribution within the system were noted throughout the calculation. These errors are believed to be associated mainly with the calculation of clearance of the pump suction pipe work, though other more detailed errors in the calculation of the water distribution within the core may also be important.
4. The critical flow model in RELAP5/MOD1.5/Cycle 34 gave significantly lower discharge flow rates than the corresponding model in RELAP5/MOD1, when two-phase conditions exist upstream of the break. In this calculation special modelling was used to avoid this feature. It is believed that the anomaly has been removed from more recent versions of the code.

ACKNOWLEDGMENT

This paper is published by permission of the Central Electricity Generating Board and the United States Nuclear Regulatory Commission. The work reported here was performed whilst the author was on attachment with EG&G (Idaho) Inc at the Idaho National Engineering Laboratory, under the USNRC/UKAEA Code Validation Agreement.

The author wishes gratefully to acknowledge the assistance afforded by numerous members of Semiscale staff, as well as members of Reactor Simulation and Analysis Branch, at EG&G (Idaho) Inc.

REFERENCES

1. M T Leonard, Post Test RELAP5 Simulation of the Semiscale S-UT Series of Experiments, EGG-SEMI-5622, October 1982.
2. M T Leonard, Vessel Coolant Mass Depletion During a Small Break LOCA, EGG-SEMI-6061, September 1982.
3. J C Chapman and J R Wolf, ESO for Semiscale MOD-2B Power Loss Experiment Series (Appendix S-PL-4), EGG-SEMI-6061, 1982.
4. J C Chapman and J R Wolf, Quick Look Report for Semiscale Power Loss Series Experiment, S-PL-4, EGG-SEMI-6314, June 1983.
5. R A Larson, Experiment Data Report for Semiscale MOD-2B Power Loss Test Series (Tests S-PL-4 and -7), NUREG/CR-3462, September 1983.
6. M T Leonard, RELAP5 Standard Model Description for the Semiscale MOD-2A System, EGG-SEMI-5692, December 1981.

7. J E Streit, Post Test RELAP5 Simulation of the Semiscale MOD-2A Feedwater Line Break Tests, S-SF-1, 2, and 3c, EGG-SEMI-6062, October 1982.
8. G G Loomis, Summary Report, Semiscale Mod-2A Heat Loss Characterization Test Series, EGG-SEMI-5448, May 1981.
9. C B Davis, RELAP5 Calculations of the Effect of rimary Coolant Pump Operation During Semiscale SB Experiments, EGG-CAAD-5531, 1981.
10. R M Summers, RELAP5 Assessment: Semiscale MOD-3 Small Break Tests NUREG-CR-3277, July 1983
11. K H Ardron and P C Hall, Prediction of Void Fraction in Low Velocity Vertical Steam-Water Flow, Jnl. Heat Transfer, Vol. 102, No 1, pp 3-8, 1980.

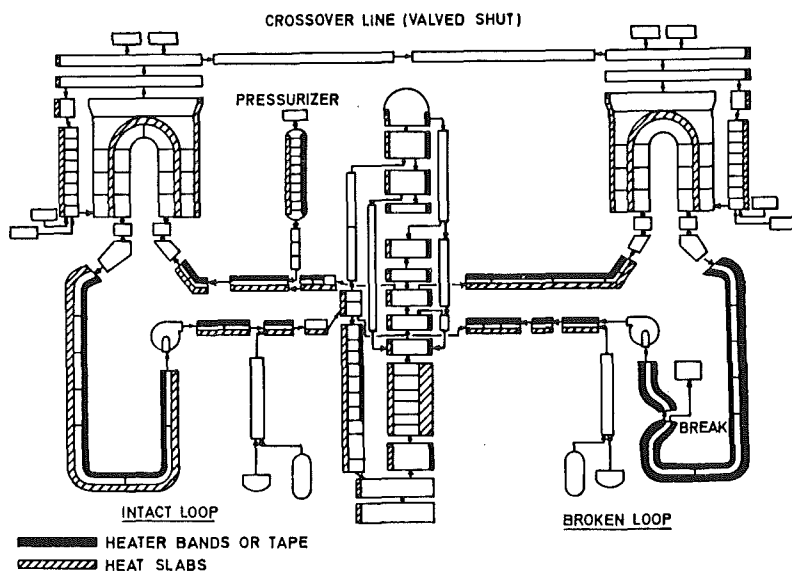


FIGURE 1 RELAP5 NODING DIAGRAM

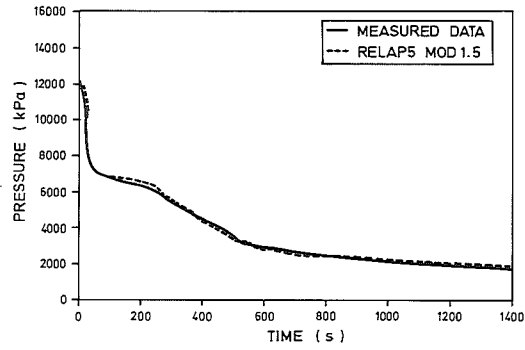


FIGURE 2 SYSTEM PRESSURE

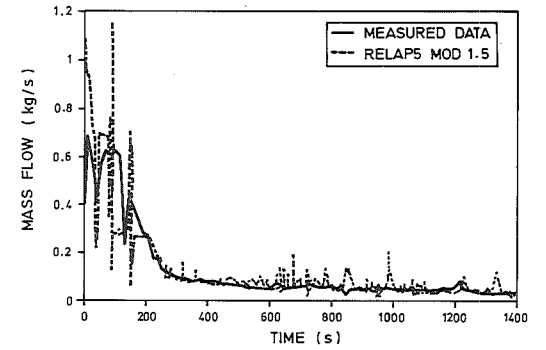


FIGURE 3 BREAK FLOW

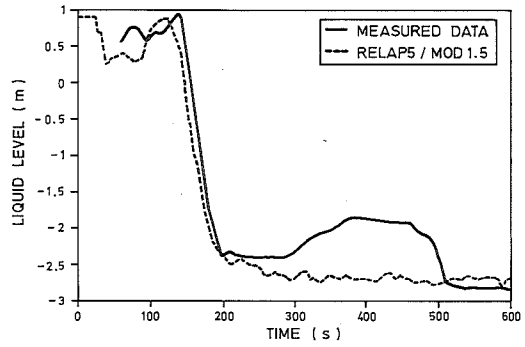


FIGURE 4 INTACT LOOP PUMP SUCTION DOWNFLOW COLLAPSED LIQUID LEVEL

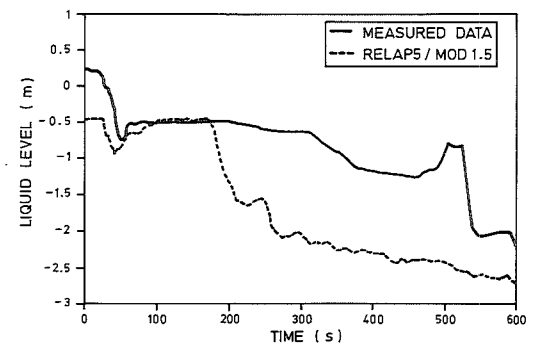


FIGURE 5 INTACT LOOP PUMP SUCTION UPFLOW COLLAPSED LIQUID LEVEL

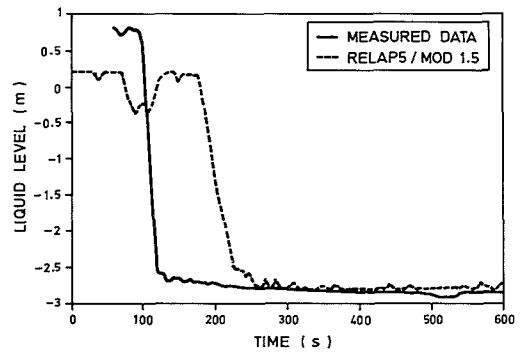


FIGURE 6 BROKEN LOOP PUMP SUCTION DOWNFLOW COLLAPSED LIQUID LEVEL

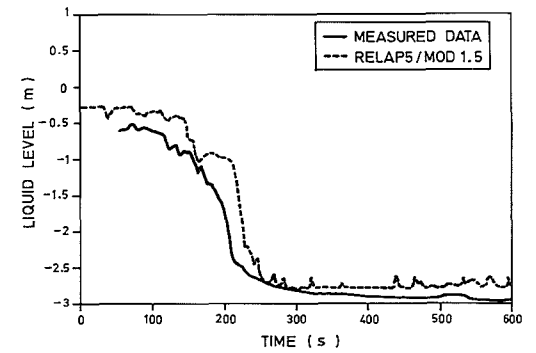


FIGURE 7 BROKEN LOOP PUMP SUCTION UPFLOW COLLAPSED LIQUID LEVEL

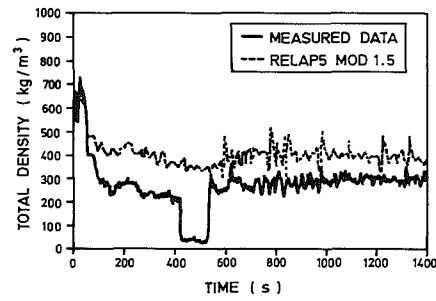


FIGURE 8 COOLANT DENSITY NEAR TOP OF CORE

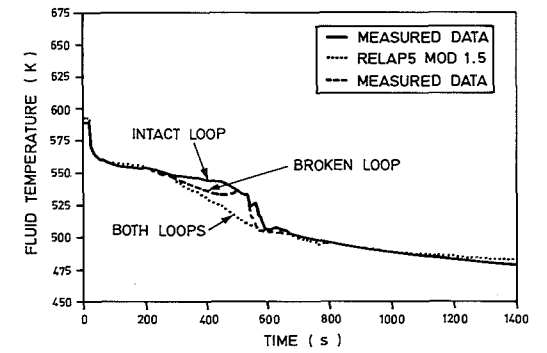


FIGURE 9 HOT LEG TEMPERATURES

SMALL BREAK ANALYSES WITH COMPUTER CODES SMABRE AND RELAP5/MOD1

J. Miettinen

Technical Research Centre of Finland
Nuclear Engineering Laboratory
P.O. Box 169, 00181 Helsinki, Finland

ABSTRACT

The LOFT small break tests L3-5 and L3-6 and the LOBI test SD-SL-03 have been analysed using the large system code RELAP5/Mod1 and the simplified, fast running code SMABRE. The comparison against the experimental results and comparison between the results of the codes indicate, that the simplified solution method used in SMABRE is satisfactory, when small break transients are calculated. Because SMABRE computes at least ten times faster than RELAP5, it is a practical tool in extensive studies of parameter effects during small break LOCA (SBLOCA) transients both in scaled experimental facilities and real plants. RELAP5 is used parallel for calculation of some parameter conditions. SMABRE has also been installed to the full scope training simulator of the Loviisa plant.

INTRODUCTION

The development of light water reactor (LWR) transient analysis capabilities has produced large system codes like RELAP4, RELAP5, TRAC, DRUFAN and CATHARE for analysis of loss of coolant accidents (LOCA). The solution methods of the thermohydraulics are developed to handle most severe LOCA transients as well as milder LOCA transients in LWR's. The size of the code systems is typically large, and hundreds of man-years may be used for code development. Computation needs large computers and computation times are typically at least ten times longer than real time. For code modifications specialists are needed.

In the case of a small break LOCA (SBLOCA) the possibilities for different event paths are nearly infinite. Then the large codes are not practical tools for plant response studies with many parameter combinations and a simpler model with the following features is needed in addition to the large system codes:

- o Real time simulation capability to allow large parameter studies. Interactive computer periphery gives a feeling about the real time sequences.
- o The process parameters are simulated with sufficient accuracy: Very high accuracy is not needed.
- o All possible control functions affecting the thermohydraulics are simulated.

These may be seen as the main ideas in the development of the SBLOCA code at the Technical Research Centre of Finland (VTT). The development of this code started in 1980 after TMI. The Finnish PWR's have some differences compared to Western PWR plants and thus own code development was well argued. The SBLOCA transients with leak sizes from 0 to 10% are significant from plant safety point of view.

The code is called SMABRE (SMAll BREAK) /1/. SMABRE may be used for 0 to 10 % SBLOCA analyses of PWR plants and for plant transients where neutron kinetics are not important. The secondary side model is simple describing water and steam parts as fully separated volumes. The modelling capability of the code is versatile allowing calculation of the various systems including simple separate test facilities as well as large nuclear power plants.

SMABRE is capable to simulate the transients in real time with a process computer like PDP 11/70 and the modified version of the code has been implemented as a primary side two-phase model to the Loviisa full scope training simulator having two parallel PDP 11/70 computers for plant physical simulation /2/.

In thermohydraulic analyses of the Finnish PWR's the large computational tools are the RELAP4 and RELAP5/Mod1 codes and in the near future the RELAP5/Mod2 version is expected to be installed. The computer used for assessment and independent plant analyses at VTT is Cyber 173. The parallel use of RELAP5 and SMABRE has been seen beneficial both in plant applications and in code assessment. If a large set of parameter variations is needed, a few selected common cases are calculated with both codes after parameter variations with SMABRE.

DIFFERENCES BETWEEN SMABRE AND RELAP5

Both the numerical solution methods and the set of physical correlations are quite different in SMABRE and RELAP5. In Table 1 the main features of the codes regarding SBLOCA calculations are compared.

The field equations in SMABRE are written for the conservation of mixture mass, steam mass, integrated mixture momentum and water or steam energy. The two-phase separation is calculated using the drift flux model. In RELAP5/Mod1 the conservation equations for water and steam mass, water and steam momentum and mixture energy are solved. The calculation of the two-phase flow is based on interfacial friction correlations dependent on the flow regime map.

In SBLOCA calculations the accuracy of the heat transfer correlations has minor significance, but the heat transfer logic must be complete, however. Typically the wall temperatures follow closely the fluid temperatures. Some heat transfer features, which often are not well modeled in large break LOCA (LBLOCA) blowdown codes, but may become significant in SBLOCA transients, are:

- o Steam condensation on the wall e.g. in the steam generator primary side.
- o Heat transfer mode transition from film boiling to nucleate boiling.
- o Interfacial condensation when a stagnant water level is separating water and steam.

Feature	SMABRE	RELAP5/Mod1
Local fluid variables	α, u_m, u_g, h_l or h_g	α, p, u_l, u_g, h_l or h_g
Integrated fluid variables	p, u_m at region boundaries	-
Interfacial equations	Drift flux velocity, Condensation or flashing heat and mass transfer.	Interfacial drag, Condensation or flashing heat and mass transfer.
Simplifying assumptions	$h_l = h_{ls}$ or $h_g = h_{gs}$, enthalpies are calculated, but practically the result is this.	$h_l = h_{ls}$ or $h_g = h_{gs}$, least massive phase is defined to be saturated.
Wall heat transfer	Forced convection, nucleate boiling (NB), film boiling (FB), critical heat flux, transition boiling for transition FB to NB, and wall condensation in simplified forms.	Like in SMABRE, but the correlation set includes many parallel correlations.
Critical flow model	Only for the break solved with Moody model having two contraction coefficients.	For break and junctions the model based on the method of characteristics, Two contraction coefficients
Main coolant pump model	2 quadrant head and torque curves for single phase (1ϕ) water, two-phase (2ϕ) multiplier.	4 quadrant head and torque homologous curves, 2ϕ multiplier for the head and torque $\phi/2\phi$ difference.
Core model	Input heating power generation.	Point neutron kinetics.

Table 1. A comparison between characteristic features of SMABRE and RELAP5/Mod1 codes

During SBLOCA transients the separation of water and steam phases becomes the most dominating process. By comparing the results of RELAP5 and SMABRE a difference has been seen in the calculated water level void gradients. The RELAP5/Mod1 version cannot calculate sharp void gradients of water level without very large number of nodes, like SMABRE does. The modelling of water level becomes significant in the calculation of e.g. core uncover, drying of steam generator primary side and steam venting through vessel bypass connections.

SMABRE uses a simplified solution method for the calculation of the pressure distribution. It is assumed that the local pressure differences are very small compared to the absolute pressures. This feature is the main reason, why the present version of SMABRE is not recommended for larger LOCA transients.

The numerical solution of RELAP5 is described as a linear, semi-implicit finite-difference integration scheme. The equation set is solved with matrix operations. The discretization in SMABRE for local variables is based on upwind discretizing and the solution method is semi-implicit. In the present code version no matrix operations are used in the solution.

COMMON TEST CASES

A part of the SMABRE assessment work has been performed in the frame of the internordic SÅK-3 project between Denmark, Norway, Sweden and Finland. The capabilities of three codes, RELAP5, TRAC and SMABRE has been compared calculating common SBLOCA test cases. The tests calculated both with RELAP5 and SMABRE codes are:

1. LOFT L3-6 2.5 % PWR cold leg break in operating intact loop. Primary coolant pumps left running during the transient. Test facility scaling about 1:60, Coolant volume to break area ratio 38300 m³/m² /4,7/
2. LOFT L3-5 2.5 % PWR cold leg break. Same as L3-6, but pumps stopped in the beginning /5,8/.
3. LOBI-SD-SL-03 0.4 % PWR cold leg break in the LOBI/Mod1 test facility. Test facility scaling 1:712. Coolant volume to break area ratio 235000 m³/m² /6,9/

The comparison between the codes and experimental results was performed by choosing twenty most significant parameters describing the transient behaviour. The set of chosen parameters includes primary and secondary pressures, average densities in the cold and hot sides of the loops, fluid temperatures in the loops, core cladding temperatures, loop mass flow rates and the break flow rate. The main conclusions concerning calculations with SMABRE and RELAP5 are listed in Table 2 for LOFT L3-6, in Table 3 for LOFT L3-5 and in Table 4 for LOBI SL-SD-03. Figure 1 presents the SMABRE nodalization for the LOBI facility and Figure 2 for the LOBI facility. The comparison of few parameters between SMABRE and RELAP5 are presented in Figures 3 to 11. The comments to the results in Figures may be found in Tables 2, 3 and 4.

In the comparison presented in Tables 2, 3 and 4 only those parameters are mentioned, which were found most significant. E.g. the fluid temperatures followed typically the saturation temperature during the transient, both in the experiment and in the calculation, and were not important in the comparison. The experimental data of LOBI SD-SL-03 showed strong subcooling effects for water in uninsulated parts of the loop, but these local heat losses were not modeled.

The primary side nodalizations in the RELAP5 and SMABRE runs for all the three cases were quite similar. With SMABRE several calculations were done for all of the cases and during different runs usually only the contraction coefficient of the break flow was varied. Several changes in the nodalization of the bypass connections and in the upper plenum as well as variations of the pump two-phase model were needed before the final run.

Additional comparisons in the SÄK-3 project were performed later using a different set of parameters and then some misunderstandings with respect to the experiment were found. The SMABRE results were not good with respect to the natural circulation and horizontal stratification in the L3-5 and LOBI SD-SL-03 experiments, but the calculations with a modified nodalization are expected to give better results.

CONCLUSIONS

The development of the SBLOCA code SMABRE has proved to be successful. The assessment of SMABRE has shown, that it is a very fast code and capable of predicting the behavior of integral test facilities in SBLOCA transients usually as accurately as large codes like RELAP5/Mod1.

ACKNOWLEDGMENTS

The RELAP5/Mod1 analyses have been performed by Mr. H. Holmström and Mr. M. Hänninen. The SMABRE analyses have been performed by the author, by Mr. P. Hyvönen and by Mr. H. Ollikkala.

REFERENCES

1. Miettinen, J., SMABRE - Code Manual: Numerical methods and constitutive Equations, VTT, Helsinki, Finland
2. Miettinen, J., Hänninen, M., Experiences about a Two-phase Model SMABRE in a full scale PWR Simulator, International Meeting on Thermal Reactor Safety, Chicago, August 1982.
3. Ransom, V.H. et al., RELAP5/Mod1 Code Manual, Volumes 1 and 2 (Draft), NUREG/CR-1826, EGG-2070, Revision 1, March 1981.
4. Bayless, P.D., Carpenter, J.M., Experimental Data Report for LOFT Nuclear Small Break Experiment L3-6 and Severe Core Transient Experiment L8-1, NUREG/CR-1868, EGG-LOFT-2075.

5. Dao, L.T.L., Carpenter, J.M., Experimental Data Report for LOFT Nuclear Small Break Experiment L3-5/L3-5A, NUREG/CR-1695, EGG-2060.
6. Ohlmer, E., Fortesque, T., Experimental Data Report on LOBI Test SD-SL-03, LEC 81-04, JRC Ispra, May 1981.
7. Hänninen, M. et al., Small Break LOCA Analysis Code Comparison Report for Test Case LOFT L3-6, SÄK-3-F(84)4, VTT, Finland, September 1984.
8. Astrup, P., Small Break LOCA Analysis Code Comparison Report for Test Case LOFT L3-5, SÄK-3-D(84), Risoe, Denmark, March 1984.
9. Astrup, P., Small Break LOCA Analysis Code Comparison Report for Test Case LOBI SD-SL-03, SÄK-3-D(84)6, Risoe, Denmark, March 1984.

NOMENCLATURE

Symbols

u Velocity m/s
 p Pressure N/m²
 h Enthalpy J/kg
 α void fraction

Subscripts:

l liquid
 g gas, steam
 s saturated
 m mixture

Parameter compared	Evaluation of result	
	SMABRE	RELAP5
Transient calculated	0 ... 2500 s	0 ... 1300 s
Secondary pressure	Satisfactory prediction (MSIV data insufficient)	Satisfactory prediction (MSIV data insufficient)
Primary pressure	Good prediction, strong secondary effect	Good prediction, strong secondary effect
Pump mass flow rate	Close to RELAP5 results, no measurements	Remark: RELAP5 pump data is based on LOFT and SEMISCALE results
Leak flow rate	Well predicted, contrac- tion coefficient for Moody model =0.9 (subc.) or =0.45 (satur.)	Well predicted, contrac- tion coefficient for RELAP5 model =0.72
Loop densities	Good for broken loop, not good for intact loop	Satisfactory for both loops, less for broken loop

Table 2. Comparison of predictions for the LOFT test L3-6

Parameter compared	Evaluation of result	
	SMABRE	RELAP5
Transient calculated	0 ... 2030 s	0 ... 1300 s
Secondary pressure	Like for L3-6	Like for L3-6
Primary pressure	Good prediction, strong secondary effect	Good prediction, strong secondary effect
Natural circulation, bypass flow	Natural circulation overpredicted, steam bypass underpredicted	Same comments as for SMABRE
Leak flow rate	Well predicted, contraction coefficient like for L3-6	Well predicted, contraction coefficient like for L3-6
Loop densities	Good for hot legs, overpredicted for cold legs	Overpredicted for hot and cold legs

Table 3. Comparison of predictions for the LOFT test L3-5

Parameter compared	Evaluation of result	
	SMABRE	RELAP5
Transient calculated	0 ... 4500 s	0 ... 2750 s
Secondary pressure	Defined by input	Defined by input
Primary pressure	Good prediction, strong secondary effect	Good prediction, strong secondary effect
Natural circulation and vessel bypass	Natural circulation strongly overpredicted, steam venting through bypass underpredicted	Similar comments as for SMABRE results
Leak flow rate	No measurement, contraction coefficients of Moody =0.85 and =0.45	No measurement, contraction coefficient of RELAP5 model =1.0
Loop densities	Good for hot legs, overpredicted for cold legs	Similar comments as for SMABRE results

Table 4. Comparison of predictions for the LOBI test SD-SL-03

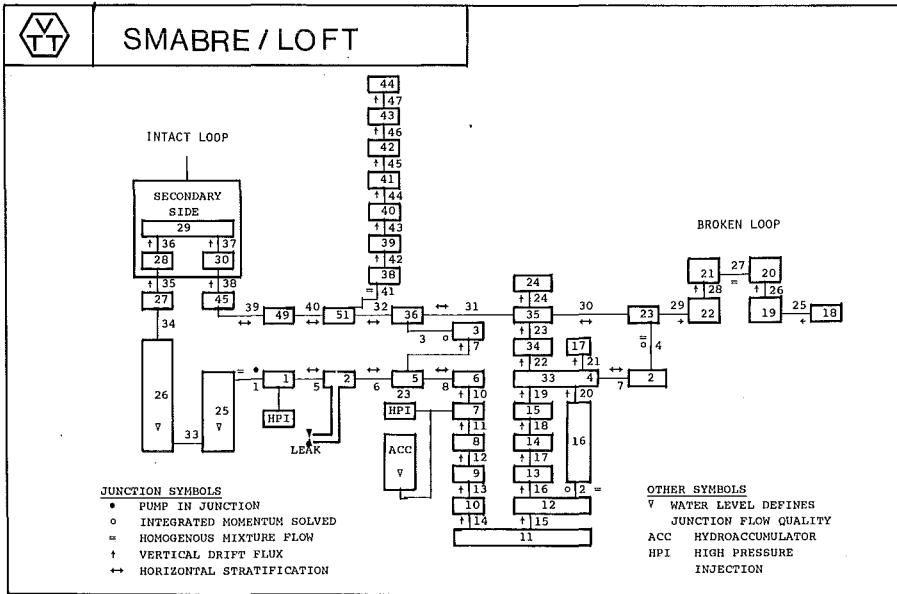


Figure 1. SMABRE nodalization for LOFT facility. RELAP5 nodalization for the primary side was nearly the same.

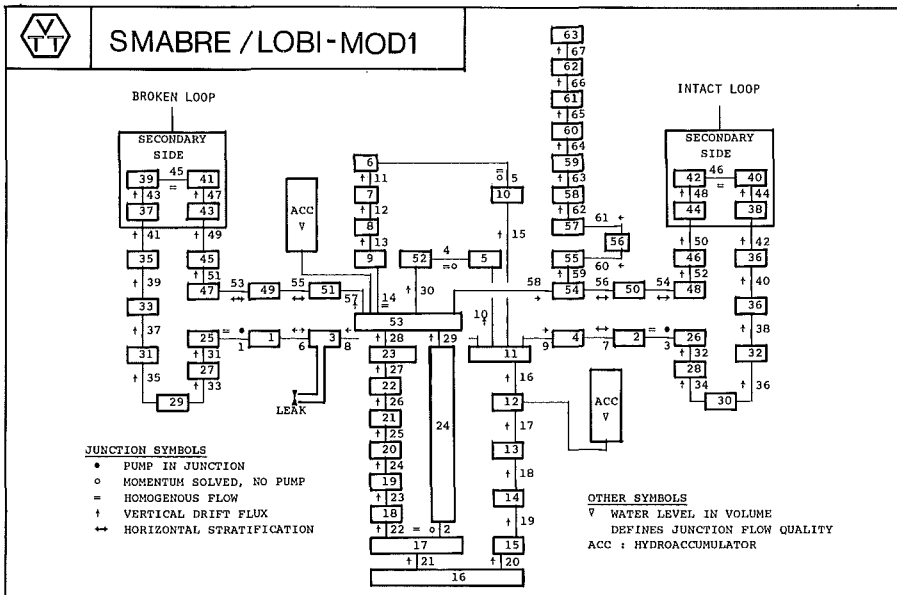


Figure 2. SMABRE nodalization for LOBI facility. RELAP5/Mod1 nodalization for the primary side was the same.

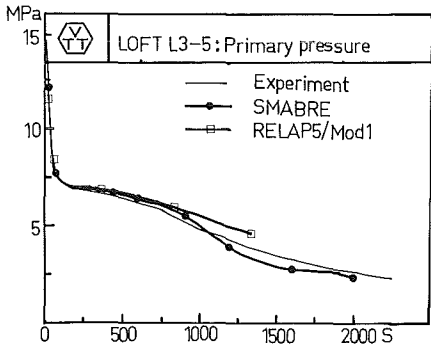


Figure 3. LOFT L3-5, see Table 3.

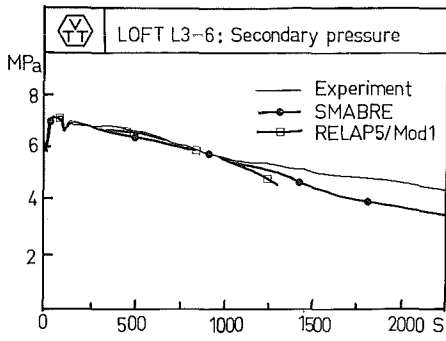


Figure 6. LOFT L3-6, see Table 2.

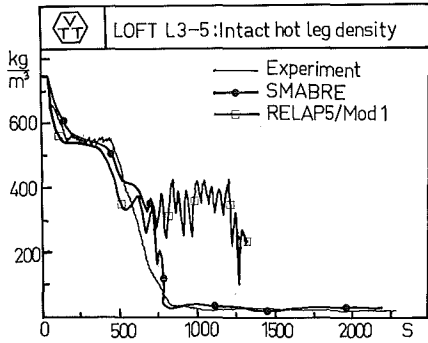


Figure 4. LOFT L3-5, see Table 3.

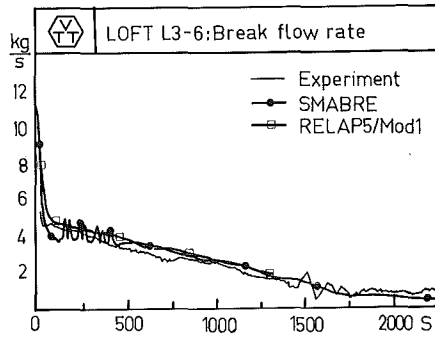


Figure 7. LOFT L3-6, see Table 2.

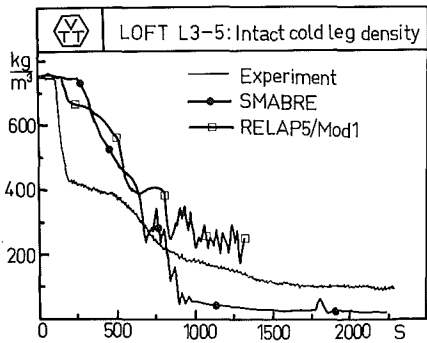


Figure 5. LOFT L3-5, see Table 3.

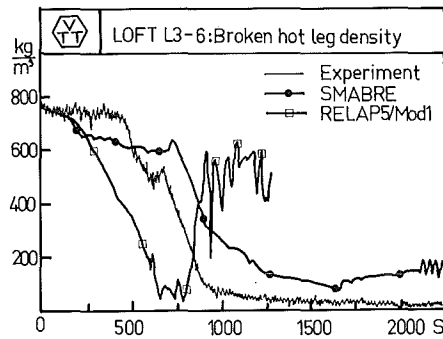


Figure 8. LOFT L3-6, see Table 2.

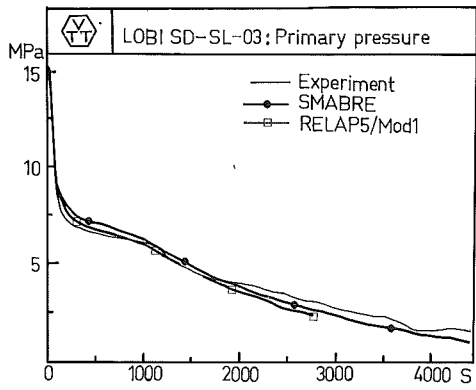


Figure 9. LOBI SD-SL-03, see Table 4.

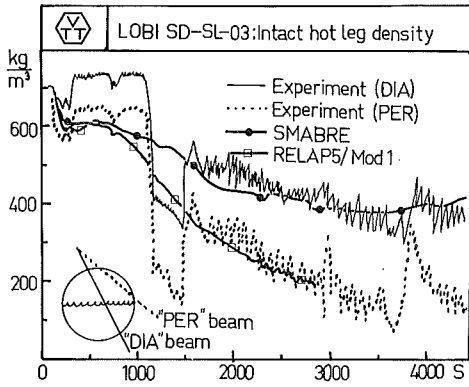


Figure 10. LOBI SD-SL-03, see Table 4.

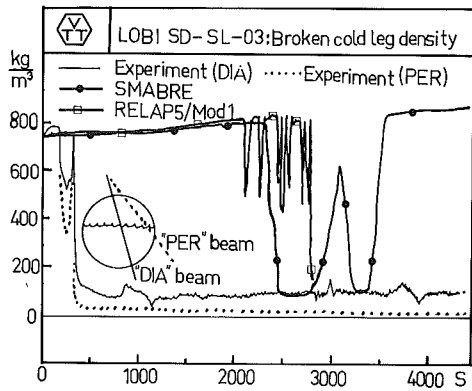


Figure 11. LOBI SD-SL-03, see Table 4.

THE ANALYSIS OF LOFT TEST L9-3 USING RELAP 4/MOD 6 AND
ALMOD-JRC COMPUTER CODES

M. Andreani^(°), P.C. Cacciabue^(*), M. Mazzini^(°), F. Oriolo^(°)

(°) Dipartimento di Costruzioni Meccaniche e Nucleari,
University of Pisa

(*) Engineering Division - Joint Research Centre, ISPRA

ABSTRACT

The paper presents the post-test analysis of the LOFW/ATWS experiment L9-3 on LOFT apparatus, performed using RELAP 4/MOD 6 and ALMOD-JRC computer codes.

Attention is given to their ability to simulate on ATWS incident; in this connection parametric studies about modelling of core, pressurizer, secondary side of the steam generator and heat slabs effect are described.

Limits and merits of the codes are also discussed from the point of view of adequacy of the computed results to the experimental data as well as for their flexibility and running times.

INTRODUCTION

The experiment L9-3, performed on the LOFT [1] reactor simulated a loss of feedwater without scram (LOFW/ATWS) in a commercial PWR [2,3].

In accordance with the programmatic aim to provide experimental data for benchmarking PWR computer codes, the experiment L9-3 specific objectives were to:

1. Assess the applicability of the point kinetics model, used in predicting transient reactor power;
2. Determine the steam generator secondary dry-out behaviour and its effect on the primary system response characteristics;
3. Determine the two-phase and subcooled flow characteristics of the pressurizer valves PORV and SRV at high pressures (17 MPa).

The post-test analysis of the experiment (for the first 200 seconds) has been performed using two computer codes: RELAP 4/MOD 6 and ALMOD-JRC.

The main objective of the work has been the evaluation of the capability of the two codes for PWR plant ATWS simulation.

A second aim was the comparison of the performances of a computer code (ALMOD-JRC), specially developed for PWR transients analysis [4,5] with those of the RELAP 4 [5]; this last code, even if specially suited for large LOCA simulation, has been used successfully at Pisa University for the analysis of a larger class of accidents, particularly small break LOCA [7].

DESCRIPTION OF THE EXPERIMENT

The sequence of events is given in Table I.

The experiment starts by tripping the feedwater pump, at a power level of 48.7 MWth; other experimental conditions are:

- hot leg temperature of 557.7 °K;
- pressurizer pressure of 14.98 MPa;
- pressure in the SG secondary side of 5.61 MPa.

Table I: Sequence of events for experiment L9-3

EVENT	TIME AFTER EXPERIMENT INITIATION (s)
.Main feedwater pump tripped off	0.0
.Pressurizer spray valve cycling initiated	29.5 ± 2.0
.Steam generator steam control valve closed	67.3 ± 1.0
.Experiment PORV opened	73.8 ± 0.2
.Pressurizer liquid reached top of indicating range (1.83 m above bottom)	90.0 ± 0.4
.Steam generator liquid level reached bottom of indicating range (0.25 m above tube sheet)	94.5 ± 4.0
.Experiment SRV opened	96.8 ± 0.2
.Experiment SRV closed	107 ± 1
.Experiment PORV closed	123 ± 1
.Experiment PORV cycling initiated	125.4 ± 0.2

SIMULATION MODELS

Calculations using RELAP 4/MOD 6 code

The aim of the analysis performed by the RELAP 4/MOD 6 computer code has been not only to get as close as possible to the experimental results, but also to begin the development of a code utilization strategy suitable for prediction calculations: for this reason no dial has been used to "fit" the experimental data and none of the measured responses of the variables have been considered as boundary conditions.

Sensitivity studies

The driving variable of the transient is the primary average temperature: it is determined by the balance of the nuclear power and the extracted power by the secondary fluid in the steam generator.

The former may depend on the axial nodalization of the fuel and the moderator regions (the reactivity feedback is a function of the temperature distribution in the core), the latter depends on the SG thermal-hydraulic and on the nodalization of the steam bundle, so that the modelling of the secondary side (much more than the primary side) becomes a crucial part of the calculation.

The relationship between the primary average temperature and the pres-

surizer (and system) pressure is strongly affected by the nodalization of the pressurizer: the RELAP 4 computer code has no special non-equilibrium model for the pressurizer, so that only an adequate subdivision in volumes allows to account for the temperature stratification.

Core model - A parametric study has been made with a varying number of control volumes, each heated by one nuclear slab, to evaluate code sensitivity on this respect. The results indicate that the nodalization of the core does not affect very strongly the relationship between the average temperature of the primary fluid and the generated power; however a good selection is important in order to get a steady-state power as close as possible to the experimental one.

SG secondary side model - Two types of nodalization have been tested. The first had several volumes: 4 for the steam generator boiling region, 1 volume for the downcomer and 1 volume for the steam separator-steam dome zone; it is the result of a parametric study intended to simulate the complex thermal-hydraulic phenomena occurring in SG secondary side during the boil-off transient.

The single node description, usually adopted for calculations of both transients and LOCAs, involves several limitations in simulating the behaviour of the secondary variables:

- 1) The true relationship between the water volume and level cannot be preserved because in RELAP 4 each control volume has a constant trasversal area, that, on the contrary, varies in real SG secondary side; an incorrect calculation of the level in the secondary side involves errors in the evaluation of SG heat removal capacity.
- 2) The equilibrium assumption forces the entire secondary side to be at saturated conditions, so that all the energy input into the secondary side is used to produce steam (rather than superheating it or taking to saturated conditions the subcooled water initially present in the downcomer of the steam generator); this involves an incorrect partitioning of the water between the two pahses, and then an incorrect calculation fo the mixture level.
- 3) The single volume model neglects the recirculation flow in the steam generator; therefore, the mass flow across the boiling region cannot be calculated correctly.

The inadequacy of the second schematization is proved by the behaviour of the calculated pressure, showing an increase less rapid than esperimentally observed [8]. This result is almost independent from the bubble rise model used in the secondary side, but it is strongly affected by the way we describe its geometrical configuration and the initial distribution of the masses of water above and below the top of the tube bundle [8], in order to overcome the first limitation (it is impossible to preserve all the parameters simultaneously).

Pressurizer - As a result of parametric studies, the pressurizer has been described by three volumes: at least two volumes are necessary in order to get a qualitative agreement of the pressure response to the fluid expansion with the experimental one. The third volume on the top, in which initially homogeneous conditions are assumed, allows a better quantitative agreement with the experiment; it accounts for the real situation of turbulence, which occurs in the upper part of the pressurizer when the cold water is injected, across the spray valve, into the steam space.

Final nodalization

The nodalization finally used consists of 36 control volumes and 42 junctions, as shown in Fig. 1; the heat transfer is simulated by 28 heat slabs.

The LOFT vessel is modelled by 8 control volumes; one for the downcomer, the lower plenum and the core bypass, two for the upper plenum and three for the core.

The structures of the vessel have been described in detail, in order to calculate accurately the heat storage effect.

Piping between vessel and steam generator is modelled by two volumes, because the insurge flow temperature is suited to be calculated with good precision.

The primary side of the steam generator (tube bundle) is described with 7 control volumes and heat transfer is simulated by 7 heat slabs.

Piping between steam generator and pump inlet, as well as from pump outlet to reactor vessel, is simulated by one volume. Steam generator plena are conglobed in piping volumes.

The two primary coolant pumps are modelled by a single homogeneous control volume, so as the spray line, which is connected to the pressurizer by a valve, moved by a pressure trip.

The inactive broken hot and cold legs are described by the volumes 15 and 14, respectively.

The experimental valve on the top of the pressurizer is modelled by two separate valves, whose flow areas have been established so that, at the same pressures, the calculated steam mass flows are consistent with the measured target flow rates for the PORV and the combined PORV and safety valves.

Two valves connect the volume, simulating the SG secondary side steam dome, with two time-dependent volumes, simulating the condenser and the containment free space.

Physical models and options

The HF-HEM critical flow models with transition quality 0.02, have been chosen to compute the mass flow rate at the junctions equipped with valves.

The vertical slip between liquid and steam is calculated only for junctions concerning the pressurizer.

It has been established MVMIX=0 for single path junctions and MVMIX=3 for double-path junctions.

The enthalpy transport model is activated only for junction, 26.

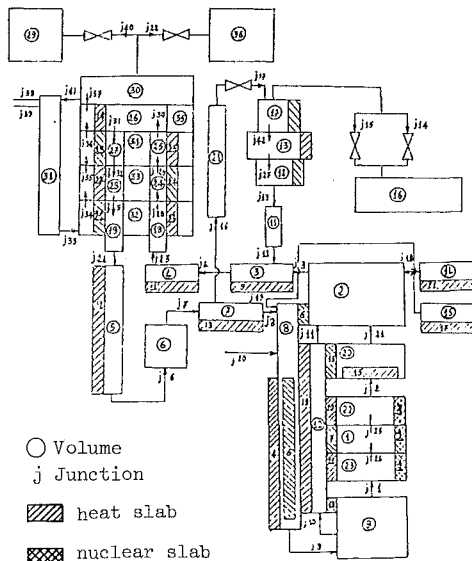


Fig. 1: Nodalization of LOFT apparatus used in RELAP 4/MOD 6 calculation.

The Wilson model, with a bubble density gradient equal to 0.8, is used in the volumes simulating the pressurizer: it is activated for volume 17 when the mixture level in volume 13 approaches the height of junction 42. As regards the steam generator secondary side, a fixed bubble rise velocity and gradient (3 ft/sec and 0.8, respectively) has been used in downcomer and boiler, whereas the complete separation model has been chosen for the steam-separator region (volume 30).

The MOD 6 blowdown correlations package has been used to calculate heat transfer; the heat exchange by natural convection is also accounted for the slabs concerning the steam generator.

The CHF correlation selected is the W3, Hsu-Beckner and Zuber modified, while the transition boiling and film boiling correlations are those of Tong-Young and Condie-Bengston, respectively.

Calculations using ALMOD-JRC code

The objective of this analysis has been the assessment of the capability of ALMOD-JRC to simulate accidents like the one postulated in the L9-3 test; a particular attention has been paid to the heat slabs model, recently implemented in the code, and to the AKW model, a new simplified model for the steam generator, developed in order to simulate transients involving tube bundle dry-out.

Parametric studies of input values for some constants, affecting the behaviour of the steam generator and the pressurizer, have been performed.

Moreover, the importance of accounting for the heat exchanges with the structural materials has been estimated. The representation of LOFT by ALMOD-JRC code is shown in Fig. 2.

Steam generator - A series of parametric runs has been executed over the constants and the quantities not exactly known from the experimental data report, in order to optimize the results.

The most interesting results are:

- the ratio between the mixture level (swell level) and the density compensated level (collapsed level) in the boiling region (riser) is a function of the input value for the inverse of the average void fraction (CCO). CCO value has been varied from 1.25 to 1.65; the pressure and the level in the secondary side are better represented for the high value (but not greater than 1.65 because, otherwise, meaningless results would be obtained for the mixture levels). Also the pressure peak in the primary side approaches the experimental one;
- the heat removed by steam generator depends on BETA, ratio between the heat transmission numbers for the tubes on both sides of the SG: varying it from

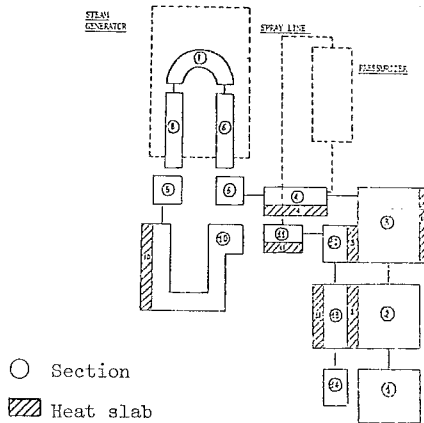


Fig. 2: Nodalization of LOFT apparatus used in ALMOD-JRC calculation.

0.5 to 0.9 a very small influence on the transitory has been observed. The value assumed for the calculation (0.809) has been obtained as the mean value of the corresponding quantities evaluated by the RELAP 4/MOD 6 for the hot and cold legs for the steady-state plant conditions.

Pressurizer - The condensation is modelled in the code ALMOD-JRC as a non-equilibrium phenomenon, governed by a coefficient (the constant C) given in input. For the pressure range in object (150-180 bars), the order of magnitude of this constant is in the range of 1-10 kg/sec (if referred to power reactors, accounting for the relative surfaces of water-steam in the pressurizer). A parametric analysis of C, varying between the above values, has shown that the best simulation of the pressure behaviour during the transient occurs for C=5 kg/sec. Greater values of C correspond to a faster level rise in the pressurizer, which quickly fills-up, causing therefore a greater maximum pressure peak. The reverse is true for lower values of C.

Another input datum is the fraction of water insurge in the pressurizer directly, given to the buffer volume (EPS). The value 0.2, used in reactors where the surge line is laterally connected to the pressurizer, is not suited to the LOFT plant, where the surge line has a different geometrical arrangement. Because no experimental data were found for the evaluation of this quantity, the value best suited, from a parametric analysis varying EPS between 0.01 and 1, to represent the maximum pressure peak has been selected; the minimum value has been chosen.

Heat slabs - The results of the calculation performed, with and without slabs (with all the other input data unchanged), clearly show that the heat exchanges with the structures play a very important role in transients such as a LOFW/ATWS; this is specially true in small geometrical configurations (high surface to volume ratio), as in the experimental LOFT reactor. As self-explanatory example of this observation, the primary coolant temperature behaviour in both cases is shown in Fig. 3.

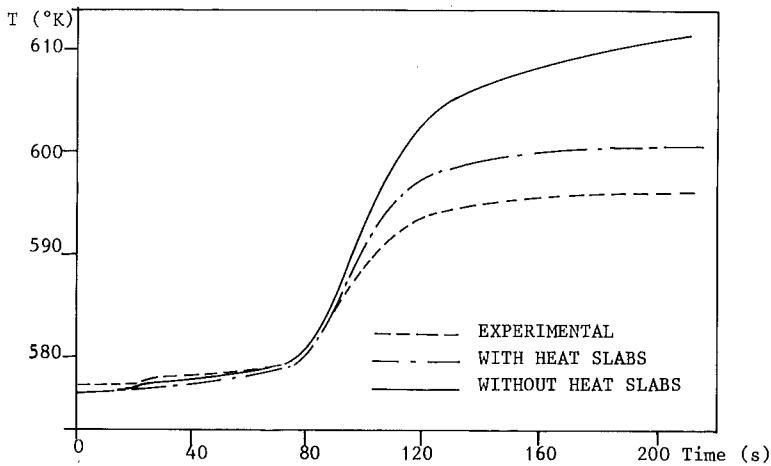


Fig. 3 - Hot leg temperature obtained by ALMOD-JRC code with and without heat slabs.

RESULTS

In this section, the results obtained using RELAP 4/MOD 6 and ALMOD-JRC codes are briefly discussed, comparing them with the measured data.

Ten seconds of steady-state are added to 200 seconds of real transient in all the plots.

Hot leg temperature - The hot leg temperature transitory is shown in Fig. 4: both RELAP and ALMOD codes simulate the progression of events reasonably well.

In the first part of the transient (0:50 seconds), the only relevant discrepancy of ALMOD calculation is the anticipation of the first rise of temperature; this is due to the inability of the code to account for the effects of the recirculation flow and of the presence of a large mass of subcooled water in the SG secondary side: for this reason, the secondary pressure (and then the temperature), in disagreement with the physical reality, increases as soon as the feedwater flow has been interrupted (Fig. 5).

More important discrepancies occur from 50 seconds onwards.

In RELAP 4 calculation, the temperature increases as quickly as the one in experimental results and its behaviour is not affected by a poor estimation of some of the secondary variables. The pressure has higher values than experimental ones (Fig. 5), so that a larger amount of water is calculated to escape from the steam generator through the open valve: this involves a quicker drop of the downcomer level (Fig. 6), but not of the level in the boiling region, so that the heat transfer rate can be computed correctly; we can say that an incorrect distribution of water between downcomer and boiler compensates for the discrepancy in the pressure trend.

Also the calculation by ALMOD code shows a quicker SG depletion, due to the overestimation of the secondary pressure, and, then, a larger slope in the calculated curve of the level in the downcomer: in this case, however, the difference of the levels in the downcomer and in the boiling region is estimated accounting only for the different density, so that the tube bundle discovers more quickly.

As the power extracted from the primary fluid by steam generator is calculated, as proportional to the mixture level in the riser, the heat exchange drops too quickly and the primary temperature has a larger increase rate.

In the later part of the examined transient (from 100 seconds onwards) RELAP 4 calculates a slight but continuous increase, whereas ALMOD calculation shows a flat curve since 160 seconds.

The difference (with the heat sink completely lost in both cases) may be due to a little lower generated power level (Fig. 7) calculated by ALMOD, as a consequence of the more abrupt increase of the primary temperature in the first part of the transient, which can be balanced by the heat storage into the structures.

Generated power - The generated power is shown in Fig. 7. We can say that the behaviour calculated, by both codes agrees with the experimental one reasonably well, and it is consistent with the temperature transient: this shows that the reactivity feedback is well estimated.

The adequate response of power versus the core inlet temperature of the coolant (Fig. 8), although it cannot be considered a rigorous proof, shows the applicability of the point kinetics (the same model is implemented in both codes) in predicting LOFT reactor power in this transient.

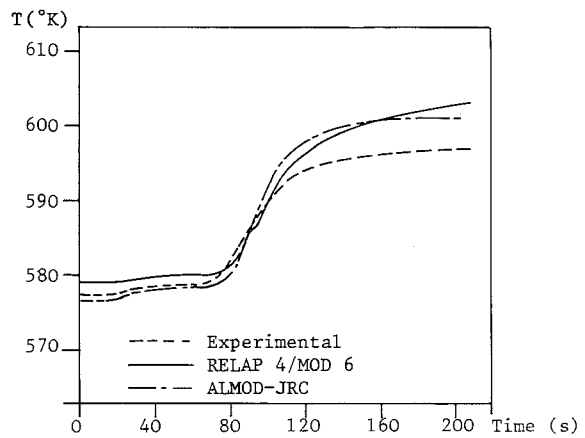


Fig. 4: Hot leg temperature.

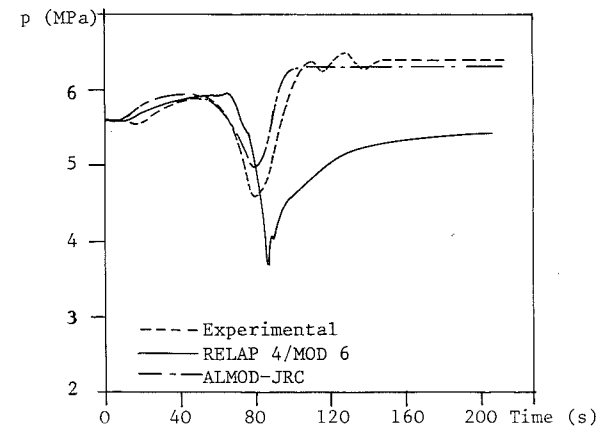


Fig. 5: Secondary pressure.

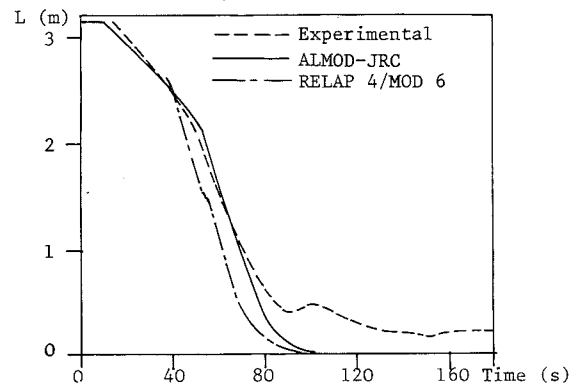


Fig. 6: Downcomer collapsed level.

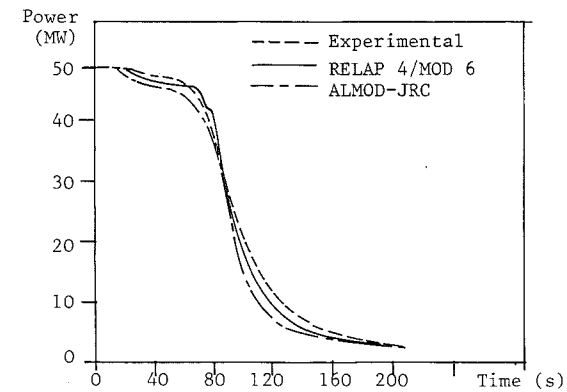


Fig. 7: Generated power.

Pressurizer pressure - The calculated pressure responses (Fig. 9) are in accordance with the temperature ones: an overestimation of the increase rate in the ALMOD-JRC case, a larger increase after the closing of the safety valve, in the RELAP calculation.

The pressure peak calculated using ALMOD-JRC is higher than the experimental one by 4 bars, whereas the RELAP 4/MOD 6 code calculates almost the same value as the measured one.

Owing to the relevant differences of temperature responses, the comparison between the pressurizer model of the RELAP 4 (assuming thermodynamic equilibrium everywhere) and that one used by ALMOD-JRC (non equilibrium phenomena are described) is not significative. It might be interesting, however, to observe that, at the time of PORV opening, the value of the derivative of pressure against temperature, in the test and in the calculations by RELAP 4 and ALMOD-JRC are 3.2 ± 0.3 , 3.5 ± 0.1 and 4.3 ± 0.1 bar/°C respectively; the better agreement is found for the RELAP calculation.

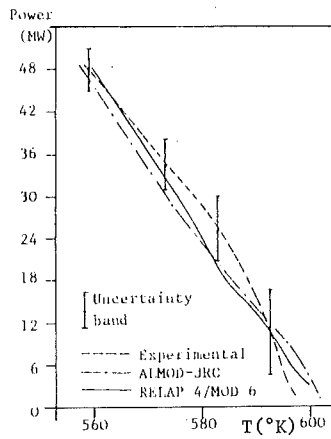


Fig. 8: Power versus core inlet fluid temperature.

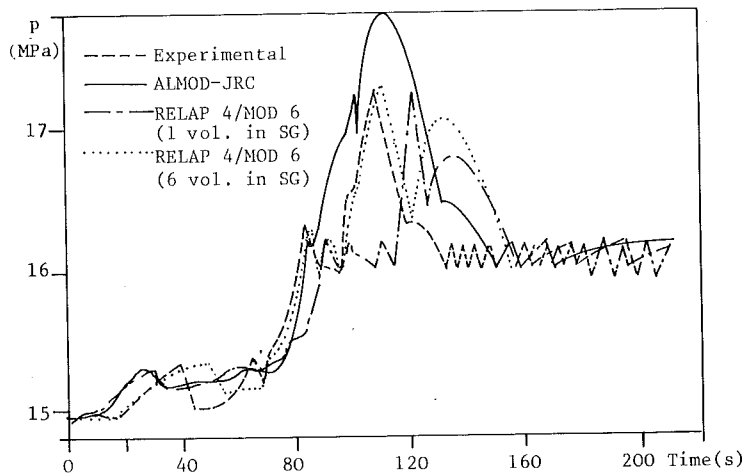


Fig. 9: Pressurizer pressure.

The main limitation of the non-equilibrium model implemented in ALMOD-JRC lies in computing the condensation rate by the same constant C during the whole transient, independently of the pressurizer thermodynamic conditions.

Valves flow characterization - The issue concerns only RELAP 4 code, because in ALMOD-JRC empirical formulas are implemented for the calculation of water and steam flow.

The Henry-Fauske model allows a good agreement between the calculated sub-cooled mass flow-rate and the experimental one, at the highest pressure (172 MPa): 4.2 kg/sec against 4.5 ± 0.5 kg/sec.

CONCLUSIONS

The analysis of the LOFT L9-3 experiment has shown the capability of both RELAP 4/MOD 6 and ALMOD-JRC computer programs to simulate correctly accidents such as loss of feedwater flow ATWS.

Disagreement points originate, for both codes, from the simulation model of the steam generator behaviour: the effect on the primary system response is, fundamentally, an error in estimating the primary temperature increase rate, after the secondary side dry-out has begun in ALMOD case, and in the later transient in RELAP case.

From the point of view of the ability to evaluate accidents in commercial plants, the results obtained by ALMOD-JRC can be considered more suitable, because of the conservative evaluation of the pressure peak. A calculation using RELAP 4 is more accurate because can better simulate the thermal-hydraulic behaviour, of the steam generator, but it is very expensive (CPU ratio = 40).

Moreover, the non-equilibrium model implemented in ALMOD-JRC in order to simulate the pressure response of the pressurizer, does not appear to be completely adequate to the aim, so that the RELAP 4 three-node equilibrium model can be considered better (the pressure trend in the RELAP 4 calculation approaches qualitatively better the experimental results).

Another significant consideration concerns the most significant events; their progression can be reasonably well simulated, provided that the loss of heat to the structural materials is taken into consideration.

REFERENCES

1. D.L. REEDER, "LOFT System and Test Description"-NUGER/CR-0247, TREE-1208, July 1978.
2. P.KUAN, "LOFT Experiment Definition"-EGG-LOFT-5732 (1982).
3. P.D. BOYLESS, J.M. DIVINE, "Experiment data report for LOFT anticipated transient without steam experiment L9-3"-NUREG/CR-2717 (1982).
4. W. FRISCH, K. SCHMIDT, "A PWR plant model for the analysis of large amplitude transients"-3rd Power Plant Dynamics Control and Testing Symposium, Knoxville Sept. (1977).
5. P.C. CACCIABUE, B. LISANTI, A. TOZZI, "ALMOD-JRC Computer Program. Part.1: Implementation of new models for the analysis of heat transfer during PWR accidental transients"-Report to be published.
6. RELAP 4/MOD 6: A Computer Program for Transient Thermal-Hydraulic Analysis of Nuclear Reactors and Related Systems"-ANCR-NUREG-1335.
7. N. CERULLO, G. GALASSI, M. MAZZINI, F. ORIOLO, "Experience in small break LOCA calculations by RELAP 4/MOD 6 code"-Int. Meet. on Thermal Nuclear Reactor Safety, Chicago (Ill.), August 29-Sept. 3, 1982.
8. M. ANDREANI, P.C. CACCIABUE, M. MAZZINI, F. ORIOLO, "Analysis of LOFT Test L9-3 Using RELAP 4/MOD 6 and ALMOD-JRC Computer Codes". Dipartimento di Costruzioni Meccaniche e Nucleari, Università di Pisa, RL 065(83).

ANALYSIS OF RECOVERY PROCEDURES FOR A SINGLE STEAM GENERATOR
TUBE RUPTURE

Charles L. Nalezny and Tien-Hu Chen

EG&G Idaho, Inc.
P.O. Box 1625
Idaho Falls, ID 83415

ABSTRACT

The LOFT Experiments L6-8C-1 and L6-8C-2 simulated a single steam generator tube rupture, a transient that is likely to occur during the lifetime of a commercial pressurized water reactor (PWR). These experiments were designed to evaluate an alternative procedure for recovery from such an accident, and to evaluate techniques used to analyze reactor transients. Experiment L6-8C-1 was the alternative procedure, conducted with the reactor coolant pumps on while depressurizing the primary coolant system by feed and bleed of the unaffected steam generator, and operation of the pressurizer spray. Experiment L6-8C-2 simulated the standard procedure used in commercial PWRs and was conducted with the reactor coolant pumps off while depressurizing the primary coolant system by feed and bleed of the unaffected steam generator, and operation of the power-operated relief valve. The results of the study indicate that the pressurizer spray is as effective as the power operated relief valve for reducing the primary system pressure, and can be used to reduce the release of primary system coolant to the environment. The results of the posttest calculations agreed very well with the data, and indicated that the RELAP5/MOD1 code could be a capable analytical tool for studying reactor safety problems.

INTRODUCTION

Understanding the behavior of commercial pressurized water reactors (PWRs) during anticipated transients is a major objective of the Nuclear Regulatory Commission (NRC) Reactor Safety Research Program. This concern with anticipated transients stems from the relatively high rate at which they challenge the reactor protection and reactivity shutdown systems, the stringent safety goals that are specified for reactors, and the increasing number of nuclear power plants. Anticipated transients are a significant source of risk because of the relatively high probability of occurrence, and the possibility of combining an anticipated transient with an equipment malfunction or operator error which could lead to an inadequate core cooling situation.

One of the most important anticipated transients is a steam generator tube rupture which is also a possible source of accidental radioactive release from commercial PWRs.

LOFT Experiments L6-8C-1 and L6-8C-2 simulated a single steam generator tube rupture, and were used to evaluate an alternative recovery procedure.

The Experiments were conducted on August 26 and 29, 1982, respectively at the Loss-of-Fluid Test (LOFT) facility by EG&G Idaho, Inc., for the U.S. Nuclear Regulatory Commission.

The major objectives specified for the two experiments were to evaluate a primary coolant system (PCS) recovery technique for a primary system-to-secondary system break, which avoids a challenge to the power-operated relief valve (PORV); and to assist the NRC in evaluating reactor transient analysis techniques used in reactor licensing by applying the same techniques to transients performed in the LOFT facility [1].

The remainder of this paper presents a short description of the LOFT facility, an overview of the experiments, a description of the RELAP5 computational model used for the posttest calculations, a comparison between calculations and data, and conclusions.

DESCRIPTION OF THE LOFT FACILITY

The LOFT facility [2] consists of a containment structure, support buildings, and a test assembly that contains a 55-MW(t) experimental PWR which is designed to simulate the major components and system responses of a commercial PWR during a hypothetical loss-of-coolant accident (LOCA). The nuclear core is approximately 1.7-m long, 0.6-m in diameter, and contains 1300 fuel pins of 4.0 wt% U^{235} . The four control assemblies are of typical PWR design.

The PCS consists of an intact loop and a broken loop. The intact loop, simulating three loops of a PWR, contains an operating steam generator, two primary coolant pumps, and a pressurizer. The broken loop, which simulates the fourth loop, contains: a steam generator simulator; a pump simulator; and two quick opening blowdown valves. The experiment assembly is shown in Figure 1.

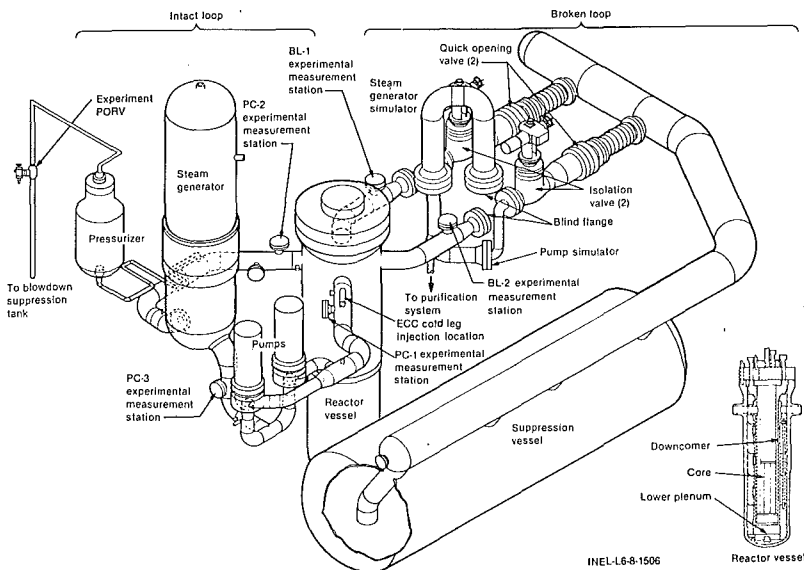


Figure 1. LOFT system geometry.

EXPERIMENT OVERVIEW

Experiment L6-8C-1 simulated a single steam generator rupture to evaluate a recovery technique that does not involve use of the PORV to depressurize the system [3]. L6-8C-2 simulated an identical steam generator rupture with a conventional recovery technique, involving use of the PORV. The results of L6-8C-1 were then compared to the results of Experiment L6-8C-2 to evaluate the procedures.

Following a steam generator tube rupture in a commercial PWR, primary coolant immediately enters the secondary system. The normal steam path then transports the primary coolant (in the form of steam) and any radioactive gases present through the turbine to the condenser where they are vented to the atmosphere.

Normal procedure, in a commercial PWR, involves isolating the steam generator with the ruptured tube(s), and using the other unaffected steam generators and the PORV to depressurize the system. The disabled steam generator's atmospheric relief valves and code safety valves operate, as required, during the depressurization and are a major release path along with the PORV. The U.S. NRC requires termination of the release as soon as possible but within 30 minutes. This is accomplished by reducing primary system pressure to below the steam generator relief valve set point. A major objective of the recovery procedure is to minimize the amount of primary system coolant released to the environment. The total amount of primary system coolant released during L6-8C-1 was to be compared to the amount released during L6-8C-2 to evaluate the alternate procedure, that does not involve use of the PORV.

Experiment L6-8C-1 was initiated by opening the purification system letdown valve (to approximate the rupture of a single steam generator tube), turning off the pressurizer heaters, and beginning steam generator feed and bleed to establish the required plant cooldown rate (55.6 k/h). Initial conditions for L6-8C-1 were: hot leg pressure = 15.5 MPa, cold leg temperature = 562.1 K, PCS flow rate = 476.4 kg/s, decay heat = 0.34 MW. Under the combined effects of the secondary system feed and bleed, and the simulated break, the system began to cooldown and depressurize (as shown in Figure 2). The specified cooldown rate was established by 72 ± 5 s. At 115 ± 3 s into the transient, the pressurizer level reached zero, which indicated that the pressurizer was almost empty (there is approximately 0.04 m^3 below the bottom tap of the pressurizer). By 200 s, calculations indicate that only an additional 0.02 m^3 of volume were lost from the primary system and a small amount of coolant was still in the bottom of the pressurizer. This was due to

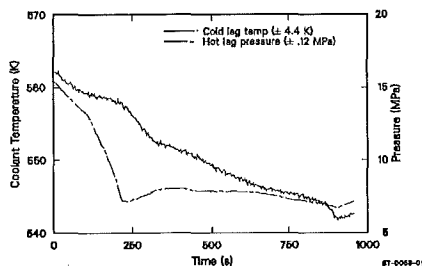


Figure 2. Coolant temperature in cold leg and pressure in hot leg during LOFT Experiment L6-8C-1.

expansion of the primary coolant as the pressure dropped. As soon as the pressurizer spray came on at 200 ± 2 s, the primary system depressurization rate increased and a positive pressure liquid level was restored.

When emergency coolant injection from the high pressure injection system (HPIS) started at 219.3 ± 0.7 s, the pressure began to increase, because the HPIS injection rate exceeded the break flow rate. Once the pressurizer liquid level was restored to approximately 0.10 m, the HPIS flow was reduced to maintain a constant pressurizer level. After the HPIS flow was reduced the system pressure began to drop until the target pressure of 6.8 MPa was reached at 876.2 ± 1 s. The primary coolant pumps were operated continuously during L6-8C-1 in order to monitor PCS mass inventory after the pressurizer emptied.

Initial conditions for L6-8C-2 were hot leg pressure = 15.4 MPa, cold leg temperature = 562.4 K, PCS flow rate = 473.7 kg/s, and decay heat = 0.28 MW. The main difference was the initial pressurizer liquid level which was higher for L6-8C-2 than it was for L6-8C-1. The experiment was initiated in a manner similar to L6-8C-1, by opening the purification system letdown valve, and using steam generator feed and bleed to cool and depressurize the plant in a controlled manner (the cooldown rate was 55.6 K/hr as it was during L6-8C-1). Figure 3 shows pressure and coolant temperature in the intact loop hot leg.

The pressurizer level indicated zero at 157 s. The pressurizer took longer to drain during L6-8C-2 than during L6-8C-1 because the initial liquid level was higher (0.48 ± 0.04 m vs 0.35 ± 0.04 m). At 217.6 ± 0.4 s the primary coolant pumps were tripped, at 219.4 ± 1.0 s the PORV was latched open, and at 220.0 ± 0.3 s HPIS flow was initiated. The pressurizer level increased into the indicating range at 231.8 ± 2.0 s.

As shown in Figure 3, the pressure continued to decrease after HPIS flow was initiated because the PORV was opened. The system pressure continued to decrease because the flow out the PORV was steam with high energy content, even though the steam flow rate from the PORV was much lower than the HPIS flow. As a result, the liquid level in the pressurizer was increasing while the pressure decreased. The rapid energy flow from the PORV resulted in the system reaching saturation temperature at 267 ± 5 s, which stopped the rapid pressure decrease (see Figure 3). HPIS flow was decreased at 270.7 ± 1 s to maintain pressurizer level. The primary system pressure reached 6.80 MPa at 282 ± 2 s.

The objective of L6-8C-1 and L6-8C-2 was to evaluate an alternate procedure for recovering from a steam generator tube rupture. Experiment L6-8C-2 used the standard procedure employed by commercial PWRs to recover from a

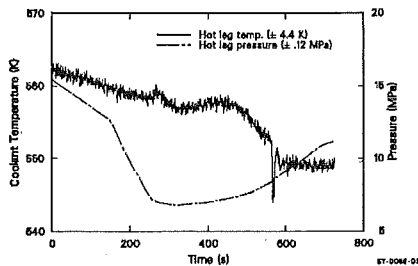


Figure 3. Hot leg coolant temperature and pressure during LOFT Experiment L6-8C-2.

steam generator tube rupture. The alternate procedure used during Experiment L6-8C-1 consisted of establishing a controlled cooldown with steam generator feed and bleed, and turning on the pressurizer sprays instead of opening the PORV when the pressurizer drained to depressurize the system.

Latching open the PORV during L6-8C-2 released 42 ± 5 kg of steam from the pressurizer and increased the total coolant loss during L6-8C-2 compared to L6-8C-1 for the first 376 s. Better control of the pressurizer spray and/or the HPIS flow during L6-8C-1 would have prevented the repressurization that delayed the termination of the test. However, the experiments demonstrated that the pressurizer spray can be as effective as the PORV for depressurizing the primary system.

ANALYTICAL RESULTS AND COMPARISON WITH EXPERIMENTAL DATA

RELAP5 is a reactor analysis code that can be used to predict the transient behavior of water cooled nuclear reactors (or simulators) subjected to postulated accidents such as those resulting from a loss-of-coolant accident (LOCA) or anticipated transient without scram (ATWS). The RELAP5/MOD1/CYCLE22 computer code [4] was used for posttest calculations of system thermal-hydraulic response for LOFT Experiments L6-8C-1 and L6-8C-2. The results were then compared with the measured data from the two experiments.

The purpose of performing these comparisons was to evaluate whether the experimental results could be calculated with acceptable accuracy by the RELAP5 code. Most of the measured initial and boundary conditions compared well with the specified values used for performing the experiment predictions [5-6]. The only boundary condition changes in the RELAP5 input model used for the posttest calculations were: pressurizer spray flow rate, which was about 25% high and injected 25 s early in the pretest prediction; HPIS flow rate, which was about 6% low and initiated 44 s too early in the pretest prediction; and break mass flow rates, which were about 20% high in the pretest prediction. The input model changes also included correction of the steam generator U-tube equivalent diameter, Inconel 600 volumetric heat capacity, and steam separator modeling.

Experiment L6-8C-1

Figure 4 compares the calculated and measured hot leg and steam generator secondary pressures for Experiment L6-8C-1. The posttest calculations pressures were in very good agreement with the experimental data. The slight

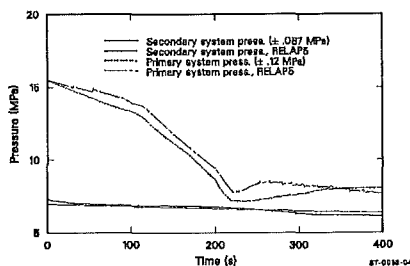


Figure 4. Comparison between measured and calculated primary and secondary system pressure during LOFT Experiment L6-8C-1.

repressurization that occurred in the primary system after about 220 s was also calculated reasonably well. The primary system repressurization that occurred during Experiment L6-8C-1 is attributed to the fact that pressurizer spray flow and HPIS injection were initiated later than specified. This repressurization would not have occurred if the specified operation conditions were rigorously followed.

Figure 5 shows the comparison of measured and calculated hot leg coolant temperature. The calculated coolant temperature agreed very well with the measured data. The slight difference between the measured and calculated cooldown rate after about 220 s is related to the slight difference in the repressurization response (see Figure 4). The difference between the calculated and measured coolant temperatures is within the ± 4.4 K uncertainty limit for temperature measurements.

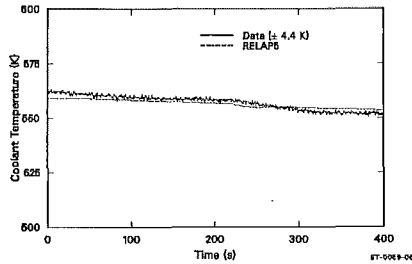


Figure 5. Comparison between measured and calculated coolant temperature in primary system hot leg during LOFT Experiment L6-8C-1.

Figure 6 presents the comparison between measured and calculated pressurizer liquid level. The calculated pressurizer liquid level response was in excellent agreement with the experimental data. Although the calculation is slightly overpredicted, the difference is small and well within the measurement uncertainty of ± 0.06 m (± 0.20 ft). Figure 7 compares the calculated and actual measured break mass flow rates. The calculated and measured flow rates were generally in good agreement, although slight differences from the measured data can be seen between 80 and 160 s. The overpredicted break mass flow rate during that period was mainly due to the break flow control problem. The measured data clearly shows that the operator was unable to maintain the desired flow rate specified for the experiment. The slight difference between the calculated and measured break flow do not significantly affect the transient response.

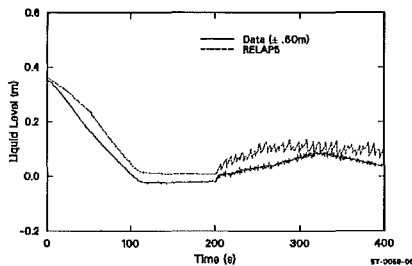


Figure 6. Comparison between measured and calculated pressurizer liquid level during LOFT Experiment L6-8C-1.

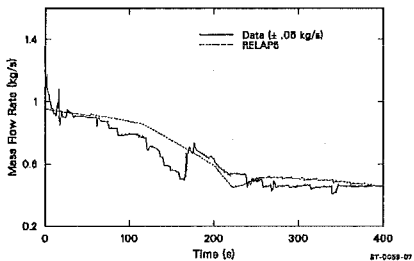


Figure 7. Comparison between measured and calculated break flow rate during LOFT Experiment L6-8C-1.

Experiment L6-8C-2

Figure 8 shows the comparison of the calculated and measured primary and secondary pressures for Experiment L6-8C-2. Figure 9 shows the comparison of calculated and measured temperature in the hot leg. As indicated in these figures, the calculated pressures and coolant temperature were in very good agreement with the experimental data. While a slight difference is noted in primary pressure and coolant temperature, the general response characteristics agree well with the experimental results.

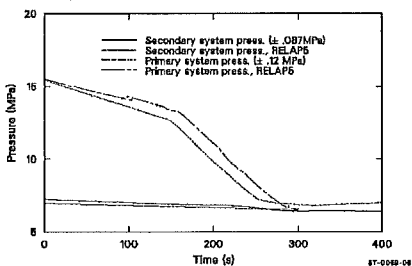


Figure 8. Comparison between measured and calculated primary and secondary system pressure during LOFT Experiment L6-8C-2.

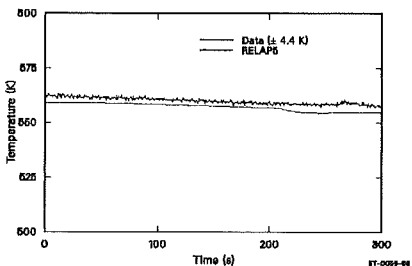


Figure 9. Comparison between measured and calculated coolant temperature in primary system hot leg during LOFT Experiment L6-8C-2.

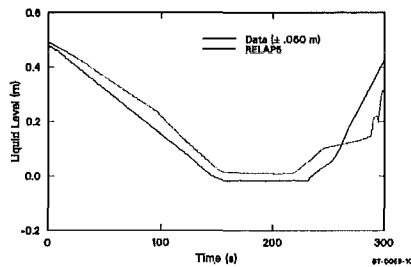


Figure 10. Comparison between measured and calculated pressurizer liquid level during LOFT Experiment L6-8C-2.

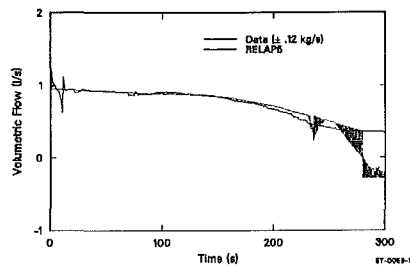


Figure 11. Comparison between measured and calculated break flow rate during LOFT Experiment L6-8C-2.

Figures 10 and 11 present comparisons of the calculated and measured pressurizer liquid level and break mass flow rate. These comparisons show clearly that the calculated pressurizer levels and the calculated break mass flow rates were in almost perfect agreement with data.

CONCLUSIONS

The comparison between L6-8C-1 and L6-8C-2 demonstrated that the pressurizer spray is as effective as the PORV in depressurizing the primary system, and can result in less mass loss from the primary system during recovery from a steam generator tube rupture accident. However, it is more sensitive to operator control, and will require more investigation before it can be qualified as an alternative procedure.

The comparison between calculated and measured data for Experiments L6-8C-1 and L6-8C-2 demonstrated that RELAP5/MOD1 can accurately model the major phenomena associated with a single steam generator tube rupture transient. Those results add to the qualification data base for RELAP5/MOD1, and increase user confidence that the code can be used to accurately predict the response of PWRs to small break transients and alternate recovery procedures.

REFERENCES

1. S. Silverman, "LOFT Experiment Operating Specification LOFT Anticipated Transient Series L6, Test L6-8," EGG-LOFT-5733, July 1982.
2. D. L. Reeder, LOFT System and Test Description (5.5-ft Nuclear Core 1 LOCEs), NUREG/CR-0247, TREE-1208, July 1978, EG&G Idaho, Inc.
3. D. B. Jarrell et al., Experiment Data Report For LOFT Anticipated Transport Experiment Series L6-8, NUREG/CR-2930, EGG-2219, November 1982.
4. V. H. Ransom et al., RELAP5/MOD1 Code Manual Vol 1; System Models and Numerical Method, EGG-2070, November 1980. The analysis was performed using Cycle 22. A production version of the RELAP5/MOD1 code which is maintained at Idaho National Engineering Laboratory Computer Center.

5. K. G. Condie, Best Estimate Prediction for LOFT Experiment Series L6-8C, EGG-LOFT-5982, August 1982.
6. J. P. Adams, Quick-Look Report on LOFT Nuclear Experiment Series L6-8, EGG-LOFT-6031, September 1982.

NOTICE

This paper was prepared as an account of work sponsored by an agency of the United States Government. Neither the United States Government nor any agency thereof, or any of their employees, makes any warranty, expressed or implied, or assumes any legal liability or responsibility for any third party's use, or the results of such use, of any information, apparatus, product or process disclosed in this paper, or represents that its use by such third party would not infringe privately owned rights. The views expressed in this paper are not necessarily those of the U.S. Nuclear Regulatory Commission.

Work supported by the U.S. Nuclear Regulatory Commission, Office of Nuclear Regulatory Research under DOE Contract No. DE-AC07-76ID01570.

STEAM GENERATOR TUBE RUPTURE IN AN EXPERIMENTAL
FACILITY SCALED FROM A PRESSURIZED WATER REACTOR

G. G. Loomis

Idaho National Engineering Laboratory
Idaho Falls, Idaho U.S.A.

ABSTRACT

Results from an experimental investigation of steam generator tube rupture in the Semiscale Mod-2B system are presented. From the experimental results, the characteristic system response signature for a wide range of number of tubes ruptured has been described. The tube rupture was assumed to occur during normal full power operation (15.6 MPa system pressure, 37 K core differential temperature). In addition, recovery scenarios involving operator actions were examined. The recovery scenarios included use of pressurizer auxiliary spray and internal heaters, steam generator feed and steam, primary feed and bleed, and main cooling pump operation. Recovery scenarios suggested by typical U.S. pressurized water reactor emergency operating procedures were followed.

INTRODUCTION

This paper presents results from an experimental investigation of steam generator tube rupture as it pertains to the safety aspects of pressurized water reactors (PWRs). Steam generator tube rupture transients are important to study because the tube rupture allows a primary to secondary system flow path which can eventually result in a release of radioactive fluid to the atmosphere. The experimental investigation was conducted in the Semiscale Mod-2B facility which is a small, nonnuclear, high pressure, experimental facility modeled from a PWR. The Semiscale facility is located at the Idaho National Engineering Laboratory and is operated by EG&G Idaho for the Nuclear Regulatory Commission. Examined in this paper are the characteristic system response signature, for a wide range of number of tubes ruptured, and the effectiveness of emergency operator recovery techniques.

In actual PWR plant experience several tube rupture transients have occurred in the United States. These include: Point Beach, Surry, Prairie Island, St. Lucie and Ginna [1]. However, limited system response data was available from those transients and the only experimental simulation of tube rupture events were conducted by Semiscale in 1977 [2]. Those experiments involved studying tube rupture concurrent with large primary pipe breaks. Code calculational results have been published [3-6] but the calculations have not been compared to experimental results. Therefore, the Semiscale steam generator tube rupture experiments provide a needed and unique data base for code verification and development.

SYSTEM DESCRIPTION AND TEST PROCEDURE

Semiscale Mod-2B is a scaled model representation of the primary system of a PWR plant, with a fluid volume of about 1/1705 of a PWR. The scaling

philosophy followed in the design of the Mod-2B system (modified volume scaling) preserves most of the first-order effects thought important for small break loss-of-coolant transients. Most notably, the 1:1 elevation scaling of the Semiscale system is an important criterion for preserving the factors influencing signature response to a tube rupture transient. The Mod-2B system consists of a pressure vessel with external downcomer and simulated reactor internals, an "intact loop" with a tube and shell inverted U-tube active steam generator, pressurizer, and pump; and a "broken loop" including an active pump, active steam generator, and associated piping which allows break simulations. The intact loop simulates three "unaffected loops" of a 4-loop PWR and the broken loop simulates an "affected loop" in which the tube rupture is assumed to occur. The tube rupture is simulated by a line and break assembly connecting the primary and affected loop secondary systems in the vicinity of the tube sheet. The break assembly consists of a break orifice, break valve and venturi flowmeter. The break orifice is an interchangeable symmetric conical flow tube. Three orifice sizes were used in the Semiscale experiments to simulate double-ended offset shear breaks of either one, five, or ten tubes in a PWR near the tube sheet. The entire break assembly was locatable on either the hot or cold side of the steam generator to simulate either hot or cold side breaks. Vessel internals included a simulated core which consisted of a 5 x 5 array of internally heated electric rods, of which 21 to 23 were powered. The rods are geometrically similar to nuclear rods with a heated length of 3.66 m and an outside diameter of 1.072 cm. External heaters are installed in a relatively uniform manner on the vessel and loop piping to offset environmental heat loss. In addition, core power was augmented by a continuous 20 kW during the transients to make up for heat loss unaccounted for by external heaters. The pressurizer included internal heaters for pressure control and a scaled power operated relief valve (PORV) which allowed simulation of PORV operations in a PWR. In both unaffected and affected loop steam generator secondaries special effluent flow controls were included to give properly scaled steam relief flow rates. These included a power operated atmospheric dump valve (ADV) and a staged safety relief valve (SRV) both situated on the main steam line upstream of the main steam isolation valve (MSIV).

Conditions in the system were monitored by an extensive network of metal and fluid thermocouples and differential pressure transducers. In the affected steam generator a long and short tube are extensively instrumented with both primary and secondary side fluid thermocouples and several primary side differential pressure transducers. Average fluid density was measured in the loops and vessel with gamma densitometers while volumetric flow was measured with turbine meters. Condensing systems and catch tanks were included to measure secondary effluent from the steam generator ADVs and SRVs and the pressurizer PORV.

As a general procedure prior to initiation of the transient, the system was filled with demineralized water and vented to ensure a liquid-filled system. The system was heated to initial conditions using core power and pumped flow, and pressurized using pressurizer internal heaters to draw a steam bubble. The steam generator secondaries dissipated the core heat by steaming to atmosphere. The Semiscale initial conditions were typical of PWR full power operation hydraulic conditions in the primary and secondary systems (15.6 MPa primary pressure, 37 K core differential temperature).

Most transients were initiated at 0 s by opening the tube rupture break block valve allowing primary fluid to flow into the affected loop secondary. The primary system depressurized to the low pressurizer trip pressure (13.1 MPa) which initiated core scram and MSIV closure. As the primary system further depressurized to the safety injection pressure trip (12.51 MPa), the

following automatically occurring events transpired: safety injection initiated, main feedwater terminated, auxiliary feedwater start-up, and main coolant pumps off (start coastdown).

All experiments involved a 600 s operator diagnostic period during which time only automatically occurring events, as discussed above, transpired. The 600 s time period was thought reasonable to determine which steam generator had suffered the tube rupture and to initiate a planned recovery of the system.

Recovery involved first attempting to reduce primary pressure below the affected generator ADV set point pressure (5.85 MPa in Semiscale) to isolate secondary fluid release to atmosphere via the ADV and then to establish primary pressure and mass inventory control. Recovery techniques started with terminating auxiliary feedwater to the affected loop generator and then involved, either separately or in combination, the following: intact loop generator feed and steam (using auxiliary feed and ADV steam), primary feed and bleed (using safety injection and pressurizer PORV operation), pressurizer auxiliary spray, pressurizer internal heaters, and intact loop pump operation.

RESULTS

The discussion of Semiscale experimental results are divided into two areas: System signature response and system recovery. The system signature response covers the early operator identification time period (0-600 s) when only automatically occurring events transpire. The system recovery section includes one of several specific recovery scenarios studied in the Semiscale simulations.

System Signature Response

The occurrence of a tube rupture in the Semiscale system during typical PWR type operating conditions has a very distinctive signature response. The system signature response can be characterized by such parameters as primary and secondary system pressure, system liquid levels, fluid flow rates and temperatures. The signature response is discussed for a time period of 600 s which was assumed to include only automatically occurring events without operator action. A time of 600 s was chosen as representative of the time required for an operator to identify the occurrence of a tube rupture transient. For discussion purposes, a single cold side tube rupture in the Semiscale system is used for this section.

The tube rupture, occurring at 0 s, caused a primary system depressurization and loss of primary mass to the broken loop steam generator secondary system. Figure 1 compares the primary and secondary pressures early in the transient. Primary fluid, originally at 15.54 MPa flowed through the conical flow tube break orifice into the broken loop steam generator secondary originally at 5.58 MPa. The loss of mass from the primary system caused a steady primary depressurization until the pressurizer emptied at about $t = 134$ s (Figure 2) at which time the primary depressurization rapidly increased. The increase in primary depressurization corresponded exactly in time to the interfacial liquid level¹ of the pressurizer reaching the bottom of the pressurizer. When the pressurizer level reached the surge line connecting the pressurizer to the hot leg there was a large change in the amount of free surface area for flashing of saturated pressurizer fluid. As long as the interfacial level was above the bottom of the pressurizer and not in the surge line, the interfacial surface area was high and promoted flashing which in turn retarded the primary depressurization. When the interfacial liquid level depleted to the surge line (due to break flow), the interfacial surface area

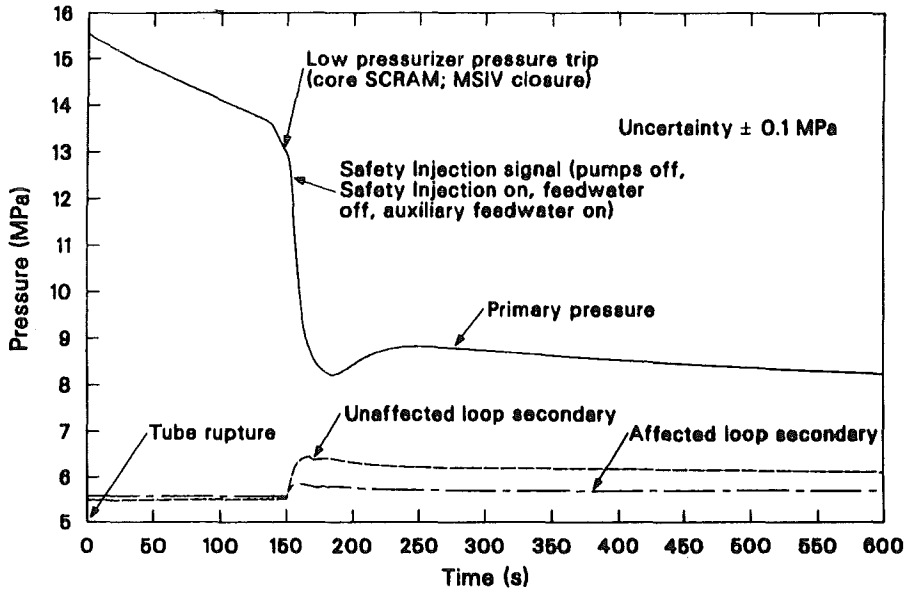


Figure 1. Comparison of primary and secondary pressure during a cold side, one-tube rupture transient.

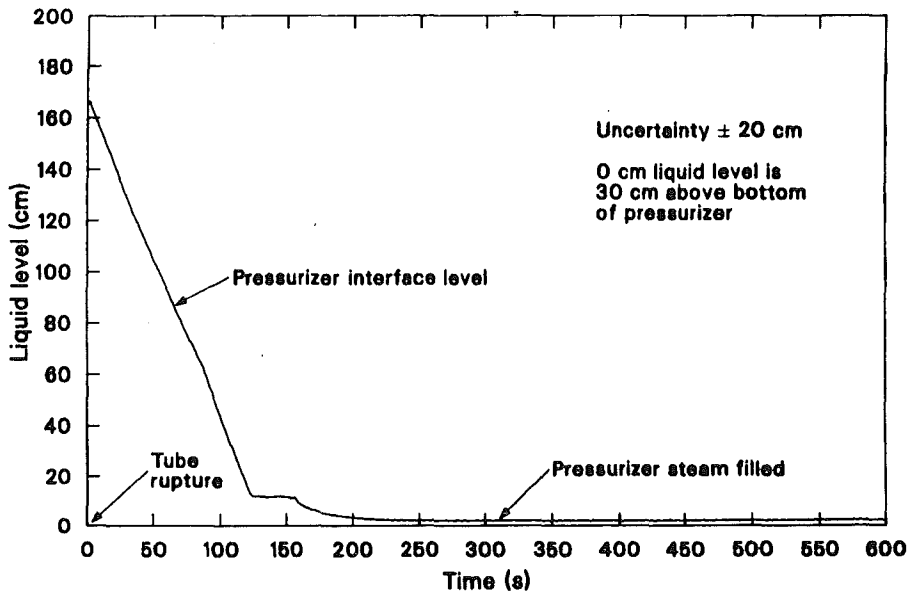


Figure 2. Pressurizer interfacial liquid level during a cold side, one-tube rupture transient.

decreased which retarded flashing resulting in an increase in depressurization. Shortly after the pressurizer interfacial level cleared the bottom of the pressurizer, the low pressurizer pressure set point of 13.1 MPa was achieved, which automatically caused core power scram to the ANS decay curve and the MSIV closure on both steam generators.

Upon MSIV closure, primary to secondary heat transfer in both the broken and intact loop steam generators caused a rapid pressurization of the secondaries as shown in Figure 1. Prior to achieving the low pressurizer pressure trip, both the intact and broken loop steam generator secondary pressure remained fairly constant as full core power was removed via normal secondary steaming conditions through a full open MSIV. The energy addition due to tube rupture break flow from the primary to broken loop secondary caused a negligible rise in broken loop secondary pressure prior to MSIV closure. Following MSIV closure the pressure rose quickly in both generator secondaries to the ADV set point pressures and the ADVs were cycled several times. The secondary pressure soon leveled out below the ADV set point as primary to secondary heat transfer was reduced due to a reduction in primary heat source after core scram.

Following core scram, the system primary pressure showed an increase in depressurization rate due to a shrinkage of the primary fluid caused by primary to secondary heat transfer. No major change in primary depressurization occurred when the primary pressure reached the safety injection signal (12.51 MPa) which automatically induced termination of power to the primary coolant pumps, initiation of safety injection, termination of main feed-water, and start-up of auxiliary feed-water to the secondaries. The effects of the automatic safety injection events were overshadowed by the rapid reduction of core power and resulting primary fluid shrinkage due to primary-to-secondary heat transfer. Eventually, the primary system depressurization was sufficient for the hot leg fluid to reach saturation conditions at about 220 s, (Figure 3). Flashing in the system then caused a major reduction in the depressurization rate. The primary pressure made a slight recovery between 190 and 240 s. This repressurization was caused by a combination of: superheated steam in the pressurizer due to heat transfer from the pressurizer walls to the pressurizer fluid (Figure 3), and the change from forced circulation to natural circulation heat transfer in the steam generators that occurs as the primary pumps coast down. Following pump coastdown, the core decay heat removal mechanism was single-phase natural circulation and the magnitude of the flow rate is typical of single-phase results found previously in Semiscale separate effects experiments [7].

Following the slight primary repressurization period (190-240 s), the primary pressure first stabilized then followed a slow depressurization but remained above the broken loop ADV set point for the entire initial 600 s period. This slow depressurization was supported by a combined energy balance including safety injection flow, primary to secondary heat transfer, break flow, and primary and secondary heat loss.

During the first 600 s, only minor system mass voiding occurred as shown in Figure 4 which compares a primary unaffected loop steam generator tube collapsed level and the vessel upper head collapsed level.² The primary tubes remained essentially full and the vessel upper head level was reduced from 421 cm to 375 cm above the cold leg. Because of the positive differential pressure between the primary and broken loop secondary, a positive break flow persisted throughout the early period; however, safety injection flow, once initiated, was slightly higher than break flow. A slightly larger safety injection flow than break flow resulted in the slight filling trend in vessel upper head level during the first 600 s as shown in Figure 4.

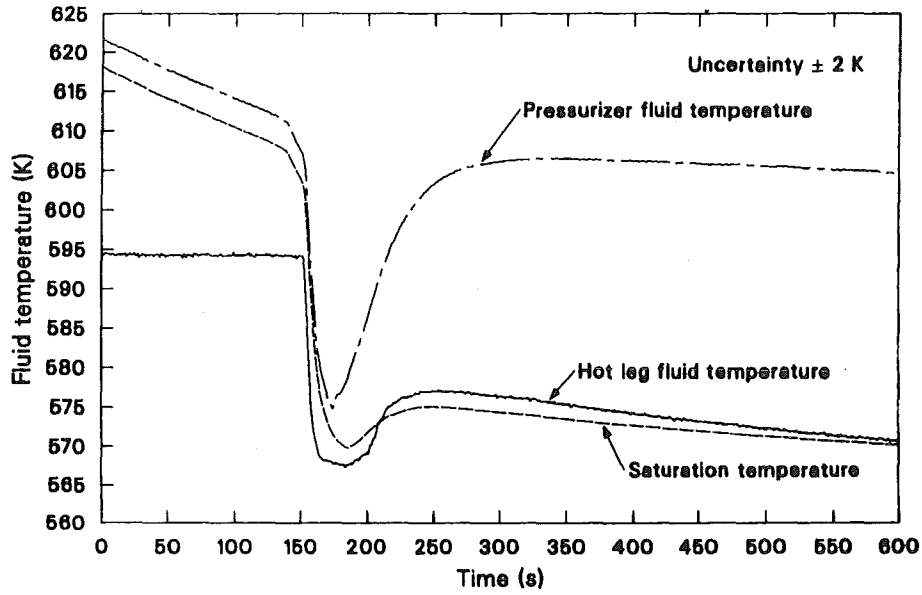


Figure 3. Comparison of fluid temperatures and saturation temperature for a cold side, one-tube rupture transient.

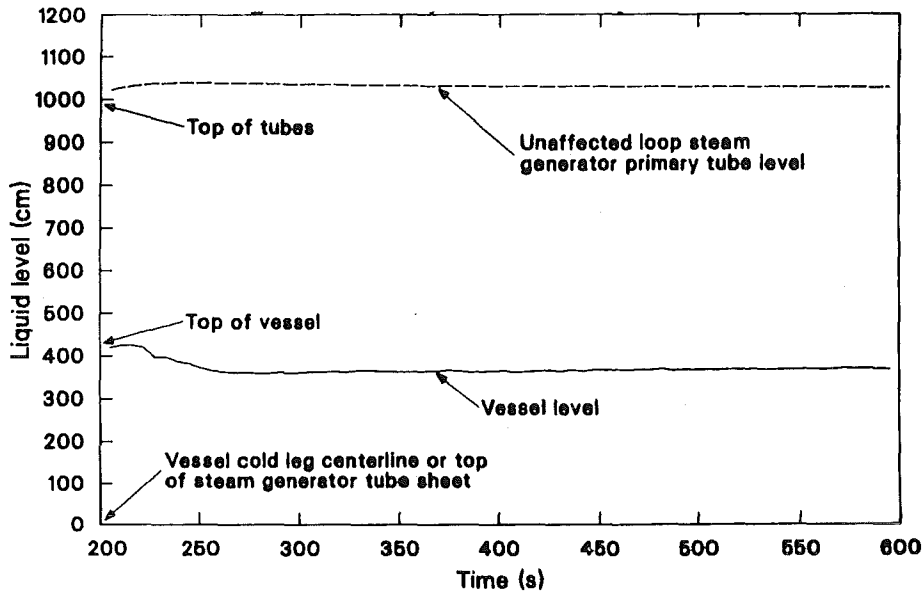


Figure 4. Comparison of collapsed liquid level for unaffected loop steam generator primary tube and vessel upper head during a cold side, one-tube rupture transient.

This basic signature response was found to be typical for one-, five- and ten-tube ruptures; only the timing of events such as core scram, MSIV closure, and safety injection were different. In addition, the signature response was found to be essentially identical for hot side and cold side tube ruptures. The fundamental difference for the break spectrum studied was the relationship of safety injection and break flow. For the five- and ten-tube breaks, the vessel liquid inventory was considerably less than for the one tube case due to a much higher break flow in relation to safety injection flow. At 600 s, the one tube break had a system mass inventory of about 87%; the five-tube break had an inventory of 60%; and the 10-tube break had an inventory of 52%. Even though the vessel liquid collapsed level was reduced to the top of the core during the ten-tube rupture and within 15 cm of the top of the core for the five-tube rupture, no core rod heatup occurred.

System Recovery

Recovery scenarios studied in the Semiscale experiments included a variety of simulated operation actions and compounding failures aimed at first reducing the primary pressure below the affected loop ADV set point, thus isolating the affected loop secondary from atmospheric release, and then cooling the system fluid. A complete listing of the recovery scenarios studied in the Semiscale experiments is found in Reference 8. Most of the operator recovery scenarios in Semiscale started at 600 s and included test termination criteria dictated by test length. Normal recovery combinations suggested by typical U.S. PWR emergency operation procedures (9) were followed; however deviations were made to allow meaningful code comparison and to complete the experiments in a timely manner.

One recovery scenario studied in Semiscale involved a combination of: pressurizer auxiliary spray for primary pressure reduction and fluid inventory control, including use of pressurizer heaters for pressure control and to establish subcooling; use of unaffected loop secondary ADV with auxiliary feedwater for subcooling control; safety injection flow for primary inventory control; and the use of primary coolant pump operation to redistribute system fluid energy and promote core cooling. Figure 5 presents the primary and secondary pressures during a complicated multiphase recovery procedure. Starting at 600 s pressurizer auxiliary spray was initiated and cycled on pressurizer level for the remainder of the transient. The spray caused a primary depressurization from 6.2 MPa which is above the affected loop generator ADV set point (5.85 MPa) to 5.6 MPa which is below the ADV set point. Pressurizer heaters were then used to establish pressure control and increase the primary pressure from 5.6 to 5.85 MPa. The unaffected loop pump was then turned on (the pump had coasted down to zero speed starting at the safety injection signal) which effectively mixed hot and cold fluid in the loop. This mixing resulted in establishing hot leg subcooling as shown on Figure 6. Next, unaffected loop feed and steam was initiated by latching open the unaffected loop ADV and continuing auxiliary feedwater. Figure 5 shows a rapid decrease in the unaffected loop secondary pressure which supported a rapid increase in loop subcooling shown on Figure 6. The increased heat sink increased primary to secondary heat transfer and subcooled the primary fluid. During the entire recovery procedure the affected loop secondary pressure followed the primary pressure closely. However, a small positive break flow persisted as the primary pressure was slightly higher than the secondary. After 7000 s the primary pressure was lower than the secondary and an actual backflow of affected loop generator fluid to the primary pressure occurred. Throughout the recovery procedure, the combined mass balance between safety injection flow, break flow, pressurizer auxiliary spray, and break flow to the affected loop secondary resulted in a vessel collapsed level no lower than the top of the core heated length. With this level there was no core rod heatup.

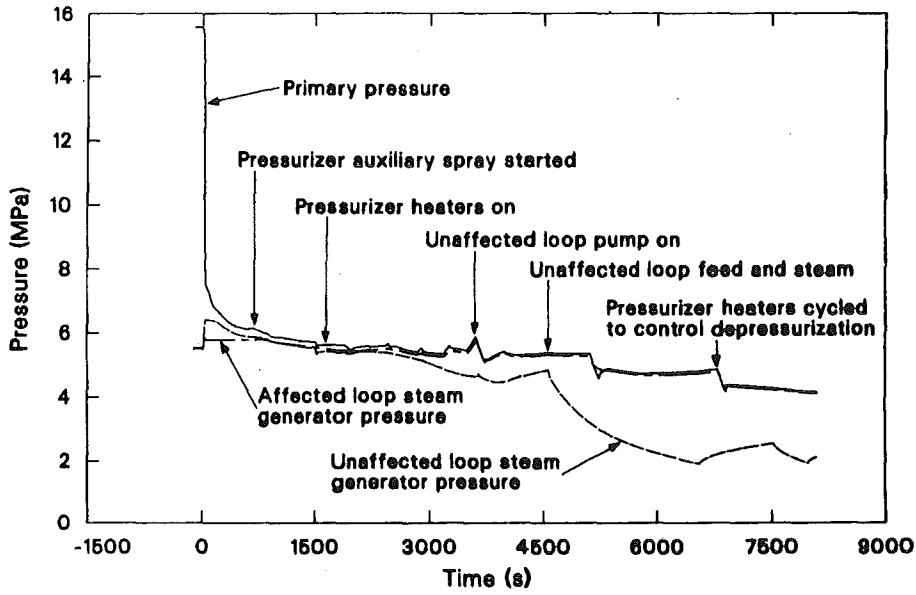


Figure 5. Primary and secondary pressure during recovery from a cold side, one-tube rupture transient.

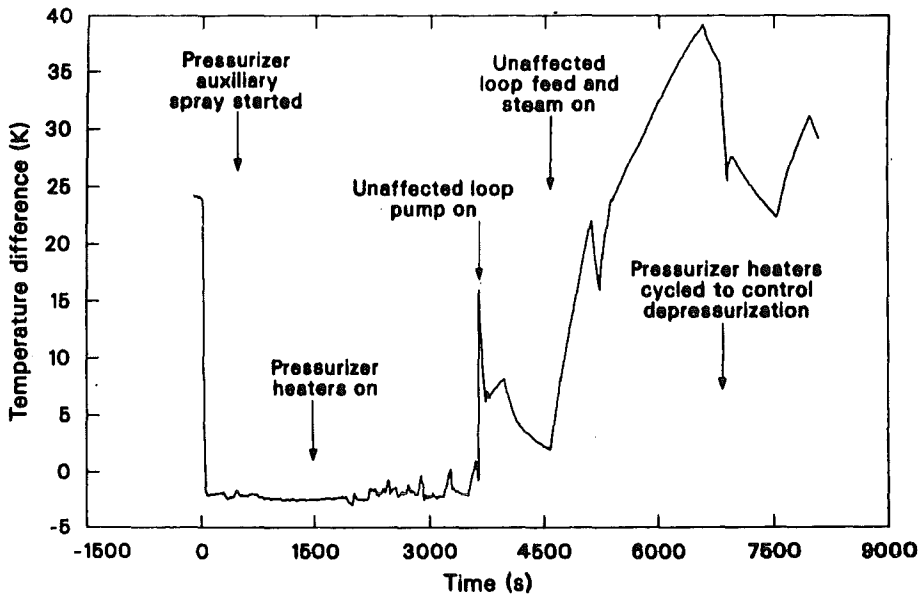


Figure 6. Hot leg subcooling during recovery from a cold side, one-tube rupture transient.

CONCLUSIONS

The Semiscale steam generator tube rupture experimental results provide a unique data set for use in code development and verification. The experiments can be used for both system signature response analysis involving only automatically occurring events and analysis of operator induced recovery procedures.

A tube rupture transient has a very distinct signature response. The signature response is characterized by a rapid primary depressurization to saturation conditions followed by a gradual slow saturated depressurization as primary fluid flows through the tube rupture to the affected loop generator secondary system. As part of the signature response the steam generator secondaries show a rapid increase in pressure when the main steam isolation valves are closed at core scram due to primary-to-secondary heat transfer without steam relief. The pressure rose in the secondaries to relief valve set points and relief valves were opened (atmospheric dump valves). The signature response was found to be similar for a wide spectrum of number of tubes ruptured (one, five, and ten tubes) however the timing of automatically occurring events such as core scram and safety injection initiation are different. In addition, the relationship between safety injection and break flow left the primary mass inventory lower for the larger number of breaks. However, for the break spectrum studied in Semiscale vessel liquid, inventory remained high enough to preclude a core rod heatup.

-
1. Interfacial level is a "pooled" liquid level with saturated steam above and saturated liquid below and is determined using a differential pressure measurement.
 2. Collapsed level refers to all the fluid (both steam and liquid) between the differential pressure measurement taps being treated as saturated liquid only.

REFERENCES

1. L. J. Martinez and D. J. Shimech, Experimental Operating Specification for the Semiscale Mod-2B Steam Generator Tube Rupture Experiment Series, EGG-SEMI-6285, July 1983.
2. J. M. Cozzual, O. M. Hammer, and G. G. Loomis, Investigation of Simulated Steam Generator Tube Ruptures During Loss-of-Coolant Experiments in the Semiscale Mod-1 System, TREE-NUREG-1213, May 1978.
3. D. Dobranich, Steam Generator Tube Rupture Analysis for Zion-1, LA-SSTS-TN-2, September 1981.
4. D. Dobranich, R. J. Henninger, and N. S. DeMuth, "Steam-Generator-Tube-Rupture-Transients for Pressurized Water Reactors," International Meeting on Nuclear Reactor Safety, Chicago, Illinois, August 29-September 2, 1982.
5. D. Dobranich, N. S. DeMuth, R. J. Henninger, and R. D. Burns III, "Special Small-Break Applications with TRAC," ANS Specialists Conference on Small Breaks in LWRs, Monterey, California, LA-UR-81-1519, August 25-27, 1981.

6. W. G. Shier and M. M. Levine, PWR Steam Line Break Analysis Assuming Concurrent Steam Generator Tube Rupture, BNL-NUREG-26903, 1980.
7. G. G. Loomis and K. Soda, Results of the Semiscale Mod-2A Natural Circulation Experiments, NUREG/CR-2335, September 1982.
8. G. G. Loomis, Results of the Semiscale Mod-2B Steam Generator Tube Rupture Experiments (to be published December 1984 NUREG Report).
9. Emergency Operating Procedures for Zion Nuclear Power Plant (EOP-10).

NOTICE

This paper was prepared as an account of work sponsored by an agency of the United States Government. Neither the United States Government nor any agency thereof, or any of their employees, makes any warranty, expressed or implied, or assumes any legal liability or responsibility for any third party's use, or the results of such use, of any information, apparatus, product or process disclosed in this paper, or represents that its use by such third party would not infringe privately owned rights. The views expressed in this paper are not necessarily those of the U.S. Nuclear Regulatory Commission.

Work supported by the U.S. Nuclear Regulatory Commission, Office of Nuclear Regulatory Research under DOE Contract No. DE-AC07-76ID01570.

A RAMONA-3B CODE DESCRIPTION AND NODALIZATION STUDY
FOR THE PEACH BOTTOM-2 TURBINE TRIP TEST 3*

G. C. Slovik and P. Saha

Department of Nuclear Energy
Brookhaven National Laboratory
Upton, New York 11973, U.S.A.

ABSTRACT

A brief description of the BWR transient analysis code RAMONA-3B and the results of a nodalization study for simulation of the Peach Bottom-2 Turbine Trip Test 3 using this code are presented. The code employs a 1-1/2 group, three-dimensional diffusion model for neutron kinetics, coupled with a one-dimensional, nonequilibrium, nonhomogeneous two-phase flow model for thermal hydraulics. Furthermore, the reactor core is presented with parallel hydraulic channels, and the code accounts for the acoustic effects due to valve closure in the steam line.

The nodalization study indicates that even for a highly non-uniform control rod pattern, RAMONA-3B can adequately predict the transient reactor power and vessel pressure for an overpressurization event with relatively large neutronic nodes, each containing four (2x2) fuel assemblies and a control rod.

INTRODUCTION

RAMONA-3B¹ is a best-estimate Boiling Water Reactor (BWR) core and systems transient code with three-dimensional neutron kinetics coupled with one-dimensional, nonhomogeneous, nonequilibrium thermal hydraulics. To be compatible with 3-D neutron kinetics and power generation, the code employs parallel hydraulic channels in the reactor core. It includes a boron transport model and all necessary BWR components such as jet pump, recirculation pump, steam separator, steam line with all necessary valves and a limited plant control and protection system. The code is particularly suitable for analysis of BWR transients such as Control Rod Drop Accident (CRDA), Abnormal Transients Without Scram (ATWS) and partial ATWS, where a space-time neutron kinetics coupled with an adequate thermal hydraulics is required because of strong void-reactivity feedback.

The purpose of this paper is to provide: (1) a brief description of the RAMONA-3B models and solution method, and (2) the results of a recent noding study that was performed using the Peach Bottom-2 Turbine Trip Test 3² as the model transient.

RAMONA-3B MODELS AND SOLUTION METHODS

Neutron kinetics and thermal hydraulics are the two major parts of the RAMONA-3B code. Heat conduction in the fuel rod links them together. Figure 1 shows the coupling and interaction among these parts as employed in RAMONA-3B.

*Work performed under the auspices of the U.S. Nuclear Regulatory Commission.

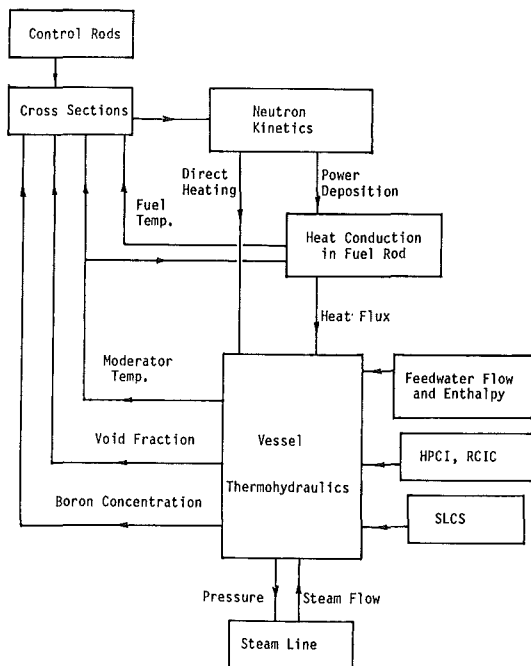


Figure 1 Simplified Flowchart of RAMONA-3B Computational Logic.

Neutron Kinetics

The neutron kinetics model of RAMONA-3B starts from the following two-group, three-dimensional, time-dependent diffusion equations:

Fast Neutrons:

$$\frac{1}{v_1} \frac{\partial \phi_1}{\partial t} = \nabla \cdot D_1 \nabla \phi_1 - \Sigma_{21} \phi_1 - \Sigma_{a1} \phi_1 + (1-\beta) [v_1 \Sigma_{f1} \phi_1 + v_2 \Sigma_{f2} \phi_2] + \sum_{i=1}^I \lambda_i c_i \quad (1)$$

Thermal Neutrons:

$$\frac{1}{v_2} \frac{\partial \phi_2}{\partial t} = \nabla \cdot D_2 \nabla \phi_2 + \Sigma_{21} \phi_1 - \Sigma_{a2} \phi_2 \quad (2)$$

Delayed Precursors:

$$\frac{\partial c_i}{\partial t} = \beta_i [v_1 \Sigma_{f1} \phi_1 + v_2 \Sigma_{f2} \phi_2] - \lambda_i c_i \quad (3)$$

$i=1$ to I where $I=6$

However, in RAMONA-3B, it is assumed that the thermal neutron leakage term, i.e., $\nabla \cdot D_2 \nabla \phi_2$, can be either neglected or assumed to be constant. Thus, RAMONA-3B uses the well-known 1-1/2 group, coarse mesh diffusion model³. The boundary conditions at the core periphery are specified with parameters related to the extrapolation length for the fast flux and the albedo for the thermal flux.

The three-dimensional power generation is the sum of prompt and delayed energy deposition rates. The prompt component is proportional to the instantaneous fission rate, whereas the delayed energy deposition rate is calculated from the 1979 ANS Standard 5.1 for decay heat. As shown in Figure 1, the cross section dependence on fuel and moderator temperatures, void fraction, boron concentration and control rod positions is taken into account in the neutron kinetics calculation. The code uses the following form of the two-group cross sections and diffusion coefficients:

$$\Sigma = (1 - f_d) \sum_{n=1}^3 a_n^o \alpha^{n-1} + f_d \sum_{n=1}^3 a_n^c \alpha^{n-1} + a_\ell (T_\ell - T_{\ell o}) + a_f (\sqrt{T_f} - \sqrt{T_{fo}}) + \delta \Sigma(c_B, \alpha) \quad (4)$$

The first two terms account for the effect of void feedback and the presence of control rods. The third term accounts for the effect of moderator temperature feedback, while the fourth term accounts for Doppler feedback. Finally, the term $\delta \Sigma(c_B, \alpha)$ accounts for the effect of standby soluble boron injection should it occur.

Heat Conduction in Fuel Rod

Thermal energy storage and heat conduction in the fuel elements (pellet, gas gap and cladding) are computed using the following discrete-parameter model:

$$\rho c \frac{\partial T}{\partial t} = \nabla \cdot k \nabla T + q''' \quad (5)$$

No axial conduction is allowed; heat capacities (ρc) in the pellet and cladding, along with the thermal conductivity in the cladding, are assumed to be constants. The gas gap conductance is a prescribed function of pellet temperature.

Thermal Hydraulics

The reactor vessel thermal-hydraulics model of RAMONA-3B starts from the following one-dimensional, four-equation model:

Vapor Mass:

$$\frac{\partial}{\partial t} (\alpha \rho_g) + \nabla \cdot (j_g \rho_g) = \Gamma_v \quad (6)$$

Mixture Mass or Volumetric Flux:

$$\nabla \cdot j_m = \frac{\rho_l - \rho_g}{\rho_l \rho_g} \Gamma_v - \left[\frac{\alpha}{\rho_g} \frac{D_g \rho_g}{Dt} + \frac{(1-\alpha)}{\rho_l} \frac{D_l \rho_l}{Dt} \right] \quad (7)$$

Mixture Momentum:

$$\frac{\partial G_m}{\partial t} + \frac{\partial}{\partial Z} [\alpha \rho_g v_g^2 + (1-\alpha) \rho_l v_l^2] = - \frac{\partial p}{\partial Z} - g \rho_m - f_l \phi_m^2 \frac{G_m |G_m|}{2 \rho_l D_h} \quad (8)$$

Mixture Energy:

$$\frac{\partial}{\partial t} [\alpha \rho_g u_g + (1-\alpha) \rho_l u_l] + \frac{\partial}{\partial Z} [\alpha \rho_g v_g h_g + (1-\alpha) \rho_l v_l h_l] = \frac{q_w'}{A} + q'''(1-\alpha) \quad (9)$$

Two further simplifications are made before the above set of equations are solved in RAMONA-3B. First, the mass and energy equations for the entire reactor vessel are combined (along with equations of state) to yield an equation for the average vessel pressure. This pressure, which is a function of time, but not of space, is used to compute the steam-water properties inside the reactor vessel.

The second simplification calls for integration of the momentum equation, i.e., Equation (8), through each of the parallel channels in the core to obtain a number of closed-contour integral momentum equations. These equations along with the volumetric flux equations, i.e., Equation (7), are solved first to calculate the flow field in the entire vessel. The vapor mass and mixture energy equations, i.e., Equations (6) and (9), are then solved to calculate the void fractions and liquid temperatures in the vessel. Thus, the above two simplifications reduce the computation burden of RAMONA-3B without significant loss in accuracy.

The code uses a slip model of the form:

$$v_g = S v_l + v_o \quad (10)$$

to calculate the relative velocity between the vapor and liquid phases. Non-equilibrium vapor generation and condensation are accounted for through appropriate correlations. However, the vapor phase is assumed to be at saturation, while the liquid phase can be either subcooled, saturated or superheated. Appropriate correlations are also used for wall friction, form losses and wall heat transfer, including the post-CHF regime.

The code uses a boron transport equation. However, boron is assumed to move with the liquid velocity, and no boron stratification is allowed.

The code employs models for typical BWR components, namely, jet pump, recirculation pump, steam separator and steam line with all necessary valves. However, all circulation loops and steam lines are lumped together to one recirculation loop and one steam line, respectively. The code also tracks the two-phase mixture and collapsed water levels in the reactor vessel downcomer. The latter is used to activate some of the control and safety systems. For the steam line, it uses the mass and momentum equations with the assumption of an adiabatic process. Note that the steam line pressure is a function of both time and space. Therefore, the acoustic effects in the steam line due to valve closure and/or opening are taken into account.

Plant Control and Protection Systems

RAMONA-3B has simplified but adequate models for the plant control and protection systems which directly affect the main steam supply system. Specifically, RAMONA-3B simulates the actions of the pressure regulator, the Safety and Relief Valves (SRV), the Main Steam Isolation Valve (MSIV), and the plant protection system through trip logics. It also includes the High Pressure Coolant Injection (HPCI) and the Reactor Core Isolation Cooling (RCIC) systems. The feedwater and recirculation flow controls are being implemented in RAMONA-3B at this time. A balance-of-plant code, MINET⁴, is also being interfaced with RAMONA-3B so that an entire BWR plant can be simulated.

Solution Method

In RAMONA-3B, all partial differential equations are first transformed into ordinary differential equations. The initial or steady-state conditions are then obtained by setting the time derivatives to zero, and iterating to obtain the eigenvalues of the system of equations. For the transient calculation, different methods are used for the different parts of the code. Specifically, the Gauss-Seidel iteration is used to integrate the fast neutron equations, explicit integration for delayed neutron equations, an iterative predictor-corrector method for heat conduction, the explicit first-order Euler method for vessel thermal hydraulics, and finally, the fourth-order Runge-Kutta-Simpson for the steam line dynamics. The neutron kinetics and fuel heat conduction equations are integrated with a master time step, whereas the thermal-hydraulic equations use a substep. There are several time step controls to assure stability and accuracy of the calculation. The details of the RAMONA-3B code can be found in References 1 and 5.

NODALIZATION STUDY

Ideally, a nodal code such as RAMONA-3B should represent each fuel assembly by a separate neutronic channel. However, this could be quite expensive in terms of the computer running time for a systems calculation such as Anticipated Transient Without Scram (ATWS). Therefore, a detailed core nodalization study has been performed in order to provide user guidelines on the optimum number of computational cells that should be used for a RAMONA-3B systems calculation. One of the Peach Bottom-2 Turbine Trip Tests, namely Test No. 3, was selected as the reference test. These were severe overpressurization tests, and particularly challenging for the nodalization study because of highly non-uniform initial control rod pattern. The initial conditions for Test 3 are shown in Table 1. The test was initiated by the closure of the turbine stop valves and was terminated by the delayed scram. The details of the test can be found in Reference 2.

Five calculations with decreasing number of nodes in the core have been performed using a quarter core symmetry. The number of neutronic and hydraulic nodes as used in these calculations are presented in Table 2. Note that the number of hydraulic nodes outside the core was kept constant at 99 in all five calculations.

Case 1 is the reference case with 4584 neutronic and 843 hydraulic cells which had earlier provided the best agreement with the test data (Section 7.4 of Reference 1). In this nodalization, each fuel assembly along with the appropriate control blade was explicitly modeled as a separate neutronic channel having the dimensions of $\Delta X = \Delta Y = 15.24$ cm. With 24 axial levels in the

Table 1. Initial Conditions for Test 3

Reactor Power	2275 MW
Core Pressure	6.95 MPa
Total Core Flow	12841 kg/s
Bypass Flow	1059 kg/s
Feedwater Flow	1148 kg/s
Core Inlet Subcooling	7.4°C
Initial Power Level	69.1% of Rated Power
Scram Level	77.0% of Rated Power

Table 2. Noding Details for the RAMONA-3B Nodalization Study

Case	Core Nodalization			Total Neutronic Nodes	Total Hydraulic Nodes	CPU/Real Time
	Axial Level	Neutronic Channels	Hydraulic Channels			
1(Ref)	24	191	31	4584	843	789
2	12	191	31	2292	471	410
3	24	55	31	1320	843	341
4	12	55	31	660	471	192
5	12	22	23	264	375	149

core, the height of each neutronic and hydraulic node was also 15.24 cm. However, several neutronic channels were grouped together to form thirty coolant channels in a core octant. Thus, the total number of core hydraulic channels including a bypass channel was thirty one (31).

Case 2 was made by changing Case 1 axial levels from 24 to 12. The same extrapolation lengths used in the reference run, i.e., Case 1, were used to represent the reflectors, but new albedos were calculated to match the initial average axial power distribution. This type of adjustment was made for each nodalization. The only other modification made to the nuclear data was to add a fuel parameter data set. This was done to collapse two zones in the fuel which became necessary in reducing the number of axial levels from 24 to 12 in the core. This particular collapsed node contained a region which was made up of a section containing burnable poison (i.e., gadolinium) while the other section did not. The new fuel data set was generated by taking the volume average for each of the coefficients in the diffusion coefficients and cross sections. This new set was then used in every calculation that used 12 axial levels in the core.

The next modeling change (for Cases 3 and 4) was made by combining four fuel assemblies into one neutronic channel. This was a relatively straightforward process because each control blade controls four assemblies; hence, the positioning of the fuel and its associated control blade was completely consistent with the reference case. This produced neutronic nodes that had dimensions of $\Delta X = \Delta Y = 30.48$ cm while $\Delta Z = 15.24$ and 30.48 cm to represent the core with 24 (Case 3) and 12 (Case 4) axial levels, respectively.

The final core model (Case 5) in this nodalization study had 12 axial levels and 22 neutronic channels. Difficulties arose in this nodalization because the nodes contained an equivalent of about 9 assemblies. Also, the hydraulic channels and control blades had to be remodeled since the reference case had 31 hydraulic channels and 54 control blades. Because of large neutronic nodes, the model lost its direct relationship to the details of the reactor core. Hence, the control blade pattern from the test data was abandoned and the control blade positions were adjusted to yield the most accurate initial average power distribution. Each node was assigned a unique hydraulic channel and control blade to preserve as much of the three-dimensional effect as possible. For the neutronic nodes, this coarse mesh representation crossed many fuel zones and no clear collapsing was possible. However, the fuel types were arranged as appropriately as possible using the same fuel types as in the reference case. The dimensions of these neutronic nodes were $\Delta X = \Delta Y = 45.72$ cm and $\Delta Z = 30.48$ cm.

The initial relative axial power distributions for each of the different core nodalizations and the main global parameters predicted for this transient can be seen in Figures 2 through 5. The BNL CDC-7600 CPU to real time ratios to run each model out to 2.0 seconds are also presented in Table 2.

It can be seen from Figures 2 and 3 that the core models that used either 191 or 55 neutronic channels were able to represent the initial power distribution reasonably well. This ability stems from the fact that in the 191 neutronic channels representation, each assembly was represented along with its assigned control blade, which in turn, controls the four nearest assemblies. This symmetry was taken into account when constructing the 55 channel case which grouped the four assemblies into one neutronic node; hence, the same control blade pattern as used in the test was employed in these models, thus contributing to good agreement with the transient data shown in Figures 4 and 5. Case 1 and 2 with 24 and 12 axial levels, but with 191 neutronic channels, predicted almost identical results. However, in Figure 4 the relative power for Case 3 with 24 axial levels (and 55 neutronic channels) predicts the peak to within 6 percent, while Case 4 with 12 levels (and 55 neutronic channels) predicts the maximum value to within 10 percent. While these differences did exist, hydraulically the results of the 55 channel cases were very similar to the reference case because the total integrated power was still close to the reference case. In Figure 5, this fact is borne out since the system pressure for the cases with 191 and 55 neutronic channels (Cases 1 through 4) predicted the same pressure response.

For Case 5 with 12 axial levels and 22 neutronic channels, the results were not as good. In Figure 3 it can be seen that the initial average relative axial power distribution was underpredicted in the lower part of the core and overpredicted near the top. This situation existed because a neutronic node encompassed about 9 fuel assemblies on the horizontal plane. Hence, the effect of inserting a control blade into the node affected a larger area. RAMONA-3B was not designed to control this type of node since the control blades are represented explicitly in the core, which means that as the control blade moves into a core, the node preceding it must be completely controlled. While this is appropriate when representing one assembly in a node, it greatly underpredicts the nodal power when used in neutronic nodes containing 9 assemblies, particularly when each assembly may have a different control blade pattern. This problem can be circumvented by using the control density in a node; however, that option is not presently available in RAMONA-3B. The same problem caused the underprediction of the transient relative power and system pressure as shown in Figures 4 and 5, respectively.

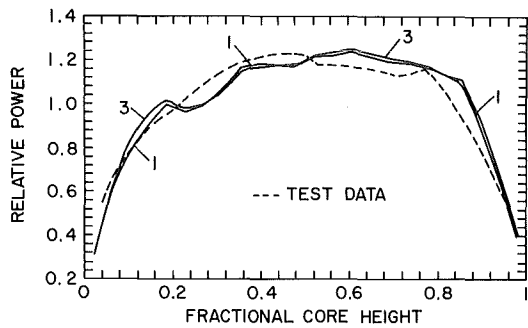


Figure 2 Comparison Between the Measured (---) and RAMONA-3B (—) Steady-State Axial Power Distribution

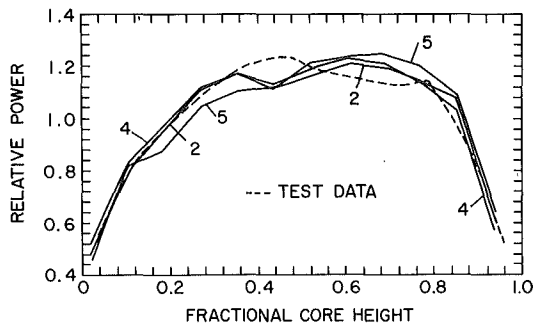


Figure 3 Comparison Between the Measured (---) and RAMONA-3B (—) Steady-State Axial Power Distribution

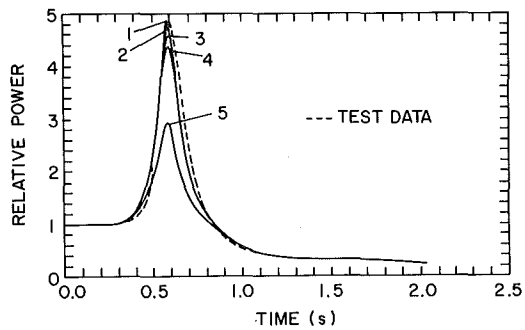


Figure 4 Comparison Between the Measured (---) and RAMONA-3B (—) Transient Total Power

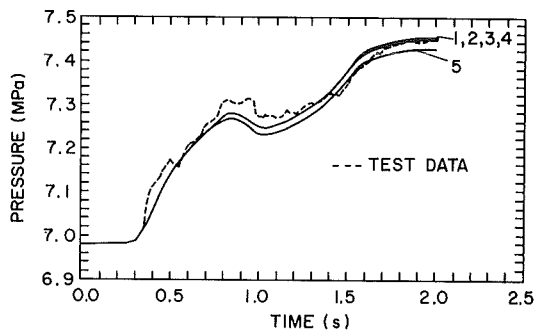


Figure 5 Comparison Between the Measured (---) and RAMONA-3B (—) System Pressure

In conclusion, the Peach Bottom Turbine Trip Test 3 can be best simulated with a quarter core representation of one node per assembly (i.e., 191 neutronic channels) with either 24 or 12 axial levels in the core with almost identical results. This test can also be represented by using 55 neutronic channels, i.e., grouping four assemblies around a control blade, because the control blade pattern can still be explicitly expressed. Hence, a RAMONA-3B user can represent the Peach Bottom-type reactor cores with reasonable accuracy by using a neutronic channel containing four fuel assemblies. This would result in a significant saving in the computer running time. Also, it was found that for a highly non-uniform control rod pattern, the number of assemblies in a node should not exceed four (4) since such a pattern cannot be accurately defined in RAMONA-3B. This could be alleviated if a control density option was added to RAMONA-3B. It will be included in the future improvement.

ACKNOWLEDGEMENTS

The authors would like to thank Dr. Fuat Odar, the NRC program monitor, for his suggestions and encouragement. Thanks are also due to Ms. A. C. Fort and L. Zaharatos for the fine typing of this manuscript.

REFERENCES

1. Wulff, W., Cheng, H. S., Diamond, D. J., and Khatib-Rahbar, M., "A Description and Assessment of RAMONA-3B MOD.0 Cycle 4: A Computer Code with Three-Dimensional Neutron Kinetics for BWR System Transients," NUREG/CR-3664, BNL-NUREG-51746, January 1984.
2. Carmichael, L. A., and Neimi, R. O., "Transient and Stability Tests at Peach Bottom Atomic Power Station Unit 2 at End of Fuel Cycle 2," EPRI NP-564, 1978.
3. Borresen, S., "A Simplified, Coarse-Mesh, Three-Dimensional Diffusion Scheme for Calculating the Gross Power Distribution in a Boiling Water Reactor," Nuclear Science and Engineering, 44, pp. 37-43, 1971.

4. Van Tuyle, G. J., Nepsee, T. C., and Guppy, J. G., "MINET Code Documentation," NUREG/CR-3668, BNL-NUREG-51742, February 1984.
5. Connell, H. R., Neymotin, L., Saha, P., and Slovik, G. C., "User's Manual for RAMONA-3B: A Computer Code with Three-Dimensional Neutron Kinetics for BWR Systems Transients," BNL Draft Report, February 1984.

NOMENCLATURE

a	Coefficients in two-group cross sections
A	Flow cross-sectional area, m^2
c_i	Delayed neutron precursor concentration, m^{-3}
c_B	Boron concentration per unit liquid mass
D	Diffusion coefficient, m
D_h	Hydraulic diameter, m
f	Friction factor
f_d	Control fraction
G	Mass flux, kg/m^2s
g	Acceleration due to gravity, m/s^2
h	Specific enthalpy, J/kg
j	Volumetric flux density, m/s
k	Thermal conductivity, W/m-K
p	Pressure, Pa
q'	Heat transfer per unit length, W/m
q'''	Heat generation or deposition per unit volume, W/m^3
S	Slip parameter
T	Temperature, K
t	Time, s
u	Specific internal energy, J/kg
v	Velocity, m/s
v_o	Bubble rise velocity, m/s
Z	Axial coordinate, m
α	Void fraction
β	Total delayed neutron fraction
Γ_v	Vapor generation rate, kg/m^3s
λ	Decay constant for delayed neutrons, s^{-1}
Σ	Macroscopic neutron cross section, m^{-1}
ϕ	Neutron flux, $m^{-2}s^{-1}$
ϕ_m	Two-phase multiplier
ρ	Density, kg/m^3
ν	Mean number of neutrons in fast or thermal group

Subscripts

1	Fast-group neutrons
2	Thermal-group neutrons
a	Absorption
f	Fission or fuel
g	Vapor (saturated)
i	Index for delayed precursors
l	Liquid
m	Mixture
o	Reference
w	Wall

"SYSTEMATIC PROCEDURES FOR CORE NEUTRONICS MODELLING
IN THE 3-D BWR SYSTEM TRANSIENT CODE RAMONA-3B"

S. Børresen and L. Moberg

Scandpower A/S
Kjeller, Norway

ABSTRACT

RAMONA-3B is a BWR System Transient Code with a full 3-D core neutronics model. The neutronics modelling is based on the PRESTO nodal method extended for kinetics. Established procedures exist for cross-section and kinetic parameter generation. The methods are fully compatible with state-of-the-art static methods for 3-D LWR core simulation and produces results with a high accuracy.

The neutronics model and cross-section data generation methods are described. Results from 3-D calculations are presented in comparison with experimental data, to illustrate the accuracy under steady state as well as transient conditions.

Procedures for generating consistent 1-D and point kinetics data, also applicable in RAMONA-3B, are being described.

INTRODUCTION

RAMONA-3B¹ is a BWR system transient code. It is unique in that it can calculate the core with 3-D neutronics, while also simulating the remainder of the nuclear steam supply system. The core neutronics are based on the PRESTO nodal method, a 1 1/2 group coarse mesh diffusion model. The hydraulics model describes the core with several parallel flow channels and is based on a 4 equation two-phase flow nonhomogeneous, nonequilibrium model. The steam supply system is described by e.g. recirculation pumps, steam separators, steam-lines, plant protection and control systems.

This paper emphasizes the core neutronics modelling in RAMONA-3B. The systematic FMS (Fuel Management System) methods of generating 2 group macroscopic cross-section data are described as well as the interaction with the 3-D static simulator, PRESTO, used to determine the actual core burnup state.

Benchmarks and qualification against experimental data are presented in order to demonstrate RAMONA-3B's ability to accurately predict 3-D power distributions both under steady state and transient conditions.

RAMONA-3B may also be used with a 1-D (axial) core model. Such a model requires plane average cross-section data, producing consistent 1-D power distributions. Procedures for generating 1-D cross-sections are described together with results from a qualifying benchmark case.

NEUTRONICS MODEL

The neutronic model of RAMONA-3B is based on the two-group, time-dependent diffusion equations combined with six delayed precursor group equations. The equations are differenced with the PRESTO² coarse mesh method, in general using a mesh spacing equal to the assembly pitch. The equations are solved with the assumption of asymptotic thermal flux, but with a corrective method accounting for the thermal flux leakage between the nodes. Albedo boundary conditions are defined on the core periphery. In the steady state application, the RAMONA-3B model is identical to that of the PRESTO Static simulator³.

Nuclear data are represented by two group macroscopic cross-sections, defined for each fuel bundle design. To account for various feedback effects the cross-sections are represented as functions of

- burnup state
 - exposure
 - void history
- instantaneous conditions
 - coolant density
 - coolant temperature
 - fuel temperature
- control rod presence
- Xenon concentration

The cross-sections are evaluated for each node; the burnup and Xenon effects are determined at the initial conditions only, whereas the instantaneous parameters and control rod feedback is updated at each time-step throughout the transient. Delayed neutron parameters are treated in analogy with the cross-sections, but with the instantaneous variation with void and temperatures neglected.

INTERACTION WITH NUCLEAR DATA AND CORE STATE FILES

RAMONA-3B is a part of Scandpower's integrated code system (FMS) for LWR core analysis⁴. As such it interfaces directly with cross-section data files as well as data files describing the actual core burnup state.

The basic code for cross-section generation is RECORD⁵. It is a fast production code for calculation of neutron spectrum, group cross-section data, kinetic parameters and reactivity as functions of fuel burnup in LWR fuel assemblies. With individual treatment of each fuel pin, the code calculates reaction rates, power and burnup distributions in two dimensions, taking into account most features which arise in present-day LWR designs.

Two-group macroscopic cross-sections, homogenized over the assembly, are taken from a series of RECORD runs, processed by a data processing code and stored as polynomials in a nuclear data bank for access by RAMONA-3B, cf. Fig. 1.

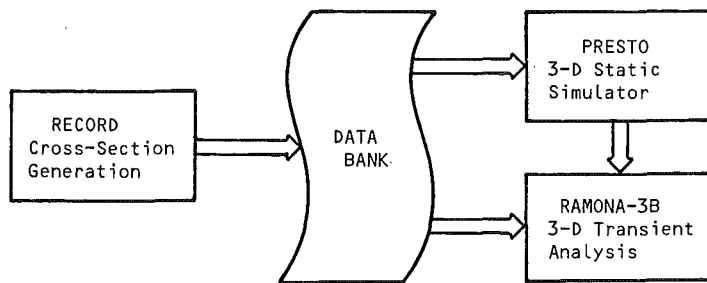


Fig. 1 FMS Code System

The reactor core state, defining the initial conditions for RAMONA-3B, is generated by static simulations with PRESTO, updating the burnup, void history as well as Xenon state on a nodal basis. The role of PRESTO in this approach is also illustrated in Fig. 1.

QUALIFICATION OF 3-D POWER DISTRIBUTIONS

A wide experience exists in calculating 3-D power distributions using the Scandpower codes in steady state (i.e. RECORD/PRESTO). Since RAMONA-3B and PRESTO are identical in the static application, these data also serve as the basis for qualification of RAMONA-3B's ability to predict the initial conditions of any transient. The qualification base consists of core follow calculations of about 30 reactor cycles, along with comparisons with measured TIP-data. In addition, measured γ -scan data from 4 different BWR reactors have been analyzed. A representative measure of the achievable accuracy can be found in Ref. 6, and is summarized in Table 1. The data refer to comparisons between calculated and measured nodal power distributions, and show an accuracy of roughly 8-9 %, as compared to TIP data. The γ -scan data, which has a lower measurement uncertainty, show an even better agreement (4 - 6 %).

Of equal importance in RAMONA-3B, is the ability to calculate the shifts in power distribution during the transient. Experimental data on detailed transient power distributions are sparse, but the recorded detector response from the Peach Bottom Trubine Trip Transients form an important experimental data base. Results from the RAMONA-3B analysis⁷ of these tests are shown in Fig. 2 (examples of individual detector readings), Fig. 3 and Table 2 (axial average detector response).

PROCEDURES FOR GENERATION OF A CONSISTENT 1-D AXIAL NEUTRONICS MODEL

Many BWR system transients show power shifts only in the axial direction. It may therefore be cost-beneficial to perform the simulation of such transients using a 1-D axial core model. The nodal neutronics model of RAMONA-3B also applies in 1-D and a systematic procedure for generating average cross-section data for such a model has been developed.

By use of a stand-alone computer code, PETRA, nodal distributions of cross-sections and associated state variables are being collapsed to average planar values. Appropriate averaging schemes with e.g. adjoint flux/flux weighting is used and with the reflector effects taken into account. A radial buckling term is introduced in order to reproduce the 3-D solution exactly (in the average sense). The functional dependence in the 1-D cross-sections from coolant density and temperature as well as fuel temperature is calculated by fitting the data to several reactor states.

In addition to the 1-D data, PETRA also produces core average point kinetics parameters.

A qualification of these methods was done by applying them to the Peach Bottom Turbine trip Test (cf. § 4. above). Fig. 4 shows the result of the 1-D simulation in comparison to the original 3-D result*.

SUMMARY

RAMONA-3B combines the state-of-the-art methods of 3-D LWR core simulation with that of an advanced system transient code. Its application to a variety of transients, such as pressurization, ATWS, and control rod drop transients have been demonstrated and documented^{1, 7, 8, 9}.

* This work was performed under a contract for Brookhaven National Laboratory.

REFERENCES

1. W. Wulff, et.al., "A Description and Assessment of RAMONA-3B : A Computer Code with Three-Dimensional Neutron Kinetics for BWR System Transients", BNL-NUREG-51746, Brookhaven National Laboratory, Jan. 1984.
2. S. Børresen, "A Simplified, Coarse Mesh, Three-Dimensional Diffusion Scheme for Calculating the Gross Power Distribution in a Boiling Water Reactor", Nucl. Sci. & Eng., 44 (1971).
3. S. Børresen, L. Moberg, J. Rasmussen, "Methods of PRESTO-B, A Three-Dimensional, LWR Core Simulation Code". NRC Topical Report, NF-1583.03 (1983).
4. S. Børresen, T. Skardhamar, S. Wennemo-Hansen, "Applications of FMS RECORD/PRESTO for Analysis and Simulation of Operating LWR Cores", Proc. NEA Specialists Mtg., Paris, (Nov. 1979).
5. H.K. Ness and T. Skardhamar, "Methods of RECORD : An LWR Fuel Assembly Burnup Code", NRC Topical Report, NF-1583.02, (1983).
6. K.E. Karcher, W.K. Cantrell, D.W. Schroeder, "A Description and Validation of Steady-State Analysis Methods for Boiling Water Reactors" NRC Topical Report, NF-1583.01, (1983).
7. L. Moberg, J. Rasmussen, T.O. Sauar, O. Øye : "RAMONA Analysis of the Peach Bottom-2 Turbine Trip Transients", EPRI NP-1869, June 1981.
8. D.I. Garber, D.J. Diamond, H.S. Cheng, "Calculation of a BWR "Partial ATWS" using RAMONA-3B", Proc. of the International Meeting on Thermal Nuclear Reactor Safety, Chicago, Sept. 1982.
9. G. Slovik, P. Saha, "A RAMONA-3B Code Description and Nodalization Study for the Peach Bottom-2 Turbine Trip Test 3", Proc. of the International Meeting on Thermal Nuclear Reactor Safety, Karlsruhe, Sept. 1984.

TABLE 1. COMPARISON BETWEEN CALCULATED AND MEASURE NODAL POWER DISTRIBUTIONS (REF. 3 AND 6)

Experiment	Standard deviation, calculation vs. measurement
<u>TIP-Measurements</u>	
Brunswick-1, cycle 1-4 } Brunswick-2, cycle 5 }	0.087
Quad Cities-1, cycle 1-2	0.093
<u>y-Scan Measurements</u>	
Quad Cities-1, EOC2	0.037
Hatch-1, EOC1	0.064

TABLE 2. TRANSIENT POWER PEAK VALUE ON VARIOUS AXIAL LEVELS

	PEAK VALUE / INITIAL VALUE				
	On Detector Level				Total Average
	A	B	C	D	
RAMONA	3.65	4.50	5.01	5.24	4.67
TT1 Measurement	3.47	4.46	5.23	5.56	4.68
RAMONA	3.54	4.45	4.76	4.88	4.46
TT2 Measurement	3.53	4.56	4.94	5.09	4.53
RAMONA	3.35	4.47	5.29	5.26	4.58
TT3 Measurement	3.63	4.87	5.44	5.55	4.87

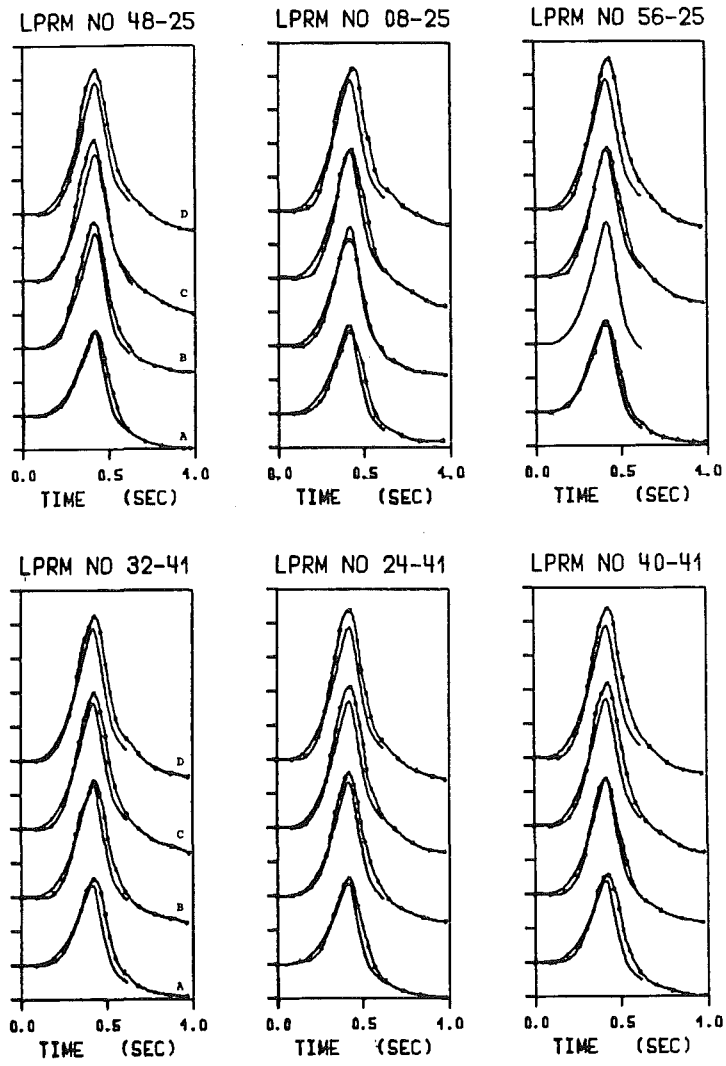


Fig. 2 Calculated and Measured LPRM response, Peach Bottom Turbine Trip Test TT2

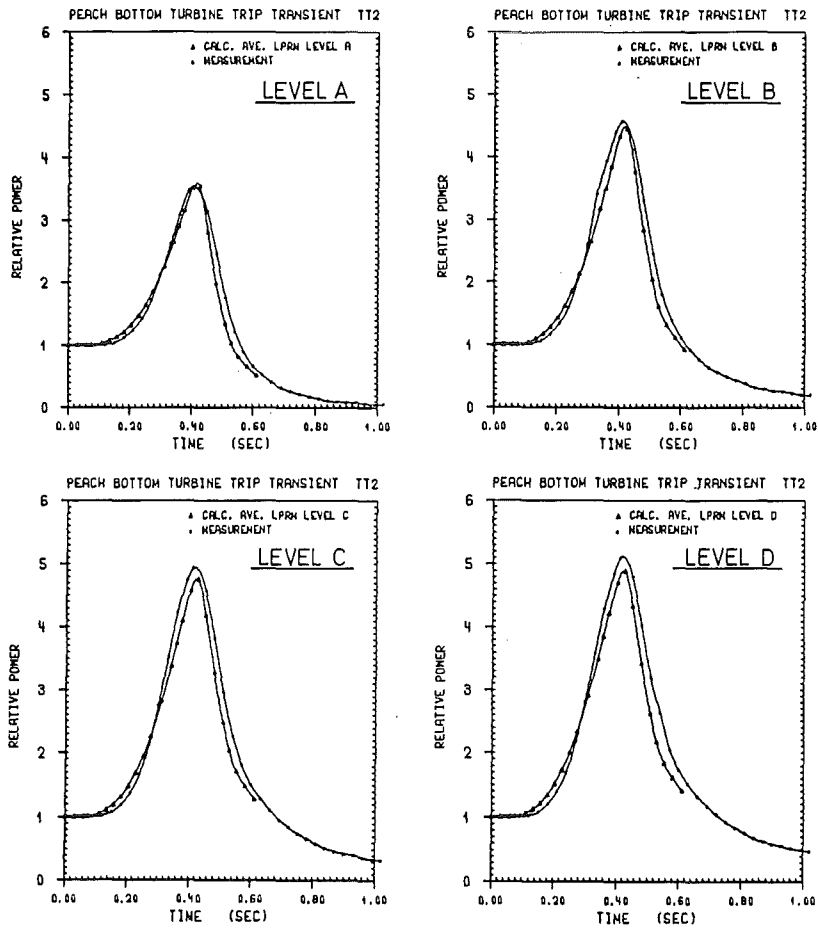


FIGURE 3 Average LPRM Response on Various Axial Levels, Peach Bottom Turbine Trip, TT2.

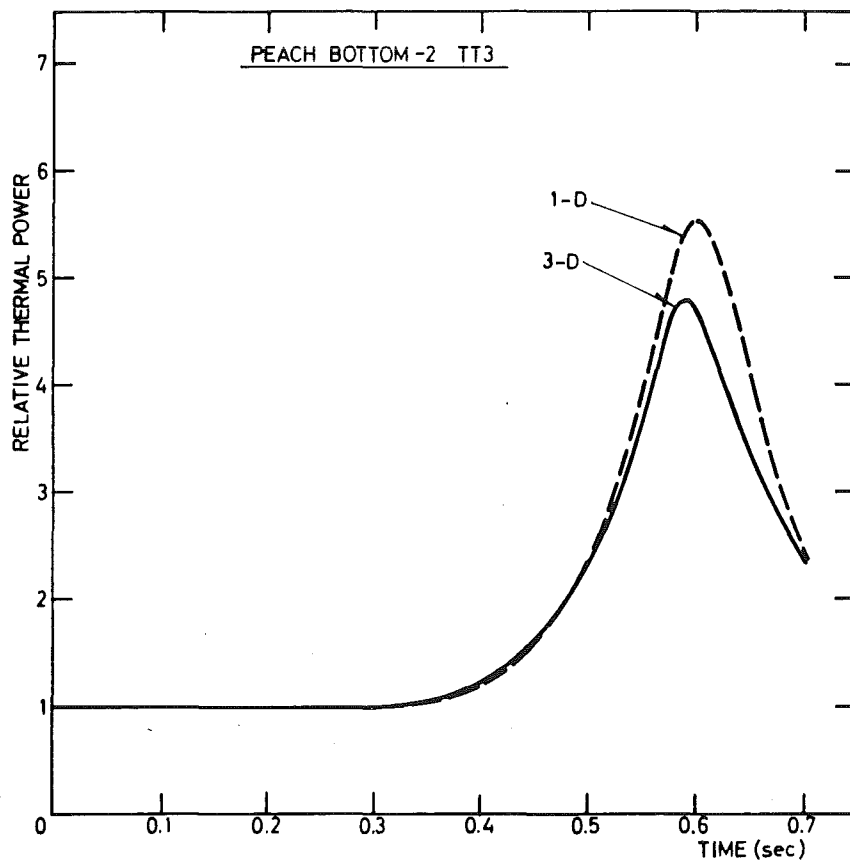


FIGURE 4 Fission Power vs. Time, Comparison between 1-D and 3-D Results, Peach Bottom Turbine Trip Test TT3.

A QUICK RUNNING DYNAMIC SIMULATION
CODE FOR BWR TRANSIENTS

C.S. Lin and W.E. Kastenberg

Mechanical, Aerospace and Nuclear Engineering Department
University of California, Los Angeles
Los Angeles, California 90024

ABSTRACT

A quick running computer code for the analyses of BWR system transients has been developed. The code is based on a four equation flow model which accounts for non-homogeneous two phase flow and a five equation flow model which accounts for non-homogeneous, non-equilibrium two phase flow. Several transients have been analyzed, including turbine trip with and without bypass, and a step reactivity insertion. For the case of turbine trip without bypass, steam flow reversal is predicted, consistent with more recent calculations for this transient.

INTRODUCTION

A number of computer codes have been developed for the simulation and analysis of nuclear reactor system transients. These system codes are important for design, research and assessment of safety. The capabilities and limitations of existing system codes are reviewed and summarized in detail by Wulff [1].

The purpose of this paper is to present a fast-running simulation model for BWRs. Important goals in this effort have been (a) to provide better understanding of complex two-phase flow phenomena under transient conditions, (b) to strive for real time simulation. These considerations require balance between modeling detail and computing time required for application.

In order to meet these goals, a four equation flow model which accounts for non-homogeneous two phase flow and a five equation flow model which accounts for non-homogeneous, non-equilibrium two phase flow were developed. The four equation model is an improvement over the homogeneous equilibrium model found in such codes as RELAP [2] and RETRAN [3,4] yet is more simple than the five and six equation models found in such codes as TRAC [5].

FLUID DYNAMICS

One of the improvements represented by this model lies in the development of two-phase flow models and numerical solution methods which are used to solve the flow field equations. It has been recognized that modeling of two-phase flow is the central issue of system simulation because it determines both capabilities and limitations, and it dominates the cost of computing. This is particularly true for BWRs since they always encounter two-phase flow under normal operation as well as under transient conditions. Hence, in order to more accurately determine the dynamic response of BWRs, to increase the understanding

of the two-phase flows that are encountered, and to extend the capability of simulation, non-homogeneous (NH) and non-homogeneous, non-equilibrium (NHNE) models are developed. Both models are derived from the rearrangement of the six-equation two-fluid model.

The non-homogeneous four-equation model employed has been derived by Lin and Kastenberg [6] and can be expressed as follows:

(1) Mixture Continuity Equation

$$\dot{M}_i = \sum_{v \in T_i} (W_{lv} + W_{gv}) - \sum_{v \in I_i} (W_{lv} + W_{gv}) \quad (1)$$

(2) Total Internal Energy Equation

$$\dot{U}_i = \sum_{v \in T_i} [(W_{lv} H_{lv} + W_{gv} H_{gv})] - \sum_{v \in I_i} [(W_{lv} H_{lv}^* + W_{gv} H_{gv}^*)] + Q_i \quad (2)$$

(3) Liquid Momentum Equation

$$\dot{W}_{lk} = f_{lk}(t, P_i, P_j, W_{lk}, W_{gk}) \quad (3)$$

(4) Vapor Momentum Equation

$$\dot{W}_{gk} = F_{gk}(t, P_i, P_j, W_{lk}, W_{gk}) \quad (4)$$

where $i, j=1, \dots, N$; $v, k=1, \dots, K^*$

The subscripts i, j represent volume indices, and v, k junction indices. The flow in a critical junction is determined by an algebraic relationship:

$$\dot{W}_k = g_k(P_i), \quad k = K+1, \dots, K^* \quad (5)$$

The equation of state is given by

$$P_i = P_i(U_i, M_i), \quad i=1, \dots, N. \quad (6)$$

Using vector notation, Equations (1)-(6) can be written as

$$\dot{y} = F(t, y) \quad (7)$$

where $y = \text{col}: [W_{l1} \dots W_{lK} W_{g1} \dots W_{gK} \dots U_1 \dots U_N M_1 \dots M_N]$ and $F = \text{col}: [F_1 \dots F_{2K+2N}]$. We introduce the following Jacobian matrix:

$$dF(t,y) = [\partial F_i / \partial y_j], \quad (8)$$

where the elements are assumed to be continuous functions, and H_{lk} , H_{gk} , Q_i , f_{lk} , and f_{gk} are also continuous with time.

By differencing Equation (7) and using Equation (8), we obtain

$$(y^{n+1} - y^n) / \Delta t = F(t^n, y^n) + dF(t^n, y^n)(y^{n+1} - y^n). \quad (9)$$

Rewrite Equation (9) as

$$[I - (\Delta t) dF(t^n, y^n)] y^{n+1} = [I - (\Delta t) dF(t^n, y^n)] y^n + (\Delta t) F(t^n, y^n) = G^n \quad (10)$$

where I is a unit matrix of $(2K+2N)$ order and Δt is a time step. The one-step integration method, Equation (10), has been proven to be consistent and convergent [7] for a large Δt . In Equation (10), the numerical time advancement could be accomplished by simultaneous solution of the $2K+2N$ system of linear equations. However, because of the simple nature of the continuity and energy equations, all of the variables except the liquid flow rate (or vapor flow rate) can be eliminated.

The elimination process is described in Reference [6] and a reduced system of K equations containing only the unknown W_{ℓ}^{n+1} is obtained:

$$\underline{A} \underline{W}_{\ell}^{n+1} = \underline{Z}, \quad (11)$$

where $\underline{A} = [A_{kv}]$ is a $K \times K$ matrix; $\underline{W}_{\ell} = \text{col}: [W_{\ell 1} \dots W_{\ell K}]$; $\underline{Z} = \text{col}: [Z_1, \dots, Z_K]$.

The detailed formulations of A_k and Z_k can also be found in Reference [6].

The NHNE model contains five-equations: two for continuity, two for momentum and one for energy. The one energy equation is supplemented by the constraint that the least massive phase is always at saturation. The numerical solution of the NHNE model is similar to the NH model and will not be given here.

GEOMETRIC NODALIZATION

With the fluid dynamics developed above, a free system topology is achievable. However, in order to save computer storage and computing time, a fixed system topology is used. Only two fixed types of geometric nodalizations are utilized to represent a primary system for BWRs.

The simplified nodalization (type 1) is shown in Figure 1. This type utilizes 14 control volumes and 19 junctions or flow paths. The twenty jet pumps and two recirculation loops are combined into one loop to reduce the number of control volumes and junctions required. The steam line piping is divided into four volumes to provide an accurate determination of the pressure at the turbine valve, bypass valve and safety relief valves. The values of the pressure at those valves are important because they determine the control logic of the valve action. In other words, the timing and the number of valves to be opened or closed are controlled by the pressure signals. The core is modeled using one control volume. The rod drive flow and the cleanup demineralizer flow can be accounted for by in-

increasing the feedwater flow slightly to establish a mass and enthalpy balance with the assumed main steam flow.

The simplified nodalization described above actually combined two recirculation loops into one loop. Therefore, it cannot simulate a number of important transients, such as a recirculation pump failure and a LOCA in any recirculation loop. In these transients, the system response in the two recirculation loops are different and it is necessary to utilize two loops. Figure 2 shows the complicated nodalization (type 2) of the primary system for BWRs. There are 17 control volumes and 24 flow junctions.

It can be shown that the structures of the matrix A corresponding to the networks of Figure 1 and 2 are close to diagonal matrices (Figures 3 and 4). Hence Equation (11) can be efficiently solved by a combination of the block elimination [7] and factorization methods [8].

REACTOR CORE POWER GENERATION AND THERMAL ANALYSIS

The point model is used for the neutron kinetics and the power generated is assumed to be distributed uniformly over the fuel cross section; however a certain fraction is given directly into the coolant. The feedback reactivity effects include fuel temperature (the Doppler effect), water temperature and moderator density. Power generation continues after the reactor is shutdown because of fission product decay. It has been widely assumed that decay heat can be fitted to a polynomial of eleven exponentials. By defining a 'concentration' for each group, we can model fission product decay heat as 11 decayed neutron groups. The fission heat generated in the fuel is transferred from the fuel across the gap between fuel and cladding, and then through the cladding to the coolant. In addition, the fuel temperature contributes to the reactivity feedback through the Doppler effect. The thermodynamic behavior of a reactor core is represented by a "single channel" model. A whole-core lumped parameter model for heat conduction equation is employed [9].

SYSTEM COMPONENT MODELS

The system component models include centrifugal pumps, jet pumps, valves, trip controls, steam separators, critical flow models and constitutive correlations.

Pumps. For Boiling Water Reactors, two kinds of pumps should be modeled. They are centrifugal pumps and jet pumps. A pump model is given to calculate the pressure difference between both sides of a centrifugal pump and are described by homologous curves. The development of the homologous curves are for single-phase flow conditions. The pump model also allows the option of accounting for cavitation or two-phase degradation effects on pump response. A separate set of homologous two phase curves for heat and torque ratios which are in the forms of difference curves are also supplied.

Apart from the centrifugal pumps, a compressible two-stream flow with one-dimension momentum mixing equation is utilized for a jet pump. This equation is based on single stream flow equation, with some modifications.

Valves. Simple valves and check valves can be modeled to simulate the turbine stop valves, main steam isolation valves and steam bypass valves. Once a trip action occurs, the flow area for the valve is given from an input area-versus-time table. Two types of check valves are modeled. One exhibits a

hysteresis behavior one does not. Both types are controlled by flow-dependent pressure drops of the formula.

Trip Controls. The trip logic of a reactor system can be simulated by trip control data. An arbitrary number of these control data can be input. These signals are, in general, the following: 1) reactor power, 2) volume pressure or temperature, 3) elapsed time, 4) mixture level, 5) liquid level, 6) water temperature, 7) fuel temperature, 8) mass flow at junctions.

These controlling signals can be used to perform a number of reactor system actions such as reactor scram, valve open or close, ECC fill water injections and pump shut off. When the signal reaches the setpoint, the trip is actuated after the specified delay.

Steam Separator Model. In the conventional separator design for BWRs, two phase mixture leaving the upper plenum region enters the steam separator from the bottom and impinges on vanes which impel the liquid radially and allow vapor to pass vertically through the device. The separated liquid is collected by gravity and returned downward to the reactor downcomer region. The shortcoming of this approach is it assumes the quality of the outlet steam flow path to a value of 1.0 for all inlet flow conditions and does not reflect the actual efficiency of a separator nor its variability of separation performance as a function of flow condition. Since the separation is not perfect, some liquid (carryover) is entrained in the vapor path and some vapor (carryunder) is entrained in the liquid path. The separator model defines the values of carryover and carryunder in terms of the significant parameters which affect its performance. The separator performance varies with inlet quality and mixture level in the separation.

Critical Flow Models. Many theories on critical flow rate have been proposed and are produced in a number of tables. Currently, these tables are transferred into a set of empirical formulas as shown in Reference [4]. These polynomials are functions of stagnation pressure, P , and stagnation specific enthalpy, h . They are explicit and convenient to use.

Constitutive Correlations. The governing equations derived in the fluid dynamics indicate that individual models are required for mass exchange and, interphase and wall-to-phase momentum and energy transfer. It is evident that the number of constitutive models required is dependent on the complexity of the two-phase flow models. The constitutive correlations are thus dependent on the topology or structure of the flow field, i.e., flow regimes. Models for the flow regimes are also required. A detailed review and discussion of flow regimes and constitutive models which have been widely applied to simulation codes can be found in a number of References [2,4,5,10]. Those employed here are given in Reference [11].

CODE VERIFICATION

The BWR plant modeled is a General Electric BWR-4. Three different transients, i.e., a turbine trip without bypass (TTWOB), a turbine trip with bypass (TTWB) and a positive reactivity insertion (PRI) are analyzed. Although each of the three transients requires slightly different models, the major initial conditions for each are identical. Table 1 lists the initial conditions used for each transient. They are the same as assumed in the Safety Analysis Report (SAR) for the La Salle Plant [12]. End-of-core (EOC) conditions are used

to develop the physics parameters including the scram curve worth. Most of the results from this study will be compared with the La Salle SAR [12] and RETRAN predictions [13,14] for various transients. Comparisons with the plant SAR and RETRAN predictions are made on a qualitative basis to check general trends and not from a quantitative viewpoint. The qualitative comparisons are made only to assure that no major errors exist in the simulation code.

Turbine Trip Without Bypass (TTWOB). A variety of turbine or nuclear system malfunctions can initiate a turbine trip. Once a turbine trip is initiated, all turbine stop valves achieve full closure within about 0.10 second. The TTWOB transient represents the fastest possible steam flow shutoff and a severe nuclear system pressure increase. In this transient, the turbine is tripped and it is assumed that steam bypass valves (which will normally open to relieve pressure) fail to operate.

The system response for TTWOB is shown in Figures 5-7. The transient is initiated by the closure of the turbine stop valves. Once these valves are closed, a pressure shock appears in the steam line. Hence, the steam flow leaving the vessel decreases. Since the core is continuing to generate power with a reduced steam flow, the reactor vessel pressure increases. The pressure continues to increase until the safety/relief valves open. This rise in pressure causes a reduction in the core voids which, in turn, results in a core power increase. The power continues to rise until the new voids generated by the higher power, the Doppler reactivity feedback and the scram reactivity feedback override this positive effect and then begins to reduce the core power. The steam flow is reversed twice because of a large pressure shock induced by the fast closure of the turbine stop valves and failure of the steam bypass valves. The flow reversals occur at $t=0.44$ second and $t=1.46$ seconds.

Comparisons with vendor calculations of La Salle County Station nuclear power plant are also shown in Figures 5-7. The results indicate that the system pressure and power responses compare reasonably well with the plant SAR predictions. However, the plant SAR predictions do not show the flow reversals. In the SAR, the steam flow was reduced only to 25% but did not reverse or exhibit any oscillations. The steam flow reversals were also predicted by the RETRAN study. This discrepancy has been carefully evaluated and a conclusion was made that the momentum and inertia effects in the steam line were not accounted for in the vendor calculations. The finding of the new-simulation model presented here also enhances the confidence of this conclusion.

In this simulation, a uniform time step (0.02 sec) is used. The computing time needed to simulate up to two seconds of real time is 6 CPU seconds using an IBM 3033 computer (compared with 33 CPU seconds in the RETRAN study). It is believed that if error control criteria were included for variable time steps (as in RETRAN), computing time will be further reduced.

Turbine Trip with Bypass (TTWB). The TTWOB transient discussed above is an unlikely event because the steam bypass valves will normally open. Consequently the turbine trip with bypass (TTWB) is a more likely event. From the plant SAR, this transient is estimated to occur with a moderate frequency. The assumptions and conditions are the same as the TTWOB transient except the steam bypass valves are assumed to function normally. The steam bypass system capacity is set to 26% of the rated steam flow as listed in Table 1.

Figures 8-10 show the results expected from 105% of rated power for this transient. As can be seen from these Figures, this transient is less severe than the TTWOB transient. The core power increases rapidly because of the void reduction caused by the pressure increase. However, the power increase is limited

only to 132% of its rated value. The peak pressure at the steam dome does not exceed 1116 psia. The steam flow exhibits oscillations as the TTWOB transient. However, unlike the TTWOB transient, steam flow reversals never occur during the time period of the transient because the effect of the steam bypass flow greatly reduces the magnitude of the pressure shock. Comparisons with vendor calculations of La Salle County Station plant are also shown in Figures 8-10. The results indicate that the system pressure, core power and flow responses compare reasonably well with the SAR predictions for this transient.

Positive Reactivity Insertion (PRI). It is assumed that this transient is produced by an earthquake. The acceleration forces of the earthquake can cause compaction of the reactor core due to closing the radial gaps between the fuel assemblies. This can result in a net positive step reactivity insertion to the core. When the control rods are scrambled, the rate of inward motion is decreased from the normal rate. This is because a retarding force resulting from the seismic event, delays the motion of control rods. A 60¢ step reactivity insertion is assumed in this case. Figure 11 shows the power response for the PRI transient. The reactor power rapidly increases to 240% after the positive reactivity insertion takes place at 0.1 sec. Then, the increase of the core power becomes slowly saturated due to the negative feedback reactivity of the Doppler effect. After the reactor scram signal is initiated, the core power begins to decrease. Recently, more validations of the simulation model presented have been carried out. They include the simulation [15] of Peach-Bottom TTWOB experiments and sensitivity studies for each transient described above.

CONCLUSION

A fast running simulation model for BWR transients has been presented which emphasizes computer cost, ease of use and sufficient accuracy for most transients of interest. The simulation is expected to be capable of predicting the most important parameters of pressure, flow, coolant enthalpy and temperature as a function of time. Since all reactor plant transients take place in real time, the new code is designed to strive for the same goal. Several transients have been analyzed, including a turbine trip with and without bypass, and a step reactivity insertion. The results are in good agreement with the La Salle SAR and RETRAN predictions.

REFERENCES

1. W. Wulff, EPRI Report, EPRI WS-81-212, p. 5-1 (May 1981).
2. Staff Report, "RELAP4", Idaho National Engineering Laboratory, ANL-NUREG-1335 (Sept. 1976).
3. Staff Report, "RETRAN", EPRI, EPPRICGM-5 (Dec. 1978).
4. Staff Report, "RETRAN-02", EPRI, NP-1850-CCM (May 1981).
5. Staff Report, "TRAC-PIA", LA-7777-MS, NUREG/CRO665 (May 1979).
6. C.S. Lin and W.E. Kastenberg, Nuclear Science and Engineering, April (1984).
7. T.A. Porsching et. al. "FLASH-4, A Fully Implicit Fortran IV Program", Bettis Atomic Power Laboratory, WAPD-TM-840 (March 1969).
8. E. Isaacson and H.B. Keller, "Analysis of Numerical Methods", John Wiley and Sons, Inc., New York (1966).
9. E.E. Lewis, "Nuclear Power Reactor Safety", Wiley, New York (1977).

10. E.D. Hughes, et.al. EPRI NP-143 (1976).
11. C.S. Lin, "A Fast Running Simulation Code for BWRs". Ph.D in Engineering, UCLA, 1983.
12. Staff Report, "Final Safety Analysis Report," La Salle County Station, Commonwealth Edison Company.
13. Staff Report, "RETRAN Sensitivity Studies of Light Water Reactor Transients," EPRI NP-454 (June 1977).
14. K. Hornyik and J.A. Naser, "RETRAN Analysis of the Turbine Trip Tests at Peach Bottom Atomic Power Station Unit 2 at the End of Cycle 2," EPRI NP-1076-SR (April 1979).
15. H.C. Yeh, "Analysis of the Peach Bottom 2 Turbine Trip Transients", M.S. in Engineering, UCLA 1984.

NOMENCLATURE

H_l = junction total liquid energy per unit mass	H_g = junction total vapor energy per unit mass
M = total mass	W_g = vapor flow rate
U = total internal energy	Q = heat source term
P = thermodynamic pressure	Δt = time step
W_l = liquid flow rate	θ = a number between 0 and 1
k, v = junction index	i, j = volume index
T_i = set of in-coming junctions	I_i = set of out-going junctions
N = total # of control volumes	K = total # of normal flow junctions

TABLE 1
Initial Conditions for the Simulation Code

<u>Parameter</u>	<u>Units</u>	<u>Value</u>
Thermal Power	MW	2533
Steam Flow	10E+6 lb/hr	10.99
Core Flow	10E+6 lb/hr	77.0
Core Bypass Flow	10E+6 lb/hr	4.83
Recirculation Flow	10E+6 lb/hr	34.2
Jet Pump N Ratio	-----	1.25
Steam Dome Pressure	psia	1020
Feedwater Temperature	$^{\circ}$ F	427.3
Bypass Valve Capacity	%	26
Scram Curve	MWD/T	EOC
Scram Worth	\$	-32.0
Void Coefficient	ζ /%	-15.1
Doppler Coefficient	ζ / $^{\circ}$ F	0.173

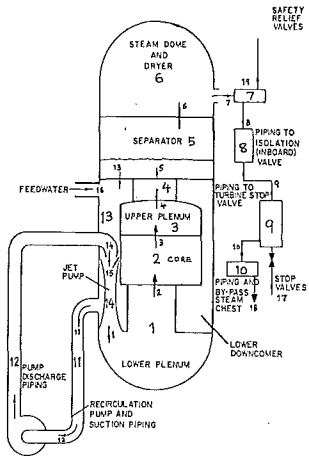


Figure 1. Geometric Nodalization of BWR Primary System (Type 1)

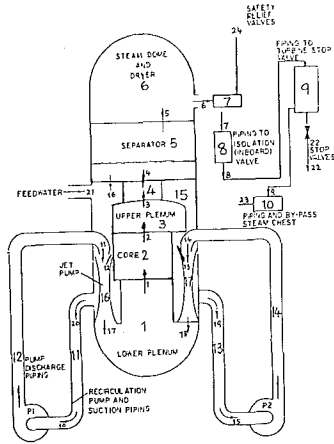


Figure 2. Geometric Nodalization of BWR Primary System (Type 2)

	1	2	3	4	5	6	7	8	9	10	11	12	13	14	15	
1	X	X													X	X
2	X	X	X													
3	X	X	X													
4		X	X	X												
5		X	X	X	X										X	
6			X	X	X	X									X	
7				X	X	X	X									
8					X	X	X	X								
9						X	X	X	X							
10							X	X	X	X						
11								X	X	X	X					
12									X	X	X	X				
13				X	X					X	X	X	X			
14	X										X	X	X	X		
15	X											X	X	X	X	

Figure 3. Structure of Matrix A (Type 1)

	1	2	3	4	5	6	7	8	9	10	11	12	13	14	15	16	17	18	19	20		
1	X	X																		X	X	
2	X	X	X																			
3	X	X	X																			
4		X	X	X																		
5			X	X	X															X		
6				X	X	X														X		
7					X	X	X															
8						X	X	X														
9							X	X	X													
10								X	X	X											X	
11									X	X	X								X			
12										X	X	X						X	X	X	X	
13											X	X	X					X	X	X	X	
14												X	X	X				X				
15													X	X							X	
16				X	X									X	X				X	X	X	
17	X														X	X						
18	X															X	X					
19																X	X		X	X	X	
20																	X	X	X		X	X

Figure 4. Structure of Matrix A (Type 2)

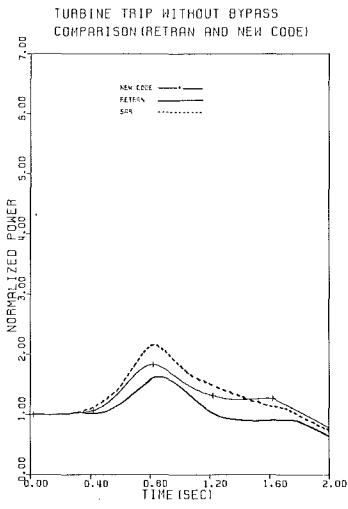


Figure 5. TTWOB Comparison-Power (Base Case)

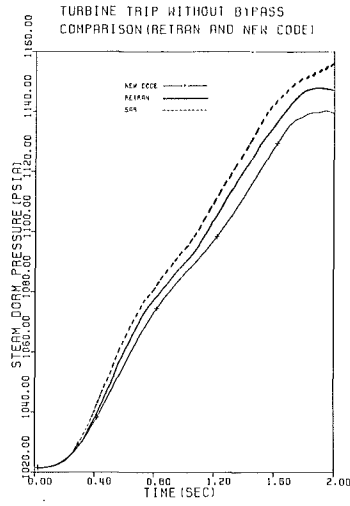


Figure 6. TTWOB Comparison-Pressure (Base Case)

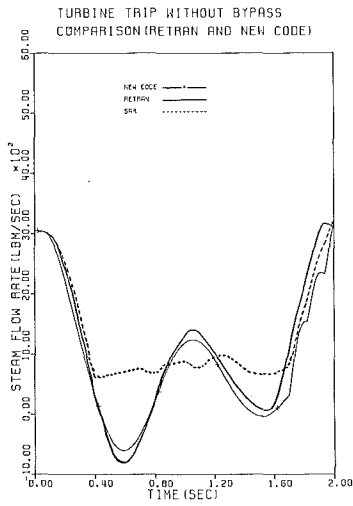


Figure 7. TTWOB Comparison-Steam Flow (Base Case)

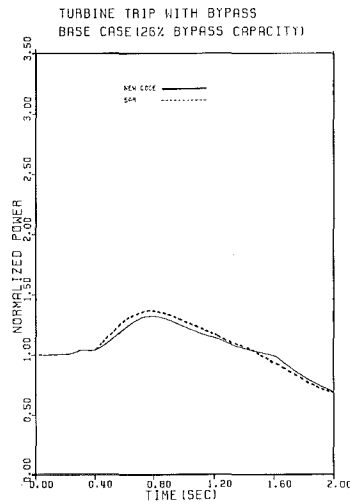


Figure 8. TTWB Normalized Power (Base Case)

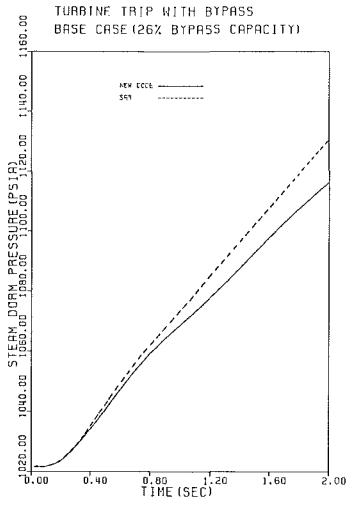


Figure 9. TTWB Steamdome Pressure (Base Case)

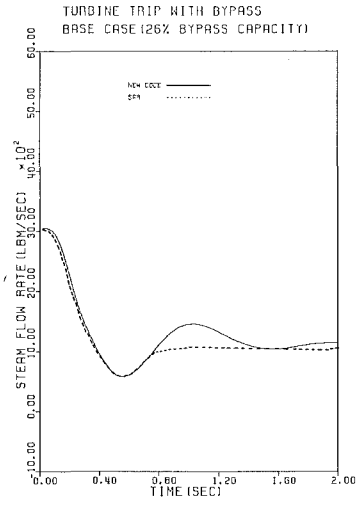


Figure 10. TTWB Steam Flow (Base Case)

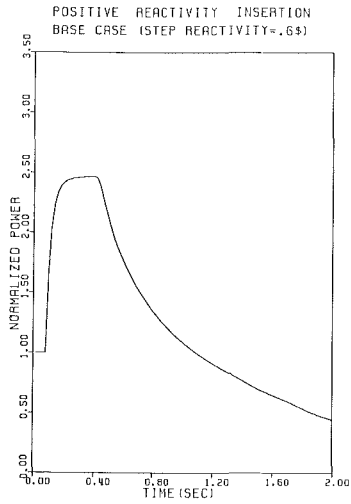


Figure 11. PRI Normalized Power (Base Case)

A BWR STABILITY PREDICTION MODEL AND ITS QUALIFICATION AGAINST TESTS IN OPERATING REACTORS.

Yngve Waaranperä and Håkan Svensson

AB ASEA-ATOM
Box 53 S-71204 Västerås, Sweden.

ABSTRACT

This paper describes briefly a time-domain stability prediction code in the form of a general-purpose BWR transient analysis code, which has been developed under an EPRI contract, starting from the existing code BISON. The code has a four equation slip model with core and bypass channels, one-dimensional two-group diffusion neutron kinetics, fuel heat transfer model, steam line model, and balance-of-plant models. Briefly outlined is also the stability prediction validation against tests in Peach Bottom-2, ASEA-ATOM BWRs and the FRIGG loop.

INTRODUCTION

The stability of the coolant flow and the power is weakened, when the operating state is altered in the direction of increasing power/flow ratio. Nuclear parameter modifications such as a reduced fuel time constant, more negative void reactivity coefficient, smaller delayed neutron fraction, and hydraulic design changes such as increased steam separator pressure losses or reduced core inlet orificing have an unfavourable effect on stability. Thermal-hydraulic dynamic instability is caused by interaction between opposite phase oscillations of non-boiling and boiling flow pressure losses, driven by a flow-induced density head variation, and has to be considered at the design of the individual core channels. Nuclear coupled flow and power instability is caused by a density head feedback loop in which density reactivity directly affects the fission power, and via the fuel time constant and the related time integrated evaporation rate variation alters the core density head with a phase lag of about 180°. This reactivity coupled instability phenomenon also has to be considered in the core and coolant loop design. Thanks to the high operating pressure of commercial BWRs, which reduces density variations in the boiling flow, and the long time constant of the Zircaloy-clad UO₂ fuel, which attenuates the gain in the feed-back loop from power to void, adequate stability can be ascertained by proper design and imposed operational constraints.

The stability of the operating state of a BWR is primarily a concern of availability. Operational constraints and possible transients originating from oscillatory operating modes have a negative impact on the capacity factor of the plant. Reduced fuel pin radius, extended operating range or Pu recycling may be used for improvement of fuel characteristics and the overall economy provided that stability is not unduly impaired. Accordingly there are economic incentives to improve the accuracy of stability predictions by the development of prediction tools validated against experiments in commercial power stations. Ultimately stability is also a concern of safety, inasmuch as instability may lead to operational transients, and transients may be precursors to more severe incidents. On the other hand a transient may bring the reactor into a state of degraded stability, which brings the question of stability into focus in ATWS considerations.

THE STABILITY PREDICTION MODEL

The BISON code has a one-dimensional hydrodynamic model for the reactor pressure vessel coolant flow paths, in which the core is represented by a heated channel and a bypass channel. Recirculation pumps are modelled by a homologous model and jet pumps can be represented. A four-equation model of the slip model type is employed, in which the momentum and energy balances are solved for the mixture and the mass balance for vapour and

mixture. Constitutive equations preserving thermal non-equilibrium describe boiling or condensation anywhere in the loop. The steam generation in the core is described by two alternative models, Lellouche-Zolotar's mechanistic model (1) and Solberg's model (2).

The ASEA-ATOM void correlations AA74 and AA78 and Lellouche-Zolotar's void correlation (1) are available for the core. For the other loop parts Bryce and Holmes' correlation modified by ASEA-ATOM (3) is used. The code provides also several choices for the two-phase friction multiplier, the most important being Chisholm's correlation of Baroczy type and ASEA-ATOM's two-phase friction correlation based on FRIGG data. Steam separator pressure loss and steam carry under from the separators can be calculated from special correlations based upon experiments.

The mathematical model forms a set of partial differential equations in one space dimension and time. This system is reduced into a system of ordinary first order differential equations by discretization of the space variable and finite difference approximation of spatial derivatives. The flow loop thus is subdivided into subsections, and a set of first order ordinary differential equations is obtained for the mass of liquid and vapour, internal energy and momentum in these subsections. The momentum balance is space integrated and solved for entire loop sections. Integral momentum balance or subdivided momentum balance can be chosen. The hydrodynamic model can handle reversed flow and counter-current flow.

Time integration is made by a general explicit time integration method in the code, which includes first order (Euler) or second-order (Heun) methods as options. The mass and momentum balance equations may be time integrated by a so called θ -method, which incorporates implicit time integration as a special case. Seeing that the energy equation is integrated by an explicit method, the material transport Courant limit required for numerical stability applies to the time step size, i. e. (time step) $<$ (node mass) / (mass flow rate). The time step length is adjusted within prescribed limits so as to keep the error in each step within specified bounds. The initial state is calculated by iterative solution of the system of equations, which is obtained by setting all time derivatives equal to zero.

The neutron kinetics model is a two-group finite difference diffusion model with space dependence in the axial dimension. Each core subsection in the hydrodynamic model and the top and bottom reflector are discretized into a user-specified number of mesh intervals. The time integration of the fluxes is made by a θ -method or a prompt jump approximation method. Up to six groups of delayed neutrons may be represented. The neutron kinetic properties are calculated directly from cross section data specified as polynomials in the density and temperatures of moderator and fuel. These data can be given on a disc file from which data sets can be selected to describe the axial variation of the properties. The properties of several fuel types can be weighted arithmetically. The axial burnup distribution may be determined by a search procedure in the code for a specified axial power shape and k_{eff} -value and a given control rod distribution. Similarly the control rod distribution can be searched to give a target power shape and k_{eff} -value for a given distribution of neutron kinetic properties. These options are valuable for the code user, since the axial power shape is very important in stability analysis as well as transient analysis in general. Manual trial-and-error search for desired axial profiles tends to be tedious and time-consuming.

Fission power is calculated as prompt power, proportional to the fission rate and delayed power, released at the radioactive decay of fission products. A fraction of the fission power is generated directly in the core and bypass channels. Bypass void reactivity may be accounted for at user's option. Control rod movements specified by the user or calculated by the hydraulic scram system model are taken into account.

The void coefficient predicted by a given set of neutronics data may be adjusted by means of a user-specified void factor, which does not affect the steady state solution. This extends the range of applicability of a neutron cross section data set, and is very useful, since a complete data set covering equilibrium core conditions is quite expensive and rather time-consuming to produce. Similarly a doppler factor can be used to modify the doppler reactivity coefficient.

The fuel thermodynamics model represents the average pin, and applies a finite difference solution of the time dependent radial heat conduction in the fuel, gasgap and cladding. The gasgap heat transfer coefficient may be supplied as a function of pellet temperature or calculated by use of two alternative models, based on the solid pellet and the cracked pellet concepts, respectively. The second model has a small radial gap with a rather large heat transfer coefficient, but the pellet heat conductivity is deteriorated by a crack pattern containing fission gas. The heat transfer from the cladding to the coolant is described by flow regime dependent heat transfer correlations.

The steady state solution for the coupled hydrodynamic, neutronic and fuel temperature models is obtained by power-void iterations, after which the initial state is calculated for the external system models. The steam lines model calculates the mass flow and pressure in a multinode model assuming isentropic behaviour of the steam. Time integration is made by the θ -method. Relief and safety valves can be located in the steam line and the turbine valves and dump valves can be connected to it. The balance-of-plant models include all the systems that are required for the analysis of the time-dependent behaviour of a BWR power station. They embody the trip and interlock system, process monitoring systems, scram system, pressure, water level and power control systems, turbine and generator, condensate and feedwater systems and relief and safety valves.

The decay ratio predicted by the code is to some extent time step dependent and also affected by the spatial discretization. This is an inherent feature of a discretized model employing low order integration schemes, as the decay ratio error depends on the truncation error. The first order Euler's method gives an almost linear overprediction of the decay ratio with the time step size, whereas the second order Heun's method makes a rather small overprediction, quadratically dependent on the time step size. Furthermore method studies on one-component second order systems as a part of the code development work show that a first order implicit method underpredicts decay ratios, with a linear dependence on the time step size. A θ -method time integration scheme predicts a rather time step independent decay ratio for $\theta = 0.5$ according to these method studies, and so does also Heun's method. The truncation error affects stability predictions but not transient analysis. Although slightly inconvenient this time step effect does not present any serious problems once the code user is made aware of it and corrects for it, as has been done in the calculations presented in this report. The error is practically negligible for Heun's method but nevertheless use of Euler's method appears suitable with corrections based on sensitivity studies using different time steps.

The code can be used to analyse hydrodynamic and nuclear-coupled stability, all kinds of non-LOCA events, and the initial phase of LOCA events. Channel stability and the transient behaviour of individual channels can be analyzed by a slave channel version of BISON using time-dependent boundary conditions from the complete BISON. Besides that the loop independent core stability option in the complete BISON can be selected to analyse core stability.

VALIDATION OF THE STABILITY PREDICTION MODEL

The code validation plan includes the following stability tests:

1. Peach Bottom-2 end-of-cycle 2 stability tests (4)
2. Peach Bottom-2 cycle 3 stability tests (5)
3. TVO I 1978 stability tests
4. Forsmark 1 1980 stability tests
5. FRIGG loop hydrodynamic stability tests.

This paper discusses the code validation against the tests in Peach Bottom-2 at end-of-cycle 2 and in TVO I.

Nuclear coupled oscillations mechanism

As a background for discussions below the basic mechanisms behind reactivity coupled thermal-hydraulic flow and power oscillations in a BWR are briefly described. This is done by

reference to the phase relationships between crucial process variables in a BISON case with limit cycle oscillations. The core outlet flow oscillation lags 90° behind the inlet flow in this case, and the core average density lags 90° behind the inlet flow, as expected from a mass balance consideration. Core power oscillates in phase with the core density reactivity, and changes the core heat flux to the coolant, attenuated and phase retarded about 90° by the fuel time constant. In phase with the heat flux is the evaporation it generates, and lagging 90° behind it the time integral of this evaporation, corresponding to a void variation, which is in phase with the void variation generated by the opposite phases of the inlet and outlet flows. This forms a feedback loop with a 180° phase shift and a gain dependent on the reactivity coefficient, the delayed neutron fraction, the fuel time constant, the flow rate, the steam velocity, the power level and power distribution. The flow oscillations are sustained, since the dominating single-phase and two-phase pressure losses are at opposite phases, with the phase of the core density head in between and opposite to the temporal acceleration pressure losses of the oscillating flows. The high steam velocity in the riser and steam separators attenuates the density head variation above the core and gives a small phase lag between core two-phase pressure losses and the steam separator pressure losses. Furthermore the normalized power distribution fluctuates at opposite phase with the void distribution variation, the relative power at the top and bottom of the core being 180° apart. However, in absolute terms the power at the core outlet lags only about 90° behind the inlet power, since the normalized variation is superimposed by the global variation.

Peach Bottom-2 stability tests

Peach Bottom-2 is a BWR/4 product line reactor of GE design, having a rated thermal power of 3293 MW and a rated flow of 12 915 kg/s driven by jet pumps. The fuel inventory of the 764 assembly core was 576 7x7-type assemblies of the initial load and 188 8x8-type reload assemblies during cycle 2. A number of 404 initial load assemblies remained in the core during cycle 3. All fuel assemblies contained burnable absorber rods. The stability tests were conducted as a series of small pressure perturbation tests composed of pseudo-random binary switching (PRBS) of small step (about 0.5 bar) inputs to the pressure regulator set point (4). Decay ratio and natural frequency at the test points were estimated by least square fits of transfer function models to the transfer functions from the core pressure to fission power, which were estimated from the recorded data using Fast Fourier Transform.

The coolant loop model was based upon data in reference 6 and some additional information supplied by EPRI. Bypass boiling was predicted by the code in all the four tests for the flow fractions given in reference 6. The core exposure distribution, calculated for incore fuel management purposes, was also supplied by EPRI. The neutron cross section data versus burnup were calculated by the ASEA-ATOM cell code PHOENIX for four fuel types. The corresponding cross section polynomial sets were derived for each fuel type, exposure void and burnup level, and stored on a disc file. This file was used to prepare additional coefficient sets by interpolation with respect to burnup so as to get data for the average burnup of each fuel type in each axial subsection in the core. The fuel type data were weighted arithmetically to obtain the average neutron cross section data in each subsection to be stored on a temporary disc file for the current case. Delayed neutron data, inverse velocities and bypass void reactivity data were also obtained from the PHOENIX calculations. Fuel gasgap heat transfer data, which are rather important for stability predictions, were calculated by ASEA-ATOM's code STAV4 for 7x7 and 8x8 fuel for the solid pellet concept and STAV5 for the cracked pellet concept.

The steam dome pressure was given as a boundary condition, and a perturbation was prescribed as a triangular pressure pulse, generating a damped nearly sinusoidal oscillation in the state variables. The decay ratio of the response of a process variable described by the time function $f(t)$ was defined as $(f(t+T) - \langle f \rangle) / (f(t) - \langle f \rangle)$, where t corresponds to maxima or minima, $\langle f \rangle$ is the equilibrium value and T is the period. In general the decay ratio was not quite constant for consecutive periods, and suitable averaging had to be made. The perturbation and evaluation method is consistent with the experimental stability data, which are based upon transfer functions from core pressure to average neutron flux signal.

Results of the code validation analysis versus Peach Bottom-2 EOC2 tests are given in table 1 for the cracked pellet fuel model and Lellouche-Zolotar's void model. Similar results were obtained for the solid pellet model, whereas AA74 void correlation gave higher decay ratios. Experimental data in the A columns are given in reference 6, and those in the B columns were evaluated by an ASEA-ATOM method (7) referred to previously.

Table 1. Measured and calculated stability data for Peach Bottom-2 EOC2 tests

Test-point	Flow %	Power %	Experimental Results				Theoretical Results	
			Decay ratio		Natural frequency (Hz)		Decay ratio	Natural frequency (Hz)
			A	B	A	B		
PT1	52.3	60.6	0.26	--	0.45	--	0.19	0.44
PT2	43.8	51.7	0.30	0.23	0.45	0.46	0.21	0.40
PT3	40.4	59.2	0.33	0.35	0.43	0.41	0.36	0.41
PT4	40.3	43.5	0.27	0.24	0.39	0.37	0.25	0.37

Unfortunately the transfer functions are not sufficiently accurate for an evaluation using the ASEA-ATOM method at and above the resonance frequency for PT1 and PT2, the recording interval, which was doubled in PT3 and PT4, being too short. Thus no data could be evaluated for PT1, and for PT2 rather uncertain figures could be obtained only with difficulty. For PT3 and PT4, however, the two methods for the experimental results in columns A and B agree reasonably well, the differences indicating the range of uncertainty. With these circumstances in view credit should be given to the good agreement between experimental and calculated results for PT3 and PT4, and less attention be paid to the deviations for the two other test points, PT2 in particular. Extensive sensitivity analyses have been made, showing among other things that deviations may also be caused by errors in power and flow.

TVO I stability tests

TVO I & II in Finland and Forsmark 1 & 2 in Sweden are internal pump BWRs of ASEA-ATOM's design. Rated thermal power is 2000 MW for TVO and 2700 MW for Forsmark. The fuel assemblies are of the standard ASEA-ATOM 8x8 design. Stability tests using the normal instrumentation including a transient data acquisition system were integrated with normal startup testing. The reactor stability was evaluated by Fourier inversion of the transfer function from reactor pressure to average neutron flux, determined by use of sinusoidal perturbation of the turbine admission valve positions. Inherent process noise in 18 process variables was also recorded, and the APRM signal was used for an alternative determination of stability characteristics (7). These tests at minimum pump speed and natural circulation continued a stability test program that had started by tests in Barsebäck (8).

The TVO I stability tests were conducted on 17-18 October 1978 preceded by a nine hour hot standby following commissioning tests at 0-20 % power. After start at 1.45 pm on October 17 equilibrium conditions were established at 5.45 pm for test point 1 at minimum pump speed and 28 % power. A 12 minute noise recording was followed by a pressure perturbation test lasting from 6.45 until 8.15 pm, while recordings were made successively for 13 perturbation signals in the frequency range 0.012-1.5 Hz.

Thereafter the six internal pumps were tripped one by one, and the plant operation was continued at natural circulation with stationary pump wheels. Noise recordings were taken at test point 2 at 23 % power, and control rod withdrawal commenced at 9.45 pm. Temporarily

halted by a turbine trip at 9.57 pm, during which the full steam load capacity condenser served as heat sink, the power ascension was resumed at 1.21 am on October 18, when the the generator was brought back on the grid. Documented by use of plant process computer loggings at 10 minute intervals, the power raise was carried on, until limit cycle oscillations were observed at 4.30 am in core flow and power signals at 50 % power. Noise recordings were made at this point, test point 3. Subsequently Xenon build-up caused a power redistribution and a drop to 48 %, test point 4, where a pressure perturbation test was made during 8.00-9.30 am, followed by a 12 minute noise recording.

Pump restart began at 10.00 am, and noise recordings were made at test point 5 at 63 % power with four pumps operating at minimum speed. Before the remaining two pumps were started, control rods were inserted to compensate for the steep flow control line between test points 4 and 5, the steepness bearing evidence of bypass channel boiling. All six pumps operating at minimum speed, test point 6 at 62 % power was established at 12.00 am after some further control rod insertion. Noise recordings followed by a pressure perturbation test during 0.30-1.30 pm concluded the test program.

Using the recorded process variables and six computer loggings Mr Stig Andersson (8, similar TVO II tests), identified a higher core state oscillation mode at limit cycle conditions in test point 3. Thus the oscillation pattern of the core flow and power evidently had been azimuthal, dividing the core along a diagonal, which shifted as a function of time , the flow and power being at opposite phases in the core halves. Furthermore the dividing diagonal at a given axial plane shifted azimuthally about 180° from inlet to outlet at a given time. Accordingly the inlet and outlet flows to any arbitrary core half were at opposite phases, and the power at the top lagged about 180° behind the power at the bottom. The data analysis confirmed that the channel flows had been within permissible ranges, as could be deduced from the eight core channel inlet differential pressure cell signals, which form the flow monitoring system together with hard-wired square-rooting, summation and averaging circuits.

In contrast to later tests the eight individual channel flow signals were not registered. Nevertheless it can be concluded that a large scattering in the channel flow amplitudes occurred in test point 4. This conclusion is based upon the behaviour of the transfer function G_{wd} , from the above mentioned hard-wired flow signal to the pressure difference over the internal pumps, and the transfer function G_{pw} , from the steam dome pressure signal to the flow signal. At the core resonance frequency the gain of G_{wd} drops to about 20 % of its off-resonance value for test point 4, while on the contrary the gain of G_{pw} increases drastically. Absolute amplitudes are also affected, since the steam dome pressure amplitude is relatively constant. For test point 6 there is a small, hardly significant dip at core resonance, and at other test points in this test sequence and at other occasions no such dip can be discovered. To judge from the phase at core resonance of relevant transfer functions there is no reason to suspect transmitter dynamic effects in G_{wd} . Therefore differences in channel or zone flow amplitude and phase in test point 4 is the logical explanation, bearing in mind the variation of channel power level and axial distribution, the radial orificing distribution, and the fact that the peripheral channels are not represented in the flow signal.

The calculations show that the core and bypass channel flows are in phase with each other, and that the bypass flow amplitude is about 10 %, nearly the same as in the hard-wired flow signal. As the eight channel flow devices are evenly distributed in the central orificing zone of the core, they should give a good measure at least of the average zone flow variation, but they are few enough to overemphasize individual channel flow variations. Obviously the relative flow signal amplitude is much greater than the pump flow amplitude, the true magnitude of which is revealed by the pump pressure difference signal. Accordingly the flow signal in test point 4 has to be dominated by channel flow signals, the amplitude of which is greater than the average relative core flow amplitude. As a hypothesis it is therefore suggested that the flow amplitude increases in the channels or zones which are closest to their natural frequency. The downcomer flow, restricted by static and dynamic pump head losses, which are considerable for higher power levels at natural circulation with stationary or windmilling pumps in the main flow path, is diverted to the resonance channels, reducing and in some cases even reversing the flow variation in the other channels. This conclusion about unequal channel flow amplitudes is supported by the test recordings in the natural circulation

tests in TVO II (8), where the large number of recorded signals - 70 - included the eight channel flow signals and 38 neutron detector signals. The standard deviation of the eight flow signals varied from 1 % to 12 % at limit cycle, in which no higher instability mode developed. Flow signal spectral densities showed two pronounced peaks, one at the global core resonance frequency, 0.34 Hz, and the other one in the range 0.26 - 0.31 Hz. Plots of oscillations in local fluxes and channel flows showed beats, indicating that they were produced by superposition of two oscillations with frequencies close to each other. Minimum flow amplitude in a rather peripheral channel nearly coincided with maximum amplitude in a central channel.

The fact that the downcomer flow amplitude may be highly unevenly distributed to the core channels complicates the task of predicting the stability using a model with one or a few core channels at such operating points where the stability of the fundamental mode oscillations is highly dependent on the downcomer flow restrictions, as will be seen below.

Results for test point 6 at 62 % power and minimum recirculation pump speed are shown in table 2 for the cracked pellet fuel model (A) and the solid pellet model (B). The difference between the fuel model options is greater than in the Peach Bottom-2 calculations for nearly equilibrium core burnup conditions. The measured transfer function G_{pq} from pressure to average neutron flux indicates an overtone at 0.8 Hz, and a tendency to a secondary resonance peak at the possible ground tone 0.4 Hz, the frequency predicted by the cracked pellet model (A). Since the core resonance frequency, 0.33 Hz, is close to the frequency predicted by the solid pellet model (B), this could be an indication that only a minor part of the fuel pellets have cracked at this early stage. However, a more plausible interpretation will be presented below.

Table 2. Measured and calculated data for TVO I 1978 stability test point 6

Case	Power MW	Flow kg/s	Stability characteristics	
			Decay ratio	Natural frequency (Hz)
Exp. data	1226	2890	0.25	0.33
A	1226	2890	0.26	0.40
B	1226	2890	0.22	0.32

For test point 4 at 48 % power and natural circulation the measured transfer function G_{pq} from pressure to average neutron flux shows an overtone at about 0.67 Hz, roughly twice the core resonance frequency, 0.33 Hz, and an overtone at 1.1 Hz, corresponding to a ground tone of 0.28 Hz, where the transfer function gain curve has a weak tendency to a secondary peak. The observed phase curve appears to be composed of the phase curves of two overlapping resonance peaks. Below 0.2 Hz and above 0.36 Hz the phase curve resembles the phase curve of a rather stable second order system with resonance peak at 0.28 Hz and transition from phase advanced to phase retarded occurring between 0.2 and 0.35 Hz. From the slope of this inferred phase curve at resonance a damping factor of 0.20 and a decay ratio of 0.24 is estimated. In the frequency range 0.3 - 0.4 Hz the phase is dominated by the observed, pronounced peak and its rapid phase transition. From the steep slope of this phase curve at the peak resonance a decay ratio of 0.73 is calculated. A transition between the two phase curves occurs in the frequency range 0.2 - 0.3 Hz. Compared to test point 6 the two overlapping resonance peaks have been shifted towards lower frequency and the higher one now corresponds to the core resonance peak. As observed above, the two resonance frequencies might be the effect of cracked and solid pellets, but more likely the higher frequency corresponds to resonance channels or core sections, which are weakly revealed in test point 6, and the lower one to the fundamental mode, which is suppressed in test point 4.

The results for test point 4 are summarized in table 3. Reversed core bypass channel

flow, leading to boiling and counter-current steam flow, was predicted. As hinted above case 1 underpredicts the decay ratio calculated from measured data for the pronounced resonance peak. The stability data inferred for the secondary peak at 0.28 Hz are, however, well predicted by case 1b, the fundamental mode BISON calculation using the solid pellet fuel model, whereas case 1 with the cracked pellet model, which is used for the cases in table 3 unless otherwise stated, underestimates the period and overestimates the decay ratio.

Table 3. Measured and calculated data for TVO I 1978 test point 4 at natural circulation and 48 % power.

Case	Comment	Power MW	Flow kg/s	Decay ratio	Natural period sec	Case characteristics
Exp.	Test data	960	1845	0.74	3.0	
Exp.	Fundamental mode			0.24	3.6	Inferred fundamental mode data for secondary resonance peak
1		960	1826	0.35	2.60	Dynamic and static downcomer losses equal.
1b		960	1826	0.22	3.35	As 1, but solid pellet model
2	Core stab.	960	1826	0.42	2.45	
3	"-	960	1826	0.47	3.00	Less bottom-peaked power ¹⁾
4	"-	1150	1826	0.54	2.22	Relative power = 1.20
5	"-	1150	1600	0.63	2.34	As 4, but reduced flow
6	"-	1150	1600	0.69	2.90	As 5, but central zone orifice ²⁾ and less bottom-peaked power ¹⁾
7		960	1826	0.49	2.65	Minimum measured dynamic pump loss slope ³⁾
8		960	1826	0.57	2.62	As 7, but central zone orifice
9		960	1826	0.75	3.18	As 8, but less bottom-peaked ¹⁾
10		960	1826	0.75	2.62	Constant pump losses
11		960	1826	0.89	2.62	Constant downcomer restriction losses
12		960	1826	1.05	2.60	As 11, but central zone orifice ²⁾
13		960	1826	0.88	3.12	As 11, but solid pellet model
14		960	1826	1.08	3.10	As 12, but solid pellet model

Note 1 The measured bottom-peaked power distribution has a maximum of 2.06 at 12.5 % core height. The profile in this case is adjusted to a peak of 1.45, more representative for an annular core region with high control rod density.

Note 2 Orifice pattern: Central zone 368 channels 60 velocity heads
 Intermediate zone 64 channels 100 "-
 Peripheral zone 68 channels 140 "-

A weighted restriction coefficient is normally used in BISON input.

Note 3 Deduced from the transfer function G_{wd} from measured flow to pump pressure difference, the slope interpreted as a measure of the true dynamic restriction.

Attempts were made to reproduce the stability characteristics corresponding to the observed, pronounced core resonance peak in the following manner. The option for loop

independent core stability analysis was used in cases 2 - 6 to simulate the core, or actually a part thereof, with constant boundary conditions, and the effect of less bottom-peaked power distributions, power level, and flow rate was analysed for this option. For the complete BISON model the dynamic downcomer flow restriction was reduced to the slope deduced from the dip at core resonance frequency in the gain of the transfer function G_{wd} from flow to pump pressure difference in cases 7 - 9, and to zero or near zero values in cases 10 - 14. Noteworthy is that the constant core boundary conditions in case 2 give a higher decay ratio, although the destabilising effect of steam separator pressure losses is not present as in case 1 and 1b. The reduced downward tilt of the power in cases 3, 6 and 9 increases the decay ratio and the period, which otherwise is somewhat underpredicted as in table 2 for the cracked pellet fuel model. However, a further reduction of the downward tilt makes the decay ratio decrease again. Increased power in the core section simulated in case 4 also gives a higher decay ratio and a smaller period, and so does the reduced flow in case 5. Case 6 predicts a central zone decay ratio of 0.69, for a relative power of 1.20, if the measured flow would be overestimated by as much as 15 %.

Since the transfer function G_{wd} actually does not give a true measure of the dynamic flow resistance of the pumps at core resonance, according to the previous discussion, the justification for cases 7 - 9 is questionable, and they are more to be considered as part of the sensitivity studies, with regard to the dynamic single-phase flow restrictions. Case 9, which predicts the measured decay ratio, represents resonance channels located in a less bottom-peaked area of the central zone, whose response is assumed to dominate the entire loop. Contrary to the core stability cases 2-6, this core section interacts with a reduced dynamic flow resistance in the downcomer and a full flow resistance in the steam separators.

In case 10 zero dynamic pump flow restriction is assumed at resonance, and in cases 11 and 13 even the small remaining downcomer restriction pressure loss is assumed constant. Finally cases 12 and 14 show the result when the central orificing zone is chosen as representative for the entire core. The solid pellet model in cases 13 and 14 give a natural period close to the measured value, whereas the cracked pellet model in the corresponding cases 11 and 12 underpredict the period. The decay ratios are equal, in contrast to the fundamental mode cases.

CONCLUDING REMARKS

Satisfactory results were predicted for the forced circulation stability tests in jet pump and internal pump reactors. Further validation analysis of tests with intermediate and high decay ratios is desirable. At natural circulation in internal pump reactors the single core channel model predicts the inferred fundamental mode decay ratio and frequency, but the core resonance does not occur at this mode, which is very stable thanks the large flow restrictions of the stationary or windmilling pumps in the main flow path. Instead the core resonance corresponds to resonance channels or core sections in an oscillation mode, which appears not to be restricted by the downcomer dynamic pressure losses. For jet pump reactors which do not have large downcomer flow restrictions at natural circulation, as shown by their higher flow rate at natural circulation, the core resonance can be expected to occur at the fundamental mode resonance at least below the limit cycle threshold.

The merits of the idea of using zero or low dynamic flow resistance in the downcomer for the predictions of the limit cycle threshold at natural circulation are doubtful, in particular due to the inconsistent assumption that the steam separator dynamic pressure loss is not influenced. To a certain extent this assumption may be justified by the fact that the density head variation in the resonance channels generates a power variation of a more global nature and causes steam flow variations at the outlet of other channels, creating a global two-phase flow variation through the steam separators at opposite phase with the resonance channels inlet flows. The drawback is that this method always will predict a higher decay ratio than the fundamental mode. Even if the limit cycle threshold would be predicted, the decay ratio would be overpredicted for operating states not too far from instability. For the code to be used as an independent prediction tool, it should rather not depend on measured data, which are likely to be plant and operating state specific. Therefore this concept would be truly useful if the zero dynamic flow resistance assumption would turn out to be adequate, but the problem of

deciding when to use this approach would remain. Based on an assumption of loose neutronic coupling between oscillating core sections, the core stability option with constant boundary conditions has some potential to predict the instability mode corresponding to the core resonance peak at natural circulation in internal pump reactors, predicting a higher decay ratio than the fundamental mode, when the latter is stable thanks to downcomer flow restrictions. Further studies with increased radial buckling and control rod density and actual power profiles may improve the agreement with experimental data. Some interaction with the steam separators is, however, bound to be caused by the large global power variation superposed to the fundamental mode. In the end, therefore, brute force in the form of a three-dimensional multi-channel model such as ASEA-ATOM's code ANDYCAP may be required.

At limit cycle conditions the large dynamic pump restriction loss presumably is instrumental for the development of the higher instability mode observed in test point 3. The reason for the absence of a higher instability mode of the same kind at limit cycle in TVO II may be the two windmilling pumps, the higher flow rate, the less bottom-peaked power profile, and/or the different radial control rod distribution, especially since all these factors probably affect the degree of suppression of the fundamental mode. To judge from the predicted natural frequency the solid pellet concept is valid for the fresh core in the TVO I tests. The degree of pellet cracking during fuel exposure might therefore be inferred from the resonance frequency determined from noise recordings.

ACKNOWLEDGEMENT

The work on the development and validation of the stability prediction model is partially funded by Electric Power Research Institute, Palo Alto, USA, under project RP 1384-1. The support from EPRI by Dr Robert N. Whitesel, Dr Gerald S. Lellouche and Dr Patrick G. Bailey is gratefully acknowledged. The author wishes also to thank fellow ASEA-ATOM employees Mr Stig Andersson and Dr Jan H. Blomstrand for use of valuable results - mainly unpublished - of work on boiling water reactor stability of theoretical and experimental nature, Mr Henrik Nerman for fuel model information, and Dr Dusan Babala for method discussions.

REFERENCES

1. G S Lellouche, B S Zolotar, "Mechanistic Model for Predicting Two-Phase Void Fraction for Water in Vertical Tubes, Channels, and Rod Bundles". EPRI NP-2246-SR (Febr 1982).
2. P Bakstad, K O Solberg, "A Model for the Dynamics of Nuclear Reactors with Boiling Coolant with a New Approach to the Vapour Generating Process", Kjeller Report KR-121, IFA, Kjeller, Norway (1967)
3. W M Bryce, "A New G-dependent Slip Correlation which gives Hyperbolic Steam-Water Mixture Flow Equation", AEEW-R1099 (1977).
4. L A Carmichael, R O Niemi, "Transient and Stability Tests at Peach Bottom Atomic Power Station Unit 2 at End of Cycle 2", EPRI NP-564 (June 1978)
5. F B Woffinden, R O Niemi, "Low Flow Stability Tests at Peach Bottom Atomic Power Station Unit 2 Cycle 3", EPRI NP-972 (April 1981)
6. N H Larsen, "Core Design and Operating Data for Cycles 1 and 2 of Peach Bottom-1", EPRI NP-563 (June 1978)
7. Jan H Blomstrand and Sven-Åke Andersson, ASEA-ATOM, "BWR Core Response to Fluctuations in Coolant Flow and Pressure with Implications on Noise Diagnosis and Stability Monitoring", Topical Meeting on Advances in Reactor Physics and Core Thermal Hydraulics, Kiamesha Lake, NY, September 22-24, 1982, NUREG CP-0034 vol 1, pp 220-235.
8. Yngve S Waaranperä, Stig Andersson, ASEA-ATOM, "BWR Stability Testing: Reaching the Limit Cycle Threshold at Natural Circulation", Trans. ANS, 39, 868(1981)

A COMPARISON OF RELAP5/MOD1.6, TRAC-BD1/VERSION 12,
AND TRAC-BD1/MOD1 ASSESSMENTS WITH DATA FROM A
ROSA III SMALL BREAK TEST

K. C. Wagner and R. J. Dallman

EG&G Idaho, Inc.
Idaho Falls, Idaho 83415, U.S.A.

ABSTRACT

A comparative analysis of three assessment studies of Run 912 from the ROSA-III small break LOCA test series has been performed. Two of the studies were done using the TRAC-BD1 computer code, while the RELAP5 code was used for the third study. The studies are part of INELs support to the United States Nuclear Regulatory Commission for the independent assessment of reactor safety codes. The ability of each computer code to calculate pertinent thermal-hydraulic phenomena in the experiment is presented. The run time assessment statistics are also presented.

INTRODUCTION

A comparison of three assessment studies of the Rig of Safety Assessment (ROSA)-III, Run 912 is made. In each study, an advanced, best estimate, reactor safety code was used to calculate the transient. Two of the studies used the TRAC-BD1 computer code [1,2], while the RELAP5 code [3] was used for the third study. They were performed at the Idaho National Engineering Laboratory (INEL) in support of the United States Nuclear Regulatory Commission (USNRC) for the independent assessment of reactor safety codes. The object of this paper is to compare the ability of each code to predict the pertinent thermal-hydraulic phenomena measured in the experiment, discuss the improvements from the earlier version of TRAC-BD1 to the more recent version, and compare the run time statistics of each code.

FACILITY AND TEST DESCRIPTION

The ROSA-III facility was a well instrumented, volumetrically scaled (1/424) BWR system with an electrically heated core [4]. There were four half-length power bundles in the core. One bundle simulated a high power channel while the other three bundles simulated average power channels. Each bundle contained 62 heated rods and 2 water rods in an 8 x 8 array.

There were two recirculation loops attached to the pressure vessel. Each loop had two jet pumps and one recirculation pump. A prototypical BWR has the jet pumps inside the pressure vessel in the downcomer region. However, the ROSA-III jet pumps were placed external to the vessel due to modeling constraints imposed in scaling the downcomer flow area. The break location was in the recirculation loop and just upstream of the recirculation pump.

The ROSA-III facility has a prototypical BWR Emergency Core Cooling System (ECCS) which includes a High Pressure Core Spray (HPCS), a Low Pressure Core Spray (LPCS), and a Low Pressure Coolant Injection (LPCI).

The main steam line at the top of the vessel serves three functions. First, it simulates the resistance of a steam turbine during steady state operations. Secondly, it acts as a Safety Relief Valve (SRV) during transient situations to maintain the vessel pressure below 8.47 MPa. Finally, it acts as an Automatic Depressurization System (ADS) during a Loss of Coolant Accident (LOCA) to reduce the system pressure.

Run 912 simulated a 5% break of the recirculation pump suction piping [5]. The transient was initiated when the break valve was opened. The pump power was turned off and the core power was controlled to simulate a prototypical BWR power decay. The system pressure decreased until 24 s when the Main Steam Isolation Valve (MSIV) was closed. Following MSIV closure, the system pressure rapidly increased until the SRV was manually operated to keep the system pressure below 8.47 MPa. The ADS valve opened at 158 s and caused a rapid depressurization. The heater rods began to heatup from 206 s to 261 s. The LPCS and LPCI were initiated at 318 s and 406 s, respectively. All heater rods were quenched between 328 s and 433 s. The peak cladding temperature of 839 K occurred at 410 s at the midplane of the high power rod.

COMPUTER CODE AND MODEL DESCRIPTIONS

This paper compares assessment studies using three different computer codes. Two studies were performed using different versions of the TRAC-BD1 code [6] and one study used the RELAP5 code [7]. A description of the computer code and the computer models is given below.

The two versions of the TRAC-BD1 computer code were written specifically to examine various transients in a BWR. TRAC-BD1/Version 12 was released in late 1981 and represents the oldest code in this comparison. Conversely, TRAC-BD1/MOD1 was released in June 1984 and represents the state-of-art BWR transient code at the INEL. Both TRAC-BD1 codes feature a full nonhomogeneous, nonequilibrium two fluid thermal-hydraulic model in all portions of a BWR system and multi-dimensional treatment of a BWR vessel. The major improvements of the code from TRAC-BD1/Version 12 to TRAC-BD1/MOD1 that would influence the present calculation include: a comprehensive control system model; a two phase level tracking model; a moving mesh quench front tracking model for the fuel rods and both sides of the channel wall; and improved constitutive relations for heat, mass, and momentum transfer between the fluid phases and the structure surface [1,2].

The TRAC-BD1/Version 12 vessel nodalization is shown in Figure 1. The two dimensional vessel model featured twelve axial levels and three radial rings. No azimuthal dependency was simulated in the vessel. The two inner rings between levels four and seven represented the high and average power channel and bypass regions. The annular downcomer was modeled in the outer ring. The guide tubes and the channels were modeled internally in the vessel by using one dimensional components and source connections to the vessel.

The advent of the level tracking model in TRAC-BD1/MOD1 permitted a coarser vessel nodalization than the Version 12 model. In the new model, to reduce costs, levels two and three, six and seven, and nine and ten were combined to reduce the number of axial levels from twelve to nine. Use of the level tracking model in the downcomer region of the vessel permitted the axial location of the one dimensional components to be specified independent of the cell location. In the newer model, the liquid level was tracked in a continuous manner throughout the downcomer region. Hence, the correct void fraction (above or below the liquid level) was always donored to the vessel source connections.

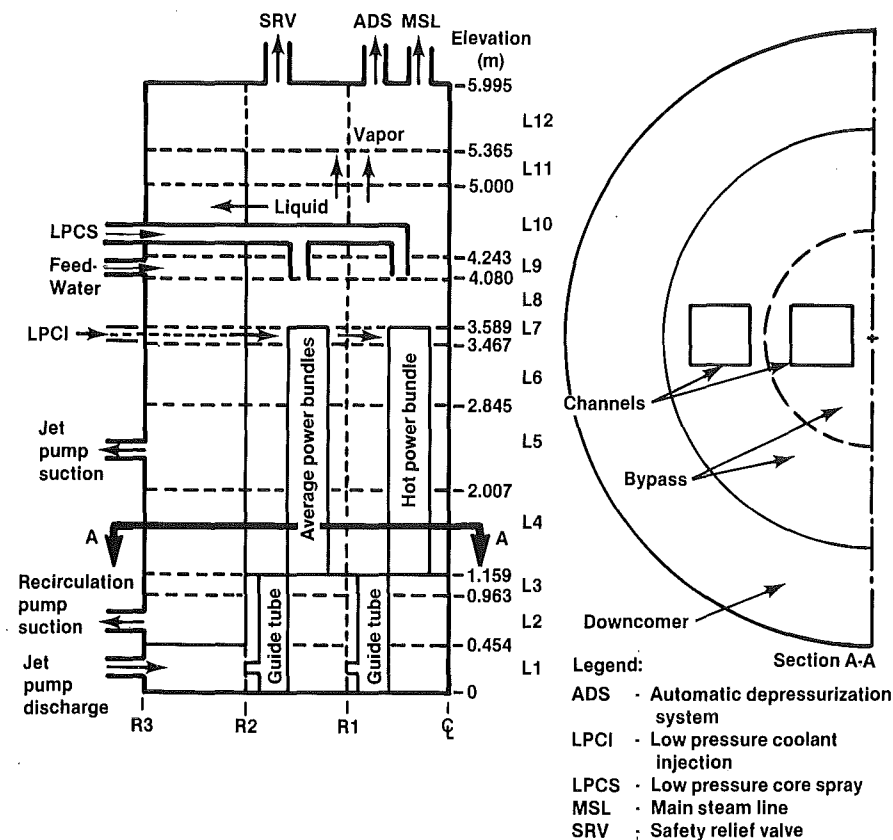
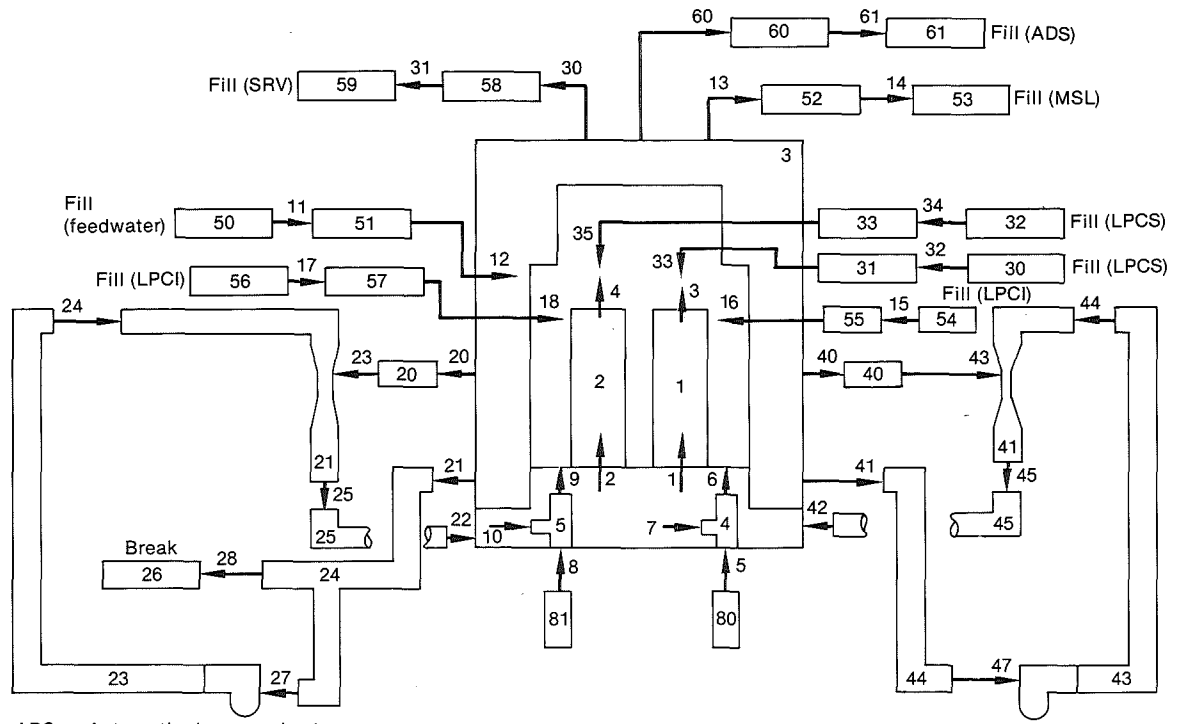


Figure 1. TRAC-BD1 vessel nodalization of ROSA-III.

The core regions in the TRAC-BD1 models were simulated using the CHAN component. A CHAN component in ring 1 of the vessel simulated the high powered bundle, while another CHAN in ring 2 modeled three average power bundles. In the TRAC-BD1/Version 12 model, four rod groups were used in the CHAN component of the high power rod. Three groups corresponded to the three radial peaking factors while one group corresponded to the two water rods. The average power channel used two groups. One group simulated all the heated rods while the other group modeled the two water rods. The advantage of using several rod groups in the CHAN component is for radiation calculations at elevated temperatures. After examining the results from the Version 12 calculation, it was determined that radiative heat transfer in the bundle was not a dominant heat transfer mode. Therefore, it was decided to only use one rod group per channel in the MOD1 model.

The TRAC-BD1 system nodalization is shown in Figure 2. Both the intact and broken loops were modeled. One JET PUMP component was used in each loop to



ADS - Automatic depressurization system
 LPCI - Low pressure coolant injection
 LPCS - Low pressure core spray
 MSL - Main steam line
 SRV - Safety relief valve

Notes:
 1 Junction 1
 1 Component 1

INEL 3 3561

Figure 2. TRAC-BD1 system nodalization of ROSA-III.

model the two jet pumps in the facility. The small break was modeled at junction 26. The LPCS and LPCI were connected to both ring 1 and 2 to assure uniform mixing. Flow versus pressure tables from the test data were input as boundary conditions for the ECCS flows. The LPCI and LPCS components were activated when the calculated system pressure was below 2.38 and 1.81 MPa, respectively.

Ambient heat loss from the facility was also modeled. No experimental data was available for the ROSA-III heat loss distribution. However, the total heat loss was measured to be roughly 150 kW. The Version 12 model used a 50 kW heat loss from the vessel and 50 kW from each of the two recirculation loops. The Version 12 results indicated the vessel heat loss distribution should have been increased. Therefore, a higher heat loss from the vessel (75 kW from the vessel and 38 kW from each of the two loops) was used in the MOD1 model to achieve better agreement with the data.

Several other boundary conditions were put into the model. A flow versus time table derived from the experimental data was used for the main steam line (MSL) and feed water flows. A rotational speed versus time table for the two recirculation pumps was used after the pump power termination. Pressure versus flow tables were used for the SRV and ADS flows. The SRV was activated only when the system pressure was greater than 8.40 MPa. The ADS was activated 120 s after the downcomer level reached 4.25 m.

The RELAP5/MOD1.6 computer code was used in the third study [3]. RELAP5/MOD1.6 was an intermediate version of RELAP5, satisfying internal modeling requirements at the INEL until RELAP5/MOD2 [8] was completed. It contained many of the same models found in RELAP5/MOD2. RELAP5/MOD1.6 did not have multi-dimensional capability, hence, a one dimensional solution was used throughout the model. The code was released at the INEL in early 1983.

The RELAP5 model nodalization was similar to the TRAC-BD1 models except for a one dimensional pressure vessel. Similarly, the core was divided into two channels. The heater rods were modeled in groups similar to the TRAC-BD1/Version 12 model. The water rods were not modeled. The guide tubes and the bypass regions were also modeled using PIPE components. A RELAP5 SEPARATOR component was used to simulate the ROSA-III steam separator. Heat structures were used to model the ambient heat loss from the vessel and the recirculation loops. A 150 kW steady state ambient heat loss was calculated from the system. The RELAP5 heat loss distribution was similar to the TRAC-BD1/Version 12 model, 50 kW from the vessel and 50 kW from each loop.

The RELAP5 recirculation loops, ECCS, and MSL nodalization were similar to the TRAC-BD1 models. The same boundary conditions used in the TRAC-BD1 models were used in the RELAP5 model.

RESULTS

This section compares the results from three assessment studies with the measured data. An uncertainty analysis was not performed on the data, hence, most of the measured results are presented without an uncertainty range. Although no uncertainties were given for the heater rod temperatures, the data were processed by elevation and linear heat rate (high or low power channel) to determine the minimum and maximum data. Both curves are presented with the calculated results to illustrate the range of data.

Several comparisons are presented in order to judge the ability of the codes to predict the pertinent thermal hydraulic phenomena during the experiment. The system pressure and heater rod response were determined to be important parameters that characterize a small break simulation. These parameters are directly influenced by an accurate calculation of the steam line flow, break flow, and regional mass distribution. To facilitate the discussion of the code and data comparisons, the calculated results from the three analyses will be referred to as V12 for the TRAC-BD1/Version 12 analysis, MOD1 for TRAC-BD1/MOD1 analysis, and RELAP5 for RELAP5/MOD1.6 analysis.

Figure 3 compares the calculated and measured steam dome pressures. The pressure remained fairly constant at the initiation of the transient until the core power decay began at 8.8 s. Subsequently, the pressure decreased until the MSIV closure at 24 s and then rapidly repressurized to the SRV set point (8.40 MPa). The experimental and V12 results showed a slight depressurization after 100 s until the ADS was actuated at 158 s (164 s in V12). The RELAP5 and MOD1 results remained near the SRV set point until the ADS valve was opened. The calculated break flow for these two calculations was lower than the measured break flow and V12, which appeared to contribute to the calculated pressure hold up.

After ADS actuation, there was a rapid depressurization until 318 s when the feedwater line flashed and LPCS liquid fell into the core and vaporized. The measured depressurization was greatly reduced after the initiation of the LPCS, thus LPCI was delayed until 406 s when the system pressure reached 1.81 MPa. In each of the calculations, the ECCS was also initiated by a system pressure trip. Consequently, variations in the calculated depressurization rate from the measured value caused variances in the initiation of the LPCS and the LPCI. The RELAP5 results showed an over calculation of the depressurization rate and no influence of the feedwater flashing or the LPCS initiation. Excessive condensation in the RELAP5 upper plenum after LPCS initiation caused the calculated depressurization to be too high. Consequently, the RELAP5 LPCI initiation was 80 s premature. The V12 calculated depressurization rate agreed with the data until 318 s. There was feedwater flashing in the V12 results but the LPCS fluid was held up in the upper plenum by high steam velocities at the core exit. As a result, the V12 LPCI initiation was also earlier than measured. The MOD1 depressurization rate matched the measured value and had the best agreement with the data after 318 s. Several improvements in the MOD1 interfacial drag package permitted the LPCS liquid to drain into the core after LPCS initiation and improved the agreement with the data. The MOD1 results were above the data at the beginning of the ADS blowdown due to an over calculated initial pressure and a slight delay in the actuation of the ADS (158 s in the experiment versus 165 s in MOD1).

The break mass flow is compared in Figure 4. The measured break flow had a long subcooled blowdown until the ADS valve opened and the flow transitioned to saturated flow. The MOD1 and RELAP5 results also show the transition to saturated flow after ADS actuation. The V12 break flow went saturated 47 s prior to the measured time. The sharp decrease in the V12 break flow, however, was not reflected in the calculated system pressure response which continued to decrease after the transition. Conversely, the MOD1 and RELAP5 calculated system pressures appeared more sensitive to the break flow. It appeared the MOD1 and RELAP5 break flows were underpredicted during the subcooled portion of the transient and caused the repressurization rate to be too high. It was believed that the V12 subcooled break flow was too high and contributed the slightly premature depressurization at 80 s and the early transition to saturated flow.

Several factors influenced the differences between the MOD1 and V12 break flow calculations. In the V12 simulation, the critical flow model was not used

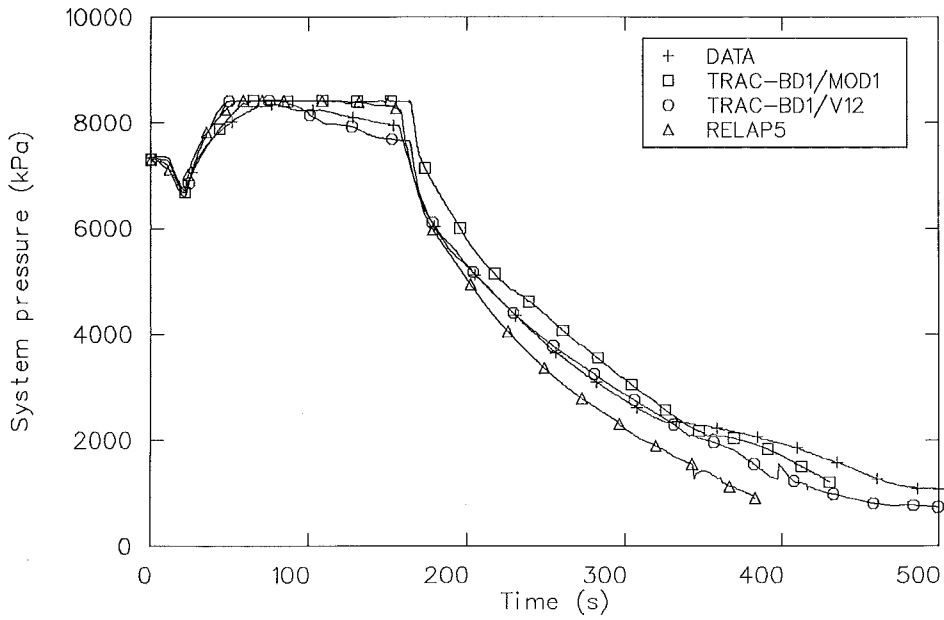


Figure 3. Comparison of measured and calculated steam dome pressures.

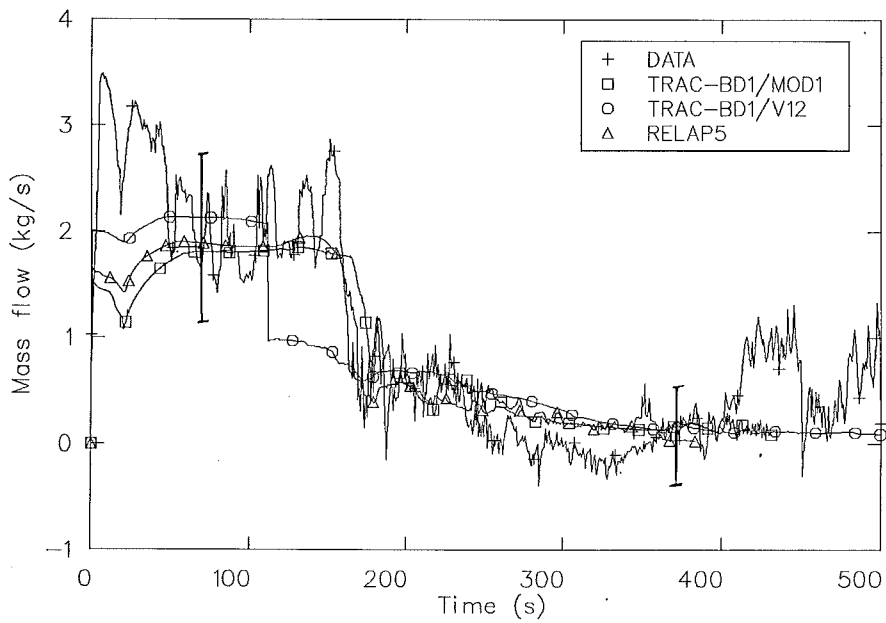


Figure 4. Comparison of measured and calculated break mass flows.

at the break plane because there were severe flow oscillations. Consequently, a characteristic analysis of the break flow was used until 111 s when the flow went saturated. The critical flow model was revised in MOD1 and worked satisfactorily for the entire transient. The MOD1 critical subcooled flow model was extremely sensitive to the amount of liquid subcooling. The MOD1 steady state lower plenum subcooling was approximately 6 K, whereas, the measured value was 11 K. Several attempts were made to lower the amount of liquid subcooling, however the model always converged to approximately 6 K subcooling. A hand calculation using the MOD1 subcooled critical flow equations showed a 15% increase in break flow with 11 K subcooling versus 6 K subcooling. The lower amount of liquid subcooling in the MOD1 model may indicate insufficient ambient heat loss or an incorrect heat loss distribution. The MOD1 model had less heat loss in the loops than the V12 model and that may have contributed to the discrepancy. The total ambient heat loss in the two models was identical. The additional amount of heat loss in the MOD1 vessel did improve the agreement with the measured pressurization rates.

A comparison of the high power channel thermocouple data at the core mid-plane with the calculated surface temperatures is shown in Figure 5. The measured results remained near saturation conditions until 200 s and then departed from nucleate boiling conditions. The measured thermocouples were quenched between 380 s and 440 s after the ECCS fluid entered the core. The RELAP5 and MOD1 results show reasonable agreement with the data whereas the V12 results have three distinct heatups versus one in the data. A discussion of each calculations' heater rod response follows.

The RELAP5 core dried out at a slightly higher rate than was measured and caused a premature heatup. The calculated heatup rate was approximately the

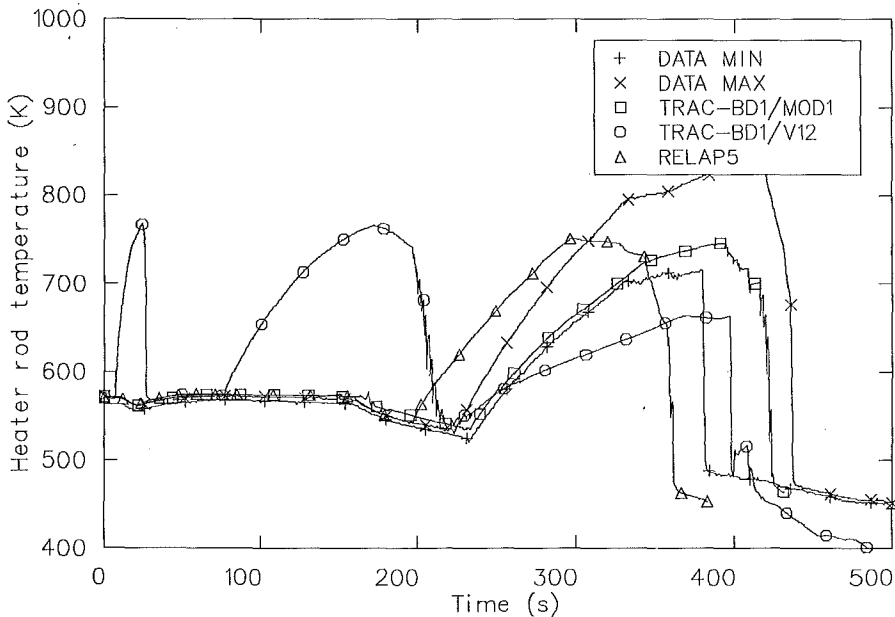


Figure 5. Comparison of measured and calculated high power bundle midplane temperatures.

same as the measured value. The calculated PCT was 751 K at 297 s versus a measured value of 839 K at 410 s. The RELAP5 temperature turned around shortly after the calculated LPCS initiation and rapidly quenched after LPCI started (325 s). The variances in the calculated and measured pressure response directly influenced the premature rod quench and event timing during the reflood portion of the transient.

The V12 results indicated three heatups during the transient. The first departure from saturation conditions was caused by an underprediction of the core inlet flow during the pump coast down. The ROSA-III external jet pumps were rather atypical of a prototypical BWR and were not satisfactorily modeled in V12. During the pump coast down, the total jet pump flow was underpredicted and caused a departure from nucleate boiling in the core. The rods returned to nucleate boiling upon the initiation of the core power decay. The second heatup was caused by restrictive Counter Current Flow Limiting (CCFL) at the core upper tieplate. Liquid was retained in the upper plenum during the V12 calculation whereas liquid was measured to hold up in the upper plenum and subsequently drain back into the core. The V12 heater rods were quenched by flashing of liquid following ADS. The final V12 heatup also was slightly delayed from the data. A reduced calculated heatup rate was attributed to an overprediction of the forced convection heat transfer in the core region. A calculated PCT of 665 K occurred in the final heatup at 397 s. The calculated core quench preceded the experiment because of the premature LPCI initiation.

The MOD1 heater rod response was in excellent agreement with the data. The MOD1 heater rod temperatures and core inventory results represent a significant improvement over the V12 simulation. The improvements in the interfacial drag and heat transfer relationships provided a better simulation of the phenomena in this transient. The jet pump model was improved and no anomalous heatup was calculated early in the transient. A comparison of the behavior at the upper tie plate revealed good agreement between the calculated and measured results. The fine mesh model was used in the MOD1 reflood. As seen in Figure 5, the quench occurred in successive reductions in the heater rod temperature. This corresponded to individual fine mesh nodes quenching as liquid entered into the core. The MOD1 model also adverted a calculated pressure spike observed in V12 (395 s) during the core quench.

CODE RUN TIME STATISTICS

The pertinent run time statistics are given in Table I. An indication of how fast a computer code runs is found by taking the ratio of the Central Processor Unit (CPU) time divided by the calculated transient Real Time (RT). The CPU/RT ranged from 18 in the RELAP5 calculation to 65 in V12. The TRAC-BD1 two dimensional vessel calculations add significantly to the expense of the simulation. The MOD1 calculational cost was greatly reduced from the V12 calculation

TABLE I. SUMMARY OF RUN TIME STATISTICS

Parameter	TRAC-BD1/V12	TRAC-BD1/MOD1	RELAP5/MOD1.6
Transient time (RT)	500	425	387
Number of cells (C)	142	131	140
Number of heated surfaces	201	186	146
Number of time steps (DT)	84116	28546	17138
CPU time (CPU)	32500	14922	6969
CPU/RT	65	35	18

by the economizations in the vessel and ChAN components. The MOD1 and RELAP5 simulations were allowed to run near the calculational Courant limit whereas the V12 simulation was limited to a maximum of 0.01 s time steps.

CONCLUSIONS

The overall trends of the Run 912 transient were well predicted by the three respective codes. Each code did a reasonable job predicting pertinent thermal-hydraulic phenomena and the sequence of events. Many of the deficient areas observed in the V12 simulation were corrected in the MOD1 version. The areas of discrepancy in the MOD1 simulation may be directly attributable to modeling sensitivities rather than to code deficiencies. RELAP5 provided a good simulation of the phenomena in the core, however, the system depressurization after ADS and excessive condensation after LPCS affected the sequence of events. On the other hand, the RELAP5 simulation ran much faster than the TRAC simulations. A significant improvement in the runtime statistics was obtained in the MOD1 simulation from the earlier version.

REFERENCES

1. J. W. Spore et al., TRAC-BD1: An Advanced Best Estimate Computer Code Program for Boiling Water Reactor Loss-of-Coolant Accident Analysis, NUREG/CR-2178, EGG-2109, October, 1981.
2. INEL TRAC-BD1 Development Group, TRAC-BD1/MOD1: An Advanced Best Estimate Computer Code for Boiling Water Reactor Analysis, NUREG/CR-3633, April 1984.
3. V. H. Ransom et al., RELAP5/MOD1.5: Models, Developmental Assessment, and User Information, EGG-NSMD-6035, October, 1982.
4. Yoshinari Anoda et al., ROSA-III System Description for Fuel Assembly No. 4, JAERI-M 9363, February 1981.
5. Yoshinari Anoda et al., Experimental Data of ROSA-III Integral Test Run 912 (5% Split Break Without HPCS Actuation), JAERI Data Report, July 1981.
6. R. J. Dallman, TRAC-BD1 Analysis of a Small Break Test in the ROSA-III Facility, A.S.M.E., 83-WA/HT-17, November 1983.
7. K. C. Wagner, RELAP5 Assessment Using ROSA-III Data, EGG-NTAP-6328, June 1983.
8. INEL RELAP5 Development Group, RELAP5/MOD2 Code Manual, EGG-SAAM-6377, April 1984.

Work supported by the U.S. Nuclear Regulatory Commission, Office of Nuclear Regulatory Research under DOE Contract No. DE-AC07-76ID01570.

ROSA-III LARGE BREAK TEST ANALYSIS BY TRAC-BD1

M. Kato and N. Abe
Nippon Atomic Industry Group Co., Ltd.
System Analysis Department
Kawasaki, Japan

and

H. Aoki
Toshiba Corporation
Nuclear Design Engineering Department
Yokohama, Japan

and

K. Tasaka
Japan Atomic Energy Research Institute
Reactor Safety Laboratory 1
Tokai-mura, Ibaraki-ken, Japan

ABSTRACT

TRAC-BD1 is a best-estimate system code, developed at INEL for BWR LOCA analysis. ROSA-III program at JAERI conducts the LOCA integral system experiment on a BWR. The large break test, Run 926, was analyzed by TRAC-BD1 to assess the predictive capability of the system behavior on a BWR during LOCA. A comparison between calculation and experiment indicated that TRAC-BD1 predicted overall data trends and key phenomena very well. However, the peak cladding temperature was overpredicted. The heat transfer correlations in the code were reviewed. The peak cladding temperature, calculated by the modified heat transfer correlation, was in good agreement with the data.

INTRODUCTION

TRAC-BD1 code [1] is a best estimate system code developed at the Idaho National Engineering Laboratory (INEL) for Boiling Water Reactor (BWR) loss-of-coolant accident (LOCA) analysis. This code features a three dimensional treatment of the BWR pressure vessel and a one dimensional treatment of fuel bundles and pipings. The thermal hydrodynamic model is a nonhomogeneous, nonequilibrium two-fluid formulation for two-phase flow.

The Rig of Safety Assessment (ROSA)-III test program at the Japan Atomic Energy Research Institute (JAERI) conducts the LOCA integral system experiment on a BWR. Run 926, which is a 200 % guillotine break at the inlet side of a recirculation pump with assumption of HPCS failure, was analyzed by TRAC-BD1 to assess the predictive capability of the system behavior for a BWR during LOCA. The results are discussed in this paper.

ROSA-III AND TEST DESCRIPTION

The ROSA-III test program, which has been conducted at JAERI, is a LOCA integral system experiment on a BWR. The test facility is designed to simulate LOCA in BWR/6. The volume of each component is scaled to 1/424. Figures 1 and 2 show the schematic test facility and internal structures in the vessel, respectively. The facility consists of pressure vessel, steam line, feedwater line, recirculation loops and ECCS. The core is simulated by four half length bundles with electric heater rods heated indirectly. Each bundle has 62 heated rods and 2 water rods in an 8 x 8 array. The total maximum heater power is 4.2 Mw. Three of four bundles have the same power, while the other has 1.4 times larger power. Each bundle has radial power distribution. The axial power distribution for each rod is chopped cosine with a peaking factor of 1.4. There are two primary recirculation loops. Each loop has a recirculation pump and two jet pumps, respectively. Jet pumps are located outside of the vessel. The facility has three coolant injection systems as ECCS, namely high pressure core spray (HPCS), lower pressure core spray (LPCS) and lower pressure coolant injection (LPCI) systems. The flow rate for each system is scaled to 1/424 of the actual plant condition.

The break is simulated by two orifices or nozzles, two quick opening valves and one quick shut-off valve, to enable simulating the various break conditions from a small diameter split break to a double ended-break. The discharge flow rates are measured by using 2-beam gamma-densitometers and drag disk upstream from the break locations.

RUN 926 TEST

Run 926 [2] is a 200 % guillotine break at the inlet side of the recirculation pump with assumption of HPCS failure. Breaks are simulated by nozzles. Primary initial conditions were the 7.37 MPa steam dome pressure, 10.0 K lower plenum subcooling, 16.3 kg/s core inlet flow and 3.967 MW total bundle power.

After the break, the feedwater stopped at 4.0 seconds and the steam flow stopped at 5.4 seconds by the level trip signal. LPCS and LPCI initiated at 71.0 seconds and 96.3 seconds, respectively. A 783.5 K peak cladding temperature (PCT) was reached at 118.5 seconds after the break, during a reflood phase. The entire core was completely quenched and cooled by ECCS and the ECCS effectiveness was confirmed.

ANALYTICAL MODEL

TRAC-BD1 (version Boo2) was used. Figure 3 shows a TRAC-BD1 noding for ROSA-III large break test. The pressure vessel is modeled by a VESSEL component with fourteen axial levels and three radial rings (no azimuthal dependency). The inner two rings in levels 5 through 9 model the bypass region. The steam-separator model was applied to level 13. Two CHAN components are used to simulate the four bundles. One in the inner ring simulates the high power bundle. The other one in the second ring simulates the three average power bundles.

The radial power distribution in each bundle was accounted for by specifying four rod groups. Three groups corresponded to the different peaking factors and the fourth modeled two water rods.

The countercurrent flow limiting (CCFL) model with side entry orifice

(SEO) coefficient was utilized at the inlet of both CHAN components. The CCFE model with upper tie plate (UTP) coefficient was used at the outlet of both CHAN components.

Jet pumps were modeled by TEE components, since the jet pump component, JETP, has problems in regard to simulating the external jet pumps {3}.

In the CHAN component, several user-specified heat transfer options are provided. In the present calculation, the following options were used. Critical heat flux (CHF) was calculated with the CISE-GE critical quality CHF correlations. The minimum stable film boiling temperature was taken to the maximum of those calculated by homogeneous nucleation and Iloeje correlation. A threshold void fraction value of 0.9 was used for radiation calculation. The calculation included steam and droplets, and correct view factors were used for anisotropic reflection.

Before transient calculation, a steady state calculation was performed using the initial heater power, pump speeds, main steam flow and feedwater flow. Table I shows comparisons of the measured and calculated steady state conditions. The calculated steady state conditions are very close to the measured values.

Calculated break flow was dependent on the nodalization at the break in TRAC-BDL calculation [3]. The nodalization at break was decided upon as a straight pipe model, after sensitivity calculations on a truncated cone model and a straight pipe model.

In the transient calculation, measured steam, feedwater, LPCS and LPCI flows were used for boundary conditions.

RESULTS AND DISCUSSIONS

The transient calculation was performed until all heater rods were quenched. In this calculation, a speed ratio of central processor unit (CPU) seconds divided by transient seconds, was 72:1 for blowdown phase (before 70 seconds) and 210:1 for reflood phase (after 70 seconds). The time step sizes were limited by Courant limit during blowdown phase and by convergence speed during reflood phase.

Figure 4 shows a comparison between the measured and calculated pressure histories in the lower plenum. Up to 35 seconds after the break, the calculated pressure is in good agreement with the measured data. After 35 seconds, the calculated depressurization becomes higher than the measured data. This is probably due to a overprediction of a break flow shown later. At around 70 seconds, the depressurization rate is decreased due to flashing of water in the feedwater line. This phenomena is also observed in the calculation.

Figure 5 shows comparisons between the measured and calculated break flow rates. In the vessel side break, the calculation is in good agreement with the measured data, before the recirculation suction is uncovered (about 18 seconds). After approximately 18 seconds, the calculated break flow rate is slightly greater than the measured data. In the pump side break, the calculated break flow rate is slightly greater than the measured data.

Figure 6 shows a comparison of differential pressure between the lower plenum and steam dome. The calculation agrees well with the experiment,

during the blowdown phase. However, the calculation is lower than the measured data, during the reflood phase (after 90 seconds).

Figure 7 shows a comparison of bundle differential pressure. The calculation agrees with the experiment during the blowdown phase. The measured data drops at around 70 seconds. This is caused by the bundle draining into the lower plenum which was produced by reduced steam generation from depressurization decrease at the feedwater flashing. However, this phenomena is not observed in the calculation. In the experiment, the differential pressure starts to increase soon after LPCS initiating. However, in the calculation, it starts to increase soon after LPCI initiating. This discrepancy was caused by preventing LPCS water from draining into the bundle shown Fig. 10.

Figure 8 indicates upper tie plate fluid temperatures of the high power channel. Above the upper tie plate, fluids are always saturated in both the calculation and experiment. Below the upper tie plate, superheated fluids appeared soon after the break and disappeared at the lower plenum flashing in both calculation and experiment. At around 50 seconds, superheated fluids again appeared. In the experiment, the superheated fluid temporarily disappeared at the time of feedwater flashing but this phenomena is not observed in the calculation. Times at which superheat appeared are almost the same in the calculation and experiment. This means that core uncover times are almost the same in the calculation and experiment.

Figures 9 and 10 show calculated channel inlet and outlet velocities of the high power bundle, respectively. The inlet flow are co-current upward before LPCI initiation. Then, velocities oscillate. All bundles were completely uncovered soon after the feedwater flashing in the experiment, but were not uncovered in the calculation. Probably the high interfacial shear prevented fluid from draining into the lower plenum from bundles in the calculation. The bundle outlet flow is also co-current upward during both blowdown phase and reflood phase. This indicates that HPCS spray did not fall into the bundle in the calculation.

Figure 11 shows comparisons of heater surface temperatures of the average power bundle. At the top position, the heater surface temperature started to increase at about 10 seconds and rewetted at the lower plenum flashing in the experiment. This temperature history is well simulated by TRAC. At around 45 seconds, the temperature again increased in both the experiment and calculation. The dryout time is almost the same in the calculation and experiment. The measured temperature dropped at the feedwater flashing, but the calculation did not. At the middle point, The calculated dryout time is slightly later than in the experiment. Calculated heatup rates at the top and middle positions also agree with the data. Rods at the bottom position did not heatup in the calculation, since the bottom position was not uncovered.

Figure 12 shows comparisons of heater surface temperatures of the high power bundle. In the high power bundle, the first and second dryout times at the top and middle positions agreed well in the calculation and experiment. However, the bottom position did not heatup in the calculation. These results are similar to those of the average power bundle. The FCT was observed at the middle position of the higher bundle. The heater surface at the middle position was not quenched in the original TRAC-BD1 calculation. The reason

for this is probably problem in the heat transfer model of TRAC, since the calculated bundle differential pressure agrees with the measured data as shown in Fig. 7.

In the original TRAC-BD1, quenching occurs when the cladding temperature, T_{clad} , decreases below the minimum stable film boiling temperature, T_{min} , calculated as follows:

$$T_{min} = \min (T1, \max (T2, T3)) \quad (1)$$

where $T1$ = Hsu's maximum rewet temperature (811 k)
 $T2$ = homogeneous nucleation minimum stable film boiling temperature
 $T3$ = Iloeje's correlation

In Eq. (1), T_{min} is independent from surface properties. However, Groeneveld and Snock [4] indicated that T_{min} was dependent on surface properties in all experiment reviewed and that T_{min} increased with a decrease in $k\rho c_p$ of the wall. Therefore, the authors incorporated Henry's correlation [5]^D for T_{min} calculation in TRAC-BD1, that is:

$$T_{min} = \max (T2, T3, T4), \quad (2)$$

where $T4$ is Henry's correlation, including the effect of surface properties:

$$T_4 = T_{Ber} + 0.42 \cdot (T_{Ber} - T_f) \left[\sqrt{\frac{(k\rho c_p)_l}{(k\rho c_p)_w}} \cdot \frac{h_{fg}}{c_w \Delta T_{Ber}} \right]^{0.6} \quad (3)$$

$$T_{Ber} = T_f + 0.127 \cdot \frac{\rho_l h_{fg}}{k} \left[\frac{g(\rho_l - \rho_g)}{\rho_l + \rho_g} \right]^{2/3} \cdot \left[\frac{\sigma}{g(\rho_l - \rho_g)} \right]^{1/2} \cdot \left[\frac{h}{g(\rho_l - \rho_g)} \right]^{1/3} \quad (4)$$

$$\Delta T_{Ber} = T_{Ber} - T_f \quad (5)$$

In the present calculation, $(k\rho c_p)_l / (k\rho c_p)_w$ is the order of 0.1. Therefore, T_{min} from Henry's correlation^D is larger than that from Iloeje's correlation by about 100 K. In Fig. 12, the heater surface temperature transient at the middle position calculated using modified T_{min} , is in excellent agreement with the measured PCT.

CONCLUSIONS

The following conclusions were obtained in this study,

- 1) TRAC-BD1 can predict the overall trends and key phenomena very well.
- 2) Investigations are necessary on
 - a) Correlation for T_{min}
 - b) Interfacial shear at CHAN inlet and outlet

ACKNOWLEDGEMENT

The authors are grateful to Dr. W. L. Weaver of EG&G Idaho, Inc. and Dr. J. W. Spore of EG&G Service, Inc. for their useful recommendations.

REFERENCES

1. J. W. Spore, et al., "TRAC-BD1 : An Advanced Best Estimate Computer Program for Boiling Water Reactor Loss-of-coolant Accident Analysis," NUREG/CR-2178, Oct. 1981

2. H. Nakamura et al., "ROSA-III 200% Double-Ended Break Integral Test Run 926 (HPCS Failure)", JAERI-M 84-008, Feb. 1984
3. R. J. Dallman, "TRAC-BD1 Calculation and Data comparison of International Standard Problem 12", EGG-CAD-5860, May 1982.
4. D. C. Groenveld and C. W. Snock, "A Review of Current Heat Transfer Correlations used in Reactor Safety Assessments", Second International Topical Meeting on Nuclear Thermal-Hydraulics, Santa Barbara, USA, 1983
5. R. E. Henry, "A Correlation for the Minimum Film Boiling Temperature", AIChE Symposium Series, 80 (138) : 81-90, 1974

Nomenclature

T ; Temperature
 c ; specific heat
 k ; thermal conductivity
 g ; acceleration of gravity
 h ; enthalpy
 μ ; viscosity
 ρ ; density

Subscript

l ; liquid
 g ; vapor
 f ; film
 fg ; heat of vaporization

Table I Comparison between Calculated and Measured Initial Conditions

Parameter	Measured Data	TRAC-BD1
Steam Dome Pressure (Pa)	7.3×10^6	7.29×10^6
High Power Channel Inlet Flow (kg/s)	3.9	3.40
Average Power Channel Inlet Flow (kg/s)	3.9	3.85
Bypass Flow (kg/s)	0.72	0.82
Intact Jet Pump Discharge Flow (m^3/s)	1.1×10^{-3}	1.02×10^{-3}
Broken Jet Pump Discharge Flow (m^3/s)	1.1×10^{-3}	1.05×10^{-3}
ΔP between Upper Plenum and Steam Dome (Pa)	4×10^4	3.81×10^4
ΔP between Lower Plenum and Upper Plenum (Pa)	5×10^4	5.09×10^4

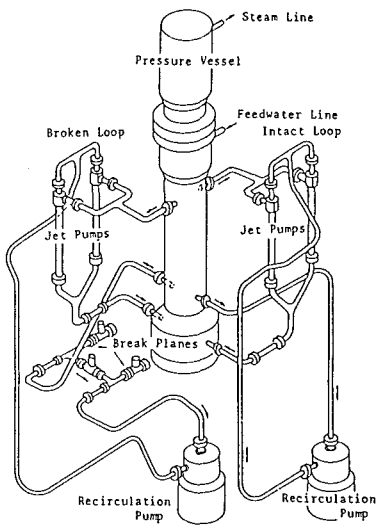


Fig. 1 Schematic Diagram of ROSA-III Test Facility

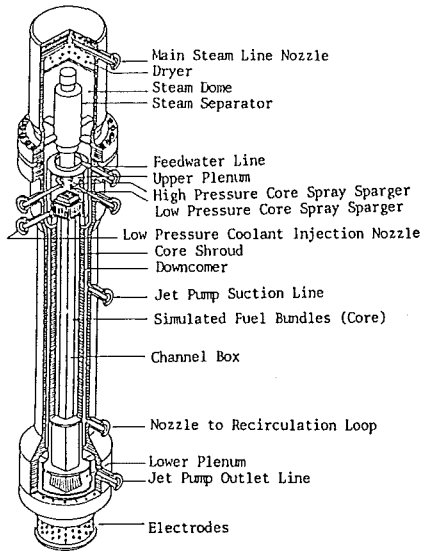


Fig. 2 Internal Structure of Pressure Vessel of ROSA-III

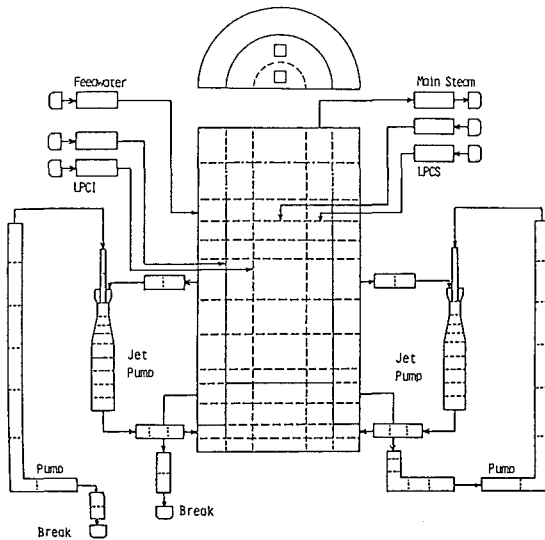


Fig. 3 TRAC-BD1 Noding for ROSA-III Large Break Test

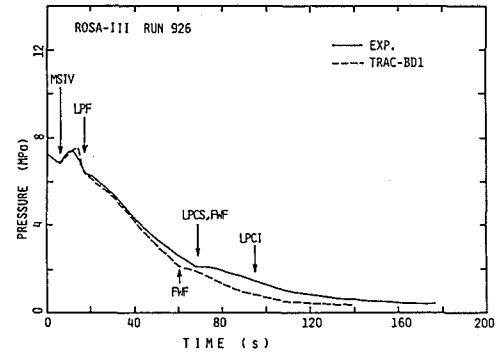


Fig. 4 Pressure in Lower Plenum

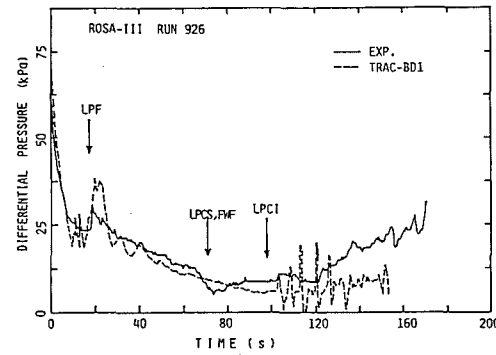


Fig. 6 Differential Pressure between Lower Plenum and Steam Dome

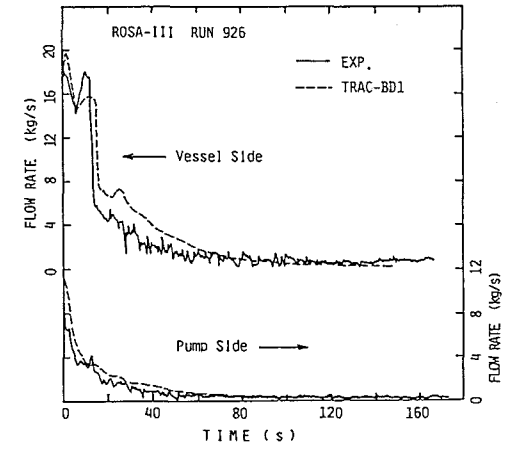


Fig. 5 Break Flow Rates

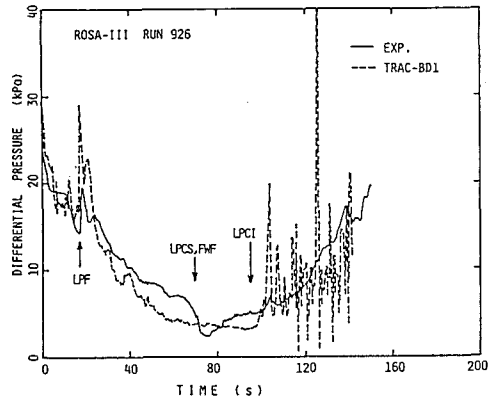


Fig. 7 Bundle Differential Pressure

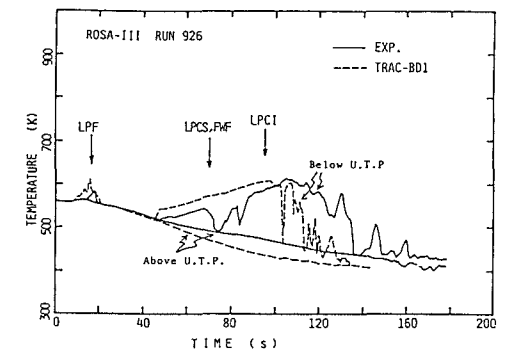


Fig. 8 Upper Tie Plate Fluid Temperatures

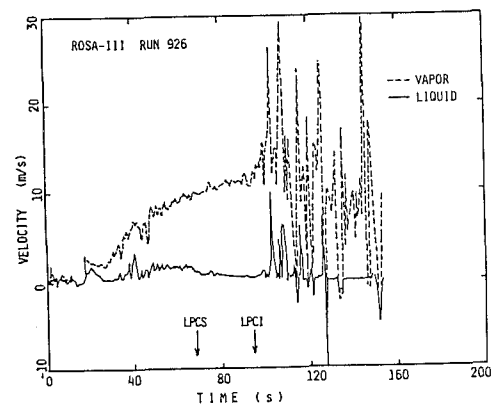


Fig. 9 Calculated Velocities at CHAN Inlet

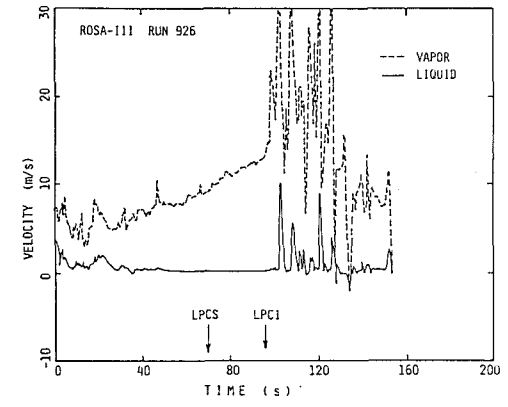


Fig. 10 Calculated Velocities at CHAN Outlet

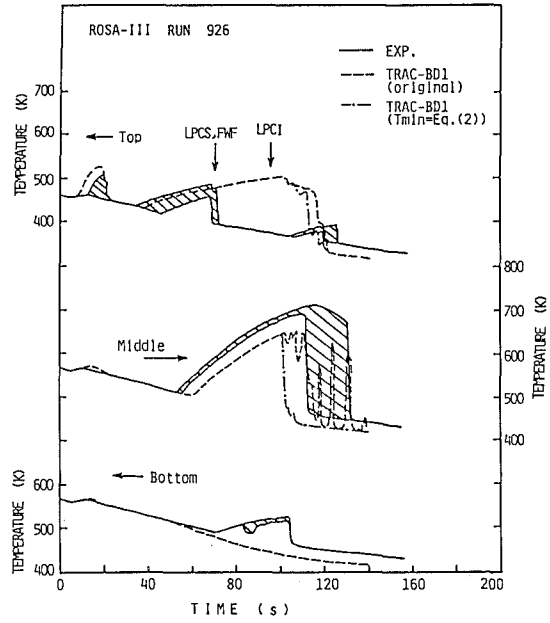


Fig. 11 Heater Surface Temperatures of Average Power Bundle

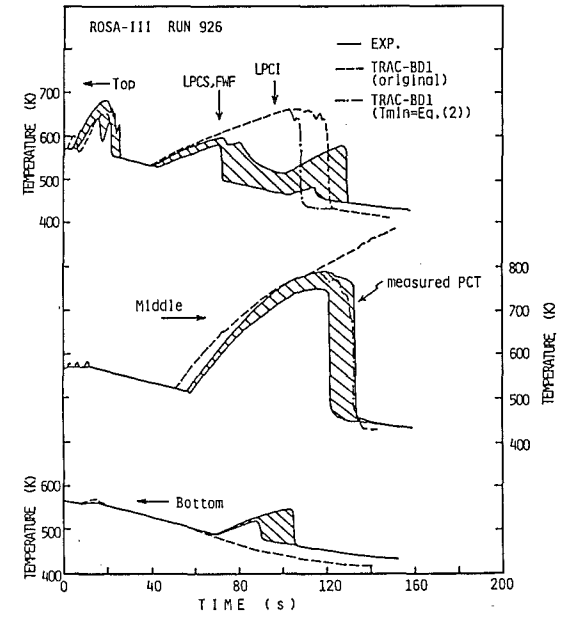


Fig. 12 Heater Surface Temperatures of High Power Bundle

TRAC-BD1 ASSESSMENT UNDER SEVERE
ACCIDENT BOIL-OFF CONDITIONS

G. Th. Analytis and S. N. Aksan

Swiss Federal Institute for Reactor Research (EIR),
5303 Würenlingen,
Switzerland

ABSTRACT

Postulated small break loss of coolant accidents in PWRs may involve partial core uncovering. It is important to be able to predict histories of dry-out point and resulting fuel temperature during the transient. In this work, we shall compare experimental data obtained during boil-off experiments in the NEPTUN test facility at EIR and calculations performed with the best estimate thermal hydraulic code TRAC-BD1 version 12. The TMI-type accident conditions which led to boil-off of the coolant and subsequent uncovering of the core were chosen for this comparison. In general, TRAC-BD1 predicts well the temperature histories of the boil-off experiments; though, some problem areas have been identified and are discussed.

INTRODUCTION

After the occurrence of the TMI-2 accident, in LWR safety analysis, increased attention has been paid to low flow and intermediate or low pressure transients which, if no remedial measures are taken, may sequentially lead to uncovering, overheating and damage of the core. When the reactor power is at decay heat levels and the coolant entering the core is subcooled, uncovering of the core is likely to occur only at relatively low coolant mass flow rates. As a result of TMI-2, hydraulic and heat transfer mechanisms associated with cooling of fuel rods in a pool of water without external circulation is needed to be understood. In particular, there is an obvious need for assessing thermal hydraulic safety codes as far as their ability to correctly predict the level swell (or expansion of the boiling pool) and the fuel rod temperatures in the uncovered region is concerned. Consequently, considerable effort is being spent not only in improving and extending the available transient thermal hydraulic codes, but also in performing carefully controlled experiments in test facilities; the results of these simulations can be directly utilized for assessing the predicting capabilities of these codes or even for developing new models, hence giving a direct feed-back to the code developers.

At the Swiss Federal Institute for Reactor Research (EIR), the NEPTUN heater rod bundle was originally designed for low pressure ($\leq 5 \cdot 10^5$ Psc) reflood experiments whose aim was to study the heat transfer characteristics between the rod and the coolant. Additionally, a number of core-uncovery (boil-off) experiments have been performed to investigate the mixture level decrease and resulting fuel rod heat-up above that level that may occur in a PWR during a small break LOCA. These boil-off tests have been performed under defined conditions using different initial parameters (eg. rod power, system pressure, coolant subcooling etc.). In this work, we shall report on comparisons between experimental data obtained in five boil-off tests in the NEPTUN facility with the corresponding predictions obtained by using the best estimate thermal hydraulic code TRAC-BD1 version 12 / 1 /. Although reasonable agreement between experimental results and code predictions was obtained, specific problem areas which resulted in considerable deviations in transition regions between flow regimes where the models of the code change have been identified and discussed in some detail.

DESCRIPTION OF THE NEPTUN FACILITY AND TEST PROCEDURE

The NEPTUN heater rod bundle was originally built to simulate a PWR core. It contains 33 electrically heated rods and four guide tubes. Each heater rod has an axial height of 1.68m and radial dimensions similar to PWR nuclear fuel rods. There are five fuel assembly spacer grids, axially located at equal distances. Additionally, a continuously variable axial power profile can be achieved. The instrumentation allows the measurement of cladding (at eight equi-distant axial levels), housing, thermal insulation and coolant temperatures, absolute and differential pressures at several axial positions, flow rates, carry-over rates and heating power. The differential pressure measurement stations at eight axial levels were intended for tracing the two-phase mixture level. For a complete description of the NEPTUN facility, the interested reader is referred to / 2 /.

Although NEPTUN was originally designed to simulate a PWR core, the presence of the housing enclosing the heater rods opens the possibility of comparing experimental measurements in NEPTUN with predictions of system codes specially developed for modeling BWRs. Consequently, the boil-off experiments were analyzed by using TRAC-BD1. We shall report on the comparison between measurements and code predictions in the following section.

The NEPTUN boil-off tests were initiated by turning on the full defined power and terminating the coolant flow to the bundle at a given pressure. The coolant swells in a rather unknown manner in the boiling length of the test section and a certain amount of water is expelled out, depending on the power supplied to the heater rods. As the upper parts of the test section are uncovered, due to the transition from nucleate boiling to steam cooling, heat-up of the rods is initiated. Experimental rod surface temperature data shows that no multi-dimensional effects are present and that the movement of the mixture level can be described as a one-dimensional

process. Finally, we should point out that each experiment was performed more than once and the data was found to be consistent.

COMPARISON OF EXPERIMENTAL RESULTS WITH CODE PREDICTIONS

The TRAC-BD1 code was developed for the detailed thermal hydraulic analysis of design basis LOCAs in BWRs. The basic features of the code / 1 / include a full non-homogeneous, non-equilibrium, two-fluid thermal hydraulic model of the two-phase flow in all parts of the BWR system, with a three-dimensional thermal hydraulic treatment of the reactor vessel which could be of importance in asymmetric transients.

In relation to the NEPTUN boil-off experiments, the important feature of TRAC-BD1 which was developed to enable modeling of a BWR core heat transfer and coolant flow is the channel (CHAN) component, which also includes a package of constitutive relations specific to BWRs. The CHAN component simulates a rod bundle and channel box assembly and is therefore closely representative of the NEPTUN bundle geometry. Here we should mention that while implementing the code to our system, certain changes had to be made to enable the calculation of temperature dependent material properties for materials used in the NEPTUN heater rods. These additional materials are Inconel 600, aluminium dioxide, copper and Kanthal / 3 /.

For the comparison between the NEPTUN boil-off tests and the TRAC predictions, five representative experiments were chosen in which different parameters have been varied; these experiments are summarized in Table I.

TABLE I

Experim. Nr.	Total bundle power (kW)	Pressure (Psc)	Initial Subcooling (°K)
5002	24.6	1.10^5	0
5005	42.1	5.10^5	32
5006	42.1	5.10^5	12
5007	24.6	5.10^5	12
5008	10.5	5.10^5	12

Summary of the 5 boil-off experiments.

The model chosen to simulate the NEPTUN facility is shown in Fig. 1. There are 18 hydrodynamic volumes in the CHAN component, and a BREAK and FILL component for supplying the no-flow and constant pressure boundary conditions respectively. The number and sizes of the cells were chosen to coincide with the 8 axial measured data levels. The cross-section of the CHAN model is also shown in Fig. 1; we have modelled the NEPTUN bundle by a 2X2 rod array. Finally, the Biasi local CHF correlation and the maximum of the Henry-Berenson and the Dooeje correlation for the minimum stable film boiling temperature were chosen as the user options.

The comparisons between measurements and code predictions are shown in Fig. 2 - 6. Here we should point out that all TRAC calculations were performed by turning-off the heat transfer due to radiation; the necessity for doing this was dictated by findings reported in a previous work / 4 / according to which with the radiation heat transfer turned-on, there were discrepancies between measured and predicted rod surface temperature histories.

In Fig. 2, the measured rod surface temperature history at the peak axial power level (level 4 in Fig. 1) and computed collapsed liquid level for Exp. 5007 are compared with the corresponding TRAC-BD1 predictions. One can readily recognize two problem areas, the first one at approximately 30 sec. into the transient at the onset of nucleate boiling; this can be seen both in the temperature history curve in which case the code calculates the onset approximately 10 sec. earlier than the data shows, and in the collapsed liquid level where the sudden voiding of the test section is also predicted to occur earlier. The second problem area is related to the fact that the code predicts an earlier (by 75 sec.) CHF or dry-out; consequently, the predicted peak rod surface temperature is approximately 155 °K higher than the measured one. As we shall see, these two problems persisted throughout our calculations for all cases. Similar discrepancies have been reported by other authors / 5 /; though, due to the fact that the experiments reported there were performed under high pressures typical of a BWR, the differences between measurements and predictions were much smaller. We shall briefly discuss this point in due course.

In Fig. 3, we compare the time histories of the same variables for Exp. 5006 with the code predictions. As it can be seen from Table I, in this experiment, the power was higher than in Exp. 5007 but the pressure and the initial water subcooling were the same. Similar differences between measurements and predictions can be seen, although now the agreement is somehow better than with Exp. 5007. In particular, the onset of nucleate boiling and the voiding of the test section are very well predicted, while the CHF is now predicted to occur 30 sec. earlier than the data shows; the difference between predicted and measured peak rod surface temperature is 120 °K.

In Fig. 4, we compare the measured rod surface temperature histories at the axial levels 3, 5, 6 and 7 (cf. Fig. 1) for Exp. 5007 with the

corresponding code predictions. For all 4 axial levels, the CHF is predicted to occur approximately 70 sec. earlier. Though, the differences between predicted and measured peak rod surface temperatures change as one moves to higher axial levels and while below the peak axial power level (level 3, Fig. 4a) this difference is 155 °K, at levels 5, 6 and 7 (Fig. 4b, c, d resp.) the difference is 100 °K, 13 °K and -82 °K respectively; in particular, at axial level 7, the predicted peak rod surface temperature is lower than the measured one. These differences also persisted throughout all our comparisons and would indicate that at the later stages of the transient, in the upper parts of the voided section, the heat transfer is over-predicted.

Finally, in Fig. 5 and 6 we show comparisons between measured and calculated rod surface temperature (at the peak axial power level 4) and collapsed liquid level histories for Exp. 5008 and Exp. 5005 respectively. For Exp. 5008 (low power; cf. Table I), the voiding of the test section is predicted to occur 40 sec. earlier than the data show while up to 700 sec. into the transient, both measurements and calculations show that at level 4, the CHF has not yet been reached. Also here, TRAC-BD1 underpredicts the rod surface temperature after the nucleate boiling transition by approximately 4 °K. In Fig. 6, the same comparisons are shown for Exp. 5005 (high power, high subcooling). All the differences between measurements and code predictions we have already discussed also persist in this case. In this experiment, the measurements were stopped before the power was turned off and hence, the subsequent decrease of the rod surface temperature is not shown. Lastly, we should point out that due to space limitations, we do not show the comparisons between measurements and TRAC predictions for Exp. 5002. For this low pressure experiment, TRAC predicted an almost immediate CHF, as much as 260 sec. earlier than it actually occurred, while it overpredicted the peak rod surface temperature at level 4 by as much as 250 °K; though, surprisingly enough, it predicted much lower void fraction in the test section than the measurements showed. Clearly, the differences between measured data and TRAC-BD1 predictions increase as the pressure decreases; this is also supported by comparisons reported elsewhere / 5 /.

CONCLUDING DISCUSSIONS

Rod surface temperature and collapsed liquid level histories from 5 boil-off experiments in the NEPTUN test facility at EIR have been compared with the corresponding predictions obtained by using the best estimate thermal hydraulic code TRAC-BD1 version 12. Although in general the code does relatively well in predicting the time histories of the aforementioned variables, certain problem areas have been identified; these can be summarized as follows:

- (a) TRAC-BD1 predicts an earlier voiding of the test section and onset of nucleate boiling.
- (b) TRAC-BD1 predicts an earlier CHF than the measurements show; the

differences between measured and predicted CHF are much larger for the low pressure Exp. 5002 and also for the low power experiments. The earlier CHF predicted by the code is clearly related to the fact that the code also predicts an earlier voiding of the test section.

A third problem area reported in a previous work / 4 / was related to the difference in slope between measured and calculated temperature history curves indicating that some high temperature phenomena such as radiation heat transfer were not accurately predicted. This was rectified by turning-off the heat transfer due to radiation; with radiation heat transfer included, the temperature history curves cross the measured ones somewhere above the CHF and the predicted peak rod surface temperatures are lower than the measured ones.

Concluding, we can say that TRAC-BD1 does well in predicting the uncover and heater rod heat-up behaviour for the NEPTUN boil-off experiments, characteristic of conditions experienced during a small break LOCA in a PWR. Some of the aforementioned difficulties and problem areas may be due to the fact that TRAC-BD1 is designed for a BWR in which real flow conditions exist; in the NEPTUN boil-off experiments, we are dealing with a no-flow situation for which the code may not be well-suited. The incorporation of specific correlations would probably improve the predicting capability of the code in this type of transients.

REFERENCES

1. J. W. Spore et al., TRAC-BD1: An advanced best estimate computer code program for Boiling Water Reactor loss-of-coolant accident analysis, Vol. 1, 2, 3, NUREG/CR-2178 (1981).
2. H. Grütter, F. Stierli, S. N. Aksan and G. Varadi, NEPTUN bundle reflooding experiments: Test facility description. EIR Report Nr. 386 (1981).
3. L. Nielsen, Adaptation of TRAC-BD1 to the ETH Computer System. EIR internal report (1983).
4. S. N. Aksan, L. Nielsen, S. Güntay and G. Varadi, Comparison of NEPTUN boil-off and reflooding data with computer code calculations. Paper presented at the European Two-Phase Flow Group Meeting, 14 - 17 June 1983, Zürich, Switzerland (1983).
5. R. E. Phillips, R. W. Shumway and K. H. Chun, Improvements to the prediction of boiling transition during boiling water reactor transients. Thermal Hydraulics in Nuclear Power Technology, Vol. 15, pp 53 - 62 (1981).

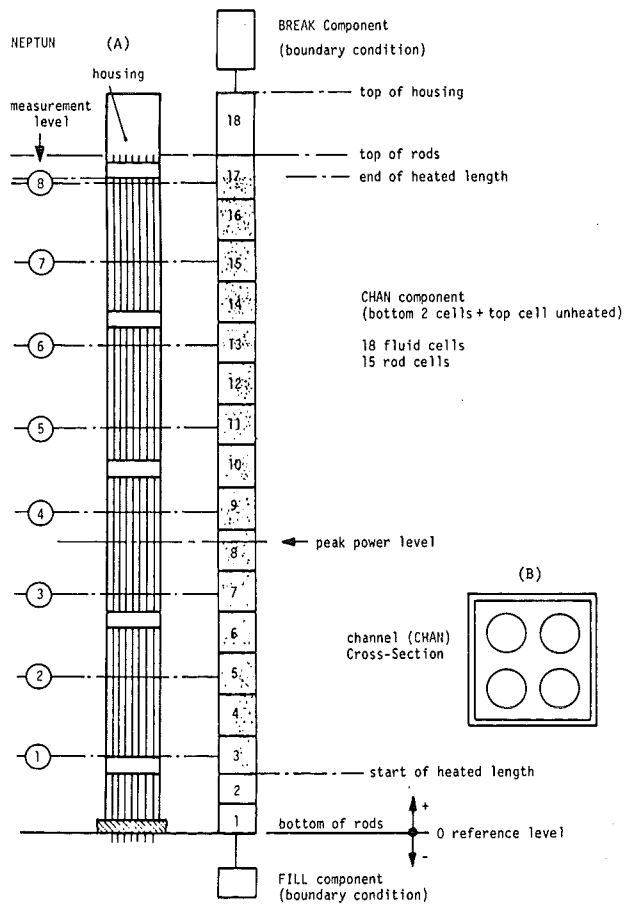


Fig. 1 TRAC-BD1 three-component nodalization for NEPTUN boil-off tests; (A) Vertical nodalization; (B) Cross-sectional modeling of the CHAN component.

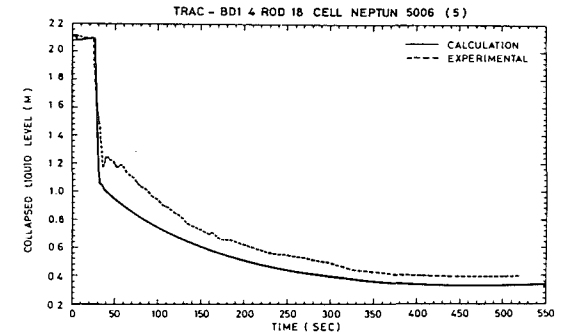
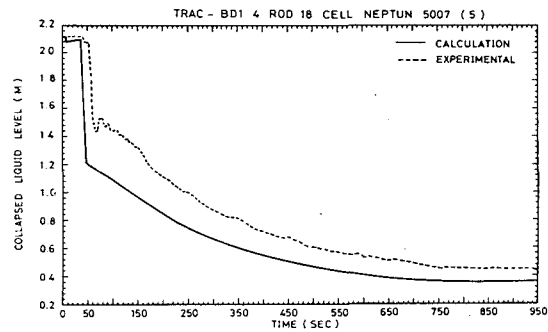
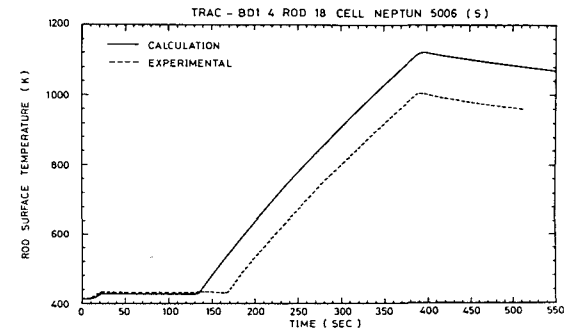
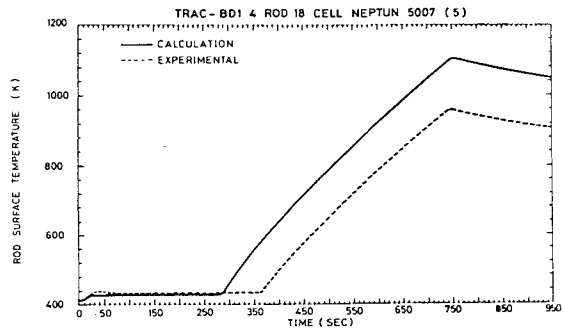


Fig. 2 Measured and calculated rod surface temperature and collapsed liquid level histories for Exp. 5007. Temperatures measured at level 4.

Fig. 3 Measured and calculated rod surface temperatures and collapsed liquid level histories for Exp. 5006. Temperatures measured at level 4.

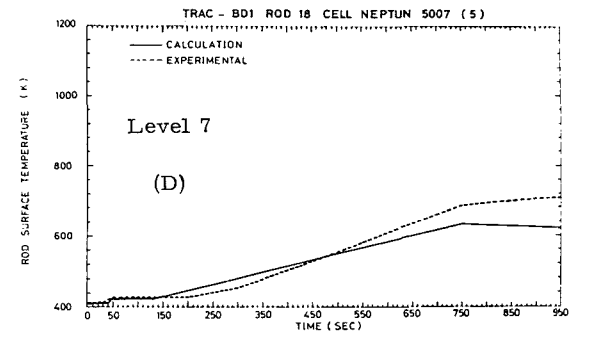
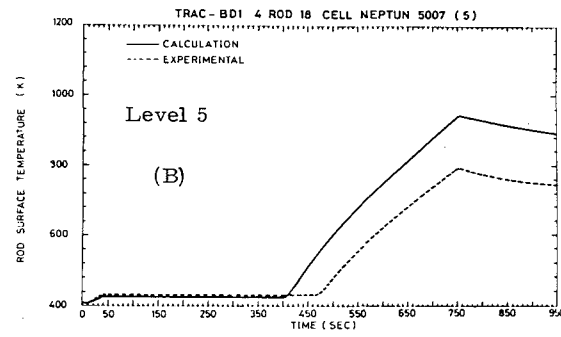
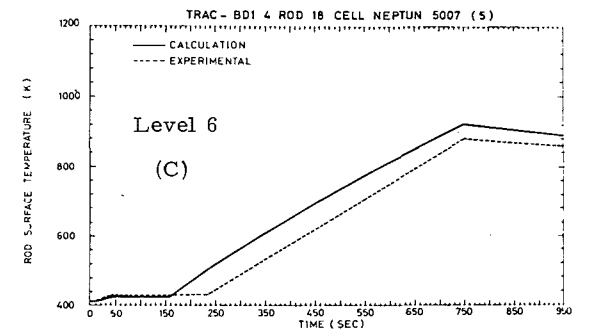
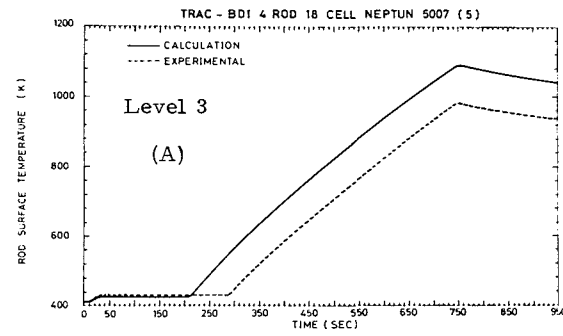


Fig. 4 Measured and calculated rod surface temperature histories for Exp. 5007 at axial levels 3, 5, 6 and 7 (cf. Fig. 1).

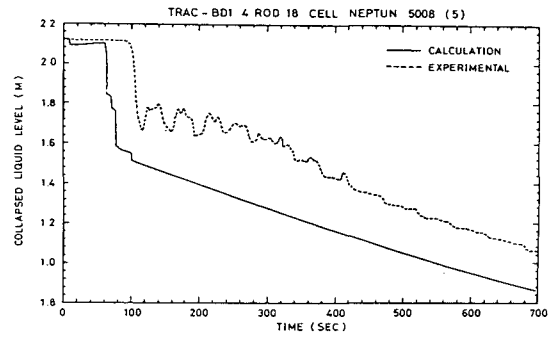
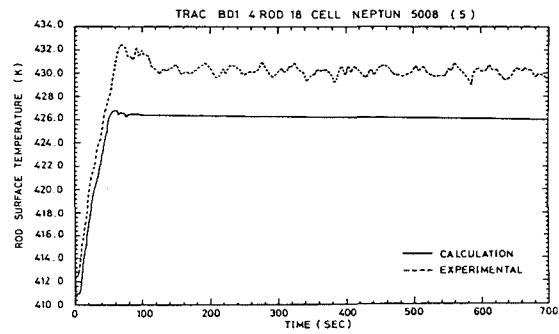


Fig. 5 Measured and calculated rod surface temperature and collapsed liquid level histories for Exp. 5008. Temperatures measured at level 4.

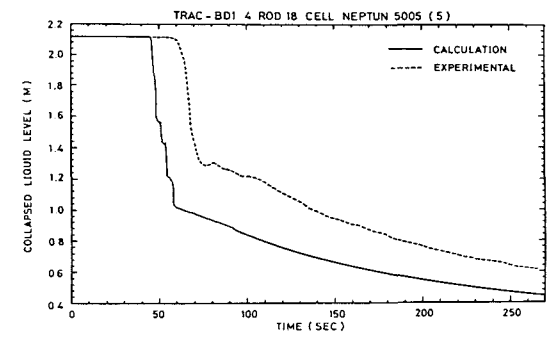
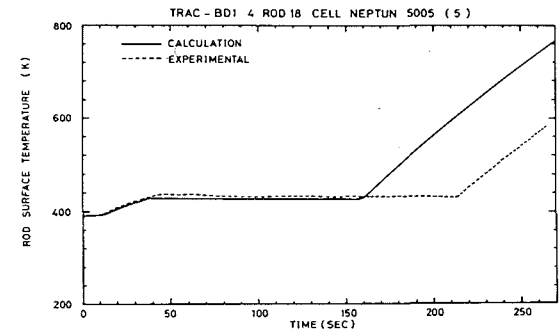


Fig. 6 Measured and calculated rod surface temperature and collapsed liquid level histories for Exp. 5005. Temperatures measured at level 4.

ANALYSIS OF SINGLE AND PARALLEL TUBE COUNTER-CURRENT
FLOW LIMITING EXPERIMENTS WITH TRAC-BD1 CODE*

P. Saha, L. Neymotin and U. S. Rohatgi

Department of Nuclear Energy
Brookhaven National Laboratory
Upton, New York 11973 U. S. A.

ABSTRACT

Simulation of single and parallel tube Counter-Current Flow Limitation (CCFL) tests conducted at Dartmouth College has been performed using the TRAC-BD1 (Version 12) code. Comparison between the code predictions and the experimental data presented in this paper indicates that the code is capable of predicting most of the qualitative aspects of the experiments. However, there are significant disagreements between the code results and the data which warrant improvement of the interfacial shear package of the code, particularly for the annular flow regime. The improved package should consist of correlations developed from the counter-current flow experiments and should be valid for the entire annular flow regime map, i.e., wavy-transition-rough film regimes.

INTRODUCTION

It is well known that Counter-Current Flow Limitation (CCFL) is one of the controlling phenomena during a Loss-of-Coolant Accident (LOCA) in both Pressurized and Boiling Water Reactors (PWRs and BWRs). Therefore, the advanced safety codes such as TRAC-PF1¹, TRAC-BD1² and RELAP5/MOD1³ are expected to predict this phenomenon with reasonable accuracy. As a part of the independent code assessment program at Brookhaven National Laboratory (BNL), these codes were applied to several basic CCFL tests. This paper will present the results of the TRAC-BD1 code for single and parallel tube CCFL tests^{4,5} conducted at Dartmouth College. (RELAP5/MOD1 results were in poor agreement even with the single tube test data, and TRAC-PF1 did not produce useful results for the parallel tube test.)

In order to concentrate on the hydrodynamic aspect of CCFL, only the air-water tests were simulated using the TRAC-BD1 (Version 12.0) code. Liquid entrainment was minimal during these tests; water was injected into a liquid filled upper plenum from where it flowed down to a lower plenum through the test section. Thus the tests were suitable to assess the interfacial shear package of TRAC-BD1 in counter-current flow situations which might be expected during the refill/reflood stage of a BWR LOCA.

TEST DESCRIPTION

The basic test apparatus consisted of an upper plenum which could be connected to a lower collection chamber by one, two or three vertical tubes up to 1.52 m in length. A schematic diagram of the apparatus is presented in Figure 1. The upper plenum and lower collection chamber were constructed of

*Work performed under the auspices of the U.S. Nuclear Regulatory Commission.

0.33 m I.D. lucite cylinders. Water was introduced into the upper plenum by means of an annular injection ring to minimize asymmetrical entrance effects in the tubes. A drain was installed to provide a constant water level of approximately 10 cm in the upper plenum for all tests. The upper portion of the plenum was open to the atmosphere through a disentrainment device designed to minimize splashing during operation.

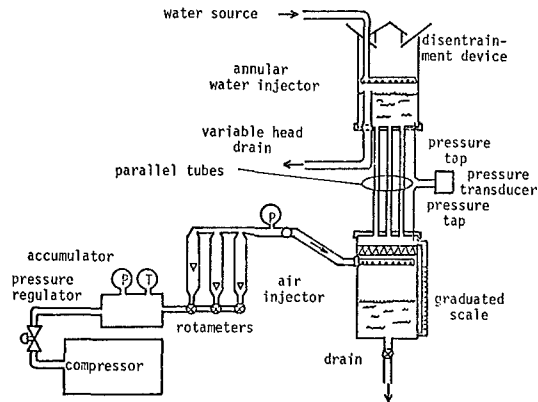


Figure 1 Schematic Diagram of Experimental Apparatus.

The lower chamber was sealed at both ends and was 0.71 m in depth. A drain was provided to expel water accumulated during testing, and a port in the side of the chamber accepted an air injection system. An aluminum honeycomb baffle was installed above the air injector to reduce asymmetrical entrance effect in the tubes being tested. All tubes tested were machined with square edges at both ends and were mounted vertically in the apparatus with the end surfaces aligned flush with the end plate surfaces of the upper and lower chambers.

During the experiment, the air flow rate was changed stepwise. After each step, a sufficiently long time was allowed for the flow to establish. The air flowrate was changed either in the ascending or descending order with the only requirement that none of the tubes experienced a solid water downflow regime. Therefore, throughout the experiments each tube remained in either a counter-current flow or a pure air upflow regime. After a steady-state condition was achieved, the pressure drop across the tubes, i.e., the pressure difference between the top of the lower chamber and the bottom of the upper plenum, the air flow rate and the integrated water downflow rate were measured. The water downflow rate was measured by means of a graduated scale installed in the lower chamber. All experiments were conducted at near-atmospheric pressure and room temperature.

Two sets of experiments, each conducted in round tubes of 0.0254 m I.D. and 1.52 m in length, were simulated with the TRAC-BD1 code. However, the first set used only one tube, whereas the second set employed three identical tubes. Thus a direct comparison between the test results and the code predictions is possible for both single and multi-tube CCFL phenomena. The details of the test procedure and results can be found in Reference 5.

TRAC-BD1 INPUT MODELS

Single Tube Test

The test apparatus was modeled by connecting three TRAC-BD1 TEE components in series as shown in Figure 2a. Part of the upper plenum and drain pipe were modeled with the upper TEE, part of the upper plenum with water injection, the test section and part of the lower plenum were modeled with the middle TEE, and the bottom TEE represented part of the lower plenum and the air injection pipe. The water and air injection pipes and the closed end at the bottom were modeled with FILL components where the water or air flow rates were specified. The upper open end and the end of drain pipes were modeled with BREAK components where the atmospheric pressure was specified. The test section was divided into 18 computational volumes or cells whose lengths varied from 0.074m to 0.1m.

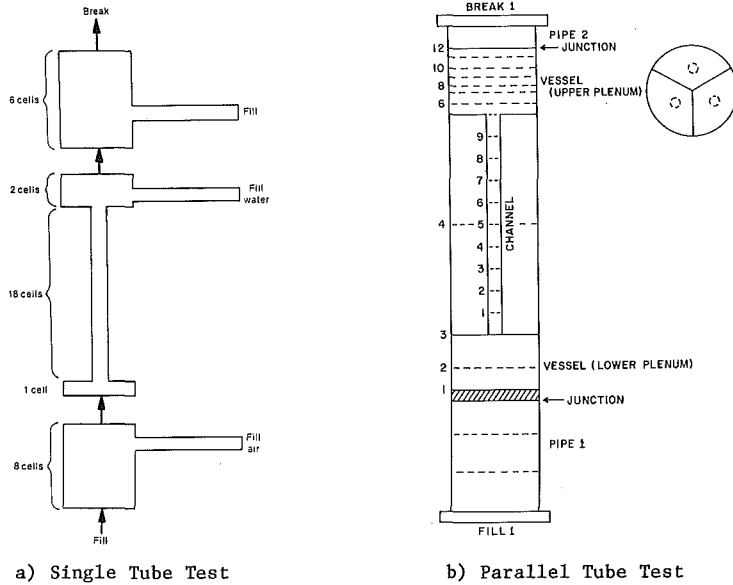


Figure 2 TRAC-BD1 Nodalization for the Dartmouth College CCFL Tests.

Steady state calculations were performed for different air flow rates. Each calculation produced one point on the flooding or $\sqrt{j_g^*}$ versus $\sqrt{j_f^*}$ curve where j_g^* and j_f^* are defined as

$$j_g^* = (Q_g/A) \sqrt{\rho_g} / \sqrt{(\rho_l - \rho_g)} gD \quad (1)$$

$$j_f^* = (Q_l/A) \sqrt{\rho_l} / \sqrt{(\rho_l - \rho_g)} gD \quad (2)$$

(In the above equations, Q_g , Q_l , A and D represent the volumetric gas and liquid flow rates, tube flow area and the tube diameter, respectively. Standard symbols are used for phasic densities and acceleration due to gravity.) The liquid flow rate was determined by calculating the liquid inventory in the lower plenum for a given time interval.

Parallel Tube Test

These experiments were modeled using the VESSEL, CHANNEL, PIPE, BREAK and FILL components of TRAC-BD1, and the nodalization used is shown in Figure 2b. The vessel had one radial ring divided symmetrically into three azimuthal cells each containing one vertical tube. The lower and upper plena were represented by the VESSEL component, whereas the three tubes connecting them were modeled by three CHANNEL components with ten equal cells in each channel. Air was injected into the lower plenum vertically at Cell Junction 2 using a FILL component.

In order to maintain a constant water level in the upper plenum, a vertical drain PIPE connected to atmosphere through a BREAK was attached at Cell Junction 7. Water was introduced into the upper plenum between Cell Junctions 5 and 6 horizontally in radial direction at a rate exceeding the conservatively estimated free-fall water downflow rate in a channel. The excess water was allowed to leave the upper plenum through the drain pipe. The air entering the upper plenum through the vertical channels was allowed to leave through PIPE 2 and/or the drain pipe.

PIPE 1 and FILL 1 shown in Figure 2b were not present in the experimental facility, but were added for the convenience of computation. The code had to be run for a certain period of time for each operational point (with fixed air flux) until a steady-state condition was reached. During this time water collected in the lower plenum could fill it up, thus changing the flow conditions at the entrance of the tube. During the experiment the lower plenum was periodically drained by means of a manually operated valve. This drainage was simulated by attaching PIPE 1 at the bottom of the lower plenum where the water was collected without altering the tube entrance conditions.

Another difficulty related to the size of the lower plenum had to be overcome. Since the air volume in the lower plenum would affect the time response of the system, an air shield (or restriction) was placed between the lower plenum and PIPE 1 (shaded area in Figure 2b). In order to drain the water down, but at the same time keep the air from diffusing into the drain pipe (PIPE 1), a very high value of the additional friction loss coefficient for the air was used. Thus the effective lower plenum volume in the model was kept the same as in the experiment.

CODE PREDICTIONS AND COMPARISON WITH DATA

Single Tube Test

Figure 3 shows the comparison between the data and TRAC-BD1 results for the water downflow rates in the single tube test. It is clear that TRAC-BD1 highly overpredicts the water downflow rate for a given air upflow rate. In addition, "dumping" (alternate heavy downflow of water and upflow of injected air) is predicted at a much higher air upflow rate ($\sqrt{j^*}_g \approx 0.65$) than observed in the test ($\sqrt{j^*}_g \approx 0.2$). However, the code did compute a stable countercurrent flow situation at higher air upflow rates although, as seen in Figure 3, the water downflow rates were highly overpredicted.

There are several possible reasons for this discrepancy. The most probable reason is the underprediction of interfacial shear in the annular flow regime. In TRAC-BD1, the interfacial shear correlation developed from the cocurrent data has also been used for the counter-current flow situations without sufficient verification. A correlation based on counter-current flow

data such as that due to Dukler⁶ has produced better results with TRAC-PF1 for this same experiment⁷. Other possible reasons are inadequate wall friction and a lack of automatic entrance loss at the area changes (e.g., junction between the upper plenum and the test section) in TRAC-BD1.

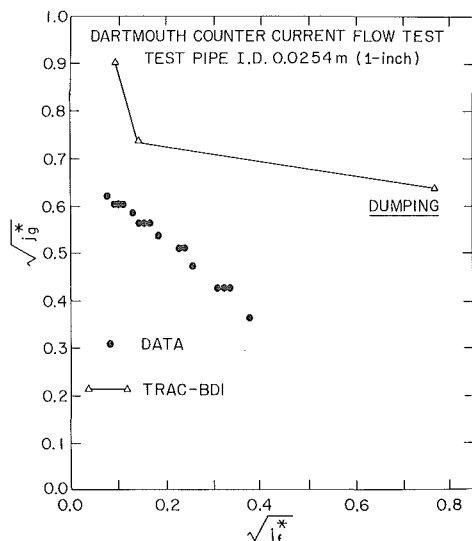


Figure 3 Comparison Between the Data and TRAC-BD1 Prediction for the Dartmouth College 0.0254 m I.D. Single Tube Test.

Parallel Tube Test

Since the water downflow rates during the parallel tube experiments were not reported, only the data on overall pressure drop across the test section were available for code comparison. Figure 4 shows the TRAC-BD1 results and the measured non-dimensional pressure drop, ΔP^* vs. J_g^* . These are defined as:

$$\Delta P^* = - \left(\frac{\Delta P}{L} + \rho_g g \right) / [g(\rho_l - \rho_g)] \quad (3)$$

$$J_g^* = (Q_{g,\text{total}}/A_{\text{total}}) \rho_g^{1/2} [Dg(\rho_l - \rho_g)]^{-1/2} \quad (4)$$

In the above equations, ΔP , L , $Q_{g,\text{total}}$, A_{total} and D represent the measured pressure difference between the lower and upper plena, tube length, total volumetric gas flow through all three tubes, total tube flow area and the tube inside diameter, respectively. Standard symbols are used for the phasic densities and the acceleration due to gravity.

In Figure 4, the alphabets A-B-C-D-E represent the experimental path as the air flow rate was decreased in steps, whereas the numbers 1-2-3-4-5 denote the TRAC-BD1 results. For J_g^* greater than approximately 1.0, the code prediction is in close agreement with the data (see Paths A-B and 1-2). This is to be expected since in this region only air flowed through all the pipes and no water was able to flow down. This also confirms that TRAC-BD1 correctly predicts the wall friction due to single phase gas flow.

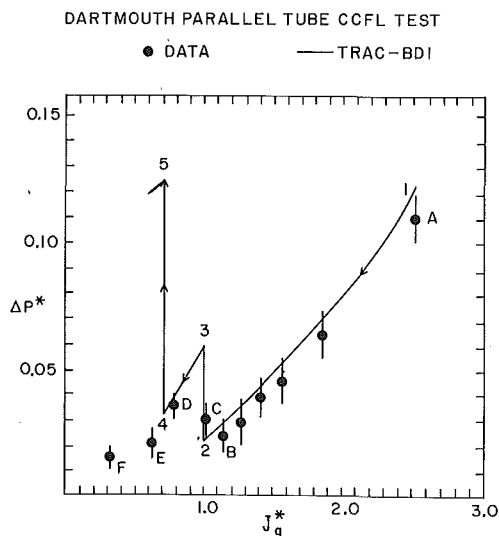


Figure 4 Comparison Between the Data and TRAC-BDI Prediction for the Dartmouth College 0.0254 m I.D. Parallel Tube Test.

As the air flow rate was decreased further, i.e., $J_g^* < 1.0$, according to TRAC-BDI, water started to flow down through one of the pipes while only air continued to flow up through the two remaining pipes. In the experiment, however, there was two-phase counter-current annular flow in one pipe and single-phase air upflow in two pipes. This corresponds to Point C in Figure 4. Notice that the non-dimensional pressure drop ΔP^* increased as the flow pattern changed from Point B to C. A change in flow pattern was also observed in the calculation (Point 2 to 3). However, instead of having one pipe in the counter-current annular flow regime, TRAC-BDI calculated the pipe to be in a low-void ($\alpha \approx 5\%$) two-phase downflow regime and the other two pipes in the single-phase air upflow regime. This resulted in higher air flow rates through the air-filled pipes and caused higher ΔP^* across the parallel tubes (compare Point 3 with C). As the total air flow rate was decreased further, the calculated ΔP^* started to decrease as it should be (Path 3-4). However, when J_g^* became lower than approximately 0.7, another pipe switched to the low-void two-phase flow regime and air was flowing up through one pipe only. This resulted in a sharp increase in the calculated value of ΔP^* (see Path 4 to 5), which was in contradiction with the experimental path D-E. Calculations could not be continued below J_g^* of approximately 0.5 because of the code failure in numerics.

In short, some qualitative aspects of the experiments were predicted by TRAC-BDI. However, there were significant disagreements between the code prediction and the experimental data regarding ΔP^* and flow pattern below J_g^* of approximately 1.0 when water starts to flow down through one or more tubes.

DISCUSSION

It is apparent that the interfacial shear stress used in the annular flow regime in TRAC-BD1 must be increased to obtain a better agreement with the single tube data. The same objective can also be met using a CCFL correlation (e.g., Kutateladze correlation) by adjusting the free coefficient(s). The code developers have recommended⁸ the use of the Kutateladze correlation

$$\sqrt{K_g} + \sqrt{K_\lambda} = \sqrt{K} \quad (5)$$

with the constant $K = 1.05$ for the single tube tests discussed in this paper. The definitions of K_g and K_λ are:

$$K_g = (Q_g/A) \sqrt{\rho_g} / [\sigma g(\rho_\lambda - \rho_g)]^{1/4} \quad (6)$$

$$K_\lambda = (Q_\lambda/A) \sqrt{\rho_\lambda} / [\sigma g(\rho_\lambda - \rho_g)]^{1/4} \quad (7)$$

where σ is surface tension. Note that the value of K suggested for this test series is quite different from the default or standard value of 3.2 which indicates that different values of K would be needed for different experiments. This is obviously a shortcoming for a best-estimate, advanced code like TRAC-BD1.

Situation is even more complicated for the prediction of parallel tube experiments due to a fundamental difference between the single and parallel tube CCFL operations. Figure 5 shows the typical ΔP^* vs. J_g^* curve for counter-current flow in a single 0.0254 m I.D. vertical tube connecting two plena. For J_g^* greater than 1.0, no water can flow down, and only air flows upward. Therefore, ΔP^* decreases as J_g^* is decreased from a high value of 1.0 (Part C of Figure 5). As J_g^* is decreased below 1.0, water starts to flow down and a counter-current rough film annular flow regime develops in the tube. Since the interfacial friction increases as the liquid film becomes thicker, the pressure drop increases with the decrease in the air flow rate. This is Part B of Figure 5 where the Wallis-type correlation⁹ for interfacial friction in the annular flow regime is valid. As the air flow rate is decreased further ($J_g^* < 0.5$), the liquid film becomes smoother or wavy, and the pressure drop starts to decrease with the decrease in the air flow rate. This is Part A of Figure 5. Although the flow is still in the counter-current annular flow regime, no established correlation for interfacial shear is available for this region.

For a single-tube J_g^* -controlled experiment, it is possible to traverse all parts of the curve shown in Figure 5. However, in a multi-tube system, where only the total J_g^* can be controlled, but not J_g^* through each tube, stable operation in Part B is not possible. Therefore, in the three-tube system discussed earlier, one tube starts to operate in Part A whereas two tubes continue to operate in Part C as soon as the total J_g^* is decreased below 1.0. It must be reiterated that the flow regime in the tube operating in Part A is still in the counter-current annular flow regime and not in the low-void downflow regime. TRAC-BD1, however, predicted a low-void mixture flowing down in one tube as soon as the J_g^* is decreased below 1.0. The code essentially uses a Wallis-type correlation for the annular flow regime which increases the interfacial shear as water starts to flow down. This tends to increase the ΔP^* and reduce the air flow rate through that tube. Since the code does not have any correlation to describe Part A of Figure 5, the calculation eventually stabilizes when the tube becomes almost water-filled and a very low-void two-phase mixture flows down. As a result, the air flow rate through the other

two tubes increases significantly (~50%) and the total ΔP^* across the tubes jumps appreciably (from Point 2 to 3 in Figure 4). Therefore, it is apparent that unless the interfacial shear package can be modified to include Part A of Figure 5, the code will not be able to predict the multi-tube CCFL data.

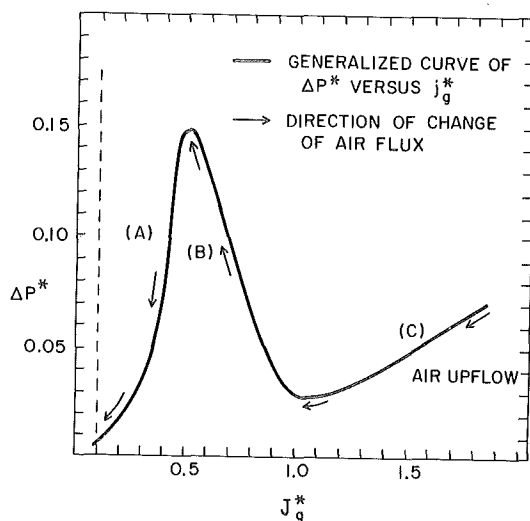


Figure 5 A Typical ΔP^* vs. J_g^* Curve for Counter-Current Flow in a Single Vertical Tube (Approximate Data for 0.0254 m I.D. Tube).

CONCLUSIONS

1. TRAC-BD1, without the use of CCFL correlation, highly overpredicts the liquid downflow rate for a single tube counter-current flow situation. The prediction for the multi-tube CCFL experiment is also inadequate.
2. Modifications in the interfacial shear package of TRAC-BD1 seem necessary for better prediction of CCFL. The new package must consider data obtained in the counter-current flow experiments, and both Parts A and B of the ΔP^* vs J_g^* curve of Figure 5.
3. Use of CCFL correlations such as that due to Kutateladze would require different constants for different experimental apparatus and hardware. This is not a desirable feature for a best-estimate, advanced code like TRAC-BD1.

ACKNOWLEDGEMENTS

The authors would like to thank Dr. Fuat Odar, the NRC program monitor, for his suggestions and comments. The fine typing by Ms. A. C. Fort is also highly appreciated.

REFERENCES

1. Liles, D. R., et al., "TRAC-PF1: An Advanced Best-Estimate Computer Program for Pressurized Water Reactor Analysis," NUREG/CR-3567, LA-9944-MS, February 1984.
2. Spore, J. W., et al., "TRAC-BD1: An Advanced Best-Estimate Computer Program for Boiling Water Reactor Loss-of-Coolant Accident Analysis," NUREG/CR-2178, EGG-2109, October 1981.
3. Ransom, V. H., et al., "RELAP5/MOD1 Code Manual," NUREG/CR-1826, EGG-2070, March 1982.
4. Bharathan, D., "Air-Water Counter-Current Annular Flow," EPRI Report NP-1165, Sept. 1979.
5. Clark, C. R., et al., "Flooding in Multi-Path Vertical Countercurrent Air-Water Flow," NRC-0193-5, Thayer School of Engineering, Dartmouth College, Sept. 1978.
6. Dukler, A. E., "Two-Phase Interactions in Counter-Current Flow," University of Houston, Annual Report, Nov. 1978-1979; 1980.
7. Rohatgi, U.S., "Assessment of TRAC Codes with Dartmouth College Counter-Current Flow Tests," ANS Transactions, Vol. 44, pp. 611-612, Detroit, Michigan, June 1983.
8. "TRAC-BD1/MOD1 Developmental Assessment," INEL Draft Report, pp. 14-19, October 1983.
9. Wallis, G. B., "Annular Two-Phase Flow, Part 1: A Simple Theory," Journal of Basic Engineering, Transactions of ASME, Vol. 92, pp. 59-72, March 1970.

POSTTEST DATA ANALYSIS AND ASSESSMENT OF TRAC-BD1/MOD1
WITH DATA FROM A FULL INTEGRAL SIMULATION TEST (FIST)
POWER TRANSIENT EXPERIMENT

P. D. WHEATLEY
K. C. WAGNER

IDAHO NATIONAL ENGINEERING LABORATORY
EG&G IDAHO, INC.
P.O. BOX 1625
IDAHO FALLS, ID 83415 USA

ABSTRACT

The FIST power transient test 6PMC2 was analyzed to further the understanding of the FIST facility and provide an assessment of TRAC-BD1/MOD1. FIST power transient 6PMC2 investigated the thermal-hydraulic response following inadvertent closure of the main steam isolation valve and the subsequent failure of the reactor to scram. Failure of the high pressure core spray system was also assumed, resulting in only the reactor core isolation cooling flow for inventory makeup during the transient. The experiment was a sensitivity study with relatively high core power and low makeup rates.

This study provides one of the first opportunities to assess TRAC-BD1/MOD1 under power transient and natural circulation conditions with data from a facility with prototypical BWR geometry. The power transient test was analyzed with emphasis on the following phenomena; (a) the system pressure response, (b) the natural circulation flows and rates, and (c) the heater rod cladding temperature response. Based on the results of this study, TRAC-BD1/MOD1 can be expected to calculate the thermal-hydraulic behavior of a BWR during a power transient.

INTRODUCTION

Interest in boiling water reactor (BWR) plant behavior during transients, with a failure to scram, has increased in recent years due to several events at commercial sites. This interest has led to the development or enhancement of several computer codes to calculate plant behavior, and an experimental program which in part investigated the BWR response during power transients. The Full Integral Simulation Test (FIST) program, co-sponsored by the United States Nuclear Regulatory Commission (USNRC), Electric Power Research Institute (EPRI) and the General Electric Company (GE), included several experiments during phase I testing to investigate BWR thermal-hydraulic response during a power transient. FIST is well suited to investigate power transients as it is a full height facility with a full sized bundle. Being full height, FIST provides the prototypical water level movement, static head, for fidelity in natural circulation flow. FIST provides some of the first experimental data that can be utilized to assess and benchmark computer codes.

TRAC-BD1/MOD1 (Reference 1), an advanced best estimate thermal-hydraulic computer code, was used to simulate the FIST power transient. The code results were then compared with the data to assess the code's capabilities to simulate a power transient. FIST test 6PMC2 was chosen for analysis as it provides the

power transient for the first part of the experiment and a refill/reflood during the later part of the experiment. Thus two very different type transient phenomena were assessed using one set of experimental data.

FACILITY DESCRIPTION

The FIST facility was designed and constructed to represent the nuclear steam supply system (NSSS) of a BWR/6 with a vessel diameter of 5.537 m (218 inch). The facility includes two complete, independent recirculation loops. Pump inertia is adjusted for each loop to achieve proper core flow coastdown which is characteristic of a BWR. A heated feedwater system capable of delivering make-up water at BWR rated temperature and scaled flow rates is also featured in the FIST facility to allow steady state operating conditions and provide characteristic downcomer temperature gradients. Other systems included in the facility which were used during power transients are: reactor core isolation cooling (RCIC) system and the safety relief valves (SRV). Five SRVs are used to simulate the five banks of SRVs in the BWR.

The FIST pressure vessel is shown in Figure 1 with the BWR vessel for comparison. The FIST facility is full BWR height with volume scaling (1/624) to a single full sized fuel bundle. All flow areas were scaled based on the single bundle in FIST to the 624 bundles in a BWR. Thus the fluid volumes are also representative of the BWR on a 1 to 624 basis. The simulated downcomer annulus and part of the lower plenum form a separate region connected to the main vessel. The main vessel contains the remainder of the lower plenum and downcomer, along with the other simulated BWR regions. This division of the vessel allows installation of two scaled jet pumps as well as maintaining a scaled cross-sectional area in the downcomer. The jet pumps are designed to provide the appropriate core flow and are the same height as a BWR which provides a prototypical core liquid level and proper natural circulation flow.

The core region contains a single, full size, electrically powered 8 x 8 bundle employing direct heaters. The bundle is surrounded by a typical BWR zircaloy channel which is physically and thermally in contact with the bypass region, thereby allowing bundle to bypass heat transfer typical of a BWR. The FIST bundle inlet and outlet regions are geometrically similar to those in a BWR.

The FIST facility is fully instrumented to measure pressure, temperature, differential pressure, liquid level, and other miscellaneous parameters. Table I summarizes the measurements. A complete description of the facility and the instrumentation can be found in the Facility Description Report (Reference 2).

TABLE I. FIST EXPERIMENTAL MEASUREMENT SUMMARY

<u>Parameter</u>	<u>Number of Measurements</u>	<u>Percent of Total</u>
Pressure	8	1.9
Differential pressure	126	29.9
Conductivity	45	10.1
Metal temperature	21	4.9
Fluid temperature	82	19.3
Heater rod temperature	112	26.4
Miscellaneous	32	7.5

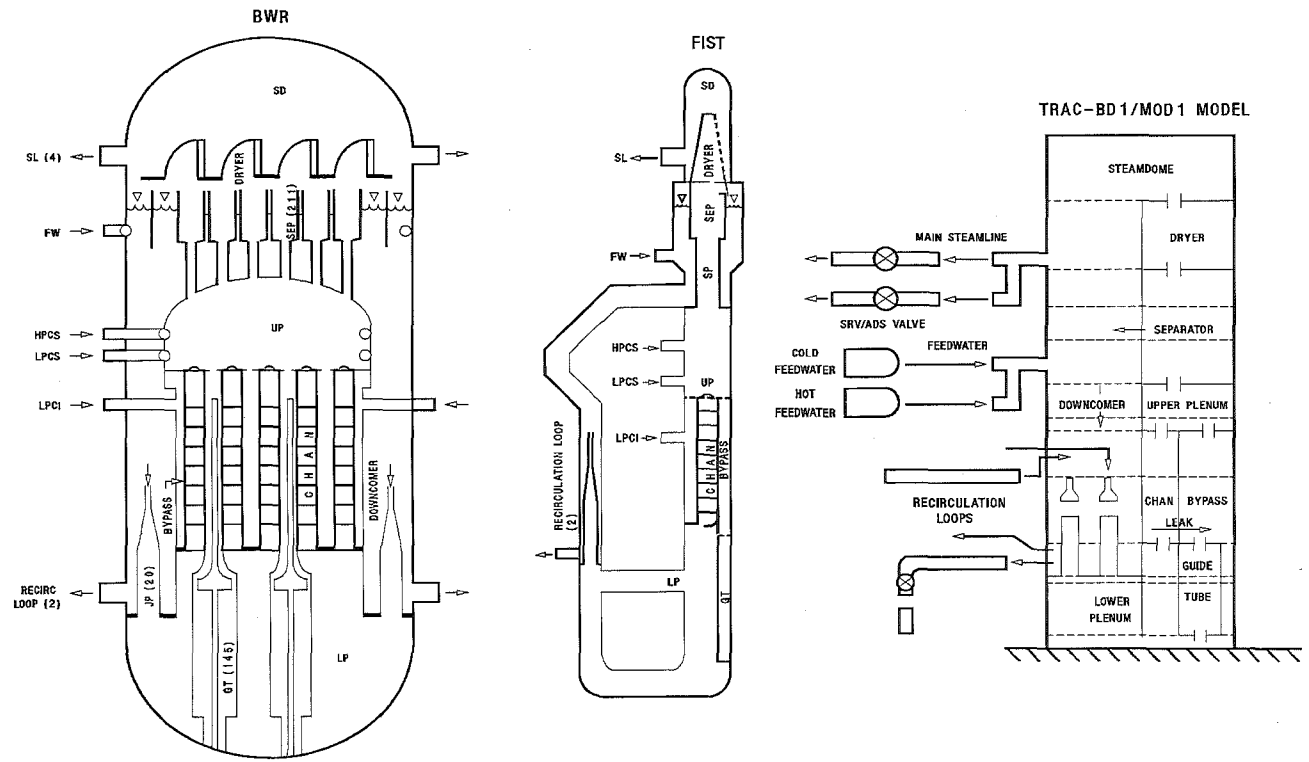


Figure 1. Comparison of FIST facility with a BWR and TRAC analytical model.

CODE AND MODEL DESCRIPTION

TRAC-BD1/MOD1 provides a best-estimate analysis capability for analyzing the full range of postulated accidents or transients in a BWR system and related experimental facilities. The code allows consistent and unified analysis capability for all areas of a large or small break loss-of-coolant accident, beginning with the blowdown phase, through heatup, reflood with quenching and finally, the refill phase of the accident.

Unique features of the code include: (a) a full nonhomogeneous, non-equilibrium two-fluid thermo-hydraulic model of two-phase flow in all portions of the BWR system, with a three-dimensional thermal-hydraulic treatment of the vessel; (b) detailed modeling of a BWR fuel bundle, including a thermal radiation heat transfer model for radiative heat transfer between multiple fuel rod groups, liquid and vapor phases, and the fuel channel wall with quench front tracking on all fuel rod surfaces and the inside and outside of the fuel channel wall for both bottom flooding and falling film quench fronts; (c) detailed models of BWR hardware such as jet pumps and separator-dryers; and (d) a countercurrent flow limiting model for BWR-like geometries. Other features of the code include a nonhomogeneous, thermal equilibrium critical flow model, and flow regime dependent constitutive relations for the interchange of mass, energy, and momentum between the fluid phases and between the phases and the structure.

The TRAC-BD1 FIST model nodalization is also shown in Figure 1. The model used a vessel component to simulate the lower plenum, bypass, downcomer, upper plenum, separators, dryers, and the steam dome. The FIST vessel had one radial ring and two azimuthal sectors separating the downcomer from the core region. This configuration allowed one-dimensional flow through the vessel and modeling of the vessel walls for both the downcomer and core regions. Double sided heat slabs were used to model the vessel walls and an average heat transfer coefficient was applied to the outside of the heat slab modeling heat losses to the surroundings.

A CHAN component was placed in the core region (Cell 2) at Levels 5 and 6. It simulated an average power bundle with two rod groups, one group representing the water rods and one group for the 62 heated rods. Other systems modeled included (a) the main steamline, main steam isolation valve (MSIV) and the SRVs, (b) the feedwater and the RCIC system, and (c) both recirculation loops with each driving a JET PUMP component.

The FIST TRAC model was run in the steady state mode to establish pretest conditions similar to those in the experiment. A summary of the code calculated initial conditions and those measured prior to the start of the experiment are given in Table II. Several boundary conditions were

TABLE II. FIST INITIAL CONDITIONS FOR TEST 6PMC2

<u>Parameter</u>	<u>Measured Data</u>	<u>TRAC</u>
Steamline flow (kg/s)	2.37 ± 0.12	2.49
Feedwater flow (kg/s)	2.44 ± 0.12	2.44
Power (kW)	4640. ± 30.0	4640.0
Jet pump flow (kg/s)	17.8 ± 0.53	17.9
Bypass flow (kg/s)	1.7 ± 0.34	1.67
Steamdome pressure (kPa)	7173.0 ± 50	7199.0
Downcomer level (m)	10.72 ± 0.13	10.77
Downcomer temperature (K)	552.0 ± 2.0	552.0

specified as tabular input or a time trip. The following were input in a tabular form; the feedwater flow rate and the RCIC flow rate. The recirculation pumps were tripped on high pressure and the loops were isolated at 73 s by a time trip. The core power was terminated on high heater rod cladding temperature similar to the experiment.

The SRV flow was calculated by the code during the transient after the valve area had been sized during sensitivity runs. The sensitivity runs were necessary as TRAC allows the user to input a single value of the hydraulic diameter and valve area. This method is adequate as long as the valves being modeled are identical (such as in an actual BWR). However, the FIST facility used 5 valves to represent the 16 valves in a BWR. Each FIST valve modeled a valve bank prototypical of a BWR/6 and was therefore of a different size.

The TRAC code assumes the hydraulic diameter varies linearly with valve area. This is a good assumption if multiples of identical valves are being modeled. However the five FIST SRVs were scaled to represent one, three, four, and seven valves. In this case, the hydraulic diameter would vary more like the square root of the flow area. Thus the valves were sized during sensitivity runs to match the flow at the design point of the BWR valves.

TEST DESCRIPTION

FIST power transient 6PMC2 investigated the thermal-hydraulic response following the inadvertent closure of the main steam isolation valves (MSIV) and the subsequent failure of the reactor to scram. Test 6PMC2 was a sensitivity experiment with relatively high core power and low inventory makeup rates. The core power history was calculated using a BWR/6 plant deck and a one-dimensional neutronic code. Assumptions in the neutronics calculation were boron injection at 120 s and the high pressure core spray (HPCS) system was available. When the 6PMC2 experiment was conducted the HPCS system was inhibited. Therefore, the power curve was higher than the RCIC system would be expected to handle. The effects of this will be discussed shortly.

The experiment was initiated, after a short period at steady state by activating the preprogrammed bundle power controller. The steam valve (MSIV) closed 2 s after test initiation. The programmed bundle power peaked at 7300 kW (157% nominal) at 5.5 s. The bundle power was terminated at 357 s when an administrative limit of 895 K on rod cladding temperatures was reached. The rod cladding heatup was a direct result of using a power curve generated assuming HPCS operation and conducting the experiment with only RCIC operational. A rod heatup is not expected during a power transient in which only RCIC is available, see test 6PMC2A of the FIST test series (Reference 3).

As system pressure increased, after steam valve closure, the SRVs opened to halt the pressure rise. The SRVs opened and closed on pressure setpoints identical to the BWR settings. The high system pressure tripped the recirculation pumps at 4 s and started the timer for loop isolation which occurred at 73 s. The feedwater system was operated as close to a BWR as possible within the FIST feedwater pump shut-off head restrictions. Liquid level in the downcomer decreased as system inventory was lost through the SRVs. Level 2 was reached at 70 s and the RCIC flow was activated at 85 s. RCIC flow was not large enough to restore the downcomer level until core power was terminated and the SRVs closed.

The rod cladding temperatures above the 1.448 m level in the core underwent heatup. The peak cladding temperature of 895 K was reached at the 2.972 m elevation. The cladding temperatures turned around and decreased due to the

bundle power trip at 357 s and the following reflood by the RCIC system. The core uncover and rod heatup was a result of the mismatch in the programmed power and the unavailability of the HPCS system in the experiment, as discussed previously.

RESULTS

The power transient calculation was analyzed and compared with data in what were considered to be the areas of most interest to individuals using the code in the field of severe accident analysis. This section will provide a review of the code's capabilities in the following areas: (a) system pressure response, (b) natural circulation flow rates, and (c) the heater rod cladding response.

A key parameter during the power transient is the system pressure response, as this parameter has a large influence on the void feedback in a nuclear plant. The FIST power transient pressure is compared with the TRAC calculated pressure response in Figure 2. The system pressure increased in response to the MSIV closure. The code calculated a peak of 8525 kPa versus a measured peak of 8425 kPa at about 6 s. The pressure rise was halted by the opening of all the SRVs in both the calculation and the experiment. The pressure oscillated between 6650 kPa and 7800 kPa, the setpoint for the SRVs. The pressure response of the facility lagged that of the calculation after the SRV closing as the system repressurized. During the fifth pressurization the calculated pressure reached the setpoint of the third and fourth SRVs and they opened unlike the experiment. The experiment was very close to the setpoint (within 300 kPa) but the SRVs in the facility did not open. The programmed power decreased shortly thereafter and the measured pressure decreased. It is believed that the large flanges in the FIST facility damped the pressure response slightly and were enough to prevent the system pressure from reaching the SRV setpoint before the programmed power decreased. The large flanges, which are not prototypical, were not modeled in the TRAC calculation. Consequently a higher pressurization rate was calculated.

The system pressure after bundle power termination was approximately 7000 kPa in both the calculation and the experiment. Subsequent to the power termination, the calculated pressure remained higher than the experiment during the remainder of the transient. There were several reasons for the higher pressure. First, the ambient heat loss for the calculation was half that actually measured prior to the experiment. The generic heat loss value was used, later the actual test specific heat loss was available. Second, the separator may have provided mixing of the superheated vapor from the core with the saturated liquid present; the mechanical mixing is not accounted for in TRAC. Most important of all, the reflood rate of the core after bundle power trip was much higher in the calculation and the increased rate of energy addition caused the pressure to remain higher than the measured value. The reflood rate will be discussed as part of the heater rod response discussion.

Next, the calculated natural circulation rate was compared with the experiment. The bundle inlet flow rate was examined as a function of the liquid level in the downcomer. The code calculated values were in good agreement with those measured during the experiment, as shown in Figure 3. At the lower elevations, around seven meters, the code calculated flow was slightly less than the measured flow. The ambient heat loss was smeared over the entire vessel, due to the limitation of the code, whereas the downcomer was the highest heat loss region experimentally. The downcomer temperatures were slightly lower in the experiment leading to the higher flow rate. The heat

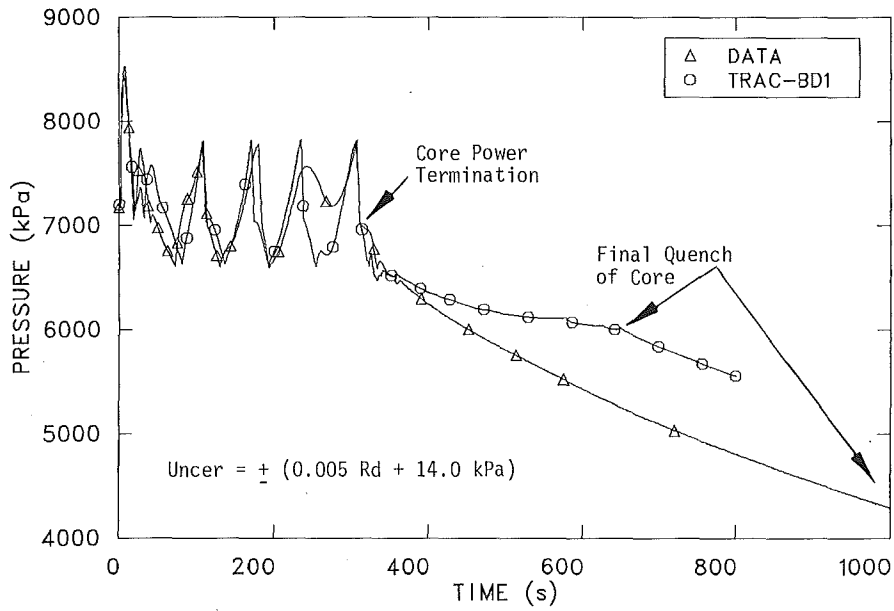


Figure 2. Comparison of calculated and measured steam dome pressure through 1000 s.

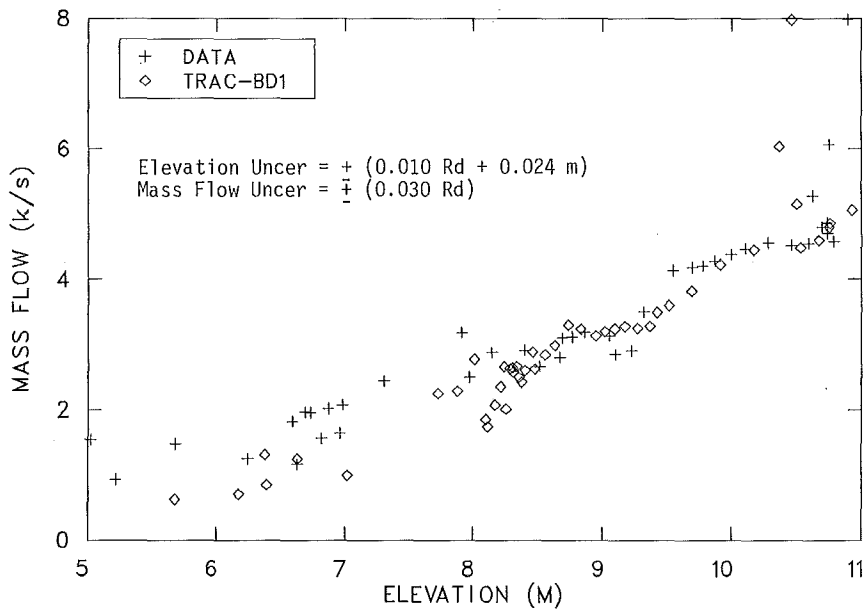


Figure 3. Comparison of calculated and measured natural circulation flow versus downcomer level.

loss of the FIST facility, much like all subscaled experiments, is not prototypical of the BWR and therefore the code should calculate BWR natural circulation better at lower downcomer elevations.

The downcomer water level is interrelated with the natural circulation flow rate. The code may calculate the correct flow for a given elevation in the downcomer but the code must also track the level movement with time to provide a truly accurate description of the transient phenomena. Figure 4 compares the calculated and measured downcomer liquid levels. Early in the transient there was excellent agreement between the two. At 41 s the measured level decreased as the level passed the bottom of the separator skirt. The calculated level did not show a similar decrease as the separator still had a reasonably low void mixture which drained into the downcomer. The liquid drainage from the separator was due to the nodalization of the facility. Subsequent models have moved the separator liquid discharge to Level 11 eliminating the liquid storage in the separator. Though the measured and calculated levels differ for the remainder of the transient, the level movement does show similar slope and trends.

Overall TRAC calculated both the level movement and the natural circulation flow very well. The code also calculated the pressure response of the facility well during the early portions of the transient until bundle power termination. The discussion will now shift to the refill/reflood of the core after the bundle power termination and the phenomena which is usually associated with loss-of-coolant accidents but may be important during a power transient with several auxiliary system failures.

The heater rod cladding response was examined and a typical TRAC calculated rod temperature and several measured cladding temperatures at the same elevation are shown in Figure 5. The TRAC calculated temperature shows a departure from saturation conditions approximately 35 s earlier than the measured values. The early heatup is due to the higher integrated vessel mass loss when the SRVs opened during the fifth vessel repressurization, as discussed earlier.

Both the calculated and measured temperatures peaked at 895 K when the bundle power was terminated. The measured temperatures rolled over as the bundle power was terminated and decreased as the core was reflooded. The calculated temperatures rapidly decreased 25 K before showing a cooling rate similar to the experiment. The differences were due to the location of the measured versus the calculated temperatures. The measured temperatures were on the inside of the cladding and thus exhibited a delay in cooling after bundle power trip, whereas the calculated temperatures were for the outside of the cladding. Due to code limitations on where cladding temperature can be monitored and plotted it was necessary to use the calculated outside temperatures and inside measured temperatures. After the initial turnaround the temperatures are believed to differ very little from inside to outside.

The TRAC calculation showed quenching earlier than the experiment. The core quench front position versus the core liquid level is shown in Figure 6. The liquid level and quench position were the same for the experiment. The TRAC calculation showed a quench front preceding the liquid level. Entrainment of fluid in the bundle caused the quench front to precede the liquid level. The top three nodes in the channel quenched as fluid in the lower downcomer flashed forcing liquid into the bundle. The flashing was apparently caused by too little heat loss in that portion of the downcomer; therefore liquid flashed as the pressure decreased.

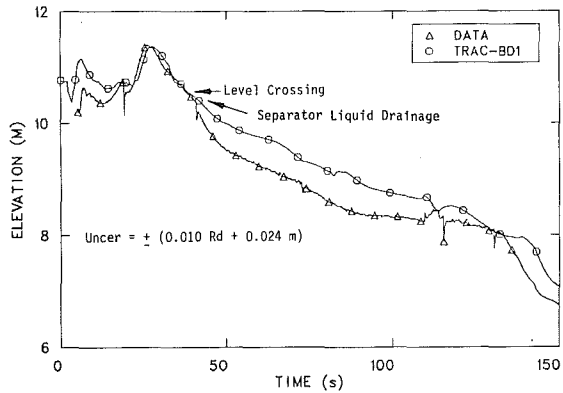


Figure 4. Comparison of calculated and measured downcomer level.

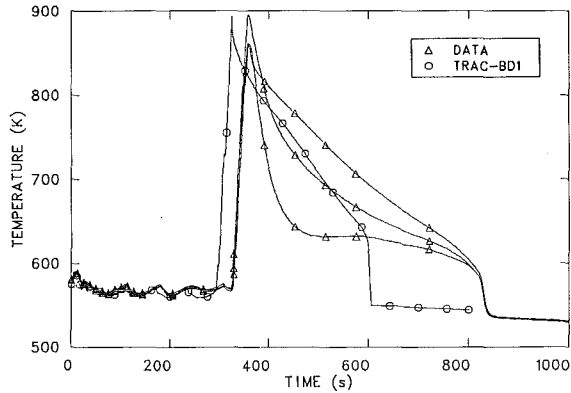


Figure 5. Comparison of calculated and three typical measured heater rod temperatures at 2.972 m (117 inch) level.

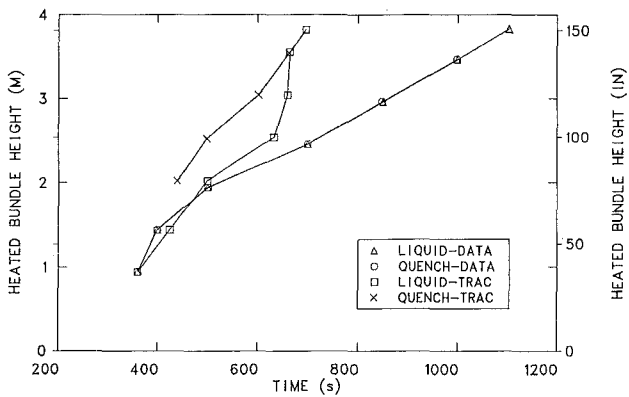


Figure 6. Comparison of calculated and measured heater rod quench front and core liquid level.

CONCLUSIONS

TRAC-BD1/MOD1 was capable of calculating the thermal-hydraulic phenomena in the FIST facility during a power transient event. Both the natural circulation and downcomer liquid level were well calculated. The heater rod response and peak cladding temperature were also in good agreement with the data. Calculated system pressure matched the experiment well enough that pressure effects should be represented adequately for the neutronics package in TRAC when used for plant calculations. Quench front propagation and time to quench were not in good agreement with the data due to entrainment within the bundle. Modeling of subscale SRV systems should be undertaken with care due to the code limitation on the hydraulic diameter. It is suggested that the valve area and hydraulic diameter be sized during sensitivity runs using data or valve design conditions.

REFERENCES

1. D. D. Taylor et al., TRAC-BD1/MOD1: An Advanced Best Estimate Computer Code for Boiling Water Reactor Transient Analysis, NUREG-CR-3633, EGG-2294, April 1984.
2. A. G. Stephens et al., Full Integral Simulation Test Facility Description Report, General Electric, to be published July 1984.
3. W. S. Hwang et al., BWR Full Integral Simulation Test (FIST) Phase I Test Results, General Electric, to be published July 1984.

Work supported by the U.S. Nuclear Regulatory Commission, Office of Nuclear Regulatory Research under DOE Contract No. DE-AC07-76ID01570.

TRANSIENT CONDENSATION HEAT TRANSFER COEFFICIENT
EXPRESSIONS DURING AND AFTER BLOWDOWN*

Dale A. Schauer

Gesellschaft für Reaktorsicherheit (GRS) mbH
Köln GermanyLawrence Livermore National Laboratory
P.O. Box 808, L-125
Livermore, CA 94550, U.S.A.

ABSTRACT

Analytical expressions are presented for calculating condensation heat transfer coefficients during and after blowdown at specific locations in a containment structure. A forced convection model is used during and immediately after blowdown when much turbulence exists, and a free convection model is used after blowdown end when the turbulence subsides. The forced convection expression depends primarily on a turbulent velocity relationship which is dependent on the distance from the break. The free convection expression depends on the wall-mixture temperature difference and the ratio of air partial pressure to total air-steam pressure. Experimental results were used to refine both of these expressions. Recommendations are given on how they are to be used. Calculations are compared with experimental values.

INTRODUCTION

During a loss of coolant accident (LOCA), the blowdown effluent results in a pressure increase of the atmosphere inside the reactor containment structure. This pressure rise could possibly damage the containment structural integrity and allow the release of radioactive material into the environment. The maximum pressure is highly dependent on the heat transfer from the fluid to the interior surfaces of the structure. Condensation heat transfer is the dominant mechanism for energy removal from the incoming fluid. Therefore, an accurate estimate of the containment pressure response requires an accurate estimate of the condensation heat transfer coefficient during blowdown.

At the start of blowdown, the containment air mixes in a turbulent manner with incoming steam. For a short time very high values are measured for the heat transfer coefficient which are typical of dropwise condensation. However, shortly thereafter as the surfaces become covered with water from the condensing steam, and the wall temperature increases, the heat transfer mechanism is dominated by filmwise condensation. After

* Completed at Gesellschaft für Reaktorsicherheit (GRS) mbH (Köln) while on research leave of absence from Lawrence Livermore National Laboratory, Livermore, California.

blowdown ends, the high mass flow rate ceases and the containment atmosphere becomes less and less turbulent. During this time free convection condensation dominates which is dependent on the mass ratio of air to air and steam.

A review of heat transfer coefficient values (h-values) in a LOCA completed by Slaughterbeck⁽¹⁾ recommended the use of the Tagami-Uchida^(2,3) correlation to determine the containment pressure response for reactor licensing assessment. This approach provides an average h-value to be used for the entire containment structure and generally results in calculated pressures greater than those measured. For a more detailed multi-room model, a h-value that could vary depending on location would enable a more realistic calculation.

FORCED CONVECTION CONDENSATION

The filmwise condensation model by Whitley⁽⁴⁾ considers a liquid film forming on a vertical wall at uniform temperature and then running downwards. The analysis assumes laminar flow in the liquid but turbulent flow in the vapor and a ripple free liquid-vapor interface. The resistance through the liquid layer is small compared with that through the vapor. A closed form solution is presented that contains a velocity term. The solution applies to arbitrarily oriented surfaces for irregular dropwise and filmwise condensation because for forced convection, gravity plays a major role in the steam condensation. When the solution was evaluated using experimental data, it was observed that many of the temperature varying properties were nearly self compensating. Also, it was found that a log-term could be closely approximated by the wall-atmosphere temperature difference multiplied by 0.051. This simplified the equation to only 3 terms, velocity, characteristic length and density.

This solution was compared with local experimental h-values from various test facilities^(5,6,7) for times through blowdown to 300-600 seconds afterwards. When the h-values were referenced relative to the distance from the break, it was noted that the maximum h-values were proportional to $z^{-2.5}$, where z is the distance in meters from the blowdown break location.

When using the experimental h-values in the closed form solution, to determine the turbulent velocity, it was observed that the velocity could be defined as a function of the distance from the break. During blowdown, the velocity was relatively constant but decreased exponentially with time after the end of blowdown. Combining the velocity relationship with the closed form solution yields the following equation for the condensation heat transfer coefficient during and immediately following blowdown. Here L is the film length (m), ρ is the containment atmosphere density (kg/m^3), and t_b is the end of blowdown time (s). In these expressions the velocity term is enclosed by square brackets. Containment velocity measurements⁽⁸⁾ made in a small opening (800x600mm) between the break room and an adjacent room were used to refine the velocity term. At 0.2 seconds after the start of blowdown, the maximum measured velocity was 160 m/sec, but at 2 seconds had decreased to 60 m/sec, at 18 sec to 30 m/sec and at 28 sec to 16 m/sec. Therefore, the velocity term was modified to limit the maximum velocity to 35 m/sec which is in the range of reasonable measured containment velocities.

$$h = \frac{630}{L^{0.2}} \rho \left[\frac{7045}{z^{3.6} + 200} \right]^{0.8} \text{ (during blowdown)} \quad (1)$$

$$h = \frac{630}{L^{0.2}} \rho \left[\frac{7045 e^{-0.054(t-t_b)}}{z^{3.6} + 200} \right]^{0.8} \text{ (for } t > t_b) \quad (2)$$

Experimental values for L, z and density were used in eq (1) to calculate maximum h-values (W/m²K) during blowdown and compared with experimental values as shown in Figure 1.

FREE CONVECTION CONDENSATION

After the end of blowdown the turbulent steam-air atmosphere quickly attains more or less still conditions and the heat transfer is dominated by free convection. When vapor and a non-condensable gas are present, the vapor (steam) must diffuse through this gas film to reach the cold surface. Henderson and Marchello⁽⁹⁾ performed a controlled experiment with steam-air and toluene-nitrogen mixtures condensing on a horizontal pipe. Experimental data from HDR, Marviken, and Battelle allowed evaluation of their h-expression, as well as a comparison to the actual experimental values as shown in Figure 2. In this figure, H is the ratio of the actual h (W/m²K) to the Nusselt h for the pure condensable. Y was calculated by estimating the partial pressure of steam assuming saturated steam at the measured bulk temperature. This value was subtracted from the bulk pressure to obtain the air partial pressure and then divided by the containment pressure to give Y. For the experimental conditions representative of the blowdown environment, the limited property variations allowed the Nusselt h to depend only on D (m), the characteristic dimension (water film length) and the temperature difference (K) between the bulk atmosphere and the wall surface. It was found that a value of 66 produced a good fit to the data. This was slightly larger than 51 as suggested by Henderson and Marchello. It is possible that the difference was due to the sharp contrast of the clean glass cylinder compared to the containment structure with its dust and other debris. The final free convection condensation expression in simplified form is given by,

$$h = \frac{8100}{1 + 66 \frac{P_A}{P}} \left[\frac{1}{D(T - T_W)} \right]^{0.25} \quad (3)$$

Eq (3) can be used to estimate h at times long after blowdown, or in rooms far removed from the break during blowdown. It is valid only when there is no turbulence in the atmosphere and for conditions of condensation formation on the structure walls.

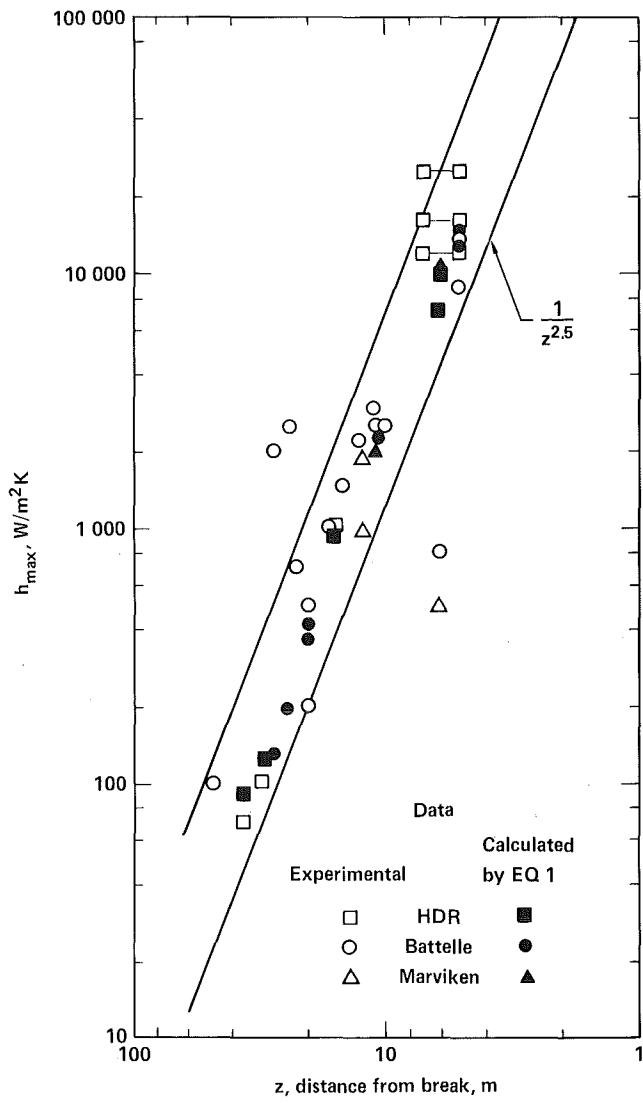


Fig. 1: Comparison between experimental and calculated maximum heat transfer coefficient

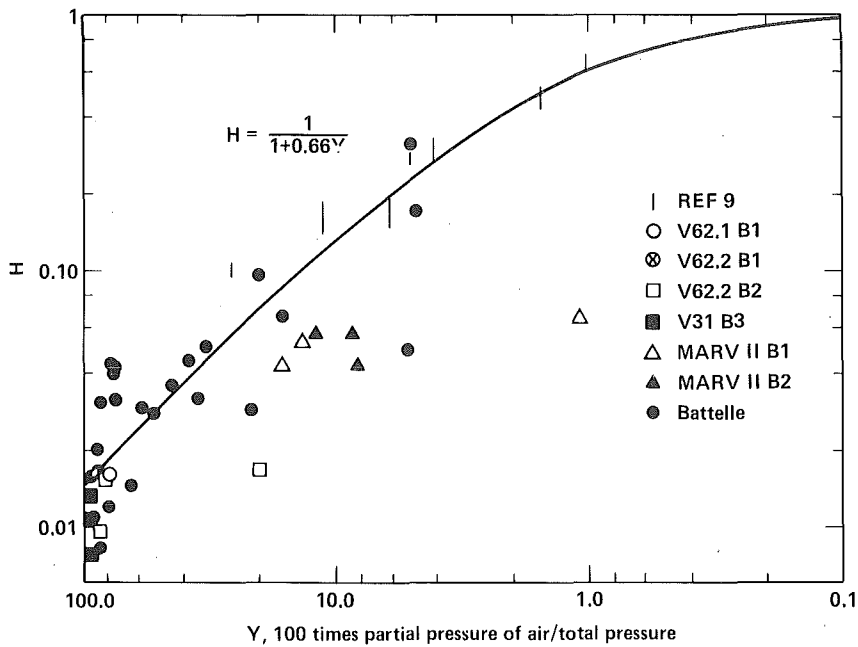


Fig. 2: Heat transfer ratio for filmwise condensation under conditions of free convection for a steam-air mixture

COMPARISON OF h -EXPRESSIONS WITH EXPERIMENTAL DATA

Equations (1) and (2) were used to calculate h -values during and immediately after blowdown when turbulence dominates. Eq (3) was used after blowdown end or when conditions are characteristic of free convection with condensation. A transition time was defined as the time at which the h -value calculated by eq (2) is equal to that simultaneously calculated by eq (3). Figure 3 shows a qualitative plot of the h -values and equations during and long after blowdown.

Figures 4-6 compare calculated h -values with experimentally measured h -values at various distances from the break. These distances are $z = 5\text{m}$, 11m and 31m . Note that the transition time occurs nearer blowdown end as the distance from the break increases. These examples show that the condensation expressions adequately represent the actual measured data. Typically, the greatest differences are at early time near the break location. Considering that the experimental data is from different test facilities with differing measurement systems and experimental design, the agreement is quite good.

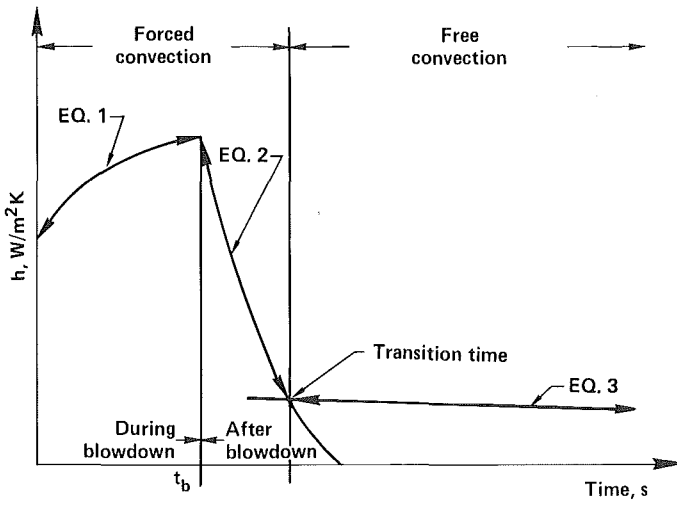


Fig. 3: Heat transfer coefficient indicating time that equations 1, 2, and 3 apply

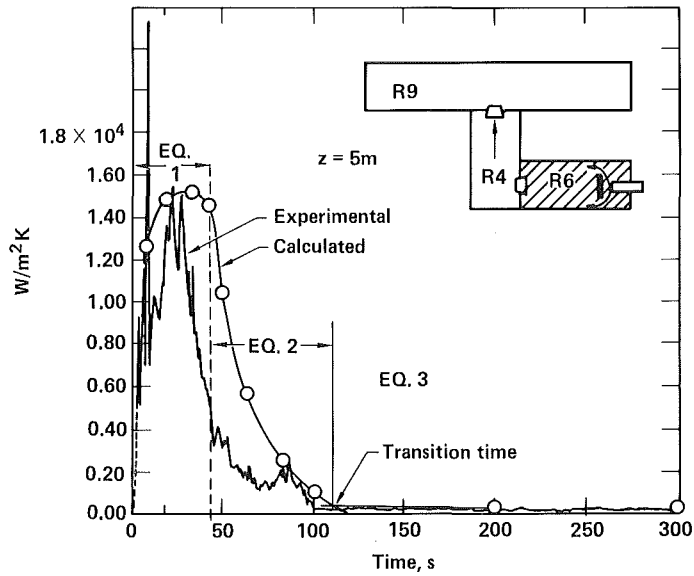


Fig. 4: Experimental and calculated heat transfer coefficient for Battelle D3 - Room 6

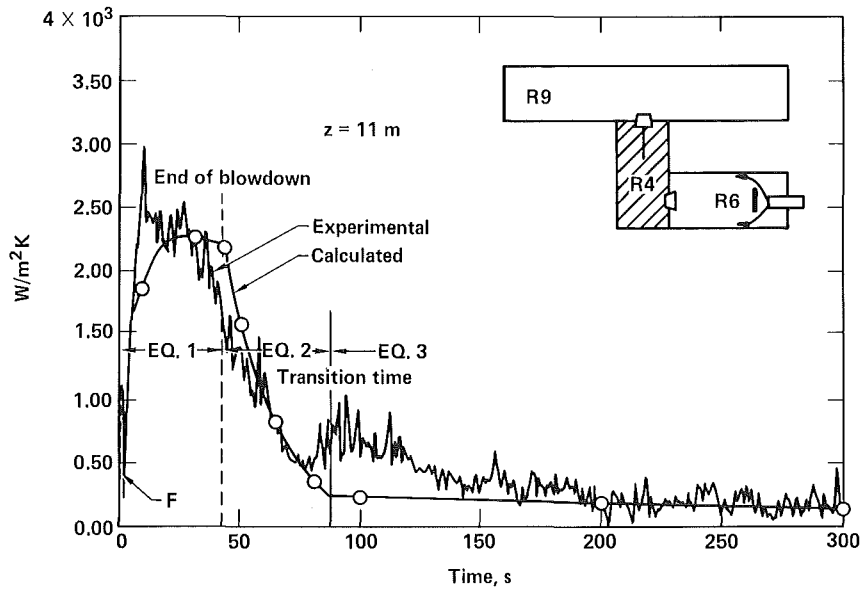


Fig. 5: Experimental and calculated heat transfer coefficient for Battelle D3 - Room 4

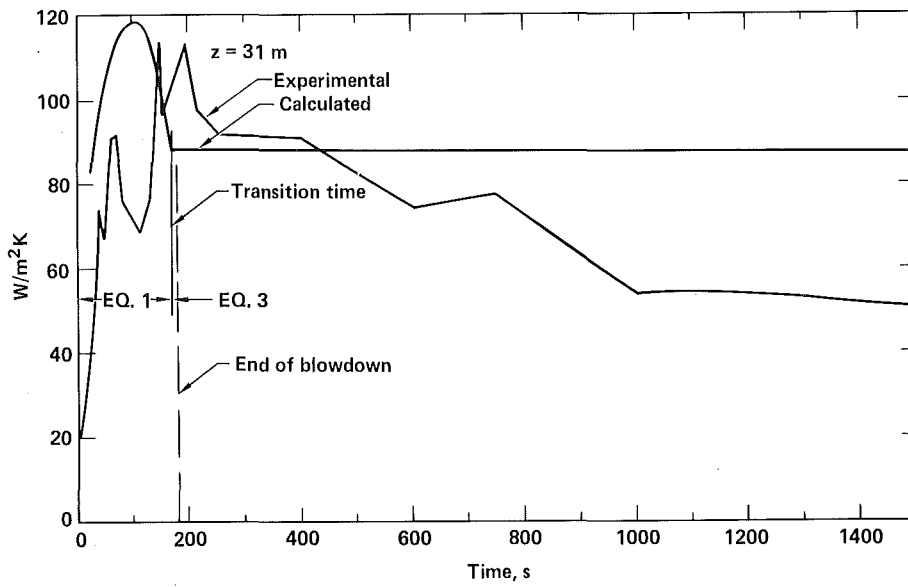


Fig. 6: Experimental and calculated heat transfer coefficient for HDR V62.2 Block 2

DISCUSSION

This analysis used data representing bare steel surfaces (HDR), painted concrete surfaces (Battelle and Marviken), and a painted steel liner on a concrete surface (Marviken). The heat transfer coefficient expressions presented are to be used without any special factor for painted concrete or steel. Comparisons of maximum h-values reported⁽⁷⁾ and those calculated for HDR⁽⁵⁾ suggest no significant difference between painted concrete and bare steel.

Others^(10,11,12) have reported conflicting opinions on this subject. This lack of consensus is in all probability due to the difficulty in determining the correct surface temperature from measurements located in the substrate material. For example, the temperature drop across a 0.15 mm paint layer ($k = .225 \text{ W/mK}$) for a typical early time heat flux of $2 \times 10^4 \text{ W/m}^2$ is 12°C . If the bulk fluid is at 120°C and the substrate surface is actually at 100°C one obtains $\Delta T = 20^\circ\text{C}$ when the 12°C ΔT in the paint layer is neglected, and a $\Delta T = 8^\circ\text{C}$ when it is not neglected. The experimental h-value ($h = Q/\Delta T$) is dependent on the true atmosphere-surface temperature difference. The above example results in a h-value ratio of 0.4 (1000/2500). This is the same ratio as that suggested for the difference between concrete and steel.

Equations (1) and (2) contain two variables L, and z and are valid for the walls as well as the ceiling. A value for L should be chosen that has physical significance in relationship to each containment room. As a first approximation, the radius of an equivalent spherical room volume should be used. The variable z, the distance from the break, also requires judgment. In a complex containment structure, the value chosen should represent a rather direct path from the actual break to the center of the room in question. In the break room, use the radius of the equivalent spherical volume. Equation (3) contains D. In practice one may choose to use the diameter of an equivalent volume for each containment room.

A final problem in judgment is estimating values for L and z in a simple one room model calculation. Until many one room calculations have been completed, one should use the diameter of an equivalent spherical volume of the entire containment for L, D and z.

CONCLUSIONS

1. The maximum value for h decreases in a well-defined manner as z increases.
2. During blowdown a turbulent velocity can be defined that is constant at a specific containment location.
3. Immediately following the end of blowdown, the turbulent velocity decays rapidly in an exponential manner.
4. At times after blowdown end, the heat transfer is characterized by free convection with condensation.
5. The expressions to use for h during and after blowdown is that which provides the largest value using eqs (1), (2), or (3).
6. The expressions defined estimate values of h that show reasonable agreement with those determined experimentally.
7. These expressions enable realistic local values to be estimated for h in a large break.

REFERENCES

- (1) D. C. Slaughterbeck, Review of Heat Transfer Coefficients for Condensing Steam in a Containment Building Following a Loss-of-Coolant Accident, Idaho Nuclear Corporation, Rep. No. IN-1388, 1970
- (2) T. Tagami, Interim Report on Safety Assessments and Facilities Establishment Project in Japan for Period Ending June 1965, (No. 1). Unpublished work.
- (3) H. Uchida, A. Oyama, Y. Togo, Evaluation of Post Incident Cooling Systems of Light-Water Power Reactors, Proc. of the 3rd Int. Conf. on the Peaceful Uses of Atomic Energy (Held in Geneva, August 31-Sept. 9, 1964), Vol. 13, N.Y. United Nations, 1965 (A/Conf. 28/P/436) pp 93-104.
- (4) R. H. Whitley, C. K. Chan, and D. Okrent, On the Analysis of Containment Heat Transfer Following a LOCA, Annals of Nuclear Energy, Vol. 3, 1976, pp 515-525.
- (5) B. Böhm and H. Lorenz, Experimentelle Bestimmung der Wärmeübergangskoeffizienten im Containment bei den HDR-Blowdown-Versuchen V 62.1/2 HDR-Sicherheitsprogramm - EV 3000, Battelle Report BF-R-63.690-1 (PHDR-Nr. 12-80) Dec. 1979.
- (6) Blowdown 11 Results, the Marviken Full Scale Containment Experiments, Containment Response to a Loss of Coolant Accident, Joint Reactor Safety Experiments in the Marviken Power Station, Sweden, Nov. 1973, U.S. Atomic Energy Commission, Washington D.C. 20545, Report No. MXA-1-211.
- (7) B. Böhm and H. Lorenz, Bestimmung der Wärmeübergangskoeffizienten aus den Modellcontainment-Versuchen der Reihe D Battelle Report BF-RS 50-23-3, August 1979.
- (8) D. Barschdorff and M. Neumann, Einsatz der Infrarotabsorptionsmesseinrichtungen und Messergebnisse bei den Versuchen V 62.1 und V 62.2, Institut für Thermische Strömungsmaschinen, Universität Karlsruhe, Oktober 1979.
- (9) C. L. Henderson and J. M. Marchello, Film Condensation in the Presence of a Noncondensable Gas, Journal of Heat Transfer, Trans. ASME, Aug. 1969 pp. 447-450.
- (10) A. Kolflät and W. A. Chittenden, A New Approach to the Design of Containment Shells for Atomic Power Plants, Proceedings of Amer. Power Conf., Vol. 19, (1957) pp 651-659.
- (11) P. Griffith and M. S. Lee, The Effect of Surface Thermal Properties and Finish on Dropwise Condensation, Int. J. Heat Mass Transfer, Vol. 10, 1967, p. 697.
- (12) J. W. Rose, Effect of Condenser Tube Material on Heat Transfer During Dropwise Condensation of Steam Int. J. Heat Mass Transfer, Vol. 21, 1978, pp. 835-840.

MULTIVENT EFFECTS IN A LARGE SCALE
BOILING WATER REACTOR PRESSURE SUPPRESSION SYSTEM*

Edward W. McCauley

Lawrence Livermore National Laboratory
Livermore, California 94550, U.S.A.

E. Aust and H. Schwan

GKSS-Forschungszentrum Geesthacht GmbH
D-2054 Geesthacht, FRG

ABSTRACT

The steam-driven GKSS pressure suppression test facility, which contains 3 full scale vent pipes, has been used for 5 years to investigate the postulated loss-of-coolant accident in a Mark II and Type 69 boiling water reactor. Using the results from several of these tests, wetwell boundary load data (peak pressures and spectral power) during the chugging stage, have been evaluated for "sparse" pool response (one and two vents in the three vent pool) and for "full" pool response (one, two, or three vent operation in pools of constant wetwell pool area per vent). The "sparse" pool results indicate the pool-system, chug event boundary loads are strongly dependent on wetwell pool area per vent, with the load increasing with decreasing area. The "full" pool results show a substantial increase in the pool-system, chug event boundary loads upon a change from single cell to double cell operation; only minor change occurs in going from double to triple cell operation.

INTRODUCTION

The postulated loss-of-coolant accident (LOCA) in a commercial boiling water reactor (BWR) has been the subject of extensive and detailed international study for several years. Because of its complex thermodynamic nature, the most fruitful information regarding the related two phase condensation phenomena and dynamic load production of the LOCA has come from full-scale tests.

*This work was supported in part by the United States-Nuclear Regulatory Commission under a memorandum of understanding with the United States Department of Energy.

Experimental results from full scale, "single cell", one vent tests have provided an important data base for design of reactor containment structures. The actual reactor system, however, contains about 70-100 such vent pipes and therefore much effort has gone into study of the relation between one vent "single cell" test results and the expected behavior of an actual multivent system. The small scale (1:7.5) concrete cell tests of Kraftwerk Union¹ provided, for that scale, information regarding dynamic loading resulting from tests with 1, 2 or 6 vents operating in a 10 vent pool as well as results from tests using "full" pools containing 2, 6 and 10 vents. These small scale tests (80 mm diameter vent pipes) tended, in a qualitative sense, to confirm the conservative nature of full scale "unit cell" tests. Lack of complete scaling of the two phase flow in this small system prevented quantified confirmation.

The GKSS-PSS tests reported here, were conducted in a three vent test facility² shown schematically in Fig. 1. The full scale (600 mm diameter) vent pipes have an L/D ratio of 11.3-18.1. In a KWU type 69 containment, L/D is ca. 18.7; in a G.E. MK-II, the L/D is ca. 23. The standoff distance (vent exit to pool floor) is one meter in the GKSS facility; for a plant it is ca. 2 meters. The vent pipe lengths and standoff distance of the test facility are considered sufficient, however, to avoid distortion of the two phase flow and resulting condensation effects at the vent exit during the chugging stage. (This is particularly so with regard to the standoff distance since the condensation-induced rarefaction, which excites the pool-system frequency and gives rise to the higher frequency dynamic loads seen during chugging, occurs inside each vent pipe near its exit /3/, rather than below the vent pipe. The shorter vent pipes of the GKSS-PSS facility increase the acoustic (organ-pipe) frequency over that expected in a plant, where the acoustic frequency is expected to be ca. 8-10 Hz. In the PSS tests this frequency is found to be ca. 12-14 Hz from vent A and 16-18 Hz from vents B and C. This acoustic frequency, observable in both pool and boundary pressure histories, is characteristic of the condensation oscillation stage (CO) and is often triggered in a steam filled vent pipe during the chugging stage. According to the schematic of Fig. 1, the 3.8 m deep wetwell pool provides a uniform vent submergence depth of 2.8 m, typical of plant design, so that no distortion due to pool pressure-head effects are expected.

The pool-system frequency is that facility dependent frequency which is excited by the steam-ring collapse (condensation). It is in this domain that the strong chugging loads are found. The pool system frequency of earlier single-cell and multivent experimental studies has ranged from 14-52 Hz. The GKSS-PSS pool-system frequency has been both observed and measured to be about 38 Hz. The GKSS-PSS facility thus provides an adequate basis for tests investigating further the multivent effect (MVE).

SELECTION OF EXPERIMENTS AND DATA

This study into the multivent effect is based on four tests selected from the larger GKSS-PSS test series. These tests were conducted under similar thermodynamic conditions, using no drywell preheat. The analysis matrix is shown in Table 1.

The results of several repetitions of the standard-conditions test M1 show that although the CO to chugging transition time may vary, for a given time into a blowdown the chugging character of a test type (which decreases in strength and frequency with time) is effectively reproducible. This observation suggests that evaluations of simulated LOCA tests, intended to investigate a multivalent effect, could become substantially distorted if only the strongest chug events from selected tests were evaluated. Rather it appears necessary to investigate under conditions of constant mass flux in the vent pipe(s).

The threshold mass flux for onset of the chugging stage in the GKSS-PSS tests is about $10 \text{ kg/m}^2\text{s}$. Because the in-vent steam flux decreases with time in a simulated LOCA experiment, and more rapidly with a larger delivery orifice, efforts to provide evaluations within a reasonably narrow band of mass flux dictate a shorter rather than longer evaluation time period. Therefore, to obtain a reasonable set of statistics with a nearly constant mass flux, ten successive chug events, beginning at a conveniently chosen steam mass flux of 5 or $3 \text{ kg/m}^2\text{s}$, were evaluated for each of the selected tests.

Table I. TEST MATRIX FOR DATA EVALUATION

Test No.	Active Vents No.	Vents Name	Steam Orifice Dia.,mm	DW vol. per vent m^3	WW area per vent m^2	WW air vol. per vent m^3	Special Features
M1-5	3	A,B,C	100	19.9	5.4	23.7	(a)
Z1-AB	2	A,B	70	29.2	8.1	36.3	(b)
E1-A	1	A	50	56.9	16.2	74.0	(c)
M1-Z.B-2	1/2	B/A,C	100	19.9	5.4/5.4	23.7/23.7	(d)

- a) standard or basis test
- b) vent pipe C blocked
- c) vent pipes B and C blocked
- d) "unit cell" boundary placed around vent B

Thermodynamic conditions for these tests were:

initial water mass in steam generator	7600 kg
steam source	319 C, 111 bar
initial drywell/wetwell pressure	1 bar
initial drywell/wetwell temperature	25 C
final drywell/wetwell pressure	2 bar

The evaluated results are based on pressure histories measured on the submerged wetwell boundaries. As shown in Fig. 1, the primary "load" is taken as pressure, measured on the wetwell floor directly under each of the three vent pipes. In addition, one wall pressure history measured at vent-exit level is also included. The dynamic pressure data which provide the basis for these evaluations are PCM data digitized with a time step of 0.15 ms after being low-pass filtered at 1600 Hz; no further data filtering is imposed.

Because of the strong and variable nature of the frequencies resulting from chugging events, our analyses of the boundary pressure histories also include development and study of the power spectral density (PSD). For a time window of about 0.75 s, the complete original data are analyzed for each chug event. The pool-system peak overpressure and peak underpressure are determined relative to the local prechug event mean pool pressure.

EVALUATION OF THE EXPERIMENTAL DATA

Loading in the three-vent pool with one, two, or three active vents

Figure 2 shows, on identical ordinate scales, the peak overpressures (POP) and peak underpressures (PUP) from tests M1-5, Z1-AB and E1-A plotted versus the nominal time of rarefaction for each event. These data indicate a clear and systematic reduction in boundary pool-system loading as the number of active vents in the three vent pool is decreased. The data also demonstrate a strong periodicity of the chug strength with time.

Loading in one-, two-, and three-vent pools

In order to further study the multivent effect, the PSS facility was modified by placement of a steel single-cell boundary around vent B. This provided a wetwell configuration suitable for conducting simultaneous double cell and single cell tests; each vent pipe has a pool area of 5.4 m². The geometry of this modified wetwell and the location of the pressure transducers used to evaluate its response are shown in Fig. 3. In general, the same measurement evaluation method is applied; however, the floor transducers PA42 and PA50, along with the lateral boundary transducer PA43, are now associated only with the double cell (vents A and C) operation. For the single cell (vent B), floor transducer PA47 and a new lateral boundary transducer PA56 are used in the evaluations.

The peak over- and underpressure from the one-, two-, and three-vent "full pool" tests plotted against the rarefaction time, are shown in Figs. 4a and 4b. These data indicate a somewhat stronger response from the two-vent pool than from the three-vent pool. The one-vent pool response is rather weaker than in either the two- or three-vent pools.

DISCUSSION OF RESULTS AND CONCLUSIONS

This study into the multivent effect is perhaps the first to be based on well modeled, steam driven LOCA experiments conducted with full scale vent pipes.

Evaluation of both floor and wall boundary data taken from selected GKSS-PSS multivent experiments indicates a pronounced multivent effect exists during the chugging stage of a postulated loss-of-coolant accident.

Consideration of the peak overpressure and underpressure (POP and PUP) or chug event spectral power shows that for steam mass fluxes of 5 to 3 kg/m² s the chug strength is strongly cyclic in time with, in general, a strong chug being followed by a weak chug (or vice versa). From the viewpoint of boundary pressure, the multivalent effect has been observed in several ways. First, the mean peak differential boundary pressure is found to increase monotonically, and with an increasing slope, with a decrease in pool-area-per-vent. Second, the mean peak differential boundary pressure tends to increase with an increase in the number of vents-per-full-pool (constant pool-area-per-vent). Both of these effects are consistent for overpressure and for underpressure. In addition, study of the power spectral density associated with the chug events indicates not only a consistency in these findings with regard power delivered to the boundaries, but also a strong variability in the relative frequency content from the boundary loads produced by the consecutive chug events.

LIST OF REFERENCES

1. KWU-Reaktortechnik (Hrsg.), "Forschungsprogramm Reaktorsicherheit: Kondensation V, Teil II - Betonzellenversuche", unveröffentlichter Abschlußbericht zum Förderungsvorhaben BMFT RS 78 E, KWU-RE 23/016/78, Erlangen (July 1978).
2. E. Aust, H. D. Fürst, H. R. Niemann, "Basisprogramm über experimentelle Untersuchungen an Ein- und Mehrrohranordnungen für Druckabbausysteme von Kernkraftanlagen", GKSS 79/E/8, Geesthacht (February 1979).
3. E. McCauley and G. Holman (LLNL), E. and Aust, H. Schwan, and J. Vollbrandt (GKSS), "The Physical Model of Lean Suppression Oscillation Phenomena-Steam Condensation in the Light Water Reactor Pressure Suppression System", presented at the International Nuclear Reactor Safety Heat Transfer Seminar, Dubrovnik, Yugoslavia, September 1980, Lawrence Livermore National Laboratory, Rpt. UCRL-84151 (April 1980).

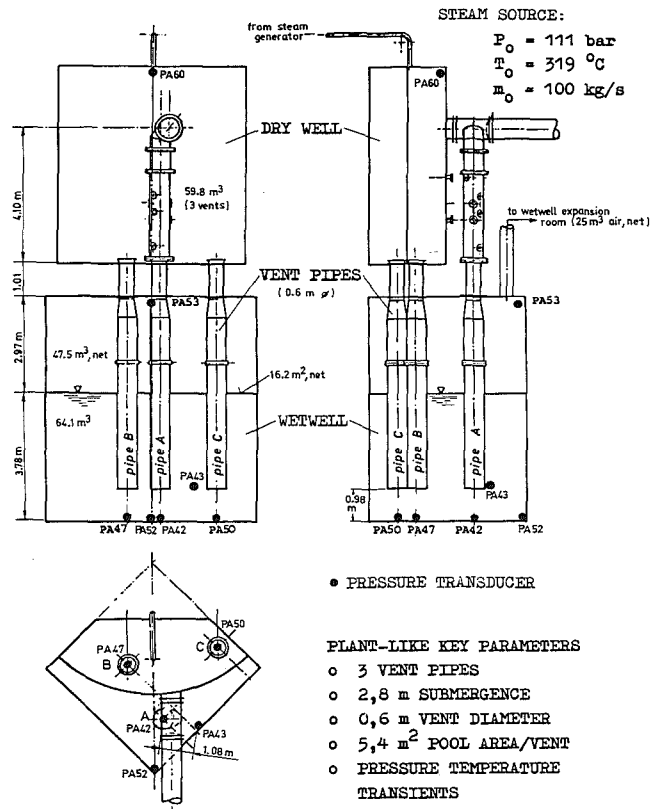


Fig. 1: GKSS Pressure Suppression Test Facility
 (steam generator and wetwell expansion room not shown)

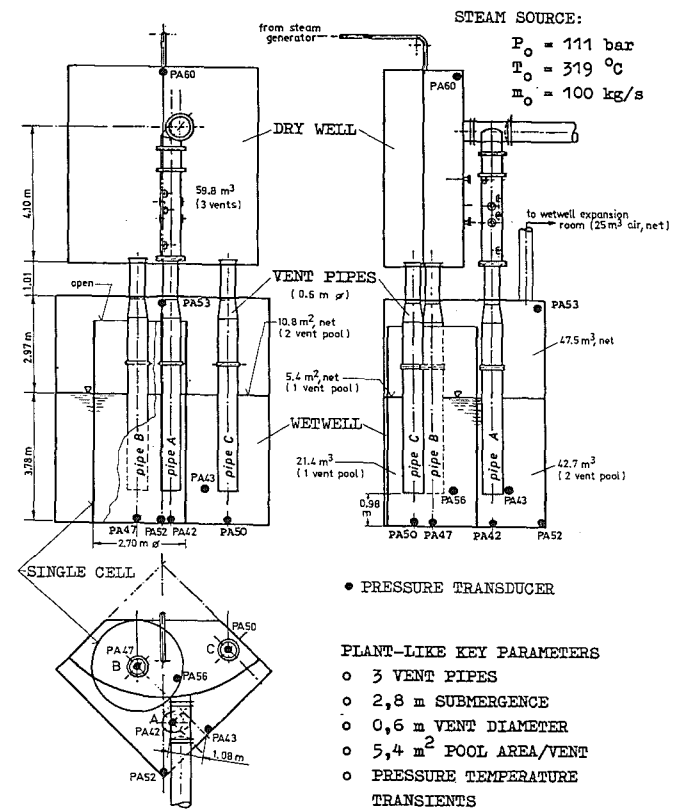


Fig. 3: Modified GKSS Pressure Suppression Test Facility
 (steam generator and wetwell expansion room not shown)

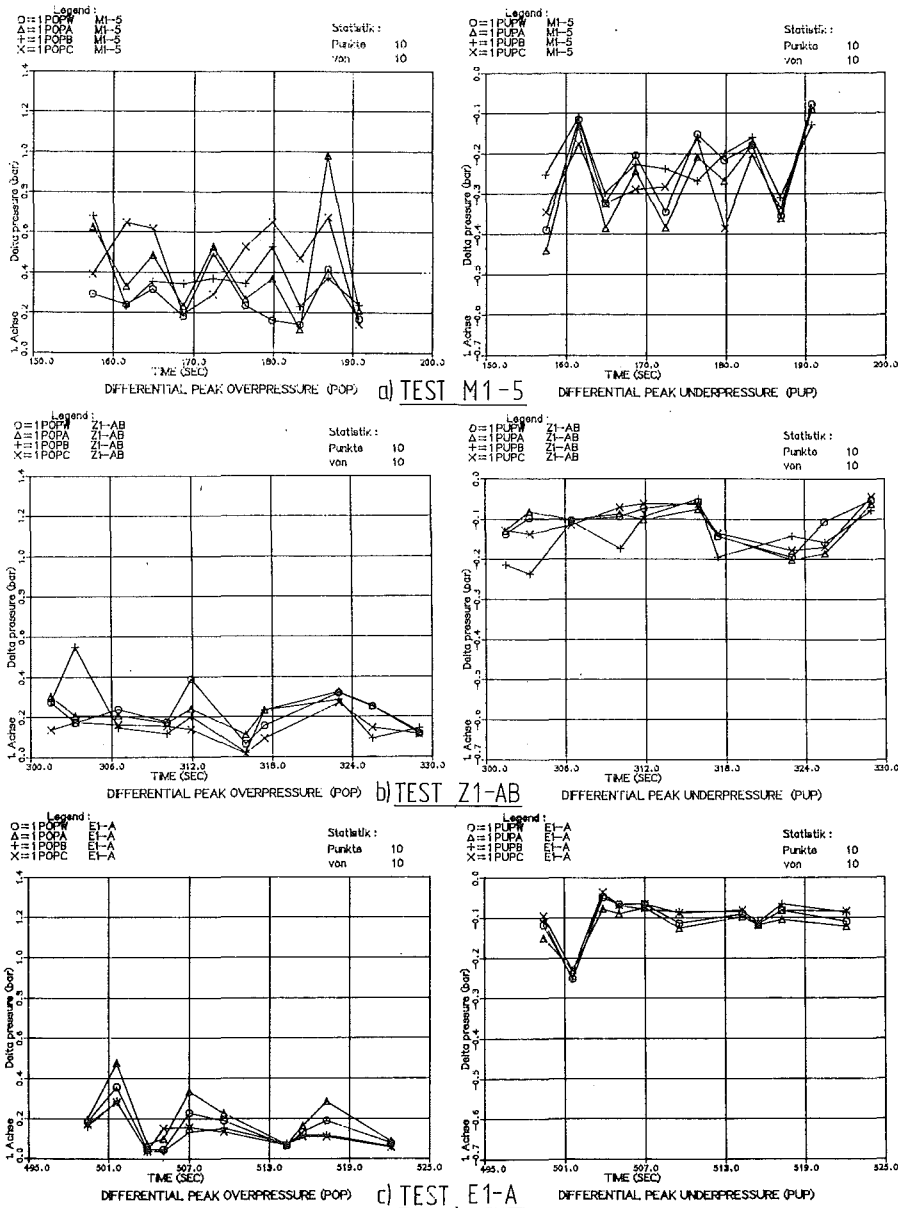


Fig. 2: History of peak pressure in the three vent pool
 $\phi_s = 5 \text{ kg m}^{-2} \text{ s}^{-1}$ (GKSS tests M1-5, Z1-AB, E1-A)

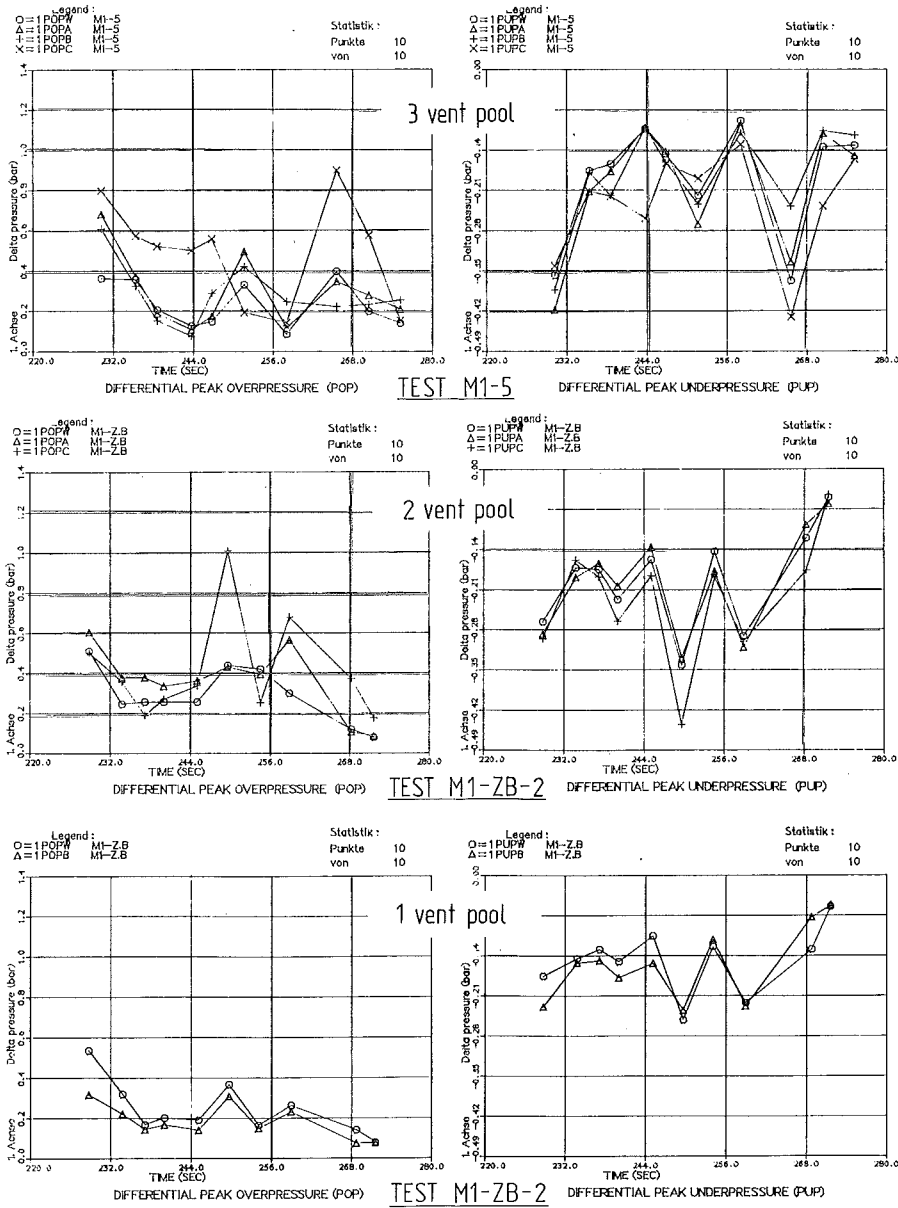


Fig. 4: History of peak pressure in the filled pool
 $\phi_s = 3 \text{ kg m}^{-2} \text{ s}^{-1}$ (GKSS tests M1-5, M1-ZB-2)

VERIFICATION OF THE 3-D, 2-FLUID, 3-FIELD CONTAINMENT CODE
COBRA-NC WITH HDR- AND BATTELLE-FRANKFURT DATA SETS

M.J. Thurgood
Battelle Pacific Northwest Laboratory
Richland, WA 99352, U.S.A.

K. Fischer and L. Wolf
Battelle-Institut e.V.,
Am Römerhof 35, 6000 Frankfurt/Main 90, FRG

ABSTRACT

Pressure differences between subcompartments in a nuclear reactor containment during blowdown are dependent upon intensity and direction of the blowdown jet, as well as upon the geometrical arrangement of obstacles in the jet vicinity. This was shown in recent HDR experiments. The computer code COBRA-NC was used to perform a pre-test calculation for the 3-D flow distribution in the break subcompartment for the first time as well as to simulate the entire containment flow distribution in a lumped parameter mode. Preliminary results are given for the 3-D calculation, helping to understand the flow structure and the deficiencies of the lumped-parameter approach. Results of the comparison between measured data and lumped parameter calculation are presented in detail.

INTRODUCTION

Recent HDR-containment experiments indicated a high dependency of differential pressure built-up and water carry-over through vent flow openings between containment subcompartments upon details of the break room internal flow structure. It was found, that the flow inside the break room is affected by subcompartment internal structures such as the jet impingement plate (distance and inclination with respect to break position) as well as local subcompartment flow resistances posed by metallic structures such as piping etc. These distributed effects cannot be a priori accounted for by present lumped-parameter containment codes used for design and licensing purposes. In fact, it could be shown that the selection process of important input parameters to those codes - although resulting in sometimes perfect agreement with data - does not rest on a concise physical rationale.

Besides of these unresolved issues, a variety of local special measurement techniques applied for the HDR-tests such as local heat transfer, local steam/air concentration and steam/air concentrations as well as droplet velocities within the vents connecting the break room with its neighbours have not been consistently assessed by computations simply because most of these phenomena necessitate highly local discretization as well as advanced fluid modeling. This situation calls for the application of a truly three-dimensional containment code with advanced best-estimate models for the fluid conditions expected in realistic containment atmospheres after LOCA. COBRA-NC is such a code.

DESCRIPTION OF COBRA-NC

The COBRA-NC computer code has been developed by the Battelle Pacific Northwest Laboratory for the U.S. Nuclear Regulatory Commission. It provides a two-component, two-fluid, three-field representation to allow the modelling of water and its vapor as well as a noncondensable gas mixture. The two-fluid capability is needed to account for condensation of steam in the containment atmosphere and on structural surfaces, containment sprays, pressure suppression pools etc. The three fields represent the vapor-gas mixture, the continuous-liquid phase and the liquid-drop phase. The continuous-liquid phase is used to model liquid films on containment structures, pools on containment floors and film built-up in vents, whereas the liquid-drop phase is used to model the two-phase blowdown jet, containment sprays as well as drop entrainment and de-entrainment between subcompartments. COBRA-NC features an extremely flexible noding scheme that allows the code to be run in a traditional lumped-parameter mode, one-dimensional, two-dimensional, three-dimensional mode or a mixture thereof, i. e. 3-D breakroom, 1-D vents, lumped-parameter for neighbouring rooms. The code has a finite-difference slab conduction model for structural heat conduction which allows to use any number of materials in each slab. A mixing-length turbulence model has been incorporated to model turbulent shear flows and turbulent diffusion of gas species due to concentration gradients.

COBRA-NC has been already assessed against a large set of experimental containment data. The present paper focuses on some selected applications in connection with recent HDR investigations.

THREE-DIMENSIONAL MODEL OF THE HDR BLOWDOWN SUBCOMPARTMENT

In order to study the effects of multidimensional flow patterns in the HDR blowdown room for HDR experiment T31.3, a three-dimensional model has been developed. Figure 1 shows a vertical plane of the model. The grid spacing ranges from 0.225 m to 1.0 m. In the upper section the locations of the blowdown nozzle and the impingement plate are indicated as they are represented by the computational grid. The model consists of 898 spatial control volumes and 81 heat slabs representing structural heat transfer surfaces.

The histories of mass and enthalpy discharge rates into the blowdown subcompartment were specified by PHDR based on past experimental evidence. Later evaluations of the mass flow data showed that the actual blowdown rate was up to 20 % lower than the pre-specified one. Therefore, the present results are of preliminary nature and are given without comparison to experimental data. The computations will be repeated with the corrected blowdown rate in the near future. However, important general features of the flow patterns in the blowdown room can already be observed on the basis of the present results.

The blowdown subcompartment is connected with its neighbours via a number of complex vent flow openings. The boundary conditions for these vents were taken from a separate lumped-parameter model calculation of the entire containment. This calculation was similar to the one described in the subsequent section.

The three-dimensional model calculation was carried out up to a point in time of 0.113 s within 1 hour of CRAY-1 computer time. During this time period, pure steam discharge occurs in the blowdown nozzle. Figure 2 shows a horizontal plane of the upper model section with the impingement plate representation. At the time of 0.113 s, about half of the break subcompartment space is filled with steam. Near the main vent, a homogeneous pressure of 2.1 bar is calculated which is higher than the calculated pressure in the blowdown room of the lumped-parameter model (1.85 bar). One possible reason for this difference is the lower heat removal by structures in the 3-D model, because only half of the structures has come in contact with steam at the time of 0.113 s. The local pressure in the area where the deflected jet hits the wall is enhanced to maximum of 3.3 bar. Figure 3 shows some horizontal steam velocities in the upper section. The deflected blowdown jet causes some additional entrainment flow into the lower right corner of the room. The approach velocities of the main vent are much larger in the lateral direction (92 m/s) than in the straight direction (32 m/s). This means that a certain increase of the vent loss coefficient may be expected, resulting from an enhanced dynamic restriction of the flow path due to non-uniform inflow conditions.

Further applications of the 3-D model shall be undertaken with the corrected discharge rates, extending the model time up to the occurrence of droplet flow (0.5 s).

LUMPED-PARAMETER MODEL OF THE HDR CONTAINMENT

As a contribution to the International Standard Problem No. 16, a lumped-parameter post-test prediction of HDR experiment V44 was performed. The control volumes and flow paths of the model are shown in figure 4. Some of the control volumes were further subdivided into two or more nodes. The model comprises a total of 81 nodes in 9 vertical sections, together with 112 heat slabs. A transient of 5 s model time took 154 s of computer time on a CRAY-1.

Vent flow loss coefficients were taken as specified by GRS except for the vents ÜÖ 140 and 143 where an enhanced coefficient was used in order to account for the additional flow resistance caused by the blowdown jet. For the two-phase part of the blowdown jet, a drop size of 200 μm was specified. For the base case calculation, it was assumed that no drop deposition occurred in the vents. Steam condensation at the structures was calculated according to the Uchida correlation.

The enthalpy history of the blowdown jet specified by PHDR between 0.3 s and 2 s was slightly modified to give a continuous steam discharge rate, which seems to be more realistic than the original values for ISP 16.

Figure 5 shows the comparison of calculated and measured pressure in the break compartment during 5 seconds after blowdown initiation. The experimental data show large scattering bandwidths caused by different measured pressure values at different locations induced by pressure waves and/or sensor vibrations. The calculated values tend towards the upper boundary of the measured data bandwidth.

Local pressure variations within the blowdown subcompartment as shown e. g. in figure 2 cannot be represented by a lumped-parameter model. Therefore, the pressure differences calculated in the lumped-parameter model are not strictly comparable to the experimental data which are locally measured quantities.

Figure 6 shows measured and calculated pressure differences adjacent to the blowdown subcompartment. Because the experimental reference pressure in the blowdown room shows considerable local variations, a better agreement between data and calculated results should not be expected.

The long-term pressure variation in the containment is displayed in figure 7 and shows excellent agreement between experiment and COBRA-NC. It can be concluded that the distribution of energy between steam, droplets, water films and structures is modeled in an acceptable way. The plot of the atmospheric temperature in the dome region, figure 8, shows that the lumped-parameter model does not fully represent the mixing induced by natural convection currents at later time, thus giving a too low temperature in the upper region. It would be possible to reach some improvements in the calculations by changing the noding connections; however, the only safe way of predicting the actual mixing process would be to use a finite difference model with a large number of nodes.

Additional informations about COBRA-NC application to the HDR-experiment V44 and a detailed discussion of the results of sensitivity studies are contained in /1/.

CONCLUSIONS

The computer code COBRA-NC has been verified for lumped-parameter and multidimensional mode applications. Due to lack of space, comparisons of hydrogen distribution experiments with COBRA-NC calculations cannot be shown in the present paper. The interested reader is referred to /2/. Parameter variations have been performed to show the model sensitivity to the major input variables. The model results lead to an improved understanding of the thermohydraulics in a containment.

REFERENCES

- /1/ M.J. Thurgood, "COBRA-NC Post Test Prediction for HDR Steam Blowdown Test V44 (International Standard Problem 16)". NUREG/CR-3749, May 1984.
- /2/ M.J. Thurgood, "COBRA-NC: An Advanced Containment Code", Proc. 11th Water Reactor Safety Research Information Meeting, NUREG/CP-0048, Vol. 3, p. 361-399 (1983).

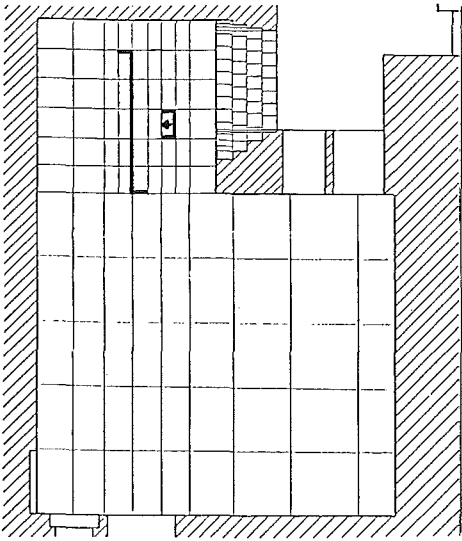


Figure 1. Threedimensional model grid of HDR blowdown room

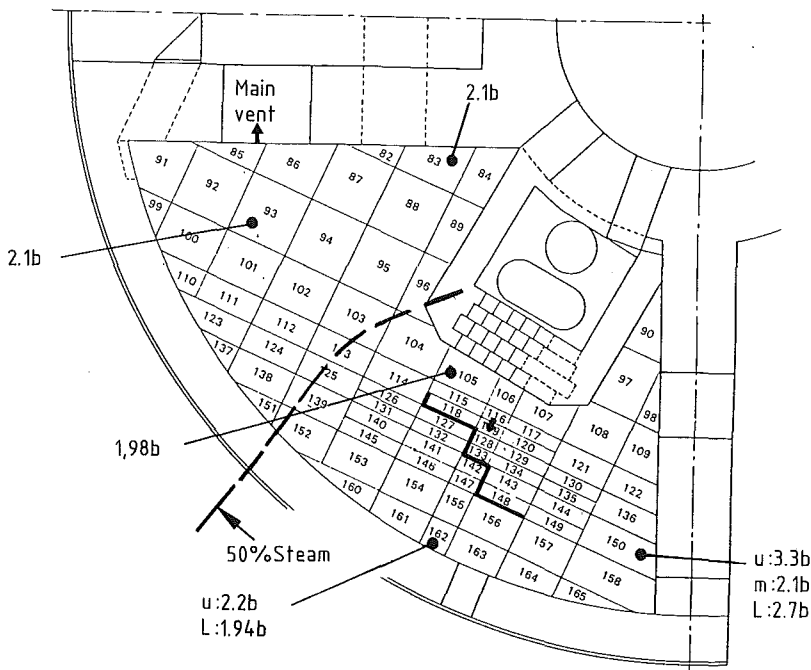


Figure 2. Horizontal distribution of pressure and steam in the upper section at time $t = 113$ ms
(u = upper, m = medium, l = lower level)

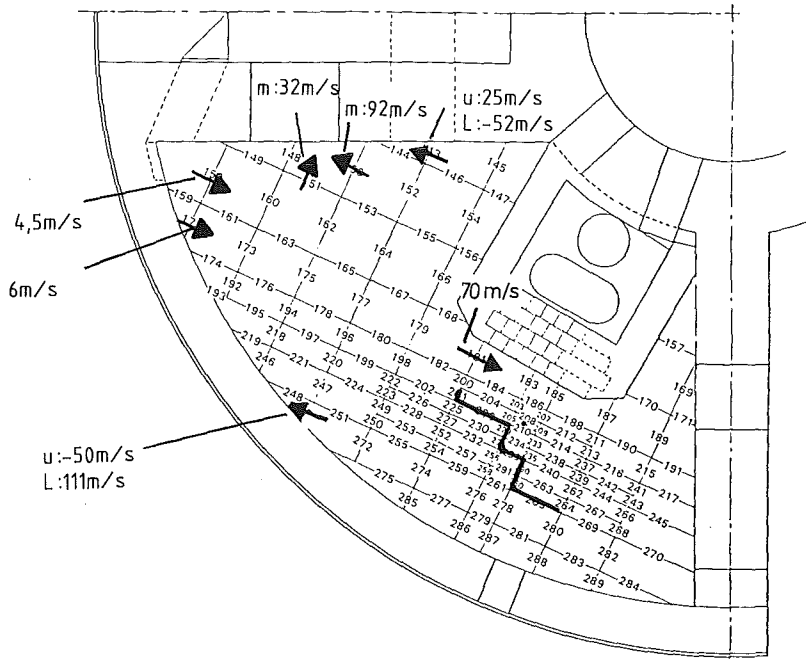


Figure 3. Horizontal velocity distribution in the upper section

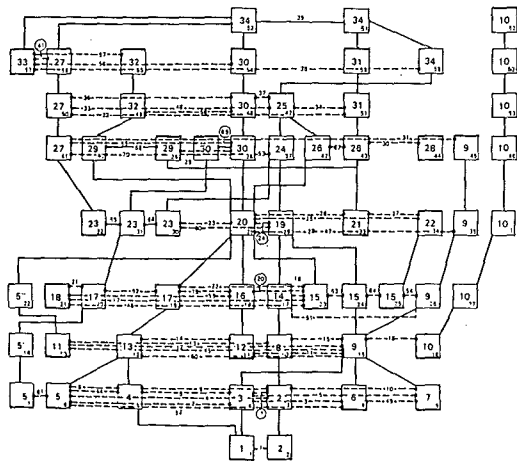


Figure 4. Lumped-parameter model of HDR containment

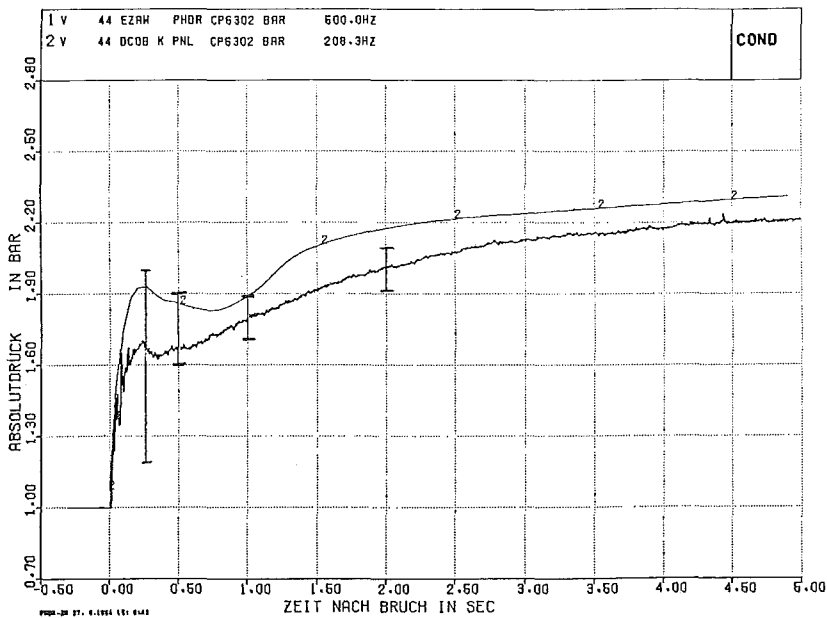


Figure 5. Pressure in the blowdown room

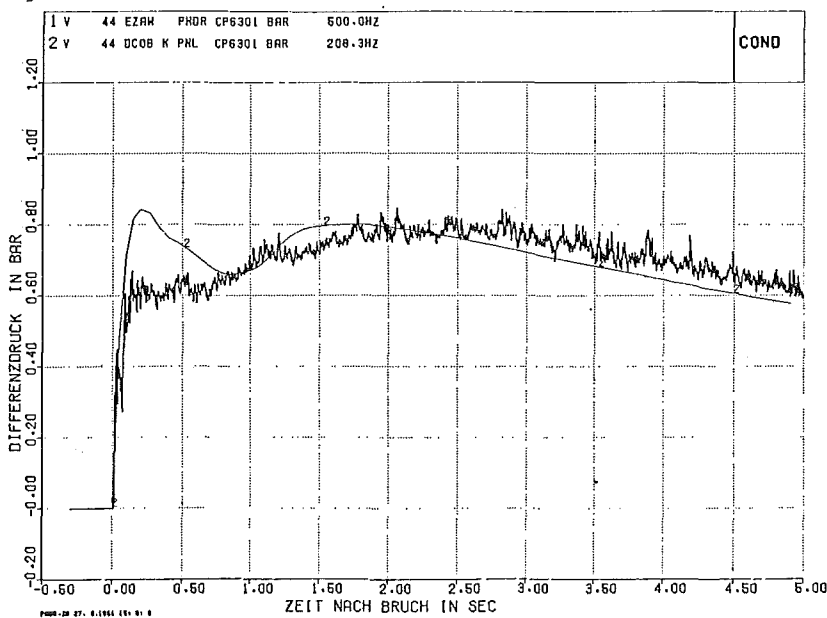


Figure 6. Differential pressure blowdown room - neighboring room R 1708

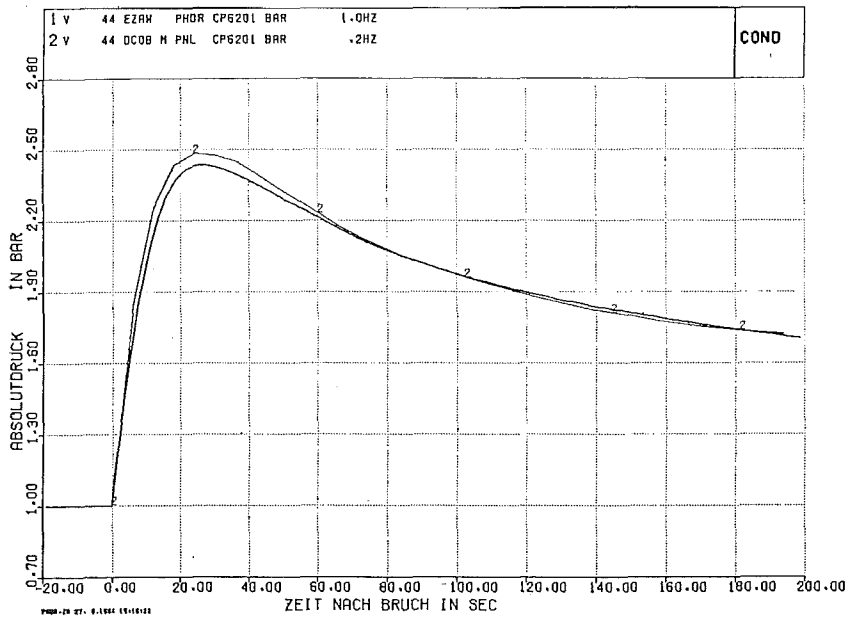


Figure 7. Containment pressure

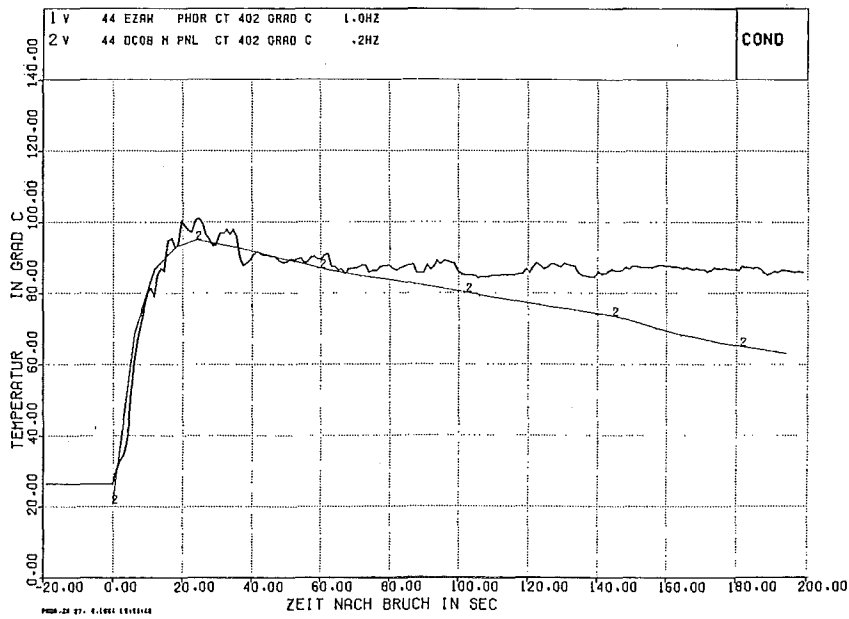


Figure 8. Atmospheric temperature in the dome region

Chapter 11

Probabilistic Risk Assessment

	pages
11.1 A. Thadani, F. Rowsome, T. Speis: Applications of Probabilistic Techniques at NRC	1881 - 1890
11.2 E.P. O'Donnell, T.J. Raney: A Proposed Approach to Backfit Decision-Making Using Risk Assessment and Benefit-Cost Methodology	1891 - 1897
11.3 L. Cave, W.E. Kastenberg, J.N. Tweedy: The Development and Application of Quantitative Methods in Licensing Nuclear Power Plants	1898 - 1907
11.4 M.P. Rubin, B. Atefi, D.W. Gallagher, R.T. Liner: Application of Probabilistic Risk Assessment Techniques as a Decision Tool in the U.S. Nuclear Regulatory Commission's Systematic Evaluation Program	1908 - 1917
11.5 H. Fuchs, L. Miteff: PRA - to what Depth? (The "Bed of Nails" Effect)	1918 - 1926
11.6 A.S. Benjamin, V.L. Behr, F.E. Haskin, D.M. Kunsman: Severe Accident Reactor Risks and the Potential for Risk Reduction	1927 - 1936
11.7 R.A. Bari, I.A. Papazoglou, W.T. Pratt, K. Shiu, H. Ludewig, N. Hanan: Severe Accident Analysis and Risk Assessment for two Boiling Water Reactors	1937 - 1946
11.8 J.E. Wells: Seismic Risk Assessment as Applied to the Zion Nuclear Generating Station	1947 - 1956
11.9 F.T. Harper, M.T. Drouin, E.A. Krantz: Classification of United States Light Water Reactors by Dominant Core Melt Frequency Contributors	1957 - 1966

- 11.10 G. Bars, J.M. Lanore, G. Villeroux: 1967 - 1973
Introduction of Operator Actions in the Event Trees
- 11.11 G. Ericsson, S. Hirschberg: 1974 - 1982
Treatment of Common Cause Failures in the Barsebäck 1
Safety Study
- 11.12 J.C. Luxat, A.P. Firla, E. Hussein, A.P. Mazumdar, 1983 - 1991
B.C. Choy:
Probabilistic Transient Simulation Methodology in Support
of Probabilistic Safety Evaluation Studies for Ontario
Hydro Reactors
- 11.13 S.L. Israel: 1992 - 1999
How Firm are PRA Results?
- 11.14 P.J. Amico, W.L. Ferrell, M.P. Rubin: 2000 - 2008
The Significance of Water Hammer Events to Public Dose
from Reactor Accidents: A Probabilistic Assessment
- 11.15 H. Fabian, A. Feigel, O. Gremm: 2009 - 2015
The Probabilistic Approach and the Deterministic
Licensing Procedure
- 11.16 P. Wittek, W.G. Hübschmann, S. Vogt: 2016 - 2024
Influence of the Atmospheric Dispersion Model
Modifications on the Results of the German Reactor Risk
Study
- 11.17 J.A. Martin, Jr.: 2025 - 2027
Effectiveness of Early Evacuation of Small Areas, Shelter
and Relocation in Reducing Severe Accident Consequences
- 11.18 R.P. Burke, D.C. Aldrich, N.C. Rasmussen: 2028 - 2037
Modeling the Economic Consequences of LWR Accidents

- 11.19 D.A. Lappa: 2038 - 2047
Impact of Assumptions Concerning Containment Failure
on the Risk from Nuclear Power Plants
- 11.20 J.G. Kollas: 2048 - 2056
An Estimation of the LOCA Consequences of a Research
Reactor Located Within a Large Population Centre

APPLICATIONS OF PROBABILISTIC TECHNIQUES AT NRC

A. Thadani, F. Rowsome, and T. Speis

U. S. Nuclear Regulatory Commission
Washington, D.C. 20555

ABSTRACT

The NRC is currently making extensive use of probabilistic safety assessments in the reactor regulation. Most of these applications have been introduced in the regulatory activities in the past few years. Plant Probabilistic Safety Studies are being utilized as a design tool for applications for standard designs and for safety assessment of plants located in regions of particularly high population density. There is considerable motivation for licensees to perform plant-specific probabilistic studies for many, if not all, of the existing operating nuclear power plants as a tool for prioritizing the implementation of the many outstanding licensing actions on these plants as well as recommending the elimination of a number of these issues which are judged to be insignificant in terms of their contribution to safety and risk. Risk assessment perspectives are being used in the prioritization of generic safety issues, development of technical resolution of unresolved safety issues, assessing safety significance of proposed new regulatory requirements, assessment of safety significance of some of the occurrences at operating facilities and in environmental impact analyses of license applicants as required by the National Environment Policy Act.

NRC's regulatory and licensing decisions are based on the defense-in-depth concepts emphasizing quality and high standards for design, construction, and operation. These concepts are focused towards prevention of accidents by requiring reliable shutdown and cooling systems, provisions for reduction in the amount of fission products that could be released to the environment, and siting in areas that are not in close proximity to highly populated areas. Since the publication of the Reactor Safety Study (WASH-1400) in 1975 and more so in the aftermath of the Three Mile Island accident, greater attention was given to the value of probabilistic safety analysis

for systematic and integral evaluation of plants to identify vulnerabilities and as a tool for making safety trade-off studies.

The NRC is currently making extensive use of probabilistic safety assessments in the regulation of nuclear power plants. The scope of the probabilistic studies performed is governed by the intended application of the assessment. For standard designs where the PRA is used as a design tool, a thorough probabilistic analysis of the integral design is performed where as only limited, narrow assessments are conducted for evaluating risk significance of changes in plant technical specifications.

PRA provides the central theme of the development of NRC policy concerning requirements to improve protection from risk posed by severe reactor accidents. The policy for the generic approval, by rulemaking, of new standard plant designs requires the applicant to employ risk assessment techniques as a design tool, and to include a PRA in his license application. Near term Construction Permit applications must supply a PRA within two years of the granting of a construction permit. This PRA is to include consideration of alternative designs for core and containment heat removal systems which would enhance the safety of the plant in a cost effective manner. In the safety evaluation of standard nuclear island design proposed by General Electric as GESSAR II, the PRA is being used to supplement the conventional staff safety analysis and to guide in formulating any new requirements for this standard design. Current plans call for similar application of PRA in evaluating the advanced PWR design proposed by Westinghouse.

Concern that reactors located in regions of particularly high population density might pose a disproportionate share of the societal risk has lead the NRC to consider special provisions to mitigate severe reactor accidents at such plants. The owners of plants, Indian Point Units 2 and 3, and Zion 1 and 2 volunteered PRAs to develop a rational basis for such decisions.

The owners of Limerick and Millstone-3 were required by NRR to supply a PRA. In each case, where the PRA review has been completed, the PRA has identified a few alterations in plant design or operation that would be very effective in reducing the vulnerability of the plants to severe reactor accidents, and, where the NRC staff assessments have been completed, shown that expensive alterations to containment systems were not necessary. The fixes that have been adopted have had spectacularly good cost/benefit ratios. The striking success of these ventures into the use of PRA in the regulatory arena is attracting a good deal of attention in the NRC

staff as well as in the industry. It is becoming increasingly common for licensees requesting exemptions from specific requirements to document their case with PRA-based arguments. As the staff becomes more accustomed to thinking in terms of risk, it is becoming increasingly receptive to this approach.

The leading example of this approach has been the PRA of Big Rock Point submitted by Consumers Power. Initially, CPC took this approach to avert the premature shutdown of the plant. They had calculated that full compliance with all the new requirements spawned by the accident at TMI would cost more than the very small Big Rock Point plant could earn back in its remaining years of power generation. Then, too, CPC felt that many of the TMI Action Plan items were poorly suited to a plant of the unique design of BRP. CPC offered to perform a risk assessment of the plant, and to fix any prominent accident vulnerabilities revealed by the study, to the extent that their economic analysis indicated to be feasible. The staff approached the idea with deep reservations, but it has worked out very well. The staff and the licensees are now using the PRA as a source of perspective with which to resolve a wide array of outstanding license actions and generic issues on the plant. The program is serving as a pilot project for the new Integrated Safety Assessment Program. Then, too, CPC is pioneering in the use of a plant specific PRA as an operations management tool. Their risk management program is looking increasingly attractive to the NRC.

The NRC has instituted a program designed to screen newly-proposed generic safety issues by importance. It serves a dual purpose: it provides a technical basis with which to allocate staff resources to the technical resolution of safety issues, and coordinate issue resolution. Estimates of the risk attached to the proposed issues, developed using PRA-based methods and insights, plays a key role in the priority evaluation. This application of PRA is employed with liberal doses of conservatism. Since the results are only employed in staff resource allocation, little penalty accrues to overestimating the risk, but an important issue that is dropped from further study because its risk was underestimated could affect public health and safety but then if new information indicates that the issue merits further consideration it can be resurrected. Recent work in this program has been documented in NUREG-0933. NRC has also introduced a new priority ranking scheme to guide in the development of the Long Range Research Plan. It, too, entails the use of risk-assessment-based perspectives.

Many of the Unresolved Safety Issues and generic safety issues under review or recently resolved by the staff have been analyzed with risk assessment techniques. The Station Blackout issue and the DC power issue were analyzed principally using PRA. Risk perspectives were also employed in the analysis of Anticipated Transients Without Scram,

the reactor vessel thermal shock problem, water hammer events impacts, containment sump performance and many other issues, among them Systems Interactions and Decay Heat Removal are employing PRA methods or results.

Probabilistic models have also been used to perform sensitivity studies for providing insights into the bases for limiting conditions of operation (LCO), LCO extensions and testing and maintenance requirements. Some specific examples include revisions in Reactor Protection Systems testing requirements and extensions in Diesel Generator LCO. These techniques are also being applied to operating experience to identify the high-risk features of plant design and operation.

A quiet revolution has been going on within the NRC staff since the advent of the Committee for the Review of Generic Issues (CRGI). This group has been tasked by the Commissioners to serve a screening and filtering function for new generic requirements. It imposes strict standards of regulatory analysis or value/impact analysis on proposed new requirements. The sponsors of new generic requirements must document a convincing case that the risk reduction value of a ratchet must amply warrant the expense of its enforcement. This is forcing the staff to do a much more thorough job of evaluating the risks as well as the costs of new requirements than the staff was accustomed to do in years past.

In summary, the NRC staff has utilized some of the lessons learned from probabilistic safety studies and several new initiatives such as the Integrated Safety Assessment Program, the Severe Accident Policy, and the Safety Goal Evaluation Plan are underway which are expected to further illuminate the value of these studies.

SPECIFIC EXAMPLES OF APPLICATIONS OF PROBABILISTIC TECHNIQUES AT NRC

1. High Population Density Site

A staff report on population near nuclear sites, NUREG-0348, "Demographic Statistics Pertaining to Nuclear Power Reactor Sites" (NRC, November 1979) documented the population distribution around all U.S. nuclear power stations on the basis of the 1970 census. The NRC staff concerns that plants located in high population density zones may present a disproportionately high segment of the total societal risk from reactor accidents has led to the completion of full scope PRAs for four sites (Indian Point Units 2 and 3, Zion Units 1 and 2, Limerick, and Millstone Unit 3). The staff has completed its review of all but the Millstone 3 PRA and the summary results of the staff assessment are provided in figures 1, 2, and 3. Questions concerning scope, consistency of approach, adequacy of data, level of detail, and analytical quality assurance are being raised as potential areas where

comparison between studies could be faulted. The state of the art of the PRAs is evolving rapidly and continuously. Thus the more important use of these studies should be from the insights gained and the value of potential improvements considering uncertainties. One such application of the PRA is the case of improvements made at Indian Point Units 2 and 3.

The licensees for the Indian Point plants submitted probabilistic assessments to the staff to provide perspective on the safety of their plants. Subsequent to a review of the PRAs, the staff had several interactions with the licensees regarding dominant contributors to core-melt likelihood and severe offsite consequences. Several design and operations modifications that addressed the dominant contributors were implemented prior to restart of the plants. For Indian Point 2, these modifications included 1) installation of a bumper between the control room building and an adjacent structure and the ceiling tiles connected to the grid structure to reduce the potential of an earthquake to disable the control room; 2) installation of alternate power lines for a charging pump, component cooling water pump and two service water pumps to reduce the potential of a fire resulting in a reactor coolant pump seal failure and loss of ECCS and leading to core-melt; 3) modification of the Technical Specifications to require a plant shutdown in the event of a severe hurricane off of the New Jersey coast to reduce the potential for loss of all AC power, because of loss of high wind sensitive structures, that would lead to core-melt. Subsequent analyses indicated that these modifications had a high value-impact.

For Indian Point 3, the modifications included connecting the ceiling tiles to the grid structure and providing alternate power to charging, component cooling water, and service water pumps similar to that done for Unit 2.

2. Big Rock Point

The licensee performed a probabilistic assessment of the Big Rock Point plant in order to address the relative safety concerns of the TMI action items. As a result of the study, the licensee initiated several plant modifications to reduce the likelihood of core-melt as indicated by his study. These voluntary actions which addressed the dominant sequences included 1) replacement of a manual valve (located inside containment) with an automatic DC powered valve to provide alternate makeup to the emergency condenser which would reduce the potential for overpressure events and a stuck open safety valve; 2) revise procedures to utilize the high pressure feedwater system with recirculation from the containment to reduce dependence on the reactor depressurization system; 3) installation of position locks on seven valves in the post LOCA recirculation system to reduce the potential for misalignment of the system after test or maintenance; 4) elimination of the 15 minute delay for the containment spray actuation to reduce the potential failure at high temperatures of essential systems inside containment.

Subsequently, the NRC staff concurred that the licensee could be relieved of making additional modifications to improve control room habitability and adding an additional senior reactor operator based on probabilistic arguments. Both of these items were from the TMI Action Plan. Additional relief from TMI Action items is under consideration by the staff.

3. Auxiliary Feedwater Studies

After the TMI accident, the NRC's Office of Nuclear Reactor Regulation sponsored a series of studies to review the design of auxiliary feedwater systems in U.S. PWRs. These studies used PRA techniques to identify potential failures that could dominate the unreliability of auxiliary feedwater systems during transients caused by a loss of main feedwater, including the station blackout sequence. (The ability to cope with this particular sequence had not been a licensing requirement for the earlier licensed plants.) This study, which demonstrated the value of applying PRA techniques when at the system level, led to changes in the safety review process. A quantitative requirement on auxiliary-feedwater availability was added to in the standard review plan, and studies of auxiliary-feedwater reliability have become a routine requirement for licensing.

4. Station Blackout

Two studies addressed the unresolved safety issue A-44, "Station Blackout." Together they provide the technical bases for resolving the A-44 issue. The first study, "The Reliability of Emergency AC Power Systems in Nuclear Power Plants," when combined with the relevant loss-of-offsite-power frequency, provides estimates of station-blackout frequencies for 18 nuclear power plants and 10 generic designs. The study also identified the design and operational features that are the most important to the reliability of AC power systems.

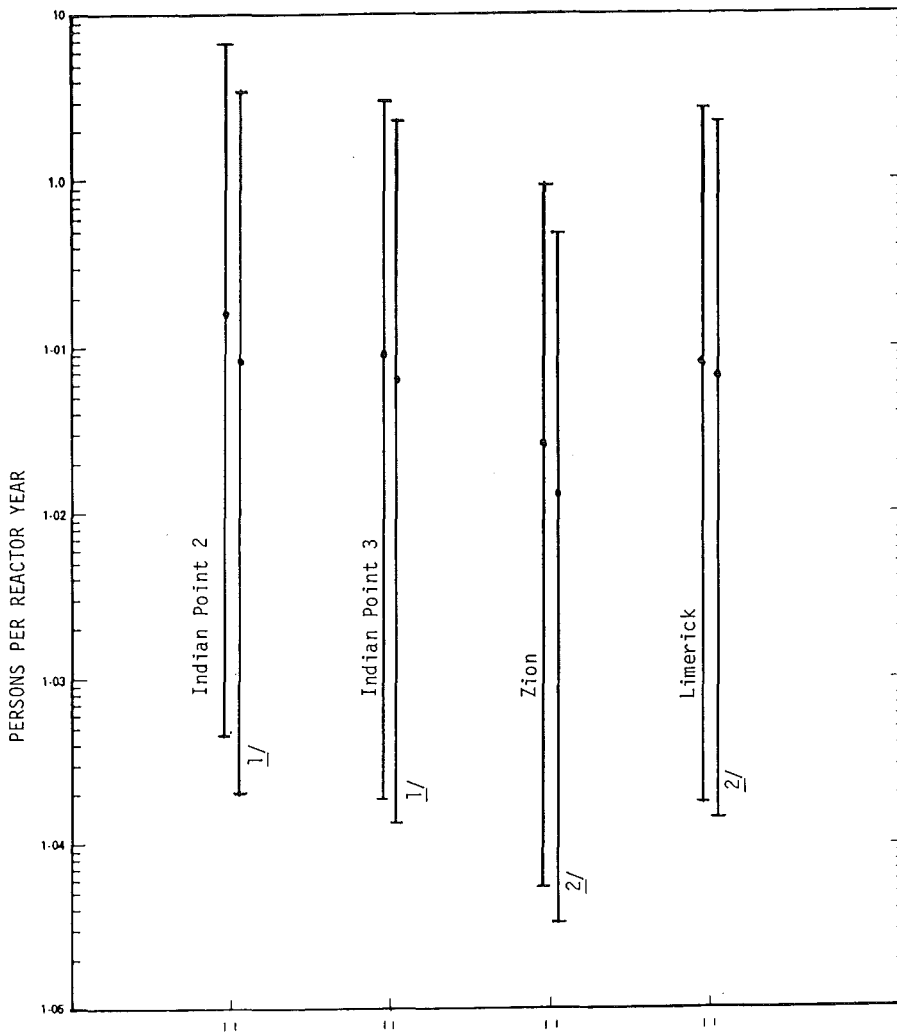
The second study, "Station Blackout Accident Analysis," (NUREG/CR-3226) focused on the relative importance to risk of station-blackout events and the plant design and operational features that would reduce this risk.

The technical bases supplied by these PRA-type special issues studies are currently being used to formulate the NRC strategy for resolving of the station-blackout issue.

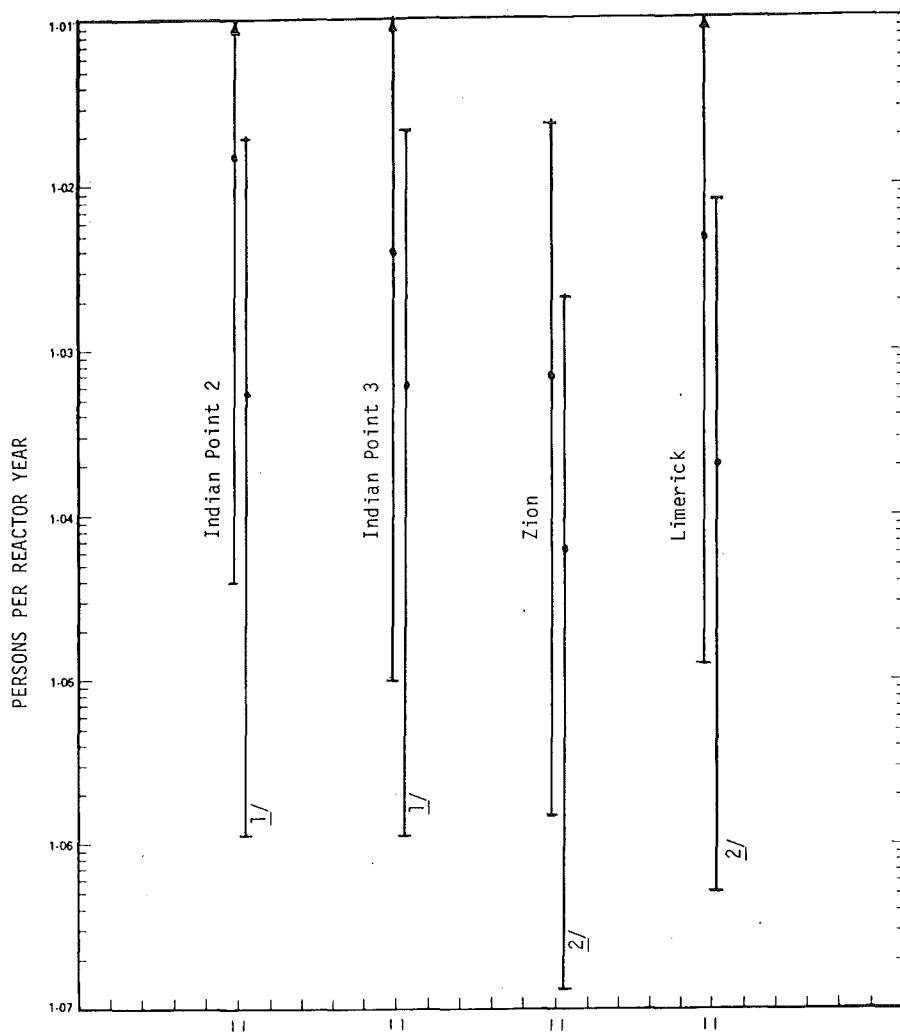
Anticipated Transients without Scram (ATWS)

The NRC staff evaluation of anticipated transients without scram in NUREG-0460 was one of the first applications of PRA techniques to an unresolved safety issue. The evaluation highlighted the relative frequency of severe ATWS events for various reactor types and estimated the expected reduction in frequency for various postulated plant modifications. The study also proposed quantitative goals for resolving this issue.

Other notable examples of PRA application to the ATWS issue are the NRC-sponsored survey and critique of the reactor protection system (RPS) and the quantitative evaluation of proposed ATWS-related modifications sponsored by a consortium of U.S. utilities. The RPS survey reviewed some 16 reliability studies, mostly in published PRAs, to compare the predicted failure probability per unit demand, the anticipated-transient frequency, and primary influences on RPS unavailability. There was a surprising degree of agreement among the 16 studies. The second study quantified the relative improvement to be gained by implementing a set of recommendations being proposed by the utility consortium in an ATWS petition to the NRC.



NOTE: Estimates are obtained from staff review, exclude thyroid cancers and are for the entire region of the plant sites. 1/ Estimate excludes severe seismic and hurricane events. 2/ Estimate excludes severe seismic events.



NOTE: Estimates are obtained from staff review, are based on supportive medical treatment and are for the entire region of the plant sites. 1/ Estimate excludes severe seismic and hurricane events. 2/ Estimate excludes severe seismic events.

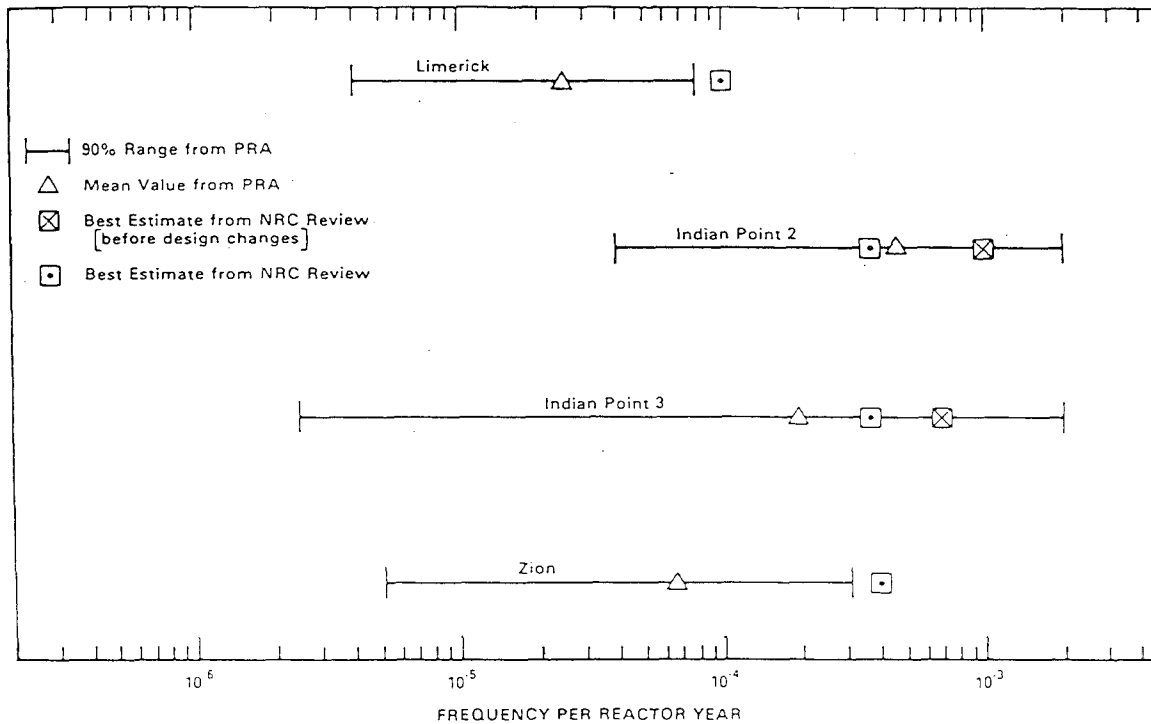


Figure 1 Core damage frequency with high density population plants - uncertainty range of internal and external events.

NOTE: The PRAs were not necessarily performed using consistent methodologies or assumptions. Many of the PRAs evaluate designs that have subsequently been altered.

Figure 1 Core damage frequency with high density population plants - uncertainty range of internal and external events.

A PROPOSED APPROACH TO BACKFIT DECISION-MAKING
USING RISK ASSESSMENT AND BENEFIT-COST METHODOLOGY

E. P. O'Donnell and T. J. Raney

Ebasco Services Incorporated
Two World Trade Center
New York, New York 10048, U.S.A.

ABSTRACT

This paper outlines a proposed approach to backfit decision-making which utilizes quantitative risk assessment techniques, benefit-cost methodology and decision criteria. In general terms, it is structured to provide an objective framework for decision-making aimed at ensuring a positive return on backfit investment while allowing for inclusion of subjective value judgments by the decision-maker. The distributions of the independent variables are combined to arrive at an overall probability distribution for the benefit-cost ratio. In this way, the decision-maker can explicitly establish the probability or level of confidence that a particular backfit will yield benefits in excess of cost. An example is presented demonstrating the application of methodology to a specific plant backfit.

INTRODUCTION

Backfitting of nuclear power plants is required for a variety of reasons. Changing regulatory requirements throughout the operating life of the plant may impose changes to plant design as a condition of continued operation. Utilities may also initiate plant modifications aimed at improving plant performance or availability. In either event, decisions have to be made by regulators, plant designers or owners with respect to whether, when and in what manner a backfit should be implemented. The issues involved rarely permit straightforward decisions without analysis of impacts on safety, plant performance and economics. Risk assessment techniques, combined with benefit-cost methodology, provide a method for rationally approaching backfit decision-making which can aid the regulator or utility in arriving at the optimum solution to a wide variety of problems. This paper describes one approach and presents an example of methodology as applied to a hypothetical backfit problem.

CONCEPT DESCRIPTION

The concept of a benefit-cost analysis is simple - the benefits and costs of the item of interest are established and compared. There are two common ways of comparing benefits and costs. One is the net worth, where the cost is subtracted from the benefit. The other is the benefit-cost ratio, where the benefit is divided by the cost. The latter is considered more useful because it gives a rate of return rather than absolute return. However, either must be considered in conjunction with the total cost because a Utility has limited capital available for improvements.

Benefits are defined as the expected returns from the change and costs as expected outlays required to implement the change, although either can turn out to be positive or negative. For a nuclear plant backfit, candidate changes are usually proposed based on a perceived benefit(s) of increased plant availability (B_1), reduced economic risk of plant loss (B_2), reduced public radiological risk (B_3) or reduced inplant exposure (B_4). These benefits are calculated directly in units other than dollars, so a valuation factor (U) must be applied to each to convert the benefit to the common denominator of dollars for comparison to cost. Costs include engineering and design services (C_1), material and equipment purchases (C_2), installation and construction (C_3), operation and maintenance activities (C_4) and any plant downtime required for installation (C_5).

The benefit-cost ratio (R) is determined by multiplying each benefit by its respective valuation factor, summing these products then dividing by the summation of the costs. In equation form this is:

$$R = \frac{\sum B_i U_i}{\sum C_k}$$

Quantitative information required for the analysis comes from a variety of sources. The effect on plant availability comes from the operating history of the plant (or similar plant) coupled with a reliability analysis of the changed system. Both the plant loss and public radiological risk change come from a sensitivity study of the plant PRA. Inplant exposure change comes from operating experience or is calculated from time and motion studies of installation, operating, test and maintenance actions associated with the proposed change coupled with plant radiation zone information.

Valuation factors come mostly from the Utility. The value of plant availability is usually available from the Utility's economic dispatch program. Economic risk can include the plant capital cost, cleanup costs and replacement power if this cannot be readily passed on to the consumer. The NRC has stated a value for public radiological risk in the Safety Goal Policy of \$1000/man-rem, but the Utility may wish to propose values that are more in line with other implicit societal values for averted deaths. The Utility must also place a value on a change in inplant exposures.

It is understood that the parameters involved have significant uncertainties. The traditional approach to dealing with this has been to use conservative or best estimate values in the model. However, this has two severe drawbacks. First, differing studies of the same problem can yield widely differing results. Second and more important, those charged with making decisions based on the results have no idea of what level of confidence to place on the results.

The best way of dealing with uncertainties is to recognize and accept their existence and treat them explicitly. This involves expressing uncertain input parameters as probability distributions rather than single numbers and propagating these distributions through the analysis. The techniques for doing this do exist and should be used.

The essential link between PRA and benefit-cost analysis should not be apparent. PRA is the only means available to quantify plant loss and public radiological risks, so it is an irreplaceable input to the analysis. Also, the operating history studies and reliability analyses required to quantify

plant availability changes are usually considered to fall under the general heading of PRA. The same is true for the uncertainty characterization and propagation.

EXAMPLE BENEFIT-COST ANALYSIS OF BACKFIT

The best way to demonstrate the usefulness of PRA based benefit-cost analyses for backfit decision-making is to show an example. A PRA for an operating plant showed that the dominant causes of core melt were complete electric power losses (caused by fires, earthquakes or high winds) that lead to both a Reactor Coolant Pump (RCP) seal failure LOCA through loss of electric powered seal cooling and a loss of safety injection. Containment cooling was lost as well, although this does not affect core melt probability.

De-coupling the seal failure LOCA from the loss of electric power would prevent the core melt because Auxiliary Feedwater is partially independent from electric power and is by itself sufficient for core cooling as long as the reactor coolant pressure boundary is intact. This could be accomplished by adding a steam turbine driven pump for emergency RCP seal cooling, as the French PWR designs have. This would reduce the frequency of these dominant sequences enough to essentially eliminate them as dominant.

Losses of RCP seal cooling that cause seal damage but do not proceed to core melt have occurred at operating plants. Replacement of badly damaged seals can take a month, causing a substantial availability loss. Since the standby seal cooling system could avert seal damage in such instances, the system has the potential benefit of increased availability as well.

This problem was set into the benefit-cost framework using the parameter values given on Table I. Reduction in core melt frequency was determined by multiplying the core melt frequency (ranges) of the sequences involving seal failure LOCAs given in the PRA by the average unavailability on demand of a steam turbine driven pumping system. Population dose ranges from these accidents were taken directly from the PRA. Plant availability changes were estimated from operating data on seal failure frequency and repair times.

The value of increased availability was taken from published replacement power costs. Value of avoiding core damage was taken from cleanup cost estimates (adjusted for insurance compensation) and replacement power costs. Value of averted man-rem exposure was taken as a range between the proposed AIF and NRC values. Costs were taken from engineering and construction estimates of the proposed change. All costs were annualized over a five-year payback period, which is typical of what a Utility desires (maximum) when making a backfit investment decision.

Known uncertainties that were not treated probabilistically in the model are:

- Whether a loss of RCP seal cooling actually does result in a small LOCA. There is evidence that it does not and tests are ongoing to investigate this area, but the PRA used for parameter quantification for the model assumed that it does.
- Whether Auxiliary Feedwater by itself is adequate for core cooling following a small LOCA. Recent analyses have shown that it may be, but the PRA assumed that it is not.

TABLE I: STANDBY RCP SEAL COOLING
BENEFIT COST ANALYSIS PARAMETERS

VARIABLE	DISTRIBUTION
- BENEFITS -	
AVAILABILITY INCREASE (%)	UNIFORM (5E-3, 1E-2)
CORE MELT FREQ REDUCTION (yr ⁻¹)	LOGNORMAL (3E-5, 2)
POP DOSE FROM CORE MELT (man-rem)	LOGUNIFORM (6E+6, 3E+8)
- VALUES -	
AVAILABILITY INCREASE (\$/%)	SINGLE VALUE (2.5E+6)
CORE MELT EVENT AVOIDANCE (\$/event)	UNIFORM (6E+9, 1E+10)
POP DOSE AVOIDANCE (\$/man-rem)	UNIFORM (1E+2, 1E+3)
- COSTS -	
ENGINEERING & DESIGN	UNIFORM (120, 180)
MATERIALS & EQUIPMENT	UNIFORM (210, 270)
CONSTRUCTION & INSTALLATION	UNIFORM (400, 900)

* All costs are initial costs in 1983 k\$
annualized over five-year payback period

- Whether the Utility actually sees indirect benefits such as reduced public risk by recovering them through the rate structure. This is highly dependent on the Utility and Public Utility Commission, but the model implicitly assumes that they can.
- Whether the backfit can be installed within a planned refueling outage. The model assumed that it could.

The first two were not included because they are essentially binary and one answer of each simply validates the results where either of the other answers render the analysis moot. The third is also binary, and one answer was simply chosen as an assumption of the analysis. The fourth was not

included for a lack of available information. The model assumptions for each of these uncertainties used in the analyses enhance the benefits of the fix. Thus, the resultant distribution of benefit-cost ratio is conservative to the high side by the known but untreated uncertainties.

The parameter distributions were propagated through the benefit-cost model using a simulation technique. The resultant benefit-cost curve, given on Figure 1, shows that at the best estimate (50%) point the value of the fix is slightly below the break even point. The curve exhibits a long tail to improbable but high benefit-cost ratios because of the lognormal function that describes the decrease in core melt probability.

Analysis of the results showed that at the best estimate, 73% of the total benefits were from offsite risk reduction. This stems from the facts that the sequences affected by the backfit involved severe radionuclide releases. The high fraction for this benefit underscores the importance of the structural uncertainty that the Utility can recover investments for public protection. Otherwise, this benefit is not seen by the Utility in a strict accounting sense and may not be appropriate for inclusion in the analysis.

Twenty-five percent (25%) of the total benefits were from plant economic risk reduction and the remaining 2% were from increased plant availability. Thus, the backfit is primarily "insurance", with probabilistic rather than expected return.

Based on this analysis, the backfit would appear attractive to a Utility that is averse to low probability-high consequence risks. Re-doing the analysis to increase this risk aversion would shift the benefit-cost curve to the left, thereby increasing the probability of a benefit-cost ratio greater than one. However, it must be remembered that there are two uncertainties not treated in the analysis that could render the study moot (devoid of benefits). The costs of further tests and/or analyses to eliminate these uncertainties should be considered against the cost of backfit before making a decision.

PROS AND CONS OF APPROACH

The benefits of using the approach described are decreased costs of backfitting for existing plants and reduced capital costs for new plants. This is deemed achievable because the structure of the benefit-cost analysis forces consideration of all costs and benefits of a backfit and assures proper balancing of the two. Given the present proven high level of safety at today's nuclear plants, very few backfits would survive such a test. Any backfits that were recommended would be money well spent, as return on this money is assured.

The principal drawbacks of using a PRA based benefit-cost approach for backfit decision-making are money and time. Regarding money, a high quality baseline PRA is required to assure a sound basis for benefit calculations. The PRA must include external events since many older plant backfits and some of the existing criteria to be examined concern external event protection. It also must include a highly detailed treatment of human reliability because many proposed backfits are for instrumentation and operator training/qualification. Such a PRA would cost several million dollars. Also, it is not hard to envision a group of five or more full-time professionals to perform the benefit-cost analyses, and maintaining this

staff is a cost of the approach. However, the cost of engineering feasibility and cost studies are not properly assigned to the benefit-cost approach because these would be performed for a backfit regardless.

Regarding time, the benefit-cost studies are not trivial and do require time to perform, which delays the decision on a backfit. This time is not always available, particularly if the backfit is related to a shutdown order or is a restart issue. The work required to justify exclusion of the existing regulatory criteria could take one or two years not even including NRC review. However, this time is available today for most Utilities while the need for new capacity is not imminent.

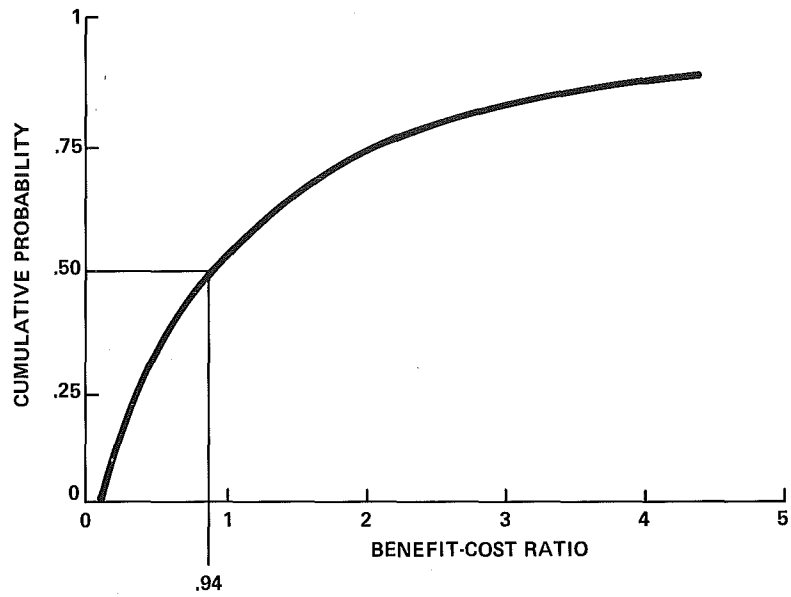
On the balance, the potential benefits should far outweigh the costs. Many plants are engaged in backfit programs costing several hundred million dollars, even exceeding the original plant costs in many cases. If the benefit-cost analysis eliminated even a few percent of this backfitting, it would more than pay for itself. The same is true for using PRA to determine criteria for a new plant. Indeed there is so much money at stake that any effective method to moderate regulatory requirements should be pursued by the Utilities.

A significant uncertainty of this approach is acceptance by the NRC. The NRC presently uses some form of benefit-cost analyses in the CRGR review of new generic requirements, but this does not assure acceptance of benefit-cost analyses for plant-specific backfits, especially those that may stem from generic requirements. The NRC has accepted such an approach to some extent at Big Rock Point, but it is not reasonable to extrapolate the experience of that unique plant to today's typical plants. Although some senior NRC officials have individually expressed willingness to consider such an approach, there is no definitive policy. Such a policy will probably not be forthcoming until and unless a Utility makes a proposal on an active plant docket.

CONCLUSIONS

PRA based benefit-cost analyses are an effective means of judging backfits and existing criteria for nuclear power plants. They permit such decisions to be made based on solid value and technical bases with explicit consideration of uncertainties. Incorporating provisions for such an approach in the regulatory process, although not a panacea, could greatly contribute to restoring nuclear power's competitive edge.

Figure 1
BENEFIT-COST RESULTS FOR
STANDBY RCP COOLING



THE DEVELOPMENT AND APPLICATION OF QUANTITATIVE METHODS
IN LICENSING NUCLEAR POWER PLANTS

L. Cave*, Risk Assessment Ltd., Tunbridge Wells, United Kingdom
W.E. Kastenber, University of California, Los Angeles, California, 90024
J.N. Tweedy, South of Scotland Electricity Board, Glasgow

* Currently Adjunct Professor, University of California, Los Angeles

ABSTRACT

The development and application of two quantitative methods, which could be used as part of the decision making process in nuclear power plant licensing, are described. These methods are the use of quantitative screening criteria to assess the adequacy of the safety functions in existing plants and the use of cost/benefit analysis to determine limits to the cost effective expenditure on "back-fitting" to improve safety. It is shown that the results obtained by the two methods are not necessarily compatible with one another. The need for clear guidance from regulatory bodies on the choice of some major parameters used in cost/benefit analysis is demonstrated.

1 INTRODUCTION

In the US, the UK and elsewhere there is currently a considerable interest in the development of quantitative methods for evaluating the safety of existing nuclear power plant (NPP), particularly in relation to severe accidents (i.e. those leading to extensive core damage, or core melt, possibly accompanied by severe failure of the containment), and in the development of methods for assessing the cost effectiveness of possible improvements in safety.

The authors have been involved in several aspects of these developments and in this paper we show that, when used as part of the decision making process in the licensing of nuclear power plant (NPP), different approaches can lead to dissimilar conclusions concerning the desirability of "back-fitting" to improve the safety of existing plants.

The first of the two approaches discussed in this paper is the application of quantitative safety goals, or quantitative design objectives (QDO), to develop "Quantitative Screening Criteria" (QSC) criteria which could be used for a simple preliminary assessment of the adequacy of the DHR function in a large number of existing plants. These QSC would be used in a flexible manner (as described in Section 5.2, below) without prejudice to any subsequent regulatory action.

The second approach is the application of cost/benefit (or, in US terms, value/impact) analysis. These approaches are described at some length in [1 and 2], accordingly in this paper only an outline of each method is provided so that more space can be given to discussion of the differences between the conclusions that might be reached by the two methods.

2 THE APPLICATION OF QUANTITATIVE DESIGN OBJECTIVES

2.1 Possible Difficulties in the Practical Application of QDOs

In principle, given a QDO expressed in suitable terms and a probabilistic risk assessment (PRA) for the plant in question, it should be a simple matter to decide whether that plant meets the QDO.

In practice a number of difficulties may arise, for example:-

- (i) The QDO may not be stated in a form which is directly comparable with the results of the PRA.
- (ii) If there is more than one QDO, it may not be immediately obvious which is the more limiting.
- (iii) The possible extent of the uncertainties in the results of the PRA may make interpretation of the comparison with the QDO difficult.

- (iv) The fact that FRAs, of any sort, may be available for only a small fraction of the plant population which is of interest.
- (v) In a particular problem, interest may be limited to the adequacy of only one safety function e.g. removal of decay heat.

Each of these potential difficulties is discussed below:-

2.2 The Choice of QDOs

At the present time the situation in the US is that the NRC have not yet decided whether to adopt the concept of using QDOs for regulatory purposes, they are carrying out an evaluation program which should be completed in 1985 (3 and 4). For the purposes of this paper we have assumed that, if a decision is made to adopt the concept, the QDO used would be the same as those which are currently being evaluated. Two of the QDOs define acceptable limits to the risk to the public and a third, which is described as a "subordinate objective", defines a limit to the probability of core melt, p_m (median value, 1×10^{-4} per reactor year, r. yr.). Thus the QDO for p_m is in a form which is immediately comparable with the results of a FRA. However, since the QDOs for Individual Risk and Societal Risk are expressed in terms of percentages of the US fatal accident rate and of the naturally occurring rate for fatal cancers respectively, they are not directly comparable with the results of a typical FRA, nor is it immediately obvious which of the three QDOs is most limiting in relation to p_m .

Following the procedure adopted in other areas of radiological protection it is therefore convenient to define parameters, which may be described as "derived QDOs" (analogous to the "derived working levels" for, say, surface contamination in radiological protection practice), which can readily be compared with the results of a FRA.

Since both of these QDOs are related primarily to the amount of radioactivity released into the atmosphere in the event of a severe accident the most convenient parameter for the "derived QDOs" is "probability" of a large release, denoted here by p_r . "Large release" in this context is a release large enough to cause early fatalities at a distance of 1.6 km (1 mile) from the plant, which is the basis of the QDO for Individual Risk. This corresponds to a minimum release of about 5 per cent of the inventory of the more volatile fission products (e.g. iodine and caesium) in the core of a 1000 MW(e) reactor. In the UK, p_r has been used successfully for several years as the principal quantitative parameter for specifying safety requirements for NPP(5).

The Individual Risk QDO can be translated into a requirement that the additional probability of accidental death, due to the presence of an NPP, should not exceed 5×10^{-7} per r. yr. for an individual living in the vicinity. Taking into account the random direction of the plume from a severe accident, this corresponds to a value of about 5×10^{-6} per r. yr. for p_r .

The Societal Risk QDO can be translated into a requirement that the additional probability of death due to cancer, averaged over a radius of 80 km (50 miles) around an NPP, should not exceed 2×10^{-6} per r. yr., due to the presence of the NPP. A simple analysis, assuming a uniform population distribution around the NPP, shows that this QDO would be met if p_r were as high as 2×10^{-4} per r. yr. This conclusion should also be valid for non-uniform population distributions.

Thus, even if the containment were completely ineffective, the QDO for Societal Risk would be met if the QDO for probability of core melt were achieved (i.e. $p_m < 1 \times 10^{-4}$ per r. yr.). However the QDO for Individual Risk is considerably more restrictive and it can be seen that unless the conditional probability of severe containment failure following a sequence leading to core melt, q_c , were less than 5×10^{-2} per event,

the Individual Risk QDO would not be met if p_m were as high as 1×10^{-4} per r. yr. Thus meeting the QDO for core melt would not necessarily be a sufficient condition for ensuring that the QDO for Individual Risk would also be met. Thus the contributions to both p_r and to p_m must be considered in the quantitative evaluation of the adequacy of the DHR or other safety functions.

Summarising these derived QDOs, we have:-

QDO for probability of large release to atmosphere, p_r , 5×10^{-6} per r. yr.

QDO for probability of core melt (if $q_c < 5 \times 10^{-2}$), p_m , 1×10^{-4} per r. yr.

It may be noted that in the UK the two utilities with NPP (The Central Electricity Generating Board and the South of Scotland Electricity Board) have adopted a "design guide line" in their purchasing specifications of 1×10^{-6} per r. yr. for large releases and wish to see this achieved with a minimum reliance on the containment, the design targets for the safety functions are therefore based on a value of 1×10^{-6} per r. yr. for p_r (6). This design guide line is compatible with the UK legal requirement that, in all industrial activities, the risk to the public and to employees should be made "as low as reasonably practicable", the interpretation of this requirement is discussed further in Section 3.3.4, below.

2.3 Treatment of Uncertainty in the Development of Quantitative Screening Criteria

It is generally agreed that estimates of p_m , or of large releases to atmosphere, p_r , are subject to large uncertainties. The sources of uncertainty in estimating p_m and p_r can be classified in 3 broad groups, namely:-

- Group 1 The uncertainties in the parameters, such as failure rates of plant items, used in calculations of the probability of core melt and containment failure due to faults within the systems and plant items themselves, where the modelling of the system behaviour is well established.
- Group 2 The uncertainties relating to the probability distributions for, and the effects of, events external to the systems (e.g. cable race fires, floods, seismic disturbances) and those relating to faults within the system where the modelling is not well established.
- Group 3 The uncertainties arising from relatively rare causes which can be visualised but have not yet been experienced in the operation of NPP, for example, specific design errors; obscure common mode faults and system interactions; bizarre behaviour of the operator.

It will be seen that the great majority of existing probabilistic risk assessments (PRAs) only include the Group 1 uncertainties; efforts are being made to develop methods for tackling the Group 2 uncertainties and in some recent US PRAs (e.g. those for Zion and Indian Point) it has been found that the contribution to core melt due to "external" events is comparable with that due to the "internal" faults.

As more operating experience is obtained and analysed it should be possible to reduce the importance of the Group 2 and 3 uncertainties but at the present time they should be regarded as making a substantial contribution to the probability of core melt.

Thus in order to derive a QSC which can be applied to a large number of plants at the present time, it is necessary to base it on a fraction of the QDO which corresponds to the Group 1 conditions defined above. The problem of sub-dividing the overall QDO between the 3 groups is discussed in Ref. 1. Any division must be somewhat arbitrary but some semi-quantitative arguments suggest that a 40:30:30 allocation between the groups would be reasonable. This has the merit that, on the one hand, it avoids extreme situations in which the importance of the Group 2 and 3 uncertainties could be so over-estimated that the system reliabilities required in the conditions of Group 1 uncertainty would be unrealistically high. On the other hand, if the proposed allocation does represent an over-estimate of the importance of Group 2 and 3, the maximum short fall (a factor of 2.5) in the Group 1 allocation could not be regarded as very significant.

Using this allocation we can proceed to develop QSC for the DHR function from a derived QDO for p_m of 4×10^{-5} per r. yr. and a derived QDO for p_r of 2×10^{-6} per r. yr.

2.5 Sub-division of the "Derived QDO" for p_m and p_r Between the Safety Functions

Core melt can occur as a result of:-

- (i) Failure of the reactor to trip in response to an adverse change in the ratio of heat removal to heat input.
- (ii) Failure to remove heat at an adequate rate after the reactor has tripped.
- (iii) Failures of certain "critical structures" which lead to a situation in which the reactor shutdown or heat removal systems are made ineffective.

It is convenient to sub-divide (ii) into two parts, so that we can consider separately the initial phase after a large or medium LOCA, when the main problem is to ensure that reflooding of the core occurs quickly enough to prevent damage to the fuel, and the later phases of these LOCA's, together with the entire post-trip behaviour in other types of fault, where the main requirement is to remove the decay heat. In this paper we are concerned only with the second part.

The proposed sub-division of p_m between the 4 safety functions is based on the following:-

- (a) Published results of PRAs.
- (b) Consideration of the frequencies of events which create a demand for each of the functions.
- (c) Relative difficulties of achieving high reliability in the different functions.

As described in Ref. 1, these considerations have led to the following allocations for the DHR, in the post reflood phase, in Group 1 conditions of uncertainty:-

PWR 75 per cent i.e. $p_m = 3 \times 10^{-5}$ per r. yr.

BWR 50 per cent i.e. $p_m = 2 \times 10^{-5}$ per r. yr.

A similar sub-division is proposed for p_r but in this case it is necessary to distinguish between those cases in which core melt is followed by severe containment failure due to random events and those in which there is a common cause (the latter are described here as "Special Cases"). It is proposed that 20 per cent of the derived QDO of 1.5×10^{-6} per r. yr. should be allocated to the "Special Cases" and 80 per cent to the rest. These allocations are then sub-divided amongst the functions in the same way as the QDO for p_m . Thus the proposed QSC for the DHR function, for PWR, in Group 1 conditions of uncertainty are:-

General Case $p_r = 1.2 \times 10^{-6}$ per r. yr.

Special Case $p_r = 3 \times 10^{-7}$ per r. yr.

The corresponding values for BWR are two-thirds of those for PWR.

(Note: 'Severe Containment Failure' in this context is one which, associated with core melt, would give rise to a release large enough to cause early fatalities in the vicinity of the plant).

A further sub-division of the QSC, between the early and later stages in which the DHR systems are required to function is described in Ref. 1 but this is not required for the purposes of this paper.

2.5 Application of the QSC for the DHR Function

It is visualised that by various devices (e.g. grouping, synthesis of FRAs from existing assessments, or reliability analyses of limited scope) estimates of the contributions to p_m and to p_r due to failures of the DHR function, in Group 1 conditions of uncertainty, will become available for many more of the existing US plants than those for which FRAs have been carried out. Thus it should be possible to apply the QSC to most of the population.

It is recognised that the QSC are somewhat arbitrary and are probably conservative. Thus, if these contributions to p_m or p_r for a particular plant are observed to be greater than the corresponding QSC, this should only be regarded as an indication that the plant in question should be examined more closely. For example, if it can be seen that p_m and p_r for the plant as a whole meet the corresponding QDOs from which the QSC have been derived, no further action would be necessary. The interpretation of the results of this comparison with the QSC is discussed further in Section 5.2 below.

3 THE APPLICATION OF COST/BENEFIT ANALYSIS

3.1 Sources of Data on Benefits

A nuclear reactor accident can cause harm to the health and property of the public ('off-site' costs) and to the plant itself and to the health of the operators ('on-site' costs). A further important cause of on-site costs is the need to replace nuclear power from plant with higher operating costs. Since improvements to the plant to reduce the probability of an accident, or to reduce its effects, have the effect of averting damage, these 'averted costs' can be regarded as the 'benefit' resulting from the expenditure on the improvement, which can then be compared with the actual costs which would be incurred by the utility in making the improvements.

The detailed make-up of the 'benefits' and the 'costs' are described in [7 and 8] and more recently in [9]. However, for the purposes of this paper a particularly useful compilation is that of [10], which summarises the avertable 'off-site' and 'on-site' costs, for each of the existing and proposed NPP in the US, for each of 3 'standard' accidents. The same assumptions are made for each NPP. Thus, although there may be disagreement about some of the assumptions, the set of data is self-consistent. A review of the assumptions in [10] suggests that the absolute values of the costs for each plant are unlikely to be an error by a factor of more than 3 [9]. This set of data is therefore suitable for illustrating the argument which we wish to develop in this paper.

3.2 Summary of the Benefits Associated with 'Avertable Costs'

Some broad conclusions which can be drawn from the data of [10] are as follows:-

- (a) "On-site" costs per MW(e) of installed capacity show little variation over the whole set. Given that core melt has occurred, a representative value is $\$4 \times 10^6$ per MW(e) installed; the maximum variation about this value is about +50 per cent. The "on-site" costs, for an accident which leads to core melt, are virtually independent of the size of the release to atmosphere.

(b) "Off-site" costs per MW(e) of installed capacity show a substantial site to site variation. This variation depends mainly on population density so that it is possible to distinguish between 3 types of site, for each of which a representative value can be identified, for an accident of given severity. Given that the most severe accident considered in Ref. 1101 (Accident "SST1", which corresponds to releases of from 45 to 67 per cent of the more important volatile isotopes, notably Cs¹³⁷ and I¹³¹) has occurred, these values are as follows:-

- Low Population Site (e.g. Palo Verde or Surry) about \$ 1 x 10⁶ per MW(e)
- Medium Population Site (e.g. Peach Bottom or Millstone) about \$ 3 x 10⁶ per MW(e)
- High Population Site (e.g. Indian Point or Limerick) about \$10 x 10⁶ per MW(e)

For our purposes it is sufficient to consider a central value of \$3 x 10⁶ per MW(e) installed and to examine the sensitivity of conclusions based on this value to increases and decreases by a factor of 3.

(c) The "off-site" costs are almost linearly proportional to the fractional release to atmosphere of the more important volatile isotopes, notably Cs¹³⁷. Thus the results of the analysis which relate to "off-site" costs are very sensitive to the performance and reliability of the containment. Consequently, "off-site" costs based on the "SST1" type of accident are likely to be greater than those which would result from nearly all the accidents which might occur in practice.

(d) Apart from the "high population" sites, the "on-site" costs are larger than the "off-site" ones, even for the most severe accidents. However, since the latter are likely to be more important from the regulatory point of view it is desirable to keep the two sets of costs separate.

From these broad conclusions we can now estimate the maximum expenditure on improvements to achieve given reductions in p_m and p_r that would be cost effective.

3.3 Limits on Cost Effective Expenditure for Improvements to Avert Losses

3.3.1 Limit to Cost Effective Expenditure for Improvement, C_E, based on "Off-Site Costs"

If a proposed improvement can be shown to reduce the probability of a large release, of given size, S₁, by an amount Δp_{r1}, the maximum sum that would be strictly cost effective, in terms of averted off-site costs, C_E, can be determined from the following equation:-

$$C_E = n \sum_{t=1}^{\text{all } t} \Delta p_{r1} B_1 \dots\dots\dots (1)$$

where n is the effective number of years of plant life remaining, taking into account any discounting policy, and B₁ is the benefit arising from the cost averted by preventing release S₁.

In 1101 a discount rate of 4 per cent per annum is used, which is consistent with the assumptions that all benefits are measured in constant (1981) value dollars. The use of a 4 per cent discount rate leads to effective plant lives of 17 to 21 years for nearly all the existing and projected US plants. For our purposes it is sufficient to assume a uniform value of 20 years.

In the case of off-site costs the relative importance of the contributions to C_E from the SST1, 2 and 3 types of accident depends on the performance and reliability of the containment after core melt. For Indian Point, for example, which is a PWR with a large dry containment, NRC have taken the view that the conditional probabilities of SST1, 2 and 3 releases, given core melt, are 0.03, 0.01 and 0.96 (111). Since the off-site costs attributable to SST2 and SST3 releases are of order 1 per cent and 0.1 per cent respectively of those due to an SST1 release, it can be seen that the smaller releases would not contribute significantly to C_E. The results of the RSS (112) suggest that for other PWRs the conditional probability for SST1 releases may be higher than 0.03, possibly about 0.1).

For BWRs with Mark 1 containments, the RSS predicts a conditional probability of about 0.95 for releases about one third of the size of an SST1 release, the corresponding off-site costs would be 30 per cent of those for an SST1 release (8). However, if the operator were able to prevent severe containment failure by venting, as now appears to be the case, the conditional probability of a large release should be similar to that estimated for Indian Point.

This uncertainty concerning containment performance and reliability can be a major source of uncertainty in estimating C_E.

3.3.2 Limit to Cost Effective Expenditure for Improvement, D_E , Based on "On-Site" Costs

It follows from the preceding discussion that there is an equation similar to Eqn (1) above for D_E . However, in this case we are concerned with the reduction in core melt probability, Δp_m , rather than Δp_r . Since B_S , the on-site cost averted by prevention of core melt, is virtually independent of the size of release, thus we have:-

$$D_E = n \Delta p_m B_S \dots\dots\dots (2)$$

It follows that estimates of D_E are subject to less uncertainty than those of C_E .

3.3.3 Comparison of Limits to Cost Effective Expenditure Based on "Off-Site" and "On-Site" Costs

Some conclusions which can be drawn from the preceding discussion are as follows:-

- (a) Since B_S is greater than B_r for nearly all plants and since p_m is equal to, or greater than p_r for all plants, D_E is less than C_E for only a few plants; for most plants D_E is much larger than C_E . Thus a clear understanding is required as to the extent to which regulatory decisions based on consideration of cost effectiveness should take account of on-site costs. (See next section).
- (b) A general reduction in source terms would accentuate the importance of on-site costs, compared to off-site costs, in relation to establishing the limits on cost effective expenditure. However, inclusion of a "risk aversion factor" in estimating the benefit obtained by averting off-site costs would have the opposite effect.

3.3.4 Numerical Values for Limits to Cost Effective Expenditure on Improvements

Equations (1) and (2) can be used to find values of C_E and D_E corresponding to selected values of B and Δp . The range of values of Δp which has been used to prepare Table I provides some insight into the extent of improvement that might be possible within the limits of cost effectiveness. The Table is based on the avertable costs for 1,000 MWe plant with an effective remaining life of 20 years, on an average US site. It is assumed that the additional probability of severe containment failure, given core melt q_c is 0.1.

Table I Some Representative Values for the Limits to Cost Effective Expenditure on the Reduction of p_r to the QOO Value of 5×10^{-6} per r. yr.

Initial Values of p_r	Factor of Improvement to Achieve QOO	Δp_r	C_E^a \$E	Likely Extent of Cost Effective Improvement ^b	Δp_m^c	D_E^d \$E	Likely Extent of Cost Effective Improvement ^d
6×10^{-6}	1.2	1×10^{-6}	6×10^4	None possible	1×10^{-5}	8×10^5)
1×10^{-5}	2.0	5×10^{-6}	3×10^5	Operating Procedure	5×10^{-5}	4×10^6) Minor sub-system changes
3×10^{-5}	6	2.5×10^{-5}	1.5×10^6	Minor sub-system changes	2.5×10^{-4}	20×10^6) Major sub-system changes
1×10^{-4}	20	$\sim 1 \times 10^{-4}$	6×10^6) Major sub-system changes	$\sim 1 \times 10^{-3}$	80×10^6) Substantial additional sub-systems
3×10^{-4}	60	$\sim 3 \times 10^{-4}$	18×10^6)	$\sim 3 \times 10^{-3}$	240×10^6) Major design changes

Notes, see overleaf

Notes

- (a) Could be spent on "prevention" or "mitigation".
- (b) Assuming expenditure is used for "prevention", i.e. reduction of p_m .
- (c) Assuming conditional probability of severe containment failure, given core melt, is 0.10.
- (d) Assuming that whole of expenditure is used to reduce p_m ; since the limit for expenditure on reduction of p_r by mitigation is determined by Δp_r , not Δp_m .

It can be seen from Table 1 that if the limit to cost effective expenditure were determined by off-site costs alone then:-

- (a) The sums available for improvement would probably be too small to obtain any substantial reduction in p_r , unless the initial value of this probability were at least ten times larger than the QDO value of 5×10^{-6} per r. yr. suggested in Section 2.2 above.

This implies that the suggested QDO for Individual Risk would not be fully consistent with the concept of a cost effective limit on expenditure, based on off-site costs, unless a substantial "risk aversion" factor were introduced. In the UK the relevant legal requirements do, in effect, necessitate the use of such a factor. This is because it is necessary to show that all "reasonably practicable" steps have been taken to reduce the risk. The interpretation of this phrase by the Courts, in other industries, has been that the limit to expenditure on improvement is only reached when the cost of the improvement is becoming "grossly disproportionate" to the reduction in risk which would be achieved. Achievement of the UK design target

(i.e. p_r less than 1×10^{-6} per r. yr. with limited reliance on the containment) on a site with high

population density would imply a cost effective limit of about $\$2 \times 10^6$ to reduce p_r from 1×10^{-5} to 1×10^{-6} per r. yr., based on averted off-site costs. Even in a new design it is most unlikely that an improvement of this magnitude could be achieved at a cost of less than $\$10 \times 10^6$. Thus this choice of design target should also satisfy the 'ALARP' requirement.

- (b) The effect of a substantial decrease in the source term for most sequences would have the effect of reducing p_r , in any given design, since fewer sequences would give rise to 'large' releases, so that the question of further improvement to meet the QDO would be less likely to arise.
- (c) An alternative interpretation of the results in Table 1 is that the proposed QDO for Individual Risk is more severe than would be necessary to comply with the "ALARA" concept, as used in the US. However, it could also be argued that, if the public were offered a QDO for Individual Risk, decisions whether or not to meet that QDO for a specific plant should not be influenced by cost effectiveness considerations based on societal effects.

It can also be seen from Table 1 that if the limit to cost effective expenditure to meet the proposed QDO for Individual Risk were determined by on-site costs then, for a plant with the same initial value of p_r , the sums available for reducing p_r could be very much larger if, as in our example, the conditional probability of severe containment failure is reasonably low (0.1 per demand). Of course, if this probability were high, this would not be true. In the extreme case, if it were unity (i.e. $p_r = p_m$) the cost effective limit, for an average plant on an average site, based on on-site costs would be only 30 percent greater than that based on off-site costs. However, such extreme cases should be uncommon. In the case of a site in an area with a high population density, if the conditional probability of severe containment failure were high, the avertable off-site costs could exceed the on-site ones. Nevertheless even for the worst site in the US (Indian Point), the off-site costs would be only a factor of 2 greater if q_c were equal to unity. However in that particular case we have $p_r \sim 0.03 p_m$, so that the on-site limit would, in practice, be dominant.

It is apparent from this large difference in the limits on cost effective expenditure that, if a regulatory body decides to use cost/benefit considerations in decision-making, it must decide at the outset whether or not to include avertable on-site costs in the cost/benefit analysis and whether or not to include some form of risk aversion factor. Differences in conditions between countries may, of course, lead to different decisions on these aspects, e.g. in the UK, a substantial risk aversion factor is introduced; in a country with a State owned electricity generating industry inclusion of the on-site costs would be easier to justify than if the industry were privately owned.

4 COST EFFECTIVE LIMITS TO THE EXPENDITURE ON IMPROVEMENT OF THE DHR FUNCTION

It is now possible to combine the results obtained in Sections 2 and 3 in order to compare the extent of the improvement that might be made in the DHR function, as determined by cost effectiveness considerations, with the extent of improvement that might be required in order to meet the "derived QDOs" discussed in Section 2, e.g., for PWR:-

(I) Contribution to p_r , in Group 1 conditions of uncertainty, of 1.5×10^{-6} per r. yr.

(II) Contribution to p_m , in Group 1 conditions of uncertainty, of 3×10^{-5} per r. yr.

Proceeding as in Section 3 it will be seen that the limits to cost effective expenditure will be one third of those shown in Table 1. However, in those cases where it can be shown that an improvement aimed at reducing the contribution to Δp_r , or Δp_m , in Group 1 conditions of uncertainty should also be effective in some Group 2 or Group 3 conditions of uncertainty, then clearly the overall value of Δp_r , or Δp_m , would be greater, so that a larger benefit would be obtained by the modification and thus the cost effective limit should be higher.

This implies that, on the basis of off-site costs, the maximum sum available for improvement of the DHR function, in Group 1 conditions of uncertainty, would be unlikely to exceed $\$10 \times 10^6$ (i.e., corresponding to Δp_r , in Group 1 conditions of uncertainty, of 1×10^{-4} and some benefit in Group 2 and/or 3 conditions of uncertainty) for a 1,000 MW(e) plant, of average age, on an average US site. Major changes to an existing sub-system should be possible for a sum of this size but it is unlikely that it would cover the cost of an additional DHR sub-system such as an independent high pressure injection train (13).

However, if on-site costs were used as a basis for estimating limits to cost effective expenditure, it is possible that, in the total population of US plants, there might be a few in which the addition of a further DHR sub-system would be cost-effective.

In the "Special Cases" identified in Section 2.4, where the same initiating event (e.g., prolonged "Station Black-out") could lead to core melt and to severe containment failure, p_r would be small since the frequency of the initiating event would be small (of order 10^{-3} per r. yr.), thus the value of Δp_r corresponding to complete elimination of the sequence would also be small (less than 1×10^{-5} per r. yr). Consequently the cost effective limit on improvement would be small also (less than $\$6 \times 10^5$ for our average case). Moreover, since the conditional probability of severe containment failure would be unity, by definition, we would have $p_m = p_r$ and $\Delta p_m = \Delta p_r$. Thus the cost effective limit based on on-site costs would also be relatively small (less than $\$8 \times 10^5$).

For BWR the limits would be two-thirds of those for PWR in similar conditions.

5 COMPARISON OF REQUIREMENTS FOR DHR RELIABILITY BASED ON QSC AND ON COST/BENEFIT CONSIDERATIONS

5.1 Formulation of Quantitative Screening Criteria for the DHR Function

We have shown that from a set of QDOs for individual and societal risk, such as those proposed by NRC for evaluation in 1983, a corresponding set of "derived QDOs", expressed in terms of maximum acceptable probability of large release to the atmosphere (p_r) or maximum acceptable probability of core melt (p_m), can be obtained.

The NRC's QDO for individual risk imposes a more stringent safety requirement than that for societal risk and, unless the conditional probability of severe containment failure (q_c) is less than 0.05 per demand, the "subordinate QDO" for p_m proposed by NRC (1×10^{-4}) per r. yr., medium value would not be a sufficient criterion to meet the QDO for p_r .

In the application today of these derived QDOs to a practical problem, such as assessing the adequacy of the DHR function in a large population of existing plants, it is necessary to take account of the quality and scope of the FRAs which are available. The majority of these only provide estimates of p_m and, in some cases, p_r for sequences arising from "internal" initiating events (i.e., those occurring within the plant systems themselves). Thus at present it is only possible, in many cases, to evaluate the adequacy of the DHR function in these conditions, which correspond to the "Group 1 conditions of uncertainty" defined in Section 2.3 above.

Thus in order to obtain a set of quantitative screening criteria (QSC) against which the plants can be compared it is necessary to sub-divide the "derived QDOs" in two stages:-

Firstly, to take account of the limited scope of the existing PRA's. We have suggested a 40:30:30 division between our 3 groups.

Secondly, to take account of the contribution to the overall values of p_r and p_m due to the failure of safety related functions other than DHR. We have suggested 75 per cent for DHR in PWR and 50 per cent in BWR, in each of the 3 groups.

These proposals lead to QSC (median values) for the DHR functions, in Group 1 conditions of uncertainty, which are as follows:-

$$p_r(\text{DHR}, 1) = 1.5 \times 10^{-6} \text{ per r. yr. for PWR and } 1.0 \times 10^{-6} \text{ per r. yr. for BWR}$$

$$p_m(\text{DHR}, 1) = 3 \times 10^{-5} \text{ per r. yr. for PWR and } 2 \times 10^{-5} \text{ for BWR, if } q_c < 5 \times 10^{-2} \text{ per demand}$$

For the "Special Cases" in which the same initiating fault leads to core melt and to severe containment failure, $p_r(\text{DHR}, 1) = p_m(\text{DHR}, 1) = 3 \times 10^{-7} \text{ per r. yr. for PWR and } 2 \times 10^{-7} \text{ per r. yr. for BWR.}$

5.2 Cost Effectiveness of Improvements to the DHR Function

The brief analysis of the limits to cost effective expenditure for reducing p_r and p_m shows that avertable off-site costs can only justify a relatively small expenditure on improvements but a substantially larger expenditure could be justified on the basis of avertable on-site costs. If we assume that the maximum value of Δp_r required to meet the suggested QSC for the DHR function, in Group 1 conditions of uncertainty, were 1×10^{-4} per r. yr. the sum available for improvement of the DHR function (in an existing 1,000 MW(e) plant with a 20 year effective life, on an average US site) would be about $\$6 \times 10^6$, if based on avertable off-site costs. The modifications which could be made for a sum of this size would not be extensive and would not necessarily be sufficient to reduce p_r by 1×10^{-4} per r. yr.

Thus a situation could arise in which the "cost effective" concept would not be fully compatible with the suggested QSC for the DHR function. In this situation it might be possible to show that the proposed modification would also be effective in reducing p_r sufficiently in conditions of uncertainty other than Group 1 to meet the overall QSC for the DHR function. In this situation the limit to cost effective expenditure would be correspondingly higher. Alternatively the possibilities of reducing the contribution to p_r due to failures of the other safety functions (e.g. the scram system) or of increasing the mitigation of the effects of core melt could be examined, as a means of meeting the derived QDO for p_r at minimum cost. These options for improving systems other than the DHR, or for increasing the extent of mitigation, should also be open to the licensee as an alternative means of meeting the derived QDO for p_r , without fully meeting the QSC for the DHR function, if these options provided a less expensive method for meeting the derived QDO for p_r .

If the avertable on-site costs were used as a basis for establishing the limit to cost effective expenditure, this limit could be higher by a factor of order 10 than in the previous case so that the likelihood of an unresolvable incompatibility between the QSC for the DHR function and the "cost effective" concept would be greatly reduced.

A reduction in the "source terms" would reduce the initial value of p_r , for any given plant, since fewer sequences should lead to "large releases", as defined in Section 2.2 above. Thus a situation could be reached in which the suggested QSC for the DHR function derived from p_r would be met without difficulty by most, if not all, of the existing plants, even though the QSC derived from p_m were exceeded.

Nevertheless, the limit to cost effective expenditure for improvement would also be reduced, if this were based on avertable off-site costs. Thus the possibility of an incompatibility between the suggested QSC for the DHR function which is based on p_m and the "cost effective" concept would be greater. However, if on-site costs were used as a basis for the expenditure limits, the sum available for improvement of the DHR function would not be affected by the change in the source terms.

It will be seen that a regulatory body which intends to use the concept of cost effectiveness as a major factor in reaching decisions about improvements to existing plant should decide at the outset whether to consider only avertable off-site costs or whether to consider on-site costs as well. If it is also intended to adopt a set of QDOs for existing plants, the compatibility of these with the concept of cost effectiveness of improvements should be examined.

6 CONCLUSIONS

The main conclusions to be drawn from the work described above are as follows:-

- (a) If the quantitative screening criteria for the DHR function, suggested here, which are based on the US NRC's proposed QDO for Individual Risk, were applied to existing US LWR, it is likely that some plants would fail to meet the criteria unless the 'source terms' can be reduced. However, since the QSC are intended to be used in a flexible manner, an initial failure to meet them should be regarded only as an indication that a range of possible alternatives for meeting the overall QDOs should be examined in order to find the optimum solution.
- (b) If the limit to cost effective expenditure for improvement of the DHR function were based on avertable off-site costs only, and given the existing 'source terms' for severe accidents to US LWR, it is doubtful whether sufficient improvement could be made in all cases to meet the suggested QSC, even if this were the least expensive solution for meeting the overall QDO. However, if the limit to expenditure were based on avertable on-site costs, the limits would be substantially higher and thus the possibility of failing to meet the QSC within the limits of cost effective expenditure would be reduced. This difference between the two limits on expenditure would be accentuated by a decrease in the "source terms" for severe accidents.
- (c) The concept of limiting the cost of back-fitting to a level which is cost effective may be a useful one in regulatory analysis but a clear definition of the basis for calculating the limits to the expenditure is required at the outset.
- (d) The design target adopted by the UK utilities should be severe enough to ensure compliance with the legal requirements that the risks from reactor accidents should be made 'as low as reasonably practicable'. This design target implies the use of a large risk aversion factor, of order 10; a reduction in the 'source terms' for severe accidents would increase this factor still further.

ACKNOWLEDGMENT

The views expressed in this paper are those of the authors and do not necessarily represent those of their parent organisations or other bodies.

REFERENCES

- 1 Cave L. and Kastenbergh W.E. "The Development of Quantitative Criteria for the Decay Heat Removal Function of LWRs", Proc. of CSNI Specialist Meeting on "Decay Heat Removal Systems", Wurenlingen, Switzerland, April 1983.
- 2 Lin K.Y., Cave L. and Kastenbergh W.E. "A Value/Impact Assessment for Alternative Decay Heat Removal Systems", Proc. of this Meeting.
- 3 USNRC, "Policy Statement on Safety Goals for the Operation of Nuclear Power Plants", 14 March 1983.
- 4 USNRC, "Plan to Evaluate the Commission's Safety Goal Policy Statement", 14 March 1983.
- 5 Cave L., Harrison J.R. et al "The Practical Application of Quantitative Safety Criteria for NPP", Proc. of ANS/ENS Topical Meeting on "Probabilistic Risk Assessment", New York, September 1981.
- 6 Central Electricity Generating Board, "Pressurized Water Reactor Design Safety Guidelines", D962, Issue A, April 1982.
- 7 Heaberlin S.W. et al "A Handbook for Value/Impact Assessment", NUREG/CR-3568, December 1983.
- 8 Aldrich D.C. et al "Technical Guidance for Siting Criteria Development", NUREG/CR-2239, December 1982.
- 9 Burke R.P. and Aldrich D.C. et al "Economic Risks of Nuclear Power Reactor Accidents", NUREG/CR-3673, April 1984.
- 10 Strip D.R. "Estimates of the Financial Consequences of Nuclear Power Reactor Accidents", NUREG/CR-2723, September 1982.
- 11 Meyer J.F. Testimony given at the Hearings on Indian Point Units 2 and 3, New York, 1983.
- 12 Reactor Safety Study, US Nuclear Regulatory Commission WASH-1400 (NUREG-75/014), 1975.
- 13 Berry D.L. and Sanders F.A. "Study of Alternate Decay Heat Removal Concepts for LWRs - Current Systems and Proposed Options", NUREG/CR-1556, April 1981.

APPLICATION OF PROBABILISTIC RISK ASSESSMENT TECHNIQUES AS A
DECISION TOOL IN THE U.S. NUCLEAR REGULATORY COMMISSION'S
SYSTEMATIC EVALUATION PROGRAM

Mark P. Rubin

U.S. Nuclear Regulatory Commission
Washington, D.C. 20555

B. Atefi, D. W. Gallagher, R. T. Liner
Science Applications, Inc.
McLean, Va. 22102

ABSTRACT

Probabilistic risk assessment techniques are finding increasing application as decision tools in regulatory programs of the US NRC. One area where they are being applied is in the Systematic Evaluation Program, which is a review and evaluation of older operating nuclear power plants in the United States against current licensing criteria and safety standards. In this program deviations against current safety requirements are identified and assessed. Where necessary, modifications are suggested in plant hardware, operating procedures or Technical Specifications. For selected issues within this program, probabilistic risk assessment techniques were applied to identify the significance of deviations from current safety requirements. These techniques were also utilized to determine the risk/benefit from various proposed corrective actions and to help select the most effective of various alternatives.

BACKGROUND

In the later 1960s and early 1970s, the U.S. Atomic Energy Commission's (now Nuclear Regulatory Commission) scope of review of proposed power reactor designs was evolving and somewhat less defined than it is today. The requirements for acceptability evolved as new facilities were reviewed. In 1967, the Commission published for comment and interim use proposed General Design Criteria for Nuclear Power Plants (GDC) that established minimum requirements for the principal design standards. The GDC were formally adopted, though somewhat modified, in 1971, and have been used as guidance in reviewing new plant applications since then. Safety guides issued in 1970 became part of the Regulatory Guide Series in 1972. These guides describe methods acceptable to the staff for implementing specific portions of the regulations, including certain GDC, and formalize staff techniques for performing a facility review. In 1972, the Commission distributed for information and comment a proposed "Standard Format and Content of Safety Analysis Reports for Nuclear Power Plants," now Regulatory Guide 1.70. It provided a standard format for these reports and identified the principal information needed by the staff for its review. The Standard Review Plan (SRP, NUREG-75/087) was published in December 1975 and updated in July 1981 (NUREG-0800) to provide further guidance for

improving the quality and uniformity of staff reviews, to enhance communication and understanding of the review process by interested members of the public and nuclear power industry, and to stabilize the licensing process. For the most part, the detailed acceptance criteria prescribed in the SRP are not new; rather they are methods of review that, in many cases, were not previously published in any regulatory document.

Because of the evolutionary nature of the licensing requirements discussed above and the developments in technology over the years, operating nuclear power plants embody a broad spectrum of design features and requirements depending on when the plant was constructed, who was the manufacturer, and when the plant was licensed for operation. The amount of documentation that defines these safety-design characteristics also has changed with the age of the plant--the older the plant, the less documentation and potentially the greater the difference from current licensing criteria.

SYSTEMATIC EVALUATION PROGRAM OBJECTIVES

The Systematic Evaluation Program (SEP) was initiated by the U.S. Nuclear Regulatory Commission (NRC) in 1977 to review the designs of older operating nuclear power plants in order to reconfirm and document their safety. The review provides (1) an assessment of the significance of differences between current technical positions on safety issues and those that existed when a particular plant was licensed, (2) a basis for deciding on how these differences should be resolved in an integrated plant review, and (3) a documented evaluation of plant safety.

The original SEP objectives were:

- (1) The program should establish documentation that shows how the criteria for each operating plant reviewed compares with current criteria on significant safety issues, and should provide a rationale for acceptable departures from these criteria.
- (2) The program should provide the capability to make integrated and balanced decisions with respect to any required backfitting.
- (3) The program should be structured for early identification and resolution of any significant deficiencies.
- (4) The program should assess the safety adequacy of the design and operation of currently licensed nuclear power plants.
- (5) The program should use available resources efficiently and minimize requirements for additional resources by NRC or industry.

Many of the plants selected for review were licensed before a comprehensive set of licensing criteria had been developed. They include five of the oldest nuclear reactor plants and seven plants under NRC review for the conversion of POLs and FTOLs. The plants to be considered under the original Phase II program were

- (1) Yankee
- (2) Haddam Neck

- (3) Millstone 1
- (4) Oyster Creek
- (5) Ginna
- (6) La Crosse
- (7) Big Rock Point
- (8) Palisades
- (9) Dresden 1
- (10) Dresden 2
- (11) San Onofre

REVIEW METHOD

Overview

The Systematic Evaluation Program (SEP) review procedure represents a departure from the typical NRC staff reviews conducted to support the granting of a construction permit or operating license for a new facility or a license amendment for an operating facility. A typical licensing review starts with the submittal by the utility of a safety analysis report (SAR) that describes the design of the proposed plant. The staff reviews the SAR on the basis of the Standard Review Plan (SRP), Regulatory Guides, and Branch Technical Positions (found in the SRP) that constitute current licensing criteria. The guidelines in the SRP represent acceptable means of complying with licensing regulations specified in Title 10 of the Code of Federal Regulations (10 CFR).

The SEP was initiated by NRC, and not by the licensee as part of an application for a license or request for a license amendment. The SEP procedure involves several phases of data gathering and evaluation so that an integrated assessment of the overall plant safety can be made. The various phases and their interrelationships are described below.

Selection of Topic List

A list of significant safety topics was derived from existing safety issues during Phase I of the program. More than 800 items were considered in the development of the original list; however, a number of these were found to be duplicative in nature or were deleted for other reasons. The number of remaining issues varied by plant. Generally, approximately 100 significant issues remained for the detailed SEP review.

Topic Evaluation Procedures

Each remaining SEP topic was reviewed to determine whether the corresponding plant design was consistent with current licensing criteria such as regulations, guides, and SRP review criteria, or the equivalent of such criteria. Where the plant was not consistent with current licensing criteria, and no acceptable utility actions have been taken, the differences from these criteria were evaluated as potential candidates for modification. The final phase of the SEP involved an "integrated assessment" of topics not in compliance with current regulations.

INTEGRATED PLANT SAFETY ASSESSMENT

The objective of the integrated plant safety assessment is to make balanced and integrated decisions on when to modify SEP facilities to current licensing criteria. Factors considered important in reaching decisions on modification include safety significance, radiation exposure to workers, and, to a lesser extent, implementation impact and schedule. To provide insights on the safety significance of the various areas of nonconformance with current NRC regulations, probabilistic risk assessment techniques were utilized in the integrated assessment phase.

Where possible, PRA techniques were applied to the SEP topics. Not all of the issues identified are easily addressed by well-defined PRA techniques. In particular, issues which address the ability of the power plant to safely deal with events for which the frequency and/or effects on plant systems are unknown are not evaluated in this study. PRAs generally examine accident scenarios for which the initiating event frequencies are relatively well known and probabilities of system failures are estimated by detailed consideration of system configuration, random component failures, and system interactions. Thus the issues evaluated are those which address systems or plant features during normal operation or accident situations of relatively well-known frequency. Examples of these topics is given in Table 1 below.

TABLE 1

A Partial List of Typical SEP Issues Evaluated Using PRA Techniques

1. Thermal - Overload Protection for Motors of Motor-Operated Valves
2. Requirements for Isolation of High and Low Pressure Systems
3. ESF Switchover From Injection to Recirculation Mode (Automatic ECCS Realignment)
4. Independence of Redundant Onsite Power Systems
5. Testing of Reactor Trip System and Engineered Safety Features, Including Response-Time Testing

Issues excluded are those dealing with seismic, tornado, or flooding events for which the frequency of a given severity event, or any such event, is not well known. Also excluded are issues dealing with high energy line breaks, where it is not the frequency, but the effects on systems, which is not known. Treating these issues in the framework of PRA would generally be at the edge of the state-of-the-art (since event frequencies, etc., are not well known) and thus our confidence in the risk-based categorization of these issues would be less than for the results of our analysis of those issues

which fit well into present PRA considerations. Table 2 below indicates topics which fall into these categories.

TABLE 2

A Partial List of Typical SEP Issues Not Evaluated Using PRA Techniques

1. Classification of Structures, Components and Systems (Seismic and Quality)
2. Wind and Tornado Loadings
3. Design Codes, Design Criteria, Load Combinations and Reactor Cavity Design Criteria
4. Pump Flywheel Integrity
5. Organic Materials and Post-Accident Chemistry

RISK ASSESSMENT

The probabilistic assessment technique adopted in this study (for those topics amenable to PRA analysis) was to examine the impact of the proposed resolution of each issue on the reliability of plant components or systems or on the likelihood of accident sequences. The impact of an issue on component unavailabilities was determined first. The changes in component unavailabilities were used to calculate system unavailability changes and these were used to estimate core melt frequency changes. If the changes in component or system unavailabilities as a result of resolution of an issue were determined to be insignificant, the analysis was not carried to the next level. Fault tree methodology was used for modelling of the systems or subsystems under consideration.

The above process provided an assessment of the impact of a proposed SEP modification upon the availability of plant systems.

The same multilevel procedure was used to rank the significance of resolution of an issue with respect to risk. If the resolution of an issue had an insignificant effect on the unavailability of a component or system under consideration, the risk significance of the issue was ranked low. If the resolution of the issue had a significant effect on the unavailability of the system under consideration, plant specific or surrogate PRAs were utilized to determine if the systems impacted by proposed SEP modifications would likely appear as important elements in dominant core melt accident sequences. If the effect of resolution of the event was found to be insignificant with respect to the core melt sequence frequency, the risk significance of the issue was ranked low. If the effect on the particular core melt sequence frequency was found to be significant but not dominant to the overall core melt probability, the risk significance of the issue was ranked as medium. Finally, if the resolution of the issue had a significant

effect on the overall core melt frequency, the significance of the issue was ranked high with respect to risk.

If an existing PRA was available for the plant under consideration, the fault trees and quantitative results of the PRA were utilized. Otherwise, when necessary, fault trees were developed and quantified for the systems under consideration. For the plants that a PRA was not available, results of other PRAs performed in the Interim Reliability Evaluation Program (IREP), Reactor Safety Study Methodology Application Program (RSSMAP) and Reactor Safety Study on similar plants were considered. These were used for insights on the importance of systems and accident sequences. In almost all the plants studied the measure of importance of an issue was its contribution to the total core melt frequency. The only exceptions were for the cases of Big Rock Point and Millstone 1 where PRAs, including offsite risk estimates, were available for our study. For these plants the existence of plant specific PRAs allowed the quantification of risk reduction potential and estimation of man-rem reduction due to the resolution of each issue evaluated.

With the exceptions above, although the analysis was quantitative, results were reported as high, medium or low with respect to risk significance. This was done because uncertainties and lack of confidence in approximations such as the use of "similar" PRAs do not warrant the precision that numerical results might suggest or imply. Figure 1 provides an overview of the methodology used in this study.

EXAMPLE OF TOPIC EVALUATION

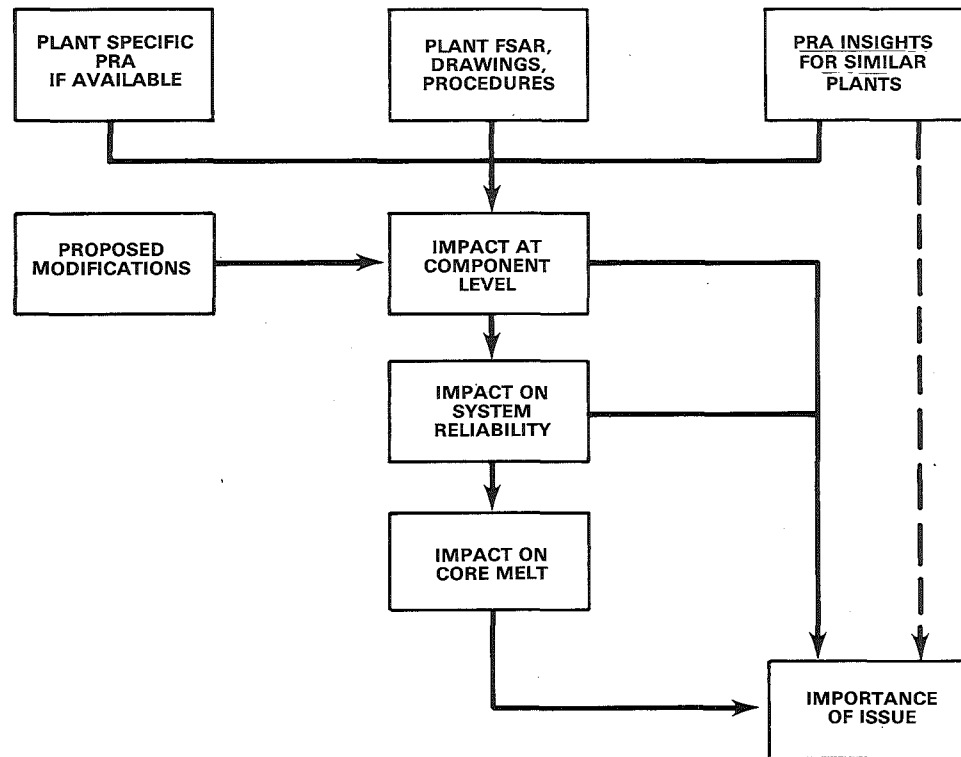
An example of one of the issues analyzed for the Haddam Neck Plant, a 582 MWe PWR with full power operation in 1968, follows.

The Standard Review Plan (SRP) guidelines for ECCS switchover from injection to recirculation states that automatic transfer is preferable to manual transfer. However, in case of manual transfer, the guidelines suggest that there should be sufficient time (about 20 minutes) for the operator to complete this action.

The switchover from Emergency Core Cooling injection to recirculation in the Haddam Neck Plant is currently performed manually. The time available to the operator to perform this task, given a large LOCA and full flow operation of the high and low pressure safety injection pumps and charging pump, is of the order of 6 minutes. If the switchover from injection to recirculation is not performed in time, the water level in the Refueling Water Storage Tank (RWST) would become low enough for the safety injection pumps and charging pumps to be cavitated and possibly damaged. The charging pumps are required for the long-term two-path recirculation of the water so that boric acid precipitation can be avoided. Given that the plant does not satisfy the letter of the SRP guidelines, the issue is whether any of several proposed modifications should be required of the licensee.

To resolve this issue, the core melt frequency as a result of operator failure to switchover from ECCS injection to recirculation following a LOCA

FIGURE 1 Overview of the Methodology Used in this Study



must be evaluated. If the contribution of core melt frequency due to this scenario is determined to be significant with respect to the total core melt frequency, system modification that could reduce the core melt frequency must be analyzed.

A fault tree for the failure of the recirculation system was developed and quantified. A simplified version of this fault tree is shown in Figure 2. The results showed that the failure probability of the current Haddam Neck recirculation mechanism, considering both hardware failures and human error, is 3.1×10^{-2} . Based on an assumed large LOCA frequency of 1.0×10^{-4} per year, this leads to a frequency of 3.1×10^{-6} /year for this particular core melt scenario. The total core melt frequency for the Haddam Neck Plant has never been calculated; hence the importance of the scenario is evaluated by comparing the above core melt probability with the typical core melt probabilities developed for similar PWRs in the IREP, RSSMAP and Reactor Safety Study. Based on these evaluations, the overall core melt frequency is in the range of 3×10^{-5} to 2×10^{-4} /year. At the lower end of this range, complete elimination of the injection-to-recirculation switchover failure scenario would have an effect on core melt frequency of approximately 10%, but it would not change the order of magnitude of the frequency. This issue is therefore ranked as having medium significance from the risk point of view.

Two alternatives to this configuration were analyzed. In the first case, addition of a set of redundant annunciator level instruments to the RWST was considered. The licensee has in fact made a commitment to add a redundant set of alarmed level indicators. This change resulted in reduction of the estimated failure probability of the recirculation system to 3.9×10^{-3} , which is an order of magnitude smaller than for the present configuration. This leads to a core melt frequency of 3.9×10^{-7} /year, due to recirculation failure. Judging from previous PRAs, this is insignificant at the available level of precision.

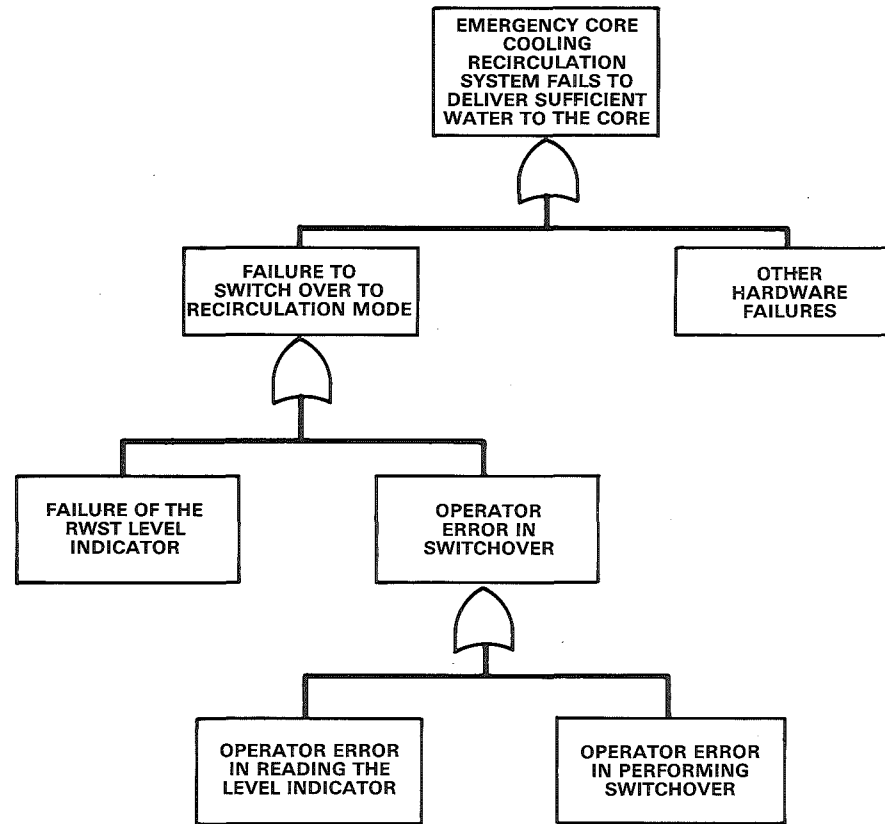
A second modification involving redundant alarms and an automatic switchover mechanism was also evaluated. Although some further benefit (reduction in system failure probability) was derived from the addition of the automatic switchover, the addition of redundant alarmed sensors alone was deemed adequate. The same PRA based approach was applied to all SEP topics amenable to these techniques. The final risk importance of all evaluated topics on Haddam Neck are given below in Table 3. It should be understood that these risk results were only one of several decision tools utilized by the US NRC for determination of modification requirements. Due to limitations and uncertainties in the risk results, deterministic analysis, and engineering judgment were also heavily relied upon for guidance. Details of the SEP plant evaluations can be found in NUREGs 0820-0827.

TABLE 3

Classification of Issues Importance to Risk

<u>HIGH</u>	VI - 7.C.1	Independence of Redundant Onsite Power Systems
	VIII - 3.A	Station Battery Test Requirements
	VIII - 3.B	DC Bus Voltage Monitoring
	IX - 5	Ventilation Systems

FIGURE 2 Simplified Fault Tree of Switchover Process



MEDIUM

- V - 11.A Requirements for Isolation of High and Low Pressure Systems
- VI - 7.B ESF Switchover from Injection to Recirculation Mode (Automatic ECCS Realignment)

LOW

- III - 8.A Loose Parts Monitoring
- III - 10.A Thermal Overload Protection for Motors of Motor Operated Valves
- IV - 2 Reactivity Control System Including Functional Design and Protection Against Single Failure
- V - 5 RCPB Leak Detection
- V - 10.A Residual Heat Rmoval System Heat Exchanger Tube Failure
- V - 10.B RHR System Reliability
- V - 11.B RHR Interlock Requirements
- VI - 4 Containment Isolation System
- VI - 10.A Response Time Testing
- VII - 2 Onsite Emergency Power Systems - Diesel Generator
- XV - 16 Radiological Consequences of Failure of Small Lines Carrying Primary Coolant Outside Containment
- XV - 17 Steam Generator Tube Rupture (System and Radiological Consequences)

CONCLUSIONS

Our experience has shown that this kind of analysis can be quite valuable in prioritization of different issues when dealing with a large number of topics. This will enable the analyst to focus the deterministic and more detailed probabilistic analysis on those issues which are important with respect to risk. More specifically, it was found that many proposed modifications that might intuitively be expected to be important may in fact be quite insignificant when viewed in the context of public risk associated with the operation of a plant. However, when a proposed modification does turn out to be important from the standpoint of risk, the quantitative probabilistic analysis usually provides very strong and convincing support to be considered along with other deterministic factors. Overall, we believe that probabilistic analysis can often be used very effectively in evaluating different regulatory requirements and in choosing among alternative ways of meeting the requirements.

PRA - TO WHAT DEPTH?
(The "Bed of Nails" Effect)

H. Fuchs and L. Miteff

Motor-Columbus Consulting Engineers
Parkstrasse 27, CH-5401 Baden, Switzerland

ABSTRACT

A common feature of probabilistic risk studies for nuclear power plants is a very uneven distribution of the main contributors to the core melt risk.

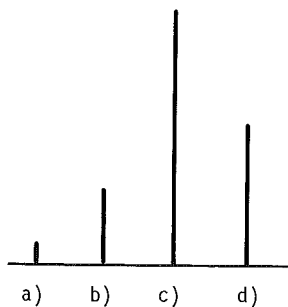
A partial PRA for a 3-loop PWR confirmed this picture of an imperfect "bed of nails": having shortened the most prominent "nail" (risk contributor) by further analysis/plant improvements, an ever increasing number of the next-longest nails called for suitable treatment. Realistic analysis and plant improvements may well bring down the calculated core melt risk by more than an order of magnitude compared to Rasmussen but the many "nails" to be treated lead to diminishing returns for the sharply increasing amount of work required.

INTRODUCTION

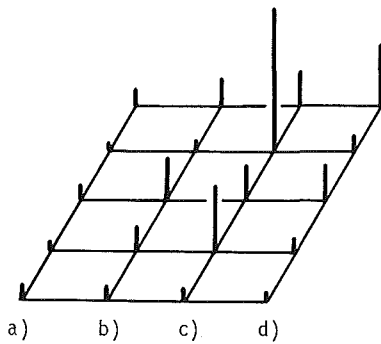
Both the Rasmussen report [1] and the German risk study [2] show a very uneven distribution of the main contributors to the risk of core melt. Looking at the risk contributions from the initiating events:

- a) large LOCA
- b) intermediate LOCA
- c) small LOCA
- d) transients

the small LOCA represents by far the most prominent contributor for a PWR as illustrated qualitatively below:



Each of these four contributors to the core melt risk is composed of a number of components (sequences) with widely varying risk contributions, so that the detailed risk profile for a) - d) looks like a very imperfect "bed of nails":



The length of the nails corresponds to the core melt frequency per year induced by the various sequences. Each sequence describes a combination of failures in the safety systems which might lead to core melt.

Which amount of effort should be spent by the PRA-team/plant operator towards a reduction of the most prominent risk contributors, i. e. towards a more usable "bed of nails"?

Having shortened the most prominent nail by deeper analysis and/or modifications in the plant - one drops upon the next highest nails and so on - until one realizes that the way to a more perfect bed of shorter nails is paved with a rapidly increasing amount of effort needed.

The paper describes some lessons learned from PRA work which was started to dig deeper (or to improve a "bed of nails"...).

HOW THE PRA STARTED

In 1978 a working group, including members from Swiss licensing bodies, nuclear utilities and a consultant started to tackle the questions:

- What is the appropriate basis for emergency planning, especially for cases with ground contamination?
- How far can results from the Rasmussen study be transferred to reactor plants in Switzerland?

Taking as a reference plant a 3-loop PWR, both differences in containment and systems to the Surry-1 plant were taken into account, as described in [3]. The result was a core melt probability about an order of magnitude smaller than for Surry. Meanwhile, more results from the German Risk Study became available and were taken into account. This resulted in 1981 in a core melt frequency of $1.7 \cdot 10^{-5}/a$ as compared to $8.6 \cdot 10^{-5}/a$ (German Risk Study) or $1.3 \cdot 10^{-4}/a$ (Rasmussen).

The most important contributors to this figure of $1.7 \cdot 10^{-5}/a$ were:

Small LOCA	71 %
Intermediate LOCA	12 %
ATWS	12 %

The small LOCA included the following main sequences:

Cooldown with 100 K/h	57 %
HP Injection	25 %
LP Injection	12 %

HOW THE "BED OF NAILS" WAS ATTACKED (Incentives for a deeper analysis)

The working group and especially the plant owner felt that the analysis had not gone to sufficient depth to take credit of various extra features of the reactor under investigation. On the other hand, new evidence [4] showed that the (licensing) criteria for success of ECCS functions in case of a small LOCA were overly pessimistic. It was therefore decided to refine the analysis, especially for cooldown and for HP injection. In order to limit total expenditure, no major computer effort was planned, no new tools were to be developed.

Work thus concentrated upon differences in plant features, which were critically evaluated. As far as available, new results on realistic success criteria (instead of the licensing criteria) were used (so-called "best-estimate" criteria).

COOLDOWN WITH 100 K/H

If a "small leak" is smaller than about half the upper limit of the small LOCA in the German Risk Study, then the primary circuit has to be cooled down by auxiliary feedwater, so that low pressure (10 bar) is reached before the reactor water storage tanks are empty (a bigger "small leak" loses energy fast enough so that no excessive heat-up of the core occurs before low pressure conditions are reached - in this case, the 100 K/h - cooldown is not absolutely necessary). However, since the size of the break cannot be determined shortly after the onset of the break, the cooldown would be started even for the smaller "intermediate break".

In the reference plant of the German Risk Study (Biblis B), a manual procedure was foreseen for cooling down with 100 K/h: the temperature/time gradient had to be derived from a strip chart and was the basis for the manual control of the valves. The 3-loop plant investigated in this paper uses a semiautomatic procedure:

- special type of a acoustical and optical alarm
- upon this special alarm, the operator triggers...
- ... the automatic cooldown devices

If, for whatever reasons (e. g. because of a faulty control system), the cooldown is too rapid, then the protection logic interpretes this as a break in the secondary side and isolates containment. The 3-loop plant has introduced a special feature which allows a timely reset of containment isolation, provided the operators correctly and timely identify the alarms for containment isolation.

There are two different ways to remove heat during the cooldown: by blowing off steam from the main steam lines to the atmosphere or to the condenser.

Neglecting the latter possibility, the failure probability of the 100 K/h-cooldown was assessed to roughly $5 \cdot 10^{-4}$. Two "nails" (main risk contributors) showed up:

- the risk contribution by the only device giving the set point for the cooldown gradient to all of the 3 loops/control systems
- the risk of failure to reset containment isolation

As a consequence

- all three control systems for the cooldown were equipped with independent set point devices
- reset of containment isolation was made possible from the control room

As a result of these modifications, the failure probability was reduced by a factor of 5 to $1 \cdot 10^{-4}$. If the possibility for blow down of steam to the condenser is taken into account, the failure probability for the 100 K/h-cooldown decreases to about $6 \cdot 10^{-5}$. This figure is in good agreement with the corresponding results from [5].

HIGH PRESSURE (HP) INJECTION

In the case of a small or intermediate leak, the high pressure injection system has to compensate for the water loss through the leak until the low pressure injection system can take over (at about 10 bar primary pressure) the task to remove afterheat.

The main features of interest for the investigation were:

- the peculiarities of a 3 primary loops - 4 x 50 % HP injection trains - combination
- the use of more realistic success criteria for HP injection based on "best estimate" emergency core cooling calculations [4]
- the location of the "small" or "intermediate" leak
- the behaviour of the 3-way valves which direct the HP water to the hot or the cold leg of the primary circuit
- the effect of a potential miscalibration of the pressure sensors which trigger the switch over from high pressure to low pressure injection mode

For the 3 loop - 4 trains problem, leak locations and sizes may deterministically be postulated where the (n-2) criterion might not be literally met. However, taking into account:

- the behaviour of the 3-way valves (pressure drop needed for a switch-over, relative pressure drop of the valves)
- the probability for "special" break locations for which the (n-2) criterion might not be fully met (because too much water is lost)
- realistic (best estimate) success criteria
- the efficiency of the procedure to calibrate the pressure sensors,

it turned out that "special" break locations accounted for less than 10 % of the total risk contribution of the HP injection, the failure probability of which was calculated to lie within the interval

$1.8 \cdot 10^{-4}$ $4.5 \cdot 10^{-4}$ (small leak)
 $7.0 \cdot 10^{-5}$ $3.5 \cdot 10^{-4}$ (intermediate leak)

depending on the assessment of the calibration procedure for the pressure-sensors. The higher numbers refer to a rather conservative judgment as in [2], the lower ones to a "realistic" approach for the common-mode probabilities for

- incorrect switching over from HP to LP injection
- nonactivation of the ECCS

The numbers quoted above show that the "nail" HP injection could be shortened; however, it remains a prominent nail - this points to the potential merits of a 3 loop - 3 train configuration.

SHORTENING FURTHER "NAILS"

The following items led to further risk reduction ("nail-shortening"):

- effect of 6 accumulators instead of 4 as in the reference plant of the German Risk Study: some risk reduction for large and intermediate leaks
- ATWS: a more detailed investigation of pressure peaks during transients allowed a reduction of this risk contribution
- intermediate leaks: the combined effects of the accumulators and the HP injection were taken into account

These considerations led to some further reduction of the total frequency per year of core melt. This gave the following rounded results:

100 K/h cooldown:	$3 \cdot 10^{-7}/a$
HP injection:	$5 \cdot 10^{-7}/a$
Other small LOCA sequences:	$2 \cdot 10^{-6}/a$
Intermediate LOCA:	$8 \cdot 10^{-7}/a$
ATWS:	$1 \cdot 10^{-6}/a$
All other sequences:	$5 \cdot 10^{-7}/a$

giving a total core melt frequency of about $5 \cdot 10^{-6}/a$.

MORE OF THE "BED OF NAILS" EFFECT

The numbers quoted above show clearly the evolution of the relative importance ("length of nail") of the various sequences and subsequences leading to core melt: having succeeded in shortening the most prominent nails by deeper analysis/plant improvements, the next longest nails call for similar treatment - or they become dominant. We experienced that the effort needed to shorten further nails increases sharply while the resulting decrease of the total risk gets more and more modest. The assessment of human failure becomes more important, as illustrated by the 100 K/h cooldown:

In the assessment of 1981, the subsequences

- failure of the special alarm calling for cooldown
- failure of the operator to initiate automatic cooldown upon the special alarm signal

contributed roughly 10 % to the core melt frequency of the 100 K/h cool-down. After deeper analysis and the above-mentioned plant modifications, their relative contribution jumped to about 50 %. This may be somewhat artificial because we took over the lower limit for human failure probability of 10^{-5} (median) of WASH-1400.

Another example is the analysis of the HP injection where the two common-mode (CM) failures probabilities mentioned in Chapter 5 accounted for 43 % of the risk of the HP sequence - as long as success criteria were defined according to licensing requirements. When "best estimate" criteria were adopted, the two CM probabilities increased their relative contribution to over 75 % - again with a strong influence of operator behaviour.

The "bed of nails" effect does not only show up within an accident sequence, but also for the set of sequences leading to core melt. An example to that is the relative contribution of the LP injection to the small LOCA: it jumps from 12 % in the 1981 version to almost 60%! Another example are ATWS: their contribution to core melt rose from 12 % to around 20 %.

Considering the amount of work involved: a reduction of core melt frequency by a factor of around 5 ($8.6 \cdot 10^{-5}/a$ in the German Risk Study; $1.7 \cdot 10^{-5}/a$ as per 1981) needed a substantial effort - the further reduction by a factor of around 3 (i. e. to $5 \cdot 10^{-6}/a$) even more so!

We feel that a further reduction by a factor of 2 would require at least the same effort as for the previous factor of 3. For budgetary reasons this work should therefore be stopped way before an asymptotic, comfortable "bed of nails" is reached.

Coming to the lessons learnt during the study, one should recall that the "big" risk studies [1] and [2] gave rise to a large number of modifications in various plants and to design changes for newly designed reactors. A transfer of the results of those studies is therefore very worthwhile and - in the case of the 3-loop PWR investigated here - led also to some modifications in the plant. For the purpose of emergency planning, the work proved to be helpful, but could have been terminated somewhat earlier. Areas for further study for the benefit of plant operators and designers could be:

- more accurate and more specific values for the failure probabilities of important mechanical and electrical hardware
- better assessment of human failure (operator behaviour, maintenance, calibrations, tests ...)
- better analysis of anticipated transients/without scram

CONCLUSIONS

- The approach to attack in each successive step the most prominent risk contributors ("nails") is a very sound procedure at least for comparative PRA's
- The 3-loop PWR investigated in this study proved to have a number of positive features (mainly in systems) and some more were added as a result of the PRA study
- Although it was possible to shorten the most prominent nails in the "bed of nails", still a rather uneven distribution of risk contributors remained. The effort necessary for the analyses increased progressively, indicating some "law of diminishing returns" for the effort in analysis, discussion, consensus finding, etc.
- As the risk contributions from the systems and components decrease due to deeper analysis and plant improvements, the human failure contribution gains relative weight
- The results were instrumental in limiting the scenarios used for emergency planning. Further progress is expected from the world-wide source term work where some important risk reduction ("nail-cutting") is in progress.

ACKNOWLEDGMENTS

Important contributions to this study came from Messrs. R. Gubler, J. Landolt and S. Chakraborty. The work of Motor-Columbus was funded by a group of Swiss utilities (GSKL).

REFERENCES

- [1] US NRC: Reactor Safety Study: An Assessment of Accident Risks in US Commercial Nuclear Power Plants, October 1975; WASH-1400 (NUREG 75/014, PB 248 201)
- [2] Deutsche Risikostudie Kernkraftwerke, Verlag TUV Rheinland 1979/80
- [3] R. Gubler, H. Fuchs, S. Chakraborty: Determination of Accident Source Terms for the Nuclear Power Plant Gösgen on the Basis of WASH-1400; IAEA-CN-39/9 (October 20 - 24, 1980)
- [4] Abschlussbericht, Förderungsvorhaben BMFT RS 306: Best-Estimate Notkühlrechnungen für hypothetische Ausfallkombinationen des Notkühlsystems bei DWR's, Kraftwerk Union RE 23/012/79 (October 1979)
- [5] H. Fabian, H. Sobotka: Valuation of Heat Removal Systems of a More Recent KWU PWR 1300 MWe Plant; Sobotka
Proc. CSNI Specialist Meeting, April 25 - 29, 1983, EIR Würenlingen, Switzerland

SEVERE ACCIDENT REACTOR RISKS AND
THE POTENTIAL FOR RISK REDUCTION

A. S. Benjamin, V. L. Behr, F. E. Haskin, and D. M. Kunsman

Sandia National Laboratories
Albuquerque, New Mexico, USA 87185

ABSTRACT

Sandia National Laboratories is performing the Severe Accident Risk Rebaselining and Risk Reduction Program (SARRP) in order to incorporate insights from ongoing programs and task forces toward a rebaselining of reactor risks and of the overall uncertainty. A second objective is to evaluate the benefits and costs of proposed new safety features designed to reduce the frequencies and/or consequences of severe accidents. Results to date indicate that onsite financial risks are generally higher than offsite financial risks, that the uncertainties in the offsite risks are much larger than those in the onsite risks, and that expensive safety options are probably not cost-effective. These results will be a key input to the Nuclear Regulatory Commission's upcoming decision making on severe accidents.

INTRODUCTION

During 1985-1986, the U. S. Nuclear Regulatory Commission (NRC) will decide which of several possible directions it will take on the subject of severe accidents. Various possibilities include a rulemaking for fission product source terms, special provisions for safety backfits, and the establishment of probabilistic safety goals. To provide the proper technical basis for these decisions, the NRC is sponsoring the following activities: (a) a variety of severe accident research programs, combined under the Severe Accident Research Plan; (b) nation-wide task forces on containment loading, containment response, and fission product source terms; (c) reviews of the state-of-the-art by organizations such as the American Physical Society; and (d) technical exchange meetings with the Industry Degraded Core (IDCOR) program.

One of the means for integrating this developing array of technical information is the Severe Accident Risk Rebaselining and Risk Reduction Program (SARRP), which is a part of the Severe Accident Research Plan (SARP). The objectives of this program are as follows:

- (1) Incorporate insights gained from the sources mentioned above toward a rebaselining of reactor risks and of the overall uncertainty in reactor risks.

*This work is supported by the United States Nuclear Regulatory Commission and performed at Sandia National Laboratories which is operated for the US Department of Energy under contract number DE-AC04-76DP00789.

- (2) Evaluate the benefits and costs of proposed new safety features designed to reduce the frequencies and/or consequences of severe accidents.

The first objective (risk rebaselining) is being accomplished first for specific plants that have been analyzed previously in probabilistic risk assessments, and then for generic plant categories derived by a risk-based grouping of plant designs. Both a plant-specific and a generic perspective on reactor risks will result from these analyses.

The plant-specific part of the rebaselining covers six reference plants having the following types of containments: (a) PWR large-dry, (b) PWR subatmospheric, (c) PWR ice condenser, (d) BWR Mark I, (e) BWR Mark II, and (f) BWR Mark III. The generic part involves a cooperative effort with the Accident Sequence Evaluation Program (Ref: F. T. Harper, these proceedings) to establish general risk profiles on the basis of system design, containment design, and siting factors. ASEP performs the systems evaluations, while SARRP focuses upon the containment and siting aspects.

For the second objective (cost-benefit analysis) we are comparing the risk reduction benefits of a variety of safety options to the costs of implementation. We are directing the cost-benefit analyses primarily toward existing plants, although some of the results can be extrapolated to new plants.

The safety options under consideration include systems that prevent the core from melting and systems that mitigate the consequences. Mitigation options include: (a) hydrogen control systems, (b) filtered or unfiltered containment venting systems, (c) increased containment pressure or temperature capability, (d) additional containment cooling capability, (e) independent containment spray trains, (f) passive or active core retention devices, (g) containment water management schemes, and (h) missile shields. Prevention options include: (a) additional trains of emergency core cooling or auxiliary feedwater, (b) incorporation of feed-and-bleed capability, (c) automatic primary system depressurization capability for PWRs, (d) reactor protection system improvements, (e) improved onsite ac power reliability, (f) improved service water reliability, (g) improved logic for crossover to recirculation, (h) improved maintenance of check valves and floor drains, and (i) other plant-specific modifications.

The first phase of SARRP will be completed during summer 1985. The work to be accomplished by that time includes a complete iteration on the objectives described above. This paper describes the fundamentals of our methodology and presents some preliminary results for two of the reference plants -- the PWR subatmospheric containment and the BWR Mark III containment.

PLANT-SPECIFIC REBASELINE

To discuss the elements that contribute to the rebaselining of reactor risks, it is convenient to represent the risk in the following way, as the sum of a product of factors:

$$RISK_K = \sum_{I,J} \text{FREQ}_I \cdot \text{CFM}_{I,J} \cdot \text{CONS}_K(\text{FP}_{I,J})$$

Here $RISK_K$ is the mean risk associated with consequence K, and

FREQ_I = frequency of accident sequence I.

- $CFH_{I,J}$ = probability of containment failure mode J, conditional upon occurrence of accident sequence I.
- $CONS_K(FP_{I,J})$ = mean magnitude of consequence K, given fission product releases $FP_{I,J}$ for containment failure mode J of sequence I.

Our evaluations of risk include societal risks (e.g., early fatalities and latent cancer fatalities per year) and individual risks (e.g., mortality probability for an individual living close to the plant).

When considering plant modifications that have the potential for reducing risk, and for which the risk reduction benefit must be weighed against the cost of implementation, it is convenient to generalize the risk equation, above, to a "financial risk" equation. Financial risk may be defined as follows:

$$FRISK_L = \sum_{K,L} RISK_K \cdot COST_{K,L}$$

where $FRISK_L$ is the mean financial risk based on a method of evaluation L, expressed as dollars per year or per life of the plant, and $COST_{K,L}$ is the cost associated with consequence K in evaluation method L. Four evaluation methods that we use in cost-benefit analyses of plant modifications are:

- (1) Offsite Financial Risk -- The mean financial risk resulting from the offsite costs of severe accidents (e.g., offsite property damage and the cost of early and latent fatalities).
- (2) Onsite Financial Risk -- The mean financial risk resulting from onsite costs (e.g., replacement power and cleanup costs).
- (3) Total Financial Risk -- The sum of offsite and onsite financial risks.
- (4) Financial Risk ALARA Guideline -- A surrogate measure of financial risk, based on evaluating population dose at \$1,000 per person-rem.

Accident Sequence Frequencies

The rebaselining of plant-specific sequence frequencies is being provided to us by the Accident Sequence Evaluation Program. ASEP utilizes insights obtained from probabilistic risk assessment (PRA) experience and from reported precursor events to update the accident sequence frequencies provided in the original PRAs.

A sampling of ASEP results is given in Table I. In general, ASEP has found that core melt accidents resulting from reactor coolant pump seal failures and station blackouts are more probable than originally estimated, while certain other sequences are less probable.

At this time, the ASEP plant-specific frequency rebaselining includes some but not all of the plant modifications that have occurred since the PRAs were originally performed, and some but not all of the credits for improved procedures. ASEP will more fully evaluate the potential effects of post-PRA improvements on sequence frequencies during the next several months. As a result, some of the numbers in Table I may change.

Table I. Sampling of Interim Rebaselined Accident Sequence Frequencies

<u>Sequence Notation</u>	<u>Sequence Description</u>	<u>Original PRA Frequency</u>	<u>ASEP Rebaselined Frequency</u>
<u>PWR Subatmospheric Containment</u>			
S ₃ D	Reactor coolant pump seal leak resulting in plant shutdown, followed by failure of emergency core cooling in the injection phase.	Not Evaluated	9x10 ⁻⁵
TMLB'	Loss of offsite and onsite ac power (station blackout).	3x10 ⁻⁶	2x10 ⁻⁵ 1x10 ^{-4*}
TKMU	Transient followed by failure to scram, loss of main feedwater, and failure of high pressure emergency core cooling injection.	<10 ⁻⁶	1x10 ⁻⁵
TML	Transient with loss of main and auxiliary feedwater.	6x10 ⁻⁶	4x10 ⁻⁶
<u>BWR Mark III Containment</u>			
TQW	Transient event with loss of main feedwater and residual heat removal.	2x10 ⁻⁵	9x10 ⁻⁶
TC	Transient event followed by failure to scram.	5x10 ⁻⁶	5x10 ⁻⁶
TQUV	Transient event followed by failure of all water delivery systems. Station blackout is included in this sequence.	2x10 ⁻⁶	4x10 ⁻⁶

*Higher frequency for TMLB' applies if loss of reactor coolant pump cooling causes a large pump seal LOCA.

Containment Failure Mode Probabilities

SARRP is performing a study for the NRC Accident Source Term Project Office (ASTPO) to reassess the various ways in which containments are threatened and to reevaluate the failure mode probabilities. To perform this analysis, we are developing comprehensive containment event trees for each of the six reference plants. The event trees delineate the various pathways that the accident can take following the loss of core cooling (or in some cases the loss of containment cooling). Thus, they include not only containment failure events but also events that describe the progression of core degradation and the state of the plant.

To quantify the event trees, and hence to determine the probabilities of the various accident pathways, we are drawing upon information from a wide variety of sources. These include NRC-sponsored studies, such as the Containment Loads Working Group, Containment Performance Working Group, Battelle source term analysis for ASTPO (BMI-2104), and Severe Accident Sequence Analysis (SASA) program; also Industry-sponsored sources, such as the Industry

Degraded Core (IDCOR) program. The study will be completed at the end of this year and documented as a part of the ASTPO final report (NUREG-0956).

Figure 1 shows some sample results. Each probability in Figure 1 is the summation of the probabilities of the various accident pathways that lead to a particular containment failure mode, given the occurrence of a particular initiating accident sequence. The containment failure mode probabilities for each accident sequence sum to unity.

Three separate estimates are given in Figure 1 -- optimistic, central, and pessimistic. Basically, these correspond to the low, medium, and high estimates of containment loading and response provided by the Containment Loads and Performance Working Groups. In some cases, the differences between the three estimates reflect differences between sources (e.g., BMI-2104 results compared to IDCOR results).

The analysis at this time is quite preliminary and somewhat incomplete. For example, containment failure from steam explosions and from direct coupling of core debris energy to the atmosphere ("direct heating") have not yet been included. They will be included before the study is completed.

In general, we are finding that the original PRAs underestimated the probability that containment survives a core melt without failure. They may also have underestimated the probability of containment leakage resulting from penetration failures at high pressure or temperature. For some sequences, the original PRAs overestimated the probability of containment failing early during the accident timeline, a situation which can lead to high consequences. In other cases they may have underestimated that probability.

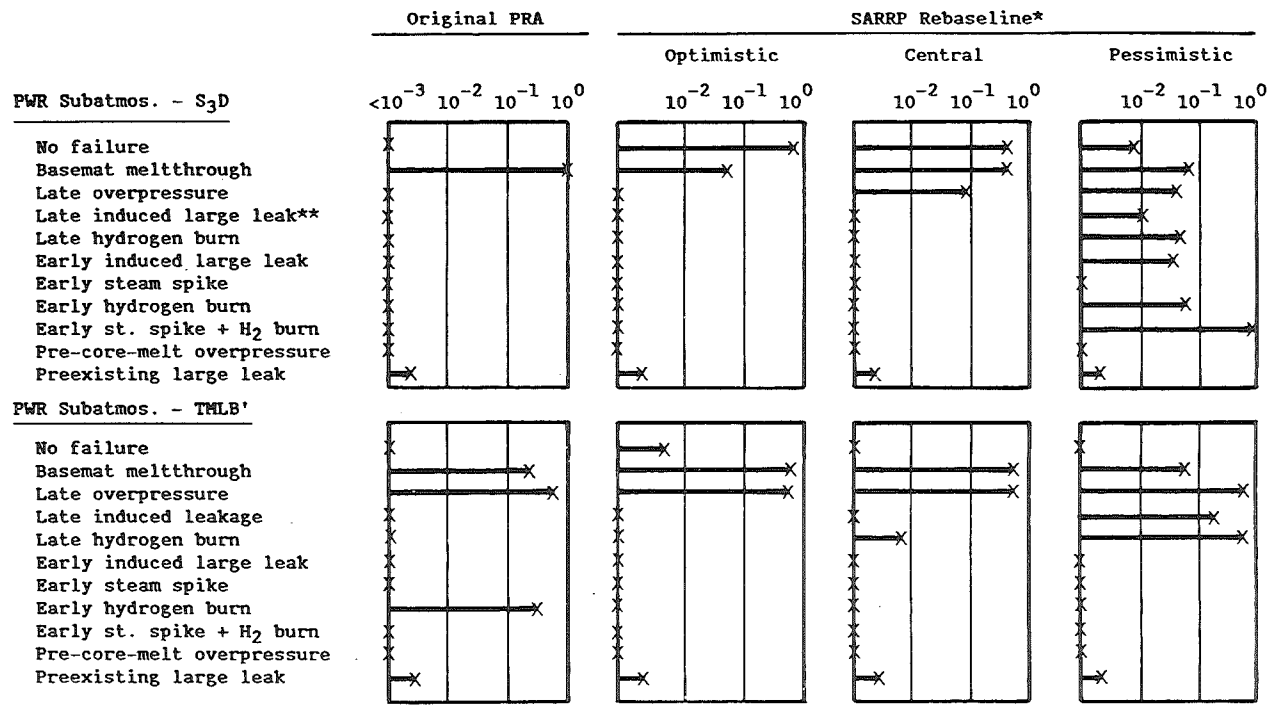
Fission Product Source Terms

The plant-specific rebaselining of fission product releases to the environment are provided by the Battelle calculations for ASTPO in BMI-2104 and by the NRC-sponsored project entitled Quantitative Uncertainty Estimate of the Source Term (QUEST). We use the BMI-2104 calculations for the central estimate and the QUEST calculations for the optimistic and pessimistic estimates. Sample results from these studies are given in Figure 2.

In general, the BMI-2104 calculations have produced lower source terms than those used in the original PRAs, which were based on WASH-1400. The amount of difference varies strongly between reactor plants, accident sequences, and containment failure modes. The calculations indicate that the source term is very small if the containment sprays continue to operate through the sequence or if the containment survives to late times. However, these calculations do not account for late-time reevolution of fission products from the primary system due to decay heating of the surfaces.

Accident Costs

The Regulatory Analysis Program provides us with information about the costs that would be incurred from severe reactor accidents (Ref: R. K. Burke, these proceedings). Briefly, the costs of early and latent fatalities are inferred from the expenditure that society has traditionally been willing to make to prevent deaths (typically \$10⁵ to \$10⁷ per death, based on data from various sources). Property damage costs are obtained from CRAC-2 code calculations. Onsite consequence costs, such as the costs of replacement power and post-accident cleanup, are estimated from industry



*Containment failure from steam explosions and direct atmospheric heating are not yet included in the rebaseline; see text.

**A large leak is defined as one which precludes containment failure from gradual overpressurization-- i.e., at least 25 sq. cm.

Figure 1. Sampling of Interim Rebaselined Containment Failure Mode Probabilities

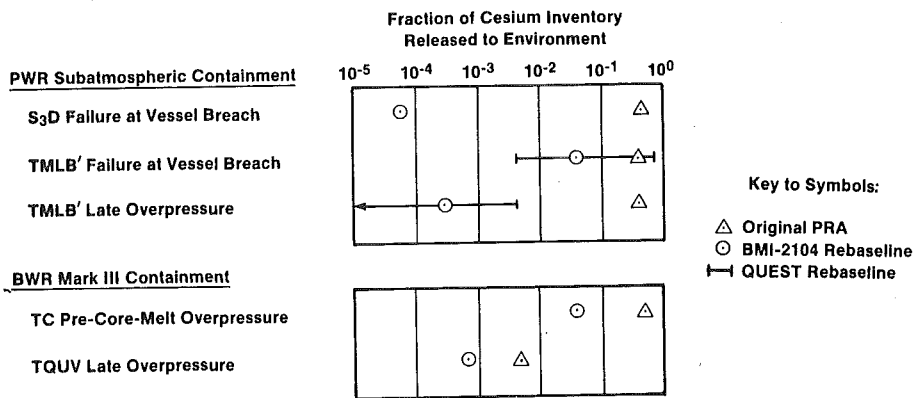


Figure 2. Sampling of Interim Rebaselined Fission Product Source Terms

experience. The costs are usually present-value discounted at a fixed percentage rate (e.g., 4 percent per year) to account for the difference between the prevailing interest rate and the rate of inflation.

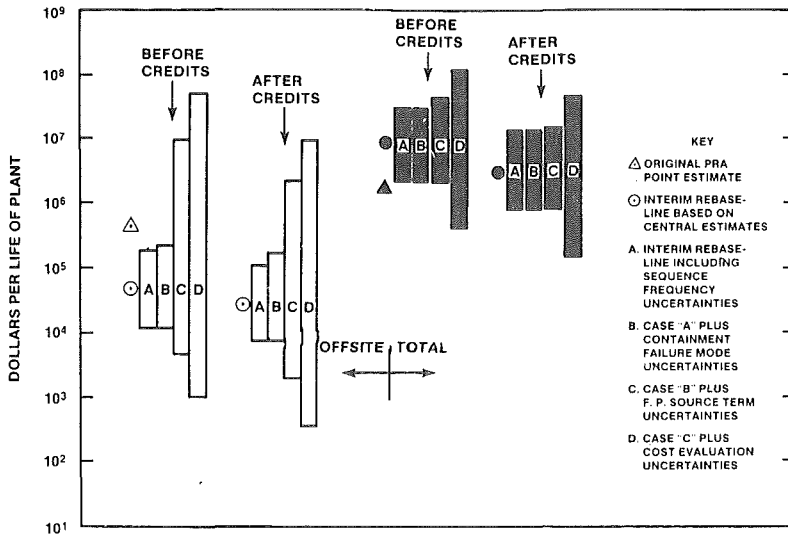
Financial Risk

Figure 3 shows some estimates of offsite and total financial risk for the PWR subatmospheric and BWR Mark III reference plants. The results should be considered preliminary and subject to modification as new information becomes available. We present them as sample interim results which depict the general character but not necessarily the final values of the results to be published in 1985.

Two point estimates and four uncertainty bands are illustrated for each case. The first point estimate (△) provides a financial risk estimate corresponding to the results provided by the original PRA. The second point estimate (○) derives from rebaselined central estimates of the sequence frequencies, containment failure mode probabilities, fission product source terms, and accident costs. The first uncertainty band (A) examines the effects of sequence frequency uncertainties on the rebaselined central estimate. The others add to each previous band the uncertainties associated with (B) containment failure mode probabilities, (C) fission product source terms, and (D) accident costs.

Two plant configurations are examined. The first includes only those post-PRA plant improvements which have been formally included in the ASEP frequency rebaselining. The second estimates the potential effects of credits that are currently being considered by ASEP but have not yet been incorporated into their estimates. For the PWR subatmospheric plant, these post-PRA credits include (a) reactor protection system improvements, (b) auxiliary feedwater cross-tie, (c) primary system feed-and-bleed capability, (d) emergency procedures for depressurizing the secondary system, and (e) credit for attaining cold shutdown during certain slow-to-develop sequences. For the BWR Mark III plant, they include (a) reactor protection system improvements, (b) new operating procedures for automatic depressurization system, (c) emergency procedures for unfiltered containment venting (low volume), and (d) incorporation of a hydrogen igniter system (ac power dependent).

(a) PWR Subatmospheric Containment



(b) BWR Mark III Containment

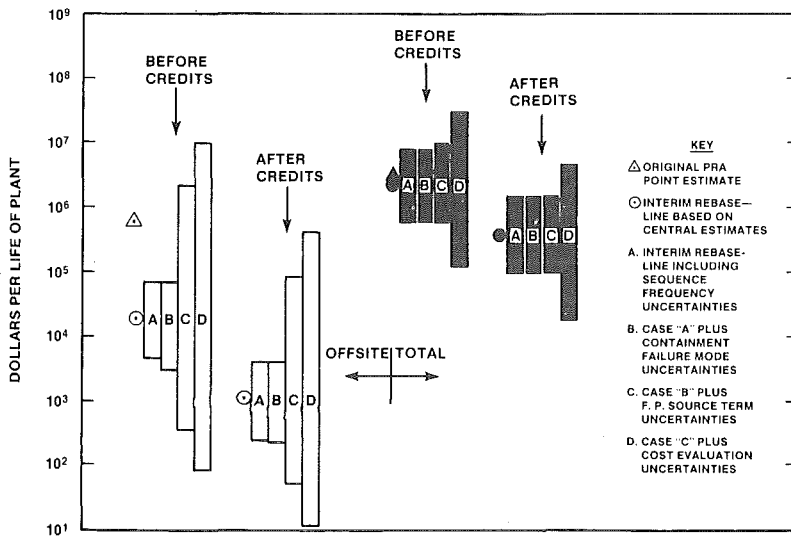


Figure 3. Interim Rebaselined Offsite and Total Financial Risks

It is apparent from Figure 3 that the total financial risk for these plants is considerably larger than the offsite financial risk, indicating the importance of onsite costs such as power replacement and cleanup. The overall uncertainty in the total financial risk, however, is considerably smaller than that for offsite financial risk, because the onsite costs are basically independent of containment failure mode and fission product source term. The rebaselining based on central estimates results in a considerable reduction in the offsite financial risks, compared to the original PRAs, primarily because of the less conservative containment and source term treatment. However, the central-estimate rebaselining for the PWR plant leads to an increase in the total financial risk because of the higher core melt probability. The post-PRA credits discussed above have a potential for reducing both offsite and total financial risks by an order-of-magnitude or more for the BWR, somewhat less for the PWR. Generally, the estimates of financial risk based on the original PRAs fall within the overall uncertainty range of the rebaselined estimates.

Benefits Versus Costs

Figure 4 shows some preliminary estimates of benefit versus cost for three safety options applied to the two reference plants. To conserve space, only the two point estimates and the total uncertainty band (D) are included in the illustrations. The benefit is evaluated as the difference between the financial risks before and after the implementation of the safety option (i.e., the averted financial risk). The cost is the expenditure required for retrofitting the safety option into the reactor plant, including possible down-time costs. The cost estimates were provided by vendors and architect-engineering firms.

Figure 4 illustrates that despite the large uncertainties, certain proposed backfits can strongly be shown to be not cost-effective. These are the cases for which the benefit is unequivocally less than the cost. (i.e., the filtered venting system and auxiliary feedwater train in Figure 4(a) and the residual heat removal train in Figure 4(b).) In cases where the benefit and cost uncertainties overlap, the determination of cost-effectiveness is less clear.

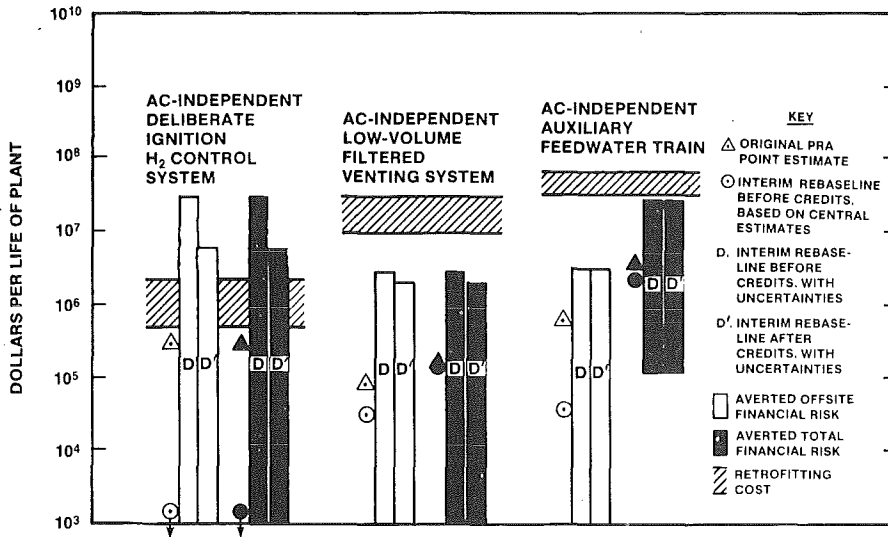
CLOSURE

The information being generated in this program will address severe accident issues in the following ways:

- (1) By displaying the state-of-the-art of risk assessment, it will help to clarify whether risk assessment can be used as a tool for regulatory decision making.
- (2) By portraying quantitatively how the overall uncertainty in financial risk is distributed between various sources, it will help to prioritize phenomenological research.
- (3) By providing a ranking of potential safety options in terms of relative costs and benefits, it will indicate which safety options ought to be considered for further analysis and possible implementation.

The results will thus provide a key input to NRC's upcoming severe accident decision making.

(a) PWR Subatmospheric Containment



(b) BWR Mark III Containment

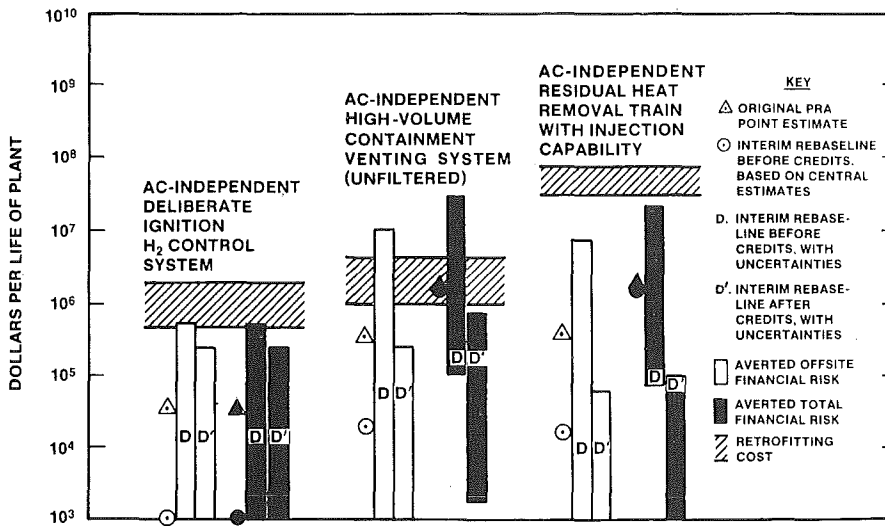


Figure 4. Interim Rebaselined Cost-benefit Comparisons for Three Safety Options

SEVERE ACCIDENT ANALYSIS AND RISK ASSESSMENT
FOR TWO BOILING WATER REACTORS*R. A. Bari, I. A. Papazoglou, W. T. Pratt,
K. Shiu, H. Ludewig, and N. HananDepartment of Nuclear Energy
Brookhaven National Laboratory
Upton, New York 11973, U.S.A.

ABSTRACT

Brookhaven National Laboratory (BNL) has been involved in two comprehensive probabilistic risk assessment (PRA) activities for boiling water reactors. Specifically, detailed reevaluations of the PRAs have been performed for the Limerick Generating Station and for the General Electric Standard Plant, GESSAR-II. The purpose of this paper is to present the insights and conclusions from these studies, and in particular, to focus on the similarities and differences between these studies in terms of methodologies, assumptions, and results.

I. INTRODUCTION

Brookhaven National Laboratory (BNL) has been involved in two comprehensive probabilistic risk assessment (PRA) activities for boiling water reactors. Specifically, detailed reevaluations of the risks have been performed for the Limerick Generating Station and for the General Electric Standard Plant, GESSAR-II relative to those presented in the initial studies. The initial studies were performed by the Philadelphia Electric Company [1], and the General Electric Company [2], respectively, and BNL was chartered by the U.S. Nuclear Regulatory Commission to perform the independent peer reviews.

The purpose of this paper is to present the insights and conclusions from these peer review studies, and in particular, to focus on the similarities and differences between these studies in terms of methodologies, assumptions, and results. In addition, we discuss the peer review processes for these studies.

The risk assessments were performed for two distinct purposes. The Limerick PRA was performed as a condition for the operating license because it was perceived by the NRC that, because of the plant's location near a high population density area, it might pose risks that would be a disproportionately high component of total societal risk from U.S. commercial nuclear reactor operation. The construction of Limerick-I is essentially complete and public hearings are currently being held in connection with (and prior to) its operation. The GESSAR PRA was performed as part of the standard

*This work was performed under the auspices of the U.S. Nuclear Regulatory Commission.

plant safety analysis report which is being reviewed by NRC in connection with its final design approval process for new construction permit applications. The GESSAR PRA is also being evaluated in connection with NRC's activities on severe accident rulemaking [3] for standard plant design certification.

References 1 and 2 did not include within their scopes the assessment of the risks from in-plant fires or from seismic initiators. However, in subsequent studies, both organizations did supplement their initial PRAs with assessments of the risk from in-plant fires and from seismic initiators. These subsequent studies were also reviewed by Brookhaven National Laboratory. The external events analysis for Limerick was reported in the Severe Accident Risk Assessment [4]. The GESSAR-II external events analysis was reported in supplements to Reference 2.

In the case of Limerick, BNL performed a limited review of the Severe Accident Risk Assessment [4] and this is reported in Reference [5]. In Reference 5, BNL concluded that Reference 4 appeared to carry out a state-of-the-art evaluation of the core melt frequency due to seismic and fire initiating events. A limited requantification of the core melt frequency was performed in an attempt to replicate results and to highlight sensitivities to model assumptions.

BNL also performed an assessment of the containment failure modes and fission product release related to seismic initiators and this is reported in Reference [6]. Reference 6 provided technical support information for the Draft and Final Environmental Statements on the Limerick Generating Station by the U.S. Nuclear Regulatory Commission. As per request by NRC, BNL performed an assessment of the fission product source terms in which the WASH-1400 methodology was followed to compute the radionuclide releases to the environment.

In the case of GESSAR, the BNL assessment of the risks from seismic and fire initiators is ongoing at the time of this writing and therefore will not be discussed further here. Thus the remainder of this paper will focus on the internal event contributors to the risk assessments.

II. DESCRIPTION OF PLANTS

A brief description of the plants is presented in this section.

Limerick is a BWR/4 with a MARK-II containment and is rated at 3293 MWt. It is sited in eastern Pennsylvania, near the city of Philadelphia. Details of the plant design can be obtained from Reference 1 and from the Final Safety Analysis Report on Limerick.

GESSAR-II is a BWR/6 with a MARK-III containment and is rated at 3579 MWt. Much of the GESSAR-II design description can be obtained from the Safety Evaluation Report [7] on GESSAR-II. In that report, it can be seen that GESSAR-II is similar to other BWR/6, MARK-III plants such as Grand Gulf, Clinton, and particularly, Perry. The GESSAR-II PRA was performed for a given Nuclear Island Design which does not include the following balance of plant facilities: turbine building; service water building; switchyard. In addition, the offsite consequence analysis was not performed for an actual site but, rather, it was performed with reference to Composite Site #6 of WASH-1400.

Both the Limerick and GESSAR-II designs represent modern BWR technology. In particular, both plants utilize high and low pressure coolant injection systems with automatic depressurization and both plants have reactor protection systems which feature alternate rod insertion, recirculation pump trip and standby liquid control.

III. METHODS AND RESULTS FOR THE TWO STUDIES

In this section a synopsis of the principal methods and results of each study is presented.

III.1 The Limerick PRA

The Limerick PRA used the methods and approaches of WASH-1400 as per request from the U.S.N.R.C. Specifically, the U.S.N.R.C. requested the Philadelphia Electric Company to produce a study which used the basic approach and techniques of WASH-1400, but which accounted for plant-specific design differences between Limerick and the WASH-1400 plant (Peach Bottom) and included site-specific analyses of offsite consequences.

The accident sequences that dominate the core melt frequency are transients (and not accidents initiated by loss of coolant inventory). These include: 1) transients that do not cause feedwater and power conversion system unavailability, coupled with failure of these systems, failure of the high pressure injection systems and failure to timely and manually depressurize the reactor; 2) loss of offsite power transients coupled with failure of the high pressure injection system and failure of either the low pressure injection system or failure to timely and manually depressurize the reactor; 3) transients that imply loss of feedwater and power conversion system, followed by failure of the high pressure injection system and failure of either the low pressure injection system or failure to timely and manually depressurize the reactor; 4) a transient coupled with a failure of the containment heat removal function that leads to containment failure; 5) a transient coupled with failure to scram.

In contrast, WASH-1400 concluded that transients coupled with a loss of containment heat removal function are the type of accidents with the highest frequency. Next, in the WASH-1400 assessment come anticipated transients without scram (ATWS) sequences, and last, transients followed by loss of high and low pressure injection functions. This inversion in the order of importance is due partly to differences in the methodology used, as well as to differences in the design of the plants. The methodology employed in the Limerick study is more detailed and realistic than that employed in WASH-1400, particularly in its inclusion of the possibility of recovering unavailable systems. This is important for the containment heat removal system since there is a period of 20 hours after the initiation of the accident during which the system can be recovered. The system for containment heat removal in the Limerick station is more reliable than that considered for the WASH-1400 plant. Finally, the ATWS sequences do not contribute significantly to the frequency of core damage for the Limerick station because the design of the plant incorporates the alternate-3A modification in the ATWS prevention/mitigation system suggested by the NRC staff, and because the modeling and quantification of the ATWS sequences in the Limerick PRA are more realistic and, hence, less conservative than in WASH-1400.

The core meltdown analysis for Limerick [1] was performed with a modified version of the MARCH code (INCOR). The CORRAL and CRAC codes were used

to compute fission product transport and offsite consequences, respectively. Four accident classes were defined:

Class I: core damage sequences with loss of coolant makeup; core damage before containment failure;

Class II: sequences with failure of long-term heat removal function; containment failure before core damage;

Classes III & IV: ATWS sequences with core damage prior to and following containment failure, respectively.

In the Limerick PRA, Class I contributed almost 90% of the total core damage frequency and Class IV contributed less than 1%; Classes II & III contributed almost equally to the remainder of the total core damage frequency. Based on these accident classes, containment event trees were developed and five characteristic fission product release categories were defined. The (point estimate) source term analysis was similar to the treatment in WASH-1400 except that the design specific features of the MARK-II containment were accounted for in the Limerick PRA and suppression pool decontamination factors of 100 and 10 were used for both elemental iodine and particulates for subcooled and saturated pools, respectively.

The influence of newer source term methods (beyond WASH-1400 methods) was given limited consideration, in terms of an uncertainty analysis, in Reference 1. A more extensive source term sensitivity study was included in Reference 4.

The offsite health effects for Limerick are given in Table I. The Class I sequences contribute significantly to latent fatalities which the Class IV sequences are important for early fatalities.

Table I Comparison of Risks for Limerick PRA, GESSAR-II PRA and WASH-1400 BWR

RISK INDEX	LIMERICK PRA	GESSAR-II PRA	WASH-1400 BWR
Core Damage Frequency	1.5×10^{-5}	5.0×10^{-6}	5.7×10^{-5} (a)
Expected Early Fatalities (per plant year of operation)	2.4×10^{-6}	0 (c)	3.0×10^{-5} (b)
Expected Latent Fatalities (per plant year of operation)	1.2×10^{-2}	1.7×10^{-5} (c)	2.1×10^{-2} (b)

(a) Mean Value assuming log-normal distribution, median, and error factor reported in WASH-1400.

(b) From Table 5-6, Main Report, WASH-1400.

(c) Based on newer source term approaches than Limerick PRA or WASH-1400.

III.2 The GESSAR-II PRA

A summary of the GESSAR-II PRA is presented in Reference [8] and this synopsis is extracted from there.

The methodology used in the PRA is essentially the WASH-1400 approach, but it is augmented by the use of recent developments in the computation of the core melt frequency and of the consequences of postulated accidents. A combined fault tree/event tree procedure is used to delineate accident sequences. Transient and loss of coolant accidents define the initiators and demand failures of the water makeup systems, decay heat removal systems, and reactor protection systems are computed. As in this case of the Limerick PRA, realistic success criteria are used to model system response.

The accident sequences are grouped into accident classes which are then related to radionuclide release categories with the aid of containment event trees.

The physical phenomena associated with core meltdown, containment loading, and fission product transport are modeled with the MARCH and CORRAL computer codes. However, unlike the Limerick PRA, the GESSAR-II PRA uses current information (e.g., NUREG-0772) to develop its (point estimate) accident source terms. Offsite consequences were determined with the GRAC code.

The GESSAR-II PRA predicted that there would be no early fatalities from the accident sequences studied. This is due, according to GE, to the effectiveness of fission product scrubbing in the suppression pool (relative to that assumed in WASH-1400) and to their analysis of in-vessel retention of fission products (which was ignored in WASH-1400).

Table I gives the computed risk indices for the Limerick and GESSAR-II PRAs and the WASH-1400 BWR results are given for comparison.

IV. THE PEER REVIEWS BY BROOKHAVEN NATIONAL LABORATORY

IV.1 The Peer Review of the Limerick PRA

In NUREG/CR-3028 [9], we reported that our point estimates of the core damage frequency, expected acute fatalities, and expected latent fatalities are greater than those given for the Limerick PRA (see Table 1) by factors of 6.7, 20, and 15, respectively.

In the BNL revision, both a point value of the frequency of core damage and the associated uncertainties were assessed. The 90% probability range for the frequency of core damage of the BNL revision spans almost two orders of magnitude from 6.6×10^{-6} (5% percentile) to 3.3×10^{-4} (95% percentile). The median value is equal to 3.7×10^{-5} . It is noteworthy that according to the uncertainty assessment of the BNL version there is an 80% chance that the core-damage frequency will be lower than the BNL point estimate, a 65% chance that the core-damage frequency will be lower than the mean value of the Reactor Safety Study BWR estimate, and a 22% chance that it will be lower than the Limerick study estimate.

The difference between the Limerick and Brookhaven point values for the core-damage frequency is mainly due to three factors. The first is related to the dependences between reactor safety functions that exist as a result of the use of common support systems for different safety systems, as well

as dependences between the initiators and mitigating systems. The BNL revision accounted for some of these dependences that were not in the Limerick study. Second, Brookhaven found it necessary to make several corrections and modifications to the event trees and fault trees. The third key factor that led to a difference in the Limerick and Brookhaven results was that different values were used for the frequencies of some of the twelve accident initiators.

The BNL revision is in qualitative agreement with the Limerick study on the identification of the highest frequency accident sequences. These accident sequences were outlined in Section III.1.

The increase in health consequences in the BNL study resulted largely from the difference in the assessments of the core-damage frequency. A re-evaluation by Brookhaven of the containment event tree analysis also increased both acute and latent fatalities, but with less impact than the new core-damage frequencies. The BNL analyses of fission product behavior had little effect on acute fatalities and reduced latent fatalities. An in-depth review of the consequences (site) model used in the LGS-PRA was outside the scope of the BNL review. The consequence model used in the Limerick PRA was based on the WASH-1400 model, but with changes to reflect population and meteorology appropriate to the Limerick site. The BNL health consequences were also based on the WASH-1400 model. However, because different versions of the computer code (CRAC) were used to determine consequences for the Limerick PRA and by BNL, the increases in the health consequences also reflect differences in the mathematical models. The BNL CRAC model increased total mean acute and latent fatalities by a factor of approximately 3 relative to the version of CRAC used for the Limerick PRA.

The complementary cumulative distribution functions (CCDF) for acute and latent fatalities are presented in Figures 1 and 2, respectively. The figures depict the "point estimate" CCDF of the BNL version, the 5% and 95% limits of the BNL uncertainty assessment, the point estimate of the Limerick study, and the point estimate of the WASH-1400 (RSS) BWR CCDF. The BNL uncertainty assessment reflected in Figures 1 and 2 does not include uncertainty associated with the consequence (site) model. The prediction of acute fatalities is very sensitive to the assumed evacuation model. Based on an NRC staff model for evacuation, we recomputed the expected early fatalities and found them to be approximately one order of magnitude greater than those predicted with the WASH-1400 model.

Importance analysis was conducted for the frontline safety systems, their support systems, and for other significant events with respect to the frequency of core damage. Various importance measures were used: the Fussell-Vesely measure, the risk degradation worth, and the risk improvement worth and our results for these are given in Reference [10]. Recently, the results of these importance analyses have been used by BNL in the development of a prioritization scheme for startup and preoperational testing at Limerick. The NRC regional staff must conduct these tests on systems and components and, because of limited resources, these tests must be prioritized according to their importance to safe operation of the plant. This is a very useful application to safety activities of PRA results which goes beyond the conventional statement of the "bottom line" risk results.

IV.2 The Peer Review of the GESSAR-PRA

At the time of this writing, the review of the GESSAR-II PRA has not been completed due to redefinitions of schedules by the interested parties.

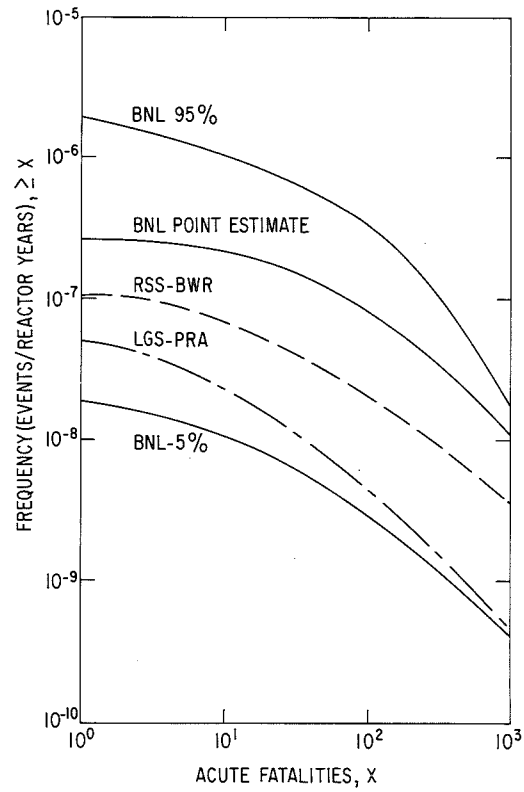


Figure 1 Complementary Cumulative Distribution Functions for Acute Fatalities.

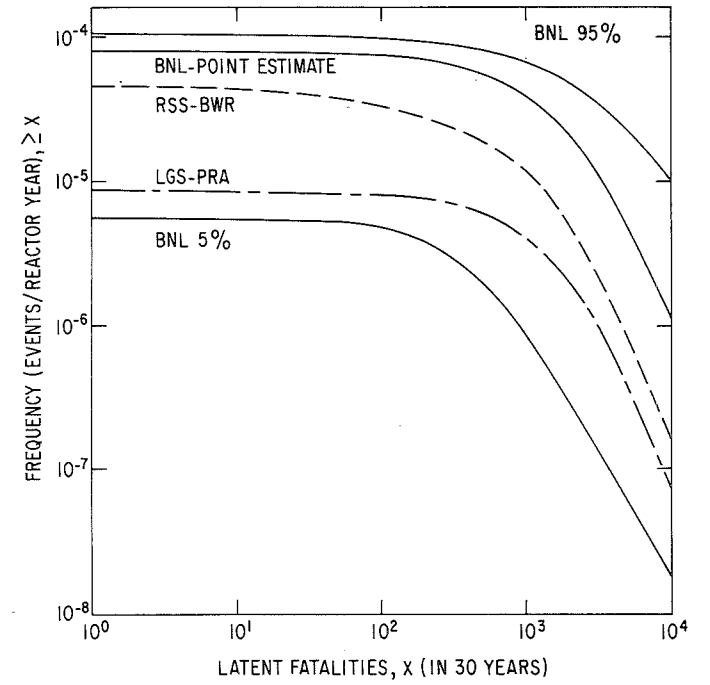


Figure 2 Complementary Cumulative Distribution Functions for Latent Fatalities.

Furthermore, because of the commercial proprietary nature of the General Electric Company's work on GESSAR-II, we must refrain from reporting material that is not already in the open literature (until a determination is made to do otherwise).

The review of the GESSAR-II PRA required several staff years of effort at BNL, over an approximately two year period. Several meetings were held with NRC staff and cognizant GE staff. The review process approximated an interactive review in which BNL findings were presented to the GE staff at meetings and in interim reports and this resulted in an open exchange on some of the technical issues associated with the PRA. As was the case for the Limerick PRA, BNL differed with the GESSAR-II PRA on the modeling of support system dependences. Importance analysis was also performed on the basis of BNL's revision of the GESSAR-II PRA.

In the areas of containment response to severe accidents and fission product behavior, BNL reassessed the source terms for GESSAR-II by accounting for the most current, technically defensible, information on this subject. This included surveys and reviews of 1) GE's work, 2) the work of IDCOR (U.S. Nuclear Industry's activity on rulemaking with respect to degraded cores), 3) the work done under the auspices of the U.S. NRC's Accident Source Term Program Office.

With regard to the latter, BNL acquired most of the computer codes produced by that program and used them, in part, in the GESSAR-II source term reassessment. Thus BNL's evaluation of the GESSAR-II source is in marked contrast to BNL's assessment (as well as Philadelphia Electric Company's assessment) of the Limerick source term. The latter basically followed a WASH-1400 prescription, which is generally regarded to be conservative. BNL did not do an offsite consequence assessment for GESSAR-II. Rather, BNL supplied its accident source terms to the NRC staff who then performed the consequence evaluation.

V. DISCUSSION

The peer review activities for the Limerick and GESSAR-II PRAs were very detailed, manpower intensive, lengthy activities. Complex results were replicated in detail. Computer codes (e.g., WAMCUT, WAMBAM, SETS, MARCH, CORRAL, CRAC) were extensively used to verify results and to develop alternatives. Furthermore, the codes themselves and their input data sets were scrutinized. Many meetings and conference calls were held in order to obtain information and exchange differences of technical views. In the case of Limerick, site visits were made by BNL staff.

Based on this review experience, several questions can be posed about the peer review process for PRAs. Some of these are: 1) What is the proper level of depth for a review? 2) Can the review process be standardized? 3) How should differences between review results and the initial study be resolved? We provide our opinions on each of these.

With regard to Item 1, it has been the experience of BNL that there is a need to verify the specific quantitative claims made in a PRA i.e., it is not enough to ascertain that, for example, a state-of-the-art tool was used in a particular area - one must verify that the appropriate analysis was indeed performed. We are not implying that performers of PRAs are devious. Rather, because PRA is still an emerging technology, there is much room for differences in interpretations and/or assumptions.

With regard to Item 2, we believe that some aspects of a PRA review can be standardized and we at BNL have attempted [11] to do this. However, before a standard review process can be optimized, one would need standard procedures for reporting the results of PRAs. Again, we have attempted [12] to develop such standard procedures.

Finally, it appears to us that Item 3 would need to be answered if closure of the PRA performance/review process is desired. However, this may not be needed on all issues for which differences may exist. For example, if differences on a particular issue lead to minor differences in overall risk, then it may not be worth the resources required to achieve resolution [13]. On the other hand, if a particular end use of a PRA result requires resolution of some issue, then it may be worthwhile to have the view of a third (non-interested) party. If the issue involves one (or a limited number) of the many disciplines that are spanned by a PRA analysis, then perhaps a panel of experts in that field could render a judgment on the narrower issues.

ACKNOWLEDGMENTS

We thank M. A. Azarm, J. L. Boccio, C. Ruger, J. Reed, M. McCann and J. W. Yang for various discussions related to these PRAs. We also thank E. Chelliah, M. Rubin, B. Hardin, J. F. Meyer, J. Mitchell, F. Coffman, R. Frahm, and J. Rosenthal (all from the NRC staff) for their support.

REFERENCES

1. "Probabilistic Risk Assessment of the Limerick Generating Station," Philadelphia Electric Co., March, 1981.
2. "BWR/6 Standard Plant Probabilistic Risk Assessment," 238 Nuclear Island, GESSAR-II, General Electric Co. (Rev. 2), February, 1982.
3. "NRC Policy on Future Reactor Designs: Decisions on Severe Accident Issues in Nuclear Power Plant Regulation," NUREG-1070 (Draft).
4. "Severe Accident Risk Assessment," Limerick Generating Station, Philadelphia Electric Co., April, 1983.
5. "A Preliminary Review of the Limerick Generating Station Severe Accident Risk Assessment," M. A. Azarm et al., NUREG/CR-3493, Brookhaven National Laboratory, June, 1984.
6. "Containment Failure Mode and Fission Product Release Analysis for the Limerick Generating Station: Base Case Accident," H. Ludewig et al., BNL-33835, BNL Informal Report, April, 1984.
7. "Safety Evaluation Report Related to the Final Design Approval of the GESSAR-II BWR/6 Nuclear Island Design," NUREG-0979, U.S. Nuclear Regulatory Commission, April, 1983.
8. "The General Electric BWR/6 MARK-III Standard Plant PRA," K. W. Holtzclaw et al., Trans. Am. Nucl. Soc. 45, 542 (1983).

REFERENCES (Cont'd)

9. "A Review of the Limerick Generating Station Probabilistic Risk Assessment," I. A. Papazoglou et al., NUREG/CR-3028, Brookhaven National Laboratory, February, 1983.
10. "Importance Analysis of Safety Systems in the Limerick Generating Station," I. A. Papazoglou et al., Trans. Am. Nucl. Soc. 45, 391 (1983).
11. "PRA Review Manual," I. A. Papazoglou et al., NUREG/CR-3485, Brookhaven National Laboratory, September, 1983 (Draft).
12. "Probabilistic Safety Analysis Procedures Guide," I. A. Papazoglou et al., NUREG/CR-2815, Brookhaven National Laboratory, January, 1984.
13. For example, a difference of interpretation of loss of offsite power experience led BNL analysts to revise their assessment of the core-damage frequency at Limerick; the reassessed value would be 5.7 times greater than the Limerick PRA value rather than 6.7 times greater. See R. A. Bari, Letter to the Editor, Nuclear News, Vol. 26, No. 12, September, 1983, p. 31.

SEISMIC RISK ASSESSMENT AS APPLIED TO THE
ZION NUCLEAR GENERATING STATION*

James E. Wells

Lawrence Livermore National Laboratory
Livermore, California 94550, USA

ABSTRACT

To assist the U.S. Nuclear Regulatory Commission (NRC) in its licensing and evaluation role, the NRC funded the Seismic Safety Margins Research Program (SSMRP) at Lawrence Livermore National Laboratory (LLNL) with the goal of developing tools and data bases to evaluate the risk of earthquake caused radioactive release from a commercial nuclear power plant. This paper describes the SSMRP risk assessment methodology and the results generated by applying this methodology to the Zion Nuclear Generating Station. In addition to describing the failure probabilities and risk values, the effects of assumptions about plant configuration, plant operation, and dependence will be given.

INTRODUCTION

A nuclear power plant is designed to ensure the survival of all buildings and emergency safety systems in a worst-case ("safe shutdown") earthquake. The assumptions underlying this design process are deterministic. In practice, however, these assumptions are clouded by considerable uncertainty. It is not possible, for example, to accurately predict the worst earthquake that will occur at a given site. Soil properties, mechanical properties of buildings; and damping in buildings and internal structures vary significantly among plants. To properly analyze seismic risk it is necessary to consider all significant sources of uncertainty as well as all significant interactions. Total risk is obtained by considering the entire spectrum of possible earthquakes and integrating their calculated consequences.

There are five steps in the SSMRP methodology [1] for calculating the seismic risk at a nuclear power plant:

1. Determine the local earthquake hazard.
2. Identify potential accident scenarios for the plant which lead to radioactive release.
3. Determine failure modes for the plant emergency safety systems.
4. Compute failure probabilities of the critical components in the emergency safety systems.
5. Compute probability of radioactive release using information from Steps 1 through 4.

* This work was performed under the auspices of the U.S. DOE by LLNL under contract number W-7405-ENG-48.

A brief discussion of each of these steps is given below.

Step 1 - Determine the Earthquake Hazard

The earthquake hazard at a given power plant site is characterized by a frequency plot which gives the probability of occurrence (per year) of earthquakes causing different peak ground accelerations. For the Zion Nuclear Generating Station, located at Zion, Illinois, approximately 40 miles north of Chicago, this curve is derived from a combination of recorded earthquake data, estimated earthquake magnitudes of known events for which no data are available, review of local geological investigations, and use of expert opinion based on a survey of seismologists and geologists familiar with the region in question.

In addition to computing the seismic hazard curve, a number (usually 30) of random synthetic earthquakes are generated using the HAZARD computer code. These earthquake time histories provide the random ground motion uncertainty inherent in real earthquakes, and are used as input to the building response calculations described below.

Step 2 - Identify Accident Sequences

In this step we identify the possible paths that a reactor system could follow during a shutdown, given that an earthquake-related event has occurred which causes shutdown. These paths usually involve an accident and a subsequent failure of one or more safety systems and are referred to as "accident sequences".

All the accident sequences result from one or more seismically-induced initiating events (events requiring immediate shutdown of the plant). For the Zion plant, seven classes of initiating events were considered. For each of these initiating events, an event tree is constructed. Each branch of an event tree is an accident sequence.

Step 3 - Determine Failure Modes of Safety Systems

To determine failure modes for the plant safety systems, fault tree methodology was used. Construction of a fault tree begins by identifying the immediate causes of system failure. Then each of these causes is examined for more fundamental causes, until one has constructed a downward branching tree, at the bottom of which are failures not further reducible, i.e., failures of mechanical or electrical components due to all causes such as fault tree are called basic events. Fault trees are required for each safety system identified on the event trees. For Zion, seven safety systems were modeled. Most of the systems modeled required both electric power and service water, so detailed fault trees were also developed for both these systems.

The basic failure events contained in the fault trees fell into three categories: (1) human and maintenance errors, (2) other random failures, and (3) seismically-induced component failures.

Step 4 - Compute Failure Probabilities of Critical Components in the Safety Systems

To compute the failure of critical components and safety systems, it is necessary to have both a measure of the maximum load or acceleration that the component experiences during an earthquake as well as a measure of the load or acceleration level at which it fails. Both the maximum load and the strength at failure are random variables. The strength at failure of the buildings and

the mechanical and electrical equipment is never known exactly, for there is usually wide variation in the results of tests to determine their failure characteristics. Uncertainties in material properties, soil layering, wall dimensions and joint connectivity influence the response of the building to an earthquake. All of these uncertainties give rise to uncertainties in calculating the response and onset of failure of each building and component in the power plant. The most important feature of the SSMRP is that these uncertainties are explicitly recognized and propagated through the calculational scheme, so that the result is not a single number, but rather, the statistical probability of the occurrence of core melt and radioactive release.

(a) Response Calculations

The buildings, foundations, major components, and piping systems are all modeled by the finite element method. SSI and structure response were calculated by the substructure approach. Piping analysis was performed by multi-support time history analysis. To incorporate the uncertainties, multiple analyses of the entire power plant are made. In each of these repeated calculations, the magnitudes of the input parameters are varied in a random fashion, and each calculation is performed using a different set of three input time histories.

(b) Determination of Fragility Functions

Component failure is defined as either loss of operability or pressure boundary integrity. Failure (fragility) is characterized by a cumulative distribution function which describes the probability that failure has occurred given a value of load. Loading may be local spectral acceleration or moment, depending on the component and failure mode under consideration. Contrary to previous work, fragility is related to the appropriate local response, rather than being related to the free-field peak ground acceleration.

A data base of the necessary fragility functions was developed. As a first step, all components identified on the fault trees were grouped into 37 generic categories. Fragility functions for each generic category were developed based on a combination of design analysis reports, experimental data, and an extensive expert opinion survey. Statistical methods were used to combine data from several sources.

Step 5 - Compute Probability of Core Melt and Radioactive Release

Accident sequence probabilities are calculated to determine radioactive release probabilities. Core melt probability is the sum of the probability of all accident sequences leading to core melt.

(a) Calculation of Cut Set Probabilities

Each accident sequence consists of the statistical union of sets of events (successes or failures of components) which must occur together (min cut sets). The computer code SEISIM [2] was written expressly to calculate the probability of such component failure groups including all common-cause failures. Given the individual component responses and fragilities (in terms of the means and variances of their distributions) and given the computed correlations between the responses (obtained from the 30 time history response calculations at each earthquake level), SEISIM constructs a multi-variate lognormal distribution for each component failure group, and then uses n-dimensional numerical integration to compute the probability of the component failure group occurring.

(b) Calculations of Probability of Radioactive Release

Once the component failure group probabilities have been computed, the probability of each accident sequence can be found using the expression for the statistical union of independent cut sets, which is an upper bound to the accident sequence probability. Then each accident sequence probability is multiplied by the probability of the earthquake's occurrence and the probability of failure of the containment to obtain the probability of radioactive release. Several different containment failure modes of different severity were identified, ranging from rupture of the containment shell to leakage of the containment isolation valves. Different containment failure modes are assigned to different accident sequences depending on the understanding of the physical processes involved. One accident sequence can result in one or more containment failure modes.

Finally, accident sequence probabilities are assigned to different release categories to reflect their severity with respect to radioactive release to the surrounding population. These release categories relate to the type and energy content of the radioactive fission product release, as well as the mode and timing of the release. They range from rupture of the top of the containment with a rapid, high energetic release (due to a fuel/water explosion or steam overpressure) to slow melt-through of the containment concrete foundation, which is expected to have the least effect on the surrounding population. The containment failure modes and the release categories are those derived and used in the Reactor Safety Study [3].

RESULTS

This section presents the results of the seismic risk analysis of the Zion Nuclear Generating Station [4]. The calculations of the median core melt probability and the confidence bounds are also described.

The base case described in this section is our best estimate of the configuration of the Zion plant and its emergency procedures. A number of important assumptions have been made as described below.

1. It is assumed that "feed and bleed" emergency core cooling can be performed after an earthquake. In this procedure, which is employed if the auxiliary feedwater system has failed, the operator makes use of the emergency safety pumps to pump cooling water to the core. The resulting steam is bled-off through the pressurizer relief valves.
2. The identified structural failure modes are assumed to have their most serious consequences. Two structural failure modes play crucial roles.
 - (i) The failure of the service water pump enclosure roof (at top of the crib house) is assumed to fail all six service water pumps beneath it. This results in loss of the emergency AC power diesel generators, due to lack of cooling water.
 - (ii) The failure of the wall between the turbine building and the auxiliary building is assumed to cause loss of all electrical wiring and control circuits, so both power and control to the reactor building are lost.

3. Soil failure under the toe of the containment is assumed to result in sufficiently large rocking motions so as to fail the SIS, CHG, RHR, CSIS and CSRS piping between the AFT building and the reactor building.
4. Failure of the vertical column supports under the steam generators and reactor coolant pumps assumed to result in a break in the primary coolant piping equivalent to a large LOCA initiating event. It was assumed that failure of supports in two different loops results in a reactor vessel rupture initiating event.

These assumptions play an important role in the base case results.

Probability of Radioactive Release

The median frequency of radioactive release for the base case was computed to be 3×10^{-5} per year. This value reflects inherent randomness in all the input variables and the hazard curve, as well as modeling uncertainties in all the input variables due to lack of exact knowledge of their mean values. The 10% and 90% confidence bands on the release frequency were found to be about 3 orders of magnitude apart. The median values and confidence bounds were obtained by making repeated calculations of the release frequencies for the base case, while varying the median values of all input variables according to an experimental design. Fourteen repeated calculations were performed, with new sets of structural responses, fragility curves, and hazard curves used for each. The median value and confidence bounds were inferred from these fourteen runs, as seen in Fig. 1. The core melt frequency is due primarily to the failure of certain structural elements which result in common-cause failures of the safety systems.

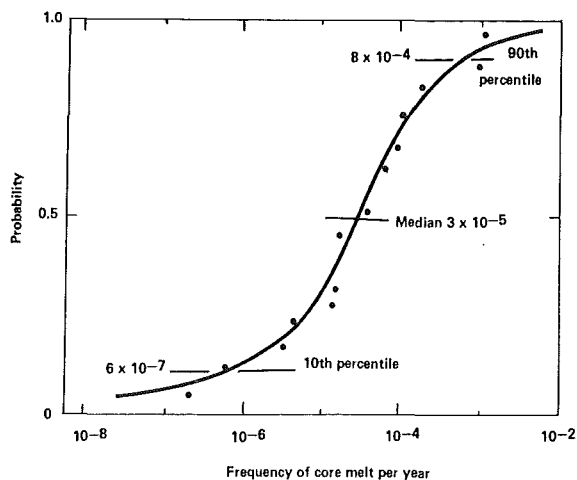


Fig. 1. Uncertainty intervals on frequency of core melt (best estimate).

Results for the Base Case with Random Uncertainty Only

To illustrate the important accident scenarios, the results of a single analysis of the base case are presented below. In these calculations all input variables were assigned best estimate values for their medians and standard deviations. The median hazard curve was used. In effect, this base case calculation gives the risk at Zion with no effects of modeling uncertainty.

Table 1 summarizes the results of the risk calculations for the base case. This table presents the probabilities per year of occurrence of the seven release categories and the man/REM per year associated with each release category. As can be seen from this table, the release categories having the highest probability of occurrence are release categories 2 (containment failure due to steam water explosion) and 7 (melt-through of basemat) with probabilities of occurrence of $1.4\text{E-}6$ and $1.5\text{E-}6$ per year, respectively. The man-REM/year released comes from release categories 2 and 3 (containment failure due to overpressure). Note that the conversion of release category probabilities to man-REM/year released is based on averaged values for a PWR taken from NUREG/CR-2800 and are not specific to Zion. The total probability of core melt is seen to be $3.6\text{E-}6$ per year and the total release is 9.6 man-REM/year. These release category probabilities were found to be due primarily to the failures of certain local structural elements and inter-building piping which resulted in common-cause failures of the safety systems.

Table 1. Base Case (With Feed and Bleed and Structural Failures) Summary of Release Probability and Dose

Release Category	Release Probability	Man-REM/year
1	$2.9\text{E-}8$	0.16
2	$1.4\text{E-}6$	6.50
3	$5.4\text{E-}7$	2.91
4	$9.2\text{E-}11$	0
5	$8.3\text{E-}10$	0
6	$1.7\text{E-}7$	0.02
7	$1.5\text{E-}6$	0.03
Total	$3.6\text{E-}6$	9.6

In terms of both core melt probability and dose, it was found that, of the six earthquake levels studied, earthquake levels 2, 3, and 4 are dominant and the probabilities and dose were significantly smaller at earthquake levels 1 and 6. This indicates that we captured the bulk of the risk in the middle earthquake levels (2 to 4 SSE), and that the range of earthquakes considered is adequate.

It was found that, at the three lower earthquake levels, the initiating events are dominated by the transients. At earthquake level 4, it is primarily the small and small-small LOCAs which are important. At earthquake level 5 the initiating event probabilities are fairly evenly spread over the initiating events and the LLOCA and RPV initiating events have become significant. Finally, at level 6 the dominant initiating events are the RPV and LLOCA events. Thus, we see that as we increase the level of earthquake excitation the contribution of the more severe initiating events increases.

Out of the total 9.6 man-REM/year, approximately 6.1 man-REM/year is due to accident sequences caused directly by the uplift and crib house pump room roof failures, and 2.7 man-REM/year is due to failures of pairs of pipes between the reactor and AFT buildings. Thus it is seen that, for the base case computations of the seismic risk at Zion, the structural failures and the assumptions as to their consequences play an overriding role.

Sensitivity of Risk Results to Basic Assumptions

To test the fundamental assumptions on which the base case results were predicated, three additional risk assessments of Zion were performed, with the results shown on Table 2. In case I, the effects of the structural failures (the service water pump enclosure room roof, auxiliary building shear wall, and soil failure and basemat uplift) were removed, but the "feed and bleed" capability was retained. In this case, both the probability of core melt and radioactive dose decreased by 50% relative to the base case.

In case II, both the effects of structural failures and the "feed and bleed" cooling capability were removed. For this case, the core melt probability increased by a factor of 2-1/2 over the base case. This is because if "feed and bleed" cooling cannot be performed, the auxiliary feedwater system (AFWS) has no back-up, and thus electrical component failures in the AFWS became melt-through (which is relatively benign) rather than over-pressure failure of the containment.

In case III, the effects of the structural failures are included, but no "feed and bleed" capability is assumed. This results in the highest (point estimate) values of both core melt probability and radioactive release. The core melt probability is 3 times higher than in the base case, and the radioactive release is 13% higher than for the base case.

In summary, it can be seen that, depending upon the assumptions made as to the consequences of the localized structural failures and the credibility of performing "feed and bleed" cooling, the core melt probability can vary by an order of magnitude, and the release can vary by 250%.

Correlation Effects on Seismic Risk

In this section, we present the results of two sets of calculations which show that correlation can change the final risk result by an order of magnitude if the risk is dominated by pairs of component failures, while in contrast, correlation has little effect if the total risk is due primarily to structural failures. These cases are illustrated in Table 3.

For the cases where structural failures are included and where these structural failures dominate the total calculated risk, one is dealing with a situation in which the most important terms in the accident sequences are single failures, and hence the dominant cut sets. Correlation only affects the computation of the union of cut sets. And since the effects of correlation on the union of cut sets are usually relatively small, correlation need not be considered for those cases that are dominated by single structural failures since the final risk numbers will vary by only a small amount.

By contrast, however, in those cases in which the risk is dominated by failures of pairs of equipment, one finds correlation to have a large effect because correlation affects the probability of the component pairs which constitute the most important cut sets in the accident sequences. Thus, for these cases we find that correlation plays an important role in evaluating the total risk of the plant.

Table 2. Comparison of Cases Analyzed to Test Effects of Fundamental Assumptions

Base Case (with Feed & Bleed, with Structural Failures)			Case I (with Feed & Bleed, No Structural Failures)	
Release Category	Probability per year	man-REM per year	Probability per year	man-REM per year
1	2.9E-8	0.2	1.9E-8	0.1
2	1.4E-6	6.5	1.9E-7	0.9
3	5.4E-7	2.9	6.1E-7	3.3
4	0	0	0	0
5	8.3E-10	0	8.8E-10	0
6	1.7E-7	0	1.2E-7	0
7	1.5E-6	0	5.3E-7	0
Total	3.6E-6	9.6	1.5E-6	4.3

Case II (w/o Feed & Bleed w/o Structural Failures)			Case III (w/o Feed and Bleed, with Structural Failures)	
Release Category	Probability per year	man-REM per year	Probability per year	man-REM per year
1	2.4E-8	0.1	3.3E-8	0.2
2	5.7E-7	2.7	1.5E-6	7.2
3	6.6E-7	3.6	6.0E-7	3.2
4	0	0	0	0
5	0	0	0	0
6	2.8E-7	0	2.9E-7	0
7	7.6E-6	0.2	8.6E-6	0.2
Total	9.1E-6	6.6	1.1E-5	10.8

Table 3. The Effects of Correlations of Structure Responses and Fragility Functions on Release Frequencies and Dose, with the Assumption of no Structure Failures and no Feed and Bleed.

	Release Category	Frequency/yr	Man-rem/yr
Case 1 (with full correlation for fragility functions and calculated correlations for structure responses)	1	3.1E-8	0.2
	2	7.4E-7	3.6
	3	6.5E-7	3.5
	4	0	0
	5	2.5E-11	0
	6	3.3E-7	0.1
	7	1.8E-5	0.4
	Total	2.0E-5	7.8
Case 2 (with no correlation for fragility functions and with calculated correlations for structure responses)	1	2.4E-8	0.1
	2	5.7E-7	2.7
	3	6.6E-7	3.6
	4	0	0
	5	8.8E-10	0
	6	2.8E-7	0
	7	7.6E-6	0.2
	Total	9.1E-6	6.6
Case 3 (with no correlation for fragility functions or structure responses)	1	1.5E-8	0.1
	2	2.5E-7	1.2
	3	7.4E-7	4.0
	4	4.5E-13	0
	5	2.5E-11	0
	6	1.8E-7	0
	7	1.3E-6	0
	Total	2.5E-6	5.3

REFERENCES

- [1] P. D. Smith, et al., "Seismic Safety Margins Research Program Phase I Final Report," Lawrence Livermore National Laboratory, Livermore, CA, UCRL-53021, Vols. 1-10, NUREG/CR-2015, Vols. 1-10 (1982).
- [2] J. E. Wells, "SEISM: A Probabilistic Risk Assessment Tool Used in Evaluating Seismic Risk," Proceedings of the Conference on Seismic Risk and Heavy Industrial Facilities, Lawrence Livermore National Laboratory, Livermore, CA (1983).
- [3] U.S. Nuclear Regulatory Commission, "Reactor Safety Study: An Assessment of Accident Risks in U.S. Commercial Nuclear Power Plants, WASH-1400," NUREG-75/014 (October 1975).
- [4] M. P. Bohn, et al., "Application of the SSMRP Methodology to the Seismic Risk at the Zion Nuclear Power Plant," Lawrence Livermore National Laboratory, Livermore, CA, UCRL-53483, NUREG/CR-3428 (1983).

SAND83-2594C

CLASSIFICATION OF UNITED STATES LIGHT WATER REACTORS BY
DOMINANT CORE MELT FREQUENCY CONTRIBUTORS*F. T. Harper
Sandia National Laboratories (U.S.A.)M. T. Drouin
Science Applications International Corporation (U.S.A)E.A. Krantz
EG&G Idaho, Inc. (U.S.A.)

ABSTRACT

In the past ten years a relatively small number of Light Water Reactors (LWRs) in the United States (U.S.) have been the object of intense risk analysis. These plants have been used as surrogates to evaluate generic safety issues at other plants. There are many problems with the surrogate approach to generic nuclear safety research, the most obvious being that nuclear plants in the U.S. are almost always different from one another in ways that affect plant risk. To address this problem, the Accident Sequence Evaluation Program (ASEP) is classifying LWRs in the U.S. by dominant core melt sequence contributors -- excluding external events. These contributors are identified through examination of approximately 100 U.S. LWRs. Although the ASEP grouping scheme is complex, it should be considered in generic studies to better understand generic safety issues.

I. OBJECTIVES OF THE ACCIDENT SEQUENCE EVALUATION PROGRAM

The ASEP is a critical element of the Severe Accident Research Program (SARP) which is sponsored by the United States Nuclear Regulatory Commission (U.S.N.R.C.). The SARP was established to support the U.S.N.R.C. in evaluating severe accidents. There are four overall objectives for the ASEP:

- 1) to provide a comprehensive general set of accident sequences (excluding external events initiators) for all Light Water Reactors (LWRs) in the United States,
- 2) to develop associated likelihoods for these sequences,

*This work is supported by the United States Nuclear Regulatory Commission, Office of Nuclear Regulatory Research, and performed at Sandia National Laboratories which is operated for the United States Department of Energy under contract number DE-AC04-76DP00789.

- 3) to ascertain the dominant contributors to these sequences, and
- 4) to group LWRs by design and operational similarities.

The completion of the fourth objective is highly significant. In the past, surrogate plants--grouped by vendor, by containment type, or by other characteristics--have been used to simplify generic analyses. However, there have always been questions concerning the proper method to classify plants when studying a particular issue. Many of these accident analysts now depend on ASEP for guidance when choosing surrogate plants. We are currently classifying plants by core melt frequency and by dominant core melt contributors. A scheme has been developed in which different plant classes will be established for different severe accident issues. This paper will summarize the methodology that is being used to establish plant classes and will present the insights that come from this plant classification.

II. PREVIOUS ATTEMPTS AT CLASSIFICATION OF U.S. LWRs

Our first attempt to classify the LWRs in the U.S. was to group them by their functional responses to severe accident situations. Because the functional responses of most reactors in accident situations are the same, this effort did not produce very many groups. Functionally, LWRs can be classified into three groups: two Pressurized Water Reactor (PWR) groups and one Boiling Water Reactor (BWR) group. We then classified reactors by considering their systemic responses to severe accident situations -- although the functional response may be the same, the systems that perform the functions vary from plant to plant. We classified the U.S. LWRs in seventeen different groups: six BWR groups and eleven PWR groups. Within each group the systems that would respond to any accident initiator are the same.

We then tried to group reactors at the next level of detail: by system configurations. We knew that the configurations of the systems used to mitigate accidents had evolved over the years although the system names and the system functions may have stayed the same. We therefore looked at differences within the systems at plants. We found that, even though some front line systems in different plants look similar, every plant is unique.

The usefulness of the three different grouping schemes described so far is extremely limited. Grouping at the functional level is of limited use because the groups are too large and too many differences exist within the groups. Grouping considering differences within systems is also of limited use because each plant is a group by itself. Grouping by systems can be useful for many purposes but has the disadvantage that no support system information is considered when the groups are formed -- many past Probabilistic Risk Assessments (PRAs) have found that support systems, which have the potential to fail several systems at once (e.g. the service water system or the electrical system), are very important to core melt frequency.

We therefore developed an approach to support those programs that needed more specific grouping information: we grouped plants by core melt frequency and by dominant core melt contributors. In principle, the grouping of plants by dominant core melt contributors should be the optimum grouping scheme. Any

present or future research effort that addresses safety issues across the LWR industry should be able to use this grouping format.

To group by dominant core melt contributors, it was first necessary to find out what the contributors are. The methodology that we used to find the dominant core melt contributors is summarized below.

III. SUMMARY OF THE METHODOLOGY USED TO OBTAIN DOMINANT CORE MELT CONTRIBUTORS

The methodology used to obtain dominant core melt contributors consisted of two major tasks: 1) the selection of accident sequences to be analyzed; and 2) the modeling and quantification of these accident sequences.

III.1 Accident Sequence Selection

Because the ASEP scope includes such a large selection of plants, we decided to limit the number of sequences to be analyzed for each plant. To determine the sequences to be analyzed, we used information from past PRAs published in the U.S. and from recent studies that provided new accident sequence insights. The core melt accident sequences from the PRAs were requantified using the most recent insights. Some examples of the new insights that were used in the requantification are listed below:

- o The potential for recovering offsite power is less than previously thought.
- o Small loss of coolant accidents with failure of the recirculation cooling mode in PWRs are thought not to be as important as previously thought.
- o There are many sources of cooling in BWRs that have not been considered in past PRAs that could render some previously dominant sequences insignificant.
- o The recovery time for loss of decay heat removal sequences in BWRs may be longer than previously thought.

This requantification has shown that only a few sequences contribute significantly to the core melt frequency. Sequences initiated by transients and small loss of cooling accidents, followed by failure of early core cooling (PWR and BWR) or long term heat removal (BWR only), and Anticipated Transients Without Scram (PWR and BWR) are the types of sequences that have been shown to be dominant. A study of actual events that have occurred in U.S. LWRs reinforces the view that these sequences are the most likely sequences.

III.2 Modeling and Quantification

The ASEP sequences (with the exception of the Anticipated Transient Without Scram sequences*) were modeled and quantified as follows: 1) Seventy percent of operating and soon to be operating plants were surveyed (104 plants). 2) Simplified diagrams were drawn for the mitigating systems of the identified dominant sequences. 3) Fault tree models at the pipe segment level were constructed for those systems and their support systems; simplified actuation and control systems were also modeled. 4) The accident sequences were solved by Boolean reduction using the Set Equation Transformation System (SETS) computer code and then quantified using the Set Evaluation Program (SEP) computer code -- statistical uncertainties were propagated throughout the SEP analysis. 5) A bounding analysis addressing the non-statistical uncertainties was conducted after the initial quantification.

IV. RESULTS OF LWR CLASSIFICATION BY CORE MELT FREQUENCY AND DOMINANT CORE MELT FREQUENCY CHARACTERISTICS

To illustrate the results of this grouping effort; we will look at plant grouping in two PWR sequences and in two BWR sequences. Because of the length limitations of this paper we will only be able to compare four PWRs and four BWRs. The four PWRs and four BWRs represent actual plants -- the system differences important to core melt frequency for each plant are described in Table I**. Due to the preliminary nature of these results, the plants are not identified by their names.

IV.1 PWR Results

The two PWR sequences that are considered for PWR grouping in this paper are a transient induced Loss of Cooling Accident (LOCA) with a failure of the high pressure injection systems to cover the core (T-LOCA-HPI) and a transient event with loss of all feedwater (T-LOFW). The relative frequencies of the two sequences are presented in Table II for the four plants considered.

Table II. PWR Relative Sequence Frequency

<u>Plant</u>	<u>T-LOCA-HPI</u>	<u>T-LOFW</u>
W4-A	300	5000
W4-B	300	7000
W4-C	300	5000
BW-2	1000	8000

(All frequencies are normalized to lowest frequency presented in this paper.)

*The Anticipated Transient Without Scram sequences will not be discussed in this paper.

**Table I can be found at the end of the paper.

The frequencies for the T-LOFW sequence are comparable and the four plants could be classified as one group for that sequence. The plants would be divided into two groups considering the T-LOCA-HPI sequence frequencies: Group 1 -- W4-A, W4-B, W4-C, Group 2 -- BW2. When considering this sequence, the Westinghouse reactors group together, but are separate from the Babcock and Wilcox reactor.

The classification of plants is not as simple as it appears in the preceding paragraph. Each sequence actually consists of five subsequences with different initiating events. The five initiating events considered are: 1) a transient with the power conversion system initially available (T-PCS), 2) a transient with the power conversion system initially unavailable (T-NOPCS), 3) a loss of offsite power transient (T-LOSP) 4) a loss of a DC bus transient (T-DC), and 5) a loss of an AC bus transient (T-AC).

Considering the five subsequences, the number of grouping possibilities increases tremendously. If the order of importance of the five initiating events is considered for each of the two sequences, each plant would be considered unique. If the frequency of the subsequence is used as a classification criterion, then the plants can be grouped. However, the grouping looks different for each subsequence. The grouping also looks different for each subsequence if the dominant contributors to core melt frequency are used to group the plants. The PWR grouping possibilities considering the five subsequences are presented in Table III*.

There are, however, some consistent grouping patterns that can be found in Table III:

- A) Sequence T-LOCA-HPI insights
 - 1. When grouped by dominant core melt contributors, plants W4-A and W4-B group together for all initiators except T-AC.
- B) Sequence T-LOFW insights
 - 1. When grouped by subsequence frequency, plants W4-B and BW2 always group together.
 - 2. When grouped by subsequence frequency, plants W4-A and W4-C group together except in the T-DC subsequence.
 - 3. When grouped by dominant contributors to core melt, plants W4-A and W4-C always group together.

IV.2 BWR Results

The two BWR sequences that are considered for BWR grouping in this paper are a transient event with loss of all reactor core injection (T-LI) and a transient event with a loss of the decay heat removal function (T-LDHR). The frequencies of the two sequences are presented in Table IV for the four plants considered.

*Table III can be found at the end of the paper.

Table IV. BWR Relative Sequence Frequency

<u>Plant</u>	<u>T-LI</u>	<u>T-LDHR</u>
GE6-A	300	10000
GE6-B	700	4000
GE4-A	300	6000
GE4-B	3000	70

(All frequencies are normalized to the lowest frequency presented in this paper.)

The BWR plants can be classified into the same two groups for both sequences: Group 1 -- GE6-A, GE6-B, GE4-A, and Group 2 -- GE4-B. It is interesting to note that the T-LI frequency for GE4-B is much higher than for the other three plants and that the T-LDHR frequency for GE4-B is much lower.

The same five initiating events that were analyzed for PWRs are analyzed for BWRs. Like the PWR sequences, the two BWR sequences consist of five subsequences each and the problems of BWR classification while considering the different subsequences are similar to the problems of PWR classification. If the order of importance of the five initiating events is considered, plants GE6-A, GE4-A, and GE6-B group together for the T-LDHR sequence. The plants do not group for the T-LI sequence. When considering core melt frequency or dominant core melt contributors, the same sort of complex grouping pattern that was seen in the PWR grouping emerges. The BWR subsequence grouping possibilities are presented in Table V*. As in the case of the PWR some consistent grouping patterns can be found:

A) Sequence T-LI insights

1. When grouped by dominant core melt contributors, plant GE6-A and GE6-B always group together.

B) Sequence T-LDHR insights:

1. When grouped by subsequence frequencies, plants GE6-A and GE4-A always group together; plant GE6-B groups with plants GE6-A and GE4-A except for T-NOPCS subsequences.
2. When grouped by dominant core melt contributors, all four BWRs usually group together. The only exception to this occurs in the T-PCS subsequence when plant GE4-B cannot be grouped with the other three.

V. CONCLUSION

To simplify safety research, LWRs must be grouped. In the past LWRs have been grouped by many different descriptors -- systemic response to accident

*Table V can be found at the end of the paper.

situations, containment differences, vendor, utility, etc. Whereas some of these grouping schemes are adequate for specific programs, none of the schemes are adequate for the large majority of nuclear safety research programs. The ASEP grouping scheme -- the classification of plants by dominant core melt contributors -- appears to be applicable to a large number of nuclear safety programs. Our grouping scheme has one large disadvantage: the presentation of the groups is complex. One particular plant may fall into many different groups depending on what sequence is considered and what initiating event is considered.

A thorough classification of LWRs requires a multi-dimensional matrix that includes both the set of grouping descriptors used in the past and the descriptors used to describe dominant core melt sequence contributors. Accident analysts who are basing their generic analyses on groups classified using an incomplete set of descriptors may be unintentionally producing misleading results. To avoid presenting misleading results, analysts should consider all grouping schemes before limiting their studies to a particular plant or type of plant.

System Acronyms and Definitions:

AC -- AC Power
 ADS -- Automatic Depressurization System (BWR primary side pressure relief)
 AFW -- Auxiliary Feedwater (PWR secondary heat removal system)
 DC -- DC Power
 EP -- Electric Power
 HP -- Either High Pressure Coolant Injection (HPCI) or High Pressure Core Spray (HPCS) -- (BWR high pressure injection systems)
 HPIS -- High Pressure Injection System (PWR high pressure injection system)
 LPCI -- Low Pressure Coolant Injection (BWR low pressure injection system)
 LPCS -- Low Pressure Core Spray (BWR low pressure injection system)
 PCS -- Power Conversion System (BWR and PWR primary and secondary side heat removal, respectively)
 PORV -- Power Operated Relief Valve (PWR primary side pressure relief system)
 RCIC -- Reactor Core Isolation Cooling (BWR high pressure injection system)
 SRV -- Safety Relief Valve (PWR primary side pressure relief system)
 SWS -- Service Water System (BWR and PWR cooling water support systems)

Failure Modes Definitions:

ACT -- Actuation Failure
 BUS -- Electric Power Bus Failure
 CE -- Common Element Failure (common component -- e.g., valve -- shared between trains of a system or shared between systems)
 CM -- Common Mode Failure
 HE -- Human Error Failure
 HW -- Hardware Failure
 LOSP -- Independent Failure of Loss of Offsite Power
 TM -- Test and Maintenance Failure

Table I. Summary of Plant System Differences

PWR PLANT TYPE	AFW	HPIS	EP	SWS		
W4-A	<ul style="list-style-type: none"> Common suction between two MDP and one TDP trains 	<ul style="list-style-type: none"> Common suction and common injection between pumps trains 	<ul style="list-style-type: none"> Two AC and DC divisions per unit Two DGs per unit 	<ul style="list-style-type: none"> Eight open loop pumps (four per unit) for two units Five closed loop pumps for two units 		
W4-B	<ul style="list-style-type: none"> Separate suction for each pump train (2 MDP trains, 2 TDP trains) 	<ul style="list-style-type: none"> Same as W4-A 	<ul style="list-style-type: none"> Three AC and DC divisions per unit Five DGs between two units 	<ul style="list-style-type: none"> Four open loop pumps (two per unit) Three closed loop pumps for one unit 		
W4-C	<ul style="list-style-type: none"> Common suction between two MDP and TDP trains 	<ul style="list-style-type: none"> Same as W4-A 	<ul style="list-style-type: none"> Same as W4-B 	<ul style="list-style-type: none"> Six open loop pumps for two units Five closed loop pumps for two units 		
BW2	<ul style="list-style-type: none"> Dual common suction between two MDP and one TDP trains 	<ul style="list-style-type: none"> Common suction between pump trains Separate injection per pump train 	<ul style="list-style-type: none"> Three AC and DC divisions per unit Common hydro-generator shared between all units 	<ul style="list-style-type: none"> Two open loop pumps for one unit 		
W4 - Westinghouse Four Loop Reactor BW2 - Babcock & Wilcox Two Loop Reactor MDP - Motor Driven Pump TDP - Turbine Driven Pump SG - Steam Generator DG - Diesel Generator						
BWR PLANT TYPE	RCIC	HPCS/HPCI	LPCS	LPCI/RHR	EP	SWS
GE6-A	<ul style="list-style-type: none"> Common suction from CST with HPCS 	<ul style="list-style-type: none"> HPCS Common suction from CST with RCIC 	<ul style="list-style-type: none"> Single MDP train 	LPCI: <ul style="list-style-type: none"> Three single MDP trains RHR: <ul style="list-style-type: none"> Two single MDP trains 	<ul style="list-style-type: none"> Three AC and DC divisions per unit Three DGs per unit 	<ul style="list-style-type: none"> Three open loop pumps (one per train) for one unit
GE6-B	<ul style="list-style-type: none"> Separate suction than HPCS from CST 	<ul style="list-style-type: none"> HPCS Separate suction than RCIC from CST 	<ul style="list-style-type: none"> Same as GE6-A 	<ul style="list-style-type: none"> Same as GE6-A 	<ul style="list-style-type: none"> Same as GE6-A 	<ul style="list-style-type: none"> Four open loop pumps for one unit
GE4-A	<ul style="list-style-type: none"> Common suction from CST with HPCI 	<ul style="list-style-type: none"> Common suction from CST with RCIC Common injection path with LPCS 	<ul style="list-style-type: none"> Two trains two MDPs per train Common injection path with HPCI 	LPCI: <ul style="list-style-type: none"> Four single MDP trains RHR: <ul style="list-style-type: none"> Same as GE6-A 	<ul style="list-style-type: none"> Four AC and DC divisions per unit Four DGs per unit 	<ul style="list-style-type: none"> Four open loop pumps (two per train) for one unit
GE4-B	<ul style="list-style-type: none"> Common suction from CST with HPCI 	<ul style="list-style-type: none"> Common suction from CST with RCIC 	<ul style="list-style-type: none"> Two trains, two MDPs per train 	LPCI/RHR: <ul style="list-style-type: none"> Two trains, two MDPs per train 	<ul style="list-style-type: none"> Same as GE4-A 	<ul style="list-style-type: none"> Twelve open loop pumps (three per train) for three units

GE6 - General Electric BWR 6 Reactor
 GE4 - General Electric BWR 4 Reactor

MDP - Motor Driven Pump
 CST - Condensate Storage Tank

DG - Diesel Generator

Table III. PWR Classification Possibilities

SEQUENCE INITIATORS	TRANSIENT INDUCED LOCA WITH FAILURE OF HIGH PRESSURE INJECTION (T-LOCA-HPI)				TRANSIENT WITH LOSS OF ALL FEEDWATER (T-LOFW)			
	SUBSEQUENCE FREQUENCY GROUP		DOMINANT CORE MELT CONTRIBUTORS GROUP		SUBSEQUENCE FREQUENCY GROUP		DOMINANT CORE MELT CONTRIBUTORS GROUP	
	PLANT GROUPS	RELATIVE GROUP FREQUENCY*	PLANT GROUPS	GROUP CHARACTERISTICS	PLANT GROUPS	RELATIVE GROUP FREQUENCY*	PLANT GROUPS	GROUP CHARACTERISTICS
T-PCS	1. W4-A	1. 1	1. W4-A	1. PORV	1. W4-B	1. 3000	1. W4-A	1. PCS Failure
	BW2		W4-B	AC-HW,HE,Bus	BW2		W4-C	AFW-HW,TH,CM
	2. W4-B	2. 10	2. W4-C	2. PORV, SRV	2. W4-A	2. 300	2. W4-B	2. PCS Failure
	W4-C		BW2	SW-CE,TH,CH	W4-C		BW2	AFW-HW,CH
T-NOPCS	1. W4-A	1. 2	1. W4-A	1. PORV, SRV	1. W4-B	1. 2000	1. W4-A	1. AFW-CE,CM,HW,TH
	W4-B		W4-B	SW-CH,HW	BW2		W4-C	
	BW2		W4-C	HPIS-CH,CE,HW	2. W4-A	2. 700	2. W4-B	2. AFW-CH,HW,TH
	2. W4-C	2. 3	BW2		W4-C		BW2	
T-LOSP	1. W4-A	1. 10	1. W4-A	1. PORV	1. W4-A	1. 700	1. W4-A	1. AFW-CE,CM,HW
	W4-B		W4-B	AC-CH,HW,TH	W4-B		W4-B	DC-TH,CM
	2. W4-C	2. 2	W4-C		W4-C		W4-C	AC-HW
	BW2		2. BW2	2. PORV	BW2		2. BW2	2. AFW-CH,CE,HW
T-DC	1. W4-A	1. 3	1. W4-A	1. PORV, SRV	1. W4-A	1. 3000	1. W4-A	1. AFW-HW,TH,CM
	W4-B		W4-B	2. SW-CE,HW,TH	W4-B		W4-B	
	BW2		BW2	3. HPIS-HW,TH	BW2		W4-C	
	2. W4-C	2. 1	2. W4-C	2. HPIS-HW,ACT	2. W4-C	2. 300	BW2	
T-AC	1. W4-B	1. 7	1. W4-B	1. PORV	1. W4-A	1. 300	1. W4-A	1. AFW-CH,HW,TH
	W4-C		W4-C	HPIS-TH,HW	W4-B		W4-B	
	BW2		BW2	SW-HW,TH	W4-C		W4-C	
	2. W4-A	2. 30	2. W4-A	2. PORV, SRV	BW2		BW2	
DOMINANT INITIATORS FOR TRANSIENT INDUCED LOCAe WITH FAILURE OF HIGH PRESSURE INJECTION SEQUENCE IN ORDER OF IMPORTANCE (T-LOCA-HPI)				DOMINANT INITIATORS FOR TRANSIENTS WITH LOSS OF ALL FEEDWATER SEQUENCE IN ORDER OF IMPORTANCE (T-LOFW)				
W4-A	W4-B	W4-C	BW2	W4-A	W4-B	W4-C	BW2	
PLANT TYPE	PLANT TYPE	PLANT TYPE	PLANT TYPE	PLANT TYPE	PLANT TYPE	PLANT TYPE	PLANT TYPE	
1. T-AC	1. T-LOSP	1. T-PCS	1. T-AC	1. T-NOPCS	1. T-DC	1. T-LOSP	1. T-DC	
2. T-LOSP	2. T-AC	2. T-AC	2. T-DC	2. T-DC	2. T-NOPCS	2. T-NOPCS	2. T-PCS	
3. T-DC	3. T-PCS	3. T-NOPCS	3. T-LOSP	3. T-LOSP	3. T-LOSP	3. T-DC	3. T-NOPCS	
4. T-NOPCS	4. T-DC	4. T-LOSP	4. T-PCS	4. T-PCS	4. T-AC	4. T-AC	4. T-LOSP	
5. T-PCS	5. T-NOPCS	5. T-DC	5. T-NOPCS	5. T-AC	5. T-PCS	5. T-PCS	5. T-AC	

Notes:

W4-A,B,C -- Westinghouse four loop plants.
 BW2 -- Babcock & Wilcox two loop plant.

*All frequencies are normalized to the lowest frequency presented in this paper.

This table is divided into two major grouping possibilities:

A) The top half of the table groups the plants by both core melt frequency and dominant core melt contributors for each sequence initiator of the two sequences, T-LOCA-HPI and T-LOFW. The dominant core melt characteristics are those failures that dominate the core melt frequency. The failures are presented with system designators and failure mode designators. The applicable system is listed first with the specific failure mode(s) following (see Section V for system and failure modes definitions).

B) The bottom half of the table lists, in the order of importance, the initiators for each plant type.

Table V. BWR Classification Possibilities

SEQUENCE INITIATORS	TRANSIENT WITH LOSS OF REACTOR CORE INJECTION (T-LI)				TRANSIENT WITH LOSS OF DECAY HEAT REMOVAL (T-LDHR)			
	SUBSEQUENCE FREQUENCY GROUP		DOMINANT CORE MELT CONTRIBUTORS GROUP		SUBSEQUENCE FREQUENCY GROUP		DOMINANT CORE MELT CONTRIBUTORS GROUP	
	PLANT GROUPS	RELATIVE GROUP FREQUENCY*	PLANT GROUPS	GROUP CHARACTERISTICS	PLANT GROUPS	RELATIVE GROUP FREQUENCY*	PLANT GROUPS	GROUP CHARACTERISTICS
T-PCS	1. GE6-A 2. GE6-B 3. GE4-A 4. GE4-B	1. 30 2. 200 3. 20 4. 300	1. GE6-A GE6-B GE4-A 2. GE4-B	1. PCS LOSP AC-CH SW-CH ADS HP, RCIC-HW 2. LOSP AC-HW ADS DC-TM	1. GE6-A GE6-B GE4-A 2. GE4-B	1. 70 2. 20	1. GE6-A GE6-B GE4-A 2. GE4-B	1. PCS SW-HW, CH RHR-HW, CH AC-HW LOSP 2. PCS RHR-CH, HE AC-HW LOSP
T-NOPCS	1. GE6-A GE6-B 2. GE4-A 3. GE4-B	1. 10 2. 30 3. 100	1. GE6-A GE6-B GE4-A 2. GE4-B	1. ADS SW-CH RCIC-HW HP-HW 2. LOSP SW-HW AC-HW ADS	1. GE6-A GE4-A 2. GE6-B GE4-B	1. 3000 2. 100	1. GE6-A GE6-B GE4-A GE4-B	1. RHR-CH, HW, TM SW-HW, CH
T-LOSP	1. GE6-A GE4-A 2. GE6-B 3. GE4-B	1. 200 2. 700 3. 3000	1. GE6-A GE6-B GE4-B 2. GE4-A	1. AC-CH, HW DC-CH, HW SW-CE, HW 2. DC-CH AC-CH SW-CH HP-HW RCIC-HW	1. GE6-A GE6-B GE4-A 2. GE4-B	1. 100 2. 20	1. GE6-A GE6-B GE4-A GE4-B	1. AC-HW SW-HW, CE, HE, CH RHR-HW, CH
T-DC T-AC	1. GE6-A GE6-B GE4-A 2. GE4-B	1. 30 2. 1000	GE6-A GE6-B GE4-A GE4-B	1. ADS HP-HW RCIC-HW 2. SW-HW SW-TM	1. GE6-A GE6-B GE4-A 2. GE4-B	2. 3000 2. 30	1. GE6-A GE6-B GE4-A GE4-B	1. RHR-HW, CH, TM SW-HW, CH, TM
DOMINANT INITIATORS FOR TRANSIENTS WITH LOSS OF REACTOR CORE INJECTION SEQUENCE IN ORDER OF IMPORTANCE (T-LI)				DOMINANT INITIATORS FOR TRANSIENTS WITH LOSS OF DECAY HEAT REMOVAL SEQUENCE IN ORDER OF IMPORTANCE (T-LDHR)				
GE6-A PLANT TYPE	GE4-A PLANT TYPE	GE6-B PLANT TYPE	GE4-B PLANT TYPE	GE6-A PLANT TYPE	GE4-A PLANT TYPE	GE6-B PLANT TYPE	GE4-B PLANT TYPE	
1. T-LOSP	1. T-LOSP	1. T-LOSP	1. T-LOSP	1. T-AC	1. T-AC	1. T-AC	1. T-NOPCS	
2. T-AC	2. T-NOPCS	2. T-PCS	2. T-DC	2. T-DC	2. T-DC	2. T-DC	2. T-AC	
3. T-DC	3. T-DC	3. T-AC	3. T-PCS	3. T-NOPCS	3. T-NOPCS	3. T-NOPCS	3. T-DC	
4. T-PCS	4. T-PCS	4. T-NOPCS	4. T-AC	4. T-LOSP	4. T-LOSP	4. T-LOSP	4. T-LOSP	
5. T-NOPCS	5. T-AC	5. T-DC	5. T-NOPCS	5. T-PCS	5. T-PCS	5. T-PCS	5. T-PCS	

Notes:

GE6 -- General Electric BWR6 Plants.
GE4 -- General Electric BWR4 Plants.

*All frequencies are normalized to the lowest frequency presented in this paper.
**Insights and frequencies are the same for both T-AC and T-DC initiators.

This table is divided into two major grouping possibilities:

A) The top half of the table groups the plants by both core melt frequency and core melt contributors for each sequence initiator of the two sequences, T-LI and T-LDHR. The core melt contributors are those failures that dominate the core melt frequency. The failures are presented along with system designators and failure mode designators. The applicable system is listed first with the specific failure mode(s) following (see Section V for system and failure modes definitions).

B) The bottom half of the table lists, in the order of importance, the initiators for each plant type.

INTRODUCTION OF OPERATOR ACTIONS IN THE EVENT TREES

G. BARS, J.M. LANORE, C. VILLEROUX.

CEA/IPSN/DAS

ABSTRACT

In the PRA in progress in France for a 900 MW PWR plant, an effort is done for introducing operator actions during accident sequences. A first approach of this complex problem relies on an extensive use of existing methods and knowledge in diverse fields.

Identification of actions is based on the operating procedures, and in particular on the existence of special emergency procedures which define the optimal actions during severe accidents. This approach implies the introduction in the event trees of the notion of procedure failure.

Quantification of the corresponding probabilities leads to several problems including physics of the sequences, systems availability and human behaviour for decision making and actions. This treatment is illustrated by the example of the small break event tree.

INTRODUCTION

In the PRA in progress in France for a 900 MW PWR plant, an effort is done for being as realistic as possible in the treatment of accident sequences. For this purpose, it is obvious that operator actions must be introduced although it is certainly one of the most difficult fields in a PRA.

In a first step, our approach is not the development of very new methods or models, but a tentative to gather and structure all the means available for a more systematic and homogeneous treatment of identification, introduction and quantification of operator actions.

OPERATOR ACTIONS IN A PRA

Type of actions : Among the actions which can have an effect on risk probability, a main distinction can be made between actions during normal operation of the plant and actions in accidental situation.

The first type is mainly errors during test and maintenance tasks with an effect on system availabilities. This aspect is the best known today (Ref 1, 2). The THERP method (Ref 3) is generally recognized as suitable for this problem which will not be developed further in this paper.

On the contrary, during an accident, the operator actions are no more routine tasks but involve thinking process and knowledge. Human actions can either increase or reduce the risk. This aspect is much more complex both for identifying the possible actions and for assessing the corresponding probabilities.

Identification : For identifying the significative human actions during an accident, it would be necessary to imagine a priori all the possibilities, and these may be extremely numerous.

An important investigation in this field is being performed for the development of special emergency procedures. Indeed the safety approach in France for severe accidents management is to complete the current accidental and incidental procedures (A and I) by a set of emergency procedures (H and U) (Ref 4) which identify the optimal actions even for out of design accidents.

Particularly an emergency procedure called "U1 procedure" is conceived to assure best possible conditions for RCS cooling and core safety, during any situation for which event specific procedures may be inappropriate. This procedure is based on the NSSS physical states (Ref 6).

Taking into account the existence of these emergency procedures we assume that in any situation, even very degraded, the operator (or the team of operators) will always follow an existing procedure, without having to define a strategy by himself. With such an assumption the identification of human errors, even during an accident, can be based on an analysis of the operating procedures (correctly or incorrectly applied). By this way, we can include in the PRA an important set of operator actions, which are at least the most likely.

Introduction in the PRA : The actions of the H and U procedures (including the use of complementary equipments) initiate sequences different from the branches of the initial system event tree.

The possibility for the operator to change the course of an accident sequence makes necessary the introduction of the notion of procedure success or failure in the event tree. The construction of the event tree needs then a systematic investigation of all procedures involved in the accident.

QUANTIFICATION

The term procedure is a global notion including diagnosis, decision, task execution and efficiency. To avoid complex and unuseful studies (and taking into account the large uncertainties), the treatment is in a first step simple and schematic in order to select the really important problems.

Definition of a procedure failure : To define clearly what is the failure of a procedure, we introduce the notion of key-action. Generally the key-action is the important action (which may consist of several elementary tasks) which must be achieved correctly and in time for the success of the procedure. The procedure failure is then the failure of the key-action.

For some procedures, the key-action may be on the contrary an action to be avoided. In some cases, there are two or more key-actions and, for a same procedure, the key-action may differ according to the accident sequence.

Fault tree of a procedure failure : The possible causes of a procedure failure are represented by a generic fault tree for each type of key-action (key-action to achieve or to avoid). As an example, the fault tree fig 1 corresponds to the first case.

This representation is very schematic, since various correlations exist between the causes. However this simple model is clear and allows a rough assessment for selecting the most significant contributions.

Probability of the causes : On fig 1 appear very different types of causes, needing very different approaches for assessing their probabilities. For instance :

- . Leaves n° 6 and 9 are systems failures, assessed by reliability calculation. These reliability studies must take into account possible changes in reliability parameters due to the accidental situation.

- . Leaf n° 2 is an error during execution of a task. This problem can be treated by the THERP method.

- . Leaf n° 8 is the physical efficiency of a procedure needing thermohydraulics calculations for some particular situations. The statement of the problem is generally clear but leads to very numerous parametric studies. For limiting the calculations to a reasonable level, a careful selection of the parameters is necessary.

- . The most difficult problem is the sub-tree 5, which includes diagnosis and decision. Recent studies (Ref 3, 5) indicate that in this case the most important parameter is the time available for acting. So according to the literature we intend to use as a first approach a curve giving the probability of failure versus time, established by a compilation of foreign results, experts opinion, and some specific data (simulator or experience).

In a further step we intend to list all the human failures retained in the PRA, and to ask to experts a relative ranking of the corresponding probabilities. This global approach will provide a complementary information.

EXAMPLE

Fig 2 is the event tree related to a small break initiating event. Procedures involved : In this event tree three operating procedures have been introduced.

- . H2 is the procedure related to a total loss of feed water. A feed and bleed cooling mode is initiated by opening manually the relief valves of the pressurizer.

- . U1 is a general procedure defining the best actions for cooling the core when the event procedures are inappropriate (multiple system failures - operator errors). U1 covers then a wide range of situations. In our example the U1 action of interest is, in case of HPSI failure, a fast depressurization by the steam generators which allows the operation of the LPIS system.

- . A1.1 is the small break procedure which states that the use of the containment spray system can be replaced by using the RHRS for cooling the primary water. This long term cooling configuration can be established either directly (case of very small LOCAs) as soon as RHRS operating conditions are reached, or delayed in case of a previous actuation of the spray system (for more important LOCAs).

Related studies : The assessment of failure probabilities for these three procedures leads to different type of studies, according to the specific problems related to each one.

- For U1, the first question is the physical efficiency of the procedure. More precisely for what break size, and within what delay is it possible to reach the LPSI conditions before a core damage.

For this purpose a thermohydraulics study has been initiated and is presently in progress.

- For H2, the most important parameter seems the human factor. The time available for acting before unreversible damage is short (about 30 minutes) and for several reasons the operator task is difficult :

. in this sequence there are two simultaneous accidents (a small break and a loss of steam generators), so an increased difficulty for diagnosis,

. the key-action (opening of the pressurizer valves) is not a current action and the operator may be reluctant for accomplishing it. So investigations in the field of human behaviour are necessary.

- For A1.1, an important contribution to the procedure failure is the system failure, since the RHRS is located inside the containment and will have to run under accidental conditions.

Expected effects : In a general way it is important to note that the introduction of these procedures will have an obvious effect on the risk probability related to the small break event tree by reducing the probability of three dominant sequences.

Indeed the procedures appear as redundancies for systems.

The introduction of H2 and U1 will reduce the probabilities of core melt for S2L and S2D3 sequences (respectively) by factors which are about the ratio of success to failure of the procedures. The utilization of A1.1 leads to a much lower benefit, since the failure of LPIS long term recirculation is dominant. The importance of this procedure becomes obvious when considering as a separate initiating event the case of steam phases breaks (PORV stuck open).

CONCLUSION

In the field of operator actions, and in a general way in the PRA in progress, we do not intend to develop very new technics, but rather to integrate extensively our present knowledge in the field of PRA and also in other fields like operating procedures, human factors, operating experience.

By a systematic research of the procedures involved in each sequence, a clear identification of the key-actions and of the failure causes, and an assessment of probabilities by use of all the means available, we obtain a treatment which seems more complete and less arbitrary, where the really important problems appear more clearly. The approach still needs numerous improvements, but even a limited step in this complex field would be already an interesting result.

REFERENCES

- 1 - PRA Procedures Guide - NUREG/CR.2300
- 2 - IREP Procedures Guide - NUREG/CR.2728
- 3 - Handbook of Human Reliability Analysis - NUREG/CR.1278
A. Swain and H.E. Guttman.
- 4 - French regulatory requirements concerning severe accidents in PWR
A. L'Homme and J. Pelcé - Meeting Cambridge. August 1983.
- 5 - Post event human decision errors : operation action tree/time reliability
correlation.
R.E. Hall, J. Fragola and J. Wreathall - NUREG/CR.3010.
- 6 - Additional emergency procedure based on NSSS physical states approach.
P. Cadiet, G. Depond and H. Sureau- International Meeting on Thermal
Nuclear Reactor Safety - Chicago. August 1982.

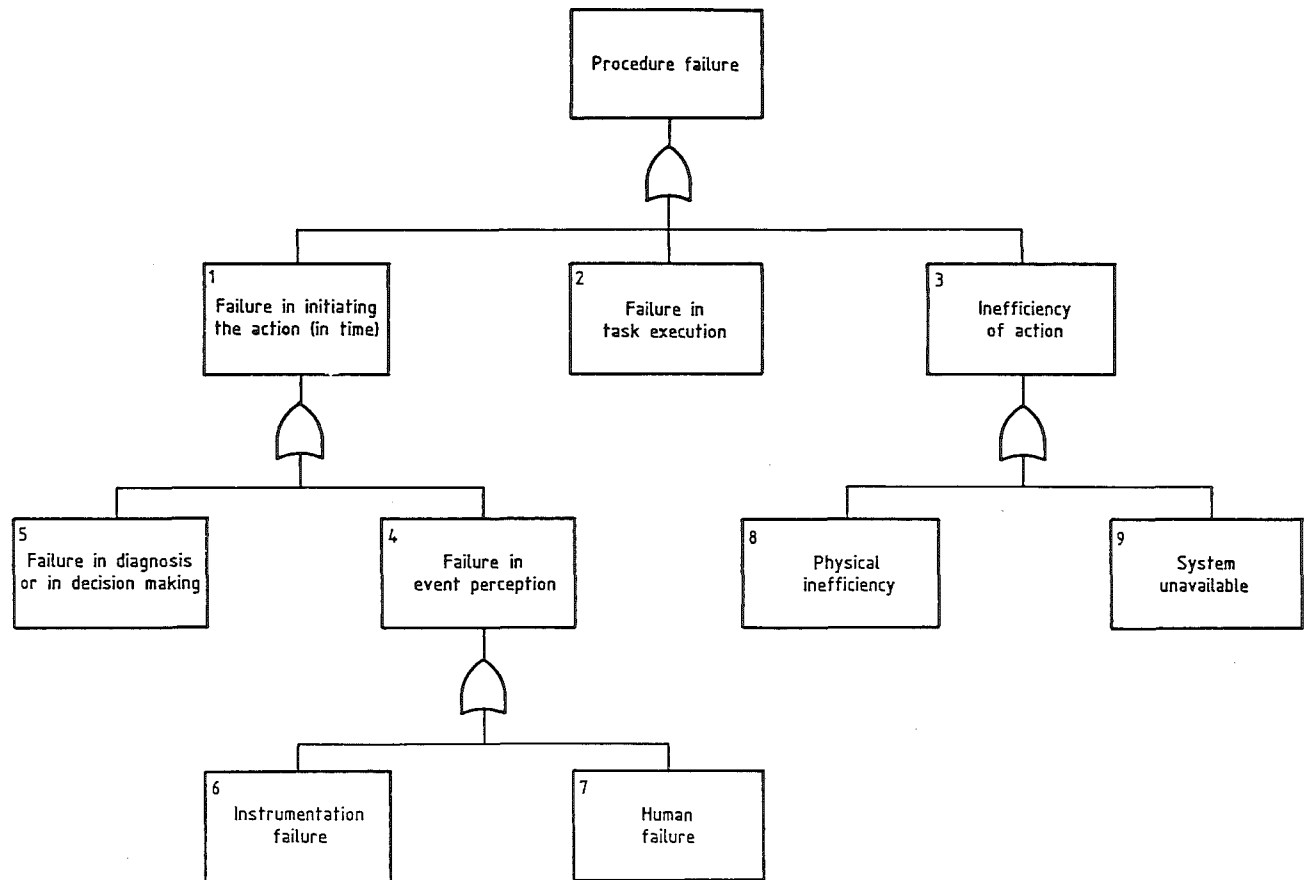
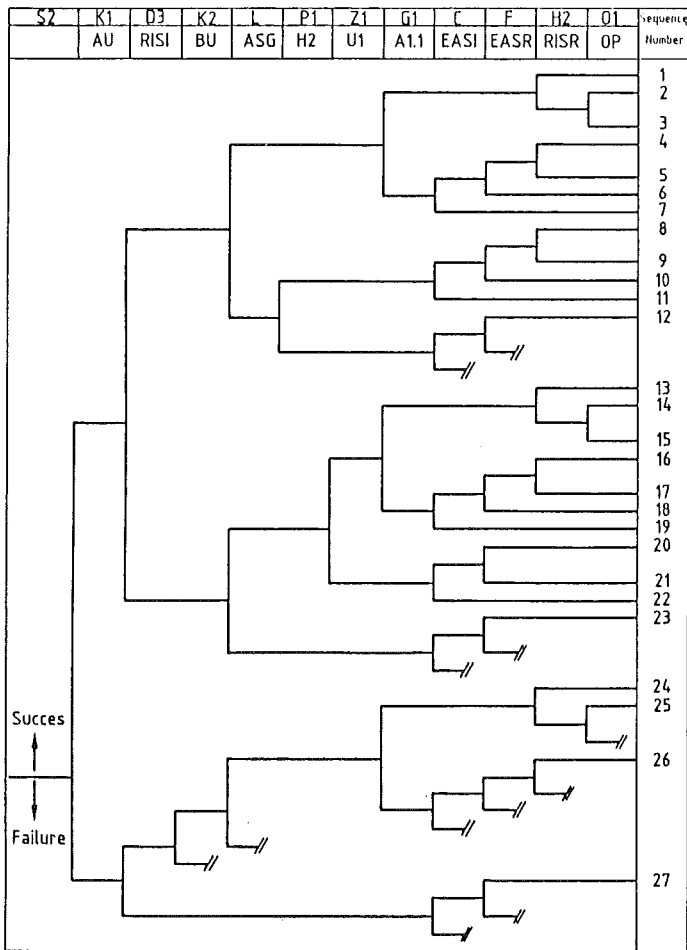


Fig. 1 - PROCEDURE FAILURE FAULT TREE

Fig. 2 - SMALL LOCA EVENT TREE



- AU Reactor Protection System
- RISI High Pressure Injection System
- BU Emergency Borication
- ASG Auxiliary Feed Water System
- H2 H2 Procedure
- U1 U1 Procedure
- A11 A11 Procedure
- EASI Containment Spray Injection System
- EASR Containment Spray Recirculation System
- RISR High Pressure Recirculation System
- OP Manual Operation of Containment Spray System

TREATMENT OF COMMON CAUSE FAILURES
IN THE BARSEBÄCK 1 SAFETY STUDY

G. Ericsson and S. Hirschberg

AKTIEBOLAGET ASEA-ATOM
S-721 04 Västerås, Sweden

ABSTRACT

This paper presents the main features of the common cause failure analysis in the Barsebäck 1 safety study. The qualitative part of the analysis has been given the highest priority. A procedure, based on the generic cause approach, has been developed for systematic performance of think-through and walk-through analyses. The method is relatively simple, requires reasonable resources and allows identification of significant common cause failures. Results of the qualitative analysis form the basis for assignment of varying beta-factors which are extensively used in the quantitative analysis of dependencies. Generally, the estimated common cause failure probabilities contribute significantly to the analysed core melt sequences.

INTRODUCTION

The reactor safety study for the Barsebäck 1 nuclear power plant has been jointly carried out by AB ASEA-ATOM and the utility (Sydkraft). The reactor, a BWR, is of ASEA-ATOM design and started commercial operation in 1976.

The importance of dependent failures has been clearly demonstrated by reactor operating experience. Dominating accident sequences frequently involve dependent failures. Therefore, treatment of dependencies should constitute a crucial part of any PRA study. General assumption of independence between systems (components) is non-conservative and usually leads to excessively optimistic results.

There are many factors which make the analysis of potential dependencies difficult. Some of them are as follows:

- definition dilemma
- existence of several systems of classification of dependent failures
- controversies regarding the use of qualitative models for identification of dependencies
- immense number of potential dependencies
- treatment of human errors
- lack of reliable data sources
- limitations of methods for quantification of dependencies
- uncertainties in the treatment of external events.

In view of these difficulties the need of thorough treatment of dependencies was acknowledged at the initial stage of the project.

EVALUATION OF AVAILABLE METHODS

As a first step in the analysis of dependencies the available models were evaluated [1]. This activity was motivated by prevailing lack of guidance on how the dependency analysis should be incorporated into a PRA-study. Several methods have been developed for treatment of dependencies. The available models have varying degree of complexity, are based on different assumptions, and consequently differ with respect to applicability. The following conclusions were drawn:

- 1) Common cause failures (CCFs) constitute an important group of dependencies, which requires special treatment. According to a general definition, CCFs are multiple failures occurring at the "same" point of time (i.e. simultaneously or in a short time interval), attributable to a common cause. Such a rather inclusive definition seems adequate for the performance of PRA studies, where all potentially significant CCFs are to be identified.
- 2) If handling of large fault trees is possible, it is often advantageous to model dependencies originating from the system design directly in the fault trees. This implies that the control signals, power supply, auxiliary systems, etc., are modelled for each component served by these.
- 3) The qualitative analysis should be given highest priority in the study of dependencies. As a result of identification of potential critical dependent failures, immediate measures are usually taken in order to eliminate (or reduce) the risks. Furthermore, the qualitative analysis constitutes the starting point for a possible quantification.
- 4) Available methods for qualitative analysis of dependencies can be divided into three groups:
 - think-through and walk-through analyses
 - fault tree modification
 - generic cause approach.

Detailed knowledge of the plant and of the involved processes is a prerequisite for a meaningful use of the methods.

- 5) Relatively small resources are needed for think-through and walk-through analyses. These types of approach should lead to identification of significant dependencies given that systematic procedures are used.
- 6) Fault tree modification, traditionally the most popular of the qualitative methods, requires rather extensive resources and does not guarantee identification of all significant CCFs.
- 7) Use of generic cause approach, based on identified minimal cut sets (MCS), offers good chances to identify significant dependencies. Computer codes may be used to automate the analysis to a large extent. The method is systematic, which creates a potential danger that the analyst is systematically missing some important items.

- 8) Independently of which method is chosen great importance must be given to the screening procedures for elimination of insignificant dependencies. Otherwise the problem becomes impossible to handle. The necessary sorting can make use of assignment of ranks to primary events, knowledge of components' physical location, the existing barriers, etc.
- 9) There is a number of reliability models for quantification of dependencies. The following examples may be mentioned: square root method, beta-factor method, Marshall-Olkin specializations, common load model, Markov models.
- 10) None of the quantitative methods is universal. All models suffer from lack of reliable CCF-data. Therefore, sensitivity analysis is a very useful tool for the assessment of CCF-significance.
- 11) The final choice of method for qualitative CCFA depends upon the available resources (personnel, time, funding, computer codes and computer capacity) and upon the objectives of the study.

PRINCIPLES FOR QUALITATIVE ANALYSIS

Based on the conclusions given above, a program for practical carrying out of the CCFA has been formulated [2].

The postulated dependencies have been classified according to their potential causes:

- 1) Systems interaction
- 2) Normal external environment
- 3) Facility-related external phenomena
- 4) Site-related external phenomena
- 5) Design limitations and functional deficiencies
- 6) Human factor.

A much more detailed classification, explicitly specifying physical sources of dependencies, has been presented [2].

Before going into details concerning the practical treatment of the different types of dependencies, some general comments regarding principles of fault tree construction in the Barsebäck 1 safety study, are in place.

- 1) The fault trees are developed to an extremely detailed level (even component fault trees are included), which facilitates identification of dependencies between components.
- 2) Certain human errors are included in the fault trees.
- 3) Tests and maintenance are represented in the fault trees.
- 4) Equipment shared between several systems may be easily identified since a unique code is allocated to each component.

- 5) Dependencies which originate from the system-design features, e.g. signal exchange, auxiliary systems, power supply, etc., are included in the fault trees.
- 6) Common cause failures in redundancies are represented in the fault trees as basic events (mainly in component fault trees, whenever they are available). However, the nature of the common cause is not specified.

As a result of the principles governing construction of fault trees, no separate treatment of systems interactions is necessary, since interactions associated with the system design have been earlier incorporated into the fault trees.

Identification of dependencies which may arise through influence of normal external environment has been performed using systematic think-through and walk-through analyses. A general description of the applied methodology will be given in next paragraph. Facility-related external phenomena are in principle handled in the same way as normal external environment.

Analysis of site-related external phenomena is outside the scope of the Barsebäck 1 safety study.

A large part of potential dependencies which originate from design limitations is covered by systems interactions. Identification of functional deficiencies is a standard part of the continuous safety work performed by utilities and by the plant supplier. The procedures developed for think-through and walk-through analyses allow that searching for such deficiencies is performed in a systematic way.

A simplified treatment of human errors as a source of dependencies has been a part of think-through and walk-through analyses. In addition, a separate study [3] concerning potential dependencies caused by planned and unplanned maintenance, has been performed. For the analysed cases, it was concluded that dependencies generated by human factor (and not modelled in the fault trees), give negligible contributions to unavailability of redundant equipment.

PROCEDURE FOR QUALITATIVE ANALYSIS

A special procedure has been developed for systematic identification of dependencies [4]. Concepts and terminology of the generic cause approach [5] have been transferred to walk-through analysis. The methodology is based on:

- examination of system documentation for safety systems of interest
- study of developed fault trees
- experience from treatment of CCFs in earlier reactor safety studies
- use of check lists covering all important special conditions and secondary causes for all relevant redundancies
- use of questionnaires prepared for each special condition and for each secondary cause
- on-site inspection of the system under consideration.

The main practical steps in the procedure are:

- 1) Identify redundancies within each system
- 2) Make a preliminary estimate of potential dependencies using the check list
- 3) Answer the questions in the questionnaires, but only for the special conditions and secondary causes which were pointed out on the check list
- 4) Go back to the check list and assign ranks to each common cause candidate. Use a six-degree scale extending from 1 (insignificant) to 6 (large significance)
- 5) Make a final choice of common cause candidates.

The same procedure may be applied to identification of dependencies between redundant systems. In these cases more attention must be directed towards potential dependencies between components with diverse functions. The analysis of dependencies between redundant systems has been performed parallelly with the study of CCF-contributions within individual systems. The proximity and physical separation between systems of interest has been considered during the walk-through analysis.

SCOPE AND RESULTS OF QUALITATIVE ANALYSIS

The described method for systematic identification of dependencies is especially suitable for analysis of mechanical systems with relatively few components within each redundancy. Core cooling systems and residual heat removal systems in Barsebäck 1 fulfil these conditions. The walk-through analysis of these systems [6] has been carried out by a working group including personnel with long operating experience as well as analysts with "PRA-background". In this way there was a good chance to cover all important angles of the analysis. Two types of dependencies have been considered:

- 1) Dependencies between redundancies within individual systems.
- 2) Dependencies between redundant systems.

The following systems from the first group have been analysed:

- 1) Core cooling systems
 - Feedwater lines (312)
 - Condensate system (462)
 - Low pressure coolant injection system (323)
 - Auxiliary feedwater system (327).
- 2) Residual heat removal systems
 - Shutdown cooling system (321)
 - Containment vessel spray system (322)
 - Shutdown cooling water system (712)
 - Shutdown secondary cooling system (721).

Analysis of dependencies between redundant systems has been performed for the following combinations:

- 312/462, 327
- 327, 323
- 312, 323
- 322, 321
- 461 (condenser and vacuum system), 721/712
- 461, 322
- 461, 321.

205 potential dependencies have been identified, including 198 dependencies between redundancies within individual systems and 7 dependencies between redundant systems. None of the dependencies motivates immediate application of measures such as design modifications or procedural changes.

There are 13 cases with moderate significance (the remaining 192 dependencies are less significant). Most of them appear in the auxiliary feedwater system. This result is not unexpected since the redundancies in this system are characterized by lack of separation and are particularly susceptible to dependencies.

Generally, facility-related external phenomena appear more frequently as source of dependencies than the normal external environment.

These components which are most sensitive to dependencies have been listed [6], separately for each system. Furthermore, the dominating factors in the normal external environment as well as the facility-related external phenomena which are expected to be insignificant, have been pointed out.

Here, only the results obtained for the auxiliary feedwater system are accounted for. The checklist is shown in attachment 1. In principle it is possible that all types of dependency may occur but the majority of these does not influence the system reliability. Therefore, none of the dependencies with rank one (insignificant) has been indicated in the checklist. A questionnaire concerning fire of auxiliary feedwater pumps is also enclosed (attachment 2).

QUANTITATIVE ANALYSIS

The beta-factor model [7] has been chosen for quantification of CCF-contributions. The method is simple to apply, employs only a single CCF-parameter and is considered to be adequate for calculations concerning systems with two redundant channels. The beta-factor method is, however, expected to result in excessively pessimistic results when applied to systems with higher redundancy levels [8].

The choice of the beta-factor is in each particular case dependent on the significance factors assessed in the qualitative analysis. Three different values have been used (0.01, 0.05, 0.10). Principles for assignment of beta-factors to identified redundancies have been described [9].

The preliminary results of the Barsebäck 1 safety study show that CCFs contribute 14 % of the total estimated core melt probability. The loss of residual heat removal is dominated by CCF-contributions. Some of the dependencies identified in the study have low significance but are in disagreement with basic design principles. In most cases, modifications may be carried out at low costs.

CONCLUSIONS

The characteristic features of common cause failure analysis in the Barsebäck 1 safety study have been described. The main efforts have been concentrated on the qualitative part of the analysis. A practical approach to the problem, based on the principles of the generic cause method, has been developed. The described procedure for identification of dependencies is simple, systematic and requires rather small resources. In spite of certain limitations it is expected that the important dependencies have been identified. Future developments may involve improved quantification of CCF-contributions from redundancies with three or more channels and detailed analyses of site-related external phenomena.

ACKNOWLEDGEMENTS

The authors are grateful to Peter Ljöfberg, Lars Thuring and Kenneth Zander (Sydkraft), who participated in performing this study.

REFERENCES

1. S. Hirschberg, Dependent Failure Analysis: Inventory and Evaluation of Available Methods (in Swedish), AB ASEA-ATOM, Report KPA 82-315, September 1982 (internal document).
2. G. Ericsson, S. Hirschberg, Barsebäck 1 - Safety Study. Program for Practical Carrying Out of the Dependency Analysis (in Swedish), AB ASEA-ATOM, Report KPA 82-488, November 1982 (internal document).
3. G. Ericsson, Barsebäck 1 - Safety Study. Human error in Connection with Planned and Unplanned Maintenance - an Inventory of Sources of Dependency (in Swedish), AB ASEA-ATOM, Report KPA 83-269, September 1983 (internal document).
4. S. Hirschberg, Barsebäck 1 - Safety Study. Qualitative Common Cause Failure Analysis - Development of Procedures for Identification of Dependencies (in Swedish), AB ASEA-ATOM, Report KPA 83-34, February 1983 (internal document).
5. R. B. Worrell, D. W. Stack, Common Cause Analysis Using SETS, SAND 77-1832, Sandia Laboratories, Albuquerque (1977).
6. S. Hirschberg, Barsebäck 1 - Safety Study. Identification of Dependencies. Analysis of Core Cooling Systems and Residual Heat Removal Systems (in Swedish), AB ASEA-ATOM, Report KPA 83-157, May 1983 (internal document).
7. K. N. Fleming, A Reliability Model for Common Mode Failures in Redundant Safety Systems, Proceedings of the Sixth Annual Pittsburgh Conference on Modeling and Simulation, General Atomics Report GA-A13284, April 1975.
8. S. Hirschberg, Workshop on Dependent Failure Analysis, Västerås, April 27-28, 1983. Summary Report: Conclusions and Recommendations for Future Work, AB ASEA-ATOM, July 1983.
9. L. Thuring, Quantitative CCF-analysis (in Swedish), Sydkraft, Report 8305-102, June 1983 (internal document).

Attachment 2

SYSTEM: 327
DATE: 83-05-04
SIGN: SH

REDUNDANCY: P1, P2

CAUSE OF DEPENDENCY: FIRE

Fuel load. Which combustibles can be found in the room?

Oil in the pumps.

Which redundant components are affected by fire?

Almost all.

Effect on the system?

Loss of function.

Risk of ignition?

Lot of traffic, but fuel load concentrated to the pumps.

Fire detectors?

Yes.

Extinguishing equipment?

Automatic sprinklers.

Fire propagation from and into the room?

Fire can propagate through the doors if they are left open. The turbine oil-system is located in the adjacent room (separated by thick concrete walls).

Final opinion:

Fire has a moderate significance as a cause of dependency.

PROBABILISTIC TRANSIENT SIMULATION
METHODOLOGY IN SUPPORT OF PROBABILISTIC SAFETY
EVALUATION STUDIES FOR ONTARIO HYDRO REACTORS

J.C. Luxat, A.P. Firla, E. Hussein, A.P. Muzumdar, B.C. Choy

Ontario Hydro
Toronto, Ontario, Canada M5G 1X6

ABSTRACT

A system of computer codes for probabilistic transient event analysis is described. The system is designed as a versatile and flexible tool that addresses the total analytical process within a probabilistic framework. The major elements in the system are discussed and the potential applications of the codes to various aspects of safety evaluation for Ontario Hydro nuclear generating stations are outlined.

INTRODUCTION

Analysis of the progression of events following a postulated initiating failure forms an important part of safety evaluations for Ontario Hydro's CANDU reactors. A key element in this analysis is characterizing the event sequences which, in turn, involves determining the probable timing of state transitions and estimating the resultant consequences associated with the transitions. The analytical tools used for this purpose are deterministic transient simulations employed in conventional accident analysis, and fault tree/event tree methodology employed in probabilistic safety evaluation (PSE). Transient simulation analysis explicitly evaluates time dependent process system responses and the transitions in the physical process states but, traditionally, has not been developed to directly handle uncertainties within a probabilistic framework. PSE techniques, on the other hand, explicitly account for the probabilistic nature of changes in plant state due to system or component failures and operator interventions, but do not directly incorporate modelling of the underlying physical processes and the time dependency of process system responses. Despite these inherent differences the two tools play important complementary roles in the safety evaluations of nuclear generating stations.

In reality there is a vast shared common ground linking the two analytical tools. At the most fundamental level the plant systems, the underlying physical processes and the safety concerns are common elements of the analysis. Similarly, the potential state of the plant at the time a failure event occurs, the state of various systems that are called upon during the progression of events and the underlying physical processes are all sources of uncertainty with respect to characterizing the event sequences. An overall probabilistic approach represents, perhaps, the most effective analytical framework to rationalize and quantify uncertainties.

The above observations have motivated the development at Ontario Hydro of a system of computer codes for PRObabilistic Transient Event Analysis (PROTEAN).

The major elements of the PROTEAN system are described in this paper. Since it is a system designed to address the total analysis process, the following discussion is not limited to probabilistic transient modelling. Ultimately, probabilistic modelling is neither more nor less important than deterministic modelling of fundamental physical processes.

OBJECTIVES AND METHODOLOGY

The analysis of event sequences and evaluation of physical process uncertainties potentially requires many transient simulations spanning a wide range of times with varying scope and complexity of system and physical process modelling. Furthermore, any new analytical tool should not attempt to replace existing tools that are established and effective in their respective areas of application. Rather, a new tool should complement and augment existing tools. In addressing these general requirements and constraints the following objectives were adopted for the code development:

- (a) Capability must be implemented to allow rapid generation of simulation models and input data for interconnected and interacting systems within a station. This capability must allow easy reconfiguration of the structure of the models.
- (b) The models must be kept as simple as possible to provide inexpensive but acceptably accurate simulation capability. The models should directly incorporate probabilistic modelling of uncertainty propagation.
- (c) There should be a flexible, easily configured facility to interface models of a particular system that have different levels of modelling complexity.

In order to meet these objectives the PROTEAN system is being developed as a set of interacting codes that perform specific tasks in the analysis process, as shown in Figure 1. A key element in meeting the first objective is automating, to the greatest extent possible, the generation of system models and their associated input data. This requires a data base which contains detailed design data for the various systems and a set of procedures that will accept a user-input model specification and generate the required model and data. These procedures would access and process data from the data base and provide the linkage between the input data and the code subroutines that implement the model. The models may be used either in the transient simulations or in subsequent analysis that uses the output generated by the transient simulations. The ultimate objective of this development is to provide an analytical tool that allows more of the user's effort to be directed toward the analysis with less effort required to put the analytical models in place.

Additional details of the subsystems identified in Figure 1 are described in subsequent sections.

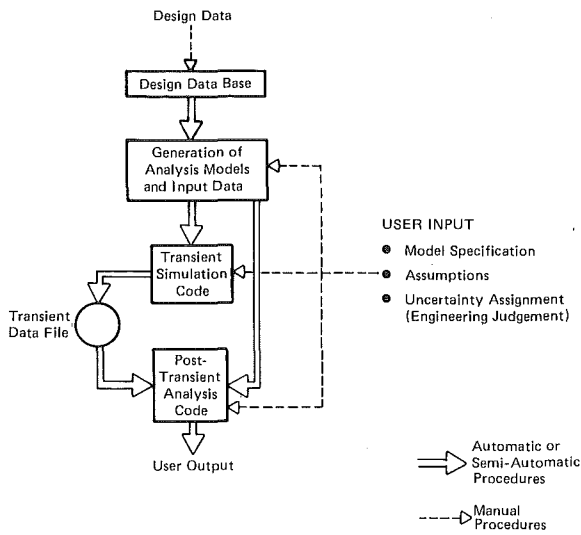


FIGURE 1
Structure of the System of Computer Codes
for Probabilistic Transient Event Analysis

THE DATA BASE

The data base contains detailed design data pertaining to the many interconnected systems in a CANDU nuclear generating station. Each of these systems may be considered as a network in which some physical quantity, such as an electric current or fluid, flows in specified directions according to the arrangement of the components in the network and their operating state. Consequently, the data base has been designed with a logical classification of the data into sets that form a complete description of the network structure and components in a system. These sets of data are organized into four files associated with each system. As shown in Figure 2, there are three files describing, respectively, the network topology, physical characteristics of components and network-to-network interconnections and a fourth file that is a relational table providing the linkage between the three descriptor files.

The network structure of a system is contained in the topology file. The top level of description consists of specifying the network topology in terms of a directed graph which identifies the unique node points in a network and the branches connecting the nodes. Each branch is subdivided into a number of unique component types arranged in an ordered sequence that corresponds to the manner in which the components are physically connected. Figure 2 shows the directed graph and part of the ordered sequence of component types, arranged in data records indexed by branch identifiers, for the example network (System 1). It is important to recognize that there is a limited set of basic component types. A particular component need only be identified by a "type" character and unique numeric index value.

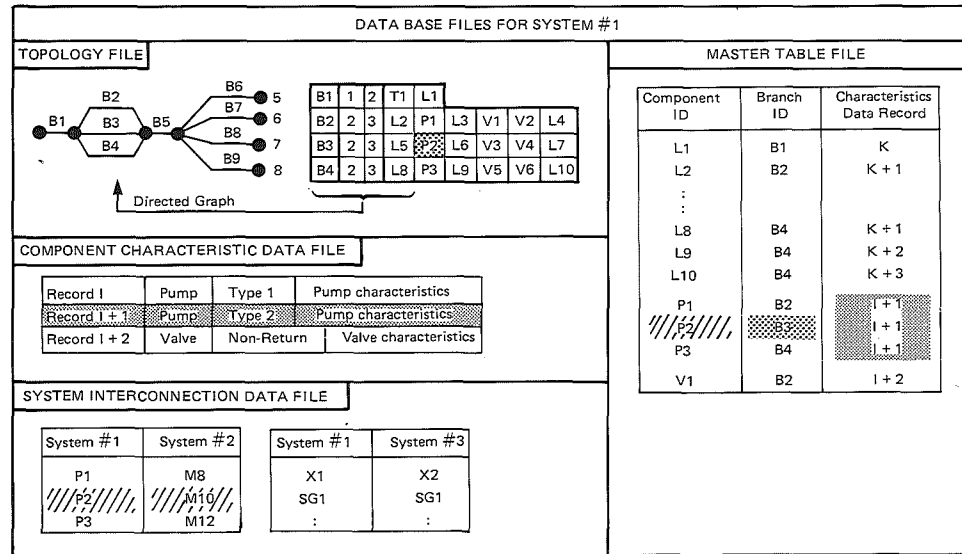
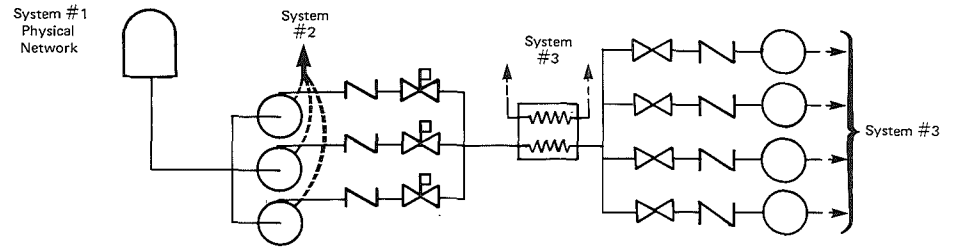


FIGURE 2
The Structure of Files in the Data Base Showing
the Relationships between Data in the Files

The description of a component in terms of physical attributes such as length, diameter, material etc is not required in the description of the network structure. Consequently, the physical characteristics of a component are specified in the component characteristic data file. The data in this file is not related to the location of the component in the network. In fact there may be identical components located in different sections of the network; for example the pumps in the three branches B2, B3 and B4 of the example network. The linkage between the network structure and component physical data is provided by the master table file. The data in this file links each uniquely identified component in the network to an associated branch in the topology file and to a record in the component characteristics data file.

The final, logically separate set of data is the system interconnection data file. The data in this file consists of sets of component identifiers that specify which components in the system network being described are connected to components that are part of another system. The linkage of this data to the data describing the network is, once again, provided via the master table file. Indexed sequential data file structures are employed with data access and retrieval via "keys" [1].

ANALYTICAL MODELS AND DATA GENERATION

The general structure of the procedure to generate models and input data for analysis purposes is shown in Figure 3. The model structure is specified in a similar manner to the network description in the data base. It consists of a topological description of the model and the identification of the component model subroutines that are to be used. Associated with this description is information identifying a one-to-one relationship between a section of the model and a section of the system network description in the data base. This information is used to retrieve the design data from the data base and to control the subsequent procedures that perform the mathematical operations to generate the derived data for the model.

Automating the process of model generation involves linking the sets of derived data to the appropriate model subroutine and linking the model subroutines to a network solution control procedure. These linkages are structured by the user-specified model topology. This task is the most difficult one to implement. The approach that has been adopted is to implement this function in stages. The first stage involves automating the input data generation procedure. This will be followed by semi-automation of the model generation procedure. Finally the experience gained from the preceding stages will result in the refinement and ultimate integration into an automated procedure. This approach is dictated, in part, by the need to perform analysis at the same time that development is being performed.

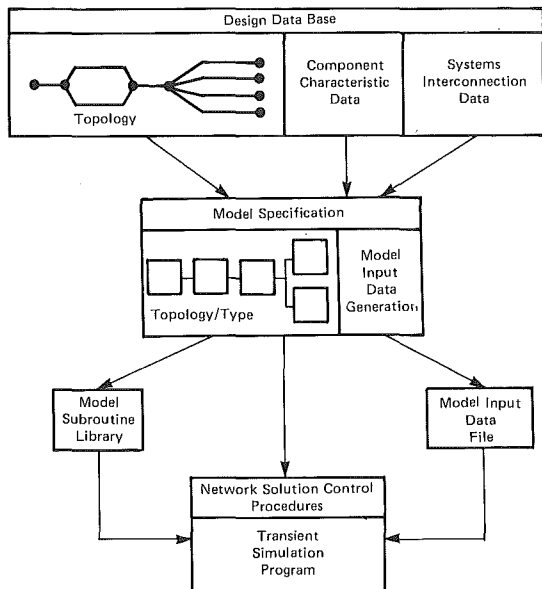


FIGURE 3
Procedure for Automated Generation of System Models
for Transient Simulation Analysis

TRANSIENT AND POST-TRANSIENT ANALYSIS

As stated earlier, the intent of the code is to utilize low order analytical approximation models to the greatest extent possible. The network solution control procedure is also based upon applying analytical or semi-analytical iterative solution schemes analogous to lumped parameter solution methods employed in electrical network and feedback control systems analysis. These solution schemes are essential for ensuring the code meets the objective of being an inexpensive and flexible simulation tool. Figure 4 shows the trends in pressure and flow in a CANDU heat transport loop following a loss of coolant accident discharging coolant at a rate of 400 kg/s, as predicted with an approximate model for the heat transport system. The model consists of four lumped nodes with an explicit solution for the heat transport loop flows. These loop flows couple the mass and energy balance solutions for the four nodes. This modelling approach yields pressure and flow distributions in the heat transport system that are within 5 percent of the results obtained with a large code containing hundreds of nodes.

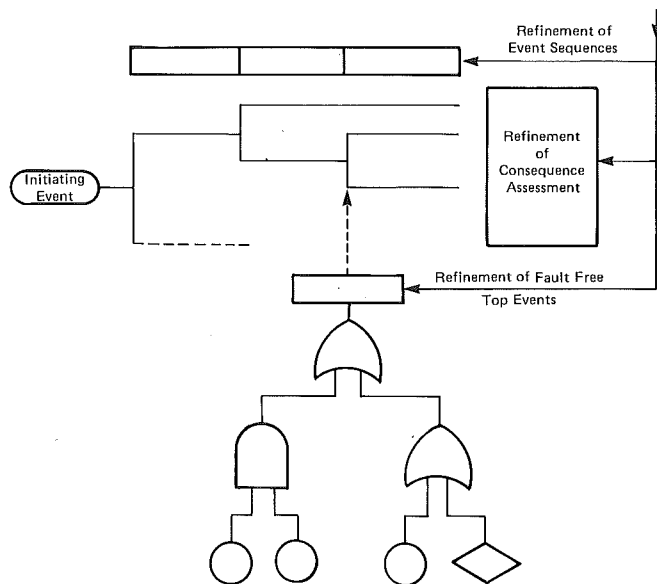
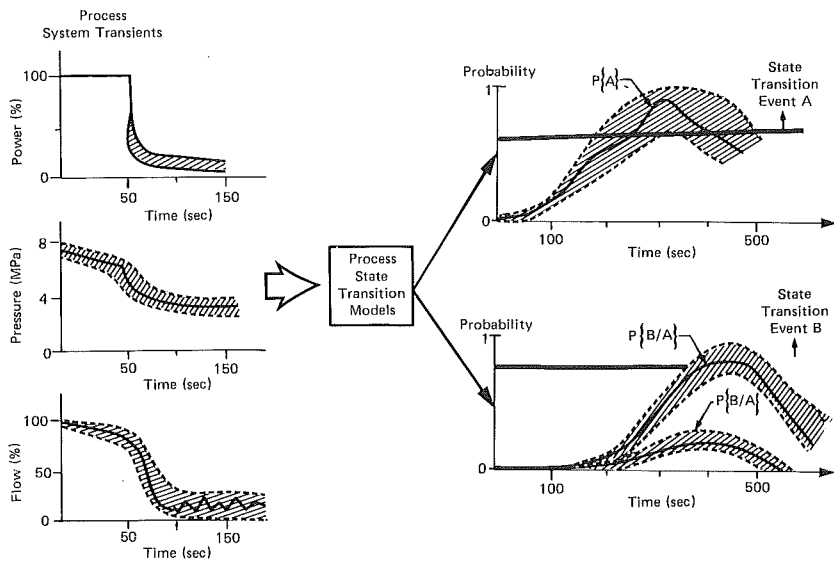


FIGURE 4
 Depiction of Probabilistic Process State Transition Modelling
 and its Application within a PRA Framework

Similar considerations are applied in uncertainty propagation modelling. The uncertainties of interest can be classified as plant state, empirical knowledge and physical process model uncertainty [2,3]. Plant state uncertainties arise from the spectrum of possible operating states and conditions in the various plant systems. They influence the conditions at, and the timing of plant state transitions. The uncertainties in empirical knowledge influence the prediction of transitions in the physical process states (for example flow and heat transfer regimes) and the physical process responses following these transitions. Finally, model uncertainties relate to the ability of a particular model to provide a reasonable representation of reality, within the constraints of the state of empirical knowledge. Approaches to the treatment of plant state and empirical knowledge uncertainties include Monte Carlo and response surface methods [3,4] which treat a code essentially as a black-box and derive distribution functions connecting the outputs to be inputs of the box.

In the PROTEAN code an alternative approach is adopted. Firstly, uncertainty in characterizing transitions in physical states is differentiated from uncertainty propagation in process variables and parameters. The former is concerned with quantifying the probability of a state transition occurring and the range in probable timing of the transition. The latter, however, is continuous in time and, while potentially influencing state transitions, is in part dependent upon the process state. Secondly, process variables and parameters (code input and outputs) have underlying causal relationships that are directly related to the models; which, in turn, are conditioned by the process state. Fundamental changes in the propagation of process variable uncertainties occur at discrete time intervals when process state or plant state transitions occur. The termination of one state provides the initial conditions for the next state. In a given state, the uncertainties in the set of input variables and parameters are first transformed into equivalent uncertainties in the following fundamental physical quantities: mass, energy, mass transport rate (flow) and energy transfer rate (power). The transformations are determined directly from the models associated with the particular process state. The transformed uncertainties can then be propagated to other variables, for example coolant pressure or fuel temperature, by quasi-linearized sensitivity analysis.

A simple, intuitive example is shown in Figure 4 where the mean trends and uncertainty ranges in selected process variables are shown as a function of time during a small loss of coolant accident in which delayed injection of emergency coolant is postulated. The state transition models indicated in this figure evaluate the probability of a transition to a stratified flow regime in the fuel channels (state transition A) and the conditional probability of any fuel element exceeding some elevated temperature (transition B), given either stratified or non-stratified flow. In the example, state transition B is only probable if state transition A occurs within a limited time following reactor shutdown. Although this is an oversimplified and somewhat contrived example, it demonstrates that, in quantifying uncertainties with a probabilistic code, the results must be broadly consistent with engineering judgments that can be made by independent deterministic analysis.

APPLICATIONS

A major application of the code will be in quantifying the effects of uncertainties in system states and process parameters on both the probable timing of transition events and the potential consequences associated with the transitions. This probabilistic transient information can, for example, be utilized within the context of probabilistic safety evaluations in the manner depicted in Figure 4. Another major application area is in the assessment of the effectiveness of safety system actions. The objective in this application is to quantify the effect of uncertainties in the safety systems, for example instrumentation response, the phenomenological safety criteria employed and the effects of process and control system states and actions, on the ability of these systems to meet safety design objectives or production reliability targets. Finally, elements of the system, such as the front-end data base and input data generation procedures, can potentially be employed by other analysts to assist in data preparation for codes employed in accident analysis.

REFERENCES

- [1] Muzumdar, A.P. and J.C. Luxat, "Design of a Nuclear Power Station Data Base for Analysis Applications", Proc. CNS 10th Ann. Symp. on Simulation of Reactor Dynamics and Plant Control, St. John, New Brunswick, April 1984.
- [2] Parry, G.W. and P.W. Winter, "Characterization and Evaluation of Uncertainty in Probabilistic Risk Analysis", Nucl. Safety, 22 (Jan-Feb 1981) pp. 28-42.
- [3] Chu T.L. and G.E. Apostolakie, "Assessment of the Uncertainties Associated with the Core Uncovering Time in TMI-Type Accidents", Reliab. Engineering, 8 (1984) pp. 23-56.
- [4] Vaurio, J.K. and C. Mueller, "Probabilistic Analysis of LMFBR Accident Consequences with Response Surface Techniques", Nucl. Sci. Eng., 65 (February 1978), pp. 401-413.

HOW FIRM ARE PRA RESULTS?

Sanford L. Israel

U.S. Nuclear Regulatory Commission
Washington, D.C. 20555

ABSTRACT

The results of several PRAs and their peer reviews are discussed in terms of changes in likelihoods and identification of dominant sequences. Overall core-damage likelihoods appear to be affected by the scope of the study and some of the underlying assumptions in the analyses. Assumptions also play an important role in identifying dominant contributors to core-damage or offsite consequences. This paper presents examples of the impact of study scope and assumptions on the results of PRAs. These examples highlight the need for more attention to be given to the bases that support the more sensitive assumptions.

INTRODUCTION

There have been numerous probabilistic assessments performed in the United States over the past few years with many different objectives in mind. Most of those sponsored by the utilities and submitted to the Nuclear Regulatory Commission (NRC) in support of an ongoing licensing or regulatory activity received rather intensive peer reviews to assess the validity of the findings. In order to confirm the PRA results, the reviews examined the event trees/fault trees, component failures, human errors, common cause failures, assumptions, and interdependencies and also looked for omissions. Many of these areas were simply audited and compared with the existing state-of-the-art treatment; however, the more searching portions of the review required gaining some independent familiarity with the plant design and operation and a questioning attitude to ferret out marginal assumptions or lapses in logic. Reviews of the various studies generally resulted in different estimated core-damage likelihoods and differences in dominant contributors to core-damage or risk.

Differences in PRA results are expected. The Lewis Committee [1] noted "WASH-1400 is defective in many important ways. Many of the calculations are deficient when subject to careful and probing analysis, with the result that the accuracy of many of the absolute probabilities calculated therein is not good as claimed." Further, the Committee said that they didn't know whether the results were high or low and that the uncertainties were understated. Uncertainty has become a hallmark of probabilistic assessments and considerable attention has been focused on shortcomings of PRAs. At various times, the culprits have been identified as insufficient data, inadequate treatment of common cause failures and human errors, and modeling errors.

In the following discussion, I have tried to highlight the observations from peer reviews that led to different perceptions of core-damage likelihoods or dominant accident sequences. Hopefully, this information will provide some insight on where to focus attention when performing a PRA or reviewing one in the future. In addition, I will discuss some of the more significant findings of a recent survey [2] of the impact of various aspects of PRA methodology on identifying dominant accident sequences. This survey, sponsored by the NRC, attempted to pinpoint those aspects of the PRA methodology which appeared to drive the PRA results.

My comments are directed primarily at core-damage assessments which have received the most attention and presumably are the most mature. Similar concerns about uncertainty and bias could be addressed in the containment and consequence analysis. These analyses entail much more detailed phenomenological modeling with its associated uncertainty than the core-damage assessments.

DISCUSSION

Protestations of large uncertainties notwithstanding, the one parameter that receives the most attention in a probabilistic assessment is the estimated core-damage likelihood. It fixes our perception of risk. In the United States, the core-damage likelihoods estimated by the various plant studies range from $2 \times 10^{-6}/\text{RY}$ to $2 \times 10^{-3}/\text{RY}$. This wide spread in estimates reflects differences in plant design and operation as well as differences in methodology (including the choice of the estimators). There are several documented studies and peer reviews of the same plants in the United States which allow us to examine the potential impact of different methodologies on the estimated core-damage likelihoods. The comparisons of the studies presented below are meant to identify the types of methodological considerations that appear to influence the results without passing judgment on the validity of any particular approach or result.

The Indian Point plants (Units 2 and 3) have been the subject of considerable scrutiny over the past four years because of their location in a high population density area. The first probabilistic study of the plants [3] used an abbreviated characterization of the important plant systems, a small prescribed set of sequences for internally initiated events, and a simplified quantification based on failure probabilities from the Reactor Safety Study [4]. The second study was a thorough investigation of the plants that considered both internal and external events [5]. The third study [6] was a quick estimate of core-damage likelihoods for internally initiated events based on simplified event trees, a cursory knowledge of the plant design, and an analyst's gross estimates of system unavailabilities (no fault tree characterization). The fourth study [7] was a rather intensive peer review of the in-depth probabilistic study. The estimated core-damage likelihoods for internally initiated events from these studies ranged from about $10^{-4}/\text{RY}$ to $10^{-5}/\text{RY}$ with the low estimates obtained by the rudimentary studies and the higher estimates obtained by the more sophisticated study and peer review.

Why the difference in the core-melt estimates? One's initial reaction would be to suspect that the detailed event tree and fault tree analyses

uncovered some hidden vulnerability; however, this is not the underlying cause. The differences are attributable to assumed LOCA frequencies and different analysts perceptions. The analyst's perceptions that were significant were assumptions that loss of reactor coolant pump seal cooling would result in a seal failure (LOCA); its corollary that a break in the component cooling water system would also result in a consequential seal failure and loss of ECCS; and the quantification of human error probabilities associated with switchover from injection to recirculation following a LOCA. The assumptions regarding the reactor coolant pump seal failure and the component cooling water system are not unique to these plants; however, they may have been illuminated by the more thorough studies. The different estimates of human error probabilities that had an impact on the results do not appear to correlate with the level of effort expended since widely different estimates were obtained from similar efforts in References 5 and 7. The analyst's role and impact is reenforced by the treatment of external events in Reference 5 and its review in Reference 7. The review resulted in about an order of magnitude increase in the estimated core-damage likelihood associated with external events. Differences in judgment and knowledge accounted for the different estimates and these judgments were not associated with features particularly unique to the plants. Thus, in this instance, the analysts appear to be a dominant factor in core-damage estimates.

A similar set of probabilistic assessments and reviews for the Zion plants are reported in References 8 through 11. The estimated core damage likelihoods ranged from roughly $10^{-4}/RY$ to $10^{-5}/RY$ for plants that are somewhat similar to the Indian Point units. Again, the differences in the estimates were attributable to assumed LOCA frequencies and assumptions about equipment operability under degraded conditions, not to weaknesses uncovered by in-depth event tree and fault tree treatments. These results may not be entirely independent since the study groups were essentially the same as those used in the various Indian Point studies.

A peer review [12] of the Big Rock Point probabilistic assessment did not yield any changes in core-damage likelihoods; however, a review of the Limerick study [13] resulted in a factor of six increase in the estimated core-damage likelihoods for internally initiated events. The principal reasons for the differences are discovery of dependencies between initiators and mitigating systems; interdependencies between major safety systems (because of support systems); modifications to event trees and fault trees; and different assumptions about initiating frequencies. The major impacts were assumptions about initiating frequencies with deviations in the fine structure having less significance.

The reviews cited above resulted in increases in the estimated core-damage likelihoods by factors up to ten. The potential impact of a review is controlled by the thoroughness of the originators and reviewers and the regulatory process in general (we regulators may have a bias towards the conservative). A factor of ten is certainly a significant difference in

estimated core-damage likelihood, but it is not my intent to start a new round of reviews to validate this finding. The important points to be noted are that these reviews have confirmed the fidelity of the event tree/fault tree analyses and have highlighted the analyst's judgment as a significant variable in the process. These judgments can affect the estimates because of omissions, assumptions about initiating frequencies, and human errors. These judgments may have some plant-specific origin but for the most part are generic in nature. While these judgments may inject uncertainty in the quantification process, they are also a rich source of insights regarding potential weaknesses associated with severe accidents and as such should be considered a significant product of the PRA if properly illuminated. The influence of the analyst on core-damage estimates is also supported by a recent survey of six PRAs [2]. This survey indicated that quantification of human actions (both beneficial and adverse) had a potentially significant impact on the estimates. It is well known that human error assessment is very sensitive to the analyst performing the evaluation.

Our perception of dominant contributors to core-damage and offsite consequences is also strongly influenced by the analyst. An assumption that has attained prominence in recent PRA studies performed in the United States is the loss of reactor coolant pumps (RCP) seals when seal cooling is lost. This assumption impacts events involving loss of all AC power (station blackout) initiated by a simple loss of offsite power or caused by fire, seismic, wind, or flood events that produce the same effect. Prior to about 1980, the station blackout accident sequence in PWRs considered only decay heat removal through the steam generator and the independent failure of the turbine driven auxiliary feedwater (AFW) train. If the RCP seals fail in a station blackout, the resulting LOCA cannot be mitigated because the emergency core cooling pumps depend on AC power. Thus, the estimated core-damage likelihood for a station blackout is increased by whatever credit one takes for the availability of the turbine driven AFW pump. Until recently, there has not been a serious investigation of the failure modes of the seals used in the different RCP designs. One manufacturer had results from a single test indicating that the seal integrity could be maintained for at least 50 hours without cooling, while another manufacturer had operating experience that the seal would survive at least 30 minutes. Using this limited information and their own judgments, analysts assume that the seals either fail or not subsequent to a station blackout type event. If one assumes that the seals fail, then significant contributors to core-damage are Loss-of-Offsite-Power events at Zion (about 30% [11]); component cooling water pipe breaks at Zion (about 50% [11]), Indian Point, Unit 2 (about 10% [7]), and at Indian Point Unit 3 (about 30% [7]); hurricanes at Indian Point, Unit 2 (about 10% after technical specification change); and fires at Indian Point Unit 2 and 3 (about 5% before modification [7]). These sequences would not be dominant contributors to core-damage if one assumes that the seals do not fail in a short time frame upon loss of cooling. The contribution of the simple loss-of-offsite-power events associated with this assumption is small at the Indian Point plants because of the high degree of redundancy in emergency power which is not typical of most plants.

System success criteria can also influence our perception of dominant core-damage sequences. At the Zion plants the component cooling water and service water support systems are shared by the two units. The success criteria for the minimum number of pumps required to operate in each system

following a loss-of-offsite-power event has an important influence on the importance of this sequence. A sensitivity study reported in the review [11] indicated a 50% reduction in the core-damage likelihood of loss-of-offsite-power events if the criteria changed from 2 CCW pumps and 2 SW pumps to one CCW pump and 3 SW pumps.

An example somewhat related to the subject of success criteria is the loss of long term heat removal sequence for Peach Bottom in the Reactor Safety Study [4]. This accident sequence was built on the assumption of no operator action for over 20 hours while the reactor building overpressurized and the subsequent rapid depressurization was assumed to fail the core cooling pumps. Subsequent PRAs such as Limerick [13] have identified additional operator actions which would reduce the potential significance of this accident sequence in BWRs. In this instance, the relative importance of the sequence appears to be dependent on the analyst's persistence in discovering alternate recovery modes for a sequence that evolves over a long time frame.

Assumptions can also influence our perception of dominant accident sequences leading to potentially severe offsite consequences. Both the Indian Point and Zion plants have redundant containment cooling systems through the use of either the containment sprays or fan coolers. Several accident sequences in these plants involved the loss of the low pressure safety recirculation system which also provides the containment spray function during the recirculation phase. Thus, the functionability of the fan coolers for these sequences are an important factor in reducing the probability of slow overpressure failure of the containment and significant offsite releases. The fan coolers were not designed to operate in a post core-melt environment so the analyst must judge the plausibility of their operability under degraded conditions. Sensitivity studies presented in the reviews of the Zion [11] and Indian Point [7] PRAs indicated that the frequency of the plant damage state - core-melt without containment cooling - could increase by up to a factor of three if the fan coolers have a conditional failure probability of one in the degraded environment.

Omissions are another source of missing dominant contributors to core-damage accident sequences. Omissions occur because of the limited scope of the study or oversights. The impact of study scope was highlighted by the Indian Point and Zion studies [5,10] which showed externally initiated events, such as earthquakes, were important contributors to core-damage. Prior to these studies, most PRAs conducted in the United States had little or no treatment of external events because the relevant methodologies were in an embryonic stage. Analysis of externally initiated events relies heavily on judgment and modeling approximations which result in large uncertainties and reduced confidence in the central estimates.

The inclusion of externally initiated events in the Indian Point and Zion studies [5,10] increased the estimated core-damage likelihoods by a factor up to five. More importantly, these events were dominant contributors to offsite consequences because the resulting effect defeated core cooling and containment cooling simultaneously. A peer review of the Indian Point PRA [7] provided different judgments about hazards curves, component fragilities, and accident sequence definition that resulted in a substantial increase in the estimated likelihoods of seismic, fire, and wind events. Fortunately,

simple modifications were implemented to reduce the probability of the dominant sequences so that extended debate about the correctness of the judgments was not necessary.

The depth of the fault tree development can also be considered under the scope of the study. The more detail included in the study, the greater the opportunity for discovering vulnerabilities in the plant. The probabilistic assessment of Millstone Unit 1, sponsored by the NRC [14], examined control logic in greater detail than is normally pursued in a PRA (except for the reactor protection system). During the course of the study, the analysts uncovered a single failure in the logic that would have precluded automatically loading equipment on the emergency buses following a loss of offsite power event. This vulnerability, which was subsequently corrected, resulted in a dominant accident sequence which would have been missed in most PRA studies.

Another example of the importance of the depth of the study was flagged in the review of the Zion PRA [11]. In this instance it was noted that continued operation of pumps needed to mitigate certain events was dependent on room cooling and that the thermostat which controlled the cooling system was never tested to determine its operability. Surveillance procedures for the room coolers have since been modified to include testing of the thermostat.

Oversights can also have a significant impact on the identification of dominant sequences. The Indian Point and Zion studies illuminated the significance of the loss of reactor coolant pump seal cooling as noted earlier. Peer reviews of these studies [7,11] flagged an overlooked accident sequence (involving a break in the component cooling water system) that stems directly from the RCP seal cooling concern. The seals are cooled by high pressure injection of seal water from the charging pumps and cooling of the seal housing by component cooling water. Component cooling water is also used to cool the charging pumps and the high pressure safety injection pumps. Thus, a break in the component cooling water system could result in loss of all RCP seal cooling, a consequential small LOCA, and loss of ECCS needed to mitigate a small LOCA.

Most of the examples cited above had shortcomings related to the scope of the study or engineering judgements that are outside of the formal event tree - fault tree - statistics portion of the assessment. Expanded study scopes usually entail treatment of external events which are also sensitive to the analyst's judgement. In large measure, all of these judgements concern faults outside the design envelope of the plant and/or components.

CONCLUSION

The analyst has been shown to be a strong influence on the PRA results - both core-damage estimates and identification of dominant contributors to core-damage or risk. This influence is a significant variable in the analysis because judgements are generally in areas outside of the design envelope and may not be supported by available data. Thus,

more attention needs to be given to the engineering bases for these sensitive judgements. However, developing empirical support for these judgements could be more resource intensive than the basic PRA itself.

An alternate approach is to provide a truly independent peer review of the PRA. This would introduce a reasonable amount of skepticism that may ferret out marginal assumptions. Past peer reviews have been successful in identifying differences of opinion regarding plant/component response under degraded conditions. A peer review is not foolproof because it relies on the PRA documentation, to a large extent, for developing an understanding of the plant design and operation. Thus it is important that the documentation be fairly complete and unbiased in illuminating assumptions used in the analysis.

Does this lack of firmness in the PRA results impair its usefulness? I think not. The process of performing a PRA and the interaction with a peer review group provides a very constructive framework for illuminating potential weaknesses in plant design and operation that may warrant remedial action. The interactions sharpen the focus on subtle nuances that may have significant safety impact. This interaction should include utility personnel who have the most knowledge about plant operation and who also have the most to gain from the risk perspectives obtained from the safety analysis.

REFERENCES

1. H. Lewis et al, Risk Assessment Review Group Report to the U. S. Nuclear Regulatory Commission, NUREG/CR-0400, September 1978
2. D. Gallagher et al, Insights into PRA Methodologies, NUREG/CR-3852, August 1984
3. Offshore Power Systems, An Evaluation of the Residual Risk from the Indian Point Nuclear Power Plants, Report No. 35A96, May 1980
4. Reactor Safety Study, An Assessment of Accident Risks in U. S. Commercial Nuclear Power Plants, WASH-1400, October 1975
5. Indian Point Probabilistic Safety Study, April 1982
6. R. Bernero et al, Task Force Report on Interim Operation of Indian Point, NUREG-0715, August 1980
7. G. Kolb et al, Review and Evaluation of the Indian Point Probabilistic Safety Study, NUREG/CR-2934, December 1982
8. Offshore Power Systems, An Evaluation of the Residual Risk from the Indian Point and Zion Nuclear Power Plants, Report No. 36A75, February 1980
9. A. Buslik and R. Bari, A Critique of the Offshore Power Systems Risk Study for the Zion Nuclear Power Plant, BNL-NUREG-28750, December 1980

10. Zion Probabilistic Safety Study, September 1981
11. D. Berry et al, Review and Evaluation of the Zion Probabilistic Safety Study NUREG/CR-3300, May 1984
12. J. Poloski et al, A Review of Consumers Power Company Probabilistic Risk Assessment of the Big Rock Point Plant, EGG-EA-5765, April 1982
13. I. Papazoglou et al, A Review of the Limerick Generating Station Probabilistic Risk Assessment, NUREG/CR-3028, February 1983
14. A. Garcia et al, Interim Reliability Evaluation Program: Analysis of the Millstone Point Unit 1 Nuclear Power Plant, NUREG/CR-3085, May 1983

THE SIGNIFICANCE OF WATER HAMMER EVENTS TO PUBLIC DOSE
FROM REACTOR ACCIDENTS: A PROBABILISTIC ASSESSMENT

Paul J. Amico

Applied Risk Technology Corporation
P.O. Box 175
Columbia, Maryland 21045, USA

Walter L. Ferrell

Science Applications, Inc.
505 Marquette Ave., NW, Suite 1200
Albuquerque, New Mexico 87102, USA

Mark P. Rubin

RRAB-DST-NRR
U.S. Nuclear Regulatory Commission
Washington, DC 20555, USA

ABSTRACT

A probabilistic assessment was made of the effects on public dose of water hammer events in light water reactors. The analysis utilized actual historical water hammer data to determine if the water hammer events contributed either to system failure rates or initiating event frequencies. Representative PRAs were used to see if changes in initiating events and/or system failures caused by water hammer resulted in new values for the dominant sequences in the PRAs. New core melt frequencies were determined and carried out to the subsequent increase in public dose. It is concluded that water hammer is not a significant problem with respect to risk to the public for either BWRs or PWRs.

INTRODUCTION

This paper summarizes a probabilistic assessment that was made of the effects of water hammer events that occur in light water reactors (LWRs). It is taken from work performed for the U.S. Nuclear Regulatory Commission in support of their evaluation of Unresolved Safety Issue (USI) A-1: Water Hammer. The opinions represented in this paper are those of the authors, and do not necessarily represent the official position of the NRC.

In the recent report NUREG/CR-2781 [1], the results of actual and potential water hammer events occurring in LWR power plants is presented. NUREG/CR-2781 also presented methods for their prevention and mitigation. Water hammer damage appears to be primarily limited to the piping support systems. The frequency and severity of water hammer events is greater in BWRs

than in PWRs. The predominant cause of water hammer events is the presence of voids or steam bubbles in pumped water lines. A detailed list of known and suspected water hammer events is given in NUREG/CR-2059 [2]. To date, no water hammer event has placed a plant in an emergency condition. However, 18 of the reported 82 events in BWR plants did disable a safety system train. A methodology was developed which was capable of utilizing the information in these two reports to estimate, in a conservative way, the potential contribution to public dose from core melt accidents involving water hammer induced system failures.

METHODOLOGY

A general methodology was developed to evaluate the effect of water hammer on plant risk from core melt. In order to do this, it was necessary to compare the water hammer contribution to some baseline measure of plant risk. It was decided that the best way to do this was to see what affect could be seen on the results of an already performed probabilistic risk assessment (PRA) if water hammer events were incorporated into it. This was necessary since PRAs performed to date have not included water hammer as a specific event. It was also decided that for the purpose of this analysis the measure of plant risk utilized should be dose to the public, measured in man-rem. This was selected because it is a useful measure for providing a generic bounding quantification of societal risk, and also because this is the measure which the NRC had selected to use for ranking the importance of generic unresolved safety issues. Three specific power plants were selected for the study, based on the availability of PRAs representing these plants. The plants selected were a BWR-3 with isolation condenser, a BWR-4, and a Westinghouse PWR [3]. The selection of two BWRs and one PWR was based on the review of water hammer studies which indicated, as previously mentioned, that water hammer was a more important consideration in BWRs and further, that water hammer experience could be different for differing BWR types. The analysis itself was carried out in the following series of steps.

Step 1 - Frequency of Water Hammer Events

The frequency of water hammer events was determined for various systems by plant type. The information used to do this was taken from NUREG/CR-2781 [1] and NUREG/CR-2059 [2]. The list of systems considered were those systems for which there was some history of water hammer occurrence (at least one known or suspected water hammer event). The number of events having occurred in each system were determined directly from the listings in the reference documents. Only events which occurred during commercial operation were counted. It was felt that events during start-up testing and system checkout were not representative of actual plant performance. Classical point estimates for water hammer frequency were generated for each system and plant type based on the event count and the number of reactor-years of commercial operation in each population. For BWRs, frequencies were developed for three groupings, all BWR 3s and 4s, BWR 3s only, and BWR 4s only. The purpose of this was to determine if there were actually any statistically significant differences between the frequency of water hammer events in the same systems in each plant type. In order to determine if there was a difference, 90 percent Chi-squared confidence bounds were generated for the water hammer frequencies developed. Then, for each system, a subjective judgement was made as to whether there was a significant difference between the frequency

determined for the individual BWR 3 and 4 groups and the overall BWR population. The judgement was based to a large extent on the overlap of the 90 percent confidence bounds. In general, if the confidence bounds of the individual plant groups completely overlapped the confidence bounds of the overall population, then it was felt that there was no significant difference between the individual plant group frequencies for that system and the population frequency estimate was used (the individual frequency estimates were rejected). Otherwise, the individual plant group frequencies were used and the overall population frequency was rejected. As stated above, this was based on analyst judgement and was very subjective in nature. However, it was felt that any error induced would be minimal, and though more complex statistical analysis was theoretically possible, the marginal size of the data base did not justify such treatment. For PWRs, the analysis of data by plant groupings was not utilized since we had chosen to perform only one PWR analysis. All PWR data was combined into a single data base and the point estimate frequencies were determined. Since the PWR plant analyzed was a Westinghouse plant, it would have been reasonable to use just Westinghouse data had it differed significantly from Combustion Engineering and Babcock and Wilcox data. However, this was not the case, thus the system water hammer point estimate frequencies determined for all PWRs were used throughout the analysis.

Step 2 - Frequency of Water Hammer Induced Failures

In order to determine the frequency of water hammer induced failure, it was necessary to combine the frequencies of water hammer events from step 1 with a calculated value for the fraction of water hammer events in each system which result in failures. This fraction was based on a detailed examination of the descriptions of the water hammer events contained in the two NUREG documents. The event descriptions provided the necessary information to determine if any system failure had resulted from the water hammer occurrence. Once again a simple classical calculation was utilized, that is, the point estimate system damage fraction was determined by dividing the number of water hammer events resulting in system failure by the total number of water hammer events for that system. For systems where a failure had not occurred but where the historical data indicated that it was possible to develop sufficient force through water hammer to cause failure, a conservative bounding value was used, based on the assumption that the next water hammer event in that system would result in a failure. Depending on the system, the frequencies were determined for various contributions to and types of systems failure. For normally operating systems essential to plant operation, the frequency of a water hammer induced transient initiator was determined. For standby systems, the frequency of a water hammer induced failure in response to a demand was determined. In this case, the failure frequencies were converted from per year to per demand, based on the estimated number of tests per year, since this is the number required for quantification these of systems in the PRAs. The number of tests per year was assumed to be 10 per train for safety systems, based on the standard technical specifications requirement for one test per month and allowing for two months for refueling (no tests performed). This is obviously a conservative assumption which would yield a higher than actual demand failure rate. For all systems which interface with the reactor coolant system, if the data indicated that water hammer forces could be sufficient to cause a pipe break, a LOCA contribution from water hammer was determined, based on the same calculational technique. However, in this case it was important to consider the expected location of the water hammer

effects, since the location of the pipe break determined if any additional failures (such as check valves) would be required for the pipe break to result in a LOCA. Thus, the frequency of the water hammer induced pipe break was adjusted to account for these additional failures and a water hammer induced LOCA frequency was determined. The data for these additional failures was taken from the Interim Reliability Evaluation Program (IREP) data base.

Step 3 - Contribution of Water Hammer to Total Event Frequencies

At this point, the potential contribution of water hammer induced failure to system failures and initiating events was determined. The system demand failure rates and initiating event frequencies excluding water hammer were extracted from the three PRAs used for this evaluation (the previously referred to BWR-3 with isolation condenser, BWR-4, and Westinghouse PWR PRAs). The water hammer induced frequencies or demand failure rates determined in Step 2 were added to the appropriate initiating event frequency or system failure rate extracted from the PRAs. The new numbers determined were compared with the old (water hammer excluded) numbers to determine if there was a measurable increase due to water hammer. Only those initiating events and systems which showed a measurable increase were retained to the next step in the analysis. Thus, the rest of the analysis was simplified by screening out those events and systems for which the water hammer contribution was not measurable.

Step 4 - Consideration of Event Phenomenology

In the previous steps, no evaluation was made of the precise conditions which lead to the water hammer event. It was simply assumed, conservatively, that these water hammer events could occur randomly at any time. Thus, the new values calculated in the previous step were the maximum expected values including water hammer effects. In order to further refine the analysis and reduce the number of cases which needed to be quantified in the final analysis, it was necessary to account for the fact that these water hammer events were not possible under all conditions. Therefore, the phenomenology of water hammer in the particular systems was examined to determine under which conditions they were possible. In order to illustrate this idea, let us consider the following example. It was determined that water hammer was a potentially significant contributor to isolation condenser (IC) failures. However, an examination of the IC water hammer events and the system design showed that due to the location of the IC, which is located very high in the containment and has a steam riser line located at a nozzle above the level of the steam lines, and the nature of IC water hammer, which requires that water be forced into the steam riser, the only way this event can occur is if there is an extremely high water level in the reactor vessel (above the steam lines). Water levels this high can only occur from level surge due to reactor trip before feedwater trip, which is not possible during sequences initiated by loss of feedwater or loss of offsite power. Therefore, sequences from the PRA which were initiated by these two transients were not reevaluated for the effects of isolation condenser water hammer events.

Step 5 - Requantification of Release Category Frequencies

Each of the PRAs utilized contained a list of dominant sequences which accounted for essentially all of the core melt frequency at that plant. Further, these sequences had been carried out to the expected release

category, such that release category frequencies were shown. In order to determine the contribution of water hammer to these frequencies, it was necessary to requantify these release categories to include water hammer events. Using the values calculated in step 3 and the phenomenological considerations developed from step 4, the frequencies of the dominant sequences from each of the three PRAs were requantified by applying the new (water hammer included) system demand failure rates and initiating event frequencies to the calculation of the sequence frequencies. The calculation was carried out to the release categories, and new values were obtained for the release categories which represented the inclusion of water hammer. Those release categories which showed a measurable increase in frequency due to the inclusion of water hammer were retained for the final step of the evaluation.

Step 6 - Determination of Effect on Public Dose

The release category frequencies, both before and after inclusion of water hammer (the "old" and "new" values, respectively), were converted to public dose in man-rem per year. This was done by multiplying the release category frequencies by the expected whole body dose to the public (in man-rem) for the given category. These dose levels were obtained from two sources, thus two calculations were performed. The first calculation used dose levels from a draft version of NUREG-0933 [4]. For the sake of comparison, the other calculation used the dose levels from the draft version of WASH-1400, the Reactor Safety Study [5,6]. The major difference between the two sets of values is in two areas. The NUREG-0933 values were based on a population dose model truncated at a 50 mile radius from the plant while the WASH-1400 values are based on an "infinite" population dose model (no truncation). Also, the NUREG-0933 model assumed an exclusion area of 1/2 mile and a uniform population density of 340 persons per square mile beyond that while the WASH-1400 model used the Indian Point population demographics and divided the final result by two. The dose estimates taken from each source are shown on Table I. The old values were subtracted from the new values to determine the contribution of water hammer to dose to the public for both scales. These "delta-values" also represent the potential maximum reduction in public dose from the elimination of water hammer as an event.

RESULTS-BWRs

The analysis of water hammer in BWRs included the effects of water hammer events on nine BWR systems which had a history of occurrence. Table II shows the results of the systems analysis for both BWR-3s and BWR-4s. The values shown on the table are the values selected for the quantification after the application of the statistical test performed on the samples as described in the methodology section. Thus, in some cases a single number representing both BWR types is shown and in some cases the water hammer histories were sufficiently different as to require the use of specific values for each plant type. As can be seen, the failure frequencies due to water hammer are relatively small. The historical data showed that for most of the systems, the most serious effect possible was a loss of system function. In only one case, the feedwater system, was there any need to consider the potential for a water hammer induced pipe break and subsequent LOCA. This was because the other systems are not subject to water hammer forces sufficient to cause pipe ruptures. However, the frequency of LOCA due to feedwater system water hammer was small because the location of feedwater system water hammer events has

TABLE I

Estimated Public Dose (Man-Rem) by Release Category

Release Category	Dose (NUREG-0933)	Dose (WASH-1400)
PWR 1	5.4E+6	3.8E+7
PWR 2	4.8E+6	3.6E+7
PWR 3	5.4E+6	3.9E+7
PWR 4	2.7E+6	2.2E+7
PWR 5	1.0E+6	6.0E+6
PWR 6	1.5E+5	6.5E+5
PWR 7	2.3E+4	9.5E+3
PWR 8	7.5E+4	2.6E+5
PWR 9	1.2E+2	3.6E+2
BWR 1	5.4E+6	3.9E+7
BWR 2	7.1E+6	7.5E+7
BWR 3	5.1E+6	4.6E+7
BWR 4	6.1E+5	3.1E+6
BWR 5	2.0E+1	1.3E+2

TABLE II

System Failure Frequencies Due to
Water Hammer Events in BWRs

System	Plant Type	Water Hammer Failure Frequency	Event Type	Sig. Contrib. to Sys. Fail?
HPCI	BWR-3	4.5E-4/demand	demand failure	No
	BWR-4	5.5E-3/demand	demand failure	Yes
IC	BWR-3	3.2E-2/demand	demand failure	Yes ^b
	BWR-3	1.9E-7/year	LOCA initiator	No
LPCI/RHR ^a	BWR-3	1.6E-4/demand	demand failure	Yes
	BWR-4	7.0E-4/demand	demand failure	Yes
LPCS ^a	BWR-3	2.6E-3/demand	demand failure	Yes
	BWR-4	5.7E-4/demand	demand failure	No
RCIC	BWR-3	2.9E-3/demand	demand failure	Yes
	BWR-4	7.0E-4/demand	demand failure	Yes
RWCU	BWR-3, 4	8.0E-3/year	transient initiator	No
SCW	BWR-3	7.5E-2/year	transient initiator	No
	BWR-4	3.0E-2/year	transient initiator	No
PCS	BWR-3, 4	3.5E-2/year	transient initiator	No
FW	BWR-3	1.2E-2/year	transient initiator	No
	BWR-3	9.6E-8/year	LOCA initiator	No
	BWR-4	3.5E-3/year	transient initiator	No
	BWR-4	2.8E-8/year	LOCA initiator	No

(a) values are per train

(b) failure does not apply to LOFW or LOFP events

been in the area of the feedwater control valves. A pipe break in this area would lead to a LOCA only if the additional failure of the downstream check valves allowed backflow from the reactor coolant system to the break area. When these additional failures were added to the feedwater water hammer pipe break frequency, the overall water hammer induced LOCA frequency did not increase the frequency of the large LOCA initiator.

Propagating the results shown in Table II throughout the PRAs yields the new values for release category frequency and total core melt frequency shown in Table III. As can be seen from this table, the effect of water hammer on total core melt frequency is negligible for both types of BWR. By negligible, we mean that there is no change in the frequency when the calculated values are rounded to two significant digits (i.e., the calculated change is less than one percent). The table also shows that for the BWR-3 evaluated, the effect of water hammer is negligible for each individual release category. In the case of BWR-4s, there was a measurable effect due to water hammer on the frequencies of release categories 1 and 2, the high consequence categories. The change was on the order of 7% for each of the two categories. In tracing back the cause of the effect, it was determined that it was due almost entirely to water hammer induced failures in the residual heat removal (RHR) system.

The final results of the BWR analysis are shown in Table IV. This table shows the increase in public dose when water hammer is included in the PRA analyses utilized. As discussed in the methodology section, this result is shown using two dose models. As would be expected, the BWR-3 results indicate no change in public dose due to the consideration of water hammer. The BWR-4 results indicates an approximately 2% contribution on both scales from the consideration of water hammer, which resulted from the 7% increase in the frequency of release categories 1 and 2.

RESULTS--PWRs

The PWR analysis turned out to be significantly easier than the BWR analysis. Due to space limitations the results cannot be presented here on the same level of detail as the BWR results, however, the results proved to be quite interesting. The analysis of water hammer events at PWR plants showed that water hammer did not have any noticeable effect on either systems failure probabilities or initiating event frequencies. Thus, once the analysis reached this point it was obvious that it was not necessary to carry out this calculation to release category frequency or subsequently to public dose. Water hammer can be said to have a negligible effect on core melt frequency and public dose for PWRs.

CONCLUSIONS

A methodology for the probabilistic assessment of the significance of water hammer was developed and applied. The technique was kept simple in keeping with the sparse nature of the available data. Because of this, the answers obtained have very substantial uncertainties attached to them. In order to control the effect of these uncertainties, the analytical technique used for the analysis utilized a number of very conservative assumptions, thus even the substantial uncertainties involved should not change the conclusions

TABLE III

Increase in Release Category Frequencies Due to
Water Hammer Events in BWRs

	Release Category				Sum
	1	2	3	4	
BWR 4					
Category total					
with water hammer	1.4E-7	4.2E-5	1.7E-4		2.1E-4
w/o water hammer	1.3E-7	3.9E-5	1.7E-4		2.1E-4
increase	7%	7%	negl.		negl.
BWR 3 w/isolation condenser					
Category total					
with water hammer	1.3E-6	8.2E-6	1.0E-4	2.3E-4	3.4E-4
w/o water hammer	1.3E-6	8.2E-6	1.0E-4	2.3E-4	3.4E-4
increase	negl.	negl.	negl.	negl.	negl.

TABLE IV

Increase in Public Dose Due to
Water Hammer Events in BWRs
(all values in man-rem/reactor-year)

	BWR 3s with isolation condenser		BWR 4s	
	NUREG- 0933	WASH- 1400	NUREG- 0933	WASH- 1400
Total Public Dose With Water Hammer Included	715	5,979	1,169	10,956
Total Public Dose Without Water Hammer Included	715	5,979	1,147	10,735
Increase in Public Dose	0	0	22	221

since it is more likely that the results are too high rather than too low. However, it is extremely important to keep in mind that it is not possible to prove this, and thus one must still consider the uncertainties to be statistically significant. Bearing this in mind, we can present what we feel to be reasonable conclusions based on the analysis.

The PWR analysis showed that water hammer did not even contribute to the individual system failure probabilities or initiating event frequencies. The BWR analysis showed that although water hammer did contribute to some events, this did not significantly impact the overall results. The BWR-3 results showed no change in overall core melt frequency or public dose. The BWR-4 results showed no change in overall core melt frequency and a 2% change in public dose. Further, the absolute man-rem per reactor-year change for the BWR-4s was quite small for both dose models used. Therefore, based on the results of this analysis, it is the conclusion of the authors that, within the limitations cited previously, it is possible to state that water hammer is not a significant problem with respect to core melt frequency or public dose from reactor accidents in either PWRs or BWRs.

REFERENCES AND FOOTNOTES

- [1] S. Banerjee, et al., Evaluation of Water Hammer Events in Light Water Reactor Plants, NUREG/CR-2781, July 1982.
- [2] R. L. Chapman, et al., Compilation of Data Concerning Known and Suspected Water Hammer Events in Nuclear Power Plants, NUREG/CR-2059, May 1982.
- [3] This study is intended to estimate the contribution of water hammer generically by plant type, not by specific plant. In order that there be no misunderstanding of the applicability of the results to any specific plant, at the request of the U.S. Nuclear Regulatory Commission the authors have agreed to withhold the identity of the plant PRAs utilized in the study.
- [4] U.S. Nuclear Regulatory Commission, NUREG-0933, preliminary review draft, 1982.
- [5] U.S. Nuclear Regulatory Commission, Reactor Safety Study—An Assessment of Accident Risks in U.S. Commercial Nuclear Power Plants, WASH-1400, Draft, 1974.
- [6] These dose levels by release category were only shown on a table in the draft version of WASH-1400. This table was removed from the final report.

"THE PROBABILISTIC APPROACH AND THE DETERMINISTIC LICENSING
PROCEDURE"

H. Fabian, A. Feigel, O. Gremm

Kraftwerk Union AG
Hammerbacher Str. 12+14, 8520 Erlangen

INTRODUCTION

The following is an attempt to show systematically the relationship between the deterministic and probabilistic approach, which are often incorrectly seen as being fundamental opposites.

Very often a discussion of the advantages of

- probabilistic methods
- risk assessment
- safety goals

is started with the question

"How safe is safe enough?"

Even in the case safety goals exist, which give definite answers to this question, this is not enough, because it is not known, what a safe plant looks like. Therefore a second question arises:

"What does a safe plant look like?"

This question is at least of the same importance as the first one. Whereas the answer to the first question is normally given in probabilistic categories, the answer to the second question is normally given in deterministic categories. This leads us to the question to be handled in this paper:

"How fit the deterministic and probabilistic ways
together"

REMARKS TO DEFINE THE TERMS USED

The term "deterministic" is used in the field of nuclear technology in two meanings:

- in the scientific/technological meaning, "deterministic" means that a technical process or the result of a calculation is determined by clear scientific/technical causal relationships;
- in the licensing process the term "deterministic" is used to point out that the actual design of the engineered safety features is derived from pre-determined postulates. Such

postulates may be design basis accidents or other design basis principles such as those of redundancy, diversity, safety factors, calculation prescriptions and the like. They also include the radiological exposure limits established by the radiological protection ordinance. In so far as such postulates have been validated and have proven expedient, they can be established in the form of detailed design specifications in technical rules and regulations.

The nuclear licensing procedure is largely based on the establishment and application of deterministic principles in the derivation of the safety concept; the application of probabilistic procedures is of a complementary nature only (/1/, criterion 1.1).

The term "probabilistic" is used in a variety of combinations and meanings, some of which are:

- qualitative or quantitative evaluation of the frequencies of events
- event tree and/or fault tree analysis, the task of such studies can be different
 - . to optimize systems by comparison of different alternatives
 - . calculation of systems reliability as part of an overall risk assessment
- risk assessment to get an overall picture of the risk in connection with nuclear power plants

In this paper we deal with the trends to give more importance to probabilistic methods in licensing procedures. We would like to show, that it makes no sense to replace deterministic criteria by probabilistic criteria only.

We also would like to show that probabilistic methods are helpful as additional tool, but they should not replace the traditional deterministic way in the licensing procedure.

If we now go ahead with the comparison of deterministic and probabilistic approaches, this concerns only that area in which the term "deterministic" is used in the sense of the licensing context (see above).

KNOWLEDGE OF CAUSAL RELATIONS AS A PRESUMPTION OF BOTH THE DETERMINISTIC AND PROBABILISTIC METHOD

The knowledge and application of causal relationships, that is the determinism in the scientific/technological meaning of the word, is a requirement both to the deterministic and to the probabilistic approach.

This fact is evident for the deterministic method, but has to be explained for the probabilistic way:

The main tools used in the probabilistic method, which are

- event trees and
- fault trees

are representations of the causal relationships between the behaviour of the components, the different boundary conditions and their consequences.

This deterministic picture presented in event and fault trees is transformed into a probabilistic tool only after insertion of failure rates, which give statistical information only in one respect of the behaviour of the components and this is the frequency of component failures. There is a fundamental problem with this statistical information, but we will come back to this later on. Additional examples for deterministic information in the scientific/technical meaning necessary for probabilistic studies are

- efficiency conditions
- consequences of failures
- results of transient calculations (e.g. pressures, temperatures)
- limiting conditions for components
- materials specifications to be met

PROBABILISTIC EVALUATION OF DETERMINISTICALLY DERIVED CONCEPTS

It is possible to evaluate and quantify the safety concept, which has been gained on a "deterministic" basis, by means of probabilistic risk studies. This involves posing the question as to the

- frequency of occurrence and
- consequences

of event sequences that can not be kept under control by the engineered safety features. Such a study related to German conditions is available in the form of the German Risk Study, Phase A /2/.

This and similar studies validate the deterministic procedure used to a certain degree, as is evident from the fact that these studies have not given reason to make any drastic changes to the existing safety concept.

We can conclude that the risk assessment has confirmed the safety concept in the following way

- No important accident sequences have been forgotten
- The deterministic requirements were checked with the possibility of
 - . Optimization of details of the overall safety concept
 - . Reduction of extrem requirements

At the same time as they confirm the safety concept, the risk studies also essentially validate the nuclear engineering rules and regulations which establish the deterministic principles and requirements on which the safety concept is based.

Thus, the safety level derived from the safety concept is also the safety level defined by the body of technical rules and regulations, at least to the extent to which this has already been established. These relationships are shown in Figure 1, from which two statements can be derived:

1. In principle it is equivalent whether the requirements are specified in the form of safety goals to be complied with or by a set of deterministic specifications in the form of technical rules and regulations. Reference has already been made to this elsewhere /3/. The type of approach to be used should be decided solely from the point of practicability.
2. Safety goals cannot be established isolated from
 - the deterministic requirements of the existing criteria, guidelines, rules and regulations
 - the safety level of plants already licensed on the basis of the above mentioned requirements.

The safety goals have to be consistent with these, if they define the same safety level. If this consistency should not yet be existing, it must be established.

Thus, the establishment of safety goals is not a fundamental problem but a problem of "conversion", provided the above mentioned consistency is given. The conversion can be done by valuation of the safety concept of licenced plants by means of probabilistic risk analysis.

PRIORITY OF THE DETERMINISTIC APPROACH FOR LICENSING

For engineering purposes, it is more practical to derive a safety concept from a catalogue of deterministic requirements /3/.

The step from a given safety goal for instance $10^{-4}/a$ for core melt down events as proposed in the US/5/, to a real safety concept is not possible without additional information. It is necessary to know which measures are available for the designer to reach the safety level required by the safety goal. The safety goals give an information how safe is safe enough but not what a safe plant looks like. To know this the creativity of engineers is necessary in addition to the safety goal to reach the safety level required by the safety goal.

In some fields it is possible to describe processes in statistical terms according to the nature of these processes. One example is the field of human actions. According to the statistic nature it is not possible to standardize human actions, even in the case of high sophisticated operator training and things like that. The results are uncertainties in the safety analysis. In order to prevent imponderabilities for the safety concept as a result of such uncertainties, it may be advisable to introduce special techniques with clearly defined causal structures.

The German safety philosophy has gone this way by reducing the human influence by means of automation of all important safety functions.

Now we come back to the problem of using failure rates as a statistical description of the behaviour of components as inputs for event trees and fault trees. It is clear that the actual behaviour is determined by boundary and systems conditions. What we do is, to treat unknown or complex deterministic situations statistically in order to simplify the problem. This method is well established and has its big advantages especially in the case of highly complex situations. But it seems necessary to remember this from time to time in order to prevent incorrect conclusions as the result of probabilistic calculations.

In the light of these arguments, it is understandable that in the licensing procedure in accordance with the BMI-safety criterion 1.1 /1/ the probabilistic approach should be attributed only a complementary role. Risk studies

- for the quantification of the residual risk
- to determine the balance nature of the safety concept

need not be performed in connection with each specific licensing procedure.

The German practice with the German Risk Analysis was satisfactorily in this respect. The study was performed without any connection to any actual licensing procedure.

When the results were available, some of them were helpful in connection with fundamental discussions

- to prove the actual safety concept of the German PWR
- to give hints for further optimization in details as mentioned above

As another result the study identified some fields where need for more information exists. Especially to get better understanding of

- core melt events and
- identification of conservatism

and therefore a lot of R + D-Work was started. This has also nothing to do with actual licensing procedures but hopefully will be helpful in fundamental safety discussions in the future, especially in the sense of reducing such requirements which are the results of overestimating the consequences of safety problems.

CONCLUSION

Remember the following

- If safety goals are given, the creativity of the engineers is necessary to transform the goals into actual safety measures. That is, safety goals are not sufficient for the derivation of a safety concept.

- The licensing process asks
"What does a safe plant look like?"
The answer cannot be given by a probabilistic procedure, but need definite deterministic statements.

The conclusion is, that the licensing process needs a deterministic approach.

The probabilistic approach should be used in a complementary role in cases where

- deterministic criteria are not complete, not detailed enough or not consistent
- additional arguments for decision making in connection with the adequacy of a specific measure are necessary.

But also in these cases the probabilistic answer has to be transformed into a clear deterministic statement.

REFERENCES

- /1/ Federal Minister of the Interior
Safety Criteria for Nuclear Power Plants
published 21. October 1977
- /2/ German Risk Study
published by Verlag TÜV-Rheinland, Cologne 1979
- /3/ A. Birkhofer, F. W. Heuser
What do Risk Studies Effect?
Information conference of the Swiss Association
for Atomic Energy and of the Austrian Nuclear Forum
Safety and Risk Lines of Thought in the age of
nuclear energy
Zurich, 22nd/23rd November 1982
- /4/ W. Braun
Limitation of Probabilistic Risk Assessment
Journal Atomkernenergie (Kerntechnik Vol. 41 (1982)
Lfg. 2, p. 73)
- /5/ Safety Goals for Nuclear Power Plants
NUREG - 0880, Febr. 1982

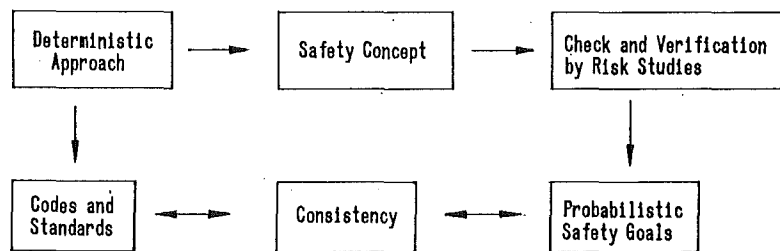


Fig. 1: Consistency between deterministic and probabilistic procedure in the derivation of a safety concept and for rule making.

INFLUENCE OF THE ATMOSPHERIC DISPERSION MODEL MODIFICATIONS ON
THE RESULTS OF THE GERMAN REACTOR RISK STUDY

P. Wittek, W.G. Hübschmann, S. Vogt

Kernforschungszentrum Karlsruhe GmbH
Postfach 3640, D-7500 Karlsruhe 1
Federal Republic of Germany

ABSTRACT

Improvements of the atmospheric dispersion model of the German Reactor Risk Study (GRS), Phase B, are presented. Washout model variations show the need of a realistic as well as practicable modeling. Emphasis is further given to the lift off criterion in the plume rise model, to the height dependent dispersion parameters and to the mixing layer height. The partially antagonistic effects of these modifications on the results of the Reactor Risk Study (in terms of early and late fatalities) are discussed.

1. INTRODUCTION

The German Reactor Risk Study (GRS) [1] applies the accident consequence model UFOMOD [2] to assess the collective damage of the population associated with potential nuclear power plant accidents. Phase A of UFOMOD development was restricted by the requirements of comparability with the U.S. Reactor Safety Study (RSS) [3] concerning methodology and basic assumptions. In Phase B this restriction is omitted for the benefit of an advanced methodology and recent results of research work.

The accident consequence model consists of four main components : the atmospheric dispersion model, the dosimetry joined with the protective action model and the health effect model. This report is confined to the meteorological model

2. THE METEOROLOGICAL MODEL

Proceeding from the accidental release of radionuclides the atmospheric dispersion model calculates the spatial and temporal

distribution of the activity concentration in the air and the contamination on the ground downwind of the reactor site. The temporal distribution of the activity is determined by varying meteorological conditions. This is realized in the model using sequences of weather data measured hourly. The spatial distribution is affected by the rise of the activity plume, by dispersion parameters, and by the depletion of the activity inventory due to washout and dry deposition.

2.1 WASHOUT

The washout model in UFOMOD is based on the assumption that precipitation will remove the airborne activity uniformly throughout the depth of the activity plume. The amount of activity being washed out is proportional to the local activity concentration of the plume. Accordingly the fraction of activity remaining in the plume is given by equation (1)

$$f_w = e^{-\lambda \cdot t} \quad (1)$$

t is the duration of rain and λ is the washout coefficient. The washout coefficient is regarded to be a function of the rain intensity and is invariant in space and constant for each hour.

A considerable part of the precipitation data used in the GRS are not available in form of recorded intensities but defined as key numbers according to the world weather watch code. Due to this qualitative classification three intensity bands have been introduced in Phase A each represented by a washout coefficient (Tab.I).

TAB. I WASHOUT PARAMETERS USED IN UFOMOD

	Washout Coefficient in s^{-1}		Rain Duration in h
	Aerosol	Iodine	
Phase A	$1 \cdot 10^{-4}$ a		0.5
	$5 \cdot 10^{-4}$ b		
	$10 \cdot 10^{-4}$ c		
Phase B	$2,9 \cdot 10^{-5}$	$3,7 \cdot 10^{-5}$ a	0.5
	$1,22 \cdot 10^{-4}$	$1,1 \cdot 10^{-4}$ b	
	$3,40 \cdot 10^{-4}$	$2,37 \cdot 10^{-4}$ c	

^arain intensity 0 - 1 mm/h

^brain intensity 1 - 3 mm/h

^crain intensity > 3 mm/h

With the exception of the intermediate band the coefficients of the Phase A agree with those of the RSS. In Phase B it is differentiated additionally between the wet deposition behaviour of iodine and aerosols. The washout coefficients evaluated by Brenk [4] and Schrödel/Urban [5] are based on literature reviews.

The average duration of rainfall during one hour was assumed to be 0.5 h in agreement with the RSS. Evaluations for the site of the Kernforschungszentrum Karlsruhe (KfK) however show that this assumption is only partially justified. From 10 570 hours of rainfall data recorded from 1973 to 1982 with a resolution of 10 minutes an average rainfall duration occurring within one hour has been calculated for each of the intensity bands. As can be seen from Tab. II the duration of the lowest band remains below the assumption mentioned above while the others exceed it [6].

TAB. II AVERAGE RAINFALL DURATION AND INTENSITY WITHIN ONE HOUR
(BASIS 10570 HOURS OF RAIN)

Precipitation Intensity I in mm/h	Average of Rainfall Duration in h	Average of Rain Intensity in mm/h
0 - 1	0.43	0.35
1 - 3	0.75	1.60
> 3	0.72	5.86

The best approximation of the reality is to calculate the washout coefficient as a function of the rain intensity \bar{I} given during the process of rainfall, and its actual duration by equation (1). This procedure requires the measurement of precipitation and its duration in time steps of at maximum 10 minutes. Using KfK data the model named in the following the "realistic" approach has been applied to UFOMOD.

Since precipitation data of this degree of resolution usually are not available at nuclear power plant sites an additional model is needed for general application. So KfK data again have been used to approach the realistic model mentioned above. From rainfall intensities averaged across each intensity band a washout coefficient has been calculated according to equation (2)

$$\bar{\lambda} = a \left(\frac{1}{K} \sum_{i=1}^K \bar{I}_i \right)^b \quad (2)$$

The constants a,b are different for iodine and aerosol. K is the number of rain hours recorded within 10 years.

Assuming that each rain event affects another activity plume the duration of rainfall \bar{t} is obtained according to the expression

$$\frac{1}{K} \sum_{i=1}^K e^{-\lambda_i t_i} = e^{-\lambda \bar{t}} \quad (3)$$

The results are presented in Tab. III. The rain duration of the second and third band is increased, while the rain duration of the lowest band and the washout coefficients are changed slightly.

TAB. III IMPROVED WASHOUT PARAMETERS FOR PHASE B

Precipitation Intensity I in mm/h	Washout Coefficient in s ⁻¹	Rain Duration in h
0 - 1	Aerosol 0,34•10 ⁻⁴	0.50
	Iodine 0,42•10 ⁻⁴	0.47
1 - 3	Aerosol 1,17•10 ⁻⁴	0.73
	Iodine 1,06•10 ⁻⁴	0.73
> 3	Aerosol 3,33•10 ⁻⁴	0.58
	Iodine 2,33•10 ⁻⁴	0.62

In order to demonstrate the effect of these washout models on the number of early fatalities calculations have been performed with the release category " core melt down followed by steam explosion " (FK1). FK1 is the release category, in which the number of early fatalities is most sensitive to precipitation.

The first of the four models presented in Tab. IV applies the conservative washout coefficients of Phase A and a rainfall duration of half an hour, while the remaining models apply the more realistic Phase B washout coefficients of Tab. I. This explains the result of the first model to exceed the other results by one order of magnitude. The Phase B model II illustrates that an underestimate occurs compared to the realistic approach if only the coefficients are substituted and no attention is paid to the rainfall duration. The improved Phase B model III agrees well with the realistic approach.

The washout model III is derived from the data basis of KfK and has been applied in this comparison only to the nuclear power plant locations of the site region Upper Rhine Valley.

TAB. IV INFLUENCE OF WASHOUT MODELS ON EARLY FATALITIES

Washout-Model	Early Fatalities in rel. units
Phase A	15.5
Phase B, model II	0.2
Phase B improved, model III	1.3
realistic approach, model I	1.0

A general application to other sites is proposed but the parameters have to be verified as soon as appropriate precipitation data are available.

2.2 DISPERSION PARAMETER

UFOMOD uses basically a bi-gaussian function to describe the distribution of the radioactive effluents within the plume perpendicular to the transport direction. The related dispersion parameters σ_y and σ_z characterize the horizontal and vertical extension of the plume. They are determined by experiment and depend on meteorological and local topographical conditions. Appropriate experiments have taken place at KfK in different emission heights between 60m and 195m and at KfA Jülich in heights of 60m and 100m. From all these experiments a dependence of the dispersion parameters on the emission height is indicated. In order to take into account this fact dispersion parameters assigned to four emission height ranges have been introduced to UFOMOD. In Fig. 1 the σ -parameters are shown for a neutral atmospheric stratification. For the range below 250m experiments of appropriate release height have been combined [7], while the curves of the range above 250m are the result of an extrapolation procedure [8]. The dispersion parameters σ_y , σ_z reflect in general the surface roughness as well as the release height of the plume. The effect of roughness however decreases with increasing emission height. Because the occurring plume heights are ranged up to 1000 m the use of height dependent parameters is regarded to be reasonable. Nevertheless UFOMOD offers alternatively the option to use further dispersion parameters related to surface conditions.

2.3 MIXING HEIGHT

The vertical extension of the plume is in general confined by an interception layer, which reduces considerably the turbulent exchange upwards. The height up to this layer, the so-called mixing height is considered to be dependent on the stratification of the atmosphere. Compared to Phase A the mixing heights have been decreased by factors of 1.25 up to 5 in order to be compatible with meteorological soundings [9].

2.4 LIFT OFF CRITERION

The prediction of early health effects is strongly influenced by the plume rise. An effect frequently discussed in this context is that the buoyant plume may become entrapped in the wake of the reactor building. The plume fails to lift off the ground if the windspeed u exceeds the critical windspeed u_{crit}

$$u_{crit} = 2.09 (\pi F / H_b)^{1/3} \quad (4)$$

where F is the buoyancy flux in $[m^4/s^3]$ and H_b is the building height [10].

3. RESULTS

In order to demonstrate the influence of the modifications discussed before, UFOMOD calculations have been performed for each reactor site of the GRS. The three release categories "core melt down followed by steam explosion" (FK1), "core melt down with a large containment leak of ϕ 300 mm" (FK2) and "core melt down followed by late overpressure failure of the containment" (FK6) have been selected from the group of eight categories defined in the Phase A of the GRS. The results in terms of the relative number of early and late fatalities are presented in order to highlight the meteorological effects and to exclude the influence of modifications in other parts of the model (Tab. V). As a reference the results of version UFOMOD/B3 have been taken [11].

The dominant FK1 exposure pathway contributing most to the number of early fatalities is the external exposure by radioactivity deposited on the ground. The increased washout rate therefore causes an enhanced number of early fatalities in case of FK1. For FK2 weather sequences without rain account predominantly for early fatalities, so there is no change to be noted. No early fatalities are calculated in case of FK6.

The height depending σ -parameters have replaced the roughness dependent. This accounts for a reduction of the calculated early fatalities in case of FK1, where the plume heights exceed in general 250m and the parameter set valid for this height range is used most frequently. For FK2 the calculated height covers a broad range of heights assigned to different parameter sets, which again accounts for a considerable reduction of early fatalities.

The reduced mixing heights do not affect early fatalities in case of FK2, while for FK1 an increase of 18% has to be stated. The mixing layer height determines the maximum σ_z -parameter. For neutral atmospheric

TAB. V RESULTS DUE TO MODIFICATIONS IN THE METEOROLOGICAL MODEL

Modification	Release category	Early Fatalities in rel. units	Late fatalities
Washout	FK1	1.76	1.00
	FK2	1.00	0.99
	FK6	-	1.01
height dep. σ -Parameter	FK1	0.57	1.01
	FK2	0.47	1.01
	FK6	-	1.08
reduced Mixing Height	FK1	1.18	1.04
	FK2	1.00	1.02
	FK6	-	0.97
Lift off	FK1	1.46	1.01
	FK2	1.03	1.01
	FK6	-	1.01
all effects inckuded	FK1	2.00	1.03
	FK2	0.49	1.00
	FK6	-	1.04

stratification these bounds are reached in a few kilometers distance from the reactor site. Combined with the extended plume heights of FK1 this results in an increased number of early fatalities.

The application of the lift off criterion causes an enhancement of early fatalities for FK1 and FK2 respectively. In case of FK1 additional weather sequences become effective.

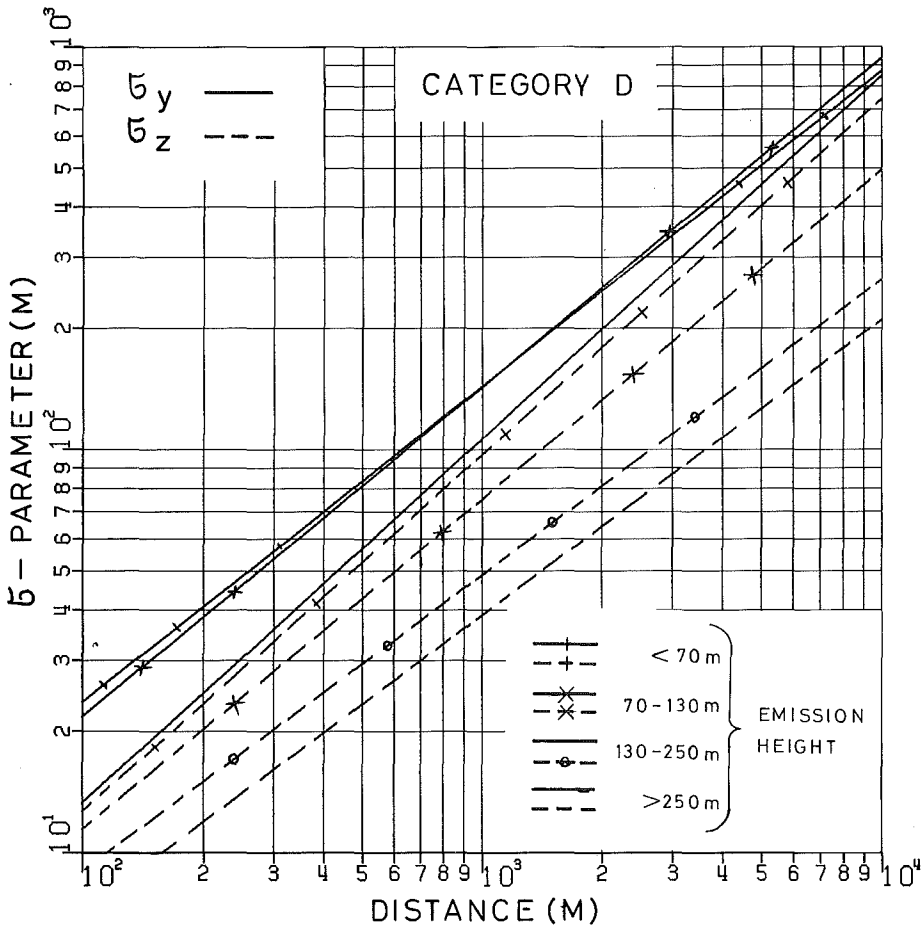
Having introduced all modifications into UFOMOD the number of collective early fatalities for FK1 is doubled whereas it is reduced in case of FK2. The number of late fatalities only varies between 0.97 and 1.08 and is turned out to be relatively insensitive to variations of meteorological parameters.

With respect to a more realistic approach compared to Phase A a series of modifications have been introduced to the meteorological submodel of UFOMOD for Phase B. While the collective damage of early fatalities is influenced considerably, late fatalities are only slightly affected.

References

- [1] Deutsche Risikostudie Kernkraftwerke
Fachband 8
Unfallfolgenrechnung und Risikoergebnisse
Verlag TÜV Rheinland, 1981
- [2] UFOMOD
Programm zur Berechnung der radiologischen Folgen von
Reaktorunfällen im Rahmen von Risikostudien
M. Schückler, S. Vogt; KfK-Bericht 3092, Januar 1981
Kernforschungszentrum Karlsruhe GmbH
- [3] Reactor Safety Study
An Assessment of Accident Risks in U.S. Commercial Nuclear
Power Plants
N.C. Rasmussen; NUREG - 75/014, WASH 1400, October 1975
U.S. Nuclear Regulatory Commission, Washington
- [4] The Calculation of Wet Deposition from Radioactive Plumes
H.D. Brenk, K.J.Vogt; Nuclear Safety Vol. 22, Nr.3 (1981)
- [5] Literaturstudie zum Kurzzeit-Washout-Faktor von Aerosolen
E. Schrödel, H. Urban; GRS-Bericht A - 609, Mai 1981
Gesellschaft für Reaktorsicherheit mbH
- [6] Niederschlag und Washout im Unfallfolgenmodell der Deutschen
Risikostudie Kernkraftwerke
S.Vogt, W.Hübschmann, P.Wittek; KfK-Bericht 3548, Juli 1983
Kernforschungszentrum Karlsruhe GmbH
- [7] Ausbreitung von Schadstoffen in der Atmosphäre
H. Geiß; KTG-Seminar Band 1
Kerntechnische Gesellschaft e.V., Verlag TÜV Rheinland
- [8] Jahresbericht 1980 der Hauptabteilung Sicherheit
KfK-Bericht 3113, April 1981
Kernforschungszentrum Karlsruhe GmbH
- [9] Untersuchung des Einflusses geänderter Parameter im Teilmodell
atmosphärischer Ausbreitung auf die Ergebnisse der Deutschen
Risikostudie Kernkraftwerke(DRS)
S.Vogt, P.Wittek; KfK-Bericht 3209, April 1982
Kernforschungszentrum Karlsruhe GmbH
- [10] Commonwealth Edison Company, 1981
Zion Probabilistic Safety Study, Chicago IL.
- [11] Unfallfolgenrechnungen und Risikoabschätzungen für Druck-
wasserreaktoren mit dem Rechenprogramm UFOMOD/B3
J. Ehrhardt, S. Vogt
KfK-Bericht 3373, Mai 1983
Kernforschungszentrum Karlsruhe GmbH

FIG. 1 HORIZONTAL AND VERTICAL DISPERSION PARAMETERS FOR DIFFERENT HEIGHTS



Effectiveness of Early Evacuation of Small Areas,
Shelter and Relocation in Reducing
Severe Accident Consequences

James A. Martin, Jr.
U.S. Nuclear Regulatory Commission
Washington, DC 20555

ABSTRACT

Relatively moderate scale emergency response actions by the public can provide substantial reductions in the number and chance of early and continuing health effects in the event of a major release of radionuclides from a nuclear power plant. In the event of a core melt accident scenario, early, precautionary evacuation of areas within 2 to 3 miles and sheltering elsewhere in the early time frame can substantially reduce the risk of early fatalities--to close to zero in some cases. In the further event of an actual major release of radioactivity to the atmosphere, expeditious relocation from highly contaminated areas would be necessary. This paper will discuss the calculations and emergency response assumptions that lead to these insights. Since emergency response is unlikely, the applications of these insights are more likely to be found in other areas such as emergency planning, siting and probabilistic risk analyses.

Light water nuclear reactor (LWR) risk studies in the United States have conventionally assumed evacuation by the public from an area within 10 miles of a nuclear power plant in the event of a large accidental release.¹ This study has examined the benefits of a protective action strategy employing an early evacuation of a relatively small area near the site, plus sheltering by the public in the remaining areas, and relocation from highly contaminated areas (hot spots) in the intermediate time frame.

The calculations were performed conditional upon a postulated SST1¹ release. This release is currently considered by the U.S. Nuclear Regulatory Commission to be characteristic of the most severe accidental releases possible from a light water reactor and would result from a core melt accident sequence where no fission product removal systems are assumed to be operable, where the containment fails early, and material is released directly to the atmosphere in a puff. The expected frequency of a release of this nature has been estimated to be about one per 100,000 reactor-years.¹ In this accident, 100 percent of the inventory of noble gases, 45 percent of radioiodine, and 65 percent of cesium and tellurium in a reactor core are postulated to be released to the atmosphere at a height of 10 meters, over a two hour period beginning 1.5 hours after accident initiation. An initial protective action warning is assumed to be given by the plant operators one half hour before the presumed release begins.

A version of the CRAC2 code² providing for three emergency response zones was used for the calculations. The washout coefficient₃ (for rainfall) in CRAC2 was reduced to 10^{-4} /sec per mm/hr of rainfall (from 10^{-3} for stability categories A thru D) to realistically bound observations.³ No other revisions to CRAC2 were made. Meteorology typical of the New York City area, in the CRAC2 data sets, was used for the calculations.

Differing public emergency responses were assumed for three radial zones as follows: (i) In the near zone, an evacuation at an effective speed of 10 mph of areas within 1, 2, 3 or 5 miles, with a one hour delay after warning was assumed. Thus, movement begins one half hour after the beginning of the release. (ii) In both the mid and far zones people were assumed to take shelter until after passage of the puff. People in these areas were assumed to be exposed to the full plume and, additionally, to four and eight hours of contaminated ground in the mid and far zones, respectively. (Note that in earlier estimates, people in the far zone were assumed to conduct normal activities for 24 hours before relocation from hot spots.⁴) The mid zone extended from the outer radius of the near zone to 10 miles while the far zone extended to all distances beyond 10 miles. Protection factors for the early evacuees were taken to be 0.5 for cloud and ground exposure and 1. for inhalation.

Protection factors of 0.33 were used for each pathway for those people in shelters. These protection factors are considered to be representative of one or two-story wood frame houses with basements, e.g., as would pertain for the northeastern United States.⁴ The sheltering times were chosen as estimates of the time that would be required for hot spots to be identified by radiological monitoring teams and for people to relocate from them. Because of delays before release and plume travel time, the elapsed time from accident initiation exceeds four (or eight) hours from the beginning of the accident, extending to six to twelve hours depending on wind speed and distance.

The potential mitigating effectiveness of early evacuations within 1, 2, or 3 miles is shown in Figure 1 for an 800 MW(e) reactor located at a coastal site in the U.S. With a three mile early evacuation (immediate shelter/relocation elsewhere), no acute fatalities were calculated. The results for several other U.S. sites studied (not shown) can be briefly summarized as follows: For low power levels, e.g., 550 MW(e), no acute fatalities were calculated assuming a two mile early evacuation. For the highest reactor power levels, most acute fatalities occurred at 0.5 to 1.0 miles where people were caught by the front of the puff release. For one relatively high population density site, where zero early fatalities was calculated for the highest reactor power level [1100 MW(e)], there were no residents within three miles in the CRAC2 data set. This illustrates the potential benefits of leaving the nearby area before a major release. Small numbers of acute injuries were calculated for all cases, but at low probability levels. These occurred within ten miles in most cases, but never beyond twelve miles. Peak acute fatalities and injuries were always associated with rain, a sudden calm after transport, or stable meteorology (low wind speeds, narrow plumes).

These results are in marked contrast to the large numbers of acute fatalities estimated in earlier studies for an accident of the SST1 type^{1,4}. Large absolute uncertainties must be associated with all such calculations. In particular, not all sites would have the same shelter characteristics as assumed here. Nevertheless, the relative worth of the emergency response strategies assumed in this study are clear. Such perspectives should be considered in emergency response planning and LWR risk studies.

REFERENCES

1. U.S. Nuclear Regulatory Commission, "Technical Guidance for Siting Criteria Development," NUREG/CR-2239 (December 1982).
2. U.S. Nuclear Regulatory Commission, "CRAC Calculations for Accident Sections of Environmental Statements," NUREG/CR-2901 (March 1983).
3. H. D. Brenk and K. J. Vogt, "The Calculation of Wet Deposition from Radioactive Plumes," *Nuclear Safety*, v. 22, n. 3, pp. 362-371 (May-June 1981).
4. U.S. Nuclear Regulatory Commission, "Calculations of Reactor Accident Consequences," WASH-1400/NUREG-75/014 (Reactor Safety Study), Appendix VI, October 1975.

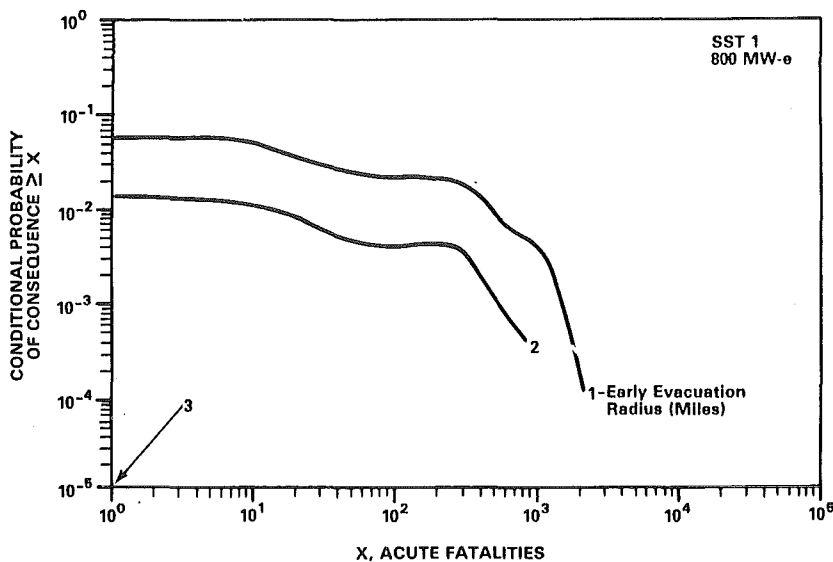


Figure 1. Conditional probabilities of various numbers of acute fatalities, assuming SST 1 accident, early evacuation of small areas, and a slow relocation from highly contaminated areas.

NOTE: There are large uncertainties in the absolute values of the scales in this figure.

MODELING THE ECONOMIC CONSEQUENCES OF LWR ACCIDENTS

Richard P. Burke and David C. Aldrich

Division 6415
Sandia National Laboratories
Albuquerque, New Mexico 87185 USA

Norman C. Rasmussen

Massachusetts Institute of Technology
Cambridge, Massachusetts 02139 USA

ABSTRACT

Models to be used for analyses of economic risks from events which may occur during LWR plant operation are developed in this study. The models include capabilities to estimate both onsite and offsite costs of LWR events ranging from routine plant outages to severe core-melt accidents resulting in large releases of radioactive material to the environment. The models can be used by both the nuclear power industry and regulatory agencies in cost-benefit analyses for decisionmaking purposes.

The newly developed economic consequence models are applied in an example to estimate the economic risks from operation of the Surry Unit #2 plant. The analyses indicate that economic risks from U.S. LWR operation, in contrast to public health risks, are dominated by relatively high-frequency forced outage events. Even for severe (e.g., core-melt) accidents, expected offsite costs are less than expected onsite costs for the Surry site. The implications of these conclusions for nuclear power plant operation and regulation are discussed.

INTRODUCTION

The purpose of this study was to develop models to be used for analyses of economic risks from unanticipated events which occur, or might occur, during LWR plant operation [1]. The models estimate the economic consequences of LWR forced outages and accidents from the societal perspective and can be used together with estimates of event frequencies to calculate the expected losses from LWR operational events of various severities. Both "onsite" costs, which either occur at onsite locations or most directly affect the plant licensee, and "offsite" costs, which most directly affect the public surrounding the plant, are estimated in the models. The models are used in an

example analysis to estimate the expected losses from both routine forced outage events and severe accidents during the remaining lifetime of the Surry #2 plant. The results of the analyses have important implications for both LWR plant licensees and regulatory agencies.

MODEL DESCRIPTIONS

The economic consequence models estimate the following onsite costs which either occur at onsite locations or most directly affect the plant licensee:

- power production cost increases (replacement power costs) due to LWR outage time,
- physical plant capital losses caused by severe accidents,
- plant decontamination costs,
- plant repair costs,
- early decommissioning costs after severe accidents,
- plant worker health impact costs.

The power production cost increases caused by the need for using generating facilities with higher fuel cycle costs during LWR outages are the dominant loss contributors for unanticipated forced outage events which do not result in core damage. These costs are estimated using models developed at Argonne National Laboratory which account for regional variations in the mix of generating facilities used to provide replacement power and the costs of replacement fuels [2]. These costs range from approximately \$250/MWe-day to \$1000/MWe-day of outage depending on the LWR plant location in the U.S. Plant repair cost estimates for forced outage events which do not result in core damage are based on operating experience in the U.S. The costs of plant repair for these events have generally been small relative to replacement power costs.

For more severe accidents, power production cost increases, physical plant capital losses, and plant decontamination costs are the most important onsite cost contributors. Plant decontamination costs are modeled based on experience with the Three Mile Island Unit #2 cleanup program and engineering studies of post-accident decontamination [3]. These costs are estimated to range between $\approx \$1 \times 10^9$ and $\approx \$2 \times 10^9$ depending on the physical progression and severity of the accident. Costs associated with decommissioning before the end of the planned plant lifetime and the costs of plant worker health effects do not contribute significantly to the expected onsite losses from either routine forced outage events or severe accidents. In addition to the onsite cost components included in the consequence models, electric utility business costs, nuclear power industry losses, and onsite litigation costs were addressed in the development of the consequence models. These costs could be very important to specific organizations after severe accidents.

Economic consequence models were also developed to estimate the offsite costs of severe accidents. Offsite costs are calculated probabilistically based on the estimated frequencies of specific releases of radioactive materials (source terms) and the meteorological conditions at the time of a release. The economic consequence models can utilize information regarding atmospheric dispersion, deposition, and public health effects calculated with CRAC2, UFOMOD, MARC, or other similar consequence calculation codes [4,5,6]. The models include the following offsite costs of public protective measures and health impacts for severe LWR accidents which might result in a significant release of radioactive material to the environment:

- evacuation costs,
- additional temporary population relocation costs,
- agricultural product disposal costs,
- land and property decontamination costs,
- land interdiction costs,
- permanent population relocation costs,
- health impact and medical care costs.

The costs of evacuation and temporary population relocation include the food, housing, and transportation costs to move individuals either prior to a release of radioactivity or from areas contaminated immediately after a release occurs. The loss of productivity of individuals moved from contaminated areas is also included in the relocation costs. Agricultural product disposal costs are the estimated market value of contaminated goods which are not suitable for consumption. Land and property decontamination costs are based on cost estimates for achieving specific exposure reduction factors in rural and urban areas. In addition, the cost of population relocation during decontamination is also included in the offsite cost models. The costs of land interdiction are estimated using present value discounting and the estimated tangible wealth contained within areas which cannot be decontaminated to acceptable levels for habitation. The costs of permanent population relocation from interdicted areas, including possible periods of productivity losses, are also calculated in the models. Finally, the purely economic costs of offsite health effects, including lost productivity and medical care costs, are included in the models.

Analyses performed using the above models indicate that the costs of population evacuation, temporary relocation, and possible agricultural product disposal are important for severe accidents which result only in very small releases of radioactive material to the environment. The costs of decontamination or interdiction of offsite land and property become important for severe accidents resulting in larger releases of radioactive material, and dominate the offsite costs of low probability accidents with very large releases of radioactive material.

A data base of U.S. LWR operating experience was developed as part of this study to estimate the frequency-severity spectrum of unanticipated forced outage events. The data base includes only forced outage events with causes related directly to plant operation. Forced outages caused by direct regulatory orders were not included in the data base but were analyzed separately. The forced outage data base includes a total of 367 reactor-years of operation which occurred during the period 1974-1980 at 67 U.S. plants. Table I shows the forced outage frequency statistics for the 67 plants during this period. Both the mean and median plant-specific forced outage frequencies for this period are approximately 10 events per reactor-year, with a range of forced outage frequencies from 2 events per reactor-year to 24 events per reactor-year. The mean duration for all forced outages during this period is approximately 83 hours, and the median duration is approximately 15 hours. Thus, during the 1974-1980 period of study, forced outages occurred frequently at U.S. LWRs causing an average plant availability loss of 10% per reactor-year of operation. The broad distributions of plant forced outage frequencies and durations demonstrate that certain plants have been successful at minimizing forced outage losses, while others have experienced very significant forced outage problems.

Table I. Statistical Parameters of Forced Outage Frequency
Data for 67 U.S. LWR Plants, 1974-1980

<u>Statistical Parameter</u>	<u>PWRs</u>	<u>BWRs</u>	<u>All LWRs</u>
Total Number of Plants	41	26	67
Mean Plant-Specific Forced Outage Frequency (per Reactor-Year)	11.3	9.4	10.6
Median Plant-Specific Forced Outage Frequency (per Reactor-Year)	11.2	9.6	10.4
Variance of Plant-Specific Forced Outage Frequency	24.4	17.0	22.1
Standard Deviation of Plant-Specific Forced Outage Frequency (per Reactor-Year)	4.9	4.1	4.7
Minimum Plant-Specific Forced Outage Frequency (per Reactor-Year)	2.8	2.3	2.3
Maximum Plant-Specific Forced Outage Frequency (per Reactor-Year)	24.3	21.0	24.3

EXAMPLE APPLICATIONS AND ANALYSES

The onsite and offsite economic consequence models have been combined with the 1974-1980 forced outage data base and the severe accident frequencies from the Reactor Safety Study (RSS) [7] to estimate the economic risks from plant operation over the remaining lifetime of the Surry #2 plant (uncertainties associated with the analyses are discussed in Reference [1], and, in general, are not expected to influence the conclusions presented here). Table II shows the expected losses from both routine forced outage events and severe (core-melt) accidents for the remaining lifetime of the plant (estimated to be approximately 30 years). The present values of expected losses for the remaining plant lifetime are expressed in 1982 U.S. dollars and are shown for discount rates of 0%, 4%, and 10%. The expected losses for routine forced outage events are based on the average operating experience for all plants in the 1974-1980 data base and estimated replacement power costs for the Surry #2 plant. The expected severe accident losses are based on the median core-melt accident frequencies and source terms from the RSS [7] with onsite and offsite economic consequence calculations performed with the new models in conjunction with the CRAC2 code [4]. Table II shows that the expected losses from severe accidents are small (\$1-\$6 million dollars) relative to the expected losses from routine outage events (\$84-\$270 million dollars) for the remaining lifetime of the Surry plant. This results from the relatively high frequency of forced outage events and the substantial power production cost increases for LWR forced outages. Table II also shows that even for core-melt accidents, expected onsite losses are substantially larger than expected offsite losses for the Surry plant.

Estimated complementary cumulative distribution functions (CCDFs) of core-melt accident economic costs for the remaining lifetime of the Surry #2 plant are shown in Figure 1. Each CCDF shows the probability of an accident with costs greater than a specified magnitude occurring at some time during the remaining lifetime of the Surry #2 plant. CCDFs are shown for (1) offsite costs excluding health effects, (2) offsite costs including health effects, (3) onsite replacement power and capital costs only, (4) onsite replacement power, capital, and plant decontamination costs, and (5) total onsite and offsite costs. The curves for onsite costs show that the most likely core-melt accidents are predicted to result in onsite costs much larger than offsite costs. The variations in onsite costs shown in the distribution function result from the dependence of replacement power costs and capital losses on the timing of an accident in the plant life. A core-melt accident which occurs near the end of plant life, when most of the capital cost of the plant has been recovered, would have smaller onsite costs than one which occurs near the beginning of plant life. The variations in offsite costs shown in the distribution functions result from the dependence on the specific release of radioactive materials and the weather conditions at the time of the release. The distributions of offsite costs show that only for very low probability events are offsite costs predicted to be larger than onsite costs. The offsite cost distributions also show that the costs of offsite health effects are predicted to be small relative to offsite property damage costs. This conclusion is supported by the results of previous studies [8] which have augmented dollar values for offsite health effects (e.g., \$1,000,000 per fatality) to represent all of the negative attributes of health impacts rather than only the purely economic costs which are included in this study.

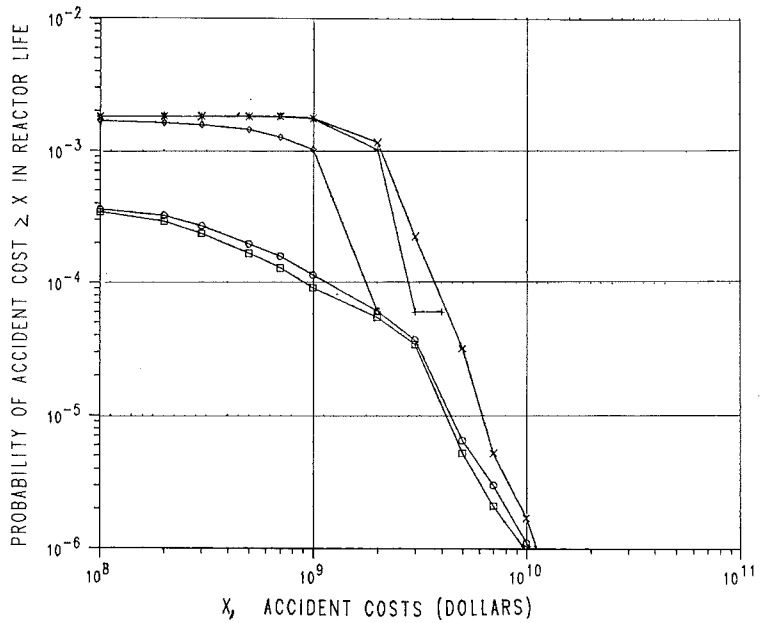
A breakdown of offsite cost components estimated using the economic consequence models for both a large release of radioactive material (the PWR-2 release category in the RSS) and a smaller release (the PWR-5 release category in the RSS) is shown in Table III. All costs are expressed in 1982 dollars

Table II. Present Value of Routine Outage and Severe Accident
Economic Risks for Remaining Life of Surry Unit #2 Plant

<u>Discount Rate</u>	<u>Routine Forced Outage Events</u>	<u>Core Melt Accidents</u>		
	<u>(No Core Damage)</u> <u>(≈10/reactor-year)</u>	<u>(≈6x10⁻⁵/reactor-year)*</u>		
		<u>Offsite</u>	<u>Onsite</u>	<u>Total</u>
0%	\$2.7x10 ⁸	\$4.4x10 ⁵	\$5.5x10 ⁶	\$5.9x10 ⁶
4%	\$1.6x10 ⁸	\$2.5x10 ⁵	\$3.3x10 ⁶	\$3.6x10 ⁶
10%	\$8.4x10 ⁷	\$1.3x10 ⁵	\$1.7x10 ⁶	\$1.8x10 ⁶

*Estimated risks for core-melt accidents based on RSS PWR core-melt accident frequencies and source terms with consequence calculations performed for the Surry #2 plant with new economic consequence models.

Figure 1. Complementary Cumulative Distribution Functions of Core-Melt Accident Economic Consequences for the Remaining Lifetime of the Surry #2 Plant.



□ OFFSITE COSTS EXCLUDING HEALTH EFFECTS	MEAN = 3.7E+05
○ OFFSITE COSTS INCLUDING HEALTH EFFECTS	MEAN = 4.3E+05
◇ ONSITE R. POWER AND CAPITAL COSTS ONLY	MEAN = 1.9E+06
⊕ ONSITE R. POWER, CAPITAL, AND CLEANUP COSTS	MEAN = 5.3E+06
× TOTAL ONSITE AND OFFSITE ACCIDENT COSTS	MEAN = 5.6E+06

Table III. Onsite and Offsite Accident Costs Conditional Upon RSS Category
PWR-2 and PWR-5 Releases, Surry Site

<u>Offsite Cost Component</u>	Mean Costs (1982 U.S. Dollars)	
	<u>PWR-2 Release</u>	<u>PWR-5 Release</u>
Evacuation	\$4.4x10 ⁶	\$4.4x10 ⁶
Emergency Phase Relocation	\$2.2x10 ⁷	\$5.9x10 ⁵
Intermediate Phase Relocation	\$7.6x10 ⁷	\$1.7x10 ⁶
Agricultural Product Disposal	\$9.1x10 ⁷	\$2.3x10 ⁶
Population Relocation During Decontamination	\$7.1x10 ⁷	\$2.8x10 ⁵
Land and Property Decontamination	\$6.4x10 ⁸	\$8.9x10 ⁶
Land and Property Interdiction	\$1.6x10 ⁸	\$9.9x10 ⁴
Interdicted Population Relocation	\$2.7x10 ⁷	\$2.4x10 ²
<u>Offsite Health Effects and Health Care</u>	<u>\$1.7x10⁸</u>	<u>\$6.8x10⁶</u>
Total Offsite Cost	\$1.3x10 ⁹	\$2.5x10 ⁷
<u>Total Onsite Cost</u>	<u>\$3.3x10⁹</u>	<u>\$3.3x10⁹</u>
<u>Other Attributes from Economic Models</u>	<u>PWR-2 Release</u>	<u>PWR-5 Release</u>
Total Population Dose Incurred, 0-100 Years	1.5x10 ⁵ Person-Sv	5.9x10 ³ Person-Sv
Total Population Dose Avoided by Protective Measures	3.1x10 ⁵ Person-Sv	1.3x10 ³ Person-Sv
Total Dose to Decontamination Workers	2.6x10 ³ Person-Sv	1.7x10 ¹ Person-Sv
Labor Required for Decontamination Program	1.1x10 ⁴ Person-Years	1.7x10 ² Person-Years
Number of Decontamination Workers Required for Completion of Program in 90 Days	4.6x10 ⁴ Persons	6.9x10 ² Persons

and are mean estimates conditional upon release occurrence. The table shows that costs associated with land and property decontamination and interdiction are the most important contributors to offsite costs for a large release of radioactive material, and that costs associated with evacuation, agricultural product disposal, and health effects and health care costs become more important for smaller releases. However, the comparison of total offsite and onsite costs in Table III shows that offsite costs are negligible relative to onsite costs for the PWR-5 source term. Even for the PWR-2 source term, onsite costs are larger than total offsite costs for the Surry site. Table III also shows other attributes of the post-accident recovery program which are calculated in the economic consequence models. The estimates of population exposures avoided by protective measures are useful for performing cost-benefit analyses in developing protective action criteria. The attributes of the required decontamination program, including exposures to workers and labor requirements, are useful for determining if resource limitations would be a problem in post-accident recovery operations. For example, Table III shows that a large number of decontamination workers would be required to complete the recovery program in a short period of time following a very large release (PWR-2) of radioactive material.

CONCLUSIONS AND DISCUSSION

The analyses of LWR outage frequencies and economic risks from LWR operation performed with the models developed in this study lead to the following conclusions:

1. In contrast to public health risks, economic risks from U.S. LWR operation are dominated by high frequency, small consequence forced outage events. Most of the costs of these events result from reduced plant availabilities and capacity factors and the need for use of higher marginal cost fuel sources for generation of electricity.
2. The economic risks from U.S. LWR operation are dominated by onsite losses resulting from replacement power costs for short-term outages. Severe accident economic risks are also dominated by onsite losses including replacement power costs, plant capital losses, and plant decontamination costs. For Surry, only very low probability core-melt accidents with large releases of radioactive material could result in offsite costs as large as onsite costs.
3. There is a strong economic incentive to reduce the frequency and durations of unanticipated forced outage events. Reduction of forced outage frequencies should result in a reduction in economic and public health risks from transient-induced severe accidents as well.

These conclusions have important implications for LWR licensees and operators. The analyses indicate that reduction of the frequencies and durations of forced outage events would result in large economic benefits from increased plant availabilities. Thus, an increased emphasis on improving LWR plant operations and maintenance to reduce forced outage losses is warranted on an economic basis. Reduction of forced outage frequencies should also result in a reduction of economic risks from transient-induced severe accidents. The analyses also indicate that risk management programs in the LWR industry should direct special attention to plants in the first few years of operation when the potential for large onsite losses is highest.

The conclusions of this study also have important implications for regulation of the LWR industry. Although reduction of core-melt accident frequencies and consequences is important for controlling public health risks, economic analyses indicate that limited societal resources might be more productively used in controlling routine forced outage losses. Reduction of routine outage frequencies would also reduce the frequencies of plant transients and thus might have some impact on core-melt accident frequencies and public health risks as well. Finally, expenditures for core melt accident prevention are likely to produce larger economic benefits than expenditures for systems which only mitigate the offsite consequences of core-melt accidents since a large portion of the expected costs result from onsite losses (replacement power, capital, and cleanup costs).

ACKNOWLEDGEMENTS

This work is supported by the United States Nuclear Regulatory Commission, Office of Nuclear Regulatory Research, and performed at Sandia National Laboratories which is operated for the United States Department of Energy under contract number DE-AC04-76DPO0789. This work was also supported by the U.S. Department of Energy Nuclear Engineering and Health Physics Fellowship program.

REFERENCES

1. Burke, R.P., Aldrich, D.C., and Rasmussen, N.C., Economic Risks of Nuclear Power Reactor Accidents. Albuquerque, NM: Sandia National Laboratories, NUREG/CR-3673 (SAND84-0178), April 1984.
2. Buehring, W.A., and Peerenboom, J.P., Loss of Benefits Resulting from Nuclear Plant Outages. Argonne, IL: Argonne National Laboratory, NUREG/CR-3045 (ANL/AA-28), March 1982.
3. Murphy, E.S., and G.M. Holter, Technology, Safety, and Costs of Decommissioning Reference Light-Water Reactors Following Postulated Accidents. Richland, WA: Pacific Northwest Laboratories, NUREG/CR-2601, September 1982.
4. Ritchie, L.T. et al., CRAC2 Model Description. Albuquerque, NM: Sandia National Laboratories, NUREG/CR-2552 (SAND82-0342), March 1984.
5. Bayer, A. et al., "The German Risk Study: Accident Consequence Model and Results of the Study." Nuclear Technology, Volume 59, October 1982.
6. Clark, R.H., and Kelly, G.N., MARC - The NRPB Methodology for Assessing Radiological Consequences of Accidental Releases of Activity. Chilton, England: National Radiological Protection Board, NRPB-R137, 1981.
7. U.S. Nuclear Regulatory Commission, The Reactor Safety Study, Main Report. Washington, D.C.: WASH-1400 (NUREG-075/14), October 1975.
8. Strip, D.R., Estimates of the Financial Consequences of Nuclear Power Reactor Accidents. Albuquerque, NM: Sandia National Laboratories, NUREG/CR-2723 (SAND82-1110), September 1982.

Impact of Assumptions Concerning Containment Failure
on the Risk from Nuclear Power Plants*

David A. Lappa

Lawrence Livermore National Laboratory
Livermore, California 94550, U.S.A.

ABSTRACT

We describe the containment failure mode and release category assumptions used in the seismic risk study of the Zion nuclear power plant, which was performed by the Seismic Safety Margins Research Program (SSMRP). We then, for the dominant accident sequences, reassign containment failure modes and release categories based upon current thinking. We recalculate the seismic risk from the Zion facility using the new assumptions. Lastly, we discuss the impact of the new assumptions on the results and the relevance of the assumptions to value/impact analyses.

INTRODUCTION

In 1978, the United States Nuclear Regulatory Commission began the Seismic Safety Margins Research Program at Lawrence Livermore National Laboratory. The primary goals of the SSMRP were to develop tools and data bases for evaluating the risk of earthquake induced radioactive releases from commercial nuclear power plants. In order to perfect and demonstrate SSMRP methods, a seismic risk assessment was performed for the Zion Nuclear Power Plant, a twin 1040 MWe Pressurized Water Reactor facility located on Lake Michigan 40 miles north of Chicago, Illinois.

Limited demonstration calculations were made as part of Phase I of the SSMRP. The calculations were completed in February, 1981. A 9-volume final report was issued during 1981-1982. The containment failure modes and release categories are discussed in the report for the systems analysis portion of the project [1]. The Zion plant seismic risk assessment was completed in October 1982 and reported in November 1983 [2]. All references to the SSMRP report in this study are for the Phase II results and final methodology.

* This work was supported by the U.S. NRC under a Memorandum of Understanding with the U.S. Department of Energy.

The general methodology employed in the SSMRP is a familiar one in the probabilistic risk assessment field. Using the general design of the plant as a guide, analysts defined a set of initiating events which could result from an earthquake at the Zion site. There were seven of these initiating events: 1) Reactor Vessel Rupture; 2) Large LOCA; 3) Medium LOCA; 4) Small LOCA; 5) Small-small LOCA; 6) Class 1 Transient; and 7) Class 2 Transient. Each of the events is capable of initiating reactor accident sequences which lead to a core melt and a release of radioactivity from the plant.

For each initiating event, an event tree was defined by the analysts based upon the safety systems at the plant, which are designed to mitigate the effects of reactor accidents. The event trees define the combinations of successes and failures of safety systems which make up the various accident sequences. A total of 219 accident sequences were defined and evaluated in the study. Of these, 178 lead to a core melt.

DEFINITION OF TERMS

Containment Failure Modes:

The SSMRP defined 5 ways in which the containment could fail. These five failure modes are represented by the first five letters of the Greek alphabet: ALPHA, BETA, GAMMA, DELTA, and EPSILON.

ALPHA: Reactor Pressure Vessel Steam Explosion

In this mode, the molten core contacts water in the vessel. This produces a steam explosion which fractures the reactor pressure vessel and disperses large amounts of core material into the containment atmosphere. The result is a sudden, large increase in containment atmosphere pressure and temperature which could fail the containment structure. Additionally, energetic missile fragments may be produced which can fail the containment spray equipment and, possibly, penetrate the containment.

BETA: Containment Leakage

In this mode, one or more of the normal penetrations into the containment fail to seal properly, thereby providing a leakage path for the radioactivity. This mode includes the passage of radioactivity from the containment to the outside via normal piping which may not be isolated effectively.

GAMMA: Hydrogen Detonation

In this case, hydrogen which has accumulated in the containment building over the course of the accident is ignited. This ignition produces a rapid temperature and pressure spike which ruptures the containment.

DELTA: Containment Overpressure

In this mode, the gradual buildup of pressure within the containment atmosphere results in a failure of the containment walls. This pressure can be due to the steam being generated by the degraded core as well as by other processes, especially the production of hydrogen and carbon dioxide during a core/concrete interaction.

EPSILON: Containment Basemat Melt Through

In this mode, the molten core, which has melted through the bottom of the pressure vessel and come to rest on the basemat floor beneath the vessel, eats completely through the containment basemat. Once it has done so, it continues to move through the supporting soil for several feet before finally coming to a halt.

Release Categories:

In addition to the containment failure modes, the SSMRP specified what the severity of the radioactive release would be given a particular accident sequence and containment failure mode. These release categories are numbered 1 through 7, each one representing a different type of release. Table I lists the release categories along with the public exposure assumed to be associated with them by the SSMRP [4].

 Table I

Public Consequences of the
 WASH-1400 Release Categories

<u>Release Category</u>	<u>man-rem per Release</u>
1	5.4E+6
2	4.8E+6
3	5.4E+6
4	2.7E+6
5	1.0E+6
6	1.5E+5
7	2.3E+4

ORIGINAL CONTAINMENT FAILURE ASSUMPTIONS

In the SSMRP, the assignment of the containment failure modes and release categories for each of the accident sequences was based largely upon the analyses from WASH-1400, the Reactor Safety Study [3]. This was possible because the WASH-1400 study included an analysis of a Pressurized Water Reactor whose safety systems were similar to those at the Zion Nuclear Power Plant. In fact, the SSMRP event trees list, for each accident, an equivalent accident sequence definition from the WASH-1400 study.

Table II below lists the most probable accident sequences from the Base Case of the SSMRP. (The Base Case is one of several case studies made and represents the best point estimate of seismic risk at Zion.) Together, these eight accident sequences account for an annual probability of core melt of $3.0e-6$, which is 85% of the total core melt annual probability of $3.5e-6$.

 Table II
 Dominant^a SSMRP Accident Sequences

	<u>Initiating Event</u>	<u>Accident Sequence</u>	<u>Definition</u>	<u>Probability</u>
1)	Class 2 Transient	T2-4a	<u>K</u> L B <u>P</u> <u>Q</u> C	$1.3e-6$
2)	Small-small LOCA	S2-35	<u>K</u> L C F	$4.1e-7$
3)	Small LOCA	S1-21	<u>K</u> C <u>D</u> <u>J</u> F <u>H</u>	$3.4e-7$
4)	Small LOCA	S1-28	<u>K</u> C D F	$3.2e-7$
5)	Large LOCA	A-13	<u>C</u> D <u>E</u>	$2.3e-7$
6)	Reactor Vessel Rupture	R-7	C F	$1.6e-7$
7)	Large LOCA	A-28	C D F	$1.3e-7$
8)	Small-small LOCA	S2-21	<u>K</u> <u>L</u> C <u>D</u> <u>J</u> F <u>H</u>	$1.2e-7$

^a Based upon contribution to core melt frequency.

Key to Accident Sequence Definitions:

B = Bleed & Feed System (B&FS)
 C = Containment Spray Injection System and Containment Fan Cooler System - Injection Phase (CSIS & CFCS(I))
 D = Emergency Coolant Injection (ECI)
 E = Containment Fan Cooler System - Recirculation Phase (CFCS(R))
 F = Residual Heat Removal System (RHRS)
 H = Emergency Coolant Recirculation (EGR)
 J = Emergency Core Functionability
 K = Reactor Protection System (RPS)
 L = Auxiliary Feedwater System & Secondary Steam Relief
 P = Safety/Relief Valves - Open (S/RV-O)
 Q = Safety/Relief Valves - Reclose (S/RV-R)

Note: X - underscore implies system success.

Table III below lists the eight dominant accident sequences identified in Table II along with the containment failure and release category assumptions made during the SSMRP. For each of the eight dominant accident sequences, the probability of the various containment failure modes is given along with the release category assumed for that containment failure mode. For example, the fifth entry, A-13 (Large LOCA sequence #13) is assumed to have a 1% chance of failing the containment via the ALPHA mode. In that case, there would be a category 3 release. Likewise, A-13 is assumed to have a 99% chance of failing the containment via the EPSILON mode, with a category 7 release resulting in that case. Finally, the BETA mode of failure was considered possible, but had less than a 1% chance of occurrence.

Note that, for each accident sequence, the containment failure mode probabilities are normalized to 1.0. This reflects the assumption by the SSMRP that, given an accident sequence that leads to a core melt, containment failure must occur at some point.

Table III

SSMRP Containment Failure Mode Assumptions
for Dominant Accident Sequences

	Accident Sequence	Containment Failure Mode Assumptions				
		ALPHA	BETA	GAMMA	DELTA	EPSILON
1)	T2-4a	1(.01)		2(.24)	2(.56)	6(.19)
2)	S2-35	1(.01)	2(*)	2(.12)	2(.04)	7(.83)
3)	S1-21	1(.01)			3(.99)	
4)	S1-28	1(.01)			7(.49)	7(.50)
5)	A-13	3(.01)	5(*)			7(.99)
6)	R-7	1(.06)	2(*)	2(.91)	2(.03)	
7)	A-28	1(.01)	4(*)		7(.49)	7(.50)
8)	S2-21	1(.01)	6(*)		3(.99)	

Note: a * implies less than .01 probability of occurrence.

SSMRP RESULTS

Using the above assumptions regarding containment failure modes, release categories, and public doses resulting from radioactive releases, the SSMRP calculated the seismic risk, in man-rem/yr, from the Zion Nuclear Power Plant. This risk was found to be 9.6 man-rem/yr.

The seismic risk found at Zion is unquestionably small. If the seismic risk at Zion is truly on the order of 10 man-rem/yr, then we need not concern ourselves with the seismic integrity of the plant. Unfortunately, all probabilistic risk assessments contain some degree of uncertainty. The SSMRP Zion study is no exception.

We are uncertain about both the core melt frequency and the public risk at Zion. The SSMRP Phase II report [2] contains the results of an uncertainty calculation which was performed as an integral part of the Zion seismic risk assessment. The uncertainty calculation resulted in a 90th percentile core melt frequency $8 \cdot 10^{-4}$ /yr, i.e., there is a 90% probability that the actual core melt frequency is $8 \cdot 10^{-4}$ /yr or less. This value is roughly a factor of 200 larger than the mean value of $3.6 \cdot 10^{-6}$ /yr.

We cannot say how the total risk scales with increasing core melt probability in the uncertainty study. For a single accident sequence, the probability of core melt is merely a linear factor in the expression for man-rem/yr. Thus, if the probability of the accident sequence increases by a factor of 5, then so does the man-rem/yr risk from that accident sequence. However, as total core melt probability increases, the relative contributions from the various accident sequences may change, causing the risk in man-rem/yr to scale in an unpredictable fashion.

Nevertheless, given that a core melt frequency estimate 200 times larger than the mean is within credible limits, and given that the uncertainty study performed in the SSMRP did not involve many facets of the methodology, including the systems analysis and the containment failure assumptions, we can see that it is important to reexamine the consequence models used in the SSMRP in light of the experience gained since the WASH-1400 study was performed.

REVISED CONTAINMENT FAILURE ASSUMPTIONS

Using results available to us from the ongoing source term assessments at the U.S. NRC, as well as other experience gained in the years since the WASH-1400 study was performed, particularly the Three Mile Island accident, we have updated the assumptions of containment failure probabilities and release categories. Table IV presents the results of our reassessment.

Table IV

Revised SSMRP Containment Failure Mode Assumptions

	Accident Sequence	Containment Failure Mode Assumptions				
		ALPHA	BETA	GAMMA	DELTA	EPSILON
1)	T2-4a		2(.01)		7(.79)	7(.20)
2)	S2-35		2(.01)		7(.79)	7(.20)
3)	S1-21		2(.01)	2(.01)	3(.98)	
4)	S1-28		2(.01)		7(.79)	7(.20)
5)	A-13		5(.01)			7(.99)
6)	R-7	1(.01)	2(.01)		6(.78)	7(.20)
7)	A-28		2(.01)		6(.79)	7(.20)
8)	S2-21		2(.01)	2(.01)	3(.98)	

In general, we notice that the probability of having ALPHA, GAMMA and EPSILON containment failure modes is now smaller. In contrast, the BETA and DELTA mode probabilities have increased. Notice that, as before, we assume that containment failure must occur, i.e., the total probability of containment failure is normalized to 1.0 for each accident sequence.

Notice also, that, for some accident sequences, the release categories have decreased in severity for a given containment failure mode. This reflects the effects of delaying containment failure upon the severity of release.

RESULTS USING REVISED ASSUMPTIONS

Recalculating the seismic risk at Zion using the assumptions given in Table IV yields a value of 3.6 man-rem/yr. Comparing against the original SSMRP risk value of 9.6 man-rem/yr, we see that the best estimate of seismic risk has decreased by 6 man-rem/yr because of our new assumptions. The probability of core melt is, of course, not affected by the assumptions and, thus, does not change.

Table V below presents the contribution to risk from each of the dominant accident sequences, using both the original and revised containment failure assumptions. Notice that, under the original assumptions, over half of the total seismic risk was contributed by the Class 2 Transient sequence T2-4a. Under the revised assumptions, this sequence is almost negligible. Consequently, we find that almost all of the risk is contributed by only two sequences: Small LOCA sequence S1-21, and Small-small LOCA sequence S2-21.

Please note that the total of 8.6 man-rem/yr risk from the dominant sequences examined is less than the total seismic risk of 9.6 man-rem/yr, the difference being the contribution of the remaining 170 accident sequences studied in the SSMRP.

 Table V
 Risk Contribution from Dominant^a Accident Sequences

	<u>Initiating Event</u>	<u>Accident Sequence</u>	<u>Contribution to Risk (man-Rem/yr)</u>	
			<u>Original</u>	<u>Revised</u>
1)	Class 2 Transient	T2-4a	5.1	0.1
2)	Small-small LOCA	S2-35	0.3	0.0
3)	Small LOCA	S1-21	1.8	1.8
4)	Small LOCA	S1-28	0.0	0.0
5)	Large LOCA	A-13	0.0	0.0
6)	Reactor Vessel Rupture	R-7	0.8	0.0
7)	Large LOCA	A-28	0.0	0.0
8)	Small-small LOCA	S2-21	0.6	0.6
		TOTAL:	8.6	2.5

^a Based upon contribution to core melt frequency.

CONCLUSIONS

The original point estimate of seismic risk at Zion of 9.6 man-rem/yr is too low to be of any concern. Thus, what we are primarily concerned with is the possibility that the containment failure mode and release category assumptions would, upon being updated, induce a sizable increase in the estimated risk from the facility. Certainly, one of the most obvious conclusions which can be drawn from the results is that this is not the case.

The other conclusion we can draw relates to the effects of containment failure mode and release category assumptions upon value/impact assessments.

Relevance to Value/Impact Assessments

In 1983, a value/impact assessment was performed to determine the effects of proposed changes to the U.S. NRC Standard Review Plan sections 3.7.1, 3.7.2 and 3.7.3, dealing with seismic design criteria [5]. As part of that assessment, a study was made of the effect upon seismic risk of strengthening the Refueling Water Storage Tank (RWST). It was found that strengthening the tank actually increased the seismic risk at the hypothetical PWR being studied. This result was directly attributed to assumptions concerning the containment failure modes and release categories which would follow the defined accident sequences.

Briefly, the phenomenon which was observed was the following. As the RWST was strengthened, the probability of having successful Emergency Coolant Injection increased. However, the stronger RWST had no impact on the probability of successful Emergency Coolant Recirculation or heat removal from containment. Thus, strengthening the RWST only served to insure a supply of water with which to produce steam in the containment. This served to increase the likelihood of containment overpressure, the DELTA mode, followed by rather severe releases.

In contrast, a failure to inject emergency coolant resulted in a "dry" reactor cavity. Thus, when the core melts through the reactor vessel, it reacts only with the concrete basemat, eventually ending with an EPSILON mode of failure, which is thought to have generally less severe consequences than the containment overpressure mode.

Table V above shows that the majority of the seismic risk under the new containment failure assumptions arises from sequences S1-21 and S2-21. Each of these sequences is characterized by successful Emergency Coolant Injection followed by unsuccessful heat removal from containment. Thus, under the new assumptions, we would expect that we would see the same type of relationship between risk and RWST strength as for the hypothetical PWR.

Clearly, there are a great deal of assumptions operative in the analysis; for example, the assumption that a failure to have successful emergency coolant injection results in a "dry" reactor cavity. If there is a total failure of the ECI system pumps, then this may be a valid assumption. If, instead, a partial pumping failure results in classifying the injection phase a failure, then we might still have a considerable volume of water available in the reactor cavity.

Another major assumption involves the severity of release which follows when the containment fails due to steam overpressurization. It is not clear whether the presence of large amounts of steam in the containment atmosphere at the time of rupture will act to improve or worsen the degree of radioactive release. Clearly, this assumption would impact the results of the above analysis.

At present, the U.S. NRC is engaged in a major reassessment of the source term from a nuclear power plant accident. When this work is completed, it may be possible to obtain more definitive results from value/impact assessments which involve consequences other than core melt frequency.

REFERENCES

1. J.E. Wells, L.L. George, and G.E. Cummings; Seismic Safety Margins Research Program: Phase I Final Report - Systems Analysis (Project VII); NUREG/CR-2015 Volume 8; UCRL-53021 Volume 8, November 1981
2. M.P.Bohn, L.C.Shieh, J.E.Wells, L.C.Cover, D.L.Bernreuter, J.C.Chen, J.J.Johnson, S.E.Bumpus, R.W.Mensing, W.J.O'Connell, and D.A.Lappa; Application of the SSMRP Methodology to the Seismic Risk at the Zion Nuclear Power Plant, NUREG/CR-3428; UCRL-53483, November 1983.
3. U.S. Nuclear Regulatory Commission; Reactor Safety Study: An Assessment of Accident Risks in U.S. Commercial Nuclear Power Plants, WASH-1400, NUREG-75/014, October 1975.
4. W.B. Andrews, R.H. Galucci, and G.J. Konzek; Guidelines for Nuclear Power Plant Safety Issue Prioritization Information Development, NUREG/CR-2800, Battelle Memorial Institute, Pacific Northwest Laboratory, May 1983.
5. D.W. Coats and D.A. Lappa; Unresolved Safety Issue A-40 Value/Impact Assessment, NUREG/CR-3480, UCRL-53489, November 1983.

AN ESTIMATION OF THE LOCA CONSEQUENCES OF A RESEARCH REACTOR
LOCATED WITHIN A LARGE POPULATION CENTRE

J.G. Kollas

N.R.C. "Democritos"
Greek Atomic Energy Commission
Aghia Paraskevi, Attiki, Greece

ABSTRACT

The LOCA consequences of a 5 MW swimming pool type research reactor located within the limits of Athens, Greece - a large population centre - are estimated. Twenty isotopes are taken into consideration in the source term. Doses and individual cancer risk from exposure to the radioactive cloud are calculated to a distance of about 20 km from the reactor site. Collective exposure and latent health effects due to early and chronic exposure are estimated for the over three million inhabitants of the Athens region.

INTRODUCTION

Many studies have been done in the past on the risk associated with nuclear power plants. However, little emphasis has been placed on the risk of research reactors and especially on the social risk of those research reactors located within a large population centre, which in some instances can not be neglected. This issue is dealt with in this present study and attention is focused to delimiting the consequences of a severe accident of the Greek Research Reactor (GRR).

GRR is a swimming pool type, light water moderated and cooled, research reactor with MTR type fuel elements¹. It is located near the north-western foot of the Immitos mountain in the district of Aghia Paraskevi, Fig. 1, at a distance of about 8 km from the centre of Athens city. The reactor is operated by the Greek Atomic Energy Commission and went critical in July 1961 at low power. In April 1964 the reactor started its operation at maximum power of 1 MW and seven years later in June 1971 the reactor reached its current maximum operation level of 5 MW. GRR is fueled with highly enriched uranium (about 90%) and is used for a number of purposes such as radioisotope production, reactor physics experiments, neutron diffraction and spectroscopy works, cross section measurements, solid state physics and radiation damage studies, activation analysis etc., and as a large gamma source for sterilization purposes during the shut-down period.

GRR has operated since 1961 without any major incident with adverse consequences either for the personnel of the Greek A.E.C. or the population around the reactor site. Nevertheless and in the framework of an ongoing safety analysis it was decided to estimate the potential consequences of a severe accident in order to delimit the consequences of the reactor's presence within Athens area, the largest population centre of Greece with over three million inhabitants and to assess the necessity of installing or not special engineered safeguards, assuring thus that an adequate level of safety is provided by the design of the reactor.



Fig. 1. Larger Athens area with GRR site.

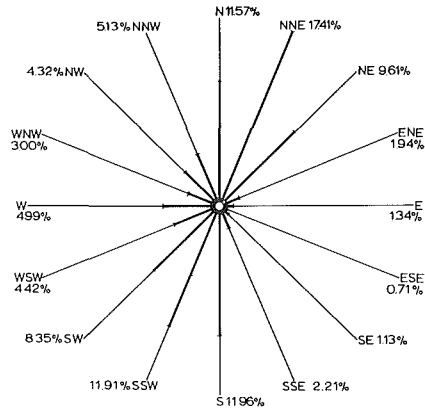


Fig. 2. Typical wind rose used for the calculations.

REACTOR ACCIDENT SOURCE TERM

The accident consequence calculations described in this study were performed using a version of the CRAC2 code^{2,3}, the improved version of the U.S. Reactor Safety Study consequence model⁴. The model describes the progression of the radioactive cloud released from the reactor building and predicts its interaction with and influence on the environment and man. One-year weather data are input to the dispersion model in the form of hourly observations of wind speed and direction, atmospheric stability and accumulated precipitation and radionuclide concentrations within the cloud are depleted by wet and dry deposition and by radioactive decay. Integrated air and ground concentrations are calculated for downwind distances. The consequence model uses the calculated airborne and ground radionuclide concentrations to estimate the population exposure to both external and internal radiation, the latter being calculated over the lifetime of the exposed population. From the calculated exposure the number of early and late health effects that would result from the accident are estimated. The early effects include fatalities and injuries and the late effects latent cancer fatalities plus benign and malignant thyroid nodules.

Among the accidents postulated for GRR the one with the most severe potential consequences on the environment and the public is a Loss-of-Coolant-Accident (LOCA) accompanied by a partial melting of the reactor core. This accident is designated as the design basis accident (DBA) of GRR, i.e. as the postulated accident for which the potential risk to the public is greater than that from any credible accident and for the mitigation of the consequences of which engineered safety systems may be needed. The credibility of the DBA is not under consideration and in the analysis we just postulate its occurrence.

In order to assess quantitatively the core melt level¹ an analysis of the accident in which either the outlet or the inlet coolant pipe connected to the bottom of the reactor tank is completely ruptured is performed, using the current version of a three-dimensional computer code THEAP-1, developed in NRC "Democritos"⁵. From a whole core analysis of GRR under the most severe LOCA conditions it was concluded that the core is likely to enter the melting conditions, and the amount of melting is roughly and conservatively estimated to be

Table I. Inventory of radionuclides in the 5 MWth GRR core and associated parameters

No.	Radionuclide	Radioactive inventory source (Ci x 10 ⁻⁴)	Half-life (days)	Deposition velocity(m/s)	Rain depletion
1	Krypton-85	0.03822	3919	0.0	0.0
2	Krypton-85m	4.738	0.1867	0.0	0.0
3	Krypton-87	8.477	0.05278	0.0	0.0
4	Krypton-88	13.76	0.1167	0.0	0.0
5	Strontium-89	4.940	52.00	0.01	1.0
6	Strontium-90	0.3007	10260	0.01	1.0
7	Strontium-91	13.26	0.3950	0.01	1.0
8	Yttrium-91	6.102	58.80	0.01	1.0
9	Zirconium-95	6.608	65.50	0.01	1.0
10	Niobium-95	6.725	35.10	0.01	1.0
11	Ruthenium-103	3.000	39.59	0.01	1.0
12	Ruthenium-106	0.2974	369.0	0.01	1.0
13	Tellurium-131m	0.7030	1.250	0.01	1.0
14	Tellurium-132	5.700	3.250	0.01	1.0
15	Iodine-131	3.250	8.040	0.01	1.0
16	Iodine-132	17.29	0.09521	0.01	1.0
17	Iodine-133	11.52	0.8667	0.01	1.0
18	Iodine-135	15.86	0.2744	0.01	1.0
19	Xenon-133	7.587	5.290	0.0	0.0
20	Xenon-135	14.47	0.3821	0.0	0.0
21	Cesium-136	0.0067	13.00	0.01	1.0
22	Cesium-137	0.2803	10990	0.01	1.0
23	Barium-140	6.800	12.79	0.01	1.0
24	Cerium-141	6.096	32.53	0.01	1.0
25	Cerium-144	5.309	284.4	0.01	1.0

of the order of 20%.

To calculate the source term resulting from this accident twenty-five isotopes were taken into consideration. GRR has an operating schedule of eight hours/day, five days/week. Under these conditions the source term was estimated at the time of maximum fission product inventory, i.e. immediately after the weekend shutdown preceding a fuel loading. Table I presents the inventory of radionuclides in the 5 MW GRR core and its associated parameters.⁶ The calculation of the source term emerges from a conservative estimate of fission product release to the reactor operating floor and further under the conservative assumptions of no filter mitigation and a ground release to the environment through leaks of the reactor building. Specifically the following figures, which represent the upper limit of the release fractions, are used:

Noble gases : 100%
 Iodines : 50%
 Other fission products: 1%

In order to estimate the DBA consequences of GRR the following additional assumptions are made: (a) the duration of the release is ten hours and its initiation is immediately after the accident, (b) the sensible heat of the release is negligible, (c) an exclusion area of 400m around the reactor is established excluding thus the Greek A.E.C. personnel from the analysis, and (d) no emergency measures are taken to mitigate the accident consequences.

For estimating doses and health effects the following factors are adopted:

Cloud shielding factor : 0.75
 Ground shielding factor : 0.33
 Individual breathing rate : $2.66 \cdot 10^{-4}$ m³/s

Table II. Summary of one year Athens area meteorological data using weather categories

<u>Weather category definitions³</u>			
R- Rain starting within indicated interval (km)			
S- Slowdown occurring within indicated interval (km)			
A-C, D,E,F- Stability categories			
1(0-1), 2(1-2), 3(2-3), 4(3-5), 5(>5)- Wind speed intervals (m/s)			
<u>No.</u>	<u>Weather category</u>	<u>Number of sequences</u>	<u>Percent of sequences</u>
1	R (0)	272	3.105
2	R (0-8)	143	1.632
3	R (8-16)	139	1.587
4	R (16-24)	149	1.701
5	R (24-32)	96	1.096
6	R (32-40)	62	0.708
7	R (40-48)	73	0.833
8	S (0-16)	55	0.628
9	S (16-24)	51	0.582
10	S (24-32)	47	0.537
11	S (32-40)	78	0.890
12	S (40-48)	87	0.993
13	A-C 1,2,3	2524	28.813
14	A-C 4,5	1286	14.680
15	D 1	536	6.119
16	D 2	245	2.797
17	D 3	148	1.690
18	D 4	294	3.356
19	D 5	355	4.053
20	E 1	0	0.0
21	E 2	0	0.0
22	E 3	131	1.495
23	E 4	92	1.050
24	E 5	0	0.0
25	F 1	1400	15.982
26	F 2	399	4.555
27	F 3	98	1.119
28	F 4	0	0.0
29	F 5	0	0.0
		8760	100.00

Furthermore for estimating latent health effects the BEIR method is employed.

METEOROLOGY AND POPULATION

The meteorological record used in the consequence calculations consists of the site wind rose, Fig. 2, and 8760 hourly observations of wind speed, atmospheric stability and accumulated precipitation. The record is completed by an unstable mixing height taken equal to 1,200m. An analysis of 6 years of meteorological data of the National Observatory of Athens led to the selection of 1979 as the most representative meteorological year of the Athens region for the period analyzed, and its meteorological record is used in the calculations.

To take properly into account the very low probability sequences with high consequences, such as the rain sequences, the importance sampling method is used^{3,8}. The entire year of meteorological data is sorted into the twenty-nine weather categories (bins) defined in Table II. Each of the 8760 potential meteorological sequences is categorized and placed in the corresponding weather category. Sequences are then sampled from each of these for use in the consequence estimation. In this present analysis sixteen sequences were selected from each weather category.

Finally, the demographic data were drawn from the most recent 1981 census. Athens area, the large population centre under consideration, contains about 3,081,000 people, which amounts to 32% of the population of Greece. (Details of the population distribution are included in Ref. 9).

LOCA CONSEQUENCES OF GRR

The consequences that could result from a severe reactor accident include short-term effects such as early fatalities and long-term effects such as latent deaths. The consequence analysis performed in this present study has shown that only long-term effects are expected from the DBA of GRR and in fact that most of the effects are not significant.

In this section we present certain characteristic aspects of the social and individual consequences resulting from GRR's LOCA which are due: (a) to the initial (early) exposure to the radioactive cloud, which includes direct irradiation by the passing cloud, exposure from inhaled radionuclides and exposure to deposited radioactive material, and (b) to both initial and chronic exposure from inhalation of resuspended radionuclides and exposure to groundshine from contaminated ground. Fig. 3,4 and 5 present the variation of doses and individual cancer risk from initial exposure with distance from the reactor site. Figs. 6,7 and 8 present individual risk results at certain distances from GRR in the form of complementary cumulative distribution functions (CCDF's), i.e. the probability that a consequence such as a dose or cancer risk of a given magnitude will be equalled or exceeded. Figs. 9,10,11, and 12 present social risk results such as the whole body collective exposure and latent health effects for the total Athens area population of 3,081,000 inhabitants.

Finally, in Table III a summary of the expected mean and peak values of the latent health effects for various organs and the whole body collective exposure of the population is presented.

CONCLUSIONS

The results presented in the previous section indicate that most of the consequences of GRR's design basis accident are of a rather limited magnitude with the exception of the nonfatal thyroid health effects. However, these consequences can not all be deemed minor and this creates the need of miti-

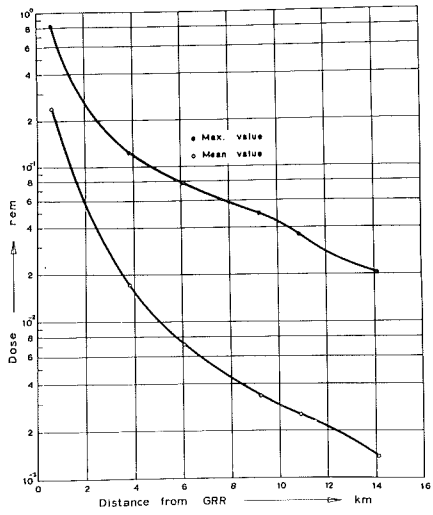


Fig 3. Acute bone marrow dose vs distance from GRR.

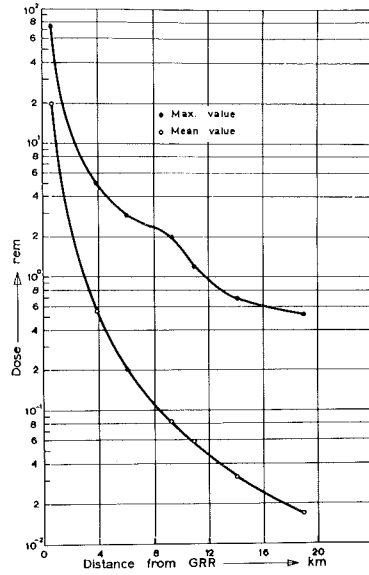


Fig 4. Acute thyroid dose vs distance from GRR.

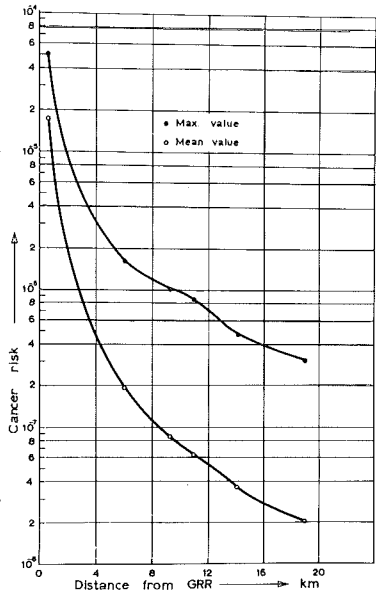


Fig 5. Cancer risk vs distance from GRR.

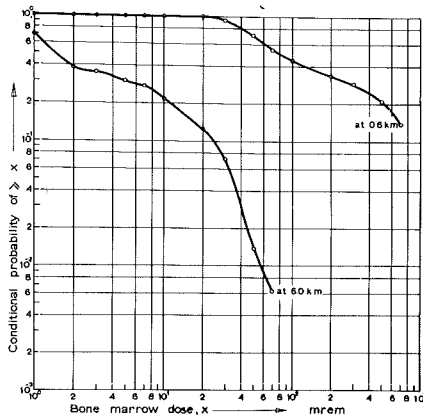


Fig 6. Acute bone marrow dose CCDF

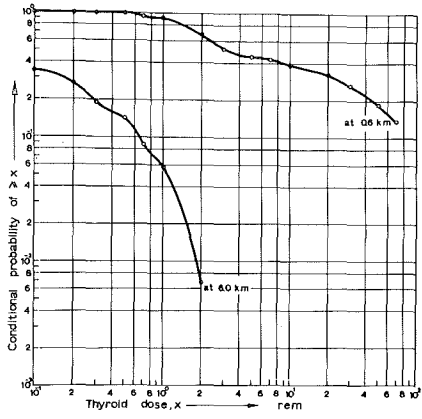


Fig. 7. Acute thyroid dose CCDF.

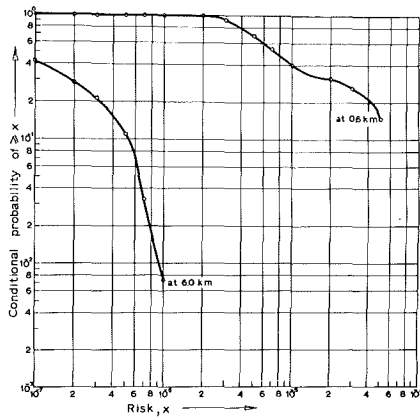


Fig. 8. Cancer risk from initial exposure CCDF

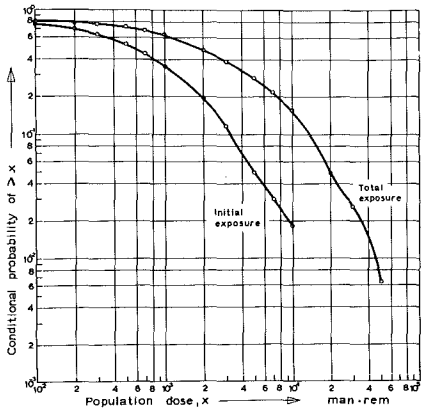


Fig. 9. Whole body population dose CCDF.

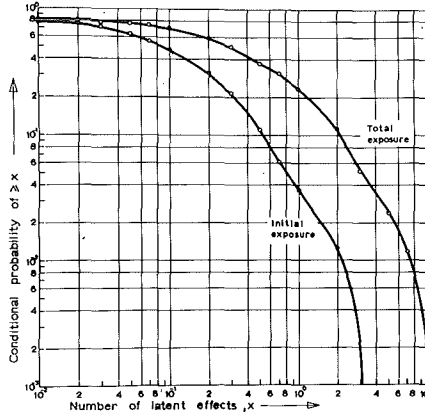


Fig. 10. Whole body latent effects CCDF.

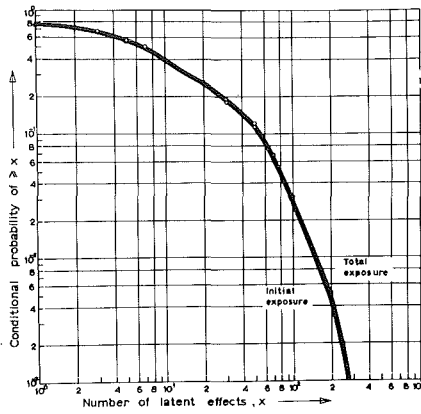


Fig. 11. Thyroid latent effects CCDF.

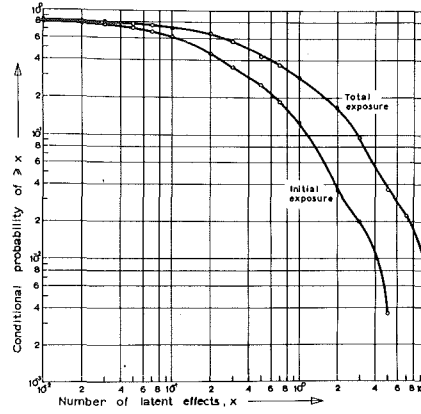


Fig. 12. Other latent effects CCDF.

Table III. Summary of latent health effects and collective exposure

Effect	Initial exposure		Initial and chronic exposure	
	Mean value	Peak value	Mean value	Peak value
Whole body	0.22	3.91	0.79	14.5
Thyroid	18.5	374	19.3	388
Leukemia	0.04	0.73	0.17	3.09
Lung	0.26	5.30	0.38	7.42
Breast	0.05	0.79	0.18	3.32
Bone	0.02	0.34	0.08	1.45
GI Tract	0.02	0.38	0.06	1.15
Other	0.05	0.80	0.19	3.37
<u>Whole body col- lective exposure</u> (man·rem)	1,340	25,000	5,030	91,800

gating them with appropriate engineered safety systems. It would seem reasonable also to assume that such a need would be borne for any similar research reactor of equal or larger magnitude, which is located within the limits of a large population centre. In the case of GRR to satisfy this need a simple emergency core cooling system (ECCS) was installed¹⁰, which by spraying large quantities of water on the reactor core and cooling it, would prevent its melting and exclude thus the release of radioactive materials to the environment in the event of a LOCA.

REFERENCES

1. C.N. Papastergiou, et al., Hazards Evaluation Report of the Greek Research Reactor-1, Greek Atomic Energy Commission, Aghia Paraskevi, Attiki, Greece, 1970.

2. L.T. Ritchie, J.D. Johnson, and R.M. Blond, Calculations of Reactor Accident Consequences, Version 2 (CRAC2):Computer Code User's Guide, NUREG/CR-2326, SAND 81-1994, Sandia National Laboratories, 1983.
3. L.T. Ritchie, et al., CRAC2 Model Description, NUREG/CR-2552, SAND 82-0342, Sandia National Laboratories, 1984.
4. Reactor Safety Study, Appendix VI : Calculation of Reactor Accident Consequences, U.S. Nuclear Regulatory Commission, WASH-1400 (NUREG-75/014),1975.
5. J.G. Bartzis, Whole Core Analysis of an Open Pool Research Reactor under the Most Severe Loss of Coolant Accident Conditions , DEMO 84/3, 1984.
6. J. Anoussis, and J. Armyriotis, Fission Product Releases from a Partial or Total Coremelt after a GRR Loss of Coolant Accident (in Greek), Reactor Safety Committee Internal Report, 1983.
7. Prof. D. Assimakopoulos, School of Meteorology, University of Athens, private communication.
8. L.T. Ritchie, D.C. Aldrich, and R.M. Blond, Weather Sequence Sampling for Risk Calculations, Trans. Am. Nucl. Soc., 38, p.113-15, 1981.
9. J. Kollas, et al., An Assessment of the Individual and Social Risk Resulting from a Hypothetical GRR-1 LOCA Release for Athens Population, DEMO 84/2, 1984.
10. C. Papastergiou, and C. Mitsonias, Emergency Core Cooling System for the Greek Research Reactor-1 'Democritos' (in Greek), DEMO 84/1G, 1984.